Woodhead Publishing Series in Energy:
Number 103

Handbook of Generation IV Nuclear Reactors

Edited by

Igor L. Pioro



ELSEVIER

AMSTERDAM • BOSTON • CAMBRIDGE • HEIDELBERG
LONDON • NEW YORK • OXFORD • PARIS • SAN DIEGO
SAN FRANCISCO • SINGAPORE • SYDNEY • TOKYO
Woodhead Publishing is an imprint of Elsevier



List of contributors

M. Allibert LPSC/IN2P3/CNRS - Université Grenoble Alpes, Grenoble, France

M. Aufiero LPSC/IN2P3/CNRS - Université Grenoble Alpes, Grenoble, France

F. Aydogan University of Idaho, Idaho Falls, ID, United States

M. Brovchenko Institut de Radioprotection et de Sûreté Nucléaire, Fontenay aux Roses, France

S.K. Chande Atomic Energy Regulatory Board, Mumbai, India

P. Chellapandi BHAVINI, Kalpakkam, India

L. Cinotti Hydromine Nuclear Energy S.à.r.l, Luxembourg

G. Clark Nuclear Adviser, Pell Frischmann Group, Manchester Square, London, UK

S. Delpech IPNO/IN2P3/CNRS, Orsay, France

A. Dragunov University of Ontario Institute of Technology, Oshawa, Ontario, Canada

R.B. Duffey DSM Associates Inc., Ammon, Idaho Falls, ID, United States

I. Dulera BARC, Mumbai, India

K. Gabriel University of Ontario Institute of Technology, Oshawa, Ontario, Canada

V. Ghetta LPSC/IN2P3/CNRS - Université Grenoble Alpes, Grenoble, France

D. Hahn Korea Atomic Energy Research Institute, Daejeon, Republic of Korea

D. Heuer LPSC/IN2P3/CNRS - Université Grenoble Alpes, Grenoble, France

M. Hosseiny University of Ontario Institute of Technology, Oshawa, Ontario, Canada

D. Hughes Hughes and Associates, Amsterdam, NY, United States

B. Ikeda University of Ontario Institute of Technology, Oshawa, Ontario, Canada

O.A. Jianu University of Ontario Institute of Technology, Oshawa, Ontario, Canada

H. Kamide Japan Atomic Energy Agency, Ibaraki, Japan

P.L. Kirillov State Scientific Centre of the Russian Federation - Institute of Physics and Power Engineering (IPPE) named after A.I. Leipunsky, Obninsk, Russia

S. Kubo Japan Atomic Energy Agency, Ibaraki, Japan

A. Laureau LPSC/IN2P3/CNRS - Université Grenoble Alpes, Grenoble, France

L. Leung Canadian Nuclear Laboratories, Chalk River, Ontario, Canada

E. Merle-Lucotte LPSC/IN2P3/CNRS - Université Grenoble Alpes, Grenoble, France

M. Morishita Japan Atomic Energy Agency, Ibaraki, Japan

G.F. Naterer Memorial University of Newfoundland, St. John's, NL, Canada

H. Ohshima Japan Atomic Energy Agency, Ibaraki, Japan

R. Panchal University of Ontario Institute of Technology, Oshawa, Ontario, Canada

D.V. Paramonov Nizhny Novgorod Atomenergoproekt, Moscow, Russia

E.D. Paramonova École Polytechnique Fédérale de Lausanne, Lausanne, Switzerland

W. Peiman University of Ontario Institute of Technology, Oshawa, Ontario, Canada

I.L. Pioro University of Ontario Institute of Technology, Oshawa, Ontario, Canada

M.A. Rosen University of Ontario Institute of Technology, Oshawa, Ontario, Canada

T. Sakai Japan Atomic Energy Agency, Ibaraki, Japan

Eu. Saltanov University of Ontario Institute of Technology, Oshawa, Ontario, Canada

T. Schulenberg Karlsruhe Institute of Technology, Karlsruhe, Germany

R.K. Sinha Department of Atomic Energy, India

C.F. Smith Naval Postgraduate School, Monterey, CA, United States

G. Srinivasan IGCAR, Kalpakkam, India

P. Tsvetkov Texas A&M University, College Station, TX, United States

G. Van Goethem European Commission, DG Research and Innovation, Energy - Euratom - Fission

P.K. Vijayan BARC, Mumbai, India

X.L. Yan Japan Atomic Energy Agency, Oarai-Machi, Ibaraki-ken, Japan

D. Zhang Xi'an Jiaotong University, Xi'an, People's Republic of China

C.O. Zvorykin National Technical University of Ukraine, Kyiv Polytechnic Institute, Peremohy Ave, Kiev, Ukraine

Woodhead Publishing Series in Energy

1 **Generating power at high efficiency: Combined cycle technology for sustainable energy production**
Eric Jeffs

2 **Advanced separation techniques for nuclear fuel reprocessing and radioactive waste treatment**
Edited by Kenneth L. Nash and Gregg J. Lumetta

3 **Bioalcohol production: Biochemical conversion of lignocellulosic biomass**
Edited by Keith W. Waldron

4 **Understanding and mitigating ageing in nuclear power plants: Materials and operational aspects of plant life management (PLiM)**
Edited by Philip G. Tipping

5 **Advanced power plant materials, design and technology**
Edited by Dermot Roddy

6 **Stand-alone and hybrid wind energy systems: Technology, energy storage and applications**
Edited by John K. Kaldellis

7 **Biodiesel science and technology: From soil to oil**
Jan C. J. Bart, Natale Palmeri and Stefano Cavallaro

8 **Developments and innovation in carbon dioxide (CO_2) capture and storage technology Volume 1: Carbon dioxide (CO_2) capture, transport and industrial applications**
Edited by M. Mercedes Maroto-Valer

9 **Geological repository systems for safe disposal of spent nuclear fuels and radioactive waste**
Edited by Joonhong Ahn and Michael J. Apted

10 **Wind energy systems: Optimising design and construction for safe and reliable operation**
Edited by John D. Sørensen and Jens N. Sørensen

11 **Solid oxide fuel cell technology: Principles, performance and operations**
Kevin Huang and John Bannister Goodenough

12 **Handbook of advanced radioactive waste conditioning technologies**
Edited by Michael I. Ojovan

13 **Membranes for clean and renewable power applications**
Edited by Annarosa Gugliuzza and Angelo Basile

14 **Materials for energy efficiency and thermal comfort in buildings**
Edited by Matthew R. Hall

15 **Handbook of biofuels production: Processes and technologies**
Edited by Rafael Luque, Juan Campelo and James Clark

16 **Developments and innovation in carbon dioxide (CO_2) capture and storage technology Volume 2: Carbon dioxide (CO_2) storage and utilisation**
Edited by M. Mercedes Maroto-Valer

17 **Oxy-fuel combustion for power generation and carbon dioxide (CO_2) capture**
Edited by Ligang Zheng

18 **Small and micro combined heat and power (CHP) systems: Advanced design, performance, materials and applications**
Edited by Robert Beith

19 **Advances in clean hydrocarbon fuel processing: Science and technology**
Edited by M. Rashid Khan

20 **Modern gas turbine systems: High efficiency, low emission, fuel flexible power generation**
Edited by Peter Jansohn

21 **Concentrating solar power technology: Principles, developments and applications**
Edited by Keith Lovegrove and Wes Stein

22 **Nuclear corrosion science and engineering**
Edited by Damien Féron

23 **Power plant life management and performance improvement**
Edited by John E. Oakey

24 **Electrical drives for direct drive renewable energy systems**
Edited by Markus Mueller and Henk Polinder

25 **Advanced membrane science and technology for sustainable energy and environmental applications**
Edited by Angelo Basile and Suzana Pereira Nunes

26 **Irradiation embrittlement of reactor pressure vessels (RPVs) in nuclear power plants**
Edited by Naoki Soneda

27 **High temperature superconductors (HTS) for energy applications**
Edited by Ziad Melhem

28 **Infrastructure and methodologies for the justification of nuclear power programmes**
Edited by Agustín Alonso

29 **Waste to energy conversion technology**
Edited by Naomi B. Klinghoffer and Marco J. Castaldi

30 **Polymer electrolyte membrane and direct methanol fuel cell technology Volume 1: Fundamentals and performance of low temperature fuel cells**
Edited by Christoph Hartnig and Christina Roth

31 **Polymer electrolyte membrane and direct methanol fuel cell technology Volume 2: *In situ* characterization techniques for low temperature fuel cells**
Edited by Christoph Hartnig and Christina Roth

32 **Combined cycle systems for near-zero emission power generation**
Edited by Ashok D. Rao

33 **Modern earth buildings: Materials, engineering, construction and applications**
Edited by Matthew R. Hall, Rick Lindsay and Meror Krayenhoff

34 **Metropolitan sustainability: Understanding and improving the urban environment**
Edited by Frank Zeman

35 **Functional materials for sustainable energy applications**
Edited by John A. Kilner, Stephen J. Skinner, Stuart J. C. Irvine and Peter P. Edwards

36 **Nuclear decommissioning: Planning, execution and international experience**
Edited by Michele Laraia
37 **Nuclear fuel cycle science and engineering**
Edited by Ian Crossland
38 **Electricity transmission, distribution and storage systems**
Edited by Ziad Melhem
39 **Advances in biodiesel production: Processes and technologies**
Edited by Rafael Luque and Juan A. Melero
40 **Biomass combustion science, technology and engineering**
Edited by Lasse Rosendahl
41 **Ultra-supercritical coal power plants: Materials, technologies and optimisation**
Edited by Dongke Zhang
42 **Radionuclide behaviour in the natural environment: Science, implications and lessons for the nuclear industry**
Edited by Christophe Poinssot and Horst Geckeis
43 **Calcium and chemical looping technology for power generation and carbon dioxide (CO_2) capture: Solid oxygen- and CO_2-carriers**
Paul Fennell and E. J. Anthony
44 **Materials' ageing and degradation in light water reactors: Mechanisms, and management**
Edited by K. L. Murty
45 **Structural alloys for power plants: Operational challenges and high-temperature materials**
Edited by Amir Shirzadi and Susan Jackson
46 **Biolubricants: Science and technology**
Jan C. J. Bart, Emanuele Gucciardi and Stefano Cavallaro
47 **Advances in wind turbine blade design and materials**
Edited by Povl Brøndsted and Rogier P. L. Nijssen
48 **Radioactive waste management and contaminated site clean-up: Processes, technologies and international experience**
Edited by William E. Lee, Michael I. Ojovan, Carol M. Jantzen
49 **Probabilistic safety assessment for optimum nuclear power plant life management (PLiM): Theory and application of reliability analysis methods for major power plant components**
Gennadij V. Arkadov, Alexander F. Getman and Andrei N. Rodionov
50 **The coal handbook: Towards cleaner production Volume 1: Coal production**
Edited by Dave Osborne
51 **The coal handbook: Towards cleaner production Volume 2: Coal utilisation**
Edited by Dave Osborne
52 **The biogas handbook: Science, production and applications**
Edited by Arthur Wellinger, Jerry Murphy and David Baxter
53 **Advances in biorefineries: Biomass and waste supply chain exploitation**
Edited by Keith Waldron
54 **Geological storage of carbon dioxide (CO_2): Geoscience, technologies, environmental aspects and legal frameworks**
Edited by Jon Gluyas and Simon Mathias
55 **Handbook of membrane reactors Volume 1: Fundamental materials science, design and optimisation**
Edited by Angelo Basile

56 **Handbook of membrane reactors Volume 2: Reactor types and industrial applications**
Edited by Angelo Basile

57 **Alternative fuels and advanced vehicle technologies for improved environmental performance: Towards zero carbon transportation**
Edited by Richard Folkson

58 **Handbook of microalgal bioprocess engineering**
Christopher Lan and Bei Wang

59 **Fluidized bed technologies for near-zero emission combustion and gasification**
Edited by Fabrizio Scala

60 **Managing nuclear projects: A comprehensive management resource**
Edited by Jas Devgun

61 **Handbook of Process Integration (PI): Minimisation of energy and water use, waste and emissions**
Edited by Jiří J. Klemeš

62 **Coal power plant materials and life assessment**
Edited by Ahmed Shibli

63 **Advances in hydrogen production, storage and distribution**
Edited by Ahmed Basile and Adolfo Iulianelli

64 **Handbook of small modular nuclear reactors**
Edited by Mario D. Carelli and Dan T. Ingersoll

65 **Superconductors in the power grid: Materials and applications**
Edited by Christopher Rey

66 **Advances in thermal energy storage systems: Methods and applications**
Edited by Luisa F. Cabeza

67 **Advances in batteries for medium and large-scale energy storage**
Edited by Chris Menictas, Maria Skyllas-Kazacos and Tuti Mariana Lim

68 **Palladium membrane technology for hydrogen production, carbon capture and other applications**
Edited by Aggelos Doukelis, Kyriakos Panopoulos, Antonios Koumanakos and Emmanouil Kakaras

69 **Gasification for synthetic fuel production: Fundamentals, processes and applications**
Edited by Rafael Luque and James G. Speight

70 **Renewable heating and cooling: Technologies and applications**
Edited by Gerhard Stryi-Hipp

71 **Environmental remediation and restoration of contaminated nuclear and NORM sites**
Edited by Leo van Velzen

72 **Eco-friendly innovation in electricity networks**
Edited by Jean-Luc Bessede

73 **The 2011 Fukushima nuclear power plant accident: How and why it happened**
Yotaro Hatamura, Seiji Abe, Masao Fuchigami and Naoto Kasahara. Translated by Kenji Iino

74 **Lignocellulose biorefinery engineering: Principles and applications**
Hongzhang Chen

75 **Advances in membrane technologies for water treatment: Materials, processes and applications**
Edited by Angelo Basile, Alfredo Cassano and Navin Rastogi

76 **Membrane reactors for energy applications and basic chemical production**
Edited by Angelo Basile, Luisa Di Paola, Faisal Hai and Vincenzo Piemonte
77 **Pervaporation, vapour permeation and membrane distillation: Principles and applications**
Edited by Angelo Basile, Alberto Figoli and Mohamed Khayet
78 **Safe and secure transport and storage of radioactive materials**
Edited by Ken Sorenson
79 **Reprocessing and recycling of spent nuclear fuel**
Edited by Robin Taylor
80 **Advances in battery technologies for electric vehicles**
Edited by Bruno Scrosati, Jürgen Garche and Werner Tillmetz
81 **Rechargeable lithium batteries: From fundamentals to applications**
Edited by Alejandro A. Franco
82 **Calcium and chemical looping technology for power generation and carbon dioxide (CO_2) capture**
Edited by Paul Fennell and Ben Anthony
83 **Compendium of hydrogen energy Volume 1: Hydrogen production and purification**
Edited by Velu Subramani, Angelo Basile and T. Nejat Veziroglu
84 **Compendium of hydrogen energy Volume 2: Hydrogen storage, transmission, transportation and infrastructure**
Edited by Ram Gupta, Angelo Basile and T. Nejat Veziroglu
85 **Compendium of hydrogen energy Volume 3: Hydrogen energy conversion**
Edited by Frano Barbir, Angelo Basile and T. Nejat Veziroglu
86 **Compendium of hydrogen energy Volume 4: Hydrogen use, safety and the hydrogen economy**
Edited by Michael Ball, Angelo Basile and T. Nejat Veziroglu
87 **Advanced district heating and cooling (DHC) systems**
Edited by Robin Wiltshire
88 **Microbial electrochemical and fuel cells: Fundamentals and applications**
Edited by Keith Scott and Eileen Hao Yu
89 **Renewable heating and cooling: Technologies and applications**
Edited by Gerhard Stryi-Hipp
90 **Small modular reactors: Nuclear power fad or future?**
Edited by Daniel T. Ingersoll
91 **Fuel flexible energy generation: Solid, liquid and gaseous fuels**
Edited by John Oakey
92 **Offshore wind farms: Technologies, design and operation**
Edited by Chong Ng & Li Ran
93 **Uranium for nuclear power: Resources, mining and transformation to fuel**
Edited by Ian Hore-Lacy
94 **Biomass supply chains for bioenergy and biorefining**
Edited by Jens Bo Holm-Nielsen and Ehiaze Augustine Ehimen
95 **Sustainable energy from salinity gradients**
Edited by Andrea Cipollina and Giorgio Micale
96 **Membrane technologies for biorefining**
Edited by Alberto Figoli, Alfredo Cassano and Angelo Basile
97 **Geothermal power generation: Developments and innovation**
Edited by Ronald DiPippo

98 **Handbook of biofuels' production: Processes and technologies (Second edition)**
Edited by Rafael Luque, Carol Sze Ki Lin, Karen Wilson and James Clark
99 **Magnetic fusion energy: From experiments to power plants**
Edited by George H. Neilson
100 **Advances in ground-source heat pump systems**
Edited by Simon Rees
101 **Absorption-based post-combustion capture of carbon dioxide**
Edited by Paul Feron
102 **Advances in solar heating and cooling systems**
Edited by Ruzhu Wang and Tianshu Ge
103 **Handbook of Generation IV nuclear reactors**
Edited by Igor L. Pioro

Foreword

Dear Readers:

Elsevier is presenting this new *Handbook of Generation IV Nuclear Reactors*, which has been written by nuclear engineering experts throughout the world. The need for this Handbook is based on the absence of any such comprehensive text, and has the following rationale.

Currently, nuclear power plants (NPPs), with about 436 nuclear-power reactors[1], generate about 11.2% of electricity around the world, and demand for this essential and reliable energy source, free from greenhouse gases, is and will be growing. Interest in the use of nuclear energy for electricity generation is leading to new nuclear reactors being built in many countries: currently, 31 countries have operating nuclear power reactors, and 4 countries without reactors presently work on adding new builds.

The safe and efficient operation of the current fleet of NPPs is essential, as is their life extension for global sustainability and human well-being. These current generation reactors/NPPs, largely water-cooled, have and are serving the world well. The remaining challenges include advances in thermal efficiency, managing rare event safety, fuel cycle enhancements, improved economic competitiveness, ensuring that nuclear weapons proliferation concerns are addressed, and radioactive waste management with full public and political participation. These technical developments are against the global backdrop of concerns and issues over climate change, economic growth, sustainable and renewable energy use, optimal resource development, political stability, international security, and environmental conservation.

The future, therefore, also lies in the development of the next generation of nuclear energy: Generation IV nuclear power reactors and other advanced reactor concepts/designs, which offer potential solutions to many of these problems, including advances in the use of risk-informed decision making and safety regulations. New reactor/NPP designs and regulations will incorporate the latest developments and understanding in this important engineering/scientific discipline.

Therefore, to place the latest developments in context and elaborate the global technical and social issues, the Handbook consists of the following sections:

1. Introduction, in which all industrial methods of electricity generation in the world are listed, with the emphasis on nuclear energy and its role in future electricity generation.

[1] This number includes 43 reactors from Japan from which only 3 currently in operation; however, more reactors are planned to put into operation soon.

2. Part One, which is completely dedicated to six Generation IV concepts: (1) Gas-cooled Fast Reactor (GFR) or just High Temperature Reactor (HTR); (2) Very High Temperature Reactor (VHTR); (3) Sodium-cooled Fast Reactor (SFR); (4) Lead-cooled Fast Reactor (LFR); (5) Molten Salt Reactor (MSR); and (6) SuperCritical Water-cooled Reactor (SCWR); and which is started with the official information from the Generation IV International Forum (GIF).
3. Part Two, which is a summary of Generation IV activities in the following countries: (1) USA; (2) European Union; (3) Japan; (4) Russia; (5) South Korea; (6) China; and (7) India.
4. Part Three, which is dedicated to related topics for Generation IV reactors including: Safety of advanced reactors; non-proliferation for advanced reactors – political and social aspects; thermal aspects of conventional and alternative fuels; hydrogen co-generation with Generation IV NPPs; and advanced small modular reactors.
5. Technical Appendices, which provides readers with additional information and data on current nuclear power reactors and NPPs: thermophysical properties of reactor coolants, thermophysical properties of fluids at subcritical and critical/supercritical pressures, heat transfer and pressure drop in forced convection to fluids at supercritical pressures, world experience in nuclear steam reheat, etc.

Our editorial and author team consists of senior international experts in the corresponding nuclear engineering areas, which represents the following countries: (1) Canada; (2) China; (3) European Union; (4) France; (5) Germany; (6) India; (7) Japan; (8) Russia; (9) South Korea; (10) Ukraine; (11) United Kingdom; and (12) US. Members of the editorial team are from academia, industry including nuclear vendors and NPPs, international organizations, government research, and scientific establishments, etc.

We welcome you to the *Handbook of Generation IV Nuclear Reactors*, and we are looking forward to seeing your comments, suggestions, and criticism to improve our future editions. Also, please enjoy reading the chapters that follow.

This unique international handbook edition combines history of development, research, industrial operating experience, new designs, systems and safety analysis, and applications of nuclear energy and many other related topics that help change the world and our lives for the best!

This Handbook is recommended for a wide range of specialists within the areas of nuclear engineering, power engineering, mechanical engineering, environmental studies, and for undergraduate and graduate students of the corresponding departments as a textbook.

Igor L. Pioro and Romney B. Duffey on behalf of the editorial team

Preface

The inspiration for creating a forum for international collaboration on advanced reactor research came out of a meeting in Washington, D.C., in 2000. The nine founding members of the Generation IV International Forum (GIF) carefully set about establishing system performance goals, identifying 6 major development tracks from more than 100 competing concepts using a screening methodology along with four goal areas (sustainability, economics, safety and reliability, proliferation resistance and physical protection), 15 criteria, and 24 metrics. Chartered in 2001, GIF formally began collaborative research in 2006 after a legal framework, a technology roadmap, and detailed initial project plans were completed.

The 2015 United Nationals Conference on Climate Change (COP21) helped highlight the essential role of nuclear energy in climate-friendly electricity production. The International Energy Agency (IEA) estimated that current global use of nuclear energy avoids 1.7 Gt of CO_2 emissions annually. Going forward, in order for nuclear energy to meet its potential in abating climate change, new plants will employ advanced technology. Notably, the next generation of nuclear power systems will produce electricity at competitive prices while assuring a concerned public that the issues of safety, waste management, proliferation resistance, and resource optimization have been satisfactorily addressed.

These concerns are the very issues that guide Generation IV research and development. When successfully deployed, the robust safety of Generation IV systems will assuage public anxiety and assure protection of capital investment. Coupled with an advanced fuel cycle, Generation IV reactors will reduce the volume of nuclear waste and improve uranium resource utilization by two orders of magnitude, without increasing proliferation risk.

This *Handbook of Generation IV Nuclear Reactors* is organized along the lines of the six systems originally selected by GIF in 2002 (and reaffirmed in 2012). It summarizes the collective progress made under the GIF banner, as well as the status of development in countries with substantial advanced reactor and fuel cycle research and development programs. Both are important. The bulk of the global funding and effort goes into the national programs, which ultimately produce the costly prototypes and demonstrations that will lead to commercialization of these systems. On the other hand, GIF fosters collaboration in the earlier stages of research and technology development by arranging joint projects and sharing key research facilities. GIF also takes the lead on developing criteria and guidelines for Generation IV designs, and supports regulatory bodies in developing rational strategies for licensing advanced reactors.

GIF welcomes Elsevier's publication of this *Handbook of Generation IV Nuclear Reactors*, which is a significant addition to the growing body of literature on advanced nuclear power systems. A convenient overview of all Generation IV systems, it will meet the information needs of those who seek a basic familiarization as well as those who want a solid basis for further study. GIF congratulates the editor and Elsevier for undertaking this ambitious project.

Generation IV International Forum (GIF)

Nomenclature

Symbols

P, p	Pressure, Pa
s	Specific entropy, J/kg K
Q	Heat-transfer rate, W
T, t	Temperature, °C or K

Subscripts

cr	Critical
el	Electrical
in	Inlet
max	Maximum
out	Outlet
pc	Pseudocritical
sat	Saturation
th	Thermal

Acronyms/Abbreviations

ABWR	Advanced boiling water reactor
ADS	Accelerator driven system
AECL	Atomic Energy of Canada Limited
AGR	Advanced gas-cooled reactor
AHFP	Axial heat flux profile
ANS	American Nuclear Society
AP	Advanced plant
AR	Advanced reactor
ASME	American Society of Mechanical Engineers
ASTRID	Advanced Sodium Technological Reactor for Industrial Demonstration
BISO	Bi-ISOtropic (nuclear fuel)
BN	Fast sodium (Быстрый Натриевый in Russian abbreviations) (reactor)
BOR	Fast test reactor (Быстрый Оцытный Реактор in Russian abbreviations)

BR	Fast reactor (Быстрый Реактор in Russian abbreviations)
BREST	Fast reactor with lead coolant (Быстрый Реактор со Свинцовым Теплоносителем in Russian abbreviations)
BSS	Basic Safety Standards
BWR	Boiling water reactor
CANDU	CANada Deuterium Uranium (reactor)
CCS	Carbon-dioxide capture and storage
CDF	Core damage frequency
CEA	Commissariat à L'énergie Atomique et aux énergies Alternatives (in English: Atomic Energy and Alternative Energies Commission, France)
CEFR	China Experimental Fast Reactor
CFD	Computational fluid dynamics
CFR	Commercial fast reactor
CHF	Critical heat flux
CHP	Combined head and power
CNNC	China National Nuclear Corporation (People's Republic of China)
CNSC	Canadian Nuclear Safety Commission
DFR	Dual fluid reactor
DOE	Department of Energy (USA)
EBR	Experimental breeder reactor
EC	European Commission
EEC	Electrical energy consumption
EGP	Power heterogeneous loop reactor (in Russian abbreviations)
ENEA	Agenzia Nazionale per le Nuove Tecnologie, l'Energia e lo Sviluppo Economico Sostenibile (in English: National Agency for New Technologies, Energy and Sustainable Economic Development, Italy)
EPR	European Pressurized Reactor (AREVA) or Evolutionary Power Reactor
EPRI	Electric Power Research Institute
ESBWR	Economic simplified boiling water reactor
ESFR	European SFR
EU	European Union
Euratom	European Atomic Energy Community (EAEC)
FBTR	Fast breeder test reactor
FFTF	Fast flux test facility
GCR	Gas-cooled reactor
GE	General Electric
GFR	Gas-cooled fast reactor
Gen-IV	Generation-IV
GIF	Generation IV International Forum
GNEP	Global Nuclear Energy Partnership
GT	Gas turbine
GTHTR	Gas turbine high temperature reactor
HDI	Human development index

HEC	High efficiency channel
HFR	High flux reactor (NRG, Petten, The Netherlands)
HERC	High efficiency re-entrant channel
HP	High pressure
HTGR	High temperature gas-cooled reactor
HTR	High temperature reactor
HTR-PM	High temperature reactor-pebble-bed modules
HTTR	High-temperature engineering test reactor
HWR	Heavy water reactor
HX	Heat exchanger
IAEA	International Atomic Energy Agency
I&C	Instrumentation and control
ID	Inside diameter
IHX	Intermediate heat exchanger
INPRO	INternational PROject on Innovative Nuclear Reactors and Fuel Cycles
IP	Intermediate pressure
IRSN	Institut de Radioprotection et de Sûreté Nucléaire (in English: Institute for Radiation Protection and Nuclear Safety, France)
ITER	International thermonuclear experimental reactor
JAEA	Japan Atomic Energy Agency
JSFR	Japan sodium-cooled fast reactor
KNK	Kompakte Natriumgekühlte Kernreaktoranlage (in German) (Compact Sodium-cooled nuclear reactor plant)
LFR	Lead-cooled fast reactor
LGR	Light-water graphite-moderated reactor
LMFBR	Liquid-metal fast-breeder reactor
LMFR	Liquid metal-cooled fast reactor
LNG	Liquefied natural gas
LP	Low pressure
LWR	Light-water reactor
MAs	Minor actimides
MHI	Mitsubishi Heavy Industries
MIT	Massachusetts Institute of Technology (USA)
MOX	Mixed oxide (nuclear fuel)
MSF	Multistage flushing
MSFR	Molten salt fast reactor
MSR	Molten salt reactor
NEA	Nuclear Energy Agency (under OECD, Paris)
NEI	Nuclear Energy Institute
NGNP	Next generation nuclear plant
NIST	National Institute of Standards and Technology
NPP	Nuclear power plant
NRC	Nuclear Regulatory Commission (USA)
OD	Outside diameter
OECD	Organization for Economic Co-operation and Development

PBMR	Pebble bed modular reactor
PFBR	Prototype fast breeder reactor
PFR	Plug flow reactor
PGSFR	Prototype Generation-IV sodium-cooled fast reactor
PHWR	Pressurized heavy water reactor
PRISM	Power reactor innovative small modular
PSA	Probabilistic safety analysis
PUREX	Plutonium uranium redox extraction
PV	Photo voltaic
PWR	Pressurized water reactor
RBMK	Reactor of large capacity channel type (in Russian abbreviations)
R&D	Research and development
RPV	Reactor pressure vessel
S.	South
SC-HTGR	Steam cycle high-temperature gas-cooled reactor
SCWR	Supercritical water reactor
SDC	Safety design criteria
SDGs	Safety design guidelines
SFR	Sodium fast reactor
SMR	Small modular reactor (used in USA)
SMRs	Small and medium-sized reactors
TD	Theoretical Density
THTR	Thorium high-temperature reactor
TRISO	Tri-isotropic (nuclear fuel)
TWR	Traveling wave reactor
UK	United Kingdom
US	United States
USA	United States of America
VVER	Water−water power reactor (in Russian abbreviation)

1 Introduction: a survey of the status of electricity generation in the world*

I.L. Pioro [1], R.B. Duffey [2], P.L. Kirillov [3], R. Panchal [1]
[1]University of Ontario Institute of Technology, Oshawa, Ontario, Canada; [2]DSM Associates Inc., Ammon, Idaho Falls, ID, United States; [3]State Scientific Centre of the Russian Federation - Institute of Physics and Power Engineering (IPPE) named after A.I. Leipunsky, Obninsk, Russia

1.1 Statistics on electricity generation in the world

It is well known that electric power generation usage is the key factor for advances in industry, agriculture, and the socioeconomic level of living (see Table 1.1 and Fig. 1.1; Pioro and Duffey, 2015; Pioro and Kirillov, 2013a; Pioro, 2012). In addition, a strong power industry with diverse energy sources is very important for a country's independence. In general, electrical energy (see Fig. 1.2) can be generated from burning mined and refined energy sources such as coal, natural gas, oil, and nuclear as well as from harnessing energy sources such as hydro, biomass, wind, geothermal, solar, and wave power.

Today, the main sources for global electrical energy generation are

1. thermal power, primarily using coal (39.9%) and secondarily natural gas (22.6%);
2. large hydraulic power from dams and rivers (17.2%); and
3. nuclear power from various reactor designs (11.2%).

The remaining 9.2% of the electrical energy is generated using oil (4.2%) and the rest 5%—with biomass, wind, geothermal, and solar energy in selected countries. In addition, energy sources, such as wind (see Fig. 1.3) and solar (see Fig. 1.4) and some others, such a wave power, are intermittent from depending on Mother Nature.

Table 1.2 lists 11 top largest power plants of the world, and Table 1.3 lists the largest power plants of the world by energy source. Figs. 1.5, 1.6, 1.8−1.10, and 1.12−1.14 show photos of selected power plants of the world, mainly, hydro and renewable energy power plants. Figs. 1.7 and 1.11 show maps of wind speed and annual average direct normal solar resource data distributions over the United States. Thermal and nuclear power plants (NPPs) are discussed in Sections 1.2 and 1.3, respectively.

It should be noted that the following two parameters are important characteristics of any power plant: (1) the overall (gross) or net efficiency[1] of a plant and (2) the capacity

* This chapter is mainly based on the following publications: Pioro and Duffey (2015), Pioro and Kirillov (2013a,b,c,d), and Pioro (2012).

[1] The gross efficiency of a unit during a given period of time is the ratio of the gross electrical energy generated by a unit to the energy consumed during the same period by the same unit. The difference between gross and net efficiencies is the internal needs for electrical energy of a power plant, which might be not so small (5% or even more).

Handbook of Generation IV Nuclear Reactors. http://dx.doi.org/10.1016/B978-0-08-100149-3.00001-X
Copyright © 2016 Elsevier Ltd. All rights reserved.

Table 1.1 Electrical energy consumption per capita in selected countries

No.	Country	Population in millions (July 2015)	EEC[a]		HDI (2014)[b]	
			TWh (2012−2014)	W/ capita	Rank	Value
1	Norway	5.21	120.5	2618	1	0.944
2	Australia	22.75	222.6	1116	2	0.935
3	Germany	80.85	540.1	762	6	0.916
4	United States	321.37	3832.0	1360	8	0.915
5	Canada	35.10	524.8	1706	9	0.913
6	United Kingdom	64.09	319.1	568	14	0.907
7	Japan	126.92	921.0	828	20	0.891
8	Italy	61.86	303.1	559	27	0.873
9	France	66.55	451.1	773	22	0.888
10	Russia	142.42	1037.0	831	50	0.798
11	Brazil	204.26	483.5	270	75	0.755
12	Ukraine	44.43	159.8	410	81	0.747
13	China	1367.49	5523.0	461	90	0.727
14	World	7256.49	19,710.0	310	103	0.711
15	South Africa	53.68	211.6	450	116	0.666
16	India	1251.70	864.7	79	130	0.609
17	Pakistan	199.09	80.3	46	147	0.538
18	Afghanistan	32.56	3.9	14	171	0.465
19	Chad	11.63	0.2	2	185	0.392
20	Niger	18.05	0.9	6	188	0.348

Selected countries listed here just for reference purposes (CIA, 2016a,b; UN, 2016). Data for all countries in the world are listed in Appendix 7, Table A7.1.

[a] *EEC*, electrical energy consumption. $\mathrm{EEC}, \frac{\mathrm{W}}{\mathrm{Capita}} = \frac{\left(\mathrm{EEC}, \frac{\mathrm{TWh}}{\mathrm{year}}\right) \times \frac{10^{12}}{365\ \mathrm{days} \times 24\,\mathrm{h}}}{(\mathrm{Population},\ \mathrm{Millions}) \times 10^{6}}$.

[b] *HDI*, Human Development Index by the United Nations. The HDI is a comparative measure of life expectancy, literacy, education, and standards of living for countries worldwide. HDI is calculated by the following formula: $\mathrm{HDI} = \sqrt[3]{\mathrm{LEI} \times \mathrm{EI} \times \mathrm{II}}$, where LEI = Life Expectancy Index, EI = Education Index, and II = Income Index. It is used to distinguish whether the country is a developed, a developing, or an underdeveloped country and to measure the impact of economic policies on quality of life. Countries fall into four broad human development categories, each of which comprises ~42 countries: (1) very high, 42 countries; (2) high, 43 countries; (3) medium, 42 countries; and (4) low, 42 countries (Wikipedia, 2016).

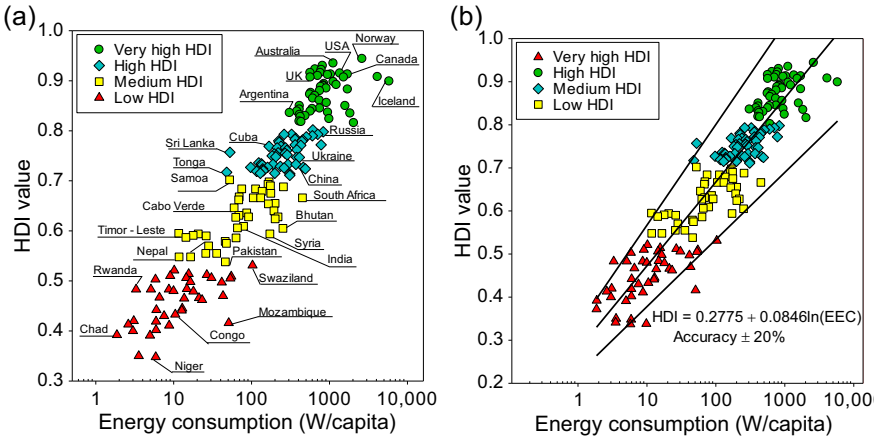


Figure 1.1 Effect of electrical energy consumption (EEC) on Human Development Index (HDI) for all countries of the world: (a) graph with selected countries shown and (b) HDI correlation. In general, the HDI correlation might be an exponential rise to maximum (1), but based on the current data it is a straight line in regular Y; logarithmic coordinates X.
Based on data from United Nations (UN), 2016. Table 1: Human Development Index and its Components, United Nations Development Programme. (Online). Available:http://hdr.undp.org/en/composite/HDI (accessed 16.01.16.) and The World Fact Book (2013).

factor[2] of a plant. Some power plant efficiencies are listed in the captions to figures, and those for thermal plants and NPPs will be discussed in Sections 1.2 and 1.3. The average capacity factors of power plants are listed in Tables 1.2 and 1.4.

Thermal power plants and NPPs usually operate semicontinuously because of a high capital cost and low operating costs. The relative costs of electrical energy generated by any system are not only dependent on building capital costs and operating expenses, but they are also dependent on the capacity factor. The higher the capacity factor the better because generating costs fall proportionally. However, some renewable energy sources with the exception of large hydroelectric power plants can have significantly lower capacity factors compared with those of thermal power plants and NPPs. Consequently, in today's politico-socio-economic world, many governments subsidize selected low-capacity factor sources, such as wind and solar, using preferential rates, enforced portfolios, artificial tariffs, market rules, and power-purchase agreements to partly offset the competitive advantage of lower cost generation from natural gas, coal, and nuclear. It is against the market background of low-cost natural gas and of directly or indirectly subsidized alternatives that today's and tomorrow's NPPs must operate.

[2] The net capacity factor of a power plant is the ratio of the actual output of a power plant over a period of time (usually during a year) and its potential output if it had operated at full nameplate capacity the entire time. To calculate the capacity factor, the total amount of energy a plant produced during a period of time should be divided by the amount of energy the plant would have produced at full capacity. Capacity factors vary significantly depending on the type of a plant.

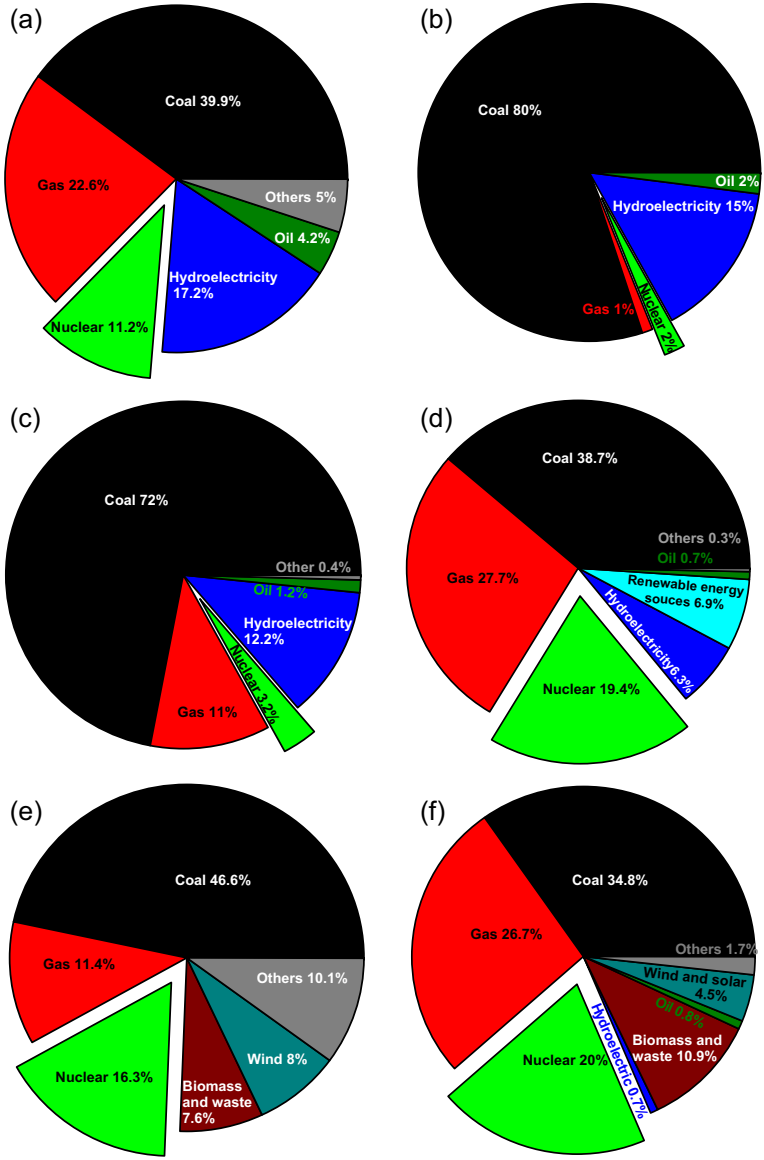


Figure 1.2 Electricity generation by source in the world and selected countries. (a) World: population 7256 million; EEC 19,710 TWh/year or 310 W/capita; HDI 0.711 or HDI rank 103. (b) China: population 1367 million; EEC 5523 TWh/year or 461 W/capita; HDI 0.727 or HDI rank 90. (c) India: population 1252 million; EEC 865 TWh/year or 79 W/capita; HDI 0.609 or HDI rank 130. (d) United States: population 321 million; EEC 3832 TWh/year or 1360 W/capita; HDI 0.915 or HDI rank 8; renewables (6.9%); wind (4.4%); biomass (1.7%); geothermal (0.4%); and solar (0.4%). (e) Germany: population 81 million; EEC 540 TWh/year or 762 W/capita; HDI 0.916 or HDI rank 6. (f) United Kingdom: population 64 million; EEC 319 TWh/year or 568 W/capita; HDI 0.907 or HDI rank 14. (g) Russia: population 142 million; EEC 1037 TWh/year or 831 W/capita; HDI 0.798 or HDI rank 50. (h) Italy: population 62 million; EEC 303 TWh/year or 559 W/capita; HDI 0.873 or HDI rank 27. (i) Brazil: population 204 million; EEC 484 TWh/year or 270 W/capita; HDI 0.755 or HDI rank 75. (j) Canada: population 35 million; EEC 525 TWh/year or 1706 W/capita; HDI 0.913 or HDI rank 9. (k) Ukraine:population 44 millions; EEC 160 TWh/year or 410 W/capita; HDI 0.747 or HDI Rank 81. (l) France: population 67 millions; EEC 451 TWh/year or 773 W/capita; HDI 0.888 or HDI Rank 22. *EEC*, Electrical energy consumption; *HDI*, Human Development Index.
Data from 2010 to 2014 presented here just for reference purposes (Wikipedia, 2015).

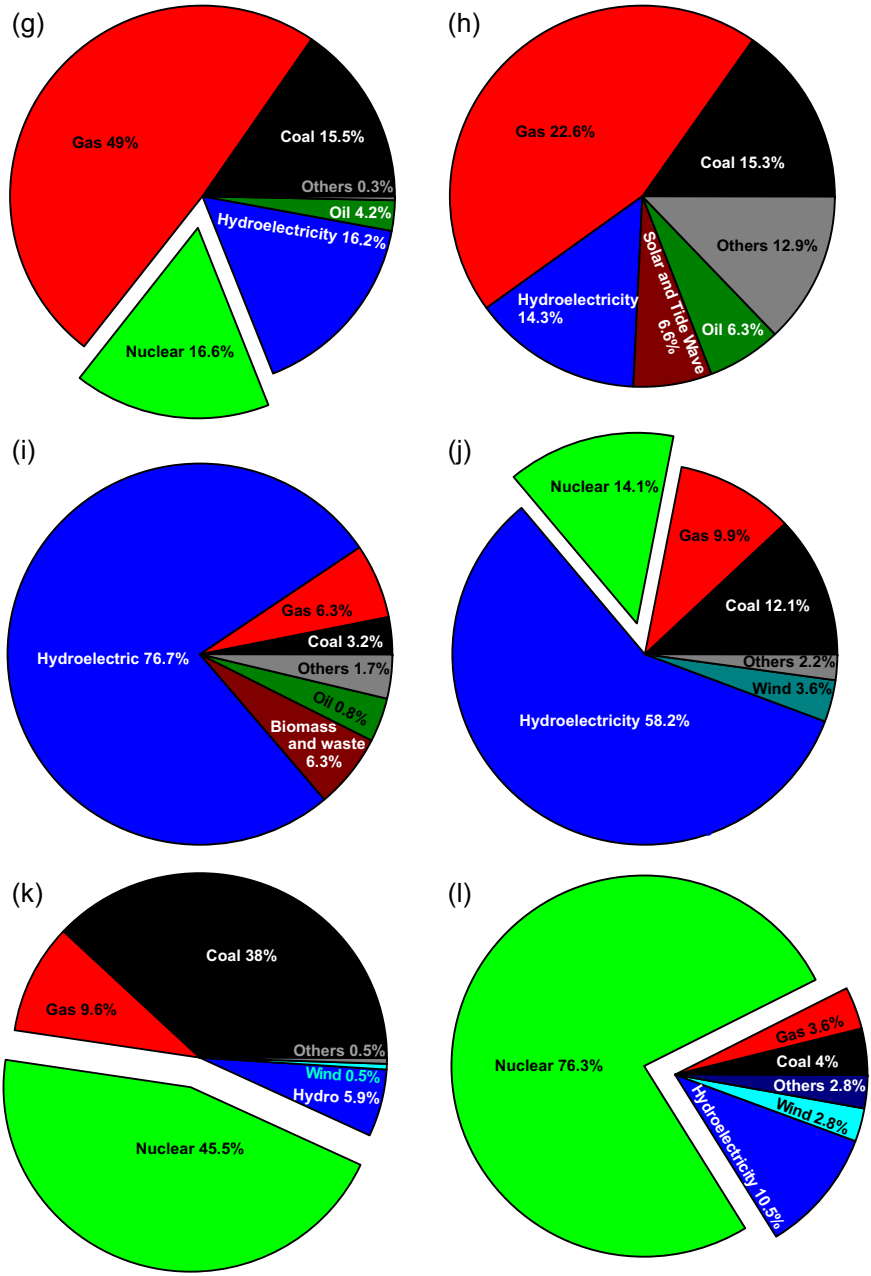


Figure 1.2 Continued.

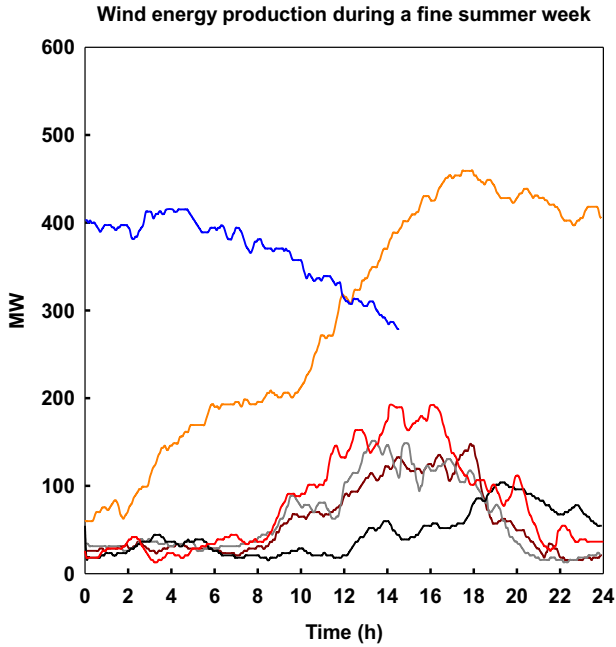


Figure 1.3 Power generated by 650-MW_{el} wind turbines in the western part of Denmark. Data shown represent a summer week (6 days, ie, various color lines) of wind power generation. Based on data from www.wiki.windpower.org.

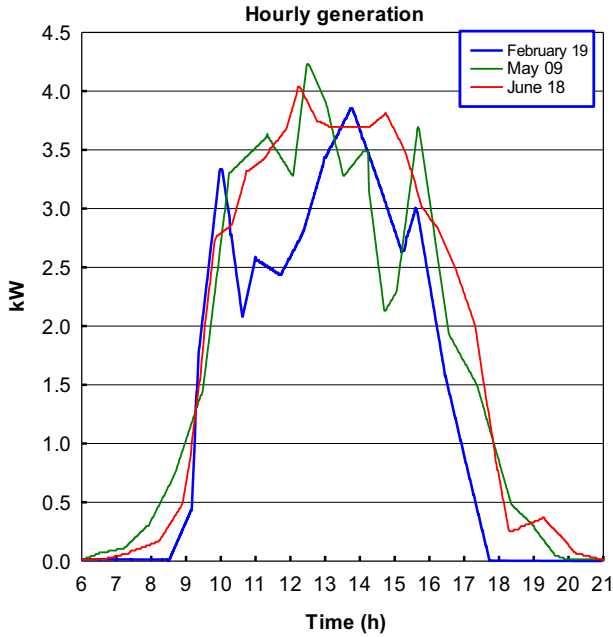


Figure 1.4 Power generated by photovoltaic system in New York State (United States). Data shown represent three mostly sunny days: February 19, May 9, and June 18.
Based on data from www.burningcutlery.com/solar.

Table 1.2 Eleven top power plants of the world by installed capacity[a]

No.	Plant	Country	Capacity (MW_{el})	Average annual generation (TWh)	Capacity factor (%)	Plant type
1	Three Gorges dam	China	22,500	98.8	50	Hydro
2	Itaipu dam	Brazil/ Paraguay	14,000[b]	98.6	72	Hydro
3	Xiluodu	China	13,860	57.1	47	Hydro
4	Guri dam	Venezuela	10,200	–	–	Hydro
5	Tucurui dam	Brazil	8370	–	–	Hydro
6	Kashiwazaki-Kariwa	Japan	7965[c]	–	–	Nuclear
7	Grand Coulee dam	United States	6809	21.0	35	Hydro
8	Longtan dam	China	6426	18.7	33	Hydro
9	Sayano-Shushenskaya	Russia	6400	24	43	Hydro
10	Bruce nuclear power plant	Canada	6231[d]	45.6	83	Nuclear
11	Krasnoyarsk dam	Russia	6000	23	44	Hydro

[a]Information provided in Table 1.2 is considered to be correct within some timeframe. New units can be added and/or some units can be out of service; for example, as of January 2016 the Kashiwazaki-Kariwa NPP is out of service after the earthquake and tsunami disaster and the resulting severe accident at the Fukushima NPP in Japan in March 2011.
[b]The maximum number of generating units allowed to operate simultaneously cannot exceed 18 (12,600 MW_{el}).
[c]Currently not in operation.
[d]Currently, the largest fully operating nuclear power plant in the world.
From Wikipedia, 2015.

Two examples of how various energy sources generate electricity in a grid can be illustrated based on the system of the province of Ontario (Canada). Fig. 1.15(a) shows installed capacity and Fig. 1.15(b) shows electricity generation by energy source in Ontario (Canada) in 2012. Analysis of Fig. 1.15(a) shows that in Ontario the major installed capacities in 2012 were nuclear (34%), gas (26%), hydro (22%), coal (8%), and renewables (mainly wind; 8%). However, electricity (see Fig. 1.15(b)) was mainly generated by nuclear (56%), hydro (22%), natural gas (10%), renewables (mainly wind; 5%), and coal (2%).

Fig. 1.16(a) shows power generated by various energy sources in Ontario (Canada) on June 19, 2012 (a peak power on a hot summer day, when major air conditioning was required) and corresponding to that Fig. 1.16(b) shows the capacity factors of various

Table 1.3 Largest operating power plants of the world (based on installed capacity) by energy source

Rank	Plant	Country	Capacity (MW_{el})	Plant type
1	Three Gorges dam power plant (Fig. 1.5)	China	22,500	Hydro
2	Bruce nuclear power plant	Canada	6231	Nuclear
3	Taichung power plant	Taiwan	5780	Coal
4	Shoaiba	Saudi Arabia	5600	Fuel oil
5	Surgut-2	Russia	5597	Natural gas[a]
6	Eesti power plant	Estonia	1615	Oil shale
7	Shatura power plant	Russia	1500	Peat[a]
7	Gansu	China	5160	Wind
8	Ivanpah solar power facility (Fig. 1.8)	United States	392	Solar (thermal)
9	The Geysers	United States	1808	Geothermal
10	Drax power plant	United Kingdom	660	Biofuel[a]
11	Sihwa Lake tidal power plant	South Korea	254	Tidal
12	Topaz	United States	550	Solar (photovoltaic)
13	Vasavi Basin Bridge diesel power plant	India	200	Diesel
14	Islay Limpet	United Kingdom	0.5	Marine (wave)

[a]It should be noted that actually some thermal power plants use multifuel options, including Surgut-2 (15% natural gas), and Shatura (peat 11.5%, natural gas 78%, fuel oil 6.8%, and coal 3.7%).
From Wikipedia, 2015.



Figure 1.5 Largest hydroelectric power plant in the world by installed capacity (21,100 MW_{el}; planned power = 22,500 MW_{el}; 700 $MW_{el} \times 30 + 2 \times 50$ MW_{el} Francis turbines),Yangtze River, China. The project cost $26 billion. The height of the gravity dam = 181 m, length = 2.335 km, top width = 40 m, base width = 115 m, flow rate = 116,000 m^3/s, artificial lake capacity = 39.3 km^3, surface area = 1045 km^2, length = 600 km, maximum width = 1.1 km, normal elevation = 175 m, and hydraulic head = 80.6−113 m. Courtesy of Chinese National Committee on Large Dams.

energy sources. Analysis of Fig. 1.16 shows that electricity that day from 12:00 am until 3:00 am was mainly generated by nuclear, hydro, gas, wind, "other," and coal. After 3:00 am wind power fell because of Mother Nature, but electricity consumption started to increase. Therefore "fast-response" gas-fired power plants and later, hydro and coal-fired power plants plus "other" power plants, started to increase electricity generation to compensate for both the decrease in wind power and the increase in demand for electricity. After 6:00 pm energy consumption slightly dropped in the province, and at the same time wind power started to be increased by Mother Nature. Therefore gas-fired, hydro, and "other" power plants decreased energy generation accordingly ("other" plants dropped power abruptly, but their role in the total energy generation is small). After 10:00 pm energy consumption dropped even more. Therefore coal-fired power plants with the most emissions abruptly decreased their electricity generation followed by gas-fired and hydro power plants.

However, the province of Ontario (Canada) currently has completely eliminated coal-fired power plants from the electrical grid. Some of them were closed, and others were converted to natural gas. Fig. 1.17(a) shows installed capacity and Fig. 1.17(b) shows electricity generation by energy source in the province of Ontario (Canada) in 2015. Analysis of Fig. 1.17(a) shows that in Ontario the major installed capacities in 2015 were nuclear (38%), gas (29%), hydro (25%), and renewables (mainly wind;



Figure 1.6 Second largest in the world 781-MW_{el} onshore Roscoe wind turbine power plant (Texas, United States). Plant equipped with 627 turbines: 406 MHI 1 MW_{el}, 55 S 2.3 MW_{el}, and 166 GE 1.5 MW_{el}. The project cost more than $1 billion, provides enough power for more than 250,000 average Texan homes, and covers an area of nearly 400 km^2, which is several times the size of Manhattan, New York, NY, United States. In general, wind power is suitable for harvesting when an average air velocity is at least 6 m/s (21.6 km/h). (It should be noted that the latest and the largest in the world wind turbine by Alstom (6-MW_{el} net wind turbine for the Haliade Offshore Platform has a rotor with the diameter of 150 m and tower 100 m high) can operate within the following range: from 3 m/s (10.8 km/h) and up to 25 m/s (90 km/h; http://www.alstom.com/power/renewables/wind/turbines/).) (See wind speed distribution over the United States in Fig. 1.7.)
From Wikimedia Commons, photo by author/username: Fredlyfish4.

8%). However, electricity (see Fig. 1.17(b)) was mainly generated by nuclear (60%), hydro (24%), natural gas (8.7%), and renewables (mainly wind; 4.9%).

Fig. 1.18(a) and (b), shows the power generated by various energy sources in Ontario (Canada) on June 17, 2015 and corresponding to that the capacity factors of various energy sources. Analysis of Fig. 1.18 shows that electricity that day from 12:00 am until 3:00 am was mainly generated by nuclear, hydro, gas, wind, and biofuel. After 3:00 am biofuel power plants slightly increased electricity generation followed by hydro and gas-fired power plants. In addition, at the same time wind power plants started to generate slightly more electricity because of Mother Nature. However, after 7:00 am wind power started to fluctuate and, eventually, significantly decreased. After 6:00 am solar power plants started to generate some electricity. During a day, hydro, gas-fired, and biofuel power plants had variable electricity generation to compensate for changes in consumption of electrical energy and variations in generating electricity with wind and solar power

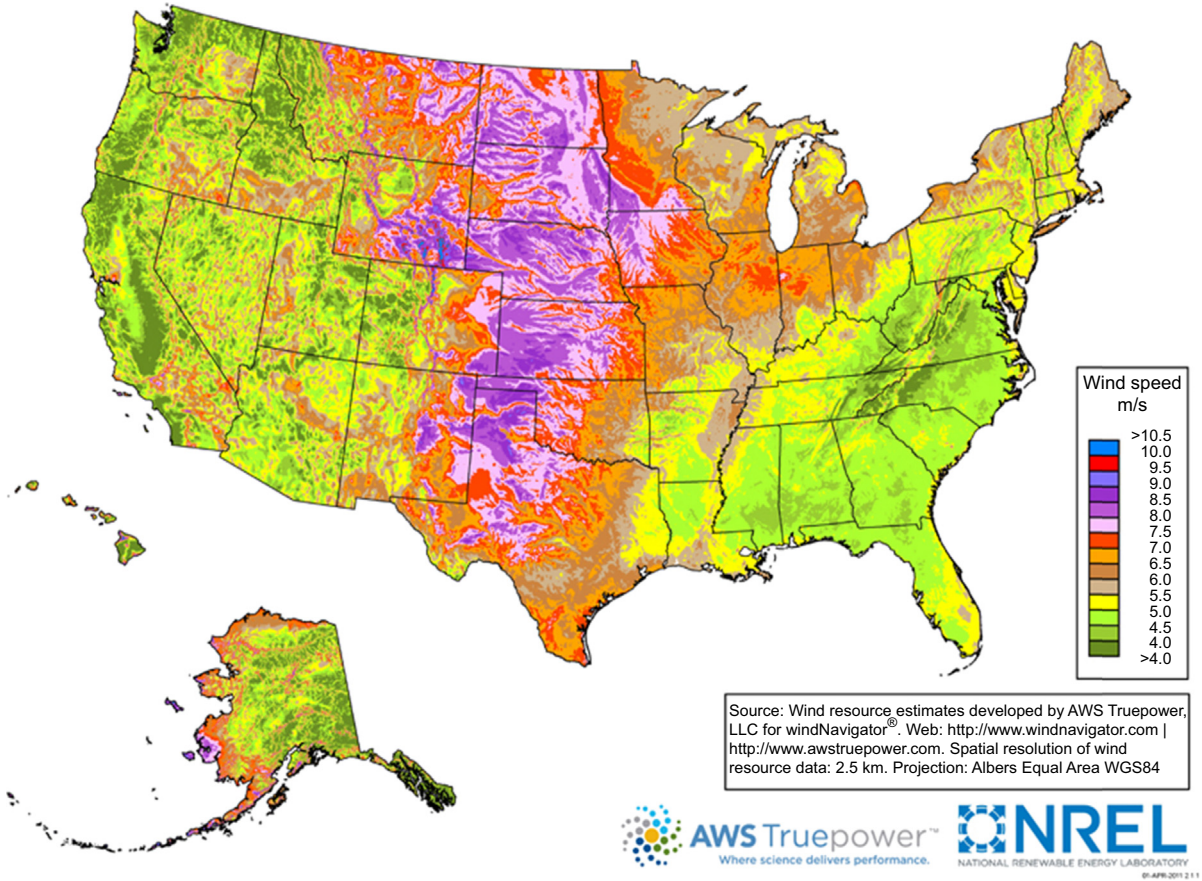


Figure 1.7 Map of wind speed distribution over the United States (shown here just for reference purposes and as an example). Figure shows that winds with average speed of 6 m/s and above (brown, red, and purple colors) have been uncovered only over the central part of the United States from north to south. However, average wind speed along the US shores of the Great Lakes, Atlantic and Pacific oceans, and the Gulf of Mexico is usually higher than 6 m/s at the height of 90 m from sea level.
Courtesy of US Department of Energy.



Figure 1.8 Aerial view of the largest concentrated solar thermal power plant in the world—the Ivanpah Solar Electric Generating System, Mojave desert, California, United States. Installed capacities: Gross = 392 MW_{el} and net = 377 MW_{el}; capacity factor = 31%; planned annual generation ~1040 GWh; site area = 16 km^2 (4000 acres); deploys 173,500 sun-tracking heliostats, and each has two mirrors (reflecting surface area is $7.02 \times 2 = 14.04$ m^2; total reflecting area is 2.4 km^2). The intercepted average solar heat flux is ~310 W/m^2. However, after taking into consideration reflection, transmission, radiation, and absorption losses, it is ~170 W/m^2 (efficiency is ~55%). The heliostat mirrors focus sunlight on receivers located on solar power towers (~140-m height). The receivers generate steam to drive single-casing reheat turbines (~130 MW [174,000 hp]). The gross thermal efficiency of the plant is ~29%. The plant is equipped with air-cooled condensers. The project cost is $2.2 billion (US). The electricity generated by the complex is enough to serve more than 140,000 homes in California during the peak hours of the day. The plant will reduce carbon dioxide emissions by more than 400,000 t/year. The negative impacts: (1) birds are killed by burning and because of crashing into mirrors (150 birds were killed in 1 month) and (2) it cannot operate at night (no thermal storage system).
From Wikipedia, 2014 and Wikimedia Commons: photo by Craig Butz.

plants. After 9:00 pm energy consumption started to drop in the province, and at the same time wind power increased by Mother Nature. Therefore gas-fired, hydro, and biofuel power plants decreased energy generation accordingly. In both cases (ie, June 19, 2012 and June 17, 2015) NPPs operated at approximately 100% of installed capacity, providing reliable basic power to the grid. The latest 2015 report by the Ontario Auditor General states the cost of using wind and solar is "Expensive wind and solar energy—We calculate that electricity consumers have had to pay $9.2 billion (the IESO calculates this amount to be closer to $5.3 billion, in order to reflect the time value of money) more for renewables over the 20-year contract terms under the Ministry's current guaranteed-price renewable program than they would have paid under the previous program" and "From 2004 to 2014, the amount that residential and small-business electricity consumers pay for the electricity commodity portion (includes Global Adjustment fees) of their bill has increased by 80%, from 5.02 cents/kWh to 9.06 cents/kWh." (For details on electricity cost, see Appendix A).



Figure 1.9 Aerial view showing portions of Solar Energy Generating Systems (SEGS; California, United States). SEGS is one of the largest solar energy power plants in the world. SEGS consist of nine concentrated solar thermal plants with 354-MW_{el} installed capacity. The average gross solar output of SEGS is ~75 MW_{el} (capacity factor is ~21%). At night turbines can be powered by combustion of natural gas. NextEra claims that the SEGS power 232,500 homes and decrease pollution by 3800 t/year (if the electricity had been provided by combustion of oil). The SEGS have 936,384 mirrors, which cover more than 6.5 km^2. If the parabolic mirrors would be lined up, then they will extend more than 370 km. In 2002 one of the 30-MW_{el} Kramer Junction sites required $90 million to construct, and its operation and maintenance costs are approximately $3 million/year, which are 4.6 ¢/kWh. However, with a considered lifetime of 20 years, the operation and maintenance costs and investments interest and depreciation triples the price to approximately 14 ¢/kWh (see annual average direct normal solar resource data distribution over the United States in Fig. 1.10).
From Wikimedia Commons: photo by A. Radecki.

These examples show clearly that any grid that includes NPPs and/or renewable energy sources must also include fast-response power plants such as gas- and coal-fired and/or large hydro power plants. This is due not only to diurnal and seasonal peaking of demand but also the diurnal and seasonal variability of supply. Thus, for any given market, the generating mix and the demand cycles must be matched 24 h a day, 7 days a week, 365 days per year, independent of what sources are used, and this requires flexible control and an appropriate mix of base-load and peaking plants.

In addition, it should be noted here that by having a large percentage of variable power sources, such as wind, solar, and other (ie, the generating capacity of which depends on Mother Nature), an electrical grid can collapse due to significant and unpredicted power instabilities. In addition, the following detrimental factors are usually not considered during the estimation of variable power source costs: (1) the costs of fast-response power plants with service crews on site 24 h per



Figure 1.10 Aerial view of the first of such kind, Gemasolar, a 19.9-MW_{el} concentrated solar power plant with a 140-m high tower and molten salt heat storage system (Seville, Spain). The plant consists of 2650 heliostats (each 120 m^2 and total reflective area = 304,750 m^2), covers 1.95 km^2 (195 ha), and produces 110 GWh each year, which equals 30,000 t/year carbon dioxide emission savings. This energy is enough to supply 25,000 average Spanish houses. The storage system allows the power plant to produce electricity for 15 h without sunlight (at night or on cloudy days). The capacity factor is 75%. Solar receiver thermal power is 120 MW_{th}, and the plant thermal efficiency is approximately 19%. Molten salt is heated in the solar receiver from 260 to 565°C by concentrated sunlight reflected from all heliostats, which follow the Sun, and transfers heat in a steam generator to water as a working fluid in a subcritical pressure Rankine steam power cycle.
Courtesy of SENER/TORRESOL ENERGY.

day/7 days per week as back-up power and (2) the faster amortization/wear of equipment of fast-response plants.

1.2 Thermal power plants[3]

In general, all thermal power plants (Pioro, 2012; Pioro and Kirillov, 2013b) are based on one the following thermodynamic cycles:

1. *Rankine steam-turbine cycle*: The most widely used in various power plants; usually for solid, gaseous, and liquid fuels, but other energy sources can also be used (eg, geothermal, solar, etc.).

[3] For thermal power plant layouts and T-s diagrams, see Appendix A1.

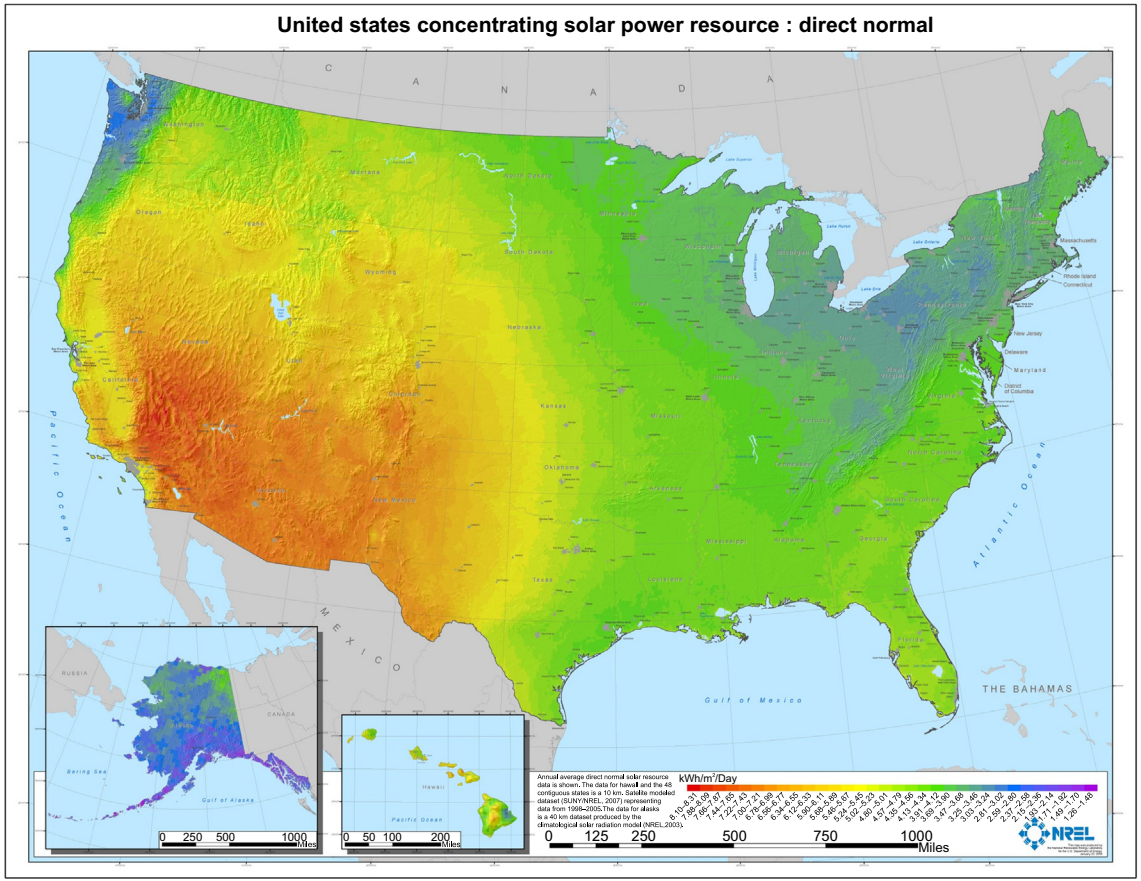


Figure 1.11 Map of annual average direct normal solar resource data distribution over the United States (shown here just for reference purposes and as an example). In general, the amount of solar radiation that reaches any one spot on the Earth's surface varies according to geographic location, time of day, season, local landscape, and local weather.
Courtesy of US Department of Energy.



Figure 1.12 Photo of fifth in the world 1.2-MW_{el} concentrated photovoltaic (PV) solar power plant (Spain). The plant has 154 two-axis tracking units, consisting of 36 PV modules each, which cover an area of 295,000 m^2 with a total PV surface area of 5913 m^2. The plant generates 2.1 GWh each year, and the conversion efficiency is 12%.
From Wikimedia Commons, author/username: afloresm.

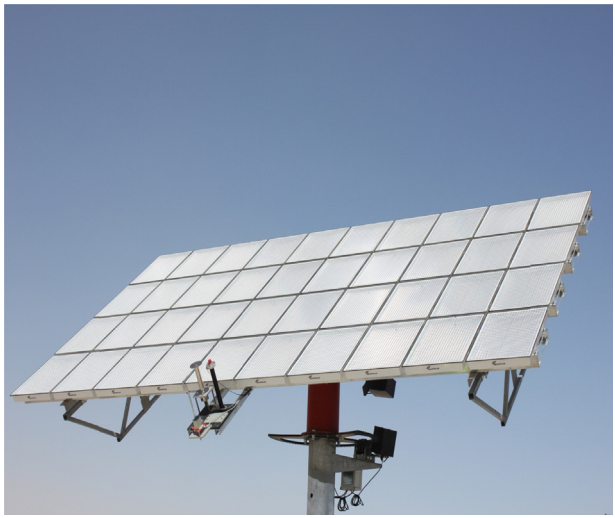


Figure 1.13 Photo of a test system consisting of 40 high-concentrating photovoltaic (PV) modules with ~34% efficiency. This test system is a joint effort of Semprius (Durham, North Carolina, United States) and Siemens in collaboration with the Spanish Institute of Concentration Photovoltaic Systems (ISFOC) and the University of Madrid. Leading modules' manufacturers of conventional PV technologies achieved the maximum module efficiency of ~20% with monocrystalline PV modules and ~16% with polycrystalline technology.
From Siemens press photo; copyright Siemens AG, Munich/Berlin, Germany.

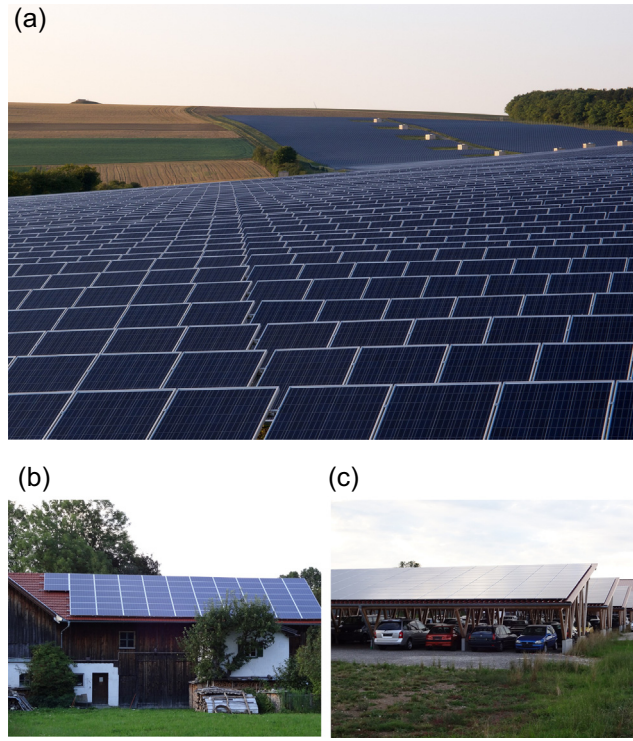


Figure 1.14 "Improper" (a) and "proper" (b and c) installation of photovoltaic panels. (a) Photo of a typical flat-panel photovoltaic power plant (19-MW_{el}) located near Thüngen, Bavaria, Germany. From Wikimedia Commons: photo by OhWeh. (b) Photovoltaic panels installed on roof of house. (c) Photovoltaic panels installed on roof of parking lot.
Photos b and c by I. Pioro, Bavaria, Germany.

2. *Brayton gas-turbine cycle*: The second one after the Rankine cycle in terms of application in power industry; only for clean gaseous fuels.
3. *Combined cycle*: The combination of Brayton and Rankine cycles in one plant (only for gaseous fuels).
4. *Diesel internal combustion engine cycle*: For diesel fuel used in diesel generators.
5. *Otto internal combustion engine cycle*: Usually for natural or liquefied gas, but gasoline can also be used for power generation (however, it is more expensive fuel compared with gaseous fuels) and used in internal combustion engine generators.

The major driving force for all advances in thermal power plants is directed toward increasing thermal efficiency to reduce operating fuel costs and minimize specific emissions. Typical ranges of thermal efficiencies of modern thermal power plants are listed in Table 1.5 for reference purposes and can reach up to 62% in the combined cycle mode.

Table 1.4 Average (typical) capacity factors of various power plants

No.	Power plant type	Location	Year	Capacity factor (%)
1	Nuclear	United States	2010	91
		United Kingdom	2011	66
2	Combined cycle	United States	2009	42
		United Kingdom	2011	48
3	Coal-fired	United States	2009	64
		United Kingdom	2011	42
4	Hydroelectric[a] (see Fig. 1.5)	United States and United Kingdom	2011	40
		World (average)	–	44
		World (range)	–	10–99
5	Wind (see Fig. 1.6)	United Kingdom	2011	30
		World	2008	20–40
6	Wave	Portugal	–	20
7	Concentrated solar thermal (see Figs. 1.8–1.10)	United States California	–	21
		Spain	–	75
8	PV solar (see Fig. 1.14)	United States Arizona	2008	19
		United States Massachusetts	–	12–15
		United Kingdom	2011	5–8
9	Concentrated solar PV (Figs. 1.12 and 1.13)	Spain	–	12

Data listed here just for reference purposes. *PV*, photovoltaic.
[a]Capacity factors depend significantly on a design, size, and location (water availability) of a hydroelectric power plant. Small plants built on large rivers will always have enough water to operate at full capacity.
Table partially based on US Energy Information Administration (2013).

Despite the advances in thermal power plant design and operation worldwide, they are still considered as not of minimum environmental impact because of significant carbon dioxide emissions[4] and air pollution as a result of the combustion process. In addition, coal-fired power plants also produce virtual mountains of slag and ash, and other gas emissions may contribute to acid rains.

[4] For example, the largest in the world 5780-MW_{el} Taichung coal-fired power plant (Taiwan) is the world's largest emitter of CO_2 with more than 40 million tons per year.

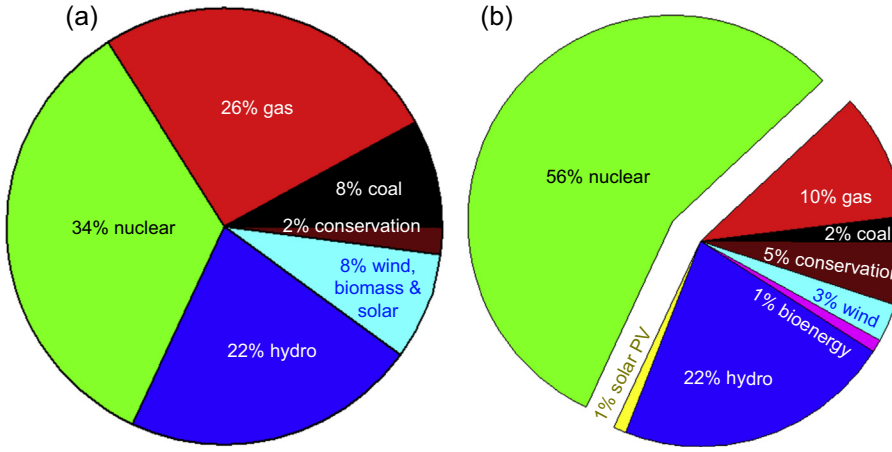


Figure 1.15 (a) Installed capacity and (b) electricity generation by energy source in Ontario (Canada), 2012−2013.
Based on data from Ontario Power Authority (http://www.powerauthority.on.ca) and Ontario's Long-Term Energy Plan.

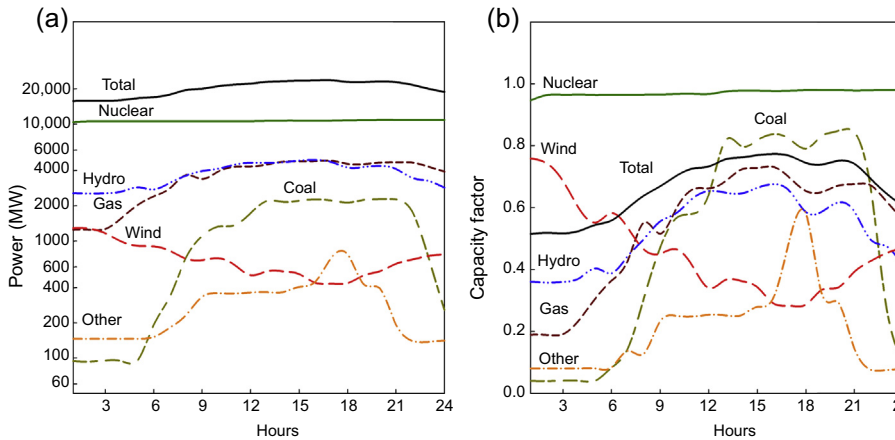


Figure 1.16 (a) Power generated and (b) capacity factors of various energy sources in Ontario (Canada) on June 19, Tuesday 2012.
Based on data from http://ieso.ca/imoweb/marketdata/genEnergy.asp (shown here just for reference purposes).

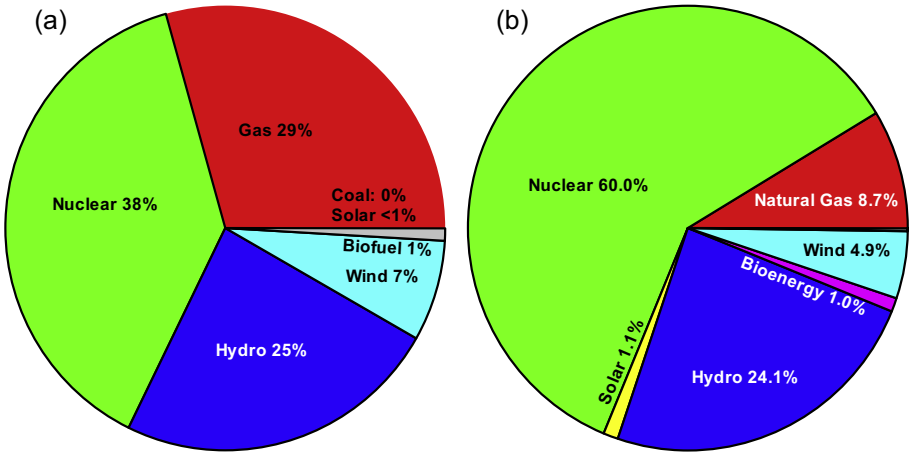


Figure 1.17 Installed capacity (a) and electricity generation (b) by energy source in Ontario (Canada), 2014−2015.
Based on data from Ontario Energy Board: http://www.ontarioenergyboard.ca/ and Ontario Energy Report http://www.ontarioenergyreport.ca/.

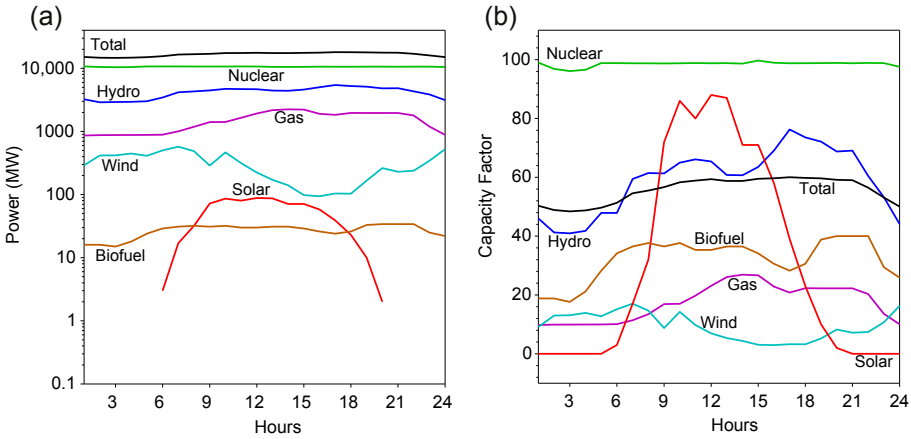


Figure 1.18 (a) Power generated and (b) capacity factors of various energy sources in Ontario (Canada) on June 17, Wednesday 2015.
Based on data from http://ieso.ca/imoweb/marketdata/genEnergy.asp (shown here just for reference purposes).

Table 1.5 Typical ranges of thermal efficiencies (gross) of modern thermal power plants (Pioro and Duffey, 2015; Pioro and Kirillov, 2013; Pioro, 2012)

No.	Thermal power plant	Gross efficiency (%)
1	Combined-cycle power plant (combination of Brayton gas-turbine cycle [fuel = natural gas or liquefied natural gas; combustion product parameters at the gas-turbine inlet: $T_{in} \approx 1650°C$] and Rankine steam turbine cycle [steam parameters at the turbine inlet: $T_{in} \approx 620°C$ {$T_{cr} = 374°C$}]).	Up to 62
2	Supercritical pressure coal-fired power plant (Rankine-cycle steam inlet turbine parameters: $P_{in} \approx 25-38$ MPa [$P_{cr} = 22.064$ MPa], $T_{in} \approx 540-625°C$ [$T_{cr} = 374°C$], and $T_{reheat} \approx 540-625°C$).	Up to 55
3	Internal combustion engine generators (diesel cycle and Otto cycle with natural gas as a fuel).	Up to 50
4	Subcritical pressure coal-fired power plant (older plants; Rankine-cycle steam: $P_{in} \approx 17$ MPa, $T_{in} \approx 540°C$ [$T_{cr} = 374°C$], and $T_{reheat} \approx 540°C$).	Up to 40
5	Concentrated solar thermal power plants with heliostats, solar receiver (heat exchanger) on a tower, and molten salt heat storage system (for details, see Fig. 1.10). Molten salt maximum temperature is ~565°C. Rankine steam turbine power cycle used.	Up to 20

1.3 Modern nuclear power plants[5]

Although nuclear power is often considered to be a nonrenewable energy source as the fossil fuels, such as coal and gas, nuclear resources can be used for significantly longer or even indefinite time than some fossil fuels, especially, if recycling of unused uranium fuel, and thoria-fuel resources and fast reactors are used. The major advantages of nuclear power are as follows:

1. High capacity factors are achievable, often in excess of 90% with long operating cycles, making the units suitable for semicontinuous base-load operation alongside intermittent windmills backed by gas peaking plants.
2. Essentially negligible operating emissions of carbon dioxide into the atmosphere compared with alternative thermal plants.

[5] For NPP layouts and T-s diagrams, see Appendix A1; and for thermophysical properties of reactor coolants see Appendix A2.

3. A relatively small amount of fuel required. For example, a 500-MW_{el} coal-fired supercritical pressure power plant requires 1.8 million tons of coal each year, but a fuel load into a 1300-MW_{el} pressurized water reactor is 115 t (3.2% enrichment) or into a 1330-MW_{el} boiling water reactor is 170 t (1.9% enrichment). Therefore this source of energy is considered as the most viable one for electrical generation for the next 50−100 years.

Despite all current advances in nuclear power, NPPs have the following deficiencies: (1) Generate radioactive wastes; (2) Have relatively low thermal efficiencies, especially water-cooled NPPs (up to 1.6 times lower than that for modern advanced thermal power plants; see Tables 1.5 and 1.6); (3) Risk of radiation release during severe accidents; and (4) The production of nuclear fuel is not an environmentally friendly process. Therefore all of these deficiencies should be addressed.

The first success of using nuclear power for electrical generation (Pioro, 2012; Pioro and Kirillov, 2013c) was achieved in several countries within the 1950s, and currently generations II, III, and III+ nuclear power reactors (see Fig. 1.19) are operating around the world (see Tables 1.6 and 1.7 and Figs. 1.20−1.23). In general,

Table 1.6 Typical ranges of thermal efficiencies (gross) of modern nuclear power plants (Pioro and Duffey, 2015; Pioro and Kirillov, 2013; Pioro, 2012)

No.	Nuclear power plant	Gross efficiency (%)
1	Carbon dioxide−cooled reactor NPP (Generation III; reactor coolant $P = 4$ MPa and $T = 290$−$650°C$; steam $P = 17$ MPa [$T_{sat} = 352°C$] and $T_{in} = 560°C$)	Up to 42
2	Sodium-cooled fast reactor NPP (Generation IV; steam $P = 14$ MPa [$T_{sat} = 337°C$] and $T_{in} = 505°C$)	Up to 40
3	Pressurized water reactor NPP (Generation III+, to be implemented within next 1−10 years; reactor coolant $P = 15.5$ MPa and $T_{out} = 327°C$; steam $P = 7.8$ MPa and $T_{in} = 293°C$)	Up to 38
4	Pressurized water reactor NPP (Generation III, current fleet; reactor coolant $P = 15.5$ MPa and $T_{out} = 292$−$329°C$; steam $P = 6.9$ MPa and $T_{in} = 285°C$)	Up to 36
5	Boiling water reactor NPP (Generation III, current fleet; $P_{in} = 7.2$ MPa and $T_{in} = 288°C$)	Up to 34
6	RBMK (boiling, pressure-channel; Generation III, current fleet; $P_{in} = 6.6$ MPa and $T_{in} = 282°C$)	Up to 32
7	Pressurized heavy water reactor NPP (Generation III, current fleet; reactor coolant $P = 11$ MPa and $T = 265$−$310°C$; steam $P = 4.7$ MPa and $T_{in} = 260°C$)	Up to 32−34

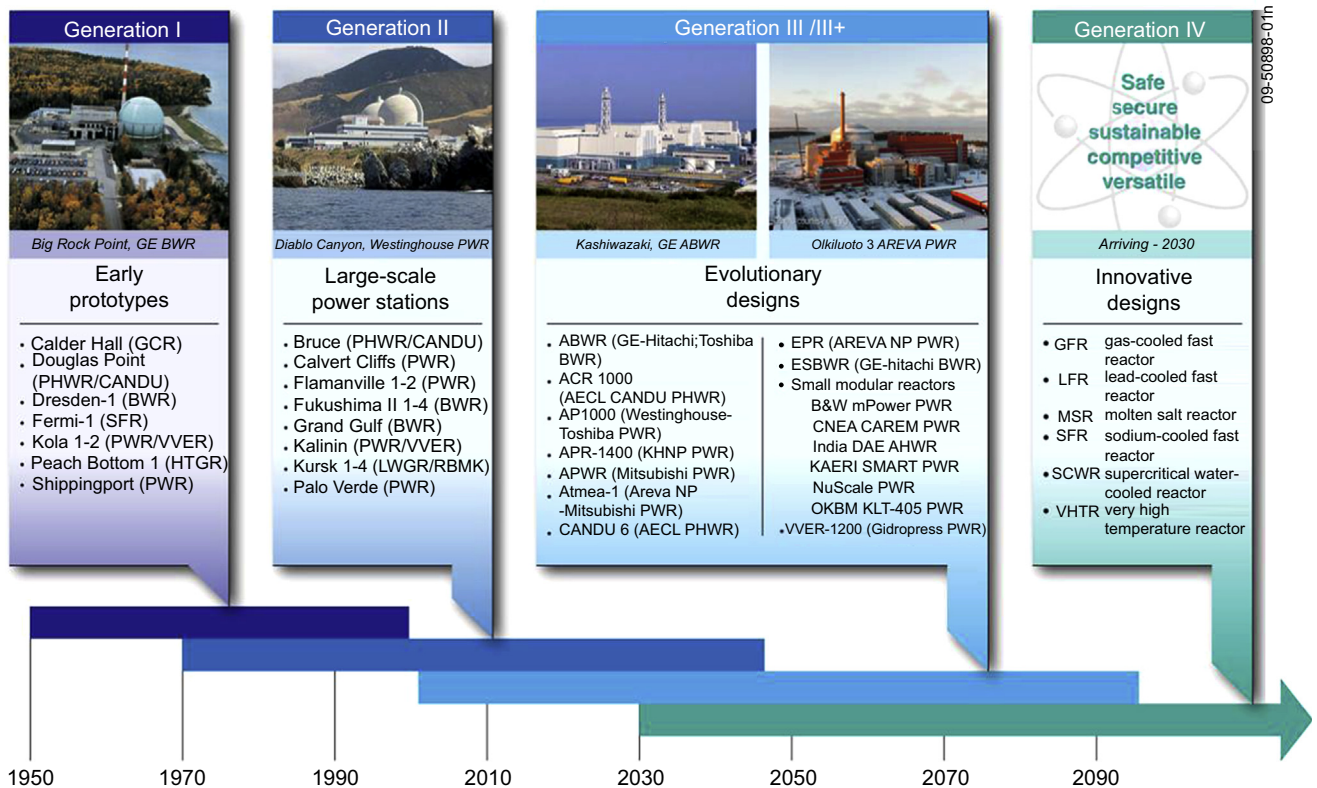


Figure 1.19 Generations of nuclear reactors.
Courtesy of Generation IV International Forum.

Table 1.7 Number of nuclear power reactors in operation and forthcoming as per March 2016 (Nuclear News, 2015) and before the Japan earthquake and tsunami disaster (March 2011; Nuclear News, 2011)

No.	Reactor type (some details on reactors)	Number of units		Installed capacity (GW_{el})		Forthcoming units	
		As of March 2015	Before March 2011	As of March 2015	Before March 2011	Number of units	GW_{el}
1	**Pressurized water reactors (PWRs**; largest group of nuclear reactors in the world—63%)	**280** ↑	268	**262** ↑	248	86	91.4
2	**Boiling water reactors (BWRs) or advanced BWRs** (second largest group of reactors in the world—19%; advanced BWRs are the only Generation III+ operating reactors)	**78** ↓	92	**75** ↓	84	6	8.1
3	**Pressurized heavy water reactors (PHWRs**; third largest group of reactors in the world—11%; mainly CANDU reactor type)	**48** ↓	50	**24** ↓	25	9	5.8
4	**Gas-cooled reactors (GCRs**[a]; United Kingdom, Magnox reactor) **or advanced gas-cooled reactors (AGRs**; United Kingdom, 14 reactors): all of these carbon dioxide−cooled reactors will be shut down in the near future and will not be built again	**14** ↓	18	**8** ↓	9	1	0.2[a]
5	**Light-water, graphite-moderated reactors (LGRs**; Russia, 11 RBMKs and 4 EGPs[b]; these pressure-channel boiling water−cooled reactors will be shut down in the near future and will not be built again)	**15**	15	**10**	10	**0**	**0**
6	**Liquid-metal fast-breeder reactors (LMFBRs)** (Russia, SFR—BN-600; the only Generation IV operating reactor)	**1**	1	**0.6**	0.6	5	1.6
In total		**436** ↓	**444**	**379** ↑	**378**	**107**	**107**

Additional data on reactors are shown in Figs. 1.20−1.23. Data in table include 43 reactors from Japan, the vast majority of which are currently (ie, January 2016) not in operation.
Arrows indicate decrease or increase in number of reactors.
[a]Forthcoming gas - cooled reactor is a helium-cooled reactor.
[b]EGP is an abbreviation for power heterogeneous loop reactor (in Russian), a channel-type, graphite-moderated, light-water coolant, boiling reactor with natural circulation.

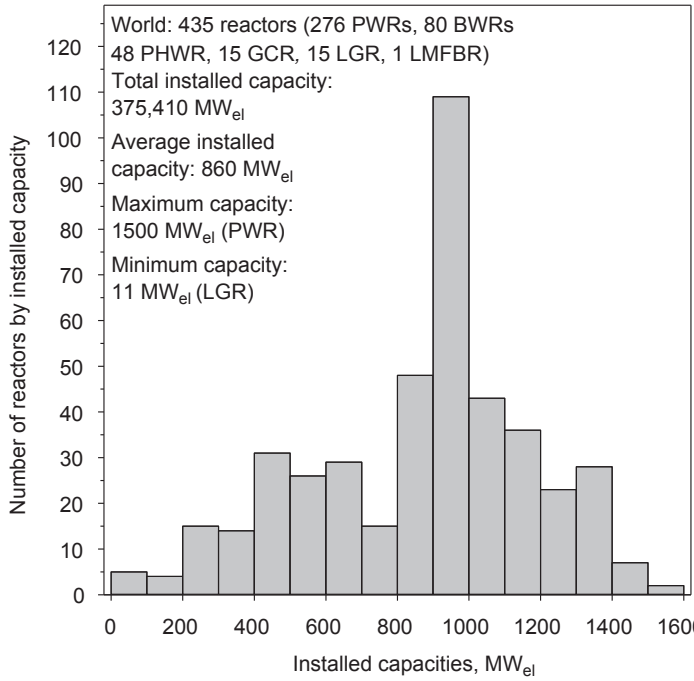


Figure 1.20 Number of nuclear power reactors in the world by installed capacity as per March 2015 (Nuclear News, 2015). For better understanding of this graph, most reactors have installed capacities within the range of 900–999 MW_{el}.

definitions of nuclear reactor generations can be defined as the following: (1) Generation I (1950–65) – early prototypes of nuclear reactors; (2) Generation II (1965–2010) – commercial power reactors; (3) Generation III (1995–2010) – modern reactors (water-cooled NPPs with thermal efficiencies within 30–36%, carbon dioxide–cooled NPPs with thermal efficiencies up to 42%, and liquid sodium–cooled NPPs with thermal efficiencies up to 40%) and Generation III+ (2010[6]–25) – reactors with improved parameters (evolutionary design improvements; water-cooled NPPs with thermal efficiencies up to 36–38%; see Table 1.8); and (4) Generation IV (2025–) – reactors in principle with new parameters (NPPs with thermal efficiencies within 40–50% and even higher for some types of reactors; see Chapters 2–18 in Part I; Pioro and Duffey, 2015; Pioro and Kirillov, 2013d; Pioro, 2012).

Slightly different definitions of nuclear reactor generations by the Generation IV International Forum are shown in Fig. 1.19.

[6] Actually, first two Generation III+ reactors put into operation (ie, "commercial start") were advanced BWRs (ABWRs) at the Kashiwazaki Kariwa NPP (Kishiwazaki, Nigata, Japan) in 1996 (reactor supplier Toshiba/GE) and in 1997 (reactor supplier Hitachi/GE).

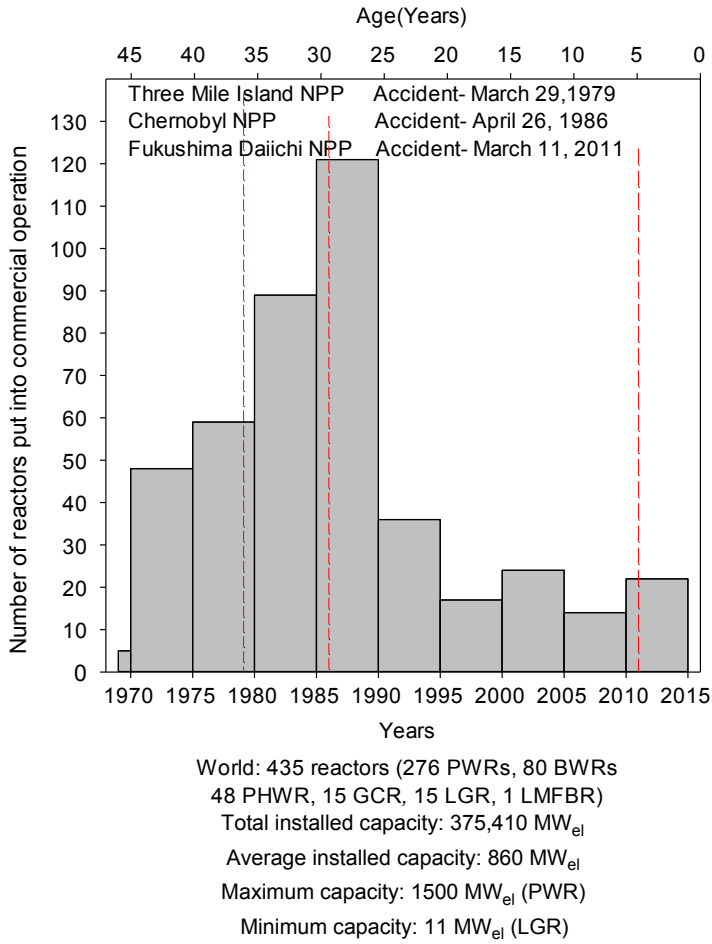


Figure 1.21 Number of nuclear power reactors of the world put into commercial operation versus years and age of operating reactors as per March 2015 (Nuclear News, 2015). Five reactors have been put into operation in 1969 (ie, they operate for more than 47 years). It is clear from this diagram that the Chernobyl NPP accident had tremendous negative impact on the nuclear power industry that lasted for decades. We currently have additional negative impact from the Fukushima Daiichi NPP accident.

Currently, 31 countries in the world have operating nuclear power reactors (Nuclear News, 2016; for details see Tables 1.7–1.9 and Table A7.2 in Appendix. Analysis of the data listed in Table 7.2 shows that 16 countries plan to build new reactors, 15 countries do not plan to build new reactors, and 4 countries without reactors (Bangladesh, Belarus, Turkey, and United Arab Emirates) are working toward introducing nuclear energy on their soils.

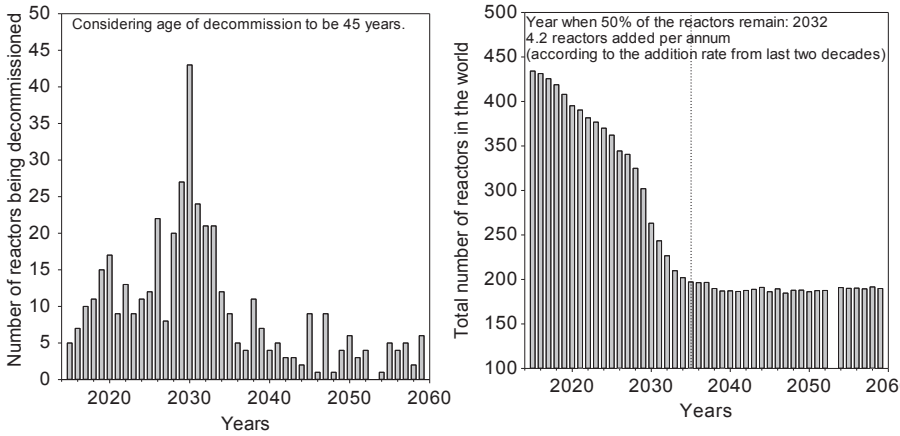


Figure 1.22 One of the possible scenarios for the future of nuclear power based on 45 years in service of current reactors and adding new reactors with a rate of ~21 reactors every 5 years.

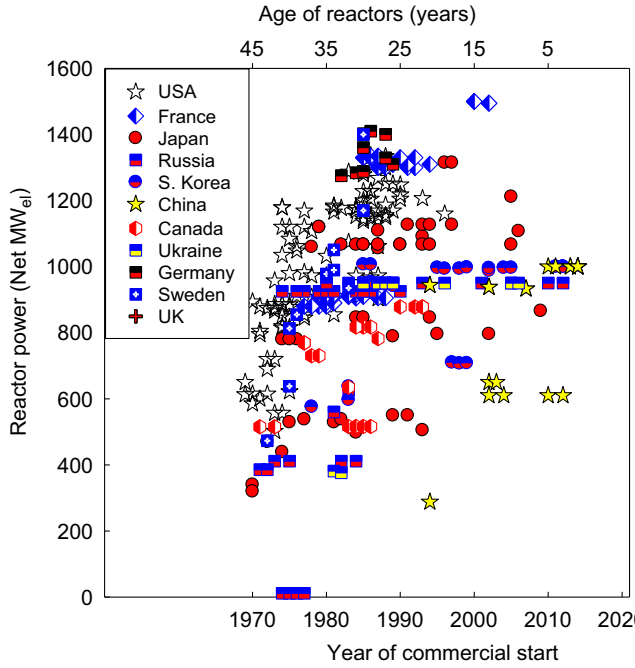


Figure 1.23 Age of nuclear power reactors in selected countries (11 nations with the largest number of reactors) as per March 2015 (Nuclear News, 2015). Shown here are data on 352 reactors with the total installed capacity of 326.5 GW_{el} Net. For other details, see Table 1.8. Some symbols might represent more than one reactor because in some cases several reactors with the same installed capacity (power) have been put into commercial operation within the same year.

Table 1.8 **Number of nuclear power reactors by nation (11 nations with the largest number of reactors ranked by installed capacity) as per March 2016 (Nuclear News, 2016) and before the Japan earthquake and tsunami disaster (March 2011; Nuclear News, 2011)**

No.	Nation	Number of units (PWRs/BWRs)		Installed capacity (GW_{el})		Changes in number of reactors from March 2011
		As of March 2016	Before March 2011	As of March 2015	Before March 2011	
1	United States	**99** (65/34)	104	**101**	103	↓ decreased by 5 reactors
2	France	**58** (58/—)	58	**63**	63	No changes
3	Japan[a]	**43** (24/23)	54	**42**	47	**↓ decreased by 6 reactors**
4	Russia	**34** (18/—/15[b]/1[c])	32	**25**	23	↑ increased by 1 reactor
5	China	**28** (26/—/2[d])	13	**19**	10	**↑ increased by 9 reactors**
6	South Korea	**24** (20/—/4[d])	20	**21**	18	**↑ increased by 3 reactors**
7	Canada	**19** (—/—/19[d])	22	**13**	15	↓ decreased by 3 reactors
8	Ukraine	**15** (15/—)	15	**13**	13	No changes
9	Germany	**8** (6/2)	17	**12**	20	**↓ decreased by 8 reactors**
10	Sweden	**10** (7/3)	10	**9.3**	9.3	No changes
11	United Kingdom	**15** (1/—/14[e])	19	**9.2**	10	↓ decreased by 3 reactors
In total		**353**	364	**326.5**	331.3	↓ decreased by 12 reactors

Selected data of this table are shown in Fig. 1.17. Data for all countries with nuclear power reactors are listed in Appendix 7, Table A7.2.
Arrows indicate decrease or increase in a number of reactors. *PWRs*, pressurized water reactors; *BWRs*, boiling water reactors.
[a]As of January 2016, the vast majority of nuclear power reactors are not in operation. However, there are plans to put them into operation in the nearest future.
[b]Number of light-water graphite-moderated reactors.
[c]Liquid-metal fast-breeder reactors.
[d]Pressurized heavy water reactors.
[e]Advanced gas-cooled reactors.

Table 1.9 Selected Generation III+ reactors (deployment in 5−10 years)

No.	Reactor type	Nuclear vendor
1	ABWR	Toshiba, Mitsubishi Heavy Industries (MHI), and Hitachi-GE (Japan−United States; the only Generation III + reactor design already implemented in the power industry)
2	Advanced CANDU reactor (ACR-1000)	Candu Energy Inc. (formerly AECL) − a member of the SNC-Lavalin Group
3	Advanced plant (AP-1000)	Toshiba-Westinghouse (Japan−United States; 6 under construction in China and 6 more planned to be built in China and 6 in United States)
4	Advanced PWR (APR-1400)	South Korea (4 under construction in South Korea and 4 planned to be built in United Arab Emirates)
5	European pressurized-water reactor (EPR)	Areva, France (1 should be put into operation in Finland, 1 under construction in France, and 2 in China; 2 are planned to be built in the United States)
6	ESBWR	GE-Hitachi (United States−Japan)
7	VVER[a] (design AES[b]-2006 or VVER-1200 with ~1200 MW_{el})	GIDROPRESS, Russia (4 under construction in Russia and several more planned to be built in various countries, including Belarus, Finland, Turkey, Vietnam, etc.)

ABWR, advanced boiling water reactor; *CANDU*, CANada deuterium uranium; *PWR*, pressurized water reactor; *BWR*, boiling water reactor; *VVER*, water-water power reactor (Russian abbreviation); *ESBWR*, economic simplified boiling water reactor.
[a]VVER or WWER are abbreviations for water-water power reactor (in Russian).
[b]AES is an abbreviation for atomic electrical station (NPP; in Russian).
Table data partially based on Nuclear News, March 2015, Publication of American Nuclear Society (ANS), 39−72.

An important question for widespread use of nuclear-based electrical energy generation is how reactors are safe. Table 1.10 lists selected accidents with casualties in power and chemical industries, transportation, and from firearms. Analysis of data in Table 1.10 clearly shows that the major cause of many deaths in the world is car accidents, which are apparently deemed socially acceptable because of the necessity for rapid, convenient transport. Nevertheless, the international nuclear and political communities have to do everything possible and impossible to prevent any future severe accidents at NPPs with radiation release and other consequences.

Table 1.10 Casualties due to various accidents in power and chemical industries, transportation, and from firearms

No.	Accidents/causes of death	Year	Region	Number of deaths
1	Fukushima NPP accident (deaths due to earthquake, not radiation)	2011	Japan	Few workers
2	Chernobyl NPP accident	1986[a]	Ukraine	56
		1986-now[b]		**>4000**
3	Kyshtym radiation release accident (Chelyabinsk region)	1957[c]	Russia	>>200
4	Sayano-Shushenskaya hydro-power plant accident	2009	Russia	75
5	Banqiao dam[d]	1975	China	**>26,000**
6	Vajont dam	1963	Italy	~2000
7	Bhopal Union Carbide India Ltd. accident[e]	1984	India	
	Immediate deaths (official data)			2259
	By government of Madhya Pradesh			3787
	Other estimations (since the disaster)			**8000**
8	Car accidents[f] (in (…) population in millions)]	**Annually** / **daily**	World (7035)	~1,300,000 / ~3560
		2013	United States (316)	**33,808**
		2013	European Union (503)	**26,000**
9	Shipwreck accidents	2011	World	3335
10	Railway accidents	2009	European Union	1428
11	Air accidents[g]	2014	World	>990
		2013		459
		2012; 2011		~800
		2010		1130
		1972		3344
		September 11, 2011	New York, United States	**>4500**

Table 1.10 Continued

No.	Accidents/causes of death	Year	Region	Number of deaths
12	Firearms casualties[h] (60% suicides and 40% homicides)	Annually	United States	**~32,000**

NPP, nuclear power plant.
[a]56 direct deaths (47 NPP and emergency workers and 9 children with thyroid cancer); ie, deaths due to the explosion and initial radiation release.
[b]Deaths from cancer, heart disease, birth defects (in victims' children), and other causes, which may result from exposure to radiation. Various sources provide significantly different estimations starting from 30,000 to 60,000 casualties and up to 200,000 and even up to 985,000 casualties. However, these deaths may also result from other causes not related to the accident (eg, pollution from non-nuclear sources— industry, transportation, etc.). In general, accurate estimation of all deaths related to the Chernobyl NPP accident is impossible.
[c]Similar to the Chernobyl NPP accident, it is impossible to accurately estimate all casualties. Some other sources estimate casualties from cancer within 30 years after the accident up to 8000.
[d]Based on information from http://www.sjsu.edu/faculty/watkins/aug1975.htm. In addition, 145,000 died during subsequent epidemics and famine. In addition, ~11 million residents were affected. Some other sources estimate casualties as high as 230,000 people.
[e]Based on information from http://news.bbc.co.uk/2/hi/south_asia/8725140.stm.
[f]In addition to fatalities in car accidents, ~50 million people become invalid each year in the world (Global Status Report on Road Safety, 2013). Therefore driving a car is a quite dangerous mode of travel!
[g]In 2000 commercial air carriers transported ~1.1 billion people on 18 million flights but there were only 20 fatal accidents. Therefore air transportation remains among the safest modes of travel.
[h]Based on information from http://www.gunpolicy.org/firearms/region/united-states.
Data listed here just for reference purposes and are from Wikipedia (2014).

1.4 Conclusions

The basis for nuclear energy for future electric power generation must take into account the key influences of the global, political, financial, and social pressures in the evolving energy marketplace. The competitive pressures and political factors are likely to dominate future usage and deployment, including national attitudes about and international issues arising from energy security and climate change.

1. The major advantages of nuclear power are well known, including cheap, reliable, base-load power; a high capacity factor; low emissions; and minor environmental impact. However, these factors are offset today by a competitive disadvantage with natural gas and the occurrence of three significant nuclear accidents (Fukushima, Chernobyl, and Three Mile Island), which caused significant social disruption and high capital costs.
2. Major sources for electrical-energy production in the world today are
   a. thermal, including primary coal (39.9%) and secondary natural gas (22.6%);
   b. "large" hydro (17.2%); and
   c. nuclear (11.2%).

   The remaining 9.2% of the electrical energy is generated using oil (4.2%) and other sources (biomass, wind, geothermal, and solar energy; 5%) in selected countries. Other energy sources have visible impact only in some countries, especially where there are government incentives for wind and solar power portfolios with electricity prices guaranteed by legislation and power-purchase contracts.

3. The attractive renewable energy sources such as wind, solar, tidal, etc., are not really reliable as full-time (24 h per day/7 days per week/365 days per year) sources for industrial power generation. Therefore a grid must also include "fast-response" power plants such as gas- and coal-fired and/or large hydro-power plants.
4. In general, the major driving force for all advances in thermal power plants and NPPs is thermal efficiency and generating costs. Ranges of gross thermal efficiencies of modern power plants are (1) combined-cycle thermal power plants (up to 62%); (2) supercritical-pressure coal-fired thermal power plants (up to 55%); (3) CO_2-cooled reactor NPPs (up to 42%); (4) sodium-cooled fast reactor NPPs (up to 40%); (5) subcritical-pressure coal-fired thermal power plants (up to 40%); and (6) modern water-cooled reactors (30−36%).
5. Despite the advances in coal-fired thermal power plant design and operation worldwide, they are still considered as not particularly environmental friendly because they produce gaseous CO_2 emissions as a result of combustion process, plus significant tailings of slag and ash. Legislated measures have recently been proposed to limit such emissions, going beyond voluntary and regional emission credits and allowable portfolios.
6. Combined-cycle thermal power plants with natural gas fuel are considered as relatively clean fossil fuel−fired plants compared with coal and oil power plants, and they are dominating new capacity additions because of lower gas production costs using "fracking" technology, but they still emit CO_2 because of the combustion process.
7. In general, nuclear power is a nonrenewable source as the fossil fuels unless fuel recycling is adopted, which means that nuclear resources can be used significantly longer than some fossil fuels, plus nuclear power does not emit CO_2 into the atmosphere. This source of energy is currently considered as the most viable one for base-load electrical generation for the next 50−100 years.
8. However, all current and oncoming Generation III+ NPPs are not very competitive with modern thermal power plants in terms of thermal efficiency, and the difference in values of thermal efficiencies between thermal power plants and NPPs can be up to 20−25%, with NPPs having higher generating cost and construction times than that of natural gas turbines.
9. Therefore enhancements are needed beyond the current builds, which are now mainly in Asia, to compete in the future marketplace, especially without government subsidies or power price guarantees. New-generation (Generation IV) NPPs must have thermal efficiencies close to those of modern thermal power plants (ie, within a range of at least 40−50%) and improved safety measures and designs to be built in the nearest future.

Abbreviations

Ann.	Annual
av.	Average
el.	Electrical
Eff.	Efficiency
gen.	Generation
Rep.	Republic
UAE	United Arab Emirates

Acknowledgments

The authors thank the unidentified authors of Wikipedia website articles and authors of photos from the Wikimedia Commons Website for their materials used in this chapter in tables, figure captions, and footnotes. Materials and illustrations provided by various companies and used in this paper are gratefully acknowledged.

References

Central Intelligence Agency (CIA), 2016a. The World Factbook: Electricity Consumption, in CIA.Org (Online). Available: https://www.cia.gov/library/publications/the-world-factbook/rankorder/2233rank.html (accessed 16.01.16.).

Central Intelligence Agency (CIA), 2016b. The World Factbook: Population, in CIA.Org (Online). Available: https://www.cia.gov/library/publications/the-world-factbook/rankorder/2119rank.html (accessed 16.01.16.).

Global Status Report on Road Safety, 2013. World Health Organization, Luxembourg, 318 p.

Nuclear News, March 2016, Publication of American nuclear Society (ANS), 35–67.

Nuclear News, March 2015, Publication of American Nuclear Society (ANS), 39–72.

Nuclear News, March 2011, Publication of American Nuclear Society (ANS), 45–78.

Pioro, I., 2012. Nuclear power as a basis for future electricity production in the world. In: Mesquita, A.Z., Rezende, H.C. (Eds.), Chapter #10 in Book: Current Research in Nuclear Reactor Technology in Brazil and Worldwide. INTECH, Rijeka, Croatia, pp. 211–250. Free download from: http://www.intechopen.com/books/current-research-in-nuclear-reactor-technology-in-brazil-and-worldwide/nuclear-power-as-a-basis-for-future-electricity-production-in-the-world-generation-iii-and-iv-reacto.

Pioro, I., Duffey, R., 2015. Nuclear power as a basis for future electricity generation. ASME Journal of Nuclear Engineering and Radiation Science 1 (1), 19. Free download from: http://nuclearengineering.asmedigitalcollection.asme.org/article.aspx?articleID=2085849.

Pioro, I., Kirillov, P., 2013a. Current status of electricity generation in the world. In: Méndez-Vilas, A. (Ed.), Chapter in the Book: Materials and Processes for Energy: Communicating Current Research and Technological Developments, Energy Book Series #1. Formatex Research Center, Spain, pp. 783–795. Free download from: http://www.formatex.info/energymaterialsbook/book/783-795.pdf.

Pioro, I., Kirillov, P., 2013b. Current status of electricity generation at thermal power plants. In: Méndez-Vilas, A. (Ed.), Chapter in the Book: Materials and Processes for Energy: Communicating Current Research and Technological Developments, Energy Book Series #1. Formatex Research Center, Spain, pp. 796–805. Free download from: http://www.formatex.info/energymaterialsbook/book/796-805.pdf.

Pioro, I., Kirillov, P., 2013c. Current status of electricity generation at nuclear power plants. In: Méndez-Vilas, A. (Ed.), Chapter in the Book: Materials and Processes for Energy: Communicating Current Research and Technological Developments, Energy Book Series #1. Formatex Research Center, Spain, pp. 806–817. Free download from: http://www.formatex.info/energymaterialsbook/book/806-817.pdf.

Pioro, I., Kirillov, P., 2013d. Generation IV nuclear reactors as a basis for future electricity production in the world. In: Méndez-Vilas, A. (Ed.), Chapter in the Book: Materials and Processes for Energy: Communicating Current Research and Technological Developments,

Energy Book Series #1. Formatex Research Center, Spain, pp. 818−830. Free download from: http://www.formatex.info/energymaterialsbook/book/818-830.pdf.

United Nations (UN), 2016. Table 1: Human Development Index and its Components. United Nations Development Programme (Online). Available: http://hdr.undp.org/en/composite/HDI (accessed 16.01.16).

US Energy Information Administration, 2013. Washington, DC, USA.

Part One

Generation IV nuclear-reactor concepts

Preface to Part One

Part One presents the current officially available information from the Generation IV International Forum (GIF) website (https://www.gen-4.org/gif/jcms/c_9260/public) covering all six Generation IV nuclear power systems (concepts): very-high−temperature reactor (VHTR), gas fast reactor (GFR), sodium-cooled fast reactor (SFR), lead-cooled fast reactor (LFR), molten salt reactor (MSR), and supercritical water-cooled reactor (SCWR). Corresponding to that, Part One consists of seven chapters (Chapters 2−8) written by top international experts—specialists in research and development of these six concepts. For clarity, the sequence of these chapters/Generation IV concepts corresponds to the type of reactor coolant: firstly VHTR and GFR, which are helium cooled; next SFR and LFR, which are liquid-metal cooled; next the MSR, molten-salt cooled; and then finally the SCWR, which is supercritical-water cooled. It should be noted that in other publications/websites the sequence of Generation IV concepts can be different; for example, on the GIF website (https://www.gen-4.org/gif/jcms/c_59461/generation-iv-systems) these concepts are often simply put in alphabetical order (ie, GFR, LFR, MSR, SCWR, SFR, and VHTR).

Introduction: Generation IV International Forum

2

I.L. Pioro
University of Ontario Institute of Technology, Oshawa, Ontario, Canada

This chapter consists of materials and figures taken directly from the Generation IV International Forum (GIF) website: https://www.gen-4.org/gif/jcms/c_9260/public (accessed January 17, 2016) with the permission of the GIF. In general, the GIF and its six Generation IV nuclear reactor concepts are not the only next generation or advanced reactors (ARs) currently under development in the world. Advanced small modular reactors (SMRs) can be considered under the class of ARs or next generation reactors. Therefore, advanced SMRs are considered in chapter "Advanced small modular reactors (SMRs)" of this handbook.

In addition, it should be noted that other nuclear reactor concepts of the next generation or ARs are being researched and developed by various nuclear engineering companies worldwide, for example, the traveling wave reactor by TerraPower (http://terrapower.com/pages/technology) in the USA. However, for the purpose of this handbook, we will mainly rely only on the GIF six Generation IV nuclear reactor concepts (see further).

The GIF website lists a number of publications dedicated to each GIF nuclear power system. Therefore, it is recommended to look through these publications for more details.

2.1 Origins of the Generation IV International Forum

GIF meetings began in January 2000 when the US Department Of Energy's (DOE) Office of Nuclear Energy, Science and Technology convened a group of senior governmental representatives from the original nine countries to begin discussions on international collaboration in the development of Generation IV nuclear energy systems.

This group, subsequently named the GIF Policy Group, also decided to form a group of senior technical experts to explore areas of mutual interest and make recommendations regarding both research and development (R&D) areas and processes by which collaboration could be conducted and assessed. This senior Technical Experts Group first met in April 2000.

The founding document of the GIF, a framework for international cooperation in R&D for the next generation of nuclear energy systems, are set out in the GIF Charter, first signed in July 2001 by Argentina, Brazil, Canada, France, Japan, Republic of Korea, South Africa, the UK, and the US.

Handbook of Generation IV Nuclear Reactors. http://dx.doi.org/10.1016/B978-0-08-100149-3.00002-1
Copyright © 2016 Elsevier Ltd. All rights reserved.

The Charter has since been signed by Switzerland (2002), the European Atomic Energy Community (Euratom) (2003), and most recently, by the People's Republic of China and the Russian Federation in November 2006.

In July 2011, the 13 members agreed to sign an extension of the Charter, signaling the wish to continue to cooperate in the R&D of Generation IV.

2.2 Generation IV goals

Eight technology goals have been defined for Generation IV systems in four broad areas: sustainability, economics, safety and reliability, and proliferation resistance and physical protection. These ambitious goals are shared by a large number of countries as they aim at responding to the economic, environmental, and social requirements of the 21st century. They establish a framework and identify concrete targets for focusing GIF R&D efforts.

Goals for Generation IV nuclear energy systems	
Sustainability-1	Generation IV nuclear energy systems will provide sustainable energy generation that meets clean air objectives and provides long-term availability of systems and effective fuel utilization for worldwide energy production.
Sustainability-2	Generation IV nuclear energy systems will minimize and manage their nuclear waste and notably reduce the long-term stewardship burden, thereby improving protection for the public health and the environment.
Economics-1	Generation IV nuclear energy systems will have a clear lifecycle cost advantage over other energy sources.
Economics-2	Generation IV nuclear energy systems will have a level of financial risk comparable to other energy projects.
Safety and Reliability-1	Generation IV nuclear energy systems operations will excel in safety and reliability.
Safety and Reliability-2	Generation IV nuclear energy systems will have a very low likelihood and degree of reactor core damage.
Safety and Reliability-3	Generation IV nuclear energy systems will eliminate the need for offsite emergency response.
Proliferation Resistance and Physical Protection	Generation IV nuclear energy systems will increase the assurance that they are very unattractive and the least desirable route for diversion or theft of weapons-usable materials, and provide increased physical protection against acts of terrorism.

These goals guide the cooperative R&D efforts undertaken by GIF members. The challenges raised by GIF goals are intended to stimulate innovative R&D, covering all technological aspects related to design and implementation of reactors, energy conversion systems, and fuel cycle facilities.

In light of the ambitious nature of the goals involved, international cooperation is considered essential for a timely progress in the development of Generation IV systems. This cooperation makes it possible to pursue multiple systems and technical options concurrently and to avoid any premature down selection due to the lack of adequate resources at the national level.

2.3 Selection of Generation IV systems

For more than a decade, GIF has led international collaborative efforts to develop next generation nuclear energy systems that can help meet the world's future energy needs. Generation IV designs will use fuel more efficiently, reduce waste production, be economically competitive, and meet stringent standards of safety and proliferation resistance.

With these goals in mind, some 100 experts evaluated 130 reactor concepts before GIF selected six reactor technologies for further R&D. These include: the gas-cooled fast reactor (GFR), lead-cooled fast reactor (LFR), molten salt reactor (MSR), supercritical water-cooled reactor (SCWR), sodium-cooled fast reactor (SFR), and very high temperature reactor (VHTR).

The latest information on a status of GIF system arrangements and memoranda of understanding is shown in Fig. 2.1 and system development timelines as defined in the original roadmap in 2002 and in the 2013 update in Fig. 2.2.

The goals adopted by GIF provided the basis for identifying and selecting six nuclear energy systems for further development. The selected systems rely on a variety of reactor, energy conversion, and fuel cycle technologies. Their designs feature thermal and fast neutron spectra, closed and open fuel cycles as well as a wide range of reactor sizes from very small to very large. Depending on their respective degrees

System	CA	CN	EU	FR	JP	KR	RU	CH	US	ZA
SFR		✓	✓	✓	✓	✓	✓		✓	
VHTR		✓	✓	✓	✓	✓		✓	✓	
SCWR	✓		✓		✓		✓			
GFR			✓	✓	✓			✓		
LFR			P		P		P			
MSR			P	P			P			

✓ = Signatory to the system arrangement; P = Signatory to the memorandum of understanding; Argentina, Brazil, and the United Kingdom are inactive.

Figure 2.1 Status of the GIF system arrangements and memoranda of understanding (as of January 1, 2014). Also, China has signed the SCWR System Arrangement in May of 2014. Courtesy of Generation IV International Forum.

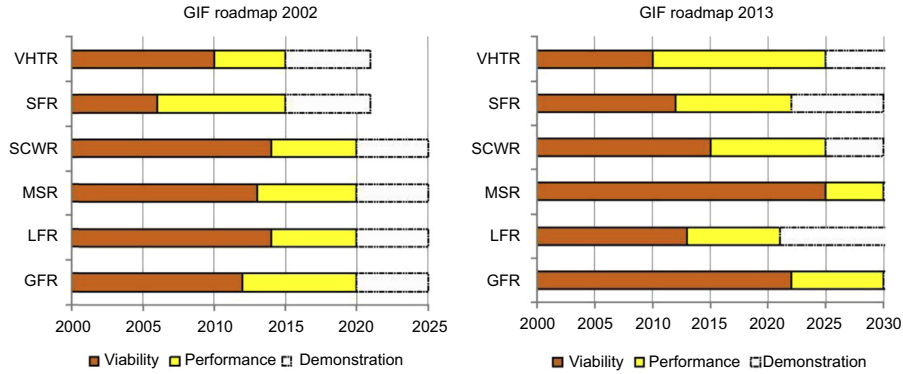


Figure 2.2 System development timelines as defined in the original roadmap in 2002 and in the 2013 update.
Courtesy of Generation IV International Forum.

of technical maturity, the Generation IV systems are expected to become available for commercial introduction in the period around 2030 or beyond. The path from current nuclear systems to Generation IV systems is described in a 2002 roadmap report entitled "A Technology Roadmap for Generation IV nuclear energy systems," which is currently being updated.

All Generation IV systems aim at performance improvement, new applications of nuclear energy, and/or more sustainable approaches to the management of nuclear materials. High-temperature systems offer the possibility of efficient process heat applications and eventually hydrogen production. Enhanced sustainability is achieved primarily through the adoption of a closed fuel cycle, including the reprocessing and recycling of plutonium, uranium, and minor actinides in fast reactors and also through high thermal efficiency. This approach provides a significant reduction in waste generation and uranium resource requirements. Table 2.1 summarizes the main characteristics of the six Generation IV systems.

It should be noted that on the GIF website, the sequence of referencing six nuclear reactor concepts can be based on their alphabetical order (see Section 2.3), or other sequences have been used (eg, see Figs. 2.1 and 2.2). However, to be consistent with the sequence of six Generation IV concepts, it was decided to list them according to the type of reactor coolant, ie, first two reactors (VHTR and GFR) are helium cooled; the next two concepts (SFR and LFR) are liquid metal cooled; the next one concept (SMR) is molten salt cooled; and the last concept (SCWR) is supercritical water (SCW) cooled.

2.4 Six Generation IV nuclear energy systems

2.4.1 Very high temperature reactor

The VHTR (see Fig. 2.3) is a further step in the evolutionary development of high temperature reactors (HTRs). The VHTR is a helium gas-cooled, graphite-moderated,

Table 2.1 Overview of Generation IV systems

No.	System	Neutron spectrum	Coolant	Outlet temperature, °C	Fuel cycle	Size (MW_{el})
1	VHTR	Thermal	Helium	900−1000	Open	250−300
2	GFR	Fast	Helium	850	Closed	1200
3	SFR	Fast	Sodium	500−550	Closed	50−150 300−1500 600−1500
4	LFR	Fast	Lead	480−570	Closed	20−180 300−1200 600−1000
5	MSR	Thermal/ fast	Fluoride salts	700−800	Closed	1000
6	SCWR	Thermal/ fast	Water	510−625	Open/ Closed	300−700 1000−1500

Courtesy of Generation IV International Forum

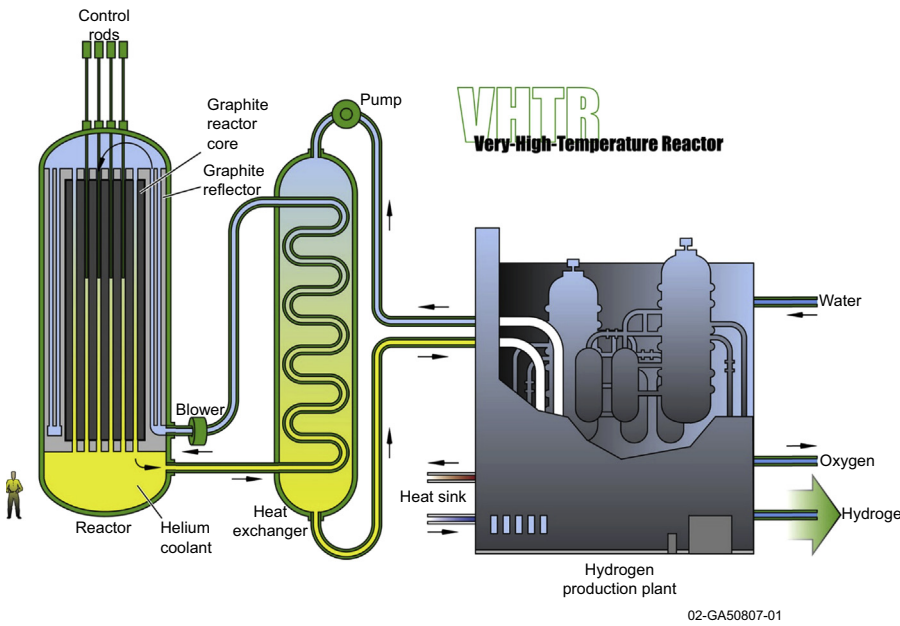


Figure 2.3 VHTR: Helium gas cooled, graphite-moderated, thermal neutron spectrum reactor with core outlet temperature 900−1000°C (shown with hydrogen cogeneration). Courtesy of Generation IV International Forum.

thermal neutron spectrum reactor with a core outlet temperature higher than 900°C and a goal of 1000°C, sufficient to support high-temperature processes such as production of hydrogen by thermochemical processes. The reference thermal power of the reactor is set at a level that allows passive decay heat removal, currently estimated to be about 600 MW_{th}. The VHTR is useful for the cogeneration of electricity and hydrogen, as well as to other process heat applications, eg, for the chemical, oil, and iron industries. It is able to produce hydrogen from water by using thermochemical, electrochemical, or hybrid processes with reduced emission of CO_2 gases. At first, a once-through low-enriched uranium (<20% ^{235}U) fuel cycle will be adopted, but a closed fuel cycle will be assessed, as well as potential symbiotic fuel cycles with other types of reactors (especially light water reactors (LWRs)) for waste reduction purposes. The system is expected to be available for commercial deployment by 2020.

The technical basis for VHTR is the TRI-ISOtropic (TRISO)-coated particle fuel. The VHTR has potential for inherent safety, high thermal efficiency, process heat application capability, low operation and maintenance costs, and modular construction.

In general, the reactor-core type of the VHTR can be a prismatic block core, such as the Japanese high-temperature test reactor, or a pebble bed core, such as the Chinese HTR-10. For electricity generation, a helium gas turbine system can be directly set in the primary coolant loop, which is called a direct cycle, or at the lower end of the outlet temperature range, a steam generator can be used with a conventional Rankine cycle. For nuclear heat applications, such as process heat for refineries, petrochemistry, metallurgy, and hydrogen production, the heat application process is generally coupled with the reactor through an intermediate heat exchanger, the so-called indirect cycle. The VHTR can produce hydrogen from only heat and water by using thermochemical processes (such as the sulfur–iodine (S–I) process or the hybrid sulfur process), high-temperature steam electrolysis, or from heat, water, and natural gas by applying the steam reformer technology.

While the original approach for VHTR at the start of the Generation IV program focused on very high outlet temperatures and hydrogen production, current market assessments have indicated that electricity production and industrial processes based on high-temperature steam that require modest outlet temperatures (700–850°C) have the greatest potential for application in the next decade and also reduce technical risk associated with higher outlet temperatures. As a result, over the past decade, the focus has moved from higher outlet temperature designs such as Gas Turbine-Modular Helium Reactor and Pebble Bed Modular Reactor to lower outlet temperature designs such as High Temperature Reactor-Pebble Bed Modules in China and the Next Generation Nuclear Plant in the USA.

The VHTR has two typical reactor configurations, namely the pebble bed type and the prismatic block type. Although the shape of the fuel element for two configurations are different, the technical basis for both configuration is same, such as the TRISO-coated particle fuel in the graphite matrix, full ceramic (graphite) core structure, helium coolant, and low power density, in order to achieve high outlet temperature and the retention of fission production inside the coated particle under normal operation condition and accident condition. The VHTR can support alternative fuel cycles such as U–Pu, Pu, mixed oxide (MOX), and U–thorium (Th).

2.4.2 Gas-cooled fast reactor

The GFR (see Fig. 2.4) is a high-temperature helium-cooled fast spectrum reactor with a closed fuel cycle. The core outlet temperature will be of the order of 850°C. It combines the advantages of fast spectrum systems for long-term sustainability of uranium resources and waste minimization (through fuel multiple reprocessing and fission of long-lived actinides), with those of high-temperature systems (eg, high thermal cycle efficiency and industrial use of the generated heat for hydrogen production). It requires the development of robust refractory fuel elements and appropriate safety architecture. The use of dense fuel, such as carbide or nitride, provides good performance regarding plutonium breeding and minor actinide burning. A technology demonstration reactor needed for qualifying key technologies could be in operation by 2020.

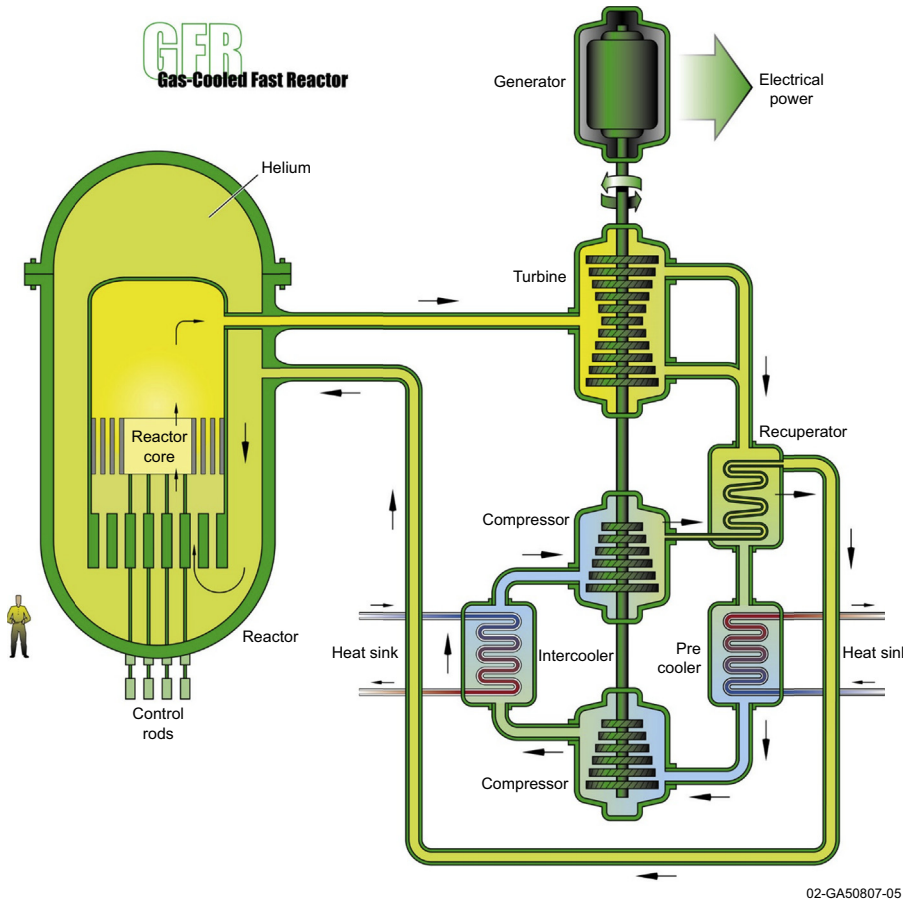


Figure 2.4 GFR: Helium gas-cooled, fast neutron spectrum reactor with closed fuel cycle and outlet temperature of about 850°C (shown with direct gas turbine Brayton power cycle). Courtesy of Generation IV International Forum.

The GFR uses the same fuel recycling processes as the SFR and the same reactor technology as the VHTR. Therefore, its development approach is to rely, insofar as feasible, on technologies developed for the VHTR for structures, materials, components, and power conversion systems. Nevertheless, it calls for specific R&D beyond the current and foreseen work on the VHTR system, mainly on core design and safety approach.

The reference design for GFR is based around a 2400-MW_{th} reactor core contained within a steel pressure vessel. The core consists of an assembly of hexagonal fuel elements, each consisting of ceramic-clad, mixed carbide-fueled pins contained within a ceramic hex tube. The favored material at the moment for the pin clad and hex tubes is silicon−carbide fiber-reinforced silicon carbide.

As a new approach, the latest GFR concept will have the indirect cycle. A heat exchanger transfers the heat from the primary helium coolant to a secondary gas cycle containing a helium−nitrogen mixture, which in turn drives a closed-cycle gas turbine. The waste heat from the gas turbine exhaust is used to raise steam in a steam generator, which is then used to drive a steam turbine. Such a combined cycle is common practice in natural gas-fired power plants, so it represents an established technology, with the only difference in the GFR case being the use of a closed-cycle gas turbine.

2.4.3 Sodium-cooled fast reactor

The SFR (see Fig. 2.5) uses liquid sodium as the reactor coolant. It features a closed fuel cycle for fuel breeding and/or actinide management. The two primary fuel recycle technology options are advanced aqueous and pyrometallurgical processing. A variety of fuel options are being considered for the SFR, with MOX preferred for advanced aqueous recycle and mixed metal alloy preferred for pyrometallurgical processing. Owing to the significant past experience accumulated with sodium-cooled reactors in several countries, the deployment of SFR systems is targeted for 2020.

Using liquid sodium as the reactor coolant, allowing high power density with low coolant volume fraction and operation at low pressure. While the oxygen-free environment prevents corrosion, sodium reacts chemically with air and water and requires a sealed coolant system.

Plant size options under consideration range from small, 50−300 MW_{el} modular reactors to larger plants up to 1500 MW_{el}. The outlet temperature is 500−550°C for the options, which allows the use of the materials developed and proven in prior fast reactor programs.

The SFR closed fuel cycle enables regeneration of fissile fuel and facilitates management of minor actinides. However, this requires that recycle fuels be developed and qualified for use. Important safety features of the Generation IV system include a long thermal response time, a reasonable margin to coolant boiling, a primary system that operates near atmospheric pressure, and an intermediate sodium system between the radioactive sodium in the primary system and the power conversion system. Water/steam (Rankine cycle) and supercritical carbon dioxide or nitrogen (Brayton cycle) can be considered as working fluids for the power conversion system to achieve high performance in terms of thermal efficiency, safety, and reliability. With innovations to reduce capital cost, the SFR is aimed to be economically competitive in future

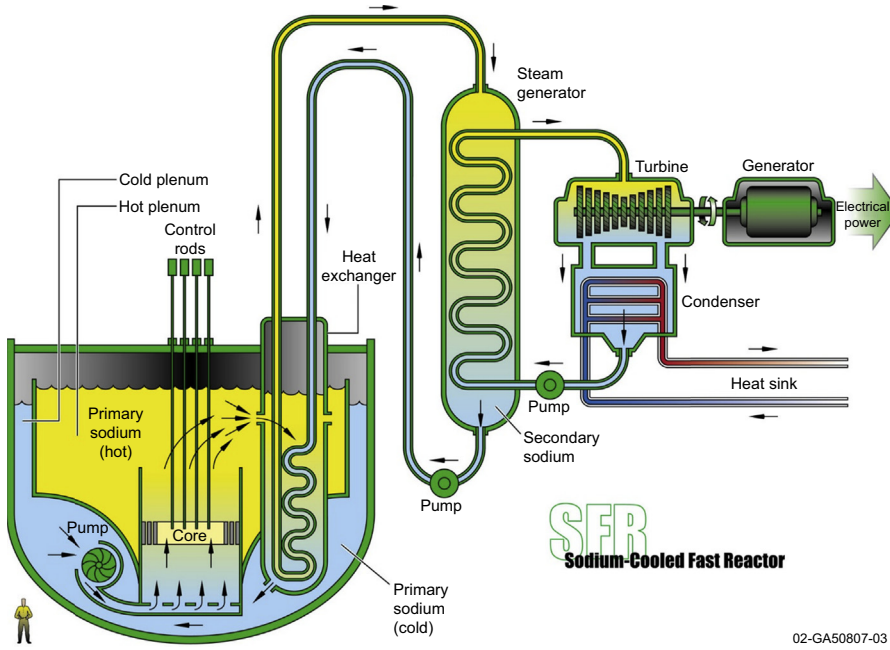


Figure 2.5 SFR: Molten sodium-cooled, fast neutron spectrum reactor with closed fuel cycle and outlet temperatures within 500−550°C (shown pool-type reactor with indirect steam turbine Rankine power cycle).
Courtesy of Generation IV International Forum.

electricity markets. In addition, the fast neutron spectrum greatly extends the uranium resources compared to thermal reactors. The SFR is considered to be the nearest-term deployable system for actinide management.

Much of the basic technology for the SFR has been established in former fast reactor programs, and was confirmed by the Phenix End-of-Life tests in France by operation of Monju reactor in Japan and the lifetime extension of BN-600 in Russia. New programs involving SFR technology include the China Experimental Fast Reactor, which was connected to the grid in July 2011, India's Prototype Fast Breeder Reactor, and the latest success in Russia with putting into operation the BN-800 reactor.

The SFR is an attractive energy source for nations that desire to make the best use of limited nuclear fuel resources and manage nuclear waste by closing the fuel cycle.

Fast reactors hold a unique role in the actinide management mission because they operate with high-energy neutrons that are more effective at fissioning actinides. The main characteristics of the SFR for actinide management mission are:

- Consumption of transuranics in a closed fuel cycle, thus reducing the radiotoxicity and heat load, which facilitates waste disposal and geologic isolation; and
- Enhanced utilization of uranium resources through efficient management of fissile materials and multirecycling.

A high level of safety achieved through inherent and passive means also allows accommodation of transients and bounding events with significant safety margins.

The reactor unit can be arranged in a pool layout or a compact loop layout. Three options are considered:

- A large size (600−1500 MW_{el}) loop-type reactor with mixed uranium−plutonium oxide fuel and potentially minor actinides, supported by a fuel cycle based upon advanced aqueous processing at a central location serving a number of reactors;
- An intermediate to large size (300−1500 MW_{el}) pool-type reactor with oxide or metal fuel; and
- A small size (50−150 MW_{el}) modular-type reactor with uranium−plutonium−minor actinide−zirconium metal alloy fuel, supported by a fuel cycle based on pyrometallurgical processing in facilities integrated with the reactor.

2.4.4 Lead-cooled fast reactor

The LFR (see Fig. 2.6) is characterized by a fast neutron spectrum, a closed fuel cycle with full actinide recycling, possibly in central or regional fuel cycle facilities, and

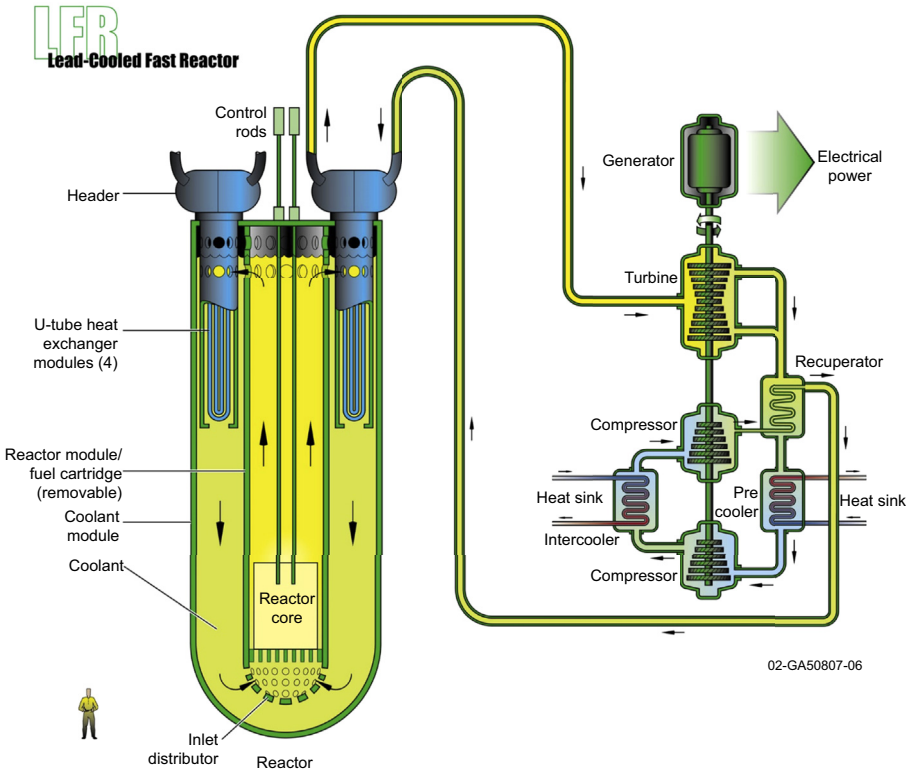


Figure 2.6 LFR: Molten lead-cooled, fast neutron spectrum reactor with closed fuel cycle and outlet temperatures within 500−550°C (shown with indirect Brayton power cycle). Courtesy of Generation IV International Forum.

high-temperature operation at low pressure. The coolant may be either lead (preferred option), or lead−bismuth eutectic (LBE). The LFR may be operated as a breeder, a burner of actinides from spent fuel using inert matrix fuel, or a burner/breeder using thorium matrices. Two reactor-size options are considered: a small 50−150 MW_{el} transportable system with a very long core life, and a medium 300−600 MW_{el} system. In the long term, a large system of 1200 MW_{el} may be envisaged. The LFR system may be deployable by 2025.

Lead and LBE are relatively inert liquids with very good thermodynamic properties. The LFR would have multiple applications including production of electricity, hydrogen, and process heat. System concepts represented in plans of the GIF System Research Plan are based on the European Lead-cooled Fast Reactor, Russia's BREST-OD-300 (fast reactor with lead coolant; Быстрый Реактор со Свинцовым Теплоносителем in Russian abbreviations) and the Small Secure Transportable Autonomous Reactor concept designed in the US.

The LFR has excellent materials management capabilities since it operates in the fast neutron spectrum and uses a closed fuel cycle for efficient conversion of fertile uranium. It can also be used as a burner to consume actinides from spent LWR fuel and as a burner/breeder with thorium matrices. An important feature of the LFR is the enhanced safety that results from the choice of molten lead as a relatively inert and low-pressure coolant. In terms of sustainability, lead is abundant and hence available, even in case of deployment of a large number of reactors. More importantly, as with other fast systems, fuel sustainability is greatly enhanced by the conversion capabilities of the LFR fuel cycle. Because they incorporate a liquid coolant with a very high margin to boiling and benign interaction with air or water, LFR concepts offer substantial potential in terms of safety, design simplification, proliferation resistance, and the resulting economic performance. An important factor is the potential for benign end state to severe accidents.

The LFR has development needs in the areas of fuels, materials performance, and corrosion control. During the next 5 years, progress is expected on materials, system design, and operating parameters. Significant test and demonstration activities are underway and planned during this timeframe.

2.4.5 Molten salt reactor

The MSR (see Fig. 2.7) embodies the very special feature of a liquid fuel. MSR concepts, which may be used as efficient burners of transuranic elements from spent LWR fuel, also have a breeding capability in any kind of neutron spectrum ranging from thermal (with a thorium fuel cycle) to fast (with a uranium−plutonium fuel cycle). Whether configured for burning or breeding, MSRs have considerable promise for the minimization of radiotoxic nuclear waste.

The MSR is distinguished by its core in which the fuel is dissolved in molten fluoride salt. The technology was first studied more than 50 years ago. Modern interest is on fast reactor concepts as a long-term alternative to solid-fueled fast neutrons reactors. The onsite fuel reprocessing unit using pyrochemistry allows breeding plutonium or uranium-233 from thorium. R&D progresses toward resolving feasibility issues and

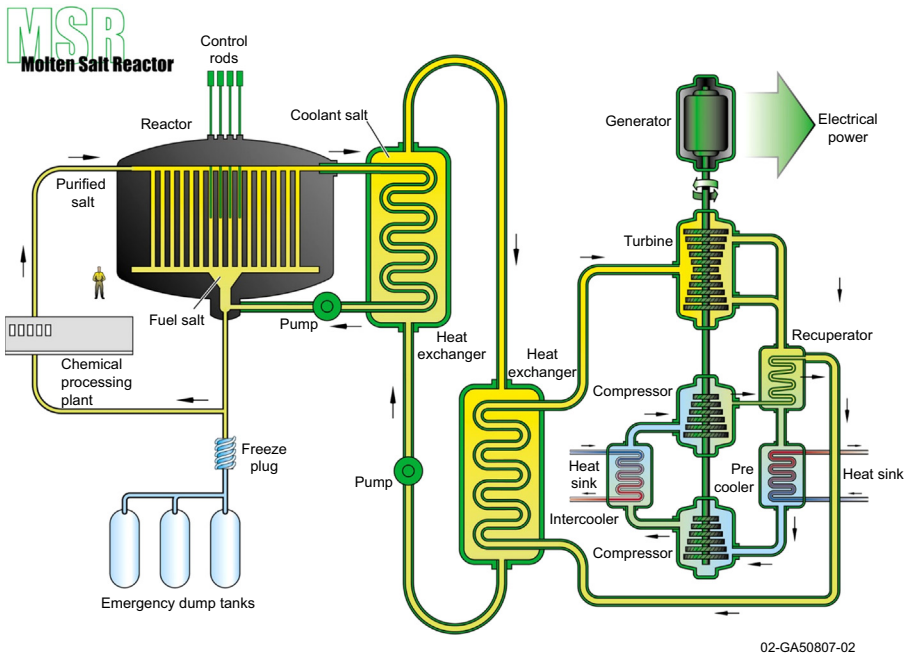


Figure 2.7 MSR: Molten salt-cooled reactor with outlet temperatures within 700−800°C (shown with indirect Brayton power cycle).
Courtesy of Generation IV International Forum.

assessing safety and performance of the design concepts. Key feasibility issues focus on a dedicated safety approach and the development of salt redox potential measurement and control tools in order to limit corrosion rate of structural materials. Further work on the batchwise online salt processing is required. Much work is needed on molten salt technology and related equipment.

MSR technology was partly developed, including two demonstration reactors, in the 1950s and 1960s in the USA (Oak Ridge National Laboratory). The demonstration MSRs were thermal neutron spectrum graphite-moderated concepts. Since 2005, R&D has focused on the development of fast-spectrum MSR concepts (MSFR) combining the generic assets of fast neutron reactors (extended resource utilization, waste minimization) with those relating to molten salt fluorides as fluid fuel and coolant (low pressure and high boiling temperature, optical transparency).

In contrast to most other MSRs previously studied, the MSFR does not include any solid moderator (usually graphite) in the core. This design choice is motivated by the study of parameters such as feedback coefficient, breeding ratio, graphite lifespan, and ^{233}U initial inventory. MSFR exhibit large negative temperature and void reactivity coefficients, a unique safety characteristic not found in solid fuel fast reactors.

Compared with solid fuel reactors, MSFR systems have lower fissile inventories, no radiation damage constraint on attainable fuel burn-up, no requirement to fabricate and handle solid fuel, and a homogeneous isotopic composition of fuel in the reactor. These and other characteristics give MSFRs potentially unique capabilities for actinide burning and extending fuel resources.

MSR developments in Russia on the Molten Salt Actinide Recycler and Transmuter aim to be used as efficient burners of transuranic waste from spent UOX and MOX LWR fuel without any uranium and thorium support and also with it. Other advanced reactor concepts are being studied, which use the liquid salt technology as a primary coolant for fluoride salt-cooled high-temperature reactors, and coated particle fuels similar to high-temperature gas-cooled reactors.

More generally, there has been a significant renewal of interest in the use of liquid salt as a coolant for nuclear and nonnuclear applications. These salts could facilitate heat transfer for nuclear hydrogen production concepts, concentrated solar electricity generation, oil refineries, and shale oil processing facilities, among other applications.

2.4.6 Supercritical water-cooled reactors

SCWRs (see Fig. 2.8) are a class of high-temperature, high-pressure water-cooled reactors operating with a direct energy conversion cycle and above the thermodynamic critical point of water (374°C and 22.1 MPa). The higher thermodynamic efficiency and plant simplification opportunities afforded by a high-temperature, single-phase coolant translate into improved economics. A wide variety of options are currently considered: both thermal neutron and fast neutron spectra are envisaged, both pressure vessel and pressure tube configurations are considered, and thus use light water or heavy water can be used as a moderator. The operation of a 30 to 150 MW_{el} technology demonstration reactor is targeted for 2022.

Unlike current water-cooled reactors, the coolant will experience a significantly higher enthalpy rise in the core, which reduces the core mass flow for a given thermal power and increases the core outlet enthalpy to superheated conditions. For both pressure vessel and pressure tube designs, a once-through steam cycle has been envisaged, omitting any coolant recirculation inside the reactor. As in a Boiling Water Reactor (BWR), the "superheated" steam will be supplied directly to the high-pressure steam turbine, and the feed water from the steam cycle will be supplied back to the core. Thus, the SCWR concepts combine the design and operation experiences gained from hundreds of water-cooled reactors with those experiences from hundreds of fossil-fired power plants operated with SCW. In contrast to some of the other Generation IV nuclear systems, the SCWR can be developed incrementally step-by-step from current water-cooled reactors.

These general features offer the potential of lower capital costs for a given electric power of the plant and of better fuel utilization, and thus a clear economic advantage compared with current LWRs.

In general, SCWR designs have unique features that offer many advantages compared to state-of the-art water-cooled reactors. However, there are several

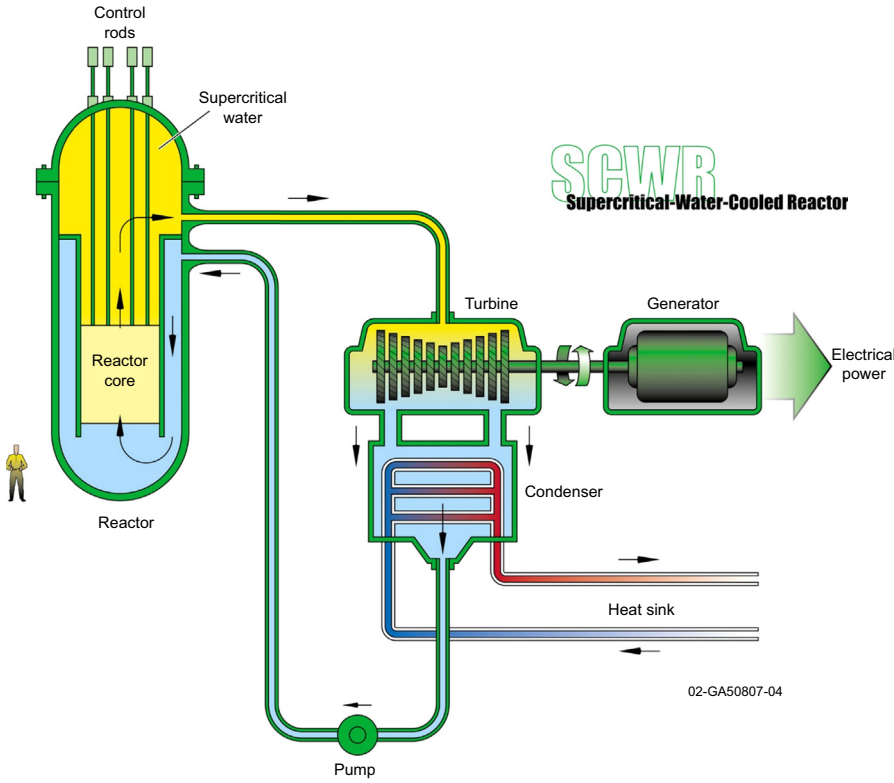


Figure 2.8 SCWR: Supercritical water-cooled, thermal neutron spectrum reactor with outlet temperatures within 510−625°C (shown with direct steam turbine Rankine power cycle). Courtesy of Generation IV International Forum.

technological challenges associated with the development of the SCWR, and particularly the need to validate transient heat transfer models (for describing the depressurization from supercritical to subcritical conditions), qualification of materials (namely, advanced steels for cladding), and demonstration of the passive safety systems.

SCWR designs have unique features that offer many advantages compared to state of-the-art water-cooled reactors:

- SCWRs offer increases in thermal efficiency relative to current generation water-cooled reactors. The efficiency of an SCWR can approach 44% or more, compared to 34−36% for current reactors.
- Reactor coolant pumps are not required. The only pumps driving the coolant under normal operating conditions are the feed water pumps and the condensate extraction pumps.
- The steam generators used in pressurized water reactors and the steam separators and dryers used in boiling water reactors can be omitted since the coolant is superheated in the core.

- Containment, designed with pressure suppression pools and with emergency cooling and residual heat removal systems, can be significantly smaller than those of current water-cooled reactors.
- The higher steam enthalpy allows to decrease the size of the turbine system and thus to lower the capital costs of the conventional island.

Preconceptual core design studies for a core outlet temperature of more than 500°C have been performed in Japan, assuming either a thermal neutron spectrum or a fast neutron spectrum (Oka et al., 2010). Both options are based on a coolant heat-up in two steps with intermediate mixing underneath the core. Additional moderator for a thermal neutron spectrum is provided by feed water inside water rods. The fast spectrum option uses zirconium-hydride (ZrH_2) layers to minimize hardening of the neutron spectrum in case of core voiding. A preconceptual design of safety systems for both options has been studied with transient analyses.

A preconceptual plant design with 1700 MW net electric power based on a pressure vessel-type reactor has been studied by Yamada et al. (2011) and has been assessed with respect to efficiency, safety, and cost. The study confirms the target net efficiency of 44% and estimates a cost reduction potential of 30% compared with current pressurized water reactors. Safety features are expected to be similar to advanced boiling water reactors.

A preconceptual design of a pressure vessel-type reactor with a 500°C core outlet temperature and 1000 MW electric power has been developed in Europe, as summarized by Schulenberg and Starflinger (2012). The core design is based on coolant heat-up in three steps. Additional moderator for the thermal neutron spectrum is provided in water rods and in gaps between assembly boxes. The design of the nuclear island and of the balance of the plant confirms results obtained in Japan, namely an efficiency improvement up to 43.5% and a cost reduction potential of 20−30% compared with latest boiling water reactors. Safety features as defined by the stringent European Utility Requirements are expected to be met.

Canada is developing a pressure tube-type SCWR concept with a 625°C core outlet temperature at the pressure of 25 MPa. The concept is designed to generate 1200 MW electric power (a 300-MW concept is also being considered). It has a modular fuel channel configuration with separate coolant and moderator. A high-efficiency fuel channel is incorporated to house the fuel assembly. The heavy water moderator directly contacts the pressure tube and is contained inside a low-pressure calandria vessel. In addition to providing moderation during normal operation, it is designed to remove decay heat from the high-efficiency fuel channel during long-term cooling using a passive moderator cooling system. A mixture of thorium oxide and plutonium is introduced as the reference fuel, which aligns with the GIF position paper on thorium fuel. The safety system design of the Canadian SCWR is similar to that of the Economic samplified BWR(ESBWR). However, the introduction of the passive moderator cooling system coupled with the high-efficiency channel could reduce significantly the core damage frequency during postulated severe accidents such as large break loss-of-coolant or station blackout events.

Preconceptual designs of three options of pressure vessel SCWRs with thermal, mixed, and fast neutron spectrum have been developed in Russia, which joined the SCWR System Arrangement in 2011.

Outside of the GIF framework, two conceptual SCWR designs with thermal and mixed neutron spectrum cores have been established by some research institutes in China under framework of the Chinese national R&D projects from 2007 to 2012, covering some basic research projects on materials and thermohydraulics, the core/fuel design, the main system design (including the conventional part), safety systems design, reactor structure design, and fuel assembly structure design. The related feasibility studies have also been completed and show that the design concept has promising prospects in terms of the overall performance, integration of design, component structure feasibility, and manufacturability.

Prediction of heat transfer in SCW can be based on data from fossil-fired power plants, as discussed by Pioro and Duffey (2007). Computational tools for more complex geometries like fuel assemblies are available, but still need to be validated with bundle experiments. System codes for transient safety analyses have been upgraded to include SCW, including depressurization transients to subcritical conditions. Flow stability in the core has been studied numerically. As in BWRs, flow stability can be ensured using suitable inlet orifices in fuel assemblies.

A number of candidate cladding materials have been tested in capsules, autoclaves, and recirculating loops up to 700°C at a pressure of 25 MPa. Stainless steels with more than 20% chromium (Cr) are expected to have the required corrosion resistance up to a peak cladding temperature of 650°C. More work is needed to develop alloys suitable for use at the design peak cladding temperatures of 850°C for the Canadian SCWR concept. Further work is also needed to better identify the coolant conditions that lead to stress corrosion cracking. It has been shown that the creep resistance of existing alloys can be improved by adding small amounts of elements, such as zirconium (Zr), as reported by Kaneda et al. (2011). In the longer term, the steel experimental oxide dispersion strengthened alloys offer an even higher potential, whereas nickel-base alloys that are being considered for use in ultra-supercritical fossil-fired plants are less favorable for use in SCWRs due to their high neutron absorption and associated swelling and embrittlement.

Key water chemistry issues have been identified by Guzonas et al. (2012): predicting and controlling water radiolysis and corrosion product transport (including fission products) remain the major R&D areas. In this regard, the operating experience using nuclear steam reheat at the Beloyarsk nuclear power plant (NPP) in Russia is extremely valuable.

2.5 Summary

In summary, Table 2.2 lists estimated ranges of thermal efficiencies (gross) of Generation IV NPP concepts for reference purposes (Pioro and Duffey, 2015).

Table 2.2 Estimated ranges of thermal efficiencies (gross) of Generation-IV NPP concepts (Generation IV concepts are listed according to thermal efficiency decrease) (shown here just for reference purposes)

No	Nuclear power plant	Gross efficency, %
1	Very high temperature reactor NPP (reactor coolant − helium: $P = 7$ MPa, and $T_{in}/T_{out} = 640/1000°C$; primary power cycle − direct Brayton gas-turbine cycle; possible back-up − indirect Rankine steam cycle).	≥55
2	Gas-cooled fast reactor or high temperature reactor NPP (reactor coolant − helium: $P = 9$ MPa and $T_{in}/T_{out} = 490/850°C$; primary power cycle − direct Brayton gas turbine cycle; possible backup − indirect Rankine steam cycle).	≥50
3	Supercritical water-cooled reactor NPP (one of Canadian concepts; reactor coolant − light water: $P = 25$ MPa and $T_{in}/T_{out} = 350/625°C$ ($T_{cr} = 374°C$); direct cycle; high-temperature steam superheat: $T_{out} = 625°C$; possible backup − indirect supercritical-pressure Rankine steam cycle with high-temperature steam superheat).	45−50
4	Molten salt reactor NPP (reactor coolant − sodium-fluoride salt with dissolved uranium fuel: $T_{out} = 700/800°C$; primary power cycle − indirect supercritical pressure carbon dioxide Brayton gas turbine cycle; possible backup − indirect Rankine steam cycle).	~50
5	Lead-cooled fast reactor NPP (Russian design BREST-OD-300[a]; reactor coolant − liquid lead: $P \approx 0.1$ MPa and $T_{in}/T_{out} = 420/540°C$; primary power cycle − indirect subcritical pressure Rankine steam cycle: $P_{in} \approx 17$ MPa ($P_{cr} = 22.064$ MPa) and $T_{in}/T_{out} = 340/505°C$ ($T_{cr} = 374°C$); high-temperature steam superheat; (in one of the previous designs of BREST-300 NPP primary power cycle was indirect supercritical-pressure Rankine steam cycle: $P_{in} \approx 24.5$ MPa ($P_{cr} = 22.064$ MPa) and $T_{in}/T_{out} = 340/520°C$ ($T_{cr} = 374°C$); also, note that power-conversion cycle in different lead-cooled fast reactor designs from other countries is based on a supercritical pressure carbon-dioxide Brayton gas turbine cycle.	~41−43
6	Sodium-cooled fast reactor NPP (Russian design BN-600: reactor coolant − liquid sodium (primary circuit): $P \approx 0.1$ MPa and $T_{in}/T_{out} = 380/550°C$; liquid sodium (secondary circuit): $T_{in}/T_{out} = 320/520°C$; primary power cycle − indirect Rankine steam cycle: $P_{in} \approx 14.2$ MPa ($T_{sat} \approx 337°C$) and $T_{in\ max} = 505°C$ ($T_{cr} = 374°C$); steam superheat: $P \approx 2.45$ MPa and $T_{in}/T_{out} = 246/505°C$; possible backup in some other countries − indirect supercritical pressure carbon dioxide Brayton gas turbine cycle).	~40

[a]BREST-OD-300 is Fast Reactor with "NATural safety" test demonstration in Russian abbreviations (БРЕСТ-OD-300 − Быстрый Реактор с ЕСТественной безопасностью − Опытно −Демонстрационный).

Acknowledgments

The author would like to express his great appreciation to Dr. H. McFarlane, Dr. H. Paillere, Ms. G. Grosch, and Generation IV International Forum (GIF) Secretariat for their materials used in this chapter.

References

Guzonas, D., Brosseau, F., Tremaine, P., Meesungnoen, J., Jay-Gerin, J.-P., 2012. Water chemistry in a supercritical water-cooled pressure tube reactor. Nuclear Technology 179.

Kaneda, J., Kasahara, S., Kano, F., Saito, N., Shikama, T., Matsui, H., 2011. Material development for supercritical water-cooled reactor. In: Proc. ISSCWR-5, Vancouver, BC, Canada, March 13−16.

Oka, Yo, Koshizuka, S., Ishiwatari, Y., Yamaji, A., 2010. Super Light Water Reactors and Super Fast Reactors. Springer, Germany, 416 p.

Pioro, I., Duffey, R., 2015. Nuclear power as a basis for future electricity generation. ASME Journal of Nuclear Engineering and Radiation Science 1 (1), 19 pages. Free download from: http://nuclearengineering.asmedigitalcollection.asme.org/article.aspx?articleID=2085849.

Pioro, I.L., Duffey, R.B., 2007. Heat Transfer and Hydraulic Resistance at Supercritical Pressures in Power Engineering Applications. ASME Press, New York, NY, USA, 334 p.

Schulenberg, T., Starflinger, J. (Eds.), 2012. High Performance Light Water Reactor. Design and Analyses. KIT Scientific Publishing, Germany, 241 p.

Yamada, K., Sakurai, S., Asanuma, Y., Hamazaki, R., Ishiwatari, Y., Kitoh, K., 2011. Overview of the Japanese SCWR concept developed under the GIF collaboration. In: Proc. ISSCWR-5, Vancouver, BC, Canada, March 13−16.

Very high-temperature reactor

3

X.L. Yan
Japan Atomic Energy Agency, Oarai-Machi, Ibaraki-ken, Japan

3.1 Development history and current status

Development of high-temperature gas-cooled reactor (HTGR), also known as very high-temperature gas-cooled reactor (VHTR) for its Generation IV designs, has continued for over half a century. Several reactors have been built or being constructed. These are identified in Table 3.1. Still others are being developed at various stages, including more units of high-temperature reactor-pebble bed module (HTR-PM) power reactor in China, multipurpose GTHTR300C in Japan, NuH2 for nuclear hydrogen and process heat in Korea, next generation nuclear plant (NGNP) cogenerating reactor in the United States, and an experimental power reactor in Indonesia.

Dragon, the first reactor built, pioneered the use of tri-isotropic (TRISO)-coated particle fuel, still the standard fuel form today. The AVR (Arbeitsgemeinschaft Versuchsreaktor) tested additional fuel designs and accumulated extensive performance data. The prototypical FSV (Fort St. Vrain) validated the prismatic core physics design with high burnup (90 GWd/t) on thorium fuel and demonstrated steam turbine power generation at 39% thermal efficiency and easy load following. Yet the component failures, such as with the primary coolant circulator, forced excess outage and undermined its economics. The THTR-300 (thorium high-temperature reactor 300) of a pebble bed core design encountered technical problems after only a brief period of operation, and their scrutiny led to protracted shutdown. The FSV and THTR-300 were prematurely decommissioned largely as business decision.

Asia then became home to the latest builds. The high-temperature engineering test reactor (HTTR) in Japan and the high-temperature test reactor (HTR-10) in China were constructed and started up around the turn of the millennium. Both remain operational today. The 30-MW_{th} HTTR demonstrated operation of 950°C reactor outlet coolant and export of 863°C process heat. Such high-temperature capability would raise reactor thermal efficiency and support advanced applications as reported by the plant design of GTHTR300 by Japan Atomic Energy Agency (JAEA) (Sato et al., 2014; Yan et al., 2014). The Generation IV system employs a 600-MW_{th} reactor with outlet coolant temperature of 950°C to power a gas turbine for electricity generation and a thermochemical process for hydrogen production, yielding thermal efficiency of 50% or higher.

Based on the experience of HTR-10 and extensive engineering development of the reactor components, China is constructing the world's first prototype modular

Handbook of Generation IV Nuclear Reactors. http://dx.doi.org/10.1016/B978-0-08-100149-3.00003-3
Copyright © 2016 Elsevier Ltd. All rights reserved.

Table 3.1 High-temperature gas-cooled reactors built worldwide

	Test HTGRs				Prototype HTGRs			
								
	Dragon	**AVR**	**HTTR**	**HTR-10**	**Peach bottom**	**FSV**	**THTR-300**	**HTR-PM**
Country	UK (OECD)	Germany	Japan	China	USA	USA	Germany	China
Period of operation	1963–1976	1967–1988	1998–Present	2000-Present	1967–1974	1976–1989	1986–1989	2017 planned
Reactor core type	Tube	Pebble bed	Prismatic	Pebble bed	Tube	Prismatic	Pebble bed	Pebble bed
Thermal power, MW_{th}	21.5	46	30	10	115	842	750	2 × 250
Coolant outlet temperature, °C	750	950	950	700	725	775	750	750
Coolant pressure, MPa	2	1.1	4.0	3.0	2.25	4.8	3.9	7.0
Electrical output, MW_e	–	13	–	2.5	40	330	300	211
Process heat output, MW_{th}	–	–	10	–	–	–	–	–
Process heat temperature, °C	–	–	863	–	–	–	–	–
Core power density, W/cm^3	14	2.6	2.5	2	8.3	6.3	6.0	3.2
Fuel design	UO_2 TRISO	(Th/U, U)O_2, C_2 BISO	UO_2 TRISO	UO_2 TRISO	ThC_2 BISO	(Th/U, Th)C_2 TRISO	(Th/U)O_2 BISO	UO_2 TRISO

BISO, Bi-isotropic coating of fuel particle

reactor plant HTR-PM in the northeastern Shandong province (Fu et al., 2014). Although not a VHTR by coolant temperature, the twin-unit (2×250 MW_{th}) power plant with reactor coolant temperature of 750°C shares some of the design approaches of VHTR, including passive safety features and high-temperature heat application potential. The construction began in December 2012 and the operation is expected in 2017.

In 2001, the GIF endorsed six nuclear system concepts, which will deliver affordable energy products while satisfactorily addressing the issues of nuclear safety, waste, and proliferation (Petti, 2014). Recognizing the VHTR to be nearest term deployable and exceptionally suitable, not only for electricity generation, but also for hydrogen production and other industrial applications, the US Department of Energy (DOE) has placed the Generation IV priority on the VHTR. The Energy Policy Act of 2005 formally established the NGNP as a DOE project to demonstrate commercial high-efficiency generation of electricity and hydrogen (The US Energy Policy Act of 2005, 2005). At present, the advanced gas reactor (AGR) fuel development and qualification program at the US Idaho National Laboratory is qualifying uranium oxide/uranium carbide (UCO) TRISO fuel (Petti, 2014). And the NGNP Industry Alliance, a consortium of HTGR designers, utility plant owner/operators, suppliers, and end users, is promoting the reactor commercialization and industrial applications (ngnpalliance). In 2012, the Alliance selected AREVA's prismatic SC-HTGR of 625 MW_{th} that provides steam and electricity cogeneration as its primary choice of reactor design for prototype implementation in mid-2020s (Shahrokhi et al., 2014).

3.2 Technology overview

3.2.1 Reactor design types

The two primary types of core design are prismatic and pebble bed. Both are in use today. They employ the same particle fuel but differ in the method of packaging the fuel particles and subsequently loading the fuel in the core. Fig. 3.1 compares the design approaches of the pebble bed HTR-10 (Wu et al., 2002) and the prismatic HTTR (Saito et al., 1994).

The spherical fuel particle measuring about 1 mm in diameter consists of an inner nuclear kernel coated in successive layers of carbon and ceramics. Thousands of the particles are packed in graphite matrix into a spherical pebble of roughly tennis ball size or a cylindrical compact about the size of man's thumb. A pebble bed core contains a large number of fuel pebbles (for example, 27,000 in the HTR-10 core), and the helium coolant flows in the void volume formed in the pile of the pebbles. On the other hand, a prismatic core contains many hexagonal graphite blocks (150 in the HTTR core) in which the fuel compacts are embedded and the helium coolant flows in the channels provided in the block. Both cores are surrounded by graphite reflector and enclosed in steel pressure vessel. Reactivity control rods (RCRs) are inserted from above the reactor pressure vessel (RPV).

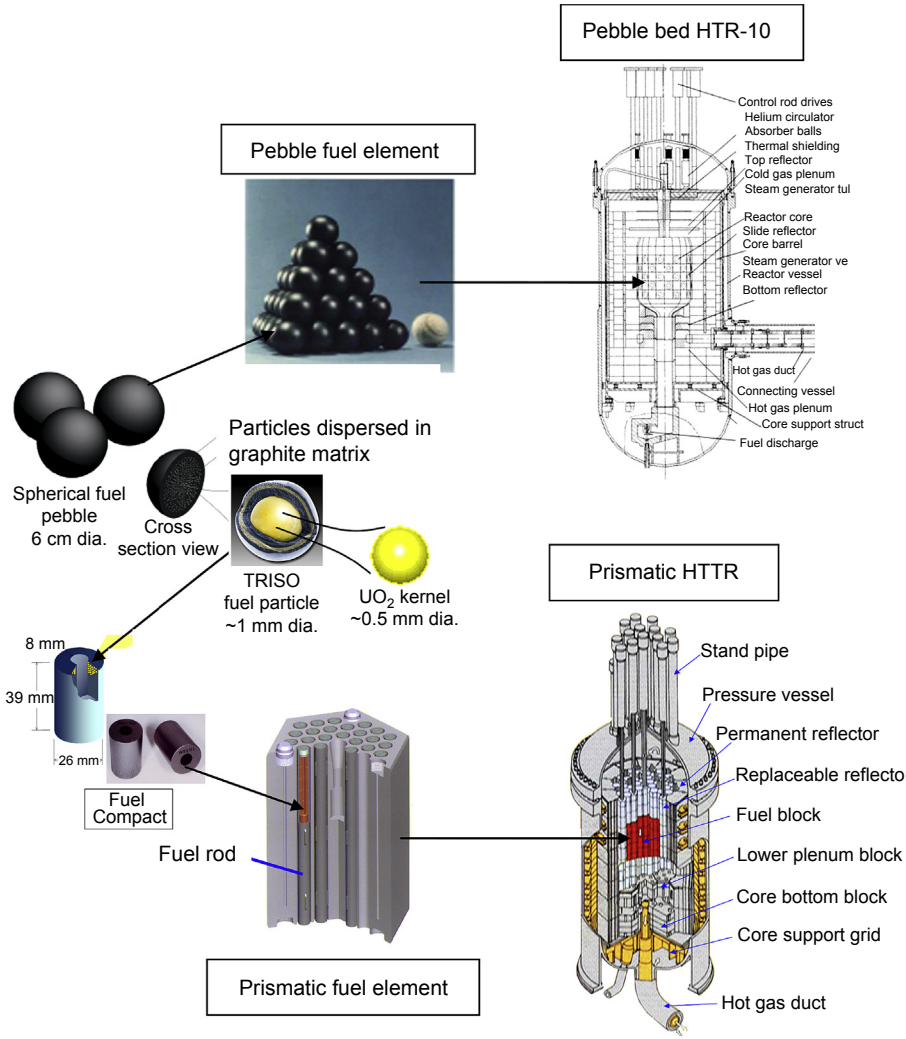


Figure 3.1 Pebble bed reactor design and prismatic reactor design.

3.2.2 Design features

3.2.2.1 Safety

Constructed entirely of highly heat resistant materials, the HTGR fuel and core structure maintain their integrity at extreme temperatures. Most reactor designs set the fuel temperature limit to 1600°C based on proof of fuel performance data. The reactor temperature is then capped under it by a combination of inherent design choices made. Starting with the choice of low power density and of the large quantity of graphite materials used in the core, it limits the extent and rate of reactor temperature excursion

in an accident. This is aided by the further choice of negative temperature coefficient of reactivity in the core, which would shut the reactor down upon any occurrence of abnormal rise in temperature. Decay heat is then removed from the core by thermal conduction. Finally, helium is the choice of reactor coolant. Remaining in single phase as well as being neutronically transparent and chemically inert, use of helium would mitigate the consequences such as radioactive coolant release or hydrogen generation in the case of a loss of coolant accident. Together, these inherent design features prevent core melt and significant radioactivity release in any licensing basis events. Such safety performance has been demonstrated in the anticipated transient without scram (ATWS) tests carried out on the HTR-10 (Hu et al., 2004) and HTTR (Takamatsu et al., 2014).

3.2.2.2 Fuel cycle

HTGR offers various options of fuel cycle. Typically, low-enriched (<20%) uranium is used as is in the HTTR and HTR-10, both of which select fuel form of uranium dioxide (UO_2). An alternative form of uranium oxycarbide (UOC) is currently under development and qualification (Petti, 2014).

Thorium is attractive regionally or in longer term, since the world reserve of thorium is more abundant than that of uranium. Although not fissile, Th-232 is fertile and breeds fissile U-233 by absorbing neutrons produced, for example, by fission of initial U-235. Various forms of thorium fuel have been operated in the reactors (see Table 3.1).

More fuel options exist but require development (Greneche, 2003; Kuijper et al., 2006). The fuel cycles that can effectively destruct weapons-grade plutonium and transmute minor actinides while engaging in energy production have been studied (Oak Ridge National Laboratory, 2008; Fukaya et al., 2014). The particle fuel has demonstrated up to 700 GWd/t burnup, an important asset in the plutonium and transuranium (TRU) fuel cycles, since the high burnup provides deep burn and thus reduces the quantity and cost of reprocessing (Richards et al., 2008). Since 2015 Japan has launched a study of PuO_2−YSZ (yttria-stabilized zirconia) fuel and core design with a burnup limit of 500 GWd/t with the aim to validate clean burning of plutonium in HTGR (Goto et al., 2015).

Spent fuel may be directly disposed or recycled. In the case of direct disposal, separation and reduction of waste streams could be made prior to disposal. Separated graphite blocks may be treated and reused. Separated fission products and actinides can be confined in stable matrices such as glasses. In the case of recycling, mechanical separation of spent fuel compacts from bulk graphite block, pulsed currents to free the fuel particles from the compact, and subsequent removal of ceramic coating layers by high-temperature oxidation or by carbochlorination to access spent kernels of the particle have been studied (Masson et al., 2006).

The fuel is proliferation resistant. Not only does the TRISO structure make it difficult to illicitly access the isotopes of spent fuel kernel, but also the high burnup target in commercial systems will leave little and poor isotopes in spent fuel such that it would require diversion of large material quantities to pose a nuclear risk.

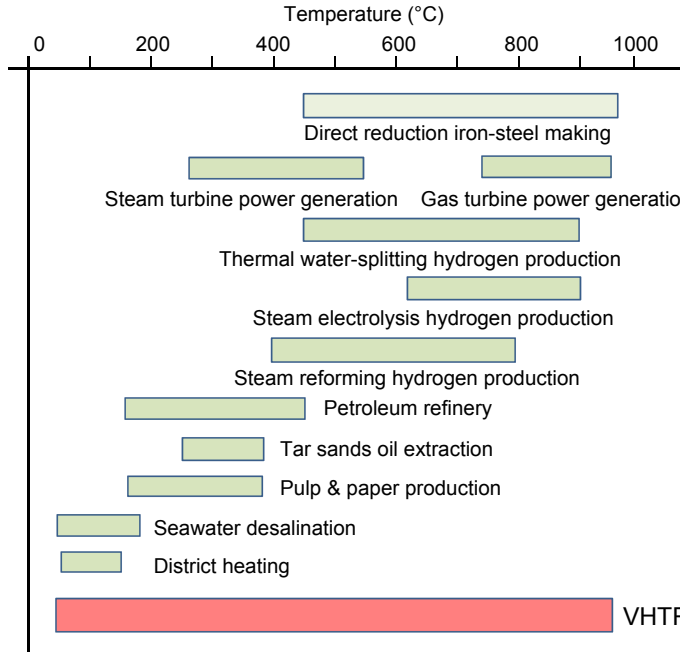


Figure 3.2 Temperature range of VHTR and heat demand of industries.

3.2.2.3 Multipurpose

Fig. 3.2 identifies a number of applications that fall in the supply temperature range of the VHTR. Power generation can be performed by steam turbine with efficiency at about 40% or by gas turbine at about 50%. Industrial heat applications have been extensively studied, including thermochemical hydrogen production, reforming of fossil fuels and biomass, steelmaking, desalination, and district heating. The VHTR is well posed for cogeneration. As an example, a 600-MW_{th} reactor could simultaneously produce 200 MW_e electricity using gas turbine, 66 t/day hydrogen from thermochemical decomposition of water, and 40,000 t/day potable water from desalination. The utilization of the reactor thermal power would reach 85% through cogeneration.

3.3 Detailed technical description

3.3.1 Fuel design

TRISO-coated particle is the standard fuel used today. As shown in Fig. 3.3, the innermost of the particle is a low-enriched fuel kernel of usually UO_2 and sometimes UOC. The kernel is coated by a buffer layer of porous carbon and then by the successive TRISO layers, including the inner layer of high-density pyrolytic

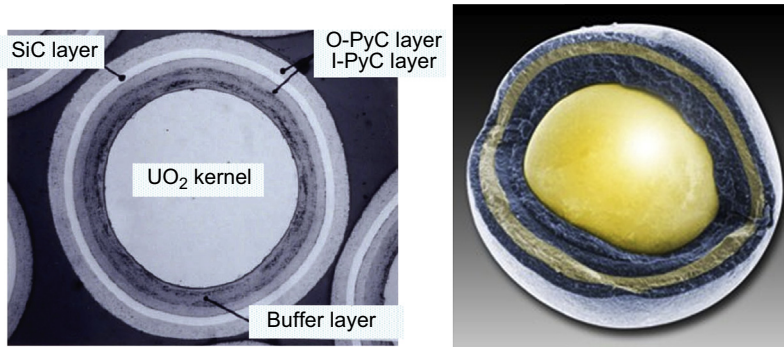


Figure 3.3 TRISO-coated fuel particle.

carbon (IPyC), the silicon carbide (SiC) layer, and the outer layer of high-density pyrolytic carbon (OPyC).

The buffer layer acts a container for the fission product gases and the CO gas resulting from fuel burnup. The IPyC layer protects the kernel during the manufacture coating of the outer SiC layer and also provides a gas barrier for the inner buffer. The SiC layer, being the hardest of the structural layers, acts as both a pressure container for the gases generated in the kernel and a material barrier for the metallic fission products. The OPyC provides a protective cushion for the SiC layer during the binding and pressing of the particles into the cylindrical compact or spherical pebble.

A compact, as used in the HTTR, contains about 13,000 particles of 0.92 mm diameter. The particles are dispersed in the graphite matrix in a packing fraction of about 30%. Each compact includes about 14 g of heavy metal. Table 3.2 lists further details of the fuel design for the HTTR and also for the GTHTR300.

A pebble as used in the HTR-10 contains about 12,000 particles. The fuel zone is a ball of binding graphite matrix in a particle packing fraction of about 10%. The fuel zone measured in a diameter of 50 mm is wrapped by a fuel-free layer of graphite with a thickness of 5 mm, resulting in an overall diameter of 60 mm for the pebble. The heavy metal loading of each pebble is around 7 g.

The high level of safety performance provided by the VHTR requires a high level of fabrication quality for the fuel. This is judged with the failure rates of the TRISO ceramic layers in manufacture. An acceptance criterion for the HTTR fuel, for example, is through-coating defect in 1.5 per 10,000 particles, or 0.015% as fabricated. The operation of the HTTR first loading of fuel has proved that the actual fraction of fabrication defect is about two orders of magnitude less than the specification.

The technology of TRISO particle fuel has been established for the UO_2 kernel type at commercial production scale in Germany, China, and Japan and for the UOC kernel type at pilot production scale in the US. France, Korea, and South Africa have pursued fuel technology development programs including fuel manufacturing and irradiation tests.

Table 3.2 Fuel design specification

	Burnable poison pin diameter (mm) HTTR	**GTHTR300**
Burnup up limit (GWd/t)	33	150
Fuel rod		
Rod structure	Graphite sleeved	Graphite cladded
Length (mm)	546	1050
Diameter (mm)	34	26
Fuel compact		
Length (mm)	39	83
Inner diameter I.D./ Outer diameter O.D. (mm)	10/26	9/24
Cladding thickness (mm)	–	1
Particle packing fraction (vol%)	30–35	21–29
Coated fuel particle		
Coating type	TRISO	TRISO
Diameter (μm)	920	1010
Fuel kernel		
Material	UO_2	UO_2
Enrichment (wt% average)		14
Diameter (μm)	600	550
Density (g/cm^3)	10.80	10.80
Buffer layer		
Thickness (μm)	60	140
Density (g/cm^3)	1.15	1.15
IPyC layer		
Thickness (μm)	30	25
Density (g/cm^3)	1.85	1.85
SiC layer		
Thickness (μm)	25	40
Density (g/cm^3)	3.20	3.20
OPyC layer		
Thickness (μm)	45	25
Density (g/cm^3)	1.85	1.85

Advanced fuel designs are proposed in the US and Japan. One such design replaces the SiC layer with zirconium carbide (ZrC), which increases heat resistance by about 200°C over the limit of the SiC layer (Goto et al., 2015). Another design adds a thin layer of ZrC over the buffer layer. This layer acts as a reactive oxygen getter to remove the oxygen gas freed in fission and thus mitigates the gas pressure buildup associated with high burnup.

3.3.2 Fuel burnup

Fuel burnup in the VHTR is explained using the example of core physics design calculation for uranium and plutonium fuels as follows.

3.3.2.1 Uranium fuel

Table 3.3 includes the core design parameters and burnup calculation conditions for the for the 600-MW_{th} reactor of the GTHTR300 (Nakata et al., 2003). The calculation procedure considers effective averaged six-group macroscopic cross sections in each of the burnup regions of the core. A one-dimensional lattice burnup cell calculation code, DELIGHT, is used to generate the group constants of fuel blocks, reflector blocks, etc. A transport code, TWOTRAN-2 (Lathrop and Brinkley, 1973), is used to generate details of flux distributions in the regions containing the control rods, where the neutron flux may vary suddenly. With these six-group macroscopic cross sections, a spatial power distribution is calculated by CITATION, a diffusion code (Fowler et al., 1971), for a 3-D one-sixth core model. The calculated spatial power distribution is used as an input to calculate the next burnup step.

From the core analysis, it becomes clear that the excess reactivity has to be compensated by the burnable poisons until the middle of an operation cycle so that the design target of a 2-year refueling cycle (730 days) is achievable. A half core of fuel blocks is exchanged with fresh fuel every 2 years. As seen in Table 3.3, the residual uranium enrichment is reduced to 4.42% below the design target of 5% from the initial uranium enrichment of 14%.

3.3.2.2 Plutonium fuel

Table 3.4 details the fuel burnup calculation conditions for a proposed plutonium fuel cycle concept for the GTHTR300 core. The proposal by JAEA, called the Clean Burn concept (Fukaya et al., 2014; Goto et al., 2015), is intended to consume the plutonium recovered from reprocessing Japan's commercial light water reactor(LWR) spent fuel while relying on fuel design features that enhances proliferation resistance. The concept requires modification to the above-described uranium core design. A major change is that more fuel columns are added in the inner reflector region, increasing the total number of the fuel columns in the core to 144 from 90.

To limit the plutonium enrichment in fresh fuel to the allowable level in Japan, the Clean Burn concept employs PuO_2 in an inert YSZ microsphere kernel. It avoids mixing with uranium so that no additional plutonium is generated during a fuel burnup

Table 3.3 Result of uranium fuel burnup calculation for a 600-MW_{th} VHTR

Item	Unit	Value	
Reactor power	MW_{th}	600	
Core cross section			
Number of fuel blocks		90	
Inner graphite blocks		73	
Outer graphite blocks		48	
Core height	m	8.4	
Fuel blocks in core height		8	
Fuel block			
Height/across flat	mm	1050/410	
Number of fuel rods		57	
Fuel rod diameter	mm	26	
Coolant channel diameter	mm	39	
Number of burnable poison rods		3	
Average core power density	W/cm^3	5.4	
Fuel cycle length	EFPD	1460	
Refueling batches (w/axial shuffling)		2	
Fuel enrichment	%	14	
Average fuel burnup	GWd/t	120	
Fuel design		UO_2	
Full-core initial heavy metal	kg	7090	wt% of initial heavy metal
U-235		993	14.0
U-238		6097	86.0
Full-core discharged heavy metal	kg		
Uranium		5839	82.4
U-235		258	3.6
U-236		0	0.0
U-238		5581	78.7
Plutonium		155	2.2
Pu-239		72	1.0

Table 3.3 Continued

Item	Unit	Value	
Pu-240		27	0.4
Pu-241		37	0.5
Pu-242		19	0.3
Residual uranium enrichment	%	4.42	
Fissile plutonium isotope rate	%	70.2	
Natural uranium requirement	kg/(GW_e * d)	467.0	
Natural uranium utility rate	%	0.57	

cycle. As shown in Table 3.4, about 95% of initial plutonium-239 is consumed during 250 EFPD (effective full power day). In order to target the fuel burnup of 500 GWd/t, the traditional SiC TRISO fuel architecture is modified by coating a thin (about 10 μm) layer of ZrC over the PuO_2−YSZ kernel. The ZrC layer acts as oxygen getter to remove oxygen gas freed from the kernel burnup and is the key to permitting the targeted level of burnup. Presently, JAEA, in cooperation with its technical partners, is validating the fuel design by test fabrication (Goto et al., 2015).

3.3.3 Reactor design

3.3.3.1 Prismatic core reactor design

Fig. 3.4 depicts the HTTR reactor design (Saito et al., 1994; Fujimoto et al., 2004). The cylindrical core consists of columns of removable hexagonal graphite blocks. Thirty of the columns are fuel columns stacked in five blocks high. Dowels are used to align fuel blocks in a column. There are a total of 150 fuel blocks of varying uranium enrichments as identified in the table included in the figure. The other columns in the core are control rod guide columns provided for insertion of RCRs and release of reserved core shutdown system. The permanent graphite reflector blocks embrace a ring of replaceable side reflector blocks that surround the central core. The control rods containing boron carbide (B_4C) are moved in and out of the core from atop of the RPV. The control rods are used for adjustment and shutdown of core power in addition to compensating for reactivity due to changes in core temperature, fuel burnup, and concentration of fission products such as ^{149}Sm and ^{135}Xe with large neutron absorption cross sections. The reserved core shutdown system is provided as backup for reactor shutdown with the releasing of B_4C pellets into the channels bored in the control rod blocks. The entire core is affixed by the lateral restraint mechanism from the outer side of the permanent reflector to the inner wall of the RPV. The RPV is made of low alloy steel of 2.25 Cr−1 Mo and sized to 5.5 m in diameter and 13.2 m in height.

Unlike test reactors such as the HTTR, larger commercial-scale reactor design tends to select annular, instead of cylindrical, active core configuration, mainly to minimize

Table 3.4 Result of plutonium fuel burnup calculation for a 600-MW_{th} VHTR

Item	Unit	Value	
Reactor power	MWt	600	
Core cross section			
Number of fuel blocks		144	
Inner graphite blocks		48	
Outer graphite blocks		19	
Core height	m	8.4	
Fuel blocks in core height		8	
Fuel block			
Height/across flat	mm	1050/410	
Number of fuel rods		57	
Fuel rod diameter	mm	26	
Coolant channel diameter	mm	39	
Number of burnable poison rods		3	
Average core power density	W/cm^3	5.4	
Fuel cycle length	EFPD	1000	
Refueling batches (w/axial shuffling)		4	
Fuel enrichment	%	58.6	
Average fuel burnup	GWd/t	500	
Fuel design		PO_2−YSZ	
Full-core initial heavy metal (IHM)	kg	1200	
		Fresh fuel	Spent fuel
^{237}Np	wt% IHM	4.6	2.4
^{238}Pu	wt% IHM	1.3	7.4
^{239}Pu	wt% IHM	51.0	2.8
^{240}Pu	wt% IHM	20.8	9.1
^{241}Pu	wt% IHM	7.6	9.1
^{242}Pu	wt% IHM	4.9	10.6
^{241}Am	wt% IHM	8.2	1.2
^{242}Am	wt% IHM	0.0	0.0
^{243}Am	wt% IHM	1.5	2.9

Table 3.4 Continued

Item	Unit	Value	
^{242}Cm	wt% IHM	0.0	0.7
^{243}Cm	wt% IHM	0.0	0.1
^{244}Cm	wt% IHM	13.2	1.8
^{245}Cm	wt% IHM	4.4	0.1
Fissile nuclides	wt% IHM	58.6	12.0
Neptunium (Np) and precursor	wt% IHM	20.4	12.8

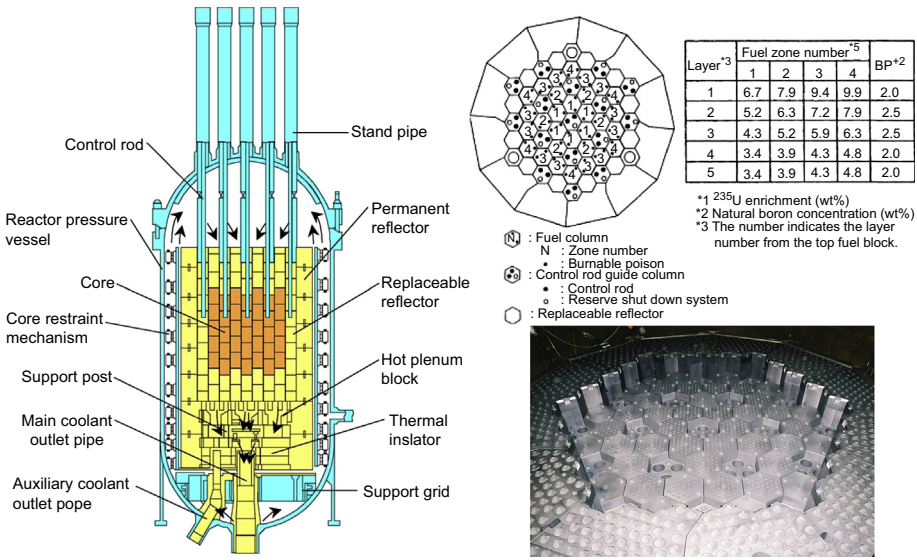


Figure 3.4 The HTTR test reactor design (photo is the top view of the reactor core).

fuel temperature in the event of passive core conduction cooldown. This design choice is highlighted by the GTHTR300 reactor design shown in Fig. 3.5 (Nakata et al., 2003). The commercial reactor is designed using the code system and design procedure that have been validated by the HTTR operation.

The annular core of the GTHTR300 reactor consists of 90 fuel columns with each column stacked of 8 hexagonal fuel blocks high and is capped at top and bottom with reflector blocks. The active core is surrounded by inner and outer side graphite reflector columns, some of which also serve as control rod guide columns. The core is enclosed by a steel core barrel, which is in turn housed in the steel RPV. The coolant enters the reactor via the inner pipe of the horizontal coaxial duct on the left of the vessel and travels upwards in the flow channels embedded in the outer side reflector,

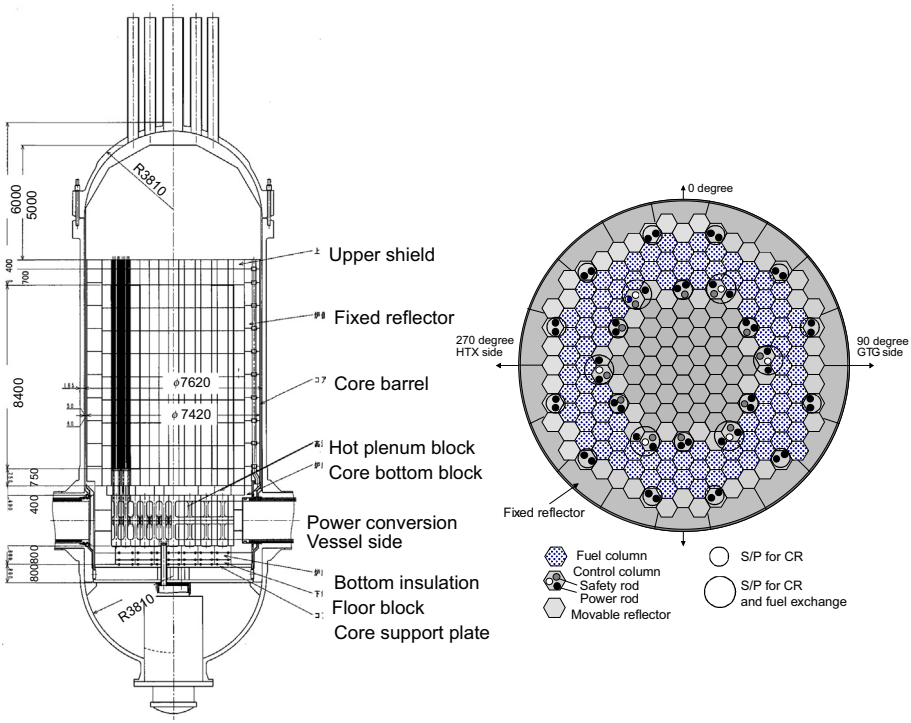


Figure 3.5 GTHTR300's prismatic core reactor design.

turns in the top plenum of the core, then flows downward into the active core and then exits into the bottom plenum of the core, and finally exits through the inner pipe of the horizontal coaxial duct on the right of the RPV.

Table 3.5 compares the design parameters for the HTTR test reactor and GTHTR300 commercial reactor. The table includes three sets of commercial design parameters. The two sets pertain to the core outlet temperature of 850°C, while the third set pertains to 950°C. The main difference is the number of enrichments used. In the baseline design with uniform enrichment for the whole core, the resulting peak operating fuel temperature is higher than the other sets with multiple enrichment count. In general, the number of enrichments placed in the core may be varied and optimized to minimize power peaking and thus peak fuel temperature throughout a core burnup period. The refueling interval is shortened to 1.5 years in the case of the 950°C core design from the 2 years in the 850°C core designs.

3.3.3.2 Pebble bed core reactor design

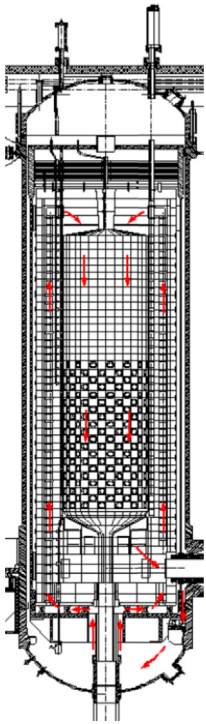
Rated at relatively small thermal power of 250 MW_{th} per reactor unit, the HTR-PM still allows for the use of a cylindrical pebble bed core (see Fig. 3.6). The active core is 3 m in diameter and 11 m in height and contains a loose pile of approximately 420,000 spherical fuel pebbles. The core geometry is maintained by side graphite

Table 3.5 Reactor design specification

		HTTR	GTHTR300
Reactor rating	MWt	30	600
Coolant inlet temperature (°C)	°C	395	587, 587, 594
Coolant outlet temperature (°C)	°C	850, 950	850, 850, 950
Coolant pressure (MPa)	MPa	4	7.0, 7.0, 5.1
Coolant (helium) flow rate (kg/s)	kg/s	12.7/10.4	439, 439, 322
Fuel type		TRISO U_2O	TRISO U_2O
Refueling interval (days)	day	660	730, 730, 548
		Full core	Half core
Number of fuel blocks (columns × stacks)		150 (30 × 5)	720 (90 × 8)
Core height (m)	m	2.9	8.4
Effective core inner/outer diameter	m	0/2.3	3.7/5.6
Average power density (W/cm^3)	W/cm^3	2.5	5.4
Average burnup (GWd/t)	GWd/t	22	120
Maximum burnup	GWd/t	33	155
Fuel block height/across flat (mm)	mm	550/360	1050/410
Fuel rods per block		33	57
Fuel rod diameter (cm)	mm	34	26
Core enrichment count		12	1/8/7
Average enrichment (%)	wt%	6	14.0, 14.3, 14.5
Burnable poison count		2	1, 6, 5
Burnable poison pin diameter (mm)			4.8, 4.8, 3.6
Max fuel temperature (nominal) (°C)		1350	1150, 1108, 1244
Max fuel temperature (loss of coolant accident) (°C)		–	1562, 1546, 1535

reflectors and carbon bricks. The pebbles are continuously recirculated downward through the core for more than a dozen times using a pneumatic fuel transport line, until reaching the design burnup of 100 GWd/t. The spent fuel pebble is discharged through the core bottom center tube and transported into the spent fuel storage tank.

Two reactivity control systems are provided in the side reflector. One consists of eight RCRs that are inserted to regulate the core reactivity for power modulation and to shut down the reactor in hot condition, and the other consists of 22 small absorber sphere shutdown units used to provide backup shutdown and to maintain



Parameter	Unit	Value
Reactor total thermal power	MWt	2 × 250
Rated electrical power	MW_e	210
Average core power density	MW/m^3	3.22
Electrical efficiency	%	42
Primary helium pressure	MPa	7
He temperature at reactor inlet/outlet	°C	250/750
Helium flow rate	kg/s	96
Heavy metal loading per fuel element	g	7
Enrichment of fresh fuel element	%	8.5
Active core diameter	m	3
Equivalent active core height	m	11
Diameter of the RPV	m	~6.0
Number of fuel elements in a module		420,000
Number of fuel cricle in the core		15
Average burnup	GWd/tU	90
Main steam pressure	MPa	13.9
Main steam temperature	°C	571
Main feedwater temperature	°C	205
Feedwater flow rate for a module SG	kg/s	98

Figure 3.6 HTR-PM's pebble bed core reactor design and technical parameters.

cold shutdown. Besides, 30 gas boreholes are provided in the outer area of the side reflector as coolant flow channels. The core support structure consists of a steel core barrel, steel bottom supporting structure, and top thermal shield. It supports the ceramic structure of the pebble bed core by transferring various loads to the RPV. During operation, the annular area between the RPV and the core barrel is filled with cold helium to guarantee the temperature of pressure vessel not exceeding the limitation.

3.3.4 Reactor safety

Fig. 3.7 highlights the safety approaches taken generally by the VHTR, which relies on three inherent design features:

1. The ceramic-coated fuel particle, which maintains the integrity of containment for fission products under a design temperature limit of 1600°C;
2. The helium coolant that is chemically inert and thus absent of explosive gas generation or phase change; and
3. The graphite structured and moderated core, having characteristics of negative reactivity coefficient, low power density, and high thermal conductivity.

Owing to these features, the VHTR reactor core, whether it is prismatic or pebble bed geometry, may be removed of decay heat by thermal conduction through the

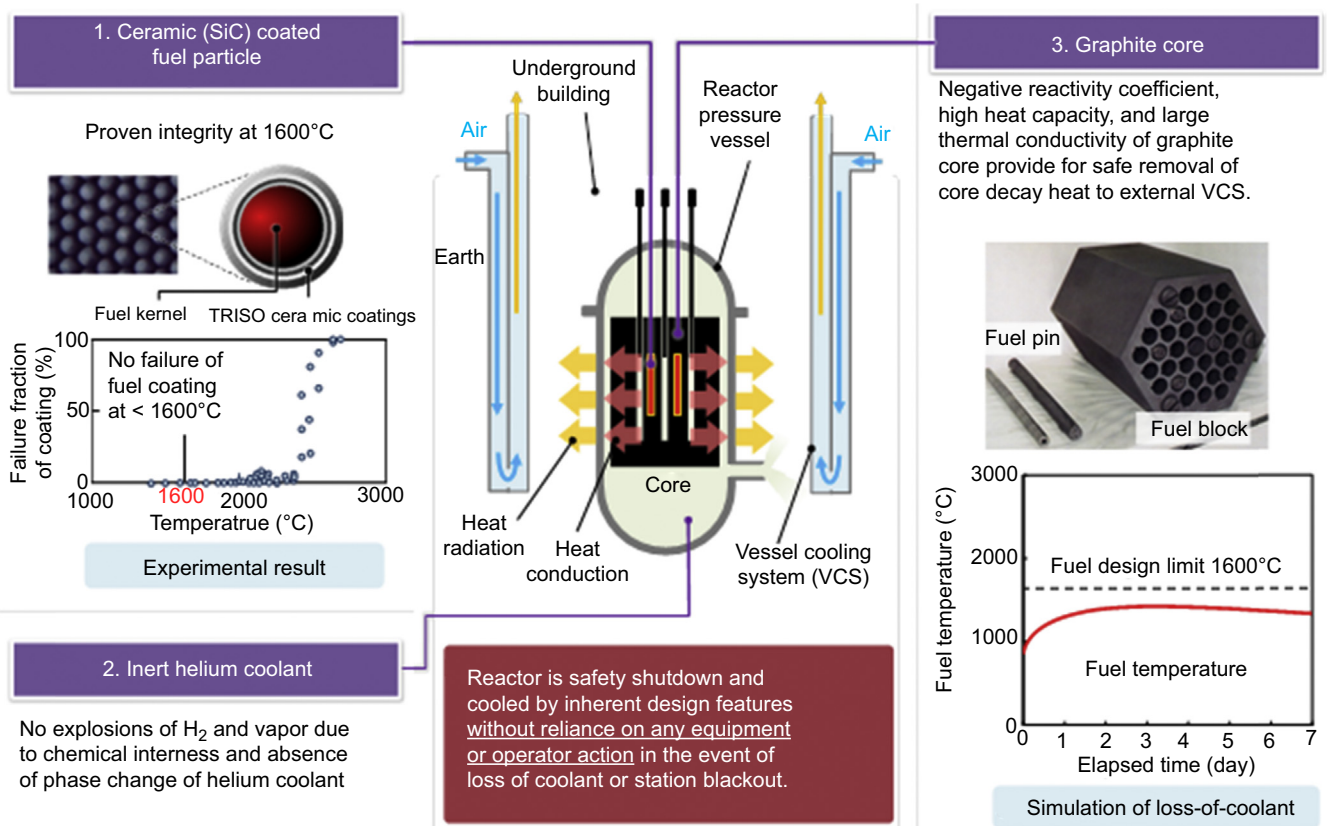


Figure 3.7 Inherent safety features of VHTR.

graphite core to the RPV and further, in the case of GTHTR300 design, by heat radiation to a naturally circulated vessel cooling system. As shown by the simulation result in the lower right side of Fig. 3.7, such decay heat removal process is capable of keeping the fuel from exceeding its design temperature limit for a period of days, or months if necessary, without reliance on any equipment or operator action, even in such severe accidents as loss of coolant or station blackout.

3.3.5 Plant design

GTHTR300 is a multipurpose, inherently safe, and site flexible small modular reactor(SMR) that JAEA is developing for commercialization. As shown in Fig. 3.8, the reactor system combines an HTGR with helium gas turbine to generate power while circulating the reactor coolant. The system consists of three pressure vessel units housing the reactor core, gas turbine, and heat exchangers, respectively. The multivessel system facilitates modular construction and independent maintenance access to functionally oriented equipment and systems in the vessel units. The reactor system is placed below grade in the reactor building.

The HTR-PM shown in Fig. 3.9 contains two parallel trains of nuclear steam supply system (NSSS) of identical design, each consisting of a 250-MW_{th} pebble bed reactor and a steam generator. The two NSSS systems have independent primary loops but share auxiliary facilities, such as fuel handling system and helium purification system. The two trains jointly supply superheated steam to a common steam turbine power generator rated at 200 MW_e.

3.3.6 Plant operations

3.3.6.1 Startup, rated operation, and shutdown

This sequence of reactor power operation is explained using a high-temperature (950°C) rise-to-power test carried out on the HTTR (Fujikawa et al., 2004).

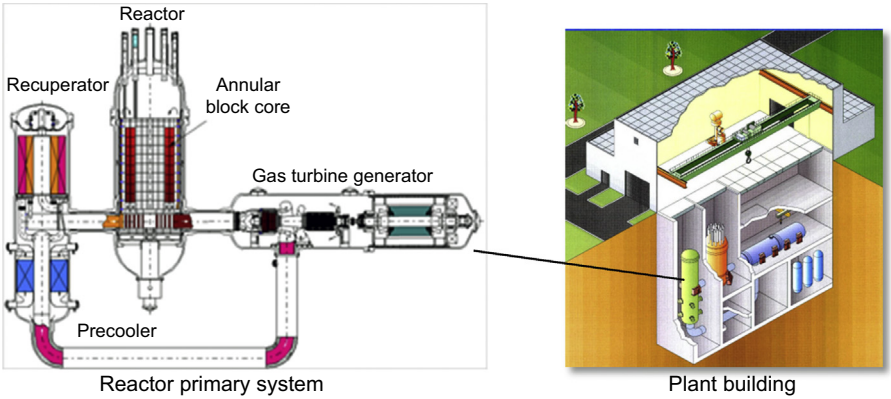


Figure 3.8 GTHTR300 plant design (600-MW_{th} reactor).

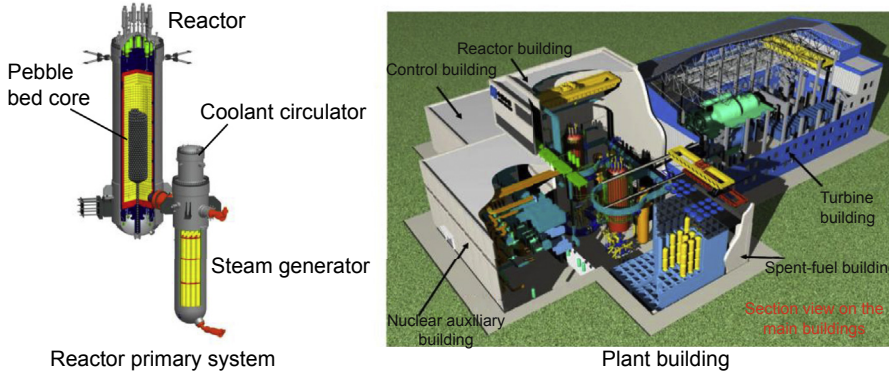


Figure 3.9 HTR-PM plant design (2 × 250 MW_{th} reactors).

The reactor power control device consists of control systems for the core power and for core outlet coolant temperature. These control systems are cascade connected; the latter control system ranks higher to give demand to the reactor power control system. The signals from each channel of the power range monitoring system are transferred to three controllers using microprocessors. In the event of a deviation between the process value and set value, a pair of control rods is inserted or withdrawn at the speed from 1 to 10 mm/s, according to the deviation. The relative position of the 13 pairs of control rods, except for three pairs of control rods used only for a scram, are controlled within 20 mm of one another by the control rod pattern interlock to prevent any abnormal power distribution. The plant control device controls plant parameters such as the coolant temperature of the reactor inlet, flow rate of the primary coolant, pressure of the primary coolant, and differential pressure between the primary cooling system and pressurized water-cooling system. The schematic diagram of the plant control system is shown in Fig. 3.10. The reactor power, the reactor inlet coolant temperature, and the primary coolant flow rate are controlled to constant values by each control system. The reactor outlet coolant temperature is adjustable by the control system of the primary coolant flow rate.

Fig. 3.11 are measurements of the sequence of startup, rated operation, and shutdown of the HTTR operating test, which began on March 31, 2004. The reactor power was increased in steps with monitoring all of the parameters, ie, thermal parameters and coolant impurities. To minimize thermal stress in high-temperature components, the temperature was raised within the rate of 35°C/h when the outlet coolant temperature is less than below 650°C and 15°C/h when the coolant temperature is above 650°C. The reactor power was kept at 50% (15 MW_{th}), 67% (20 MW_{th}), and 100% (30 MW_{th}), each step for more than 2 days in a steady temperature condition in order to measure the power coefficients of the reactivity. The reactor power was also kept at 82%, at which the reactor outlet coolant temperature is slightly below 800°C, in order to remove the chemical impurity in the coolant by helium purification system. The calibration of the neutron instrumentation system with the reactor thermal power was performed at the 97% power level.

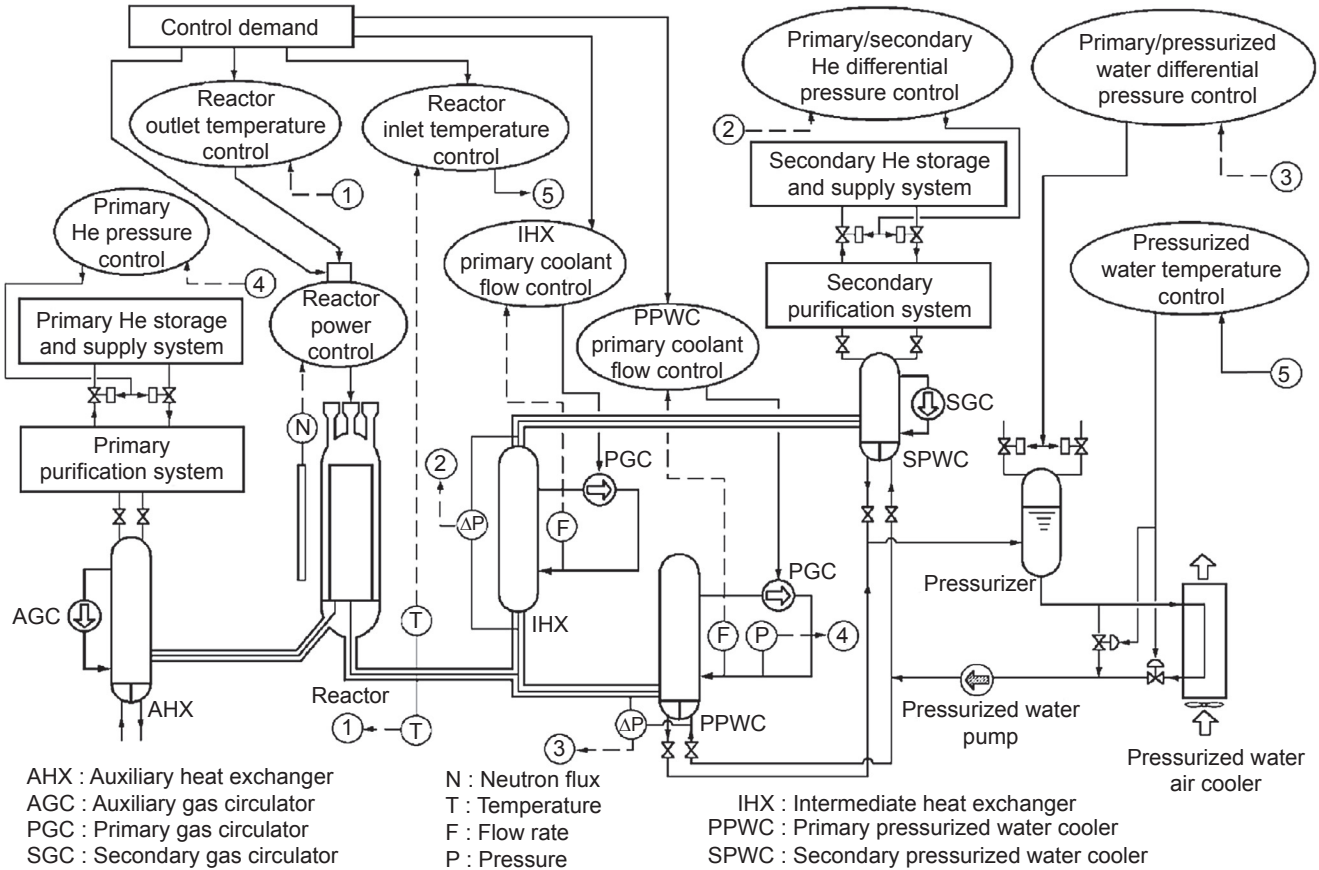


Figure 3.10 The HTTR reactor control system.

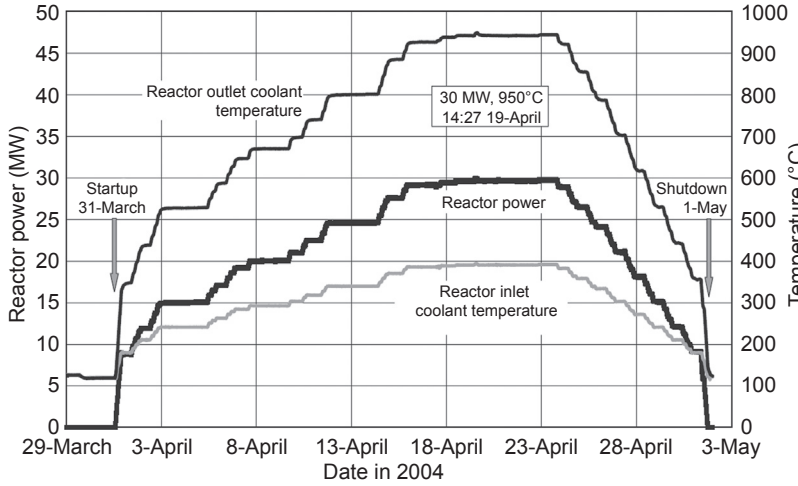


Figure 3.11 Measured HTTR operation sequence: startup, rated operation, and shutdown.

The reactor outlet coolant temperature of 950°C was achieved on April 19, 2004, during the single loaded operation mode. During the parallel loaded operation mode, the reactor outlet coolant temperature reached 941°C, and the secondary helium temperature at the IHX outlet reached 859°C on June 24, 2004. The difference of the reactor outlet coolant temperature from the design value of 950°C was caused by a permitted margin for error of the flow rate indicators of the primary cooling system. The temperature deficiency implied that the flow rate in the parallel loaded operation mode was about 1% higher than that of the single loaded mode.

3.3.6.2 Dynamic operation

Dynamic simulation was done on the GTHTR300C plant. Fig. 3.12 illustrates the plant process and associated control system. The GTHTR300C consists of a 600-MW_{th} HTGR with outlet coolant temperature of 950°C, an intermediate heat exchanger (IHX) to supply 900°C process heat to a thermal plant to produce hydrogen or other industrial products, and a direct-cycle recuperated gas turbine to generate power while circulating reactor coolant (Kunitomi et al., 2007). Section 3.4.2.1 details an example of this system to coproduce electricity and hydrogen.

The overall approach to dynamic operation integrates the following four load control strategies (Yan et al., 2012a):

1. Control of turbine speed, Sd, through flow bypass valve CV1.
2. Control of recuperator low-pressure side inlet temperature, Tx, through flow bypass valve CV2.
3. Control of turbine inlet temperature, Tt, by flow bypass valve CV3.
4. Control of turbine inlet temperature and pressure, Tt and Pt, by bypass valve CV4, and inventory flow valves IV1 and IV2.

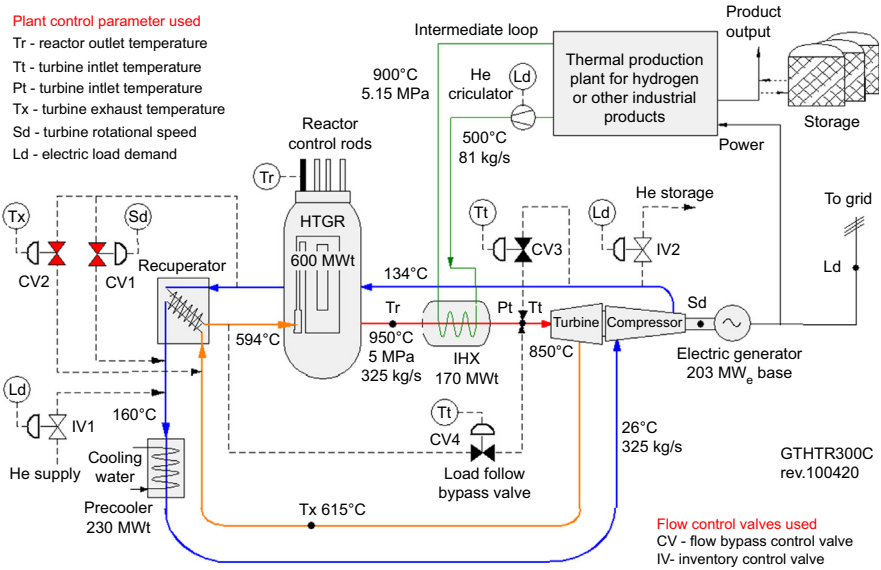


Figure 3.12 Control system for a 600 MW_{th} power and heat cogenerating VHTR.

The first two strategies are used to control rapid transients, such as a sudden loss of electric generator load. They are effective to protect the gas turbine from excess overspeed and prevent thermal shock in the recuperator.

The third strategy is used to automate heat rate to follow slow or fast changes of heat load in the IHX perturbed from the thermal production plant. As the IHX primary exit flow temperature rises or falls in response to a change in the IHX secondary heat load, the flow valve CV3 opens or closes to introduce more or less of cold flow to upstream of the turbine from the compressor discharge to the turbine inlet so as to keep the turbine inlet temperature constant. The overall control strategy aims to continue normal power generation, unaffected by any heat load change in the IHX.

The fourth control strategy is applied to automate cogeneration load follow. The conditions to be met include: (1) constant reactor temperature to avoid thermal stress in high-temperature structure; (2) constant reactor thermal power to yield base load economics; and (3) constant power generation efficiency over a broad range of load follow. The ability to follow variable power and heat loads is simulated with the results given in Fig. 3.13. The simulation examines the plant response to an electric demand increase of 5% of the base rate per minute with corresponding reduction of the heat rate, which is the maximum requirement for cogeneration load follow. The reactor remains at 100% power at all times. Starting from the base cogeneration rates, turbine power generation is raised to follow the electric load demand increase by increasing the primary coolant inventory through the inventory control valve IV1. The IHX heat rate to the thermal production plant is lowered by lowering the intermediate loop flow circulation rate with the variable speed gas circulator. As the primary exit temperature of the IHX begins to rise, the valve

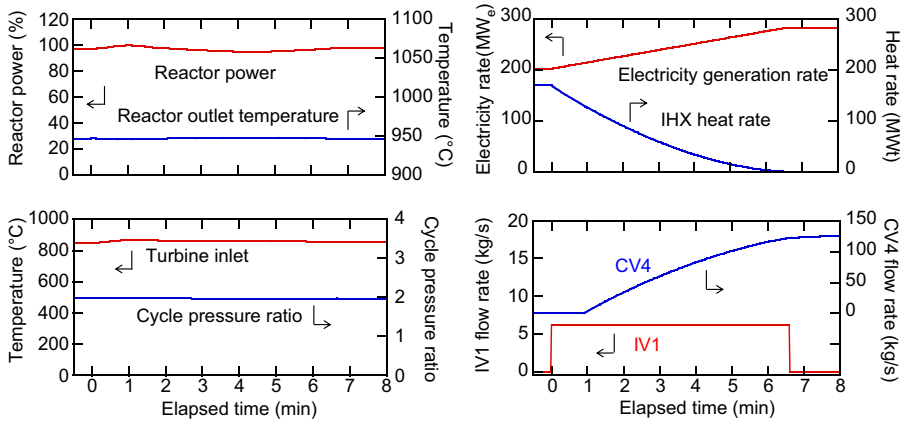


Figure 3.13 Simulation of VHTR cogeneration load follow to +5%/min electric load increase.

CV4 is opened by active or prescheduled control to follow load demand to direct cold flow from compressor discharge to mix with the hot exit gas of the IHX primary side. The goal of applying flow bypass via CV4 to maintain turbine inlet temperature near the rated 850°C is achieved, as shown in Fig. 3.13. The power sent out to external grid increases to 276 MW_e from 178 MW_e in as little as 7 min. The pressure in the reactor and at turbine inlet increases to 7 MPa from 5 MPa. To return to the base cogeneration rates, the control is reversed by reducing primary coolant inventory through another inventory control valve IV2 and simultaneously by closing the bypass valve VC4.

One attractive feature of the above-described control scheme is that the reactor operates at full power with little changes in the core and fuel temperatures, despite the rapid and wide-ranging load following. Under this condition, the control rod position is essentially unchanged. The core coolant temperatures are not changed. Neither is the core coolant flow rate. The rise in coolant pressure has large effect on the core and fuel temperatures. The heat transfer conditions in the core remain in the well-developed turbulent flow regime in the entire load range of interest.

Another merit of the control scheme is that the operating points of the gas turbine, including turbine inlet temperature and pressure ratio, are unchanged as shown in Fig. 3.13 such that aerodynamic performance of both turbine and compressor remains at their optimum design conditions. This allows for constant power generation efficiency of 46% over the entire load following range.

3.4 Applications and economics

Proven at coolant temperature of 950°C, the highest among the Generation IV reactors, the VHTR enables not only high-efficiency electric power generation, but also broad cogeneration and industrial heat applications.

3.4.1 Power generation

A nuclear system supply steam may be used to power a steam turbine to produce electricity. This is done in HTR-PM. At reactor outlet temperature of 750°C, the plant thermal efficiency is 40%.

More attractive performance features are possible with the VHTR to power a gas turbine. Fig. 3.14 shows the direct gas turbine cycle of Japan's GTHTR300 design. The cycle attains thermal efficiency in the range of 46–51%, corresponding to the range of reactor outlet temperatures of 850–950°C (Yan et al., 2003). Further, the plant simplification is achieved due to eliminating essentially all water and steam systems from the plant. Dry cooling also becomes economically feasible because the rejection of the waste heat from the gas turbine cycle occurs from around 200°C, creating a large temperature difference from ambient air. As a result, the dry cooling tower size required per unit of power generation is comparable to the wet cooling towers used in nuclear plants today. The economical dry cooling would permit inland and remote reactor siting even without a large source of cooling water.

3.4.2 Cogeneration

Cogeneration may improve the plant economics because systems and operations are shared between multiple production activities or because overall thermal efficiency is usually increased from when power is produced alone.

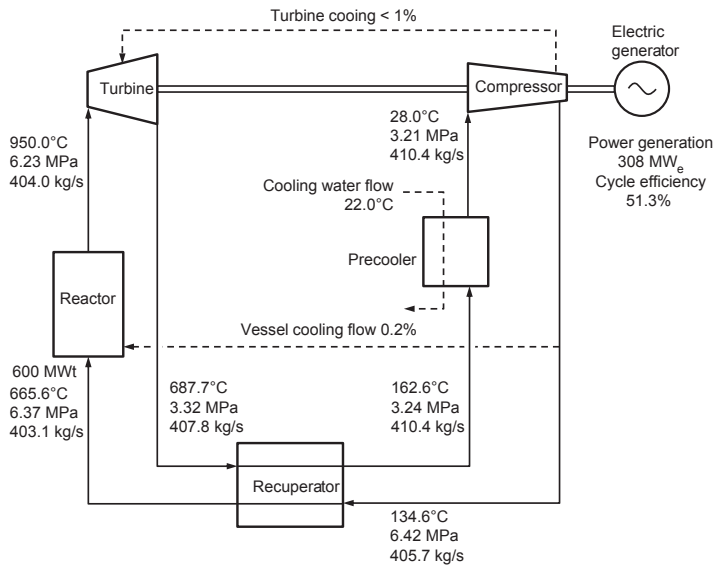


Figure 3.14 A gas turbine power generation cycle based on VHTR.

3.4.2.1 Hydrogen cogeneration

Hydrogen may be efficiently produced in the system illustrated earlier in Fig. 3.12, where nuclear heat is transferred from the primary side coolant in the IHX and then transported in a closed heat transport loop to the thermal hydrogen production plant (Yan et al., 2005). The process parameters in Fig. 3.15 indicates that the IHX transfers 170 MW_{th} of the total 600 MW_{th} reactor thermal power to the hydrogen process. The balance of the reactor thermal power is used by the gas turbine to generate 203 MW_e electricity.

While many hydrogen processes have been proposed, the most studied include the copper–chlorine cycle in the process temperature range of 200–600°C (Orhan et al., 2012), the iodine–sulfur (IS) process of 450–850°C (Kasahara et al., 2014), and the hybrid sulfur cycle of 600–850°C (Gorensek and Summers, 2011).

Fig. 3.15 illustrates the principle of the IS process. The energy and material balance correspond to the heat rate of 175 MW_{th}, of which 170 MW_{th} is supplied in the IHX, and 5 MW_{th} is input from the helium circulator heating in the secondary loop that connects the reactor and the hydrogen plant. The electricity consumption is 25.4 MWe, accounting for the process electric utilities for helium gas circulator, process fluid pumps, and the electro-electrodialysis (EED) to concentrate the hydrogen iodide(HI) flow stream. Accordingly, the thermal efficiency of the IS process plant is estimated to be 48.6% higher heating value(HHV) as detailed below.

$$\text{IS process thermal efficiency} = \frac{H_2 \text{ production rate} \times \text{HHV}(H_2)}{\text{net heat consumed} + \frac{\text{net electricity consumed}}{\text{power generation efficiency}}}$$

$$= \frac{\frac{30{,}655\ \text{Nm}^3/\text{h}}{3600\ \text{s}} \times 12.76\ \text{MJ}/\text{Nm}^3}{170\ \text{MW}_{th} + \frac{25.4\ \text{MW}_e}{47.3\%}} = 48.6\%$$

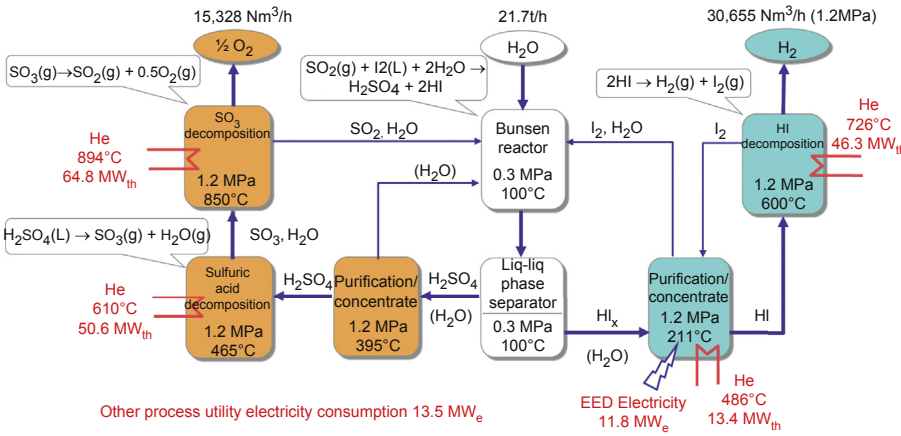


Figure 3.15 Thermochemical iodine sulfur process for hydrogen production.

A key factor that contributes to the high process efficiency is use of the innovative cobalt-reactive HI decomposing process developed by Japan's Toshiba Corporation. The test of the process has yielded nearly 100% HI decomposition rate in one pass through the Co and HI reaction. Another factor is that electricity used by the hydrogen plant is most efficiently cogenerated in-house by the nuclear reactor power plant. The thermal efficiency is 47.3% for power generation.

3.4.2.2 Desalination cogeneration

Fig. 3.16 shows a desalination cogeneration process designed for efficient recovery of the waste heat from a VHTR. Table 3.6 summarizes the design parameters of the process. A multistage flash (MSF) system is connected to the reactor plant cycle via

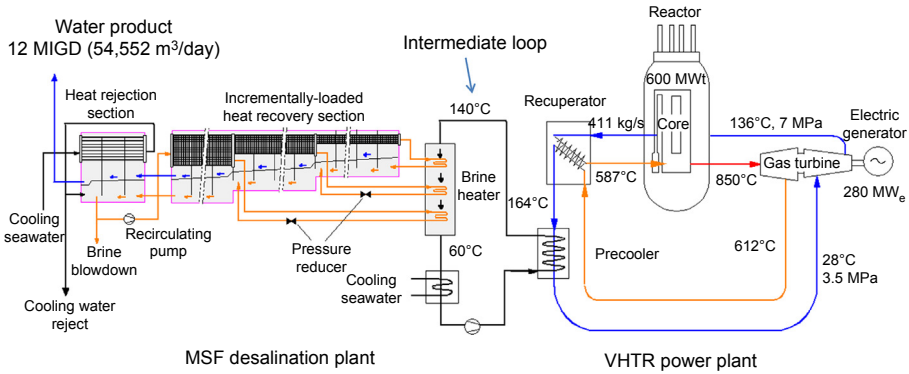


Figure 3.16 VHTR desalination cogeneration process.

Table 3.6 Desalination cogeneration performance

Reactor thermal power	**600 MW_{th}**
Reactor outlet temperature	850°C
Power generation rate	280 MW_e
Seawater desalination rate	12 MIGD (54,552 m^3/day)
Effective thermal input to desalination	220 MW_{th}
Heat supply (hot water) temperature	140°C
Hot water return temperature	60°C
Top brine temperature	112°C
Design seawater temperature	25°C
Seawater temperature rise at HRJ	10°C
Design seawater salinity	45,000 ppm
Recycle brine concentration	62,000 ppm

HRJ, heat rejection section

a closed intermediate loop that transports the waste heat from the reactor to the desalination plant while acting as a barrier to prevent accidental material exchange between the two plants. To efficiently recover the waste heat, the MSF increments the thermal load of the multistage heat recovery section in a number of steps as opposed to keeping it constant in the traditional MSF process (Yan et al., 2013). As the number of steps increases, more waste heat becomes recoverable, while the top brine temperature, a sensitive MSF process parameter, is also increased. Both lead to increased water yield. Operating with a similar number of stages, the present MSF process is shown to produce 45% more water than the traditional process operating over the same temperature range. Connected to a 600-MW_{th} VHTR gas turbine power plant, the desalination yield is 54,552 m^3/d without penalizing to the power generation. The overall utilization of the nuclear reactor thermal power is increased to 83% from 47% in power generation alone.

3.4.3 Industrial application

The heat supply from the VHTR covers the temperature range of heat demands in many industries, some of which, such as large-scale hydrogen production and desalination, are described earlier, and the others that have been frequently studied include oil extraction, coal gasification, oil refinery and petrochemical, and steelmaking. The inherent safety of the VHTR makes the industrial heat applications economically attractive, as it permits siting proximity to the industry customers, in particular to high-temperature heat users so as to minimize the cost and loss of heat transmission.

Fig. 3.17 shows a system that ties a direct reduction steelmaking plant to a VHTR (Yan et al., 2012b). The latter supplies the former all energy and feedstock with the

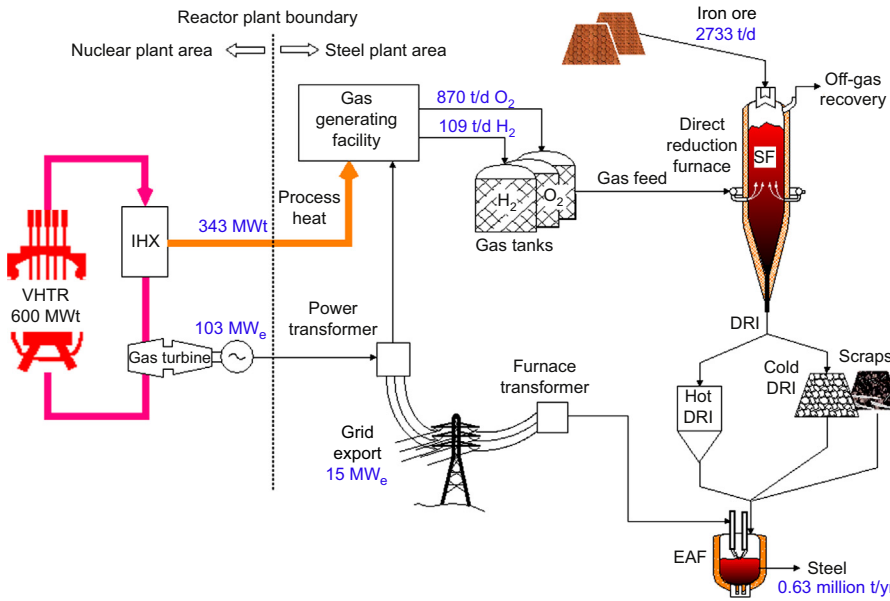


Figure 3.17 Energy and material balance of a VHTR-based steelmaking process.

exception of iron ore. The process takes on a multidisciplinary approach: the reactor plant employs a VHTR with 950°C outlet temperature to produce electricity and heat. The steelmaking plant employs conventional furnaces but substitutes hydrogen and oxygen for hydrocarbons as reactant and fuel. Water decomposition through an experimentally demonstrated thermochemical process manufactures the feedstock gases required. Through essential safety features, particular a fully passive nuclear safety, the design achieves physical proximity and yet operational independence of the two plants to facilitate interplant energy transmission. The calculated energy and material balance given in Fig. 3.17 yields slightly over 1000 t of annual steel output per 1 MW_{th} of reactor thermal power and is essentially free of CO_2 emission.

3.4.4 Economics

3.4.4.1 Cost of electricity generation

A summary of the cost evaluation for the GTHTR300 power plant is given. Details can be found elsewhere (Takei et al., 2006). For the purpose of cost estimation, the plant construction assumes the following:

- Nth-of-a-kind plant that allows for learning effects
- replacement of LWR on existing site
- modular method of construction
- equipment shipped to exclusive port on site
- reactor building and structures similar to the HTTRs
- seismic design conditions same as that of the HTTR
- cost accounts for design, fabrication of facilities, plant construction, and commission operations
- plant siting in Japan

The capital cost estimation assumes a plant life of 40 years. The depreciation period is 20 years. Thereafter, the book value of the plant is assumed to be 5% constant for the reminder of the plant life. The financial parameters assumed are 3% discount rate, 3% interest rate, and 1.4% property tax.

Capital cost

Fig. 3.18 shows the capital cost of the plant that includes four reactor units (4×274 MW_e) comparing with the LWR. The cost for the reference LWR of 1180 MW_e was estimated by Federation of Electric Power Companies (FEPC) of Japan. The cost of decommissioning GTHTR300 is higher because the number of systems and structures, such as pressure vessels and primary biological shielding, that become radioactive in operation and must be disposed of during decommission, are bulkier in the GTHTR300. However, the total capital cost of GTHTR300 (1.31 US ¢/kWh) is about 25% lower than the LWR (1.77 US¢/kWh) because of the greater power generating efficiency of GTHTR300.

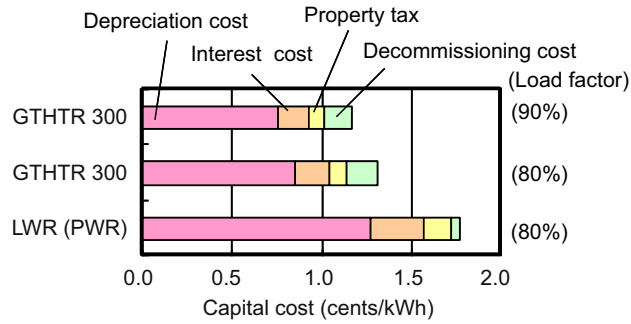


Figure 3.18 Capital cost.

Operating cost

Fig. 3.19 shows the operating cost in comparison with the LWR. The operating cost of the GTHTR300 (0.92 US¢/kWh) is about 35% lower than the LWR (1.42 US¢/kWh) since the plant generating efficiency is higher and because the maintenance cost is lower, owing to less number and material of systems to be regularly serviced.

Fuel cost

Fig. 3.20 shows the fuel cycle cost comparing with the LWR. The overall fuel cycle cost of GTHTR300 (1.22 US¢/kWh) is comparable to that of the LWR (1.23 US¢/kWh). In the front-end process, the higher enrichment and the fabrication of coated fuel particles make the cost of enrichment, conversion, and fabrication higher in the GTHTR300. In the back-end process, although unit costs in almost all processes of the GTHTR300 are higher, the back-end cost of the GTHTR300 is lower than the LWR because the material quantity of spent fuel is less as a result of higher burnup and because of the greater plant efficiency.

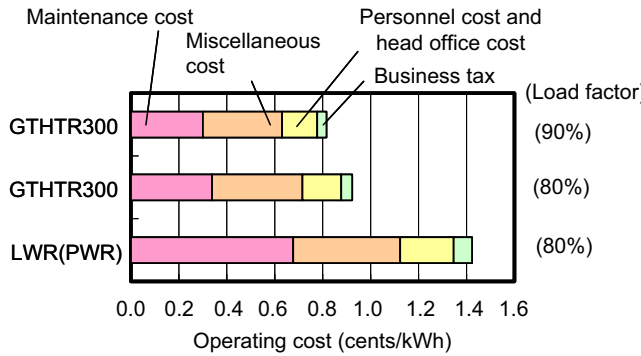


Figure 3.19 Operating cost.

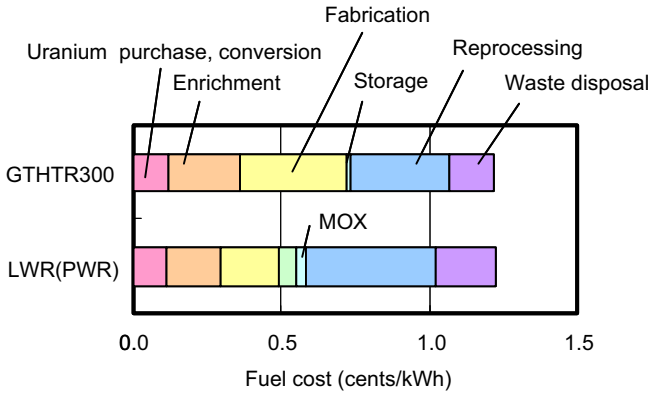


Figure 3.20 Fuel cost.

Power generation cost

Fig. 3.21 shows the power generation cost by summing up the above capital, operation, and fuel cycle costs. The power generation cost is 3.2 US¢/kWh at the load factor of 90% and increases to 3.45 US¢/kWh at a reduced factor reduced of 80%. The GTHTR300 offers a 20% cost advantage over the 4.42 US¢/kWh of LWR estimated by FEPC.

3.4.4.2 Cost of hydrogen production

Table 3.7 summarizes the estimated cost of the GTHTR300 for cogenerating hydrogen with a co-located IS process water-splitting thermochemical plant. The estimation of the plant design, referred as GTHTR300C + IS below, assumes a load factor of 90% for both the reactor and hydrogen plants. The capital cost of hydrogen plant covers equipment cost, site construction cost, and indirect cost. Nuclear heat is assumed to be cogenerated in the 600-MW_{th} reactor plant, 170 MW_{th} of which is supplied via IHX to the hydrogen plant facility, while the balance is used to generate power in the reactor plant. The utilities include the feed water to IS process, 25.4 MW_e

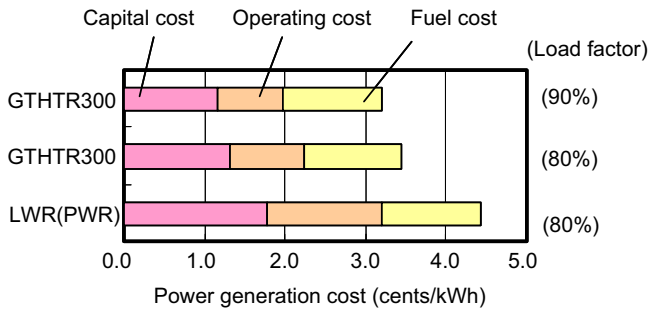


Figure 3.21 Power generation cost.

Table 3.7 Hydrogen production cost by GTHTR300C

H_2 production rate (H_2 production efficiency)		**30,655 Nm^3/h (48.8%)**	**30,655 Nm^3/h (48.8%)**
H_2 plant life	Year	15	15
H_2 plant capital	\$/kg-H_2	0.657	0.657
Nuclear heat	\$/kg-H_2	0.965	0.965
Nuclear electricity	\$/kg-H_2	0.294	0.294
H_2 plant utilities	\$/kg-H_2	0.091	0.091
By-product (O_2) credit	\$/kg-H_2	0	−0.278
Return on investment (8%)	\$/kg-H_2	0.161	0.161
Total production cost	\$/kg-H_2	2.169	1.891
	¢/Nm^3	19.5	17.0

electricity that is supplied in house by the nuclear reactor plant at a cost of 3.2¢/kWh (see Section 3.4.4.1 for detail) and consumed to power the EED, the process pumps, the helium circulator of the heat transport loop, and catalysts and chemicals used in the IS process. Return on investment is 8%. Note that the value difference in the two columns of the table results from whether a credit is taken from the sale of by-product oxygen.

Final hydrogen production cost is US \$2.169/kg-H_2, of which 64% is the cost of nuclear heat and electricity supplied in house by the co-located GTHTR300C. The cost distributors are identified in Fig. 3.22.

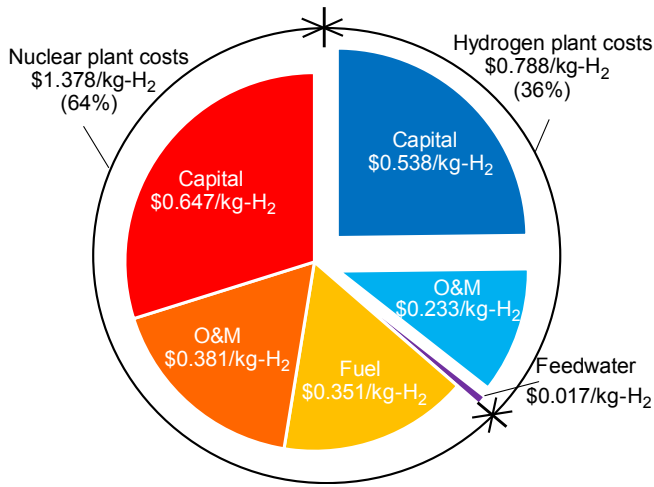


Figure 3.22 Cost share of hydrogen production by GTHTR300C + IS.

3.4.4.3 Cost of desalination cogeneration

Table 3.8 compares the estimated costs of potable water production through seawater desalination cogeneration with conventional and VHTR power plants (Sato et al., 2014). The conventional plant is based on a modern gas turbine combined cycle (GTCC) power plant at 55% power generation efficiency. The VHTR cogeneration system is that described in Section 3.4.2.2. The costs were evaluated by an original equipment manufacturer (OEM) vendor active in the Middle East desalination plant construction. The vendor carried out the plant equipment design and evaluated the required operation and maintenance. The cost estimation was then developed based on the vendor construction and operation know-how of comparable-scale MSF plants.

The prices of oil and natural gas are referred to the World Bank Commodity Prices Date (also known as Pink Data). The 10-year average (July 2004−July 2014) crude oil prices of the three primary benchmarks (Brent, Dubai, and West Texas intermediate) fall in the narrow range of 79.8−84.1 US $/bbl. During the same 10-year period, the average natural gas benchmark prices (US, Europe, and Japan) are in the range of 5.6−11.1 US $/MMBtu. For this study, the lower values of the above ranges for oil and gas are used to calculate the heat costs of the conventional plant.

The estimated water cost with the VHTR desalination cogeneration is US $0.57/$m^3$ comparing to US $2.13/$m^3$ for the oil-fired plant and US $1.14/$m^3$ in the case of the gas-fired plant. Despite the higher capital cost of the VHTR desalination plant, the considerable energy cost saving by cogeneration using the VHTR power generation waste heat provides 50% or more water cost advantage comparing the fossil-fired GTCC options widely practiced for desalination cogeneration today.

Table 3.8 Fossil-fired and VHTR seawater desalination cogeneration cost estimates

	GTCC (Gas turbine combined cycle)		VHTR desalination cogeneration
Plant ->	**Oil-fired**	**Natural gas-fired**	
Capital ($/$m^3$)	0.29	0.29	0.39
Energy ($/$m^3$)			
Heat	1.65	0.67	0.04
Electricity	0.13	0.13	0.09
Operation ($/$m^3$)			
Consumables	0.02	0.02	0.02
O&M	0.03	0.03	0.03
Water cost ($/$m^3$)	2.13	1.14	0.57

O&M, operation and maintenance

3.5 Summary

VHTR technology is well advanced through the decades of international research, development, and commercialization efforts. Several reactors have been built. Two test reactors remain operational in China and Japan. Still others are being developed.

Pebble bed and prismatic reactor are the two major design variants. Both are in use today. In either case, the basic fuel construction is the TRISO-coated particle fuel. Uranium, thorium, and plutonium fuel cycle options have been investigated and some have been operated in the reactors. Spent fuel may be direct disposed or recycled. The unique construction and high burnup potential of the TRISO fuel enhances proliferation resistance.

The VHTR safety relies mostly on passive and inherent design features. The choice of low core power density limits the decay heat generation rate to the extent that can be safely removed by thermal conduction only. The choice of the core negative reactivity coefficient provides reactor shutdown in case of accidental rise in core temperature. Helium coolant used is chemically inert and thus absent of explosive gas generation or phase change. The robust design and proven fabrication quality of the TRISO fuel prevents significant release of fission products in any licensing events.

The VHTR coolant temperature (950°C) is the highest among the Generation IV reactors. This enables not only for efficient power generation by either steam or gas turbine, but also for high-temperature heat application and attractive cogeneration. The VHTR-based hydrogen production, steelmaking, and seawater desalination have been found cost competitive.

The world first modular prototype plant, HTR-PM, consisting of two reactor units of 250 MW_{th} each at 750°C reactor outlet temperature, is being built in China. The operation is expected in 2017. The quest in the current development for the 950°C GTHTR300 reactor in Japan and for the systems in the USA, Korea, and other countries is to demonstrate the technologies of advanced fuels, power conversion, and heat applications that can satisfactorily address the set of Generation IV objectives for safety, economics, waste management, and proliferation resistance.

Acronyms

AREVA	French nuclear plant vendor company
ATWS	Anticipated transient without scram
AVR	Arbeitsgemeinschaft Versuchsreaktor, an HTGR test reactor in FZJ
CITATION	Diffusion computer code
CV	Control valve
DRI	Direct reduction iron
EED	Electro-electrodialysis

Continued

EFPD	Effective full power day
FEPC	Federation of Electric Power Companies of Japan
FSV	Fort St. Vrain, an HTGR prototype power station in the US
GTHTR300	Gas turbine high-temperature reactor 300 MW_e in Japan
GTHTR300C	Gas turbine high-temperature reactor 300 MW_e cogeneration in Japan
HTR-10	High-temperature test reactor 10 MW_{th} in Tsinghua University's INET
HTTR	High-temperature engineering test reactor, 30 MW_{th} test reactor in JAEA
IHM	Initial heavy metal
IPyC	Inner layer of (high-density) pyrolytic carbon
IS	Iodine−sulfur cycle hydrogen production process
IV	Inventory flow valve
LOCA	Loss of coolant accident
MW_e	Megawatt electric
MW_{th}	Megawatt thermal
MWD	Megawatt day
MIGD	Million imperial gallon per day
NGNP	Next generation nuclear plant in the US
NuH_2	Nuclear hydrogen and process heat demonstration reactor in Korea
NSSS	Nuclear steam supply system
OEM	Original equipment manufacturer
OPyC	Outer layer of (high-density) pyrolytic carbon
RCR	Reactivity control rod
SAS	Small absorber sphere
SC	Steam cycle or Rankine cycle
SiC	Silicon carbide
THTR-300	Thorium high-temperature reactor 300 MW_e built in Germany
TWOTRAN	Name of computer code
TRISO	Tri-isotropic coating of fuel particle
TRU	Transuranium
UCO	Uranium oxide/uranium carbide
UO_2	Uranium dioxide
VHTR	Very high temperature gas-cooled reactor

WTI	West Texas intermediate (oil benchmark)
YSZ	Yttria-stabilized zirconia
ZrC	Zirconium carbide

References

Fowler, T., et al., 1971. Nuclear Reactor Core Analysis Code. CITATION, ORNL-TM-2496. ORNL.

Fu, J., Jiang, Y., Cheng, H., Cheng, W., 2014. Overview and progress of high temperature reactor pebble-bed module demonstration project (HTR-PM), HTR2014-11125. In: Proceedings of the HTR 2014, Weihai, China, October 27−31.

Fujikawa, S., Hayashi, H., Nakazawa, T., Kawasaki, K., Iyoku, T., Nakagawa, S., Sakaba, N., 2004. Achievement of reactor-outlet coolant temperature of 950°C in HTTR. Journal of Nuclear Science and Technology 41 (12), 1245−1254.

Fujimoto, N., Nojiri, N., Ando, H., Yamashita, K., 2004. Nuclear design. Nuclear Engineering and Design 233, 23−36.

Fukaya, Y., Goto, M., Ohashi, H., Tachibana, Y., Kunitomi, K., Chiba, S., 2014. Proposal of a plutonium burner system based on HTGR with high proliferation resistance. Journal of Nuclear Science and Technology 51 (6), 818−831.

Gorensek, M., Summers, W., 2011. In: Yan, X., Hino, R. (Eds.), The Hybrid Cycle. Chapter in Nuclear Hydrogen Production Handbook. CRC Press, Florida, USA.

Goto, M., et al., 2015. Conceptual study of a plutonium burner high temperature gas-cooled reactor with high nuclear proliferation resistance. Paper 5426. In: Proceedings of Global 2015, September 20−24, 2015, Paris, France.

Greneche, D., 2003. HTR fuel cycles: a comprehensive outlook of past experience and an analysis of future options. In: Proceedings of the ICAPP.

Hu, S., Wang, R., Gao, Z., 2004. Safety demonstration tests on HTR-10. Paper HTR2004-H06. In: Proceedings of the HTR 2004, Beijing, China, September 22−24.

http://www.ngnpalliance.org/ (accessed 13.10.15.).

Kasahara, S., Tanaka, N., Noguchi, H., Iwatsuki, J., Takegami, H., Yan, X., Kubo, S., 2014. JAEA's R&D on the thermochemical hydrogen production is process. Paper HTR2014-21233. In: Proceedings of the HTR 2014, Weihai, China, October 27−31.

Kuijper, J., et al., 2006. HTGR reactor physics and fuel cycle studies. Nuclear Engineering and Design 236, 615−634.

Kunitomi, K., Yan, X., Nishihara, T., Sakaba, N., Mouri, T., 2007. JAEA's VHTR for hydrogen and electricity cogeneration: GTHTR300C. Nuclear Engineering and Technology 39 (1), 9−20.

Lathrop, K., Brinkley, F., 1973. TWOTRAN-II: An Interfaced Exportable Version of the TWOTRAN Code for Two Dimensional Transport. LA-484-MS.

Masson, M., et al., 2006. Block-type HTGR spent fuel processing: CEA investigation program and initial results. Nuclear Engineering and Design 236, 516−525.

Nakata, T., Katanishi, S., Takada, S., Yan, X., Kunitomi, K., 2003. Nuclear, thermal and hydraulic design for gas turbine high temperature reactor (GTHTR300). AESJ Transaction 2 (4), 478−489.

Oak Ridge National Laboratory, November 2008. Deep Burn: Development of Transuranic Fuel for High-Temperature Helium-Cooled Reactors. ORNL/TM-2008/205.

Orhan, M., Dincer, I., Rosen, M., 2012. Design and simulation of a UOIT copper−chlorine cycle for hydrogen production. International Journal of Energy Research. http://dx.doi.org/10.1002/er.2928.

Petti, D., 2014. Implications of results from the advanced gas reactor fuel development and qualification program on licensing of modular HTGRs. Paper HTR2014-31252. In: Proceedings of the HTR 2014, Weihai, China, October 27−31.

Richards, M., et al., 2008. VHTR deep burn applications. In: 16th Pacific Basin Nuclear Conference (16PBNC), Aomori, Japan, October 13−18. Paper ID P16P1238.

Saito, S., et al., 1994. Design of High Temperature Engineering Test Reactor (HTTR). JAERI 1332.

Sato, H., Yan, X.L., Tachibana, Y., Kunitomi, K., 2014. GTHTR300—A nuclear power plant design with 50% generating efficiency. Nuclear Engineering and Design 275, 190−196.

Shahrokhi, F., Lommers, L., Mayer III, J., Southworth, F., 2014. US HTGR deployment challenges and strategies. Paper HTR2014-11309. In: Proceedings of the HTR 2014, Weihai, China, October 27−31.

Takamatsu, K., Yan, X., Nakagawa, S., Sakaba, N., Kunitomi, K., 2014. Spontaneous stabilization of HTGRs without reactor scram and core cooling—safety demonstration tests using the HTTR: loss of reactivity control and core cooling. Nuclear Engineering and Design 271, 379−387.

Takei, M., Kosugiyama, S., Mouri, T., Katanishi, S., Kunitomi, K., 2006. Economical evaluation on gas turbine high temperature reactor 300 (GTHTR300). Transaction of AESJ 5 (2), 109−117.

The US Energy Policy Act of 2005, August 5, 2005.

Wu, Z., et al., 2002. The design features of the HTR-10. Nuclear Engineering and Design 218, 25−32.

Yan, X., Kunitomi, K., Nakada, T., Shiozawa, S., 2003. GTHTR300 design and development. Nuclear Engineering and Design 222, 247−262.

Yan, X., Kunitomi, K., Hino, R., Shiozawa, S., 2005. GTHTR300 design variants for production of electricity, hydrogen or both. In: Proc. 3rd of OECD/NEA Information Exchange Meeting on Nuclear Production of Hydrogen, Oarai, Japan.

Yan, X., Sato, H., Tachibana, Y., Kunitomi, K., Hino, R., 2012a. Evaluation of high temperature gas reactor for demanding cogeneration load follow. Journal of Nuclear Science and Technology 49 (1), 121−131.

Yan, X., Kasahara, S., Tachibana, Y., Kunitomi, K., 2012b. Study of a nuclear energy supplied steelmaking system for near-term application. Energy 39, 154−165.

Yan, X., Noguchi, H., Sato, H., Tachibana, Y., Kunitomi, K., Hino, R., 2013. Study of an incrementally loaded multistage flash desalination system for optimum use of sensible waste heat from nuclear power plant. International Journal of Energy Research 37, 1811−1820.

Yan, X., Sato, H., Kamiji, Y., Imai, Y., Terada, A., Tachibana, Y., Kunitomi, K., 2014. GTHTR300 cost reduction through design upgrade and cogeneration. Paper HTR2014-21436. In: Proceedings of the HTR 2014, Weihai, China, October 27−31.

Gas-cooled fast reactors

4

P. Tsvetkov
Texas A&M University, College Station, TX, United States

4.1 Rationale and generational research and development bridge

The history of gas-cooled fast reactors (GFRs) dates back to the dawn of the nuclear era. It needs to be noted that GFR technology is being pursued to this day and remains to be of contemporary interest in many countries worldwide (IAEA-154, 1972; Waltar et al., 2012).

The biggest potential advantage of GFRs is in their expected technological range of applications—from electricity to process heat to waste minimization. Both breeders and burners were of initial interest, taking advantage of the very nature of this concept to offer a fast spectrum system that can be tailored to the desired conversion ratios. Reactors using air, helium, CO_2, and dissociating gases as coolants have been explored (Waltar et al., 2012). General Atomics in the United States originated the initial conceptual effort. The interests in the design expanded globally after that, including Germany, France, and Russia. The former Soviet Union explored N_2O_4 as a coolant (IAEA-154, 1972; Waltar et al., 2012).

The unique robustness of the technology is unmatched in the engineering domain of nuclear reactors. There are thermal reactors and fast reactors with various coolants, but none of them offers the option to fit in all anticipated deployment domains supporting the complete range of energy system applications.

Despite of the great promise of GFRs, thus far these systems have not deployed and operated. The marketed promise of GFRs does not come without complicating factors. For GFRs to fully realize their potential and become technically feasible, enabling engineering solutions are needed to bring the GFR technology to life and ensure its commercial success (Waltar et al., 2012; A Roadmap to Deploy New Nuclear Power Plants in the United States by 2002, 2010).

The major perceived economic advantages of GFRs are in their promise to operate at high power densities and with no intermediate loops. The helium-cooled GFRs have an advantage of using chemically and neurotically inert single-phase gas, although it is characterized by its extreme mobility and the resulting challenges to contain. It should be noted that the challenges of using helium are being addressed and resolved not only in the GFR programs but also in the high-temperature reactor (HTR) programs (Waltar et al., 2012; Weaver, 2005).

These enabling solutions include materials, fuel, control, instrumentation, and other design features ensuring reliability and safety in extreme operational conditions of GFRs over the projected operational lifetimes. The significant challenges of the needed

Handbook of Generation IV Nuclear Reactors. http://dx.doi.org/10.1016/B978-0-08-100149-3.00004-5
Copyright © 2016 Elsevier Ltd. All rights reserved.

enabling technologies resulted in global GFR research and development (R&D) efforts to deliver on the GFR promise. Significant results have been achieved thus far, contributing to the expectation of GFRs to become deployable and commercially viable sometime in the future (Technology Roadmap Update for Generation IV Nuclear Energy Systems, 2014).

The achieved progress in the development, deployment, and operation of high-temperature helium-cooled thermal reactors brings GFRs closer to the time when they will be able to cross from being promising "paper reactors" to the world of real systems. Some of the needed enabling solutions have already been proposed in the feasibility programs for GFRs (Waltar et al., 2012).

However, it has also been concluded over the years that further work would be required to advance the GFR technology to the level of prototypes demonstrating its performance characteristics and commercial viability. The key research areas of contemporary GFR R&D efforts include reactor design; fuel; fuel cycles; structural materials; system optimization; and, most importantly, safety (Technology Roadmap Update for Generation IV Nuclear Energy Systems, 2014).

Developments related to GFRs based on the Generation I era accomplishments advanced the conceptual premise whereas further Generation II−III advancements and subsequent evolving operation and safety considerations allowed for refining the GFR concept and contributed some of the vital enabling technologies. The Generation IV GFR is the culmination of decades of preceding R&D efforts with an expectation of its potential deployment and commercialization by 2030 (A Roadmap to Deploy New Nuclear Power Plants in the United States by 2002, 2010; Technology Roadmap Update for Generation IV Nuclear Energy Systems, 2014).

The Generation IV GFR concept is being developed with the following objectives in mind meeting the Generation IV reactor criteria: economic competitiveness, enhanced safety and reliability, minimal radioactive waste generation, and proliferation resistance. Safety considerations are of the upmost priority for Generation IV GFRs.

The GFR cores are inherently characterized by higher core neutron leakage than liquid metals, leading to increased fissile loadings that challenge safety and proliferation resistance characteristics. Higher fissile loadings and harder spectra in GFRs further reduce the fuel Doppler coefficient relative to other fast reactors. Required pressures of GFR systems are approximately 7 MPa for helium-cooled configurations and approximately 20 MPa for supercritical CO_2-cooled configurations.

High system pressures are needed to compensate for the low heat capacity of He and to achieve high thermal efficiency for CO_2, respectively. Highly pressurized systems require special design provisions to mitigate the potential for and consequences of rapid depressurization scenarios. Generation IV GFRs have provisions for heat removal from the core in accident scenarios and in planned maintenance processes.

At reduced pressures in these systems, natural circulation may not be sufficient for adequate heat removal. This leads to the use of ceramic high-temperature materials in Generation IV designs to further substantiate the licensing case for GFRs (Waltar et al., 2012; Weaver, 2005).

The GFR concept is beyond contemporary nuclear power technologies. The 2002 technology roadmap qualified GFRs on the basis of their potential robust operational domain. The analysis and recommendations have been deeply rooted in the 2000s era nuclear renaissance expectations.

The updated 2014 roadmap accounts for the subsequent accomplishments of more than 10 years of R&D related to the Fukushima Daiichi accident lessons and contemporary economics of the 2010s. Because the required enabling technologies need to mature to the level of commercial deployment, the GFRs are no longer expected to reach the demonstration phase within the roadmap projected time range (Technology Roadmap Update for Generation IV Nuclear Energy Systems, 2014).

As already indicated, decades of technology development efforts for GFRs serve as a foundation for deployment expectations assuming that vital enabling technologies mature in the coming decades of R&D efforts. Generation IV GFRs are expected to be the result of international collaborative efforts bringing novel technologies to energy markets and customizing them according to local conditions.

It is expected that global interests in GFRs will ultimately lead to growing practical operational experiences and deployments, consequently contributing to establishing and developing the GFR safety case needed for reactor successful licensing and eventual commercialization (Technology Roadmap Update for Generation IV Nuclear Energy Systems, 2014). The objectives are for GFRs to be sustainable, safe, reliable, economically competitive, proliferation resistant, and secure (Waltar et al., 2012; Weaver, 2005).

4.2 Gas-cooled fast reactor technology

Historical GFR concepts as well as the Generation IV GFRs represent an alternative to liquid metal−cooled fast reactors (LMFRs). The use of gases leads to a harder neutron spectrum compared with the fast reactor cores of sodium- and lead-cooled fast reactors (Waltar et al., 2012).

Harder spectra in GFRs allow for a broad range of fast spectrum system applications ranging from historical breeder cores to advanced burner reactors. High breeding ratios, shorter doubling times, and high power densities are characteristic design features of historical gas-cooled fast breeder reactors (Waltar et al., 2012; Weaver, 2005).

The burner version of GFRs yields higher transmutation efficiencies in waste management application scenarios. Unlike LMFRs operating at near atmospheric pressures, GFRs require significant in-core pressurization, thus complicating reactor dynamics in transient scenarios during normal and off-normal situations as well as adding procedures to reactor maintenance schedules compared with LMFRs (IAEA-154, 1972; Waltar et al., 2012).

The Generation IV GFR design is identified in Generation IV International Forum documents as the reactor concept with significant sustainability expectations. This assertion is based on the reduced core volume and the reactor ability to minimize its own spent fuel inventory and to manage uranium resources and actinide waste streams

in various future closed fuel cycle scenarios (Technology Roadmap Update for Generation IV Nuclear Energy Systems, 2014).

Utilization of gases in GFRs leads to R&D efforts to create power units with GFRs using direct cycle balance of plant configurations based on Brayton cycle options. Gas coolants can be pumped directly through the turbine without the need for an intermediate loop (Waltar et al., 2012). Expected elevated in-core temperatures result in high energy conversion efficiencies of power units with GFRs in Brayton cycles and potential heat utilization for process heat applications. Furthermore, utilization of high-efficiency Brayton cycles minimizes the environmental impact of GFRs (Weaver, 2005).

The historical GFR concepts include designs of smaller 300- and 1000-MW_e rated units. Generation IV power units with GFRs assume 600 and 2400 MW_{th}. Lower power unit ratings enable modularity and load-follow operation modes, and they facilitate synergies with very high-temperature reactors. Higher power unit ratings facilitate neutron economy with consequent reductions of core fuel inventories, and they are more compatible with base-load operation modes (Waltar et al., 2012).

Metal-clad fuel elements with oxide or carbide fuels are traditionally considered for GFRs. Table 4.1 summarizes fuel and core configuration options that are being explored for Generation IV GFRs (Waltar et al., 2012; Meyer et al., 2006; Ryu and Sekimoto, 2000; Dumaz et al., 2007). Of note, the core concepts developed for GFRs follow the prismatic block/hexagonal lattice path as well as the pebble bed core path (Weaver, 2005; Ryu and Sekimoto, 2000). The high outlet temperatures of GFRs eliminate considerations of steel-based alloys as cladding materials. Ceramic materials and refractory metals are the most feasible in-core materials for GFRs (Waltar et al., 2012). Silicon carbide composite materials are the potential cladding choices for future GFRs assuming that sufficient performance characteristics can be achieved for in-core applications (Waltar et al., 2012).

Table 4.1 In-core design options for Generation IV gas-cooled fast reactors

Fuel	Fuel element	Core configuration
Dispersion fuels • Cylinders • Hexagons • Spheres • Arbitrary geometry	Coated compacts Coated plates	Hexagonal lattices with stacks of compacts Plate-geometry configurations Prismatic block arrays
Microparticle, HTR-type fuels • Single-size particles • Multisize particles	Microparticles Spherical pebbles Compacts with coated microparticles	Particulate beds Pebble beds Hexagonal configurations Prismatic block array configurations

HTR, high-temperature thermal reactor.

The use of helium in Generation IV GFRs stems from decades of R&D efforts for HTRs. Alternative gases are also explored, including air, steam, and CO_2. Air poses activation and corrosion concerns, but it is much easier to resupply in loss of coolant accident scenarios (Advanced Reactor Concepts, 2012). Helium and supercritical CO_2 received the most significant attention as potential coolants for GFRs. For the desired high thermal efficiencies, the use of supercritical CO_2 allows for lower outlet temperatures compared with helium-cooled designs while still operating very efficiently (Waltar et al., 2012). Because thermal decomposition of CO_2 is accelerated starting at 700°C, the oxidation/corrosion rates increase significantly beyond those temperatures, providing further performance limits for maximum operating temperatures in supercritical CO_2-cooled GFR systems not to exceed 600°C (Waltar et al., 2012; Weaver, 2005).

Steam introduces cladding compatibility challenges, the potential for positive coolant reactivity effects, and reduced conversion rates. CO_2 leads to higher pressure drops and associated forces across components, increased acoustic loadings, and economic penalties due to increased primary coolant pumping requirements. The challenges of CO_2 are potentially offset by its heat removal and energy conversion advantages (Waltar et al., 2012; Advanced Reactor Concepts, 2012).

The GFR safety case is complicated by the recognized challenges of passive heat removal during accident scenarios, fuel reliability, and in-core materials under extreme conditions of high temperature and fast neutron fields (Technology Roadmap Update for Generation IV Nuclear Energy Systems, 2014; Advanced Reactor Concepts, 2012). It is recognized that although fully passively safe GFRs are possible at lower power densities, the economic competitiveness is challenging for those designs. This can be addressed through the use of guard (or secondary) vessels for GFRs.

The economics of closed fuel cycles with GFRs as well as other reactor options are not expected to be immediately commercially viable. Closed fuel cycles will be economical at the end of the 21st century or early in the 22nd century assuming conditions of limited fuel resources (Waltar et al., 2012; Technology Roadmap Update for Generation IV Nuclear Energy Systems, 2014; Weaver, 2005). Furthermore, hybrid systems combining the advantages of GFRs with the advantages of other energy sources as well as integrating power and process heat applications may potentially make the economic case for Generation IV GFRs more competitive and bring the deployment of these systems closer to reality because it allows fuller realization of their performance potential. However, deployment of prototype systems to demonstrate both performance characteristics, including reliability and economics, is of paramount importance for the viability of GFRs. Construction of a GFR prototype would address the limited experience challenge that has impeded GFRs.

4.3 Conclusions

The Generation IV GFR is the robust nuclear reactor design offering a broad range of potential applications—from electricity to process heat to waste minimization.

The objectives are for GFRs to be sustainable, safe, reliable, economically competitive, proliferation resistant, and secure. Decades of technology development efforts for GFRs serve as a foundation for deployment expectations assuming vital enabling technologies mature in the coming decades of R&D efforts.

References

Dumaz, P., Allègre, P., Bassi, C., Cadiou, T., Conti, A., Garnier, J.C., Malo, J.Y., Tosello, A., 2007. Gas-cooled fast reactors − status of CEA preliminary design studies. Nuclear Engineering and Design 237, 1618−1627. Elsevier.

GENIV International Forum, January 2014 Technology Roadmap Update for Generation IV Nuclear Energy Systems, 2014. OECD Nuclear Energy Agency for the Generation IV International Forum.

IAEA-154, July 24−28, 1972. Gas-cooled fast reactors. In: Proc. IAEA Study Group Meeting Sponsored by the USSR State Committee on the Utilization of Atomic Energy. Institute of Nuclear Energy, Minsk.

Meyer, M.K., Fielding, R., Gan, J., 2006. Fuel Development for Gas-Cooled Fast Reactors. INL/CON-06−11085.

Ryu, K., Sekimoto, H., 2000. A possibility of highly efficient uranium utilization with a pebble bed fast reactor. Annals of Nuclear Energy 27, 1139−1145. Elsevier.

Technical Review Panel Report, Evaluation and Identification of Future R&D on eight Advanced Reactor Concepts, December 2012 Advanced Reactor Concepts, 2012. U.S. DOE Office of Nuclear Energy.

Volumes I and II, Nuclear Energy Research Advisory Committee, Subcommittee on Generation IV Technology Planning A Roadmap to Deploy New Nuclear Power Plants in the United States by 2010, 2002. U.S. DOE Office of Nuclear Energy, Science and Technology.

Waltar, A., Todd, D., Tsvetkov, P. (Eds.), 2012. Fast Spectrum Reactors. Springer, ISBN 978-1-4419-9572-8.

Weaver, K.D., 2005. Interim Status Report on the Design of the Gas-Cooled Fast Reactor (GFR). Gen IV Nuclear Energy Systems. INEEL/EXT-05-02662.

Sodium-cooled fast reactor

5

H. Ohshima, S. Kubo
Japan Atomic Energy Agency, Ibaraki, Japan

5.1 Introduction

Since the beginning of the peaceful use of nuclear energy, sodium-cooled fast reactors (SFRs) have a long history of their research and development (R&D), led by the United States, Russia (formerly Soviet Union), the United Kingdom and France followed by Japan and Germany. The focus was to utilize a uranium resources by using plutonium (PU), which is generated by transmutation of ^{238}U during operation of a reactor. After testing various materials for the coolant, sodium was selected. SFR development has slowed since the late 1980s, presumably because of the commercially successful light water reactors (LWRs) and the fact that uranium resource depletion was under the surface. Moving into the 21st century, new energy demands arise in developing countries such as China and India, whereas global warming due to the use of fossil fuels and the growing disposal problem of radioactive wastes from LWR spent fuel became major issues. Thus SFR R&D has been in the limelight again to realize their commercialization, mainly in the United States, Russia, France, the Republic of Korea, Japan, China, and India. The performance for the fuel breeding and power generation is confirmed, and the improvements are identified through the operation experiences of the current and past SFRs. The R&D is turning into the new phase for the demonstration of reactor design, construction, and operation.

5.2 Development history

Since the early days of nuclear energy development, R&D for realizing the fast reactor and the thermal reactor were conducted in parallel. In fact, it was in 1951, the very first nuclear reactor, experimental breeder reactor-I (EBR-1) produced electricity. As for the fast reactor coolant, after some trial works, it was recognized that the sodium would be the most suitable coolant among various coolant materials such as mercury and NaK. In the 1960s and 1970s, several experimental SFRs were built and operated successfully in the United States (Fermi-1, EBR-II, The Fast Flux Test Facility (FFTF)), the former Soviet Union (BR-5/BR-10, BOR-60), the United Kingdom [dounreay fast reactor (DFR)], France (Rapsodie), Germany (KNK-II), and Japan (Joyo) (Aoto et al., 2014; Cacuci, 2010).

Reflecting the valuable knowledge and experiences gained through the operation of these experimental reactors, the design and construction of prototype—or demonstration—SFR have started in some countries, such as the former Soviet Union

Handbook of Generation IV Nuclear Reactors. http://dx.doi.org/10.1016/B978-0-08-100149-3.00005-7
Copyright © 2016 Elsevier Ltd. All rights reserved.

(BN-350, BN-600), the United Kingdom (PFR), France (Phenix, Super-Phenix), and Japan (Monju) (Aoto et al., 2014; Cacuci, 2010). Through the design, construction, and operation of these SFRs, a great deal of engineering knowledge was accumulated on SFR technology, including the plutonium fuel performance, fissile material breeding, operation and maintenance, fuel handling for refueling, the related nuclear fuel cycle process, and the safety features. Concerning the safety features, incident control such as sodium coolant leakage was also attained (IAEA, 1998, 2007). It was recognized that the SFR would be a feasible nuclear technology in near future.

However, demand-and-supply balance of the uranium resources did not become as serious as it had been foreseen in the days of introduction of thermal reactors such as the LWRs. As a result, numbers of LWRs have been used all over the world to date. On the other hand, SFR development, where the sodium coolant technology and the plutonium technology are deeply involved, had slowed down or completely shut in some countries because of the economical aspect in the short term or the enhancement of the nuclear nonproliferation policy.

After entering the 2000s, the nuclear energy caught people's attention again for its capacity of supplying sustainable energy without giving harmful effects to the environment such as global warming. In France, Russia, India, China, the Republic of Korea, and Japan, each country made a development plan for the realization of the next-generation SFR technology which has an economic competitiveness in parallel with further enhanced built-in safety features. In Russia, although they have faced the slow-down phase in the past, such as a postponement of the construction of BN-800 reactor, they are now attaining excellent capacity factor in the BN-600 reactor, have completed the construction of the BN-800 reactor, and achieved the first criticality in 2014. The BN-1200 design has been in progress as the next-generation reactor (Aoto et al., 2014). In China, an experimental fast reactor has been connected to the grid in 2011 as the result of vigorous R&D as a response to the foreseen large increase in the domestic energy demand. Then a prototype reactor, CFR-600, and the following commercial reactor, CFR-1000, are planned (Zhang, 2013). India is also about to start a prototype fast breeder reactor (PFBR) operation via an experimental reactor, the fast breeder test reactor, foreseeing future construction of the next SFRs (Chellapandi, 2015). France is proceeding a Generation IV (Gen-IV) SFR prototype project called ASTRID (Advanced Sodium Technological Reactor for Industrial Demonstration; Rouault et al., 2015), and the Republic of Korea and Japan proceed in their design of Prototype Gen-IV Sodium-cooled Fast Reactor (PGSFR) and the Japanese sodium-cooled fast reactor (JSFR), respectively (Tae-Ho, 2015; Kamide et al., 2015). The United States is continuing a modular SFR development whereas 4S (Tsuboi et al., 2009), PRISM (Triplett et al., 2012), and travelling wave reactor-prototype (TWR-P) (Hejzlar et al., 2013) are being developed in the industry.

In addition to each country's domestic development project, some international frameworks of bilateral and multilateral cooperation, such as the Generation IV International Forum (GIF) (Gen-IV, 2014a,b), were established by countries conducting fast reactor technology development. Utilizing these international frameworks, each country is promoting the SFR development project while balancing international competition and international cooperation.

In the GIF, the member-states and international organization have recognized the importance of having an international safety design standard or safety design criteria

(SDC). The task force to develop the GIF, SFR, and SDC started the work in 2010 and completed the SDC had been documented and was approved in 2013. Nowadays, safety design guidelines (SDGs) is developed to support practical application of the SDC in the design process for safety improvement (IAEA, 2015).

5.3 System characteristics

5.3.1 Design features with sodium properties

Sodium properties are shown in Table 5.1 (Sodium Technology Education Committee, 2005; JSME, 1986). Sodium is used as a liquid metal coolant for the fast spectrum reactor. It has rather high atomic mass number and good neutronic features. Its neutron cross section is small enough to make a critical system with a fast neutron spectrum. For U-Pu fuel, breeding can be obtained only with a fast neutron spectrum. Using sodium as coolant, the neutron spectrum is hard enough to provide breeding performance with U-Pu fuel. A major radioactive isotope generated by neutron capture is ^{24}Na with a half-life of 15 h. Another radioactive isotope is ^{22}Na with a half-life of 2.58 years. Gamma rays from those isotopes have to be taken care for maintenance.

From the viewpoint of heat transfer, sodium has attractive features such as high boiling point (881°C) and high thermal conductivity. Thanks to these features, the reactor core can be designed with high power density without pressurization. For the power generation, high-temperature dry steam can be provided from sodium-heated steam generators with an operation temperature of approximately 500°C, and a high-performance steam turbine system similar to the one used in subcritical fossil power plant with the dry steam. From a safety point of view, the coolant inventory necessary to submerge the core can be maintained without pressurization in operating

Table 5.1 Sodium and light water properties

Item	Sodium	Light water
Mass number of natural isotope	23	H:1, O:16
Absorption cross section to thermal neutron (0.025 eV)	0.53 b	0.66 b
Total cross section to thermal neutron (0.025 eV)	3.9 b	104 b
Melting point	97.82°C	0°C
Boiling point (at atmospheric pressure)	881.4°C	100°C
Density (liquid) (g/cm^3)	0.856 (400°C)	0.77 (277°C, 15 MPa)
	0.820 (550°C)	0.66 (327°C, 15 MPa)
Thermal conductivity (liquid) (W/cm°C)	0.722 (400°C)	0.005 (327°C, 15 MPa)

and under the accidental conditions because of the high boiling point. The natural circulation capability is excellent because of the high thermal conductivity, high system temperature, and large temperature difference between the core inlet and outlet coolant. Several experimental and prototype reactors succeeded in demonstrating the full natural circulation capability of decay heat removal (Lucoff et al., 1992; Tenchine et al., 2012). Compatibility with structural materials is excellent under the deoxidization condition. Corrosion and surface changes of structural materials can be controlled during the plant lifetime by controlling and monitoring concentration of impurities such as hydrogen and oxygen. On the other hand, chemical features are active. Liquid sodium in the air burns spontaneously in certain conditions and reacts with water, producing hydrogen and heat. Measures for sodium fire and sodium-water reaction should be taken into account in the system design. In maintenance operation, the sodium temperature is maintained at approximately 200°C which is much higher than melting point of 98°C. Because of the high-temperature conditions, chemical reactivity, and liquid metal opaqueness, maintenance on SFRs requires further development of inspection and repair technologies.

5.3.2 Core configurations

Schematic views of the typical core configurations for SFRs are shown in Fig. 5.1. The core consists of core fuel, control rods, blanket fuel, and shields. In general, the core fuel is a mixture of plutonium and depleted uranium. The blanket fuel is depleted uranium. The chemical forms of fuel element, close to its final stage of development, are oxide and metal (U-Pu-Zr alloy). Nitride fuel is also available. The neutron absorber used in control rods is boron carbide (B_4C).

In the core fuel region, fissile nuclides such as ^{239}Pu and ^{241}Pu undergo fission to produce energy and excess neutrons. At the same time, in the core and blanket fuel regions, fertile nuclides such as ^{238}U and ^{240}Pu contribute to the fissile nuclides breeding by efficiently capturing excess neutrons. Compared with the LWRs, the burn-up reactivity change is rather small because of the conversion of fertile nuclides to fissile ones in the core fuel region, which results in the high fuel burn-up and long operation cycle length, and less reactivity control requirement.

A homogeneous core is shown in Fig. 5.1(a). The core fuel region is surrounded by axial and radial blanket fuels so that the leaking neutrons from the core fuel region can be captured efficiently by the blanket fuels. The core fuel region consists of a few (two in most cases) types of fuel with different plutonium enrichments. The outer core fuel has higher plutonium enrichment than that of inner core fuel to flatten the radial power distribution.

A heterogeneous core configuration uses fertile blanket fuels in the core fuel region. There are two types of core design: the axial heterogeneous core and the radial heterogeneous core, as shown in Fig. 5.1(b) and (c), respectively. The neutron leakage from the core fuel region to the internal blanket fuel region is enhanced in these core configurations, which yield higher breeding ratios and reduced sodium void reactivity compared with those of the homogeneous core, but it require higher fissile fuel inventories.

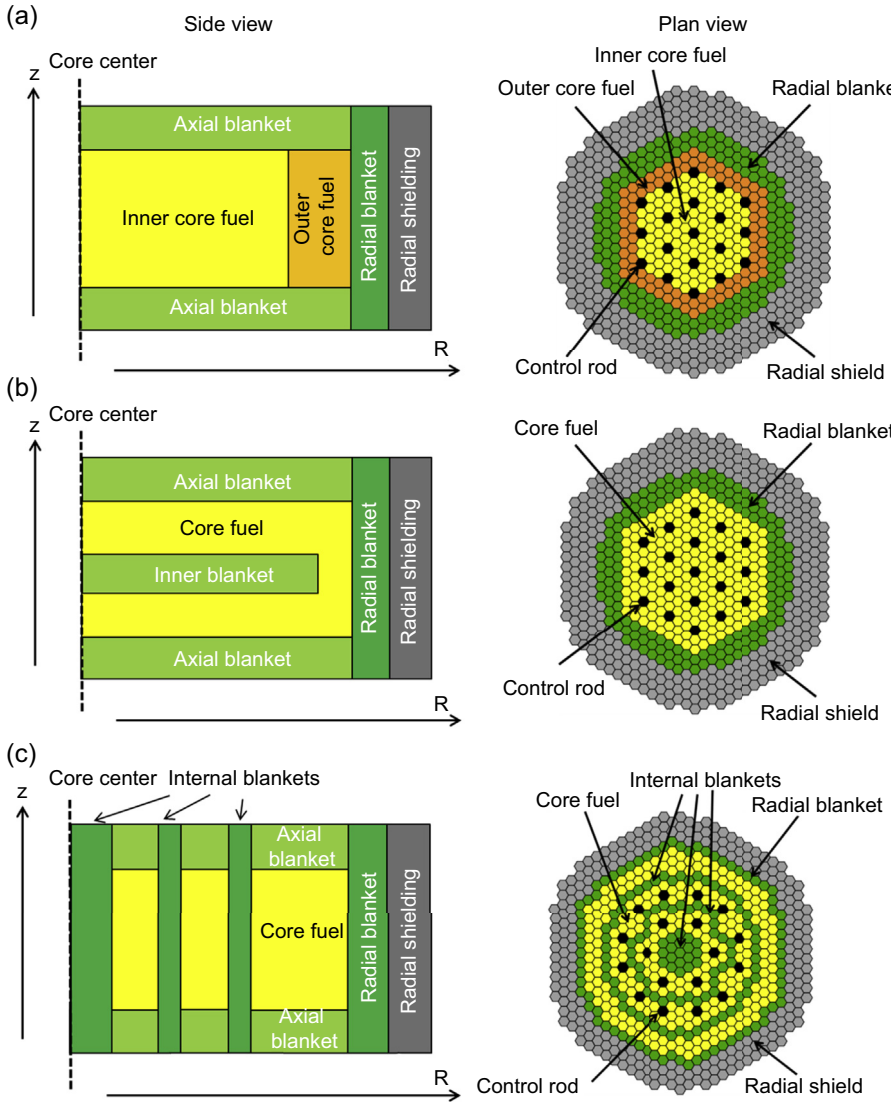


Figure 5.1 Typical homogeneous and heterogeneous sodium-cooled fast reactor core configurations: (a) homogeneous core, (b) axial heterogeneous core, and (c) radial heterogeneous core. All rights reserved by Japan Atomic Energy Agency.

Figure 5.2 shows a typical core fuel element (also called a fuel pin) and fuel assembly (also called a fuel subassembly). The core fuel element contains the core fuel, upper and lower axial blanket fuels, and a space called the fission gas plenum within a cladding tube. Then they are assembled as a fuel element bundle. The fuel assembly contains the fuel element bundle in a hexagonal assembly duct called a wrapper tube.

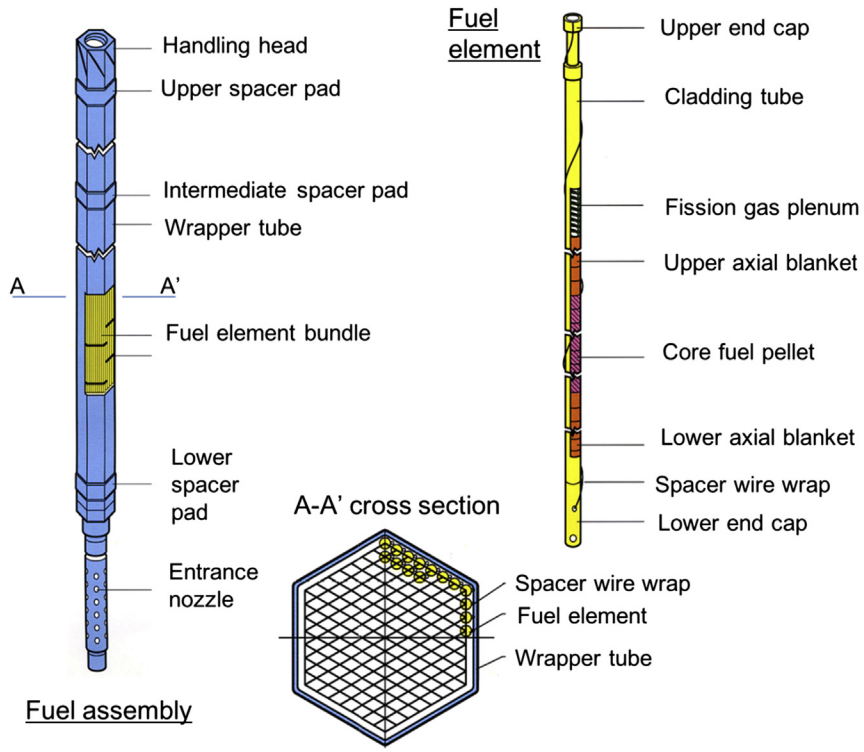


Figure 5.2 Typical sodium-cooled fast reactor core fuel element and fuel assembly.
All rights reserved by Japan Atomic Energy Agency.

The cladding and wrapper tubes are made of high-strength stainless steels that can endure the high-temperature and fast-neutron−irradiation conditions.

The fuel elements are separated by a spiral wrapping wire (alternatively, grid spacers can be used). The sodium coolant flows through the spaces between the fuel elements. The fuel elements are placed in a tight triangular lattice arrangement to maximize the fuel volume fraction for core neutron performances and to minimize the core size for the plant capital cost reduction.

In recent SFR developments, some advanced ideas have been introduced to core conceptual designs. From an economical point of view, Japan and France proposed a large homogeneous core concept with a high internal conversion rate (Mizuno et al., 2005; Buiron et al., 2007). Large-diameter fuel elements were used to increase the internal conversion ratio, which provided a high total fuel burn-up (including core and blanket fuel), a long operation period, and a sufficient breeding ratio with a small amount of blanket.

To enhance safety, France made a decision to adopt an innovative core concept with low sodium void reactivity, called *Coeur à Faible Vidange* (CFV; Sciora et al., 2011). The CFV is an axially heterogeneous core with a stepwise core height and a sodium plenum. This configuration exhibits the multiplier effect on the significant reduction

of sodium void reactivity coefficients. The concept of an upper sodium plenum had been originally proposed by Russia in the 1980s.

Because of the rich neutron economics, the SFR core has large design flexibility. Depending on the requirements of place and time, the core can be designed not only as a breeder but also as a burner. In typical burner-core designs (Languille et al., 1995, Yang et al., 2007), the blanket fuels are eliminated and the plutonium enrichment is increased to reduce the internal conversion ratio by means of, for instance, reducing the core height (pancaking the core shape), introducing diluent material, and so on.

5.3.3 Plant system

Overview of a typical SFR system is shown in Fig. 5.3 (Gen-IV, 2012) and Fig. 5.4. The core is accommodated in the reactor vessel. The reactor vessel is generally composed of a vessel and a plug because of its low-pressure conditions. Sodium generally has a liquid level in the vessel and is covered by inert gas. Sodium-contained components of the SFR including the reactor vessel are designed as thin-walled structures because the major load comes from the thermal stress due to transient temperature change under elevated temperature. Although its internal pressure is not a critical load factor, seismic load can be critical in the design of the components depending on the site condition. A seismic isolation system is useful for SFRs to reduce the seismic load on the sodium-containing components. Most plants adopt guard or safety vessels

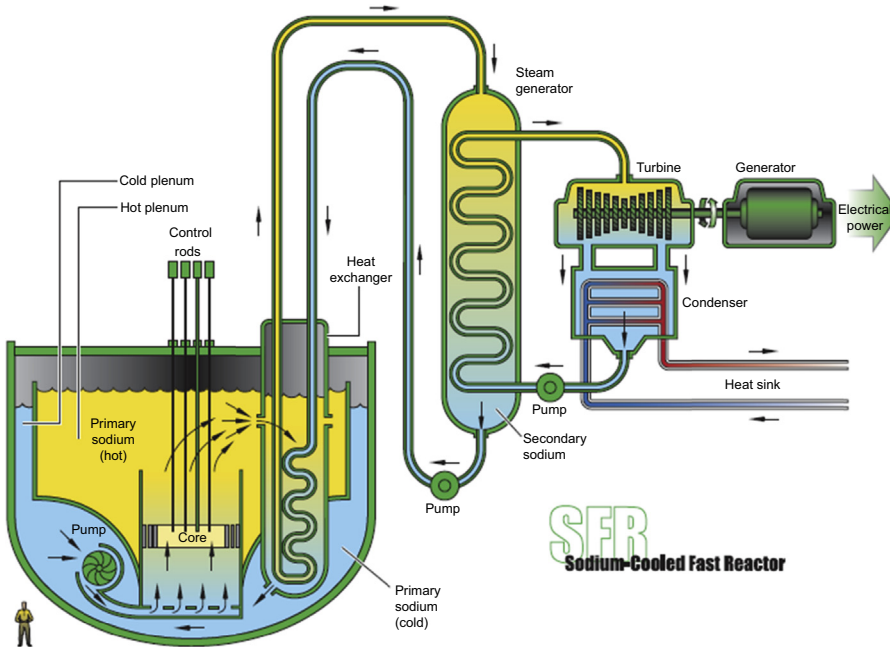


Figure 5.3 Sodium-cooled fast reactor system (pool type).

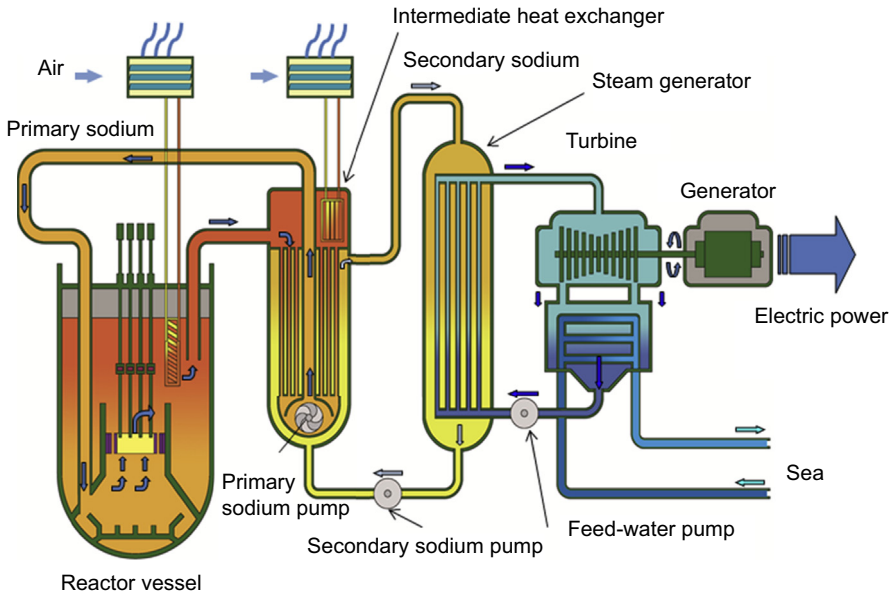


Figure 5.4 Sodium-cooled fast reactor system (loop type).
All rights reserved by Japan Atomic Energy Agency.

outside of reactor vessels that can maintain the sodium level in case of primary sodium leak. The plug is required to have functions of thermal insulation and shielding against high operation temperature and high neutron flux. On the plug, an upper core structure is installed and provides control rod driver line guides and support for core instrumentations. The control rods are inserted from above the core by gravity or other acceleration devices. Because of the chemical reactivity of sodium, fuel handling is generally operated under the plug with special fuel handling machines and rotating plugs. That fuel handling under the plug affects the diameter and height of the reactor vessel.

For the cooling system, there are the primary sodium cooling systems, secondary sodium cooling systems, and steam-water cooling systems. Because SFRs generally use steam turbines for energy conversion, system design has to take care of sodium-water reaction at sodium-heated steam generators. To protect the core from the effects of the sodium-water reaction, a sodium-cooled reactor generally has intermediate cooling systems (secondary cooling systems).

Major components in the primary cooling system are primary pumps and intermediate heat exchangers (IHXs). Primary pumps have redundancy, and mechanical pumps are generally selected. A few experimental reactors selected a single mechanical pump or electromagnetic pumps for the primary system. IHXs transport heat generated in the core from the primary sodium to the secondary one. The shell and tube type with straight tubes is generally used. Supporting the primary cooling system, a primary sodium purification system, a sodium charge-drain system and a cover gas system are required.

A major role of the secondary cooling system is to create dry steam at the sodium-heated steam generators. Because the secondary sodium temperature can be designed at approximately 500°C, the steam conditions can be similar to those of the subcritical fossil power plants and the thermal efficiency is approximately 40%. For the sodium-heated steam generator, several designs were tested as mockups or in the existing reactors (Chikazawa et al., 2008). Recent designs generally select straight or helical coil tube types based on the previous studies. Water is in the tube side and sodium is in the shell side, generally considering pressure conditions and material coexistence. In some designs, steam generators are divided into an evaporator, superheater, and reheater or an evaporator and superheater. Recent designs tendency is an integral type. In some designs, double or triple tubes are selected to prevent or mitigate the sodium-water reaction. For the secondary pump, mechanical pumps were generally selected in the past reactors. Only a few experimental reactors selected electromagnetic pumps. Supporting the secondary cooling system, a secondary sodium purification system, a sodium charge-drain system and a cover gas system are required. Those systems are independent from those of primary systems because the sodium in the primary system is radioactive.

Decay heat could be removed by the steam generators or by installing independent systems cooled by the air. Because of the lower system pressure, an emergency core cooling system such as a coolant injection system required in LWRs is not required. Furthermore, in the case of air cooling systems, because of the sodium features, several experimental and prototype reactors succeeded in demonstrating the full natural circulation capability of decay heat removal.

Because of the chemical reactivity of sodium, the fuel handling system is completely different from that of LWRs. The refueling at the reactor vessel is generally operated under the plug. For the ex-vessel handling system, various types of systems were tested in the past reactors (Chikazawa et al., 2009). For spent fuel transportation, decay heat has to be removed during transportation. Inert gas cooling or sodium pot transportation are generally selected. For the spent fuel storage, in-vessel and/or ex-vessel sodium storages are selected. Spent fuels are washed to remove active sodium and transferred to the secondary nonsodium storage or other facility such as test facilities after being stored under sodium.

Maintenance and repair under high-temperature sodium conditions of approximately 200°C have been taken into account in the plant design. Under sodium viewer or volumetric testing devices in sodium conditions have been proposed and are still under development. Access routes for such testing devices shall be provided in the plant design. Because of the high melting point, sodium heating is required to prevent sodium freeze.

5.3.4 Loop type and pool type

Sodium-cooled reactors could be categorized into two types: loop and pool types (Figs. 5.3 and 5.4). In the loop types, major components in the primary systems are connected by piping. Existing reactors have nozzles on the reactor vessels for the piping. Some advanced designs eliminate nozzles adopting piping through the plug. The pool-type system accommodates major primary components inside of the reactor vessel. Primary pumps and IHXs are located on the reactor vessel plug, and hot and

Table 5.2 Pool- and loop-type reactors in the world

	Pool	Loop
United States	EBR-II	EBR-I, Fermi, SEFOR, CRBR[a], FFTF
United Kingdom	PFR	DFR
France	Phenix, Super-Phenix	Rapsodie
Germany		KNK-II, SNR-300[b]
Russia	BN-600, BN-800	BOR-60, BN-350
India	PFBR	FBTR
China	CEFR	
Japan		Joyo, Monju

CEFR, China experimental fast reactor; *CRBR*, clinch river breeder reactor; *DFR*, dounrey fast reactor; *EBR*, experimantal breeder reactor; *FFTF*, fast flux test facility; *FTBR*, fast breeder test reactor; *SEFOR*, southwest experimental fast oxide reactor.
[a]Terminated during construction.
[b]Terminated before operation.

cold sodium are separated by reactor vessel inner structures. Advantages of the loop type are a compact reactor vessel/structure that can be fabricated in the factory and has better seismic resistance. On the other hand, those of the pool type are large thermal inertia and primary sodium contained by a simple vessel. In the recent comparative studies (USDOE and GIF, 2002; Chikazawa et al., 2011; Francois et al., 2008; Devictor et al., 2013), both concepts are technologically feasible and meet design goals. Adopting innovative cost-reduction technologies, the loop type shows slightly lower construction cost. Table 5.2 shows past and existing pool- and loop-type reactors in the world. Many experimental and prototype reactors chose the loop type. From the viewpoint of operational experiences in the prototype class, BN-350 had operational experiences and Monju is the only existing reactor as the loop prototype because CRBR and SNR-300 were terminated before operation. For the pool type, PFR, Phenix, and BN-600 accumulated operational experiences. BN-600 is still in operation and PFBR and BN-800 have started operation. As the next-generation reactors, PRISM, ASTRID, BN-1200, and PGSFR have selected the pool type. JSFR has adopted the loop type, reducing construction cost with innovative technologies.

5.3.5 Consistency with fuel cycle system (fuel cycle technology)

Fuel cycle studies showed that SFRs can contribute to the worldwide sustainable development with assurance of stable energy sources and consideration of environmental destruction issues. Currently operating LWRs with low-enriched uranium containing 3−5% of ^{235}U utilize only less than 2% of the natural uranium energy potential. Depending on the available resources and prices of natural uranium, the nuclear energy utilization of only ^{235}U has a possibility to face the limitations in approximately

100 years. However, the nuclear fuel recycling with SFRs can produce more than 50 times energy as compared to that of LWRs from the same quantity of natural uranium. This means that SFRs potentially extend the uranium resources by several thousands of years. Moreover, the SFR technology is essential not only as an energy supply but also as the prevention of greenhouse gas emission, thus it will be one of the important future energy source available for the long term global development.

Many studies discussed the timing for the deployment of the commercial SFR and the transition strategies from LWRs to SFRs (Walter et al., 2012; CEA, 2012a). LWRs have already converted (and will convert) some ^{238}U to plutonium in their operation. There already exists enough ^{238}U as depleted uranium from the uranium enrichment process. Therefore the introduction of SFRs seems consistent with the current LWR system in terms of the nuclear material supply. The breeding ratio necessary for SFRs is estimated as 1.0−1.2 and more depending on the deployment scenarios.

Another benefit for the SFR fuel cycle system is the reduction of environmental burden by recycling all actinide nuclides and partitioning selected fission products (FPs). The spent fuel contains minor actinides (MAs; ie, neptunium, americium, curium, etc.) as well as uranium and plutonium. In the conventional nuclear fuel cycle, those MAs and FPs are disposed of in a deep geological repository as high-level radioactive wastes. Because of the long-lived radioactive MAs such as ^{241}Am (half-life: 433 years) and ^{237}Np (half-life: 2.1 million years), it takes several hundred thousand years to reduce the radiotoxicity of high-level radioactive waste to the level of natural uranium.

Therefore the partitioning and transmutation approach has been studied in several SFR developing countries. SFRs are excellent in its neutronic characteristics for the capability of using MAs as the nuclear energy resources and the resulting MA minimization in the closed fuel cycle. The recycling of plutonium and MAs makes great contributions to the reduction of radiotoxicity in the waste: studies showed that it can shorten the duration to bring it into the natural uranium level down to only a few hundred years. Moreover, the high-level waste volume and necessary repository area can be reduced by removing not only the heat source nuclides such as ^{241}Am but also some influential FPs on the strength of vitrified wastes.

Note that the radiotoxicity reduction strongly depends on the nuclide losses during reprocessing. The following high-level development target is pursued in most of development projects (Sato, 2005; CEA, 2012b): the reprocessing losses of plutonium and MAs are less than 0.1%.

The high decay heat and radioactivity of MA-bearing fuel have a large influence on the fuel fabrication, transportation, and handling, which gives many development challenges to the fuel cycle system.

5.4 Safety issues

5.4.1 Safety design criteria and safety design guidelines

For LWRs, the International Atomic Energy Agency (IAEA) established comprehensive and systematic safety standards that consist of safety fundamentals

(IAEA, 2006), requirements (IAEA, 2012), and guides (IAEA, 2004a,b, 2005). The GIF has developed safety principles for the next-generation nuclear energy systems that are safety goals under the GIF technology roadmap (USDOE and GIF, 2002) and the basis for the safety approach (RSWG-GIF, 2008). These documents correspond to the upper level of the IAEA safety standards, whereas there are no documents corresponding to safety requirements and guides for Gen-IV reactors on the basis of international consensus.

SFRs are one of the most promising reactors and are expected to enter the demonstration phase sometime after 2020 (GIF, 2014a,b). Gen-IV SFR prototype/demonstration reactors are progressing into the conceptual design stage for future licensing applications. It is therefore indispensable to establish internationally harmonized safety design requirements/criteria for the realization of enhanced safety designs common to different SFR systems. With this background the development of SDC for SFRs, corresponding to the IAEA SSR-2/1, was initiated in 2011. The objective of this SDC is to provide reference criteria of the safety approach, mainly focusing on specific criteria to the fast spectrum reactor and the sodium coolant.

The Fukushima Daiichi nuclear power plant accident has emphasized the importance of designing nuclear systems with a higher level of safety than existing reactors. Lessons learned from the accident have been reflected in the SDC, in particular indicating the need for reliable decay heat removal over long periods as well as the necessity of enhancing design measures against external hazards. Taking SFR characteristics into account, the SDC was introduced to enhance safety measures against severe accidents by utilizing inherent and passive safety features. SFR safety experts developed the SDC report (Phase 1) in May 2013, and this report was referred to as the basic document for discussions between the GIF and the IAEA/INPRO (The International Project on Innovative Nuclear Reactors and Fuel Cycles) in terms of developing the international safety standardization (Nakai, 2015). Since then, external reviews of this report have been performed by regulatory authorities of the GIF-SFR member countries and the IAEA, etc. (Okano et al., 2014).

During the development, the GIF-SDC developers suggested to establish more detailed guidelines, which correspond to the IAEA safety guides, to support practical application of the SDC and to discuss further specific items, such as practically eliminated accident conditions. Since May 2013 the GIF-SFR members have been developing SDGs (Nakai, 2014). In the early stage of SDG development, the SDG on safety approach and design conditions are developed to be used as a supplementary technical document for SDC clarification in 2015. In the latter stage, the SDG on the key structures, system, and components will be developed by around 2016.

5.4.2 Safety characteristics and safety design

Each country has also been making efforts on the design study and also on R&D of SFR systems to enhance the safety depending on the safety characteristics and to satisfy the high safety demands required by the SDC.

5.4.2.1 Reactor shutdown

An SFR is operated under a critical condition with fast neutrons using liquid sodium as the reactor coolant, allowing high power density. Positive reactivity insertion might happen because of fuel compaction in the degraded core because the core is usually not designed in the most critical configuration. Although the sodium void reactivity depends on the core size and design, it is generally positive at the center of the core in a large-sized core. Active shut-down systems are provided in the existing SFR designs with diversity so that core damage caused by a design-basis accident can be prevented. To further improve the safety of SFRs, a passive shut-down mechanism or inherent negative reactivity feedback or their combination is considered as one of the core damage prevention measures even under active shut-down system failure. The effect of the inherent reactivity feedback for the mitigation of power increase has been demonstrated in EBR-II and Rapsodie (Lucoff et al., 1992), and its related R&D is undertaken for reactor application. As for the metal fuel core, R&D is underway to investigate the inherent reactivity characteristics with negative reactivity effects due to thermal expansions of control rod drive lines and fuel assemblies (Chang, 2011; Tae-Ho, 2015). For example, core designs with an upper sodium plenum and heterogeneous configuration are currently being developed for an intermediate to large-sized reactor with an oxide or nitride fuel core so as to make an effective coolant temperature reactivity coefficient negative or zero (Verrier et al., 2013; Chebeskov, 1996; Vasyaev et al., 2015). Passive reactor shut-down systems that utilize a Curie-point magnetic alloy (Nakanishi et al., 2010), thermal expansion, and hydraulic force change (Alexandrov et al., 1996; Dufour, 2015) for automatic delatching/insertion of control rods under loss of flow, and that increase neutron leakage by gas expansion under a flow reduction condition in pipes filled with gas, are under development (Triplett et al., 2012).

5.4.2.2 Decay heat removal

The large temperature margin to sodium boiling (the boiling point is 880°C, the melting point is 98°C in atmospheric pressure) enables the reactor operation in a wide range without pressurization of the reactor coolant systems. High thermal conductivity of sodium provides heat removal from the core with high power density. Because an SFR is operated at low pressure, depressurization caused by a sodium leakage accident does not lead to loss of coolant due to flashing. Therefore it enables to maintain the coolant level for reactor cooling by providing back-up structures that can retain leaked sodium as of the coolant boundary. Moreover, decay heat removal can be achieved by its natural circulation capability to an ultimate heat sink (atmosphere) utilizing the high heat transport capability and temperature difference between the core inlet and outlet coolant. These safety features had been adopted into the design since its experimental stage, then Joyo (Sawada et al., 1990) and Phenix (Guidez, 2013) have demonstrated the natural circulation capability. In addition, an SFR with the primary and secondary systems (sodium) together with the tertiary system (water/steam) allows various combinations of diversified systems because of its flexibility in items such as types of heat exchangers and the installation locations. For practical elimination of accident situations that result

in core damage from a complete loss of decay heat removal function, a cooling system design is pursued to maintain its function against extreme internal and external hazards using an appropriate combination of redundancy and/or diversity of systems and the natural circulation function (Kubo and Shimakawa, 2015; Tae-Ho, 2015; Dufour, 2015; Triplett et al., 2012).

5.4.2.3 Design measure against sodium chemical reactions

Typical influences of accidental sodium chemical reactions in SFRs are possible interruption of safety functions such as decay heat removal due to leaked sodium combustion in air and possible damage to the secondary sodium cooling system, especially on the boundary between the primary and the secondary sodium cooling system in IHX, because of the sodium-water reaction induced by heat transfer tube failure in a steam generator.

Several sodium combustion experiments have been conducted to understand the consequences and phenomenology, and analysis tools have been developed in various countries (Cherdron, 1996; Malet, 1996; Olivier et al., 2007, 2008; Yamaguchi et al., 2001; Ohno et al., 2012; Sathiah et al., 2014; Chikazawa et al., 2014). Sodium leak events experienced in the plant operation gave feedbacks on the design, manufacturing, and operation. For the prevention of sodium leak, simple design with less branching or fewer connection pipes should be pursued. Early detection of leak and mitigation of sodium combustion are important. For the mitigation, a guard vessel and a guard pipe are feasible to suppress leakage and combustion (Yamano et al., 2012). Sodium components and pipes are installed in the room which is filled with inert gas such as nitrogen, and steel liner is also provided for another design measures to mitigate sodium chemical reactions to prevent leaked sodium from contacting the floor or wall concrete.

Design measures have been developed based on the operational experiences of past and current SFRs and the relevant R&D. When a water leak happens at a steam generator, a corrosive sodium-water product jet is generated in the shell side and attacks other tubes. Because the sodium-water reaction accompanies hydrogen and heat generation, it also causes pressure elevation. Prevention and mitigation of sodium-water reaction are important in the sodium-heated steam generator design. For the steam generator leak protection, systems of leak detection, steam blow down, and pressure relief are installed. Rupture disks located in the sodium side of the steam generator passively burst by pressure increase due to the sodium-water reaction. The rupture disks are connected with the sodium-water reaction product treatment system. Because steam generators becomes larger in size as the plant power increases (Vasyaev et al., 2015), higher sensitivity for the detection systems and quicker response for the mitigation systems will be required for the future SFRs (Hune et al., 2015). Analysis tools for the sodium-water reaction, which can simulate complicated coupling of thermal hydraulics, chemical reaction, and structural response, have been developed (Takata et al., 2009). A double-walled tube is a possible measure for prevention and mitigation of the sodium-water reaction (Enuma et al., 2015). A gas turbine system is considered for elimination of the sodium-water reaction (Cachon et al., 2012).

5.4.2.4 Containment measures

By means of above-mentioned design measures, core damage can be prevented even under plant conditions beyond the design-basis accidents. However, consequences of core damage are evaluated, and design measures are provided from the viewpoint of defense-in-depth. Typical initiating events that might result in core damage situations are unprotected transients for SFRs (Walter et al., 2012). In a loss of flow type unprotected transient, the reactivity effect comes from coolant boiling characterized by the power change at the beginning, the so-called "initiating phase." The degree of the power increase depends on the core reactivity characteristics, including coolant void reactivity. Although the coolant void reactivity is positive, there are competitive negative reactivity effects such as Doppler, axial expansion of intact fuel, and failed fuel dispersion. Thus prompt criticality can be prevented. It is reported that the limit value for oxide fuel cores is approximately \$6 to prevent prompt criticality (Suzuki et al., 2014). Such kind of evaluations are made by analysis tools based on the experimental data related to fuel pin failure and failed fuel behavior obtained in the safety research reactors such as CABRI and Transient Reactor Test Facility (Nonaka and Sato, 1992; Kayser and Papin, 1998; Bauer et al., 1990; Weber, 1988). The subsequent accident phase is called the "transition phase," in which core damage progression depends on the extent of core damage in the initiating phase, net reactivity, power, and the cooling conditions. In case of insufficient cooling, degraded core materials greatly increase its mobility as core melt escalates due to wrapper tube failure and molten materials such as fuel and steel. According to analyses for oxide fuel cores, severe re-criticality might happen because of mobile fuel compaction under certain conditions (Kondo et al., 1992; Maschek and Asprey, 1983; Maschek et al., 1992; Yamano et al., 2008; Bachrata et al., 2015). The core expansion due to massive fuel vaporization, causing significant pressure load on the reactor vessel and reactor roof via the surrounding liquid sodium, might happen when the re-criticality event is so severe. Therefore prevention of such excess energy release due to re-criticality and maintaining reactor and cover gas boundary function are important. As a design measure to prevent severe re-criticality under core degradation, core designs with steel duct structures for molten fuel discharge are developed (Suzuki et al., 2014; Dufour, 2015). On the other hand, the structural response of the reactor vessel and reactor roof to the core expansion has been studied using scale models (Chellapandi et al., 2013; Nakamura et al., 2004). Sodium inside of the reactor vessel is useful to cool the degraded core. Because sodium has retention capability of radioactive materials in the core, it is desirable to submerge the core even in the case of core damage. Design measures to achieve in-vessel retention have been developed (Suzuki et al., 2014; Dufour, 2015; Osipov et al., 2013).

5.5 Future trends and key challenges

Technology and experience have been accumulated from actual reactor plant design, construction, and operation throughout the long development history of SFRs and now

it has reached the technical maturity to move toward the demonstration phase to realize the sustainable energy supply system. R&D is moving on to the important aspects in realizing closed fuel cycle as sustainable energy supply system; excel in safety and reliability, economic competitiveness, minimizing radioactive waste and radiotoxicity, and proliferation resistance and physical protection.

The basic safety design technology has been established through the history of the design, construction, and operation of SFRs, and the next step is to adopt new design features for reactor shutdown/cooling utilizing inherent characteristics or a passive mechanism. The design with a combination of conventional active safety features and inherent characteristics or passive mechanisms is pursued so that the core degradation is extremely unlikely to occur even though the design extension conditions and the design bases accidents are taken into account. Furthermore, the mitigation measures against core degradation are investigated and evaluation and design measures are studied to achieve in-vessel retention and cooling of the degraded core material by taking advantage of the sodium physical properties and the low system pressure. The following R&D activities are held in GIF (Gen-IV, 2014a).

Inherent safety features:

- Safety principles (reactivity feedback, core design goals, balanced safety approach),
- Passive or self-actuated shut-down system,
- Decay heat removal options (short and long term),
- Reactor transient behavior and testing experience, and
- Severe accident prevention.

Severe accident mitigation:

- Experiments on fuel melting behavior,
- Specialized fuel assembly design for severe accident behavior (eg, sacrificial inner duct), and
- Core catcher options.

Safety analysis tools:

- Validation and uncertainty quantification,
- Severe accident modeling, and
- Probabilistic safety assessment techniques.

Lessons learned from the Fukushima Daiichi nuclear power plant accident (AESJ, 2015) should be reflected so that sufficient countermeasures are provided for a severe external event or possible multiple events and possible subsequent events such as long-term loss of external power. Seismic isolation is effective in enhancing the structural design margin against earthquakes; for instance, a combination of laminated rubber bearings and the hydraulic dampers are developed as a seismic isolation system for the reactor building. Natural convection is a possible effective measure for decay heat removal against the long-term loss of external power. Electrical equipment important to safety should be protected against floods or tsunamis to avoid the failure as in an LWR. In addition, the area where the sodium-containing facility

is installed also needs countermeasures against flooding. Key issues in GIF are as follows (Gen-IV, 2014a):

- Robust and highly reliable systems for adequate cooling of safety-relevant components and structures,
- Geometric stability of the SFR core in case of a strong earthquake and assurance of reliable performance of the control rods,
- Seismic-resistant design of the spent fuel pools and fuel-handling devices,
- Integrity of the primary circuit and its cooling,
- Design features aimed at the risk aversion of the flooding of the reactor building, and
- Effective options for dealing with severe accidents.

Major factors for the improvement of economic competitiveness are capital cost, capacity factor, and fuel cost. One approach is to reduce construction cost-per-unit power generation (ie, increasing plant output while simplifying and making compact structures, systems, and components; Kotake et al., 2010). Extension of the plant lifetime (eg, to 60 years) is also effective in reducing the capital cost. Hence, manufacturing technology for the large components and their functional demonstration, adoption of new material such as ^{9}Cr steel, and advanced codes and standards on the design and construction have considerable attention. On the other hand, small modular reactors have another cost reduction potential through R&D cost and the manufacturing cost reductions by mass production (Triplett et al., 2012). These small modular reactors will be suitable for the small energy demand in the remote location. Longer operation cycle length and shorter maintenance period are desirable to achieve a higher capacity factor. Because the longer operation cycle length means higher burn-up, fuel cost reduction is also achievable. More than 2 years of continuous operation is possible for SFRs by making the core designed with a higher conversion ratio for its driver fuels. Because the cooling system of SFRs is kept under a deoxidization atmosphere, stress corrosion cracking is not a concern. However, technology development for inspection and repair is important because the cooling system is filled with high-temperature opaque chemically active liquid sodium. Shortened refueling time and the reliability improvement are important for the fuel-handling systems because of their remote operation under sodium. Appropriate consideration is required in handling MA-bearing fuel for slow decay heat attenuation of spent fuel and heat generation of new fuel.

Conventional SFR power conversion is made by steam turbine system connected to the secondary sodium cooling system. Water leaks in the heat transfer tube of the steam generator often became a decreasing capacity factor (Guidez, 2013). Hence gas turbine power conversion systems using supercritical carbon dioxide or nitrogen and steam generators using double-walled tubes are studied. In these fields the following R&D are in progress in GIF (Gen-IV, 2014a):

- Reduced duration of fuel loading outage through improvement of fuel-handling systems,
- Increased fuel burn-up and cycle length,
- Improved instrumentation for detection and localization of sodium leaks,

- Improved In Service Inspection and Repair capabilities, which play a key role in SFR operation (due to the opaqueness and elevated temperature of the sodium coolant), through advanced instrumentation (ultrasonic techniques, robotics),
- Extended plant lifetime to 60 years, comparable to current Generation III/III + reactors, through
  - Development and qualification of materials with enhanced resistance to aging degradation and
  - Development of improved inspection and diagnostic capabilities for verifying fitness of materials and structures for continued service,
- Codes and standards—such as the RCC-MRx code in Europe or the new ASME Section III, Division 5, which provides design and construction rules for mechanical components such as vessel, piping, and support structures (core excluded).

One of the important roles of SFRs is to contribute to minimizing radioactive waste and radiotoxicity in addition to the effective utilization of uranium resources by the establishment of a closed fuel cycle. R&D has been performed for MA-bearing fuel manufacturing, irradiation, and handling. In addition, cladding tube material such as ODS steel (Kaito et al., 2013; Logé et al., 2013) has been developed aiming for high burn-up more than 150 GWD/t. There has been R&D related to SFR core design with MA-bearing fuel in which an effective loading method of MA is investigated taking into account the influence on the fuel property and core nuclear characteristics (eg, homogeneous loading to driver fuel and loading to the blanket fuel).

References

AESJ, 2015. The Fukushima Daiichi Nuclear Accident Final Report of the AESJ Investigation Committee. Springer. http://dx.doi.org/10.1007/978-4-431-55160-7.

Alexandrov, Yu.K., Rogov, V.A., Shabalin, A.S., 1996. Main features of the BN-800 passive shutdown rods. In: Absorber Materials, Control Rods and Designs of Shutdown Systems for Advanced Liquid Metal Fast Reactors Proceedings of a Technical Committee Meeting Held in Obninsk, Russian Federation, 3–7 July 1995, IAEA TECDOC 884. IAEA, Vienna.

Aoto, K., Dufour, P., Hongyi, Y., Glats, J.P., Kim, Y.I., Ashurko, Y., Hill, R., Uto, N., 2014. A summary of sodium-cooled fast reactor development. Progress in Nuclear Energy 77, 247–265.

Bachrata, A., Bertrand, F., Lemasson, D., 2015. Unprotected loss of flow simulation on ASTRID CFV-V3 reactor core. In: Proceedings of ICAPP 2015, May 03–06, 2015-Nice (France) Paper 15356.

Bauer, T.H., Wright, A.E., Robinson, W.R., Holland, J.W., Rhodes, E.A., 1990. Behavior of modern metallic fuel in TREAT transient overpower tests. Nuclear Technology 92, 325.

Buiron, L., Dufour, Ph., Rimpault, G., Prulhiere, G., Thevenot, C., Tommasi, J., Varaine, F., Zaetta, A., 2007. Innovative core design for generation IV sodium-cooled fast reactors. In: Proceedings of ICAPP 2007, May 13–18, 2007, Nice, France.

Cachon, L., Biscarrat, Ch, Morin, F., Haubensack, D., Rigal, E., Moro, I., Baque, F., Madeleine, S., Rodriguez, G., Laffont, G., 2012. Innovative power conversion system for the French SFR prototype, ASTRID. In: Proceedings of ICAPP'12, Chicago, USA, June 24–28, 2012, Paper 12300.

Cacuci, D.G. (Ed.), 2010. Handbook of Nuclear Engineering, vol. 4. Springer.

CEA, 2012a. Rapport sur la gestion durable des matières nucléaires. http://www.cea.fr/energie/rapport-sur-la-gestion-durable-des-matieres-nucl-106009.

CEA, 2012b. Rapport sur la gestion durable des matières nucléaires. Séparation-transmutation des éléments radioactifs à vie longue, Vol. 2. p. 24. http://portail.cea.fr/multimedia/Documents/publications/rapports/rapport-gestion-durable-matieres-nucleaires/Tome%202.pdf.

Chang, W.P., Kwon, Y.M., Jeong, H.Y., Suk, S.D., Lee, Y.B., February 2011. Inherent safety analysis of the KALIMER under a LOFA with a reduced primary pump halving time. Nuclear Engineering Technology 43 (1).

Chebeskov, A.N., 1996. Evaluation of sodium void reactivity on the BN-800 fast reactor design. Physor 2, C-49.

Chellapandi, P., Srinivasan, G.S., Chetal, S.C., 2013. Primary containment capacity of prototype fast breeder reactor against core disruptive accident loadings. Nuclear Engineering and Design 256, 178–187.

Chellapandi, P., 2015. Status of PFBR. In: 5th Joint IAEA-GIF TM/WS on Safety of SFR, IAEA, Vienna, June 23–24, 2015.

Cherdron, W., 1996. Review of the Sodium Fire Experiments including Sodium-concrete-reactions and Summary of the Results, IAEA/IWGFR Technical Committee Meeting on Evaluation of Radioactive Materials Release and Sodium Fires in Fast Reactors. O-arai, Ibaraki, Japan, Nov. 11–14, 1996, IWGFR/92, pp. 39–48

Chikazawa, Y., Famer, M., Grandy, C., 2008. Technology gap analysis on sodium-heated steam generators supporting advanced burner reactor development. Nuclear Technology 164, 410–432.

Chikazawa, Y., Famer, M., Grandy, C., 2009. Technology gap analysis on sodium-cooled reactor fuel-handling system supporting advanced burner reactor development. Nuclear Technology 165, 270–292.

Chikazawa, Y., Kotake, S., Sawada, S., 2011. Comparison of advanced fast reactor pool and loop configurations from the viewpoint of construction cost. Nuclear Engineering and Design 241, 378–385.

Chikazawa, Y., Katoh, A., Yamamoto, T., Kubo, S., Iwasaki, M., Hara, H., Shimakawa, Y., Sakaba, H., 2014. Performance Evaluation on Secondary Sodium Fire Measures in JSFR. In: Proceedings of ICAPP 2014, April 6–9, 2014, Paper 14106, Charlotte, USA.

Devictor, N., Chikazawa, Y., Saez, M., Rodriguez, G., Hayafune, H., 2013. R&D in support of ASTRID and JSFR: cross-analysis and identification of possible areas of cooperation. Nuclear Technology 182 (2), 170–186.

Dufour, P., 2015. Status of the ASTRID project. In: 5th Joint IAEA-GIF TM/WS on Safety of SFR, IAEA, Vienna, June 23–24, 2015.

Enuma, Y., Kawasaki, N., Orita, J., Eto, M., Miyagawa, T., 2015. JSFR design progress related to development of safety design criteria for generation IV sodium-cooled fast reactors (3). Progress of component design. In: 23rd International Conference on Nuclear Engineering, Paper 1492, May 17–21, 2015, Chiba, Japan.

Francois, G., Serpantie, J.P., Sauvage, J.F., Lo Pinto, P., Saez, M., June 2008. Sodium fast reactor concepts. In: Proceedings of ICAPP'08, Paper 8096, Anaheim, CA, USA.

Generation IV International Forum, 2012. A Technology Roadmap for Generation IV Nuclear Energy Systems. GIF-002-00. DOE, U.S.

Generation IV International Forum, 2014a. Technology Roadmap Update for Generation IV Nuclear Energy Systems. GIF-002-00. OECD Nuclear Energy Agency, Paris.

Generation IV International Forum, 2014b. Annual Report 2014. OECD Nuclear Energy Agency, Paris.

Guidez, J., 2013. Phenix the Experience Feedback. EDP Sciences, ISBN 979-10-92041-04-0.

Hejzlar, P., et al., November 2013. Terrapower, LLC Traveling Wave Reactor Development Program Overview. Nuclear Engineering and Technology 45 (6), 731–744.

Hune, A.W., Gerber, A., Pirus, J.P., Soucille, L., 2015. ASTRID SFR prototype steam generator design evolution related to safety and cost issues. In: Proceedings of ICAPP 2015, May 03–06, 2015-Nice (France) Paper 15236.

IAEA, 1998. Unusual Occurrences During LMFR Operation. IAEA-TECDOC-1180.

IAEA, 2004a. Design of Reactor Containment Systems for Nuclear Power Plants Safety Guide. Safety Guides No. NS-G-1.10. International Atomic Energy Agency, Vienna.

IAEA, 2004b. Design of the Reactor Coolant System and Associated Systems in Nuclear Power Plants, Safety Guide. Safety Guides No. NS-G-1.9. International Atomic Energy Agency, Vienna.

IAEA, 2005. Design of the Reactor Core for Nuclear Power Plants Safety Guide. Safety Guides No. NS-G-1.12. International Atomic Energy Agency, Vienna.

IAEA, 2006. Fundamental Safety Principles. Safety Fundamentals No. SF-1. International Atomic Energy Agency, Vienna.

IAEA, 2007. Liquid Metal Cooled Reactors: Experience in Design and Operation. IAEA-TECDOC-1569.

IAEA, 2012. Safety of Nuclear Power Plants: Design. Specific Safety Requirements No. SSR2/1. International Atomic Energy Agency, Vienna.

IAEA, 2015. Fifth joint IAEA-GIF technical meeting/workshop on safety of sodium-cooled fast reactors terms of reference. In: 5th Joint IAEA-GIF TM/WS on Safety of SFR, IAEA, Vienna, June 23–24, 2015.

JSME, 1986. JSME Data Book: Heat Transfer, fourth ed. Japan Society of Mechanical Engineering.

Kaito, T., Ohtsuka, S., Yano, Y., Tanno, T., Yamashita, S., Ogawa, R., Tanaka, K., 2013. Irradiation Performance of Oxide Dispersion Strengthened (ODS) Ferritic Steel Claddings for Fast Reactor Fuels. FR'13, paper CN-199-252.

Kamide, H., Ando, M., Ito, T., 2015. JSFR design progress related to development of safety design criteria for generation IV sodium-cooled fast reactors (1). Overview. In: 23rd International Conference on Nuclear Engineering, Paper 1666, May 17–21, 2015, Chiba, Japan.

Kayser, G., Papin, J., 1998. The reactivity risk in fast reactors and the related international experimental programmes CABRI and SCARABEE. Progress in Nuclear Energy 32, 631–638.

Kondo, S., Tobita, Y., Morita, K., Shirakawa, N., 1992. Simmer-III: an advanced computer program for LMFBR severe accident. In: ANP'92, Tokyo, Japan (1992) October 25–29, No 40–5.

Kotake, S., Sakamoto, Y., Mihara, T., Kubo, S., Uto, N., Kamishima, Y., Aoto, K., Toda, M., 2010. Development of advanced loop-type fast reactor in Japan. Nuclear Technology 170, 133–147.

Kubo, S., Shimakawa, Y., 2015. JSFR design progress related to development of safety design criteria for generation IV sodium-cooled fast reactors (2). Progress of safety design. In: 23rd International Conference on Nuclear Engineering, Paper 1748, May 17–21, 2015, Chiba, Japan.

Languille, A., Gamier, J.C., Lo Pinto, P., Na, B.C., Verrier, D., Deplaix, J., Allan, P., Newton, T., Sunderland, R.E., Kiefhaber, E., Maschek, W., Struwe, D., 1995. CAPRA core studies the oxide reference option. In: Proceedings of Global 1995, September 11–14, 1995,Versailles, France.

Logé, R.E., Toualbi, L., Vanegas-Marques, E., de Carlan, Y., Mocellin, K., 2013. Optimization of the Fabrication Route of Ferritic/Martensitic ODS Cladding Tubes: Metallurgical Approach and Pilgering Numerical Modeling. FR'13, paper CN-199-380.

Lucoff, D.M., Walter, A.E., Sackett, J.I., Salvatores, M., Aizawa, K., October 1992. Experimental and design experience with passive safety features of liquid metal reactors. In: Proceedings of ANP'92, Tokyo, Japan.

Malet, J. C., 1996. Ignition and Combustion of Sodium − Fire Consequences − Extinguishment and Prevention, IAEA/IWGFR Technical Committee Meeting on Evaluation of Radioactive Materials Release and Sodium Fires in Fast Reactors, O-arai, Ibaraki, Japan, Nov. 11−14, 1996, IWGFR/92, pp. 13−37

Maschek, W., Asprey, M.W., 1983. Simmer-II recriticality analyses for a homogeneous core of the 300-Mwe class. Nuclear Technology 63, 330.

Maschek, W., Munz, C.D., Meyer, L., 1992. Investigation of sloshing motions in pools related to recriticalities in liquid-metal fast breeder reactor core meltdown accidents. Nuclear Technology 98, 27.

Mizuno, T., Ogawa, T., Naganuma, M., Aida, T., 2005. Advanced oxide fuel core design study for SFR in the "feasibility study" in Japan. In: Proceedings of Global 2005, October 9−13, 2005, Tsukuba, Japan.

Nakai, R., 2014. GIF-sdc phase 2 activity status of the safety design guideline (SDG) development. In: 4th GIF-IAEA Workshop on Safety of SFR, Vienna, June 10−11.

Nakai, R., 2015. RSWG and SFR SDC TF progress update. In: 9th GIF-IAEA/INPRO Interface Meeting, Vienna, March 4−5.

Nakamura, T., Kaguchi, H., Ikarimoto, I., Kamishima, Y., Koyama, K., Kubo, S., Kotake, S., 2004. Evaluation method for structural integrity assessment in core disruptive accident of fast reactor. Nuclear Engineering and Design 227, 97−123.

Nakanishi, S., Hosoya, T., Kubo, S., Kotake, S., Takamatsu, M., Aoyama, T., Ikarimoto, I., Kato, J., Shimakawa, Y., Harada, K., 2010. Development of passive shutdown system for SFR. Nuclear Technology 170, 181−188.

Nonaka, N., Sato, I., 1992. Improvement of evaluation method for initiating-phase energetics based on CABRI-1 in-pile experiments. Nuclear Technology 98, 54−69.

Ohno, S., Ohshima, H., Tajima, Y., Ohki, H., 2012. D Development of PIRT and Assessment Matrix for Verification and Validation of Sodium Fire Analysis Codes. Journal of Power and Energy Systems 6 (2), 241−254.

Okano, Y., Nakai, R., Kubo, S., 2014. International reviews on safety design criteria and development of safety design guidelines for generation-IV sodium-cooled fast reactors. In: The Ninth Korea-Japan Symposium on Nuclear Thermal Hydraulics and Safety (NTHAS9), Buyeo, Korea, November 16−19, Keynote Lecture 1.

Olivier, T.J., Blanchat, T.K., Dion, J.A., Hewson, J.C., Nowlen, S.P., Radel, R.F., 2008. Metal Fire Implications for Advanced Reactors. Part 2: PIRT Results. SANDIA REPORT SAND 2008−6855.

Olivier, T.J., Radel, R.F., Nowlen, S.P., Blanchat, T.K., Hewson, J.C., 2007. Metal Fire Implications for Advanced Reactors. Part 1: Literature Review. SANDIA REPORT SAND 2007−6332.

Osipov, S.L., Rogozhkin, S.A., Sobolev, V.A., Shepeleva, S.F., Kozhaev, A.A., Mavrin, M.S., Ryabov, A.A., 2013. Analytical and Experimental Study for Validation of the Device to Confine BN Reactor Melted Fuel. FR'13, paper CN-199-374.

Rouault, J., Abonneau, E., Settimo, D., Hamy, J.M., Hayafune, H., Gefflot, R., Benard, R.P., Mandement, O., Chauveau, T., Lambert, G., Audouin, P., Mochida, H., Iitsuka, T., Fukuie, M., Molyneux, J., Mazel, J.L., ASTRID, 2015. The SFR GENIV technology demonstrator project: where are we, where do we stand for? In: Proceedings of ICAPP 2015 May 03−06, 2015-Nice (France), Paper 15439.

Risk and Safety Working Group of the Generation IV International Forum, 2008. Basis for the Safety Approach for Design & Assessment of Generation IV Nuclear Systems, Revision 1. GIF/RSWG/2007/002. OECD Nuclear Energy Agency, Paris.

Sathiah, P., Roelofs, F., 2014. Numerical modeling of sodium fire—Part I: Spray combustion. Nuclear Engineering and Design 278, 723−738.

Sato, K., 2005. Conceptual Design Study and Evaluation of Advanced Reprocessing Plants in the Feasibility Study on Commercialized FR Cycle Systems in Japan. In: Proceedings of GLOBAL 2005 Tsukuba, Japan, Oct 9−13, 2005, Paper No. 502.

Sawada, M., Arikawa, H., Mizoo, N., 1990. Experiment and analysis on natural convection characteristics in the experimental fast reactor Joyo. Nuclear Engineering and Design 120, 341−347.

Sciora, P., Blanchet, D., Buiron, L., Fontaine, B., Vanier, M., Varaine, F., Venard, C., Massara, S., Scholer, A.C., Verrier, D.P., 2011. Low void effect core design applied on 2400 MWth SFR reactor. In: Proceedings of ICAPP 2011, May 2−6, 2011, Nice, France.

Sodium Technology Education Committee, September 2005. Sodium Technology Handbook. JNC TN9410 2005-001.

Suzuki, T., Kamiyama, K., Yamano, H., Kubo, S., Tobita, Y., Nakai, R., Koyama, K., January 20, 2014. A scenario of core disruptive accident for Japan sodium-cooled fast reactor to achieve in-vessel retention. Journal of Nuclear Science and Technology.

Tae-Ho, L., 2015. Fundamental approach to safety design of prototype Gen-IV SFR. In: 5th Joint IAEA-GIF TM/WS on Safety of SFR, IAEA, Vienna, June 23−24, 2015.

Takata, T., Yamaguchi, A., Uchibori, A., Ohshima, H., 2009. Computational methodology of sodium-water reaction phenomenon in steam generator of sodium-cooled fast reactor. Journal of Nuclear Science and Technology 46, 613−623.

Tenchine, Pialla, D., Gauthe, P., Vasile, A., 2012. Natural convection test in Phenix reactor and associated CATHARE calculation. Nuclear Engineering and Design 253, 23−31.

Triplett, B.S., Loewen, E.P., Dooies, B.J., May 2012. PRISM: a Competitive small modular sodium-cooled reactor. Nuclear Technology 178, 186−200.

Tsuboi, Y., Matsumiya, H., Hasegawa, K., Kasuga, S., Sakashita, Y., Handa, N., Ueda, N., Grenci, T., 2004. Development of the 4S and related technologies (1). Plant system overview and current status. In: ICAPP9. Tokyo, 2009-05. ANS, 2009, Paper 9214.

U.S. DOE Nuclear Energy Research Advisory Committee and the Generation IV International Forum, 2002. A Technology Roadmap for Generation IV Nuclear Energy Systems. GIF-002-00. OECD Nuclear Energy Agency, Paris.

Vasyaev, A.V., Shepelev, S.F., Bylov, I.A., Poplavskiy, V.M., Ashurko, I.M., 2015. Provision of safety design criteria for generation-IV sodium-cooled fast reactor system implementation in BN-1200 reactor design. In: 5th Joint IAEA-GIF TM/WS on Safety of SFR, IAEA, Vienna, June 23−24, 2015.

Verrier, D., Scholer, A.C., Chhor, M., 2013. A New Design Option for Achieving Zero Void Effect in Large SFR Cores. FR'13, paper CN-199-347.

Walter, A.E., Todd, D.R., Tsvetkov, P.V. (Eds.), 2012. Fast Spectrum Reactors. Springer.

Weber, D.P., 1988. The SAS4A LMFBR Accident Analysis Code System. ANL/RAS 83-38.

Yamaguchi, A., Takata, T., Okano, Y., 2001. Numerical Methodology to Evaluate Fast Reactor Sodium Combustion. Nuclear Technology 136, 315−330.

Yamano, H., Fujita, S., Tobita, Y., Sato, I., Niwa, H., 2008. Development of a three dimensional CDA analysis code: SIMMER-IV and its first application to reactor case. Nuclear Engineering and Design 238 (1), 66−73.

Yamano, H., Kubo, S., Shimakawa, Y., Fujita, K., Suzuki, T., Kurisaka, K., 2012. Safety design and evaluation in a large-scale Japan sodium-cooled fast reactor. Science and Technology of Nuclear Installations 2012. Article Id 614973, 14 pages.

Yang, W.S., Kim, T.K., Grandy, C., 2007. A metal fuel core concept for 1000 MWt advanced burner reactor. In: Proceedings of Global 2007, September 9−13, 2007, Boise, Idaho, US.

Zhang, D., 2015. Fast Reactor Development Strategy in China. FR'13, paper IAEA-CN-199-FRP-01.

Lead-cooled fast reactor

6

C.F. Smith [1], L. Cinotti [2]
[1]Naval Postgraduate School, Monterey, CA, United States; [2]Hydromine Nuclear Energy S.à.r.l, Luxembourg

6.1 Overview and motivation for lead-cooled fast reactor systems

Lead-cooled fast reactors (LFRs) are fast spectrum reactors cooled by molten lead (or lead-based alloys) operating at high temperature and at near atmospheric pressure, conditions enabled because of the very high boiling point of the coolant (up to 1743°C) and its low vapor pressure. The coolant is either pure lead or an alloy of lead, most commonly the eutectic mixture of lead and bismuth, also known as LBE. The predominant coolant considered in the Generation IV reference LFR systems is pure lead, though systems cooled by LBE are also under consideration and are included in this chapter as appropriate. It is noted that there are many similarities and some differences between lead and lead alloys as reactor coolants, and a discussion of some of the important differences is briefly presented. The LFR reactor core is characterized by a fast neutron spectrum, owing to the scattering properties of lead that allow the sustainment of high neutron energy and relatively low parasitic absorption of neutrons.

Lead coolants are relatively inert from a chemical perspective and possess several attractive properties that enable a high degree of inherent safety and simplification of design:

- There are no rapid chemical reactions between the lead coolants and either water or air.
- The high boiling point of lead allows reactor operation at near atmospheric pressure and eliminates the risk of core voiding due to coolant boiling.
- The high latent heat and high thermal capacity of lead provide significant thermal inertia in the event of a loss of heat sink.
- Lead shields gamma radiation and retains iodine, cesium, and other fission products (FPs) at temperatures up to 600°C, thereby reducing the source term in case of release of FPs from the fuel.
- The low neutron moderation of lead allows greater spacing between fuel pins, leading to low core pressure loss and reduced risk of flow blockage.
- The simple coolant flow path and low core pressure loss as well as the thermodynamic properties of lead allow a high level of natural circulation cooling in the primary system for DHR.

Starting in the late 1950s, LBE-cooled reactors were designed and built in the Soviet Union for the purpose of submarine propulsion. Eight such submarines were

Handbook of Generation IV Nuclear Reactors. http://dx.doi.org/10.1016/B978-0-08-100149-3.00006-9
Copyright © 2016 Elsevier Ltd. All rights reserved.

built and operated along with two on-shore reactors. The reactor power of these systems included two levels, with thermal outputs of 73 and 155 MW_{th}. From the early 1960s until decommissioning of the final submarine in 1995, a total of 15 reactor cores were operated, providing an estimated 80 reactor years of operating experience. While significant differences exist between these reactors and currently considered Generation IV LFR systems, the operational experience provided a strong base for understanding the technology and identifying solutions to the technical challenges to be overcome to exploit the significant advantages summarized above.

Since 2000, and stimulated in part by the Generation IV program, several important new initiatives have been developed by organizations in many different locations around the globe.

In Russia, two initiatives are currently being pursued. One of these is known as the SVBR (*Svintsovo-Vismutovyi Bystryi Reaktor* or "Lead−Bismuth Fast Reactor") (Zrodnikov et al., 2009). The SVBR-100 is generally considered a follow-on technology to the prior submarine propulsion technology and is a small reactor cooled by LBE. The second major initiative, known as the BREST (*Bystry Reaktor so Svintsovym Teplonositelem* or "Fast Reactor with Lead Coolant") (Dragunov et al., 2012), is a medium-sized reactor cooled by pure lead and detailed further in this chapter as one of the reference LFR reactor systems in the Generation IV program (GIF-LFR-pSSC, 2014).

In Europe, the European Sustainable Nuclear Industrial Initiative (ESNII) (SNETP Secretariat, 2010) has retained the LFR as a technology of interest. Thus, the ELSY (European Lead-cooled SYstem) project was initiated in 2006 to define the main options of an LFR of industrial size with a power of 1500 MW_{th} and 600 MW_e (Cinotti et al., 2008). This was followed in 2010 by the LEADER project (European Advanced Lead-cooled Reactor Demonstration) (De Bruyn et al., 2013); both ELSY and LEADER were projects funded by the European Commission (EC/Euratom). The LEADER project is continuing the study of an industrial-sized reactor under the name ELFR (European Lead Fast Reactor) and also is examining a demonstrator LFR of power 100 MW_e called ALFRED (Advanced Lead Fast Reactor European Demonstrator) (Frogheri et al., 2013) that is under consideration for construction in Romania. The ELFR system is detailed further in this chapter as one of the reference LFR reactor systems in the Generation IV program (GIF-LFR-pSSC, 2014). Finally, in Belgium, SCK-CEN intends to build an ADS (accelerator driven system) demonstrator, called MYRRHA (Multi-purpose hYbrid Research Reactor for High-tech Applications) (De Bruyn et al., 2007), coupling a particle accelerator with a reactor. MYRRHA would use LBE as a coolant and as a neutron source of spallation activated by a proton beam. The reactor is expected to function either in a subcritical or critical mode.

Several additional design studies have been or are being carried out in a number of other countries including the USA, South Korea, Japan, China, and Sweden. In particular, the US design of a small LFR known as SSTAR (Small Secure Transportable Autonomous Reactor) (Smith et al., 2008) is a legacy preliminary design and is included as the reference design of a small LFR in the Generation IV program (GIF-LFR-pSSC, 2014). Over the most recent 5 years, a significant development initiative has been started

by China. The China LEAd-based Reactor (CLEAR) (Wu et al., 2013) is the reference reactor for China's Lead-based Fast Reactor Development Plan.

6.2 Basic design choices

6.2.1 Lead versus LBE

Pure lead and the eutectic alloy of LBE (consisting of 44.5% lead and 55.5% bismuth) are the principal potential coolants for LFR systems. Table 6.1 shows some key properties of LBE and lead with sodium also included for reference and comparison. Further details on the properties of lead coolants can be found in OECD-NEA (2015). The shared property that both LBE and lead are essentially inert in terms of interaction with air or water is the noteworthy advantage that LFRs have in comparison with the other principal liquid metal-cooled reactor, the sodium-cooled fast reactor (SFR). This basic property has significant implications for design simplification, safety performance, and the associated economic performance of such systems in comparison with SFRs and other Generation IV systems.

When comparing lead to LBE, it should be noted that the LBE coolant has the advantage of a lower melting point (124°C) in contrast with the 327°C of pure lead. For this reason, LBE was used in early lead-cooled reactors (ie, the reactors used for propulsion of the Soviet/Russian alpha-class submarines as well as their land-based counterparts) and in research facilities investigating the use of heavy liquid metals as reactor coolants. The lower melting point of LBE (and the resulting operational advantages) made this a logical choice for such early applications and is also the chosen coolant for several more modern reactor designs (eg, the SVBR-100 design previously mentioned, the Chinese CLEAR-I system, and several others). Additionally, LBE as a coolant has been proposed for several accelerator-driven subcritical (ADS) reactor systems designed for the purpose of transmuting long-lived radionuclides from spent nuclear fuel.

While LBE continues to be considered for some future LFR concepts, reactors cooled by pure lead have become the primary focus of the Generation IV International Forum (GIF) set of reference systems, and this approach appears to represent the most promising future direction due to conspicuous advantages in comparing these options.

Table 6.1 Comparative properties of liquid metal coolants

Coolant	Melting point (°C)	Boiling point (°C)	Chemical reactivity (w/air and water)
Lead–bismuth (Pb–Bi, LBE)	124	1670	Essentially inert
Lead (Pb)	327	1737	Essentially inert
Sodium (Na)	98	883	Highly reactive

The use of LBE as a coolant has some important drawbacks (in comparison to the choice of pure lead) that are appropriate to note. First, as a raw material, LBE (due to the bismuth content) is more expensive, and there is even some doubt that the availability of bismuth could be sufficient in the event of developing a large fleet of LFRs.

Second, it is noted that LBE is somewhat more corrosive than lead (when comparing the corrosion potential of the two coolants at the same temperature), and LBE has a lower thermal conductivity: 14.3 W/m K for LBE versus 17.7 W/m K for lead, at a temperature of 500°C (OECD-NEA, 2015).

The greatest drawback of the LBE is, however, its relatively large production of polonium-210, which is generated by neutron capture of bismuth as follows:

$$^{209}\mathrm{Bi} + \mathrm{n} \rightarrow {}^{210}\mathrm{Bi}\ (\beta\text{-};\ 5\ \mathrm{days}) \rightarrow {}^{210}\mathrm{Po}$$

^{210}Po decays with a half-life of 138.4 days into ^{206}Pb by an α emission of 5.3 MeV. Therefore, it represents a potent heat load within the coolant as well as being a dangerous and radiotoxic material in the event of its leakage or release.

The polonium production in an LBE-cooled reactor is so high that in the 80 MW, LBE-cooled ADS developed in the 5th Framework Program of Euratom, the polonium inventory within the primary coolant circuit was evaluated to be 2 kg at equilibrium. This amount of polonium generates a decay heat in the primary system that, 5 days after a reactor shutdown, would equal the decay heat power of the fuel itself (Cinotti et al., 2011).

Pure lead is not completely exempt from polonium formation because ^{208}Pb (the most abundant natural isotope of lead) transmutes into ^{209}Bi, and ^{210}Po is eventually produced from neutron capture by ^{209}Bi. The rate of polonium production in pure lead is, however, much lower than in the case of LBE, and it is negligible in terms of decay heat power. In fact, the polonium inventory at equilibrium in the primary system of a 1500 MW_{th}, pure lead-cooled reactor (ie, ELSY) has been calculated to be less than 1 g after 40 years of irradiation (Cinotti et al., 2011).

The low moderating capability and low neutron absorption of lead not only enable the operation of a fast reactor with an energy spectrum that is harder than other fast reactor types, but also permit core designs in which the fuel pin lattice has a large spacing, thereby increasing the coolant volume fraction without a significant reactivity penalty. Increasing the coolant volume fraction increases the hydraulic diameter for coolant flow through the core with a corresponding reduction of the core frictional loss. As a result of the neutronic and transport properties of lead, natural circulation is effective and can remove up to 100% of the core power, depending on reactor design, and can be relied upon for passive shutdown heat removal.

6.2.2 Design choices for reactors with lead as the coolant

The favorable properties of the lead coolant and nitride fuel (a feature of some advanced LFR designs), combined with high-temperature structural materials, can extend the reactor coolant outlet temperature up the 750−800°C range in the long term (GIF, 2002, 2014), but this will require the development of new structural

materials. For that reason, most of the present LFR projects limit the mean core outlet temperature to about 550°C, which is the same core outlet temperature typically found in SFRs. In the EC/Euratom projects, the core outlet temperature is further reduced to 480°C for easier resolution of the issue of corrosion in lead, that depends strongly on temperature.

On the other hand, it is well known that the thermal efficiency of the Rankine cycle depends more on the core inlet temperature (which is linked to the steam pressure) than on the core outlet temperature (primarily affecting only the level of steam superheating), so that the efficiency of LFRs operating in the outlet range of 480−550°C can be projected to remain at a high level.

In fact, considering also that an intermediate circuit is not needed for the LFR (because there is no need to isolate the primary coolant from the steam generator (SG) circuit), and that as a result, there is no degradation of the thermal cycle from such an intermediate circuit, a net efficiency of over 40% is reached for each of the GIF reference reactor systems (see Table 6.2), despite the moderate values of the core outlet temperatures. The parameters shown in this table are representative of modern designs serving as reference designs in the LFR System Research Plan of the GIF (GIF-LFR-pSSC, 2014). Note that the use of CO_2 as a secondary coolant has been proposed in one of the Generation IV reference designs and that it also reflects a net efficiency level well above 40%.

6.2.3 Primary system concept: evolution and challenges

Although LBE-cooled reactors were initially designed and operated for the propulsion of a limited number of Soviet/Russian submarines, this design experience cannot be

Table 6.2 Design parameters of Generation IV reference LFR concepts

Parameter	ELFR	BREST-OD-300	SSTAR
Core power (MW_{th})	1500	700	45
Electrical power (MW_e)	600	300	20
Primary system type	Pool	Pool	Pool
Core inlet temperature (°C)	400	420	420
Core outlet temperature (°C)	480	540	567
Secondary cycle	Superheated steam	Superheated steam	CO_2
Net efficiency (%)	42	42	44
Turbine inlet pressure (bar)	180	180	20
Feed temperature (°C)	335	340	402
Turbine inlet temperature (°C)	450	505	553

fully extrapolated to the full range of LFR concepts, since these reactors were small, operated at low capacity factor, and featured an epithermal (as opposed to fast) neutron energy spectrum (GIF, 2002, 2014).

The designs of LFRs have profited, perhaps to an even greater degree, from the large experience in the design, construction, and operation of the SFR. It is not surprising, therefore, that several of the early LFR projects were heavily based on solutions typical of SFRs.

6.2.3.1 *Early conceptual designs derived from sodium-cooled fast reactor concepts*

Early LFR concepts initially considered both pool-type and loop-type primary coolant systems; however, more recent designs have focused on pool-type primary systems, mainly to avoid the seismic issues associated with lead-filled piping.

Owing to the low chemical reactivity of lead with water, in contrast with sodium in the SFR, current LFR projects generally dispense with the intermediate loop between the primary system and the steam−water loop or other power conversion equipment. In fact, LFR primary system designs, especially in the past, have been very similar to those normally adopted for the SFR, but with the replacement of the intermediate heat exchanger with the SG or, in the case of SSTAR, with the lead−CO_2 heat exchanger.

The opening up the fuel pin lattice, however, while providing major benefits in terms of reduced flow resistance and enhanced potential for natural circulation cooling, also results in the reduction of the core power density and would therefore require a larger core diameter than that of an SFR of the same nominal power.

In addition, to avoid excessive corrosion and erosion by flowing lead, the speed of lead has been cautiously limited by design to values much lower (less than 2−3 m/s in most of the channels) than the flow speed of sodium in SFRs. Since the heat capacity per unit volume of lead is only about 40% higher than the heat capacity of sodium, it follows that the volume of an LFR based on typical SFR solutions would be much larger than the primary system of the SFR of the same nominal power.

If, in addition, the density of lead is taken into account (it is higher than the density of sodium by more than a factor of 10), it is evident that the mass of lead of an LFR would be very large and could even become prohibitive for the seismic design of the primary system of the reactor unless a design approach different from that of an SFR is utilized.

6.2.3.2 *Primary system development and current conceptual designs*

Gradual improvements in the understanding of the properties of lead have resulted in LFR design evolution and diversification from SFR concepts to exploit the peculiarities of lead as a coolant. Considering that much of the intense design effort for modern LFR systems has taken place only during the last 10 years, it is not surprising that there are multiple approaches being considered by designers for selection from among many options.

As an example, consider the ELSY project, which is a predecessor to the ELFR concept. ELSY represented a milestone in the quest for innovative solutions, and this quest has continued as designers have explored additional improvements to be embodied in subsequent designs.

The adoption of the pool-type reactor configuration and, more importantly, the incorporation (within the reactor vessel) of a new-design, short-height SG with integrated mechanical pump, represents an important set of innovations leading to achievement of the design goal of enhanced system compactness (see Fig. 6.1).

The anticipated primary system pressure loss of this LFR is about 1.5 bar; thus a free level difference between the cold and the hot collector of only about 1.5 m is sufficient to feed the core.

Thus it is noted that in ELSY, as well as the subsequent EC/Euratom projects (ELFR and ALFRED), an unconventional solution has been adopted, namely the installation of the primary pumps (PPs) in the hot collector.

While the European design efforts leading to the ELSY/ELFR/ALFRED series of LFR concepts were being conducted, parallel efforts were being pursued to develop an array of innovative designs. Projects in Russia, Japan, Korea, the USA, and China concurrently pursued a variety of different concepts with considerable innovation and creativity with respect to primary system design as well as the entire reactor systems.

The Russian BREST-OD-300/1200 concepts (discussed further in Section 6.6) feature a multizone concrete reactor vessel with the reactor core in the central zone, and reactor coolant pumps and SGs in separate zones to which the lead coolant flows through interconnecting channels.

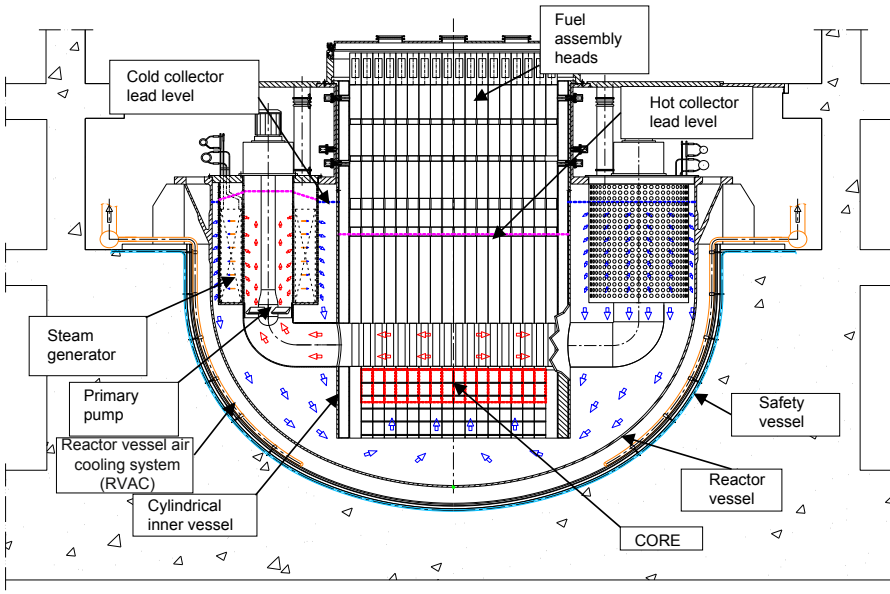


Figure 6.1 Primary system configuration of ELSY.

The SSTAR concept (also discussed further in Section 6.6) relies on natural convection for coolant flow during operational as well and shutdown conditions. It also features an in-vessel lead-to-CO_2 heat exchanger to enable power conversion by a supercritical carbon dioxide Brayton cycle system.

In summary, the primary system designs of the GIF reference reactors (as well as a multitude of other design concepts in various stages of development) provide a range of different approaches to primary system design appropriate for LFR reactor systems.

6.3 Safety principles

The fundamental safety functions (control of reactivity, core cooling, and confinement of radioactive material) are achieved and enhanced for the LFR by exploiting the favorable characteristics of the lead coolant.

For reactor shutdown, LFR designs are equipped with redundant and diversified control rod systems. Peculiar to the LFR is the high buoyancy of lead, which facilitates rod insertion from the bottom of the core (which would be more difficult from above, although still possible with active means or with use of ballast materials).

The high thermal inertia and negative reactivity feedback of lead systems offer, in general, large grace times for corrective operator action, even in case of an unprotected transient during which small positive reactivity feedbacks are counterbalanced by the strong negative core radial expansion feedback, which limits the reactor power.

For core cooling, LFR designs are generally characterized by the existence of strong natural circulation characteristics, and the provision of passive, redundant, and diverse decay heat removal (DHR) systems. The final heat sink can be stored water (as in the case of ELFR) or atmospheric air (as in the case of BREST or SSTAR), or potentially both for a higher degree of diversification.

For confinement of radioactive material, a pool-type LFR with a guard vessel would not suffer loss of primary coolant, even in the event of failure of the reactor vessel. The core would always remain covered and, by design provision, natural circulation flow paths would be maintained.

No hydrogen generation that can damage the containment system is expected in an LFR because of the relative chemical inertness of the coolant.

The containment system design pressure is not affected by the primary system and can be limited by optimizing the water inventory in the secondary system in the designs that utilize steam cycle power conversion.

The tendency of lead to retain bulk FPs, thereby reducing the source term to containment, limits the potential for release of radionuclides and may reduce the requirements for emergency planning zones and emergency evacuation plans.

The Fukushima accident has reinforced the awareness, already well appreciated by designers, of the importance of DHR systems and of the necessity that they continue to operate, even following loss of station service power.

In the LFR designs, three different DHR approaches have be considered and incorporated into LFR reactor designs:

- reactor vessel air cooling system (RVACS)
- direct reactor cooling (DRC) through dip coolers (DCs).
- heat removal through the water/steam main loops

RVACS is a reliable system, but its use can be considered only for small-size reactors, since in such systems, the vessel outer surface is relatively large in comparison with the reactor power.

DRC solutions can operate in a natural circulation mode and, new design solutions have been conceptualized, which are not only passively operated, but also passively actuated. This is possible because in an LFR, there is a margin of more than 200−300 K between the temperature of the cold collector of the reactor and the temperature that represents a safety limit; hence thermal expansion of materials, or gas expansion, can be used to initiate the operation of DHR systems.

Typical solutions include a dip cooler with water/steam at the secondary side connected to an external condenser that uses either water or air as the heat sink.

The main water−steam loops (secondary system) provide the normal route for nonsafety related DHR, but the interest in their use with safety function is questionable for the following three reasons:

- The secondary system of a reactor with superheated steam cycle is a system with relatively low reliability;
- Unlike the PWR, the secondary system of the LFR does not offer much in terms of heat capacity; and
- In the LFR, the most efficient means to mitigate the consequences of the steam generator tube rupture (SGTR) accident is the prompt, simultaneous depressurization of all secondary loops and isolation of the in-vessel SGs. Any safety-related DHR function bound with the SGs would require, instead, discrimination and isolation of the ruptured SG only, an action to be carried out preferably in a very short time (of the order of a few seconds), and this is risky if the discrimination is not fully reliable.

The SG, when functionally unavailable for heat removal, becomes a portion of the hot leg of the primary loop, and, for solutions with a cylindrical inner vessel, it is therefore necessary to use a short SG to have the proper natural draft for adequate natural circulation, without having to excessively increase the height of the reactor vessel.

The main topics of ongoing and near future research, as far as safety is concerned, are related to experimental activities for the demonstration of LFR safety system functionality and performance. Although safety system capabilities have been assessed through numerical simulations and separate effects tests have been performed, it is expected that licensing authorities will require integral testing at appropriate scale to assess the behavior of the systems to be licensed. Other experimental testing is also necessary to confirm other attributes of LFRs, such as the expected tendency for fuel dispersion instead of consolidation in case of cladding failure.

The elimination of the intermediate cooling system (in comparison to other reactor types, such as the SFR) and the installation of high-pressure SG equipment inside the reactor vessel operating at ambient pressure are features that require a rigorous approach focused to the achievement of three main objectives:

- low failure probability of the pressure boundary of the SG;
- low water/steam release in case of rupture of one or more tubes of the SG;
- low impact of any SG release of water/steam from the SG with respect to:
  - pressurization of the primary boundary;
  - mechanical loadings on the internals, core included; and
  - steam entrainment into the core.

Specific activities are currently planned or ongoing for SGTR tests at small scale with extension to larger scale in the future.

6.4 Fuel technology and fuel cycles for the lead-cooled fast reactor

6.4.1 Fuel assembly characteristics

The fuels anticipated for modern LFR concepts are generally in the form of annular pellets of (U, Pu)O_2 as in the Euratom concepts or (U, Pu, MA)N in the Russian and US concepts BREST and SSTAR.

Fuel pellets are stacked inside fuel rods (rod outside diameter of $\sim$10 mm) of stainless steel (eg, 15, 15 Ti stabilized) to form a fuel column of typical height of 0.6−1 m. The typical length of a fuel rod is at least twice the active length in order to include a lower gas plenum and an upper gas plenum with a spring to compact the fuel pellets.

Fuel rods (typically 100−300 in number) are arranged as a bundle to form the fuel assembly (FA), with a hexagonal or square cross section, which can either be open or have a flow duct (wrapper) of lateral containment of the bundle.

The solution with the wrapper has the advantage of enabling varying pressure losses through the various FA in order to control the radial distribution of core temperature, but it is disadvantageous from the neutronic viewpoint in addition to requiring greater quantities of steel and lead in the core region.

The upper head of the FA is appropriately shaped for its connection with the gripping mechanism of the handling machine. The handling machine can be designed to operate either in lead (as in BREST) or in gas (as in ELFR) to avoid the difficulties of qualification of mechanisms operated in lead.

By extending the FA with a stem that is well above the lead coolant surface level, it is possible to use a handling machine that operates exclusively in gas. This solution has also other advantages including the fact that the mass of the FA that emerges from the lead can compensate for the excess buoyancy of the immersed portion, and that the FA does not need to be connected to a lower support grid to prevent

its vertical motion. Moreover, the extended FA stem can house the core instrumentation eliminating the need for the above-core structure typical of other liquid metal-cooled reactors (ie, the SFR).

The power density, the operating temperature, the neutron flux, and the transients of the fuel of an LFR are similar to those of an SFR so that the experience gained by the large investments made for SFR fuels can be used for the LFR.

6.4.2 Fuel cycle for the lead-cooled fast reactor

The LFR is compatible with a closed fuel cycle or an open fuel cycle. Fast reactors have been conceived for either fuel cycle scenario, and LFRs can be plutonium (Pu) breeders, Pu burners, or reactors with equilibrium fuel composition and long core life.

In the present scenario characterized by a general surplus of Pu and uncertainty on nuclear power development, the designers of LFRs have devoted relatively little attention to the potential roles of LFR as a Pu breeder or burner, and the main attention has been devoted to the role of reactors with equilibrium fuel composition. This is the case for ELFR, BREST, and SSTAR, as well as other concepts under consideration.

An adiabatic core (Arteoli et al., 2010) is a fuel cycle strategy able to convert an input feed of either natural or depleted uranium (NU or DU, respectively) into energy, with FP and actinide reprocessing losses as the only output stream. This allows the full closure of the fuel cycle within the reactor (thus the term adiabatic, because of its having no ‘‘significant” exchange with the environment) with transuranics remaining at equilibrium in the core, as shown in Table 6.3, which depicts the results of an analysis carried out for the ELSY reactor.

The use of the LFR in an open cycle, loaded with enriched uranium (U), would require competitiveness with present LWR and the authors are not aware of any systematic studies, but only of promising preliminary evaluations related to the potential cost reductions made possible by recent conceptual projects.

An additional consideration exemplified in designs such as SSTAR is the ability to achieve very long core life in LFRs that operate with a conversion ratio at or slightly above one. This approach yields minimum burnup swing and thus enables long core life in such systems.

Table 6.3 Transuranic masses at equilibrium for an adiabatic ELSY (Arteoli et al., 2010)

Element	Mass (kg)
Plutonium	5971
Neptunium	27.3
Americium	225.8
Curium	56.7

6.5 Summary of advantages and key challenges of the lead-cooled fast reactor

6.5.1 Advantages of the lead-cooled fast reactor

Lead is unique among the coolants available for nuclear reactor systems for a number of reasons. As a dense liquid, it has excellent cooling properties, while its nuclear properties (ie, its low tendency to absorb neutrons or to slow them down) enable it to maintain a hard neutron energy spectrum, resulting in flexibility in fuel management and coolant flow design. These characteristics facilitate improved resource utilization, longer core life, effective burning of minor actinides (MA), and open fuel pin spacing, important features in achieving sustainability, proliferation resistance, fuel cycle economics, and enhanced passive safety by enabling fuel cooling by natural circulation.

Lead has the very high boiling temperature of 1737°C. Consequently, the problem of coolant boiling is, for all practical purposes, eliminated. The high margin to boiling leads to important safety advantages including design simplification and improved economic performance.

As a coolant operating at atmospheric pressure, the loss of coolant accident is virtually eliminated by use of an appropriately designed guard vessel. This is not only a safety advantage, but also offers additional potential for plant simplification and improved economic performance, since the complex process of simultaneous management of temperature, pressure, and coolant level (as is seen in water-cooled reactors) is not necessary.

One of the most significant advantages of lead as a coolant is its low chemical activity. In comparison with other coolants, especially sodium and water, lead presents a relatively benign coolant material that does not support chemical interactions that can lead to energy release in the event of accident conditions. Further, the tendency of lead to retain FPs and other materials that might be released from fuel in the event of an accident is another important advantage. The elimination of the need for an intermediate coolant system to isolate the primary coolant from the water and steam of the energy conversion system represents a significant advantage and potential for plant simplification and improved economic performance.

Following the Fukushima−Daiichi reactor accidents, it is important to consider future reactor technologies in light of the potential for severe accident conditions. The LFR can demonstrate superior features to avoid the consequences of such severe accidents. First, one of the primary issues was the common-mode loss of on-site diesel generators (caused by the tsunami) during an extended blackout condition (caused by the earthquake). An LFR would not need to rely on such backup power and would be resilient in the face of blackout conditions because of passively operated DHR enabled by the natural circulation capabilities of the lead coolant.

Second, the loss of primary coolant at the Fukushima−Daiichi reactors resulted from the use of pressurized water coolant. An LFR with guard vessel would not suffer a loss of primary coolant, even in the event of a failure of the reactor vessel.

The steam-cladding interactions at the Fukushima−Daiichi reactors resulted in the liberation of hydrogen and associated explosions. With the relative chemical inertness of lead as a coolant, no hydrogen generation would be enabled.

6.5.2 Key challenges of the lead-cooled fast reactor

As for all Generation IV advanced reactor technologies, there are technology challenges associated with development of the LFR. These challenges include those related to the high melting point of lead, its opacity, coolant mass as a result of its high density, and the potential for corrosion when the coolant is in contact with structural steels.

The high melting temperature of lead (327°C) requires that the primary coolant system be maintained at temperatures to prevent the solidification of the lead coolant or at least to maintain a recirculation at the core level to allow its cooling. The use of a pool-type configuration and appropriate primary system design can provide a safe and effective resolution to this issue.

The opacity of lead, in combination with its high melting temperature, presents challenges related to inspection and monitoring of reactor in-core components as well as fuel handling. This issue can also be addressed by appropriate and specific design features, for example, innovative core configurations with fuel assemblies extended above the lead free level, as implemented in the recent European projects, would serve to alleviate this issue.

The high density and corresponding high mass of lead as a coolant result in the need for careful consideration of structural design to prevent seismic impacts to the reactor system. Innovative primary systems configurations with short reactor vessels and the introduction of seismic isolation are options to address such issues.

Possibly the most difficult challenges result from the tendency of lead at high temperatures to be corrosive when in contact with structural steels. This tendency, which is accelerated at higher temperatures, will require careful material selection and component and system monitoring during plant operations.

Pending the development of materials resistant to lead corrosion at higher temperature, surface treatment, and small quantities of additional elements in the structural matrix and oxygen control are necessary to protect materials immersed in lead from corrosion and also to protect against the formation of solids in the lead coolant from oxidation processes. In the design configuration developed to date, relatively low coolant outlet temperatures serve to reduce the potential impact of this issue.

Each of the above areas of challenge is a topic of ongoing research; it is likely they can be addressed by effective research, design, and engineering.

6.6 Overview of Generation IV lead-cooled fast reactor designs

6.6.1 Reference Generation IV systems

The GIF LFR provisional System Steering Committee, which was organized in 2005, identified as reference designs the large central station design (ELSY) and the small modular system (SSTAR). In 2011, the committee was reformulated, and the new committee changed the European reference system from ELSY to the European

Lead-Cooled Fast Reactor (ELFR) and added a mid-size LFR (ie, the BREST-OD-300) as a new thrust and reference reactor system, while the SSTAR legacy system was retained as the reference small LFR. The typical design parameters of these GIF—LFR reference systems were previously summarized in Table 6.2 and are described further in the following subsections.

6.6.1.1 The European lead-cooled fast reactor

The ELFR is a design resulting from the update and modification of the earlier ELSY reactor concept. Fig. 6.2 provides an overview sketch of the primary system configuration of the ELFR reactor.

The overall primary system is contained inside a reactor vessel of stainless steel and is shaped as a cylindrical vessel with a dished bottom head. A safety vessel, anchored to the reactor pit, collects and contains lead in the event of reactor vessel leakage. The reactor vessel is a thin shell structure, the design of which is largely governed by seismic loadings and those potentially associated with lead sloshing.

Within the vessel are eight removable SG—PP assemblies, arranged symmetrically around the core close to the wall of the reactor vessel.

Under normal, steady state operation, the lead free level inside the inner shell of the SG is higher than the free level in the cold collector (outside the SG), which is higher than the free level in the inner vessel. The three equilibrium levels are the result of the

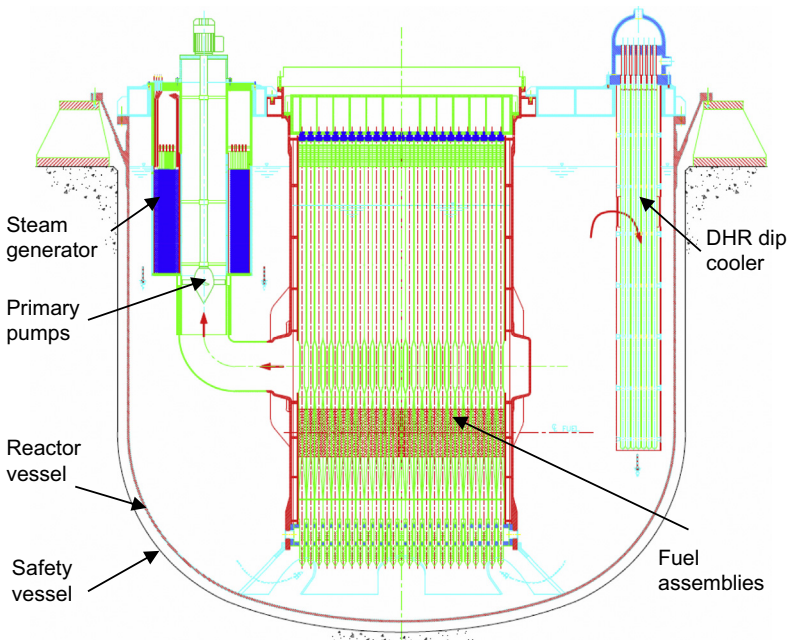


Figure 6.2 Primary system configuration of ELFR.
Dr. Alessandro Alemberti, Ansaldo Nucleare.

hydraulic head provided by the PP, the different lead density in the legs of the primary circuit and the friction in the circuit. Thus lead circulation is driven both by the hydraulic head provided by the PP and the natural draft. Lead enters the core at 400°C, where it is heated up to an average of 480°C. At the core outlet, it flows outwards entering the suction port of the eight PP and then upward into the annular space between the pump shaft and the inner shell of the SG. It flows then across the perforated inner shell and the tube bundle of the SG, where lead is cooled to 400°C and finally down to the core inlet, thereby closing the circuit.

Inside the reactor vessel, the cold collector is located in the annular space between the reactor vessel and the cylindrical inner vessel.

Two different and independent (physically separated) DHRs are provided for the ELFR. Each DHR system includes:

1. DHR1: four isolation condenser systems (ICs) connected to four SGs.
2. DHR2: four ICs connected to four DCs.

The core design has demonstrated that it is possible to provide an *adiabatic* reactor concept with equilibrium fuel so that the fuel composition remains the same between two successive loadings, ensuring the full recycling of all the actinides, with either NU or DU as only input and FPs as output. The equilibrium fuel composition is shown in Table 6.4 (Arteoli et al., 2010).

The FA is characterized by a wide pitch-to-diameter ratio favoring the establishment of natural circulation at sustainable thermal regimes during unprotected loss of flow accidents (Table 6.5).

6.6.1.2 The BREST-OD-300 reactor

The BREST-OD-300 reactor (and its companion larger system design, the BREST-1200) is a system developed by the Russian organization NIKIET in association with a number of other organizations with the goal of realizing a "naturally safe" LFR concept.

Its objectives include the elimination of severe accidents, including those related to power excursions, cooling loss, loss of external and backup power, or multiple

Table 6.4 Composition of the ELFR equilibrium fuel

Element fraction	(%)
Uranium	80.56
Plutonium	18.15
Neptunium	0.11
Americium	1.02
Curium	0.16

Table 6.5 ELFR main parameters

ELFR design options	
Electrical power, MW_e	600
Primary coolant	Pure lead
Primary system	Pool type, compact
Primary coolant circulation	Forced; decay heat removal in natural circulation is possible
Core inlet temperature, °C	400
Steam generator inlet temperature, °C	480
Secondary coolant cycle	Water−superheated steam
Feed water temperature, °C	335
Steam pressure, MPa	18
Secondary system efficiency, %	∼43
Reactor vessel	Austenitic stainless steel, hung
Safety vessel	Anchored to reactor pit
Inner vessel (core barrel)	Cylindrical
Steam generators	Integrated in the reactor vessel and removable. Preferred option: spiral tubes
Primary pumps	Mechanical pumps in the hot collector, removable
Fuel assembly	Closed (with wrapper), hexagonal
Fuel type	Mixed oxide
Maximum discharged burnup, MWd/kg-HM	100
Refueling interval, y	2
Fuel residence time, y	5
Fuel clad material	T91, coated
Maximum clad neutron damage, dpa	100
Maximum clad temperature in normal operations, °C	550
Maximum core pressure drop, MPa	0.1
Control/shutdown system	2 diverse and redundant systems: pneumatic inserted absorber rods (with backup tungsten ballast) from the top; buoyancy absorber rods from the bottom.
Refueling system	No in-vessel fuel handling machine
DHR systems	2 diverse and redundant systems (actively actuated, passively operated)
Seismic damping devices	2-D isolators below reactor building

common cause threats. It features the ability to be self-sustaining in an equilibrium operating mode and is unique in its provision for a complete fuel pyroprocessing capability co-located with the reactor.

The BREST-OD-300 is a pilot technology demonstration reactor being developed as a prototype of future commercial reactors of the BREST family, such as the larger BREST-1200. Table 6.6 provides a summary of key parameters for both the BREST-OD-300 and BREST-1200 concepts.

The BREST-OD-300 is a reactor of pool-type design. It incorporates, within the pool, the reactor core with reflectors and control rods, the lead coolant circulation circuit with SGs and pumps, equipment for fuel reloading and management, and safety and auxiliary systems. These reactor systems and items of equipment are included in a steel-lined, thermally insulated concrete vault.

Table 6.6 Technical parameters of BREST-OD-300 and BREST-1200

Characteristics	BREST-OD-300	BREST-1200
Thermal power, MW_{th}	700	2800
Electric power, MW_e	300	1200
Core diameter, mm	2400	4755
Core height, mm	1100	1100
Fuel rod diameters, mm	9.7−10.5	9.1−9.7
Fuel rod pitch, mm	13.0	13.0
Core fuel	(U + Pu + MA)N	(U + Pu + MA)N
Core charge (U + Pu + MA)N, t	19	64
Charge of (Pu + MA)/(^{239}Pu+^{241}Pu), t	2.5/1.8	8.56/6.06
Fuel lifetime, y	5	5−6
Refueling interval, y	1	1
Maximum fuel burnup % h. a.	9.0	10.2
Total margin of reactivity % ΔK/K	0.43	0.35
Lead inlet/outlet temperature, °C	420/540	420/540
Maximum fuel cladding temperature, °C	650	650
Maximum lead velocity, m/s	1.9	1.7
Steam temperature at steam generator inlet/outlet, °C	340/505	340/520
Pressure at steam generator outlet, MPa	18	24.5
Net efficiency of power unit, %	42	43
Design service life, y	30	60

BREST has a widely spaced fuel lattice with a large coolant flow area. This results in low-pressure losses, enabling natural circulation of the primary lead coolant for DHR. It does not utilize U blankets, but instead takes account of the reflecting properties of lead to improve power distribution and provide negative void and density coefficients. By design, it is not suitable for the production of weapons-grade Pu. The BREST DHR systems feature passive and very long-term residual heat removal directly from the primary coolant by natural circulation of air through air-cooled heat exchangers with the heated air vented to the atmosphere.

The fuel type planned for the first core of the BREST reactor is DU mixed with Pu and MA in the nitride form. The composition corresponds to that resulting from spent fuel from PWRs following reprocessing and a ~20 year cooling period.

The properties of lead allow for the operation with such fuel as an equilibrium composition. This mode of operation features full sustainment of the fissile nuclides in the core (the core breeding ratio is ~1) with irradiated fuel reprocessing in a closed fuel cycle. Reprocessing is limited to the removal of FPs without separating Pu and MA from the mix (U-Pu-MA). One of the unique characteristics of the BREST plant is that a reprocessing plant is co-located with the reactor. This eliminates in principle any issues or concerns due to spent nuclear fuel transportation.

Fig. 6.3 is a sketch of the BREST-OD-300 reactor.

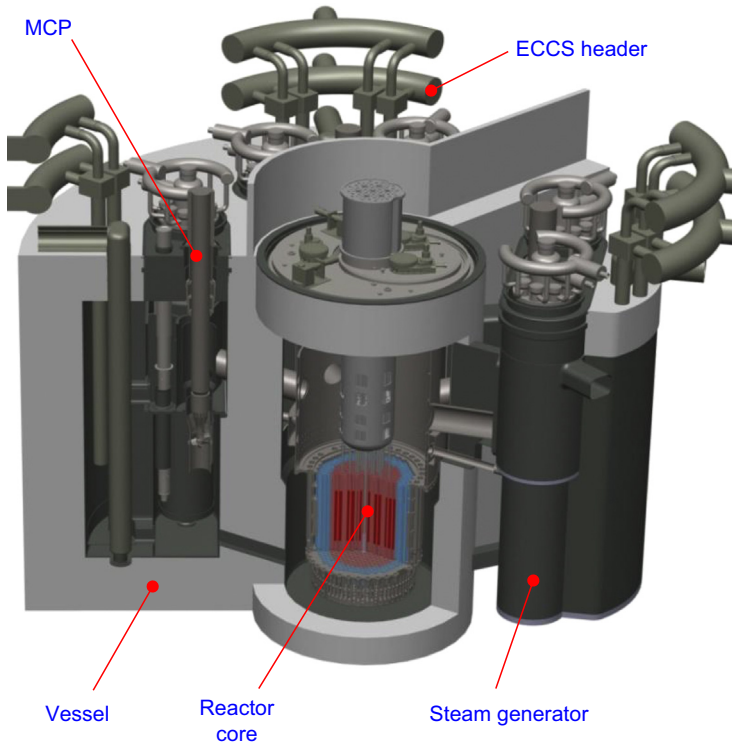


Figure 6.3 Sketch of the BREST-OD-300 reactor system.
Dr. Andrei Moiseev, NIKIET.

6.6.1.3 The Small Secure Transportable Autonomous Reactor

SSTAR is the legacy design of a reactor intended for potential deployment to countries with developing economies and infrastructures, or to sites with remote locations requiring standalone power supply. Though not currently under active development, the SSTAR design is the GIF reference design for a small modular LFR system.

The SSTAR development focused on the concept of a small transportable reactor system for international deployment, especially to remote locations or those disconnected from well-developed electricity distribution systems. SSTAR has the following features: (1) a reactor core that is designed for no refueling or whole-core replacement to eliminate or limit the need (and ability for) on-site refueling; (2) transportability: the entire core and reactor vessel would be delivered by ship or overland transport; (3) a very long-life core design: 15−30 year core life is the target; (4) the capability for autonomous load following with simple integrated controls allowing minimal operator intervention and enabling minimized maintenance; and (5) local and remote monitorability to permit rapid detection/response to operational perturbations. These features permit installation and operation in places with minimal industrial infrastructures. Additionally, they provide a facility characterized by a very small operational (and security) footprint.

Key characteristics of the SSTAR system are summarized in Table 6.7 and illustrated in Fig. 6.4. They include the following: coolant circulation is by natural convection for both operational and shutdown heat removal; there are no reactor coolant pumps. The system uses a supercritical CO_2 power conversion system providing for improved efficiency and a small footprint. The core is designed for an ultralong core life and the vessel is sealed and designed for complete cassette core replacement when refueling is required; this confers a high degree of proliferation resistance.

6.6.2 Additional Generation IV systems under study or development

In addition to the Generation IV reference systems described above, there are several other preliminary designs that are being pursued. A sample of these is presented in the following sections. Though this selection of additional systems is not exhaustive, it is representative of the diversity of approaches being considered to exploit the favorable potential of the LFR. It is also noted that, in contrast to the GIF reference designs, these additional systems under study rely primarily on LBE as the coolant. The selection includes systems being considered in Korea, China, and Japan.

6.6.2.1 The South Korea URANUS-40 system

Over the past 20 years, Seoul National University has considered the development of innovative reactor systems based on LBE cooling along with advanced fuel recycle (Choi et al., 2011). A noteworthy current result of these efforts is the small modular

Table 6.7 Technical parameters of SSTAR

SSTAR parameters, features and performance	
Coolant	Lead
Coolant circulation	Natural convection
Power conversion	Supercritical CO_2, Brayton cycle
Fuel	TRU nitride using nitrogen enriched in ^{15}N
Enrichment, %	5 radial zones; 1.7/3.5/17.2/19.0/20.7
Core lifetime, y	30
Core inlet/outlet temperatures, °C	420/567
Coolant flow rate, kg/s	2107
Power density, W/cm^3	42
Average (peak) discharge burnup, MWd/kg-HM	81 (131)
Burnup reactivity swing, $	<1
Peak fuel temperature, °C	841
Cladding	Silicon-enhanced ferritic/martensitic SS bonded to fuel pellets by lead
Peak cladding temperature, °C	650
Fuel/coolant volume fractions	0.45/0.35
Core lifetime, y	15−30
Fuel pin diameter, cm	2.50
Fuel pin triangular pitch-to-diameter ratio	1.185
Active core dimensions height/diameter, m	0.976/1.22
Core hydraulic diameter	1.371

LBE-cooled reactor designated as the Ubiquitous, Robust, Accident-forgiving, Nonproliferating, and Ultra-lasting Sustainer (URANUS-40). This system has a nominal electric power rating of 40 MW_e (100 MW_{th}), a power level selected for use as a distributed power source for production of electricity, heat supply, and desalination. It is a pool-type fast reactor with a heterogeneous hexagonal core, fueled by low-enriched uranium dioxide fuels. The primary cooling system relies on natural circulation. The system features a 3-D seismic base isolation system underneath the entire reactor building. The system also features a capsulized core design and a very long refueling period (25 y).

Table 6.8 presents a summary of the parameters of the URANUS-40 system, and Fig. 6.5 is a sketch of the concept.

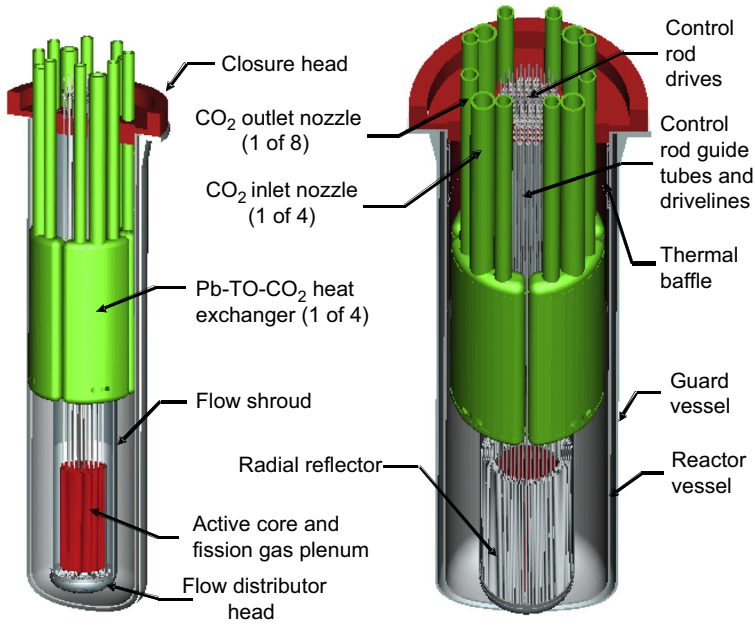


Figure 6.4 Sketch of SSTAR.
Dr. James Sienicki, Argonne National Laboratory.

Table 6.8 URANUS-40 selected parameters

Design parameter	Value or characteristic
Core power rating	40 MW_e (110 MW_{th})
Refueling interval	20 years (with 2-year inspection interval)
Primary coolant	LBE (move to pure lead coolant when advanced cladding materials available)
Primary cooling mode	Natural circulation
Core inlet/outlet temperature	305°C/441°C
Secondary coolant	Subcooled water/superheated steam
Mode of operation	Autonomous load follow mode
Fuel	Low-enriched uranium UO_2
Cladding	FGC of T91 and Si-containing ferritic steel (with advance FGC of HT-9 and Al-containing ferritic steel)
Seismic design	3-D base isolations of entire nuclear steam supply systems

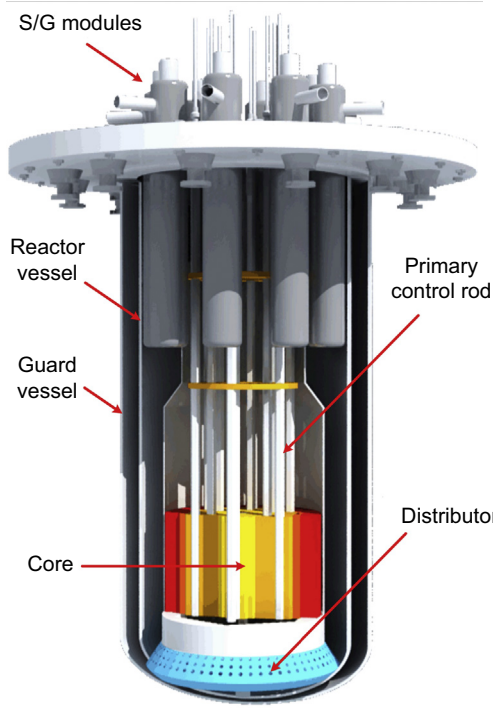


Figure 6.5 Sketch of the URANUS-40 system.
Prof. Il Soon Hwang, Seoul National University.

6.6.2.2 The Chinese CLEAR-I reactor

In 2011, the Chinese Academy of Sciences launched a project to develop ADS and LFR technology, and the CLEAR family of systems was selected as the reference for both the ADS and the LFR. CLEAR consists of three stages: a 10 MW_{th} lead-based research reactor (CLEAR-I), a 100 MW_{th} lead-based engineering demonstration reactor (CLEAR-II), and a 1000 MW_{th} lead-based commercial prototype reactor (CLEAR-III) (Wu et al., 2013).

The conceptual design of CLEAR-I was completed in 2013, and engineering design is underway. CLEAR-I has a subcritical and critical dual-mode operation. Key components of CLEAR-I, including the control rod drive mechanism, refueling system, FA, and a simulator for principle verification, have been fabricated and tested. Fig. 6.6 and Table 6.9 provide a sketch and summary of the key parameters of CLEAR-I.

6.6.2.3 The Pb–Bi-Cooled Direct Contact Boiling Water Fast Reactor

The Pb–Bi-Cooled Direct Contact Boiling Water Fast Reactor (PBWFR) is a design concept of a small-size innovative direct contact (LBE–water) LFR being developed by Takahashi et al. (2008a,b) at the Tokyo Institute of Technology. In this concept,

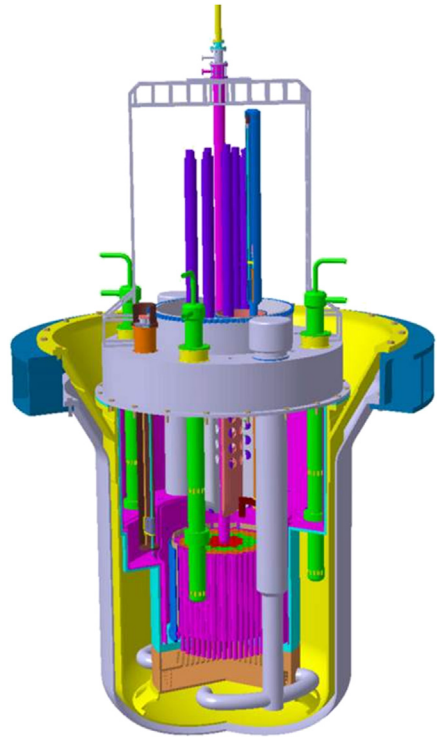


Figure 6.6 Sketch of the CLEAR-I reactor.
Dr. Tao Zhou, FDS, China Academy of Sciences.

steam is generated by direct contact between feed water and the primary LBE coolant in the upper core plenum, and is transported through the LBE coolant as a result of the buoyancy of the steam bubbles.

The idea of a direct contact system was earlier identified by Buongiorno et al. (1999, 2001) as a more compact and economical LFR than those featuring conventional forced circulation. In the PBWFR, primary pumps and SGs are eliminated. The conceptual design for the PBWFR features a long-life core with a core breeding ratio higher than unity for efficient U utilization, high proliferation resistance because of reduced risk from refueling, small size for portability, modularity and low capital investment, a negative void reactivity for safety enhancement, and reliance on steam lift and direct contact steam generation.

Table 6.10 provides a summary of selected key parameters of the PBWFR, and Fig. 6.7 is a sketch of the reactor system.

6.6.2.4 The SVBR-100 (Zrodnikov et al., 2009; Toshinsky et al., 2013)

The SVBR-100 reactor is a prototype system under active design development by a consortium of Russian organizations including OKB Gidropress, the Institute of Physics and Power Engineering, and Atomenergoproekt Moscow. It is the reactor system most

Table 6.9 CLEAR-I key parameters

Selected key parameters of CLEAR-I	
Parameter	**Value**
Thermal power	10 MW
Primary coolant	LBE
Fuel material	UO_2 (19.75%)
k_{eff} in subcritical mode	0.973
Primary system	Pool type, compact
Primary circulation	Forced
Core inlet/outlet temperature	300°C/385°C
Secondary coolant	Pressurized liquid water
Heat sink	Air cooler
Reactor height/diameter (mm)	6800/4680
Primary coolant inventory (t)	600
Heat exchangers	4 units, shell and tube heat exchanger, double-walled bayonet tube, removable
Main vessel height	6300 mm
Main vessel diameter	4650 mm
Primary pumps	2 units, mechanical pumps in the cold pool, removable

closely aligned with the previous generation of Soviet/Russian lead–bismuth cooled reactors used for submarine propulsion. As such, the SVBR draws more directly than other systems on the operational experience from that military application.

The SVBR-100 is intended for use in the remote, isolated, or coastal locations, or for dedicated industrial applications. It can be used to provide a variety of outputs, including electricity, process heat, or desalination, depending on actual system configuration. The Russian Advanced Nuclear Technologies Federal Program for 2010–15 and out to 2020 identified the SVBR-100 for pilot plant construction, and the joint venture company AKME Construction, together with VNIPIET (All-Russia Science Research and Design Institute of Power Engineering Technology) as the general architect, were selected to develop and build the pilot SVBR unit.

Table 6.11 provides a summary of selected parameters for the SVBR-100, and Fig. 6.8 is a sketch of the reactor.

6.7 Future trends

Early designs of LFR were heavily influenced by the SFR; however, over time, new solutions have been developed, recognizing the unique characteristics of the coolant.

Table 6.10 Parameters of the PBWFR

Selected key parameters of the PBWFR	
Power (thermal/electric) (MW)	450/150
Thermal efficiency (%)	33
Core inlet/outlet temperature (°C)	310/460
Core pressure drop (MPa)	0.04
Maximum cladding temperature (°C)	619
Pb−Bi flow rate (t/h)	73,970
Steam temperature (°C)	296
Steam flow rate (t/h)	863
Steam pressure (MPa)	7
Feed water temperature (°C)	220
Refueling interval (y)	10
Refueling	One batch refueling
Candidate materials for cladding and structural equipment	Aluminum−iron alloy-coated high chromium steels, high chromium steels with aluminum and silicon addition, ceramics (SiC, etc.) and refractory metals

In a similar way, the trends toward unique solutions to design issues are continuing, and this is indicated by the diversity of different designs currently under study, as shown in the previous sections of this chapter. Examples of major differences from previous designs of metal-cooled fast reactors include the following:

- the BREST reactors use of a concrete outer vessel
- the SSTAR reliance on natural circulation cooling for operational heat removal
- the ELSY/ELFR compact, integrated, and removable SG assemblies

These features are a small sample of the innovations in the current reference designs, and additional new ideas are reflected in the many designs that are being actively developed, some of which are summarized in this chapter.

Two additional projects, being developed with private funding for specific market applications, are appropriate to consider as representatives of future directions and trends. These two projects are the LFR-AS-200 project being developed by Hydromine, Inc., and the Swedish Advanced Lead Reactor (SEALER) reactor project being developed by LeadCold Reactors Inc. The descriptions below are based on private communications for these ongoing development efforts and are intended to illustrate the continuing process of innovation that is characteristic of current and future trends in LFR technology.

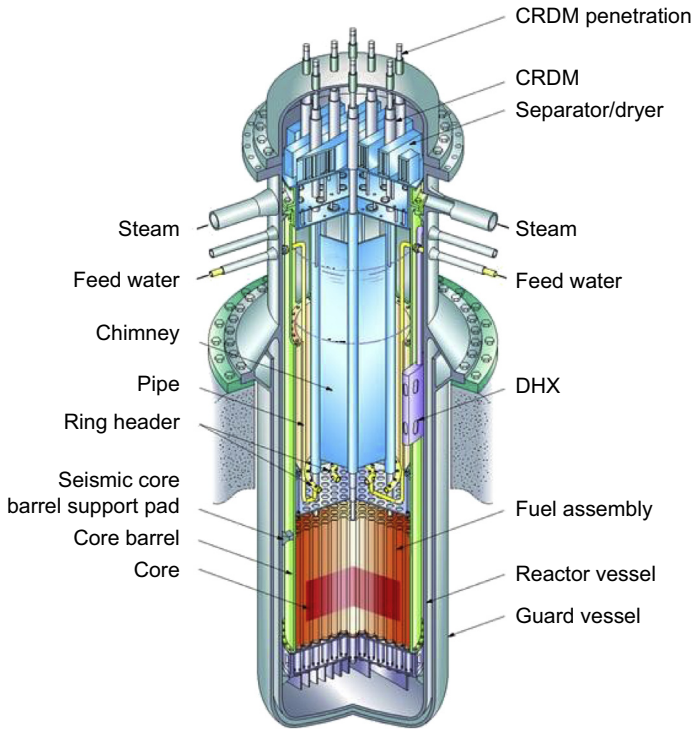


Figure 6.7 Sketch of the PBWFR.
Prof. Minboru Takahashi, Tokyo Institute of Technology.

Table 6.11 Selected parameters of the SVBR-100

SVBR-100 power plant parameters	
Reactor thermal output, MW_{th}	280
Electric power output, MW_e	100
Primary coolant temperature: inlet/outlet, °C	340/490
Steam production rate	580 t/h at pressure, 6.7 MPa, and temperature, 278°C
Average core power density, kW/dm^3	160
Fuel: type	UO_2
Uranium loading, kg	~9200
Average U-235 enrichment, %	~16.7
Core lifetime, thousands of full power hours	50,000
Time interval between refueling, years	~7–8
Reactor module dimensions	4.5/8.2 m (diameter/height)

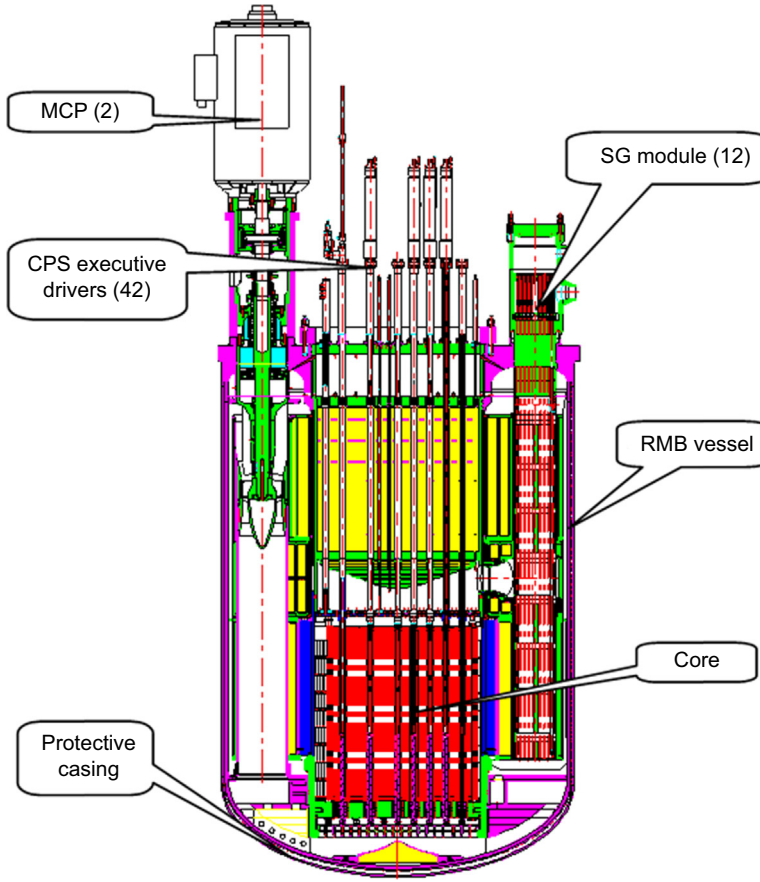


Figure 6.8 Sketch of the SVBR-100.
Prof. Georgi Toshinsky, IPPE. Received figure and table from originator, Prof Toshinsky, stating that the material is open access.

Additionally, given the importance of protection of materials from the corrosion potential of lead, this section includes a discussion of protection from lead corrosion by means of ceramic coatings.

6.7.1 The LFR-AS-200

The objective of the Lead-Cooled Fast Reactor—Amphora Shaped-200 MW_e (LFR-AS-200) project is to design and build a simple and compact reactor intended to demonstrate the competitiveness of LFR reactors for applications in open, long-lived fuel cycles based on enriched U fuel, and applications in a closed fuel cycle with equilibrium composition of fuels. AS stands for "amphora shaped," as the reactor is characterized by an amphora-shaped inner vessel and 200 is the rated electrical power of the reactor in MW.

The project builds on innovations previously proposed and evaluated for the ELSY reactor program while adding new innovations leading to a substantial further

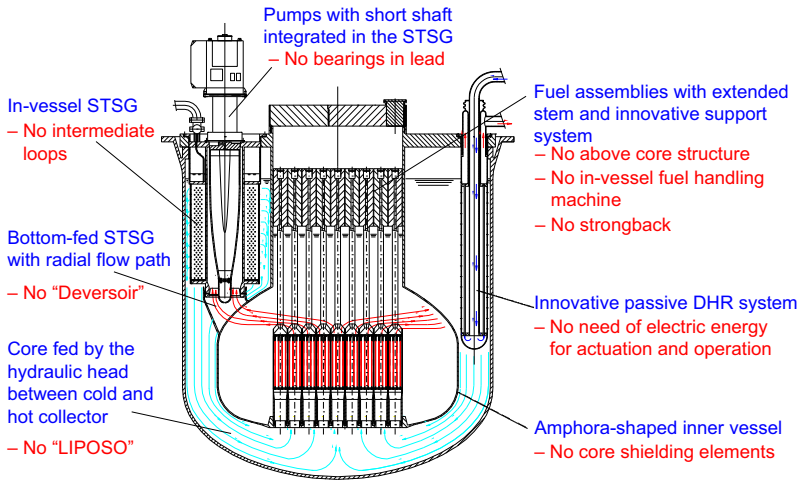


Figure 6.9 Outline of the LFR-AS-200 project showing major innovations. (Red text identifies the components typical of some LFRs and the SFR, but which are not necessary for the LFR-AS-200).
Modified from Luciano Cinotti.

compaction of the primary system with a resulting reactor vessel height of about 6 m (for a 200 MWe design) to minimize the seismic loads. The design would provide a primary system power density of about 1 MW_e/m^3.

Fig. 6.9 illustrates the LFR-AS-200 reactor assembly, highlighting the major innovations and identifying the main advantages, especially in comparison with other LFR designs and in contrast to concepts for SFR design (Hydromine unpublished work). These features of the LFR-AS-200 are described further in the following paragraphs.

- The spiral tube steam generator
  The SG for the LFR-AS-200 is characterized by a spiral-tube bundle with a 530°C lead inlet temperature and 400°C temperature at the outlet. The SG unit, as well as all other in-vessel components, is removable for in-service inspection, or replacement. The upper part of the spiral tube steam generator (STSG) is bolted to the reactor roof, and there is no equipment welded to the reactor vessel.

  The STSG feeds its outlet lower-temperature lead into the upper part of the downcomer. This keeps the reactor vessel at a uniform temperature all along its height and contributes to the primary system compactness because there is *no need for provisions such as the deversoir (ie, discharge channel)*, thermal insulation, or cooling systems.

  The STSG can be positioned at a higher level in the downcomer and the *reactor vessel* shortened accordingly because the shell perforations extend below the accidental coolant free level and provide the flow area for core cooling, even in the case of a leaking reactor vessel. By feeding the SG from the bottom, the risk of cover gas entrainment into the core is virtually eliminated.
- Pumps integrated in the STSG
  The region of the SG inside the inner shell is a free volume suitable to accommodate an axial-flow PP head. This eliminates the circumferential constraints of the pumps and contributes to the reduction of the reactor vessel diameter.

The required net positive suction head of the pumps is low, and the pump impeller can be positioned relatively high in the reactor vessel with a short shaft. Consequently, it is possible to eliminate the use of pump bearings within the molten lead coolant.

- FA with extended stem

  The reactor is equipped with FAs with stems extended well above the lead-free level to permit use of a *handling machine that operates in the cover gas at ambient temperatures under full visibility of the operator*. Via this solution, the head of the FA hangs from its support in the gas space buttressed by buoyancy, allowing for continuous monitoring.

  This approach allows:

  - *The elimination of the need to secure the FA at the core support grid.* A conventional approach might require the locking of the FAs to the core support grid;
  - The elimination of in-vessel fuel transfer equipment; and
  - *The elimination of the above-core structure* supporting the core instrumentation, a component that can interfere with the refueling system and contribute to its complexity.

  In an FA with extended stem, both the FA and the control rod can be supported from the top in gas space in full visibility. The FA vertical support system in gas is free from neutronic damage and from thermal loads; this alleviates the issue of a tricky in-service inspection of a core support grid immersed in the opaque coolant.
- Innovative passive DHR system

  The LFR-AS-200 is equipped with two independent, diverse, redundant DRCS. One system is based on a lead loop and air cooler, and is not only passively operated, but also passively actuated by means of louvers controlled by the thermal expansion of the cold leg of the lead loop.

  Thanks to the lead interposed between the enlarged lower portion and the core, the amphora-shaped inner vessel is subject to lower neutron damage, and this allows the elimination of the numerous shielding assemblies that would otherwise be necessary. The elimination of these shielding assemblies allows the reduction of the diameter of the inner vessel in its upper part, leaving a greater radial space for the installation of the SGs and allowing the *reduction of the diameter of the reactor vessel*.
- Core fed by the hydraulic head between the cold and hot collectors

  The coolant pumps are installed in the hot collector and raise the free level of the cold collector by 1 m,, sufficient to feed the core without a duct *(Liaison-POmpe-SOmmier, "LIPOSO" in French)* connecting the pump outlet with the diagrid *(Sommier)*, the pressure plenum, which feeds the core. The entire downcomer cross section is available to hydraulically connect the STSGs to the core to avoid entrained steam reaching the core in case of an SGTR.
- In-Vessel SG

  To reduce the failure probability of the pressure boundary of the SG, the tube bundle is designed to absorb large differential expansions with a reliable support system and the reduced possibility, by design, of rupture propagation to adjacent tubes.

  To reduce water/steam release in case of a rupture of one or more tubes of the SG:

  - Water and steam headers are located above the reactor roof;
  - The steam cycle has no safety-grade function for DHR. In case of any signal that might indicate a loss of water/steam within the primary system, the water/steam loops are promptly depressurized and isolated according to techniques developed for the SFR, in order to stop water/steam release into the primary system;
  - The tube bundle has few long, small-bore tubes with high water/steam-side pressure loss (about 10 bar at tube inlet plus about 10 bar along the tubes); and

- A check valve is installed on each tube inside the steam header, and a self-actuated isolating excess flow valve is placed inside the feed water header.

Pressurization of the primary boundary is limited by rupture discs through which steam is discharged into an enclosure with a pressure suppression system. The mechanical loadings on the internals are limited by minimization of lead displacement in the vessel, owing to:

- low lead inventory (a few 100 L) inside the STSG itself;
- installation of the STSG near the lead free level;
- reduced height of the STSG; and
- prevention of reverse flow between STSG and pump.

Steam entrainment into the core is prevented by the low pressure loss of the lead in the downcomer, and the difference in density between lead and steam create a *lift pipe* effect, preventing the downward flow in the region containing steam.

Other innovations are still being evaluated to further increase the safety and economic performance of the LFR-AS system. All this is possible because of the novelty of the technology for which solutions still remain that have not been yet fully explored. In particular, the success of the use of ceramic coatings (see Section 6.7.3) in preventing corrosion of metal structures are being considered to allow increases in the core outlet temperature with obvious economic benefits.

6.7.2 Swedish Advanced Lead Reactor

SEALER is a small lead-cooled nuclear battery-type reactor designed by the Swedish company LeadCold Reactors for commercial power production in off-grid applications. The dimensions of the primary system are indicated in Fig 6.10, and were established to enable transport of the vessel by cargo aircraft to destinations in the Canadian arctic. Using 2.4 tons of 19.9% enriched UO_2 fuel, the life of the core is 27 full power years when operating at 8 MW_{th} (up to 3 MW_e). Nineteen fuel assemblies (each with 91 pins) are located in the center of the core, surrounded by 12 reactivity control elements and 6 shutdown elements. Heat is removed by forced circulation of the lead coolant, using 8 pumps. Operating at a total mass flow of 1300 kg/s, the ΔT over the core is 40 K, keeping the average coolant temperature at the outlet below 430°C and the maximum cladding temperature below 450°C. One compact SG is connected to each of the pumps, using a new spiral tube design.

The anticipated fuel cladding tube material is a 15-15Ti steel, surface alloyed with Fe-10Cr-4Al-Zr. This choice is intended to ensure negligible swelling at the peak cladding dose of 60 dpa, while providing sufficient corrosion resistance.

Transient simulations of SEALER have been carried out using the SAS4A/SASSYS-1 codes as well as BELLA, a code written specifically for the purpose of safety-informed design of LFRs. Analysis shows SEALER to withstand unprotected withdrawal of a single control rod, loss of forced flow and loss of heat sink, thanks to its low power density, the capability of natural convection for decay heat removal, and reliance on thermal radiation from the vessel as the ultimate heat sink.

In the case of a full core melt, the fraction of iodine and cesium released from the lead and the primary system is sufficiently small that radiological exposure to the

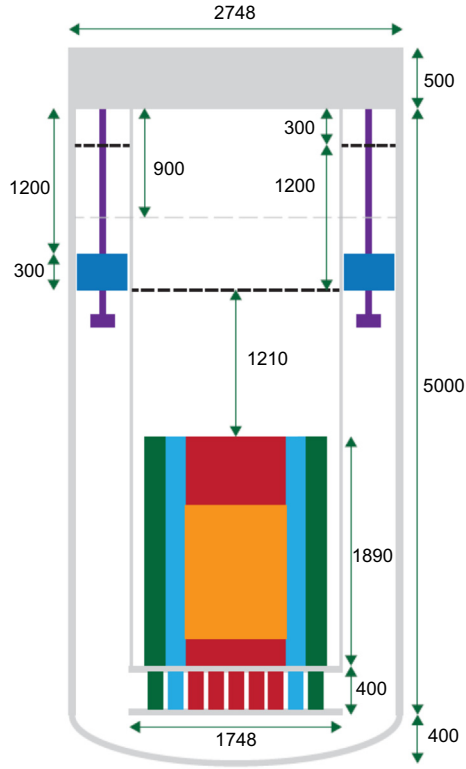


Figure 6.10 Sketch of the SEALER reactor.
Dr. Janne Wallenius, CEO LeadCold Reactors Inc.

public remains below Canadian regulatory limits at a distance of 100 m from the reactor. Hence, there is no need for evacuation or sheltering under licensing requirements for reactors sited in Arctic communities.

6.7.3 Protection from lead corrosion by means of coatings

Considerable past research has been conducted on the topics of oxygen control and protective coatings to control the potential for corrosive damage to in-vessel materials (OECD-NEA, 2015).

One of the new strategies to tackle high-temperature corrosion issues in lead is the use of ceramic coatings. Specifically, some types of oxide coatings are basically insoluble in heavy liquid metals and would allow decoupling the problem of corrosion protection at low and high temperatures. However, the structural integrity of the coating substrate system must be guaranteed at all times. Therefore, coatings are not only required to be corrosion resistant, but they must also withstand a harsh environment in which the combination of high temperature and radiation damage ultimately results in ever growing stresses and strain.

Recent studies (García Ferré et al., 2013a,b) have shown that Al_2O_3 coatings grown by pulsed laser deposition (PLD) are particularly promising. These coatings are fully dense and compact, and attain an unusual combination of metal-like mechanical properties ($E = 195 \pm 959$ GPa, $\nu = 0.29 \pm 0.02$) and ceramic hardness ($H = 10 \pm 1$ GP), together with strong interfacial bonding and resistance to wear (García Ferré et al., 2013a). The exposure of coated steel samples to oxygen-saturated lead has shown no sign of corrosion after 500 h at 550°C in stagnant conditions (García Ferré et al., 2013b). Long-term corrosion tests in low-oxygen flowing lead have already been launched, while the response of the coatings to radiation damage has been studied through irradiation with heavy ions up to 150 displacements per atom. The results show that neither the adhesion nor the structural integrity of the coatings are compromised by such extreme damage levels. Importantly, it is well established that a reasonable equivalence can be found between the damage caused by heavy-ion or neutron irradiation (Was, 2007). Last, but not least, it is worth highlighting that PLD processing can be carried out at room temperature, avoiding any microstructural rearrangement in the underlying steel components.

Sources of further information

There are four important international sources of information on the development of LFR that can be considered in expanding the information in this chapter.

- An important survey of lead coolant technology has been carried out by a working group under the auspices of the Working Party on Scientific Issues of the Fuel Cycle of the Organization for Economic Cooperation and Development—Nuclear Energy Agency. Created in 2002, this Working Group on Lead−Bismuth Eutectic (WG-LBE) coordinates and guides LBE research in participating organizations while promoting closer and broader-based collaboration. The aim of the group is to develop a set of requirements and standards as well consistent methodology for experimentation, data collection, and data analyses. Due to increasing interest in the lead-cooled option in GIF, the WG-LBE also decided to include data and technology aspects of both LBE and lead. The results are published in (OECD-NEA, 2015) the 2015 "Handbook on lead-bismuth Eutectic Alloy and Lead Properties, Materials compatibility, Thermal-hydraulics and Technologies." The publication of a revised edition of the handbook is foreseen.
- Surveys of information and coordination of international efforts on all Generation IV systems, including the LFR systems, is an important function of GIF. The Generation IV Technology Roadmap was issued in 2002 and updated in 2014 (GIF, 2002, 2014) with several annual reports published in the interim between the main documents. The roadmap provides a foundation for formulating national and international program plans on which the GIF countries may collaborate to advance Generation IV systems.
- These documents, as well as additional information on Generation IV systems, may be accessed through the Generation IV website at www.gen-4.org.
- Additional information on safety requirements and safety progress of specific designs, as well as comprehensive topical reviews, can be obtained from the International Atomic Energy Agency (IAEA). IAEA (2013) is an example of such a reference source, and additional information can be found at the IAEA website, www.IAEA.org.

Nomenclature

2-D	Two dimensional
AEP	Atomenergoproekt Moscow
ALFRED	Advanced Lead Fast Reactor European Demonstrator
Am	Americium
BELLA	a computer code written specifically for the purpose of safety-informed design of lead-cooled fast reactors
CAS	Chinese Academy of Sciences
CLEAR	China LEAd-based Reactor
Cm	Curium
CPS	Control and protection system
CRDM	Control rod drive mechanism
DC	Dip cooler
DHR	Decay heat removal
DHX	Decay heat exchanger
dpa	Displacements per atom
DRC	Direct reactor cooling
DU	Depleted uranium
el	Electrical
ECCS	Emergency core cooling system
ELFR	European Lead Fast Reactor
ELSY	European Lead Cooled System
ESNII	European Sustainable Nuclear Industrial Initiative
FA	Fuel assembly
FGC	Functionally graded composite
FP	Fission product
IC	Isolation condenser
IPPE	The Institute of Physics and Power Engineering
kg	Kilogram
kg/s	Kilograms per second
kW/dm^3	Kilowatts per cubic decimeter
LEADER	European Advanced Lead-Cooled Reactor Demonstrator
LBE	The eutectic mixture of lead and bismuth (lead−bismuth eutectic)
LFR-AS-200	Lead-cooled fast reactor—amphora shaped-200 MW_e

Continued

LIPOSO	*Liaison-POmpe-SOmmier* in French
LOCA	Loss of coolant accident
MA	Minor actinides
MCP	Main coolant pump
mm	Millimeter
MPa	Megapascal
MW_e	Megawatts electrical
MW_{th}	Megawatts thermal
MWd/kg-HM	Megawatt days per kilogram of heavy metal
MYRRHA	Multipurpose hYbrid Research Reactor for High-tech Applications
N	Nitrogen; nitride
Np	Neptunium
NU	Natural uranium
OECD-NEA	Organization for Economic Cooperation and Development—Nuclear Energy Agency
PBWFR	Pb-Bi-Cooled Direct Contact Boiling Water Fast Reactor
PP	Primary Pump
pSSC	GIF LFR Provisional System Steering Committee
Pu	Plutonium
RMB	Reactor Monoblock
RVACS	Reactor vessel air cooling system
SCK-CEN	The Belgian nuclear research center located in Mol, Belgium. The acronym comes from the Dutch: Studiecentrum voor Kernenergie; and the French: Center d'Étude de l'énergie Nucléaire
SEALER	Swedish Advanced Lead Reactor
SG	Steam generator
SGTR	Steam generator tube rupture
SNETP	Sustainable nuclear energy technology platform
SNU	Seoul National University
SS	Stainless steel
SSTAR	Small Secure Transportable Autonomous Reactor
STSG	Spiral tube steam generator
SVBR	*Svintsovo-Vismutovyi Bystryi Reaktor* in Russian, or "Lead–Bismuth Fast Reactor"
t	Ton
t/h	Tons per hour

th	Thermal
TRU	Transuranic
U	Uranium
URANUS	Ubiquitous, Robust, Accident-forgiving, Nonproliferating and Ultra-lasting sustainer
W/cm^3	Watts per cubic centimeter
WG-LBE	Working Group on Lead−Bismuth Eutectic
WPFC	Working Party on Scientific Issues of the Fuel Cycle
Y	years

References

Artioli, C., Grasso, G., Petrovich, C., 2010. A new paradigm for core design aimed at the sustainability of nuclear energy: the solution of the extended equilibrium state. Annals of Nuclear Energy 37, 915−922.

Buongiorno, J., Todreas, N.E., et al., 1999. Key features of an integrated Pb−Bi cooled reactor based on water/liquid-metal direct heat transfer. In: Trans. of the 1999 ANS Winter Meeting, Long Beach (U.S.A.).

Buongiorno, J., Todreas, N.E., et al., 2001. Conceptual Design of a Lead-Bismuth Cooled Fast Rector With In-vessel Direct-Contact Steam Generation. MIT-ANP-TR-079. Massachusetts Institute of Technology.

Choi, S., Hwang, I.S., Cho, J.H., Shim, C.B., September 28−30, 2011. URANUS: Korean Lead−Bismuth cooled small modular fast reactor activities. Paper No. SMR2011-6650. In: ASME 2011 Small Modular Reactors Symposium, Washington, DC, USA, pp. 107−112.

Cinotti, L., Locatelli, G., Aït Abderrahim, H., Monti, S., Benamati, G., Tucek, K., Struwe, D., Orden, A., Corsini, G., Le Carpentier, D., September 14−19, 2008. The ELSY project. Paper 377. In: Proceedings of the International Conference on the Physics of Reactors (PHYSOR), Interlaken, Switzerland.

Cinotti, L., Smith, C., Sekimoto, H., Mansani, L., Reale, M., Sienicki, J., August 31, 2011. Lead-cooled system design and challenges in the frame of Generation IV International Forum-Proceedings of the International DEMETRA Workshop on Development and Assessment of Structural Materials and Heavy Liquid Metal Technologies for Transmutation Systems. Journal of Nuclear Materials 415 (3), 245−253.

De Bruyn, D., Maes, D., Mansani, L., Giraud, B., July 29−August 2, 2007. From MYRRHA to XT-ADS: the design evolution of an experimental ADS system. In: Proceedings of the 8th International Topical Meeting on Nuclear Applications and Utilization of Accelerators (AccApp'07), Pocatello, Idaho.

De Bruyn, D., Alemberti, A., Mansani, L., Grasso, G., Bandini, G., Artioli, C., Bubelis, E., Mueller, G., Wallenius, J., Orden, A., April 14−18, 2013. Main achievements of the FP7-LEADER collaborative project of the European Commission regarding the design of a lead-cooled fast reactor. In: Proceedings of ICAPP 2013 Jeju Island, Korea.

Dragunov, Y., Lemekhov, V., Smirnov, V., Chernetsov, N., November 2012. Technical solutions and development stages for the BREST-OD-300 reactor unit. Atomic Energy 113 (1), 70.

Frogheri, M., Alemberti, A., Mansani, L., March 4–7, 2013. The lead fast reactor: demonstrator (ALFRED) and ELFR design. In: IAEA–International Conference on Fast Reactors and Related Fuel Cycles: Safe Technologies and Sustainable Scenarios (FR13), Paris, France.

García Ferré, F., Ormellese, M., Di Fonzo, F., Beghi, M.G., 2013a. Advanced Al_2O_3 coatings for high temperature operation of steels in heavy liquid metals: a preliminary study. Corrosion Science 77, 375–378.

García Ferré, F., Bertarelli, E., Chiodoni, A., Carnelli, D., Gastaldi, D., Vena, P., Beghi, M.G., Di Fonzo, F., 2013b. The mechanical properties of a nanocrystalline Al_2O_3/a-Al_2O_3 composite coating measured by nanoindentation and Brillouin spectroscopy. Acta Materialia 61, 2662–2670.

Generation IV International Forum (GIF), December 2002. Technology Roadmap for Generation IV Nuclear Energy Systems. GIF-002-00. https://www.gen-4.org/gif/upload/docs/application/pdf/2013-09/genivroadmap2002.pdf.

Generation IV International Forum (GIF), January 2014. Technology Roadmap Update for Generation IV Nuclear Energy System. https://www.gen-4.org/gif/upload/docs/application/pdf/2014-03/gif-tru2014.pdf.

Generation IV International Forum LFR provisional System Steering Committee, April 2014. Generation IV Nuclear Energy Systems System Research Plan for the Lead-Cooled Fast Reactor. Draft.

International Atomic Energy Agency (IAEA), October 2013. Status of Innovative Fast Reactor Designs and Concepts. Supplement to the IAEA Advanced Reactors Information System (ARIS). http://aris.iaea.org.

Organisation for Economic Co-operation and Development – Nuclear Energy Agency, 2015. Handbook on Lead-Bismuth Eutectic Alloy and Lead Properties, Materials Compatibility, Thermal-Hydraulics and Technologies – 2015 edition. NEA No.7268, 954 pp.

Smith, C., Halsey, W., Brown, N., Sienicki, J., Moisseytsev, A., Wade, D., June 15, 2008. SSTAR: the US lead-cooled fast reactor (LFR). Journal of Nuclear Materials 376 (3), 255–259.

Sustainable Nuclear Energy Technology Platform (SNETP) Secretariat, October 2010. ESNII: The European Sustainable Nuclear Industrial Initiative: Demonstration Programme for Fast Neutron Reactors, Concept Paper. http://www.snetp.eu/wp-content/uploads/2014/05/esnii-folder-a4.pdf.

Takahashi, M., Uchida, S., Kasahara, Y., 2008a. Design study on reactor structure of Pb–Bi-cooled direct contact boiling water fast reactor (PBWFR). Progress in Nuclear Energy 50, 197–205.

Takahashi, M., Uchida, S., Yamada, Y., Koyama, K., 2008b. Safety design of Pb–Bi-cooled direct contact boiling water fast reactor (PBWFR). Progress in Nuclear Energy 50, 269–275.

Toshinsky, G.I., Komlev, O.G., Tormyshev, I.V., Petrochenko, V.V., 2013. Effect of potential energy stored in reactor facility coolant on NPP safety and economic parameters. World Journal of Nuclear Science and Technology 3 (2), 59–64. www.scirp.org/journal/wjnst.

Was, G.S., 2007. Fundamentals of Radiation Materials Science, Springer. New York.

Wu, Y., Yunqing, B., Song, Y., Huang, Q., Chen, H., Song, G., Hu, L., Jiang, J., March 5, 2013. Overview of lead based reactor design and R&D status in China. In: Proceedings of the International Conference on Fast Reactors and Related Fuel Cycles: Safe Technologies and Sustainable Scenarios (FR-13), Paper INV-417, Paris, France.

Zrodnikov, A.V., Toshinsky, G.I., Komlev, O.G., Stepanov, V.S., Klimov, N.N., Kudryavtseva, A.V., Petrochenko, V.V., December 7−11, 2009. SVBR-100 module-type reactor of the IV generation for regional power Industry. In: International Conference on Fast Reactors and Related Fuel Cycles: Challenges and Opportunities. IAEA-CN-176−FR09P1132 (Kyoto, Japan).

Molten salt fast reactors

7

M. Allibert [1], M. Aufiero [1], M. Brovchenko [2], S. Delpech [3], V. Ghetta [1], D. Heuer [1], A. Laureau [1], E. Merle-Lucotte [1]
[1]LPSC/IN2P3/CNRS - Université Grenoble Alpes, Grenoble, France; [2]Institut de Radioprotection et de Sûreté Nucléaire, Fontenay aux Roses, France; [3]IPNO/IN2P3/CNRS, Orsay, France

7.1 Introduction

Molten salt reactors (MSRs) are a family of liquid-fueled fission reactor concepts using a fluid molten salt mixture as fuel. Such liquid-fueled reactors benefit from some potential advantages over solid-fueled systems, among which are

- the possibility of fuel composition (fertile/fissile) adjustment and fuel reprocessing without shutting down the reactor;
- the possibility of overcoming the difficulties of solid fuel fabrication/refabrication with large amounts of transuranic elements (TRUs); and
- the potential for better resource utilization by achieving high fuel burn-ups (with TRUs remaining in the liquid fuel to undergo fission or transmutation to a fissile element).

A circulating liquid fuel also playing the role of the coolant presents some more advantages, such as

- heat production directly in the fuel, which is also the coolant (no heat transfer delay);
- fuel homogeneity (no loading plan required); and
- rapid, passive, fuel geometry reconfiguration via gravitational draining.

This type of reactor is still at a conceptual level based on numerical modeling. However, very significant experimental studies were performed at Oak Ridge National Laboratory (ORNL) in the 1950s and 1960s, providing an experimental basis for their feasibility. In 1958 a water-based liquid fuel was used in a 5-MW_{th} homogeneous reactor experiment called HRE-2, demonstrating the intrinsic stability of homogeneous reactors. Later on the Molten Salt Reactor Experiment (ORNL-TM-728, 1965; Haubenreich and Engel, 1970; Engel et al., 1979), with a liquid fluoride-based fuel at 650°C and a graphite-moderated neutron spectrum, operated for 4 years, from 1966 to 1969, without trouble. It demonstrated the possibility of circulating a liquid fluoride mixture without corrosion problems. This was achieved by using nickel-based alloy (Hastelloy N) and oxidation control of the fuel by use of the U^{3+}/U^{4+} buffer. However, this 8-MWt thermal reactor only tested fissile isotopes (^{233}U, ^{235}U, Pu) and not fertile ones such as Th because of the capture cross sections, which are large with thermal neutrons. Nevertheless, a continuous physical processing of the fuel was successfully tested, consisting in contacting the fuel with a neutral gas to extract gaseous fission products (FPs) such as Kr and Xe before they decay into Rb

Handbook of Generation IV Nuclear Reactors. http://dx.doi.org/10.1016/B978-0-08-100149-3.00007-0
Copyright © 2016 Elsevier Ltd. All rights reserved.

and Cs (poisons for thermal neutrons). Unexpectedly, this processing also removed most of the metallic FPs. Although successful, these tests did not lead to the construction of the Molten Salt Breeder Reactor (Bettis and Robertson, 1970; Whatley et al., 1970), studied in detail by ORNL, partly because its thermal spectrum requires intensive chemical processing for FP removal and Pa extraction (related to proliferation issues due to the possible ^{233}Pa day in pure ^{233}U in such conditions) to avoid neutron captures leading to minor actinides (MAs). These drawbacks are eliminated by using a fast spectrum.

Within the MSR System Steering Committee of the Generation IV International Forum (GIF/MSR) (US DOE, 2002), two fast-spectrum MSR concepts are being studied (Serp et al., 2014; Boussier et al., 2012; GIF, 2008, 2009), both based on a liquid circulating fuel: the molten salt fast reactor (MSFR) concept initially developed at CNRS, France, and the MOlten Salt Actinide Recycler and Transmuter (MOSART) concept under development in the Russian Federation. Simulation studies and conceptual design activities are ongoing to verify that fast-spectrum MSR systems satisfy the goals of Generation IV reactors in terms of sustainability (closed fuel cycle, breeder system), nonproliferation (integrated fuel cycle, multirecycling of actinides), safety (no reactivity reserve, strongly negative feedback coefficient), and waste management (actinide burning capabilities). Compared with solid-fueled reactors, fast MSR systems have lower fissile inventories, no radiation damage constraints on attainable fuel burn-up, no reactivity reserve, strongly negative reactivity coefficients, no requirement to fabricate and handle solid fuel, and a homogeneous isotopic fuel composition in the reactor.

Here we will focus on the MSFR concept, but some elements pertaining to the MOSART concept will be provided. Regarding the MSFR, presented hereafter, its design is not fixed yet, but all important issues have been considered since the beginning, including nuclear effectiveness, safety, and proliferation resistance, to reach a design that does not encounter a major obstacle at any level of development. This is why after the presentation of the physics and chemistry aspects, deployment scenarios and safety issues are discussed. Finally, a path for future research is presented.

7.2 The molten salt fast reactor concept

7.2.1 Core and system description

Conceptual design activities are currently underway so as to ascertain whether MSFR systems can satisfy the goals of Generation IV reactors in terms of sustainability (Th breeder), nonproliferation (integrated fuel cycle, multirecycling of actinides), resource saving (closed Th/U fuel cycle, no uranium enrichment), safety (no reactivity reserve, strongly negative feedback coefficient), and waste management (actinide burner). The calculation results presented here were obtained for a reactor configuration called reference MSFR and studied in the frame of the EVOL Euratom project of the Framework Program 7 (Brovchenko et al., 2014a; Dulla et al., 2014). This is not to be taken as an optimized reactor but as a basis for interdisciplinary studies.

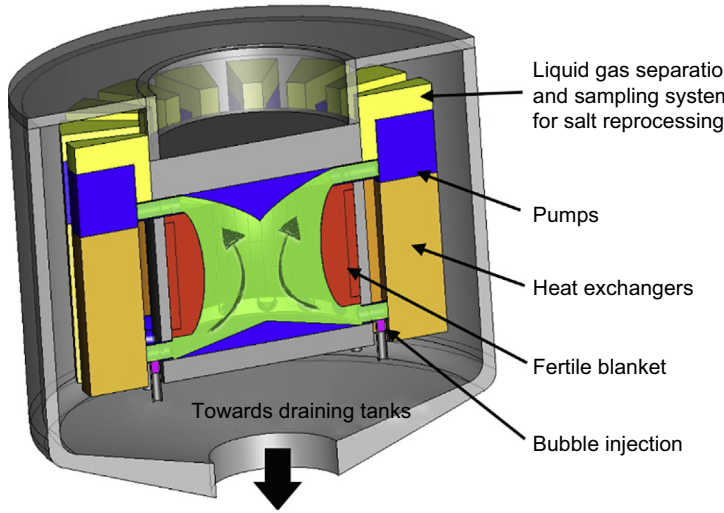


Figure 7.1 Schematic representation of the reference molten salt fast reactor fuel circuit.

The reference MSFR is a 3-GW_{th} reactor with a total fuel salt volume of 18 m^3 operated at a maximum fuel salt temperature of 750°C (Mathieu et al., 2009; Merle-Lucotte et al., 2012). The system includes three circuits: the fuel circuit, the intermediate circuit, and the power conversion circuit. The fuel circuit, defined as the circuit containing the fuel salt during power generation, includes the core cavity, the inlet and outlet pipes, a gas injection system, salt-bubble separators, pumps, and fuel heat exchangers.

As shown in the sketch of Fig. 7.1, the fuel salt flows from the bottom to the top of the core cavity (note the absence of in-core solid matter). In preliminary designs developed in relation to calculations, the core of the MSFR is a single compact cylinder (2.25 m high × 2.25 m diameter) where the nuclear reactions occur within the liquid fluoride salt acting as fuel and as coolant. Thermal-hydraulic studies performed in the frame of the EVOL project have shown that a torus-shaped core (see Fig. 7.1) improves thermal flow (Laureau et al., 2013; Rouch et al., 2014; Laureau, 2015c).

The properties of the fuel salt used in these simulations are summarized in Table 7.2. The fuel salt considered in the simulations is a molten binary fluoride salt with 77.5 mol% of lithium fluoride; the other 22.5 mol% is a mixture of heavy nuclei fluorides. This proportion, maintained throughout the reactor evolution, leads to a fast neutron spectrum in the core as shown in Fig. 7.2. Thus this MSFR system combines the generic assets of fast neutron reactors (extended resource utilization, waste minimization) and those associated with a liquid-fueled reactor.

Both contributions to the feedback coefficient (ie, the density coefficient [or void, related to the salt thermal expansion] and Doppler coefficient) are largely negative, leading to a total feedback coefficient of −5 pcm/K. This is a significant advantage for the operation and safety of the reactor as discussed in this section and in Section 7.5.2.

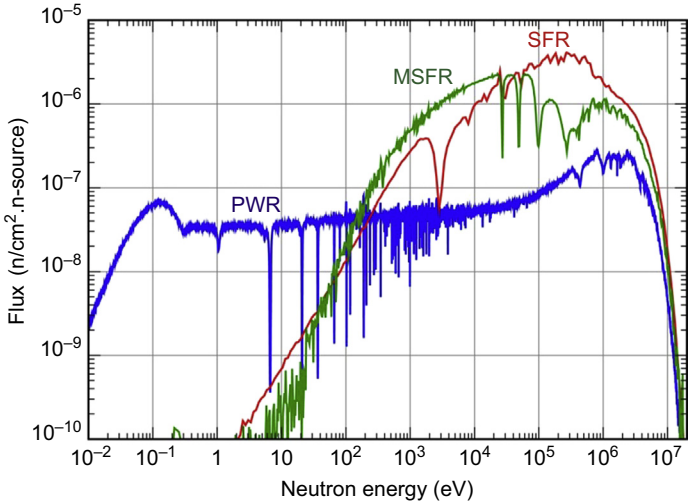


Figure 7.2 Calculated neutron spectrum of the reference MSFR (*green curve*). For comparison, a typical sodium-cooled fast neutron reactor spectrum (*in red*) and a typical PWR thermal spectrum (*in blue*) are shown. *MSFR*, molten salt fast reactor; *SFR*, sodium-cooled fast neutron reactor; *PWR*, pressurized water reactor.

Table 7.1 Characteristics of the reference molten salt fast reactor

Thermal/electric power	3000 MW_{th}/1300 MW_e
Fuel salt temperature increase in the core (°C)	100
Fuel molten salt, initial composition	LiF-ThF_4-(^{233}U or ^{enr}U)F_4 or LiF-ThF_4-(Pu-MA)F_3 with 77.5 mol% LiF
Fuel salt melting point (°C)	565
Mean fuel salt temperature (°C)	700
Fuel salt density (g/cm^3)	4.1
Fuel salt dilation coefficient (g/cm^3 °C)	8.82×10^{-4}
Fertile blanket salt, initial composition (mol%)	LiF-ThF_4 (77.5−22.5%)
Breeding ratio (steady-state)	1.1
Total feedback coefficient (pcm/°C)	−5
Core dimensions (m)	Radius: 1.1275 Height: 2.255
Fuel salt volume (m^3)	18
Total fuel salt cycle in the fuel circuit	3.9 s

Table 7.2 Physicochemical properties of the fuel salt and of the intermediate fluid measured for the salt 78%mol LiF-22%mol ThF_4 (Ignatiev et al., 2012)

	Formula	Value (at 700°C)	Validity range (°C)
Density ρ (kg/m^3)	$4094-0.882\ (T_{(K)} - 1008)$	4125	[617−847]
Kinematic viscosity ν (m^2/s)	$5.54 \times 10^{-8} \exp\{3689/T_{(K)}\}$	2.46×10^{-6}	[625−847]
Dynamic viscosity μ (Pa s)	$\rho_{(g/cm^3)}\ 5.54 \times 10^{-5} \exp\{3689/T_{(K)}\}$	10.1×10^{-3}	[625−847]
Thermal conductivity λ (W/m K)	$0.928 + 8.397 \times 10^{-5} \times T_{(K)}$	1.0097	[618−847]
Heat capacity C_p (J/kg K)	$-1.111 + 0.00278 \times 10^3\ T_{(K)}$	1594	[595−634][a]

[a]The formulas have been extrapolated up to 700°C.

In the fuel circuit, after exiting the core, the fuel salt is fed into 16 groups of pumps and heat exchangers located around the core. The salt traveling time through the whole fuel circuit is 3−4 s (Brovchenko et al., 2012). The total fuel salt volume is distributed half in the core and half in the external portion of the fuel circuit.

The external core structures and the fuel heat exchangers are protected by thick reflectors made of nickel-based alloys, which are designed to absorb more than 99% of the escaping neutron flux. These reflectors are themselves surrounded by a 20-cm thick layer of B_4C, which provides protection from the remaining neutrons. The radial reflector includes a fertile blanket (50 cm thick, *red area* in Fig. 7.1) to increase the breeding ratio. This blanket is filled with a LiF-based fertile salt with initially 22.5 mol% $^{232}ThF_4$. Because of the neutron inelastic scattering on fluorine nuclei (see Fig. 7.2), the MSFR spectrum is a bit more epithermal than that of solid-fueled fast reactors. This fact, combined with the absence of solid material in the core, results in reduced irradiation damages of the materials surrounding the core.

The fuel circuit is connected to a salt draining system that can be used for a planned shutdown or in case of any incident/accident resulting in an excessive temperature being reached in the core. In such situations the fuel salt geometry can be passively reconfigured by gravity-driven draining of the fuel salt into tanks located under the reactor and where a passive cooling and adequate reactivity margin can be implemented.

The MSFR, as a liquid-fueled reactor, calls for a new definition of its operating procedures. The negative feedback coefficient provides intrinsic reactor stability. The reactor may be driven by the heat extracted, for example, allowing a very promising flexibility for grid load-following. Unlike with solid-fueled reactors, the negative feedback coefficient acts very rapidly because the heat is produced directly in the coolant, with the fuel salt itself being cooled in the heat exchangers.

7.2.2 Transient calculations

The definition and assessment of MSFR operation procedures requires dedicated tools to simulate the reactor's behavior and assess its flexibility during normal (eg, load-following) or incidental (eg, pump failure) transients. The reactor modelization requires specific treatments to take into account the phenomena associated with the liquid-fuel circulation.

Classical calculation codes cannot be directly used because of the specificity of the core cavity's geometry and because of the precursor motion. The latter and the MSFR thermal feedback effects imply a strong coupling between the neutronics and the thermal hydraulics during reactor transient calculations. Thus dedicated tools are currently being developed. Coupled with a computational fluid dynamics (CFD) calculation code, different neutronics models are used, as detailed in this section: the transient fission matrix (TFM) approach, the diffusion model, or the direct coupling with a Monte Carlo (MC) approach for reference calculations with a reduced computational time. The use of a CFD code allows for the calculation of the three-dimensional (3D) velocity and temperature distributions. The latter, along with the density distribution, has a significant effect on the neutronic behavior through the induced variations in the neutron macroscopic cross sections. Recent studies highlighted the large effect of CFD modeling hypotheses on the MSFR analysis and the need to adopt accurate turbulence models and realistic 3D geometries (Rouch et al., 2014; Brovchenko et al., 2014a; Dulla et al., 2014). In this view, the OpenFOAM multiphysics toolkit allowed an efficient simulation of steady-state and transient cases on detailed, full-core, 3D geometries (Jasak et al., 2007).

The effective delayed neutron fraction (β_{eff}) represents an important reactor kinetics parameter. In circulating-fuel systems, because of the delayed neutron precursor drift, the β_{eff} calculation requires special techniques. The coupled neutronics/CFD simulations represent a necessary step for the accurate calculation of the effective delayed neutron fraction in the MSFR (Aufiero et al., 2014). Fig. 7.3 shows the distributions of the prompt (right) and delayed (left) neutron sources obtained in OpenFOAM and adopted to calculate β_{eff} in the nominal MSFR conditions.

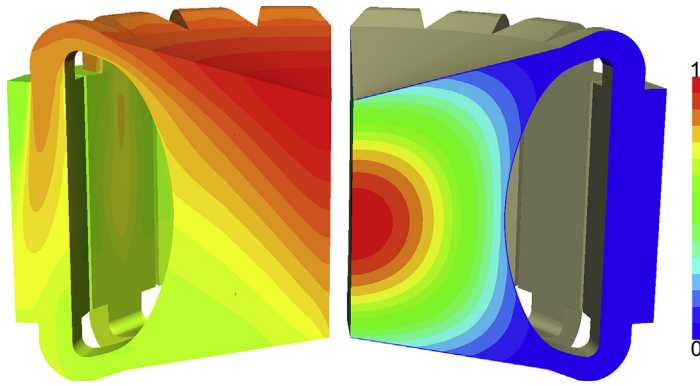


Figure 7.3 Delayed (left) and prompt (right) neutron sources in the molten salt fast reactor.

Some simplified tools were developed for the modeling of the MSFR neutronics, including the diffusion approximation of the neutron transport equation. Other tools adopted the fine-element, the finite-difference, or the finite-volume discretization of the coupled equations of the CFD/neutronics problem. All of these tools proved useful as fast-running options, during the initial MSFR design optimization phase, in identifying the specifics of the reactor physics of circulating-fuel systems confronted with thermal feedbacks on the neutronics.

The TFM approach (Laureau et al., 2015b; Laureau, 2015c) has been developed specifically as a neutronic model able to take into account the precursor motion-associated phenomena and to perform coupled transient calculations with an accuracy close to that of MC calculations for the neutronics while incurring a low computational cost. This approach is based on a precalculation of the neutronic reactor response through time before the transient calculation. The results of the SERPENT MC code (Leppänen, 2013) calculations are condensed in fission matrices, keeping the time information. These fission matrices are interpolated to take into account local Doppler and density thermal feedback effects due to temperature variations in the system. With this approach, an estimation of the neutron flux variation for any temperature and precursor distribution in the reactor can be very quickly obtained.

The results obtained with this method applied to an instantaneous load-following transient are shown in Figs. 7.4 and 7.5 (Laureau et al., 2015a). The initial condition corresponds to a critical reactor with 1.5 GW_{th} power. At the beginning of the simulation the temperature of the intermediate circuit is reduced to increase the power extracted up to 3 GW_{th}. After 1 s the feedback effect stops the increase of the neutron population, and the reactivity progressively returns to its initial value with a time constant corresponding to the balancing of the delayed neutron precursor population. An oscillation corresponding to the circulating time of the fuel salt can be observed. This application case highlights the good behavior of the reactor to load-following transients.

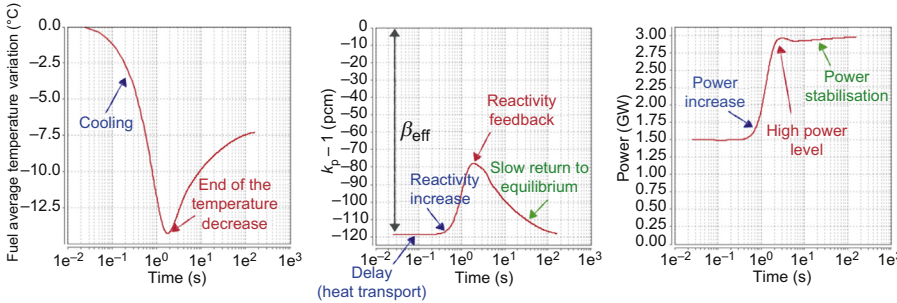


Figure 7.4 Instantaneous load-following transient of the molten salt fast reactor from an extracted power of 1.5−3 GW_{th} computed with the TFM-OpenFoam coupled code (Laureau et al., 2015a).

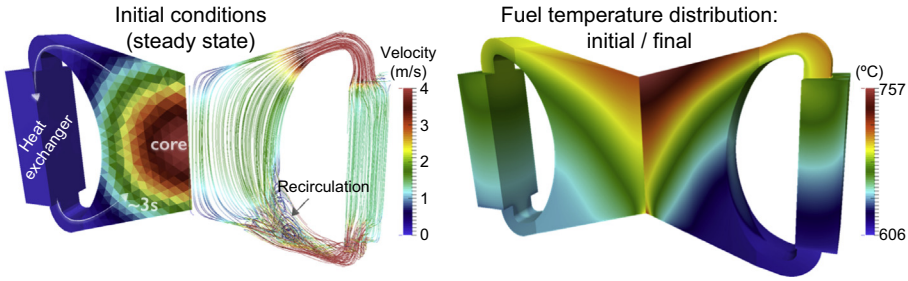


Figure 7.5 Distribution of power, velocity, and temperature in the molten salt fast reactor (Laureau et al., 2015a).

7.3 Fuel salt chemistry and material issues

7.3.1 Overview of the processing schemes

The fuel salt undergoes two types of treatment: online neutral gas bubbling in the core and delayed mini-batch on-site reprocessing (Delpech et al., 2009). These salt treatments aim at removing most of the FPs without stopping the reactor and thus securing a rather small fissile inventory outside of the core compared with present day light water reactors (LWRs). The reprocessing rate itself is assumed equivalent to the present LWR rate, although it could be possible to reprocess the fuel salt every 10 years but to the detriment of economical yield.

The salt treatment is schematically presented in Fig. 7.6. It consists of two circuits. One is a continuous gas bubbling in the core to extract the gaseous FPs and the metallic particles present in the salt (metallic FPs and corrosion products). The gaseous stream is sent to a provisional storage where most of the Kr and Xe decay into Rb and Cs, preventing their accumulation in the fuel salt. The remaining gas is recycled.

The other is a semicontinuous salt reprocessing at a rate of approximately 10 L per day to limit the lanthanide and Zr concentration in the fuel salt. The salt sample is returned to the reactor after purification and after addition of ^{233}U and Th as needed to adjust the fuel composition. This is also an opportunity to tune the oxidoreduction potential of the salt by controlling the U^{4+} to U^{3+} ratio.

These two processes are aimed at keeping the liquid-fuel salt in an efficient physical and chemical state for long time periods (decades). The gas bubbling has two objectives: removing metallic particles by capillarity (floating) and extracting gaseous FPs before their decay in the salt. The pyrochemical salt batch reprocessing avoids the accumulation in the fuel salt of large quantities of lanthanides and Zr that could be detrimental to several properties such as Pu solubility or salt volatility. Conversely to the thermal MSR, none of these processes are vital to the fast reactor operation. If they were interrupted for months or years, then the MSFR would not stop but would have a poorer breeding ratio and could suffer from partial clogging of the heat exchangers, leading to poorer efficiency. The effect of the batch pyroprocessing rate is shown in Fig. 7.7. Note that with the reactor configuration used for the calculation,

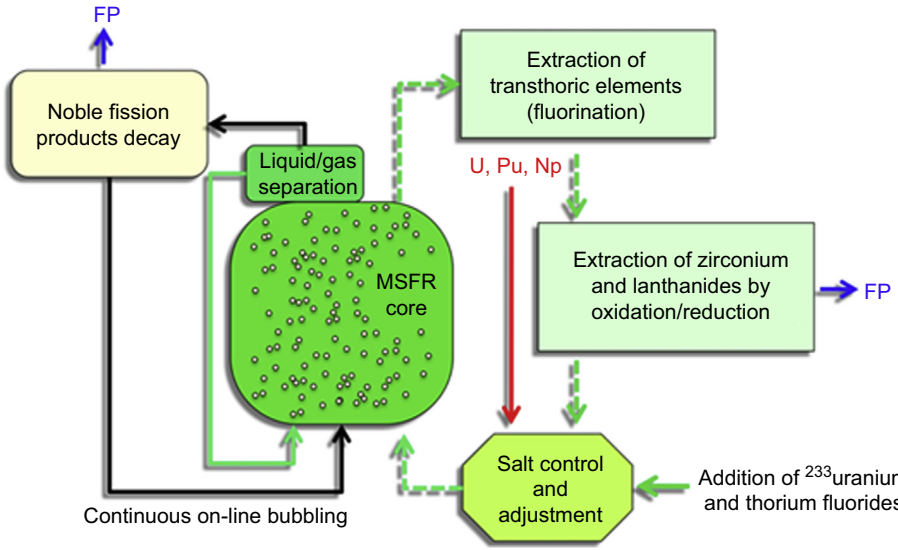


Figure 7.6 Schematic representation of the fuel salt treatment with two loops. On the left is the online treatment with gas bubbling in the core to extract noble gases and metallic particles (fission products [FPs]). On the right is the mini-batch on-site reprocessing with two objectives: removing FPs (Zr, Ln) and adjusting the fuel content in fissile and fertile isotopes. *MSFR*, molten salt fast reactor.

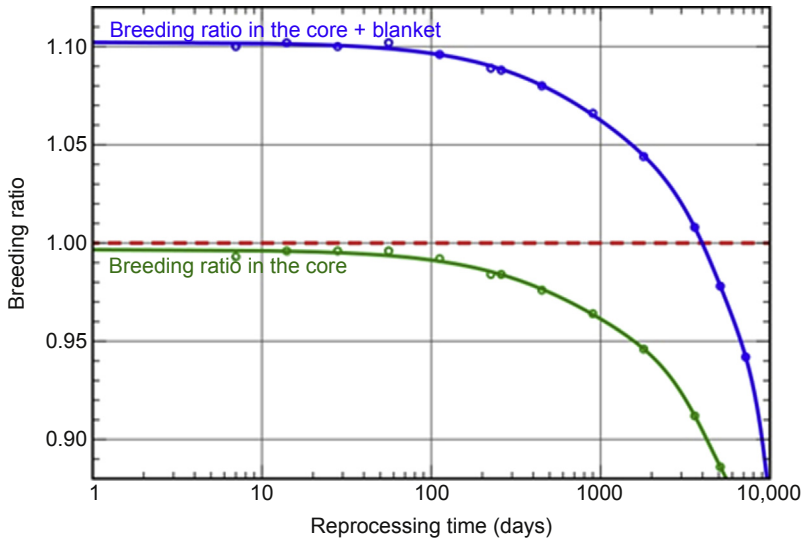


Figure 7.7 Influence of the batch reprocessing rate on the breeding ratio in the core and in the whole molten salt fast reactor system (core + fertile blanket).

the core is under-breeder. The addition of a fertile blanket secures breeding, up to a reprocessing time of the total fuel salt volume as large as 4000 days.

7.3.2 Impact of the salt composition on the corrosion of the structural materials

Material corrosion in molten salt nuclear reactors results from the evolution of the salt composition during operation: production of HF by an uncontrolled purification process or by hydrolysis reactions, production of corrosive FPs, or mass transfer in thermal gradients. Ni-based alloys have been recognized as the most suitable materials for their mechanical and chemical resistance up to approximately 700°C in the presence of fluoride salts. Graphite presents an excellent compatibility with molten fluorides, but it cannot be used for structural applications submitted to a neutron flux. Silicon carbide has a good irradiation and very high temperature resistance, and it might be an acceptable solution for corrosion. However, assembling SiC parts is not usual technology, and its long-term chemical behavior has not yet been tested in molten fluorides.

The historical tests performed at ORNL have shown that a chemical potential control of the salt was necessary to prevent two types of corrosion: Cr oxidation and intergranular corrosion by Te (an FP). This was achieved by using a chemical buffer based on the U^{4+}/U^{3+} couple. The proper U^{4+}/U^{3+} concentration ratio was obtained by contacting the salt with metallic Be from time to time to keep this ratio in a suitable range (eg, 60−20). The change of chemical potential of the fuel salt is intrinsic to the fission of fissile elements present in the fuel at valence IV because the resulting FPs have a mean valence close to III. Therefore the salt becomes more oxidizing as fissions occur; an initial chemical potential control of the salt is necessary but never sufficient to prevent corrosion. It has been shown that Cr is necessary for the mechanical properties of Ni-based alloys and not only for their chemical resistance to oxidation in air. However, its concentration should be limited to approximately 6−8 wt% to keep the corrosion rate at an acceptable level.

Before the use of the U^{4+}/U^{3+} chemical buffer a salt purification is required for the initial salt preparation or when recycling the actinides after lanthanide extraction. H_2O and HF are the most oxidizing compounds present as impurities in solid fluorides and in the molten salt. High oxidation state, H_2O, and dissolved oxides can be eliminated by using gaseous H_2/HF mixtures, but some HF may remain dissolved in the salt. Care should be taken to limit this dissolved amount. For a salt not containing Be ions the ultimate reduction can be achieved by addition of U^{3+} when recycling U into the fuel salt or by reduction with metallic Th (Th should be added anyway to compensate for neutron captures).

7.4 Molten salt fast reactor fuel cycle scenarios

To produce power, a fission nuclear reactor requires fissile material. Generation II or III reactors (pressurized water reactor [PWR], CANDU, evolutionary power reactor [EPR], etc.), being under-breeder systems (ie, using more fissile material than they

produce), need to be regularly refueled with fissile material all along their operation time. On the contrary, breeder Generation IV reactors (sodium-cooled fast reactor [SFR], MSFR, gas fast reactor, etc.) require only one (or two in the case of solid fuel reactors) initial fissile material load. They then produce at least the fissile material they need to be operated during their entire lifespan. MSRs require only one fissile load because no fuel refabrication is necessary and the fuel salt composition is controlled online without stopping reactor operation whereas two loads are necessary for solid-fueled reactors, with one fissile load inside of the reactor and the other in the reprocessing/fuel manufacturing process.

According to our simulations results, the thorium-based MSFR can be started with various initial fissile loads as follows (Heuer et al., 2014; Merle-Lucotte et al., 2009a,b, 2011):

- With U235-enriched uranium—the only natural fissile material available on Earth is ^{235}U (0.72% of natural uranium). Enriched uranium can be used directly as initial fissile material to start MSFRs with an enrichment ratio less than 20% because of proliferation resistance issues.
- With ^{233}U directly as initial fissile material; for example, assuming that this ^{233}U can be produced in fertile blankets of other reactors (SFR, etc.) or by irradiating ^{232}Th in an accelerator-driven system. Once an initial park of MSFRs based on the Th-^{233}U cycle is launched, ^{233}U will also be produced in breeder MSFR reactors, allowing the deployment of such ^{233}U-started MSFRs in a second phase even if no ^{233}U is produced elsewhere.
- With the plutonium produced in current PWRs or in future EPRs or, even better, the mix of TRU produced by these Generation II–III reactors as initial fissile load.
- With a combination of the previous starting modes. For example, ^{233}U may be produced by using special devices containing thorium and Pu-mixed oxide (Mox) in current PWRs or in future EPRs.
- Fig. 7.8 presents two examples of fuel composition evolutions for a "3 GW_{th} reference MSFR" reactor started with ^{233}U or TRU. An optimized fuel salt initially composed of LiF-ThF_4-enriched UF_4-$(TRU)F_3$ with uranium enriched at 13% in ^{235}U and a TRU proportion of 3% (see Fig. 7.9), has been selected in the frame of the EVOL project taking into consideration the neutronics, chemistry, and material issues.

Given the absence of naturally available ^{233}U, a standing question is whether a park of MSFRs can be deployed whether at the French national, the European, or the worldwide scales. In this section we illustrate the flexibility of the concept in terms of deployment and end-of-game capacities of the MSFR at the French national scale.

The deployment scenarios of a park of nuclear reactors also led to an estimation of the amount of heavy nuclei produced by such a deployment. We aim at evaluating the complexity of the management of these heavy nuclei stockpiles as well as their radiotoxicity. The French scenario, displayed in Fig. 7.10, assumes that the natural uranium resources available are large enough to require Generation IV reactors in 2070 only. The deployment scenario starts with the historical French nuclear deployment based on LWRs (PWRs followed by EPRs). By 2040 some Generation III reactors are fueled with Pu-uranium oxide (Uox) in a thorium matrix to reduce MA production and to prepare the launching of the thorium fuel cycle in MSFRs. The park of these Generation III reactors is then progressively replaced with MSFRs started with this Th-Pu Mox

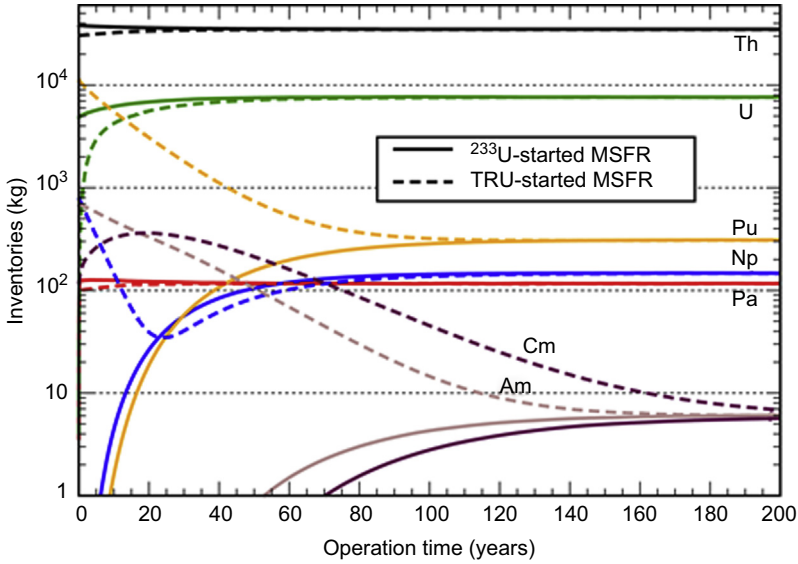


Figure 7.8 Time evolution up to equilibrium of the heavy nuclei inventory for the ^{233}U-started MSFR (*solid lines*) and for the TRU-started MSFR (*dashed lines*). Operation time is given in equivalent full power years. *MSFR*, molten salt fast reactor; *TRU*, transuranic element.

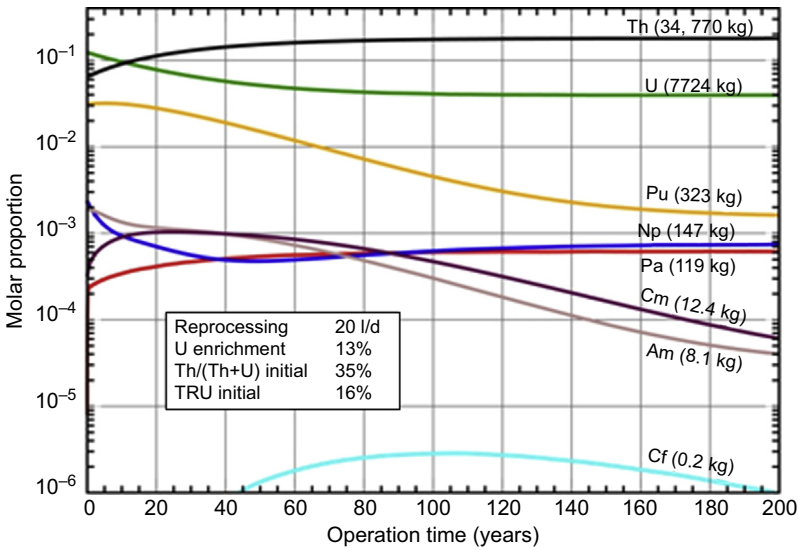


Figure 7.9 Time evolution up to equilibrium of the heavy nuclei inventory for the optimized MSFR configuration started with enriched uranium and TRUs. Operation time is given in equivalent full power years. *MSFR*, molten salt fast reactor; *TRU*, transuranic element.

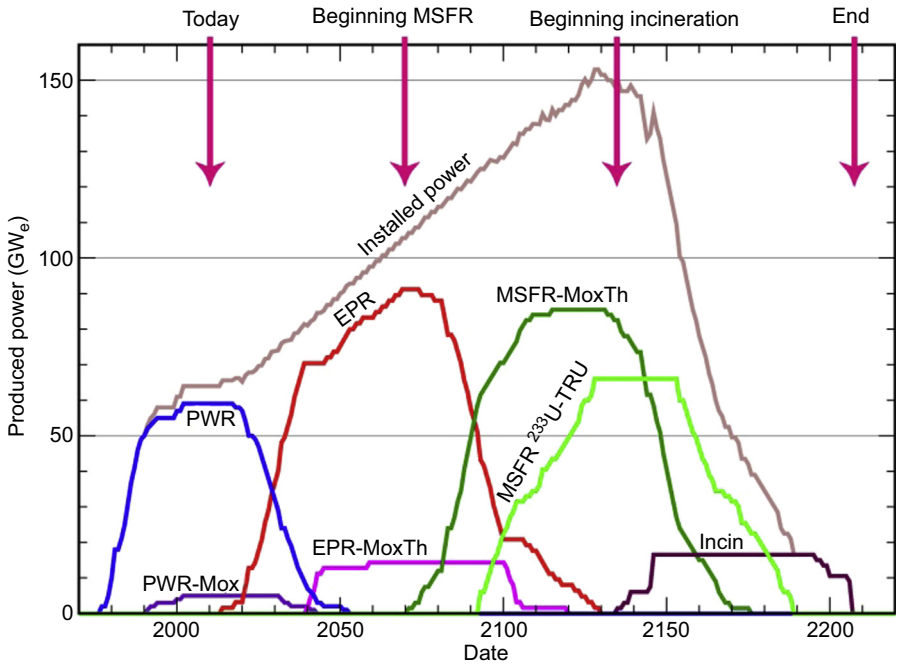


Figure 7.10 French nuclear power deployment exercise based on pressurized water reactors (PWRs), evolutionary power reactors (EPRs), and molten salt fast reactors (MSFRs).

fuel from the last Generation III reactors. The deployment is finally completed with MSFRs started with a mix of ^{233}U produced in the existing MSFRs and the remaining stockpiles of Pu-Uox and Pu-Mox irradiated in the LWRs.

Assuming that, at any time in the future, here in the first half of the 22nd century, France resolves to dispense from the production of fission-based nuclear energy, the scenario ends with the introduction of burners with a view to optimizing the end of game and further reducing the final TRU inventories after MSFR shutdown. Note that the end-of-game situation would not be different if it occurred after hundreds of years of operation; it depends only on the installed power.

The evolution of the radioactive element stockpiles other than the FPs during the scenario is shown in Fig. 7.11. The final stockpiles that will have to be managed as the scenario ends are the following:

- Depleted uranium at 0.1%: 803,700 t.
- Uranium from reprocessing (minimized by the scenario management): 3250 t.
- Irradiated thorium: 5100 t.
- Irradiated Uox fuel (minimized by the scenario management) represented in Fig. 7.10 by its Pu content (labeled "Pu-Uox"): 5 t of Pu standing for 450 t of irradiated Uox.
- Irradiated Mox fuel (minimized by the scenario management) represented in Fig. 7.10 by its Pu content (labeled "Pu + MA Mox"): 0.76 t standing for 12.4 t of irradiated MOX.

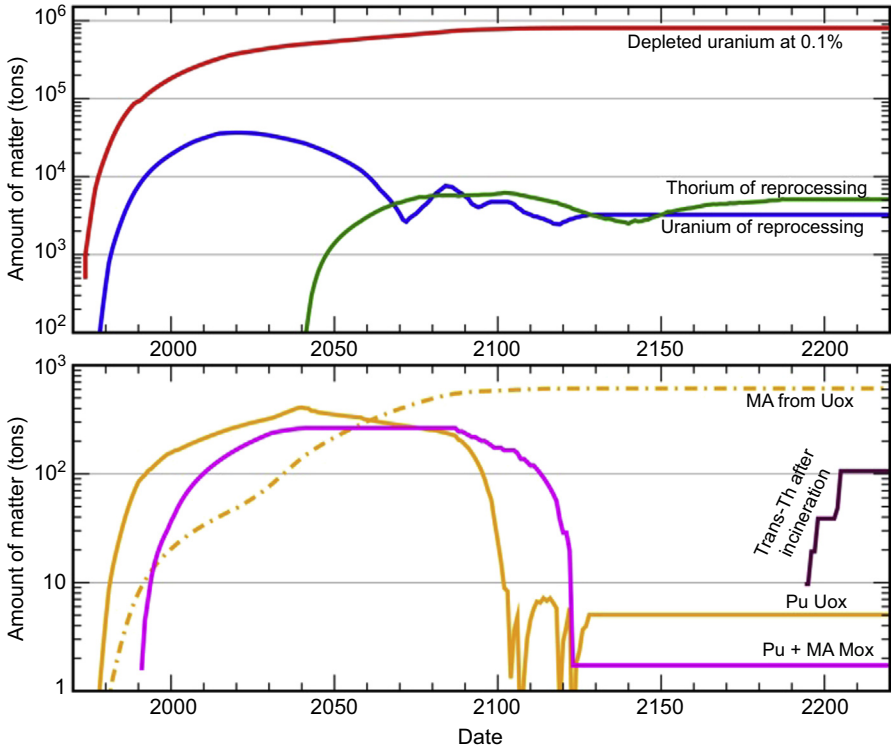


Figure 7.11 Evolution of the actinide stockpiles during the scenario considered. *MA*, minor actinides; *Uox*, uranium oxide.

- MAs separated from the Pu when the latter is used as Mox fuel in LWRs and vitrified (labeled "MA from Uox"): 612 t.
- Final burner inventories: 106 t.

The evolution of the radiotoxicity corresponding to the final radioactive stockpiles of this scenario, including the FPs, is displayed in Fig. 7.12, in which it appears that the short-term radiotoxicity (a few dozen years) is dominated by the FP whereas the long-term radiotoxicity (10^3–10^6 years) is mainly due to the vitrified MAs produced in LWRs and not reused in Mox fuel.

7.5 Safety issues

In the frame of the EVOL Euratom project in collaboration with Russian research organizations cooperating in the ROSATOM project MARS (Minor Actinides Recycling in Molten Salt; Ignatiev et al., 2012), design and safety studies of the MSFR system have been led (Brovchenko et al., 2014b; Wang et al., 2014).

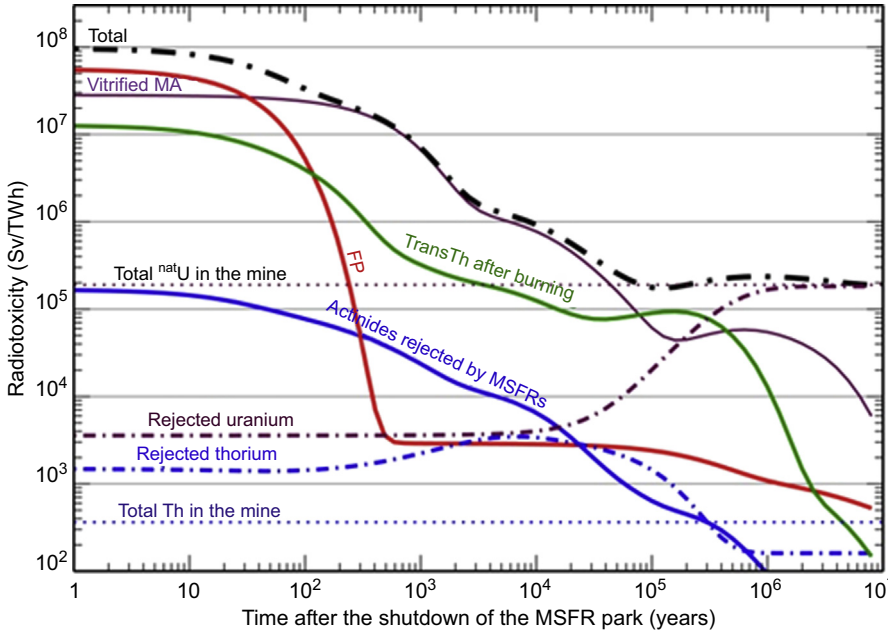


Figure 7.12 Time evolution of the various contributions to the radiotoxicity of the final radioactive stockpiles.

An MSR has some specific safety features because the fuel salt geometry can be modified quickly and passively by draining to subcritical tanks. It is possible to design the system with a maximum of passive devices to cool the fuel in all circumstances and for long times without human intervention. Moreover, the MSFR reactor stability is enhanced by its largely negative feedback coefficients. Some of these features are discussed in Section 7.5.2, but not all safety provisions are detailed.

7.5.1 Safety approach and risk analysis

The unique characteristics of a liquid-fueled reactor strongly impact its design and safety analyses. For example:

- The safety principle of defense-in-depth and multiple barriers must be re-adapted because conventional barriers (eg, clad, primary circuit, and containment in LWRs) are no longer applicable.
- The diversity and mutual independence of the MSFR reactivity control mechanisms must be demonstrated (no control or shut-down rods or burnable poisons, etc.).
- New safety criteria to evaluate reactor response during normal, incidental, and accidental conditions are needed because the MSFR fuel is in liquid state, which is not an acceptable situation for the LWR fuel.

- In the evaluation of severe accident scenarios with leakage to the environment, any interactions between the fuel salt and groundwater should be investigated in detail and the source term should be determined.
- The risk posed by the residual decay heat and the radioactive inventory in the reprocessing unit must also be evaluated.

A novel methodology for the design and safety evaluations of the MSFR is needed. Nevertheless, it would be desirable that the MSFR methodology rely on current accepted safety principles such as the principle of defense-in-depth, the use of multiple barriers, and the three basic safety functions: reactivity control, fuel cooling, and radioactive product confinement. In addition, because of the limited amount of operation experience and some of its novel features, any new methodology shall be robust and comprehensive and integrate deterministic and probabilistic approaches. To fulfill these objectives, an MSFR design and safety analysis methodology is currently being developed (Brovchenko, 2013) according to the following steps:

1. Systemic modeling of all reactor components using a model-based risk analysis tool;
2. Identification of the safety functions, which are to be defined from the components' functional criteria;
3. Identification of reactor abnormal events (failure modes and dangerous phenomena); and
4. Risk evaluation: evaluation of the probability and the severity of events.

The design and safety criteria should ensure that all of the reactor components adequately perform the safety functions to meet the requirements defined for each plant operating condition. The MSFR development being at its early stages, the idea is to adopt an inherent safety-by-design approach. Fig. 7.13 gives a preliminary view of a systematic description of the MSFR fuel circuit in terms of components and safety functions.

7.5.2 Liquid-fueled reactor specificities

The design characteristics of the MSFR have been evaluated regarding safety issues. An example has been chosen here to illustrate this approach. One of the assets of the liquid-fueled MSFR systems is the homogeneity of the fuel. In a general way this type of reactor can be placed in a category with all of the reactors that run with a circulating fluid fuel (whether gaseous or liquid). These are referred to as homogeneous reactors. Since the 1960s it has been shown that, in the case of homogeneous reactors without reactivity reserve, control rods are not necessary to control reactor operation (Briggs and Swartout, 1955). The MSFR, which is self-controlled because of its negative temperature feedback coefficients and the absence of in-core reactivity reserve, fits in this category and, consequently, control or safety rods are not included in the design being considered. Contrary to a PWR, it does not require neutron flux shape control because the fuel is permanently homogenized and the coolant, here the fuel salt itself, can undergo large temperature increases (100−200°C) with no risk of a boiling crisis susceptible to threaten the integrity of the cladding.

The three barriers traditionally used in the defense-in-depth approach were defined in the specific frame of the PWR reactor development or, more generally, in the frame

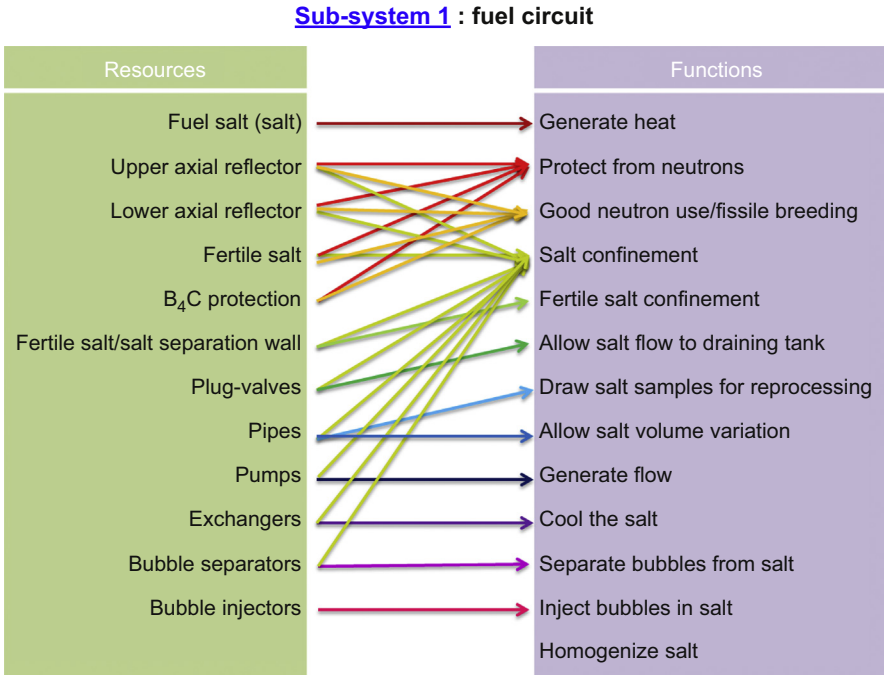


Figure 7.13 Resources and functions of the fuel circuit subsystems. The corresponding resources and functions are shown by *arrows* that are color coded to improve the legibility of the graph.

of solid-fueled reactors. Similar to other safety notions, the transposition of the confinement barriers first mandates more general consideration of the origin and application of this concept. These barriers will eventually have to be redefined according to their usefulness for each reactor design rather than seeking an equivalence with PWRs. An extensive study adapted to the sequence of potential accidental events will have to determine or confirm the number of necessary confinement barriers in the case of the MSFR as well as their configuration. However, as a first step and as a pedagogical illustration describing the overall facility, the three fuel salt confinement barriers in the MSFR can be identified by analogy with PWRs as shown in Fig. 7.14:

- *Pink*: The fuel circuit (heat exchangers, pumps, etc.) and the draining system (tanks and pipes) totally within the fuel casing.
- *Light blue*: The reactor vessel, the intermediate circuit, and the draining system's water circuit.
- *Gray*: The reactor containment structure (the building) and the emergency cooling chimney, not shown on the figure.

The first barrier (pink) includes three zones. The upper zone contains the fuel circuit (green) and the neutral gas reprocessing (yellow). A collector for salt draining is

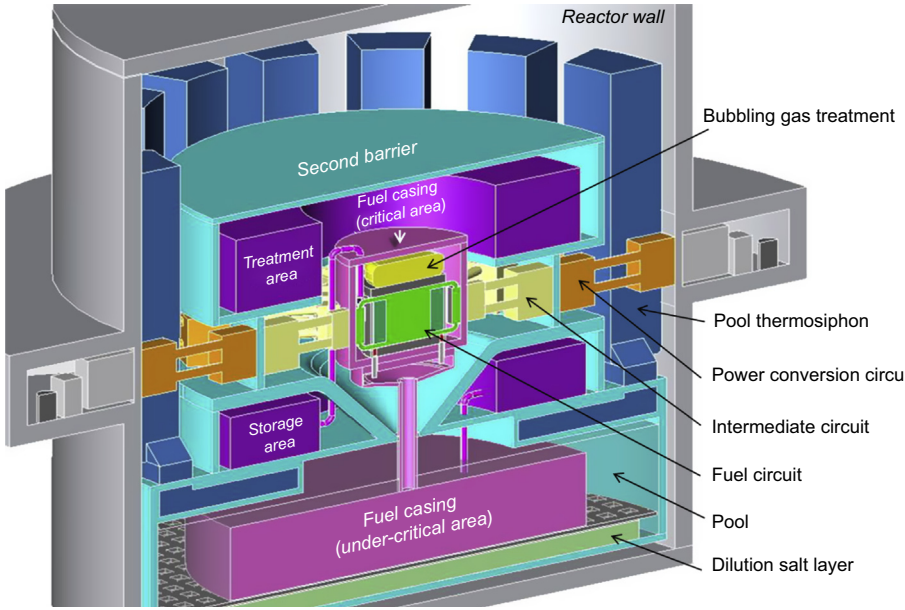


Figure 7.14 Illustration of the main functions associated with the molten salt fast reactor operation. In the middle is the green fuel salt circuit surrounded by a pink envelope representing the first confinement barrier. The cyan envelope represents the second barrier including storing and chemical salt processing units in violet. The third barrier is in gray. Two heat transfer circuits between the three barriers are represented as loops in yellow and orange.

represented (funnel and vertical tube), leading the drained salts to containers with subcritical geometry (not detailed) situated in a large water pool. This large water pool acts as a thermal buffer in case of high-temperature emergency draining. At the bottom of this pool is located a layer containing a dilution salt that can passively mix with the fuel salt in the case of a large first barrier failure. This can provide neutron poisons to the fuel and create a large salt−wall interface for passive cooling in the event of a severe accident. Heat pipes (dark blue) are used to transfer the decay heat to the atmosphere. This means that decay heat can be removed into the atmosphere in case of a heat sink failure.

Other systems that also contain radioactive materials have to be studied, in particular the fertile blanket salt system, including the storage and processing of the associated gases, and all of the related intersystem transfers.

As a brief conclusion to this section, let us recall that the global safety objectives are fully transposable to the MSFR reactor. The difficulty lies, among other things, in the identification of severe accidents for this type of reactor. Thus a core melt in the case of solid-fueled reactors is central to present safety studies and has no immediate equivalent in a liquid-fueled reactor. A safety analysis for the MSFR must then proceed from the fundamentals of nuclear safety.

7.5.3 Decay heat removal

The decay heat generation is represented versus time in Fig. 7.15. The MSFR design implies that FPs are present in two different places when the reactor is stopped. Some are in the liquid-fuel salt and some in the gas processing unit. Approximately one-third of the heat is produced in the gas processing unit and two-thirds in the liquid fuel. The power of both heat sources decreases rapidly (by a factor of 10 in ~1 day) from the value at shutdown, which depends on the history of power generation. The total amount of power at shutdown is approximately 5% of the nominal power. This value is lower compared with solid fuel reactors because FPs are continuously removed in this concept.

In case of cooling problems the fuel salt and the fluid containing FPs (salt or metal) of the gas processing unit can be drained into a subcritical tank located in a water pool. For instance, a large amount of water is used as a decay heat thermal buffer so as to reduce the heat to cold sink transfer rate need by a factor 10. This heat transfer is achieved by passive thermos siphons or heat pipes to the atmosphere through the reactor building walls (the third barrier). If unattended for a very long time, then the fuel salt will solidify.

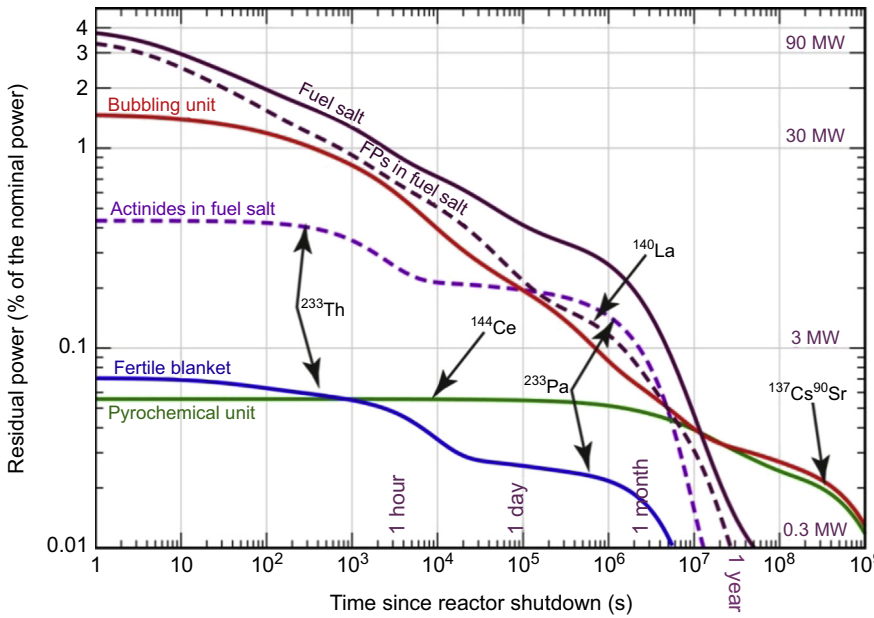


Figure 7.15 Residual heat in the different radioactive fluids of the molten salt fast reactor, after the total fission shutdown of the reactor previously in steady state (Brovchenko et al., 2012, 2013b). *FPs*, fission products.

7.5.4 Preliminary accidental transient identification

- A direct transposition to liquid-fueled reactors of the traditionally identified accidents of solid-fueled reactors is not possible. In a liquid-fueled reactor, the fuel is also the coolant so that a loss of coolant accident implies the simultaneous loss of the fuel and of the coolant. We can study these initiators by equating the primary circuit coolant to the liquid fuel while keeping in mind that the phenomena related to the accidents will not necessarily be comparable to those of a solid-fueled reactor. Another interpretation could identify the MSFR's intermediate circuit with a solid-fueled reactor's primary circuit. To retain more clarity, we prefer to redefine the accident types as outlined in the following for the fuel circuit:
- *Loss of flow*: In the fuel circuit loss of flow accident, we gather all of the accidents that are not associated with a slowing down or stalling of the intermediate fluid circulation and are not due to a loss of fuel.
- *Loss of heat sink*: In a loss of heat sink accident, the fuel salt circulation continues unchanged but its cooling is no longer ensured.
- *Total loss of power*: In the event of on-site total loss of power, all of the pumps are stalled in the fuel, intermediate, and conversion circuits, and all active systems connected to the power supply are assumed nonoperational. In this type of accident, the on-site security power supply is also considered deficient.
- *Transient overpower or overcooling*: An overcooling accident increases the reactivity and, as a consequence, the power generated because the reactor's thermal feedback coefficient is negative.
- *Loss of liquid fuel*: In the loss of liquid fuel accident, we consider a significant leak of the fuel salt outside of the fuel circuit.
- *Reactivity anomalies accident*: Because the reactivity reserve is very small in the MSFR, reactivity-related accidents have to do with reactivity anomalies rather than accidents of the transient overpower type (control bar ejection). In fact, reactivity variations incurred in this reactor are much smaller than they are in a PWR.

This preliminary list of accidents results from the application of the general safety assessment methodology mentioned earlier and currently under development for liquid-fuel reactors. The next steps for this safety evaluation will take place under the framework of the Horizon2020 European Commission project SAMOFAR starting in the second half of 2015 up to 2019.

7.6 Concept viability: issues and demonstration steps

7.6.1 Identified limits

Although the MSFR is still at the preconception design stage, several limiting factors can be identified in the development of the concept. The first, obvious, issue is materials' resistance to high temperatures under irradiation if the reactor is to be operated with a reasonably high power density. A first temperature limit is given by the fuel salt melting point (565°C), to which a safety margin should be added to avoid local solidification (eg, 50°C). To this, add 100−150°C for in-core temperature heating corresponding to a salt circulation period of 3−4 s so as to satisfy heat transfer dynamics in the heat exchangers without incurring an excessive pressure drop within these. This

leads to a temperature of approximately 750°C at the core outlet to the gas-salt separation device and the pump (hot leg). Those devices may be maintained at 700°C by cooling (ie, the same temperature as the heat exchanger plates during the heat transfer), the intermediate coolant salt being at approximately 650°C. It seems that there are today alloys that can withstand such temperatures for a long time, but this could be a limit unless the material is replaced regularly as is done with solid fuel cladding.

The second issue arises in the attempt to limit the per-gigawatt fissile inventory. This implies restricting as much as possible the proportion of fuel salt out of the core, in the tubing, pumps, and heat exchangers. One of the main constraints on the design of the MSFR fuel circuit is the ability to evacuate the heat generated while restraining the fuel salt volume mobilized for that task. It seems technically challenging to reduce this "useless" amount of salt to less than 50% of the total load, and 30% appears to be the limit.

The third issue is a question more than it is a real limit: the safety evaluation. Indeed, as discussed above, today's safety evaluation techniques apply to solid fuel water reactors but are partly irrelevant for liquid-fuel reactors. A new way of tackling the problem should find a consensus before any national safety authority can approve of a liquid-fuel reactor design, and this will take time and resources.

From the parametric studies that were performed on the MSFR, the concept does not exhibit any major stumbling blocks and the various limits can all be circumvented by reducing the power density.

7.6.2 Progression in safety demonstration and design optimization

It is possible to design a low-power demonstration reactor in which to test all of the features expected for a full-size reference MSFR with a single fuel loop, as shown in Fig. 7.16. Its fissile inventory lies in the range of 400−500 kg of ^{233}U for a zero power version and up to 670 kg for a 200-MW_{th} version.

The size of the reactor liquid-fuel loop is not a limit as shown by the calculation of a single-loop 200-MW reactor instead of a 16-loop 3-GW_{th} reactor. The low-power demonstration version (Merle-Lucotte et al., 2013) as sketched in Fig. 7.16 could be replaced by a regenerator version if the reflectors were replaced by a blanket. The size of this fuel loop assembly is approximately 2.5 m in diameter and 3 m high (core: 1.1 m diameter and 1.1 m high). The power is limited by the intermediate exchanger size, which is assumed to be the same as that of the 3-GW_{th} reactor.

Before reaching this advanced level it will be necessary to bring evidences of safety for all experiments involving nuclear materials under the supervision of nuclear safety agencies. To get the clearance of these authorities the reliability and safety of the technical solutions involved should be demonstrated first on pieces of equipment operating with non-nuclear materials (simulant salts or chemicals). Therefore the following simplified scheme is foreseen:

- basic data determination and assessment (it is the present stage up to about 2020),
- technical devices testing on non-nuclear simulants up to the full scale,

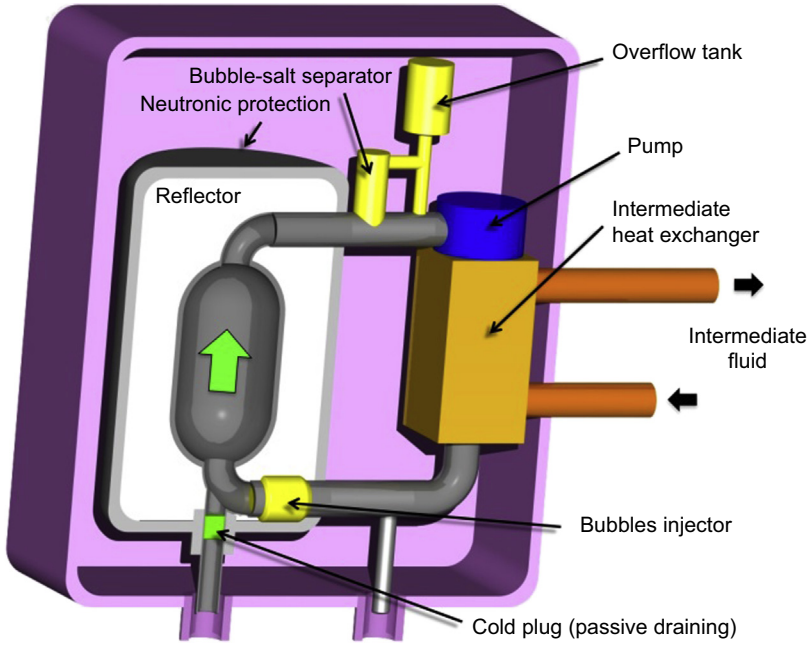


Figure 7.16 Sketch of a liquid-fuel single loop reactor for demonstration purposes or modular conception. The fuel volume (1.8 m^3) is reduced by a factor 10 from the 3-GW_{th} reactor and the power (200 MW_{th}) by a factor 15 to use the same intermediate heat exchanger.

- chemical separation tests on nuclear materials at a small laboratory scale and by remote handling, and
- development of numerical simulation tools validated on experimental equipment using circulating simulant salts at high temperature.

Obviously all of the stages mentioned here will overlap in time, not only for practical reasons but because all of the aspects of the design should be kept in mind and documented during the whole development procedure. According to present international standards, safety and proliferation resistance should be analyzed from the beginning of the conception to be inherent in the design and not "added-after."

7.6.3 Presently ongoing laboratory-scale experiments

Several experimental setups are being operated at LPSC-Grenoble-France to acquire some technical experience on the handling and processing of molten salts. One piece of equipment is called FFFER (Forced Fluoride Flow for Experimental Research). It is a 70-L FLiNaK loop with a liquid salt circulating rate of approximately 2 L/s at 600°C. This reduced-scale loop aims at studying gas injection and separation for the continuous extraction of gaseous and metallic FPs in the MSFR fuel salt. At present only the gas injection and the hydrocyclone efficiency for bubble-salt separation are being studied, but important technical devices are tested in the process.

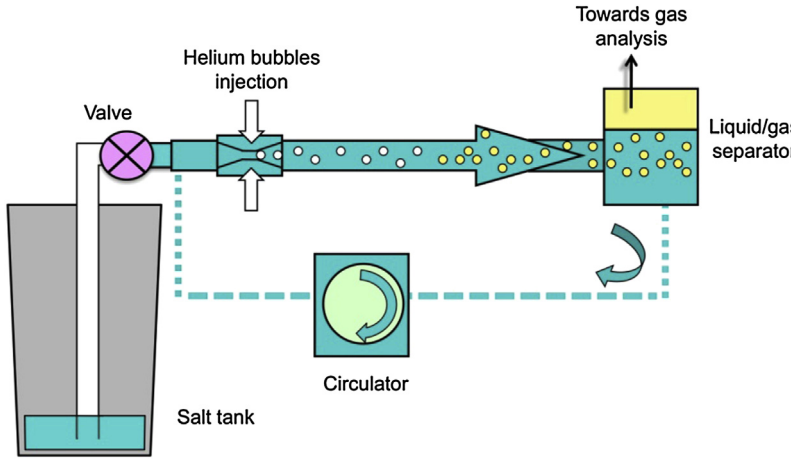


Figure 7.17 Scheme of the FFFER (Forced Fluoride Flow for Experimental Research) loop.

The FFFER loop comprises a tank where the FLiNaK load is prepared before the experiment and stored after. The circulating loop is situated above this tank and is filled with liquid salt only for the duration of the experiment. It is isolated from the tank by two valves in parallel: a mechanical ball valve and a "freeze plug." In case of electrical shutdown the freeze plug melts within a few minutes and the salt goes back in the insulated storage tank where its solidification may take place without any disturbing effects. The main elements of this equipment are shown in Figs. 7.17–7.19: the melting tank is in gray, the valves are in pink, the light blue tank contains the circulation pump, and the yellow one the hydrocyclone for bubble/salt separation. The building material is 304 and 316L steel for all of the parts. The 55-mm inner diameter pipes (mean velocity 1 m/s) are fitted with a Venturi gas injector and an ultrasonic salt velocimeter. The salt level in the three tanks (melting,

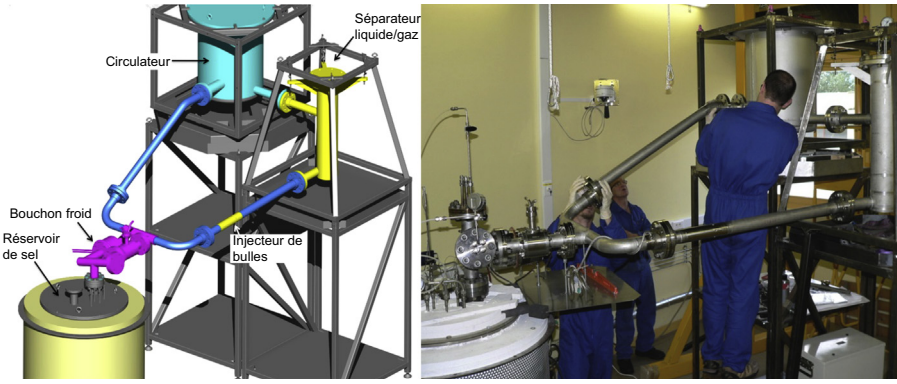


Figure 7.18 Design of the FFFER (Forced Fluoride Flow for Experimental Research) loop and view during assembly.

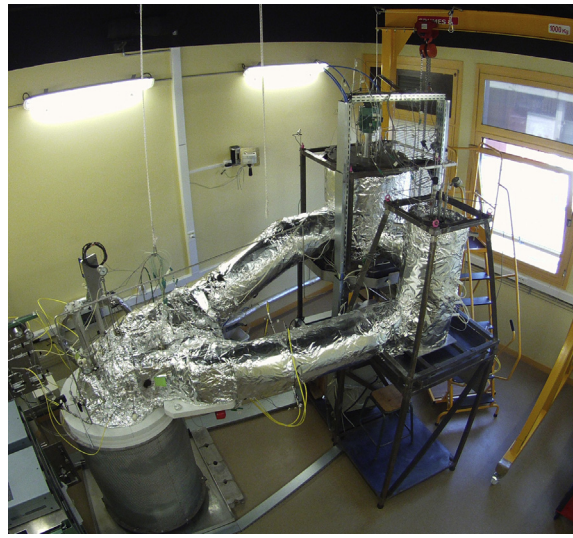


Figure 7.19 Completed loop with its thermal insulation.

separation, pump) is measured and regulated by probes, and the corresponding gas pressures are controlled according to experimental need.

The injection and separation devices were designed after a transparent water mock-up (scale 0.72) was operated, allowing to gain familiarity with the tuning of all of the parameters from the circulation pump to the separator as well as with the ultrasonic measurement of the velocity. An illustration of the vortex created by the tangential fluid inlet at the base of the separator is shown in Fig. 7.20. The bubble water separation efficiency reached approximately 85% at 0.1% volume fraction of gas and up to more than 95% for a 0.4% volume fraction of gas.

The ultrasonic velocimetric technique is based on ultrasonic reflections on bubbles to depict the velocity profile across the pipe. This gives information about the bubble distribution and their mean velocity. However, this is a new technique that requires further studies and some tuning before it can be used outside of the laboratory.

This experiment allowed casual observations of corrosion that are being studied separately on static small-scale experiments. A second loop is planned in the Euratom SAMOFAR project to identify and measure the salt's thermal behavior during thermal exchanges.

7.6.4 Other research and development activities on molten salt systems

MSR development worldwide is still at a conceptual design stage, with most investigations around these concepts based today on numerical modeling, with the notable exception of the People's Republic of China, where a large project to develop a thorium MSR prototype has very recently started.



Figure 7.20 Water mock-up of the separator showing the concentration of bubbles in the vortex center and their coalescence. The gas is evacuated at the top and the liquid through the pipe on the left.

Recent MSR developments in the Russian Federation are focused on the 1000-MW_e MOSART. The primary specifications for a MOSART core were to provide the fissile concentration and fuel salt geometry such that approximately 2.4 GW_{th} nuclear heat would be released at conditions affording efficient transmutation and recycling of TRUs from Mox PWR spent fuel (Ignatiev et al., 2012, 2014). The MOSART reference core with no graphite moderator is a cylinder 3.4 m in diameter and 3.6 m high. The fuel salt inlet and outlet pipe diameters are fixed at 1 m. Radial, bottom, and top reflectors are attached to the reactor vessel. This leaves a ring filled with fuel salt surrounding the core to cool the reflector and reactor vessel. The molten salt flow rate is 10,000 kg/s. In nominal conditions, the fuel salt enters the core at 600°C and transports 2.4 GW_{th} to the secondary salt in the primary heat exchanger. The fluoride fuel salt mixture is circulated through the reactor core by four pumps operating in parallel. Other pumps circulate the salt through the heat exchangers and return it to a common plenum at the bottom of the reactor vessel. In the reference MOSART design, the out of core salt volume is 18 m^3. The MOSART concept is being studied in different configurations, which consider different core dimensions and different compositions of the fuel salt and/or salt blanket that allow for different modes of utilization. A detailed description of MOSART can be found in Afonichkin et al. (2014).

7.7 Conclusion and perspectives

The MSFR concept has been recognized as a long-term alternative to solid-fueled fast neutron reactors because of attractive features that remain to be confirmed. It is characterized by

- Fluoride-based liquid fuels of various compositions (solvent, fertile, and fissile) allowing operation as breeder or burner with many different possible fertile and fissile compositions.
- A fast neutron spectrum.
- Homogeneous fuel composition due to fast fuel circulation (in-core turbulence and multiple heat exchanger channels). This homogeneity allows for continuous fuel monitoring.
- Continuous extraction of volatile or metallic FPs via neutral gas bubbling.
- Quasicontinuous light chemical fuel processing (rate comparable to LWR solid fuel but on a daily basis) without stopping the reactor.

These characteristics result in a reactor with a high safety potential due to

- negative temperature feedback reactivity coefficients (Doppler and density) leading to high thermal stability in operation and in all perturbing circumstances,
- homogeneous liquid state allowing passive draining of the core fuel into passively cooled geometrically noncritical tanks,
- absence of significant reactivity reserve because of the quasicontinuous adjustment of the fuel composition, and
- no pressurization required because of the absence of any volatile fluid susceptible to be contaminated by fuel leaks.

The international MSFR collaboration is presently focused on technology-independent safety issues, considering that only a high safety level may convince safety agencies to authorize the development of such a new reactor concept. Since 2001 calculations and experimental research have been conducted in Europe in national programs (CNRS-France, KI-Russia) and in a European network supported by Euratom and Rosatom (MOST, ALISIA, ACSEPT/PYROSMANI, EVOL/MOSART). This collaboration is presently continuing with the SAMOFAR/SMART-MSFR joint projects (2015/2019), in which industrial partners (EdF, AREVA) and the French technical safety organization (IRSN) will be actively involved. This common program is devoted to the acquisition of experimental data and simulation tools for safety studies. The specific objectives of the Euratom program are

- to develop and apply a new safety methodology for liquid-fuel reactors, which could also partly be woven into the safety methodology of other Generation IV reactors;
- to measure all relevant safety-related data of the fuel salt and of the whole system needed for the assessment of the MSFR;
- to design and build a software simulator to verify the safe operation of the MSFR including start-up, shut-down, and load-following operation, and to identify normal operation accident initiators;
- to extract a complete set of accident initiators and scenarios, and to evaluate these using best-estimate simulation tools including uncertainty analysis;

- to prove experimentally and numerically the safe and reliable operation of the freeze valves and the draining of the fuel salt, and to measure the natural circulation dynamics of the (internally heated) fuel salt in a loop, representing the primary circuit and drain tanks; and
- to demonstrate experimentally the reductive extraction processes for lanthanides and actinides, and to assess the safety of the high-temperature chemical processes to clean and control the fuel salt.

Since the beginning the common philosophy of the MSFR community was to give priority to knowledge over technology assuming that a long time will be devoted to assess the safety of technological solutions (ie, assuming that safety is the primary concern for public acceptance of new nuclear reactors). The resulting roadmap for future developments is presently concerned with all of the chemical and physical knowledge that help to assess the MSFR characteristics and design, including basic data measurements and multiphysics simulation tools. A second step will be the development of technological means, using simulant salts instead of real fuel, to demonstrate, at the proper scale, the validity of the proposed technology and to validate fluid flow and heat transfer models. The third step is the zero-power demonstration small reactors, with the objectives of checking the neutronic properties (eliminating data uncertainties) and testing the start-up and shut-down processes. Then, it will be possible to test a small power reactor with two new tests: the heat transfer with internal heat source and the FP extraction (continuous and quasicontinuous). This means that the pyroprocessing of the fuel by remote handling should be studied and tested in parallel to the first three steps, as well as the safety and proliferation issues. Indeed, the option of studying all of the aspects of the concept was taken from the beginning to render the safety constraints inherent to the design and not have them added after. This implies using new approaches in agreement with the GIF community for safety and proliferation resistance. All of these steps are mandatory to develop the technical and scientific background and knowledge for further practical demonstrations of the flexibility and viability of MSRs on a reactor scale. Such research and development activities are being conducted in the world, particularly by a European network supported by Euratom and ROSATOM to confirm the validity of the theoretical advantages of this concept and to assess the potential advantages of fast spectrum MSRs.

Nomenclature

Abbreviations and acronyms

3D	Three-dimensional
ACSEPT	Actinide reCycling by SEParation and transmutation
ALISIA	Assessment of LIquid salt for innovative applications
CNRS	Center National de la Recherche Scientifique
EdF	Electricité de France

Continued

EVOL	Evaluation of Viability of Liquid Fuel Fast Reactor
FFFER	Forced Fluoride Flow for Experimental Research
FLiNaK	Salt containing the following elements: F Li Na K
FP	Fission product
HRE	Homogeneous Reactor Experiment-2
IN2P3	Institut National de Physique Nucléaire et de Physique des Particules
IPNO	Institut de Physique Nucléaire d'Orsay
LPSC	Laboratoire de Physique Subatomique et Cosmologie
MARS	Minor Actinide Recycling in molten Salt
MC	Monte Carlo
MOSART	MOlten Salt Actinide Recycler and Transmuter
MOST	Review of MOlten salt technology
MOX	Mixed oxide (oxide fuel pellet containing Pu and U) for spent fuel recycling
MSFR	Molten salt fast reactor
MSRE	Molten Salt Reactor Experiment
ORNL	Oak Ridge National Laboratory
Pu-Mox	Pu- containing mixed oxide fuel
Pu-Uox	Pu-containing uranum oxide fuel
Pu + MA Mox	Pu and minor actinides mixed oxide fuel
PYROSMANI	PYROchemical processes study for minor ActiNIdes recycling in molten chlorides and fluorides
SAMOFAR	Safety assessment of MOlten salt fast reactor
SMART-MSFR	Safety of Minor Actinides Recycling and Transmuting in Molten Salt Fast Reactor
TFM	Transient fission matrix
TRU	Transuranic element
Uox	Uranium oxide (oxide fuel pellet containing only U)

Symbols

β_{eff}	Effective delayed neutron fraction
λ	Thermal conductivity in W/m °C
μ	Dynamic viscosity in Pa s

ν	Kinematic viscosity in m^2/s
ρ	Specific mass in g/cm^3
C_p	Heat capacity in J/kg °C
GW_{th}	Thermal power, GW
GW_e	Electrical power, GW
MW_{th}	Thermal power, MW

Acknowledgments

The authors thank the PACEN (Program sur l'Aval du Cycle et l'Energie Nucléaire) and NEEDS (Nucléaire: Energie, Environnement, Déchets, Société) French programs, the IN2P3 department of the National Center for Scientific Research (CNRS), the Grenoble Institute of Technology, and the European programs EVOL (Evaluation and Viability of Liquid Fuel Fast Reactor System) of Framework Program 7 and SAMOFAR of Horizon2020 for their support. The authors are also very thankful to Elizabeth Huffer for her help during the translation of this paper and to our colleagues from the MSR communities in France and Europe and in the frame of the MSR System Steering Committee of the Generation IV International Forum for all of the very interesting discussions and exchanges.

References

Afonichkin, V., Bovet, A., Gnidoi, I., Khokhlov, V., Lizin, A., Merzlyakov, A., Osipenko, A., Sannikov, I., Shishkin, V., Subbotin, V., Surenkov, A., Toropov, A., Uglov, V., Zagnitko, A., 2014. Molten salt actinide recycler and transforming system without and with Th-U support: fuel cycle flexibility and key materials properties. Annals of Nuclear Energy 64, 408−420.

Aufiero, M., Brovchenko, M., Cammi, A., Clifford, I., Geoffroy, O., Heuer, D., Laureau, A., Losa, M., Luzzi, L., Merle-Lucotte, E., Ricotti, M.E., Rouch, H., 2014. Calculating the effective delayed neutron fraction in the Molten Salt Fast Reactor: analytical, deterministic and Monte Carlo approaches. Annals of Nuclear Energy 65, 78−90.

Bettis, E.S., Robertson, R.C., 1970. The design and performance features of a single-fluid molten salt breeder reactor. Nuclear Applications and Technology 8, 190−207.

Boussier, H., et al., 2012. The molten salt reactor in generation IV: overview and perspectives. In: Proceedings of the Generation4 International Forum Symposium, San Diego, USA.

Briggs, R.B., Swartout, J.A., 1955. Aqueous homogeneous power reactors. In: Proceedings of the International Conference on the Peaceful Uses of Atomic Energy, Held in Geneva, 8−20 August, 1955, vol. III, p. 496.

Brovchenko, M., et al., 2012. Preliminary safety calculations to improve the design of molten salt fast reactor. In: Proceedings of the International Conference PHYSOR 2012 Advances in Reactor Physics Linking Research, Industry, and Education, Knoxville, Tennessee, USA.

Brovchenko, M., Heuer, D., Merle-Lucotte, E., Allibert, M., Ghetta, V., Laureau, A., Rubiolo, P., 2013. Design-related studies for the preliminary safety assessment of the molten salt fast reactor. Nuclear Science and Engineering 175, 329–339.

Brovchenko, M., Merle-Lucotte, E., Rouch, H., Alcaro, F., Allibert, M., Aufiero, M., Cammi, A., Dulla, S., Feynberg, O., Frima, L., Geoffroy, O., Ghetta, V., Heuer, D., Ignatiev, V., Kloosterman, J.L., Lathouwers, D., Laureau, A., Luzzi, L., Merk, B., Ravetto, P., Rineiski, A., Rubiolo, P., Rui, L., Szieberth, M., Wang, S., Yamaji, B., 2014a. Optimization of the Pre-conceptual Design of the MSFR, Work-package WP2. Deliverable D2.2, EVOL (Evaluation and Viability of Liquid fuel fast reactor system) European FP7 project, Contract number: 249696.

Brovchenko, M., Heuer, D., Huffer, E., Merle-Lucotte, E., Allibert, M., Feynberg, O., Ghetta, V., Ignatiev, V., Kloosterman, J.L., Lathouwers, D., Laureau, A., Rineiski, A., Rouch, H., Rubiolo, P., Rui, L., Wang, S., 2014b. Safety Approach of a Fast Liquid Fuel System, Work-Package WP2. Deliverable D2.5, EVOL (Evaluation and Viability of Liquid fuel fast reactor system) European FP7 project, Contract number: 249696.

Brovchenko, M., 2013. Etudes préliminaires de sûreté du réacteur à sels fondus MSFR (Ph.D. thesis). Grenoble Institute of Technology, France (in French).

Delpech, S., Merle-Lucotte, E., Heuer, D., et al., 2009. Reactor physics and reprocessing scheme for innovative molten salt reactor system. Journal of Fluorine Chemistry 130 (1), 11–17.

Dulla, S., Krepel, J., Rouch, H., Aufiero, M., Fiorina, C., Geoffroy, O., Hombourger, B., Laureau, A., Merle-Lucotte, E., Mikityuk, K., Pautz, A., Ravetto, P., Rubiolo, P., 2014. Sensitivity Studies of the Salt Flux in the Optimized Design of the MSFR. Deliverable D2.3, EVOL (Evaluation and Viability of Liquid fuel fast reactor system) European FP7 project, Contract number: 249696.

Engel, J., Bauman, H., Dearing, J., Grimes, W., McCoy, H., 1979. Development Status and Potential Program Development of Proliferation Resistant Molten Salt Reactors. USAEC, Oak Ridge, USA. Report ORNL/TM-6415.

GIF (Generation IV International Forum), 2008. Annual Report 2008, pp. 36–41. http://www.gen-4.org/PDFs/GIF_2008_Annual_Report.pdf.

GIF (Generation IV International Forum), 2009. Annual Report 2009, pp. 52–58. http://www.gen-4.org/PDFs/GIF-2009-Annual-Report.pdf.

Haubenreich, P.N., Engel, J.R., 1970. Experience with the molten salt reactor experiment. Nuclear Applications and Technology 8, 107–117.

Heuer, D., Merle-Lucotte, E., Allibert, M., Brovchenko, M., Ghetta, V., Rubiolo, P., 2014. Towards the thorium fuel cycle with molten salt fast reactors. Annals of Nuclear Energy 64, 421–429.

Ignatiev, V., Afonichkin, V., Feynberg, O., Merzlyakov, A., Surenkov, A., Subbotin, V., et al., 2012. Molten salt reactor: new possibilities, problems and solutions. Atomic Energy 112 (3), 157.

Ignatiev, I., et al., 2014. Molten salt actinide recycler & transforming system without and with Th-U support: fuel cycle flexibility and key material properties. Annals of Nuclear Energy 64, 408–420.

Jasak, H., Jemcov, A., Tukovic, Z., 2007. Openfoam: a C++ library for complex physics simulations. In: Proceedings of the International Workshop on Coupled Methods in Numerical Dynamics, vol. 1000, pp. 1–20.

Laureau, A., Rubiolo, P., Heuer, D., Merle-Lucotte, E., Brovchenko, M., 2013. Coupled neutronics and thermal-hydraulics numerical simulations of the molten salt fast reactor

(MSFR). In: Joint International Conference on Supercomputing in Nuclear Applications and Monte Carlo 2013, Paris, France.

Laureau, A., Aufiero, M., Rubiolo, P., Merle-Lucotte, E., Heuer, D., 2015a. Coupled neutronics and thermal-hydraulics transient calculations based on a fission matrix approach: application to the molten salt fast reactor. In: Proceedings of the Joint International Conference on Mathematics and Computation (M&C), Supercomputing in Nuclear Applications (SNA) and the Monte Carlo (MC) Method, Nashville, USA.

Laureau, A., Aufiero, M., Rubiolo, P., Merle-Lucotte, E., Heuer, D., 2015b. Transient Fission Matrix: kinetic calculation and kinetic parameters βeff and Λeff calculation. Annals of Nuclear Energy 85, 1035−1044.

Laureau, A., 2015c. Développement de modéles neutroniques pour le couplage thermohydraulique du MSFR et le calcul de paramétres cinétiques effectifs, PhD Thesis, Grenoble-Alpes University.

Leppänen, J., 2013. Serpent − A Continuous-Energy Monte Carlo Reactor Physics Burnup Calculation Code. User's Manual. VTT Technical Research Centre of Finland.

Mathieu, L., Heuer, D., Merle-Lucotte, E., et al., 2009. Possible configurations for the thorium molten salt reactor and advantages of the fast non-moderated version. Nuclear Science and Engineering 161, 78−89.

Merle-Lucotte, E., Heuer, D., et al., 2009a. Minimizing the fissile inventory of the molten salt fast reactor. In: Proceedings of the Advances in Nuclear Fuel Management IV (ANFM 2009), Hilton Head Island, USA.

Merle-Lucotte, E., Heuer, D., et al., 2009b. Optimizing the burning efficiency and the deployment capacities of the molten salt fast reactor. In: Proceedings of the International Conference Global 2009-The Nuclear Fuel Cycle: Sustainable Options & Industrial Perspectives. Paper 9149, Paris, France.

Merle-Lucotte, E., Heuer, D., Allibert, M., Brovchenko, M., Capellan, N., Ghetta, V., May 2011. Launching the thorium cycle with molten salt fast reactor. In: Proceedings of ICAPP 2011, Nice, France paper 11190.

Merle-Lucotte, E., Heuer, D., et al., 2012. Preliminary design assessments of the molten salt fast reactor. In: Proceedings of the European Nuclear Conference ENC2012, Manchester, UK paper A0053.

Merle-Lucotte, E., Heuer, D., Allibert, M., Brovchenko, M., Ghetta, V., Laureau, A., Rubiolo, P., 2013. Recommendations for a demonstrator of molten salt fast reactor. In: Proceedings of the International Conference on Fast Reactors and Related Fuel Cycles: Safe Technologies and Sustainable Scenarios (FR13), Paris, France.

ORNL-TM-728, 1965. MSRE Design and Operations Report − Part I: Description of Reactor Design. Technical report ORNL-TM-728. Oak-Ridge National Laboratory.

Rouch, H., Geoffroy, O., Rubiolo, P., Laureau, A., Brovchenko, B., Heuer, D., Merle-Lucotte, E., 2014. preliminary thermal-hydraulic core design of the molten salt fast reactor (MSFR). Annals of Nuclear Energy 64, 449−456.

Serp, J., Allibert, M., Beneš, O., Delpech, S., Feynberg, O., Ghetta, V., Heuer, D., Holcomb, D., Ignatiev, V., Kloosterman, J.L., Luzzi, L., Merle-Lucotte, E., Uhlíř, J., Yoshioka, R., Zhimin, D., 2014. The molten salt reactor (MSR) in generation IV: overview and perspectives. Progress in Nuclear Energy 1−12.

US DOE Nuclear Energy Research Advisory Committee and the Generation IV International Forum, 2002. A Technology Roadmap for Generation IV Nuclear Energy Systems, GIF-002-0.

Wang, S., Rineiski, A., Li, R., Brovchenko, M., Merle-Lucotte, E., Heuer, D., Laureau, A., Rouch, H., Aufiero, M., Cammi, A., Fiorina, C., Guerrieri, C., Losa, M., Luzzi, L.,

Ricotti, M.E., Kloosterman, J.-L., Lathouwers, D., van der Linden, E., Merk, B., Rohde, U., 2014. Safety Analysis: Transient Calculations. EVOL (Evaluation and Viability of Liquid fuel fast reactor system) European FP7 project, Contract number: 249696.

Whatley, M.E., et al., 1970. Engineering development of the MSBR fuel recycle. Nuclear Applications and Technology 8, 170−178.

Bibliography web sources

http://lpsc.in2p3.fr/gpr/gpr/publis-rsfE.htm.
https://www.gen-4.org/gif/jcms/c_9260/public.
http://www.ornl.gov/info/reports/.

Super-critical water-cooled reactors

8

T. Schulenberg [1], *L. Leung* [2]
[1]Karlsruhe Institute of Technology, Karlsruhe, Germany; [2]Canadian Nuclear Laboratories, Chalk River, Ontario, Canada

8.1 Introduction

Pressurized water reactors (PWRs) and boiling water reactors (BWRs) have been among the most successful nuclear reactors during the last 40 years. More than 300 PWRs have been built up to now, of which the latest ones exceed a net electric power output of 1600 MW_e and a net efficiency of 36%. With more than 100 units built, the BWR was almost as successful, although power and efficiency levels were somewhat lower. Both reactor types use a saturated steam cycle of approximately 7−8 MPa live steam pressure, corresponding with a boiling temperature of 286−295°C. However, these live steam conditions are still almost the same as those used in the 1960s. The few improvements in cycle efficiency are primarily because of improvements only in steam turbine blades. The situation is similar with heavy water moderated pressure-tube reactors, of which more than 60 have been built up to now. On the other hand, fossil-fired power plants have increased their efficiencies significantly since the 1960s. Steam has been superheated, and live steam temperatures and pressures have been increased stepwise to 600°C and 30 MPa, respectively. Since around 1990, all new coal-fired power plants have been using supercritical steam conditions, reaching more than 46% net efficiency today. Consequently, the application of such steam cycle technologies to the well-proven design of water-cooled nuclear reactors could offer a huge potential for further improvements.

A super-critical water-cooled reactor (SCWR) is cooled with light water at supercritical pressure (ie, >22.1 MPa) in a once-through steam cycle. It may be moderated with light water or heavy water. Feed water of the steam cycle is heated up inside of the reactor core to superheated steam, without any coolant recirculation, and the steam is supplied directly to a steam turbine. The general advantages of SCWRs, compared with conventional water-cooled reactors, are a higher steam enthalpy at the turbine inlet, which increases efficiency, reduces fuel costs, and reduces the steam mass flow rate needed for a target turbine power. This lower steam mass flow rate reduces the turbine size and the size of condensers, pumps, preheaters, tanks, and pipes and thus the costs of the overall steam cycle. Because the capital costs of nuclear power plants are usually higher than their fuel costs, this latter advantage has even a higher impact on electricity production costs than efficiency. Even more cost advantages are expected from plant simplifications such as eliminating

Handbook of Generation IV Nuclear Reactors. http://dx.doi.org/10.1016/B978-0-08-100149-3.00008-2
Copyright © 2016 Elsevier Ltd. All rights reserved.

steam separators or primary pumps in the case of a once-through steam cycle at supercritical pressure. Another advantage of using supercritical water in a nuclear reactor is that a boiling crisis is physically excluded, which adds a new safety feature to this design.

8.2 Types of supercritical water-cooled reactor concepts and main system parameters

A general sketch of the SCWR steam-cycle concept is shown in Fig. 8.1 to illustrate the once-through design principle. Feed water is heated up to 280−350°C by steam turbine extractions using several low-pressure (LP) preheaters and high-pressure (HP) preheaters. The feed-water pumps supply the feed water to the reactor at a pressure of approximately 25 MPa. The reactor may be designed with a pressure vessel or with multiple pressure tubes, but it does not require any recirculation pumps in any case. In addition to the condensate extraction pumps of the condensers, the only pumps driving the steam cycle are the feed-water pumps. The reactor produces superheated steam at a pressure of 24−25 MPa and at a temperature of 500°C or more, depending on material limitations. The superheated steam is supplied directly to the HP turbine. The steam is reheated by some extracted steam and supplied to the intermediate pressure (IP) and LP turbines.

In general, a reactor core, which is cooled with supercritical water, can be designed with a thermal or a fast neutron spectrum. The option of a thermal spectrum requires additional water as a moderator because of the low density of superheated steam, which can be provided in water rods inside of fuel assemblies or in gaps between assembly boxes. Examples can be seen in the latest boiling water reactor design or in the superlight water reactor concept using supercritical water by Oka et al. (2010). If these gaps and water rods are omitted, then the neutron spectrum will become fast, which

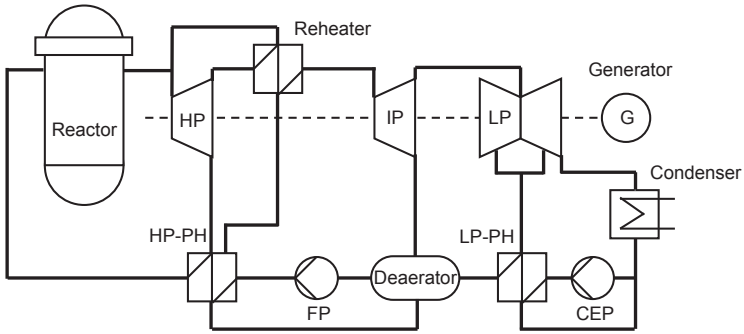


Figure 8.1 Simplified supercritical water-cooled reactor design principle with a once-through steam cycle. *HP*, high pressure; *IP*, intermediate pressure; *LP*, low pressure; *PH*, preheater; *CEP*, condensate extraction pumps; *FP*, feed-water pump; *G*, generator.

simplifies the design and increases the core power density. However, a general safety concern of the fast core option is the reactivity increase if the core should be voided under accidental conditions. Such a reactivity increase must definitely be avoided by suitable core design, for which the addition of some solid moderator, an increased neutron leakage, and a heterogeneous arrangement of seed and blanket assemblies are common measures. Oka et al. (2010) provide an example of their superfast reactor concept.

The enthalpy increase from the inlet to the outlet of the reactor exceeds those of conventional nuclear reactors by more than a factor of 8. The higher enthalpy increase of the coolant would not matter if it were uniform in the entire core. However, this can never be fully achieved. Fuel composition and distribution, water density distribution, size and distribution of subchannels, neutron leakage and reflector effects, burn-up effects, effects of control rod positioning, or effects due to the use of burnable poisons will influence the radial power profile of the core. Material uncertainties, fluid properties, uncertainties of the neutron physical modeling, heat transfer uncertainties, uncertainties of the thermal-hydraulic modeling, scattering of the inlet temperature distribution, manufacturing tolerances, deformations during operation, or measurement uncertainties will cause a statistical scatter of the enthalpy increase. Finally, some small but allowable transients might be caused by control of power, coolant mass flow, and core exit temperature and pressure. Schulenberg and Starflinger (2012) estimated that a total hot channel factor of 2 should be multiplied with the average enthalpy increase, as a first guess, to yield the maximum, local enthalpy increase under worst-case conditions. An analogue problem is also known from boiler design of fossil-fired power plants. It has been solved there by splitting the total enthalpy increase into an evaporator and two successive superheaters and by homogeneously mixing the coolant between each of these components.

Different core design concepts have been proposed to apply this technology to the SCWR (International Atomic Energy Agency, 2014). Starting from a single heat-up process of conventional nuclear reactors, as sketched in Fig. 8.2(a), the peak coolant temperatures inside of the reactor core can be reduced by a two-step process with a

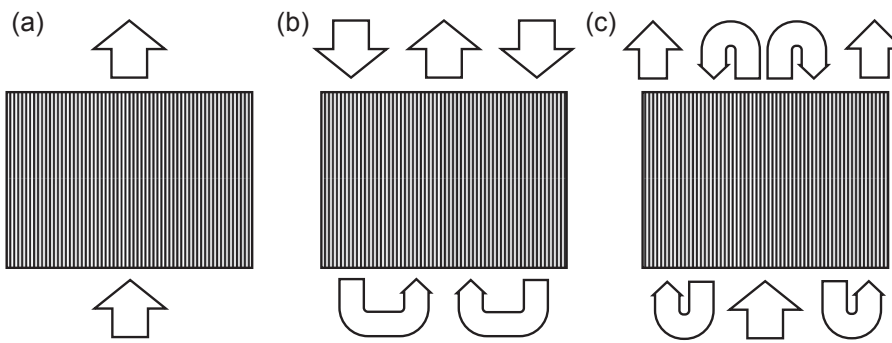


Figure 8.2 Different SCWR core design options with multiple heat-up steps. (a) Single-pass design, (b) two-pass design, and (c) three-pass design.

downward flow of coolant in the outer core region, followed by coolant mixing underneath the core and a second heat-up in the inner core region (Fig. 8.2(b)). For example, such technology has been applied by Oka et al. (2010) for their superlight water reactor concept. Even better coolant mixing is enabled with a three-pass core (Fig. 8.2(c)), with the evaporator as the first heat-up step in the inner core region, surrounded by a first superheater with downward flow and a second superheater with upward flow. The coolant is mixed between each step to eliminate hot streaks. This concept has been adopted for the high-performance light water reactor (HPLWR) and will be described in more detail in the next section. The higher the number of heat-up steps, the lower will be the peak coolant temperature at an envisaged average core outlet temperature, and thus the less stringent the material requirements, but the higher will be the complexity of core design.

8.3 Example of a pressure vessel concept

The high-performance light water reactor (HPLWR) is a pressure vessel-type SCWR with a thermal neutron spectrum, which was worked out by a European consortium in 2006–2010. Schulenberg and Starflinger (2012) summarize the design features and the analyses of the conceptual design phase. The reactor is designed for a thermal power of 2300 MW, resulting in a net electric power of 1000 MW and a net efficiency of 43.5% of the steam cycle. With a target coolant outlet temperature of 500°C, the superheated steam is thermally insulated from the reactor pressure vessel, keeping it below 350°C, as shown in Fig. 8.3. The core design applies the three-pass design concept (Fig. 8.2(c)), and mixing plena are foreseen above and underneath the core to maintain the peak coolant temperature below 600°C. Control rods are inserted from the top as in a PWR, aligned by the control rod guide tubes in the upper half of the reactor pressure vessel. The fuel assemblies of the reactor core are standing on the thick core support plate of the core barrel, which is suspended in the reactor flange. The steam plenum, including its mixing plenum in the inner region, can be removed after extraction of the hot steam pipes for yearly fuel shuffling and replacement. Feed water enters the reactor pressure vessel through four backflow limiters to minimize loss of coolant in case a feed-water line breaks. Half of the supplied feed water is purging the upper half of the reactor pressure vessel, serving afterward as moderator water inside of water rods of the fuel assemblies and inside gaps between assembly boxes. After cooling the radial core reflector, this water is mixed with the remaining feed water in the lower mixing plenum underneath the core. The mass flow split is adjusted by orifices of the lower mixing plenum.

The reactor has a total height of 14.29 m and an inner diameter of 4.46 m. The wall thickness of the cylindrical shell is 0.45 m and the spherical bottom shell has a thickness of 0.30 m. Similar to a PWR, the vessel material is 20MnMoNi55, but the hotter steam outlet must be made, for example, from P91 steel to withstand the superheated steam temperature of 500°C. The reactor internals are made from stainless steel.

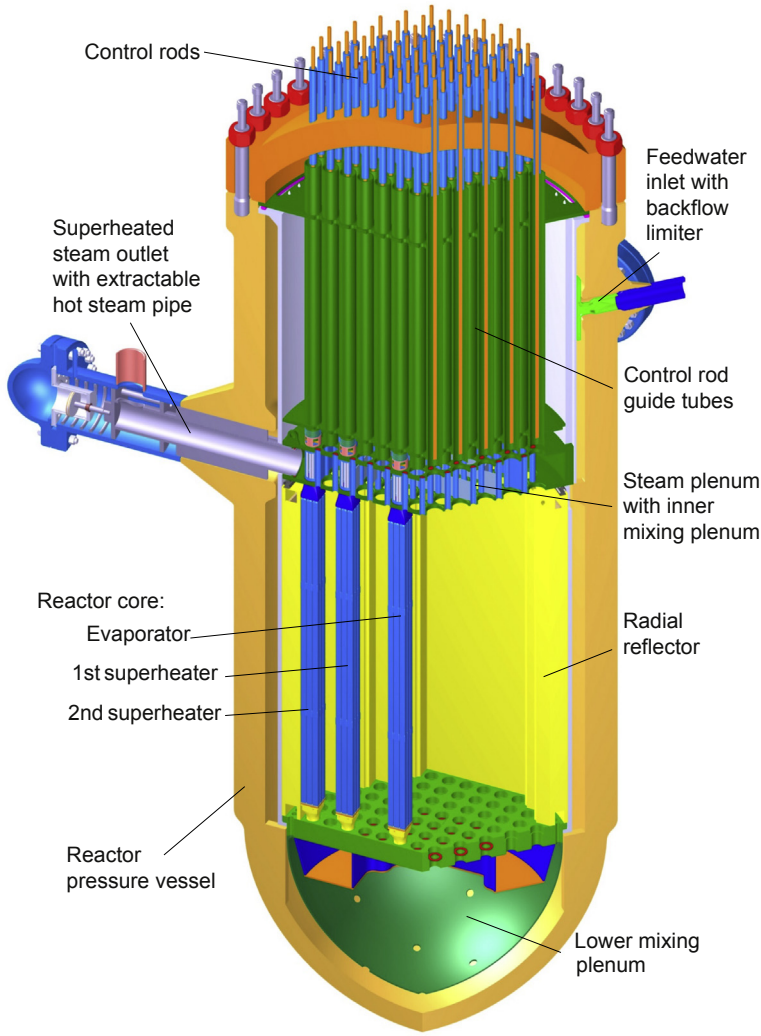


Figure 8.3 Pressure vessel design of the high-performance light water reactor with a three-pass core.
From Schulenberg, T., Starflinger, J., 2012. High Performance Light Water Reactor, Design and Analyses. KIT Scientific Publishing. ISBN:978-3-86644-817-9.

The steam cycle is designed with three LP preheaters, condensing steam that is extracted from the LP turbines, and with four HP preheaters, condensing steam from the HP and IP turbines. The reheat pressure is 4.25 MPa, achieving a reheat temperature of 442°C. The design pressure of the deaerator is 0.55 MPa. Four parallel feed-water pumps are foreseen, of which three are needed to provide the mass flow of 1179 kg/s at full power and the fourth one is kept on hot standby.

8.4 Example of a pressure tube concept

The Canadian SCWR concept is a pressure-tube type of concept. It adopts the direct cycle, which includes a 2540-MW_{th} core that receives feed water at 315°C and 1176 kg/s and generates supercritical steam at 625°C and 25 MPa. The cycle includes steam reheat using a moisture separator reheater (MSR) between the IP turbine and LP turbine. The MSR separates the moisture from the steam and reheats the steam to ensure an acceptable moisture level at the outlet of the LP turbine. Four LP condensate heaters are included in the cycle as well as a deaerator and four HP feed-water heaters. The gross electrical output is calculated as 1255 MW_e, giving a gross thermal efficiency of 49.4%. A schematic diagram of the direct cycle is shown in Fig. 8.4 (Zhou, 2009).

The Canadian SCWR core concept is illustrated in Fig. 8.5. It consists of a pressurized inlet plenum, an LP calandria vessel that contains heavy water moderator, and 336 fuel channels that are attached to a common outlet header. A counterflow fuel channel is adopted to position the inlet and outlet piping above the reactor core so that a complete break of either an inlet pipe or an outlet pipe will not result in an immediate loss of coolant at the reactor core. A nonfuel central flow channel is located at the center of the fuel channel to increase neutron moderation close to the inner fuel rings. This feature results in reasonably uniform radial power distributions across the fuel channel as well as a desirable negative coolant void reactivity throughout the burn-up cycle.

The coolant flows into the inlet plenum, around the outside of the outlet header (blue arrows in Fig. 8.5), and then it enters the pressure tube extension through a series of slots, into the fuel assembly through a crossover piece (top right figure), down through a flow tube in the center of the fuel assembly, back up through the fuel elements (bottom right figure), and then out through the outlet header.

Although the inlet plenum is a pressure vessel, none of the components are subject to high neutron fields; consequently, irradiation damage is not a major concern. A pressure-vessel steel containing approximately 3–4 wt% nickel, SA 508 grade 4N, has been selected because the operating temperature inside of the inlet plenum is only approximately 315°C. To further inhibit corrosion, the interior surfaces of the vessel could be overlaid with 308 or 309 stainless steel weld materials. The material selected for the outlet header and head is Alloy 800H, which is an Fe–Ni–Cr alloy that demonstrates excellent high-temperature properties such as strength, toughness, and corrosion resistance. Because of the low pressure differential from inlet to outlet conditions, no large forces or stresses are generated; consequently, the design requirements are relatively light. The header is supported by brackets placed on a plane running through the outlet penetrations of the inlet plenum wall, ensuring that movement due to differential thermal expansion between the plenum and header is purely in the radial direction. The outlet sleeves are decoupled from the inlet plenum wall by means of a flexible thermal isolation sleeve as shown in Fig. 8.6.

The fuel channel consists of the pressure tube extending into the moderator and an extension connecting the pressure tube to the outlet header. All internals of the pressure tube are part of the fuel assembly. The pressure tube has an open end and a closed

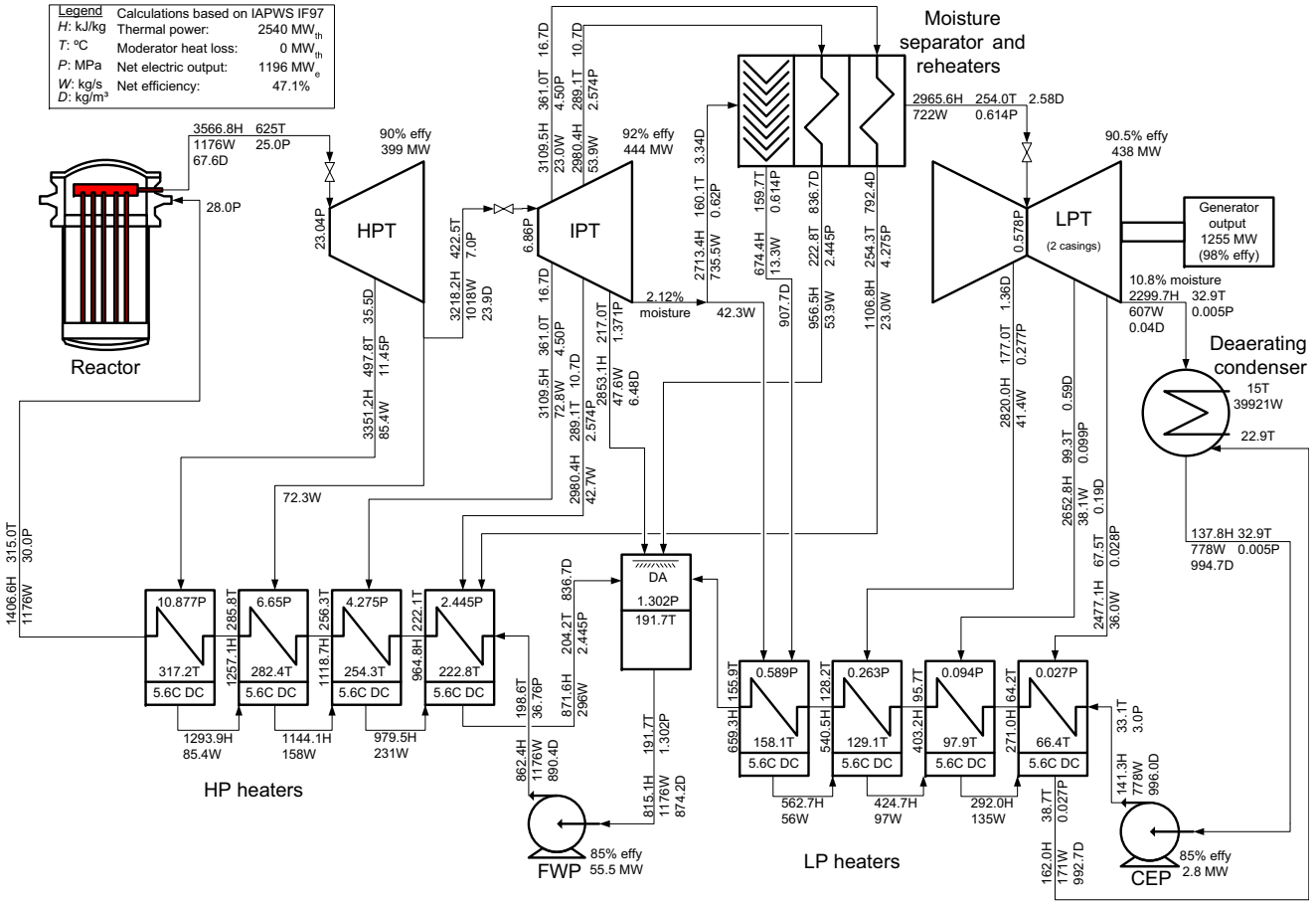


Figure 8.4 Schematic of direct steam cycle with a moisture separator reheater in a supercritical water-cooled reactor plant. *HPT*, high-pressure turbine; *IPT*, intermediate-pressure turbine; *LPT*, low-pressure turbine; *CEP*, condensate extraction pump; *LP*, low pressure; *HP*, high pressure; *FWP*, feed-water pump.

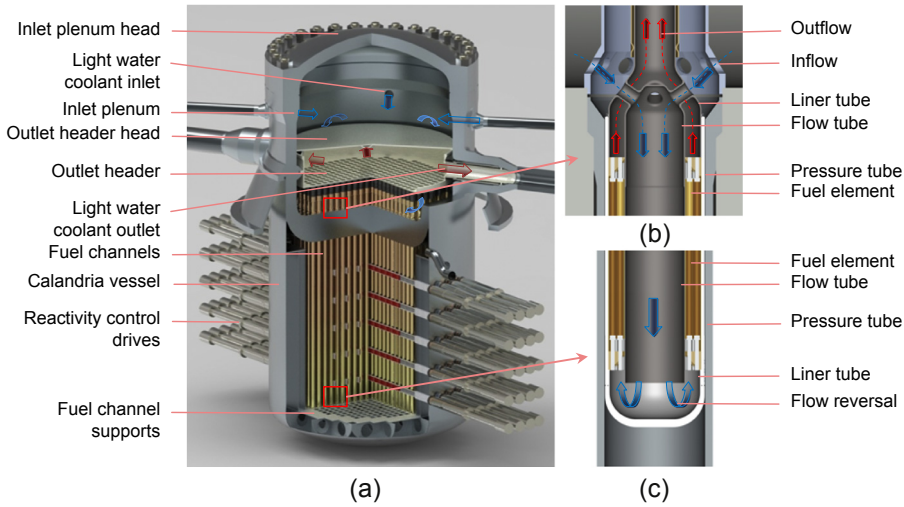


Figure 8.5 Canadian supercritical water-cooled reactor core concept. (a) Reactor core, (b) cross-over piece, and (c) bottom of fuel channel.

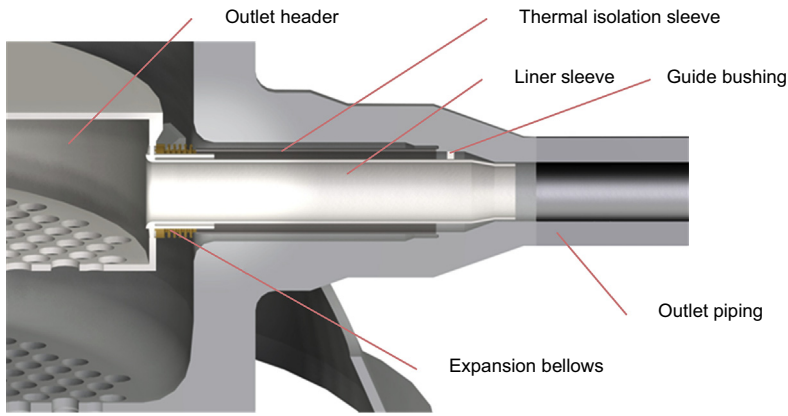


Figure 8.6 Cutaway view of outlet sleeves.

end (ie, a test-tube shape). It is inserted into one of the openings of the tubesheet of the inlet plenum with a seal weld between the HP inlet plenum and LP calandria. A pressure-tube extension is connected to the pressure tube at the top of the tubesheet and incorporates several openings near the interface with the pressure tube to allow coolant entering into the fuel channel and subsequently to the fuel assembly. These openings act as orifices to control the amount of coolant flowing into each channel and to suppress instability. The size of these openings is determined through matching the channel power output to provide an outlet coolant temperature as close to 625°C as possible. The outlet of the pressure-tube extension is attached to a corrugated bellows

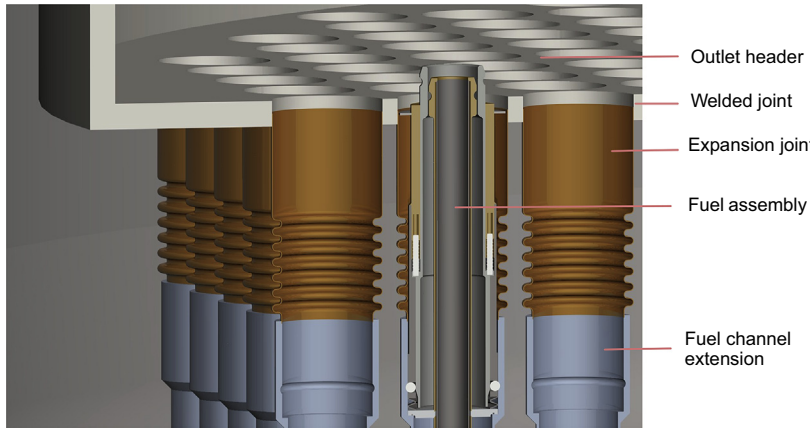


Figure 8.7 Fuel channel connection to the outlet header.

expansion joint, which in turn is welded to the bottom plate of the outlet header (see Fig. 8.7). The bellows expansion joint facilitates differential movement between the outlet header and the channel. This connection configuration would allow single-channel replacement, if required.

The calandria vessel is an LP vessel that contains the heavy water moderator, fuel channels, reactivity control mechanisms, and emergency shut-down devices. Internal structures include lateral supports for the fuel channels, reactivity control mechanism guides, and flow channels ensuring circulation of the moderator. Heavy water at low pressures and low temperatures is chosen for the moderator because of its low neutron absorption compared with light water. Additional moderator surrounding the core is included, acting as a neutron reflector and shielding. The tubesheet of the inlet plenum is located 0.75 m above the core, protecting the plenum material from radiation damage. The reactivity control mechanisms located at the sides of the core are shielded, at a minimum, with a similar volume of moderator and with an increasing amount at the reactor centerline due to the curvature of the calandria vessel. The moderator operates at subcooled temperatures using a pumped recirculation system, but in case of a station blackout, core decay heat is passively removed through the use a flashing-driven natural circulation loop. Inlet and outlet nozzles for these systems are located above the core, ensuring that the calandria will not drain because of a pipe break.

8.5 Fuel cycle technology

The pressure-vessel type of SCWR may use UO_2 in a once-through fuel cycle, with an enrichment of 5−7%, or mixed oxide (MOX) fuel if plutonium should be recycled in a closed fuel cycle. In the case of a thermal neutron spectrum, the use of MOX fuel is optional as in a conventional PWR or BWR. However, because the higher

temperatures of the SCWR require stainless steel fuel claddings instead of Zircalloy claddings, the enrichment is typically 2% points higher than for conventional water-cooled reactors to compensate for the additional neutron absorption of nickel. Therefore, the use of MOX fuel might be more economical to recycle the residual discharge fuel.

The reference fuel for the pressure-tube type of SCWR is a mix of thorium and plutonium (which is extracted from the spent light water reactor (LWR) fuel). On average, the weight percentage of plutonium is 13% in the fuel (Wojtazek, 2015). With the high neutron economy of the heavy water moderator, other fuel mixes can also be accommodated. Studies have demonstrated the feasibility of using low enriched uranium (LEU) of 7% (Yetisir et al., 2012); a mix of LEU at 7.5% with Th; a mix of transuranics at 21 wt% with Th (Winkel et al., 2013); or a mix of Pu at 8%, Th, and ^{233}U (at 2 wt%) extracted from the SCWR fuel (Magill et al., 2011).

In the case of a fast neutron spectrum, MOX fuel has been proposed by Oka et al. (2010) with an average concentration of fissile plutonium of approximately 20%. Such fuel can be produced from recycling spent fuel of LWRs with the Plutonium Uranium Redox EXtraction (PUREX) process, a mature fuel cycle technology.

8.6 Fuel assembly concept

Beyond 390°C, the coolant density is less than 200 kg/m^3, hardly enough to produce a thermal neutron spectrum. Therefore a moderator is needed for a thermal neutron spectrum, either as feed water running through moderator boxes inside of the fuel assemblies and in gaps between assembly boxes or as separate heavy water in case of a pressure tube concept. In any case the mass of structural material inside of the reactor core should be minimized to limit neutron absorption.

8.6.1 High-performance light water reactor fuel assembly concept

In case of the HPLWR (Section 8.3), the fuel assemblies are designed with 40 fuel pins each and a single moderator box in their center to enable a small wall thickness of moderator and assembly boxes, as shown in Fig. 8.8. To ease handling during maintenance, Schulenberg and Starflinger (2012) recommended grouping nine assemblies to a cluster with common head and foot pieces as shown in Fig. 8.9. The fuel rods have an outer diameter of 8 mm and a wall thickness of 0.5 mm, arranged with a pitch-to-diameter ratio of 1.18. A wire of 1.44-mm thickness is wrapped around each fuel rod to serve as a spacer and as an effective mixing device. The assembly box and moderator box are designed as a sandwich construction with a thermal insulation between two stainless steel sheets to minimize heat-up of the moderator water. Control rods, filled with boron carbide, are running inside five of the nine inner moderator boxes of a cluster. The fuel assembly has a heated length of 4.2 m. A fission gas plenum of 0.5-m length on top of the fuel pellets helps in minimizing the pressure increase during

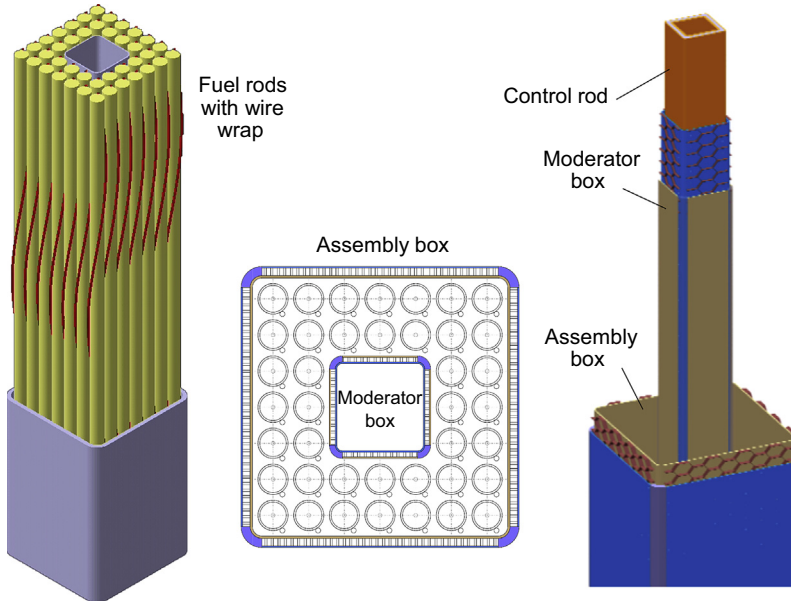


Figure 8.8 Fuel assembly concept of the high-performance light water reactor.
From Schulenberg, T., Starflinger, J., 2012. High Performance Light Water Reactor, Design and Analyses. KIT Scientific Publishing. ISBN:978-3-86644-817-9.

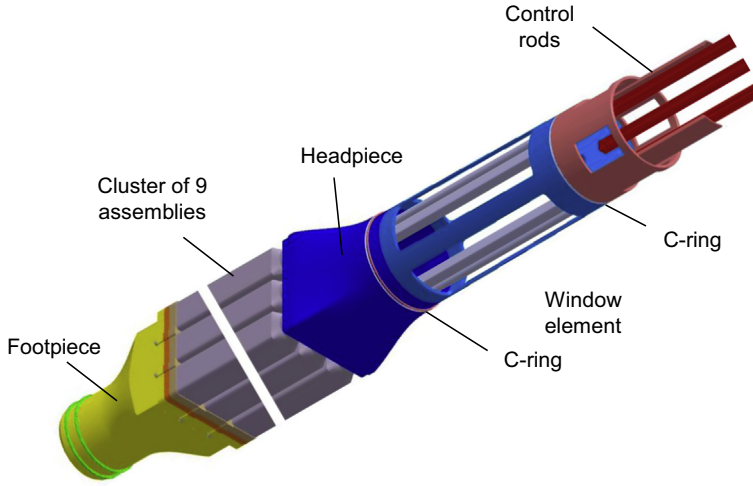


Figure 8.9 High-performance light water reactor assembly cluster design with head and foot piece; control rods are running inside five of the nine moderator boxes, inserted from the top.
From Schulenberg, T., Starflinger, J., 2012. High Performance Light Water Reactor, Design and Analyses. KIT Scientific Publishing. ISBN:978-3-86644-817-9.

burn-up. The headpiece of the assembly cluster has windows for steam release to the steam plenum, which need to be sealed with C-rings against moderator water ingress into the steam.

For a thermal power of 2300 MW, 52 of these clusters form the evaporator of the reactor core with an upward flow of coolant. They are surrounded by another 52 clusters with downward flow, serving as the first superheater. Fifty-two clusters at the core periphery, where the core power density is low enough to keep the cladding surface temperature below 650°C, provide the second superheater. The average core power density of the HPLWR is 57 MW/m^3, comparable with the power density of a BWR, and the evaporator has a power density of approximately 100 MW/m^3, comparable with a PWR.

Once a year the reactor is opened to shuffle assembly clusters, mainly from the evaporator to the first superheater and from there to the second superheater, and to replace the new assembly cluster in the evaporator. The excess reactivity of the reactor core at the beginning of each burn-up cycle is compensated with gadolinia pellets mixed with fuel pellets in four fuel rods per assembly. Boric acid, as used in a PWR to compensate for excess reactivity, may not be used for burn-up compensation because its solubility in supercritical water changes drastically when the coolant passes the pseudocritical line (384°C at 25 MPa). Instead, injection of boric acid is used only as a second shut-down mechanism in emergency cases.

8.6.2 Fast reactor fuel assembly concept

The fuel assembly design looks simpler for a reactor core with fast neutron spectrum. Oka et al. (2010) proposed using hexagonal fuel assemblies as seed assemblies with approximately 25% fissile plutonium, depending on the core size, mixed with blanket assemblies with pure ^{238}U in a heterogeneous arrangement. The coolant flow is upward or downward, depending on the headpiece, which may be designed with or without windows to the steam plenum above the core. According to Fig. 8.2, the concept may be categorized as a two-pass design with a flexible flow path. Control rod fingers are running inside of thimble tubes as in a PWR, as shown in Fig. 8.10. The stainless steel cladding of the fuel rod is designed with an outer diameter of 7 mm and a pitch of 8.12 mm. This tight hexagonal arrangement enables a high average core power density of 158 MW/m^3. For a core with 1650-MW thermal power, we would need 126 seed assemblies and 73 blanket assemblies at an active core height of 3 m.

A general problem of such fast reactor concept is an increase of the core reactivity with decreasing coolant density if the neutron spectrum is too fast. The problem may be overcome and the local void reactivity can be kept negative throughout the entire burn-up cycle by adding a solid moderator, in this case zirconium hydride (ZrH) and stainless steel around the blanket assemblies, which increases the neutron leakage and softens the spectrum. The concept is sketched in Fig. 8.10. However, as a drawback of this concept, the reactor is consuming more plutonium than breeding, which is not ideal for a sustainable nuclear energy concept.

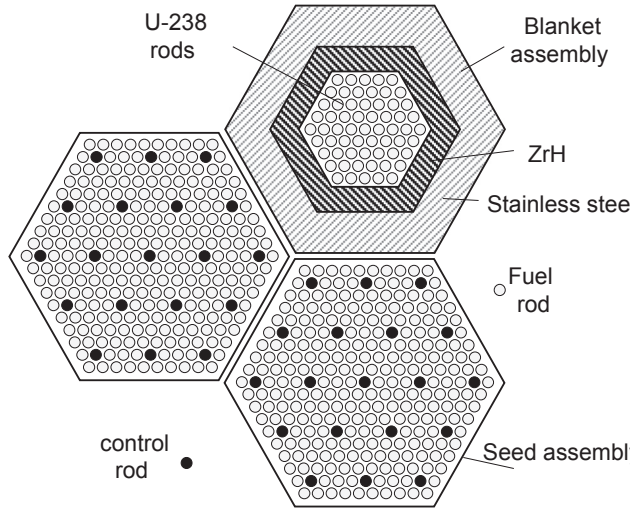


Figure 8.10 Fuel assembly design for a reactor core with fast neutron spectrum (Oka et al., 2010).

8.6.3 Canadian SCWR fuel assembly concept

The fuel for the Canadian SCWR concept is similar to existing power reactor fuel in that a ceramic pellet produces heat, which is transferred through the metallic cladding to the primary coolant. Significant differences between the Canadian SCWR concept and existing power reactor fuels, which have been considered, are the normal operating conditions and accident conditions of higher temperature and pressure. These additional considerations (combined with corrosion concerns) necessitate the rejection of zirconium-based alloys as fuel cladding candidates.

The fuel assembly consists of the fuel elements, central flow tube, encapsulated insulator, upper and lower fuel element supports, inlet/outlet flow exchanger, and outlet flow tube. The arrangement is illustrated in Fig. 8.11. Inlet coolant enters the fuel assembly from the inlet plenum and initially flows through the periphery of the fuel assembly. Above the fuel elements and upper fuel element support, a flow exchanger transfers the inlet coolant to the central flow tube. The same flow exchanger transfers the outlet coolant from the periphery of the fuel assembly to the outlet flow tube where it proceeds to the outlet header. Inlet coolant flows down the central flow tube to the bottom of the fuel assembly. The coolant reverses direction at the bottom of the fuel assembly and flows up the periphery of the fuel assembly over the fuel elements to the flow exchanger-outlet flow tube. The fuel bundle concept consists of 64 fuel elements with 32 fuel elements in each ring (see Fig. 8.12 for the cross-sectional view). The outer diameter of fuel elements is 9.5 mm in the inner ring and is 10 mm in the outer ring. Each fuel element is 6.5 m long housing the fuel pellets, an inner filler tube in the plenum area to prevent collapse under external pressure, and a spring to hold the pellets in place but allow

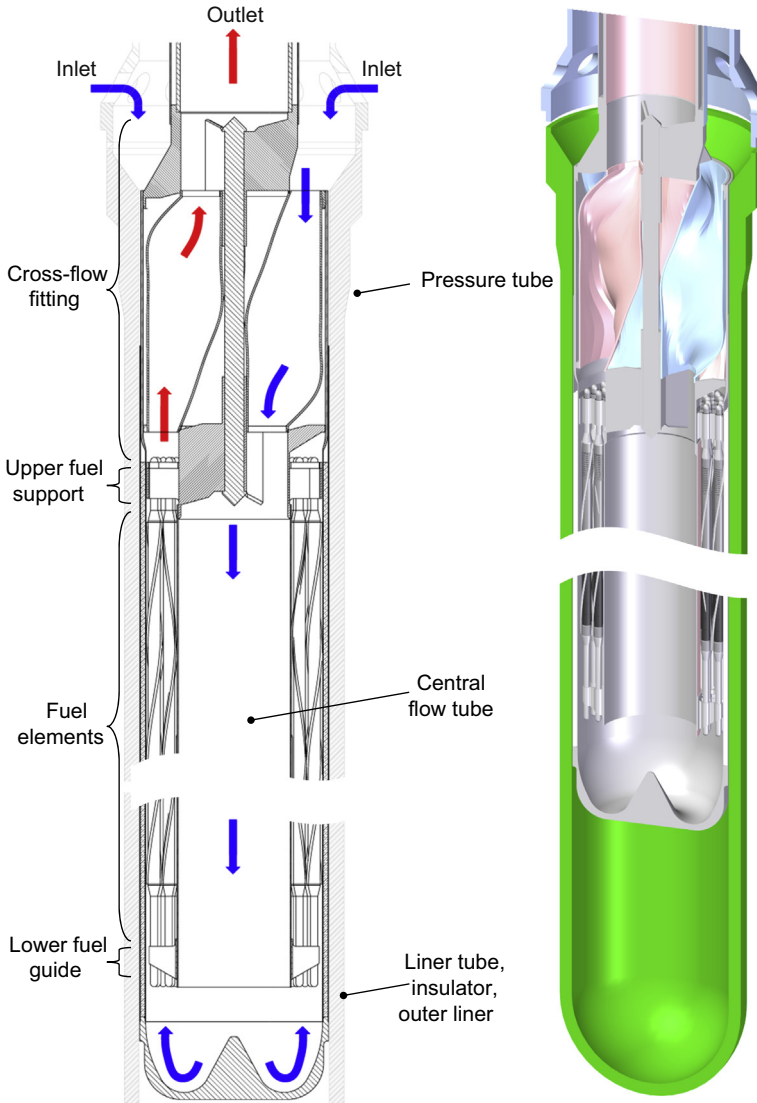


Figure 8.11 Cross-section views of the supercritical water-cooled reactor fuel assembly concept.

for pellet expansion. The active length of the fuel element is 5 m. Each end of the fuel element is closed with an end plug, which is welded to the cladding tube.

Spacings between fuel elements, between inner-ring elements and the central flow tube, and between outer-ring elements and the inner insulator liner are maintained by wires arranged in a spiral wrap around every fuel element. In addition to maintaining spacings, these wires minimize vibration of each element and enhance heat transfer

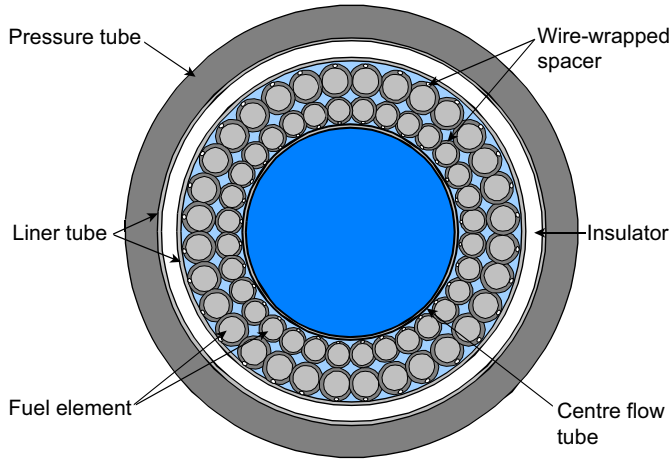


Figure 8.12 Cross-sectional view of the 64-element fuel bundle concept inside of the pressure tube.

from the cladding to the coolant. The effectiveness of wire-wrapped spacers on heat transfer enhancement has been demonstrated through experiments using tubes, annuli, and bundles. One of the concerns of using wrapped-wire spacers is fretting on the fuel cladding. In view of the relatively low channel flow, fretting is not anticipated to be an issue. Nevertheless, a confirmatory experiment may be needed.

A key feature of the Canadian SCWR fuel concept is the adoption of the proven "collapsible cladding" concept utilized in CANDU[1] fuel. This feature is especially suited to the Canadian SCWR concept because of the high temperature and pressure experienced under normal operating conditions. The choice of a collapsible cladding requires that the cladding material has sufficient ductility in the beginning of the fuel cycle to deform onto the fuel pellets. This relaxes the requirements on the creep strength and yield strength relative to a free-standing fuel cladding increasing the number of materials that can be viable for use. Five candidates of fuel cladding materials were assessed for their suitability based on various material properties (Table 8.1). Alloy 800H and Alloy 625 have been considered as prime candidates, whereas Stainless Steel 214 is excluded because of missing information on several properties.

Another feature of the current Canadian SCWR fuel element concept is the adoption of a colloidal-graphite coating of the internal surface of the cladding (Wood et al., 1980). The graphite coating of standard CANDU PHWR fuel cladding has been proven to provide additional margin to (internal) stress-corrosion cracking. Although the mechanism of this protection is not clearly understood, the most popular theories involve either the graphite acting as a "getter" for volatile corrosive fission products or because it provides a physical barrier between the fuel pellet and the cladding, protecting the cladding from fission fragment damage. In both cases, the graphite

[1] CANDU® – Canada Uranium Deuterium (a registered trademark of Atomic Energy of Canada Limited).

Table 8.1 Scorecard for fuel cladding material candidates

Material	Property							
	Corrosion	Oxide thickness	SCC (un-irradiated)	IASCC	Creep	Void swelling	Ductility (4% elongation)	Strength
800H								
310S								
625								
347								
214								

Green, available data suggest that this alloy meets the performance criteria under all conditions expected in the core; *yellow*, some (or all) available data suggest that this alloy may not meet the performance criteria under some conditions expected in the core; *gray*, there are insufficient data to make even an informed decision as to the behavior in a Canadian SCWR core concept.

coating should provide the same protection for the Canadian SCWR fuel cladding as it does for the CANDU fuel cladding.

In keeping with the collapsible cladding concept, the Canadian SCWR fuel concept will utilize the standard CANDU-type pellet configuration. Pellets will be high-density, double-dished, and chamfered. High-density pellets negate problems associated with in-reactor sintering (shrinkage); double dishes negate the problems associated with axial expansion stresses due to radial variations in pellet thermal expansion; and the chamfers avoid problems with pellet-end chipping, ease pellet loading, and ensure that pellet axial expansion is transferred via the (cooler) periphery of the fuel (at the union of the chamfer and the dish). The standard practice of pellet centerless grinding would be used to achieve very tight tolerances on pellet diameter.

The insulator consists of a series of identical plates formed on a radius. The plates are produced such that they cover 50 cm of vertical and 120 degrees of circumferential coverage around the fuel bundle. The plates have beveled edges such that they overlap at intersections vertically and circumferentially (see Fig. 8.13). The use of the plate concept is necessary for plate fabrication and fuel performance considerations. From

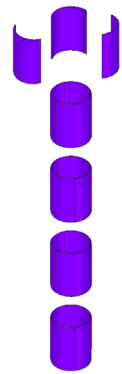


Figure 8.13 Segmented insulator concept.

a fabrication perspective, for sintered ceramic materials, the tolerances achievable are a function of the size of the part. Therefore very large/long parts cannot be fabricated to the tolerances required. From a performance perspective the plate concept allows for the following:

- the ability to minimize gaps between insulator and inner and outer liner tubes, and
- accommodating differences in thermal expansion (axial and radial) between the inner and outer liners.

The beveled edges give the plates some (limited) ability to slide past each other. This allows consideration of techniques such as heat shrinking the outer liner and/or cryoexpanding the inner liner to minimize gaps between the insulator and the liners. Because of temperature differences between the inner and outer liners at normal operating conditions and accident scenarios, differences in thermal expansion are anticipated. The plate concept allows the insulator to accommodate the thermal expansion differences while minimizing insulator gaps due to cracking.

The insulator material is yttria-stabilized zirconia, and the ceramic insulator is cladded by the inner and outer liner tubes. The insulator-liner tube assembly is attached to the fuel assembly, rather than the pressure tube, and is replaced after three fuel cycles. The insulator size and geometry are determined by the requirement that the fuel channel concept incorporates the ability to maintain core components below melting temperature even under accident scenarios that require long-term passive cooling.

8.7 Safety system concept

Defense-in-depth is one of the important principles in all safety concepts of current reactors and it shall consequently also be applied for the SCWR. Accordingly, the save operation of the power plant shall be ensured by the following measures:

Normal operation shall be safeguarded by the operating systems. Moreover, the power plant shall be based on

- conservative design with high reliability and availability and
- proven technology and quality assurance.

Operational occurrences of seldom events ($<10^{-2}$/year) shall be controlled and limited by

- surveillance and diagnostics and
- inherent safety and nuclear stability.

Design basis accidents with a probability of $<10^{-5}$/year shall be controlled by safety systems, which include

- redundancy and train separation,
- protection against internal and external hazards,
- qualification against accident conditions,
- automation, and
- autarchy of the safety systems.

Multiple failure scenarios (eg, station blackout, total loss of feed water, and loss of coolant accidents) and severe external events (eg, military or large commercial airplane crash) are included in the design extension scenarios, which shall be protected by

- diversified systems and
- design against external event loads.

If severe accidents should still occur, then the SCWR needs to be protected by

- mitigative features and
- prevention of energetic consequences that could lead to large early containment failure (eg, steam explosion, direct containment heating, and global hydrogen detonation).

8.7.1 Safety system in a pressure vessel-type supercritical water-cooled reactor concept

For a pressure vessel design of the SCWR, there are several common safety system requirements that can be taken directly from PWR or BWR designs without significant modifications. These are

- the reactor shut-down system by control rods or by a boron injection system as a second, divers shut-down system,
- containment isolation by active and passive containment isolation valves in each line penetrating the containment to close the third barrier in case of an accident,
- steam pressure limitation by pressure relief valves,
- automatic depressurization of the steam lines into a pool inside of the containment through spargers to close the coolant loop inside of the containment in case of containment isolation,
- a coolant injection system to refill coolant into the pressure vessel after intended or accidental coolant release into the containment,
- a pressure suppression pool to limit the pressure inside of the containment in case of steam release inside of the containment, and
- a residual heat removal system for long-term cooling of the containment.

An example of a containment with such safety systems is the compact HPLWR containment shown in Fig. 8.14 with 20-m inner diameter and 23.5-m inner height (Schulenberg and Starflinger, 2012). The cylindrical containment from prestressed concrete is designed for an internal pressure of 0.5 MPa. It contains the reactor pressure vessel, an annular pressure suppression pool with 900 m^3 of water and 500 m^3 of nitrogen, four upper pools with a total water volume of 1121 m^3, and a drywell gas volume of 2131 m^3. Four feed-water lines with check valves and four steam lines with containment isolation valves, each inside and outside of the containment, connect the reactor with the steam cycle. These valves are designed with a stroke time of 3 s, actively and passively closing. Four automatic depressurization systems (ADSs), each equipped with two safety relief valves and two depressurization valves, open a flow cross section of 110 cm^2 each to eight spargers in the upper pools.

Underneath the pressure suppression pool, four redundant and separated LP coolant injection pumps, with an outlet pressure of at least 6 MPa and a maximum flow rate of 180 kg/s each, supply coolant from the pressure suppression pool via a heat exchanger for residual heat removal and via a check valve to the feed-water line. Overflow pipes from the upper pools to the pressure suppression pool close the coolant loop inside

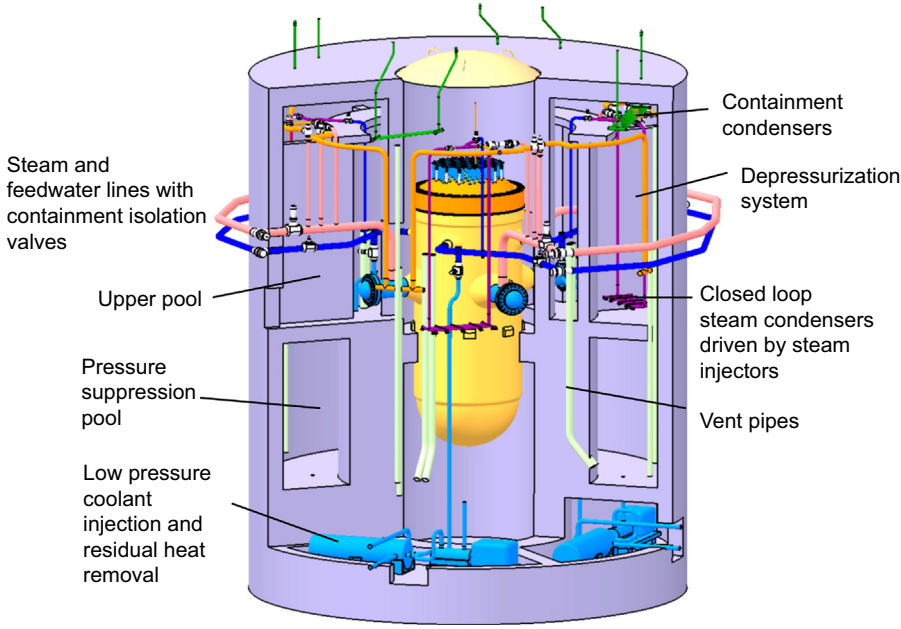


Figure 8.14 Containment of the HPLWR with safety systems.
From Schulenberg, T., Starflinger, J., 2012. High Performance Light Water Reactor, Design and Analyses. KIT Scientific Publishing. ISBN:978-3-86644-817-9.

of the containment. Sixteen vent tubes for pressure suppression in the containment connect the drywell with the pressure suppression pool.

Four emergency condensers are connected with the four steam lines and with the four feed-water lines hanging from the top in the upper pools. For example, flow through these condensers is driven by a steam injector. In addition, there are four containment condensers mounted at the ceiling of the drywell, which are connected on their secondary side to pools above the containment. Their secondary side is permanently open so that steam in the containment can condense as soon as the saturation temperature in the pools has been reached and the containment pressure is starting to increase, in the unlikely case that the heat sink of the residual heat removal system is not available. Open connecting pipes from the ceiling to the pressure suppression pools enable a discharge of hydrogen from the drywell. In turn, the pressure suppression pool can be vented to the stack through aerosol and iodine filters.

Outside the containment, a boron poisoning system on top of the containment with a tank of about 10 m^3 of B-10 with a concentration of 20−25% is connected with the feed-water lines by two lines including pumps. It serves as the second, redundant shut-down system.

8.7.2 Safety system in the Canadian SCWR concept

The safety approach adopted for the Canadian SCWR concept follows those of advanced reactors in that multiple levels of independent and diverse safety systems

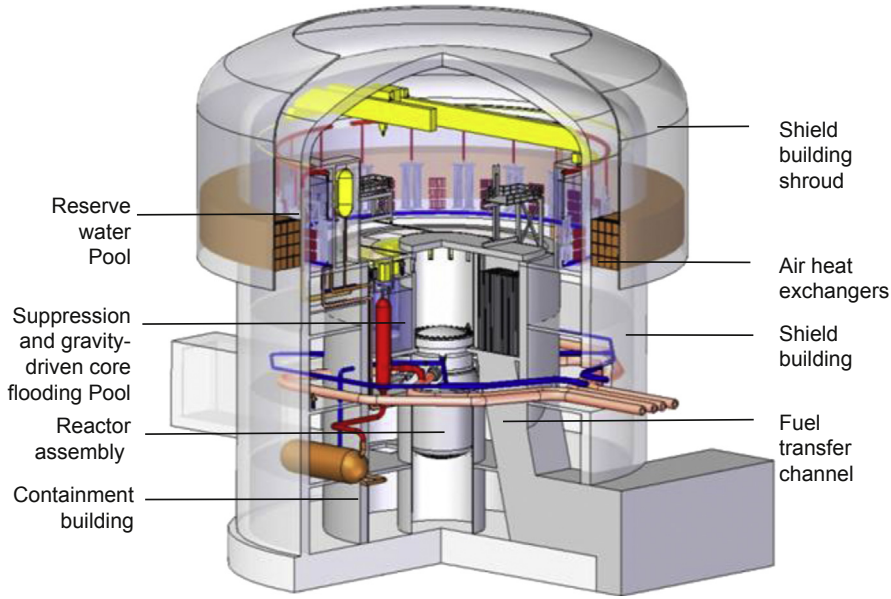


Figure 8.15 Safety system inside of the reactor building of the pressure tube-type supercritical water-cooled reactor concept.

are used as defense-in-depth and passive safety systems are adopted for increased reliability. One of the major development goals of the Canadian SCWR concept is to enhance safety such that the risk of core damage and release of radioactive materials to the environment is significantly reduced. The unique features of the pressure tube-based concept allow for an optimal balance of passive safety features on the moderator systems for emergency heat removal (eg, a prolonged station blackout event) and a combination of active and passive safety systems in the main cooling system. The primary system components are selected to provide multiple and redundant decay heat removal paths; these defense-in-depth concepts considerably reduce plant risk over existing reactors. In addition, there is a transformative improvement in core damage risk by including a further passive decay heat removal pathway for emergencies. This capability is possible through a combination of a natural circulation-driven moderator cooling system, the fuel assembly concept, fuel channel concept, and direct radiation heat transfer from the fuel to the insulator liner. The safety concept adopted for the Canadian SCWR concept is described by Novog et al. (2012), and a detailed design description of the safety systems is given by Yetisir et al. (2014) and Gaudet et al. (2014). Fig. 8.15 illustrates the safety system inside of the reactor building.

8.7.2.1 Containment pool

The primary function of the containment pool is to provide a volume of water into which steam flows from the ADS so that large-scale loss-of-coolant accidents (LOCAs) can be suppressed. In addition, the containment pool provides a gravity-driven water

flow to the reactor inlet plenum to replace inventory lost during a LOCA and subsequent decay heat boil-off. This pool consists of an annular-shaped tank and is located in the containment building above the reactor. It is divided into two sections to reflect the bilateral symmetry of the reactor and safety systems, with each half functioning independently of the other.

Located above the liquid level within the pool is the containment steam condenser gallery, which houses containment steam condenser heat exchangers and passive autocatalytic recombiner units. Physically, the condenser gallery is an annular-shaped, enclosed area, with a series of openings located on the outer wall. This outer wall forms a separation between the steam tunnel and condenser gallery. Located within these openings are the containment steam condenser heat exchangers, placed to allow condensed steam to drain directly within the condenser gallery. The condenser gallery floor is equipped with a series of drains equipped with suppression nozzles, discharging into the containment pool below the liquid level.

This layout permits the containment steam condensers and containment pool to act in unison to condense steam accumulating in the steam tunnel because of an LOCA event. In a high steam-flow regime found in a large-scale LOCA, the steam condensers will be overwhelmed, allowing steam to flow past these condensers and be injected and suppressed within the containment pool via the drains. A low steam-flow regime will result in the direct condensing of the steam by the heat exchangers, with the condensate draining into the containment pool.

The volume above the liquid level of the containment pool can be considered as a wetwell. In a high steam-flow regime from the steam tunnel to containment pool, air and gases may be entrained and deposited in the wetwell above the surface of the containment pool. To prevent the pressure in this area from rising excessively, a series of rupture panels are located above the containment pool water line, separating the drywell space from the wetwell. These panels allow gases and entrained air to escape to the larger drywell space should the wetwell volume be insufficient.

The secondary side of the containment steam heat exchangers are connected to the reserve water pool, with circulation established through gravity-driven flow. With this, heat from an LOCA event will be deposited into the reserve water pool through the containment steam condensers.

8.7.2.2 Automatic depressurization system

The ADS consists of several valves through which the reactor can be rapidly depressurized. It also provides overpressure protection to the reactor and outlet piping. The valve banks are located in the containment building steam tunnel, with the discharge flow suppressed into the containment pool.

8.7.2.3 Gravity-driven core flooding system

The gravity-driven core flooding system consists of a pipe connecting the containment pool to the reactor cold leg coolant piping. A check valve permits the reactor to operate

at its operating pressure, yet it allows water to flow into the reactor from the containment pool under accident conditions.

To ensure long-term decay heat removal in the event of a piping breach within the containment building steam tunnel, the volume of the containment pool exceeds that of the steam tunnel. Because of the seal between the reactor and steam tunnel floor, coolant will accumulate within the steam tunnel, with steam condensed and returned to the containment pool. With the steam tunnel filled with water from the containment pool, a sufficient level will remain in the containment pool to cover both the suppression nozzles and the gravity-driven core flooding system inlet pipe. This feature eliminates the need for an active pumping system and other related components (eg, sump strainers).

8.7.2.4 Isolation condensers

The primary function of the isolation condensers (ICs) is to passively remove sensible and core decay heat from the reactor, preventing reactor overpressure, and to serve as a long-term cooling system under station blackout conditions. The IC heat exchangers connect with the reactor coolant piping and remove heat from the reactor by depositing this into the reserve water pool.

The IC system is divided into two independent trains, with each train consisting of a piping loop running from the reactor outlet, to heat exchangers located in the reserve water pool, and returning to the reactor inlet. The system is pressurized and on hot standby under normal reactor operations. A connection valve is located on the system's low point near the reactor inlet and is closed under normal reactor operations. The closed valve disrupts the flow through the system to minimize heat loss.

The IC relies on the difference of densities between the IC hot leg and cold leg fluid to initiate and maintain a gravity-driven circulation. Under station blackout conditions the reactor can be depressurized and cooled by first closing the main steam and feedwater isolation valves, followed by opening the IC connection valve. The liquid column normally trapped by the connection valve is allowed to flow into the reactor inlet. As this drains into the reactor, the IC heat exchanger tubing will be exposed to steam from the reactor outlet, allowing heat transfer to the reserve water pool. Further steam produced by the reactor due to the decay heat will sustain the circulation.

Although two independent trains of ICs are considered as the reference configuration for the Canadian SCWR concept, the required capacity of the ICs varies as the reactor is cooled to prevent unnecessarily rapid cooling rates. The current two-train configuration may not allow plant operators to adequately control the cool-down rate and would require further subdivision into four independent trains, with one train attached to each of the reactor outlets. Details on the configuration will be established in future design phases.

8.7.2.5 Reserve water pool

The primary function of the reserve water pool is to serve as a buffer between the passive safety systems and the ultimate heat sink. The large mass of water available in the

pool allows heat to be absorbed and subsequently removed by the atmospheric air heat exchangers or by evaporation.

The pool is located in the upper section of the shield building and occupies an annular space against the building's outer wall. It is divided into two sections, each section housing one train of ICs and the passive moderator cooling system (PMCS). All heat exchange areas of the ICs and the passive moderator heat exchangers are located in the lower half of the pool. The pool enclosure is equipped with a filtered vent to the atmosphere to permit the release of water vapor. Pool levels can be remotely maintained by means of a fill line connected to an external emergency supply such as lake water or a water truck.

8.7.2.6 Atmospheric air heat exchangers

The primary function of the atmospheric air heat exchangers is to reject heat from the reserve water pool to the atmosphere. Although not considered as a safety system, the heat exchangers serve to extend the period of time in which the reserve water pool can function as a heat sink before intervention under a high core decay heat regime. At a lower core decay heat regime, the atmospheric air heat exchangers can reject the entire heat load, extending indefinitely the point of intervention.

The atmospheric air heat exchangers consist of a series of plate-type heat exchangers located on the periphery of the shield building. These exchangers are enclosed in a shroud, which forms a chimney to further increase gravity-driven air flow. To minimize the number of penetrations into the shield building, the heat exchangers are grouped and connected to common hot leg and cold leg headers. Valves are located on both the hot leg and cold leg headers and are closed under normal reactor operating conditions to prevent freezing in cold climates.

Under accident conditions, with the valves opened, water is drawn from the upper surface of the pool, allowed to cool in the heat exchanger, and returned to the bottom of the pool by means of a gravity-driven convection current. Likewise, cooler air is drawn through the heat exchangers from the bottom of the shroud, with the heated air escaping at the top of the shroud.

8.7.2.7 Passive moderator cooling system

The PMCS serves as an additional barrier to core damage. In an accident scenario, decay heat generated in the fuel within the fuel channel is transferred through radiation from the cladding to the inner liner of the insulator, flows through the channel insulator and pressure tube, and is deposited into the moderator. The PMCS uses a flashing-driven natural circulation loop to remove heat from the moderator, and it deposits the heat into the reserve water pool.

The PMCS is divided into two independent trains, with each train consisting of a piping loop running from the reactor calandria to heat exchangers located in the reserve water pool and returning to the calandria. The system is totally passive, and it is allowed to function during normal reactor operation. A head tank, located above the heat exchangers, maintains a constant pressure within the system.

8.8 Dynamics and control

Because the SCWR has a once-through steam cycle, in which steam from the core outlet is directly supplied to the HP turbines, it has many similarities with BWRs. However, on a closer look there is a basic difference in the coolant flow path inside of the reactor that causes a difference of the steam cycle control. In a BWR the feed-water pump is controlling the liquid level in the reactor pressure vessel, the steam pressure is controlled by the turbine governor valve, and the core power is either controlled by the control rods or by the speed of the recirculation pumps. The SCWR concepts do not include any recirculation loop. The feed-water pump can control either the steam temperature at the core outlet, if the core power is controlled by the control rods, or it can control the core power if the steam outlet temperature is controlled by the control rods. Again, the steam pressure is controlled by the turbine governor valve in both cases.

An example of control loops for operation in the load range is sketched in Fig. 8.16. Here the speed of the feed-water pump is controlled by the temperature of the superheated steam at turbine inlet, the mass flow of the HP steam extractions is controlled by the feed-water temperature, the reheat temperature is controlling the steam mass flow of the reheater, and the pressure at the reactor outlet is controlling the turbine governor valve. The thermal power of the reactor, and thus with some delay in the generator power, is controlled by the control rods of the reactor core.

A supercritical fossil-fired power plant with a once-through steam cycle is usually operated with a sliding pressure: the turbine governor valve is kept open in the upper load range and the boiler outlet temperature is kept constant such that the boiler outlet pressure increases proportionally with the steam mass flow and thus with load. Consequently, the boiler is operated at subcritical pressure below approximately 80−90% load. However, such control is not permitted for the SCWR because dryout

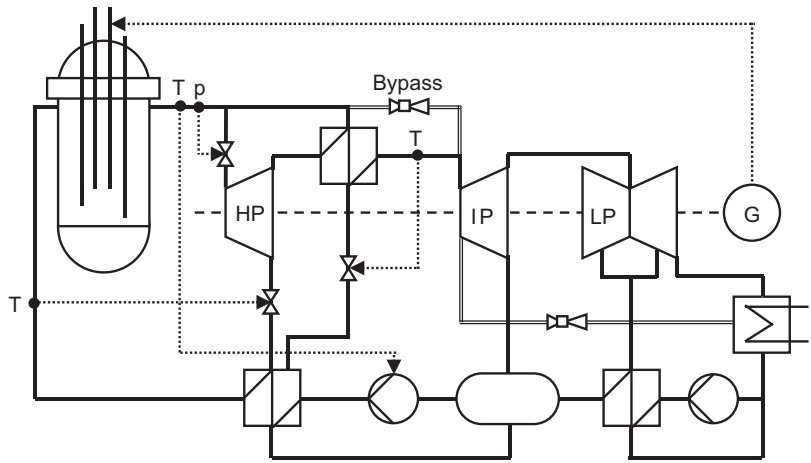


Figure 8.16 Control loops to operate the supercritical water-cooled reactor in the load range. *HP*, high pressure; *IP*, intermediate pressure; *LP*, low pressure; *G*, generator.

or even film boiling of the coolant at the fuel rods would overheat and damage them (Schulenberg and Raqué, 2014). Instead, the SCWR is operated at constant supercritical pressure in the entire load range.

The best thermal efficiency at part load can be achieved at maximum core outlet temperature. A constant temperature implies that the coolant mass flow increases proportionally with load. However, because the reactor core requires a minimal coolant mass flow, in particular for downward flow regions of the two-pass or three-pass concept (Fig. 8.2), the reactor must be operated with a colder core outlet temperature in the lower load range. Once the core outlet temperature and thus the turbine inlet temperature becomes so small that condensation and droplet erosion must be expected in the HP turbine, the steam has to bypass the turbine. Likewise, the reheat temperature is colder in the lower load range because it cannot exceed the core outlet temperature, and the steam also has to bypass the IP and LP turbines.

Oka et al. (2010) discuss the plant dynamics using such a control system. They conclude that stable operation of the thermal reactor as well as of the fast core option can be achieved by tuning the controllers.

8.9 Start-up

Starting from cold conditions, the first reactor power will be needed to warm up the steam cycle. Oka et al. (2010) suggest either to start with constant supercritical pressure by depressurizing some coolant into a flash tank or to start with a sliding, subcritical pressure by separating water and steam from the reactor core in external cyclone separators. In either case, the separated liquid is taken to preheat the feed water and the remaining steam is warming up the turbines. Because dryout will be unavoidable in the reactor core during subcritical operation, the maximum cladding surface temperature of the fuel rods needs to be checked to avoid damage.

Schulenberg and Starflinger (2012) reported about a constant pressure start-up and shut-down system for the three-pass core design of the HPLWR, trying to keep the feed-water temperature constant to minimize thermal stresses of the reactor pressure vessel. This concept also includes a warm-up procedure for the deaerator during startup from cold conditions. A battery of cyclone separators is foreseen outside of the containment to produce some steam from depressurized hot coolant of the reactor.

8.9.1 Start-up system in a pressure tube-type supercritical water-cooled reactor concept

The key requirement for the start-up system is to maintain adequate flow through the core to protect the fuel from overheating during startup. As the reactor is brought from low-pressure and low-temperature conditions to operating conditions, two-phase flow can occur within the core, giving rise to the possibility of dryout. The reduced heat transfer occurring under dryout conditions can lead to fuel overheating. For this reason the maximum allowable cladding surface temperature is set as a criterion and is determined by the cladding material.

An additional concern during reactor startup is the steam quality to the HP turbine. To avoid turbine blade damage, the moisture content in the saturated steam at subcritical temperatures is normally limited to less than 0.1%. In addition, the enthalpy of the core outlet coolant must be high enough to provide the required turbine inlet steam enthalpy.

The modified sliding pressure startup as proposed by Yi et al. (2005) can be adapted to the proposed operating conditions in the Canadian SCWR concept. To provide a starting point for future analysis of critical performance characteristics (eg, fuel cladding temperatures and thermal-hydraulic and neutron stabilities), reference operating conditions (eg, flow rates, reactor power levels, and mechanical equipment configurations) have been selected.

The recirculation flow rate chosen is to match that suggested for the superlight water reactor (Yi et al., 2005), namely 25% of full power flow, with reactor power levels and warm-up times chosen to limit temperature gradients within the pressure boundary as the reactor comes to operating temperature. The maximum feed-water temperature is adjusted to 350°C to reflect the proposed Canadian SCWR operating conditions. All start-up components are rated for a maximum operating temperature of 450°C, reducing the overall weight of the construction because of greater mechanical strength at lower metal temperatures. Finally, make-up feed-water flow during turbine warmup is to be supplied by the feed-water system because the Canadian SCWR concept does not have a reactor core isolation cooling system.

In addition to the feed water and inlet and outlet piping normally found in a reactor, the start-up system consists of a steam drum, a heat exchanger, and circulating pump, as shown in Fig. 8.17. The function of the steam drum is to provide a liquid level at which pressure equilibrium can be established based on the temperature of the water. Because no steam is allowed to escape the system, the system pressure is at the saturation temperature of the liquid. The function of the heat exchanger is to limit the coolant temperature being returned to the reactor to 350°C, and it is utilized in the start-up sequence

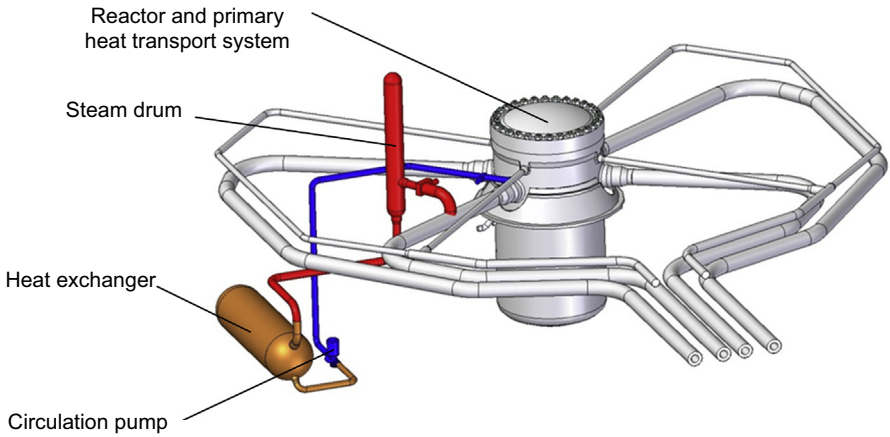


Figure 8.17 Component layout of the start-up system concept.

only after the outlet temperature exceeds this limit. To limit the thermal gradient stresses within this heat exchanger and to reduce the capacity requirement, the maximum operating temperature of the start-up components will be limited to 450°C, beyond which line switching will occur and the start-up system stopped.

To avoid additional penetrations to the reactor inlet plenum, the start-up system piping is connected to one of the four heat transport piping connections to the reactor. The connection point is within the containment building, between the reactor and main steam isolation valves and the feed-water isolation valves. The start-up system can be isolated from the reactor by means of valves located on the start-up system piping at the connection points.

A recirculation pump is to provide a constant mass flow to the reactor, regardless of the instantaneous fluid density. The pump is to be equipped with a variable-speed drive motor to maintain the desired mass flow rate throughout the start-up cycle. The pump is to be located in proximity to the heat exchanger within the shield building.

8.10 Stability

A stability problem that is well known from BWRs is the occurrence of density wave oscillations. It is caused by the large density change of the boiling coolant in the core, in particular if the local coolant pressure drop increases with decreasing mass flow. The coolant density ratio in the SCWR changes by more than a factor of 8 in the core, which is even higher than in a BWR (International Atomic Energy Agency, 2014).

Stability analyses of the coolant flow through the three-pass core of the HPLWR have been studied by Ortega Gomez (2008). As with BWRs, Ortega Gomez shows that the most effective measure to avoid density wave oscillations in the core is the installation of orifices at the inlet of fuel assemblies. These orifices need to be customized for a hot fuel assembly.

In the case of a BWR, the operation point of the average heated fuel assembly should correspond to a decay ratio less than 0.5 for a single-channel density wave oscillation, and a decay ratio less than 0.25 should correspond to the coupled thermal-hydraulic/neutronic density wave oscillation. Furthermore, the whole operation range, also including hot fuel assemblies, should be in the linear stable region of the stability map.

Ortega Gomez (2008) shows that the average and even the hot fuel assemblies of the HPLWR superheaters fulfill the stability criteria for all three types of density wave oscillations without applying any orifice. However, the average fuel assemblies of the evaporator have a decay ratio larger than 0.25 at normal operation parameters for the in-phase and out-of-phase density wave oscillation. Furthermore, hot fuel assemblies of the evaporator would operate in the linear unstable region. Thus, although the fuel assemblies of the superheaters do not need additional inlet flow restriction, all fuel assemblies of the evaporator stage must be equipped with inlet orifices.

Although the first superheater is stable with respect to density wave oscillations, even without orifices, we have to expect flow reversal in some fuel assemblies of the first superheater of a three-pass core at low mass flow rates because of an unstable stratification

of the downward flow. The mass flow control of the reactor is usually such that flow reversal is excluded, as discussed in Section 8.8. However, low mass flow rates are unavoidable during some sequences when the reactor is opened and the core is disassembled or during accident scenarios. Schulenberg and Starflinger (2012) reported about flow analyses for such scenarios, concluding that flow reversal will not be a concern for the core as long as enough margin is kept from the cladding temperature limits.

Another stability issue, which has been reported by Schulenberg and Starflinger (2012), is the xenon oscillation of the core power, such as those known from conventional LWRs. Reiss et al. (2009) studied these oscillations for a simplified HPLWR core geometry. The diameter of the core of the HPLWR is approximately 3.5 m, whereas the active height is 4.2 m. These dimensions are in the range of LWRs where xenon oscillations cannot be excluded. On the other hand, because of the large density drop of water after crossing the pseudocritical point, the migration length of the neutrons, which is an important parameter for the stability of the reactor against xenon oscillations, is larger than in current LWRs. The preliminary results of Reiss et al. (2009) indicated that the HPLWR will be unstable against xenon oscillations. Nevertheless, its stable operation can be ensured with proper control equipment (eg, partly inserted control rods), which is already well established and will be similar to today's large reactors. At the beginning of the burn-up cycle of the HPLWR, some of the control rods are inserted to compensate for excess reactivity, which makes them suitable, in addition to power control, for xenon oscillation control. At the end of the cycle some of the control rods will be still inserted because of power control and safety considerations; therefore they could also prevent large oscillations. On the other hand, partly inserted control rods could be useful not only for controlling xenon oscillations but also to fine tune the power distribution during normal operation.

8.11 Advantages and disadvantages of supercritical water-cooled reactor concepts

Differences in system configurations would lead to specific advantages and disadvantages between pressure vessel and pressure-tube types of SCWR concept. Rather than focusing on each system, the following general advantages of SCWR concepts are foreseen:

- The SCWR concepts are evolutions of the current fleet of nuclear reactors (either LWR or PHWR) combining the nuclear reactor with the balance of plant of the fossil-fired power plant. Once constructed, the SCWRs can be easily adopted into the existing systems of utilities because most utilities operate nuclear and fossil-fired power plants.
- System configurations of the SCWR concept are simpler than existing reactors; hence they can provide economic advantage.
- The SCWR concept is a water-cooled reactor, which has the distinct advantages of safeguard and proliferation resistance.
- With the introduction of a passive safety system, the safety characteristics of the SCWR concepts are as good as or better than existing reactors.
- All SCWR concepts have higher thermal efficiency than the current fleet of nuclear reactors; hence they would reduce the fuel utilization and waste stream, improving the sustainability.

The following disadvantages may be associated with the SCWR concepts:

- The high coolant temperature has led to high cladding temperature, which requires the use of stainless steels or nickel-based alloys as fuel cladding materials. Because of the high neutron absorption of these materials, the fuel burn-up is reduced or the fuel enrichment is increased. In addition, the refueling frequency is increased compared with the current fleet of nuclear reactors.
- All current SCWR concepts adopt the direct cycle to simplify the system configuration. Although the direct cycle is also being used in the BWR, the single-phase steam flow in the SCWR would transport the radioactive materials from the core to the HP turbine (the presence of liquid phase in the BWR minimizes the transfer because the radioactive materials remain in the liquid whereas the steam is directed to the turbine). This could hamper maintenance and inspection of the turbine and increase dosage to staff. Introducing the indirect cycle would alleviate the issue, but it would escalate the capital cost of the plant.
- The fuel assemblies of current SCWR concepts contain more parasitic materials than those of existing reactors, increasing the waste stream.

8.12 Key challenges

The basic idea for development of the SCWR is to use the long-term experience of PWRs and BWRs on the one hand, and the experience with supercritical fossil-fired power plants on the other hand, to derive an innovative plant concept with a minimum of research needs. Obviously, the reactor core of such a power plant will be new then, and the core outlet temperatures as well as the enthalpy increase of coolant in the core will exceed by far the current experience. However, all other components of the SCWR power plant, including the steam cycle components and the containment with its safety systems, are not considered to cause any major challenge because the latest fossil-fired power plants are operated even with a life steam temperature of 600°C at pressures above 30 MPa.

A key challenge for core design is certainly a cladding material for elevated temperatures above 600°C. Zircalloy is certainly not applicable at these temperatures. Ferritic-martensitic boiler steels used for supercritical fossil-fired power plants are hardly applicable because the small wall thickness of fuel claddings of approximately 0.5 would not provide enough corrosion margin. Austenitic stainless steels with more than 20% Cr are still among the most promising candidates; however, they have compromises in creep resistance. Nickel-based alloys can tolerate even higher temperatures in the supercritical water environment, but the high nickel concentration will cause helium embrittlement and stress-corrosion cracking under neutron irradiation. As an alternative option, the use of coatings has been considered recently such that a corrosion-resistant coating is applied on a creep-resistant substrate. Guzonas and Novotny (2014) summarize the latest status of SCWR material research.

Another key issue is the prediction of cladding surface temperatures at bulk temperature close to the pseudocritical point. The strong change of almost all coolant properties with temperature may cause a deterioration of heat transfer and associated hot spots, which can hardly be predicted with current computational fluid dynamics (Pioro and Duffey, 2007). A recent blind benchmark exercise on heat transfer in an

electrically heated rod bundle in supercritical water, summarized by Rohde et al. (2015), confirmed that we are still far from reliable predictions.

8.13 Future trends

Qualification of advanced technologies is the focus of planned research and development for the SCWR in the next years. Cladding alloys for better corrosion resistance at elevated material were recently developed, but many additional tests, including an in-pile test with supercritical water, will be required before licensing authorities can accept these materials. Likewise, neutronic and thermal-hydraulic codes as well as system codes are available, in principle, but further integral tests are needed to qualify them for these advanced nuclear applications. An in-pile test of a small-scale fuel assembly in a critical arrangement inside of a research reactor is considered to be mandatory before an SCWR prototype can be built. It has been designed by a European consortium, as outlined by Ruzickova et al. (2014), and shall be operated in a closed water loop at supercritical pressure inside of a research reactor. Although only being a small-scale fuel element, this loop must be licensed similar to a nuclear facility, including qualification of all technologies included there.

On a long-term perspective, a prototype reactor is envisaged and shall include all key technologies of the SCWR. However, different from other advanced Generation IV reactor concepts, the SCWR can also be developed in small incremental steps from PWRs, BWRs, or PHWRs, taking advantage of the long-term experience with water-cooled reactors, which would minimize the technical and financial risks of this development.

Acronyms

HPLWR	High-performance light water reactor
IC	Isolation condensers
LEU	Low enriched uranium
LOCA	Loss-of-coolant accident
PMCS	Passive moderator cooling system

Nomenclature

H	Enthalpy, kJ/kg
W	Mass flow rate, kg/s
D	Density, kg/m^3

References

Gaudet, M., Yetisir, M., Haque, Z., 2014. Physical aspects of the Canadian generation IV supercritical water-cooled pressure tube reactor plant design. In: Proc. 2014 Canada−China Conference on Advanced Reactor Development (CCCARD-2014), Niagara Falls, Ontario, Canada, April 27−30.

Guzonas, D., Novotny, R., 2014. Supercritical water-cooled reactor materials − summary of research and open issues. Progress in Nuclear Energy 77, 361−372.

International Atomic Energy Agency, September 2014. Heat Transfer Behaviour and Thermohydraulics Code Testing for Supercritical Water Cooled Reactors (SCWRs). IAEA-TECDOC-1746, Vienna, Austria, 496 pp. Free download from: http://www-pub.iaea.org/books/IAEABooks/10731/Heat-Transfer-Behaviour-and-Thermohydraulics-Code-Testing-for-Supercritical-Water-Cooled-Reactors-SCWRs.

Magill, M., Pencer, J., Pratt, R., Young, W., Edwards, G.W.R., Hyland, B., 2011. Thorium fuel cycles in the CANDU supercritical water reactor. In: Proc. 5th Int. Sym. SCWR (ISSCWR-5), Vancouver, British Columbia, Canada, March 13−16, 2011.

Novog, D., McGee, G., Rhodes, D., Yetisir, M., 2012. Safety concepts and systems of the Canadian SCWR. In: Proc. 3rd China−Canada Joint Workshop on Supercritical Water-Cooled Reactors (CCSC-2012), Xi'an, Shaanxi, China.

Oka, Y., Koshizuka, S., Ishiwatari, Y., Yamaji, A., 2010. Super Light Water Reactors and Super Fast Reactors. Springer, ISBN 978-1-4419-6034-4.

Ortega Gomez, T., 2008. Stability Analysis of the High Performance Light Water Reactor. University of Karlsruhe, FZKA 7432 (Dissertation).

Pioro, I.L., Duffey, R.B., 2007. Heat Transfer and Hydraulic Resistance at Supercritical Pressures in Power Engineering Applications. ASME Press, New York, NY, USA, 334 pp.

Reiss, T., Fehér, S., Czifus, S., 2009. Calculation of xenon-oscillations in the HPLWR. In: Proc. ICAPP 09, Tokyo, Japan, May 10−14. Paper 9067.

Rohde, M., Peeters, J.W.R., Pucciarelli, A., Kiss, A., Rao, Y.F., Onder, E.N., Mühlbauer, P., Batta, A., Hartig, M., Chatoorgoon, V., Thiele, R., Chang, D., Tavoularis, S., Novog, D., McClure, D., Gradecka, M., Takase, K., 2015. A blind, numerical benchmark study on supercritical water heat transfer experiments in a 7-rod bundle. In: The 7th International Symposium on Supercritical Water-Cooled Reactors ISSCWR-7, March 15−18 paper 2044, Helsinki, Finland.

Ruzickova, M., Schulenberg, T., Visser, D.C., Novotny, R., Kiss, A., Maraczy, C., Toivonen, A., 2014. Overview and progress in the European project: "supercritical water reactor − fuel qualification test". Progress in Nuclear Energy 77, 381−389.

Schulenberg, T., Raqué, M., 2014. Transient heat transfer during depressurization from supercritical pressure. International Journal of Heat and Mass Transfer 79, 233−240.

Schulenberg, T., Starflinger, J., 2012. High Performance Light Water Reactor, Design and Analyses. KIT Scientific Publishing, ISBN 978-3-86644-817-9.

Winkel, S., Sullivan, J., Hyland, B., Pencer, J., Colton, A., Jones, S., Sullivan, K., 2013. Discussing spent nuclear fuel in highschool classrooms: addressing public fears through early education. In: Proc. Global 2013, Salt Lake City, Utah, September 29−October 3, 2013.

Wojtazek, D., 2015. Future nuclear power generation in Canada: transition to thorium fuelled SCWRs. In: Proc. 7th International Conference on Modeling and Simulation in Nuclear Science and Engineering (7ICMSNSE), Ottawa, October 18−21, 2015.

Wood, J.C., Surette, B.A., Aitchison, I., Clendening, W.R., 1980. Pellet cladding interaction evaluation of lubrication by graphite. Journal of Nuclear Materials 88 (1), 81−94.

Yetisir, M., Pencer, J., McDonald, M., Gaudet, M., Licht, J., Duffey, R., 2012. The Supersafe© reactor: a small modular pressure tube SCWR. AECL Nuclear Review 1 (2), 13−18. http://dx.doi.org/10.12943/ANR.2012.00014.

Yetisir, M., Gaudet, M., Rhodes, D., Guzonas, D., Hamilton, H., Haque, Z., Pencer, J., Sartipi, A., 2014. Reactor core and plant design of the Canadian supercritical water-cooled reactor. In: Proc. 2014 Canada−China Conference on Advanced Reactor Development (CCCARD-2014), Niagara Falls, Ontario, Canada, April 27−30, 2014.

Yi, T.T., Ishiwatari, Y., Liu, J., Koshizuka, S., Oka, Y., 2005. Thermal and stability considerations of super LWR during sliding pressure startup. Journal of Nuclear Science Technology 42 (6), 537−548.

Zhou, T., 2009. Super-critical Water-Cooled Reactor (SCWR) Steam Cycle Design Options. AECL Report, 195-01290-ASD-001.

Part Two

Current status of Generation IV activities in selected countries

Preface to Part Two

Part Two presents the current status of Generation IV activities in selected countries, which include active research, development, and other related activities. Selected countries include the United States, the European Union [actually consists of the 28 member-states, several of which participate actively in the Generation IV International Forum (GIF) nuclear energy systems, especially France], Japan, Russia, South Korea, China, and India. Of the GIF nine original participating members, Argentina, Brazil, South Africa, and the United Kingdom are not presently active. In addition, some countries have major international nuclear vendors, many of which are majority state-owned or controlled, and national laboratories that participate in Generation IV and advanced reactor research and development. Therefore, Part II consists of seven chapters written by top international experts from these countries. The sequence of these chapters/countries corresponds mainly to installed capacities of their nuclear power plants.

Generation IV: USA

9

P. Tsvetkov
Texas A&M University, College Station, TX, United States

9.1 Generation IV program evolution in the United States

The nuclear power industry is a relatively young industrial enterprise that continues to evolve following global macroeconomic energy trends and domestic developments in countries with nuclear energy use interests. James Chadwick discovered neutrons in the 1930s. By doing so he kicked off the quest for utilizing neutron-induced fissions as an energy source in a broad range of applications.

The first critical nuclear reactor went operational on December 2, 1942, in Chicago. Since then, three generations of nuclear reactors can be distinctively identified, with the fourth generation emerging at the onset of the 21st-century energy technology developments (U.S. DOE, 2003; Weaver, 2005). These four consecutive generations of nuclear energy systems have significant historical impact on the nuclear power industry's efforts to innovate itself while remaining commercially viable and competitive in the US domestic energy markets and throughout the world (U.S. DOE, 2001):

- *Generation I* (1950−1970)—*experimental and prototype reactors*: The first power reactor generation was introduced during the period 1950−1970 and included early prototype reactors such as Shippingport, Dresden, and Fermi I in the United States.
- *Generation II* (1970−1990)—*large, central-station nuclear power reactors*: The second generation included commercial power reactors built during the period 1970−1990 such as the light water-cooled reactors (LWRs) with enriched uranium including the pressurized water reactor (PWR) and the boiling water reactor (BWR). In the United States, it includes 104 constructed nuclear power plants.
- *Generation III and III+* (1990−2030)—*evolutionary designs*: The third generation started being deployed in the 1990s and is composed of the advanced LWR, including the advanced boiling water reactor (ABWR), and the System 80+. These were primarily built in East Asia to meet that region's expanding electricity needs. New designs that are being deployed include the Westinghouse Advanced Passive AP1000 and GE economic simplified boiling water reactor (ESBWR) in the United States. These are considered as evolutionary designs offering improved safety and economics.
- *Generation IV* (2030 and beyond)—*next-generation designs*: Although the current second- and third-generation nuclear power plant designs provide an economically, technically, and publicly acceptable electricity supply in many markets, further advances in nuclear energy system design can broaden the opportunities for the use of nuclear energy. The fourth generation of nuclear reactors is expected to start being deployed by 2030. The Generation IV

Handbook of Generation IV Nuclear Reactors. http://dx.doi.org/10.1016/B978-0-08-100149-3.00009-4
Copyright © 2016 Elsevier Ltd. All rights reserved.

reactors are designed with the following objectives in mind: economic competitiveness, enhanced safety and reliability, minimal radioactive waste generation, and proliferation resistance.

While gaining power operation experience in nuclear engineering ever since 1942 through Generation I−III+ systems and including emerging Generation IV systems, it was quickly established in early industrial efforts that nuclear reactions offer not only uniquely dense power sources but also a potential for sustainable power to meet energy demands far beyond the reaches of fossil fuels, including electricity and process heat applications from district heating to potable water production to large-scale industrial uses. The nuclear energy sustainability and security over fossil fuel alternatives together with its potential for minimized environmental impact are the unique nuclear industry traits.

Retrospectively, after the end of World War II, efforts to develop and deploy nuclear power plants began worldwide. Thus far, most operating and currently under-construction power plants are with LWRs. PWRs lead the industry whereas BWRs are not far behind. This technological reality of Generation I−III+ systems dates back to early decisions related to naval propulsion applications of nuclear energy as well as water's economical characteristics as the cheap and universally abundant reactor coolant (Weaver, 2005).

The LWR technology is well understood, matured, and optimized for traditional and novel applications. Much work has been done around the world to improve the existing reactor designs (Weaver, 2005). The safety demands of LWRs led to elaborate and extensive engineered safety features in Generation II−III+ reactors. The key historical technology limitations of LWRs are (1) significant system complexity emanating from naval origins and affecting performance and reliability, (2) limited operating temperatures subsequently restricting the attainable balance of plant energy conversion efficiencies, and (3) safety characteristics of LWR cores limiting core internal survivability in accident scenarios with accident-impeded or without built-in engineered safety features, especially in loss-of-coolant accidents.

Although existing designs, which are denoted as Generation II and III, provide a reliable, economical, and publicly acceptable supply of electricity in many markets, further advances in nuclear energy system design can broaden the opportunities for the use of nuclear energy. Other coolant types have been explored, resulting in nuclear power plants with heavy water reactors, gas reactors, and liquid metal reactors. Recognizing the advantages of non-light-water systems, it is also apparent that light water early deployment and its economics determined its leading use in contemporary nuclear reactors. The large base of experience with the current nuclear plants has been used to guide development of the new Generation IV designs to contemporary readiness-for-deployment levels. Common goals are simplification, larger margins to limit system challenges, longer grace periods for response to emergency situations, high availability, competitive economics, and compliance with internationally recognized safety objectives.

Table 9.1 summarizes the contemporary reactor technologies of accepted use and relevance to Generation IV systems and beyond. Typical LWR design traits such as

Table 9.1 Contemporary nuclear power technologies

Reactor	Fuel	Core coolant	Core moderator	Turbine working fluid	Number of loops	Applications
LWR−PWR	UO_2, 3−5% ^{235}U	H_2O, 160 bars	H_2O, 160 bars	H_2O steam	2	Electricity, desalination
LWR−BWR	UO_2, 3−5% ^{235}U	H_2O, 70 bars	H_2O, 70 bars	H_2O steam	1	Electricity, desalination
CANDU	Natural uranium	D_2O, 90 bars	D_2O, 90 bars	H_2O steam	2	Electricity
HTR	UCO, 8−15% ^{235}U	He, 60 bars	Graphite	H_2O steam He	2 1	Electricity, process heat, waste management
LMFR	UO_2, UO_2-PuO_2, $(U,Pu)O_2$, UC, 10−20% fissile	Na, NaK, 5 bars	None	H_2O steam	2	Electricity, process heat, waste management

LWR, light water reactor; *PWR*, pressurized water reactor; *BWR*, boiling water reactor; *CANDU*, Canada deuterium uranium reactor; *HTR*, high-temperature reactor; *LMFR*, liquid metal fast reactor.

primary coolant doubling as a moderator, need for pressurization in PWRs to avoid bulk boiling, and enriched fuels to compensate for parasitic absorption are noted, recognizing their impact in the global nuclear technology evolution.

Moving from LWRs to high-temperature reactors (HTRs) and eventually to liquid metal fast reactors (LMFRs) progressively leads to lower pressures but potentially higher fissile content needs. Developments of HTRs and LMFRs are founded on decades of research and development (R&D) efforts in the United States and other countries since the 1950s, alongside development and successful commercialization of LWRs. Historically, the design development efforts have been driven by several major objectives, all of which target addressing and resolving the above-noted technology limitations of LWRs: (1) system design simplification trends, (2) implementation of modularity principles, (3) higher operating temperatures, and (4) (inherent) safety features. Combined, these developments enhance performance characteristics, facilitating competitiveness against other energy technologies. The development trends based on these objectives matured in the 1970s and continue to the present day (Weaver, 2005).

Enabling developments in materials and energy conversion technologies facilitate design efforts toward next generations of nuclear reactors. As nuclear engineering technologies mature, energy use efficiencies continuously increase. These studies allow benefit from the extensive operational experience of LWRs and adopting new technologies.

The US Department of Energy (DOE) has been working with the nuclear industry to establish a technical and regulatory foundation for the next generation of nuclear plants (U.S. DOE, 2003, 2001, 2002). The DOE Generation IV Initiative began in the early 2000s to facilitate developing technologies that achieve safety, performance, waste reduction, and proliferation resistance while serving as an energy option that is economically competitive and ready for deployment by 2030 (OECD NEA, 2002, 2005). The licensing process is being developed jointly with the US Nuclear Regulatory Commission (NRC) whereas proliferation resistance and physical protection are being developed and evaluated following the guidelines produced by the National Nuclear Security Administration. The initial technology roadmap was completed in 2002 for the program and subsequently updated in 2014 (U.S. DOE, 2002; OECD NEA, 2014a). The original roadmap was focused on selection methodology details and kickoff of R&D for the recommended most-promising systems. The analysis and recommendations have been deeply rooted in the 2000s-era nuclear renaissance expectations. The updated 2014 roadmap provides an overview of the original 2002 document, adds the evaluations of subsequent accomplishments of more than 10 years of R&D, and provides analyses of Generation IV systems accounting for the Fukushima Daiichi accident lessons and contemporary economics of the 2010s. Both documents discuss projected developments in the United States and throughout the world.

The Generation IV International Forum (GIF) was established in 2000 with its charter formalized in 2001 (OECD NEA, 2002). The original membership consisted of representatives from nine countries stemming from their participation in the US DOE-led intergovernmental group discussing international collaboration opportunities in nuclear energy technologies, later named as the GIF Policy Group. The nine founding

members, signatories to the original GIF Charter of 2001, are Argentina, Brazil, Canada, France, Japan, the Republic of Korea, the Republic of South Africa, the United Kingdom, and the United States. Switzerland signed the GIF Charter in 2002, Euratom in 2003, and the People's Republic of China and the Russian Federation signed in 2006, bringing the GIF membership to 13 countries.

The US DOE initiated the international program and plays the leading role in the GIF efforts whereas Argentina, Brazil, and the United Kingdom are nonactive members. The extended GIF Charter was signed by representatives from all 13 countries in 2011, reaffirming national interests in collaborative efforts toward Generation IV systems (OECD NEA, 2005, 2011). In 2015, the GIF Framework Agreement was extended for another 10 years, facilitating continued collaborative efforts. The current list of implementing agents includes NRCan (Canada), Euratom, CEA (France), ANRE and JAEA (Japan), CAEA and MOST (China), MSIP and NRF (Korea), South Africa, Rosatom (Russia), PSI (Switzerland), and DOE (United States) (OECD NEA, 2014a).

The Generation IV nuclear energy systems comprise nuclear reactor technologies that could be deployed by the mid-21st century and present significant advancements in economics, safety and reliability, and sustainability over currently operating reactors. Described in the initial roadmap are six system concepts chosen by the US DOE's Nuclear Energy Research Advisory Committee and the GIF to be investigated:

- gas-cooled fast reactors (GFRs),
- very-high−temperature reactors (VHTRs),
- supercritical water-cooled reactors (SCWRs),
- sodium-cooled fast reactors (SFRs),
- lead-cooled fast reactors (LFRs), and
- molten salt reactor (MSRs).

The GIF nations trust that development of these six concepts leads to a range of long-term benefits in the United States and worldwide. The US DOE supports domestic nuclear energy community interests in exploring and developing SFRs and VHTRs via signing formal GIF System Arrangement Documents for these designs (OECD NEA, 2014a). In addition, the US nuclear energy community participates in collaborative efforts toward developing various concepts of LFRs and MSRs. The base line enabling technologies to achieving high-performance characteristics are also accounted for and supported by the forum member's national R&D programs. These developments include novel system concepts and energy architectures, new materials, designs for online maintenance, and technological solutions needed to shorten outages.

Many related current efforts, such as improvements in man−machine interfaces using computers and information visualization systems and operator licensing program tools including simulator training exercises that have been applied at current plants, will ultimately contribute to the high performance of future nuclear power plants. In particular, taking advantage of these technological advances, the new designs also assume plant lifetimes beyond 60 years (Weaver, 2005).

Table 9.2 summarizes the principal design characteristics thought-after and represented by the identified six Generation IV design concepts (U.S. DOE, 2002;

Table 9.2 Generation IV nuclear power technologies

Reactor	Neutron spectrum	Core coolant	Maximum achievable temperature (°C)	Envisioned fuel cycle	Power rating (MW_{el})	Applications
LWR−SCWR	Thermal/fast	H_2O	510−625	Open/closed	300−1500	Electricity, process heat
HTR−VHTR	Thermal	He	650−1000	Open/closed	250−300	Electricity, H_2, process heat, waste management
LMFR−SFR	Fast	Na	550	Closed	30−2000	Electricity, process heat, waste management
LMFR−GFR	Fast	He	850	Closed	1200	Electricity, H_2, process heat, waste management
LMFR−LFR	Fast	Pb	800	Closed	20−1000	Electricity, H_2, process heat, waste management
MSR	Thermal/fast	Fluoride salts	700−800	Closed	1000	Electricity, H_2, process heat, waste management

LWR, light water reactor; *HTR*, high-temperature reactor; *LMFR*, liquid metal fast reactor; *SCWR*, supercritical water cooled reactor; *VHTR*, very-high−temperature reactor; *SFR*, sodium-cooled fast reactor; *GFR*, gas fast reactor; *LFR*, lead-cooled fast reactor; *MSR*, molten salt reactor.

OECD NEA, 2009). Of note, only one of these systems uses light water as a coolant to achieve its performance characteristics while being potentially either a thermal or fast spectrum system.

As already indicated, decades of technology development efforts for some of these systems serve as a foundation for early commercial deployment perspectives, within the next decade or so, assuming viable marketing-consumer cases can be established on a competitive basis against alternative energy technologies targeting 2030–2100. International collaborations within the GIF framework are expected to facilitate early marketing and deployment opportunities.

Generation IV advanced reactors are expected to be the result of international collaborative efforts bringing novel technologies to energy markets and customizing them according to local conditions. The universal objectives are for these systems to be sustainable, safe, reliable, economically competitive, and proliferation resistant and secure (Yang, 2014).

9.2 Energy market in the United States and the potential role of Generation IV systems: electricity, process heat, and waste management

Nuclear power has had a substantial role in the supply of electricity in the United States for more than 3 decades, reaching contributions of nearly 20% of the domestic electricity generation (U.S. DOE, 2003; Yang, 2014). There are several types of nuclear-driven power units meeting a range of applied needs and forming an overall domestic nuclear energy system market. In addition to the nuclear power plant reactors, there are several hundreds of PWRs for naval propulsion and hundreds of research and special purpose reactors of various types. The domestic energy demand projections within the major industrial sectors, including electricity and other energy products, coupled with environmental and sustainability considerations, suggest an increasing role for nuclear energy by the end of this century (U.S. DOE, 2003, 2002; OECD NEA, 2014a, 2009).

To take full advantage of fission energy, the need for greater energy efficiency is becoming an increasingly important component in development efforts toward sustainable energy resources. Cogeneration systems, producing heat and electricity, offer a solution for optimization of nuclear energy usage and increased energy security. Nuclear power plants represent a viable energy source for cogeneration options.

Currently operating nuclear power plants discard thermal energy into a heat sink at temperatures of approximately 280°C. Heat at these temperatures is suitable for desalination plants and various other process heat applications. Future VHTRs offer much higher temperatures and energy conversion efficiencies that would allow electricity generation, potable water production, and hydrogen production in a single multipurpose cogeneration system.

The coupling of a nuclear energy system with a cogeneration facility creates unique challenges as well as unique opportunities for competitive performance characteristics

(OECD NEA, 2014a). The nuclear energy source determines the maximum energy production rate for all of the coupled energy systems driven by the reactor. Following traditional Generation II−III+ operation strategies, a continuous operation mode might also be implemented as a preferable mode for next-generation nuclear reactors. Assuming the continuous operation scenarios, the interface between the various product streams will need to be dynamically managed in such a way that reactor availability to the energy grid (the key continuous operation trait) is not challenged. If electricity generation is primary and chemical processing is secondary, then the "product shifting" protocol must be responsive to the needs of the electrical grid. High-demand periods could force the chemical plants into standby mode whereas low-demand periods could see increased chemical production. If chemical processing is primary and electricity generation is secondary, then electricity would only be sold as a commodity when demand and availability coincide. These protocols could be combined dynamically to meet greed fluctuations in a novel on-demand operation mode whereas reactors would be left to operate as desired from the reactor side—in base load or load-following modes. The direct-cycle high-efficiency Generation IV VHTRs have a unique potential to offer both high-temperature process heat and electricity in an operation scenario with very high energy conversion efficiencies of modern Brayton cycles. The direct-cycle nature of the plants allows for a load-following mode with dynamic responses to energy grid fluctuations.

Because there are existing market penetration challenges for any novel energy technology, Generation IV reactors will have significant uncertainties in their ability to capture sizable energy market shares. There are significant impediments that may prevent rapid or even accelerated deployment of near-term construction-ready Generation IV systems. Natural gas price fluctuations have the potential to significantly slow down or even completely stop deployment efforts of novel nuclear technologies and lead to shutdowns of existing Generation II LWR-based plants purely based on economic considerations.

The absence of significant observable near-term focus on nuclear energy technologies in domestic energy policy considerations and predominantly decentralized market demand−driven energy grid architectures in the United States may lead to slower novel nuclear energy system deployments and increasing numbers of Generation II LWR-based plants to be decommissioned by the end of this century. The utility companies and high-energy-demand industries are expected to be naturally reluctant to become early adopters of experimental energy systems despite their actual characteristics resorting to well-known energy solutions as long as alternatives to nuclear remain available to meet energy needs.

Introduction of Generation IV systems to the US energy markets is naturally expected to be slower and more sporadic compared with developments observed in other countries, with Russia and China the most significant examples (Weaver, 2005). Generation IV technologies are being advanced there with significant federal support driven by anticipated energy needs, climate and environmental considerations, anticipated resource shortages, and the expected resulting economic demand for nuclear energy in the long term. Domestic US energy markets are driven by near-term phenomena, and nuclear technologies are not expected to see rapid market penetrations

under existing conditions. Approximately 54 GW_e of the domestic US nuclear capacity is in regulated markets whereas 45 GW_e is in deregulated markets driven by short-term competitive power sales. Early adoptions of Generation IV technologies, including those originating in the United States, will likely occur abroad and then Generation IV designs will be returning to the United States in a longer term as market conditions and licensing support deployments evolve. Emerging environmental standards and regulations are beginning to recognize the role of nuclear power as a clean energy source (OECD NEA, 2014a; Yang, 2014).

These changes will ultimately facilitate deployments of Generation IV reactors as sustainable, environmentally responsible energy sources that are clean and immune to environmental changes because of uses of non-light−water-based power cycles. It is expected that efficient electricity generation, process heat production, and waste management capabilities will be the key features of Generation IV reactors, offering opportunities and advantages for successful energy market penetrations accounting for decentralized and centralized market conditions (U.S. DOE, 2003).

9.3 Electrical grid integration of Generation IV nuclear energy systems in the United States

The US energy system is very complex. It is actually represented by not a single electrical grid but a complex architecture of state and local grids that are loosely interconnected to meet the energy needs of its customers, both in electricity demands and in process heat applications (U.S. DOE, 2003; Nordhaus et al., 2013; Massachusetts Institute of Technology, 2011).

The average capacity factors of US nuclear power plants have increased from approximately 60% attainable in the 1960s and 1970s to more than 90% attainable in the 2000s. The reliability levels of base-load contributions to the domestic electrical grid have been steadily increasing over the same period as demonstrated through substantial reductions in operating and maintenance expenses as well as reductions in personnel radiation exposure levels at the Generation II−III nuclear power plants (Nordhaus et al., 2013; Massachusetts Institute of Technology, 2011).

Although Generation II and III nuclear power plants have been operating more and more efficiently in recent years, reliably contributing base-load capacity, the US electrical grid has been getting more and more dated, requiring significant upgrades in its infrastructure. The challenges are further complicated by existing uncertainties in planning, predictions of future energy needs, forms, and infrastructure demand forecasts, from integration of renewable sources to electrical vehicles to environmentally responsible sustainable energy ecosystems to simply managing large power consumers and individual households. A range of new technologies, from smart meters to smart grids to smart houses, is already available and is expected to become available in the near future to replace aging systems and meet the energy needs by offering dynamic architectures supporting adaptable “smart” energy solutions for all customers (Araujo, 2014; Massachusetts Institute of Technology, 2011).

Emerging novel power units with Generation IV reactors must be adaptable to energy grid architectures in their ability to meet load demands faster than traditional Generation II and III power plants characterized by slow ramp rates, meeting the competitor's challenges of load changes on minutes-hours scales (Nordhaus et al., 2013; INL, 2014). Fortunately, direct-cycle power units with Generation IV reactors and so-called hybrid systems combining advanced reactors and renewable energy sources offer desired dynamic capabilities to meet load requests on-demand, operating either in a traditional load-following mode or in a dynamic mode (INL, 2014).

Hybrid systems integrate nuclear reactors, renewable sources, energy storage/recovery buffer systems, and dynamic interfaces with electrical grids (INL, 2014). Significant flexibilities in potential architectures are available and are being explored for applications in Generation IV technology deployment scenarios (OECD NEA, 2014a; INL, 2014). Flexible power ratings of Generation IV reactors, as shown in Table 9.2, facilitate the grid integration capabilities of these systems (Nordhaus et al., 2013; INL, 2014).

9.4 Industry and utilities interests in Generation IV nuclear energy systems in the United States

The US domestic nuclear industry is in the process of transforming itself toward a much more consolidated modern enterprise. The changes are driven by deregulation and economic considerations. In 1991, 101 individual utilities had ownership interests in operating nuclear power plants. In 1999 the number reduced to 87, dominated by the top 12 owning 54% of the capacity. Today the top 10 utility companies own in excess of 70% of the total domestic nuclear capacity. These changes amount to a significant consolidation of technological resources and operational expertise.

The domestic consolidated nuclear enterprise is founded on Generation II technologies supporting LWRs. There is a systemic effort driven by reactor vendors (ie, General Electric and Westinghouse) to commercialize and deploy Generation III and III+ LWRs abroad and then bring them back and introduce them into the domestic energy markets.

Although the current domestic nuclear fleet consists of Generation II and Generation III LWRs with efforts currently in progress to deploy Generation III+ LWRs, reactor vendors, plant operators, and utility companies do express their interest in novel nuclear technologies ranging from light-water-based small modular reactors to advanced reactors using gas and liquid metals. They do recognize the need for further R&D and express their expectation for federal programs targeting novel technologies.

Table 9.3 summarizes domestic commercial interests in Generation IV reactors (U.S. DOE, 2003; OECD NEA, 2014a; Yang, 2014; Nordhaus et al., 2013). The financial interests of utility companies in advanced reactors beyond Generation III+ are only sporadic and need strong marketing campaigns to secure actual buy-ins. The domestic fast reactors are envisioned to serve as advanced burner reactors in waste management scenarios or as breed-and-burn sustainable systems (Nordhaus et al., 2013).

Table 9.3 Commercial development interests in Generation IV technologies

Reactor	Reference reactor	Project	National laboratory	Industry
HTR−VHTR	GT-MHR	NGNP	INL	General Atomics, Areva, Westinghouse
LMFR−SFR	PRISM	Advanced Reactor R&D	ANL	GE
MSR	MSR AHTR	MSR FHR	ORNL ORNL	Transatomic Power, Teledyne –

AHTR, advanced high-temperature reactor; *FHR*, fluoride-cooled high-temperature reactor; *HTR*, high-temperature reactor; *VHTR*, very-high−temperature reactor; *LMFR*, liquid metal fast reactor; *SFR*, sodium-cooled fast reactor; *MSR*, molten salt reactor; *GT-MHR*, gas turbine modular helium-cooled reactor; *NGNP*, next-generation nuclear plant; *INL*, idaho national laboratory; *ANL*, argonne national laboratory; *ORNL*, oak ridge national laboratory.

The domestic VHTR is being marketed as a system for process heat applications. The MSRs are being developed as liquid-fuel systems or as reactors cooled with fluoride salt (Forsberg et al., 2011). Over the years each advanced reactor concept attracted federal and industrial interests, facilitating further R&D activities.

The commercial viability cases are expected to be realized for VHTRs by 2050, accounting for growing needs for high temperatures and potable water and then for fast reactors by 2100, accounting for waste management and sustainability demands. The MSR deployment scenarios as fluoride-cooled high-temperature reactors have similarities to VHTRs in the near term (Forsberg et al., 2011).

The longer term goal is to deploy a liquid-fuel system that is expected to have advantages beyond conventional fast reactors with solid fuels (Nordhaus et al., 2013). Although system-level domestic R&D efforts are focused on VHTRs, SFRs, and MSRs, the materials' R&D supports all six Generation IV concepts (Yang, 2014; Nordhaus et al., 2013).

9.5 Deployment perspectives for Generation IV systems in the United States and deployment schedule

Domestic nuclear power plant owners have been applying to the NRC for their license extensions since the 1990s, and many obtained approvals to operate for an additional 10−20 years or more beyond their original plant lifetimes. This trend extends LWRs and naturally delays deployment of Generation IV units. Construction of new units with LWRs will further delay the need for Generation IV units. However, the clearly emerging opposing trend is also present. Some of the domestic utilities are supportive of novel Generation IV systems and related R&D, but they do consider and may

decommission nuclear power plants with Generation II LWRs because of economic considerations (Weaver, 2005).

In the early 2000s, the US DOE engaged the nuclear industry in a joint effort to establish a technical and regulatory foundation for the next generation of nuclear plants. The DOE Generation IV program (Gen IV) produced a 30-year roadmap of R&D efforts toward advanced nuclear power plant and fuel cycle options (U.S. DOE, 2001, 2002; OECD NEA, 2014a, 2009). The roadmap underwent several revisions and has been most recently updated in 2014 to include and address new technical issues and modifications, to reevaluate the original six concepts versus any potentially emerged new concepts meeting Generation IV criteria, to incorporate the Fukushima Daiichi accident lessons for Generation IV systems, and to include the 10-year technology demonstration horizon needs (U.S. DOE, 2002, 2005, 2012; OECD NEA, 2014a, 2009).

To complement Gen IV, DOE also organized a Near-Term Deployment Group (NTDG) to examine prospects for the deployment of new nuclear plants in the United States and to identify obstacles to deployment and actions for resolution. The group commenced its work in February 2001 and evaluated a wide spectrum of factors that could affect prospects for near-term deployment of new nuclear plants. The readiness and technical suitability of various new plant designs were assessed considering these designs as candidates for near-term deployment as Generation III+.

In recent years the DOE advanced reactor programs have been evaluated to ensure that the R&D efforts are in line with existing and expected licensing processes (U.S. NRC, 2003, 2012; DOE Nuclear Energy Research and Development Program, 2007). The established DOE Nuclear Energy Technical Review Panel (TRP) gathered input from the nuclear industry and conducted evaluations of the eight reactor concepts ranging from Generation III+ LWRs to Generation IV systems: General Atomics Energy Multiplier Module (GFR), Gen4 Energy Reactor Concept (Pb-Bi fast reactor), Westinghouse Thorium-fueled Advanced Recycling Fast Reactor for Transuranics Minimization (SFR), Westinghouse Thorium-fueled Reduced Moderation BWR for Transuranic Minimization, Flibe Energy-Liquid Fluoride Thorium Reactor (MSR), Hybrid Nuclear Advanced Reactor Concept, GE-Hitachi Nuclear Energy PRISM and Advanced Recycling Center (SFR), and Toshiba 4S Reactor (SFR) (U.S. DOE, 2012). The reactor concepts ranged from small modulator reactors to large power reactors. The TRP objective was to establish federal prioritization horizons based on the established state-of-the-art and industry interests.

Through the US DOE, in April 2001 the NTDG issued a Request for Information (RFI) seeking input from the nuclear industry and the public on nuclear plant designs that could be deployed in the near term. The eight reactor design candidates were identified by international reactor suppliers in response to the RFI as near-term deployable in the United States: ABWRs, PWRs, and HTRs. Table 9.4 summarizes the general characteristics of these designs including interested industry suppliers as well as the current status of the projects (U.S. DOE, 2002; OECD NEA, 2014a).

Two of the six original Generation IV systems, ESKOM pebble bed modular reactor (PBMR) and the General Atomics gas turbine modular helium-cooled reactor (GT-MHR), come close to meet Generation IV reactor classification requirements

Table 9.4 Near-term deployable nuclear plant designs in the United States

Reactor design and R&D project	Supplier	General features	Status	
			In 2001	In 2015
ABWR	GE	1350 MW_{el} BWR	Certified in 1997 by NRC	Constructed in Japan
SWR1000	Framatome ANP (now Areva)	1013 MW_{el} BWR	Design stage	Design stage
ESBWR	GE	1380−1594 MW_{el} passively safe BWR	Under development	Certified in 2014 by NRC; industry interest for construction at North Anna by Dominion Virginia power
AP600	Westinghouse	610 MW_{el} passively safe PWR	Certified in 1999 by NRC	No orders
AP1000	Westinghouse	1090 MW_{el} passively safe PWR. This is a higher power version of AP600.	Under development	Certified in 2005 by NRC. Under construction in China and the United States; orders in other countries
IRIS	International consortium led by Westinghouse	100−300 MW_{el} integral primary system PWR	Under development	Under development; not ready for deployment
PBMR	ESKOM initially, PBMR Ltd., consortium including Westinghouse (ended by 2010)	110 MW_{el} modular direct-cycle helium-cooled pebble bed reactor	Under development	Under development; Westinghouse withdrew in 2010; not ready for deployment in the United States. Prototypes are in operation in China
GT-MHR	General Atomics initially, international group includes OKBM Africanov, Areva, Fuji	288 MW_{el} modular direct-cycle helium-cooled reactor, developed in the late 1980s and during the 1990s.	Under development	Under development; not ready for deployment in the United States. Prototype is in operation in Japan

ABWR, advanced boiling water reactor; *NRC*, US Nuclear Regulatory Commission; *BWR*, boiling water reactor; *PWR*, pressurized water reactor; *GT-MHR*, gas turbine modular helium-cooled reactor; *PBMR*, pebble bed modular reactor.

although being conceived and developed in the 1980s and 1990s. The PBMR system, as developed in South Africa, is no longer planned for construction. However, China has been actively developing the technology and is currently operating prototypes that may affect perspectives for this concept deployment in the United States. The GT-MHR evolved into the next-generation nuclear plant developed up to the conceptual design level by Idaho National Laboratory (INL). Japan has successfully been operating the prototype system for nearly 20 years. Although prospects of deploying fast reactors in the US energy markets are remote in the near future, the domestic R&D efforts continue and the relevant technology prototypes are in operation and under construction in China, India, and Russia (Nordhaus et al., 2013; U.S. DOE, 2012).

The original NTDG assessed each candidate design, including the design-specific gaps to near-term deployment, based on information provided by the respondents. From these evaluations the NTDG formed judgments regarding each candidate's potential for near-term deployment (Weaver, 2005). As illustrated in Table 9.4, the most advanced designs evaluated in 2001 by the NTDG as suitable for near-term deployment were still under development in 2015 and are not ready for deployment, although interests in design remain among industrial partners (U.S. DOE, 2001, 2002; OECD NEA, 2014a).

The 2014 roadmap update incorporates the lessons learned from the Fukushima Daiichi accident. It has been recognized that nonwater coolants of Generation IV systems offer advantages over LWRs but require further evaluations. The impact of higher operating temperatures and power densities in Generation IV systems need to be assessed from the point of view of reliable heat removal options under extreme natural and manmade accident conditions (OECD NEA, 2014a). The Generation IV systems designed for process heat applications assume co-location or integration of power, fuel cycle, and process heat facilities. Accident responses of such configurations need to be evaluated.

The 2002 version of the roadmap identifies GE ABWR and ESBWR, Westinghouse AP1000, GT-MHR, Eskom PBMR, and Areva SWR-1000 as near-term deployable in the US energy markets (U.S. DOE, 2002). The 2014 updated roadmap reevaluates the recommended six Generation IV systems and extends demonstration expectation horizons to 2030 versus original 2025. Furthermore, MSRs and GFRs are no longer expected to reach the demonstration phase within the roadmap projected time range.

The overall system development timelines are revised for all six systems to reflect up-to-date accomplishments and changes in priorities (OECD NEA, 2014a). The updated roadmap and recent GIF reports recognize that Generation IV systems are likely to be deployed globally first and then introduced into the US energy markets (OECD NEA, 2014b, 2014c).

9.6 Conclusions

Nuclear power plants emit no greenhouse gases and offer an opportunity to develop into a sustainable energy solution. This is of global importance for the US energy industry to meet international climate management commitments. Generation IV

reactors are of significant design development interest to the US nuclear engineering community for their superior design characteristics versus LWRs. The US NRC and domestic energy markets are getting ready to handle the licensing requests and novel system economics and operation of advanced nuclear reactors. It is recognized by the domestic nuclear industry that early Generation IV deployments will require significant financial resources. The US DOE Office of Nuclear Energy has been supporting the Generation IV R&D needs since the inception of the program mitigating risk factors and facilitating the commercial success of anticipated deployments. Development efforts and energy economics are expected to converge after 2030 and yield favorable domestic conditions for Generation IV reactors. At that time, it is expected to see global deployments of Generation IV systems supporting domestic licensing and marketing efforts.

Abbreviations

ABR	Advanced Burner Reactor
AHTR	Advanced high temperature Reactor
ALWR	Advanced light water Reactor
ANRE	Agency for Natural Resources and Energy, Japan
ARC	Advanced Reactor concepts
CAEA	China Atomic Energy Authority, People's Republic of China
DOE NE	DOE office of nuclear energy
FHR	Fluoride-cooled high-temperature reactor
GFR	Gas-cooled fast reactor
GT-MHR	Gas turbine modular helium-cooled reactor
HTR	High-temperature reactor
IRIS	International Reactor Innovative and Secure
JRC	European Commission's Joint Research Center, Euratom
LOCA	Loss-of-coolant accident
MOST	Ministry of Science and Technology, People's Republic of China
MSIP	Ministry of Science, ICT and Future Planning Technology, Republic of Korea
NNSA	The national nuclear security Administration
NRCan	Department of Natural Resources, Canada
NRF	National Research Foundation, Republic of Korea
NTDG	Near-Term Deployment Group
PSI	Paul Scherrer Institute, Switzerland

Continued

RFI	Request for Information
Rosatom	State Atomic Energy Corporation, Russian Federation
SWR1000	Siedewasser Reactor-1000
TRP	Technical Review Panel
VHTR	Very-high−temperature reactor

References

Araujo, K., 2014. The emerging field of energy transitions: progress, challenges, and opportunities. Energy Research and Social Science 112−121. Elsevier.

DOE Nuclear Energy Research and Development Program, 2007. Review of DOE Nuclear Energy Research and Development Program. Committee on Review of DOE Nuclear Energy Research and Development Program. Board on Energy and Environmental Systems, Division on Engineering and Physical Sciences, National Research Council of the National Academies, The National Academies Press, Washington, DC.

Forsberg, C., Hu, L., Peterson, P., Allen, T., 2011. Fluoride-Salt-Cooled High Temperature Reactors for Power and Process Heat. Integrated Research Project. U.S. DOE.

INL, 2014. Integrated Nuclear-Renewable Energy Systems Development. INL/MIS-14−32387, INL.

Massachusetts Institute of Technology, 2011. The Future of the Electric Grid. An Interdisciplinary MIT Study. Massachusetts Institute of Technology, ISBN 978-0-9828008-6-7.

Nordhaus, T., Lovering, J., Shellenberer, M., 2013. How to Make Nuclear Cheap. Breakthrough Institute.

OECD NEA, 2014a. Generation IV Program Implementing Agents List. OECD Nuclear Energy Agency for the Generation IV International Forum.

OECD NEA, 2014b. Technology Roadmap Update for Generation IV Nuclear Energy Systems. GENIV International Forum, January 2014. OECD Nuclear Energy Agency for the Generation IV International Forum.

OECD NEA, 2014c. Generation IV International Forum Annual Report. OECD Nuclear Energy Agency for the Generation IV International Forum.

OECD NEA, 2011. Extended Charter of the Generation IV International Forum. OECD NEA.

OECD NEA, 2009. GIF R&D Outlook for Generation IV Nuclear Energy Systems. OECD Nuclear Energy Agency for the Generation IV International Forum.

OECD NEA, 2005. Framework Agreement for International Collaboration on Research and Development of Generation IV Nuclear Energy Systems. OECD NEA.

OECD NEA, 2002. Charter of the Generation IV International Forum. OECD NEA.

U.S. DOE, 2012. Advanced Reactor Concepts. Technical Review Panel Report, Evaluation and Identification of Future R&D on eight Advanced Reactor Concepts, December 2012. U.S. DOE Office of Nuclear Energy.

U.S. DOE, 2005. Generation IV Nuclear Energy Systems Ten-Year Program Plan. Fiscal Year 2005 Report. Generation IV Nuclear Energy Systems, Office of Advanced Nuclear Research, U.S. DOE Office of Nuclear Energy, Science and Technology.

U.S. DOE, 2003. The U.S. Generation IV Implementation Strategy. U.S. DOE Office of Nuclear Energy, Science and Technology. September.

U.S. DOE, 2002. A Technology Roadmap for Generation IV Nuclear Energy Systems. U.S. DOE Nuclear Energy Research Advisory Committee and the Generation IV International Forum. U.S. DOE.

U.S. DOE, 2001. A Roadmap to Deploy New Nuclear Power Plants in the United States by 2010. Volumes I and II, Nuclear Energy Research Advisory Committee, Subcommittee on Generation IV Technology Planning. U.S. DOE Office of Nuclear Energy, Science and Technology.

U.S. NRC, 2003. Proposed Plan for Advanced Reactor Research. Office of Nuclear Regulatory Research, U.S. Nuclear Regulatory Commission.

U.S. NRC, 2012. Report to Congress: Advanced Reactor Licensing. U.S. NRC. August.

Weaver, K., 2005. Future nuclear energy systems: generation IV. In: 50th Annual Meeting of the Health Physics Society, July 11, 2005, Spokane, Washington, USA.

Yang, W.S., 2014. Advances in reactor concepts: generation IV reactors. In: Research Workshop on Future Opportunities in Nuclear Power, October 16−17, 2014. Purdue University.

Euratom research and training program in Generation-IV systems: breakthrough technologies to improve sustainability, safety and reliability, socioeconomics, and proliferation resistance

10

G. Van Goethem
European Commission, DG Research and Innovation, Energy - Euratom - Fission

10.1 Background: Euratom (nuclear fission research and training) within the Energy Union (European Union energy mix policy)

The European Union (EU, 28 Member States, combined population of more than 500 million inhabitants) is a major player in the world of nuclear fission. In 2014 there were 131 nuclear power reactors in operation in 14 Member States (including 18 Russian-designed VVER units in five states), with a total capacity of 120 GW_e net and a gross electricity generation of 833 TWh (ie, 27% of gross electricity production in the EU). The average age is close to 30 years. New build projects are envisaged in 10 Member States, with four reactors already under construction in Finland, France, and Slovakia. Other projects in Finland, Hungary, and the United Kingdom are under licensing process, while projects in other Member States (Bulgaria, the Czech Republic, Lithuania, Poland, and Romania) are at a preparatory stage.

Research, innovation, and education are at the heart of the European Atomic Energy Community (Euratom) Treaty[1] (Rome, 1957), dedicated to peaceful and sustainable applications of nuclear fission. Article 4.1 of the Euratom Treaty indeed mentions explicitly **research** and **training** (R&T) as a twofold objective: "The EC is in charge of promoting and facilitating nuclear research activities in the Member States and to complement them through a Community **Research** and **Training** programme."

[1] Consolidated version of the *Treaty establishing the European Atomic Energy Community* (Euratom) OJ C 327, 26.10.2012: http://eur-lex.europa.eu/legal-content/EN/TXT/?uri=CELEX:12012A/TXT (in general, summaries of EU Legislation: http://eur-lex.europa.eu/browse/summaries.html).

Handbook of Generation IV Nuclear Reactors. http://dx.doi.org/10.1016/B978-0-08-100149-3.00010-0
Copyright © 2016 Elsevier Ltd. All rights reserved.

Euratom **research** projects in the EU (in the past decades and, in particular under the current Horizon-2020 Research and Innovation Program) are implemented in three different ways:

1. Indirect actions performed and cofunded by private and public research organizations in the EU Member States concerned with nuclear energy, in the form of collaborative projects cofunded and monitored by the European Commission (EC) Directorate General (DG) Research and Innovation (RTD), Brussels (calls for proposals, information, and final reports of indirect actions initiated under FP7/2007−13/ are posted in the CORDIS website[2]).
2. Direct actions performed and funded by the institutional laboratories of the EC (ie, DG JRC/ Joint Research Centre/[3]) dedicated to Euratom issues, namely the Institute for Transuranium Elements in Karlsruhe (Germany), the Institute for Energy and Transport spread over Petten (The Netherlands) and Ispra (Italy), the Institute for Reference Materials and Measurements in Geel (Belgium).
3. National research and innovation programs in the EU Member States dedicated to nuclear fission and radiation protection (with or without Euratom cofunding, pending on national nuclear research and technological development policies).

As far as implementation of Euratom training projects is concerned, several Euratom Fission Training Schemes (EFTS) are funded through indirect actions, focusing on lifelong learning and borderless mobility. The concept of "learning outcomes" related to knowledge (ie, understanding), skills (ie, how to do), and *competence* (ie, how to be), or KSC is at the heart of the EFTS. This approach is aligned with the general EU policy in education and culture, ie, the "Bologna 1999" process for mutual recognition of academic grades and the "Copenhagen 2002" process for continuous professional development across the EU Member States. It is no surprise that the format adopted by the International Atomic Energy Agency (IAEA) training programs is based on a concept very close to the KSC approach. Following the IAEA definition (Safety Standard Series, 2001),[4] competence means the ability to apply knowledge, skills and attitudes so as to perform a job in an effective and efficient manner and to an established standard.

Of particular interest in the specific domain of education and training in Generation-IV systems is the Tentative training scheme for the development and pre-conceptual design of Generation-IV nuclear reactors proposed by SCK-CEN (Mol, Belgium) and AREVA GmbH (Offenbach, Germany) under the Euratom FP7 project ENEN-III (2009−12). The learning outcomes related to knowledge, skills, and attitudes in this training scheme (as discussed with relevant employers and training organizations) are provided in Appendix.

Originally, in the late 1950's, the Euratom Treaty proposed nuclear power plants (NPPs) as part of the solution to the energy crisis in Western Europe. It should be noted

[2] EC DG Research and Innovation/Euratom: http://ec.europa.eu/research/energy/euratom/index_en.cfm FP7 CORDIS: *Community R&D Information Service*: http://cordis.europa.eu/fp7/euratom/home_en.html.

[3] EC DG JRC—the European Commission's in-house science service (science hub): https://ec.europa.eu/jrc/.

[4] *Building competence in radiation protection and the safe use of radiation sources* (jointly sponsored by IAEA, ILO, PAHO, WHO), IAEA 2001—http://www-ns.iaea.org/standards/documents/pubdoc-list.asp.

that, already at that time, security of the energy supply was a concern (eg, oil crisis due to the closure of the Suez Canal in 1956). Severe accidents with many casualties in the fossil energy sector (in particular, in coal mines) were also a concern. Similar concerns today still exist in the energy sector not only in the EU, but worldwide. Today's energy policies are facing even bigger challenges, because of two new socioeconomic requirements:

1. Decarbonization of the global economy (connected to climate change concerns), and
2. Easy access to affordable energy for all (connected to global population growth).

Of course, in the nuclear energy sector during the last 40 years, three severe accidents happened (Three Mile Island (TMI) in 1979 in the United States, Chernobyl in 1986 in the former Soviet Union, and Fukushima in 2011 in Japan). Lessons, however, were drawn worldwide, in particular in the EU, which organized the "stress tests"[5] in all European NPPs after the Fukushima Daiichi accident on March 11, 2011 (Great East Japan Earthquake, Tohoku's coastline, magnitude 9). These "stress tests" were defined by the EC as targeted reassessments of the safety margins of nuclear power plants and were developed by the European Nuclear Safety Regulators' Group. It should be noted that many non-EU countries also conducted comprehensive nuclear risk and safety assessments based on the EU "stress test" model. These include Switzerland and Ukraine (both of which fully participated in the EU "stress tests") as well as Armenia, Turkey, the Russian Federation, Taiwan, Japan, South Korea, South Africa, and Brazil who conducted similar tests.

Euratom works in synergy with its own institutional laboratories (ie, the DG JRC)[3] and with national programs in the EU Member States concerned with applications of nuclear fission and ionizing radiation. Euratom also works in association with international organizations dedicated to nuclear fission developments, such as the IAEA (Vienna) and the Organisation for Economic Co-operation and Development/Nuclear Energy Agency (OECD/NEA, Paris). Equally important is international collaboration with nuclear research laboratories outside of the EU frontiers (industrialized countries as well as emerging nuclear energy countries).

Fission technologies can be transmitted to the next generations only within the framework of a responsible strategy regarding waste management and/or recycling of fissile and fertile materials. In this context, Euratom research and training programs insist, in particular, on the implementation of geological disposal for spent fuel and high-level radioactive waste and/or on Generation-IV developments aiming at efficient resource utilization and waste minimization. The emphasis in this article is on Generation-IV research and development (R&D) in the EU. Safety improvements in Generation-II (eg, related to long-term operation) and in Generation-III (eg, related to severe accident management) are also addressed in Euratom R&T programs. Regarding radiation protection research, the emphasis of Euratom programs is on

[5] EC Communication COM(2012) 571, dated October 4, 2012—"EC Communication on the comprehensive risk and safety assessments ('stress tests') of nuclear power plants in the EU and related activities"—http://ec.europa.eu/energy/nuclear/safety/doc/com_2012_0571_en.pdf.

better quantification of risks at low dose and how they vary between individuals (of particular interest in radiodiagnosis and radiotherapy).

The focus on sustainability in Euratom programs goes together with a better governance structure in the decision-making process (ie, more openness, participation, accountability, effectiveness, and coherence). Special efforts are dedicated to the development of a common nuclear safety and radiation protection culture at the EU level based on the highest achievable standards (eg, focusing on sense of responsibility and on questioning the attitude of all staff members in nuclear installations). Also important is public information and engagement in energy policy issues, notably in connection with nuclear decision-making (nuclear energy is the energy that generates most emotion per MWh produced!). The above focus on "soft" issues is one of the lessons learned from conducting the previously mentioned "stress tests" in the 131 nuclear units in the EU.

Euratom research, innovation, and education programs bring together—within the so-called "European Technology Platforms"—the major stakeholder groups of nuclear fission and radiation protection, namely the following:

- research organizations (eg, from public and private sectors),
- systems suppliers (eg, nuclear vendors, engineering companies),
- energy providers (eg, electronuclear utilities and industrial heat suppliers),
- technical safety organizations (TSOs) associated with nuclear regulatory authorities,
- academia and higher education and training institutions dedicated to nuclear energy,
- civil society (eg, policy-makers and opinion leaders), interest groups, and NGOs.

These stakeholder groups are instrumental in the design of the Euratom strategy, especially, under the current EU Horizon-2020 program of research and innovation. They also foster the scientific community to participate in collaborative projects wherever appropriate (Euratom projects usually involve up to 10 organizations and have a duration of up to 4 years). It is clear that in this scientific collaboration the participating TSOs strictly keep their prescribed role, powers, and independence as a support to the national regulators in decision-making. Non-EU research organizations are usually welcome to join Euratom projects provided that their scientific contribution brings a clear added value to the project and that they pay the full costs of their participation.

Euratom is not isolated in the European energy policy.[6] Nuclear fission is part of the European energy mix, together with renewable and fossil energy sources (Article 194 of Lisbon Treaty, 2007). The EU energy strategy over the current decade is defined in the "EU Energy Roadmap 2050" (issued in 2011), which proposes five scenarios toward a low-carbon economy that are based on a balance of sustainable development, security of supply, and industrial competitiveness. Two messages are important for the European nuclear fission community at the Horizon 2050. Firstly, one of the five "decarbonization scenarios" is based on a 20% share of electricity generation by nuclear fission, which represents an equivalent capacity operating of 127 GW_{el}, to be

[6] EC DG (Directorate General) ENER programs related to nuclear safety; radioactive waste and spent fuel; radiation protection; decommissioning of nuclear facilities; safeguards to avoid misuse; security (physical protection): http://www.Euratom.org/ and http://ec.europa.eu/energy/en/topics/nuclear-energy.

compared to today's total nuclear generation of 122 GW_e. Secondly, the general conclusion for all "decarbonization scenarios" is that electricity will play a much greater role than now (almost doubling its share in final energy demand, from 21% today to 40% in 2050). Doubling the electricity consumption by 2050 is a big challenge: How to produce this electricity in a "secure/diverse, clean, and efficient" way, following the requirements of the 21st century?

More recently, another important step was made in the European energy policy when the EC adopted on January 13, 2015 the *European Fund for Strategic Investments* (EFSI),[7] which is at the very heart of the €315 billion investment offensive (over the period 2015−17) of EC president Jean-Claude Juncker (length of term in office 2014−19). The EFSI is aiming at mobilizing additional public and private investments in the real economy in areas including infrastructure, education, research, innovation, renewable energy, and energy efficiency. The EFSI should target projects that promote job creation, long-term growth, and competitiveness.

In February 2015, President Juncker presented the global EU energy strategy in the "Energy Union Package."[8] One of the objectives is *An Energy Union for Research, Innovation, and Competitiveness*. Here are two excerpts related to nuclear fission:

- "putting the EU at the forefront of … all innovative energy technologies …, including … **the world's safest nuclear generation**, is central to the aim of turning the Energy Union into a motor for growth, jobs and competitiveness."
- "The EU must ensure that … **it maintains technological leadership in the nuclear domain**, including through ITER, so as not to increase energy and technology dependence."

Not surprisingly, these statements from the "Energy Union Package" about nuclear safety and EU leadership are aligned with the most recent Euratom Directives (ie, legally binding legislation for Member States in the EU), which were driven by the lessons drawn from Fukushima. Most important in this context is the *revised 2014 Euratom Safety Directive*,[9] which introduces the following requirements for nuclear installations:

- a high-level "Nuclear Safety Objective for Nuclear Installations" avoiding radioactive releases (the most stringent safety goal in the world at the time being);
- instigation of topical peer reviews by competent regulatory authorities across Member States' borders every 6 years (focusing on safety issues);
- obligation to ensure transparency of regulatory decisions and operating practices, as well as obligation to foster public participation in the decision-making process;
- requirement for role, powers, and independence of national regulatory authorities in decision-making;

[7] EC priority—investment plan: http://ec.europa.eu/priorities/jobs-growth-investment/plan/index_en.htm.

[8] Energy union package/communication from the EC to the European Parliament, The Council, the European Economic and Social Committee, the Committee of the Regions and the European Investment bank, (COM(2015) 80, Brussels, 25.2.2015) *A Framework Strategy for a Resilient Energy Union with a Forward-Looking Climate Change Policy*—http://www.consilium.europa.eu/en/policies/energy-union/.

[9] Council Directive 2014/87/Euratom of July 8, 2014 amending Directive 2009/71/EURATOM establishing a community framework for the nuclear safety of nuclear installations—(L 219/42 Official Journal of the EU 25.7.2014)—Euratom legislation: http://ec.europa.eu/energy/nuclear/safety/safety_en.htm.

- establishment of a strong safety culture (several indicators are also provided);
- obligation to obtain, maintain, and further develop expertise and skills in nuclear safety, in particular, through a special effort on education and training.

Equally important in the context of the "the world's safest nuclear generation" is the 2013 Euratom "Basic Safety Standards" (BSS) Directive,[10] which provides the following:

- Better protection of workers and the public, also taking into account economic and societal factors, as well as better protection of patients (eg, radiodiagnosis and radiotherapy).
- Emergency preparedness and response ("Emergency exposure situations" in Articles 97–99)—in the EU Member States there are variations in the levels of dose at which specified actions are required (evacuation, sheltering, iodate tablets).
- Obligations to ensure transparency (communication with undertakings and individuals).

10.2 Generation-I, -II, -III, and -IV of nuclear fission reactors: research, development, and continuous improvement for more than five decades

Several generations of nuclear fission reactors are commonly distinguished (Generation-I, -II, -III, and -IV).

- *Generation-I (Gen-I)* reactors were developed in the 1950–60s, and none are still running today. Gen-I refers to the prototype and power reactors that launched civil nuclear power using natural uranium. This kind of reactor typically ran at power levels that were "proof of concept."
- *Generation-II (Gen-II)* refers to a class of commercial reactors designed to be economical and reliable, following the model of the present US and French fleets, using enriched uranium. Gen-II systems began operation in the late 1960s and comprise the bulk of the world's more than 400 commercial pressurized water reactors (PWRs) and boiling water reactors (BWRs). They are derived from designs originally developed for naval use. As far as safety is concerned, these reactors use traditional *active* safety features involving electrical or mechanical operations that are initiated automatically or can be initiated by the operators of the nuclear reactors, using external power sources.
- *Generation-III (Gen-III)* nuclear reactors are essentially Gen-II reactors with evolutionary, state-of-the-art design improvements. These improvements are in the areas of safety systems (notably those related to severe accident management), fuel technology, thermal efficiency, and digital instrumentation and control. Improvements in Gen-III reactor technology are aiming at achieving longer operational life for NPPs (typically up to 60 years of operation) and at higher fuel burn-up (thus reducing fuel consumption and waste production). Perhaps the most significant improvement of Gen-III systems over Gen-II designs is the incorporation

[10] Council Directive 2013/59/Euratom of December 5, 2013 laying down basic safety standards for protection against the dangers arising from exposure to ionizing radiation, and repealing Directives 89/618/Euratom, 90/641/Euratom, 96/29/Euratom, 97/43/Euratom, and 2003/122/Euratom—(L 13/31 OJ 17.2.2014)—http://ec.europa.eu/energy/nuclear/radiation_protection/radiation_protection_en.htm.

in some designs of *passive* safety features that do not require active controls or operator intervention, but instead rely on gravity or natural convection to mitigate the impact of abnormal events.
Gen-III designs have advanced safety features and set the worldwide standards for the *Safety, Security, and Safeguards* concept ("3S"). However, they have also produced a legacy of significant quantities of used fuel, require relatively large electric grids, and present public acceptance challenges in some countries.

- *Generation-IV (Gen-IV)* reactor systems are nuclear alternatives, some of which still require considerable research and development efforts. Conceptually, Gen-IV reactors have all of the features of Gen-III units, as well as the ability, when operating at high temperature, to support combined heat and power generation (eg, aiming at producing economical and decarbonized hydrogen through thermal energy off-taking). In addition, these designs, when using a fast neutron spectrum, include full actinide recycling and on-site fuel-cycle facilities based on advanced aqueous, pyrometallurgical, or other dry-processing options. As a consequence, (as explained further), these designs contribute to meeting two important sustainability goals. (1) maximize the resource base by taking advantage of the abundant natural resource U-238, and (2) minimize the high-level waste to be set to a repository by transmuting heat-generating radiotoxic minor actinides. Gen-IV options include a range of plant power ratings, including "batteries" of 100 MW_e, modular systems rated at approximately 400 MW_e, and large monolithic plants of up to 2000 MW_e.

It is worth recalling the IAEA definition of advanced nuclear plant designs:

- *"Evolutionary" (Gen-III)*: The designs emphasize improvements based on proven technology and experience. No prototype is needed for their industrial deployment. From a safety point of view, the two aims of "evolutionary" reactors are a further reduction of the core damage frequency (CDF; eg, increased use of passive safety, wherever justified) and a limitation of the off-site consequences should a severe accident occur (eg, strengthening the function of the containment)
- *"Visionary" or "revolutionary" (Gen-IV)*: The designs emphasize the use of new or entirely revisited features, particularly with regard to full actinide management and enhanced safety. Prototypes will be needed for their industrial deployment. The main aim of these reactors is to integrate all Generation IV International Forum (GIF) goals in the design ("built-in" features, not "added") and, in particular, the GIF goal of safety and reliability, by developing a "robust" safety architecture to demonstrate the "practical elimination" of severe accidents.

Short history of Generation-IV (GIF and IAEA/INPRO/approaches)

In 1999 a group of nine countries, led by the US Department of Energy, launched an international project to select a series of nuclear fission systems of a "revolutionary" type that would meet 21-st-century requirements of industry and society, and would deploy industrially before 2040. The countries involved were Argentina, Brazil, Canada, France, Japan, South Africa, the Republic of South Korea, and the United Kingdom, as well as the United States. They all signed the GIF Charter in 2001, thereby creating the GIF. The charter was originally for a duration of 10 years, and in 2011 the signatories unanimously and indefinitely prolonged this duration. In 2002 Switzerland also became a forum member. The *Euratom*, which represents the EU Member States, signed the charter on July 30, 2003 by a decision of the EC pursuant to Article 101(3) of the Euratom Treaty.[1]

The main goal of GIF is to foster worldwide the multilateral collaborative effort around the next generation of nuclear fission reactor systems (ie, power reactors and associated fuel cycles) by fixing high-level goals and providing guidance in connection with viability and performance capabilities of the selected systems, as is reported in the GIF Website[11] and further discussed in Section 10.3.

Six innovative nuclear systems (composed of power reactor and associated fuel cycle) were selected in 2002 after evaluation of more than 100 different designs by more than 100 experts from 12 countries worldwide. These six systems include the following:

- sodium-cooled fast reactor (SFR) system,
- lead-cooled fast reactor (LFR) system,
- gas-cooled fast reactor (GFR) system,
- molten salt reactor (MSR) system,
- very high−temperature reactor (VHTR) system,
- supercritical water−cooled reactor (SCWR) system.

Four of the six systems use a closed fuel cycle to maximize the resource base and minimize high-level wastes to be sent to a repository. The bulk of the GIF international R&D effort is on power sizes ranging from 1000 to 2000 MW_e (or equivalent thermal). Temperatures at core outlet range from 510°C to 1000°C, compared with less than 330°C for today's light water reactors (LWRs).

The general strategy of the GIF members is to continue to build Gen-III reactors between now and 2040. For each system, three phases are planned as mentioned earlier (from preconceptual to final design): viability (between 10 and 25 years), performance (between 10 and 20 years), and demonstration (at least 10 years). The aim is to deploy the first commercial Gen-IV reactors around 2040, ie, when the demonstration phase is completed (see Fig. 10.1, taken from GIF Roadmap, 2013). Expenditure so far is in line with the initial estimate of USD six billion over 15 years for all six systems—about 80% of the cost is being met by the United States, Japan, and France.

A special mention is needed regarding small GIF systems of power under 300 MW_e that are under construction in the world (preparing the licensing process and the industrial deployment phase of larger power plants). There is indeed a revival of interest in small and medium (also called "modular") nuclear power reactors for generating electricity and/or process heat, mainly in view of export to emerging nuclear energy countries. The IAEA defines "small" as under 300 MW_e and up to approximately 700 MW_e as "medium"—together they are now referred to by IAEA as small and medium reactors (SMRs). In general, modern SMRs are expected to have greater simplicity of design, economy of series production largely in factories, short construction times, and reduced siting costs. As a result, the capital costs are reduced and electric power is provided away from large grid systems These SMRs also are expected to have lower CDFs and longer postaccident coping periods, because of a high level of passive or inherent safety. They are usually more resistant to natural phenomena and have

[11] GIF website (hosted at OECD/NEA) with GIF Annual Reports—Symposium Publications—Technology Roadmap and R&D Outlook Publications: https://www.gen-4.org/gif/jcms/c_44720/annual-reports.

potentially smaller emergency preparedness zones than currently licensed reactors. Euratom Horizon-2020 and EU national laboratories concerned are involved in some of these SMR projects.

Several SMRs of power under 300 MW_e are considered among the GIF systems and are under construction in the world, notably in the areas of VHTRs, high-temperature reactors (HTRs), LFRs, and SFRs.

- VHTR (HTR-pebble-bed modules/HTR-PM or HTR-200/designed for commercial power generation) under construction in China: the world's first modular high temperature gas-cooled reactor demonstration plant (composed of two modules of 250 MWt, driving together a steam turbine generating 200 MW_e) will be installed at the Shidaowan plant, near the city of Rongcheng in Shandong Province. Design is by the Institute of Nuclear Energy Tsinghua University and development is by China Nuclear Engineering and Construction Corporation and Huaneng. Construction began at the end of 2012, with the pour of the concrete basemat occurring in April 2014.
- LFR (pool type) planned in the United States, in Russia, and in the EU (Belgium):
  - a small size transportable system in the United States ["small, sealed, transportable, autonomous reactor" (SSTAR): 45 MWt/20 MW_e] with a very long core life;
  - a system of intermediate size in Russia (BREST-OD-300) with uranium-plutonium nitride fuel with high density of 700 MWt/300 MW_e;
  - a smaller and newer Russian design is the Lead-Bismuth Fast Reactor (SVBR) of 280 MWt/100 MW_e, with a wide variety of fuels (refueling interval 8 years);
  - a fast spectrum irradiation facility focusing on minor actinide burning in Belgium (MYRRHA—Section 4), accelerator-driven system of 50−100 MWt.
- SFR (small modular SFR configuration) planned under GIF: A small size (50−150 MW_e) modular-type reactor with uranium-plutonium-minor actinide-zirconium metal alloy fuel, supported by a fuel cycle based on pyrometallurgical processing in facilities integrated with the reactor.

A senior industry advisory panel (SIAP), comprised of executives from the nuclear industries of GIF members, was established in 2003 to provide recommendations on long-term strategic issues, including regulatory, commercial and technical aspects. In particular, the SIAP provides guidance on taking into account investor-risk reduction and incorporating the associated challenges in system designs at an early stage of development. For example, the SIAP was asked to advise the GIF on the following:

- How to ensure the supply chain for Gen-IV systems, including identification of gaps in the supply of non-LWR reactor components (eg, emphasis on availability of materials and industrial practices as well as international standards)
- How to enhance knowledge management in advanced reactor R&D, given the history of knowledge management in the LWR industry (eg, emphasis on capture of expert knowledge in a manner that "survives" changes in personnel).

Accession to GIF brings with it certain obligations, including cofunding activities conducted by the OECD/NEA's GIF technical secretariat. The NEA (OECD/NEA) is indeed the official depositary of the GIF Framework Agreement (FA). As a consequence, the NEA is in charge of coordinating the international GIF R&D program through various dedicated committees (see GIF website[11]).

In the millennium year 2000, the IAEA in Vienna launched a complementary initiative: the International Project on Innovative Nuclear Reactors and Fuel Cycles

(INPRO).[12] INPRO focuses on the needs of the "end users" of innovative systems (ie, focus on the demand side) while GIF is more concerned with the relevant international research—development and demonstration—deployment (RD&DD) collaboration (ie, focus on the supply side). The aim of INPRO is to help ensure that nuclear energy is available to contribute to meeting the energy needs of the 21-st century in a sustainable manner. This project was proposed at the UN Millennium Summit and confirmed by the United Nation's General Assembly in 2001. To achieve this, INPRO brings together mainly nuclear technology users to jointly consider international and national actions that would result in required innovations in nuclear reactors, fuel cycles, or institutional approaches.

In 2016, INPRO's membership consists of 41 Members (40 IAEA Member States and the European Commission), namely Algeria, Argentina, Armenia, Bangladesh, Belarus, Belgium, Brazil, Bulgaria, Canada, Chile, China, Czech Republic, Egypt, France, Germany, India, Indonesia, Israel, Italy, Japan, Jordan, Kazakhstan, Kenya, Republic of Korea, Malaysia, Morocco, the Netherlands, Pakistan, Poland, Romania, Russian Federation, Slovakia, South Africa, Spain, Switzerland, Thailand, Turkey, Ukraine, the United States of America, Vietnam, and the EC.

INPRO produced in the early 2000s a methodology to assess the sustainability of Innovative Nuclear energy Systems (INS). In 2005, INPRO was requested to provide guidance in using the proposed methodology in the form of an INPRO assessment manual. The resulting INPRO manual[13] comprises an overview volume (Volume 1), and eight additional volumes (available on the IAEA website) covering the areas of economics (Volume 2), infrastructure (Volume 3), waste management (Volume 4), proliferation resistance (Volume 5), physical protection (Volume 6), environment (Volume 7), safety of reactors (Volume 8), and safety of nuclear fuel cycle facilities (Volume 9).

As a result of the creation of the GIF and INPRO programs, a framework exists worldwide for all stakeholders interested in research and innovation in nuclear fission. The aim is to solve not only scientific and technological, but also political, socioeconomic, and environmental challenges related to nuclear fission systems.

International collaboration in the development of next-generation systems was also stimulated on the regulatory side. Several national regulatory authorities agreed to share the resources and the knowledge accumulated during their assessment of new reactor designs. As a result, the Multinational Design Evaluation Program (MDEP)[14] was launched in 2005 by the US Nuclear Regulatory Commission. The technical secretariat is with OECD/NEA.

[12] INPRO in Brief—International Project on Innovative Nuclear Reactors and Fuel Cycles, IAEA, 2012 "Enhancing Global Nuclear Energy Sustainability" (INPRO: 40 members in 2014)—www.iaea.org/INPRO.

[13] INPRO manual—http://www-pub.iaea.org/MTCD/publications/PDF/TE_1575_web.pdf.

[14] *Multinational Design Evaluation Program* (OECD/NEA)—https://www.oecd-nea.org/mdep/index.html. As of November 2014, the MDEP members include national regulators from Canada (CNSC); People's Republic of China (NNSA); Finland (STUK); France (ASN); India (AERB); Japan (NRA); Republic of Korea (NSSC); Russian Federation (Rostechnadzor); Republic of South Africa (NNR); Sweden (SSM); United Kingdom (ONR); United States (NRC). Current MDEP associate members include national regulators from Turkey (TAEK) and United Arab Emirates (FANR).

MDEP's main objectives can be defined as follows:

- to enhance multilateral cooperation within existing regulatory frameworks;
- to encourage multinational convergence of codes, standards, and safety goals; and
- to implement the MDEP products to facilitate the licensing of new reactors, including those being developed by the GIF.

The MDEP notably focusses on five Gen-III reactor designs: the European Pressurized Reactor (EPR), AP-1000, APR-1400, VVER, and the advanced boiling water reactor. Particular attention is devoted to "common regulatory practices and regulations that enhance safety," eg, in the areas of design-basis accidents and emergency core cooling system performances, severe accident requirements, digital, and instrumentation and control. Convergence of "codes and standards for designs" is fostered across the world. As far as GIF—IAEA (INPRO)—MDEP collaboration is concerned, it is worth mentioning, for example, that the key GIF report dedicated to safety design criteria for the sodium-cooled fast reactor was shared in 2013.

Finally, a remarkable study by the French TSO, IRSN (Institut de Radioprotection et de Sûreté Nucléaire), should be mentioned: Review of Generation-IV Nuclear Energy Systems,[15] December 2014. The IRSN performed a review of these systems from the point of view of safety and radiation protection. Their conclusion reads as follows:

> *It should be borne in mind that any industrial deployment of a Generation-IV reactor system in France will be linked to its advantages, not only regarding reactor fleet operation and safety, but also in terms of the coherence and performance of the associated fuel cycle. This concerns all aspects relating to safety, radiation protection, material management and efforts made to minimise the quantities of radioactive waste generated, without overlooking the overall economic competitiveness of the nuclear system. Ultimately, the choice of system must be made as part of an integrated approach, based on studies that cover multiple criteria and all the aspects mentioned above.*

10.3 "Goals for Generation-IV nuclear energy systems" and "technology roadmap" for the six GIF systems (2002 and 2013)

To prepare the first Gen-IV Technology Roadmap (2002),[16] it was necessary to establish goals for these innovative nuclear fission energy systems. The goals had three purposes:

[15] IRSN 2014 Report *Review of Generation-IV Nuclear Energy Systems* http://www.irsn.fr/EN/newsroom/News/Pages/20150427_Generation-IV-nuclear-energy-systems-safety-potential-overview.aspx.

[16] *GIF Roadmap 2002/"A Technology Roadmap for Generation-IV Nuclear Energy Systems" (Dec. 2002): https://www.gen-4.org/gif/upload/docs/application/pdf/2013-09/genivroadmap2002.pdf *GIF Roadmap 2013/"Technology Roadmap Update for Generation-IV Nuclear Energy Systems: Preparing Today for Tomorrow's Energy Needs," January 2014, issued by the OECD NEA for the GIF—https://www.gen-4.org/gif/upload/docs/application/pdf/2014-03/gif-tru2014.pdf.

- They served as the basis for developing criteria to assess and compare the systems in the Technology Roadmap.
- They were challenging and stimulated the search for innovative nuclear energy systems (fuel cycles and reactor technologies).
- They also served to guide the R&D on Gen-IV systems as collaborative efforts got underway.

Four broad areas were defined in 2002 in connection with the definition of the high-level "Goals for Generation-IV Nuclear Energy Systems":

1. Sustainability (optimal utilization of natural resources/in particular, U-238/, which is also related to security of supply, as well as minimization of volume, heat and radiotoxicity of high-level waste, environmental protection)/Section 10.5,
2. Safety and reliability/Section 10.6,
3. Economics (industrial competitiveness) including social aspects/Section 10.7
4. Proliferation resistance and physical protection/Section 10.8.

Eight high-level "Goals for Generation-IV Nuclear Energy Systems" were announced in the original GIF Charter of 2001[11] pertaining to these four broad areas:

Area 1: Sustainability

- Generate energy sustainability and promote long-term availability of nuclear fuel and
- Minimize radioactive waste and reduce the long-term stewardship burden.

In this area 1, broad consensus was reached, in particular, regarding the following:

- effective fuel utilization (eg, by converting nonfissile ^{238}U to new fissile fuel), thereby improving waste management and minimizing environmental impact,
- development of new energy products (eg, process heat for various applications, such as hydrogen, gas-to-liquid conversion technologies, potable water) that can expand nuclear energy's benefits beyond electrical generation.

Area 2: Safety and reliability

- excel in safety and reliability,
- have a very low likelihood and degree of reactor core damage, and
- eliminate the need for off-site emergency response.

In this area 2, broad consensus was reached, in particular, regarding the following:

- robust safety designs (eg, using passive safety wherever appropriate) that further reduce the potential for severe accidents and minimize their consequences, thereby enhancing public confidence,
- systematic consideration of human performance as a major contributor to plant safety, reliability, availability, inspectability, and maintainability.

Area 3: Economics

- have a life cycle cost advantage over other energy sources,
- have a level of financial risk comparable to other energy projects.

In this area 3, broad consensus was reached, in particular, regarding the following:

- CO_2-free generation of a broader range of energy products beyond electricity (including small and medium nuclear power reactors),

- accommodation of future nuclear energy systems to the worldwide transition from regulated to deregulated energy markets (including "smart grids" of the future).

Area 4: Proliferation resistance and physical protection (Nonproliferation Treaty):

- Be a very unattractive route for diversion or theft of weapon-usable materials, and provide increased physical protection against acts of terrorism.

In this area 4, broad consensus was reached, in particular, regarding the following:

- further improvement of the safeguards in all nuclear material inventories involved in enrichment, conversion, fabrication, power production, recycling, and waste disposal,
- design of advanced systems from the start with improved physical protection against acts of terrorism, thereby increasing public confidence in the security of nuclear facilities.

The *2002 GIF Technology Roadmap*[16] defined three phases for each GIF system:

- *Viability phase*: Basic concepts for reactor technologies, fuel cycle, and energy conversion processes, established through testing at appropriate scale under relevant conditions, with all potential obstacles identified and resolved, at least in theory; very preliminary cost analysis—preconceptual design, 10−25 years expected for viability phase.
- *Performance phase*: Assessment of the entire system, sufficient for procurement specifications for construction of a demonstration plant; validation of waste management strategy; materials capabilities are optimized under prototypical conditions; detailed cost evaluation—conceptual design, 10−20 years needed.
- *Demonstration phase*: Demonstration of safety features through large-scale testing; environmental impact assessment; safeguards and physical protection strategy for the system; application meetings with regulatory agency—preliminary design, in view of the engineering and final design for the industrial phase, at least 10 years needed.

According to the updated *2013 GIF Roadmap*,[16] the most advanced GIF systems are as follows: SFR and LFR (performance phase due to finish in the early 2020s), followed by VHTR and SCWR (2025) and GFR and MSR (after 2030)—see Fig. 10.1.

It should be noted that only the phases 1 ("viability") and 2 ("performance") are covered by the international GIF collaboration agreements. As a consequence, the multilateral collaborative effort coordinated by the GIF covers only the first two design phases for the six systems:

- Preconceptual design: A "Viability Report" is produced, involving contributions mainly from fundamental research and academic institutions and
- Conceptual design: A "Performance Report" is produced, involving contributions mainly from applied research organizations and industrial experts.

The implementation of the "demonstration" phase (based on preliminary, engineering, and final design) is left to specific arrangements among GIF members, because it is considered to be too close to commercial exploitation. At the time being, half of the GIF systems are still in the viability phase (ie, preconceptual design, namely, SCWR, MSR, and GFR), whereas the other half is well advanced in their performance phase (ie, conceptual and preliminary design, namely, SFR, LFR, and VHTR).

After establishing the GIF Roadmap 2002, the GIF members expressed a strong will to establish an international legal framework. An important step then was the

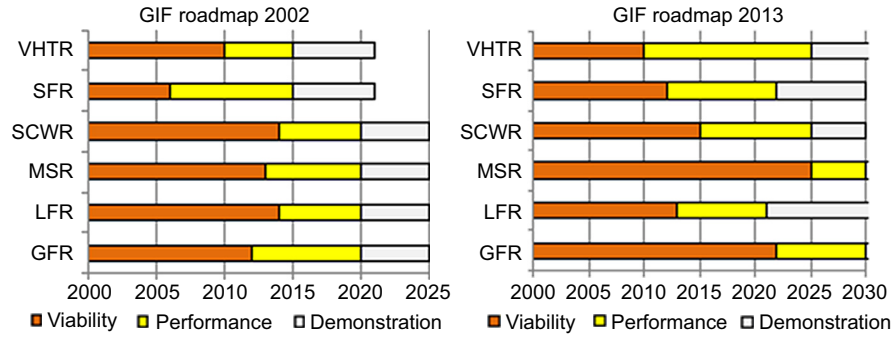


Figure 10.1 2013 Generation-IV International Forum Roadmap—viability, performance, and demonstration phases. *GFR*, gas-cooled fast reactor; *LFR*, lead-cooled fast reactor; *MSR*, molten salt reactor; *SCWR*, supercritical water reactor; *SFR*, sodium-cooled fast reactor; *VHTR*, very-high−temperature reactor.

signature of the Framework Agreement for International Collaboration on Research and Development of Generation-IV Nuclear Energy Systems (in short, the GIF FA):[17] the original version of this FA was open for signature on February 28, 2005. It is in fact an intergovernmental agreement, from a legal point of view comparable to the ITER agreement (which was officially signed in Paris on November 21, 2006 by ministers from the seven ITER Member States). On February 26, 2015 the GIF FA was extended for another 10 years, thereby paving the way for continued collaboration among participating countries.

The Russian Federation and China joined GIF in 2006. As a result, the GIF has 10 active members since 2006, ie, members who have signed the charter and signed, ratified, or/and acceded to the GIF FA and are effectively contributing to GIF work, including the United States, Canada, France, Japan, South Africa, the Republic of South Korea, Switzerland, and Euratom as well as China and the Russian Federation.

Of the six GIF systems, three are fast neutron reactors and thus have a closed fuel cycle (which makes them "sustainable"). They utilize fast neutrons, generating power from plutonium (Pu) while making more of it from the ^{238}U isotope. The SFRs, LFRs, and GFRs (helium) are designed to burn plutonium and MAs. The actinides are separated from the spent fuel and returned to the fast neutron reactors. One may consider a fourth system which can be built as fast reactor systems with full actinide recycle, namely, the MSR. Under certain conditions, even a fifth system can be considered as fast reactor, namely, SCWR.

Although the fast reactor systems of Gen-IV type get more than 60 times as much energy from the original uranium compared with the normal reactors, they are expensive to build and should still demonstrate that they are likely to offer a significantly improved level of safety compared with Gen-III reactors. Much more research is still required, eg, few studies are available on the behavior of these systems under severe accident conditions, as mentioned in the IRSN report.[15]

[17] GIF organization (partners—technology—resources): https://www.gen-4.org/gif/jcms/c_9260/public.

All of these systems operate at higher temperatures than the Gen-II and Gen-III reactors currently in operation—this is a 21st-century requirement of industry. The new systems range from an SCWR, the only one that is cooled by water, which operates above 500°C, to a helium-cooled VHTR, which has an operating temperature of 1000°C. In particular, four are designed for hydrogen production. The VHTR, GFR, LFR, and MSR are all designed to generate electricity and to operate at sufficiently high temperatures, for example, to produce hydrogen by thermochemical water cracking.

Each Gen-IV system requires challenging R&D projects: some are common to all whereas others are specific to the system. For example, the list of Gen-IV safety crosscut items comprises system optimization and safety assessment methodology, emergency planning methods, licensing and regulatory framework, radionuclide transport and dose assessment, and human factors. Additional R&D areas of common interest are proposed as instrumentation and control, human machine interface, reactor physics and thermal-hydraulics, risk management, operation and maintenance.

10.4 "European sustainable nuclear industrial initiative" and Euratom research and training program in fast neutron reactor systems

The EU Council approved the accession of Euratom to the GIF FA in its Decision no. 14929/05, Brussels, December 2, 2005. This accession was notified in EU Commission Decision C(2006)7 of January 12, 2006. On May 11, 2006, Euratom formally acceded and thus became a party to the GIF FA. As far as practical implementation is concerned, Article 2 of the latter EU Commission decision states the following:

> *The Joint Research Centre is confirmed in its role as coordinator of the Community participation in GIF and thus will represent Euratom as its own "Implementing Agent" in accordance with Article III.2 of the Framework Agreement.*

As a consequence, the EU is committed to international cooperation in Gen-IV development. Euratom participation in GIF is also aligned with the *European Sustainable Nuclear Industrial Initiative* (ESNII),which is an initiative of the *European Strategic Energy Technology* (SET-Plan, 2008), as discussed later. The European Commission named its DG JRC as Implementing Agent in representing Euratom interests in GIF. Thus the JRC is the coordinator of all contributions of EU Member States related to GIF research (ie, above-mentioned Euratom "indirect" and "direct" actions as well as national nuclear research and innovation programs).

It should be noted that in the EU, socioeconomics is at the heart of many policies. Therefore, the GIF broad area 3 (Section 10.3) "Economics" should cover a wider domain than just economics—ideally it should be renamed "Socioeconomics." In this context, it should be recalled that, in view of their decision on the Euratom part of Horizon-2020, the EU Council (Council meeting of June 28, 2011) requested that the Commission organize a symposium in 2013 on the benefits and limitations of nuclear fission for a low carbon economy. The symposium will be prepared by

an interdisciplinary study involving, inter alia, experts from the fields of energy, economics and social sciences. As a consequence, a 2012 Interdisciplinary Study was launched in April 2012, composed of two parts (scientific-technological and sociopolitical) and published on the occasion of and presented at the 2013 Symposium (Brussels, February 26–27, 2013).[18]

An Ethics study covering all energy sources was also conducted in this context and was published in the proceedings of the 2013 Symposium as well as in a separate EC/European Group on Ethics (EGE) document.[19] The title of the Ethics study is Ethical framework for assessing research, production, and use of Energy—it was issued on January 16, 2013 and referred to as "Ethics Opinion no. 27." This Ethics study advocates a fair balance between four criteria—access rights, security of supply, safety, and sustainability—in light of social, environmental, and economic concerns. The conclusion of this study also insists on more science-based support for EU energy policy in general.

The high-level Goals for Generation-IV Nuclear Energy Systems in fact are not new (eg, Enrico FERMI/1901–54/already mentioned similar goals) and are shared worldwide by many countries (more than, strictly speaking, the GIF members), as they aim to respond to several 21st-century requirements. It should also be noted that three of the GIF broad areas (areas 1, 2, and 3—Section 10.3) are crucial for many energy generation technologies (whatever the primary energy source: renewable, fossil, or fissile). Broad area 2 "Safety and reliability" as well as security in particular, are the subject of a recommendation (no. 4.2) in the previously mentioned "Ethics Opinion no. 27," which reads: "Proper impact assessment methodologies to compare the security and safety of the energy mix instruments are necessary."

In this context the important role of the Sustainable Nuclear Energy Technology Platform (SNETP)[20] should be stressed. The SNE-TP provides guidance to European research, innovation, and education programs in three domains, covering all generations of NPPs, namely, the following:

1. NUclear GENeratIon-II & -III Association (NUGENIA) dedicated to Gen-II (eg, long-term operation issues)/Gen-III (eg, severe accident management);

[18] 2012 Study: http://www.eesc.europa.eu/?i=portal.en.events-and-activities-symposium-on-nuclear-fission Synthesis report available in EU Bookshop (free of charge)—http://bookshop.europa.eu/en/benefits-and-limitations-of-nuclear-fission-for-a-low-carbon-economy-pbKINA25817/.

[19] *Ethical framework for assessing research, production, and use of Energy*, 16/01/2013—BEPA/EGE study—http://ec.europa.eu/bepa/european-group-ethics/docs/publications/opinion_no_27.pdf
*Note on BEPA/EGE. The *European Group on Ethics in science and new technologies* (EGE) in fact was asked by EC President Mr. José Manuel Durão Barroso (length of term in office: 2004–14) on December 19, 2011 to contribute to the debate on a sustainable energy mix in Europe by studying the impact of research into different energy sources on human well-being. The EGE was a team linked with the Bureau of European Policy Advisers (BEPA), reporting directly to the EC President.

[20] List of *European Technology Platforms* of interest to research and innovation in reactor safety.
SNE-TP, *Sustainable Nuclear Energy Technology Platform*—http://www.snetp.eu/
NUGENIA, *NUclear Generation-II and -III Association*—http://www.nugenia.org/
ESNII, *European Sustainable Nuclear energy Industrial Initiative*—http://www.snetp.eu/esnii/

2. ESNII dedicated to Gen-IV systems of fast neutron type and associated fuel cycle facilities; and
3. Nuclear Cogeneration Industrial Initiative dedicated to a broader range of energy products beyond electricity.

ESNII was launched on November 15, 2010 at the SET-Plan Conference in Brussels as an outcome of the above SNE-TP. It should be recalled that a more competitive resource-efficient economy (ie, moving toward a circular economy) is an important 21st-century requirement for transforming Europe. In this context the ESNII addresses the need for closed fuel cycles in nuclear fission systems, ie, their focus is on Gen-IV fast neutron technologies including the supporting research infrastructures, fuel facilities, and research work. As a result, the ESNII initiatives cover part of the Euratom contribution under the GIF Framework Agreement.

According to the ESNII, the three types of fast reactors [using, respectively, sodium (SFR), lead (LFR), or gas (GFR) as coolant] have a comparable potential for making efficient use of uranium and minimizing the production of high-level radioactive waste. When it comes to priorities, the previous work in the EU on sodium technology gives this option a strong starting position. However, as an alternative to sodium, the LFRs and GFRs also offer several interesting features.

In line with the priority put on fast neutron spectrum reactors, the ESNII is supporting the design and construction of four demonstrators:

1. Advanced Sodium Technological Reactor for Industrial Demonstration (ASTRID) demonstration reactor with sodium coolant (pool type, 600 MW_e) to be built in France ["Act for a Sustainable Management of Nuclear Materials and Radwaste," June 28, 2006; project led by French government (CEA) using a national loan of €650 million]. ASTRID is designed to pursue the R&D on SFRs and demonstrate the feasibility of transmutation of MAs. The basic design phase is planned from 2016 to 2019. CEA is associated with several industrial partners such as EDF, AREVA NP, Alstom, Bouygues, Comex Nucléaire, Jacobs France, Toshiba, Rolls-Royce, and Astrium France.
2. MYRRHA research reactor project with lead-bismuth coolant, open to the EU research community (50−100 MW_{th}). The focus is on MA burning (ie, radioactive waste minimization) through an accelerator-driven system using a subcritical fast neutron spectrum core. It will be a highly performing and versatile installation (fast spectrum irradiation facility). MYRRHA has been in the roadmap of the European Strategy Forum on Research Infrastructures (ESFRI) since 2010, and it has benefited so far by a €60 million funding. The project is led by and hosted at SCK-CEN, Mol, Belgium (end of construction is planned by 2023).
3. ALFRED (Advanced Lead Fast Reactor European Demonstrator) demonstrator with lead coolant, to be hosted in Romania. The "Fostering ALFRED Construction" consortium is composed of Romania's Nuclear Research Institute (RATEN-ICN). The project is led by Ansaldo Nucleare and Italy's National Agency ENEA.
4. ALLEGRO is designed as a *GFR* demonstrator with helium coolant, resulting from regional collaboration in the "V4G4 Centre of Excellence" *(Visegrad 4* countries for *Generation-IV* reactors) composed of Hungary (MTA EK, Centre for Energy Research), the Czech Republic (ÚJV Řež, a.s.), Slovakia (VUJE, a.s.) and Poland's National Centre for Nuclear Research (NCBJ). The research institutes of the V4G4 agreed to conduct joint research, development, and innovation in the field of Gen-IV nuclear systems. The main aim is to improve sustainability (efficient resource utilization and minimize volume, heat, and radiotoxicity of waste) and safety and reliability as well as proliferation resistance.

Three nuclear fission projects have applied officially for the previously mentioned EFSI[7]: the two fast neutron research reactor projects MYRRHA and ALLEGRO as well as the thermal neutron research reactor project PALLAS [Dutch research reactor (successor of HFR)]. It should be noted that the PALLAS reactor is aiming at taking over from the 50-year-old high-flux reactor in Petten (The Netherlands), dedicated to medical isotope production and other applications of ionizing irradiation: a national loan of maximum €82 million was provided for PALLAS in 2014 to Energie-onderzoek Centrum Nederland and their daughter company Nuclear research and consultancy group (Petten, the Netherlands).

Also worth mentioning here is the thermal neutron research reactor the Jules Horowitz Reactor (JHR), under construction at CEA Cadarache in southeastern France. When operating at its full capacity of 100 MWt, the JHR will produce, in the reflector surrounding the core area, a thermal neutron flux to study current and innovative nuclear fuels. In-core experiments will typically address material experiments with high fast flux capability up to 5×10^{14} n/cm^{2}s perturbed fast neutron flux with energy larger than 1 MeV.

NB: Historical reminder about the "European fast reactor" project (1984–93)

The bases for the "European Fast Reactor" (EFR) cooperation were laid in 1984 when the governments of Belgium, France, Germany, Italy, and the UK signed a memorandum of understanding to harmonize their fast reactor development programs and to come to a more efficient pooling of their experiences and resources.[21] Utilities, design companies, and R&D organizations were involved during a decade.

Three subsequent specific agreements were signed shortly after 1984:

- the "R&D Agreement," relating to research and development, which was signed by European R&D organizations (in particular, CEA, KfK, Belgonucléaire, ENEA),
- the "Industrial Agreement," relating to cooperation in design, construction, and marketing, which was signed by European design and construction companies (in particular, EDF, Framatome, Siemens, NTC Nuclear Technology Consult GmbH), and
- the "Intellectual Property Agreement," setting out the terms and conditions controlling the use of existing and future know-how information at the disposal of the European partners.

More than 1000 specialists worked efficiently together, even if they were located in 20 or so offices and laboratories spread across Europe, and even if they belonged to several companies of different nature, terms of reference, and management structures.

The end of the EFR project came almost unnoticed after the Concept Validation Phase, which expired at the end of 1993. First, the governments, especially, in the

[21] EFR: http://www.iaea.org/inis/collection/NCLCollectionStore/_Public/25/028/25028985.pdf—see also *The Story of the European Fast Reactor Cooperation*, Dr. Willy Marth, Kernforschungszentrum Karlsruhe KfK 5255, December, 1993—http://bibliothek.fzk.de/zb/kfk-berichte/KFK5255.pdf.

United Kingdom and in Germany, withdrew from financing the R&D program. Then the European utilities (European Fast Reactor Utilities Group) stopped financing the design companies. Nevertheless, it is believed that the EFR collaboration represented a very successful example of how an advanced technological development can be handled across nations, thereby sharing costs and taking the benefits of international skills and expertise.

10.5 Sustainability (efficient resource utilization and minimization of radioactive waste)

The GIF requirement of improved sustainability refers to the following key questions:

1. How to enhance fuel utilization? [Is spent nuclear fuel recyclable material or waste? (focus on U-238)]—Is Plutonium a valuable asset or a liability? (breeding of fissile Pu-239 fuel from nonfissionable, but fertile U-238)
2. How to minimize volume, heat, and radiotoxicity of ultimate radioactive waste? (transmutation of actinides in Gen-IV fast neutron reactor systems)

Two GIF goals (nos. 1 and 2) are defined in connection with sustainability:

1. Generate energy sustainably and promote long-term availability of nuclear fuel.
2. Minimize radioactive waste and reduce the long-term stewardship burden.

Before discussing the sustainability of Gen-IV systems, a reminder about natural uranium and the composition of spent nuclear fuel (SNF) is necessary.[22] Natural uranium is composed of 0.005% ^{234}U, 0.720% ^{235}U%, and 99.275% ^{238}U. The fuel used in a standard LWR relies on the fissile isotope ^{235}U, which is typically enriched to ^{235}U concentrations in the range of 4%. However, it should be noted that some 40% of the energy produced in the course of a nuclear fuel cycle in an LWR comes from ^{239}Pu, which is thus an excellent fissile fuel material. Moreover, ceramic-mixed oxide fuel (MOX, which is $UO_2 + PuO_2$), consisting of about 7−10% Pu mixed with depleted uranium (^{238}U), is equivalent to UO_2 fuel enriched to approximately 4.5% ^{235}U, assuming that the Pu contains approximately two-thirds fissile isotopes.

After approximately 3 years of permanence inside of the reactor core, the spent fuel of an LWR of 1000 MW_e (typical burn-up of 40,000 MWd/tHM, initial enrichment to 4% ^{235}U; 5 years cooling) is transferred to cooling pools (note: MWd/tHM, megaWatt-days per ton of heavy metal).

The average composition of this SNF (5 years after unloading) is as follows:

1. 94% ^{238}U
2. 1% ^{235}U (hence, SNF is still enriched if compared to natural uranium)
3. 1% Pu

[22] The Nuclear Fuel Cycle—Material balance for the annual operation of a 1000 MW_e NPP—http://www.world-nuclear.org/info/Nuclear-Fuel-Cycle/Introduction/Nuclear-Fuel-Cycle-Overview/.

4. 4% fission products and transuranium elements other than Pu, with the following composition on average:
   a. 3.35% of stable fission products, which pose little concern (majority of nonuranium isotopes);
   b. 0.3% of short-lived strongly thermogenic fission fragments, such as ^{90}Sr and ^{137}Cs (with half-lives on the order of 30 years), which generate most of the hazard for the first hundreds of years of disposal;
   c. 0.1% of long-lived fission fragments, such as ^{99}Tc, ^{129}I, and ^{135}Cs, that last for hundreds of thousands of years and must be isolated from the environment;
   d. 0.1% of other less long-lived fission products; and
   e. 0.15% of transuranium elements other than Pu, mainly MAs such as Np, Am, and Cm.

The core of a standard NPP of 1000 MW_e, such as the previously mentioned reactor, contains approximately 72 ton of low-enriched uranium. According to this composition of SNF, in a yearly operating cycle (refueling annually with one-third replaced, ie, 24 ton U/year), the spent fuel contains approximately 23 ton uranium (including 240 kg ^{235}U), 240 kg ^{239}Pu, and approximately 1 ton of fission products and transuranium elements other than Pu. Thus there are approximately 36 kg MAs (ie, Np, Am, and Cm, equivalent to 0.15% of the total SNF).

The radioactivity of the SNF evolves over time as the various elements decay. The same is true of its radiotoxicity (expressed in "Sv/metric tonne") versus natural uranium: that of fission products decreases very rapidly in a few hundred years and then persists at low level for millions of years, because of the presence of long-lived fission products. In fact, after approximately 600,000 years, the radioactivity of untreated spent fuel comes down to that of the natural uranium from which the fuel was made. The radioactivity of the SNF in fact decays by a factor of 65 within 1 year after unloading from the reactor core as a result of the decay of relatively short-lived fission products and actinides. The radioactivity of plutonium (mostly of half-lives 24,000, 6500, and 87 years) represents less than 10% of the total toxicity of the spent fuel when it comes out of the reactor. With the passage of time and the disappearance of the short-lived products, this proportion increases. In addition, MAs (Np, Am, Cm) significantly contribute to the radiotoxicity balance during a few thousand years. After several thousands of years, plutonium dominates and represents nearly 90% of the radiotoxicity.

A reminder about conversion (or transmutation) of fertile to fissile fuel might also be useful. The conversion ratio, C, is the ratio of the rate of production of fissile nuclei in a reactor (typically ^{233}U, ^{239}Pu, ^{241}Pu), continuously generated from fertile material (typically ^{232}Th, ^{238}U, ^{240}Pu), to the rate of consumption of fissile nuclei. If C is small, then the reactor is called a burner (eg, $C = 0.6$ in LWRs with 3−5% ^{235}U in the initial fuel); if C is between 0.7 and 1.0, it is called a converter (eg, $C = 0.75$ in LWRs with 5% Pu). If C exceeds unity, it is called the breeding ratio (BR) and then it is a breeder (eg, $C = 1.4$ in liquid metal fast breeder reactors with 15−20% Pu). It should be noted that historically the main incentive for the development of fast breeder reactors (FBRs) was the extension of uranium supplies through a better use of ^{238}U, which is nonfissionable in LWRs and is present at 99.275% in natural uranium.

Previously discussed GIF Goal No. 1 "Generate energy sustainably and promote long-term availability of nuclear fuel" leads to the issue of plutonium (in particular, ^{239}Pu) as fuel for fast neutron spectrum reactors.

In this type of reactor, a chain reaction takes place in which the neutrons are not thermalized (there is no moderator), but instead produce fission at relatively high energies (on the order of 1.0 MeV). With uranium fuel, ^{239}Pu is produced by the capture of neutrons in ^{238}U: as mentioned previously, the SNF contains 94% ^{238}U. As a result of this physical process (based on breeding of fissile ^{239}Pu fuel from nonfissionable, but fertile ^{238}U), fissile material is produced and consumed in the reactor before the fuel is removed, supplementing the original ^{235}U in the fresh fuel. To avoid thermalization of the neutrons, FBRs use a coolant with high mass number to reduce moderation, such as liquid metals (eg, ^{23}Na, Pb, or lead-bismuth eutectic , all in liquid state). The fuel of FBRs is made of pellets of mixed Pu and U oxides: PuO_2 (about 20%) and UO_2 (about 80%). Uranium depleted in ^{235}U is commonly used (residue from earlier enrichment)—nonconventional (usually more expensive) uranium ores could also be used. An alternative breeding cycle is based on thorium: this implies conversion of fertile ^{232}Th to fissile ^{233}U, which is investigated in some countries (eg, in India and Canada, thorium is four times more abundant than uranium in the Earth's crust).

According to the GIF strategy, fast neutron reactors can also be used to consume unwanted plutonium (rather than to produce plutonium as a fuel) and to destroy other heavy elements in weapons stockpiles or radioactive waste: in this case they act as burners instead of breeders (C is small).

Previously discussed GIF Goal No. 2 "Minimise radioactive waste and reduce the long-term stewardship burden" leads to the issue of recycling or circular economy, ie, separating and conserving everything that is potentially recyclable (ie, U and Pu).

Regarding to Gen-II and Gen-III, recycling nowadays is rather exceptional in the world. Recycling (or reprocessing) of civilian fuel in view of MOX fuel fabrication is performed in only few countries, namely:

- in Europe (LWR fuel at the Cap de la Hague site in France, Normandy region and at the Sellafield site in the United Kingdom, Cumbria region),
- in the *Russian Federation* (LWR fuel in the "Mayak Chemical Combine," situated in the province of Chelyabinsk in the southern Ural Mountains), and
- in Japan (LWR fuel in the long-delayed reprocessing plant at Rokkasho-mura—Japan Nuclear Fuel Ltd hopes to get an operating license by March 2016).

Smaller scale reprocessing plants are operating in Japan (FBR fuel at Tokai), in India (CANDU fuel at Tarapur and FBR fuel at Kalpakkam) and in China (LWR fuel at Lanzhou). It should also be noted that noncivilian (weapons) plutonium is used for MOX fuel fabrication (after reprocessing) in the United States (LWR-MOX fuel fabricated at Savannah River) and in Russia (LWR-MOX fuel fabricated at Tomsk).

Regarding Gen-IV, according to the GIF strategy, partitioning and transmutation techniques can be used to further improve the desired recycling process. Application of these techniques to Pu and other heavy radionuclides, such as the MAs Np, Am, and Cm, aims at reducing the volume, heat, and toxicity of ultimate radioactive waste for disposal.

As far as reprocessing in the ^{238}U/Pu fuel cycle is concerned, several chemical separation techniques have been proposed and developed in the past few decades. The most efficient process to date remains the PUREX process (Plutonium and Uranium Recovery by Extraction). This process uses nitric acid HNO_3 and organic solvents to dissolve and extract selectively U and Pu, resulting in two separate product streams (U on one side and Pu on the other side of the process chain). As far as reprocessing in the ^{232}Th/^{233}U fuel cycle is concerned, THOREX (Thorium Oxide Recovery by Extraction) technology must be used, also based on dissolution in nitric acid and solvent extraction (however, with special care for the extraction of ^{233}Pa, for the separation of ^{232}U and ^{233}U, and for the dissolution of thorium dioxide in pure nitric acid).

Much of the calculated long-term waste hazard comes from a limited set of MAs (about 0.15% of the SNF or 36 kg/year in a standard NPP of 1000 MW_e, as explained previously) with half-lives ranging from tens to millions of years such as ^{244}Cm and ^{237}Np, respectively. Exposure of these radionuclides to high neutron fluxes could transmute them into much less hazardous nuclides. In such cases, chemical separations are necessary to allow the partitioning of selected groups of radionuclides into different waste streams.

Gen-IV reactor systems of fast neutron spectrum type in fact include waste destruction as an integral part of the fuel cycle rather than as a separate process. In a still more ambitious project, based on an accelerator-driven fission system, all the waste products are continuously recycled and selected transuranium nuclides are destroyed. This is the purpose, for example, of the previously mentioned MYRRHA project.

In conclusion of this Section 10.5, to answer key questions, Gen-IV systems of the fast neutron type will manage to enhance fuel utilization (by recycling Uranium and Plutonium), while minimizing volume, heat, and toxicity of ultimate radioactive waste (by partitioning and transmutation). As a consequence, SNF is not waste, but could become a huge source of power for the future, since the current Gen-II and Gen-III of NPPs burn only a very small amount of the uranium resource. A very large amount of energy is still to be found in what has erroneously come to be known as "waste." In fact, up to 96% of the SNF (made of ^{238}U, ^{235}U, and Pu) could be recycled in Gen-IV reactor systems. Pu is thus not a liability, but a "valuable asset": there will be plenty of fuel once the ^{238}U resource can be optimally exploited, ie, when fast neutron spectrum reactors of the Gen-IV type with actinide burning capacities come into service reactors. Use of breeder reactors in a nuclear fuel cycle would extend the supply of usable fuel by a factor of about 60-fold.

10.6 Safety and reliability (maximum safety performance through design, technology, regulation, and culture)

The GIF requirement of improved safety and reliability refers to the following questions:

1. How to optimize the "risk/benefit" factor in applications of nuclear fission energy and ionizing radiation? How safe is safe enough?

2. What is the impact of human and managerial factors on safety performance? (safety culture as a complement to safety technologies and regulations)

Three GIF goals (nos. 3, 4, and 5) are defined in connection with safety and reliability:

3. Excel in safety and reliability,
4. Have a very low likelihood and degree of reactor core damage, and
5. Eliminate the "technical" need for off-site emergency response.

Before discussing the safety and reliability of Gen-IV systems, a reminder about safety principles and their implementation is necessary. A pioneering role was played in this domain by an EC document in the early 1980's, because it paved the way to later international documents (eg, those elaborated by the IAEA): "Safety principles for LWR nuclear power plants," published as COM (81)519. Later on, the TMI (1979) and Chernobyl (1986) accidents stressed the importance of the work on international collaboration in the establishment of common safety objectives, and, in particular, regarding severe accident management.

Safety objectives are fixed for every nuclear installation. These objectives should be measurable, both qualitatively and quantitatively, and they should include prevention of severe accidents and mitigation of the consequences, should prevention fail, as it has been clearly stated in a series of IAEA INSAG reports. When setting safety objectives, other factors (notably non-fatal health effects) should also be taken into account, as learned from the historical severe accidents.

In fact, there are different philosophies in the world with respect to safety goals. For example, in the EU the fear of accidents, especially of (hypothetical) severe accidents, has led some countries to propose for Gen-III very stringent safety targets implying the "practical" prohibition of large-scale evacuation and land contamination subsequent to an accident. It should be noted that, in the revised 2014 Euratom Safety Directive,[9] the EU promotes the most stringent safety principles in the world to improve nuclear safety standards. Also worth noting is that the 2013 Euratom BSS Directive[10] recommends, in particular, that social, legal, and ethical aspects should be included in addition to purely technical considerations. In the US approach for safety objectives, until recently the emphasis was placed on mortality and direct monetary costs of in- or off-site consequences, ie, cost−benefit analysis aspects were important (eg, taking into account the monetary value of human life, estimated up to several million US dollars).

Previously discussed GIF Goal No. 3 Excel in safety and reliability refers, for example, to the need of providing robust safety cases describing the safety practices. In fact, there is a good convergence of safety practices in the Member States, notably, in the following domains:

- ALARA (*As Low As Reasonably Achievable*) policy to reduce the doses of ionizing radiation to the personnel and the public;
- defense-in-depth and integrity of the successive barriers between the radioactive products and the environment (including active and passive safety systems);
- radiological consequences of postulated accidents (see eg 2013 BSS Directive);
- deterministic safety analysis => identification of postulated or design-basis accidents; and
- probabilistic safety analysis (PSA) => evaluation of the overall risk from the plant, including severe accidents analysis and management (eg, mitigation measures for high-consequence low-frequency events) => PSA levels 1, 2 and 3.

Previously discussed GIF Goal No. 4 Have a very low likelihood and degree of reactor core damage requires a reminder of the Reactor Safety Study WASH-1400[23] in the United States, which was in 1975 among the first to examine the phenomenology of severe accidents. They used methodologies developed by the Department of Defense and the National Aeronautics and Space Administration such as event trees and fault trees. They were able to compare the likelihood of nuclear and nonnuclear accidents (human-caused events as well as natural events) having similar consequences (expressed in terms of fatalities and property damage in US dollars). The main risk issues in NPPs of the LWR type were identified: molten corium behavior, fission product release, and hydrogen combustion. Several containment failure modes or challenges were identified as follows: (1) Overpressure, (2) Dynamic pressure (shock waves), (3) Internal missiles, (4) External missiles (not applicable to core melt accidents), (5) Melt through, and (6) Bypass. As a consequence of WASH-1400 and of the introduction of PSA after the TMI accident, several regulatory authorities worldwide introduced nuclear safety objectives of the probabilistic type.

Of particular interest are the following probabilistic safety criteria introduced in WASH-1400: CDF and Large Early Release Frequency (LERF—typically in the order of 100 TBq ^{137}Cs) that are calculated in Level 1 and Level 2 PSA, respectively. In INSAG-3, safety goals of the quantitative probabilistic type are proposed for CDF and LERF: the LERF value is usually 10 times smaller than the CDF value. For existing NPPs, a safety target of less than 10^{-4}/reactor year was proposed as the likelihood of occurrence of severe core damage (CDF). Accident management and mitigation measures should reduce the probability of large off-site releases (requiring short term off-site response) to less than 10^{-5}/reactor-year. Implementation of the INSAG Safety Principles at future plants should lead to safety improvements by a further factor of 10 (for all events). The latter threshold value ($<10^{-6}$/reactor-year) for unacceptable consequences is already required for existing NPPs in many OECD countries. For the radiological definition of the off-site release limits during normal operation and incidents and for the off-site release targets for accidents, other internationally widely recognized standards are usually taken, such as the IAEA and/or EU BSS.

The GIF Goal No. 5, Eliminate the need for offsite emergency response is embedded in the revised 2014 Euratom Safety Directive.[9] It is also at the heart of the European Utility Requirement (EUR)[24] organization. As far as safety requirements are concerned, the EUR organization has dedicated special attention to severe accident management since the mid-1990s. Situations and phenomena that could lead to early failure of the containment system and subsequent uncontrolled large releases of fission products into the environment should be practically eliminated by design. For

[23] N.C. Rasmussen, "Reactor Safety Study: An assessment of accident risk in US commercial nuclear power plants," AEC Report, WASH-1400-MR (NUREG-75/014), United States NRC, Washington, DC, 1975—http://www.iaea.org/inis/collection/NCLCollectionStore/_Public/35/053/35053391.pdf.

[24] European Utility Requirement (EUR): http://www.europeanutilityrequirements.org/ The EUR organization includes 17 European utilities (namely, CEZ, EDF, EDF energy, Endesa, ENEL (SOGIN), Energo-Atom Ukraine, Fortum, Gen Energija, Iberdola, MVM, NRG, RosEnergoAtom, Swissnuclear, GDF-Suez/Tractebel Engineering (now Engie), TVO, Vattenfall, and VGB Powertech).

example, for the evolutionary reactor EPR, the main safety objectives are to further reduce the core melt probability and, in the hypothetical case of a severe core melt accident, to improve the containment of fission products by excluding in a "deterministic" way any major off-site damage, that is, to "practically eliminate," by design, accident situations and phenomena that could lead to large early releases.

An integral assessment approach is provided by GIF through their Risk and Safety Working Group (RSWG). This group produced in 2011 a methodology, called the Integrated Safety Assessment Methodology (ISAM—GIF/RSWG/2010)[25] for use throughout the Gen-IV technology development cycle. ISAM allows evaluation of a particular Gen-IV concept relative to various potentially applicable safety metrics or "figures of merit." ISAM is particularly efficient to assess active versus passive safety components and systems. To help facilitate the use of the methodology, in 2014, the RSWG developed a supporting Guidance Document for ISAM (GDI—Rev 1, 2014) to provide the users with further help for the ISAM implementation.[26]

The ISAM is a tool that can be used throughout from concept development to design and then to licensing. It combines probabilistic and deterministic perspectives. It improves understanding of safety-related design vulnerabilities and the contribution to risk. It also helps identify areas for additional research and data collection. The ISAM consists of five steps: (1) Qualitative Safety Features Review, (2) Phenomena Identification and Ranking Table, (3) Objective Provision Tree, (4) Deterministic and Phenomenological Analyses, and (5) PSA.

1. *Qualitative Safety Features Review*: It is a checklist structured following the principle of the defense-in-depth, and it includes a comprehensive set of qualitative recommendations. It provides designers with useful means to help ensure that safety truly is "built-in," not "added-on," from the early phases of the design of Gen-IV systems.
2. *Phenomena Identification and Ranking Table (PIRT)*: This technique, relying heavily on expert elicitation, identifies a spectrum of safety-related phenomena or scenarios that could affect systems. Those phenomena or scenarios are then ranked on the basis of their importance (often related to their potential consequences) and of the state of knowledge.
3. *Objective Provision Tree (OPT)*: There is a natural interface between the OPT and the PIRT in that the PIRT identifies phenomena and issues that could potentially be important to safety, and the OPT focuses on identifying design provisions [in fact essential "lines of protection" (LOP)]. The purpose of the OPT is to document the implementation of essential LOPs to ensure successful prevention, control, or mitigation of phenomena that could potentially damage the nuclear system.
4. *Deterministic and Phenomenological Analyses (DPA)*: Conventional deterministic and phenomenological analyses will feed the PSA as an essential input to quantify the results. It is anticipated that DPA will be used from the late portion of the preconceptual design phase through ultimate licensing and regulation of the Gen-IV system.
5. *PSA*: It can only be meaningfully applied to a design that has reached a sufficient level of maturity. Thus it is performed and iterated beginning in the late preconceptual design phase

[25] ISAM by GIF cross-cutting methodology working group Risk and Safety—https://www.gen-4.org/gif/upload/docs/application/pdf/2013-09/gif_rsgw_2010_2_isamrev1_finalforeg17june2011.pdf.

[26] GIF—*Integrated Safety Assessment Methodology*—https://www.gen-4.org/gif/jcms/c_9366/risk-safety.

and continuing until the final design stages. Also worth mentioning is the concept of "living PSA" which is becoming increasingly accepted in Gen-IV systems.

As far as practical applications of ISAM are concerned, it is worth mentioning two limited scope trial applications to a realistic, developing advanced reactor development effort: one for a Japanese sodium fast reactor concept and one for a French sodium fast reactor concept.

Other applications of ISAM were carried out in Euratom FP7/2007−2013/projects such as the following:

- Between 2010 and 2013, the small- or medium-scale focused project LEADER (Lead-cooled European Advanced DEmonstration Reactor), coordinated by Ansaldo in Italy (total of 16 partners, total budget of €5.7 million including €3 million from EC) − application also to the ALFRED design.
- Between 2010 and 2013, the collaborative project EVOL (Evaluation and Viability Of Liquid fuel fast reactor systems) project, associated with the Rosatom project MARS ("Minor Actinides Recycling in molten Salt"), which was the main frame of international scientific co-operation on the Th-U molten salt fast reactor concepts—project coordinated by CNRS in France (total of 11 partners, total budget of €1.8 million including €1 million from EC).
- Between 2012 and 2013, the coordination and support action SARGEN-IV ("Proposal for a harmonized European methodology for the safety assessment of innovative reactors with fast neutron spectrum planned to be built in Europe"), coordinated by IRSN in France (total of 22 partners, total budget of €1.3 million including €1 million from EC).

In Gen-IV designs of very innovative type, there are several structures, systems, components, and phenomena that could bear specific risks and uncertainties. When developing the safety case (in particular, the transient and accident analysis), the applicant designer should pay special attention to the identification and assessment of the following:

- Initiating events (ie, events that create a disturbance in the plant that has the potential to lead to core damage, depending on the successful operation of required mitigating systems in the plant)—the hazard and operability (HAZOP)[27] and/or Failure Modes, Effects, and Criticality Analysis (FMECA)[28] approaches (well known in industry) seem well suited for this purpose.
- Phenomena expected to occur on the nuclear installation—the above PIRT (Phenomena Identification and Ranking Table) approach seems well suited.

In conclusion of Section 10.6, to answer the question how safe is safe enough?, a number of assessment methodologies and safety technologies do exist for existing as well as future nuclear installations. Moreover, from a nontechnical point of view, the

[27] The "*HAZard and Operability*" technique (HAZOP) is based on "intuition and good judgment"—similar to the PIRT—and provides a systematic examination of planned processes in order to identify and evaluate problems that may represent risks to personnel or equipment, or prevent efficient operation. The HAZOP technique was initially developed to analyze chemical and mining operation processes.

[28] Another widely used reliability analysis technique in the initial stages of product/system development is the "*Failure Modes, Effects, and Criticality Analysis*" methodology (FMECA). FMECA is usually performed during the conceptual and initial design phases of the system in order to assure that all potential failure modes have been considered and the proper provisions have been made to eliminate these failures.

attention is drawn to human and managerial factors and, in particular, to their impact on safety performance. This concern is at the heart of the continuous improvement of nuclear safety culture in nuclear fission installations (where inadvertent exposure of workers to excess dose should be prevented), and, in particular, in NPPs and in the fuel cycle industry. Similarly, in medical, industrial, and scientific applications of ionizing radiation (where a balance must be sought between benefits and potential harm of exposure), the focus is on radiation protection safety culture.

10.7 Socioeconomics (economic advantage over other energy sources and better governance structure in energy decision-making process)

The GIF requirement of improved socioeconomics refers to the following key questions:

1. How to evaluate the "total social cost" of energy technologies? (="private," ie, capital and O&M, fuel, "external," ie, system effects, accidents, and avoided CO_2)
2. Better governance structure in energy decision-making process (ie, more openness, participation, accountability, effectiveness, and coherence)

Two GIF goals (nos. 6 and 7) are defined in connection with economics:

6. Have a life cycle cost advantage over other energy sources and
7. Have a level of financial risk comparable to other energy projects.

To assess socioeconomics, the collaboration is needed of experts with skills in finance and accounting, hard sciences (eg, energy, environment, new technologies, life sciences), as well as soft sciences (eg, sociology, psychology, risk perception). This question is particularly complex, because of various technological and socioeconomic uncertainties and, because of the long time horizon involved (remember the horizon for NPP development "from cradle to grave" is in the order of 100 years).

The GIF Goal No. 6, Have a life cycle cost advantage over other energy sources means in fact minimizing the Levelized Unit Energy Costs (LUEC): this favors large units with economies of scale. The LUEC methodology is an economic assessment of the cost to build and operate a power-generating asset over its lifetime (usually several decades) divided by the total power output of the asset over that lifetime: typically, the unit of LUEC is Euro per milliwatt-hour (€/MWh).

A good understanding of nuclear economics is provided by the authoritative cost study of the French Court of Auditors dated January 2012 ("*Les coûts de la filière électro-nucléaire*" or "The costs of the nuclear power sector," *Cour des Comptes*).[29] This French report is a unique work in that it is the first time all of the costs of nuclear energy generation are put on the table, from construction and operation of the plants until

[29] "Cour des comptes http://www.ccomptes.fr/Publications/Publications/Les-couts-de-la-filiere-electro-nucleaire (by Jacques Percebois, chairman of "Énergies, 2050," and Claude Mandil, former DG of IEA).

decommissioning and waste treatment: there are no hidden costs. It should be noted that in NPPs, all costs are included in the price of electricity production, from upstream (exploration of ore, research, etc.) to downstream (waste management, dismantling, geological disposal, etc.). In this accounting system, however, no benefit is drawn from the avoided CO_2 emissions.

The French Court of Auditors (2012) report estimated the historical cost of electricity generation (Gen-II reactors) in France close to €50/MWh. According to the results of this analysis, the total fuel cycle cost would then represent less than 13%, and the back-end cost would be approximately 6.5% of this historical cost. However, additional costs should be taken into account by the utilities for implementing safety improvements as a consequence of the "stress tests": these costs are estimated by the EC to be in the range of €30 million to €200 million per reactor unit (in the EU, total cost of upgrade of NPPs is estimated at approximately €25 billion).

For a series of new-build reactors of the Gen-III type (eg, EPR), electricity production costs are estimated by the 2012 French report to be in the range of €70−90/MWh, taking into account the new technical characteristics: availability nearly 92% (ie, 8000 h/year), overheads amortized over power greater than that of Gen-II reactors, fuel consumption lower than that of Gen-II, service life of 60 years.

At present, cost estimates for electricity production are even higher. For example, in Turkey, the discussion with Rosatom focusses on a fixed price Power Purchase Agreement for 15 years under a Build-Own-Operate scheme: the weighted average cost is US $ 123.5/MWh and the quantity of electricity is fixed. In the UK, EDF has been offered an investment contract for Hinkley Point C (ie, the construction of UK's first nuclear plant in 28 years) with a "strike price" for its electricity output of GBP 92.50 (ie, €125 in 2012 prices) per MWh, which will be adjusted (linked to inflation) during the construction period and over the subsequent 35-year tariff period: this "strike price" for electricity from Hinkley Point C is roughly twice the current wholesale price of power.

Taking construction costs, operation and maintenance (O&M), and fuel cycle costs together, a GIF study regarding future Gen-IV systems estimated the LUEC. The results range as follows (the discount rate was set on 10%): from US $50 per MWh for SCWR to 225 for GFR (in 2009 prices).

GIF Goal no 7 Have a level of financial risk comparable to other energy projects means minimizing Capital-at-Risk (ie, investment before commercial operation): this rewards smaller units that require less capital. Capital investment costs should be seen in the context of the "total social costs" (="private" + "external costs") and the nuclear sector should be compared to renewable and fossil energy sectors.

The private and external costs can be described as follows:

- Private costs: (1) capital investment cost (60−85%); (2) O&M cost (10−25%); and (3) fuel-cycle cost (7−15%) including the natural uranium (~5%).
- External costs: (1) radioactive emissions; (2) long-term waste disposal (often already internalized); (3) accidents—liability; (4) proliferation; (5) avoided CO_2 emissions; (6) system effects (in particular, on electrical grid stability).

A large part of the external costs (outside of the fuel cycle from front-end to back-end) is included in the price of electricity production. They are, however, particularly

difficult to estimate, such as insurance to cover nuclear accident damage (eg, What are reasonable measures to implement? What is the causal link between an accident and disease occurring many years after the event?).

The uncertainty is even greater when it comes to estimating the capital expenditures for new-build reactors, be it Gen-III or Gen-IV. At the end of 2012, EDF announced that stricter regulation in the wake of the Fukushima nuclear disaster contributed to bringing the total cost of the 1600-MW_e Flamanville EPR to €8.5 billion (ie, €5300/kW_e). It should be noted, however, that these are not costs of the EPR series (-nth of a kind), which should be lower.

Construction costs have been estimated by scaling from known cost distributions and adaptation by expert judgment. In addition to scaling to power level, other considerations may lead to increase or decrease certain accounts with respect to the accounts of the reference design, such as the reactor vessel and other reactor plant equipment; space requirements; containment size; application of passive safety systems; need for an intermediate circuit; complex fuel handling in all Gen-IV systems; use of chemically highly reactive sodium as coolant in SFR; use of Rankine versus Brayton cycle. In this way, the previously discussed GIF study estimated the following ranges for overnight construction costs in Euro per kW_e: from 2500 for SCWR to 8500 for LFR (in 2009 prices).

In 2007, the Economics Modelling Working Group (EMWG)[30] of GIF prepared Cost Estimating Guidelines for Generation-IV Nuclear Energy Systems (GIF/EMWG/2007) for economic optimization during the viability and performance phases of the Gen-IV project. This project has upgraded existing nuclear economic submodels, and it developed new ones where needed, addressing each of the following five economic areas: Capital and Production Cost Models, Nuclear Fuel Cycle Model, Optimal Scale Model, and Energy Products Model. These five models have been brought together in an integrated nuclear energy economic model (INEEM). A software tool called G4-Econs (available from the GIF Secretariat at OECD/NEA) has been developed to provide a global economic assessment using the INEEM.

The GIF cost-estimating tool G4-Econs has been applied to identify and assess plant design characteristics of future nuclear reactor designs and their associated fuel cycles. All six Gen-IV designs have been investigated and compared to a reference Gen-III design. The fuel-cycle costs were divided into front-end and back-end costs. When estimating costs for Gen-IV reactor fuel cycles, nonconventional fuels should be taken into account.

In conclusion of Section 10.7, as a result of the application of the EMWG tools, the total capital investment and the LUEC can be estimated for future Gen-IV systems. Breakthrough technologies in the nuclear sector are under development worldwide; they are discussed not only among scientists and engineers, but also with national regulators and civil society (see "Science based policies and legislation" in Topic 8 of "2012 Interdisciplinary Study"[18]). Moreover, a better governance structure is needed

[30] GIF—*Cost Estimating Guidelines for Generation-IV Nuclear Energy Systems*—https://www.gen-4.org/gif/upload/docs/application/pdf/2013-09/emwg_guidelines.pdf.

in energy decision-making processes. Communication with undertakings and public participation, in particular, are crucial in the development of nuclear fission energy policies (see revised 2014 Euratom Safety Directive 9 and 2013 Euratom BSS Directive[10]).

10.8 Proliferation resistance and physical protection (protection against all kinds of terrorism)

The GIF requirement of improved proliferation resistance refers to the following key questions:

1. How to estimate the risk of nuclear proliferation? (Weapons of mass destruction, possible extension to CBRN threats.)
2. How to combat radiological terrorism? (Related to "small weapons" causing contamination.)

One GIF Goal (No. 8) is defined in connection with Proliferation resistance and physical protection:

8. Be a very unattractive route for diversion or theft of weapon-usable materials, and provide increased physical protection against acts of terrorism.

The fear of so-called "rogue nations" acquiring nuclear weapons, or terrorist organizations carrying out malevolent actions by misuse of nuclear materials, clearly remains strong. As a consequence, many political and technological experts are working on reducing the risk of dissemination of nuclear weapons. It should be recalled, however, that during the Cold War, the objective risk of proliferation was high, with more than 20 countries trying to develop nuclear weapons, 9 of which did so. In contrast, since the end of the Cold War, less than a handful of countries have attempted proliferation and only one—North Korea—has succeeded.[31]

Some experts claim that recycling plutonium in the form of MOX fuel helps combat nuclear proliferation by "burning" it in the reactor, whereas other experts claim that isolating, handling, and storing plutonium should be prohibited, because it could be easily diverted by terrorists. The ambition of Gen-IV in this domain focuses on two breakthrough technologies:

1. New reprocessing (partitioning) techniques in which U and Pu are no longer separated as is the case in the traditional PUREX process (Section 10.5), and
2. New fuel fabrication techniques for fast neutron flux reactor (transmutation) systems aiming to use (fertile) ^{238}U to breed (fissionable) ^{239}Pu, while burning the MAs neptunium, americium, and curium (the isotopes ^{237}Np and ^{241}Am, ^{242}Am, and ^{243}Am could be used in a nuclear explosive).

In this context it is worth recalling an important international political initiative: the Global Nuclear Energy Partnership (GNEP), launched by the US Department of

[31] *Nothing to Fear but Fear Itself ? Nuclear Proliferation and Preventive War*, by Debsy and Monteiroz, Pol. Science, Yale University, 2010—http://www.yale.edu/leitner/resources/papers/DebsMonteiro2011-01.pdf.

Energy in 2006. Euratom signed the GNEP agreement to become an "observer organisation" similar to the IAEA and GIF. The original aim of this international partnership was to promote the use of nuclear power and close the nuclear fuel cycle in a way that reduces waste and the risk of nuclear proliferation. The GNEP proposal would divide the world in two parts:

- fuel supplier nations, which supply enriched uranium fuel and take back spent fuel once the advanced recycle technologies are demonstrated and deployed (fuel reprocessing and burning of plutonium and MAs would occur in advanced burner reactors of Gen-IV type), and
- user nations, which operate NPPs under appropriate conditions (in addition to avoiding the capital investment of building a fuel-handling infrastructure, a comprehensive package of fuel service benefits could include "cradle-to-grave" fuel leasing that incorporates "used fuel take-back").

Some countries and analysts, however, criticized the GNEP proposal for discriminating between countries as nuclear fuel cycle "haves" and "have-nots." The partner countries of the GNEP then formally agreed in 2010 to transform the partnership into the International Framework for Nuclear Energy Cooperation (IFNEC)[32] and adopted a new mission statement. The scope of IFNEC is broader, with wider participation (34 participant countries, 4 observer organizations, including Euratom, and 31 observer countries). This allows it to explore mutually beneficial approaches to ensuring the expansion of nuclear energy for peaceful purposes in a manner that is efficient, safe, secure, and that supports nonproliferation and safeguards.

Also interesting is the international initiative on a holistic Safety, Security, and Safeguards concept ("3S") for nuclear energy that was launched with the G8 Nuclear Safety and Security Group at the G8 summit of 2008,[33] and is converging on the idea of internationally binding security and safety standards in collaboration with the IAEA. DG JRC in the European Commission is conducting many research and development actions in the "3S" domain in collaboration with the IAEA. As security threats are usually treated in separate national tracks, however, the ultimate technologies (software and hardware) in this sensitive domain are not shared on a wide scale.

As far as terrorism is concerned, the question of cyberterrorism should be raised (eg, an attack causing serious damage to a critical infrastructure). Until now only hackers were involved in cyberterrorism actions targeting industrial systems. In the nuclear sector, the computer worm Stuxnet, discovered in June 2010, was created to attack Iran's nuclear facilities: it went via Microsoft Windows and targeted Siemens industrial control systems. The widely suspected probable target was the uranium enrichment infrastructure in Iran: the Iran nuclear program has indeed been damaged.

[32] *International Framework for Nuclear Energy Cooperation* ("Steering Group," chair is the United States, Vice Chairs are France, China, and Japan; "Infrastructure Development Working Group," chairs are the United Kingdom and the United States; and "Reliable Nuclear Fuel Services Working Group," chairs are France and Japan) http://www.ifnec.org/.

[33] G8 Leaders Stress Safe, Peaceful Nuclear Development at their summit in Japan from 7 to 9 July 2008 (G8 = Canada, France, Germany, Italy, Japan, Russian Federation, the UK, and the United States—the EU also participates—https://www.iaea.org/newscenter/news/g8-leaders-stress-safe-peaceful-nuclear-development.

It has been demonstrated that other types of cyber attacks could destroy items such as vulnerable physical components of the electric grid.

In 2011, the Proliferation Resistance and Physical Protection (PR&PP) Working Group of GIF prepared a document that describes the *Evaluation methodology for PR&PP of* Generation-IV nuclear energy systems—Rev. 6 (GIF/PRPPWG/2011/003).[34] For a proposed design, the methodology defines a set of challenges, analyzes system response to these challenges, and assesses outcomes. Uncertainty of results is recognized and incorporated into the evaluation at all stages. The results are intended for three types of users: system designers, program policy-makers, and external stakeholders.

The PR&PP methodology can be applied to the entire fuel cycle or to portions of a design. It was developed, demonstrated, and illustrated by use of a hypothetical "example sodium fast reactor" (ESFR), by members of the PR&PP Working Group. The ESFR case study was the first opportunity to test the full methodology on a complete system, and many insights were gained from the process. Others, in Euratom and national programs, have adapted the PR&PP methodology to their specific needs and interests, such as the following:

- in the United States the methodology has been used to evaluate alternative spent fuel separations technologies, and
- in Belgium the PR&PP methodology was used in the proliferation resistance analysis of the MYRRHA accelerator-driven system.

10.9 Conclusion: a new way of "developing/teaching science," closer to the end-user needs of the 21-st century (society and industry)

In this chapter, Gen-IV research and training actions are discussed in the context of the Euratom Horizon-2020 program in nuclear fission and 2014 "Energy Union Package." It should be recalled that the EU energy mix policy (based on renewable, fossil and fissile primary energy sources) is based on three fundamental criteria: sustainable development, security of supply, and industrial competitiveness. The five-decade history of research, development, and continuous improvement of Gen-I, -II, -III, and -IV is briefly discussed. A number of scientific-technological and sociopolitical challenges are discussed in connection with the R&D as well as demonstration deployment of Gen-IV reactor systems and associated fuel cycle facilities.

The "Technology Roadmap" for the six GIF systems (originally in 2002, updated in 2013) is presented in connection with the main goals for Gen-IV systems, ie,:

- sustainability (efficient resource utilization and minimization of radioactive waste),
- safety and reliability (maximum safety performance through design, technology, regulation, and culture),

[34] GIF—*Evaluation methodology for PR and PP of Gen-IV*—https://www.gen-4.org/gif/jcms/c_9365/prpp.

- socioeconomics (economic advantage over other energy sources and better governance structure in energy decision-making process),
- proliferation resistance and physical protection (protection against all kinds of terrorism).

The role of the SNE-TP/ESNII in the Euratom program is explained in the context of the EU energy mix policy (following the three fundamental criteria). As a consequence, Euratom research and training actions in Gen-IV put special attention on fast neutron spectrum reactor systems. Such an economy would extract much more energy per ton of uranium than is obtained from other reactors (gain factor of 60 as compared to LWR fleet). As a consequence, Gen-IV systems of the fast neutron type contribute to satisfying the two fundamental criteria of sustainability and security of supply. As regards the last fundamental criterion of competitiveness, lots of efforts are currently dedicated by both the research community and the industrial organizations concerned: the aim is to reduce drastically costs of installed capacity (MW_e) and of power generation (MWt).

The future Euratom research and training program (after Horizon-2020) is aimed at answering the following questions raised by the Scientific and Technical Committee (Euratom Treaty—Article 7) to the Euratom community in their 2014 fall meeting:

- What should be the immediate research priorities to be considered at EU level?
- What are the key assumptions underpinning the development of these priorities?
- What is the output and impact that could be foreseen if the development of these priorities is successful?
- Which are the bottlenecks, risks and uncertainties, and how could these be addressed?
- Which science and technology gaps and potential game changers need to be taken into account?
- What are the perspectives for crossthematic activities with other areas of Euratom research and with Horizon 2020?
- What are the perspectives for supporting horizontal activities? notably: international cooperation; education and training; social sciences, and humanities.

In conclusion, currently in the EU, research and innovation programs (in particular in the nuclear fission sector) are conducted in the context of a new governance structure, based on more openness, participation, accountability, effectiveness, and coherence. Participation of all stakeholders (in particular through the "European Technology Platforms") in joint Euratom projects helps build the confidence climate that is needed to continuously improve applications of nuclear fission energy, notably Gen-IV reactor systems. A strong interaction is maintained in Euratom among research, innovation, and education actions based on the participation of all stakeholders, ie,

- research organizations (eg, public and private sectors),
- systems suppliers (eg, nuclear vendors, engineering companies),
- energy providers (eg, electrical utilities and associated fuel cycle industry),
- nuclear regulatory authorities and associated TSOs,
- higher education and training institutions, in particular universities, and
- civil society (eg, policy-makers and opinion leaders), interest groups, and NGOs.

Euratom is aiming at continuously improving collaboration between the scientific research community and policy-makers, in particular, in the context of the Gen-IV

International Forum (GIF). In fact, a new way of "developing/teaching science" is emerging in the EU, closer to the end-users' needs (ie, society and industry) of the 21st century. As a result, a strong scientific foundation is being established to support decision-making in regulatory and/or industrial organizations based on confirmed facts and research findings stemming from "best-available science" (hard and soft sciences).

Nomenclature

ALFRED	Advanced lead fast reactor European demonstrator
ALLEGRO	Gas cooled fast reactor demonstrator
BEPA	Bureau of European Policy Advisers
BOO	Build-own-operate
CAPEX	Capital Expenditures
CNRS	Centre National de la Recherche Scientifique (English: The French National Centre for Scientific Research, France)
CPD	Continuous professional development
DBA	Design basis accidents
DEVCO	International Cooperation and Development (EC Directorate General)
DG	Directorate General (Department of European Commission)
E&T	Education and training
EFSI	European fund for strategic investments
EFTS	Euratom fission training scheme (funded by EC DG RTD)
EGE	European group on ethics in science and new technologies
EMWG	Economics modelling working group (GIF methodology)
ENEN-III	"European nuclear education network" FP7 Euratom project dedicated to training schemes for Generation-III and -IV (conceptual design)
ENSREG	European nuclear safety regulators group
EQF	European Qualification framework for lifelong learning (8 levels)
ESNII	European sustainable nuclear energy industrial initiative
ETP	European technology platforms (stakeholder groups providing guidance)
EU-28	European Union (28 Member States)
EUR	European utility requirements
Euro	European currency (1€ = 1.1062 US$, average over year 2015)
FALCON	Fostering ALFRED construction
FP-7	Seventh framework program/EU research and innovation/(2007−13)

F(B)R	Fast (breeder) reactor
Horizon-2020	EU program of research and innovation (2014−20)
HM	Heavy metal
IET	Institute for energy and transport (EC DG JRC, Petten, the Netherlands)
IFNEC	International framework for nuclear energy cooperation
IRMM	Institute for reference material and Measurements (EC DG JRC, Geel, Belgium)
ISAM	Integrated safety assessment methodology (GIF)
ITU	Institute for transuranium elements (EC DG JRC, Karlsruhe, Germany)
JHR	Jules Horowitz Reactor (CEA Cadarache, France)
JRC	Joint research Center (one of the EC Directorate Generals)
KSC(A)	Knowledge, skill, and competence (attitudes)
LEADER	Lead-cooled European advanced demonstration reactor
LERF	Large early release frequency
LUEC	Levelized unit energy costs
MA	Minor Actinides [eg, neptunium (Np), americium (Am), curium (cm)]
MS	Member State
MS(F)R	Molten salt (fast) reactor system
MTA	Hungarian Academy of Science (Budapest, Hungary)
MYRRHA	Multipurpose hybrid research reactor for high-technology applications (SCK-CEN, Mol, Belgium)
NC2I	Nuclear cogeneration industrial initiative (part of SNE-TP)
NGO	Nongovernmental organization
NRG	Nuclear research and consultancy group (Petten, the Netherlands)
NSSG	Nuclear safety and security group
NUGENIA	Nuclear Generation-II and -III Association (part of SNE-TP)
PALLAS	Dutch research reactor (successor of HFR)
PIRT	Phenomena identification and ranking table
PR&PP	Proliferation resistance and physical protection group (GIF methodology)
RATEN-ICN	Regiei Autonome Tehnologii pentru Energia Nucleara—Institutul de Cercetari Nucleare Pitesti (English: Technologies for Nuclear Energy—Institute for Nuclear Research Pitesti, Romania)
RDDD	Research—Development—Demonstration—Deployment

Continued

RSWG	Risk and safety working group (GIF methodology)
R&T	Research & Training
RTD	Research and technological development (also research and innovation EC Directorate General)
3S	Safety, security, and safeguards
SARGEN-IV	Safety assessment for reactors of Gen-IV (FP6 Euratom project)
SCK-CEN	Studiecentrum voor Kernenergie—Centre d'Étude de l'énergie Nucléaire (Nuclear research centre, Mol, Belgium)
SET-plan	"Strategic energy technology" plan
SNF	Spent nuclear fuel
SMRs	Small and Medium Reactors
SNE-TP	Sustainable nuclear energy technology platform
SRA	Strategic research agenda
STC	Scientific and technical committee
TMI	Three Mile Island
TSO	Technical Safety Organization
UJV	ÚSTAV JADERNÉHO VÝZKUMU Řež, UJV REZ, Czech Republic (in English: Nuclear Research Institute plc, Husinec—Řež)

Appendix: Tentative training scheme for preconceptual Generation-IV design engineers (knowledge, skills, attitudes)

Tentative training scheme for the development and pre-conceptual design of Generation-IV nuclear reactors (preliminary version—Euratom, 2011)
Source: ENEN-III PROJECT (Contract no. FP7 - 232629)

Start date of project: 01/05/2009 Duration: 36 months.
(ENEN, *European Nuclear Education Network* - http://www.enen-assoc.org)
Deliverable no. D 1.5 (produced by SCK-CEN and AREVA GmbH/20/10/2011)

Abstract

This Euratom Fission Training Scheme (EFTS) defines in detail the competence required for engineers dedicated to development and preconceptual design of Generation-IV nuclear reactors. Three key learning categories (namely knowledge, skills, and attitudes) are structured in detail to develop the variety of 'learning outcomes' to be achieved by the participant of the training program for effective fulfillment of the respective job profile.

Bibliographic references:

1. D. Kennedy, Á. Hyland, N. Ryan, Writing and Using Learning Outcomes: a Practical Guide, EUA Handbook, March 2009.
2. IAEA Safety Series, INSAG-4, Safety Culture, Vienna, 1991.

A1. Introduction

This report defines learning outcomes for the training of engineers who are involved in the development and preconceptual design of Generation-IV nuclear reactors. The training scheme is in line with the Strategic Research Agenda (SRA) of the Sustainable Nuclear Energy Technology Platform (SNE-TP), which was published in 2009. It therefore includes areas of interest that would give the trainees the possibility to find answers to the R&D challenges mentioned in the SRA, among others:

- Primary system design simplification
- Improved materials
- Innovative heat exchangers and power conversion systems
- Advanced instrumentation, in service inspection systems
- Enhanced safety

- Partitioning and transmutation
- Innovative fuels (including MA) and core performance.

All six Generation-IV reactor types are targeted in this training scheme: the lead fast reactor (LFR), sodium fast reactor (SFR), gas fast reactor (GFR), very high temperature reactor (VHTR), super critical water reactor (SCWR), and molten salt reactor (MSR).

A2. Trainees prerequisites

The technological challenges characteristic to the design of all different Generation-IV reactor types are highly complex and demand specialized, multidisciplinary, and cross-cutting knowledge and skills. Therefore, this training scheme can only be open to at least nuclear engineers or engineers (EQF level 7) with an additional nuclear education.

A3. Knowledge, skills, and attitudes required for a Generation-IV engineer

The following domains have been identified by relevant employers and training organizations as essential for the training of Generation-IV engineers:

Knowledge: General knowledge on Generation-IV systems and technology; design specific knowledge for the LFR, SFR, GFR, VHTR, SCWR, and MSR
Skills: Working with self-developed engineering tools or off-the-shelf tools; working with nuclear design codes; cost estimates (costs, time) for the engineering work; order processing (project management)
Attitudes: formal quality control of result reports; individual, critical examination of the tasks; presentation and documentation of work results; teamwork/communication.

A4. Learning outcomes related to knowledge, skills, and attitudes for a Generation-IV engineer

A4.1 Learning outcomes in the knowledge *area* (learning to know)

A4.1.1 General knowledge on Generation-IV systems and technology

For example: LO K no. 9 related to "Structural materials for Gen-IV reactors"

1. Explain the main material challenges for the construction of Generation-IV reactors.
2. Identify the main classes of structural materials for Generation-IV reactors: steels; oxide dispersion strengthened (ODS) steels; refractory alloys; ceramics; composites.
3. Describe the main characteristics of these different structural material classes.
4. Identify criteria to select suitable structural materials for the various components of Generation-IV reactors.
5. Recall the methodology used for performing a structural integrity analysis.

6. Develop an experimental and multiscale modelling approach for Generation-IV materials research.
7. Describe the main factors which limit components lifetime and underlying phenomena: interaction with coolant; high temperatures; radiation effects; irradiation creep; …
8. Acknowledge the role of material scientists in design and licensing of Generation-IV reactors.
9. List the existing programs in material research for Generation-IV reactors (ESNII, FP7.).

A4.1.2 Design specific knowledge for the lead fast reactor

……..

A4.1.3 Design specific knowledge for the sodium fast reactor

…….

A4.1.4 Design specific knowledge for the gas fast reactor

……

A4.1.5 Design specific knowledge for the very high temperature reactor

…….

A4.1.6 Design specific knowledge for the super critical water reactor

……

A4.1.7 Design specific knowledge for the molten salt reactor

……

A4.2 Learning outcomes in the skills *area* (learning to do)

In contrast to the learning outcomes in the knowledge area, that are different when looking at Generation-III or Generation-IV reactor design, the learning outcomes in the skills area for an engineer working on Generation-IV will be similar to those in training schemes for the Generation-III design engineers. The skill categories can also be summarized in the following areas:

- Analytical Skills
  Engineers working on Generation-IV should be able to solve analytical complex thermohydraulic problems. The capability of using advanced tools like Vantage Plant Engineering Systems, eg, CATIA or thermohydraulic codes like RELAP should be a self-understood skill for this category of engineers.

- "Hands-On (Manufacturing)" Skills
  The learning outcomes in the area of "Hands-on" skills are most suitable to be achieved during experimental work and practical training at small scale facilities.
- Communication and Organizational Skills
  In an R&D environment communication and organizational skills are essential to promote successful collaboration between researchers that are part of different units or institutes. The Generation-IV projects generally are complex projects dealing with cross-cutting disciplines, involving partners from different countries. All engineers working on these projects will benefit from acquiring the skills addressed in this area of interest.

For example, LO S no. 2 related to "Hands-On (Manufacturing)"

1. Use tools required for system layout and design, such as (1) system layout: VPE, PDMS CATIA etc; (2) core prediction codes, eg, SCALE; (3) core and system thermohydraulic codes like ANSYS-CFX, RELAP, and CATHARE etc (4) drawing tools like AutoCAD, CATIA, Corel Designer; and (5) documentation tools.
2. Perform operations related to a test scale reactor such as (1) repeat procedure "reach criticality," (2) calibrate nuclear instrumentation, eg, neutron detectors, and (3) install and calibrate instrumentation for radiation detection.
3. Perform operations at a small-scale test loop such as (1) calibrate closed control loops by adjusting different deviation parameters, (2) investigate cavitation situation, (3) start/stop open-loop controllers attached to the test loop, (4) indicate the positions for the necessary instrumentation during specific tests, and (5) calibrate nonnuclear instrumentation, eg, temperature and flow rate sensors.
4. Use effectively tools required for communication purposes such as (1) MS Office Tools, (2) content management tools, (3) modern email features, and (4) language translation tools like dictionaries etc.
5. Use valid data bases of regulations, standards, components etc.

A4.3 Learning outcomes in the attitude *area* (learning to live together and/or learning to be)

As is well known, it is one of the most difficult tasks to change the behavior of an individual. Anyway this training scheme should provide a number of learning outcomes to be achieved especially, during the internship or on-the-job training period. A relatively simple separation is proposed, consisting in two categories based on the actions of the individual:

- Passive attitude
  In this context "passive" means not the absence of any kind of response, but rather reactions related directly with his or her personality. Verbs like value, accept, be aware, have confidence, listen, or embrace would be most appropriate to describe one's association with a positive attitude toward nuclear domain. This kind of attitudes could be understood under the more general term of "behavior."
- Active Attitude
  As a result of firm beliefs and convictions, an individual will not only accept and value the necessary attitude for his or her field, but he or she will act on changing the others' attitude. Again a number of verbs can help to understand the actions of such individuals: act, ask, answer, defend, justify, share, or question. This kind of attitudes could be understood under the more general term of "human performance."

For example, LO A no. 2 related to "active attitude (human performance)"

1. Promote information transmission within the project
2. Questioning attitude toward nuclear safety and safety culture
3. Act solution oriented based on principal "What is right and not who is right?"
4. Express interest in reduction of radiation exposure through intelligent and crossover disciplines design
5. Ask for support during daily activities whenever difficulties encountered
6. List the main requirements necessary for the achievement of a strong fundamental safety culture
7. Clearly state that a safety culture is connected with a proper operating/design organizations
8. Show how operating experience can reflect the weaknesses or strong points of an existing safety culture
9. Manifest interest for the changes induced by modification of safety standards and norm application
10. Respect the protocols and procedures, but keep a questioning attitude
11. Encourage an open communication spirit and channels, by interacting with people and encouraging expression of points of view (within team, between teams, departments, and businesses)
12. Point out mistakes or violation of safety rules and protocols
13. Make safety culture a daily priority by the beginning of the work

Generation IV concepts: Japan

11

H. Kamide, H. Ohshima, T. Sakai, M. Morishita
Japan Atomic Energy Agency, Ibaraki, Japan

11.1 Introduction

With respect to advanced reactor designs, Japan has put most of its resources and efforts into the development of sodium fast reactors (SFRs), which consist of a key element of the closed-loop nuclear fuel recycling system along with spent fuel reprocessing technology. Japan's efforts for SFR development go back to the 1970s, when the experimental reactor JOYO was designed and constructed with a thermal capacity of 75 MW_{th} and a loop-type system. JOYO reached its first criticality in 1978 (Maeda et al., 2005) and uprated to 140 MW_{th} in 2003 to upgrade the irradiation test capacity of the reactor. Then design and construction of the prototype power reactor named MONJU began in the 1980s, also with a loop-type system. MONJU was first taken critical in April 1994 and generated electricity for the first time in August 1995 (Kondo et al., 2013). For MONJU, efforts are now being made to prepare the application for the safety review by the regulatory authority under the new safety regulation set forth after the Fukushima-Daiichi accident in 2011.

With a purpose of probing a commercially feasible fast reactor system, a feasibility study on commercialized fast reactor cycle systems (FS) was initiated in 1999 (Aizawa, 2001). In the FS, survey studies were made to identify the most promising concept among various systems such as sodium-cooled fast reactors, gas-cooled fast reactors, heavy metal-cooled fast reactors (lead-cooled fast reactors and lead-bismuth cooled fast reactors), and water-cooled fast reactors with various fuels types such as oxide, nitride, and metal fuels. The FS concluded to select an advanced loop-type SFR with mixed oxide fuel named Japan sodium-cooled fast reactor (JSFR; Kotake et al., 2005).

On the basis of the conclusion of the FS as well as check and review by relevant government bodies, a project named the Fast Reactor Cycle Technology Development (FaCT) project was launched in 2006 by the Japan Atomic Energy Agency (JAEA) under cooperation with the Ministry of Education, Culture, Sports, Science and Technology of Japan; the Ministry of Economy, Trade and Industry of Japan; electric utilities; and vendors as an advanced stage toward commercialization of fast reactor cycle technology by 2050. In the FaCT project, both a conceptual design study of JSFR with several key innovative technologies adopted and the research and development (R&D) on these innovative technologies were conducted. The development targets related to sustainable energy production, radioactive waste reduction, safety equal to the future light water reactor, and economic competitiveness against other future energy sources

Handbook of Generation IV Nuclear Reactors. http://dx.doi.org/10.1016/B978-0-08-100149-3.00011-2
Copyright © 2016 Elsevier Ltd. All rights reserved.

were presented by the Japan Atomic Energy Commission, which is consistent with the goals of Generation IV International Forum (GIF; USDOE and GIF, 2002).

In 2010, at the end of Phase I of the FaCT project, technical assessments on the achievement of the development targets and feasibility of the innovative technologies were made. The purpose of this assessment was to evaluate the degree of achievement at that time in the midterm stage until 2015, to affirm the validity of the direction of R&D, and to identify technical challenges toward future R&Ds. As a result of the assessments, it was revealed that the development targets were mostly achieved, and some challenges that may indicate the direction of future R&D were identified (Chikazawa et al., 2015).

The finalization of the FaCT Phase I and initiation of FaCT Phase II, which is the demonstration phase of the innovative technologies, were suspended because of sociopolitical situation changes after the Great East Japan Earthquake of March 11, 2011. Since 2011, to contribute to the development of the safety design criteria (SDC), which include the lesson learned from TEPCO's Fukushima-Daiichi nuclear power plants accident, in the framework of GIF, the design study is focusing on the design measures against severe external events such as earthquakes and tsunamis. At the same time, the design study is going into detail and paying much attention to the maintenance and repair to make its feasibility more certain.

This chapter is focused on the design features of JSFR and the accompanying key innovative technologies. The conformity of JSFR design to the SDC by GIF and reflections on lessons learned from Fukushima are also discussed.

11.2 JSFR design and its key innovative technologies

11.2.1 General design features of JSFR

The very basic target of JSFR development is to achieve sustainable energy supply by SFRs by reducing radioactive materials, achieving safety equal to that of future light water reactors, and realizing economic competitiveness against other future energy sources.

With this target in mind, a plant design concept was established for JSFR. It is a loop-type plant with a two-loop heat transport system. Designs for a commercial version with 1500 MW_e and a demonstration version with 750 MW_e are pursued in the design study. A bird's eye view of the nuclear steam supply system (NSSS) of JSFR design is illustrated in Fig. 11.1, and the major design specifications are summarized in Table 11.1 for the demonstration version design.

JSFR utilizes the advantage of "economy of scale" by setting the electricity output of 1500 MW_e and it has an economic competitiveness that benefits from advanced design, such as simplified and compact structure of the reactor, integration of the intermediate heat exchanger (IHX) and the primary circulation pump, shortened piping layout, and reduction of loop number. Furthermore, a special effort has been made to meet the safety requirements, which include enhancement of passive safety capabilities and the in-vessel retention of degraded core under a core disruptive accident.

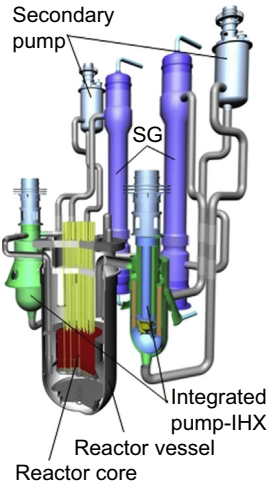


Figure 11.1 Bird's eye view of NSSS of JSFR. *IHX*, intermediate heat exchanger; *SG*, steam generator.

These measures are expected to be more realistic by introducing some innovative technologies such as Mod.9Cr-1Mo steel with high strength at high temperatures, advanced elevated temperature structural design standards, two-dimensional seismic isolation, and a re-criticality free core as well as by taking the desirable characteristics of sodium coolant such as operability in a low-pressure system and excellent heat transfer characteristics into account.

The guard pipes are provided for primary and secondary cooling systems, and those annular spaces would be filled with inert gas. There are no penetrations in the primary cooling system, and there is only one penetration for the sodium drain line in the secondary cooling system. The penetration would be covered by the guard pipes of a double boundary system. As for the steam generator (SG), a conventional single-tube helical type has been adopted. This type of SG is required to enhance the reliability of an early detection system against a water leak. The earlier detection system, especially against small leaks, would be needed to prevent the propagation of tube failures for early restarting of plant operation because the detection sensitivity would become worse in the larger SGs of the advanced loop concept.

A schematic of the reactor and cooling system is shown in Fig. 11.2. Two intermediate reactor auxiliary cooling systems (IRACSs) and one direct reactor auxiliary cooling system (DRACS) have been applied as a decay heat removal system (DHRS) suitable for the two-loop cooling system and the adopted type of SG. These systems are passive type by natural circulation.

To enhance the passive decay heat removal capability by natural circulation, the pressure drop of the core has been limited below 0.2 MPa, and the difference of elevation between the core and heat exchangers has been enlarged, such as 38.7 m between the core and air cooler of IRACSs and 37.9 m between the core and the air cooler of DRACS. The in-service inspection and repair capabilities are improved to

Table 11.1 Major design specifications of demonstration Japan sodium-cooled fast reactor

Electricity output	750 MW_e
Thermal output	1765 MW_{th}
Number of loops	2
Primary sodium	
Temperature	550/395°C
Flow rate	1.62×10^7 kg/h per loop
Secondary sodium	
Temperature	520/335°C
Flow rate	1.35×10^7 kg/h per loop
Main steam	
Temperature	497°C
Pressure	19.2 MPa
Feed water	
Temperature	240°C
Flow rate	1.44×10^6 kg/h
Plant efficiency	~42%
Fuel type	Trans-uranium mixed oxide
Burn-up (average) for core fuel	~150 GWd/t
Breeding ratio	Breakeven (1.03), 1.1, 1.2
Cycle length	26 months or less Four batches
Structural materials	
Reactor block	316FR
Heat transport system	Mod.9Cr-1Mo steel

confirm the integrity of internal structures, including core support structure, and coolant boundaries.

Fig. 11.3a shows a vertical sectional view and Fig. 11.3b shows the top of the reactor block. At the near center of the reactor vessel (RV) is a rotating plug (RP), and outside the plug is a fixed deck. At this fixed deck, there are hot legs, cold legs, a direct heat exchanger, an auxiliary core cooling system, sodium level meters, in-vessel neutron instrumentation systems, and cold traps (CTs). The height of the upper plenum is 9.3 m, including the cover gas region. In the plant operation normal sodium level (NSL) is 1.6 m below the bottom of the RV, and during the refueling sodium level (FSL) is 3.1 m below the bottom of the RV. Dip plates (DPs) are hung from the RP, and the vertical level of the DP is slightly below the FSL. The diameter of

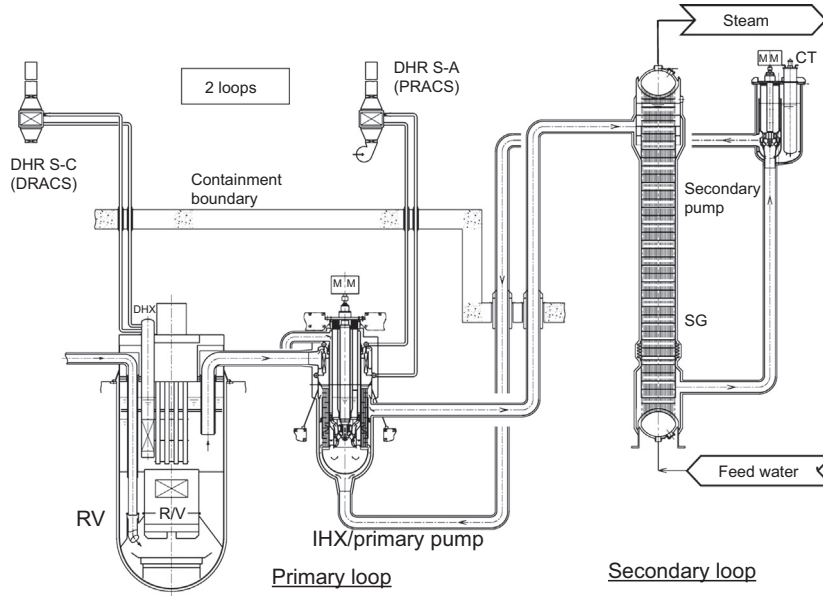


Figure 11.2 Japan sodium-cooled fast reactor and cooling system. *DHR S-C*; *DHR S-A*; *CT*, cold trap; *RV*, reactor vessel; *IHX*, intermediate heat exchanger; *SG*, steam generator; *DRACS*, direct reactor auxiliary cooling system; *PRACS*, primary reactor auxiliary cooling system.

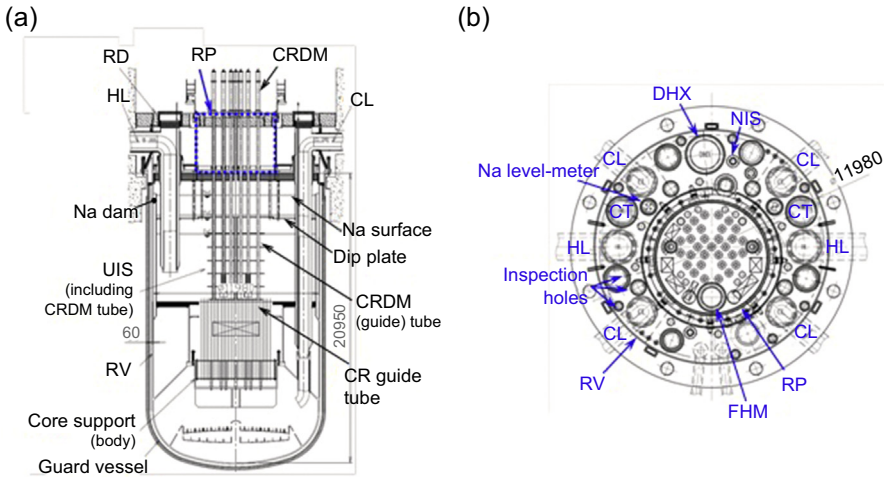


Figure 11.3 Reactor vessel (a) vertical section and (b) horizontal section at the top. *RD*; *RP*, rotating plug; *CRDM*; *CL*, cold leg; *CR*; *RV*, reactor vessel; *HL*, hot leg; *DHX*, direct heat exchanger; *NIS*, neutron instrumentation system; *FHM*, fuel handling machine.

the RV is 11.98 m, including the sodium dam, the width of which is 0.2 m. The dam is a bottom-closed dual vessel, and the highest level of the dam is slightly above the NSL. The bottom of the dam is in the middle plenum, which is under negligible creep condition.

For the safety design (Kotake et al., 2009; Kubo et al., 2011), JSFR adopts the defense-in-depth (DiD) principle according to the SDC for SFRs by the GIF. The plant states in SDC are normal operation, anticipated operational occurrences, design-basis accidents (DBAs), and design extension conditions (DECs). The deterministic approach is adopted considering DBAs to specify safety functions such as a reactor shut-down system (RSS) and a DHRS for prevention of core damage. JSFR installs several design measures against severe accidents, explicitly taking into account those accidents as DECs. In addition to the DiD principle, JSFR also adopts a risk-informed approach that plays a role in considerations on the proportion or balance of different levels of DiD.

Securing reactor shutdown, two independent RSSs (ie, primary and backup RSSs) are installed. Each RSS is initiated by independent/diversified signals from the reactor protection system. The fourth level of DiD considers design measures against DECs. In this level, including prevention and mitigation of severe accidents, the RSS provides passive shut-down capability by means of self-actuated shut-down system (SASS). Performances of the SASS had already been confirmed through the transient experiments in a sodium loop, and reliability testing has been achieved by installing SASS mock-up into JOYO (Takamatsu et al., 2007).

The re-criticality free core concept is adopted in JSFR and has the great importance to ensure the in-vessel retention scenario against whole-core disruptive accidents. Energetics due to exceeding the prompt criticality in the initiating phase must be prevented by means of restriction of the sodium void worth and the core height (Sato et al., 2011). The possibility of molten fuel compaction must be prevented by enhancing the fuel discharge from the core, adopting fuel assembly with an inner duct structure (FAIDUS).

For measures against sodium leak, all sodium and cover gas boundaries are double structured. The RV and the guard vessel (GV) are simple structures with piping penetration on the roof deck without nozzles on the vessel wall. In addition, the piping system is also simplified, eliminating branch piping as possible. With those design measures the possibility of loss of reactor level (LORL) was evaluated to be less than the target value (Kurisaka, 2006).

The DHRS consists of a combination of one loop of DRACS and two loops of the primary reactor auxiliary cooling system (PRACS). The heat exchanger of DRACS is dipped in the upper plenum within the RV. The heat exchanger of each PRACS is located in the primary-side upper plenum of an IHX. All of these systems can be operated based on a fully passive feature with natural circulation, which requires no active components such as pumps (Yamano, 2010).

Because JSFR adopts fully natural-circulation DHRS, JSFR is free from heavy electric load and quick activation of the emergency electric supply. JSFR is then capable of using a self-air−cooling gas turbine generator (GTG) independent from the components cooling water system (CCWS; Hishida et al., 2007). In fact, JSFR CCWS is nonsafety grade because of the natural convection DHRS and self-air−cooling GTG. This

configuration reinforces defense against external hazards. In the case of external hazards such as tsunamis, the CCWS could be damaged, as seen in the Fukushima-Daiichi accident, because the heat sink of CCWS depends on sea water.

For seismic design, JSFR adopts an advanced seismic isolation system for SFR that mitigates the horizontal seismic force by thicker laminated rubber bearings with a longer period and the improvement of damping performance by adopting oil dampers (Okamura, 2011).

A compact plant component layout is achieved by adopting an L-shaped hot-leg piping, a combined IHX/pump component, a once-through−type SG, and other technologies, which leads to a cost reduction through fewer plant materials.

Because SFR is a high-temperature reactor operated at creep temperature range, the selection of structural materials is very crucial. In the JSFR design, an austenitic stainless steel 316FR is used for the RV and its internal structures. 316FR is a material developed in Japan for fast breeder reactors. The chemical composition of the conventional 316 stainless steel was modified to improve creep resistance; the carbon content was lowered and nitrogen and phosphorous were added (Asayama et al., 2013; Onizawa 2013a,b; JSME, 2012). Mod.9Cr-1Mo steel is used for the primary and secondary heat transport systems, expecting its high strength at elevated temperatures and low thermal expansion. Mod.9Cr-1Mo steel is basically the same material as the ASTM/ASME Grade 91 steel (Asayama et al., 2013; Onizawa 2013a,b; JSME, 2012).

11.2.2 Key innovative technologies in the Japan sodium-cooled fast reactor design

JSFR achieves the FaCT development targets and the Generation IV reactor goals by adopting the following key technologies:

1. high burn-up core with oxide-dispersion-strengthened (ODS) steel cladding material,
2. safety enhancement with SASS and re-criticality free core,
3. compact reactor system adopting a hot vessel and in-vessel fuel handling with a combination of an upper internal structure (UIS) with a slit and advanced fuel handling machine (FHM),
4. two-loop cooling system with large-diameter piping made of Mod.9Cr-1Mo steel,
5. integrated IHX/pump component,
6. reliable SG with double-walled straight tube,
7. natural-circulation DHRS,
8. simplified fuel handling system (FHS),
9. steel plate−reinforced concrete (SC) containment vessel (CV), and
10. advanced seismic isolation system.

The technical feasibility of these technologies has been confirmed by various experimental tests and numerical computations that will be discussed hereafter.

11.2.2.1 High burn-up core

One of the important targets in the core design is to achieve a high core average burn-up up to approximately 150 GWd/ton by the ODS ferritic steel application to

the cladding material. The most important key technology for this high-performance core is advanced cladding that can stand with the target discharge burn-up of 150 GWd/ton, and the ODS steel cladding has the potential to meet this requirement. Two ODS steel claddings have been developed: a 9Cr-ODS and a 12Cr-ODS.

Fast reactor core materials including the fuel cladding tube suffer severe radiation damage by high-dose fast neutron irradiation at high temperatures. Thus irradiation resistance (ie, swelling resistance and resistance to mechanical property degradation under irradiation) and high-temperature strength are indispensable for fast reactor core materials. Conventional alloys for a fast reactor cladding tube are modified type 316 stainless steels, which have substantial industrial backgrounds, adequate strength at high temperature, and improved swelling resistance by microstructure optimization (Ukai et al., 1998; Akasaka et al., 2001). However, high-dose neutron irradiation exceeding approximately 100 dpa leads to onset of swelling in this type of alloy, thus increasing the risk of flow channel obstruction in the fuel assembly. JAEA has been developing ODS ferritic steel for the long-life fuel cladding tube that can be used in the high burn-up and high-temperature irradiation environment: average discharge burn-up to 150 GWd/ton, peak neutron dose to 250 dpa, and maximum temperature to 973 K (Shimakawa et al., 2002; Kaito et al., 2007). ODS steels have matrices highly resistant to irradiation-induced swelling (ie, tempered martensitic matrix and fully ferritic matrix). Nanosized oxide particle dispersion in the matrix improves the high-temperature creep strength for the long duration. Therefore ODS steels have a good combination of swelling resistance and creep strength.

JAEA has been developing two types of ODS steels: ODS-tempered martensitic steel (9Cr, 11Cr) and ODS recrystallized ferritic steel (12Cr). In JAEA the ODS-tempered martensitic steels are ranked as primary candidate material because of their superior irradiation resistance and manufacturability. JAEA derived neutron irradiation data of 9Cr, 12Cr-ODS steel cladding tubes using JOYO (Kaito et al., 2009; Yano et al., 2011). Postirradiation examination revealed adequate irradiation resistance of the ODS steels (ie, very small degradation of mechanical strength and ductility by neutron irradiation). ODS steels are fabricated by a powder metallurgy process, which does not necessarily have plenty of industrial background. Therefore the fabrication technology development of the ODS steel cladding tube is an important task. JAEA has already completed the development of laboratory-scale fabrication technology including tube manufacturing, welding, and inspection technology (Kaito et al., 2007; Uehira et al., 1999).

11.2.2.2 Safety enhancement

For reactor shutdown, two independent RSSs (primary and backup) are installed. In addition to the two independent systems, an additional passive shut-down system using a Curie point-type SASS is adopted. The SASS, which is schematically illustrated in Fig. 11.4, is a device that provides passive shut-down capability in the case of anticipate transient without scram (ATWS) such as unprotected loss of flow, unprotected transient over power, and unprotected loss of heat sink (LOHS). When the coolant temperature increases in ATWS, the SASS passively detaches control rods

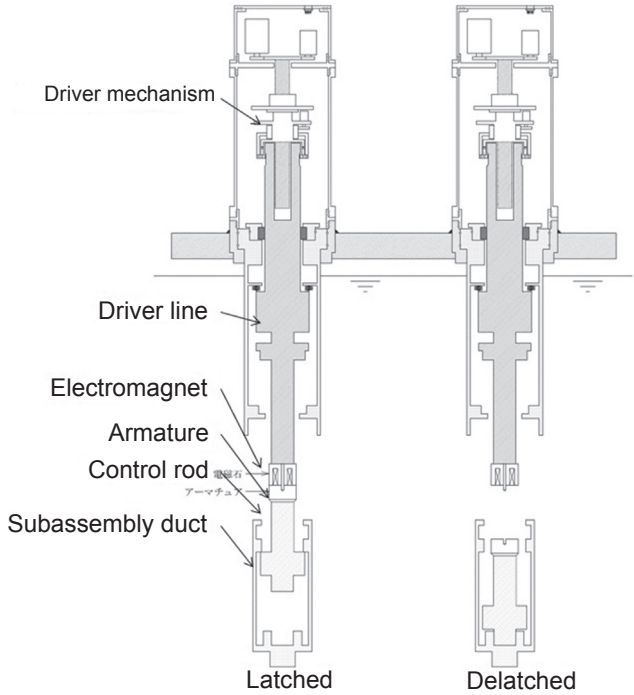


Figure 11.4 Structure and mechanism of the self-actuated shut-down system.

using the nature of ferromagnets that lose their magnetic property around their Curie points. The curie point of the temperature-sensing alloy can be controlled by using the 30Ni-31Co-Fe alloy. The other part of the magnetic route is composed of soft magnetic iron. A spacer between the electromagnet part and the armature part is made from Inconel to not affect the magnetic force of the SASS.

Several out-of-pile mock-up experiments have been conducted to demonstrate performances on holding force, response time, thermal endurance test under sodium, and measures against particle accumulation on the magnetic surface. The transient response tests with simulated ATWS conditions confirmed the time constant of the armature. In addition to the out-of-pile tests, in-pile mock-up and material experiments were conducted in JOYO (Nakanishi et al., 2010; Fujita et al., 2011). The control rod holding stability under the actual reactor-operational environment was successfully confirmed.

In the present approach for JSFR to mitigate a core disruptive accident, the core design and fuel characteristics are intended to eliminate the possibility of prompt criticality leading to mechanistic core expansion. In addition, the fuel assembly, so-called FAIDUS, is introduced as a design measure for realizing early fuel discharge before the formation of a large-scale molten pool, which has re-criticality potential because of large-scale fuel compaction (Niwa, 2007).

The concept of early fuel discharge and two design options for FAIDUS are shown in Fig. 11.5. Because the downward option involves difficulties in fabrication using a grid-type spacer, the feasibility of the upward option driven by the pressurization of the

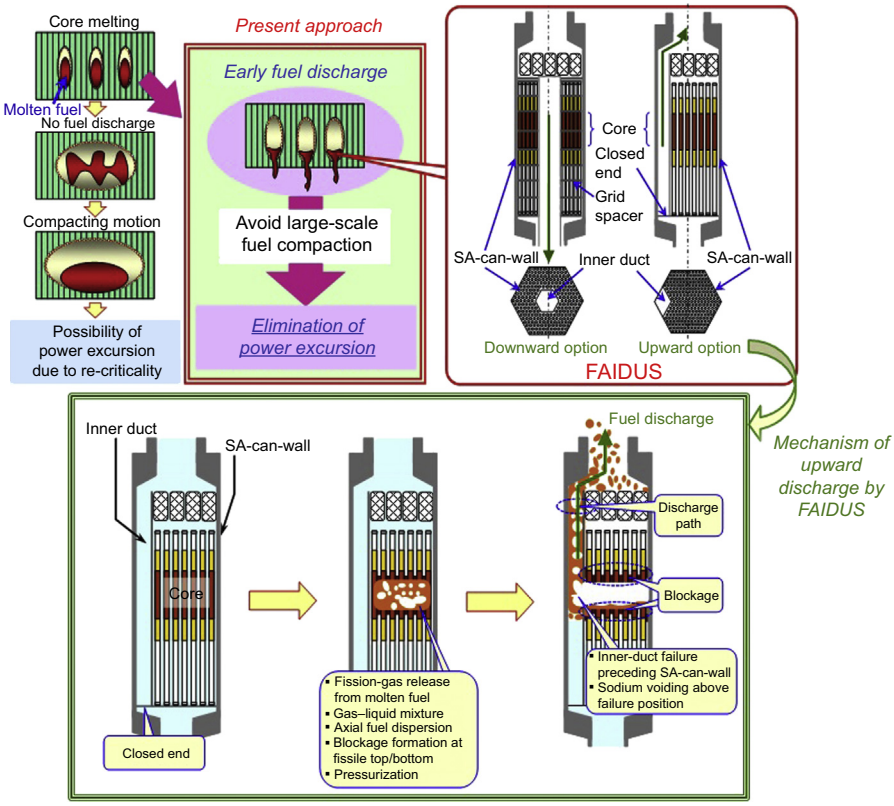


Figure 11.5 Concept of early fuel discharge and molten-fuel discharge by FAIDUS (fuel assembly with an inner duct structure). *SA*, subassembly.

disrupted core has been investigated by utilizing the phenomenological evidence obtained through well-designed experiments.

The EAGLE project, which includes out-of-pile and in-pile tests, was planned for this purpose and has been successfully conducted in the impulse graphite reactor of Kazakhstan. It was confirmed by the wall failure, fuel discharge, and integral demonstration tests of the EAGLE project that the inner-duct failure would precede subassembly-can wall failure (Konishi et al., 2007; Sato et al., 2011), and it was also confirmed by the CABRI program (Sato et al., 2004; Onoda et al., 2011) and prototype fast reactor (PFR) experiments of the TREAT program (Rothman, 1979; Bauer et al., 1986) that a sufficient driving force for upward discharge would be obtained. In addition to this experimental knowledge, the behavior of fuel discharge through the inner duct was evaluated by parametric analyses using the SIMMER code (Tobita et al., 2006), taking into account the uncertainty of wall deformation and/or failure. The effectiveness of FAIDUS as a design measure, which can eliminate the re-criticality leading to a power excursion, was confirmed through the experimental investigation and parametric analyses as previously described.

11.2.2.3 Compact reactor system

The JSFR design uses a compact RV because of a simple vessel wall structure without a cooling system (hot vessel) and a compact in-vessel FHS with a combination of a slit UIS and an advanced FHM (see Fig. 11.1a). In Japan, hot vessels without a reactor cooling system have successfully accumulated operating experience in JOYO (Hara et al., 1976) and MONJU (Yokota et al., 1991). The JSFR vessel protection is further simplified from JOYO and MONJU without an ex-vessel overflow system; JOYO and MONJU have ex-vessel overflow systems to maintain steady sodium level during start-up operation to reduce transient thermal stresses.

As an important part of the design study on sodium-cooled fast reactors, thermal-hydraulic issues in the RV are carefully addressed. At the core outlet region, temperature fluctuation due to the mixing of hot and cold flows from the core is inevitable and the potential risk of thermal fatigue is concerned. For the accurate simulation of the mixing phenomena, the key is the precise modeling of the large-scale eddy structures. Therefore the large eddy simulation (LES) modeling is demanded (Tanaka et al., 2015). Several experiments (eg, the triple jet experiment) are conducted to validate the developed simulation code (Kobayashi et al., 2015; Tanaka et al., 2016). Another concern is the vibration of structural components, especially the H/L piping, in the hot pool. The LES and model experiments are performed to investigate the vibration characteristics (ie, the amplitude and the frequency; Ono et al., 2011; Tanaka et al., 2012). At the free surface, a free surface vortex may cause gas entrainment, which should be suppressed to avoid a positive void reactivity effect in the core. Two types of evaluation methods for the gas entrainment are proposed. One is the practical evaluation method, composed of a vortex model (Burgers vortex model) with rather coarse mesh computational fluid dynamics (CFD) (Sakai et al., 2008; Ito et al., 2010). The other is a high-precision simulation method based on an interface-tracking approach, which is shown in Fig. 11.6 (Ito et al., 2013). Several

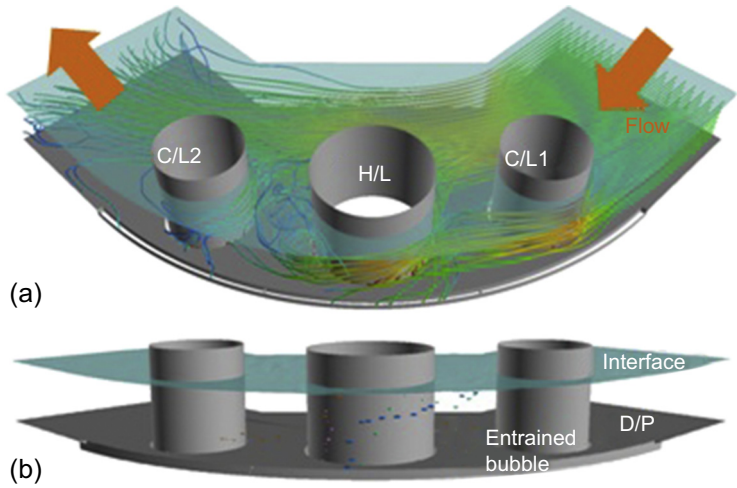


Figure 11.6 Simulation result of gas entrainment in large-scale test: (a) stream line around H/L and C/L and (b) trajectory of entrained bubble. *H/L*, hot leg; *C/L*, cold leg; *D/P*, dipped plate.

simple experiments and a large-scale water test are conducted to investigate the onset mechanism of the gas entrainment and to obtain the validation data of the evaluation methods (Kimura et al., 2008; Ezure et al., 2008).

There is another thermal-hydraulics issue induced by a vortex (ie, the vortex cavitations) at the H/L inlet. A simple vortex experiment and scaled tests are conducted to investigate (eg, the influence of the fluid property), and the obtained data are analyzed to establish a mechanistic evaluation method for the onset condition of the vortex cavitations (Ezure et al., 2013). After the scram, the primary flow rate decreases and hot sodium remains in the upper part of the upper plenum region whereas cold sodium comes from the core into the lower part (ie, the thermal stratification occurs). Since the large temperature gradient at the hot/cold interface may impact the integrity of structural objects (eg, the RV), numerical simulations of some basic tests are performed with various simulation models to establish appropriate simulation conditions (eg, the turbulence model; Ohno et al., 2011). In addition, natural-circulation decay heat removal after the scram is considered as one of most important safety characteristics of sodium-cooled fast reactors. The potential upper limit of the core fuel cladding temperature is evaluated with numerical simulation codes to confirm the feasibility of natural-circulation decay heat removal (Watanabe et al., 2015). The sodium fire and sodium-water reaction are specific accidental phenomena in sodium-cooled fast reactors. Several simulation codes (eg, the mechanistic sodium-water reaction simulation code) are developed to establish the evaluation system of those phenomena (Yamaguchi et al., 2001; Uchibori et al., 2015).

11.2.2.4 Two-loop cooling system

The two-loop cooling system contributes to a simple cooling system and a compact component arrangement. An L-shaped pipe for the primary hot-leg piping also enables a compact component arrangement. Because major issues (eg, DHRS, loss of floats (LOF), and hydraulics) were clarified and evaluated in a previous study (Yamano et al., 2010), the basic feasibility of the two-loop cooling system has already been confirmed. Recent results on DHRS are described later in this chapter. As for design basis events (DBEs), the pump seizure accident has appeared to be the most severe event, and the transient analysis taking into account the latest design has shown that the two-loop cooling system meets safety criteria (Okubo et al., 2011).

This primary cooling system increases the primary coolant flow rate per loop. As a result, a large-diameter piping system with high coolant velocity is required. That high coolant velocity may result in a flow-induced vibration issue. In the JSFR primary piping system, the number of elbows is reduced by adopting high-chromium steel with low thermal expansion characteristics. JSFR has only one L-shaped elbow for the hot-leg piping system between the RV and IHX. The curvature radius of the L-shaped elbow is equivalent to the piping diameter to configure the compact system design. On the basis of those features in the JSFR cooling system design, the flow dynamics in the piping were investigated, particularly focusing on the flow separation behavior that would be a major source of pressure fluctuations in the piping.

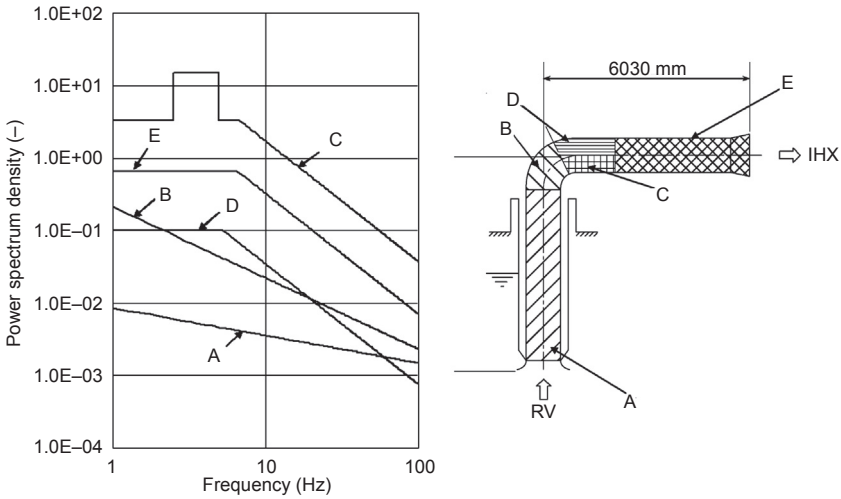


Figure 11.7 Power spectrum densities for hot-leg piping design.

Hydraulics in the large-diameter piping have been revealed by one-third scale hot-leg pipe water experiments with an acryl pipe for visualization and a stainless steel pipe for vibration data accumulation (Yamano, 2010; Yamano et al., 2009). The experiment extended the pressure loss coefficient data against Reynolds number (**Re**) up to $\mathbf{Re} = 8 \times 10^5$. The results showed that the pressure loss coefficient saturates and there is no **Re** dependency with $\mathbf{Re} > 3 \times 10^5$, showing that the real scale with $\mathbf{Re} = 3.7 \times 10^6$ could be extrapolated from the one-third scale experimental data.

Detailed vibration data were also accumulated from the water experiment with the stainless steel pipe. With the accumulated data, conservative design power spectrum density for stress analysis on random vibration has been defined as is shown in Fig. 11.7. Random vibration in the hot-leg piping has been analyzed, and the maximum stress is evaluated to be lower than the criteria of high cycle fatigue stress.

11.2.2.5 Integrated intermediate heat exchanger/pump component

The integrated IHX/pump component is one of the JSFR key technologies to achieve a compact primary cooling system. As is illustrated in Fig. 11.8, it includes a primary pump, IHX tube bundles, and PRACS heat exchange tubes. Major issues of this component are prevention of gas entrainment from the sodium free surface, sodium level control, pump shaft stability, tube wear due to vibration, temperature distribution control, and fabrication capability.

Technical feasibility of these issues are examined by various tests using a full-scale mock-up and a one-fourth scale mock-up (Hayafune et al., 2006; Handa et al., 2009). For example, the one-fourth scale mock-up experiments have revealed basic mechanisms of vibration transmission and tube wear. An evaluation method on tube wear

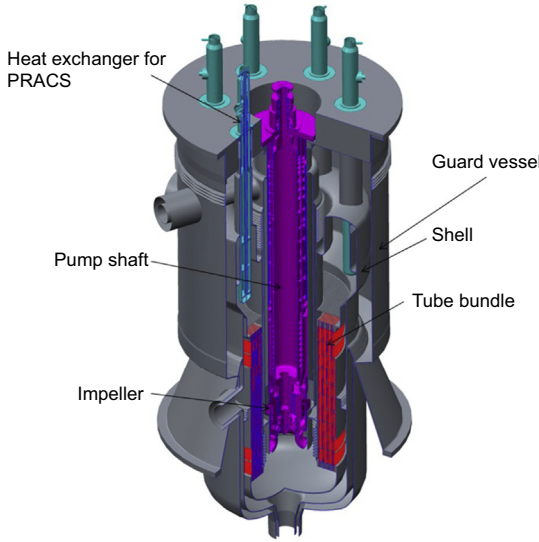


Figure 11.8 Integrated intermediate heat exchanger/pump component. *PRACS*, primary reactor auxiliary cooling system.

has been proposed (Handa et al., 2009) showing that tube wear can be accommodated by the tube thickness margin. In another recent study, several additional experiments such as a partial tube bundle model vibration test and a full-scale tube bundle water experiment have been conducted to validate and verify the proposed evaluation method.

Because the JSFR pump shaft is long ($\sim$15 m) in height, a damper is installed at the lower bearing to increase rotation stability. A full-scale mock-up of the lower pump shaft bearing with a damper has been manufactured, and water tests at 80°C with the same viscosity condition of sodium have been conducted, accumulating data of shaft holding force and damping performance.

11.2.2.6 Reliable steam generator

The JSFR design adopts a double-wall, straight-tube reliable SG for safety and investment protection. Periodical inspections on inner and outer tubes are required to maintain reliable sodium-water boundaries. Development targets of SG tube inspection devices are detection of 10% thickness defect for inner tubes and 20% for outer tubes. The JSFR double-wall tube SG can eliminate tube failure propagation as DBEs taking into account the previously mentioned inspection capabilities. The prevention of tube failure propagation has been confirmed covering the following double-boundary failure modes:

Common mode failure: Inner and outer tube failure due to a common cause.
Dependent double failure: Inner tube failure caused by outer tube failure or outer tube failure caused by inner tube failure.

Independent double failures: Inner and outer tube failure coincidently happen at the same tube.
Tube-to-tube sheet weld failure: Leak at tube-to-tube sheet weld.

For each of these failure categories, detailed assessments were made and it was shown that there is no failure propagation in the range of DBEs. Although the large leak is eliminated in the DBE, a double-ended guillotine (DEG) rupture of one double-wall tube is assumed as the maximum leak rate for a bounding event to confirm a certain design margin. SG tube failure propagation analyses using the LEAP code (Tanabe et al., 1982; Hamada and Tanabe, 1992) have been conducted with an initial leak rate from a small one DEG or DBE with hydrogen monitoring failure. The results show that the maximum tube failure propagation is within the range of five DEG, and the spike pressure on the primary-secondary and secondary sodium boundaries due to this range of sodium-water reaction has been evaluated using the SWACS code (Ono and Kurihara, 2005) and found to be in the design limits (Fig. 11.9).

11.2.2.7 Natural-circulation decay heat removal system

The JSFR design adopts fully natural convection to achieve reliable decay heat removal. All of the sodium boundaries including air cooler tubes are double walled, providing sodium leak monitoring and inspection access. Several safety analyses in various operating conditions in categories II and IV (eg, loss of off-site power for category II and one PRACS sodium leak combined with loss of off-site power and one dumper failure of the other PRACS for category IV) have been conducted confirming the performance of the JSFR DHRS system. Decay heat removal with only the DRACS has also been evaluated using a three-dimensional analysis code

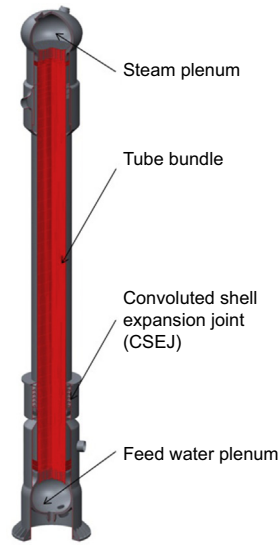


Figure 11.9 Steam generator with double-walled straight heat transfer tubes.

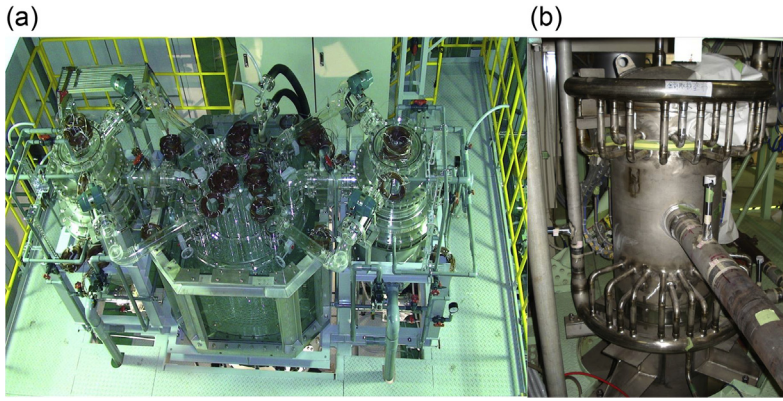


Figure 11.10 The decay heat removal system test apparatus: (a) one-tenth scale water test apparatus and (b) sodium test apparatus.

assuming failure of PRACS in loop A during loop B maintenance with sodium drain (PRACS in loop B is unavailable during maintenance). The results show that the peak temperature is lower than 700°C, meeting criteria with decay heat 7 h after the reactor trip.

For verification and validation of design and evaluation tools, a one-tenth scale water test on the whole DHRS system and a sodium test on the PRACS heat exchanger with 108 scale piping diameter have been conducted as shown in Fig. 11.10. A one-dimensional flow network analysis code and a three-dimensional analysis model using STAR-CD have been compared with those experimental data showing that they are in good agreement (Ohyama et al., 2009; Kamide et al., 2010).

11.2.2.8 Simplified fuel handling system

The JSFR design has adopted a simple FHS with advanced technologies. The JSFR in-vessel FHS consists of a combination of a UIS with a slit and a pantograph-type FHM (Fig. 11.11) to dramatically reduce the RV diameter. The FHM is removed from the RV during power operation. From the RV to the ex-vessel storage tank (EVST), a spent subassembly, which is accommodated by a sodium pot, is transported by an ex-vessel transfer machine in a similar manner as in MONJU. A two-position sodium pot has been installed for transportation of subassemblies from the RV to the EVST to reduce the refueling time and thereby increase plant availability. Active cooling is not necessary during the transportation from the RV to the EVST because of the heat capacity of the sodium pot. The sodium pot cooling system is activated only when the transportation has a malfunction or becomes stuck. The sodium pot cooling system consists of a combination of direct cooling with argon gas blow and indirect cooling with thermal emission. The EVST has a sufficient capacity for full-core evacuation to enhance the plant's in-service inspection and repair (ISIR) capability (Chikazawa et al., 2011).

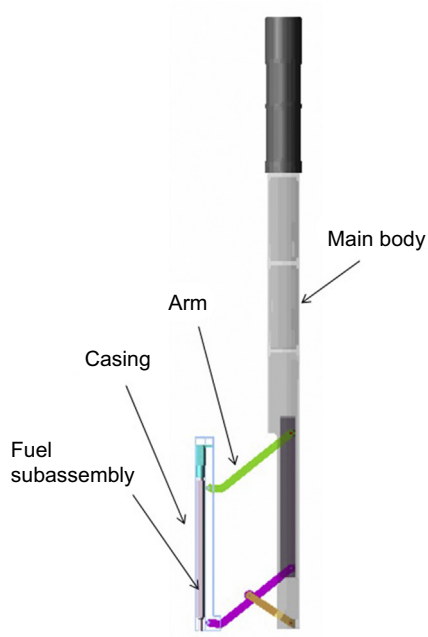


Figure 11.11 Pantograph-type fuel handling machine.

11.2.2.9 Steel plate–reinforced concrete containment vessel

The CV of the JSFR design is made of SC. The structure of SC, as shown in Fig. 11.12, consists of two steel plates facing each other and concrete filled in between. One of the advantages of the SC structure is that its steel parts can be fabricated in a factory with shorter construction period compared with on-site construction, which leads to reduction of the plant construction period and cost (Hara et al., 2009).

Experiments were performed including shear strength tests of SC beams by using two types of reinforcement specimen: tie bars and partitioning plates. In both types of specimen, temperature and amount of reinforcement material were the main parameters of the tests. The results for the tie bar type realized the degree of reduction tendency of shear strength as temperature increased. As a result of a series of experiments, sufficient data to estimate behavior under high temperatures were acquired and methods to estimate the support and the boundary function of the SCCV were developed (Katoh et al., 2011).

11.2.2.10 Advanced seismic isolation system

SFR components tend to be designed thin-walled structures because its thermal stress due to elevated temperature is much higher and its internal pressure is much lower than that of an LWR. Thin-walled structures are relatively vulnerable to severe earthquakes. The design seismic loading was greatly increased over the previous seismic condition because of the Niigata-ken Chuetsu-oki earthquake in 2007 (Nuclear Safety

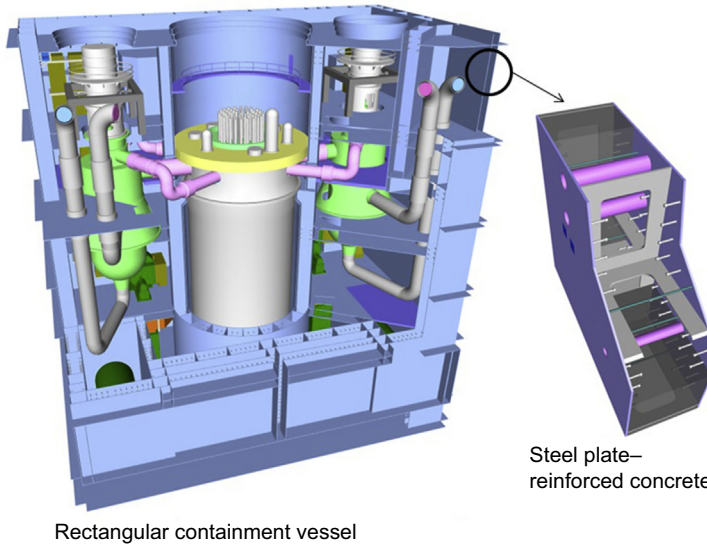


Figure 11.12 Steel plate−reinforced concrete containment structure.

Commission of Japan, 2006). Hence, the demonstration reactor of JSFR must adopt an advanced seismic isolation system, which is a practicable modification of previous technologies, because the earthquake force that affects the primary components must be mitigated more than that of the previous seismic isolation system.

The advanced seismic isolation system for SFRs adopts laminated rubber bearings, which are thicker than those of the previous design, as well as oil dampers. As a result of the examination, the specification of the advanced seismic isolation system for SFRs is that the natural frequency in the horizontal direction is 0.29 Hz and in the vertical direction it is 8.0 Hz (Okamura et al., 2011).

11.3 Update of the Japan sodium-cooled fast reactor design with lessons learned from the Fukushima-Daiichi accident

After the accident at Fukushima-Daiichi, the safety of nuclear power plants has been strongly recognized to be a common issue worldwide. Therefore enhancing nuclear safety taking into account the lessons learned from the accident has the highest and the most urgent priority. For the development of next-generation SFRs, global standards for safety criteria were expected to be established in an international framework in consideration of the lessons learned from the Fukushima-Daiichi accident. For the international safety criteria, activities on developing SDC for SFRs were undertaken and SDC created by a GIF task force were approved by the GIF policy group in May 2013 (Nakai et al., 2012).

It is recognized that there are three major points of lessons learned from the Fukushima-Daiichi accident. The first point is the enhancement of systems that may be needed to decrease the likelihood of a severe accident due to extreme external hazards. Namely, robustness should be enhanced in power supplies [direct current and alternating current (AC), if needed to power an active safety system], cooling functions (core, CV, and spent fuel pools), and the heat transportation system, including the final heat sink. The second point is the enhancement of response measures against severe accidents. The means should be provided to prevent severe mechanical loads on CVs and the instrumentation should be prepared to identify the status of the reactor core and the CV. The third point is the reinforcement of safety infrastructure by ensuring the independency and diversity of safety systems. These points are incorporated into SDC taking the characteristics of SFRs into account (Kamide et al., 2015).

Although numerous types of events, including internal and external ones, can be considered as initiators of the accident conditions, those events can be grouped into two major types of events from the viewpoints of plant responses and consequences: ATWS type and loss of heat removal system (LOHRS) type.

To contribute to the development of SDC by providing the technical solutions to be required for the higher safety level as a next-generation reactor, a series of design studies for JSFR has been conducted. As a first step, the effectiveness of the current design measures of JSFR against severe plant conditions was evaluated. Then design modifications have been investigated for the ATWS and LOHRS type events. Such design study has also been conducted for the fuel storage systems.

From the viewpoint of toughness against external events, JSFR had already improved safety features as a next-generation reactor in a preconceptual design version in 2010 (Chikazawa et al., 2015). The JSFR toughness against earthquakes and tsunamis was evaluated based on the 2010 design version. Seismic analyses showed that JSFR had a sufficient design margin for shut-down capability and integrity of major components against severe seismic conditions enveloping the Fukushima-Daiichi accident conditions. In a tsunami, the sea-water pumps for the CCWS could be totally damaged because they are located at the sea level; thus the CCWS could fail because of the tsunami because it depends on sea water as the final heat sink. In the JSFR design, safety components including DHRS and emergency power supply are independent from the CCWS because of full natural-convection DHRS and air-cooling GTG. Even in station blackout, decay heat could be removed by natural-convection DHRS. An analysis showed that the time margin was more than 10 days to LOHS because of sodium freezing in case of the damper operation failure in the air coolers. That time margin is sufficient for implementing recovery actions by operators. However, additional design improvements still have a potential to reduce core damage frequency because of LOHS.

In ATWS type events, in-balance of power and cooling might cause core damage within a shorter time period. A passive shut-down mechanism can prevent core damage even under such conditions. In addition, mitigation of core damage is considered in design because of the shorter time period to reach core damage and of the potential mechanical energy release, which might appear in the core

Table 11.2 Measures against loss of heat removal system type events

Category A	Event	Measures
LORL type	Simultaneous failure of RV and GV	Design measures and evaluation to prevent simultaneous failure of RV and GV
	Double failure in a piping system	Cooling by DRACS with low sodium level in case of double boundary failure in a piping system
LOHS type	Loss of PRACS and DRACS	AM on design base DHRS (DRACS and PRACS) • Manual operation of air cooler • Back-up power supply for air cooler control
		Alternative cooling system independent of design base DHRS (DRACS and PRACS)

LORL, loss of reactor level; *LOHS*, loss of heat sink; *RV*, reactor vessel; *GV*, guard vessel; *DRACS*, direct reactor auxiliary cooling system; *DHRS*, decay heat removal system; *PRACS*, primary reactor auxiliary cooling system; *AM*, accident management.

damage situations. JSFR adopts SASS incorporated to the two independent active shut-down systems for the prevention of core damage. To achieve in-vessel retention (IVR), FAIDUS and an in-vessel core catcher are introduced in the core and RV design as shown in Figs. 11.12.

LOHRS includes LOHS and LORL. For LOHRS, SFR has superior characteristics because of sodium coolant features such as low pressure and high natural convection capability. Utilizing those superior characteristics of sodium, the JSFR already equipped the reliable DHRS with natural convection, which does not depend on emergency AC power. The additional measures against LOHRS are summarized in Table 11.2.

For LOHS, manual control of the air cooler damper during 10 days was investigated. Transient analyses showed that the air cooler dampers were capable of being controlled manually by adopting a simple operation procedure with a sufficient operation time (Chikazawa et al., 2015). Core damage frequency due to LOHS was evaluated to be lower than 10−8/reactor-year, taking into account accident management (Chikazawa et al., 2012). Although the JSFR DHRS configuration in the 2010 version has sufficient reliability, installation of additional DHRS with independency and diversity from the DBA DHRS could improve toughness against LOHS. As a countermeasure against an LORL type event, double failure of the RV and GV is prevented by securing a margin to earthquake-resistant performance and a reliability of the RV and GV. Furthermore, function of the DRACS is extended to maintain the heat removal capability even in case of low sodium level when siphon break occurs by multiple leakages on the primary cooling circuit. It is important that RV melt-through due to LOHRS type events can be practically eliminated by those design measures in Table 11.2 to achieve IVR without significant core damage.

11.4 Concluding remarks

The design concept of JSFR, Japan's Generation IV reactor, was reviewed. It is a loop type and is characterized, in terms of safety, by a self-actuated (passive) RSS, a re-criticality free core design, and a natural-circulation DHRS. It is also characterized, from the viewpoint of economy, as a two-loop heat transport system, integrated IHX/pump component, and others.

Ten key innovative technologies were identified, and R&D was conducted to confirm the feasibilities of these technologies. These 10 key innovative technologies—high burn-up core, safety enhancement, a compact RV, a two-loop cooling system using high-chromium steel, an integrated IHX/pump component, a reliable SG, natural-circulation DHRS, a simplified FHS, a CV made of concrete that is reinforced with steel plates, and an advanced seismic isolation system—were evaluated to be suitable for implementation to the demonstration JSFR plant. The JSFR design with those key technologies has the potential to meet the targets of the FaCT project and Generation IV reactors.

To contribute to the development of the SDC of the GIF by providing the technical solutions to be required for the higher safety level as a next-generation reactor and to reflect on the lessons learned from the Fukushima-Daiichi accident to further enhance the safety of the plant against severe external events, a series of design studies for JSFR was conducted. As the first step, the effectiveness of the current design measures of JSFR against severe plant conditions was evaluated. Then design modifications were also investigated for the ATWS and LOHRS type events. Such design study has also been conducted for the fuel storage systems.

References

Aizawa, K., 2001. R&D for fast reactor fuel cycle technologies in JNC. In: Proceedings of GLOBAL 2001, Paris, France, September 9−13, 2001.

Akasaka, N., et al., 2001. Effect of irradiation environment of fast reactor's fuel elements on void swelling in P, Ti-modified 316 stainless steel. In: Effects of Radiation on Materials: 20th International Symposium, ASTM STP 1405, pp. 443−456.

Asayama, T., et al., 2013. Development of 2012 edition of JSME code for design and construction of fast reactors (1) overview. In: Proceedings of the ASME 2013 Pressure Vessels and Piping Conference PVP2013, PVP2013−98061, July 14−18, 2013, Paris, France.

Bauer, T., et al., 1986. Post-failure material movement in the PFR/TREAT experiments. In: Proceedings of International Meeting on Fast Reactor Safety and Related Physics, 1986 May 12−16; Guernsey (UK), p. 1647.

Chikazawa, Y., et al., 2011. Conceptual design study for the demonstration reactor of JSFR (6) fuel handling system design. In: Proceedings of 19th International Conference on Nuclear Engineering (ICONE19), Osaka, Japan, October 24−25, 2011.

Chikazawa, Y., et al., 2012. Evaluation of JSFR key technologies. Nuclear Technology 179, 360−373.

Chikazawa, Y., et al., November 2015. Severe external hazard on hypothetical JSFR in 2010. Nuclear Technology 192.

Ezure, T., et al., 2008. Transient behavior of gas entrainment caused by surface vortex. Heat Transfer Engineering 29 (8), 659−666.

Ezure, T., et al., 2013. Effects of fluid viscosity on occurrence behavior of vortex cavitation − vortex structures and occurrence condition. In: Proceedings of NURETH-15, Pisa, Italy, May 12−17, 2013.

Fujita, K., et al., 2011. Development of a self-actuated shutdown system for large-scale JSFR. In: Proceedings of 19th International Conference on Nuclear Engineering (ICONE19), Osaka, Japan, October 24−25, 2011.

Hamada, H., Tanabe, H., 1992. A Study of the Selection of Rational Design Basis Leak. PNC TN9410 92-097. Power Reactor and Nuclear Fuel Development Corp. (in Japanese).

Handa, T., et al., 2009. Research and development for the integrated IHX/Pump. In: Proceedings of International Conf. Fast Reactors and Related Fuel Cycles (FR09), Kyoto, Japan, December 7−11, 2009.

Hara, T., et al., 1976. JOYO construction and preoperational test experience. In: Proceedings of International Conference on Advanced Nuclear Energy Systems, Pittsburgh, Pennsylvania, March 14−17, 1976. American Society of Mechanical Engineers.

Hara, H., et al., 2009. Japan conceptual design study of JSFR (4) reactor building layout. In: Proceedings of International Conference on Fast Reactors and Related Fuel Cycles (FR09), Kyoto, Japan, December 7−11, 2009.

Hayafune, H., et al., 2006. Development of the integrated IHX/pump component 1/4-scale vibration testing. In: Presented at 14th International Conf. Nuclear Engineering (ICONE14), Miami, Florida, July 17−20, 2006.

Hishida, M., et al., 2007. Progress on the plant design concept of sodium-cooled fast reactor. Journal of Nuclear Science and Technology 44 (3).

Ito, K., et al., 2010. Improvement of gas entrainment evaluation method − introduction of surface tension effect. Journal of Nuclear Science and Technology 47 (9), 771−778.

Ito, K., et al., 2013. A volume-conservative PLIC algorithm on three-dimensional fully unstructured meshes. Computers & Fluids 88, 250−261.

JSME, 2012. Codes for Nuclear Power Generation Facilities − Rules for Design and Construction for Nuclear Power Plants, Section II: Fast Reactor Standards (2012). JSME S NC2−2012 (in Japanese).

Kaito, T., et al., 2007. Progress in the R&D project on oxide dispersion strengthened and precipitation hardened ferritic steels for sodium cooled fast breeder reactor fuels. In: GLOBAL 2007, September 9−13, 2007, Boise, Idaho, USA.

Kaito, T., et al., 2009. In-pile creep rupture properties of ODS ferritic steel claddings. Journal of Nuclear Materials 386−388, 294−298.

Kamide, H., et al., 2010. Sodium experiments on decay heat removal systems of Japan sodium cooled fast reactor − start-up transient of decay heat removal system. In: Presented at Seventh Korea−Japan Symp. Nuclear Thermal Hydraulics and Safety, Chuncheon, Korea, November 14−17, 2010.

Kamide, H., et al., 2015. JSFR design progress related to development of safety design criteria for generation IV sodium-cooled fast reactors (1) overview. In: Proceedings of 23rd International Conference on Nuclear Engineering (ICONE-23), May 17−21, 2015, Chiba, Japan.

Katoh, A., et al., 2011. Experimental investigations of steel plate reinforced concrete bearing wall for fast reactor containment vessel. In: Proceedings of 19th International Conf. Nuclear Engineering (ICONE19), Osaka, Japan, October 24−25, 2011.

Kimura, N., et al., 2008. Experimental study on gas entrainment at free surface in reactor vessel of a compact sodium-cooled fast reactor. Journal of Nuclear Science and Technology 45 (10), 1053−1062.

Kobayashi, J., et al., 2015. Water experiments on thermal striping in reactor vessel of Japan sodium-cooled fast reactor − countermeasures for significant temperature fluctuation generation. In: Proceedings of ICONE 23, May 17−21, Chiba, Japan, 2015.

Kondo, S., et al., 1992. An advanced computer program for LMFBR severe accident analysis. In: Proceedings of ANP'92; 1992 Oct 25−29; Tokyo (Japan). IV, p. 40.5-1 − 40.5-11.

Kondo, S., et al., March 2013. Recent progress and status of Monju. In: Proceedings of International Conference on Fast Reactors and Related Fuel Cycles; Safe Technologies and Sustainable Scenarios (FR-13) (USB Flash Drive), 6 pp.

Konishi, K., et al., November 2007. The results of a wall failure in-pile experiment under the EAGLE project. Nuclear Engineering and Design 237 (22), 2165−2174.

Kotake, S., et al., 2005. Feasibility study on commercialized fast reactor cycle systems current status of the FR system design. In: Proceedings of GLOBAL 2005, Tsukuba, Japan, October 9−13, 2005.

Kotake, S., et al., 2009. Safety design features for JSFR − passive safety and CDA mitigation. In: Proceedings of Annual Meeting on Nuclear Technology, Dresden, Germany.

Kubo, S., et al., 2011. Safety design requirements for safety systems and components of JSFR. Journal of Nuclear Science and Technology 48 (4), 547−555.

Kurisaka, K., 2006. Probabilistic safety assessment of Japanese sodium-cooled fast reactor in conceptual design stage. In: Proceedings of Pacific Basin Nuclear Conference (PBNC-15).

Maeda, Y., et al., 2005. Distinguished achievements of a quarter-century operation and a promising project named MK-III in Joyo. Nuclear Technology 150 (1), 16.

Nakai, R., et al., December 9−12, 2012. Development of safety design criteria for the generation-IV sodium-cooled fast reactor. In: Keynote Lecture at NTHAS8: The Eighth Japan−Korea Symposium on Nuclear Thermal Hydraulics and Safety, Beppu, Japan.

Nakanishi, S., et al., 2010. Development of passive shutdown system for SFR. Nuclear Technology 170.

Niwa, H., 2007. Safety implications of the EAGLE experimental results for the FaCT project. In: Proceedings of International Conference on Nuclear Power of Republic Kazakhstan, September 3−5, 2007, Kurchatov (Kazakhstan).

Nuclear Safety Commission of Japan, 2006. Regulatory Guide for Reviewing Seismic Design of Nuclear Power Reactor Facilities. NSCRG: L-DS-I.02.

Ohno, S., et al., 2011. Validation of a computational simulation method for evaluating thermal stratification in the reactor vessel upper plenum of fast reactors. Journal of Nuclear Science and Technology 48 (2), 205−214.

Ohyama, K., et al., 2009. Decay heat removal system by natural circulation for JSFR. In: Proceedings of International Conf. Fast Reactors and Related Fuel Cycles (FR09), Kyoto, Japan, December 7−11, 2009.

Okamura, S., et al., 2011. Seismic isolation design for JSFR. Journal of Nuclear Science and Technology 48 (4), 688−692.

Okubo, T., et al., 2011. Conceptual design for a large-scale Japan sodium-cooled fast reactor (3) core design in JSFR. In: Presented at International Congress on Advances in Nuclear Power Plants (ICAPP'11), Nice, France, May 2−5, 2011.

Onizawa, T., et al., 2013a. Development of 2012 edition of JSME code for design and construction of fast reactors (2) development of the material strength standard of 316FR stainless steel. In: Proceedings of the ASME 2013 Pressure Vessels and Piping Conference PVP2013, PVP2013−97608, July 14−18, 2013, Paris, France.

Onizawa, T., et al., 2013b. Development of 2012 edition of JSME code for design and construction of fast reactors (3) development of the material strength standard of modified 9Cr-1Mo steel. In: Proceedings of the ASME 2013 Pressure Vessels and Piping Conference PVP2013, PVP2013−97611, July 14−18, 2013, Paris, France.

Ono, I., Kurihara, A., 2005. Quasi-steady pressure analysis in intermediate water leak rate with swac-13 module in SWACS code. JNC TN9400 2005-047. Japan Nuclear Cycle Development Institute (in Japanese).

Ono, A., et al., 2011. Influence of elbow curvature on flow structure at elbow outlet under high Reynolds number condition. Nuclear Engineering and Design 241 (11), 4409−4419.

Onoda, Y., et al., 2011. Three-pin cluster CABRI tests simulating the unprotected loss-of-flow accident in sodium-cooled fast reactors. Journal of Nuclear Science and Technology 48 (2), 188−204.

Rothman, A., 1979. TREAT experiments with irradiated fuel simulating hypothetical loss-of-flow accidents in large LMFBRs. In: Proceedings of International Meeting on Fast Reactor Safety Technology, 1979 August 19−23, Seattle (USA), p. 924.

Sakai, T., et al., 2008. Proposal of design criteria for gas entrainment from vortex dimples based on a computational fluid dynamics method. Heat Transfer Engineering 29 (8), 731−739.

Sato, I., et al., 2004. Transient fuel behavior and failure condition in the CABRI-2 experiments. Nuclear Technology 145 (1), 115−137.

Sato, I., et al., 2011. Safety strategy of JSFR eliminating severe recriticality events and establishing in-vessel retention in the core disruptive accident. Journal of Nuclear Science and Technology 48 (4), 556−566.

Shimakawa, Y., et al., 2002. An innovative concept of a sodium cooled reactor to pursue high economic competiveness. Nuclear Technology 140, 1−17.

Takamatsu, M., et al., 2007. Demonstration of control rod holding stability of the self actuated shutdown system in Joyo for enhancement of fast reactor inherent safety. Journal of Nuclear Science and Technology 44 (3).

Tanabe, H., et al., 1982. Analysis Code for Failure Propagation of Steam Generator Tube -LEAPII. PNCTN952 82-04. Power Reactor and Nuclear Fuel Development Corp. (in Japanese).

Tanaka, M., et al., 2012. Numerical investigation on large scale eddy structure in unsteady pipe elbow flow at high Reynolds number conditions with large eddy simulation approach. Journal of Power and Energy Systems 6 (2), 210−228.

Tanaka, M., et al., 2016. Development of V2UP (V&V plus uncertainty quantification and prediction) procedure for high cycle thermal fatigue in fast reactor − framework for V&V and numerical prediction. Nuclear Engineering and Design 299 (2016), 174−183.

Tanaka, M., et al., 2015. Numerical simulation of thermal striping phenomena in a T-junction piping system for fundamental validation and uncertainty quantification by GCI estimation. Bulletin of the JSME, Mechanical Engineering Journal 2 (5) (2015). Paper No.15-00134.

Tobita, Y., et al., March 2006. The development of SIMMER-III, an advanced computer program for LMFR safety analysis and its application to sodium experiments. Nuclear Technology 153 (3), 245−255.

Uchibori, A., et al., 2015. Development of a mechanistic evaluation method for wastage environment under sodium-water reaction accident. In: Proceedings of NURETH-16, Chicago, Illinois, August 30−September 4, 2015.

Uehira, A., et al., 1999. Evaluation of Swelling and Irradiation Creep Properties of High Strength Ferritic/Martensitic Steel (PNC-fms). JNC report No.TN9400 99−022. Japan Nuclear Cycle Development Institute, Ibaraki (Japan) (in Japanese).

Ukai, S., et al., 1998. Irradiation Performance of FBR Monju-Type Fuel with Modified Type 316 Stainless Steel at High Burn-up. American Nuclear Society Transactions, p. 115.

USDOE and GIF, 2002. A Technology Roadmap for Generation IV Nuclear Energy Systems. GIF-002−00.

Watanabe, et al., 2015. Development of evaluation methodology for natural circulation decay heat removal system in a sodium cooled fast reactor. Journal of Nuclear Science and Technology 52 (9), 1102−1121.

Yamaguchi, A., et al., 2001. Numerical methodology to evaluate fast reactor sodium combustion. Nuclear Technology 136 (3), 315−330.

Yamano, H., et al., 2009. Unsteady hydraulic characteristics in large-diameter piping with elbow for JSFR (1) current status of flow-induced vibration evaluation methodology development for the JSFR piping. In: Proceedings of 13th International Topical Meeting Nuclear Reactor Thermal Hydraulics (NURETH-13), Kanazawa, Japan, September 27−October 2, 2009.

Yamano, H., et al., 2010. Technological feasibility of two-loop cooling system in JSFR. Nuclear Technology 170, 159.

Yamano, H., 2010. Technological feasibility of two-loop cooling system in JSFR. Nuclear Technology 170 (1), 159−169.

Yano, Y., et al., 2011. Effects of neutron irradiation on tensile properties of oxide dispersion strengthened (ODS) steel claddings. Journal of Nuclear Materials 419, 305−309.

Yokota, Y., et al., 1991. Design and construction of the reactor structure of the prototype fast breeder reactor Monju. In: Proceedings of International Conference on Fast Reactors and Related Fuel Cycles, Kyoto, Japan, October 28−November 1, 1991.

Generation IV concepts: USSR and Russia

12

D.V. Paramonov[1], *E.D. Paramonova*[2]
[1]Nizhny Novgorod Atomenergoproekt, Moscow, Russia; [2]École Polytechnique Fédérale de Lausanne, Lausanne, Switzerland

12.1 Introduction

In 2000, the Russian government published its nuclear industry strategy from 2000 to 2050 in the document: "*Strategy for developing nuclear energy in Russia for the XXI century*." Similar to the approach in the US, this strategy sets the expectation of initially continuing to rely on conventional, Generation III and III+ LWRs for the next 20−30 years. It is planned then to gradually increase the fast reactor fleet to have a portfolio of LWRs used for energy production and Generation IV (GEN-IV) fast reactors for breeding and waste disposition. It seems feasible to transition to a fast reactor fleet by about 2050 with a closed fuel cycle. Such a transition requires significant investment in GEN-IV research and development (R&D), starting with experimental and demonstration reactors and evolving to commercial plants capable to compete economically with LWRs and fossil power generation.

In 2009, Russia set a plan for how it will develop the Generation IV reactors. In the Federal Target Program, "*Nuclear energy technologies of new generation for 2010 − 2015 and up to 2020*" Rosatom (2009), the Russian Government sets the following objective to the state-owned nuclear corporation, Rosatom:

"*The main objective of the program − develop the next generation of nuclear energy technology on the basis of fast neutron reactors with a closed fuel cycle*." The Russian approach to GEN-IV reactor and fuel cycle technology development is based on the following assumptions and desired objectives (Lopatkin and Orlov, 1999; Avronin et al., 2012):

- The cost of electricity of fast reactors operating in a closed fuel cycle mode should be less than that of light water reactors (LWRs) and fossil power generation;
- Inherent safety is essential to prevent the most dangerous accidents, such as prompt runaway, loss of coolant, fire, steam and hydrogen explosions, which have historically led to core melt and catastrophic releases of radioactivity;
- Adding on numerous new "defense in depth" safety features results in even higher capital costs, which is economically counterproductive;
- Passive safety features do not alleviate other important inherent safety needs, such as waste management and nonproliferation;
- Complete reproduction of plutonium (Pu) in the core with a breeding ratio of around 1. Because of the slow growth rate of nuclear power capacity and the large amount of

Handbook of Generation IV Nuclear Reactors. http://dx.doi.org/10.1016/B978-0-08-100149-3.00012-4
Copyright © 2016 Elsevier Ltd. All rights reserved.

accumulated Pu to date, there is no need to rapidly double Pu, which makes it acceptable to have a breeding ratio ~1 and moderate core power density;
- No Pu extraction from spent nuclear fuel (SNF) while closing the fuel cycle; and
- Transmutation of the most hazardous long lived minor actinides (MAs) in SNF.

There were two alternative options for how to approach reaching the closed fuel cycle objectives, both of which mandated serious R&D investments. In the first scenario, Russia puts all of its chips on lead (Pb) fast reactors, with little to no research of other nuclear energy technologies, and almost all of the funding coming from federal sources. The second scenario is more conservative and spreads the efforts across Pb, Pb–bismuth (Bi), and sodium fast reactors (SFRs), with an increased portion of nongovernmental funding. Russia decided to take the second, portfolio-diversifying route as its nuclear strategy through 2020. Thus, three fast reactors are being developed in Russia: Pb-cooled demonstration reactor BREST-OD-300, Pb–Bi-cooled SMR SVBR-100, and a large commercial plant, BN-1200.

12.2 History of the Soviet fast reactor program

Russia has been experimenting with fast reactors since the 1950's. Table 12.1 is a snapshot of all USSR and Russian civilian fast reactor history.

Originally, the idea for creating fast breeder reactors came in the post-WWII era and was intended to ensure the sufficient supply of uranium (U) for the rapidly expanding nuclear program of the USSR. Alexander Leypunsky was one of the initial proponents of the idea and received government support in 1949. By 1955, the USSR constructed its first fast reactor: *Bystryi Reactor* or Fast Reactor (BR)-1 at the Institute of Physics and Power Engineering (IPPE) in Obninsk, Russia. This essentially was a critical assembly with a weapons Pu core and a U blanket. It had no coolant and essentially zero power. After the BR-1, a series of experimental sodium-cooled fast reactors, including BR-2, 5, and 10, was rapidly built (Pshakin, 2010).

Table 12.1 Historical timeline of USSR/Russian civilian fast reactor program (Kagramanyan, 2009)

#	Reactor	Year	Power	Coolant
1	BR-1	1955	0	*none*
2	BR-2	1956	100 kW_{th}	Hg
3	BR-5	1959	5 MW_{th}	Na, Na–K
4	BOR-60	1969	60 MW_{th}	Na
5	BR-10	1973	8 MW_{th}	Na
6	BN-350	1973	1000 MW_{th} (250 MW_{el} + desalination)	Na
7	BN-600	1980	600 MW_{el}	Na
8	BN-800	2015	880 MW_{el}	Na

In 1962−1964, the priority of conserving the U resources was confirmed, and USSR continued down the path of closed fuel cycles. It is interesting to compare the mentality 50 years ago with today's approaches:

> *[The] promising perspective is expansion of nuclear energy using fast breeder reactors starting with enriched uranium fuel and step-by-step replacement with plutonium fuel.*
>
> *Pshakin (2010)*

This closed nuclear fuel cycle strategy drove the development of a semicommercial SFR BN-350 model. While the BN-350 was under construction, the USSR started designing a larger BN-600 in parallel. Many of the lessons learned from the BN-350 demonstration project were used in the commercial design of the BN-600 (Fig. 12.1).

By the late 1970s, the USSR had accumulated significant experience in SFR technology. The USSR proceeded to designing even larger scale BNs, the BN-800 and BN-1600. The BN-800 design was a ramp-up of the BN-350 construction, but with the added bonus of using a standard turbine. IPPE had plans for building five BN-800s in the 1980s. At the same time, the BN (BN, from реактор на быстрых нейтраонах, meaning "reactor on fast neutrons") SFRs were not economically competitive with Russia's other, more traditional reactors, the LWRs and graphite-moderated thermal neutron reactors. Also, the fundamental argument in favor closing the fuel cycle on the basis of fast reactor technology was shattered when, surprisingly, vast amounts of high-grade U were found in Kazakhstan in the 1960−70s. Finally, the Chernobyl accident in 1986 undercut the nuclear energy program, and the collapse of the USSR in the early 1990s bumped nuclear energy from the list of top priorities. However, the research reactors BOR-60 and BN-600 continue to operate and form the experimental and experience base for the present time GEN-IV reactor development.

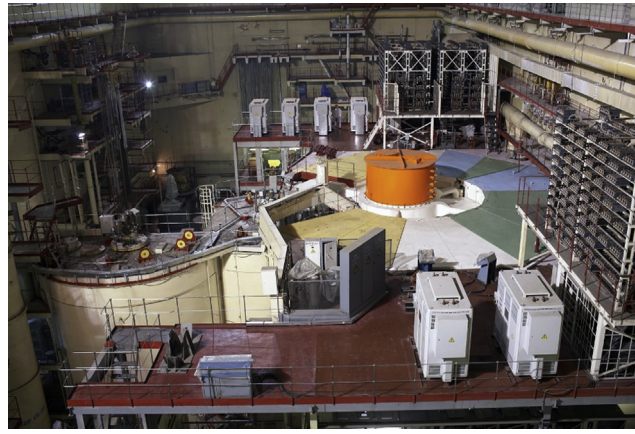


Figure 12.1 Inside reactor building of the BN-600.
http://www.rosatom.ru/wps/wcm/connect/rosatom/rosatomsite/resources/9788228047f0c3f39490bd608de3ffe0/reaktor_bn_600.jpg.

The next sections will go deeper into each one of the USSR and Russian GEN-IV reactor designs, covering the history, technological capabilities, and future plans.

12.3 Sodium fast reactors

Over the last 50 years, Russia has been designing and testing SFRs. The BN reactor concept evolved from the early test and demonstration reactors BR-1, 2, 5, and 10 in the 1950s and research reactor BOR-60 that is still in operation. The first commercial SFR was BN-350 in Shevchenko, Kazakhstan, that was used for power production and desalination. Today's BN-600 emerged out of the BN-350.

The BOR-60 still plays a vital role in reactor development in Russia and around the world, as materials testing for several research programs has been done there. It has a neutron flux of 3.7×10^{15} n/cm^{2}s and allows for testing fuel and cladding materials in the 600−1300 K 327−1027°C temperature range, as well as experiments on sodium safety systems (Diakov, 2013). Although the initial lifetime was only for 20 years starting form 1969, the license has been extended until 2020.

The BN-600 has demonstrated the feasibility of SFR technology. There were no serious safety issues with the plant that resulted in any harm to the environment or personnel. At the same time, the BN-600 experience was an opportunity to understand the limitations of the current sodium reactor technology and improve the design of the following, larger BNs. For example, R&D was done for the reactor core, electric drives for the primary and secondary sodium pumps, as well as the refueling systems, reactor vessel monitoring, and steam generators' water−sodium reaction detection systems (Bakanov et al., 2013).

The current SFR development programs include construction of commercial BN-800 power plant and multi-purpose fast neutron research reactor (MBIR), and design work on a larger commercial BN-1200.

12.3.1 BN-800

The construction of the 790 MW_{el} BN-800 started in 1984 as Unit 4 at the Beloyarsk nuclear power plant (NPP), with an estimated startup planned for 1992. However, in 1986, after Chernobyl, all nuclear plant construction was put on hold and has not resumed until 2006, once the economic situation stabilized and the design was brought to the modern safety standards (Rosenergoatom, 2015; Vasiliev et al., 2006).

Besides power generation and eventual replacement of the BN-600, the BN-800 will be used to demonstrate enhanced safety features and principles that are to be implemented in the next generation of commercial SFRs. It is planned to eventually use the plant as part of the closed nuclear fuel cycle with mixed oxide (MOX) or nitride fuel. The reactor core is planned to be recycled 20 times over the course of 40 years with 730 fuel cycle length (equivalent full power day, EFPD) fuel campaigns. The facility will also play an important role in obtaining data on the economic performance and approaches to operating cost optimization as well as the advanced fuel

performance necessary to develop future nonproliferation and closed fuel cycle strategies. The design is 100% MOX fuel capable, can burn through weapons-grade Pu at a rate of up to 3 ton/year, and produce isotopes.

The BN-800 design is largely based on BN-600. The reactor vessel was kept the same, as there were significant margins in the BN-600 vessel and sodium-to-sodium heat exchangers. The most important design changes include (Mitenkov and Sarayev, 2005; IAEA, 2000):

- Increase in the thermal power to 2100 MW_{th} from 1470 MW_{th} for BN-600;
- Additional passive safety systems employing hydraulically suspended absorber rods, which would drop into the core when the sodium flow decreases to 50% of the rated flow;
- Passive decay heat removal through air hear exchanges connected to the secondary sodium loop, with three trains at 100% capacity each;
- Core catcher that prevents core melt from interaction with the core vessel;
- Core upper axial blanket is replaced by a sodium plenum in order for the enhanced axial neutron leakage to compensate for the positive sodium void reactivity effect;
- Additional measures to prevent sodium leaks and fires including modular steam generators, leak detection systems, guard vessel, etc.; and
- Manual operations are eliminated from the refueling system to allow for use of MOX fuel.

The BN-800 reactor vessel is a cylindrical tank with spherical bottom and tapered top. A guard vessel surrounds the reactor vessel, which is necessary to localize postulated sodium leaks. Reactor cooling pumps and intermediate heat exchanges are located inside the reactor vessel. Expansion bellows compensate for difference in thermal expansion of pumps and piping. The incoming sodium cools the reactor vessel. Biological shielding consists of steel sheets, steel billets, and graphite-filled tubes. The upper section of the reactor vessel houses three rotating plugs, which are necessary for refueling and accessing the in-vessel equipment.

The implemented safety system enhancements, use of steam reheating, and reduction in the number of auxiliary systems resulted in reduction of the specific steel consumption from 4.3 ton/MW_{th} for BN-600 to 2.7 ton/MW_{th} for BN-800. The estimated core damage frequency (CDF) is 7×10^{-6} per year, and the estimated large release frequency (LRF) is below 10^{-7} per year. The main design and performance characteristics of BN-800 are given in Table 12.2.

BN-800 (Fig. 12.2) has reached minimum controlled power level in June 2014. First loading of BN-800 core includes fuel assemblies with enriched UO_2, MOX, and vibro-packed MOX.

12.3.2 Multipurpose fast neutron research reactor

Given that Russia's main experimental SFR, BOR-60, will soon be decommissioned, a new multipurpose fast neutron research reactor (MBIR) is being developed. The MBIR (Fig. 12.3) is intended to provide broader experimental capabilities compared to BOR-60 due to increasing the neutron flux, a large amount of in- and out-of-core test cells and five test loops with Pb, Pb−Bi, and sodium coolants. The reactor designer is RDIPE. The head plant designer was Atomproekt, a former subdivision of the Russian

Table 12.2 Main characteristics of the BN-800 (Vasilyeva et al., 2013; Atomenergoproekt, 2011)

Parameter	Value
Power plant	
Design life	40 years
Thermal power	2100 MW
Electric power (gross)	890 MW
Efficiency	39.3%
Auxiliary power consumption	7.4%
Capacity factor	85%
Core	
Average core power density	430 kW/L
Fuel cycle duration	140 days
Fuel rod diameter	6.9 mm
Reactor core height	900 mm
Neutron flux	8.8×10^{15} n/cm^{2}s
Fuel	PuO_2-UO_2/U-Pu-N
Average burnup	68 MW × day/kg (cold worked ChS-68 cladding and mixed oxide) 90 MW × day/kg (cold worked EK-164 cladding and mixed oxide)
Breeding ratio	1.04
Primary sodium loop	
Number of loops	3
Coolant flow rate	31,920 ton/hour
Average core inlet temperature	354°C
Average core outlet temperature	547°C
Coolant inventory	910 ton
Secondary sodium loop	
Number of loops	3
Coolant flow rate	11,500 ton/hour
Average loop inlet temperature	309°C
Average loop outlet temperature	505°C

Table 12.2 Continued

Parameter	Value
Tertiary loop	
Number of loops	Pool
Steam generator design	Once-through, sectional modular
Number of sections per steam generator	10
Steam flow	792 ton/hour
Superheated steam pressure	14 MPa
Superheated steam temperature	490°C
Feed water temperature	211°C
Turbine configuration	High-pressure cylinder + 3 low-pressure cylinders



Figure 12.2 BN-800 NPP (January 2014).
http://www.okbm.nnov.ru/images/stories/Photogalery/Site/bn-800_web.jpg.

state-owned nuclear corporation: Rosatom, and scientific guidance is provided by IPPE. The MBIR research and production program formulated to date allows (Bychkov, 2010):

- irradiation testing of structural materials;
- development of advanced fuel and absorber material for fast and thermal reactors;
- research on advanced coolants including gas, molten salt, and liquid metals;
- in-pile tests of fuel elements, fuel assemblies, absorber elements, and other core internals for water-cooled water-moderated power reactors (VVERs), GEN-IV, and other reactors;
- studies fuel behavior under transient and accident conditions;

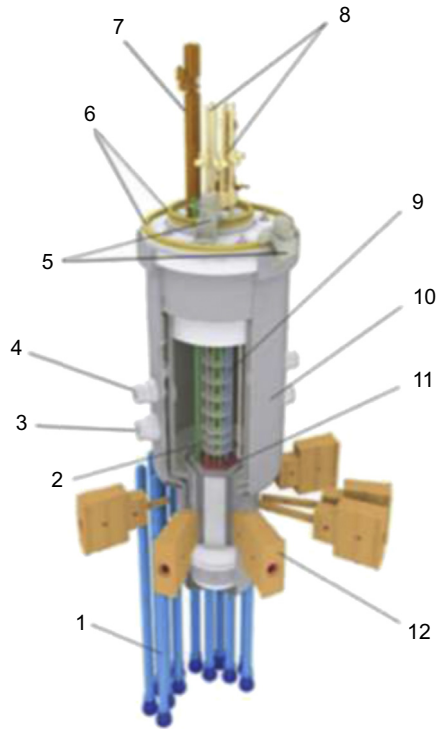


Figure 12.3 Overall view of the MBIR reactor (1 − Vertical experimental channel; 2 − Loop channel; 3 − Inlet pipeline; 4 − Outlet pipeline; 5 − Plug drives; 6 −Rotary plugs; 7 − Refueling mechanism; 8 − CPS actuator drives; 9 − Experimental channel; 10 − Reactor vessel with a safeguard vessel; 11 − Core; 12 − Horizontal experimental channel). http://nikiet.ru/eng/index.php?option=com_content&view=article&id=471%3Ap2&catid=12&Itemid=82.

- demonstration of coolant control technologies;
- verification of structural, materials, thermal−hydraulic, and other codes;
- studies of actinide transmutation for the purpose of refining the closed fuel cycle strategies;
- commercial production of radioisotopes and doped silicon;
- materials research using neutron radiography, tomography, neutron activation, etc.;
- use of neutron beams for medical applications;
- testing of reactor equipment;
- training of research reactor personnel;
- power generation; and
- process heat.

The MBIR reactor has the following in-vessel experimental facilities (Table 12.3):

- gas, sodium, heavy liquid metal (Pb, Pb + Bi), and molten salt experimental loops channels;
- instrumented test assemblies for irradiating fuel, absorber and structural materials;
- noninstrumented material test assemblies;
- noninstrumented isotope production assemblies.

Table 12.3 MBIR testing capabilities (Tretiyakov et al., 2014)

	Location	Amount	Neutron flux (n/cm^2s)
Noninstrumented materials test assemblies and isotope production assemblies	Core	Up to 14	Maximum: 4.9×10^{15} Average: 3.6×10^{15}
	Side reflector	Not limited	$0.3–2 \times 10^{15}$
Instrumented channels for experimental loops channels	Core	Up to 3	$3.2–4 \times 10^{15}$
Loop channels	Core center	1	5×10^{15}
	Side reflector	Up to 2	$1.3–2 \times 10^{15}$
Neutron radiography	Vertical out-of-the-vessel channels	1	1.14×10^{9}
Spectroscopy, activation analysis, solid state physics		2	1.08×10^{10}
		1	2.43×10^{10}
Neutron therapy		2	5.06×10^{10}
Silicon doping	Horizontal out-of-the-vessel channels	12	Up to 1.24×10^{13}
Neutron activation analysis		2	

The MBIR reactor configuration is typical for SFR with three loops with a secondary sodium loop (Tretiyakov and Dragunov 2012). MBIR safety features include a passive removal of decay heat in the primary loop by natural circulation, physical separation of the primary and secondary systems to cancel out the possibility of radioactive sodium leakage, and a fuel core catcher inside the reactor vessel. The operations and controls of MBIR also have safety features built in, such as automated process control systems to decrease the chances of operator error. CDF and LRF are estimated at 9.8×10^{-7} per reactor year and 6.1×10^{-8} per reactor year, respectively (Tretiyakov et al., 2014). The main design characteristics of the MBIR reactor are given in Table 12.4.

In 2014, NIIAR, in the city of Dimitrovgrad, obtained a site license for MBIR. A construction license was issued in May 2015, with an anticipated startup in 2020. Building in success of the BOR-60 in serving testing needs of foreign customers, Rosatom is seeking international partners to define future research programs and establish an international shared research center around the MBIR facility (Bychkov, 2010).

12.3.3 BN-1200

BN-1200 is the latest generation of sodium-cooled fast reactors intended for serial construction and transition to a closed fuel cycle nuclear power. Its fundamental engineering solutions rely on BN-600 and BN-800 experience, as far as sodium coolant

Table 12.4 MBIR design characteristics (Bychkov, 2010; Tuzov, 2015)

Parameter	Value
Thermal power, MW	150
Electric power, MW	60
Effective core diameter, mm	880
Core height, mm	550
Maximum linear power, W/cm	480
Core inlet temperature, °C	330
Core outlet temperature, °C	512
Core coolant flow rate, kg/s 650	650
Refueling interval, equivalent full power day	≥100
Neutron flux, n/cm^{2}s	5.5×10^{15} maximum 3.5×10^{15} maximum
Damage dose in the core's central plane, dpa/year	30 in the experimental loop channels 20 on the core periphery 11−17 in the side reflector's first-row
Fuel	Vibro-packed mixed oxide (24−38% Pu), (PuN + UN); Advanced fuels
Burnup, % of heavy atoms	8.65 average 12.2 maximum
Design lifetime, years	50

management, but are optimized to bring the capital costs close to water-cooled reactors for the sake of economic competitiveness.

An integral primary system layout is employed (Fig. 12.4), ie, reactor core, variable frequency submersible coolant pumps, intermediate heat exchanges, safety system heat exchangers, and cold trap filters. The reactor vessel is enclosed in a guard vessel. There are no auxiliary sodium systems in the primary circuit. The reactor core consists of fuel assemblies, boron shield assemblies, and absorber rods. The central part of the core consists of wrap-spaced hexagonal fuel assemblies and cells with absorber rods. The spent fuel is stored in the reactor vessel for up to 2 years, which facilitates spent fuel cooling and eliminates the need for spent fuel storage casks. Assemblies with boron carbide are placed behind the spent fuel to protect the reactor vessel.

The fuel composition is flexible. Core breeding for MOX fuel is facilitated by higher fuel volume fraction and increased fuel smeared density up to 9.2 g/cm^2. However, better physics parameters are provided for nitride cores, which are more compact and have higher breeding ratio and less excess reactivity.

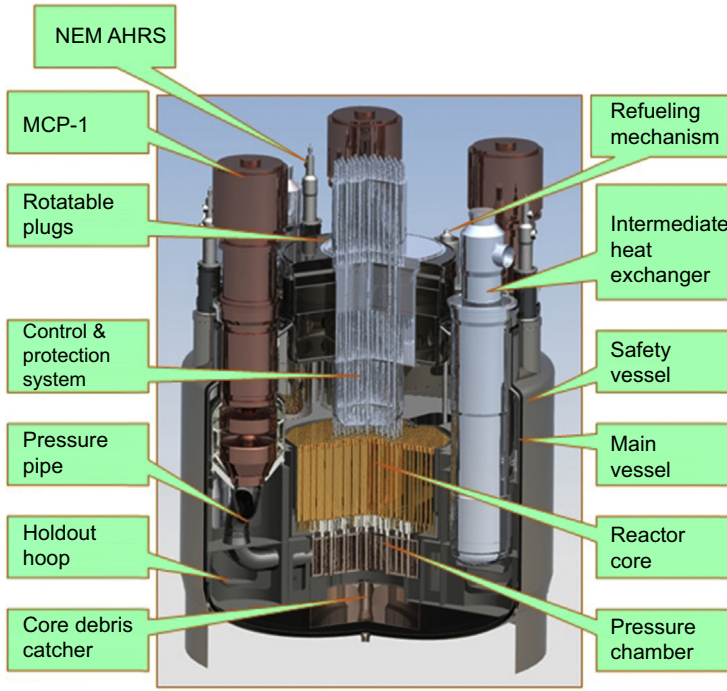


Figure 12.4 BN-1200 reactor.
http://www.okbm.nnov.ru/images/img/bn1200%20eng.jpg.

Similarly to other SFRs, BN-1200 has three circuits with four flow loops each. The primary and secondary circuits are sodium-cooled, and the third circuit coolant is water/steam. The secondary sodium pumps are single-stage vertical centrifugal pumps. The once-through steam generators are fitted with automatic protection system to guard against intercircuit leaks. There are two steam generator modules per coolant loop.

The key design parameters of BN-1200 are given in Table 12.5.

Besides the integral primary system configuration, additional safety features of BN-1200 compared to BN-800 include:

- passive emergency decay heat removal system;
- passive shutdown system with absorber rods responding to sodium temperature variations in the core; and
- reactor protection system that precludes accidental removal of more than one control rod.

As a result of the design simplification and introduction of passive safety features, both economic and safety parameters have improved. The CDF is reduced to 5×10^{-7} per reactor year, which is close to modern light water reactors. Compared with the BN-800, the BN-1200 design has less 14 systems and 900 valves. The BN-1200 design is more modular, therefore having only eight integral steam generators as compared to the 60 and 72 steam generator modules in BN-800 and BN-600,

Table 12.5 Main characteristics of the BN-1200 (Vasiliev et al., 2013; Zabudko et al., 2009; Shepelev, 2015)

Parameter	Value
Thermal power, MW	2800
Electric power, MW	1220
Reactor core height, mm	850
Fuel rod diameter, mm	9.3
Average power density, kW/L	230
Fuel type	UPuN/mixed oxide
Breeding ratio	1.2 for mixed oxide 1.08 for UpuN
Design burnup, MW-day/kg	75 cold worked austenitic steel and mixed oxide 92 for ferrite−martensitic steel and mixed oxide 74 for ferrite−martensitic steel and UPuN
Sodium temperature at reactor inlet/outlet, °C	410/550
Sodium temperature at SG inlet/outlet, °C	527/355
Steam temperature, °C	510
Steam pressure, MPa	17.5
Efficiency, gross/net	43.5/40.7
Fuel campaign, EFPD	330
Reactor system specific weight, ton/MW_{el}	5.6
Capacity factor	90%
Design lifetime, years	60

respectively. Likewise, the four BN-1200 secondary system coolant loops are standardized and symmetrically placed, thus streamlining construction and reducing the piping costs by a factor of 1.8 (Ashirmetov, 2015). These and other design simplifications yield expected capital cost close to modern VVER designs.

12.4 Heavy liquid metal reactors

The development of heavy liquid metal reactors (HLMRs) in Russia stems from its experience with Pb−Bi eutectic coolants in Soviet Alpha-class submarines. Altogether, USSR had eight nuclear submarines and two on-the-ground Pb−Bi-cooled reactor prototypes. Details of the submarine experience are extensively presented

elsewhere. An important result of the HLMR naval program was demonstration of a practical possibility of using heavy liquid metal coolant in a large-scale nuclear reactor. The most difficult technological issues were corrosion of fuel cladding and other structural components in Pb−Bi, polonium (Po) release, and primary coolant pump reliability. Experience gained with solving these problems is the basis for development of commercial Pb−Bi and Pb-cooled commercial reactors.

Advantages of heavy liquid metal coolants are well known. The choice between Pb−Bi eutectic and pure Pb depends on material reliability issues. While Pb−Bi eutectic has a lower melting temperature than Pb, which is preferable from materials standpoint, Bi is relatively expensive and transmutes into highly radioactive Po during operation. On the other hand, higher operating temperature of Pb-cooled reactor allows reaching efficiency, Pb is less corrosive compared to Pb−Bi at the same temperature, and during submarine operation, effective means to deal with Po have been developed. Given these tradeoffs, at the present time, Russia is developing both 100 MW_{el} Pb−Bi-cooled SVBR-100 reactor for regional grid applications and large Pb-cooled BREST reactors intended for closing the nuclear fuel cycle.

12.4.1 SVBR-100

SVBR-100 is the Russian entry into the SMR market. Its modular design, long refueling interval, and passive safety make it more suitable for small grids and remote locations than some of the competing LWR designs. The SVBR-100 development is a collaborative effort between the Rosatom and private En+ Group, which formed a joint venture, "AKME Engineering" (Toshinsky et al., 2011).

The most important design features of the SVBR-100 are (Petrochenko et al., 2015):

- an integral primary system configuration without primary piping and valves;
- fast neutron spectrum;
- ability to replace the reactor vessel;
- cartridge-type core with the whole fresh core loaded at once;
- repair of the primary circuit equipment and refueling are performed without coolant draining;
- decay heat removal by natural circulation;
- steam ingress into the core in an event of steam generator leak is precluded by the steam separation at the free liquid metal coolant level; and
- flexible fuel options, ie, MOX or nitride fuel with U enrichment at less than 20% and no breeding blanket.

A summary of SVBR-100 design characteristics is given in Table 12.6.

Similar to Pb, Pb−Bi eutectic is highly corrosive to reactor materials, and the corrosion potential depends on the amount of oxygen in the alloy. Corrosion resistance of the structural material can be achieved through controlling oxygen content in Pb or Pb alloy. Typically, iron (Fe) is the base element of the materials in contact with the coolant, with some chromium (Cr) and nickel (Ni) mixed in as alloying elements. Given that these three elements have a higher affinity for oxygen than for Pb−Bi, the Fe-based materials are primed with oxygen to form a protective oxide film, which

Table 12.6 Main characteristics of the SVBR-100 (AKME-Engineering, 2014; Petrochenko et al., 2015)

Parameter	Value
Thermal power, MW	280
Electric power, MW	100
Core inlet/outlet temperature, °C	340/490
Average core power density, kW/L	160
Average linear heat rate, W/cm	260
Fuel	UO_2 (16% enrichment), mixed oxide, UPuN
Core life, h	53,000
Fuel cycle, years	7–8
Steam pressure, MPa	6.7
Steam temperature, °C	278
Reactor system diameter/height, m	4.5/8.2
Reactor system weight, ton	280
Efficiency, %	36
Capacity factor, %	90
Design basis earthquake acceleration	0.12 g vertical, 0.25 g horizontal
Design lifetime, years	60

later prevents corrosion with the Pb–Bi coolant. Throughout the reactor's operation, the oxygen levels are carefully managed with the input from oxygen sensors and coolant systems. This technology has been used in the Soviet Alpha-class submarines, and its effectiveness up to 820 K 547°C has been confirmed by the EU accelerator-driven system research (Tuček et al., 2006).

Alternatively, US and European researches rely more on developing corrosion resistant steels and other materials. For example, the surface alloying by the so-called Gepulste Electronenstrahlanlage (pulsed electron beam facility) method enhances corrosion resistance at least up to 870 K 597°C (Wider et al., 2003). Nonmetallic claddings, such as SiC composites, are also being developed.

The SVBR-100 reactor (Fig. 12.5) meets the most stringent safety requirements due a combination of coolant properties, reactor, and overall plant design (Gidropress, 2011). The estimated CDF is 1×10^{-7}/year (AKME-Engineering, 2014). All of its primary equipment is housed inside a strong vessel with a protective housing to provide an integral (single unit) layout. A small free space between the main vessel and protective housing prevents the loss of coolant in the case of a postulated accident where the integrity of the reactor main vessel is lost. Also, the level of natural

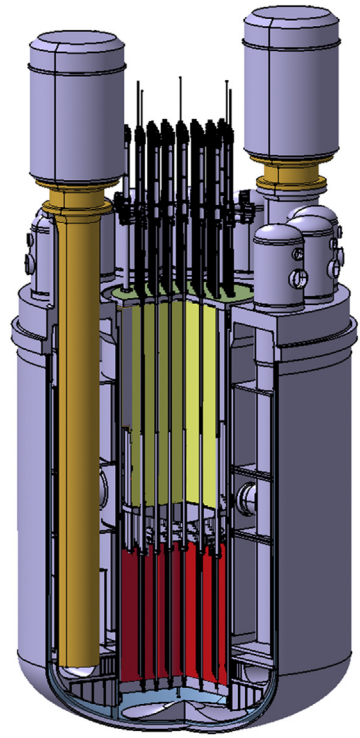


Figure 12.5 SVBR-100 reactor.
http://www.akmeengineering.com/398.html.

circulation of the primary and secondary coolant is sufficient for passive heat removal under cooldown conditions. Because the reactor vessel is located inside a water tank, passive heat transfer via the vessel to the tank water provides passive core cooling during at least 5 days without operation intervention. In addition, since the SVBR-100 secondary system pressure is higher than primary, radioactive contamination is not possible in case of steam generator tubing rapture. The low potential energy accumulated in the coolant reduces the extent of damage possibly caused by external impact. Even a postulated combination of concrete compartment destruction, a large break of primary system followed by a direct contact of Pb−Bi coolant with air does not lead to releases that might require evacuation of the local population.

As for the fuel, the SVBR has favorable neutron physical properties of its Pb−Bi coolant: a low coefficient of volumetric expansion in a combination with the control algorithms provide for a low reactivity margin during operation. The very high temperature of Pb−Bi coolant boiling ($\sim 1670^{\circ}C$) eliminates accidents due to departure from nucleate boiling in the core and makes it possible to maintain low primary pressure under normal operating conditions and in the case of hypothetical accidents. Negative reactivity feedbacks provide power reduction to the level that does not lead to core damage in case of an uncontrolled control rod withdrawal. There is a low chance of

chemical explosions and fires as a result of internal events, due to Pb−Bi inertness. Likewise, the ability of Pb−Bi to retain fission products (iodine, cesium, and some actinides) can considerably reduce the radiological consequences of a postulated loss of coolant accident (LOCA). And it avoids one of the main post-Fukushima accident concerns altogether, hydrogen explosions, as there are no materials that could generate hydrogen under any conditions.

In February 2015, the Russian regulator Rostechnadzor issued a site license for SVBR-100 in the city of Dimitrovgrad. The startup of the pilot unit is planned for 2019 followed by deployment at En+ Group's industrial sites in metallurgy and chemical and ore mining (AKME-Engineering, 2014) for power and process heat and desalination applications.

12.4.2 BREST-OD-300

The BREST-OD-300 is a 300 MW_{el} demonstration fast reactor with Pb coolant and on-site fuel reprocessing facilities (Dragunov et al., 2014). It is a precursor for a commercial BREST-1200 (Filin et al., 2000). BREST fully realizes the inherent safety concept aimed for in the Russian nuclear development program (Section 12.1). It uses Pb in an integral primary circuit to minimize LOCA, coolant fires, possibility of reactor vessel rapture, and generation of radioactive materials in the coolant itself. The high thermal capacity of the primary loop allows it to remove decay heat via natural circulation of the lead and thus mitigate loss of flow accident or other operating issues as far their impact on fuel integrity is concerned. As for the nitride U−Pu fuel, it has a high density (14.3 g/cm^3) and high thermal conductivity (20 W/m K), allowing for relatively low fuel temperature ($T_{max} < 1300°C$), low stored energy, low rate of gaseous fission products release, and low-pressure fuel rod pressure. Also, Pu breeding and small fuel temperature power effects reduce the required excess reactivity and reactivity initiated accident impacts. The reactor vessel is a steel-lined steel−concrete composite structure with build in heat exchanges for initial heating and decay heat removal, and has five hydraulically coupled cavities.

The central cavity that houses the reactor core has a side reflector, core barrel, and SNF storage (Fig. 12.6). The four peripheral cavities house steam generators, reactor coolant pumps, heat exchangers, filters, and other components. The Pb flows through the core due to differences in free levels generated by main coolant pumps. This design assures gradual decrease in the coolant flow in case of a pump trip. It also excludes the possibility of steam bubbles entering the core in case of a steam generator leak.

The reactor core is composed of hexagonal canless fuel assemblies (FAs) that facilitate handing of anticipated operational occurrences and minimize the amount of structural materials in the core. The radial power distribution is controlled by use of fuel rods of different diameters: smaller in the central zone and larger in the peripheral zone. There are two groups of absorber rods: scram and control rods. The rod drive mechanisms are attached to the upper rotary plug, and in a withdrawn condition, the rods stay below the core. For refueling, the drives are disengaged from the rods, and they float up into the core. Hexagonal channels form the side reflector where a low flow rate is maintained. Some channels are partially gas-filled such that the Pb

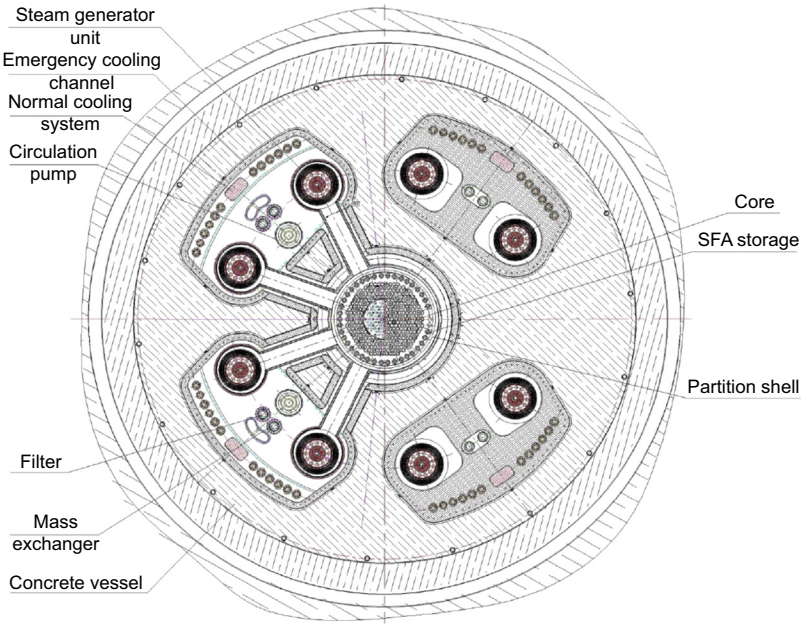


Figure 12.6 BREST-OD-300 primary system layout.
https://www.iaea.org/NuclearPower/Downloadable/Meetings/2013/2013-03-04-03-07-CF-NPTD/T3.4/T3.4.smirnov.pdf.

column level tracks the coolant pressure and affects the neutron escape, which provides for an additional feedback mechanism for the safety and control systems.

The first BREST core is likely to be nitride of depleted U mixed with Pu and MAs, whose composition corresponds to reprocessing and subsequent cooling for ~20 years, which is close to an equilibrium composition. The reloading interval is determined by cladding performance, as opposed to burnup. Reprocessing would be limited to the removal of fission products without separating Pu and MAs. The option of BREST startup on 12% enriched U with a gradual changeover to (U + Pu)N fuel is also being considered. In this case the, whole core would be reprocessed to remove only fission products (FPs) and an appropriate amount of depleted U (Bulkin et al., 2011). One of the notable characteristics of the BREST plant is that a reprocessing plant is co-located with the reactor, eliminating need for SNF transport and associated proliferation concerns.

Mononitride UN and UPuN fuel was initially tested in the BR-10 and BOR-60 reactors at 350−1045 W/cm and 4−9% burnup. Both showed good resistance to irradiation and low reaction rates with liquid metal coolants. They are also compatible with ferritic−martensitic steels, eg, EP-823 and EP-450 up to 800°C for 2000 h and 1200−1300°C for 5 h (Filin, 2000). In 2014−2015, hot cell examinations of UPuN fuel rods irradiated in BOR-60 and BN-600. Irradiation experiments on UPuN FAs for BREST and BN have started (Nikitin, 2015). The main design characteristics of the BREST-OD-300 are given in Table 12.7.

Table 12.7 Main characteristics of the BREST-OD-300 (Bulkin et al., 2011)

Parameter	Value
Thermal power, MW	700
Electric power, MW	300
Number of loops	4
Fuel	(U−Pu)N, (U−Pu−MA)N, UN, $(U-Pu)O_2$
Core diameter, mm	2650
Core height, mm	1100
Number of fuel assemblies	169
Average core power density, kW/L	200
Fuel assembly design	Canless, hexagonal
Fuel rod diameter, mm	9.7; 10.5
Fuel rod pitch, mm	13.0
Average burnup (depending on fuel type), %	3.1−5.5
Maximum burnup (depending on fuel type), %	5.6−8.3
Fuel cycle, years	5
Breeding ratio	~1.05
Coolant temperature, °C (inlet/outlet)	420/540
Maximum cladding temperature, °C	650
Steam temperature, °C	505
Steam pressure, MPa	18
Feed water temperature, °C	340
Efficiency, %	43
Design life, years	30

The BREST-OD-300 design has been developed based on naval Pb−Bi reactor experience, small- and full-scale equipment mockups for Pb coolant and numerical modeling using the existing neutronic, thermal−hydraulic, and radiation physics codes. The selection of power level, basic design features, including subcritical steam parameters, are determined by the need to demonstrate the fuel cycle closing using prototypical fuel characteristics, safety performance of the reactor system and, at the same time, maximize use of reference design solutions outside of the fuel and reactor.

The ongoing R&D program includes experimental verification of components' performance (eg, the main coolant pipe), fuel testing, transient and safety analyses, manufacturability studies, and cost optimization. The construction of a pilot fuel plant for the BREST-OD-300 has started in April 2014 at Siberian Chemical Combine in Tomsk. The plant is scheduled to begin operating in 2017, in time to produce the first fuel load by 2020. A reprocessing facility at the same site is expected to come online in 2022.

12.4.3 BREST-1200

Lessons learned from testing the BREST-OD-300 will be used to design the BREST-1200, expected to become a 1200 MW_{el} commercial Pb-cooled fast reactor. Conceptually, the BREST-OD-300 and BREST-1200 are similar. The main differences are (Filin et al., 2000):

- Use of supercritical steam cycle with parameters compatible with the Russian-made supercritical turbines K-1200-240LMZ;
- Fuel rod diameters (9.1, 9.6, and 10.4 mm) with the same Pu content in order to flatten the radial power distribution in the core;
- In the absence of coolant flow, heavy absorber rods are inserted into the core due to gravity; and
- Handling fresh and burned fuel assemblies by different mechanisms in and outside of the reactor vessel.

The main design characteristics of BREST-1200 plant are given in Table 12.8 (Filin, 2000).

The BREST-1200 design work has not been completed, as it is desirable to take into account experience of operating the demonstration plant BREST-OD-300.

12.5 Supercritical water reactor

Russian has signed the Generation IV International Forum Supercritical Water Reactor (SCWR) System Arrangements in 2011, and the work remains at a level of conceptual studies. Several SCWR concepts have been developed since the 1990's and much still remains for future investigation.

In 2006, Research and Development Institute of Power Engineering (RDIPE) developed a concept of supercritical water-cooled (25 MPa and 550°C) and graphite-moderated power reactors (VGERs). The pressure tube-type primary system and graphite moderator allow for power scaling from 850 to 1700 MW. The fuel cladding performance in the steam superheating mode was verified at experimental channels at Beloyarsk NPP. The fuel is cermet, similar to that in the steam superheating channels of the water-cooled graphite-moderated pressure-tube reactors (AMBs). The safety concept relies on a combination of active and

Table 12.8 Main characteristics of the BREST-1200

Parameter	Value
Thermal power, MW	2800
Electric power, MW	1200
Core diameter, mm	4755
Core height, mm	1100
Fuel	UN + PuN
Number of fuel assemblies	332
Fuel cycle, years	5–6
Breeding ratio	~1
Coolant temperature, °C (inlet/outlet)	420/540
Coolant flow rate, ton/s	158.4
Steam temperature, °C	520
Feed water temperature, °C	340
Efficiency, %	43
Lifetime, years	60

passive systems similar to the newer generation of VVERs (Yurmanov et al., 2009). In 2009, RDIPE proposed a more advanced concept, a fast pressure-tube supercritical water-cooler power reactor (BKER), with the following features:

- once-through core cooling; breeding ratio >1;
- annular fuel elements;
- a tight lattice with high U content and cermet fuel; and
- plant efficiency up to 45%.

Preliminary safety analyses have been performed (Barinov et al., 2009). Both RDIPE concepts rely on the following materials and water chemistry solutions: exclusion of copper-containing alloys and use a titanium condenser; neutral water chemistry with demineralization of turbine condensate and oxygen injection into condensate to reduce transport of corrosion products; and suppression of water coolant radiolysis by injection of gaseous hydrogen, ammonia, or hydrazine into feed water.

Since 00's Gydropress has developed supercritical water-cooled water-moderated power reactors (VVER-SKD) in two circuit (with steam generators) and direct cycle configurations. The more advanced direct cycle concept has the following characteristics, as shown in Table 12.9 (Sidorenko, 2010; Glebov et al., 2014; Gabriel et al., 2013).

Two options for the VVER-SKD core cooling were considered: a single pass and a two pass.

Table 12.9 Main characteristics of the BREST-1200

Parameter	Value
Thermal power, MW	3830
Electric power, MW	1700
Number of fuel assemblies	241
Coolant temperature, °C (inlet/outlet)	290/540
Efficiency, %	44−45%
Fast neutron spectrum breeding ratio	0.9−1.0
Reactor vessel diameter, mm	4800
Reactor vessel height, mm	1500
Reactor vessel thickness, mm	335
Core diameter, mm	3600
Core height, mm	4500
Fuel	MOX with austenitic alloy (ChS-68, EP-172)
Rod diameter, mm	10.7
Average linear heat rate	156 W/cm
Coolant pressure, MPa	25
Water flow rate, kg/s	1880

In the two-pass option, the core is divided into downcomer and riser sections with approximately equal number of FAs. This considerably decreases maximum fuel temperature, peaking factors, and maximum linear heat flux. However, in the two-pass coolant scheme, coolant temperature reactivity coefficient might become positive at some point during operation.

12.6 Conclusion

The future of the Russian nuclear industry is expected to be a closed fuel cycle, powered by a combination of LWR and fast reactor technology. The critical element in the Russian strategy is the GEN-IV fast reactor technology, including sodium, Pb, and Pb−Bi-cooled reactors. The USSR and then Russia have experimented with all three of these technologies, including building experimental and demonstration reactors, over the last half century.

Currently, there are several demonstration and commercial reactors under construction and design in Russia. In the SFR technology, the BN-800 will be completed in

2015, and the commercial BN-1200 by about 2030. In the Pb-cooled reactor fleet, the BREST-OD-300 is under construction, and BREST-1200 is in the design stages. The Pb−Bi-cooled SVBR-100 is targeted to capture the emerging SMR market. A combination of the BN-800/1200, BREST-OD-300/1200, and SVBR-100 will allow Russia to meet the new inherent safety goals, including accident prevention, waste disposal, and nonproliferation.

Nomenclature

DNB	Departure from nucleate boiling
dpa	Displacements per atom
EFPD	Equivalent full power day
g	Standard gravity
GESA	Gepulste Electronenstrahlanlage (pulsed electron beam facility)
HPC	High-pressure cylinder
IPPE	Institute of Physics and Power Engineering
HLMR	Heavy liquid metal-cooled reactors
LOCA	Loss of coolant accident
LOFA	Loss of flow accident
LPC	Low pressure cylinder
LRF	Large release frequency
MA	Minor actinides
MCP	Main coolant pump
n	Neutron
NIIAR	Research Institute of Atomic Reactors
RDIPE	Research and Development Institute of Power Engineering
RIA	Reactivity initiated accident
SCC	Siberian chemical combine
SNF	Spent nuclear fuel
T_{max}	Maximum temperature
USSR	Union of Soviet Socialist Republics
WWII	Second World War

References

AKME-Engineering, 2014. SVBR-100: Small Modular Multipurpose Generation IV Reactor.

Ashirmetov, M.R., 2015. BN-1200 reactor unit. In: Proceedings of the Conference: "Proruiv" Project: Results of the Project for New Technological Platform for Nuclear Energy. Moscow, Russia.

Atomenergoproekt, 2011. BN-800 NPP. JSC, St. Petersburg Research and Design Institute Atomenergoproekt, St. Petersburg, Russia.

Avronin, E., Adamov, E., et al., 2012. Conceptual Basis for Strategic Development of Russia's Nuclear Energy in the XXI Century. NIKIET, Moscow, Russia.

Bakanov, M.V., Nosov, Yu.V., Potapov, O.A., 2013. Operating experience with the BN-600 sodium-cooled fast reactor. In: FRs and Related Fuel Cycles: Safe Technology and Sustainable Scenarios (FR13). Proceedings from the International Conference on Fast Reactors and Related Fuel Cycles, vol. 2. Paris, France.

Barinov, S.V., Vikulov, V.K., Gmyrko, V.Y., et al., 2009. A concept of the fast pressure-tube power SCW reactor BKER. In: 6th International Conference "Safety Insurance for VVER Nuclear Power Plants." Podolsk, Russia.

Bulkin, S.Yu, Lemekhov, V.V., Sila-Novitsky, A.G., et al., 2011. Research and development for demonstration of fuel performance in the BREST-OD-300 core. In: IAEA Technical Meeting Design, Manufacture and In-pile Behaviour of Fast Reactor Fuel. Institute of Physics and Power Engineering, Obninsk, Russia.

Bychkov, A., 2010. MBIR Research Reactor as New Generation Multilateral Project for Third Phase of INPRO. State Scientific Centre Research Institute of Atomic Reactors. INPRO Dialogue Forum on Nuclear Energy Innovations. IAEA, Vienna, Austria.

Diakov, A., 2013. On Conversion of Research Reactors in Russia. Center for Arms Control, Energy, and Environmental Studies. http://www.armscontrol.ru/pubs/en/on-conversion-of-research-reactors-in-russia-en-corr.pdf (accessed 20.05.15.).

Dragunov, Yu.G., Lemekhov, V.V., Moiseyev, A.V., Smirnov, V.S., 2014. Lead-Cooled fast-neutron reactor BREST. In: International Scientific and Technical Conference. NIKIET-2014, Moscow, Russia.

Filin, A.I., Orlov, V.V., Leonov, V.N., et al., 2000. Design Features of BREST Reactors and Experimental Work to Advance the Concept of BREST Reactors. RDIPE, Moscow, Russia.

Filin, A.I., 2000. Current status and plans for development of NPP with BREST reactors. In: IAEA Advisory Group Meeting. RDIPE, Moscow.

Gabriel, O.O., Alade, A.M., Chad-Umoren, Y.E., 2013. Science and technology of supercritical water-cooled reactors: review and status. Journal of Energy Technologies and Policy 3 (7).

Gidropress, 2011. SVBR Reactor Plants. Podolsk, Russia.

Glebov, A.P., Klushin, A.V., Baranaev, Yu.D., 2014. Peculiarities development of nuclear energy and implementing fuel cycle closure in Russia. In: International Scientific and Technical Conference "Innovative Projects and Technologies of Nuclear power." ISTC NIKIET – 2014, Moscow, Russia.

IAEA, 2000. Transient and Accident Analysis of a BN-800 Type LMFR with Near Zero Void Effect. IAEA-TECDOC-1139.

Kagramanyan, V., 2009. Economics and Performance of Fast Neutron Systems. Panel 1 – FR09. Kyoto, Japan.

Lopatkin, A.V., Orlov, V.V., 1999. Fuel Cycle of BREST-1200 with Non-proliferation of Plutonium and Equivalent Disposal of Radioactive Waste. IAEA-SM-357/48. Research and Development Institute of Power Engineering, Moscow, Russia.

Mitenkov, F., Sarayev, O., 2005. BN-800: a key part of Russia nuclear strategy. Nuclear Engineering International 550 (608), 10−13.

Nikitin, O.N., 2015. First results of postirradiation studies of a fuel rod with mixed nitride uranium-plutonium fuel. In: Proceedings of the Conference: "Proruiv" Project: Results of the Project for New Technological Platform for Nuclear Energy. Rosatom State Corporation, Moscow, Russia.

Petrochenko, V., Toshinsky, G., Komlev, O., 2015. SVBR-100 nuclear technology as a possible option for developing countries. World Journal of Nuclear Science and Technology 5, 221−232.

Pshakin, G., February 2010. The USSR-Russia Fast-Neutron Reactor Program. Fast Breeder Reactor Programs: History and Status. Research Report 8: International Panel on Fissile Materials, ISBN 978-0-9819275-6-5.

Rosatom, 2009. Federal Target Program: Nuclear Energy Technologies of New Generation for 2010−2015 and up to 2020. Rosatom State Corporation, Moscow, Russia.

Rosenergoatom, 2015. Construction of the BN-800 Power Unit. http://www.belnpp.rosenergoatom.ru/wps/wcm/connect/rosenergoatom/belnpp_en/about/prospects-bn-800/ (accessed 08.05.15.).

Shepelev, S.F., 2015. Design of BN-1200 reactor system. In: Proceedings of the Conference: "Proruiv" Project: Results of the Project for New Technological Platform for Nuclear Energy. Rosatom, Moscow, Russia.

Sidorenko, V.A., 2010. Prospects of VVER technology development. In: 7th International Scientific Technical Conference. Moscow, Russia (in Russian).

Toshinsky, G.I., Komlev, O.G., Tormyshev, I.V., Danilenko, K.Y., 2011. Effect of potential energy stored in reactor facility coolant on NPP safety and economic parameters. In: Proceedings of ICAPP 2011. Paper 11465. Nice, France.

Tretiyakov, I.T., Dragunov, Yu.G., 2012. MBIR, an innovative reactor for validation of innovative designs. In: Nuclear Research Facilities in Russia. JSC "NIKIET", Moscow, Russia.

Tretiyakov, I.T., Romanova, N.V., et al., 2014. MBIR, a reactor facility for validation of innovative designs. In: Conference Proceeding from the International Scientific and Technical Conference "Innovative Designs and Technologies of Nuclear Power." JSC NIKIET, Moscow, Russia.

Tuček, K., Carlsson, J., Wider, H., 2006. Comparison of sodium and lead-cooled fast reactors regarding reactor physics aspects, severe safety and economical issues. Nuclear Engineering and Design 236, 1589−1598.

Tuzov, A., 2015. MBIR international research center: current progress and prospects. In: IAEA TWG-FR Meeting, Obninsk.

Vasiliev, B.A., Kamanin, U.L., Kochetkov, L.A., et al., 2006. The need for reactor-based research in developing the BN-800 project and justification of future BN projects. In: International Scientific-Engineering Conference: "Research Reactors in the 21st Century." NIKIET, Moscow, Russia.

Vasilyev, B.A., Zverev, D.L., Yershov, V.N., et al., 2013. Development of fast sodium reactor technology in Russia. In: International Conference on Fast Reactors and Related Fuel Cycles: Safe Technologies and Sustainable Scenarios (FR13). Paris, France.

Wider, H., Carlsson, J., Dietze, K., Konys, J., 2003. Heavy-metal cooled reactors—pros and cons. In: Proceedings of GLOBAL'03, New Orleans, USA.

Yurmanov, V.A., Belous, V.N., Vasina, V.N., Yurmanov, E.V., 2009. Chemistry and corrosion issues in supercritical water reactors. In: IAEA International Conference on Opportunities and Challenges for Water Cooled Reactors in the 21st Century. Vienna, Austria.

Zabudko, L.M., Poplavsky, V.M., Shkaboura, I.A., et al., 2009. Fuels for advanced sodium cooled fast reactors in Russia: state-of-art and prospects. In: International Conference on Fast Reactors and Related Fuel Cycles (FR09). Kyoto, Japan.

Generation IV concepts in Korea

13

D. Hahn
Korea Atomic Energy Research Institute, Daejeon, Republic of Korea

13.1 Current status of nuclear power in Korea

Nuclear power generation is not an option but a necessity for energy security in Korea, which is poor in natural energy resources. Nuclear energy has played a major role as the main source of power generation in Korea for the past 40 years. Korea currently operates 24 reactors, which account for 22% of its total electricity generation capacity. Prior to the Fukushima nuclear accident in Japan, the direction of nuclear power technology focused on improving the economic efficiency without exceeding the safety regulation level. However, with increased public interest in the safety of nuclear power plants, the development of technology to improve the safety rather than the economic feasibility of nuclear power plants has recently become more important.

Recognizing that nuclear safety is a top priority, Korea will continue to utilize nuclear energy as a practical solution to address issues such as rising energy demand and climate change. Under the 2nd National Energy Basic Plan, the portion of nuclear power in the total energy mix will be 29% by 2035. According to the plan, 11 nuclear power plants will be built by 2024 with the start of commercial operation of Shin Kori units 3 and 4 slated for 2015 and 2016, respectively.

Korea's Science, ICT and Future Planning Minister and the President of King Abdullah City for Atomic and Renewable Energy signed a memorandum of understanding (MoU) aimed at establishing SMART partnership for joint development and commercialization of SMART in March 2015. Under the MoU, the two countries are set to conduct a 3-year preproject engineering project to review the feasibility of constructing at least two SMART plants in Saudi Arabia. The agreement is expected to provide opportunities for Korea to commercialize, for the first time in the world, the indigenously designed SMART by constructing it in Saudi Arabia if Saudi Arabia decides to build additional reactors after a preliminary review. It is expected to help Korea exploit the global small- and medium-sized reactor market if the two countries are to cooperate on the commercialization and export of the SMART reactor to third countries.

Korea has been developing a prototype Generation IV (Gen-IV) sodium-cooled fast reactor (PGSFR) design according to the national long-term plan for the development of future nuclear energy systems. A specific safety analysis report of the PGSFR will be submitted to the regulatory authority in 2017 for its design approval by 2020. As a preliminary step before a formal safety evaluation, the Korea Atomic Energy Research Institute (KAERI) is going to submit a preliminary safety information document to the regulatory authority by the end of 2015 for an independent and authorized peer review on the safety of the PGSFR. For the successful development of the PGSFR design,

Handbook of Generation IV Nuclear Reactors. http://dx.doi.org/10.1016/B978-0-08-100149-3.00013-6
Copyright © 2016 Elsevier Ltd. All rights reserved.

Korea has been actively engaged in international collaborative research activities. As part of this effort, Korea has been actively participating in collaborative research and development (R&D) activities of the Gen-IV International Forum (GIF). Large experimental facilities have been constructed to conduct various experiments to validate thermal–hydraulic phenomena and a large sodium loop, called Sodium Test Loop for Safety Simulation and Assessment (STELLA)-1, for the test of key decay heat removal system (DHRS) components, started its operation in 2014. Design work started in early 2015 for STELLA-2, which is an integral test loop for a simulation of the thermal–hydraulic characteristics of the PGSFR primary and intermediate heat transport systems.

A very high temperature reactor (VHTR) is primarily dedicated to the generation of hydrogen, which has been dubbed as the fuel of the future and an alternative energy source to replace fossil fuels. Hydrogen production using a VHTR in conjunction with thermochemical water splitting does not emit greenhouse gases, unlike the conventional natural gas steam–methane reforming. Therefore, hydrogen production using a VHTR is a clean and efficient method to reduce dependence on fossil fuel in Korea. KAERI has been developing a VHTR and nuclear hydrogen key technologies since 2006, targeting the demonstration of nuclear hydrogen by 2030.

VHTR R&D consists of two major projects: the key technology development project of nuclear hydrogen and the nuclear hydrogen development and demonstration (NHDD) project. The key technology development project focuses on the development and validation of key and challenging technologies required for the realization of a nuclear hydrogen system. The key technologies, which are the basis of Gen-IV VHTR R&D collaboration, are mainly focused on the development of computational tools, high-temperature experimental technology, a high-temperature material database, TRI-ISOtropic (TRISO) fuel fabrication, and the hydrogen production process. The NHDD project is aimed at the design, construction, and demonstration of a nuclear hydrogen system using a VHTR. Preparation for the NHDD project began by launching an alliance for nuclear hydrogen, which consists of nine nuclear industry companies or institutes and five end users in 2009. To enhance international collaboration, a MoU with NGNP industrial alliance was signed in 2013.

13.2 Plans for advanced nuclear reactors in Korea

13.2.1 Sodium-cooled fast reactor

Although the energy supply in Korea has been ensured by nuclear power, the continuous increase of the nuclear power plants has caused a spent fuel storage problem. Therefore, a technical alternative to solve the spent fuel management is necessary to technically support the decision making process for spent fuel management.

It has been recognized nationwide that a fast reactor system is one of the most promising nuclear options for electricity generation with an efficient utilization of uranium (U) resources and a reduction of the radioactive wastes from nuclear power plants. In response to this recognition, sodium-cooled fast reactor (SFR) technology

development efforts in Korea commenced in June 1992 with the Korea Atomic Energy Commission's approval of a national mid- and long-term nuclear R&D program. At the early stages of its development, the research efforts focused on the basic R&D of core neutronics, thermal hydraulics, and sodium technology, with the aim to enhance the basic liquid metal-cooled reactor technology capabilities.

The basic R&D efforts made in the early development stage had been extended to develop the conceptual designs of KALIMER (Korea Advanced LIquid MEtal Reactor)-150 (150 MW_{el}) (Hahn et al., 2002) and -600 (600 MW_{el}) (Hahn et al., 2007), and the basic key technologies over the past 10 years since 1997 under the revised nuclear R&D program. According to the Nuclear Technology Roadmap established in 2005, an SFR was chosen as one of the most promising future types of reactors, which could be deployable by 2030.

The KALIMER-600 features a proliferation-resistant core without a blanket, and a decay heat removal circuit using natural sodium circulation cooling for a large power system. In addition, a shortened intermediate heat transport system (IHTS) piping and a seismic isolation are incorporated into the KALIMER-600 design. The KALIMER-600 conceptual design, which evolved on the basis of the KALIMER-150 (150 MW_{el}) design, was selected as one of promising Gen-IV SFR candidates. R&D efforts have been made on the development of advanced design concepts including a supercritical CO_2 Brayton cycle energy conversion system, design methodologies, computational tools, and sodium technology.

The development of the SFR technology in Korea entered a new phase from 2007 with Korea's participation in the Gen-IV SFR collaboration project. An advanced SFR design concept that can better meet the Gen-IV technology goals had developed until 2011. R&D efforts were conducted to develop the conceptual design of the advanced SFR, focusing on the core and reactor systems, and a development of the advanced SFR technologies necessary for its commercialization and basic key technologies. To develop these advanced technologies, R&D was conducted to improve the economics, safety assurance, and metal fuel performance of an SFR in the areas of safety, fuels and materials, reactor systems, and the balance of plant. To provide a consistent direction to long-term R&D activities, the Korea Atomic Energy Commission (KAEC) authorized a long-term development plan in December 2008 for future nuclear reactor systems, which include SFR, pyroprocess, and very high temperature gas-cooled reactor (VHTR). KAEC authorized the modification of the plan in November 2011, reflecting the maturity of technology achieved hitherto and the budget condition (Kim et al., 2013a,b). The modified plan includes a design development of the prototype SFR by 2017, its design approval and construction by 2020 and 2028, respectively, as shown in Fig. 13.1. This long-term plan has been implementing through nuclear R&D programs of the National Research Foundation, with funds from the Ministry of Science, ICT and Future Planning. The SFR Development Agency was organized in May 2012 to secure the budget and efficiently manage the SFR Development Project. According to the plan, KAERI, the main body responsible for the fast reactor development in Korea, is developing a design of the prototype SFR. The prototype SFR development will be extended to the commercialization phase with its initialization in around 2050.

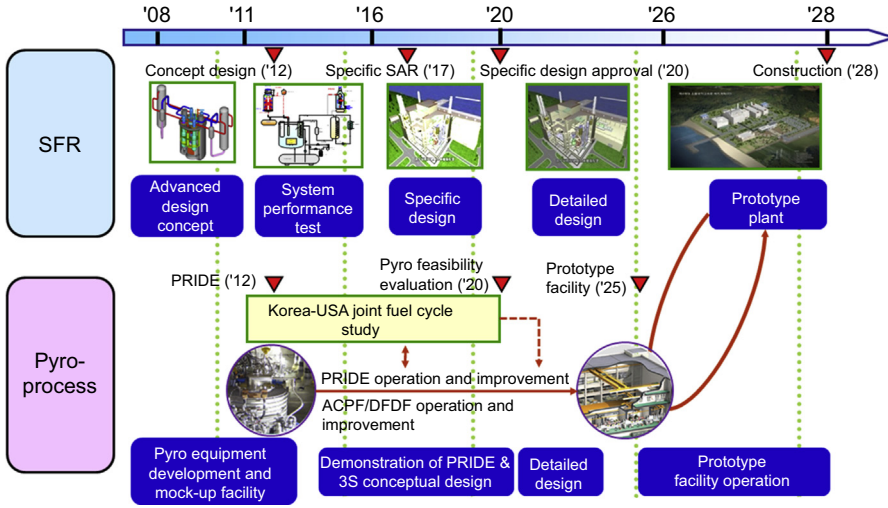


Figure 13.1 SFR pyroprocess development plan. *PRIDE*, pyroprocessing integrated inactive demonstration facility; *ACPF*, advanced spent fuel conditioning process facility; *DFDF*, dupic fuel development facility; *3S*, safety, security, safeguards.
Kim, Y.I., et al., April 2015. Internal Conference on Fast Reactors and Related Fuel Cycles (FR13).

For the development of pyroprocess, KAERI constructed the Pyroprocess Integrated Inactive Demonstration Facility, which is a mock-up facility for pyroprocessing. After engineering-scale demonstration by 2020, the Korea Advanced Pyroprocess Facility, being a prototype facility, will be constructed by 2025.

The metal fuel for the prototype SFR is being developed in accordance with the SFR and pyroprocess development plan. Fuel fabrication technology will be developed by 2018, and a U−zirconium (Zr) fuel manufacturing facility will be constructed by 2024. U−Zr fuel will be used as a starting fuel for initial core, and U−TRU−Zr fuel will replace U−Zr fuel after verification of its in-pile performance.

13.2.2 Very high temperature gas-cooled reactor

A very high temperature gas-cooled reactor (VHTR) is an inherently safe reactor that can produce heat of 750°C−950°C. By virtue of its high temperature heat, a VHTR can be used in high-temperature process heat applications, including hydrogen production and high-efficiency electricity generation. The most effective application of a VHTR is the massive hydrogen production in support of the hydrogen economy.

The rapid climate changes and heavy energy reliance on imported fossil fuels have motivated the Korean government to set up a long-term vision for transition to the hydrogen economy in 2005. One of the big challenges is how to produce massive hydrogen in a clean, safe, and economic way. Among the various hydrogen production methods, massive, safe and economic production of hydrogen by water splitting using

a VHTR can provide a successful path to the hydrogen economy. Particularly in Korea, where the use of land is limited, the "nuclear" hydrogen is deemed a practical solution, due to its high energy density.

Another merit of the nuclear hydrogen is that it is a sustainable and technology-led energy unaffected by the unrest of fossil fuel. Current hydrogen demand is mainly from oil refinery and chemical industries. Hydrogen is mostly produced by steam reforming using fossil fuel heat, which emits a large amount of greenhouse gases. Today in Korea, more than 1 Mtons/year of hydrogen is produced and consumed in oil refinery industries. In 2040, it was projected on a hydrogen roadmap that 25% of the total hydrogen demand will be supplied by the "nuclear" hydrogen, which is around 3 Mtons/year, even without considering the hydrogen iron ore reduction.

In order to prepare for the upcoming hydrogen economy, the nuclear hydrogen key technologies development project was launched at KAERI in 2006 as a national program of the Ministry of Education, Science and Technology (Chang et al., 2007). KAERI has taken a leading role in the project and the development of VHTR technologies. The Korea Institute of Energy Research (KIER) and the Korea Institute of Science and Technology (KIST) are leading the development of the SI (sulfur–iodine) thermochemical hydrogen production technology. The KAEC officially approved the nuclear hydrogen program in 2008, the amendment of which was made in 2011. The final goal of the program is to demonstrate and commercialize the nuclear hydrogen by 2030.

The nuclear hydrogen program consists of two major projects: the nuclear hydrogen key technologies development project and the NHDD project. Fig. 13.2 illustrates the plan of the nuclear hydrogen program.

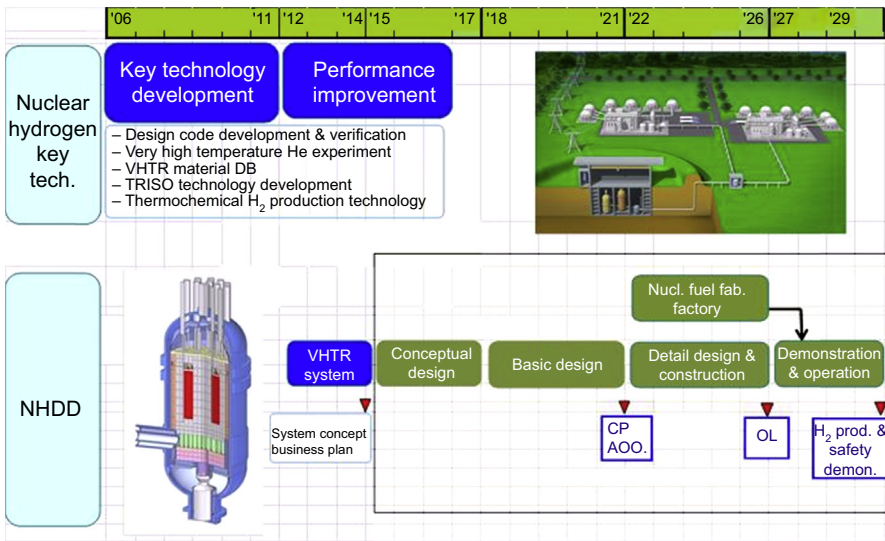


Figure 13.2 Nuclear hydrogen project plan in Korea.

The key technologies development project focuses on the development and validation of key and challenging technologies required for the realization of the nuclear hydrogen system. The key technologies selected are the design codes, high-temperature helium experiment, high-temperature material database, TRISO fuel, and thermochemical hydrogen production. This project has been carried out in phase with both the NHDD project and the GIF projects, and will continue until 2016.

The NHDD project is aimed at the design and construction of a nuclear hydrogen demonstration system for demonstration of massive hydrogen production and system safety. A VHTR systems concept study has been performed for 3 years since 2011. The main objectives of this study are to develop the VHTR systems concept for nuclear process heat and electricity supply to industrial complexes, for the massive nuclear hydrogen production required to enter into a future clean hydrogen economy, and to establish the demonstration project plan of VHTR systems for subsequent commercialization.

As part of the VHTR system concept study, (1) the plant design and functional requirements for both commercial-scale nuclear process heat and nuclear hydrogen systems are developed; (2) the design concepts, layout, and operating parameters of reactor and plant systems are optimized; (3) the design concepts of key high-temperature components and materials are investigated and assessed for manufacturing and procurement purposes; and (4) the design concepts of underground reactor building, radioactive waste management, and radiation protection are evaluated. In parallel, the design analysis systems of reactor and plant systems are constructed and applied for a performance analysis, and the system concept of a demonstration plant is developed and suggested.

As part of the demonstration project plan, commercial-scale plant concepts of both nuclear process heat and nuclear hydrogen systems were first selected reflecting the market needs and opinions of potential customers and vendors, and an economic feasibility study was carried out. Based on the above, the project structure and strategy of the demonstration project and subsequent commercialization project were established together with the relevant business model.

The project plan includes not only the project structure, schedule, budget, and project strategies to secure project financing, government support, site, and licensing, but also the technology development and validation plan required in the process of licensing of the demonstration plant. A stepwise demonstration using a single reactor system was adopted to reduce the technology and business risks, as shown in Fig. 13.3. The reactor technology is demonstrated first at the core outlet temperature of 750°C based on mature technologies. The demonstration of reactor technology will be finished in 10 years. The hydrogen production technology will be developed through international collaboration in parallel with the basic and detailed design of the reactor technology demonstration. The construction of a hydrogen production system will be finished before the demonstration of the reactor technology, which will be followed by the reactor system modification and integration. After that, the demonstration of nuclear hydrogen production will be completed in 2 years.

According to the government suggestion, VHTR systems point design started in 2015 instead of the conceptual design of the demonstration plant. The purpose of the point design is to generate design data of the stepwise and integrated demonstration

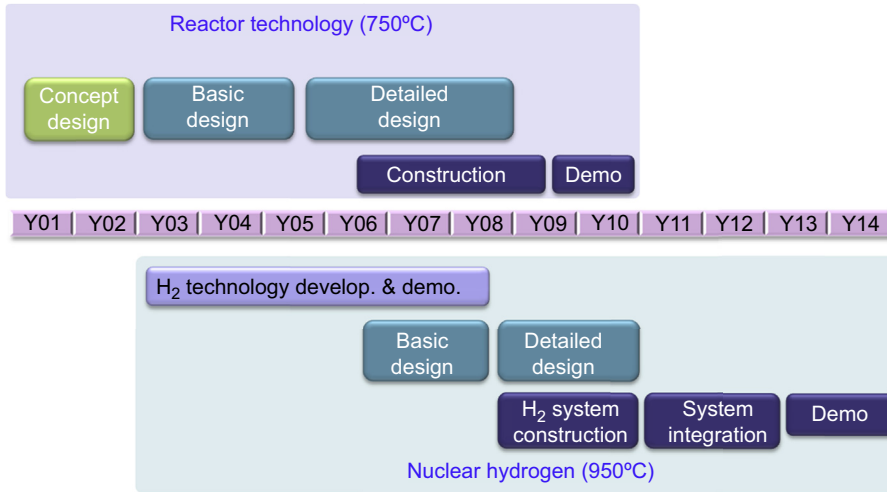


Figure 13.3 The stepwise demonstration plan of NHDD.

plant. The data will be used not only for the conceptual design, but also for a feasibility assessment of the demonstration project. KAERI will apply for prefeasibility approval to the government based on the point design results to be given support from the government. Regardless of launching the demonstration project, the GIF studies will continue because the Korean government signed an extension of the GIF framework agreement for another 10 years until 2026.

13.3 Current research and development on Generation IV reactor in Korea

13.3.1 Sodium-cooled fast reactor

13.3.1.1 Development of a 150 MW_{el} prototype sodium-cooled fast reactor

Top-tier design requirements

Based upon the experiences gained during the development of the conceptual designs for KALIMER-150 and KALIMER-600, the design of an SFR prototype plant has been carried out since 2012. The objectives of the prototype SFR (Kim et al., 2013a,b) are to test and demonstrate the performance of TRansUranics (TRU)-containing metal fuel required for a commercial SFR, and to demonstrate the TRU transmutation capability of a burner reactor as a part of an advanced fuel cycle system. The primary mission of the prototype SFR is to demonstrate the transmutation of TRU recovered from the pressurized water reactor (PWR) spent fuel, and hence the benefits of the integral recycling of all actinides (U and TRU) in a closed fuel cycle to nuclear waste management.

Based on the objectives above, the top-tier design requirements for the prototype SFR and related design parameters that were extensively discussed are given in Table 13.1. The lessons learned from fast reactor programs and the operating experience of fast reactors worldwide, particularly for metal fueled reactors, as well as the experience gained during the development of conceptual designs of KALIMER and advanced SFR design concepts and the trade-off studies, have been incorporated in the top-tier design requirements to the extent possible.

Table 13.1 Top-tier design requirements for the prototype SFR

General design requirements	Plant size	• 150 MW_{el} ($\sim$400 MW_{th})
	Plant design lifetime	• 60 years
	Seismic design	• Design basis earthquakes (SSE: 0.3 g) • Safety structures and equipments on a horizontal seismic isolation
	Fuel type	• Initial core: U−Zr metal • Reference core: U−TRU−Zr metal
Safety and investment protection	Accident resistance	• Design simplification in all aspects of design, construction, operation, and maintenance. Complexity of the plant design has been one of the main sources of high capital cost and threat to the safety of nuclear plants • A large thermal capacity of the primary system in a pool-type reactor
	Core damage prevention	• CDF $<10^{-6}$/reactor·year • A diversified core shutdown mechanism • A highly reliable and diversified decay heat removal (2 active systems and 2 passive systems) • Capable of accommodating unprotected ATWS events without any operator's action
	Accident mitigation	• A large radioactivity release frequency $<10^{-7}$/reactor·year • Core protection limits should not be exceeded for at least 7 days without any operator's action for design basis events
Plant performance and economy	Plant availability	• An annual average plant availability $\geq$75%
	Refueling interval	$\geq$6 months
	Load rejection capability	• Capable of accommodating 100% off-site load rejection without a reactor trip

Table 13.1 Continued

	Operation, maintenance, and serviceability	• Major equipments affecting the plant lifetime shall be replaceable • An occupational radiation exposure <1 man-Sv/year
	Construction cost	Competitive with that of similar types of fast reactors in future
Main components	Intermediate heat exchanger	An immerged cylindrical type
	Internal structure	Cooling facility in reactor vessel against core melting
	Primary pump	An immerged mechanical pump
	Power conversion system	• Reference: superheated steam Rankine cycle • Alternative: S−CO_2 Brayton cycle

Core design

A candidate reactor core uses a single enrichment fuel with a U−10% Zr binary metal alloy form initially and will be changed to an enrichment split core to flatten the power distribution when TRU fuel will be adopted. To accept two different types fuel in the same core dimension, the initial U core was designed with TRU core transition capability (Kim et al., 2013a,b).

Fig. 13.4 shows the layout of the U-fueled core. As shown in the figure, the core consists of two regions of fuel. Table 13.2 shows a summary of the core performance analysis results, obtained with the equilibrium cycle analysis. The beginning of equilibrium cycle (BOEC) to end of equilibrium cycle depletions were modeled with a burnup chain having descriptions for all of the U−plutonium (Pu)−MA isotopes. A zone reload without fuel shuffling was developed for the equilibrium cycle, wherein one-fourth of the inner core fuels and one-fifth of the outer core fuels were refueled at each outage.

All reactivity coefficients for U core have negative values, which means this core design holds inherent safety characteristics. In particular, the sodium void effect also shows a negative value, which is a different tendency in a typical SFR because of plutonium-free core. For the diversity of a shutdown system, two types of control assemblies are arranged to secure sufficient shutdown margin.

Fuel design

Cladding failure or damage during the steady state and transient conditions must be evaluated by appropriate predictive codes. To prevent a metallic fuel rod failure in a fast reactor, it is required to evaluate the design limits such as (1) cladding integrity including cladding strain and CDF (cumulative damage fraction); and (2) fuel melting.

Fuel melting temperature limits of 955°C and 1200°C are used for U−TRU−Zr and U−Zr fuel, respectively. It was estimated that the metallic fuel had a sufficient margin to the melting temperature.

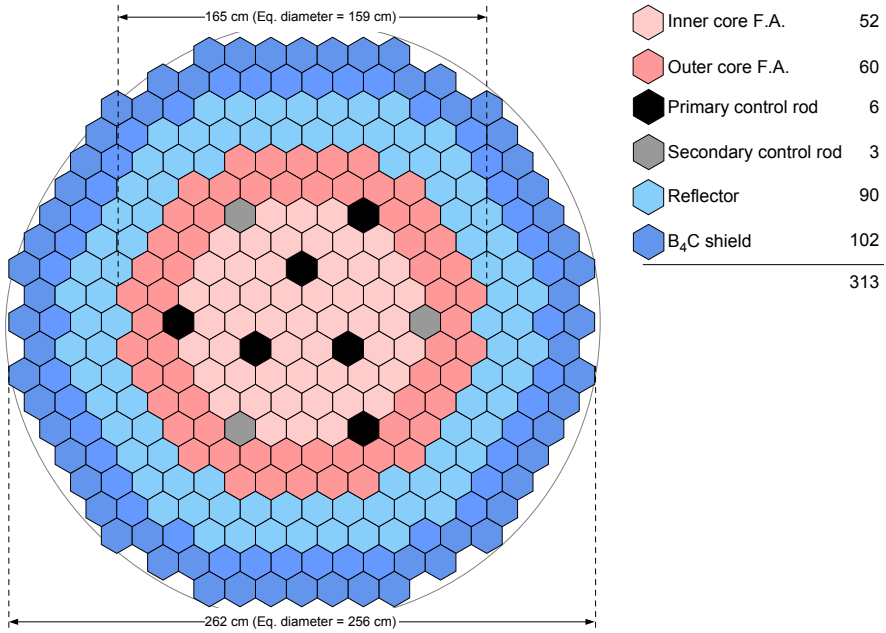


Figure 13.4 Layout of U core (150 MW_{el}).

Table 13.2 U−Zr core design and performance parameters

Design/performance parameters		Design/performance parameters	
EFPD/No. of Batch (IC/OC) (day/#)	290/4/5	*Burnup (avg./peak) (MWd/kg)*	66.4/107.1
No. of fuel assembly (IC/OC)	52/60	*Burnup reactivity swing (pcm)*	2297
Fuel pin diameter (cm)	0.74	*Fast neutron flux ($\times 10^{15}$ n/cm^2-s)*	1.43
P/D ratio	1.14	*Peak fast N. fluence ($\times 10^{23}$ n/cm^2)*	2.93
Active core height (cm)	90.0	*Ave. linear power density (W/cm)*	163.4
Lower shield height	90.0	*Peak linear power density (W/cm)*	338.7
Fission gas plenum height (cm)	125.0	*Ave. power density (W/cm^3)*	218.4
Enrichment (wt%)	19.50	*Peak power density (W/cm^3)*	452.6
Heavy metal loading (Mt)	7.33	*Bundle pressure drop (MPa)*	0.423
Charge HM mass (t/yr)	1.68	*Max. flow rate (kg/s)*	25.5

The cladding integrity including cladding strain limit, swelling limit, and CDF limit for metal fuel were evaluated by the LIFE-METAL code. In particular, CDF and cladding strain limits were estimated for the candidates for cladding material, HT9 and FC92. These limits depend on plenum-to-fuel ratio, cladding thickness/temperature, and burnup. A sensitivity analysis to evaluate these limits was carried out for the target coolant outlet temperature of 545°C. Design parameters such as maximum cladding temperature, plenum length, and cladding thickness were established to satisfy the design limits.

Fluid system design

The heat transport system is composed of a primary heat transport system (PHTS), an IHTS, and a power conversion system (PCS). The heat transport system has features such as pool-type PHTS, two IHTS loops, and a superheated steam Rankine cycle PCS, as shown in Fig. 13.5.

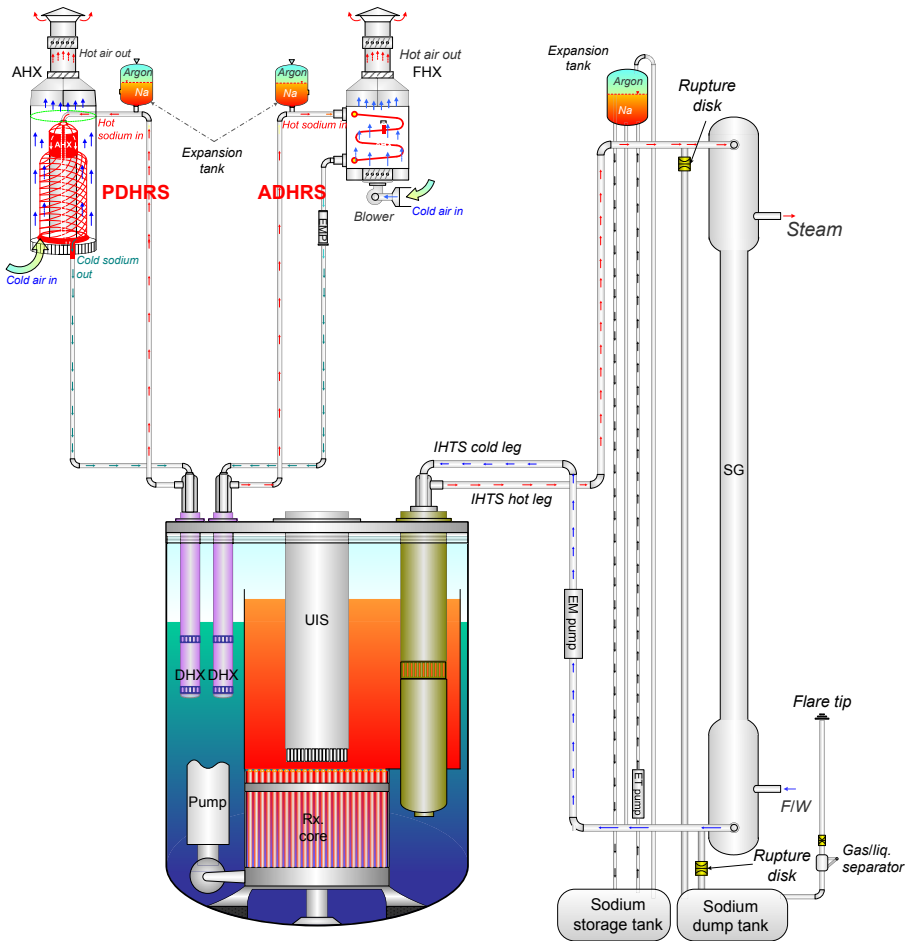


Figure 13.5 Configuration of fluid system.

The PHTS consists of two PHTS pumps, four intermediate heat exchangers (IHXs), and reactor structures. The PHTS pump is a centrifugal-type mechanical pump. The IHX is counter flow shell and tube types with a vertical orientation inside the reactor vessel where the PHTS sodium flows through the shell side and IHTS sodium flows through the tube side.

The IHTS consists of two IHTS pumps, two single-wall straight tube type steam generators, two expansion tanks, and pipings. The IHTS pump is an electromagnetic type and is located in each cold leg of the two IHTS loops. Each steam generator has a thermal capacity of 197 MW_{th} and is installed in each IHTS loop. The steam temperature and pressure at 100% normal operating condition are 503°C and 16.7 MPa, respectively.

As one of the safety design features, the DHRS is composed of two passive DHRSs (PDHRSs) and two active DHRSs (ADHRSs). It was deigned to have the sufficient capacity to remove the decay heat in all design basis events by incorporating the principles of redundancy and independency. The PDHRS is a safety-grade passive system, which comprises two independent loops with a decay Heat eXchanger (DHX) and a natural-draft sodium-to-air Heat eXchanger (AHX). The ADHRS is a safety-grade active system, which is comprised of two independent loops with a DHX, a forced-draft sodium-to-air heat eXchanger (FHX), an electromagnetic pump, and an FHX blower for each loop. The ADHRS can also be operated in natural convection mode against a loss of power supply with ~50% of its designed heat removal capacity. The heat transferred to the DHRS can be finally dissipated into the atmosphere through AHXs and FHXs by the natural convection mechanism of sodium and air only.

Mechanical structure design

The reactor structures, system, and components were designed as shown in Fig. 13.6. In this design, the reactor vessel size is determined to be 8.7 m in diameter, 1 and 5.4 m in height. The main design features are that the reactor internals are very simple, and the reactor support structure is a skirt-type structure supporting the reactor head and the reactor vessel jointed with bolts. The core support structure is a simple skirt-type structure, partly welded between keys and lugs forged with the vessel bottom head. The IHTS piping layout is established in a way to minimize the nozzle loads through the weight and seismic load analyses. The total IHTS piping length is significantly reduced using Gr91 material. The main advantage of Gr91 for IHTS piping and heat exchangers material is to avoid the dissimilar weld joints at any NSSS location.

13.3.1.2 Research and development activities

Large-scale sodium thermal–hydraulic test program

A large-scale sodium thermal–hydraulic test program called STELLA (Eoh et al., 2013) is being progressed by KAERI. As the first step of the program, the sodium component test loop called STELLA-1 has been completed, which is used for demonstrating thermal–hydraulic performance of major components, such as heat exchangers and a mechanical sodium pump, and their design code V&V. The second

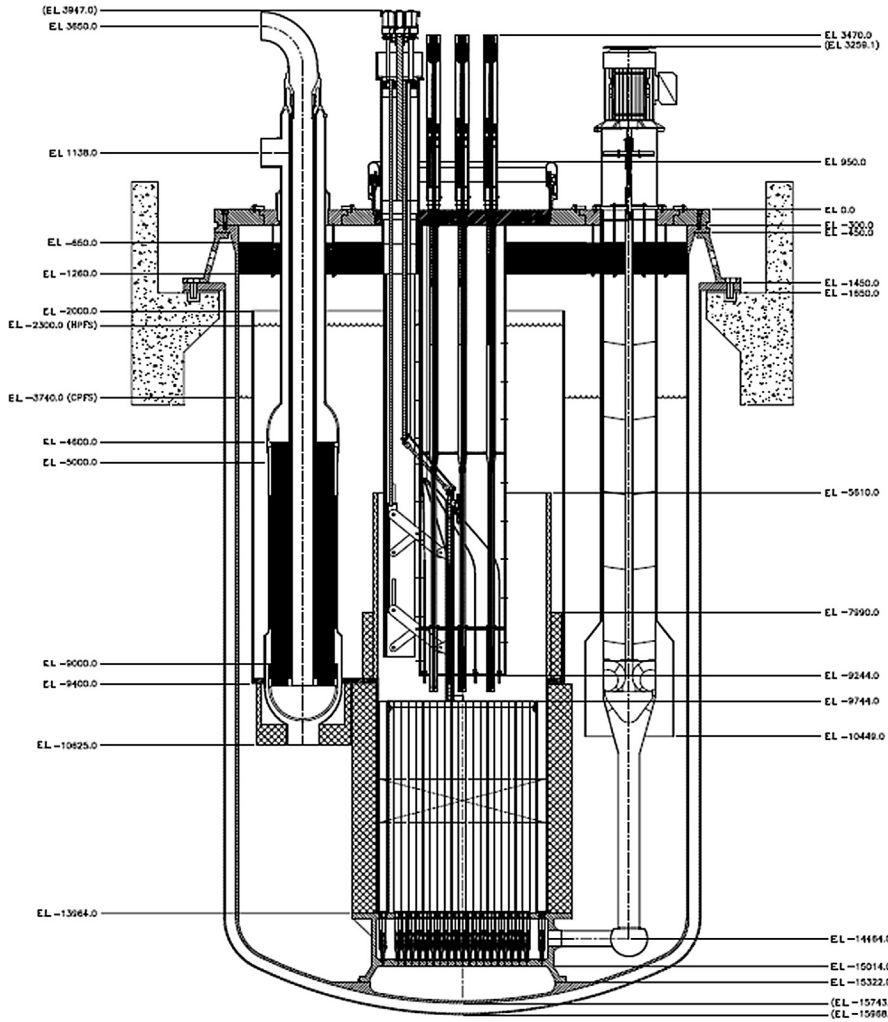


Figure 13.6 Phts arrangement (front view).

step of an integral effect test loop called STELLA-2 will be constructed to demonstrate the plant safety and support the design approval for the prototype SFR. Starting with the conceptual design of the prototype SFR, the basic and detailed design of the test facility reflecting the prototype design concept will be performed on the basis of the design requirements subject to the prototype reactor. According to the program schedule, the facility was planned to be installed by the end of 2018 and the main experiments including the start-up tests to be commenced in 2019, as shown in Fig. 13.7. The STELLA program finally aims at an integral effect test to support specific design approval for the prototype reactor.

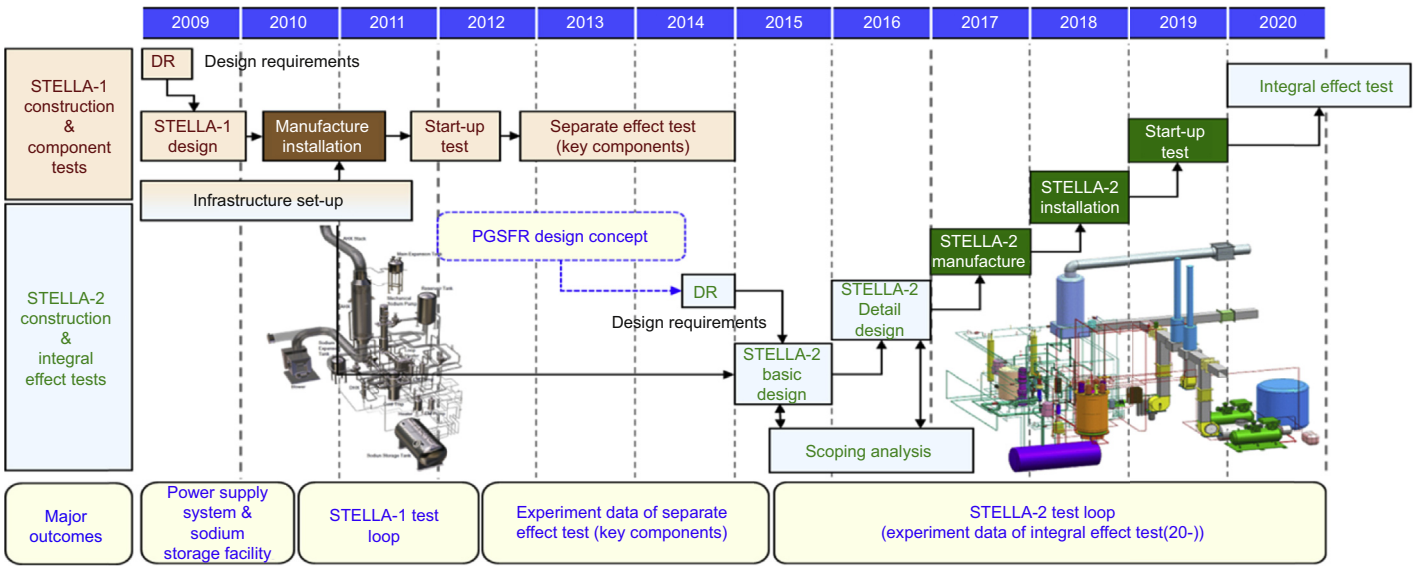


Figure 13.7 Overall schedule of the STELLA program.
Eoh, J.H., et al., April 2015. Internal Conference on Fast Reactors and Related Fuel Cycles (FR13).

Metal fuel development

Fuel slugs have been fabricated by modified injection casting and particulate fuel in KAERI to prevent the evaporation of volatile elements such as Americium (Am) (Lee et al., 2013). The U-10wt%Zr-5wt% Mn fuel slug containing a volatile surrogate element such as manganese (Mn) was soundly cast by an improved injection casting method to prevent the evaporation of volatile elements such as Am, where the volatile U alloy is melted under an inert atmosphere. The general appearance of the slug was smooth, and the diameter and length were 5.4 mm and about 250 mm, respectively, as shown in Fig. 13.8. The gamma-ray radiography of the as-cast surrogate slug was performed to detect internal defects such as cracks and pores. The mass fraction of the fuel loss relative to the charge amount after fabrication of U-10wt%Zr-5wt%Mn was low, up to 0.1%. It was seen that the losses of these volatile elements such as Am can be effectively controlled to below the detectable levels using modest argon overpressures.

For particulate fuel fabrication, it is an atomization technology considered as an alternative fabrication method of fuel slugs. Spherical U-10wt%Zr alloy particles were fabricated by centrifugal atomization at about 1500°C. Green compacts of atomized U-10wt%Zr powder were fabricated with quartz compaction dies. The compacts of U−Zr powder were sintered, ranging from 1000°C to 1100°C under a vacuum. The bonding of particles was not active in U−Zr powder pellets, mainly because of their limited interdiffusion at the sintering temperature. In addition, the use of sodium bond in the metal fuel cladding can be eliminated, owing to porous particulate fuel such that the handling of spent fuel containing radioactive sodium can be simplified.

HT9 and FC92 cladding tubes were fabricated in 2013. The ingots were melted by a vacuum induction melting process. The ingots were refined through the electro-slag remelting process. The mother tubes were fabricated by hot forging and hot extrusion. The cladding tubes were fabricated by a pilgering and drawing process. Intermediate heat treatment was carried out after cold working. The intermediate cladding tubes were normalized at 1050°C for 6 min and tempered at 800°C for 8 min. After the final cold working, the cladding tubes were normalized at 1038°C for 6 min and tempered at 760°C for 60 min. The dimensions of cladding tube, as shown in Fig. 13.9, were 7.4 mm in outer diameter, 0.5 mm in thickness, and 3000 mm in length. The mechanical tests such as creep, burst, and tensile test have been performed (Kim et al., 2013c), and irradiation tests of the cladding tubes in BOR-60 started in 2014. The irradiation test will be finished in 2019, and the PIE will be done in 2020.



Figure 13.8 U-10wt%Zr-5wt%Mn fuel slug, fabricated by improved casting method.



Figure 13.9 FC92 cladding tubes.

Reactor physics experiment

To validate the neutronic characteristics of SFRs, KAERI has been collaborating with the Institute for Physics and Power Engineering (IPPE) in Russia. Three critical assemblies were already constructed in BFS-1 and BFS-2 facilities, called as BFS-73-1, -75-1, and -76-1A. The first two critical assemblies represent the early phase of KALIMER-150 core design during the late 1990s. Recently, two more critical experiments, BFS-76-1A and BFS-109-2A, were conducted at IPPE. The BFS-76-1A critical experiment, constructed in 2010, is a mock-up experiment for the TRU burner core, which is characterized by a blanket-free concept, low conversion ratio, high burnup reactivity swing, and the consequent deep insertion of a primary control rod at BOEC. The BFS-109-2A critical experiment, constructed at 2012, is a mock-up experiment for the metallic U−Zr fueled core with various control rod positions. Another mock-up experiment for the initial U core of the prototype SFR, BFS-84-1, is ongoing in 2015. The BFS-84-1 is planned to measure key safety-related reactivity parameters such as sodium void reactivity, fuel axial expansion reactivity, and core radial expansion reactivity.

13.3.2 Very high temperature reactor

13.3.2.1 Design and analysis codes

KAERI has been developing computer code systems for graphite-moderated, helium-cooled VHTR. Fig. 13.10 shows the overall code system for VHTR licensing developed at KAERI.

KAERI has been developing a two-step neutronics analysis code system for VHTR core design (Jeong et al., 2013), in which the DeCART code (Cho et al., 2013) is used for generation of few-group cross sections together with the equivalent parameters.

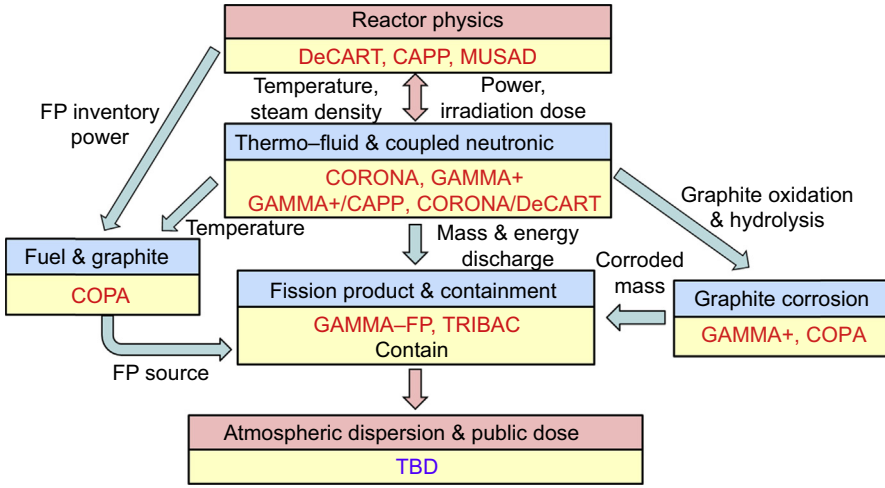


Figure 13.10 Overall code system for VHTR licensing developed at KAERI.

The CAPP code (Lee et al., 2012a,b) is used for the analysis of core physics parameters of VHTR using the few-group parameters generated by DeCART. The sensitivity and uncertainty analysis code, MUSAD (Han et al., 2015), is being developed for an uncertainty analysis of the few-group parameters generated by DeCART and eventually the uncertainty of the core physics parameters evaluated by the CAPP code. Fig. 13.11 shows the two-step neutronics analysis code system for the VHTR developed at KAERI.

The GAMMA+ code (Lim, 2014) has been developed by KAERI for system and safety analysis of VHTR. The code has the capabilities for multidimensional analyses of the fluid flow and heat conduction as well as the chemical reactions related to the air or steam ingress event in a multicomponent mixture system. As a system thermo-fluid and network simulation code, GAMMA+ includes a nonequilibrium porous media model for pebble-bed and prismatic reactor core, thermal radiation model, point reactor kinetics, and special component models such as pump, circulator, gas turbine, valves, and more.

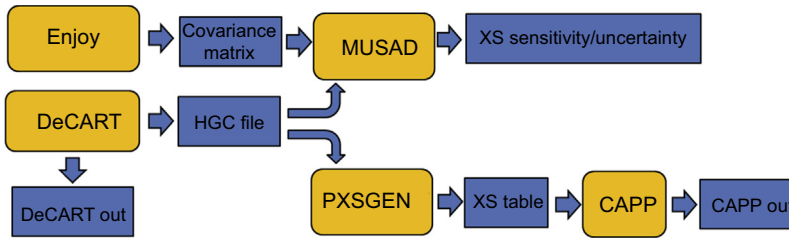


Figure 13.11 KAERI two-step neutronics analysis code system for VHTR.

KAERI has been developing the CORONA code (Tak et al., 2014) for a core thermo-fluid analysis of a prismatic VHTR. The CORONA code is targeted for a whole core thermo-fluid analysis of a prismatic VHTR with fast computation and reasonable accuracy. The computational efficiency was achieved by combining the 3-D solid heat conduction with a one-dimensional fluid flow network and adopting a block-wise parallel computation.

For a high fidelity core multiphysics analysis, KAERI has been developing a coupled code system using DeCART and CORONA (Lee et al., 2012a,b). DeCART transfers the power density and the fast neutron fluence to CORONA. On the other hand, CORONA transfers the temperature to DeCART. A separate computer code named CDECCO was developed for communication between DeCART and CORONA. No mapping is required in this coupled code system because the two codes use the same structure of the computational grids.

A neutronics/thermo-fluid coupled analysis code system is being developed by coupling the CAPP code and the GAMMA+ code (Tak et al., 2015). A server program called INTCA is utilized for the coupling of the two codes. The INTCA code not only controls the calculation procedure of the two client codes, but also performs the mapping between the variables of the two codes for coupling. Fig. 13.12 shows the neutronics/thermo-fluid coupled analysis code systems developed at KAERI.

KAERI has developed a tritium transport code, TRIBAC (Yoo et al., 2010), for the analysis of tritium behavior in a VHTR system under normal operating conditions. It can calculate the tritium distribution within the reactor system and the leakage of tritium. A fission product transport analysis code, GAMMA-FP (Yoon et al., 2013), has been developed as well for coupled analysis with GAMMA+ code. The GAMMA-FP has the capabilities of transport analyses of gaseous and aerosol FP species during postulated accident transients.

A seismic analysis code is being developed to assure the structural integrity under seismic loads. The multibody dynamic analysis of multicolumned stacks of graphite blocks was implemented in the code (Kang et al., 2011). The procedure for the thermal stress analysis of graphite fuel blocks was established using ABAQUS, a commercial FEM code, with thermal and neutron-induced material property changes of graphite (Kang et al., 2012).

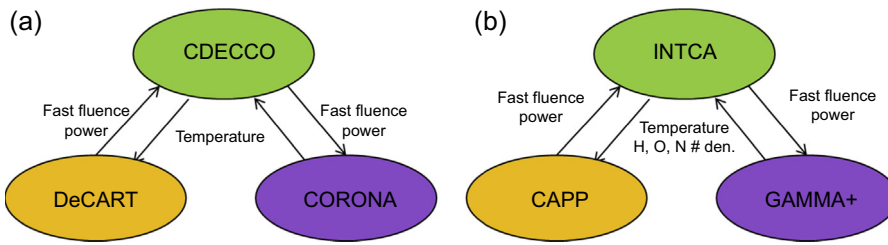


Figure 13.12 Neutronics/thermo-fluid coupled analysis code systems: (a) DeCART/CORONA System and (b) CAPP/GAMMA+ System.

13.3.2.2 TRISO fuel technology

Since 2006, KAERI has made significant progress and the manufacturing process for the TRISO-coated particle fuel has been established at the lab scale. The TRISO fuel R&D activities that have been carried out at KAERI include the development of the kernel fabrication and the TRISO coating technologies, the overcoating, and the compaction technologies of the coated fuel particles using graphite powder.

Fig. 13.13 shows a part of the lab-scale equipment for kernel fabrication. KAERI uses gel supported precipitation technology for the fabrication of spherical UO_2 kernels (Brambilla et al., 1970). The process parameters used to make up the broth solution and droplets have been studied extensively. Heating curves for the UO_2 kernel during the calcination and sintering processes were determined in the lab-scale experiments. Fig. 13.14 shows the kernel products in successive steps obtained from the kernel fabrication process at KAERI.



Figure 13.13 Kernel fabrication system.

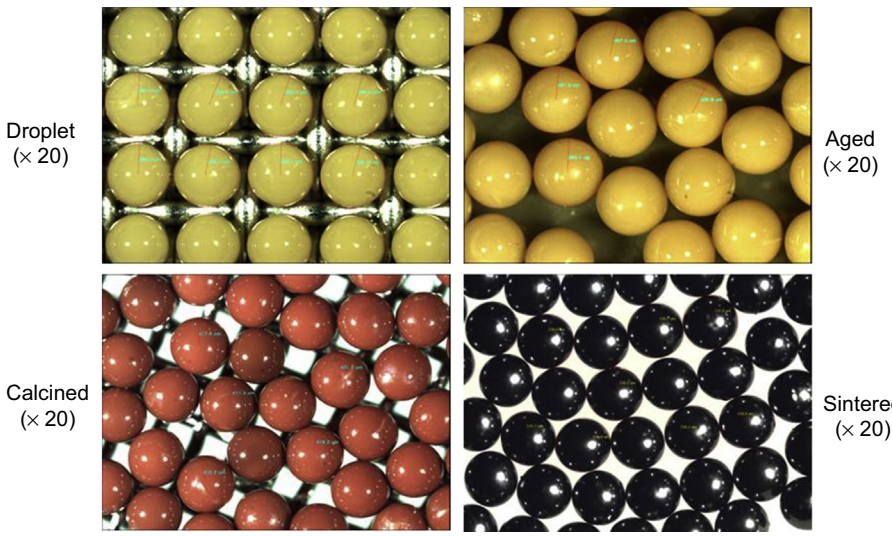


Figure 13.14 Intermediate and final products of kernel fabrication process.



Figure 13.15 TRISO coating system.

KAERI uses the fluidized bed chemical vapor deposition (FB-CVD) technology for TRISO coating (Kim et al., 2009a). Fig. 13.15 shows the arrangement of the FB-CVD furnace with the gas supply and off-gas system. Continuous coating techniques for SiC TRISO layers have been developed, and the optimization of the coating procedure has been completed at the 20−30 g/batch scale. Fig. 13.16 shows KAERI's pilot SiC TRISO-coated fuel particle.

R&D for advanced TRISO fuel technologies such as the UCO kernel fabrication and the ZrC coating has been carried out. As for the UCO kernel fabrication, a process for the carbon dissolution was established, and well-shaped discrete ADU liquid droplets were obtained using an external gelation method (Jeong et al., 2007). Currently, a new kiln-type heating furnace has been built for the heat treatment



Figure 13.16 KAERI's pilot TRISO fuel particles and a microscopic image.

experiment of the UCO kernel. KAERI's advanced pilot fuels with UCO kernels and ZrC coating layers will be produced by 2016.

In parallel, KAERI is developing a fuel performance analysis code called COPA, which estimates the thermal and mechanical behavior of a coated fuel particle, a pebble, and a fuel block and the fission product migration through a coated particle and a fuel element as well as the failure fractions of coated particles under irradiation and heating tests (IAEA, 2012). COPA has been improved to treat the behavior of the advanced fuel under irradiation and heating. A consistent calculation system has been built, which can be used to estimate the gas pressure and species in the coated fuel particle under irradiation. A software verification and validation report for COPA will be issued in 2016.

An irradiation test of KAERI's pilot TRISO particle fuel was started on October 5, 2013, and completed on March 31, 2014 (Kim et al., 2014). The average power of the fuel was evaluated to be 610 W, and the average burnup was calculated to be about 37,000 MWd/MTU. Nondestructive PIEs of the test fuel were completed, and the destructive tests are currently being carried out at KAERI's irradiated material examination facility. Simulated heat-up test equipment to perform a simulated heating test in a laboratory is under construction. It is expected to provide fundamental data for the construction of the actual heat-up test equipment for use in a hot cell.

13.3.2.3 High-temperature materials

High-temperature materials are one of the main issues for a demonstration of the VHTR, which needs to maintain the safety at very high temperatures of above 950°C to produce hydrogen with a high efficiency. The main purposes of the VHTR material R&Ds were (1) material screening/selection and qualification; (2) codifications of the relevant high temperature structural design rules to the very high temperature region and to support the licensing of a system design; (3) material characterizations and a database establishment; (4) alloy modifications and developments; and (5) Gen-IV VHTR materials collaborations and contributions. Since 2006, the material R&Ds have been being performed for graphite, alloy 617, modified 9Cr-1Mo steel, and a ceramic composite at KAERI (Park et al., 2008; Kim et al., 2009b).

Experimental data for the mechanical and physical properties of the selected graphite candidates (IG-110, IG-430, NBG-18, and NBG-25) were produced. In addition, the fracture and oxidation behaviors were estimated. To understand the radiation effects in nuclear-grade graphite, an atomistic structural change in IG-110 irradiated with 3 MeV H^+ and gamma−irradiation effects were characterized (Kim et al., 2009b; Hong et al., 2012; Corwin et al., 2008).

Creep data for alloy 617 and weldment by gas tungsten arc welding were obtained from the creep tests in air and He environments conducted in temperature ranges of 800−950°C, and creep crack growth data have also been produced. Long-term creep tests of alloy 617 weldment were conducting at 850°C for more than 13,000 h. In parallel, a constitutional equation to predict a fatigue life with strain ranges was developed for alloy 617. The creep tests for alloy 800 HT base metal (BM) and weld metal (WM)

are also being conducted in the ranges of 800−900°C. Mechanical properties of modified 9Cr-1Mo steel welded by SMAW were measured. To evaluate the degradation behavior by thermal aging, the weldment of modified 9Cr-1Mo steel was heat-treated, and the impact and tensile test were then performed (Kim et al., 2009b; Hong et al., 2012; Corwin et al., 2008; Carre et al., 2010).

Future projects are considering the use of ceramic composites where radiation doses, environmental challenges, or temperatures (up to or beyond 1000°C) will exceed the capabilities of the metallic materials (Corwin et al., 2008). However, widespread property data, standardization of the characterization methods and the development of design codes of ceramic composites are required for in-core structural components. The baseline thermal and mechanical properties of some nuclear-grade C/C composites were measured. The oxidation behaviors of composites in air and He with controlled minor impurities and irradiation effects using Si ions were also evaluated (Kim et al., 2009b; Hong et al., 2012; Corwin et al., 2008; Carre et al., 2010).

KAERI has contributed to all working groups of Gen-IV VHTR material collaboration: graphite, metal and design method, and ceramic and composite. By the end of 2014, 37 technical reports have been uploaded into the Gen-IV materials handbook. In addition, creep test records (45 data) of alloy 617 and tensile test results for the BM, WM, and weld joint of alloy 617 (32 ea) were uploaded into the Gen-IV materials handbook (Generation IV international forum annual report, 2013).

13.3.2.4 Hydrogen production

Development of the SI cycle has been pursued by several countries within the framework of the GIF for hydrogen production with the next generation of nuclear reactors. Due to its higher temperature requirements in comparison with other thermochemical cycles, the SI cycle is particularly well matched with the VHTR.

A Korean research network consisting of KAERI, KIER, and KIST is developing an integrated 50 $NL \cdot H_2/h$ scale demonstration of the SI cycle through the GIF collaboration.

Past studies have focused on not only the process evaluation using a commercial computer code, but also the screening test of the component structural materials. Experiments to develop the catalysts for sulfur trioxide and hydrogen iodide decompositions were carried out successfully, and their manufacturing technologies were established. The experimental feasibility test of a 3.5 $NL \cdot H_2/h$-scale SI test facility under atmospheric operation conditions has been performed in early 2008. As a result, we secured the continuous operation hydrogen production data for 6 h.

Few studies have examined the integration of reactions and interaction between processes. Individual unit operations have been developed, built, and tested in combination with the subsequent intermediate processes.

The computer code, KAERI−Dynamic Simulation Code (KAERI−DySCo), was developed to analyze the dynamic behavior of the VHTR−SI process coupling system. KAERI−DySCo was also verified using the code-to-code benchmark calculation through the international GIF collaboration, and steady state values

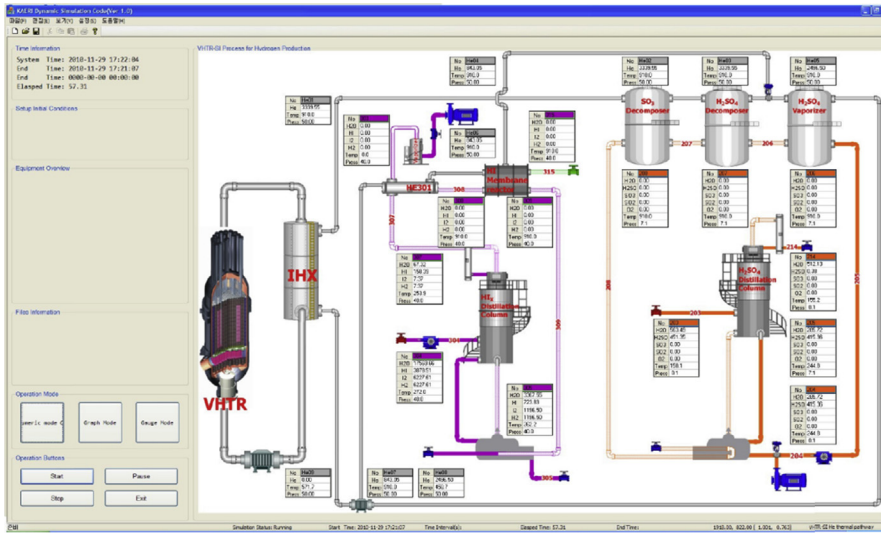


Figure 13.17 The KAERI-DySCo code main window.

calculated by the commercial computer code "ASPEN." Fig. 13.17 shows the main window of the KAERI−DySCo simulation code.

In addition, the KAERI-DySCo simulation code has been used for the dynamic startup simulations of a sulfuric acid distillation column, HIx distillation column, and its thermal decomposers, which are the main components of an SI integrated test facility with a hydrogen production rate of 50 $NL \cdot H_2/h$. Fig. 13.18 shows $50NL \cdot H_2/h$-scale SI test facilities built at KIER, which is under modification for improvements in its operational efficiency.



Figure 13.18 50 $NL \cdot H_2/h$-scale SI test facilities.

Recent advances in the thermochemical SI cycle have been reported (Bae et al., 2015; Jung et al., 2015; Lee et al., 2014). An integrated operation test of more than 8 h was successfully conducted to demonstrate the promising potential of the pressurized operation for hydrogen production in 2014.

Further research is underway to reconfirm the hydrogen productivity of the 50 $NL \cdot H_2/h$ SI test facilities for an extended operation time. On the other hand, the domestic research partners, KIER and KIST, are also investigating the scale-up technologies of SI process components to obtain the equipment design information. The goal is to establish an engineering database to design a pilot scale SI process coupled to the secondary helium loop of the VHTR.

13.3.3 Lead fast reactor

The Republic of Korea (ROK) nuclear power program has been rapidly developing since 1970s. Spent nuclear fuel management has been one of major obstacles in maintaining the public support for the Korean nuclear power program. Therefore, the minimization of high-level waste has been the principal goal of lead fast reactor (LFR) and related R&D in ROK. LFR R&D in ROK has been led by the Seoul National University (SNU), Seoul, since the 1990s, as shown in Fig. 13.19. The program has been consisted of LFR design, partitioning, and experimental benchmark and software development for design and safety analysis without discontinuity during the past two decades.

In 1996, LFR R&D was begun in ROK by a small group of researchers at SNU with the goal of developing a fast neutron based waste transmutation system, designated as PEACER with the financial support of then the Ministry of Science and Technology (Hwang et al., 2000). Medium-size transmutation reactors with electric power rating

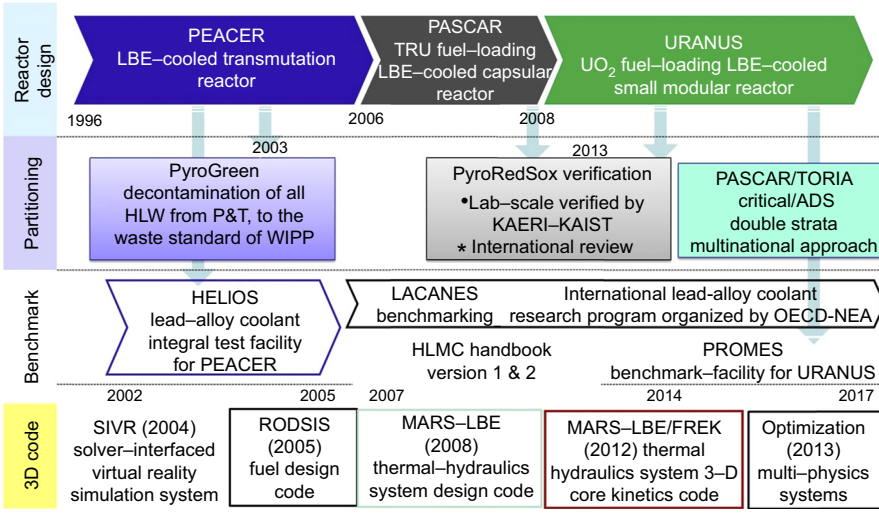


Figure 13.19 Overview of LFR R&D at SNU.

of 550 and 300 MW_{el}, respectively, were designed with loop-type system cooled by lead–bismuth eutectic (LBE). An integral closed fuel cycle was conceptualized with collocated pyrochemical partitioning and fuel recycling facilities. TRU transmutation rates of PEACER were estimated to be 2.0 for transuranic elements (TRU) and about 6 for Tc-99 and I-129. For proliferation resistance, an international control of the PEACER Park was proposed, as depicted in Fig. 13.20.

In 2002, LFR R&D was expanded by opening the Nuclear Transmutation Energy Research Center of Korea (NUTRECK) at SNU, with the support of then the Ministry of Trade, Industry and Energy. LFR design goals, criteria, and an integral modeling approach were developed by a team of about 20 researchers. Computer codes originally developed for other nuclear reactor systems were modified for neutronic modeling, thermal–hydraulic analysis, fuel rod performance analysis, and structural design, using an available database that later became Handbook on LBE and Lead from OECD/NEA, as summarized in Fig. 13.21. Materials R&D was made to determine optimal concentrations of oxygen in LBE coolant, by using yttria-stabilized zirconia (YSZ)-based membranes. Reliable oxygen sensors were developed by using metal ceramic joining technology for YSZ-tube and Type 316 stainless steel with Bi/Bi_2O_3 reference.

SNU's first international collaboration project on LFR R&D was conducted under I-NERI program for developing the conceptual design of Encapsulated Nuclear Heat Source (ENHS) (Greenspan, 2003). The ENHS design of full natural circulation of LBE was then selected as Gen-IV LFR reference design. The natural circulation concept was further developed at SNU-NUTRECK as a pool-type small modular

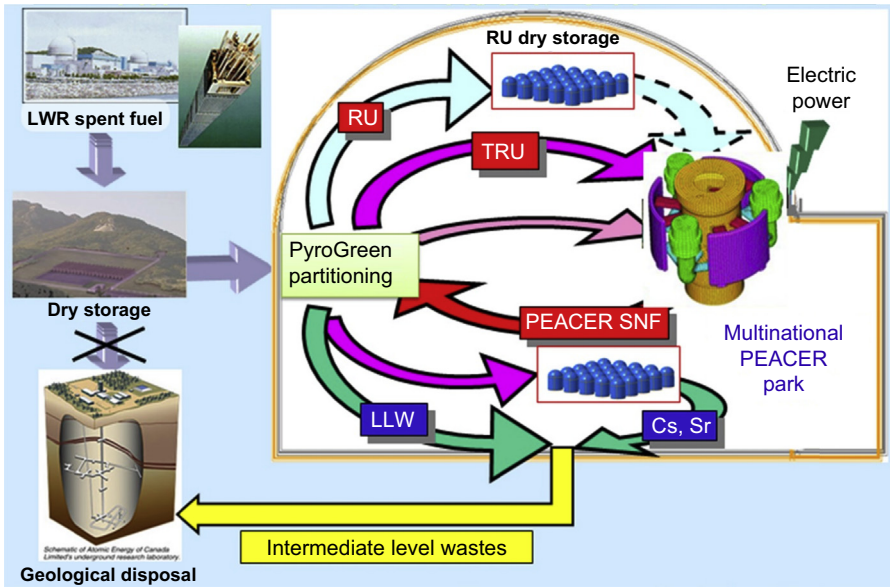


Figure 13.20 Peacer Park with multinational control.

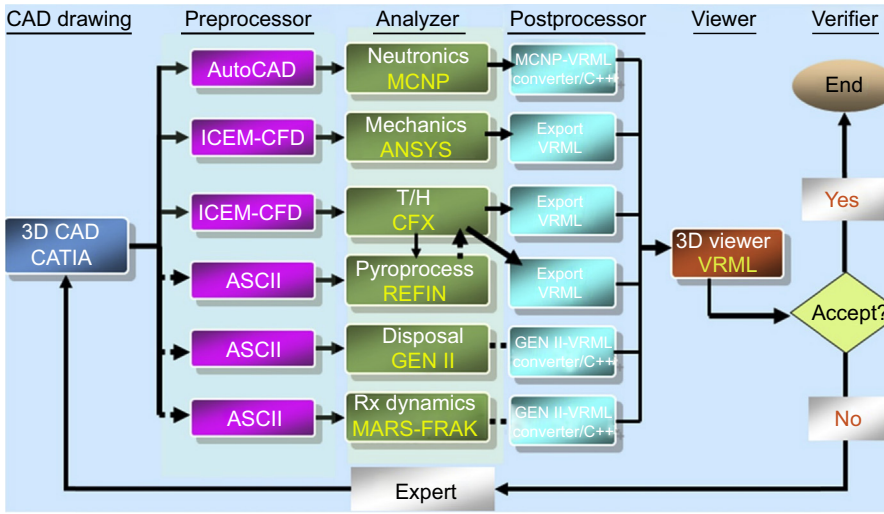
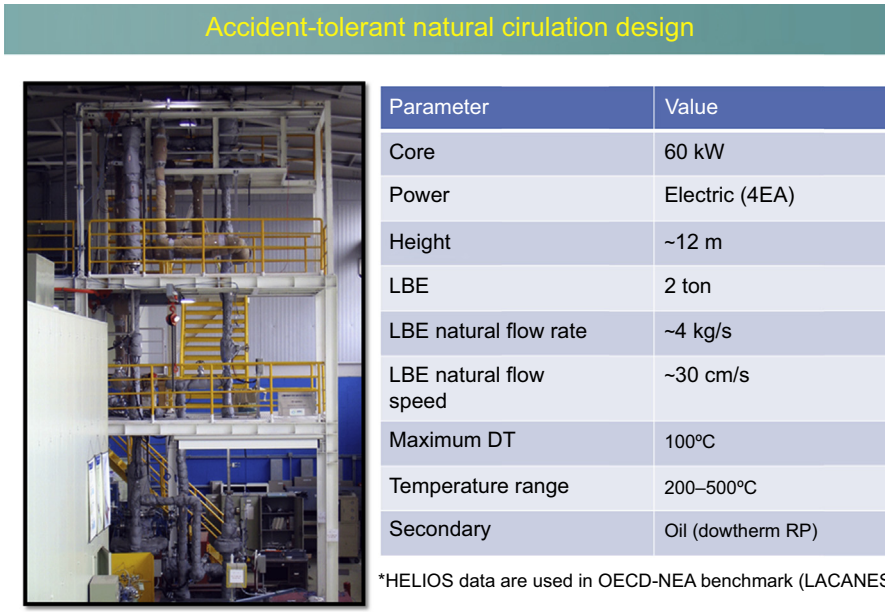


Figure 13.21 LFR design code system of SNU-NUTRECK.

transmutation reactor, designated as PASCAR, in order to meet objectives for cradle-to-grave approach of Global Nuclear Energy Partnership (Choi et al., 2011). SNU also has collaborated with Los Alamos National Laboratory on corrosion testing of materials in LBE.

In 2005, a large-scale LBE test loop, HELIOS, has been commissioned at SNU-NUTRECK. HELIOS is a thermal−hydraulic scale-down facility for PEACER-300, with the thermal power ratio of 5000:1 and the height ratio of 1:1, as shown in Fig. 13.22. HELIOS was world's tallest LBE test loop at the time with 12 m height, containing 2 Mt of LBE. The elevation difference between the heat exchanger and the mock-up core region is about 8 m, providing the same driving force for natural circulation of PEACER-300. The OECD/NEA thermal−hydraulic benchmark program, designated as Lead Alloy Cooled Advanced Energy Systems, is carried out on the isothermal forced circulation and nonisothermal natural circulation with the experimental database produced using HELIOS. OECD/NEA technical report was published from the forced circulation study where the final summary is under the progress for the natural circulation. The natural circulation capability required for normal operation as well as safety of PASCAR was demonstrated by long-term HELIOS tests (Cho et al., 2011; OECD/NEA, 2012).

In 2008, the design of a pool-type transportable small modular reactor, designated as URANUS, using enriched UO_2 fuels with a 20-year-life, has been developed for underground deployment with a 3-D seismic isolation system and the reactor vessel air cooling system, as shown in Fig. 13.23. The safety of the URANUS design in various accident scenarios was verified by a system analysis code, MARS-LBE (KAERI, 2004). 3-D seismic isolation was shown to increase the safe shutdown earthquake acceleration drastically. Corrosion mechanisms of stainless steels have been investigated by testing in LBE and subsequent examinations to find that chromium



Parameter	Value
Core	60 kW
Power	Electric (4EA)
Height	~12 m
LBE	2 ton
LBE natural flow rate	~4 kg/s
LBE natural flow speed	~30 cm/s
Maximum DT	100ºC
Temperature range	200–500ºC
Secondary	Oil (dowtherm RP)

*HELIOS data are used in OECD-NEA benchmark (LACANES)

Figure 13.22 Integral LBE test loop HELIOS and its design features.

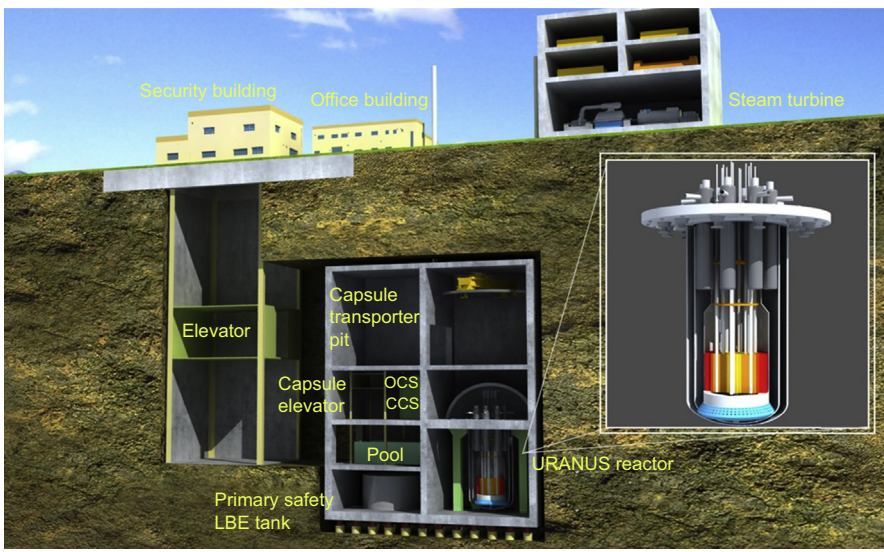


Figure 13.23 Concept of URANUS deployed underground for security enhancement.

(Cr)−iron (Fe) oxide spinel layers grow with appreciable leaching of Cr, resulting in a Cr-depleted region near metal oxide interfaces. Aluminum (Al) or silicon (Si) can greatly enhance the oxide passivity and retard leaching of metal substrate. Development of corrosion-resistant materials led to a new series of Al-containing ferritic stainless steels, which display innovative corrosion resistance in LBE, opening the way to explore the 20-year-long life core for URANUS. In order to further enhance the cost-competitiveness of URANUS, the load follow capability is fully embedded in control system designs so that its early units can enter peak-load market and can operate in symbiosis with renewable energy sources (Shin et al., 2015).

A thorium-based accelerator driven system (ADS) for TRU transmutation has been conceptually designed, as shown in Fig. 13.24. The development of pyrochemical partitioning technology for the transmutation technology R&D at SNU-NUTRECK has been aimed at the decontamination of all final waste streams into low-level waste and intermediate-level waste so that the geological repositories after several hundred years can be adequately safe, secure, and proliferation-resistant. The goal has been shown to be viable by a new flow sheet designated as PyroGreen (Jung et al., 2012). In parallel, KAERI has been developing pyrochemical partitioning technology designed for collocated sodium fast reactors, with the goal of 99.9% recovery of TRU. The high-level waste stream can be decontaminated by PyroGreen to yield TRU-rich

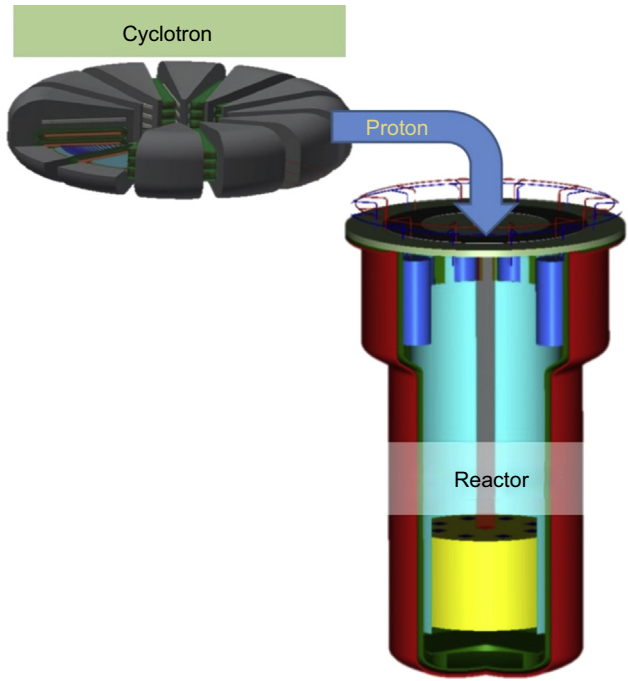


Figure 13.24 Concept of thorium-based accelerator driven system, TORIA.

fuels that can be burnt by thorium-based ADS, designated as TORIA. In its conceptual design, compact proton cyclotrons with moderate energy and beam current is coupled to LBE-cooled target in TORIA that will burn all residual TRUs from entire Korea nuclear power fleet with economic viability.

Currently, LFR R&D in ROK is focused on the further development of computer codes and corrosion-resistant materials as well as the safety design criteria. System design codes for URANUS have been focused on neutronic models and safety analysis codes. It is planned that the developed codes will be verified by independent experts. Thermomechanical processing of corrosion-resistant materials developed for long-life core will be explored to achieve desirable combination of proven mechanical properties in fast neutron environment and innovative corrosion resistance. The ROK LFR R&D community has been participating in the GIF LFR provisional Systems Steering Committee as an observer. It is planned that the safety design criteria for URANUS will be derived from the international collaboration.

13.3.4 Molten salt reactor

The beginning of molten salt reactor (MSR) research in Korea dates back to 1998. A basic concept of an MSR that burns the DUPIC fuel was first developed in Ajou University. More studies on MSR, including a recent fluoride−salt-cooled high temperature reactor, are under progress in UNIST (Ulsan National Institute of Science and Technology) and other institutes. Described below is a summary of the progress so far and future research plans of the MSR research in Korea.

Ajou University developed AMBIDEXTER-NEC (Advanced Molten-salt Breakeven Inherently-safe Dual-function EXcellenTly-Ecological Reactor Nuclear Energy Complex). The objective of the reactor is to burn DUPIC fuel, minimize minor actinides production, and of course, generate electric power. To achieve the objectives, the AMBIDEXTER reactor core consists of two parts, a blanket and a seed. The blanket consists of only molten salt fuel (LeF-BeF_2-$(Th,U,Pu)F_4$), and the seed consists of the molten salt fuel and graphite moderator channel. The blanket area has very hard neutron spectrum, almost looks like fast reactor neutron spectrum, and the seed area has a soft neutron spectrum almost looks like PWR. Therefore, AMBIDEXTER can achieve low conversion ratio, about 0.298, ie, it is a burner reactor. The code developed to analyze AMBIDEXTER is called AMBIKIN2D. The code system consists of HELIOS, AMDEC, and AMBIKIN2D.

In the area of neutronic analysis of the MSR core, UNIST is developing a code system for reactor core neutronic analysis of the MSBR, which was designed by Oak Ridge National Laboratory in the 1970s. To obtain equilibrium composition of MSR, three kinds of the equilibrium composition search methods are investigated by the nuclear reactor core analysis computer code system, which is based on MCNP6 Monte-Carlo code. The 680-cm diameter by 610-cm-high reactor vessel contains molten salt core and graphite material for neutron moderation and reflection. The fuel zone is divided into two zones of different fuel to graphite ratios. The Zone-1 has low fuel-to-graphite ratio, and most of fission reaction occurs; the Zone

2 has high fuel-to-graphite ratio, and most of breeding occurs. The first method uses the representative single unit cell for both zones. Single unit cell is set by volume-wise fuel and moderator weighting. The second method uses the representative unit cells for each zone, which are set by maintaining fuel-to-moderator ratio for each zone. The third one models directly the MSR whole core. The code system was set up with the MCNP6 Monte-Carlo code, its depletion module CINDER90, and the Python script language. The Python script is required for implementing the batch-wise reprocessing and refueling. The MSBR continuously adds fertile material and removes fission products and actinides. The core removes all volatile gases and noble metals every 20 s and separates ^{233}Pa from molten salt fuel every 3 days, allowing it to decay to ^{233}U. Other fission products have specific removal rates. After 3 days, depletion calculation is performed, and new inputs are created by using reprocessed materials. If the material compositions reach an equilibrium state, the equilibrium compositions of each method could be found. Twelve thousand days, nine thousand days, and seven thousand days are required to reach equilibrium states by using the single-cell model, two-cell model, and whole core model through depletion calculation. In the process of calculating the equilibrium fuel compositions, various parameters like multiplication factor, breeding ratio, and number density can be obtained to analyze the MSBR. The MSBR whole core analysis is performed at the initial and equilibrium core conditions for various reactor design parameters such as normalized neutron flux distribution, temperature coefficients, rod worth, and power distributions. The neutronics core characteristics were analyzed using a four-factor formula applied to the single-cell model, two-cell model, and the two zones of the whole core separately. UNIST has a plan to improve the code system to achieve higher accuracy and shorter calculation time and to design a new conceptual MSR core using the developed code system.

In the molten salt chemistry area, we are setting up a long-term experiment system to conduct the corrosion tests of structural materials under high temperature molten salt environment, and this system will be used to measure redox potential in associated test conditions. Several techniques have been adopted to obtain fundamental properties such as chronoamperometry, cyclic voltammetry, AC impedance method, and laser spectroscopy. We have also conducted a 3-D multiphysics computational analysis using parallel computing technique for multistep electrochemical processes in molten salt environment. In addition, it is required to investigate a way to safely store discharged solid spent fuel with extremely high burnup and to environmentally friendly dispose of the spent fuel. Regarding this issue, we will first investigate thermal, material, and radiological characteristics of spent nuclear fuel.

The salt used in an MSR is very noxious material, and its operating temperature is very high (710 ~ 560°C). So, simulant material, like heat transfer oils, is used at relatively low temperature in the preliminary study for safety. The interesting similarity has been found and reported first by University of California Berkeley (UC Berkeley) (Bickel et al., 2014). Thus, for understanding of high Prandtl number molten salt as a heat transfer medium, a fundamental molten salt study has been

performed using similarity technology with the simulant oils, which have a lower working temperature range. Based on UC Berkeley's previous works, using scaling law, a research will be performed with simulant oil at reduced scale with different characteristics of natural circulation condition. Also, two rectangular MSR test loops were designed for the similarity experiment with scale-down parameters. They will be used to verify the heat transfer ability of working fluid in coolant loop. Preliminary experiment for low power was conducted preferentially. Additionally, for both liquid and vapor phases, thermophysical properties of simulant oils, which are candidates of simulant, were generated and implemented into thermal−hydraulic code, which helps investigation of thermal behavior analysis with experimental data. Ultimately, our main purpose is the development of dimensionless heat transfer correlation of high Prandtl number molten salt through similarity technology application with scaled experiments and simulation of thermal−hydraulic code. Furthermore, the outcomes of the follow-up study will be used for the benchmark in terms of collaborations with UC Berkeley.

Acronyms

ADHRSs	Active DHRSs
AHX	Natural-draft sodium-to-air heat eXchanger
AMBIDEXTER-NEC	Advanced Molten-salt Break-even Inherently-safe Dual-function EXcellenTly-Ecological Reactor Nuclear Energy Complex
BOEC	Beginning of equilibrium cycle
DHRS	Decay heat removal system
DHX	Decay heat eXchanger
ENHS	Encapsulated nuclear heat source
EOEC	End of equilibrium cycle
FHX	Forced-draft sodium-to-air heat eXchanger
IHTS	Intermediate heat transport system
KAEC	Korea Atomic Energy Commission
KAERI-DySCo	Korea Atomic Energy Research Institute-Dynamic Simulation Code
KAERI	Korea Atomic Energy Research Institute
KALIMER	Korea Advance LIquid MEtal Rector
KIST	Korea Institute of Science and Technology
LACANES	Lead alloy-cooled advanced energy systems

Continued

LBE	Lead−bismuth eutectic
LMR	Liquid metal-cooled reactor
MSIP	Ministry of Science, ICT and Future Planning
NHDD	Nuclear hydrogen development and demonstration
NUTRECK	Nuclear Transmutation Energy Research Center of Korea
ORNL	Oak Ridge National Laboratory
PCS	Power conversion system
PDHRSs	Passive DHRSs
PDRC	Proliferation-resistant core without a blanket, and a decay heat removal circuit
PHTS	Primary heat transport system
PRIDE	PyRoprocess Integrated inactive DEmonstration facility
pSSC	Provisional Systems Steering Committee
RVACS	Reactor vessel air cooling system
SFRA	SFR Development Agency
STELLA	Sodium Test Loop for Safety Simulation and Assessment
TRU	TRansUranic elements
VHTR	Very high temperature gas-cooled reactor
YSZ	Yttria-stabilized zirconia

References

Bae, Ki-K., et al., 2015. Development of Key Technologies for Nuclear Hydrogen/Development of SI Hydrogen Production Process. Report # 2012M2A8A2025688. Korea Institute of Energy Research.

Bickel, J.E., et al., 2014. Design, Fabrication and Startup Testing in the Compact Integral Effects Test (CIET 1.0) Facility in Support of Fluoride-Salt-Cooled, High-temperature Reactor Technology. University of California, Berkeley.

Brambilla, G., et al., May 4−7, 1970. The SNAM process for the production of ceramic nuclear fuel microspheres. In: Symposium on Sol-Gel Processes and Reactor Fuel Cycles, Gatlinburg, Tennesses, pp. 191−209.

Carre, F., et al., 2010. Update of the French R&D strategy on gas-cooled reactors. Nuclear Engineering and Design 240, 2401−2408.

Chang, J., et al., April 2007. A study of a nuclear hydrogen production demonstration plant. Nuclear Engineering and Technology 39 (2), 111−122.

Cho, J.H., et al., 2011. Benchmarking of thermal hydraulic loop models for Lead-Alloy Cooled Advanced Nuclear Energy System (LACANES), phase-I: Isothermal steady state forced convection. Journal of Nuclear Materials 415 (3), 404−414.

Cho, J.Y., et al., 2013. DeCART2D User's Manual. KAERI/TR-5116/2013. KAERI.

Choi, S., et al., 2011. PASCAR: long burning small modular reactor based on natural circulation. Nuclear Engineering and Design 241 (5), 1486−1499.

Corwin, W.R., ORNL, et al., 2008. Generation IV Reactors Integrated Materials Technology Program Plan: Focus on Very High Temperature Reactor Materials. ORNL/TM-2008/129.

Eoh, J.H., et al., 2013. Design features of a large-scale sodium thermal-hydraulic test facility: STELLA. In: Internal Conference on Fast Reactors and Related Fuel Cycles (FR13), Paris, France.

Generation IV, 2013. International Forum Annual Report 2013. OECD/NEA for the Generation IV International Forum.

Greenspan, E., The ENHS Project Team, 2003. STAR: The Secure Transportable Autonomous Reactor System Encapsulated Fission Heat Source (The ENHS Reactor) Final Report, NERI Program Grant Number DE-FG03-99SF21889. Department of Nuclear Engineering, University of California.

Hahn, D., et al., 2002. KALIMER Conceptual Design Report. KAERI/TR-2204/2002. Korea Atomic Energy Research Institute, Daejeon, Korea.

Hahn, D., et al., 2007. KALIMER-600 Conceptual Design Report. KAERI/TR-3381/2007. Korea Atomic Energy Research Institute, Daejeon, Korea.

Han, T.Y., et al., May 03−06, 2015. Verification of a sensitivity and uncertainty analysis code based on GPT using MHTGR-350 benchmark. In: Proceedings of ICAPP 2015, France.

Hong, S.D., et al., 2012. Development of Essential Technology for VHTR. KAERI/RR-3425/2011.

Hwang, I.S., et al., 2000. The concept of proliferation-resistant, environment-friendly, accident-tolerant, continual and economical reactor (PEACER). Progress in Nuclear Energy 37 (1−4), 217−222.

IAEA, 2012. Advances in High Temperature Gas Cooled Reactor Fuel Technology. IAEA-TECDOC-1674. IAEA.

Jeong, K.C., et al., 2007. ADU compound particle preparation for HTGR nuclear fuel in Korea. Journal of Industrial and Engineering Chemistry 13, 744−750.

Jeong, C.J., et al., October 24−25, 2013. Preliminary verification calculation of DeCART/CAPP system by HTTR core analysis. In: Trans. of Korean Nuclear Soc. Autumn Meeting, Gyeongju, Korea.

Jung, H.S., et al., 2012. Environmental assessment of advanced partitioning, transmutation, and disposal based on long-term risk-informed regulation: PyroGreen. Progress in Nuclear Energy 58, 27−38.

Jung, K.-D., et al., 2015. Development of Key Technologies for Nuclear Hydrogen/Sulfuric Acid Decomposition Process for SI Cycle. Report # xxxxx. Korea Institute of Science and Technology.

KAERI, 2004. MARS Code Manual Volume I − Code Structure, System Models, and Solution Methods. KAERI/TR-2812/2004, Daejeon, Korea.

Kang, J.-H., et al., October 26−28, 2011. Development of core seismic analysis model of VHTR. In: Trans. of the Korean Nuclear Soc. Autumn Meeting, Gyeongju, Korea.

Kang, J.-H., et al., 2012. Thermo-mechanical analysis of the prismatic fuel assembly of VHTR in normal operational condition. Annals of Nuclear Energy 44 (5), 76−86.

Kim, W.J., et al., 2009a. Effect of coating temperature on properties of the SiC layer in TRISO-coated particles. Journal of Nuclear Materials 392, 213−218.

Kim, Y.W., et al., 2009b. Development of Essential Technology for VHTR. KAERI/RR-2992/2008.

Kim, Y.I., et al., 2013a. Status of SFR development in Korea. In: Internal Conference on Fast Reactors and Related Fuel Cycles (FR13), Paris, France.

Kim, Y.I., et al., 2013b. Conceptual Design Report of SFR Prototype Reactor of 150MW_{el} Capacity. KAERI/TR-4978/2013. Korea Atomic Energy Research Institute, Daejeon, Korea.

Kim, S.H., et al., 2013c. Fabrication and evaluation of SFR cladding tubes. In: International Conference on Fast Reactors and Related Fuel Cycles (FR13), Paris, France.

Kim, B.G., et al., October 27−31, 2014. Irradiation testing of TRISO-coated particle fuel in Korea. In: Proceedings of the HTR 2014, Weihai, China.

Lee, H.C., et al., April 15−20, 2012a. Development of HELIOS/CAPP Code System for the Analysis of Block Type VHTR Cores. PHYSOR 2012, Knoxville, Tennessee, USA.

Lee, H.C., et al., 2012b. Advanced Multi-physics Simulation Capability for Very High Temperature Reactor. KAERI/RR-3295/2010. KAERI.

Lee, C.B., et al., 2013. Status of SFR metal fuel development. In: International Conference on Fast Reactors and Related Fuel Cycles (FR13), Paris, France.

Lee, Y.-W., et al., 2014. Microstructural modification and porosity evolution during carbonization of fuel element compact for HTGR. Nuclear Engineering and Design 271, 244−249.

Lee, Ki-Y., et al., 2015. Development of Key Technologies for Nuclear Hydrogen/Development of Interface Technology for Nuclear Hydrogen Production System. KAERI/RR-3923/2014. Korea Atomic Energy Research Institute.

Lim, H.S., December 2014. General Analyzer for Multi-component and Multi-dimensional Transient Application (GAMMA+1.0) Volume II: Theory Manual. KAERI/TR-5728/2014.

OECD/NEA, The LACANES Taskforce, 2012. Benchmarking of Thermal-Hydraulic Loop Models for Lead-Alloy Cooled Advanced Nuclear Energy Systems − Phase I: Isothermal Forced Convection Case, 17. NEA/NSC/WPFC/DOC, p. 2012.

Park, J.Y., et al., 2008. Development of materials for a high temperature gas cooled reactor in Korea. In: Proc. of HTR2008, HTR 2008−58149, September 28−October 1, Washington DC, USA.

Shin, Y.H., et al., 2015. Advanced passive design of small modular reactor cooled by heavy liquid metal natural circulation. Progress in Nuclear Energy 83, 433−442.

Tak, N.I., et al., 2014. Development of a core thermo-fluid analysis code for prismatic Gas cooled reactors. Nuclear Engineering and Technology 46 (5), 641−654.

Tak, N.I., et al., May 7−8, 2015. Steady-state core temperature prediction based on GAMMA+/CAPP coupling. In: Trans. of the Korean Nuclear Soc. Spring Meeting, Jeju, Korea.

Yoo, J.S., Tak, N.I., Lim, H.S., 2010. Development of Tritium Behavior Analysis Code for Very High Temperature Gas-Cooled Reactor. KAERI/TR-4096/2010.

Yoon, C., Yoo, J.S., Lim, H.S., 2013. Preliminary Theory Manual for GAMMA-fp (Fission Product Module of the Transient Gas Multicomponent Mixture Analysis). KAERI/TR-4933/2013. KAERI.

Appendix: Paper list related to PEACER (including P-demo and Pyroprocess), PASCAR, URANUS, and other SNU-NUTRECK activities

Year accepted/ submitted	No.	First author	Journal/ conference	Title
2000	**001**	Il Soon Hwang	Progress in Nuclear Energy	The concept of proliferation-resistant, environment-friendly, accident-tolerant, continual and economical reactor (PEACER)
2005	002	Seung Ho Jeong	ICAPP 2005	Overview and status of HELIOS
	003	Seung Hee Chang	Global 2005	Development of LBE loop (HELIOS) for advanced materials studies
	004	Judong Bae	Global 2005	Development of an electrochemical−hydrodynamic model for electrorefining process
	005	Hyong Won Lee	ICAPP 2005	Solver-interfaced virtual reality approach for life-cycle management of nuclear energy systems
2006	**006**	Won Chang Nam	Nuclear Engineering and Design	Fuel design study and optimization for PEACER development
2007	**007**	Jae-Yong Lim	Progress in Nuclear Energy	A new LFR design concept for effective TRU transmutation
	008	Jungmin Kang	Progress in Nuclear Energy	Proliferation resistance of PEACER system
	009	Sung Il Kim	Progress in Nuclear Energy	Requirement of decontamination factor for near-surface disposal of PEACER wastes
	010	Jun Lim	ANS 2007	Corrosion experiments in large-scale LBE loop: HELIOS
	011	Jun Lim	ICAPP 2007	Progresses in the operation of Large scale LBE loop: HELIOS
2008	012	Il Soon Hwang	HLMC 2008	Passive safety characteristics of demo version of PEACER
	013	Il Soon Hwang	KNS 2008	PASCAR-DEMO − a small Modular reactor for PEACER demonstration

Continued

Continued

Year accepted/ submitted	No.	First author	Journal/ conference	Title
	014	Il Soon Hwang	ICAPP 2008	Development of transportable capsule version of PEACER design
	015	Il Soon Hwang	Actinide and fission product Partitioning and transmutation	Development of PASCAR (proliferation-resistant, accident-tolerant, self-sustainable, capsular, assured reactor) design and safety analysis
	016	Jun Lim	HLMC-2008	Corrosion behaviors of commercial FeCrAl alloys in liquid lead−bismuth eutectic environments
	017	Jun Lim	ICAPP 2008	Corrosion test of Cr- and Al-containing alloys in static LBE at 550°C
2009	018	Sungyeol Choi	Global 2009	P-DEMO for demonstration of PEACER concept
	019	Jun Lim	Journal of Nuclear Materials	Corrosion behaviors of FeCrAl alloys in liquid lead−bismuth eutectic environments
	020	Kwang Rak Kim	Global 2009	Computational multiphysics analysis of a molten-salt electrolytic process for a nuclear waste treatment
	021	Hyo on nam	Global 2009	All the spent nuclear wastes to low and intermediate level wastes: PyroGreen
2010	022	Jun Lim	Journal of Nuclear Materials	A Study of early corrosion behaviors of FeCrAl alloys in liquid lead−bismuth eutectic environments
2011	023	Sungyeol Choi	Nuclear Engineering and Design	PASCAR: Long burning small modular reactor based on natural circulation
	024	Sungyeol Choi	ASME 2011 SMR Symposium	URANUS: Korean lead-bismuth cooled small modular fast reactor activities
2012	025	V. Shankar Rao	Annals of Nuclear Energy	Analysis of 316 L stainless steel pipe of lead−bismuth eutectic cooled thermo-hydraulic loop
	026	V. Shankar Rao	Corrosion Science	Characterization of oxide scales grown on 216 L stainless steels in liquid lead−bismuth eutectic

Continued

Year accepted/ submitted	No.	First author	Journal/ conference	Title
2013	027	Jun Lim	Journal of Nuclear Materials	Design of alumina forming FeCrAl steels for lead or lead−bismuth cooled fast reactors
	028	Jae Hyun Cho	HLMC-2013	Design optimization of small modular reactors with natural circulation of lead−bismuth coolant
	029	Seung Gi Lee	HLMC-2013	Corrosion of T91, HT9, and stainless steel 316 L in static cell of liquid lead−bismuth eutectic at 600°C
2014	030	Jae Hyun Cho	ICONE22	Power maximization of fully passive lead−bismuth eutectic cooled small modular reactor
2015	031	Yong-Hoon Shin	Progress in Nuclear Energy	Advanced passive design of small modular reactor cooled by heavy liquid metal natural circulation
	032	Jae Hyun Cho	Nuclear Engineering and Design	Power maximization method for land-transportable fully passive lead−bismuth cooled small modular reactor systems

Generation IV concepts: China

14

D. Zhang
Xi'an Jiaotong University, Xi'an, People's Republic of China

14.1 Current status of nuclear power in China

The development of nuclear power in China has occurred in three stages as shown in Fig. 14.1. The first stage was the starting stage represented by the Qinshan and Daya Bay nuclear power plants (NPPs) and their building and operation. With the economic development of China, and the encouraging policy issued, such as "Medium- and Long-Term Development Plan of China Nuclear Power (2005−2020)," the construction of nuclear power entered the stage of accelerated development. Before 2008, the government had planned to increase nuclear generating capacity to 40 GW_{el} by 2020, with a further 18 GW_{el} of nuclear capacity being under construction. Furthermore, projections for nuclear power then increased to 70−80 GW_{el} by 2020, 200 GW_{el} by 2030, and 400−500 GW_{el} by 2050. However, after the Fukushima accident and consequent pause in approvals of new plants, the target adopted by the China State Council in October 2012 became 58 GW_{el} by 2020, with 30 GW_{el} under construction (WNA, 2005). National policy has moved from "moderate development" of nuclear power to "positive development" in 2004 and in 2012 to "steady development with safety."

As of May 2015, China (mainland) has 26 nuclear power reactors in operation, which contribute 2.4% of the total electricity production according to the International Atomic Energy Agency (IAEA). Twenty-four reactors are under construction; this is 40% of all reactors under construction in the world. Additional reactors are also planned, including some of the world's most advanced reactors, to provide

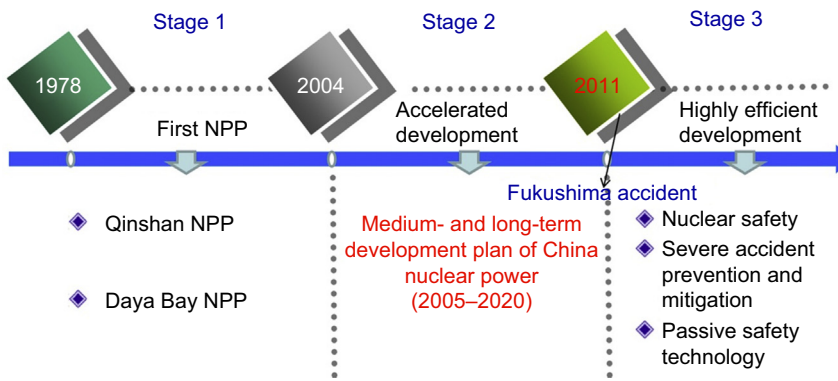


Figure 14.1 Three stages of China nuclear power development. *NPP*, nuclear power plant.

Handbook of Generation IV Nuclear Reactors. http://dx.doi.org/10.1016/B978-0-08-100149-3.00014-8
Copyright © 2016 Elsevier Ltd. All rights reserved.

more than a 3-fold increase in nuclear capacity. More than 20 NPPs are about to be approved and start construction. After the Fukushima accident, the impetus for increasing the nuclear power share in China is still increasing, mainly due to four primary reasons: (1) strong energy demand for the fast growth of the domestic economy, (2) air pollution from coal-fired plants, (3) acute fluctuation of the regular energy price creating risk for investors, and (4) increasingly intensified constraints from other energy environments and resources. The Chinese government began to learn lessons from the Fukushima accident, and nuclear safety receives more attention for the development of nuclear power. In the third stage, the advanced reactors will be developed using evolutionary technologies, such as passive safety technologies, and severe accident preventions and mitigations to ensure nuclear power safety. Therefore China is becoming largely self-sufficient in reactor design and construction, as well as other aspects of the fuel cycle, by not only making full use of Western mature technologies but also adapting and improving them. On the basis of this, China would like to go global with exporting nuclear technologies, including heavy components in the supply chain.

14.2 Plans for advanced nuclear reactors in China

China sponsors a series of programs to research, develop, and demonstrate advanced reactors, including both the Generation III reactors for commercial purposes and Generation IV reactors for nuclear sustainable development. A white paper on energy policy released by the State Council in October 2012 pointed out that China will invest more in nuclear power technological innovations, promoting application of advanced technology, improving the equipment level, and attaching great importance to personnel training. In addition, the State Council published the Energy Development Strategy Action Plan 2014−20 in November 2014, which aims to cut China's reliance on coal and promote the use of clean energy, confirming the 2012 target of 58 GW_{el} nuclear in 2020 with an additional 30 GW_{el} under construction. The plan calls for the "timely launch" of new nuclear power projects on the East coast and for feasibility studies for the construction of inland plants. It also says that efforts should be focused on promoting the use of large pressurized water reactors (PWRs) (including the CAP1400 and Huanlong-I designs), high-temperature reactors (HTRs), and fast reactors. From this plan it is seen that advanced PWRs will be the mainstream in Chinese nuclear power development, but they are not the sole reactor type.

Two Generation IV reactor concepts, HTRs and sodium-cooled fast reactors (SFRs), are considered the most promising reactors for sustainable nuclear development in China. In February 2006 the State Council announced that the small HTR was the second of two high-priority National Major Science and Technology projects for the next 15 years; this aims at exploring co-generation options in the near term and producing hydrogen in the long term. The small high-temperature reactor pebble-bed modular (HTR-PM) is now under construction at Shidaowan, Shandong province. On the basis of the successful operation of the Chinese experimental fast reactor (CEFR),

the design and relative research of the Chinese demonstration fast reactor (CDFR) are now intensively performed, and it is planned to be constructed at Xiapu, Fujian province.

In addition to HTR and SFR, the other Generation IV concepts are also supported by different government agencies. The supercritical water-cooled reactor (SCWR) was supported under the National Key Basic Research Program of China (973 project) by the China Ministry of Science. The studies of molten salt reactors (MSRs) and lead-cooled fast reactors (LFRs) are performed in the framework of the Chinese Academy of Sciences (CAS) pilot projects. In the following section, the current research and development (R&D) on Generation IV reactors in China will be briefly introduced.

14.3 Current research and development on Generation IV reactors in China

14.3.1 Sodium-cooled fast reactor research and development

SFR development in China can be generally divided into two main phases by the SFR construction, which can be divided into four subphases: (1) basic technology research phase (before 1986), (2) application technology research phase (1987−93), (3) engineering application research phase (1994−2010), and (4) large-scale commercial SFR R&D phase (2010−30). In the following section, China SFR R&D will be introduced in two parts: (1) research before SFR construction and (2) SFR development strategy.

14.3.1.1 Research before SFR construction

In the late 1960s, China began SFR research activities. The initial studies focused on neutronics, thermal-hydraulics, sodium technology, material, sodium equipment and instruments, and small sodium facilities. Later on, approximately 12 experimental setups and one sodium loop were constructed, among which a 50-kg ^{235}U zero-power neutron setup reached criticality in June 1970 (Rouault et al., 2010).

In 1986 SFR technology development was involved in the first National High Technology Research and Development Program (863 Program) of China, which started the application technology research stage aiming at the construction of the 65-MW_{th} (20 MW_{el}) CEFR. Institutes, universities, and companies such as the China Institute of Atomic Energy (CIAE), Xi'an Jiaotong University (XJTU), etc., were organized to work on the reactor design, fuel and materials, sodium technology, and safety research. Until 1993 there were in total more than 20 experimental setups and sodium loops in China. The experimental validation phase focused on sodium loop technology. Two sodium loops were imported from Italy and one sodium loop was established at XJTU. The primary design of CEFR was completed in 1997, and to test the conceptual design, a zero-power simulation experiment was performed in Russia.

14.3.1.2 SFR development strategy

The SFR development strategy in China involves three steps: the CEFR with a power of 20 MW_{el}, the CDFR with a power larger than 600 MW_{el}, and the post-CDFR commercial breeding or transmutation reactor with a power of 1000 MW_{el} (Xu, 2009).

CEFR

China's first fast reactor CEFR was constructed by CIAE in cooperation with the Beijing Institute of Nuclear Engineering. During the design of CEFR, approximately 50 tests for design verifications were conducted to confirm the performance and obtain the operation experiences.

The CEFR site excavation was started in October 1998, and it achieved criticality for the first time in July 2011. On July 21, 2011 the reactor was successfully connected to the grid. CEFR is an experimental SFR with a power of 65 MW_{th}, and the designed fuel is PuO_2-UO_2. In the first loading, UO_2 was used as the fuel with cladding, and the reactor block structure material was made of Cr-Ni austenitic stainless steel. The reactor is a pool type with two main pumps, and there are two loops in the intermediate circuit. The superheated steam in the two loops in the third circuit (water-steam) combined together before entering the turbine.

As shown in Fig. 14.2, the core of CEFR is composed of 81 fuel subassemblies (SAs), three safety SAs, three compensation SAs, and two regulating rod SAs (Xu, 2008). There are 336 stainless reflector SAs, 230 shielding SAs, and 56 spent fuel SA primary storage locations. Each fuel SA has 61 triangular arranged rods, which are located in a radial direction with a wire wrap. Hexagonal tubes are used to connect with the SA operating head at the top and the SA pin at the bottom. The pins are

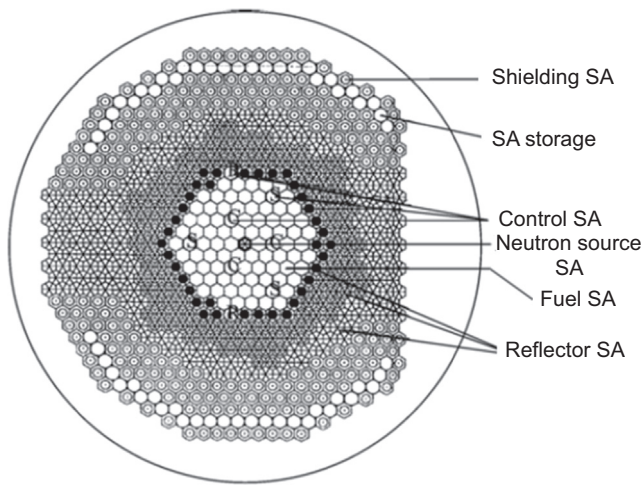


Figure 14.2 Chinese experimental fast reactor core layout. *SA*, subassembly. Reproduced from Xu, M., 2008. The status and prospects of fast reactor technology development in China. China Engineering Science 1, 70–76.

inserted into the pressure header, which has upper and lower grids. On one hand the header can locate the core axially, and on the other hand it can guide the primary sodium into the core.

The control and safety SAs have the same structure, and the reactor is controlled or shut down by their movement in the tubes. There are two separate reactor shut-down systems, both of which can quickly shut down the reactor. The compensation and regulating SAs form the first shut-down system whereas the safety SAs form the other shut-down system.

The CEFR block is shown in Fig. 14.3 (Xu, 2008). It is mainly composed of a reactor cover, a sodium pool, and internal structures. The reactor cover is an approximately 2-m-thick steel-concrete structure that acts as the reactor upper shielding and provides support for the plug, main pumps, intermediate heat exchangers (IHXs), residual heat removal heat exchangers, and the circuits and pipes of various auxiliary systems. The driving mechanisms of control and safety, the fuel manipulator, and various measurement instruments are all fixed on the small plugs of the plug system.

The sodium pools are mainly composed of a main vessel and guard vessel, with a temperature and pressure measurement instrument on the wall and a sodium leak detector in the gap of the vessels. The main vessel acting as the boundary of the primary circuit is a very important item of safety equipment. The internal structures involve the inner pool used to separate the hot and cold pools, the reactor core and its pressure header, and supports and shieldings.

The primary circuit of the CEFR in the sodium pool has two primary sodium pumps, which drives the 360°C cold sodium from the cold pool into the core and cools it. The average core outlet temperature can be as high as 530°C. Via the hot

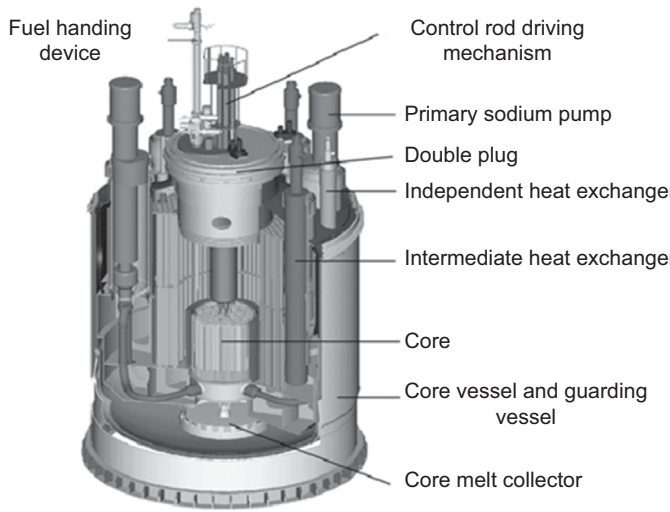


Figure 14.3 Chinese experimental fast reactor block.
Reproduced from Xu, M., 2008. The status and prospects of fast reactor technology development in China. China Engineering Science 1, 70–76.

pool, the hot sodium flows into four IHXs, where the heat is transferred to the intermediate circuit through the tube wall of the IHX. The intermediate circuit has two loops, and each has an intermediate pump, a steam generator (SG; composed of evaporator and superheater), and two IHXs connected to the primary circuit. In the third water-steam system, the 480°C superheated steam at 10 MPa from two SGs is guided into the turbine to generate electricity, and condensed water returns to the evaporator through the high-pressure heater and deaerator. The heat from the condensers is transferred to the atmosphere by cooling water. The heat transport system is shown in Fig. 14.4 (Xu, 2008).

The residual heat removal system also consists of two separate loops, and each has an independent heat exchanger, an air heat exchanger, and pipes (Xu, 1995). Totally relying on natural convection and natural circulation, the residual heat under accidental conditions is removed.

CDFR

CDFR is a pool-type SFR with a preliminary designed thermal power of 2100 MW and an electrical power of 870 MW. Mixed oxide (MOX) is used as the fuel, and sodium is the main coolant. The reactor is a three-loop, three-circuit design, and there is only one set of steam turbine generators. Fig. 14.5 shows the preliminary core layout of the CDFR (Yang et al., 2007). It was planned to be constructed in Xiapu, Fujian province, under the cooperation of the China National Nuclear Corporation (CNNC), the Fujian Investment and Development Group, and the Xiapu state-owned assets investment management company with the investigation ratio of 51:40:9.

The heat transport flowchart of CDFR is shown in Fig. 14.6 (Yang et al., 2007). The main heat transport system includes three circuits. The primary circuit is pool type and consists of three loops, each of which has a primary pump and two IHXs.

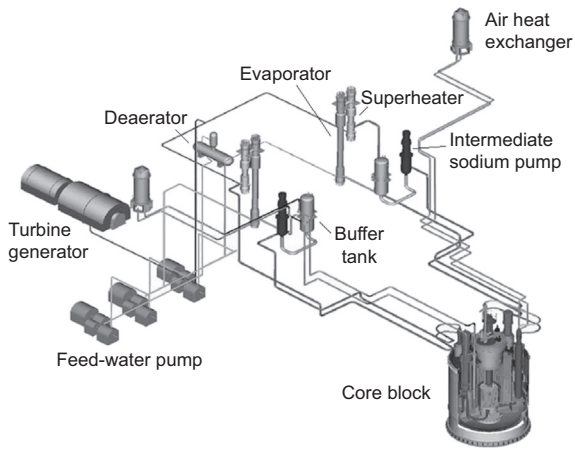


Figure 14.4 The heat transport system of the Chinese experimental fast reactor.

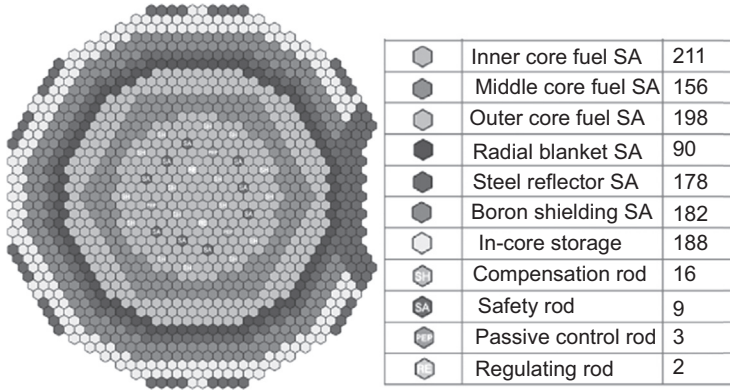


Figure 14.5 Core layout of the Chinese demonstration fast reactor. *SA*, subassembly.

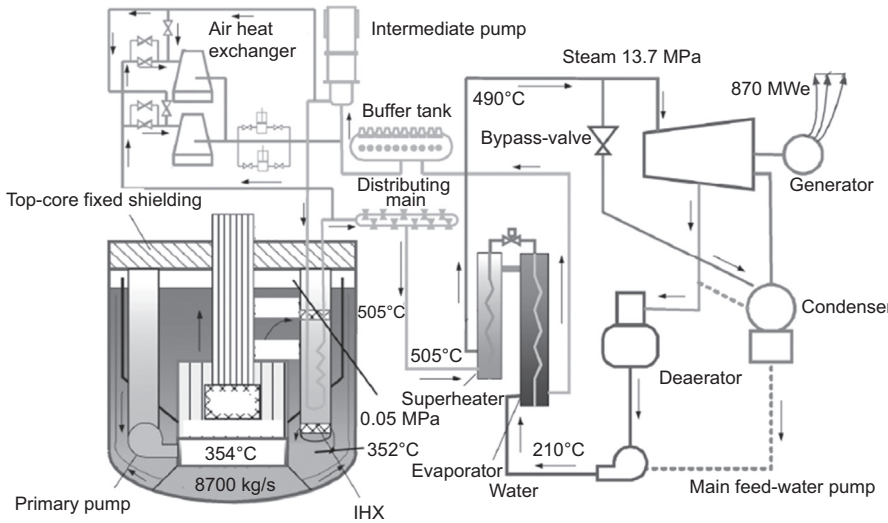


Figure 14.6 The heat transport flowchart of the Chinese demonstration fast reactor. *IHX*, intermediate heat exchanger.

These components together with the pipes of the primary circuit, grid header, core, and sodium pool constitute the primary sodium circulation system. The intermediate circuit also comprises three loops, and each loop has an intermediate pump, a SG group composed of 10 modules (each module has an evaporator and a superheater), a sodium buffer tank, two IHXs located in the main vessel, a sodium distributor, and connection pipes. The water-steam circuit is composed of three parallel SG groups and a turbine generator. Each of the SG group receives water from a water pump, and generated superheated steam from the SG groups is collected in the main steam pipe to supply the turbine.

Because the design of the CDFR is still in progress, the main technical features of the CDFR are preliminarily proposed as follows (Yang et al., 2007):

1. The primary circuit operates under atmospheric pressure.
2. The primary circuit is a pool type, and the reactor vessel has a large heat storage capacity, which guarantees that operators have sufficient time to analyze accident conditions and take necessary mitigation steps under relevant transition and accident conditions.
3. The core temperature design has a large boiling margin.
4. Fluid floating passive shut-down system is used as an emergency shut-down method, which should ensure that the reactor can shut down before exceeding the core temperature limit and a 200°C margin to boiling.
5. The heat can be removed from the main transport system and the special air cooling system connected with three loops of the intermediate circuit. The air cooling system can ensure that the residual heat is removed by natural circulation under station blackout accident.
6. A special core melting gathering unit is designed to prevent melting from contacting with the reactor vessel bottom under beyond design accident of core collapse.
7. The core top shield is used as an additional barrier of radiation.
8. Passive liquid seal device is used to prevent the reactor vessel from overpressure.
9. The passive siphon destruction device is used to prevent excessive loss of sodium when the primary circuit auxiliary system leaks.
10. The radioactive inclusive system composed of a sealing workshop and several radioactive inclusive cells is designed to guarantee the radiation emission under the national nuclear safety limit.
11. Performability is improved with the use of digital instruments and control system design and simplification of the main control room and instrument detection system.

Post-CDFR

After CDFR, there are two possibilities (Xu, 2009). CDFR can be deployed in a manner of a modular, one-site multireactor breeding nuclear reactor called the Chinese commercial breeding fast reactor (CCFR-B), which will increase the nuclear power capacity in China. The other is that if the experience with minor actinide (MA) isolation techniques and transmutation of MAs and long-lived fission products in a fast reactor is enough whereas the automatic depressurization system (ADS) technology is not mature, CDFR can be deployed in a manner of a one-site multireactor transmutation nuclear reactor called the Chinese commercial transmutation fast reactor (CCFR-T). Thus the first strategy for Chinese SFR development is to build the CDFR and deploy it in a manner of a one-site multireactor, such as five to six commercial fast reactors with a power of 800−900 MW_{el} by approximately 2030. The second strategy is to increase the nuclear power capacity to 240 GW_{el} by approximately 2050 by developing the high breeding fast reactors. The third strategy is to replace much fossil fuel with nuclear power in 2050-2100 to drastically reduce the carbon dioxide emissions.

14.3.2 Very-high−temperature reactor research and development

In China, the very-high−temperature reactor (VHTR) concept has another name, the high-temperature gas-cooled reactor (HTGR), which has been developed since the

1970s. On the basis of the intensive research, a 10-MW_{th} prototype pebble-bed HTR (HTR-10) has been built at Tsinghua University, and a demonstration HTR-PM is under construction.

14.3.2.1 Early development of the high-temperature gas-cooled reactor program in China

In China the research and development program for HTGR began in the mid-1970s. At that time the target for constructing a 100-MW_{th} thorium thermal breeder was set in place. The conceptual design of a pebble-bed HTGR with a core blanket of two zones was proposed and accomplished. This conceptual design was characterized with (1) the compactness due to high specific power, (2) a high breeding ratio (almost approaching unity in such a small reactor), and (3) operating ability (inherently stable, online refueling property, etc.).

During the Chinese sixth five-year plan (1981−85), the State Science and Technology Committee financially supported the research for the basic technology of the HTGR. The main goal was to complete the design of a high-temperature reactor module (HTR-Module); research its safety features; and develop computer codes for reactor physics, thermo-hydraulics, and safety analyses. The conceptual designs of HTR-Module-334, an HTR-Module with a thermal power of 334 MW and fuel multipass mode, as well as HTR-OTTO-200, an HTR-Module with 200 MW of thermal output and a once-through-then-out (OTTO) mode, were completed (Zhong and Gao, 1985).

In 1986 China's 863 Program was launched and the HTGR research and development program was involved in the energy field of the 863 Program. From 1986 to 1990, eight research topics for fundamental technologies were defined and put in place (Zhao et al., 2001). These eight topics were the following:

1. A conceptual design and development of computer codes for reactor physics, thermo-hydraulics, and the safety analyses;
2. Development of fuel element manufacturing;
3. The reprocessing of the thorium−uranium fuel cycle;
4. The ceramic reactor design together with a stress analysis;
5. Development of the helium technology;
6. Design of pressure vessels;
7. Development of a fuel handling system; and
8. Development of materials.

Meanwhile, many experimental facilities were set up and the theoretical calculations for the HTR-OTTO-200 t (thermal power) were completed. The intention was to begin building a real HTGR reactor after accomplishing the eight research topics mentioned here.

14.3.2.2 HTR-10 test module project

The Institute of Nuclear Energy Technology (INET) of Tsinghua University performed the conceptual design of the 10-MW_{th} HTGR test module (HTR-10) in 1990 (Steinwarz and Xu, 1990), and 2 years later the construction of HTR-10 was approved by the State Council. Supported by the Chinese 863 Program, the

construction of the HTR-10 was commenced in 1995. It reached first criticality in December 2000 with full power operation in January 2003.

The design, construction, and operation of the HTR-10 were important steps toward the commercialization of the modular HTGR in China, which may indeed influence HTGR future development.

Concept design and objectives of HTR-10

Fig. 14.7 presents the schematic diagram of the HTR-10 system. During the conceptual design of the HTR-10, the following critical issues were particularly considered (Sun and Xu, 2000):

1. A pebble-bed reactor was chosen rather than a block reactor, which has been researched for almost 20 years.
2. The 10 MW of thermal power would be suitable for both the initial investment, supported by the 863 Program, and the transition from the HTR-10 to a prototype HTR-Module.

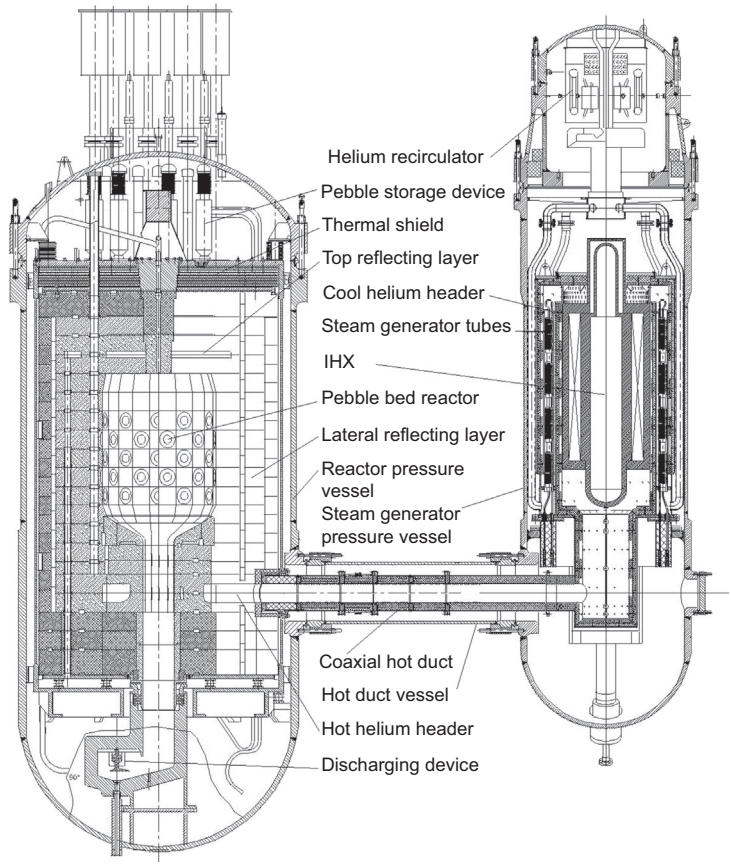


Figure 14.7 Schematic diagram of the HTR-10 system. *IHX*, intermediate heat exchangers; *SG*, steam generator.

3. To smooth the transition from the HTR-10 to the prototype HTR-Module without performing repetitive research work in the future, the HTR-10 should fundamentally represent the basic features used in the HTR-Module (eg, the multiloading mode, control rods at the reflector sides, confinement, etc.).
4. The HTR-10 was adopted to generate electricity, although its power rate might be limited. The advantages of using HTR-10 to generate electricity were to save operating costs and to present a "real power station" instead of an experimental reactor. The HTR-10 operation success would be crucial in obtaining approval from the Chinese government for the HTR-Module construction to meet the future energy needs of China.
5. During the HTGR conceptual design, its applications and safety-related experiments were taken into account. These applications and safety-related issues included the investigation of the possibility of nuclear processing heat applications and a test of the mass fuel elements at the temperature of 1600°C.

HTR-10 engineering experiments

During the HTR-10 operation, a series of engineering experiments for the test and development of the eight HTR-10 key technologies was performed on HTR-10 in INET (Xu et al., 1997). Those engineering experiments included the following:

1. The performance test of the hot gas duct,
2. The measurement test of the temperature mixture degree at the core bottom,
3. The two-phase flow instability test for the once-through SG,
4. The performance test for the pebble fuel handling system,
5. The performance test of the control rod driving mechanism,
6. The validation and verification tests for the full digital reactor protection systems,
7. The measurement test of the neutron absorption cross section in the reflector graphite, and
8. The performance test for the helium circulator.

The main objective of these engineering experiments was to validate the design characteristics and performance of the reactor components and systems and to obtain information on the design and operating experiences of the HRT-10.

Experiences learned by constructing HTR-10

Much knowledge and experience were obtained from the HTR-10 design, construction, and operation. This knowledge and experience can well guide the design of the large prototype plants, such as the HTR-Module. Most importantly, the advantages of the HTR-Module became much clearer as a result of the HTR-10 construction. It is more obvious that the HTR-Module is inherently safe and capable of achieving economic competitiveness. The primary experiences learned from the HTR-10 construction are summarized as follows:

1. It is possible to build the HTR-Module in a short period. Approximately 5 years were spent in the construction of the HTR-10 from the first concrete date (FCD) to achieving criticality. The construction period could be shortened for the HTR-Module in the future. Design delays considerably lengthened the HTR-10 construction period. In fact, the installation of all reactor components and systems only needed approximately 1 year, and the civil engineering work also required only approximately 1 year. In addition, it is also possible to complete the

installation of reactor components and systems in a short period because they are simple in the HTR-10. The adoption of the full digital reactor protection and control system can also shorten the period of precommissioning.

2. The components and systems of the HTR-Module are simple and can be produced in a modular way. There are only two slightly complex systems from the point view of the system arrangement and the number and requirement of system components, which are the pebble fuel handling system and the helium purification system. Other systems are very conventional and are easy to install.
3. The classification of all components and systems should be reconsidered because the classification for the HTR-10 during the initial design stage mainly referred to light water reactor (LWR) classifications. This is really not very proper. For example, the safety function of the helium circulator for the HTR-10 is not the same as that of the primary pump for an LWR.
4. To promote the HTGR development throughout the world, intensive international cooperation is necessary. International support speeded the construction of the HTR-10. If China had not had international support, particularly from German institutes and companies, then it would have been impossible for HTR-10 to reach criticality in the year 2000. It should be pointed out that the HTGR development level is not the same as the development of the other reactors. The prospect of the HTGR development would be uncertain if its development could not be performed with international cooperation.

14.3.2.3 High-temperature reactor pebble-bed modular project

The overall high-temperature reactor pebble-bed modular project

On the basis of the success of the HTR-10, the China State Council declared in 2006 that the small HTR was the second of two high-priority National Major Science and Technology projects for the next 15 years. It aimed to explore co-generation options in the near term and producing hydrogen in the long term. The first two 250-MW_{th} HTR-PMs with twin 105-MW_{el} reactors driving a single 210-MW_{el} steam turbine was approved (Zhang and Yu, 2002; Xu and Zuo, 2002) to be installed at Shidaowan in Weihai city of Shandong province. The reactor core is 11 m in height, and the steam will be at 566°C. The engineering of the key components, structures, and systems is based on China's own capabilities, although they include completely new technical features. It is envisaged that the thermal efficiency of 40%, localization of 75%, and 50-month construction period for the first unit can be realized. The construction of the HTR-PM started at the beginning of 2014, which was delayed after the Fukushima accident. Construction of the reactor building itself is now ongoing.

In the organization category, the China HuaNeng Group (CHNG) is the lead organization to build the demonstration Shidaowan HTR-PM with the China Nuclear Engineering and Construction (CNEC) group and the INET of Tsinghua University, which is the China HTGR R&D leader. Chinergy Company, a joint venture of Tsinghua University and CNEC, is the main contractor for the nuclear island. CNEC and Tsinghua University signed the agreement on HTR industrialization cooperation in 2003, and a further agreement on commercialization of the HTR was agreed between the two parties in March 2014. CNEC is responsible for China HTR technical implementation and is becoming the main investor of HTR commercial promotion at home and abroad.

Design of HTR-PM

HTGR uses helium as coolant and graphite as moderator as well as structural material. A single-zone core design was adopted, in which the spherical fuel elements are placed. The cylindrical active reactor core has an outer diameter of 3.0 m and effective height of 11.0 m. The effective core volume is 77.8 m^3. In the equilibrium core, the reactor core contains 420,000 fuel elements.

The reflectors include top, side, and bottom graphite reflectors. Graphite reflectors are made from graphite blocks, which are constructed layer by layer. In the circumferential direction, every layer of graphite reflectors consists of 30 graphite blocks. Inside of the side graphite reflector blocks, the corresponding numbers of channels are designed for reactor shut-down systems and for helium flow. The bottom reflector takes a cone shape at the upper surface to facilitate the pebble flow. Inside of the bottom reflector, channels are designed for the flow of hot helium. The hot helium chamber is designed in the bottom reflector area, where hot helium of different outlet temperatures is mixed and then directed to the hot gas duct in which the hot helium flows to the SG. In the center of the bottom reflector is the fuel discharge tube.

The primary helium coolant works at the pressure of 7.0 MPa. The rated mass flow rate is 96 kg/s. Helium coolant enters the reactor in the bottom area inside of the pressure vessel with an inlet temperature of 250°C. Helium coolant flows upward in the side reflector channels to the top reflector level where it reverses the flow direction and flow into the pebble bed in a downward flow pattern. Bypass flows are introduced into the fuel discharge tubes to cool the fuel elements there and into the control rod channels for control rod cooling. Helium is heated up in the active reactor core and then is mixed to the average outlet temperature of 750°C and then flows to the SG.

The reactor core and the SG are housed in two steel pressure vessels that are connected by a connecting vessel. Inside of the connecting vessel, the hot gas duct is designed. All of the pressure retaining components, which comprise the primary pressure boundary, are in touch with the cold helium of the reactor inlet temperature. The primary pressure boundary consists of the reactor pressure vessel (RPV), the SG pressure vessel (SGPV), and the hot gas duct pressure vessel (HDPV), which all are housed in a concrete shielding cavity as shown in Fig. 14.8.

Table 14.1 provides some key design parameters of the HTR-PM. Its nominal thermal power is 500 MW_{th}, and the generator power output is 210 MW_{el}. The reactor active zone has a height of 11 m and an outside diameter of 3 m. Every spherical fuel element contains 7 g of heavy metal with an enrichment of nearly 8.5%. The overall height of the reactor pressure vessel is 25 m, and the inner diameter of the vessel is 5.7 m. The reactor is designed for 40 years of operational life with a load factor of 85%.

14.3.3 Supercritical water-cooled reactor research and development

In China, the experiences and the technologies developed in the design, manufacture, construction, and operation of NPPs are mainly concentrated on water-cooled reactors.

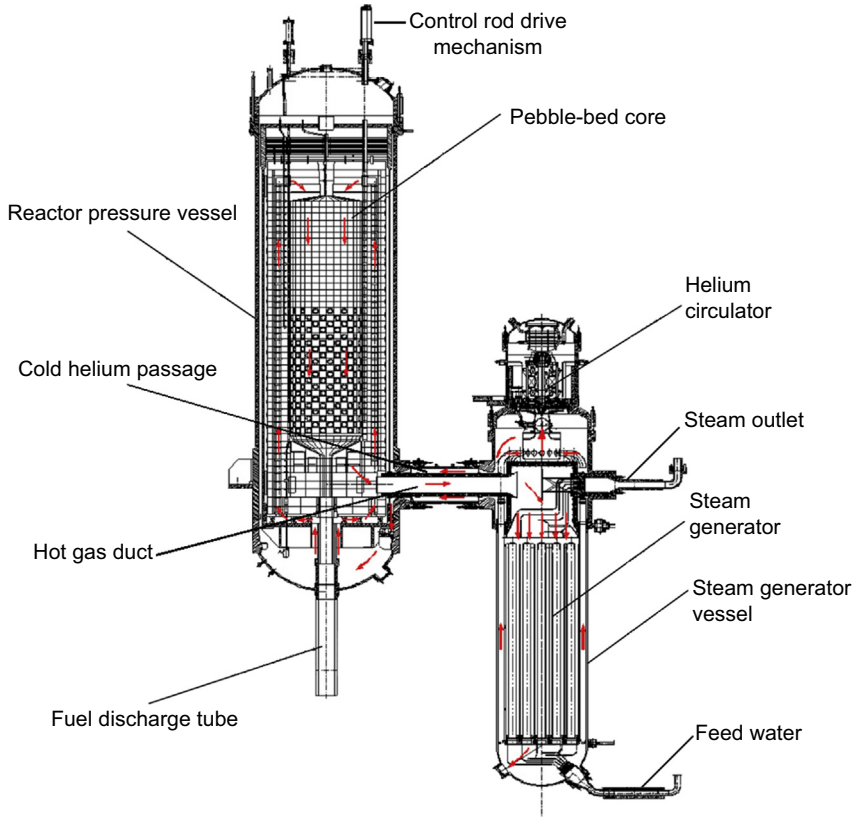


Figure 14.8 The primary loop of the high-temperature reactor pebble-bed modular.

Table 14.1 High-temperature reactor pebble-bed modular main design parameters

Category	Design parameter	Unit	Design value
General plant data	Reactor thermal power	MW_{th}	500
	Power plant output	MW_{el}	210
	Plant design life	Year	40
	Primary coolant material	–	Helium
	Expected load factor	%	85
	Moderator material	–	Graphite
	Thermodynamic cycle	–	Rankine

Table 14.1 Continued

Category	Design parameter	Unit	Design value
Reactor core	Active core height	m	11
	Fuel column height	m	11
	Average fuel power density	kW/kgU	85.7
	Fuel material	–	UO_2
	Fuel element type	–	Spherical
Primary coolant system	Mass flow rate	kg/s	96
	Operating pressure	MPa	7
	Core inlet temperature	°C	250
	Core outlet temperature	°C	750
Power conversion system	Working medium	–	Steam
	Mass flow rate	kg/s	99.4
	SG outlet pressure	MPa	14.1
	SG outlet temperature	°C	570
Fuel element	Enrichment	%	8.5
	Diameter of kernel	mm	0.5
	Diameter of sphere	mm	60
	Diameter of fuel zone	mm	50

In addition, from a technological point of view, an SCWR is a combination of the water-cooled reactor technology and the supercritical fossil-fired power generation technology. Thus the development of SCWRs is considered a smooth extension of the existing nuclear power generation in China. In 2007 a National Key Basic Research Program of China (973 Program) on SCWR was initiated by the China Ministry of Science. Since then, several universities, industrial companies, and academic institutions in China successively contribute to the SCWR-associated research activities based on which two conceptual designs have been proposed: (1) the mixed spectrum SCWR (SCWR-M) by Shanghai Jiaotong University (SJTU) and (2) the 1000-MW_{el} Chinese SCWR (CSR1000) by the Nuclear Power Institute of China (NPIC). In the following section, these two SCWR concepts are introduced.

14.3.3.1 Mixed spectrum supercritical water-cooled reactor conceptual design

The SCWR-M concept (Cheng et al., 2008) was proposed in the SCWR 973 project, which was led by SJTU and performed under the cooperation of eight institutes,

universities, and industrial companies. SCWR-M is a mixed spectrum core consisting of a thermal spectrum zone (the outer zone in Fig. 14.9) and a fast spectrum zone (the inner zone). According to the latest design (Liu et al., 2010), there are a total of 284 fuel assemblies (FAs) in the SCWR-M core, 164 of which are in the thermal zone. As schematically shown in Fig. 14.10, the water from the core inlet firstly flows downward through both coolant channels and moderator channels of the thermal zone, mixing in the lower plenum, and then it flows upward through the fast zone. The main design parameters of a SCWR-M are listed in Table 14.2.

Comparing with the PWR rods and assemblies, the rod design and assembly arrangement of SCWRs are obviously optimized (Yang et al., 2012). The assemblies

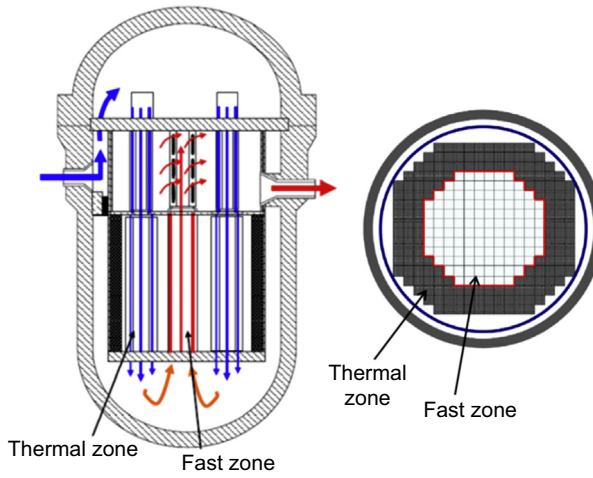


Figure 14.9 Schematic diagram of the mixed spectrum supercritical water-cooled reactor core.

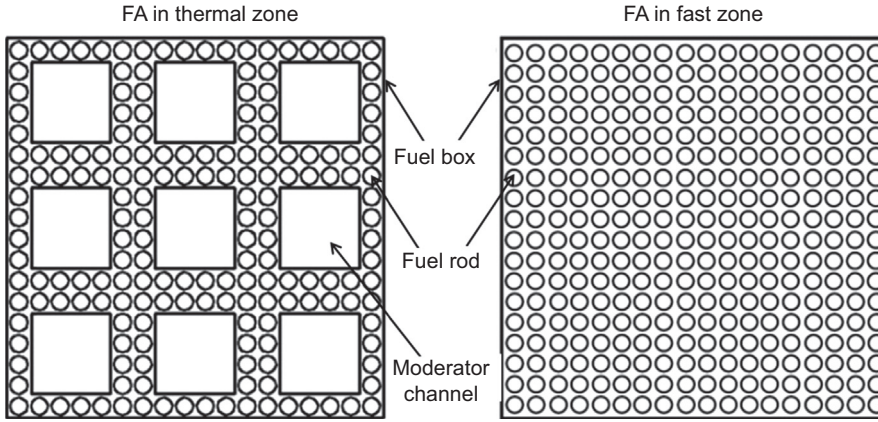


Figure 14.10 Fuel assembly (FA) structure in the thermal and fast zone of the mixed spectrum supercritical water-cooled reactor.

Table 14.2 Main design parameters of the mixed spectrum supercritical water-cooled reactor

Parameters	Units	Thermal zone	Fast zone	Entire core
Thermal power	MW	2460	1100	3560
Inlet temperature	°C	280	400	280
Outlet temperature	°C	400	510	510
Active height	m	4.0	2.0	–
Fuel assembly box size	mm	173.2	173.2	–
Number of fuel assemblies	–	180	100	280
Number of fuel pins	–	180	289	–
Fuel pin diameter	mm	8.0	8.0	–
Pitch-to-pitch ratio	–	1.20	1.27	–
Average linear power	W/cm	190	190	–
Power density	MW/m^3	114	92	102
Relative moderation capacity	–	1.53	0.15	–
Equivalent outer diameter	–	3.3	2.0	3.3
Mass flux	$kg/(m^2s)$	922	1145	–
Maximum fluid velocity	m/s	5.5	13.1	–
Pressure drop	kPa	25.0	98.0	123.0
Maximum coolant temperature	°C	550.5	526.9	550.5
Maximum cladding temperature	°C	610.4	616.7	616.7
Fuel	–	UO_2 or MOX	MOX	–
Enrichment	–	5–6%	~20%	–

MOX, mixed oxide.

in the thermal and fast zones have different structures. As illustrated in Fig. 14.10, it can be seen that additional moderator channels exist in the thermal FA to provide enough moderation. For simplification, the co-current flow mode is adopted between the coolant channels and the moderator channels in the thermal zone. The optimization work (Liu and Cheng, 2010) suggests that 20% of water flow from the inlet flows through moderation channels serving as moderator, and the rest serves as coolant through the coolant channels. To achieve a sufficiently large negative void reactivity coefficient and increase the conversion ratio, 11 layers of seed and blanket regions are introduced.

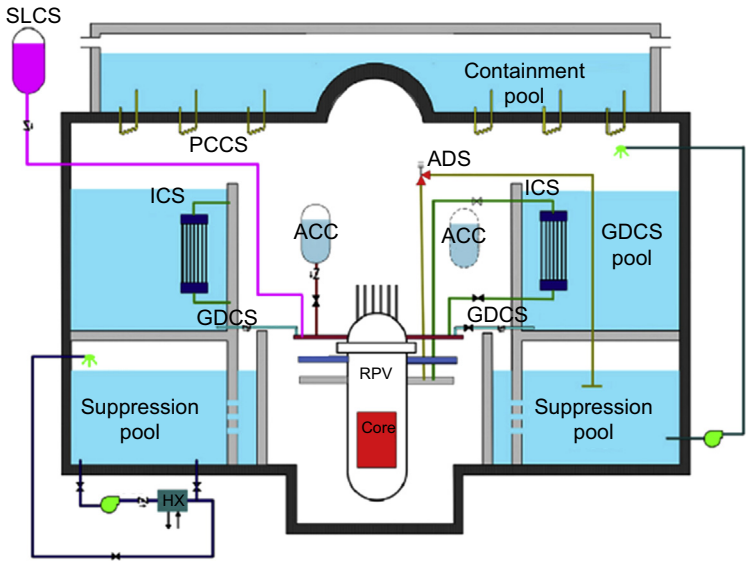


Figure 14.11 The mixed spectrum supercritical water-cooled reactor safety system. *ICS*, isolation cooling system; *GDCS*, gravity-driven cooling system; *ACC*, accumulators; *ADS*, automatic depressurization system; *PCCS*, passive core cooling system; *SLCS*, standby liquid control system.

Along with proposal of its core and assembly design, R&D activities have been extended to safety design and analysis. Some important features of SCWR-M under loss of flow accident were investigated (Xu et al., 2011; Zhu et al., 2012), and a reverse flow was observed and confirmed with the pressure keeping over the critical point in these analyses. The safety system for SCWR-M (Liu et al., 2013a,b) is derived from the passive design of AP1000 (Schulz, 2006) and the economic simplified boiling water reactor (Hinds and Maslak, 2006). It contains the isolation cooling systems, gravity-driven cooling systems (GDCS), accumulators (ACC), ADS, and standby liquid control system as schematically shown in Fig. 14.11. On the basis of the modified system code analysis of thermal-hydraulics of leaks and transients-supercritical water (ATHLET-SC), loss of coolant accident (LOCA) analysis is performed (Liu et al., 2013a,b).

14.3.3.2 The 1000-MW_{el} Chinese supercritical water-cooled reactor concept design

The 1000-MW_{el} SCWR design concept CSR1000 (Li et al., 2013; Xia et al., 2013; Zhang et al., 2013) is proposed by NPIC with China's independent intellectual property. The Phase I R&D activities on key technologies for CSR1000 began in 2010 and finished in 2013. The main objectives of Phase I are R&D on concept design, experiment, and material research for SCWRs. Its follow-up activities are ongoing. The main design parameters of CRS1000 are listed in Table 14.3.

Table 14.3 The main technical parameters of the 1000-MW_{el} Chinese supercritical water-cooled reactor core

Design parameters	Units	Value
Pressure	MPa	25.0
Electric power	MW	1000
Thermal power	MW	2300
Thermal efficiency	%	43.5
Core height	m	4.2
Number of fuel assemblies	–	177
Fuel rod diameter	mm	9.5
Pitch-to-diameter ratio	–	1.105
Flow rate	kg/s	1190.0
Fuel	–	UO_2
Cladding	–	Alloy 310S
Enrichment	%	4.3 (Conner); 5.7 (Other)

The CSR1000 is designed to be a thermal spectrum reactor based on the existing technologies of PWRs, SCWRs, and advanced boiling water reactors (ABWR). As schematically shown in Fig. 14.12, the FA in the CSR1000 core is divided into two zones, the inner zone with 57 FA clusters and the outer zone with 120 FA clusters. Entering the core from cold legs, water partially flows upward to the upper plenum, with the rest flowing downward through the down comer to the lower plenum. The water in the upper plenum divides into three parts and flows downward: (1) coolant through the outer zone coolant channels, (2) moderator through the outer zone moderator channels, and (3) moderator through the inner zone moderator channels. All of the water mixes in the lower plenum and then flows through the coolant channels of the inner zone.

As mentioned, there are a total 177 FA clusters in the core. The FA clusters in both the outer zone and inner zone are in the same structure design. To simplify the structural design and obtain more uniform moderation, the CSR1000 typical FA cluster is composed of four sub-FAs, each of which is a 9×9 fuel rod configuration with one square water channel in the center, as shown in Fig. 14.13. The rods in a sub-FA are surrounded by an assembly wall, which is made of ZrO_2 for thermal insulation covering with two 310S layers. In addition, a cruciform control rod is adopted in each FA cluster.

To hold more fissile gas with a shorter gas plenum at the ends of the fuel rod, and to decrease the highest temperature of fuel pellets as much as possible, annular fuel pellets are adopted. The outside diameter of the rod is 8.19 mm, whereas the diameter of the inner gaseous space is 1.5 mm. 310S is selected as the cladding material and other structure material.

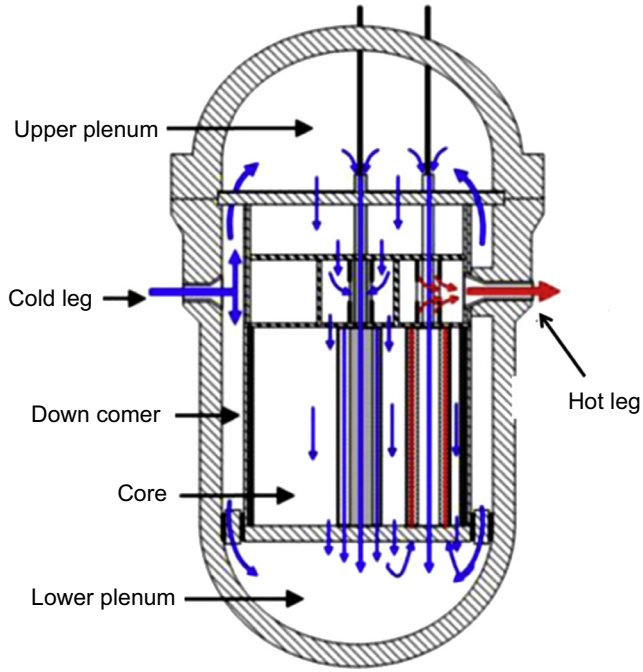


Figure 14.12 Scheme of the 1000-MW_{el} Chinese supercritical water-cooled reactor core.

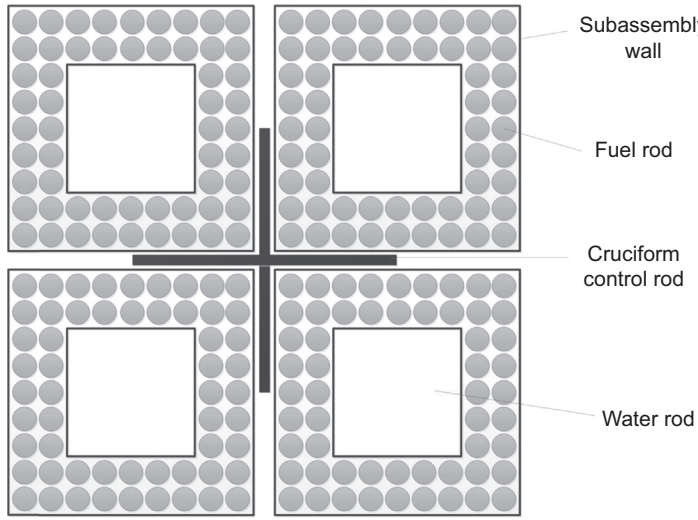


Figure 14.13 Cross section of 1000-MW_{el} Chinese supercritical water-cooled reactor fuel assembly.

According to public literature, some preliminary fundamental analyses have been performed on the CSR1000 concept. With a homemade code named FREDO-CSR1000 (FREquency DOmain analysis of CSR1000) and TIMDO-CSR1000 (TIMe DOmain analysis of CSR1000), the analysis of flow instability for CSR1000 both in the average channel and the hot channel within rated power and flow has been performed (Tian et al., 2012, 2013). The calculation results indicated that the decay ratio of the first flow path monotonically varies with power and flow. However, the decay ratio of the second flow path ascends first and then descends, the trend of which is fluctuant because of the simultaneous influence of a multitude of variables. Furthermore, it is found that the location where the flow instability happened is directly determined by the point at which the pseudocritical temperature is reached.

Subchannel analysis models have been investigated for CSR1000FA by using the experimental data available and the computational fluid dynamics (CFD) code (Du et al., 2013). The analysis results are used to improve a subchannel code. The steady-state subchannel analysis is conducted on the CSR1000 FA to obtain the temperature distribution of coolant and cladding and pressure drop in the FA. The results show that smaller pitch will flatten the profile of the coolant temperature and reduce maximum cladding surface temperatures, but it increases the pressure drop in the assembly.

Large-break accident analysis of CSR1000 was performed using the advanced process simulation software (APROS) code to clarify its characteristics and to evaluate the capability of its safety system (Dang et al., 2013). At the cold-leg large-break accident, the maximum cladding temperature is lower than the criterion 1260°C by approximately 340°C, which appears during the blow-down phase.

14.3.4 Molten salt reactor research and development

In January 2011 the CAS launched a pilot project of the thorium molten salt reactor (TMSR) nuclear energy system aiming at developing solid- and liquid-fuel MSRs. The Shanghai Institute of Applied Physics (SINAP) is in charge of this project, which strives for realizing effective thorium utilization and hydrogen production by nuclear energy within 20–30 years. The near-term goals of the TMSR project are to build two test reactors: a solid-fueled TMSR (TMSR-SF) and a liquid-fuel TMSR (TMSR-LF). Fig. 14.14 presents the strategy of the Chinese TMSR R&D. In addition, the project also includes the development of a pyro–process complex (Serp et al., 2014). The nominal power of the first solid-fuel test reactor was initially designed with power of 2 MW_{th}, and it was increased to 10 MW_{th} in 2013. The solid-fuel 10-MW_{th} test reactor will be constructed by 2020 as the initial step with the expectation of a larger 100-MW_{th} fluoride-salt–cooled high-temperature reactor (FHR) shortly thereafter. This reactor designated as TMSR-SF will be a pebble-bed FHR (PB-FHR) concept developed by the University of California–Berkeley (UCB), which may be the first FHR ever built in the world (Forsberg et al., 2014).

Before launching the CAS TMSR project, XJTU was financially supported by Natural Science Foundation of China (NSFC) to perform the fundamental research on the neutronics, thermal-hydraulic modeling, and safety analysis of MSRs. Because the

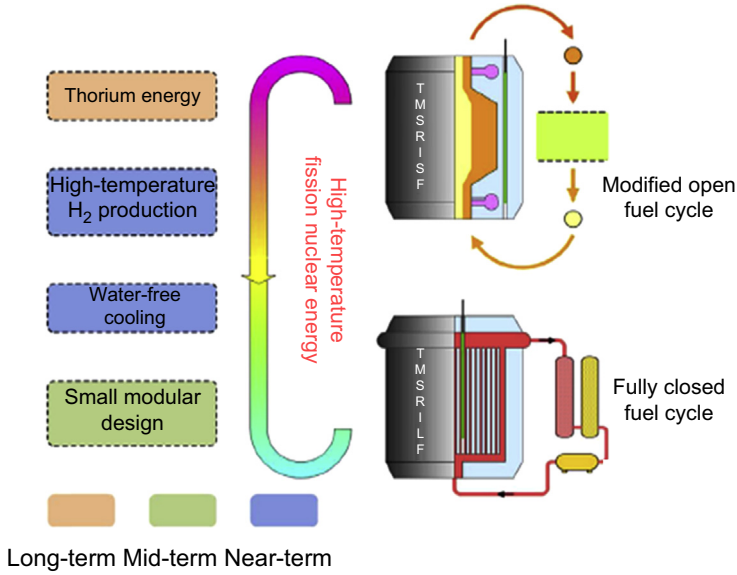


Figure 14.14 Strategy of Chinese thorium molten salt reactor research and development. *TMSR-SF*, solid-fueled thorium molten salt reactor; *TMSR-LF*, liquid-fueled thorium molten salt reactor.

TMSR designs in China change frequently and not final released, in this section only the fundamental research of MSRs under the framework of the pilot TMSR project and NSFC projects are summarized.

14.3.4.1 Thermal-hydraulic modeling and safety analysis

Several types of thermal-hydraulic models from simple to complex were developed to calculate the temperature and flow distributions in the MSR core. A one-dimensional single-phase flow model was proposed to simulate the flow and heat transfer of the fuel salt in the graphite-moderated channel-type MSR. The axial and radial power factors necessary for the thermal-hydraulic calculation were calculated by the DRAGON code (Zhang et al., 2008). A two-dimensional thermal-hydraulic model was developed to calculate the flow and heat transfer in the core, coupled with the two-group neutron diffusion equation to obtain the flux distribution (Qian et al., 2010). The steady thermal-hydraulic characteristics were also analyzed by a three-dimensional coupled neutronics/thermal-hydraulic analysis code (Zhou et al., 2014). The CFD is often adopted to simulate the multidimensional porous media flow for pebble-bed MSRs. By using simplified body center cubic (BCC) and face center cubic (FCC) models, pore scale thermal-hydraulic characteristics of pebble-bed advanced high-temperature reactor (FHR type) proposed by UCB were also investigated, in which the temperature distribution, pressure drop, and local mean Nusselt number were calculated (Song et al., 2014). Similar studies were also performed for the TMSR-SF and the 2-MW PB-FHR (Wang et al., 2014a, 2015).

Initial events analysis is necessary to be performed before the reactor safety analysis and the probabilistic safety assessment (PSA). Referring to the initial events of the LWRs, HTRs, and SFRs, the initial event lists of the TMSR-SF, containing 37 initial events, were determined and grouped into six types using the master logic diagram (MLD) (Mei et al., 2014). Table 14.4 lists the initial events and their grouping of the TMSR-SF. Through the PSA analysis of the loss of offsite power (LOOP) using the PSA process risk spectrum, the accident sequences of the radioactive material release to the core and its frequency were obtained (Mei et al., 2013).

Many efforts have also been focused on the safety analysis of MSRs. A safety analysis code was developed by establishing a kinetic model to consider the flow effects of the fuel salt coupled with a simplified heat transfer model in the core. The safety characteristics of the MOlten Salt Actinide Recycler and Transmuter (MOSART) were

Table 14.4 Initial events lists and their grouping of the solid-fueled thorium molten salt reactor

No.	Accident types	Initial events
1	Reactivity accidents	A control rod out of control under the condition of subcritical or low-power operation
		A control rod out of control under the condition of power operation
		Control rod operation in error
		Accident critical in the process of charge
2	Core heat removal increase accidents	Secondary circuit flow increase
		Secondary circuit temperature lower
3	Core heat removal decrease accidents	Primary circuit main pump stuck shaft
		Primary circuit main pump trip
		Secondary circuit circulating pump trip
		Secondary circuit circulating pump stuck shaft
		Fuel assembly entrance jam
		Loss of off-site power
		Loss of the inside and outside AC power at the same time (loss of nonemergency AC power)
		Intermediate heat exchanger leakage
		Secondary circuit air heat exchanger fault
		Air cooling tower ventilation doors get stuck
		Air heat exchanger of the cabin failure

Continued

Table 14.4 Continued

No.	Accident types	Initial events
4	Pipeline crevasse and equipment leakage accidents	Primary circuit pipeline small crevasse
		Secondary circuit pipeline small crevasse
		Primary container leakage
		Main heat exchanger tube rupture
		Fuel sphere breakage
		Isolation valve abnormal open
		Molten salt pipe rupture out of containment
		Connecting pipe between containment and the first isolation valve crevasse
		Primary circuit molten salt purification system pipeline leakage
		Radioactive waste gas disposal system leakage or breakage
		Radioactive liquid waste disposal system leakage or breakage
5	Anticipated transients without scram (ATWS)	Loss of off-site power without scram
		Control rods miss out without scram
6	Disasters (internal and external)	Earthquake
		Fire
		Flooding
		Strong wind
		Explosion
		Tsunami
		Plane crash

AC, alternating current.

investigated by simulating three types of basic transient accidents including the unprotected loss of flow (ULOF), unprotected overcooling accident (UOC), and unprotected transient overpower (UTOP; Zhang et al., 2009a). The results indicate that the conceptual design was an inherently safe one. The ULOF and the combination of ULOF and unprotected loss of heat sink (ULOHS) were studied on the MOSART by supplementing a heat sink model (Guo et al., 2013b). Using the conceptual design of the TMSR-LF as the reference case, a pump stop accident was simulated at nominal power of 2 MW_{th} by the Cinsf1D code (Wei et al., 2014). In addition, the reactivity initiated

transients of the TMSR-LF without thorium fuel, including the step reactivity initiated event, ramp reactivity initiated event, UOC, and ULOF, were analyzed as well as those of the reactor with thorium fuel (Cai, 2013).

The safety analysis of the TMSR-SF has also drawn much attention. Three types of transient conditions including ULOF, UOC, and UTOP were examined on the TMSR-SF by an FHR safety analysis code named the FHR Safety Analysis Code (FSAC; Xiao et al., 2014). The station blackout anticipated transient without scram (SBO-ATWS) accident was analyzed by the modified RELAP5/MOD 4.0 code with the responses of the passive residual heat removal (PRHR) system (Jiao et al., 2015).

Several types of PRHR system have been proposed to enhance the inherent safety of the MSRs. On the basis of the residual heat removal system for the Molten Salt Reactor Experiment (MSRE) developed by Oak Ridge National Laboratory (ORNL), a conceptual design with passive characteristics was completed using natural air cooling rather than the forced water circulation to cool the condenser (Fig. 14.15). The passive heat removal system is composed of three natural-circulation loops, including (1) the two-phase natural circulation in the bayonet cooling thimble transferring the decay heat to the second loop, (2) the two-phase natural circulation between the air cooler and the steam drum, and (3) the open loop where steam in the air cooler was condensed by the circulation of air in the chimney (Sun et al., 2014). A more detailed design was put forward with the L-type fin tube chosen as the heat exchanger tube of the air cooler (Zhao et al., 2015). Thermal-hydraulic characteristics of this type of PRHR system were investigated (Cai et al., 2014; Sun et al., 2014; Zhao et al., 2015).

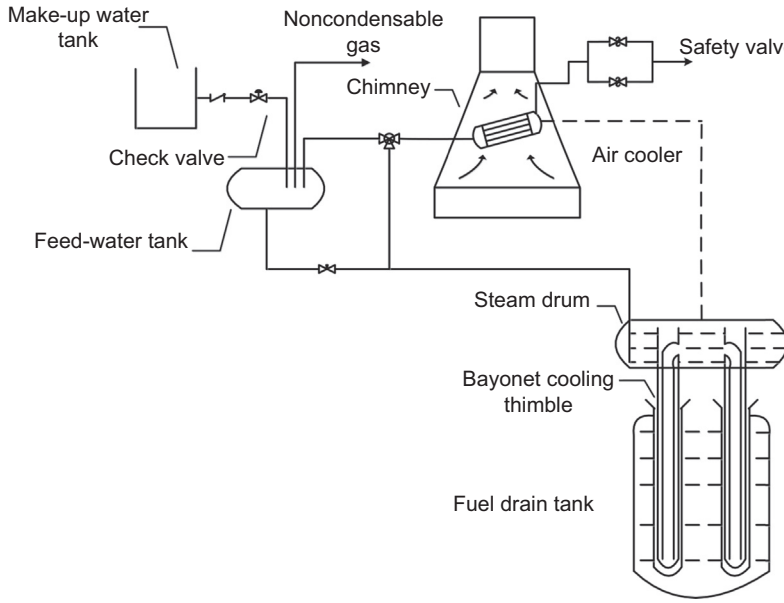


Figure 14.15 Schematic diagram of the passive residual heat removal system.

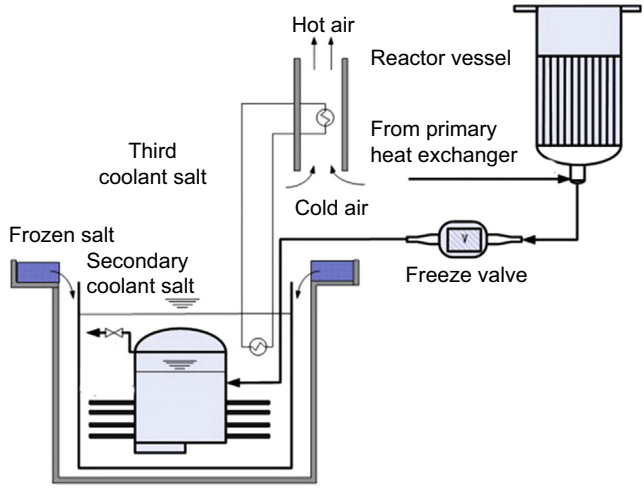


Figure 14.16 Schematic diagram of the new-concept passive residual heat removal system of molten salt reactors using the sodium heat pipe.

Using heat pipes might help to improve the heat dissipation performance of the PRHR system of MSRs. Two types of conceptual designs of PRHRs, using high-temperature sodium heat pipes and sodium-potassium alloy ones, respectively, were proposed as shown in Figs. 14.16 and 14.17. Transient analysis results indicate that the high-temperature sodium heat pipe had a successful startup and could rapidly remove the residual heat of fuel salt in the MSR accidents (Wang et al., 2013a,b).

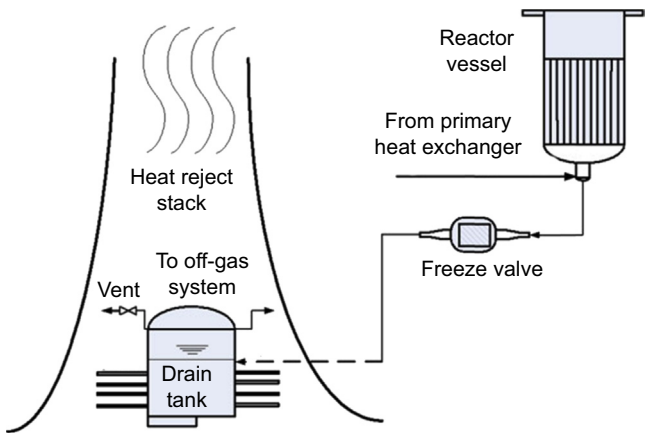


Figure 14.17 Schematic diagram of the new concept passive residual heat removal system of molten salt reactors using the sodium−potassium heat pipe.

14.3.4.2 Neutronic modeling

Neutronic characteristics of MSRs have been explored in the literature. Flow effects were considered when calculating the effective multiplication factor and fast neutron, thermal neutron, and delayed neutron precursor distribution of the liquid-fuel MSR based on the multigroup neutron diffusion equation and delayed neutron precursor conversation equation (Zhang et al., 2009b; Cheng and Dai, 2014; Zhou et al., 2014). Spatial kinetic models were developed for better neutronic analysis of the MSRs (Zhang et al., 2015; Zhuang et al., 2014).

Neutron absorption of the poisons such as ^{135}Xe and ^{85}Kr has an important impact on the reactor reactivity. The calculation method of the source terms for the MSRE with online removal of radioactive gases was developed to analyze the radioactivity of fission products and the tritium products (Zhang et al., 2014b). ORIGEN2 was applied to study the variation of the xenon and krypton fission gases varying with neutron spectrum and flux in Tri-ISOtropic (TRISO) fuel particles (Yin, 2014).

Reactor physical characteristics have also drawn much attention. The control rod worth, including the differential worth and integral worth, were calculated by the Monte Carlo code for neutron and photon transport (MCNP) for the 2 MW TMSR-SF (Zhou and Liu, 2013). The measurement of the neutron energy spectrum was also theoretically and experimentally studied (Zhou, 2013). Parametric study of the thorium-uranium conversion rate was conducted to optimize the core structure for the improvement of the economics of the TMSR using the standardized computer analyses for licensing evaluation (SCALE) code (Wang and Cai, 2013).

14.3.4.3 Thermo-hydraulics and neutronics coupling analysis

It can be noted that much work has been done on coupling thermo-hydraulics and neutronics analysis for the liquid-fuel MSRs. Neutronic models based on the multigroup diffusion theory while considering the flow effects of the liquid fuel were proposed to couple the flow and heat transfer models in performing the steady and transient analysis of the MSR (Cai, 2013; Guo et al., 2013a; Wei et al., 2014; Zhang et al., 2009a; Zhou et al., 2014). The delayed neutron precursor movement including its turbulence also was especially considered in these analyses (Cheng and Dai, 2014; Zhang et al., 2009b). COUPLE (a time-space-dependent coupled neutronics and thermal-hydraulic code), was developed on the basis of the previous work (Zhang et al., 2014a). In addition, the general MCNP is coupled with a multiple-channel analysis code (MAC) by a linking code to perform parametric studies of the MSRE (Guo et al., 2013a,c). The traditional safety analysis code CATHARE (code for analysis of thermal-hydraulics during an accident of reactor and safety evaluation) was also modified to perform the study of a single channel in the MSR core (Peng et al., 2013).

14.3.4.4 Molten salt test loops

Several experimental loops have been constructed at SINAP, including the HTS molten salt test loop (Fig. 14.18), the FLiNaK molten high-temperature salt test

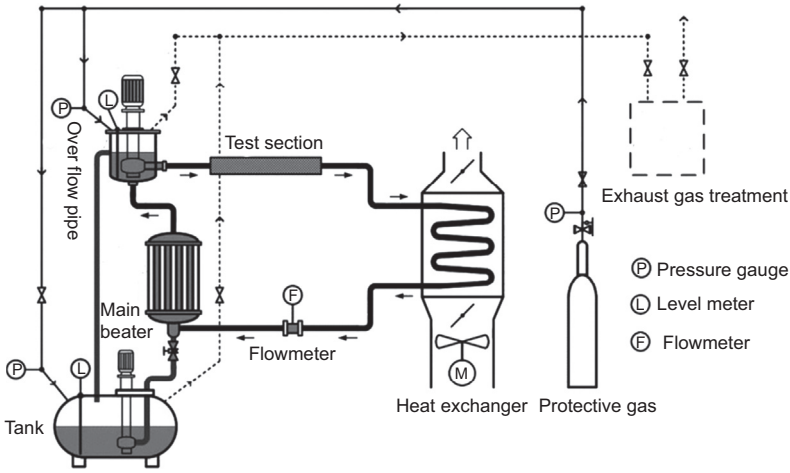


Figure 14.18 Schematic diagram of the high-temperature salt molten salt test loop.

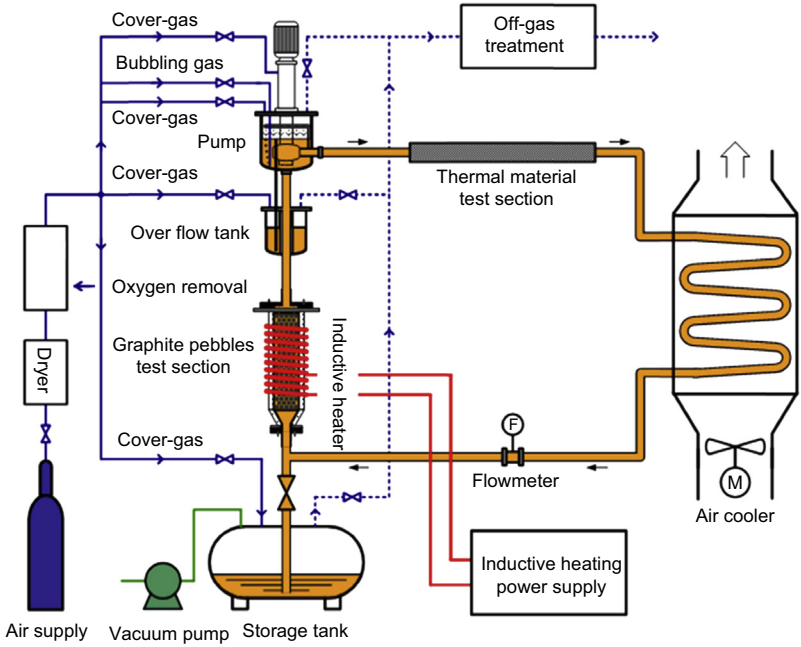


Figure 14.19 Schematic diagram of FLiNaK molten salt high-temperature testing loop.

loop (Fig. 14.19), and the nitrate natural circulation loop. The FLiNaK test loop was constructed to study the heat transfer and corrosion between the FLiNaK molten salt and fuel pebbles. Hastelloy C 276 alloy was adopted to fabricate the pipe in the loop. The FLiNaK molten salt test loop operates within the temperature range of 550−700°C whereas the heat power is approximately 200 kW (Zou et al., 2013).

The high-temperature salt molten salt test loop and the nitrate natural circulation loop operate with the liquid nitrate (Han et al., 2013).

14.3.4.5 Material and salts research

An experimental device was constructed by SINAP for measuring the density and liquidus temperature of molten fluorides typically used in the TMSR project. A candidate molten salt coolant, LiF-NaF-KF (46.5-11.5-42 mol%) was investigated (Cheng et al., 2013).

The immersion corrosion of ZrC-SiC-based ceramics was performed in molten fluoride salt FLiNaK, with the goal of assessing their capability with candidate materials in molten fluoride preparation, thermal storage, and transfer application. Results show that the ZrC-SiC composites represented better corrosion resistance than the single content of ZrC or SiC. With an increase in the SiC content, the corrosion resistance could be improved (Wang, 2013; Wang et al., 2014b). Another type of candidate high-temperature material, MAX (Mn+1AXn) phase materials, was also investigated for corrosion resistance in molten fluoride salts at the temperature of approximately 850°C, approximately the operating temperature of the MSR (Li et al., 2014). Alloys including the Chinese Hastelloy-N alloy were also examined for performance in the high-temperature FLiNaK molten salt. It can be found that temperature and the existence of water in the molten salt had significant impact on the corrosion (Liu et al., 2015).

The irradiation resistance of the structural materials used in the MSRs are of great importance. The pyrolytic carbon (PyC) coating adopted in the TRISO fuel particles was studied in the ion irradiation and static FLiNaK molten salt experiments. The results showed that irradiation defects might increase the fluorination of PyC coating in FLiNaK salt (Feng, 2014). As a candidate structural material for MSRs, the 316 austenitic stainless steel (316SS) was investigated in a high-temperature environment with Xe ion irradiation. The temperature effect of Xe ion irradiation on the 316SS was obvious (Huang et al., 2014).

The permeation behaviors of tritium in the candidate structural materials of the TMSR was studied because the tritium can easily diffuse through the structural materials at high temperatures and go into the atmosphere. The permeation process of tritium at the temperature of 400−700°C was simulated using hydrogen and deuterium with the method of gas-driven permeation. The experimental results of the permeation are similar in Hastelloy-N and GH3535 (Pi et al., 2015). Furthermore, the solubility and diffusivity of tritium in molten salts was evaluated in a two-chamber permeability apparatus separated by a nickel plate (Zeng et al., 2014). In addition to the experiments, the displacement per atom (DPA) rates for the MSRE core can and vessel were calculated and analyzed by the MCNP5, providing guidance for the MSR design and parameter selection (Liu et al., 2013a,b).

14.3.5 Lead-cooled fast reactor research and development

There is no special project on LFR research in China, which is only a constituent part of the CAS Accelerator-Driven Subcritical system project. CAS launched this

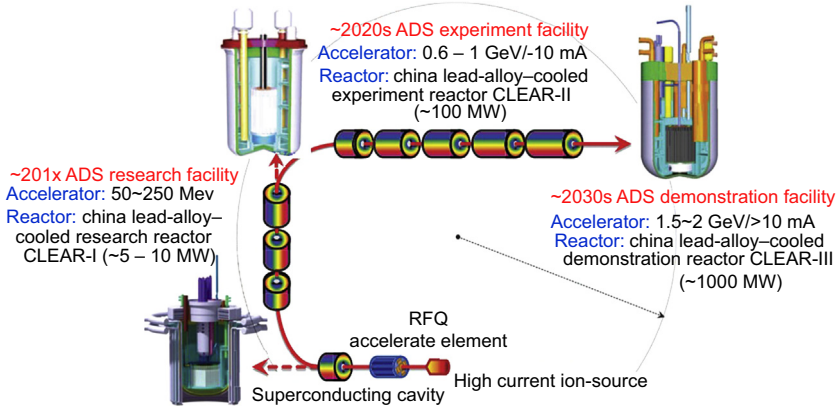


Figure 14.20 China LEad-Alloy−cooled Reactor (CLEAR) series reactor development plan in the Accelerator-Driven Subcritical system project. *RFQ*, radio frequency quadrupole.

Accelerator-Driven Subcritical system project in 2011 as another pilot project parallel with the TMSR project and planned to construct the demonstration Accelerator-Driven Subcritical transmutation system until the 2030s. The China LEad-Alloy−cooled Reactor (CLEAR) is proposed as the reference reactor in the Accelerator-Driven Subcritical system. CAS plans to develop the lead-based reactors through three phases (Wu et al., 2014): (1) a 10-MW_{th} lead-bismuth eutectic (LBE)-cooled research reactor (CLEAR-I) to be built in the 2010s, (2) a 100-MW_{th} lead-alloy−cooled experimental reactor (CLEAR-II) to be built in the 2020s, and (3) a 1000-MW_{th} lead-alloy−cooled demonstration reactor (CLEAR-III) to be built in the 2030s. As a pretesting facility, a lead-alloy−cooled zero-power reactor (CLEAR-0) is required to obtain the neutronics data for the CLEAR series reactor. However, lead-alloy material as a coolant for a reactor has some challenges that are required to be considered in the fields of neutronics, thermal hydraulics, material compatibility, physical chemistry, safety characteristics, etc. To achieve these goals, several heavy liquid metal experimental facilities have been built to investigate the critical characteristics and key technologies of lead-alloy−cooled reactors, such as material issues, thermo-hydraulics, etc. Fig. 14.20 shows the CLEAR series reactor development plan map of China along with the Accelerator-Driven Subcritical system project.

14.3.5.1 China LEad-Alloy−cooled Reactor-0

To validate the nuclear design codes and databases used in the CLEAR design, to develop the nuclear measuring methods and instruments, and to support CLEAR licensing application, it is necessary to perform the zero-power neutronics experiments. Therefore CLEAR-0, a zero-power fast spectrum experimental facility, was firstly designed to meet this requirement. The conceptual design of CLEAR-0 was finished in 2013, and the facility was planned to be built in 2015. Under its conceptual design, the facility main structure sits in the reactor pit, above which there is a removable biological shield. The cores designed in CLEAR-0 comprise a lattice of standard

SAs. By changing the simulation materials loaded in standard SAs, CLEAR-0 can simulate various cores. Meanwhile, two reactor trip systems based on a different mechanism are designed to ensure CLEAR-0 safety. CLEAR-0 has two operation modes: one is the critical mode for fast reactor validation and the other one is the subcritical operation mode driven by the accelerator neutron source for ADS validation.

14.3.5.2 China LEad-Alloy–cooled Reactor-I

CLEAR-I was designed to validate the lead-alloy–cooled research reactor and Accelerator-Driven Subcritical system coupling operation technology. Fig. 14.21 presents the overall view structure design of the CLEAR-I reactor. There are six design principles in CLEAR-I: (1) mature fuel and material technology, (2) passive heat removal system and inherent safety design, (3) pool-type reactor vessel for continuous technology, (4) remote-handling refueling system for flexible experimentation, (5) critical/subcritical dual-mode operation capability, and (6) advanced fuel test capability. CLEAR-I will be operated in critical/subcritical modes. The subcritical operation mode reactor is named CLEAR-IA and is driven by a spallation neutron source created by the proton accelerator. The critical operation mode reactor is named CLEAR-IB. The objective of CLEAR-IA research is to test the ADS integration technology. The CLEAR-IA can be changed to CLEAR-IB by replacing the target of the spallation neutron source to some FAs. The objective of CLEAR-IB research is to validate the thermo-hydraulics, neutronics, and safety characteristics of a lead-alloy–cooled fast reactor and to test the fuel and material technologies. Table 14.1 lists the main design

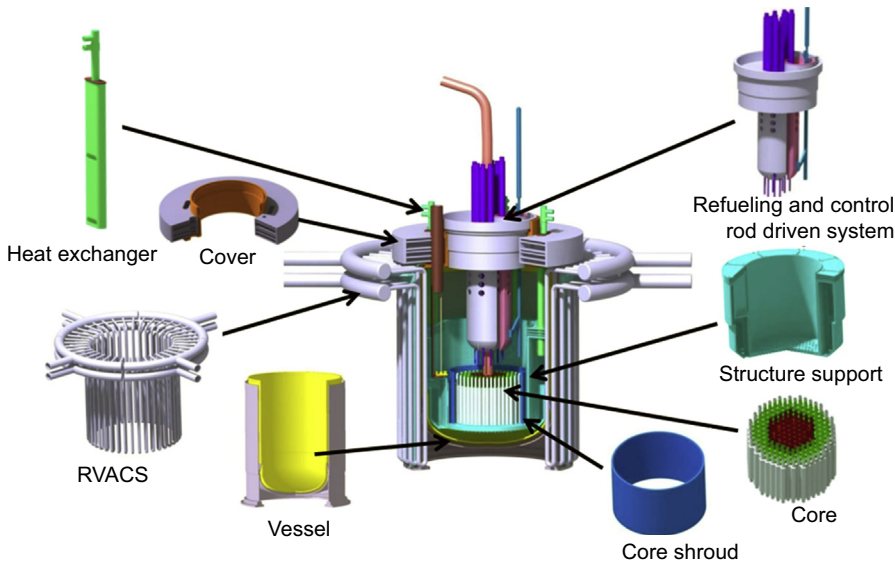


Figure 14.21 Overall view structure design for the China LEad-Alloy–cooled Reactor-I. *RVACS*, reactor vessel air cooling system.

parameters of CLEAR-I. In addition to dual-mode operation, CLEAR-I has another unique characteristic, inherent safety, which is realized primarily in two ways:

1. *Negative reactivity feedback*: The negative reactivity coefficient of fuel temperature and negative coolant reactivity feedback are achieved through proper neutronics design and passive safety system design.
2. *Two independent water-cooled secondary cooling systems are designed*: Air is used as the final heat sink by water/air heat exchangers. CLEAR-I incorporates a reactor vessel air cooling system to remove the decay heat in case the normal heat removal path is unavailable.

In the reference parametric design of CLEAR-I, the pool-type configuration is selected. The thermal power is 10 MW and no electric power is generated. LBE is chosen as the primary coolant and UO_2 with 9.75% ^{235}U enrichment is adopted as the first loading fuel. Hexagonal-wrapped FAs are used in the hexagonal lattice core, in which the cladding material is 15-15Ti steel whereas the structure material is SS316L. To satisfy the experiment flexibility requirements, the primary cooling system is driven by a mechanical pump. Large-diameter pins are designed to achieve a higher fuel volume fraction but lower core pressure drop. Table 14.5 lists the main design parameters for the CLEAR-I reactor.

Table 14.5 Main design parameters for the China LEad-Alloy–cooled Reactor-I

Parameter	Unit	Value
Thermal power	MW	10
Primary coolant	–	Lead-bismuth eutectic
Fission fuel	–	UO_2 (19.75% enrichment)
Driven force	–	Natural circulation
Subcritical mode k_{eff}	–	0.98
Primary coolant inventory	t	~700
Reactor core inlet/outlet temperature	°C	260/390
Circulation height	m	2
Secondary coolant	–	Water
Secondary coolant pressure	MPa	4
Secondary coolant temperature	°C	215/230
Primary heat exchanger	–	4 (two independent loops)
Main vessel height	–	6300
Main vessel diameter	mm	4650

14.3.5.3 China LEad-Alloy–cooled Reactor-II

For the second stage of the Chinese Accelerator-Driven Subcritical system program, an experimental facility will be built to test the platform for the Accelerator-Driven Subcritical system integration and materials experiment. It is also used as a high neutron flux test reactor for demonstration of Accelerator-Driven Subcritical system and fusion reactor materials. Therefore a 100-MW_{th} lead-cooled or LBE-cooled experimental reactor named CLEAR-II will be built coupled with a proton accelerator of approximately 600–1000 MeV/10 mA and a spallation target. On the basis of CLEAR-II success, the high-power Accelerator-Driven Subcritical system design, construction, and operation technology may be preliminarily obtained. To increase the reactor neutron flux and power density, the nuclear fuel will use high-enriched MOX fuel; FAs can partially be replaced by MA SAs to test the nuclear waste transmutation mechanism. CLEAR-II also can be used as a high neutron flux reactor to perform material irradiation experimental study.

14.3.5.4 China LEad-Alloy–cooled Reactor-III

In the third stage of the Chinese Accelerator-Driven Subcritical program, CLEAR-III is a lead-alloy–cooled demonstration reactor that aims to demonstrate the technology of nuclear waste transmutation capability of the commercial Accelerator-Driven Subcritical system. For the CLEAR-III reference scenario, an accelerator-driven lead-alloy–cooled subcritical reactor for transmutation of long-lived high-level nuclear wastes is developed based on the neutronics, thermo-hydraulics, materials, and mechanics analysis. The lead and LBE are still considered as the potential coolant for CLEAR-III to investigate the highly efficient power generation and waste transmutation. A linear accelerator produces the proton beam of 1.5 GeV/10 mA and the proton impinges on the windowless LBE target in the CLEAR-III central region. The CLEAR-III system is rated at 1000 MW of thermal power. Currently, one fuel type considered for CLEAR-III is the transuranic element (TRU)-Zr dispersion fuel, in which TRU-Zr particles are dispersed in a Zr matrix. The advanced ferritic/martensitic steel is selected as the fuel cladding and other structure materials because of its good performance under the highly corrosive and radioactive environment.

Nomenclature

Abbreviations and acronyms

863 Program	National High Technology Research and Development Program of China
973 Program	National Key Basic Research Program of China
ACC	Accumulators
BCC	Body center cubic

Continued

CAS	Chinese Academy of Sciences
CCFR-B	China commercial breeding fast reactor
CCFR-T	China commercial transmutation fast reactor
CDFR	China demonstration fast reactor
CHNG	China HuaNeng Group
CIAE	Chinese Institute of Atomic Energy
CLEAR	China LEad-Alloy−cooled Reactor
CLEAR-I	10-MW_{th} lead-bismuth cooled research reactor
CLEAR-II	100-MW_{th} lead-alloy−cooled experimental reactor
CLEAR-III	1000-MW_{th} lead-alloy−cooled demonstration reactor
CLEAR-0	A zero-power fast spectrum experimental facility
CNEC	China Nuclear Engineering and Construction
CSR1000	1000-MW_{el} Chinese SCWR
DBA	Design basis accident
DPA	Displacement per atom
FA	Fuel assembly
FCC	Face center cubic
FCD	First concrete date
FHR	Fluoride-salt-cooled high-temperature reactor
FREDO-CSR1000	FREquency DOmain analysis of CSR1000
FSAC	FHR safety analysis code
GDCS	Gravity driven cooling systems
HDPV	Hot gas duct pressure vessel
HTR	High-temperature reactor
HTR-10	10-MW_{th} prototype pebble-bed high temperature reactor of China
ICS	Isolation cooling systems
INET	Institute of Nuclear Energy Technology
LBE	Lead-bismuth eutectic
LOCA	Loss of coolant accident
LOOP	Loss of offsite power
MA	Minor actinides
MAC	Multiple-channel analysis code
MCNP	Monte Carlo code for neutron and photon transport

MLD	Master logic diagram
MOSART	MOlten Salt Actinide Recycler and Transmuter
MSRE	Molten Salt Reactor Experiment
NPIC	Nuclear Power Institute of China
NSFC	Natural Science Foundation of China
ORNL	Oak Ridge National Laboratory
OTTO	Once-through-then-out
PB-FHR	Pebble-bed FHR
PRHR	Passive residual heat removal
PyC	Pyrolytic carbon
RVACS	Reactor vessel air cooling system
SA	Subassembly
SBO-ATWS	Station blackout anticipated transient without scram
SCWR-M	Mixed spectrum SCWR
SG	Steam generator
SGPV	Steam generator pressure vessel
SINAP	Shanghai Institute of Applied Physics
SJTU	Shanghai Jiaotong University
SLCS	Standby liquid control system
TIMDO-CSR1000	TIMe DOmain analysis of CSR1000
TMSR	Thorium molten salt reactor
TMSR-LF	Liquid-fueled TMSR
TMSR-SF	Solid-fuel TMSR
TRU	Transuranic element
UCB	University of California−Berkeley
ULOF	Unprotected loss of flow
ULOHS	Unprotected loss of heat sink
UOC	Unprotected overcooling accident
UTOP	Unprotected transient overpower
VHTR	Very-high temperature gas-cooled reactor
WNA	World Nuclear Association
XJTU	Xi'an Jiaotong University

References

Cai, B., Wang, J., Sun, L., Zhang, N., Yan, C., 2014. Experimental study and numerical optimization on a vane-type separator for bubble separation in TMSR. Progress in Nuclear Energy 74, 1−13.

Cai, J., 2013. The Preliminary Analysis on Reactivity Initiated Transient of Molten Salt Reactor. Shanghai Institute of Applied Physics, CAS. The University of Chinese Academy of Sciences.

Cheng, J., Zhang, P., An, X., Wang, K., Zuo, Y., Yan, H., Li, H., 2013. A device for measuring the density and liquidus temperature of molten fluorides for heat transfer and storage. Chinese Physics Letters 30, 126501.

Cheng, M., Dai, Z., 2014. Turbulent transport effect of delayed neutron precursor in molten salt fast reactor. Atomic Energy Science and Technology 48.

Cheng, X., Liu, X.J., Yang, Y.H., 2008. A mixed core for supercritical water-cooled reactors. Nuclear Engineering and Technology 40 (2), 117−126.

Dang, G., Huang, D., Lu, J., et al., 2013. Large-break accident analysis of supercritical water-cooled reactor CSR1000 using APROS code. Nuclear Power Engineering 1, 72−82.

Du, D., Xiao, Z., Yan, X., et al., 2013. Subchannel analysis of SCWR CSR1000 assembly. Nuclear Power Engineering 1, 40−44.

Feng, S., 2014. Studies on Irradiation Damage and Molten Salt Penetration in Pyrolytic Carbon Coating on Nuclear Graphite. Shanghai Institute of Applied Physics. The University of Chinese Academy of Sciences.

Forsberg, C., Hu, L., Richard, J., Romatoski, R., Forget, B., Stempien, J., Ballinger, R., Sun, K., 2014. Fluoride-Salt-Cooled High-Temperature Test Reactor (FHTR): Goals, Options, Ownership, Requirements, Design, Licensing, and Support Facilities. Massachusetts Institute of Technology.

Guo, Z., Wang, C., Zhang, D., Chaudri, K.S., Tian, W., Su, G., Qiu, S., 2013a. The effects of core zoning on optimization of design analysis of molten salt reactor. Nuclear Engineering and Design 265, 967−977.

Guo, Z., Zhang, D., Xiao, Y., Tian, W., Su, G., Qiu, S., 2013b. Simulations of unprotected loss of heat sink and combination of events accidents for a molten salt reactor. Annals of Nuclear Energy 53, 309−319.

Guo, Z., Zhou, J., Zhang, D., Chaudri, K.S., Tian, W., Su, G.H., Qiu, S., 2013c. Coupled neutronics/thermal-hydraulics for analysis of molten salt reactor. Nuclear Engineering and Design 258, 144−156.

Han, L., Chen, Y., Zhou, D., 2013. Design of the distributed control system for HTS molten salt test loop. Nuclear Techniques 36.

Hinds, D., Maslak, C., 2006. Next-generation nuclear energy: the ESBWR. Nuclear News 49, 35−40.

Huang, H., Li, J., Liu, R., Chen, H., Yan, L., 2014. Temperature effect of Xe ion irradiation to 316 austenitic stainless steel. Acta Metallurgica Sinica 50, 1189−1194.

Jiao, X., Wang, K., He, Z., Chen, K., 2015. Core safety discussion under station blackout ATWS accident of solid fuel molten salt reactor. Nuclear Techniques 38.

Li, L., Yu, G., Zhou, X., 2014. Corrosion behavior of Ti_3SiC_2 and Ti_3AlC_2 with LiF-NaF-KF molten salt. Nuclear Techniques 37.

Liu, K., Xu, L., Liu, Z., 2015. Impact of temperature on the molten salt corrosion of Hastelloy-N alloys. Nuclear Techniques 38.

Li, X., Li, Q., Xia, B., et al., 2013. Overview on overall design of CSR1000. Nuclear Power Engineering 1, 5−8.

Liu, X.J., Cheng, X., 2010. Coupled thermal-hydraulics and neutron-physics analysis of SCWR with mixed spectrum core. Progress in Nuclear Energy 52 (7), 640−647.

Liu, X.J., Fu, S.W., Xu, Z.H., Yang, Y.H., Cheng, X., 2013a. LOCA analysis of SCWR-M with passive safety system. Nuclear Engineering and Design 259, 187−197.

Liu, Y., Mei, L., Cai, X., 2013b. Physics research for molten salt reactor with different core boundaries. Nuclear Techniques 36, 030601−030605.

Mei, M., Shao, S., Zuo, J., Yu, Z., Chen, K., 2013. Probability safety assessment of LOOP accident to molten salt reactor. Nuclear Techniques 36, 120604.

Mei, M., Shiwei, S., He, Z., Chen, K., 2014. Research on initial event analysis for solid thorium molten salt reactor probabilistic safety assessment. Nuclear Techniques 37.

Peng, C., Yan, X., Peng, J., Zeng, X., Huang, Y., Xiao, Z., 2013. CATHARE simulation on coupled neutronics/thermal-hydraulics of molten salt reactor (MSR). Nuclear Power Engineering 34.

Pi, L., Liu, W., Zhang, D., Qian, Y., Wang, G.H., Zeng, Y.S., 2015. Estimation of permeability of tritium in structural materials of molten salt reactor based on hydrogen isotope. Nuclear Techniques 38.

Qian, L., Qiu, S., Zhang, D., Su, G.H., Tian, W., 2010. Numerical research on natural convection in molten salt reactor with non-uniformly distributed volumetric heat generation. Nuclear Engineering and Design 4.

Rouault, J., Chellapandi, P., Raj, B., et al., 2010. Sodium Fast Reactor Design: Fuels, Neutronics, Thermal-Hydraulics, Structural Mechanics and Safety. In: Handbook of Nuclear Engineering. Springer, US, pp. 2321−2710.

Schulz, T.L., 2006. Westinghouse AP1000 advanced passive plant. Nuclear Engineering and Design 236, 1547−1557.

Serp, J., Allibert, M., Beneš, O., Delpech, S., Feynberg, O., Ghetta, V., Heuer, D., Holcomb, D., Ignatiev, V., Kloosterman, J.L., 2014. The molten salt reactor (MSR) in generation IV: overview and perspectives. Progress in Nuclear Energy 77, 308−319.

Song, S., Cai, X., Liu, Y., Wei, Q., Guo, W., 2014. Pore scale thermal hydraulics investigations of molten salt cooled pebble bed high temperature reactor with BCC and configurations. Science and Technology of Nuclear Installations 2014.

Steinwarz, W., Xu, Y.H., 1990. Status of design of the HTR test module China. Nuclear Engineering and Design 121, 317−324.

Sun, L., Yan, C., Fa, D., Wang, N., 2014. Conceptual design and analysis of a passive residual heat removal system for a 10 MW molten salt reactor experiment. Progress in Nuclear Energy 70, 149−158.

Sun, Y.L., Xu, Y.H., 2000. Licensing of the HTR-10 test reactor. In: Workshop on 'Safety and Licensing Aspects of Modular High Temperature Gas Reactors' Aix-en-Provence, France.

Tian, W., Tian, X., Feng, J., et al., 2013. Flow instability analysis of supercritical water-cooled reactor CSR1000 based on frequency domain. Nuclear Power Engineering 1, 45−51.

Tian, X., Tian, W., Zhu, D., Qiu, S., Su, G., Xia, B., 2012. Flow instability analysis of supercritical water-cooled reactor CSR1000 based on frequency domain. Annals of Nuclear Energy 49, 70−80.

Wang, C., Guo, Z., Zhang, D., Qiu, S., Tian, W., 2013a. Transient behavior of the sodium−potassium alloy heat pipe in passive residual heat removal system of molten salt reactor. Progress in Nuclear Energy 68, 142−152.

Wang, C., Xiao, Y., Zhou, J., Zhang, D., Qiu, S., Su, G., Cai, X., Wang, N., Guo, W., 2014a. Computational fluid dynamics analysis of a fluoride salt−cooled pebble-bed test reactor. Nuclear Science and Engineering 178, 86−102.

Wang, Y., Huang, S., Tang, Z., Xie, L., Yin, H., Zhao, S., 2014b. Corrosion behavior of ceramics immersed in LiF-NaF-KF molten salt. New Chemical Materials 42, 111−117.

Wang, C., Zhang, D., Qiu, S., Tian, W., Wu, Y., Su, G.h., 2013b. Study on the characteristics of the sodium heat pipe in passive residual heat removal system of molten salt reactor. Nuclear Engineering and Design 265, 691−700.

Wang, G., Li, W., Li, N., Han, S., 2015. Thermal-hydraulic simulation for pebble-bed fluoride salt-cooled high temperature reactor core. Atomic Energy Science and Technology 49.

Wang, H., Cai, X., 2013. Impact on breeding rate of different molten salt reactor core structures. Nuclear Techniques 36, 090601.

Wang, Y., 2013. Corrosion Behavior of Novel Ceramics Immersion in FLiNaK Molten Salt. Xiangtan University.

Wei, Q., Mei, L., Zhai, Z., Wei, G., Chen, J., Cai, X., 2014. Preliminary study on safety characteristics of molten salt reactor. Atomic Energy Science and Technology 48.

WNA, 2005. http://www.world-nuclear.org/.

Wu, Y., Bai, Y., Song, Y., et al., 2014. Design and R&D progress of China lead-based reactor. In: Proceedings of the 2014 22nd International Conference on Nuclear Engineering, July 7−11, 2014, Prague, Czech Republic. Paper No. 31136.

Xia, B., Yang, P., Wang, L., et al., 2013. Core preliminary conceptual design of supercritical water-cooled reactor CSR1000. Nuclear Power Engineering 1, 9−14.

Xiao, Y., Hu, L., Qiu, S., Zhang, D., Su, G., Tian, W., 2014. Development of a thermal-hydraulic analysis code and transient analysis for a FHTR. In: 2014 22nd International Conference on Nuclear Engineering. American Society of Mechanical Engineers pp. V005T016A005.

Xu, M., 2009. Fast reactor and sustainable nuclear energy development in China. China Nuclear Power 2, 106−110.

Xu, M., 2008. The status and prospects of fast reactor technology development in China. China Engineering Science 1, 70−76.

Xu, M., 1995. China experimental fast reactor. High Technology Letters 09, 53−59.

Xu, Y.H., Liu, J.G., Yao, M.S., Zhou, H.Z., Ju, H.M., 1997. High temperature engineering research facilities and experiments in China. In: NEA Workshop on High Temperature Engineering Research Facilities and Experiments. Petten, The Netherlands.

Xu, Y.H., Zuo, K.F., 2002. Overview of the 10 MW high temperature gas cooled reactor − test module project. Nuclear Engineering and Design 218, 13−23.

Xu, Z.H., Hou, D., Fu, S.W., Yang, Y.H., Cheng, X., 2011. Loss of flow accident and its mitigation measures for nuclear systems with SCWR-M. Annals of Nuclear Energy 38 (12), 2634−2644.

Yang, H., Zhou, P., Yu, H., et al., 2007. Preliminary consideration of overall technical scheme for China demonstration fast reactor. Annual Report of China Institute of Atomic Energy 3−5.

Yang, T., Liu, X.J., Cheng, X., 2012. Optimization of multilayer fuel assemblies for supercritical water-cooled reactors with mixed neutron spectrum. Nuclear Engineering and Design 249, 159−165.

Yin, W., 2014. Production of Radionuclide and Safety Analysis of TRISO Coated Fuel Particles. Shanghai Institute of Applied Physics Chinese Academy of Sciences.

Zeng, Y., Wu, S., Qian, Y., Wang, G., Du, L., Liu, W., 2014. Apparatus for determining permeability of hydrogen isotopes in molten-salt. Nuclear Science and Techniques 4, 040602.

Zhang, D., Qiu, S., Liu, C., Su, G.H., 2008. Steady thermal hydraulic analysis for a molten salt reactor. Nuclear Science and Techniques 19, 187−192.

Zhang, D., Qiu, S., Su, G.H., 2009a. Development of a safety analysis code for molten salt reactors. Nuclear Engineering and Design 239, 2778−2785.

Zhang, D., Rineiski, A., Qiu, S., 2009b. Comparison of modeling options for delayed neutron precursor movement in a molten salt reactor. Transactions of the American Nuclear Society 100, 639−640.

Zhang, D., Rineiski, A., Wang, C., Guo, Z., Xiao, Y., Qiu, S., 2015. Development of a kinetic model for safety studies of liquid-fuel reactors. Progress in Nuclear Energy 81, 104−112.

Zhang, D., Zhai, Z., Rineiski, A., Guo, Z., Wang, C., Xiao, Y., Qiu, S., 2014a. COUPLE, a time-dependent coupled neutronics and thermal-hydraulics code, and its application to MSFR. In: 2014 22nd International Conference on Nuclear Engineering. American Society of Mechanical Engineers pp. V003T005A019.

Zhang, Z., Xia, X., Zhu, X., Cai, J., 2014b. Source terms calculation for the MSRE with on-line removing radioactive gases. Nuclear Techniques 37.

Zhang, H., Luo, Y., Li, X., et al., 2013. Research on overall structure design of CSR1000. Nuclear Power Engineering 1, 52−56.

Zhang, Z.Y., Yu, S.Y., 2002. Future HTGR developments in China after the criticality of the HTR-10. Nuclear Engineering and Design 218, 249−257.

Zhao, H., Yan, C., Sun, L., Zhao, K., Fa, D., 2015. Design of a natural draft air-cooled condenser and its heat transfer characteristics in the passive residual heat removal system for 10 MW molten salt reactor experiment. Applied Thermal Engineering 76, 423−434.

Zhao, R.K., Yuan, K.Q., Shu, T.W., 2001. Project Progress in the Energy Field. Atomic Energy Press, pp. 121−206 (in Chinese).

Zhong, D.X., Gao, Z.Y., 1985. Study on Modular High Temperature Gas-Cooled Reactor and Its Application for Heavy Oil Recovery 1985.11 INET Report (in Chinese).

Zhou, J., Zhang, D., Qiu, S., 2014. Three-dimensional code development for steady state analysis of liquid-fuel molten salt reactor. Atomic Energy Science and Technology 48.

Zhou, X., 2013. A Study on Measurement of Neutron Energy Spectrum for Thorium Molten Salt Reactor. Shanghai Institute of Applied Physics. The University of Chinese Academy of Sciences.

Zhou, X., Liu, G., 2013. Study of control rod worth in the TMSR. Nuclear Science and Techniques 1, 010.

Zhu, D.H., Zhao, H., Tian, W.X., Su, Y.L., Chaudri, K.S., Su, G.H., Qiu, S.Z., 2012. Development of TACOS code for loss of flow accident analysis of SCWR with mixed spectrum core. Progress in Nuclear Energy 54 (1), 150−161.

Zhuang, K., Cao, L., Zheng, Y., Wu, H., 2014. Studies on the molten salt reactor: code development and neutronics analysis of MSRE-type design. Journal of Nuclear Science and Technology 1−13.

Zou, X., Dai, Z., Tang, Z., 2013. Numerical simulation of induction heating in FLiNaK molten salt high temperature testing loop. Nuclear Techniques 36.

Generation IV concepts: India

15

R.K. Sinha[1], P. Chellapandi[2], G. Srinivasan[3], I. Dulera[4], P.K. Vijayan[4], S.K. Chande[5]
[1]Department of Atomic Energy, India; [2]BHAVINI, Kalpakkam, India; [3]IGCAR, Kalpakkam, India; [4]BARC, Mumbai, India; [5]Atomic Energy Regulatory Board, Mumbai, India

15.1 Introduction

India is planning to enhance its electrical power generation capacity to 80,0000 MW_e by 2031−32 so as to significantly increase its per capita electrical consumption with a goal to reach the world average (~2700 kWh). To achieve this target, nuclear energy would have to make a significant contribution by increasing its share by approximately 15-fold. As per the government data published before the Fukushima accident (Integrated Energy Policy, 2006), the nuclear share is expected to be increased between 48,000 and 63,000 MW_e by 2032 from the current level of approximately 5800 MW_e from 21 water-cooled reactors. Five water-cooled reactors with a total capacity of 3800 MW_e and a 500-MW_e prototype fast breeder reactor (PFBR) are currently at various stages of construction and commissioning. The balance increase in capacity would be achieved by imported light water reactors under the International Atomic Energy Agency safeguard, future fast breeder reactors (FBRs), and domestic water-cooled reactors. India follows the Three-Stage Nuclear Power Program formulated by Dr. Homi Jahangir Bhabha, the designer and architect cum founder of the Indian nuclear power program, to achieve energy security with the modest indigenous natural uranium and vast thorium resources available in the country. This program has water-cooled reactors in the first stage, fast reactors in the second stage, and thorium-fueled reactors in the third stage. The first stage, with 18 pressurized heavy water reactors (PHWRs) in operation and many under construction and in the planning stages, has reached a state of commercial maturity. The second stage starts with the commissioning of PFBR by this year. Late in the second stage the program would have thorium as the fertile material along with plutonium so as to produce ^{233}U for the third stage. India has one of the largest reserves of thorium in the world. The Atomic Minerals Directorate for Exploration and Research, a constituent unit of the Indian Department of Atomic Energy (DAE), has thus far established 11.93 million tons of monazite (thorium-bearing mineral) in India, which contains approximately 1.07 million tons of thorium oxide. In view of this, the third stage of the Indian nuclear power program is based on extensive use of ^{233}U-fueled reactors with thorium as the fertile material. The reactors for the third stage are proposed to be breeder reactors and operating entirely on a ^{233}U-Th fuel cycle. The molten salt breeder reactor (MSBR) is being considered as an attractive option for large-scale deployment during the third stage, in addition to

Handbook of Generation IV Nuclear Reactors. http://dx.doi.org/10.1016/B978-0-08-100149-3.00015-X
Copyright © 2016 Elsevier Ltd. All rights reserved.

sodium fast reactors (SFRs). India has a very ambitious long-term plan of deployment of many FBRs and thorium-based reactors to achieve energy security. In addition, high-temperature reactors (HTRs) are being developed to produce hydrogen as an alternative to oil-based transport fuel. Thus India has several thermal and fast spectrum reactors on the long-term horizon. The reactors currently under design at two reactor research centers [the Bhabha Atomic Research Center (BARC) and Indira Gandhi Center for Atomic Research (IGCAR) in DAE] have design goals similar to those of Generation IV (Gen-IV) concepts. These include enhanced safety, economic attractiveness, and sustainability.

In this chapter the reactor concepts that are presented include three thermal spectrum reactors [ie, the advanced heavy water reactor (AHWR), the compact high-temperature reactor (CHTR), and the innovative high-temperature reactor (IHTR)] and two fast spectrum reactors [ie, SFRs and the Indian molten salt breeder reactor (IMSBR)]. AHWR, CHTR, IHTR, and IMSBR are being designed at BARC, and SFR is designed at IGCAR. The salient conceptual design and safety features and an overview of the current status and research and development (R&D) activities in progress/planned for these reactors are highlighted.

15.2 Advanced heavy water reactors

The AHWR is designed and developed to achieve large-scale use of thorium for the generation of commercial nuclear power. This reactor will produce most of its power from thorium, with no external input of ^{233}U in the equilibrium cycle. The reactor incorporates several passive safety features and is associated with a closed fuel cycle having reduced environmental impact. At the same time, the reactor possesses several features that are likely to reduce its capital and operating costs. Many of these features that are part of the basic goals to be achieved by Gen-IV reactors also make AHWR a demonstration reactor for Gen-IV features on the near-term time horizon. Inherent and passive safety features are used extensively to achieve enhanced safety. A prototype AHWR is being developed currently at BARC. It is a 300-MW_e, vertical, pressure-tube−type, natural-circulation−based, boiling light water-cooled, and heavy water-moderated reactor (AHWR-300). AHWR-300 is a land-based nuclear power station. The reactor is designed to produce 920 MW of thermal power, generating 300 MW(e) (gross) and 2400 m^3/day of desalinated water. The plant can be configured to deliver higher desalination capacities with some reduction in electricity generation. An AHWR-based plant can be operated in base load and in load-following mode. It is expected that this reactor will achieve commercial operation by 2027.

15.2.1 Design features of AHWR-300

The schematic of an AHWR and major systems are shown in Fig. 15.1. The reactor fuel cluster is shown in Fig. 15.2. AHWR has average burn-up of 38,000 MWd/t.

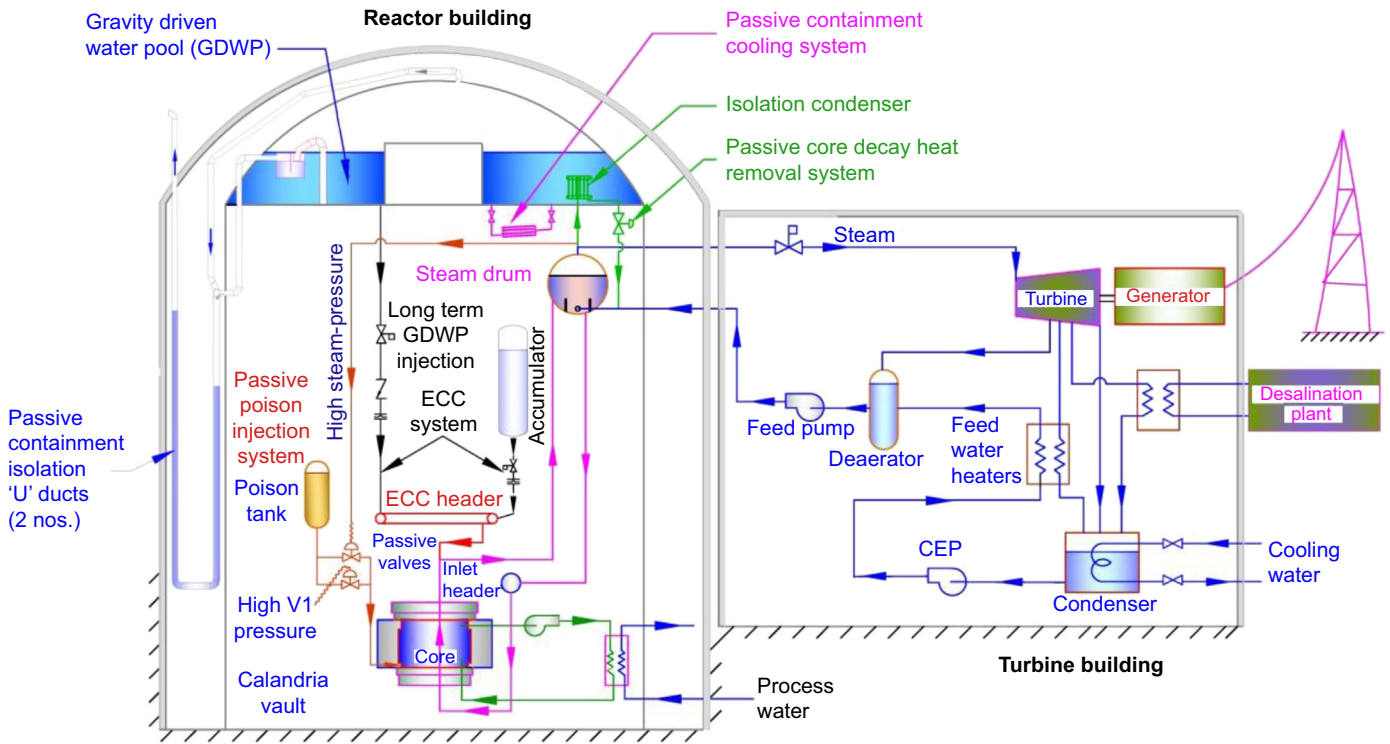


Figure 15.1 Schematic of advanced heavy water reactor and major systems.

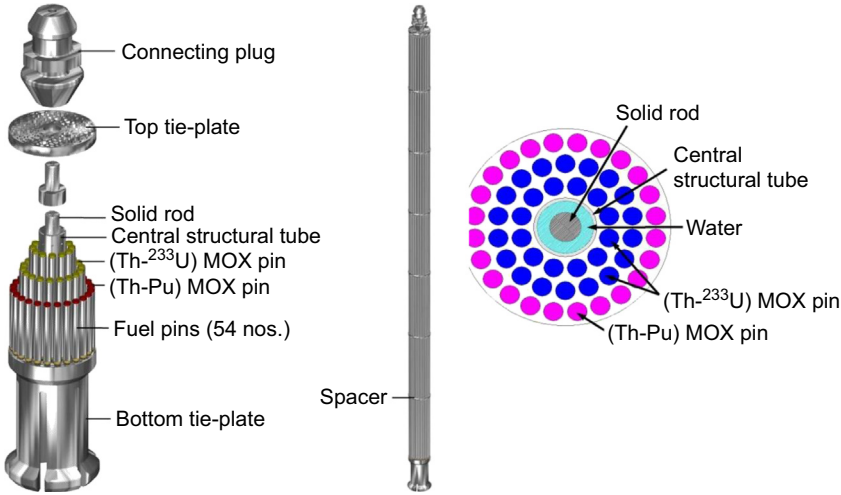


Figure 15.2 Advanced heavy water reactor fuel cluster. *mOX*, Mixed oxide.

The flexibility to adopt different fuel cycles to enhance the utilization of fuel resources: AHWR can be used for diverse fuel cycle options including once-through and closed fuel cycles. AHWRs are also optimized to achieve high burn-up with low-enriched uranium (LEU)-thorium based fuel in AHWR300-LEU. The design provides for inherent safety characteristics through achievement of the required reactivity coefficients. In the closed fuel cycle conceived, thorium, ^{233}U, and plutonium will be recovered from the spent fuel. The recovered thorium and ^{233}U will be recycled back as Th-^{233}U mixed oxide (MOX) fuel, and reprocessed plutonium will be stored and will later be used as fuel for an FBR. The plutonium requirement for the reactor will be met by reprocessing of the spent fuel of PHWRs. A schematic of the fuel cycle for an AHWR is given in Fig. 15.3. The fuel cycle facilities

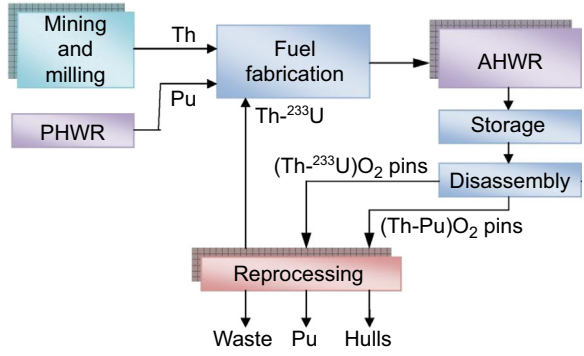


Figure 15.3 A schematic of the fuel cycle for an advanced heavy water reactor (AHWR). *PHWR*, pressurized heavy water reactor.

Table 15.1 Advanced heavy water reactors: proposed design and operating parameters

Attributes	Design parameters
Reactor power	920 MW_{th} (300 MW_e)
Fuel cluster	30 pins of (Th-Pu)O_2, 24 pins of (Th-^{233}U)O_2
Fuel discharge burn-up	40 GWd/Te (average, reference case)
Design life	100 years
Moderator	Heavy water
Coolant	Boiling light water
Core orientation	Vertical
Number of channels	452
Lattice pitch (square)	225 mm
Total core flow	2143 kg/s
Nominal operating pressure	7.0 MPa
Average core exit quality	19.1%
Total steam flow going out	408 kg/s
Feed-water temperature	403.0 K (130°C)
Coolant inlet temperature	531.4 K (258.25°C)

(fabrication and reprocessing) for AHWR will be colocated with the reactor at the same site. The design life is 100 years. The major design parameters of AHWRs are shown in Table 15.1.

15.2.2 Enhanced safety features

The emphasis in design has been to incorporate inherent and passive safety features to the maximum extent as a part of the defense-in-depth strategy. AHWR design provides a grace period of 7 days for the absence of any operator or powered actions in the event of an accident. The main objective has been to establish a case for elimination of the need for planning for evacuation in the case of an accident scenario in the plant. This is achieved through various passive and active safety systems designed to mitigate the consequences of design-basis accidents (DBAs) and features to avoid escalation of a DBA to a severe accident. An increased reliability of the control system is achieved with the use of high-reliability digital control using advanced information technology, and increased operator reliability is achieved with the use of advanced displays and diagnostics using artificial intelligence and expert systems. The main features in these categories are listed in the following subsections.

15.2.2.1 Inherent safety features

- Negative void coefficient of reactivity, low core power density, negative fuel temperature coefficient of reactivity, and low excess reactivity
- Natural-circulation–driven heat removal during normal operation and hot shutdown
- Double containment system, use of moderator as a heat sink, presence of water in the calandria vault, and large main heat transport inventory
- Four independent emergency core cooling system (ECCS) trains
- Direct injection of ECCS water into the fuel cluster
- Flooding of reactor cavity after a loss of coolant accident (LOCA)

15.2.2.2 Passive safety systems

- Passive injection of high-pressure and low-pressure emergency core coolant through the use of one-way rupture disks and nonreturn valves
- Shut-down cooling through isolation condensers in gravity-driven water pool by opening passive valve
- Passive containment isolation, after a large-break LOCA, with a water seal
- Passive shutdown by injection of poison in the moderator by use of system steam pressure in the case of failure of wired systems of shut-down system (SDS)-1 and SDS-2
- Passive containment cooling system
- Passive automatic depressurization system
- Core submergence after LOCA

15.2.2.3 Features to deal with severe accidents and Fukushima types of scenarios

- Core catcher with bottom flooding.
- Passive autocatalytic recombiners.
- Filtered hard vent system.
- Hook-up system for critical systems.
- Passive moderator and end-shield cooling systems.
- Passive union between V1 and V2 volume.
- AHWR design is found to be robust for long station blackout (LSBO) as well as LSBO with partial loss of heat sink based on analysis of postulating several scenarios relevant to the Fukushima event.

15.2.3 Safety goals

For AHWRs the goal for the frequency of severe core damage can be set at least 1 order of magnitude lower compared with the goal for new reactors of the present generation. Because the reactor uses passive heat removal systems, this goal appears to be reasonable and achievable. A peak cladding temperature value greater than or equal to 1200°C is considered to lead to core damage in a Level 1 PSA study that is performed for AHWRs. Likewise, a value of 10^{-7} per reactor per year (RY) can be set as a goal for large early release frequency. The point value for the core damage frequency (CDF) is predicted by BARC to be less than 10^{-7} per RY. This value is approximately 2 orders of magnitude lower than the value specified for the current-generation reactors.

Reliability analyses of various process systems and safety systems have been performed. The CDF was found to be approximately 5.46×10^{-8} per RY. Uncertainty analysis has also been performed taking into consideration the variability in component failure parameters. The 95% confidence value for CDF was found to be 8.13×10^{-7} per RY and the 99% confidence value was found to be 1.05×10^{-6} per RY.

15.2.4 Proliferation resistance

The technical features are incorporated to reduce attractiveness of its spent nuclear fuel material for use in any clandestine nuclear weapons program. The content of fissile plutonium in discharged fuel is very low. The radiation field from ^{233}U is very high because of the presence of ^{232}U. In the equilibrium condition, a high fraction of ^{234}U (up to 10%) will exist along with ^{233}U in the fuel. The reactor operates with low excess reactivity. Provision for nuclear material accounting is an inherent part of the AHWR-based nuclear fuel cycle, as has been the practice followed in the entire Indian nuclear program. High gamma activity in the fresh and reprocessed AHWR fuel is expected to facilitate its verification with high efficiency and reliability.

15.2.5 Physical protection

The physical protection system is an integral part of the plant layout of AHWR. The plant is divided into a nuclear island and an administrative island. The plant layout is designed with a dual-layered security arrangement to provide enhanced physical protection to the nuclear island. The nuclear island is isolated from the administrative facilities by double-wire fencing with an additional security arrangement. The double fencing also provides for electronic surveillance. Independent roads for patrolling by security personnel are also provided. The plant layout is shown in Fig. 15.4.

The passive poison injection system (PPIS) is an additional system in AHWRs to fulfill the shut-down function during a low-probability event of failure of wired SDSs [ie, anticipated transient without scram in the case of the SDS-1 and SDS-2 failure condition]. PPIS passively injects the liquid poison into the moderator by system fluid pressure during such transients to shut down the reactor. This situation may arise because of human-induced malevolent action caused by insider threat or compromise of functioning of both SDSs.

15.2.6 Improved economics

Smaller capital investment and a shorter construction period will yield lesser risk and easier funding. There are several features that the lower the capital cost of AHWRs, such as simpler and compact structures and components, elimination of the main circulation pump for the primary loop, use of light water coolant, etc. Other features such as higher burn-up of fuel, extensive use of passive features, 100 years of design life, and a higher capacity factor will help achieve reduced

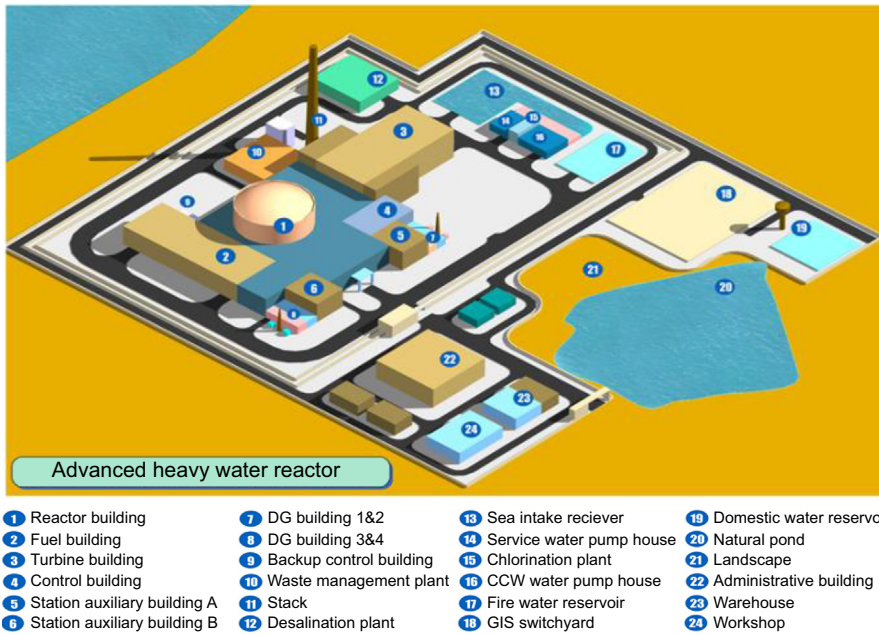


Figure 15.4 Advanced heavy water reactor plant layout.

operating costs. Preliminary assessment shows that the unit energy cost, which is the measure of the economic competitiveness, is found to be comparable to conventional energy sources.

15.2.7 Research and development activities

The development of AHWRs is being supported by R&D in various aspects of reactor technology. Many experimental facilities have been built to validate AHWR design. A critical facility, a low-power research reactor built for conducting physics experiments for validation of physics design parameters of AHWRs, was made critical in 2008 and is presently in operation. The integral test loop, which simulates the main heat transport system (MHTS) and the safety systems of AHWR, is utilized to generate steady-state and stability data, start-up procedure validation, and to study parallel channel behavior. It is also used for performance validation of isolation condensers and ECCS through LOCA tests. Other facilities include the high-pressure natural circulation loop, the 3-MW_e boiling water loop, the parallel channel instability loop, and the Calandria model test facility. A facility for proving advanced reactor thermal hydraulics, a scaled facility simulating the MHTS, is built to establish safety margins and for performance testing of the prototype fueling machine. Various facilities to validate the performance of the containment system and passive system and components are being designed. Performance validation of additional safety systems incorporated to deal with post-Fukushima safety issues such as passive autocatalytic recombiners and a hardened vent system is also being studied.

15.3 High-temperature reactors

Nuclear hydrogen production by splitting water is the main goal for the Indian HTR program. Although development of relatively lower temperature hydrogen production processes (eg, the copper-chlorine process) as well as high-temperature processes (eg, sulfur-iodine process and high-temperature steam electrolysis) are being performed in India, a decision for more a challenging goal of development of technologies for reactor systems capable of producing process heat at 1000°C was taken. Therefore under the Indian HTR program, technology development for a small-power CHTR, and a 600 MW_{th} IHTR, both capable of producing process heat at 1000°C, are being performed. For demonstration of IHTR technologies, a small-power (20 MW_{th}) version would be initially set up before deployment of large-power reactors. In this chapter, design and safety features of CHTR and a brief overview of IHTR are presented.

15.3.1 General description of compact high-temperature reactors

The CHTR is being developed as a prototype reactor for the development and demonstration of technologies associated with HTRs. The reactor is being designed to be compact in weight and size for ease in its deployment in remote locations for its use as a compact power pack. CHTR has a prismatic core. The reactor core consists of 19 hexagonal-shaped BeO moderator blocks. Each of these blocks contains a centrally located graphite fuel tube. Each fuel tube carries fuel inside of bores located on its wall. The fuel tube also serves as a coolant channel. Molten lead-bismuth eutectic (LBE) has been chosen as the coolant to enable natural-circulation–based passive cooling. Reactor physics designs for ^{233}U-Th as well as enriched ^{235}U-based fuel have been established. A design based on enriched ^{235}U-based fuel is currently being pursued. Fuel compacts are made up of TRISO (TRi-ISOtropic)-coated particle fuel, facilitating high burn-up and high-temperature applications. Eighteen blocks of BeO reflector surround the moderator blocks. Graphite reflector blocks surround these BeO reflector blocks. The reactor vessel is made of Nb-1%Zr-0.1%C alloy. A cross section of the core is shown in Fig. 15.5. Coolant plenums are provided above and below the reactor shell. Nuclear heat from the core is passively removed by natural-circulation–based flow of coolant between the two plenums, upward through the fuel tubes, and returning through the down comer tubes. Heat utilization vessels, set up above the upper plenum, act as an interface to systems for high-temperature process heat applications. A set of sodium heat pipes passively transfers heat from the upper plenum to these vessels. Another set of heat pipes transfers heat to the atmosphere in case of a postulated accident. A CHTR component layout is shown in Fig. 15.6. The major design parameters for CHTRs are shown in Table 15.2.

15.3.2 Reactor physics design

The reactor physics design of the CHTR has been performed with the main objectives of achieving high burn-up and a long refueling interval. The reactor fuel consists of

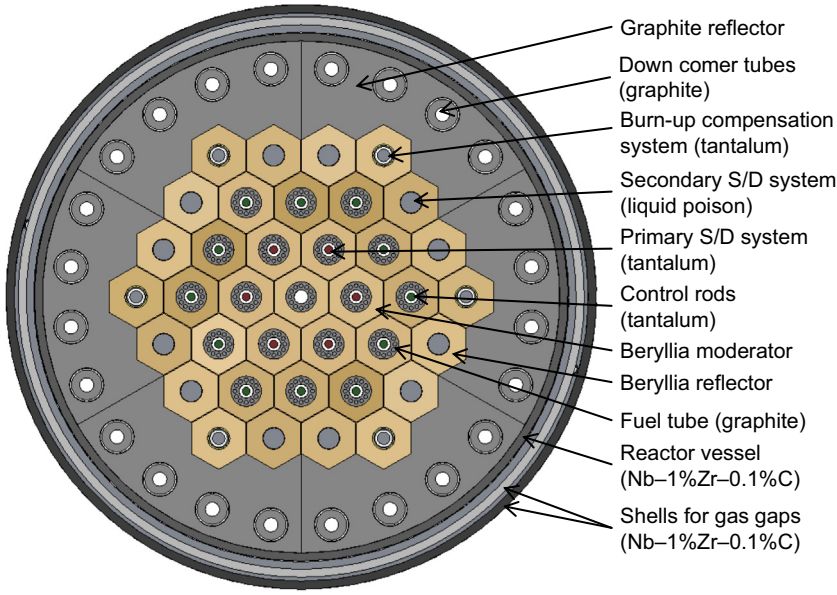


Figure 15.5 High-temperature reactor core cross section. *S/D*, Shut-down.

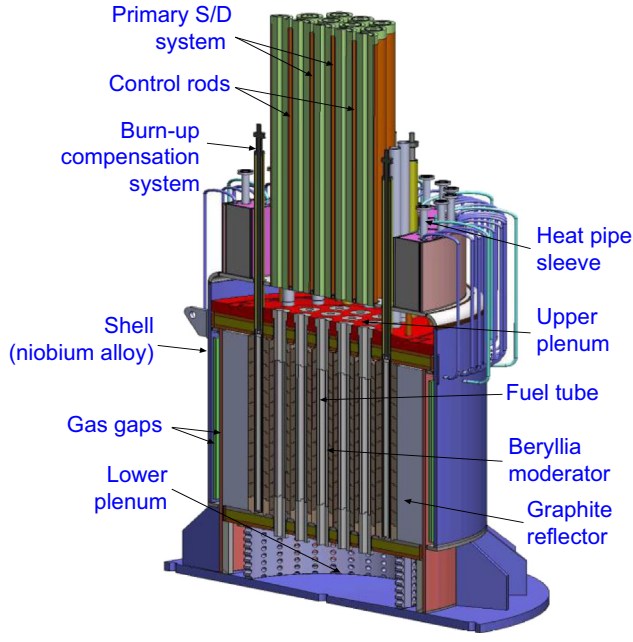


Figure 15.6 High-temperature reactor component layout. *S/D*, Shut-down.

Table 15.2 Compact high-temperature reactors: proposed design and operating parameters

Attributes	Design parameters
Reactor power	100 kW_{th}
Core configuration	Vertical, prismatic block type
Fuel	Enriched ^{235}U-based Tri-ISOtropic-coated fuel particles shaped into fuel compacts with graphite matrix
Fuel pellet size	35 mm length and 10 mm diameter
Refueling interval	15 effective full-power years
Fuel burn-up	~68,000 MWd/t of heavy metal
Fuel tube material	High-density isotropic graphite (nuclear grade)
Moderator	BeO
Reflector	Partly BeO and partly high-density isotropic graphite
Coolant	Molten Pb-Bi eutectic alloy (44.5% Pb and 55.5% Bi)
Mode of core heat removal	Natural circulation of coolant
Coolant flow rate through core	6.7 kg/s
Coolant inlet temperature	1173 °C
Coolant outlet temperature	1273 °C
Loop height	1.4 m (actual length of the fuel tube)
Core diameter	1.27 m
Core height	1.0 m (height of the fueled part and axial reflectors)
Primary shut-down system	Mechanical shut-off rods made of Ta alloy and filled with tungsten pellets, located in six channels of the first ring of the reactor core
Secondary shut-down system	Liquid poison injection in carbon−carbon composite tubes provided in 12 BeO reflector blocks
Control system	Made of Ta alloy and filled with tungsten pellets, located in 12 channels of second ring of the reactor core
Burn-up compensation rods	Made of Ta alloy, filled with tungsten pellets, and located in six BeO reflectors

8 kg of enriched ^{235}U. Variation of k_{eff} with respect to burn-up is shown in Fig. 15.7. Fertile material and the burnable poisons make the fuel temperature coefficient negative, thus making the reactor inherently safe. The primary SDS consists of a set of six tantalum alloy shut-off rods, which fall by gravity in the six coolant channels in the first ring. Twelve control rods, made of tantalum alloy, are located in the next ring.

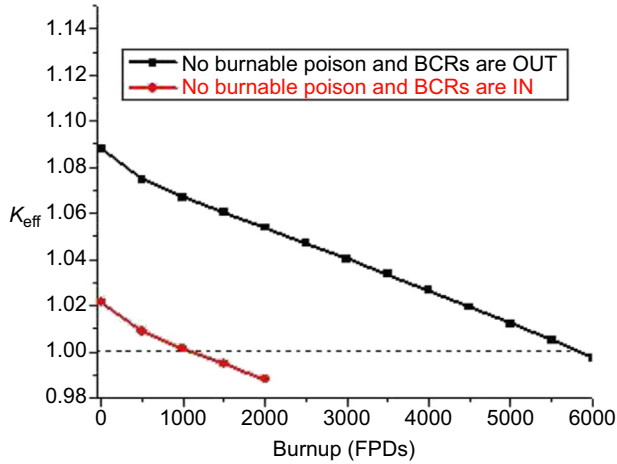


Figure 15.7 Variation of k_{eff} with respect to burn-up. *BCR*, Burn-up compensation rods.

The secondary SDS is in the form of a liquid poison injection system located in the BeO reflector region. The remaining six BeO reflectors house burn-up compensation rods, which are fully inserted in the beginning and periodically moved out.

15.3.3 Thermal hydraulics design

As mentioned earlier, the reactor heat is removed by passive natural circulation of coolant. In addition to analytical studies and the development of computer codes, two experimental LBE loops for natural-circulation studies were set up. The first one with operating temperature of 500°C has been in operation since 2009. The second loop (Fig. 15.8) with an operating temperature of 1000°C has been in operation for almost the last 1 year. In addition to these studies related to the freezing and defreezing of LBE as well as the development of oxygen sensors for LBE, level measurement probe, etc., were also carried out.

15.3.4 Fuel development

A typical CHTR fuel bed consists of a prismatic BeO moderator block with a centrally located graphite fuel tube carrying fuel compacts. Fuel compacts are made of TRISO-coated particle fuel with enriched ^{235}U-based fuel. A schematic of a single fuel bed is shown in Fig. 15.9. The technology for fuel kernel manufacture has been long established at BARC by the sol−gel technique. A facility for coating TRISO-coated particle fuel and the radiography of a typical particle is shown in Fig. 15.10. Fuel compacts with high packing density are shown in Fig. 15.11. After developing the coating technology, coatings were successfully performed on natural UO_2. Some of the coated particles have been irradiated in a fast breeder test reactor (FBTR) at IGCAR, Kalpakkam, India. In parallel, technology development for fuel compact manufacture has also been initiated. Compacts with high packing density

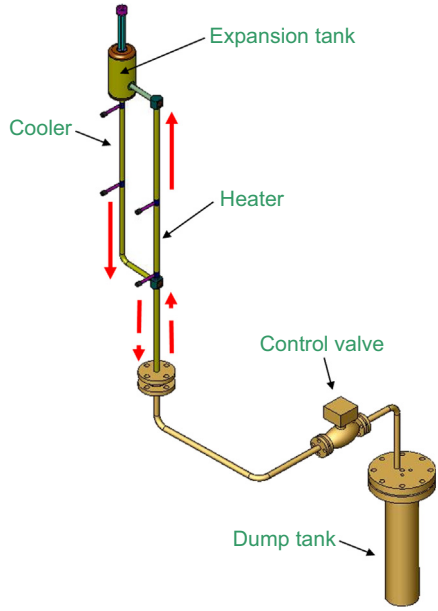


Figure 15.8 Schematic of lead-bismuth eutectic natural circulation loop (operating at 1000°C).

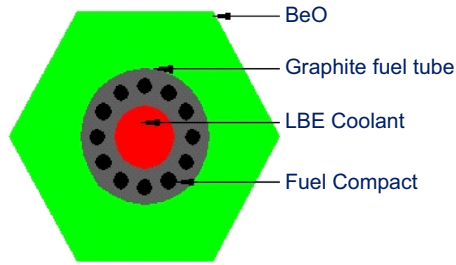


Figure 15.9 Schematic of single fuel bed for compact high-temperature reactor. *LBE*, Lead-bismuth eutectic.

(∼45%) of particles with uniform distribution could be successfully made. Further development is mainly for characterization.

15.3.5 Materials development

CHTR core materials comprise nuclear-grade high-purity materials. These are high-density isotropic BeO for moderator and reflector blocks (Fig. 15.12(a)), high-density isotropic graphite for fuel and down comer tubes, and reflector blocks (Fig. 15.12(b)). Other metallic structural materials are based on refractory metal alloys such as Nb-1%Zr-trace carbon (Fig. 15.12(c)) for reactor shell and coolant plenums and tantalum-tungsten−based alloy for safety and control rods. Graphite and these alloys are coated with oxidation-resistant coatings. These technologies have been successfully developed within DAE.

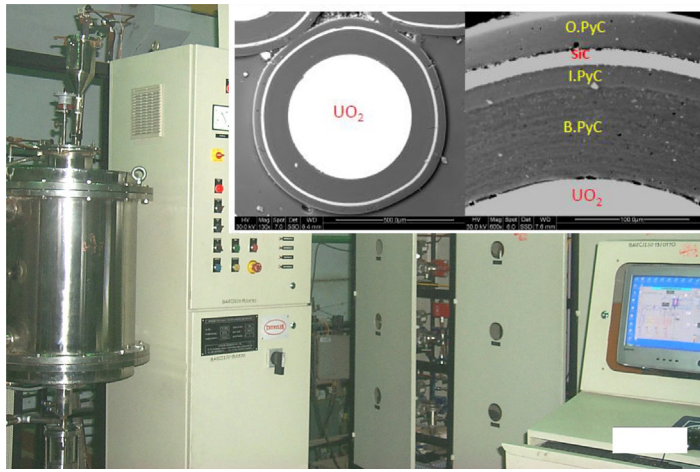


Figure 15.10 Facility for coating Tri-ISOtropic-coated particle fuel.

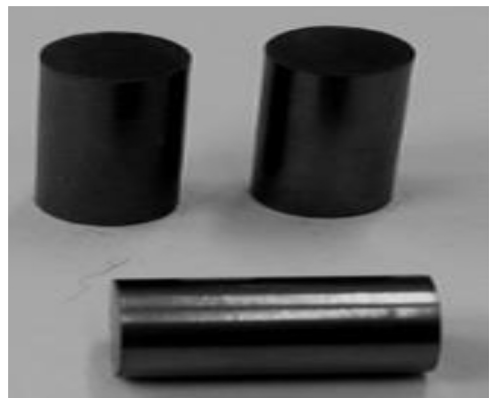


Figure 15.11 Fuel compacts for compact high-temperature reactor.

15.3.6 Inherent safety features and passive heat removal systems

CHTRs are being designed to have many features that make them inherently safe. Some of these features are a strong negative Doppler coefficient of the fuel, high thermal inertia of the all-ceramic core, low core power density, a very large thermal margin between the operating temperature and boiling point of the LBE, the chemical inertness and negative reactivity effects of LBE, low-pressure natural circulation of coolant, etc. In addition, passive systems for reactor heat removal under normal and postulated accident conditions have been incorporated. This includes natural circulation of LBE for reactor heat removal, passive heat transfer to the secondary side using high-temperature sodium heat pipes, passive SDSs, passive dissipation of heat under a postulated accident scenario, etc.

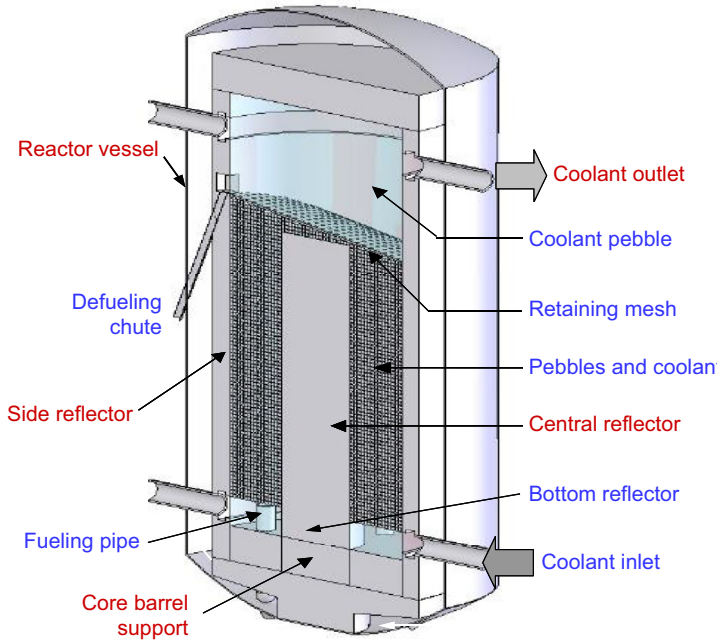


Figure 15.12 Schematic of innovative high temperature reactor.

15.3.7 Research and development activities

The major challenges to be addressed include coatings on TRISO-coated particle fuel and their characterization, production of high-density nuclear-grade BeO of intricate shapes, production of nuclear-grade high-density isotropic carbon-based materials and component manufacture, development of LBE-resistant structural material for high-temperature applications, oxidation-resistant coatings and their characterization, development of components and instrumentation for service in intimate contact with LBE coolant at high temperatures, LBE coolant technologies, and development of sodium-based high-temperature heat pipes. Most of the challenges have already been overcome, and R&D activities are in progress.

Major developmental activities planned for the future include studies related to design validation of a CHTR critical facility in the areas of high-temperature materials, thermal hydraulics, safety, and corrosion of structural materials; demonstration and testing of reactor control and SDSs; seismic qualification; qualification of passive heat removal systems under postulated conditions; development and demonstration of energy conversion technologies for utilizing high-temperature process heat; experimental facilities to demonstrate auxiliary systems such as coolant chemistry control/purification systems; and studying the irradiation behavior of new types of fuel, materials, and coatings. Subsequent to all developments, a critical facility for a CHTR would be set up.

15.3.8 Innovative high-temperature reactor

An IHTR is a pebble-bed molten salt-cooled reactor. Pebbles consist of TRISO-coated particle fuel, and the coolant is driven through natural circulation. The reactor core is a long right circular cylinder with an annular core that consists of fuel pebbles and molten salt coolant. Fig. 15.13 shows a schematic of a 600-MW_{th} IHTR. There are graphite neutron reflectors in the center and on the top, bottom, and outside of this fuel annulus. Vertical bores in the central and outer reflectors are provided for the reactivity control elements. R&D activities being pursued include a molten salt natural circulation loop, as shown in Fig. 15.14, which has been set up to perform thermal

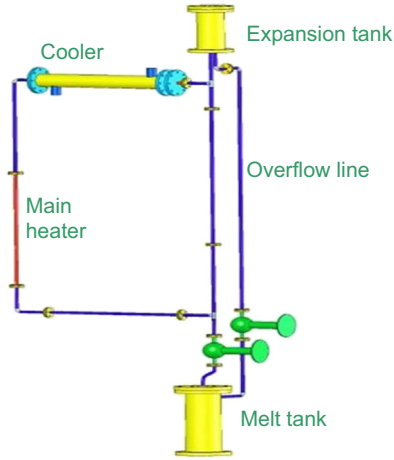


Figure 15.13 Molten salt natural-circulation loop.

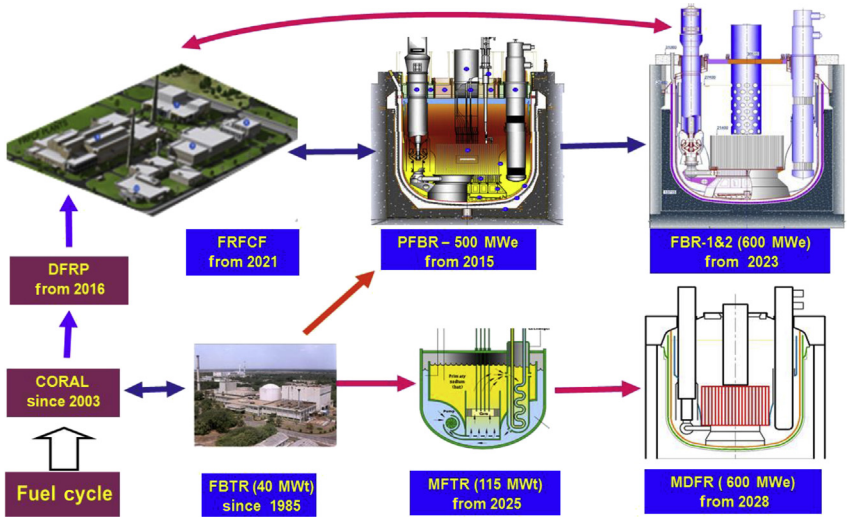


Figure 15.14 Fast breeder reactor (FBR) and associated fuel cycle program up to 2030.

Table 15.3 Innovative high-temperature reactor: proposed design and operating parameters

Attributes	Design parameters
Reactor power	600 MW_{th} for the following deliverables – Hydrogen: 80,000 Nm^3/h – Electricity: 18 MW_e – Drinking water: 375 m^3/h Optimized for hydrogen production
Coolant outlet/inlet temperature	1273/873 °C
Moderator	Graphite
Coolant	Molten salt
Reflector	Graphite
Mode of cooling	Natural circulation of coolant
Fuel	$^{233}UO_2$ and ThO_2 based high burn-up TRISO-coated particle fuel
Number of pebbles in the core	~150,000
Packing fraction of pebbles	~60%
Packing fraction of TRISO particles	~8.6%
^{233}U requirement	~7.3%
Control	Passive power regulation and reactor shut-down systems
Energy transfer systems	Intermediate heat exchangers for heat transfer to system for hydrogen production + high-efficiency turbomachinery for electricity generation + desalination system for potable water
H_2 production	High efficiency thermochemical processes

TRISO, Tri-ISOtropic.

hydraulic studies of molten salts. In addition, an experimental facility to study the corrosion behavior of molten salt on the structural materials has also been set up. Experiments on various materials have been initiated. Future R&D activities include the manufacture of pebble-based fuel, a pebble feeding and removal mechanism, thermal hydraulic studies for molten salts in pebble-bed geometry, development of large-size graphite components, a high-efficiency power conversion system, and instrumentation and other components for the molten salt environment. The major design parameters of an IHTR are shown in Table 15.3.

15.4 Fast breeder reactor

15.4.1 Fast reactor program in India

The targets and strategies of SFR development are illustrated comprehensively in Fig. 15.15. The FBR program was started by constructing a loop-type FBTR, which has been in operation since 1985. With the PHWR program well on its growth path and having established comprehensive expertise in SFR technology through successful operation of FBTR for 30 years, India is now on a robust pathway for development of the SFR-based second stage of the program with a PFBR launched in October 2003. The PFBR is undergoing stage commissioning tests and is scheduled for completion in 2015. It is envisaged that two more such units, with innovations in PFBR and based on learning experience, will be constructed by the year 2023. Subsequently, 1000-MW_e SFRs using a metallic core (has high breeding potential) will be constructed to rapidly realize the nuclear power . However, complete realization of SFR technology involves many challenges in science, design, safety, and technology, especially in fuels and core structural materials and instrumentation aspects.

15.4.2 Fast breeder test reactors and their current status

The FBTR is a sodium-cooled, loop-type fast reactor fueled with a unique high Pu mixed carbide fuel. It has two primary and two secondary sodium loops. Each secondary loop has two once-through, serpentine-type steam generators (SGs). All of the four SG modules are connected to a common steam-water circuit having a turbogenerator (TG) and a 100% steam dump condenser. The first criticality was achieved in October 1985 with a small core of 22 fuel subassemblies (SAs) of MK-I composition (70% PuC +30% UC), with a design power of 10.6 MWt and peak linear heat rating (LHR) of 250 W/cm. The core was progressively expanded by adding SAs at peripheral locations. Carbide fuel of MK-II composition (55% PuC + 45% UC) was inducted in the peripheral locations in 1996. The TG was synchronized to the grid for the first time in July 1997. The LHR of MK-I fuel was increased to 400 W/cm in 2002. Eight high-Pu MOX fuel SAs (44% PuO_2) were loaded in the core periphery in 2006. The indigenously developed unique Pu-rich mixed carbide fuel has performed extremely well, crossing a burn-up of 165,000 MWd/t. One of the important achievements is closing of the fuel cycle of the FBTR. The FBTR fuel discharged at 155,000 MWd/t has been successfully reprocessed and refabricated. This is the first time that the Pu-rich carbide fuel has been reprocessed anywhere in the world.

The FBTR is being effectively used for the PFBR subassembly irradiation of MOX fuel up to a peak burn-up of 112 MWd/kg. Furthermore, the reactor is used for generating structural material data for cladding and wrappers, calibration of sensors, neutron detectors, and some special isotope productions. Furthermore, toward designing and building future metallic fueled test reactors, the irradiation of metallic fuel pins is in progress.

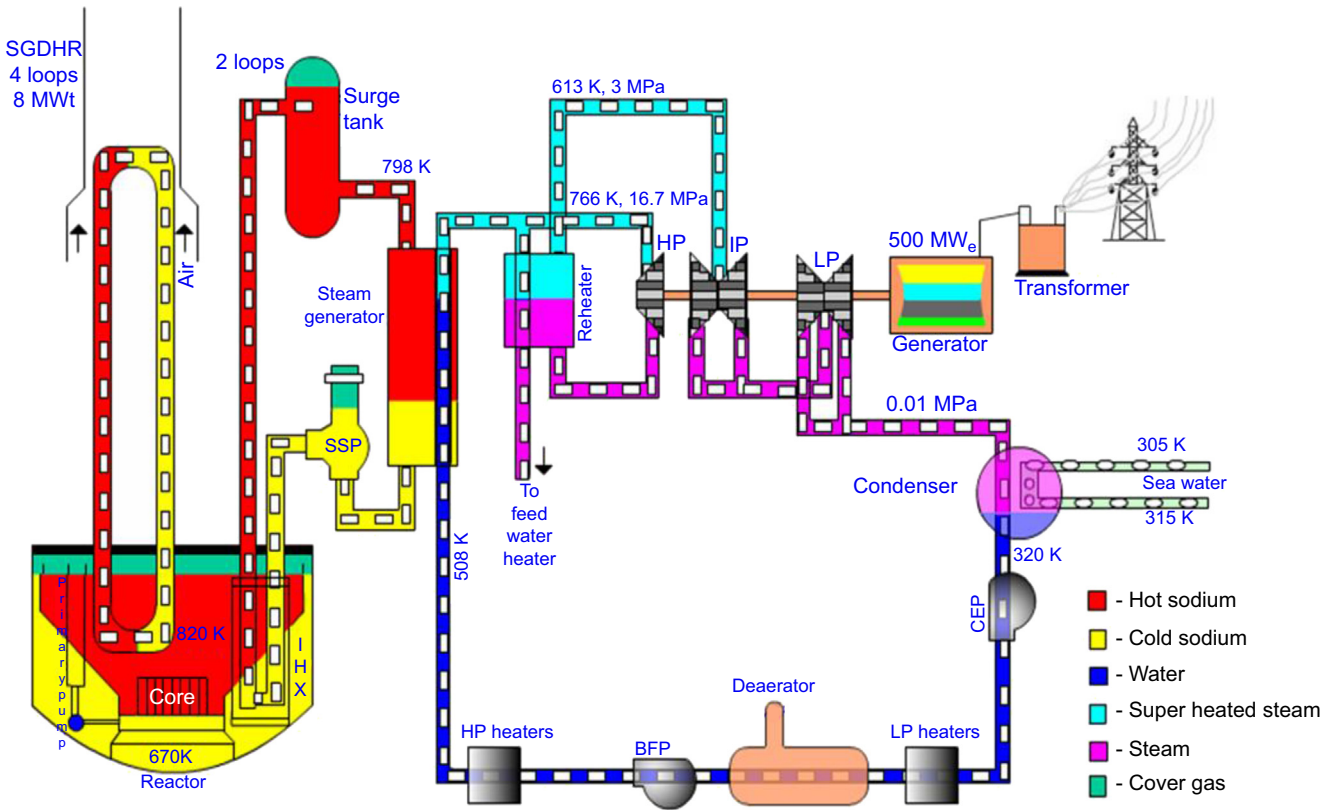


Figure 15.15 Prototype fast breeder reactor (PFBR) heat transport systems. *SGDHR*, Secondary sodium decay heat removal; *IHX*, intermediate heat exchanger.

The reactor has so far been operated up to a power level of 20 MWt. Furthermore, the reactor life is to be extended by 20 years to serve as an irradiation facility for future development. Apart from these, the FBTR has given high confidence for the successful construction, commissioning, and operation of SFRs.

15.4.3 The prototype fast breeder reactor and its current status

The PFBR is a 500-MW_e capacity pool-type reactor with two primary and two secondary loops with four SGs per loop. Pool- and loop-type concepts were studied comprehensively considering the associated merits and demerits specific to medium-size reactors such as the PFBR, and it was concluded that the pool type shall be the choice. The governing parameters meriting the choice are large thermal inertia that permits high thermal shock, higher structural reliability due to fewer associated critical welds, and the compact layout of the primary circuit components. It is also our perception that the complexities that are associated with the pool type of reactor such as thermal hydraulics, manufacturing, and handling of overdimensioned thin vessels with stringent tolerances can be successfully met by the designers and our industry. Subsequently, this has been confirmed from detailed analysis backed up with experimental validation and extensive 1:1 technology development exercise.

The overall flow diagram comprising a primary circuit housed in a reactor assembly, a secondary sodium circuit, and the balance of the plant is shown in Fig. 15.16, and the essential operating parameters of the plant are shown in Table 15.4. The nuclear heat generated in the core is removed by circulating sodium from the cold pool at 397°C to the hot pool at 547°C. The sodium from the hot pool, after transporting its heat to four intermediate heat exchangers (IHXs), mixes with the cold pool. The circulation of sodium from the cold pool to the hot pool is maintained by two primary sodium pumps, and the flow of sodium through the IHX is driven by a level difference (1.5 m of sodium) between the hot and cold pools. The heat from the IHX is in turn transported to eight SGs by sodium flowing in the secondary circuit. Steam produced in the SG is supplied to the TG. In the reactor assembly the main vessel houses the entire primary sodium circuit including the core. The inner vessel separates the hot and cold sodium pools. The reactor core consists of approximately 1757 SAs including 181 fuel SAs. The control plug, positioned just above the core, mainly houses 12 absorber rod drive mechanisms. The top shield supports the primary sodium pumps, the IHX, the control plug, and the fuel handling systems. The PFBR uses MOX fuel with depleted and natural uranium and approximately 25% Pu oxide. For the core components, 20% cold worked D9 material (15% Cr−15% Ni with Ti and Mo) is used to have better irradiation resistance. Austenitic stainless steel type 316 LN is the main structural material for the out-of-core components and modified 9Cr-1Mo (Grade 91) is chosen for the SG. The reactor is designed for a plant life of 40 years with a load factor of 75%.

The design of the PFBR calls for complete understanding of unique fuel and structural material behavior under high temperature, sodium, and irradiation environments as well as the science and technology aspects in the domains of sodium chemistry, aerosol behavior, sodium fire and sodium water reactions, special sensors for sodium

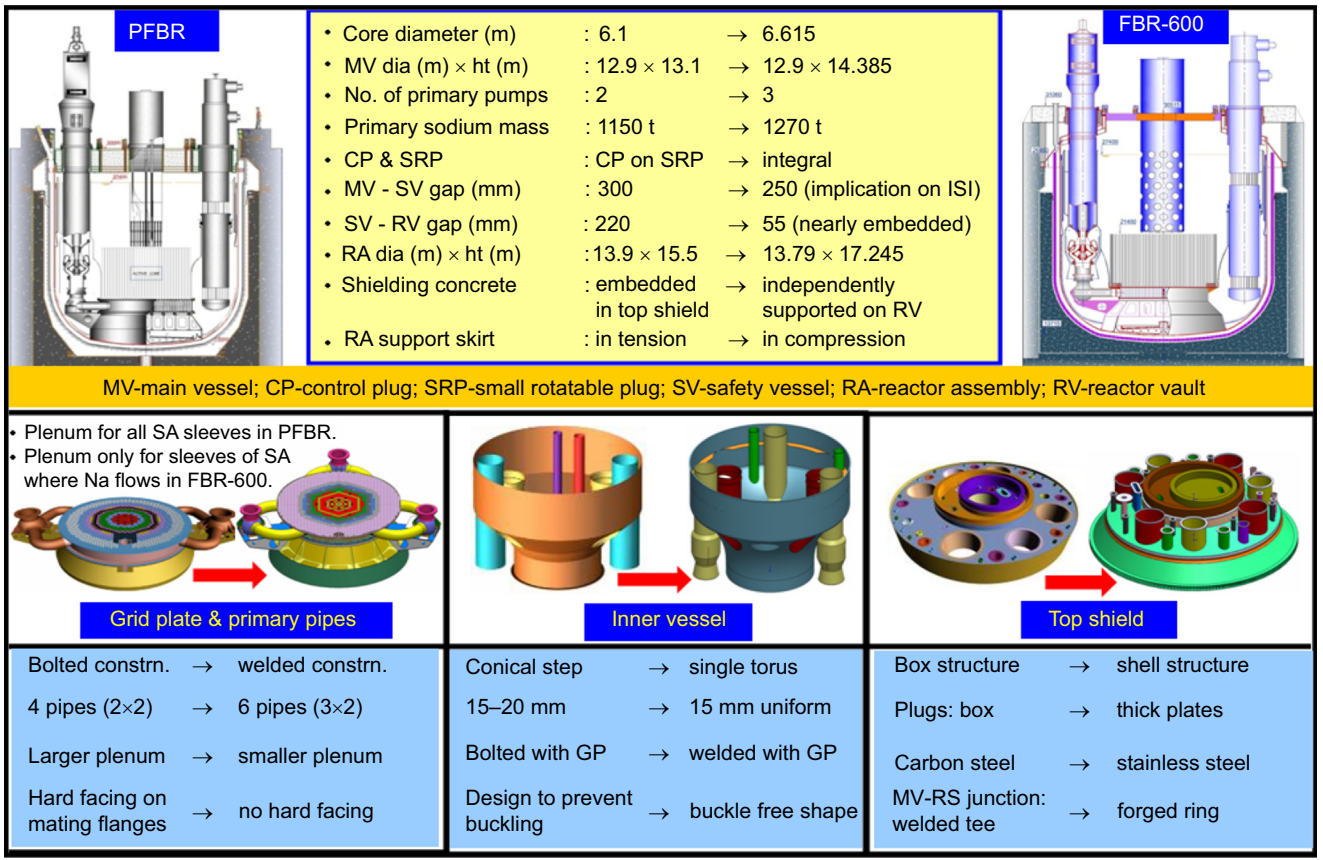


Figure 15.16 Design improvements of reactor assembly for FBR-600. *dia*, diameter; *ht*, height; *constrn*, construction; *SA*, subassembly; *PFBR*, prototype fast breeder reactor.

Table 15.4 Prototype fast breeder reactor: operating parameters

Attributes	Design parameters
Reactor thermal power	1250 MW_{th}
Electrical output	500 MW_e (gross)/470 MW_e (net)
Fuel	$PuO_2 + UO_2$
Number of fuel locations	181 (inner zone = 85; outer zone = 96)
Pu enrichment	Inner zone = 20.7% (w); outer zone = 27.7% (w)
Maximum fuel burn-up	100 GWd/t
Blanket material	Depleted UO_2
Number of blanket locations	120
Type of core	Homogenous
Core orientation	Vertical
Lattice pitch (triangular)	135 mm
Concept of primary sodium circuit	Pool type
Coolant	Liquid sodium
Total core flow	6.8 t/s
Coolant inlet temperature	397°C
Coolant outlet temperature	547°C
Total steam flow	560 kg/s
Feed-water inlet temperature	235°C
Steam temperature at HP turbine inlet	490°C
Steam pressure at HP turbine inlet	16.7 MPa
Absorber material	B_4C enriched in B-10
Breeding ratio	1.04
Design life	40 years

applications (detection of water leaks in the SG, sodium leaks, purity measurements, level detectors), thermal hydraulics, and structural mechanics (turbulences, instabilities, gas entrainments, thermal striping, stratifications, racketing, etc.). Various failure modes are identified comprehensively and analyzed in detail using validated analytical, numerical, and experimental techniques.

The construction of PFBR has been completed, and commissioning is in the advanced stage. The commissioning of the primary system is currently performed with dummy core SAs having all of the mechanical and hydraulic features with steel pellets in the place of fuel. Before replacing the dummy assemblies with actual fuel

assemblies, several tests are planned. In situ performance of primary and secondary pumps; electromagnetic pumps; in-vessel and ex-vessel fuel handling machines; and various mechanisms such as absorber rod drive mechanisms, under sodium scanners, eddy current flow meters, periscope, etc., are being qualified before and after filling sodium at various temperatures. These apart, vibrations of pumps and dummy core assemblies are checked. The first criticality is planned in the last quarter of 2015, and commercial power generation subsequently begins.

15.4.4 Motivation for improvements for future fast breeder reactors beyond the prototype fast breeder reactor (FBR-600)

The design, R&D, safety review, construction, and commissioning experience derived from PFBR have motivated the commercial exploitation of MOX-fueled SFRs with a closed fuel cycle. Accordingly, in the roadmap prepared for the FBR development beyond PFBR, two FBRs (FBR-1 and FBR-2) have been conceived to be commissioned by 2023−24. The FBR-1 and FBR-2 need to be improved with respect to the PFBR on economy (target: 20−25% material reduction and reduction of construction time by at least 2 years) and safety (target: to have features in line with emerging safety criteria, broadly Gen-IV criteria evolved after the Fukushima event). Among several measures taken to meet the requirements, an important one is that the sodium void reactivity should be kept lower than \$1. This value is \$2.7 for the PFBR, which is the lowest among the values reported for other international reactors designed before the Fukushima accident. On the basis of detailed optimization studies, it is concluded that a heterogeneous core is the most preferred solution with reference core size, fuel inventory, available knowledge, matured analysis capability, and international trend. Among a few potential options, introducing depleted uranium within the pins of a few SAs occupying the core central zone and/or introducing radial blankets in the central zones provide attractive solutions to derive a higher breeding ratio while restricting the sodium void reactivity. The heterogeneous core with only radial heterogeneity (Mark-I) has indicated that the breeding ratio of approximately 1.2 with the sodium void reactivity not exceeding \$1 is possible. Because the radial heterogeneous core occupies a little larger radial space, it has been chosen to have a flexibility to choose any heterogeneous core, which demands lesser diameter. This strategy has been adopted in a calibrated manner so that the reactor assembly dimensions do not change in the process of iterating and finally adopting the most optimized core with thorough validation including the associated core safety aspects. Accordingly, the Mark-I core with 3.4-m diameter has been chosen for the design finalization. In the subsequent design optimization studies, the reactor power has been raised to 600 from 500 MW_e for each unit. Furthermore, the main vessel diameter has been restricted not to exceed the PFBR main vessel diameter. These two FBRs will be built as one twin unit (ie, two 600-MW_e plants sharing several nonsafety-related facilities). Conceptual design documents have been prepared and reviewed independently by relevant experts.

15.4.5 Conceptual design features of FBR-600

The sodium void coefficient of the MOX core will be less than 0.9, depending upon the kind of heterogeneity that will be finalized based on the further optimization study (in progress). The two-loop concept would be retained. A twin-unit concept, optimum shielding, use of 2/1/4 Cr-1 Mo in place of 304 LN for cold pool components and piping, three SG modules per loop with increased tube length of 30 m (PFBR has four modules per loop with 23 m length), 85% load factor, 60-year design life, reduced construction time (6 years), and enhanced burn-up (up to 200 GWd/t to be achieved in stages) are being considered. Furthermore, significant improvements have been introduced in the reactor assembly design (Fig. 15.17), including (1) a welded grid plate with a smaller plenum to accommodate only those sleeves that support core SAs through which sodium flows, (2) an inner vessel having a single curved redan with uniform thickness, (3) thick-plate rotatable plugs, (4) a control plug integrated with a small rotatable plug, (5) torus-shaped thick-plate roof slab, (6) a support skirt for the reactor assembly kept under compression, (7) a safety vessel made of carbon steel embedded with the reactor vault, and (8) simplified fuel handling scheme with elimination of an inclined fuel transfer machine (Fig. 15.18). These apart, major modifications introduced in the SG are consolidated in Fig. 15.19.

These revisions call for three relatively smaller capacity primary sodium pumps instead of two larger capacity pumps. The revised parameters resulted from optimization study also include a marginal increase of operating temperatures (the mixed mean temperate of sodium outlet from the core increased by 10°C), a steam temperature of 510°C (490°C for PFBR), and an increase in load factor by 10%. The improved design concepts have indicated significant economic advantages, including a material inventory reduction by approximately 25%, a simplified fuel handling scheme, and reduced manufacture time. The new concepts introduced will be validated through executing systematic R&D, technology development exercise, testing and evaluation, etc.

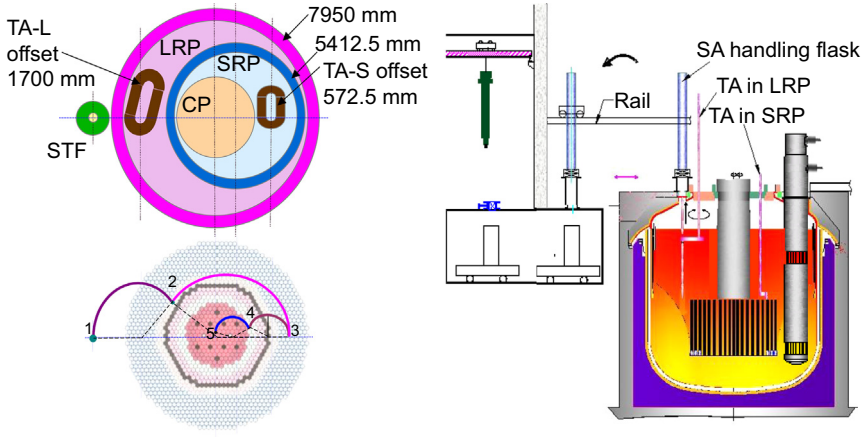


Figure 15.17 Simplified fuel handling scheme for FBR-600.

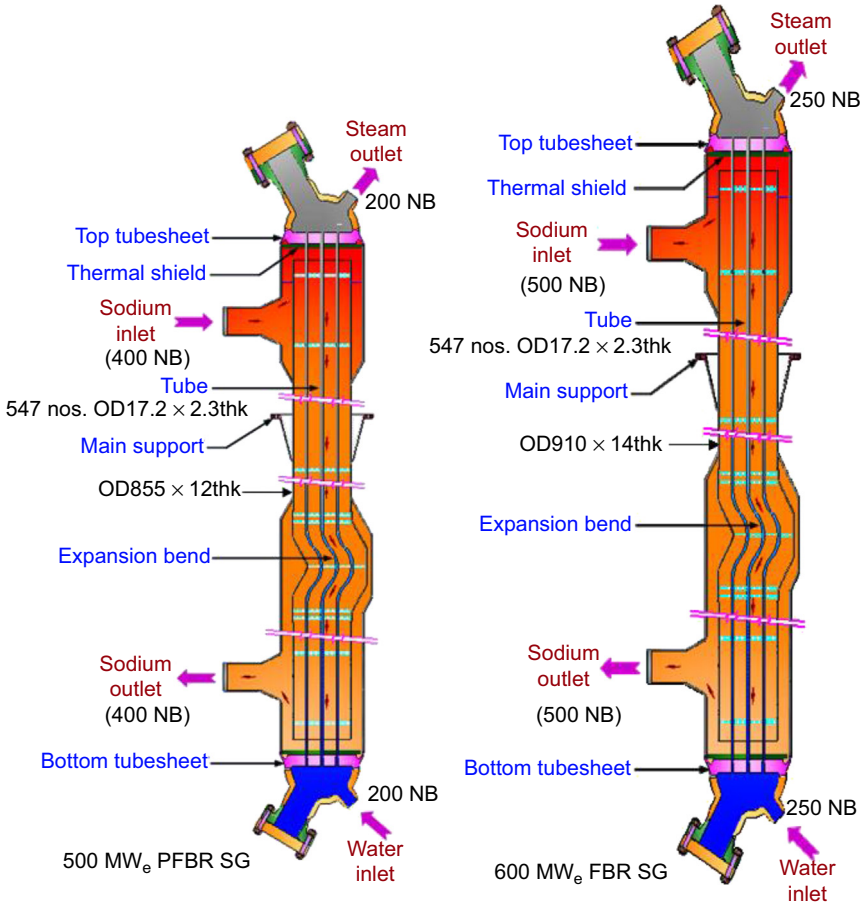


Figure 15.18 Comparison of 30-m long tube steam generator (SG) of 600-MW_e fast breeder reactor (FBR) with the prototype fast breeder reactor (PFBR) SG. *OD*, outer diameter.

15.4.6 Enhanced safety features

The safety features are introduced to meet the international safety criteria particularly evolved after the Fukushima accident. The major implication is need of detailed investigation of all beyond design-basis events (DBEs), including prolonged station blackout conditions resulting in severe core damage and large radioactivity release to the public as well as practical elimination of severe accident scenarios. The DBEs have been split into three subcategories: (1) design extension condition-1 (DEC-1) without core melting, (2) design extension condition-2 (DEC-2; which involves core meltdown), and (3) practically eliminated condition (PEC). The aim of such categorization is to ensure that even in the worst-case accident scenario no early or long-term protective measures would be needed in the public domain. For both DEC-1 and DEC-2, the radioactivity release limit is 20 mSv. DEC-1 events are those events for which the site boundary dose is only limited (20 mSv). For those coming

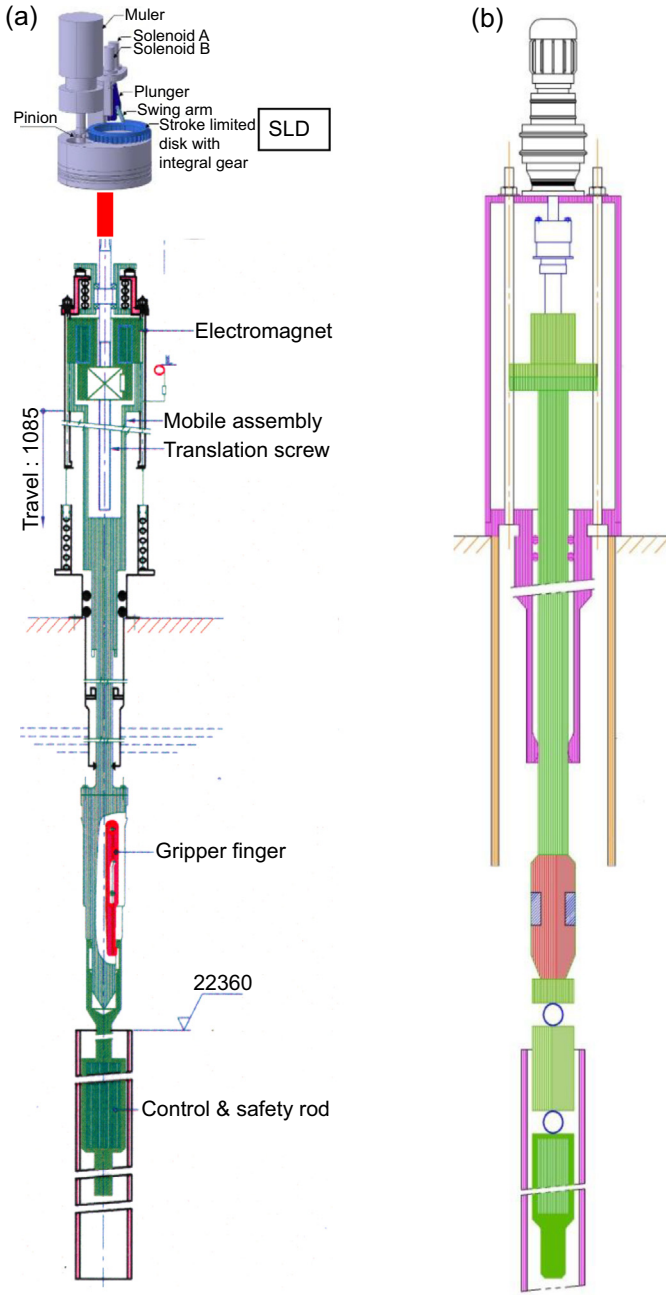


Figure 15.19 (a) Control and safety rod drive mechanism and (b) diverse shut-down rod drive mechanism with passive safety features proposed for FBR-600.

under DEC-2, the design measures should limit the event consequences within the specified time and distance. The accepted values of time and distance are yet to be internationally evolved. Events involving overheating of fuel pins (inadequate cooling of core under prolonged station blackout condition) and subsequent release of a large quantity of fission gas and fuel particles into the cover gas space are typical examples for DEC-2. Those events causing severe core damage resulting in large radioactivity release to the public come under PEC. Typical events coming under this category are (1) failure of structures lying along the core support path (roof slab, main vessel, core support structure, and grid plate), (2) simultaneous failure of the main vessel and safety vessel, (3) a core disruptive accident (CDA), and (4) re-criticality.

In the design of a SDS, the major improvements considered are (1) enhancing the reliability of SDSs (as in PFBR) with the introduction of passive safety features and (2) adequately addressing the re-criticality issue. Toward further improving reliability of SDSs (at least by one order with reference to the PFBR), active/passive safety features are introduced, including a stroke limiting device to limit the uncontrolled withdrawal of control and safety rods in their drive mechanisms (Fig. 15.20(a)) and temperature-sensitive magnet/magnetic switch (Curie point magnet) in the diverse shut-down rod drive mechanisms (Fig. 15.20(b)). These apart, introduction of hydraulically suspended absorber rods that would be dropped immediately once the primary sodium flow is reduced with the initiating events such as rupture of more than one primary pipe, seizure of all primary pumps, and total instantaneous blockage in fuel SAs is under consideration (Fig. 15.21). To avoid re-criticality, an adequate number of ultimate shut-down (USD) systems that work on liquid (Li-6) or granules (enriched B4C powder) will be introduced. The re-criticality issue and concept of the USD system are explained schematically in Fig. 15.22. The scheme of the SDSs (type, number, and location) will be finally decided based on a deterministic approach with due considerations on the probabilistic approach. However, R&D activities on the systems previously mentioned that are in progress will be continued and adequate knowledge and data will be accumulated. R&D involves introduction of such systems in the FBTR itself to increase their confidence under an actual environment (sodium, irradiation, and high temperature).

Various decay heat removal (DHR) systems are provided with high reliability to cater the needs under five situations: (1) fuel handling, (2) in-service inspection, (3) DBE, (4) DEC, and (5) postaccident conditions (Fig. 15.23). High emphasis is given to address the prolonged station blackout condition. For meeting the DHR requirements for the first three situations, dedicated DHR systems (4×10 MWt) in all of the four secondary sodium circuits (SSDHRs), an operating-grade decay heat removal (OGDHR) system in the steam-water system in the PFBR, or a combination of SSDHRs and OGDHRs are being studied. This decision is yet to be taken after detailed assessment of design, operational simplicity, availability, reliability, economics, and experience. A marginal cost increase of the SSDHR systems compared with OGDHR systems of the same capacity is to be absorbed. For taking care of DHR during DEC (situation 4), the safety-grade decay heat removal (SGDHR) system introduced in PFBR will be retained. SGDHR can be made operational by appropriate opening of the dampers in the case of any DBEs resulting in loss of power to the secondary sodium pumps. However, design studies are in progress to make the SSDHR operational

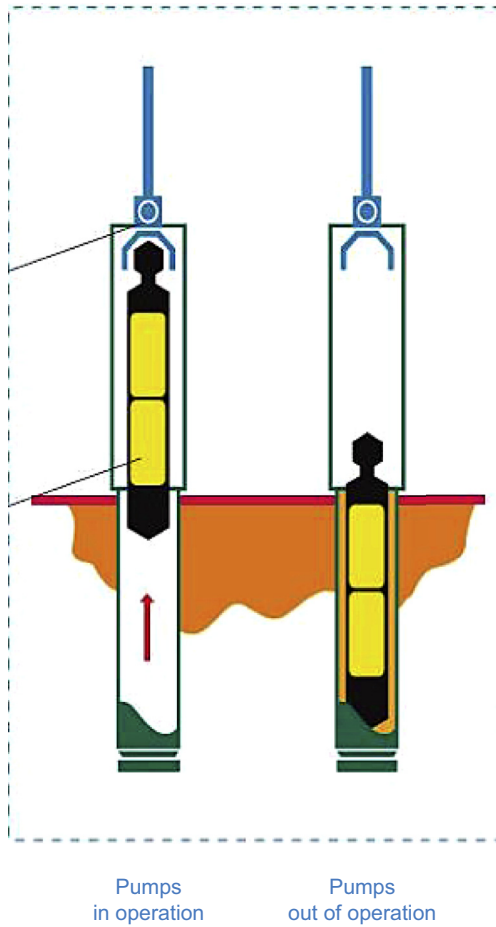


Figure 15.20 One hydraulically suspended absorber rod.

even during the loss of power to the pump to ensure high reliability of the DHR requirement. Finally, to meet the DHR requirement during postaccident situations, the current features incorporated in the PFBR will be retained (ie, ensuring heat removal capacity of the SGDHR after a CDA and a core catcher to support the core debris resulting from the CDA). Further improvements required are ensuring the heat removal capacity features in the case of core debris resulting in whole core meltdown. Although it has been shown by computational fluid dynamics analysis that a large perforation created by the molten fuel while melting through the grid plate and core support structure facilitate adequate natural circulation of sodium to remove the heat from debris settled on the core catcher and to transport to the SGDHR inlet windows through the natural-convection mode, considerations are being given to incorporate a few pipes penetrating through the inner vessel for providing alternative/additional passages for the sodium flow once the mean temperature exceeds a certain value.

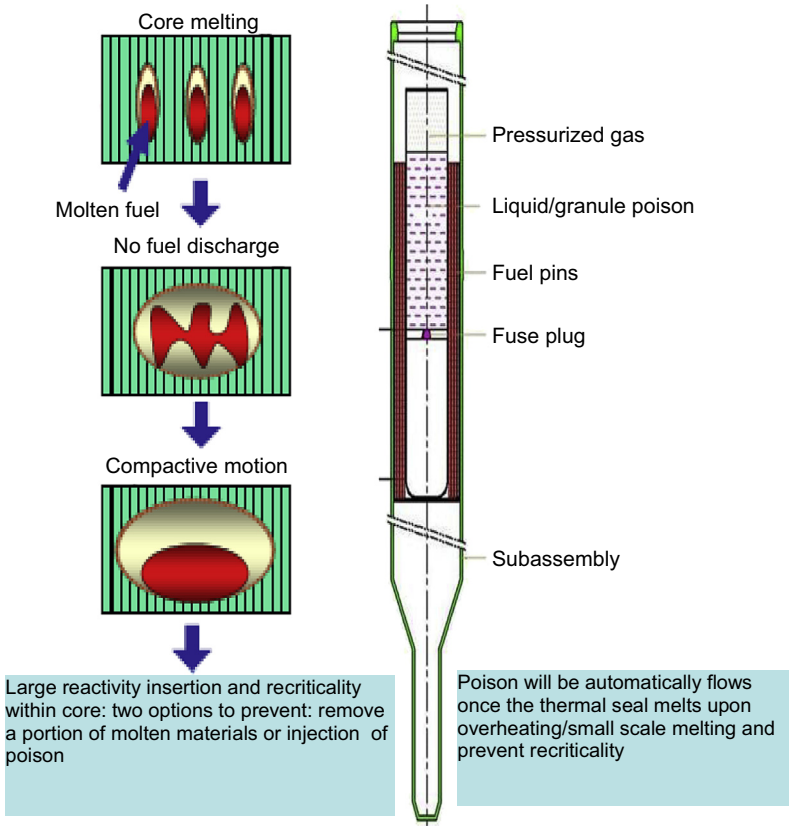


Figure 15.21 Concept of ultimate shut-down system for taking care of re-criticality.

To maintain the concrete temperature less than the applicable allowable value in the case of simultaneous leakages in the main vessel and the safety vessel, design features have been introduced to provide oil cooling coils in the intervessel spaces.

15.4.7 Research and development status

Apart from R&D on material, structural mechanics, and thermal hydraulics testing and evaluation, R&D activities are in progress for the validation of passive shut-down systems based on Curie point magnet, liquid poison injection systems, passive DHR systems, and demonstration of a postaccident heat removal system. Toward this, a few unique facilities have been built at IGCAR, including the SOdium-Fuel Interaction Facility (SOFI) for the molten fuel coolant interaction studies (Fig. 15.24), the Postaccident Thermal Hydraulics Facility (PATH) for postaccident heat removal studies (Fig. 15.25), the MINI Sodium Fire Facility (MINA) for small-scale sodium fire studies (Fig. 15.26), the Sodium Fire Experimental Facility (SFEF) for large-scale sodium fire studies (Fig. 15.27), and the SOdium CAble Interaction

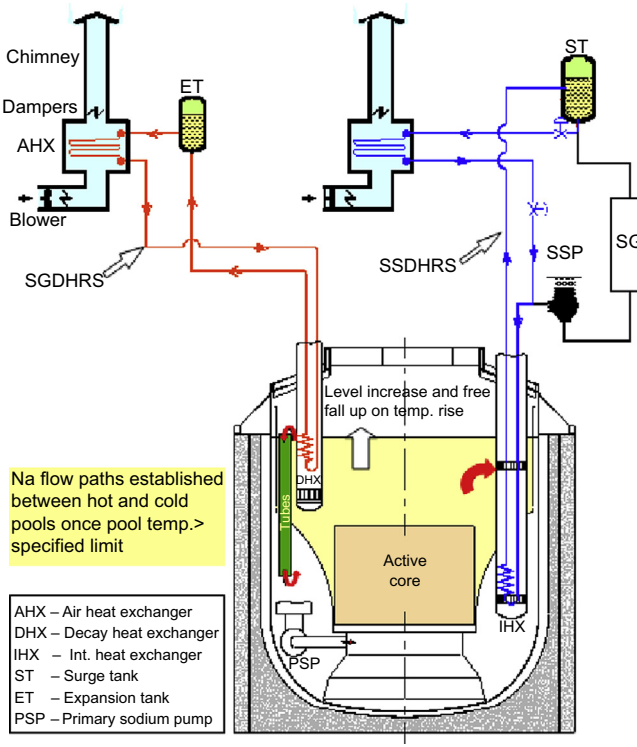


Figure 15.22 Decay heat removal systems conceived for a fast breeder reactor. *SGDHRS*, secondary sodium decay heat removal system; *SG*, steam generator; *SSP*, secondary sodium pump; *temp*, temperature.

Facility (SOCA) for simulating sodium fire scenarios on the top shield platform (Fig. 15.28). Some innovative SDSs could be introduced in the PFBR itself after thorough validations.

15.5 Molten salt reactors

India is developing two concepts of molten salt reactors. One of the concepts has a pebble-bed configuration with molten salt being used as the coolant. The pebbles are made of TRISO-coated particle fuel. This is explained in Section 13.3.8. The other configuration is the fluid-fueled MSBR. This portion of the chapter will describe Indian R&D efforts for the development of the IMSBR.

15.5.1 Conceptual designs of IMSBR

To arrive at the conceptual design, some of the design guidelines that are being followed include self-sustainability in the ^{233}U-Th cycle, enhanced and inherently safe designs, no use of beryllium and beryllium-based salts to avoid chemical toxicity,



Figure 15.23 SOdium-Fuel Interaction Facility (SOFI): Facility for molten fuel interaction studies.

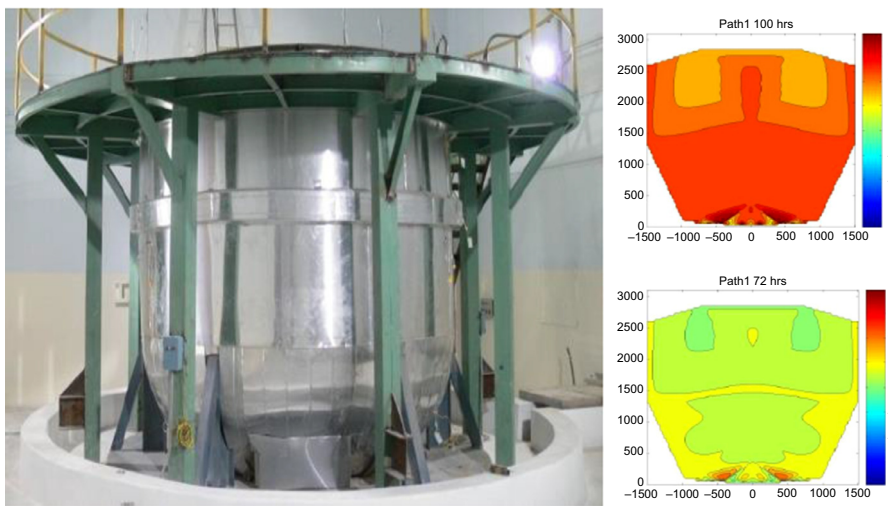


Figure 15.24 Postaccident Thermal Hydraulics Facility (PATH) for postaccident heat removal studies.

minimal waste generation and hence avoidance of the use of graphite, and the ability to replace in-core components. The IMSBR has a fuel salt and a blanket salt in the fluid form. These are made to flow through heat exchangers for ultimately transferring the high-temperature heat to the supercritical CO_2-based Brayton cycle for power generation, which can produce electricity at an efficiency of approximately 45%. Currently

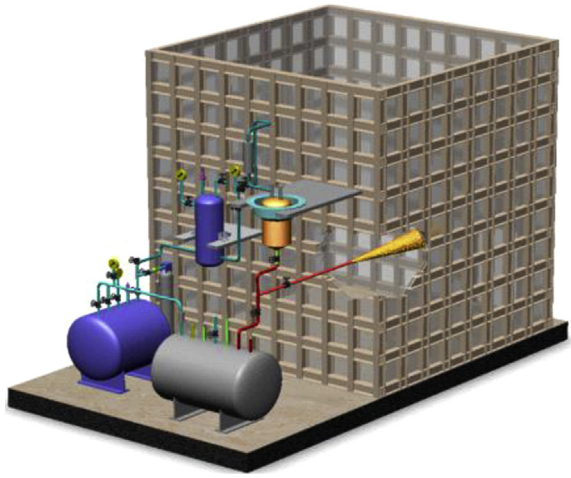


Figure 15.25 MINI Sodium Fire Facility (MINA): Facility for the sodium fire studies.

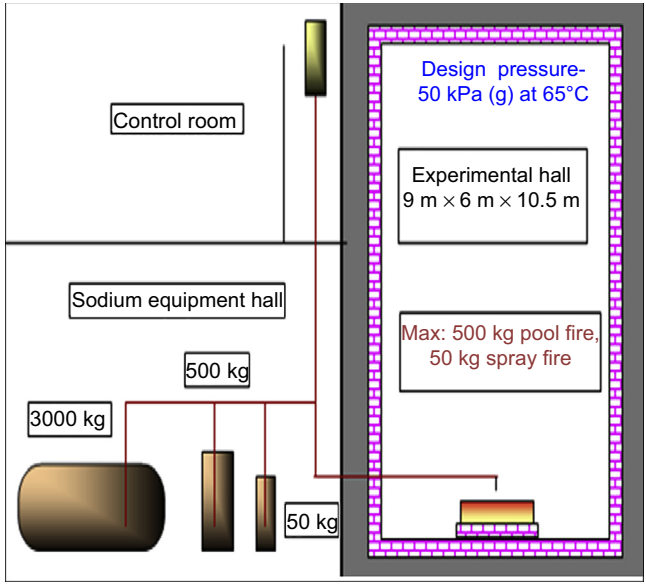


Figure 15.26 Sodium Fire Experimental Facility (SFEF): Facility for large-scale sodium fire studies.

two concepts (one loop type and another pool type) of 850 MW_e IMSBR are being established. In parallel, the design of a small-power (5 MW_{th}) technology demonstrator reactor is also being established. A schematic of the reactor is shown in Fig. 15.29, and the component layout for the pool-type concept-based reactor is shown in Fig. 15.30. The use of fluid fuel allows for removal of neutron-absorbing products

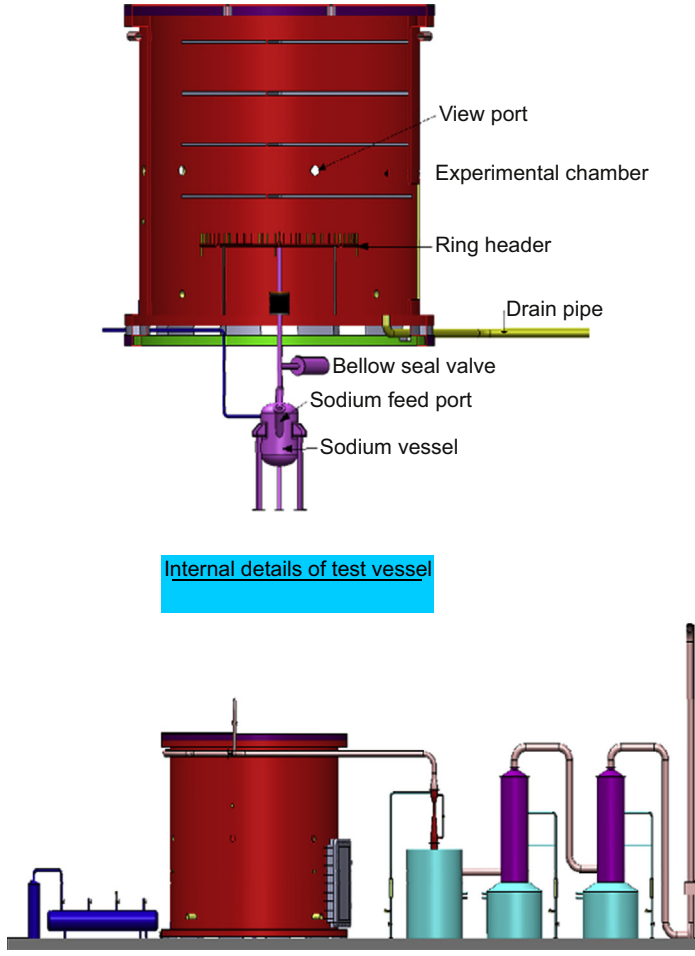


Figure 15.27 SOdium CAble Interaction Facility (SOCA): Facility for simulating sodium fire scenario at the top shield.

almost as soon as they are formed, allowing for efficient utilization of nuclear materials. The ^{233}Pa removed is allowed to decay to ^{233}U and is re-introduced into the reactor. The major design parameters of the IMSBR are shown in Table 15.5.

15.5.2 Design challenges

Some of the major challenges in which R&D has been initiated include

1. Modification of existing codes for reactor physics analysis with the capability to couple neutronics and thermal hydraulics and account for the online reprocessing system;
2. Thermal hydraulic and material compatibility studies for molten salts;
3. Large-scale salt preparation, purification, and characterization;

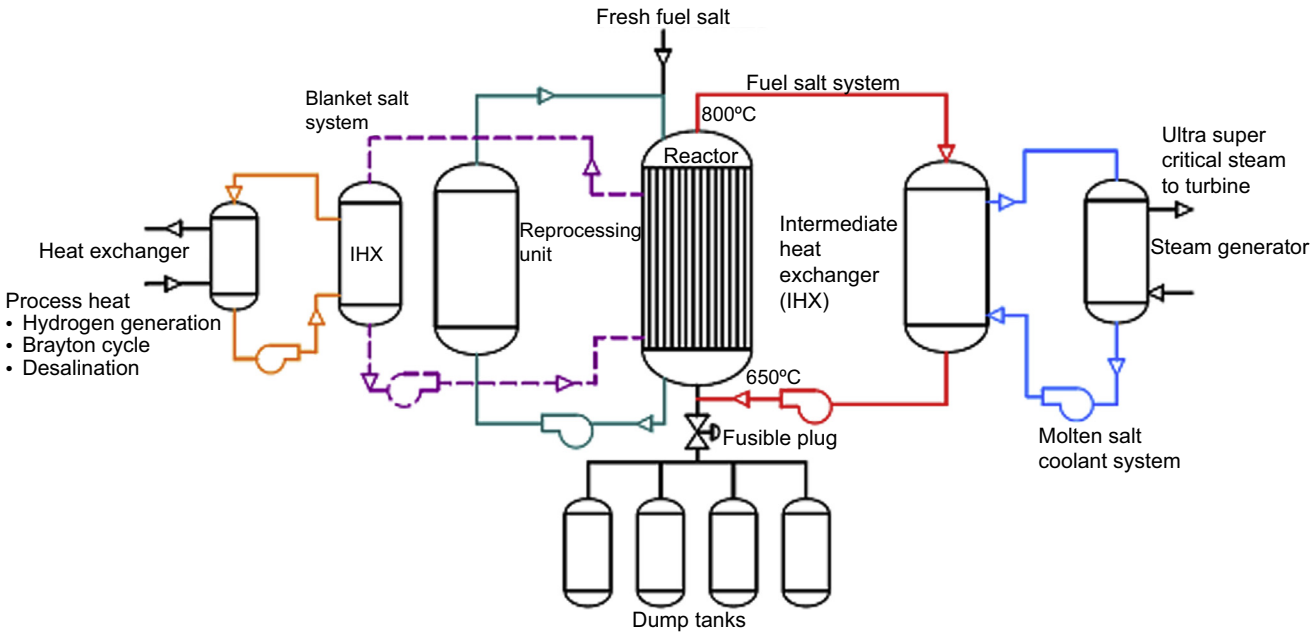


Figure 15.28 Schematic of Indian molten salt breeder reactor.

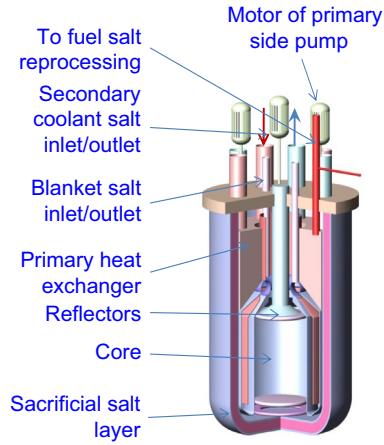


Figure 15.29 Pool-type Indian molten salt breeder reactor.

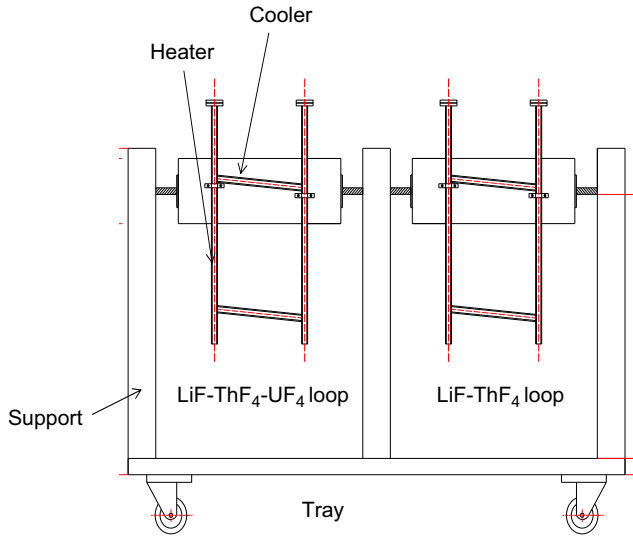


Figure 15.30 Schematic of the test facilities for a molten salt reactor.

4. Development of structural materials and qualification to meet codes and design rules;
5. Online and batch-mode offline reprocessing, without cooling of fuel salt;
6. Instrumentation for operation at high-temperature, active molten salt environment;
7. Online chemistry control techniques for salts as well as tritium capture; and
8. Development of components for high-efficiency supercritical CO_2-based power cycle.

Currently, in addition to performing fundamental studies on various salts, facilities for natural-circulation–based thermal hydraulic studies and corrosion studies under an active molten salt (using ThF_4 and natural UF_4) environment are being commissioned. A schematic of the same is shown in Fig. 15.31.

Table 15.5 Indian molten salt breeder reactor: proposed design and operating parameters

Attributes	Design parameters
Power	850 MW_e
Thermal efficiency	45%
Active core diameter/height	2/2.05 m
Core inlet/outlet	700/800°C
Fuel salt	$LiF\text{-}ThF_4\text{-}UF_4$
Blanket salt	$LiF\text{-}ThF_4$
Secondary salt	$LiF\text{-}KF\text{-}AlF_3$
Flow rate (primary)	10.9 t/s
Flow rate (secondary)	6.3 t/s
Velocity (core)	0.85 m/s
Fuel salt inventory (total)	41.1 t (2.7 t of ^{233}U)
Pumping power	5.4 MW (at 90% efficiency)
Power production system	Based on supercritical CO_2 Brayton cycle

15.5.3 Research and development activities

For the IMSBR development, all technologies have been either initiated or are being initiated. In parallel, a conceptual design of a 5-MW_{th} IMSBR is being worked out. To perform technology development for various technologies related to salts, materials, components, and power conversion systems, a Molten Salt Breeder Reactor Development Facility (MSBRDF) has been planned at the new BARC campus in the southern Indian city of Visakhapatnam.

15.6 Conclusions

Nuclear power is essential for India to meet its ambitious energy targets on the near- and long-term horizons. Introduction of innovative reactors involving thermal and fast neutron spectrums and various coolants such as water, gas, sodium, lead, and lead bismuth alloys as well as completion of R&D is the current focus of the DAE. The excellent operating experience of water reactors in the commercial domains and the FBTR, the commissioning of the PFBR, the robust roadmap for the rapid introduction of FBRs with metallic fuel, and the introduction of AHWRs and MSRs at the appropriate time to effectively utilize the vast thorium resources provide motivation and confidence to realize the targets. The reactor types developed would have several features to demonstrate economic competitiveness and enhanced safety acceptable to designers, regulators, and the public.

Development of energy systems will be largely governed by economic and environmental considerations. Relevant scientific breakthroughs and deployment of innovative technologies for meeting the challenges of long-term energy sustainability has to be the mantra for success.

Nomenclature

AHWR	Advanced heavy water reactor
AMD	Atomic minerals directorate
ATWS	Anticipated transient without scram
BARC	Bhabha Atomic Research Center
BCRs	Burn-up compensation rods
CDA	Core disruptive accident
CHTR	Compact high-temperature reactor
CSRDM	Control and safety rods in their drive mechanisms
DAE	Department of Atomic Energy
DBA	Design-basis accident
DBE	Design-basis events
DC	Dump condenser
DEC	Design extension condition
DHR	Decay heat removal
DSRDM	Diverse shutdown rod drive mechanisms
ECCS	Emergency core cooling system
FBR	Fast breeder reactor
GDWP	Gravity driven water pool
HTR	High-temperature reactor
IGCAR	Indira Gandhi Center for Atomic Research
IHTR	Innovative high-temperature reactor
IMSBR	Indian molten salt breeder reactor
ISI	In-service inspection
KWh	Kilowatt-hour
LBE	Lead-bismuth eutectic
LEU	Low-enriched uranium
LHR	Linear heat rating

Continued

LOCA	Loss of coolant accident
LSBO	Long station blackout
MHT	Main heat transport
MINA	MINI sodium fire facility
MSBRDF	Molten salt breeder reactor development facility
MWd/t	Megawatt day per ton
MW_e	Megawatt electrical
MW_{th}	Megawatt thermal
OGDHR	Operating-grade decay heat removal
PARCs	Passive autocatalytic re-combiners
PARTH	Proving advanced reactor thermal hydraulics
PATH	Postaccident thermal hydraulics facility
PEC	Practically eliminated condition
PPIS	Passive poison injection system
RY	Reactor per year
SA	Subassemblies
SDS	Shut-down system
SFEF	Sodium fire experimental facility
SG	Steam generator
SOCA	SOdium CAble interaction facility
SOFI	SOdium-Fuel Interaction facility
SSDHR	Secondary sodium decay heat removal
TG	Turbogenerator
USD	Ultimate shut-down

Reference

Integrated Energy Policy, Planning Commission, Government of India, 2006.

Bibliography

AHWR

Anantharaman, K., Ramanujam, A., Kamath, H.S., Majumdar, S., Vaidya, V.N., 2000. Thorium based fuel reprocessing & re-fabrication technologies and strategies, INSAC-2000. In: Annual Conference of the Indian Nuclear Society (Proc. of Annual Conf., Mumbai).

Anantharaman, K., Shivakumar, V., Saha, D., December 15, 2008. Utilisation of thorium in reactors. Journal of Nuclear Materials 383 (1–2), 119–121.

Hari Prasad, M., Gera, B., Thangamani, I., Rastogi, R., Gopika, V., Verma, V., Mukhopadhyay, D., Bhasin, V., Chatterjee, B., Sanyasi Rao, V.V.S., Lele, H.G., Ghosh, A.K., August 2011. Level-1, -2 and -3 PSA for AHWR. Nuclear Engineering and Design 241 (8), 3256–3269.

IAEA-TECDOC-1485, 2005. Status of Innovative Small and Medium Sized Reactor Designs, pp. 357–378.

Jain, V., Nayak, A.K., Dhiman, M., Kulkarni, P.P., Vijayan, P.K., Vaze, K.K., October 2013. Role of passive safety features in prevention and mitigation of severe plant conditions in Indian advanced heavy water reactor. Nuclear Engineering and Technology 45 (5), 625–636.

Sapra, M.K., Kundu, S., Pal, A.K., Vijayan, P.K., Vaze, K.K., Sinha, R.K., May 2015. Design and development of innovative passive valves for Nuclear Power Plant applications. Nuclear Engineering and Design 286, 195–204.

Sinha, R.K., Kakodkar, A., April 2006. Design and development of the AHWR—the Indian thorium fuelled innovative nuclear reactor. Nuclear Engineering and Design 236 (7–8), 683–700.

Sinha, R.K., 2011. Advanced nuclear reactor systems – an Indian perspective. Energy Procedia 7, 34–50.

HTRs

Basak, A., Dulera, I.V., Vijayan, P.K., 2011. Design of high temperature heat pipes and thermosiphons for compact high temperature reactor (CHTR). In: Proceedings of the 21st National & 10th ISHMT-ASME Heat and Mass Transfer Conference, December 27–30, IIT Madras, India.

Basak, A., Dulera, I.V., Vijayan, P.K., November 2012. An approach for graphite component design for nuclear reactors. In: National Conference on Carbon Materials 2012, Mumbai.

Borgohain, A., Maheshwari, N.K., Vijayan, P.K., Sinha, R.K., May 11–15, 2008. Heat transfer studies on lead-bismuth eutectic flows in circular tubes. In: Proceedings of 16th International Conference on Nuclear Engineering (ICONE), Orlando, Florida.

Dulera, I.V., Sinha, R.K., 2008. High temperature reactors. Journal of Nuclear Materials 383, 183–188.

Kanse, D., Khan, I.A., Bhasin, V., Vaze, K.K., November 2012. Micro-mechanical studies on graphite strength prediction models. In: National Conference on Carbon Materials 2012, Mumbai.

Mollick, P.K., Venugopalan, R., Roy, M., Rao, P.T., Sathiyamoorthy, D., 2012. Characterisation of buffer pyrolytic carbon of TRISO coated particle developed in hot spouted bed. In: National Conference on Carbon Materials 2012, November 2012, Mumbai.

Sinha, R.K., Dulera, I.V., October 2010. Carbon based materials – applications. In: High Temperature Nuclear Reactors, First Asian Carbon Conference (FACC 2009). 25th–27th November 2009, Indian Habitat Center, New Delhi, India. Indian Journal of Engineering and Material Sciences, 17, 321–326.

Tewari, R., Vishwanadh, B., Srivastava, D., Dey, G.K., Vaibhav, K., Jha, S.K., Mirji, K.V., Prakash, B., Saibaba, N., 2011. Development of Nb-1% Zr-0.1%C Alloy as Structural Components for CHTR. BARC. Report- BARC/2011/E/020.

FBRs

Chellapandi, P., Kumar, P., June 10–11, 2014. Implementation of practical elimination, DEC and sodium voiding effects for the future SFRs: Indian approach. In: 4th Joint IAEA-GIF Technical Meeting/Workshop on Safety of Sodium-Cooled Fast Reactors.

Chellapandi, P., Puthiyavinayagam, P., Balasubramaniyan, V., Ragupathy, S., Rajan Babu, V., Chetal, S.C., Raj, B., 2010. Design concepts for reactor assembly components of 500 MW_e future SFRs. Nuclear Engineering International 240, 2948–2956.

Chellapandi, P., June 10–11, 2014. Assessment of safety criteria of Indian SFR with respect to international scenarios. In: 4th Joint IAEA-GIF Technical Meeting/Workshop on Safety of Sodium-Cooled Fast Reactors.

Chellapandi, P., June 23–24, 2015. Enhanced safety features of FBR 1 & 2 with respect to PFBR and Gen-IV reactors. In: Fifth Joint IAEA-GIF Technical Meeting/Workshop on Safety of Sodium-Cooled Fast Reactors. IAEA HQ, Vienna.

Chetal, S.C., Chellapandi, P., Puthiyavinayagam, P., Raghupathy, S., Balasubramaniyan, V., Selvaraj, P., Mohanakrishnan, P., Raj, B., 2009. A perspective on development of future FBRs in India. In: Int. Conference on Fast Reactors and Related Fuel Cycles: Challenges and Opportunities (FR09), Kyoto, Japan.

MSBR

Dulera, I.V., Vijayan, P.K., Sinha, R.K., January 9–11, 2013. Indian programme on Molten salt cooled nuclear reactor. In: Conference on Molten Salts in Nuclear Technology. Bhabha Atomic Research Centre, Mumbai.

Vijayan, P.K., Basak, A., Dulera, I.V., Vaze, K.K., Basu, S., Sinha, R.K., 2015. Conceptual Design of Indian Molten Salt Breeder Reactor. Pramana - Journal of Physics, Indian Academy of Sciences.

Part Three

Related topics to Generation IV nuclear reactor concepts

Preface to Part Three

Part Three presents key related topics essential to the design, development, deployment, and acceptance of the Generation IV and advanced nuclear reactor concepts, which include the safety of advanced reactors, nonproliferation for advanced reactors (political and social aspects), thermal aspects of conventional and alternative fuels, hydrogen co-generation with Generation IV nuclear power plants, and advanced small modular reactors. Correspondingly, Part Three consists of five chapters (Chapters 16–20) written by top international experts working within these areas.

The safety of advanced reactors

16

R.B. Duffey[1], *D. Hughes*[2]
[1]DSM Associates Inc., Ammon, Idaho Falls, ID, United States; [2]Hughes and Associates, Amsterdam, NY, United States

> *Safeguards must be provided to prevent the use of technology from doing injury to the public health and well-being.*
>
> *Admiral Hyman G. Rickover, Hearings before the Joint Committee on Atomic Energy, 91st Congress, Second Session, March 19–20, 1970, p. 101, Washington, DC, USA*

16.1 Basic safety principles

In this chapter we review and describe the safety of new reactors, including the state of the art and challenges in analysis and testing. As pointed out long ago, safeguards must be provided against the hazards of new technology doing injury to any and all aspects of natural resources, vital services, and the entire human environment (Rickover, 1970, p. 96).

In this chapter the term *advanced reactors* (ARs) includes any that are different in design or concept from those currently licensed and commercially available. For technologically innovative and socially desirable reasons, it is generally agreed that new reactors, whatever their generation of design or operating principles, should be safer than any currently deployed. This has been particularly emphasized by the Fukushima reactor meltdowns, which were unexpected and caused significant social concern and political disruption in Japan and worldwide.

This core meltdown is, and was caused by, a rare event: a seismically induced tsunami of immense proportions that caused loss of almost all power and control. Thus the initiating event lay outside of the safety analysis envelope of what had been considered at the design stage, beyond the "design basis" of what had been considered for safety margin, and system and structural design and was more severe than considered in risk assessments for natural hazards.

16.2 Safety and reliability goals

The top-level safety requirements for new reactor concepts have been stated and internationally agreed upon by the Generation IV International Forum (GIF)

Handbook of Generation IV Nuclear Reactors. http://dx.doi.org/10.1016/B978-0-08-100149-3.00016-1
Copyright © 2016 Elsevier Ltd. All rights reserved.

(Kelly, 2014). These requirements are essentially applicable to all ARs and are given as:

1. Excel in safety and reliability,
2. Have a very low likelihood and degree of reactor core damage, and
3. Eliminate the need for off-site emergency response.

Although these aims are splendid and desirable, the safety of any new system is still subject to interesting and known questions:

- What are the actual detailed safety requirements?
- How is safety to be analyzed?
- What scenarios or accidents are to be included?
- What is a "low likelihood or degree"?
- What are the uncertainties?
- How is new technology to be licensed?
- How to respond to accidents if no response is needed?
- What is or is not an acceptable risk?

New concepts for ARs come in many different forms and are called many different names by their proponents and developers. Some basic designs, such as the many liquid-metal-cooled fast reactors, water-cooled supercritical systems, and helium-cooled high-temperature reactors, even date back 60 or more years. Many prototypes and demonstration plants were both built and operated, sometimes as part of military-related activities for nuclear propulsion and weapons material production. This plethora of acronym and naming now includes the GIF systems, small medium and/or modular reactors (SMRs), and many types and variants of ARs. The historical nomenclature has come about largely for programmatic, funding, and commercial development reasons, with varying degrees and claims for improved, passive, enhanced, inherent, and/or super safety. Fortunately, from a purely nuclear safety perspective, the issues are entirely generic and depend on establishing the chance of

- Uncontrolled events that challenge the design,
- Extensive economic and/or social damage, and/or
- Potential or actual release of radionuclides.

The basic overarching and most important Safety Objective (SO) is to keep the reactor core cooled and controlled at all times (ASME, 2012, p. 32; Howlett, 1995, p. 5) and, if not, to be able to limit and/or manage the consequences without causing undue or unacceptable risk to the public. After all, if the reactor is not controlled and cooled, then the core could melt and/or release radioactivity, which is undesirable physically and financially, wrecking the plant and the investment. The plethora of subsidiary goals, rules, criteria, assessments, regulations, and analyses are all aimed at demonstrating or supporting the achievement of this fundamental SO by a combination of design, back-up systems, and emergency measures and procedures coupled with extensive safety, risk, and structural analysis.

Licensing procedures and processes to establish the public risk also vary by country and jurisdiction, but they are simply a formal means to establish the degree of belief and justification for the chance, using safety analysis reports, methods, assessments,

reviews, or claims. The degree of detail and the exact approach adopted or expected by regulatory authorities vary widely, and today they are often specific to the country and site.

16.2.1 Subsidiary safety requirements and licensing review

The subsidiary safety requirements flowing from this fundamental objective have been promulgated as legally enforceable safety and design criteria. For example, the licensing process for new reactors in the United States is regulated under the Code of Federal Regulations (U.S. NRC, 2004). These rules provide a process for establishing a standard or "certified" design basis and require a "safety analysis report (that) describes the plant's final design, safety evaluation, operational limits, anticipated response of the plant to postulated accidents, and plans for coping with emergencies" that is used for the purposes of formal safety analysis and review.

In such design and licensing review cases, all means available and possible as sources of water and cooling are invoked for cooling purposes, including safety, nonsafety, back-up, and emergency systems. Events that are "beyond" or challenge the design basis, or were previously labeled "incredible" or "hypothetical," are now called "severe accidents" or "extended conditions." The design and operation may also be subject to "stress tests," additional measures, layered safety systems, and extensive emergency responses.

The most relevant, current, and publically available set of subsidiary safety requirements for evaluating an AR are those used for the recent review of the economic simplified boiling water reactor (ESBWR), the largest passively cooled reactor that has undergone the full licensing process. The ESBWR is more than 1200 MW_{el} and uses natural circulation of water for cooling (see Fig. 16.1).

The US Nuclear Regulatory Commission (NRC) Safety Evaluation Report (U.S. NRC, 2014) gives the criteria for risk assessment based on core damage frequency and the time scales for the use of safety and nonsafety systems, as derived from a full-scope Probabilistic Risk Assessment (PRA) analysis (Bhatt and Wachowiak, 2006). This NRC approach states the safety guidelines as follows:

> First, the focused PRA maintains the same scope of initiating events and their frequencies as that identified in the baseline ESBWR PRA. As a result, non-safety-related Structures, Systems and Components (SSCs) used to prevent the occurrence of initiating events will be subject to regulatory oversight commensurate with their Reliability/Availability (R/A) missions. Second, following an initiating event, the event tree logic of the comprehensive, Level three focused PRA will not include the effects of non-safety-related standby SSCs. This will allow the Combined Operating License (COL) applicant to determine whether the passive safety systems, when challenged, can provide sufficient capability (without non-safety-related back-up) to meet the NRC safety goal guidelines for a Cumulative Damage Function (CDF) of less than 1×10^{-4} per reactor year and for an Large Release Frequency (LRF) of less than 1×10^{-6} per reactor year.
>
> The design certification applicant will also evaluate the containment performance, including bypass, during a severe accident (SA). If the design certification applicant determines that nonsafety-related SSCs must be added to the focused PRA model to meet the safety goals, then these SSCs will be subject to regulatory oversight based on their risk significance.

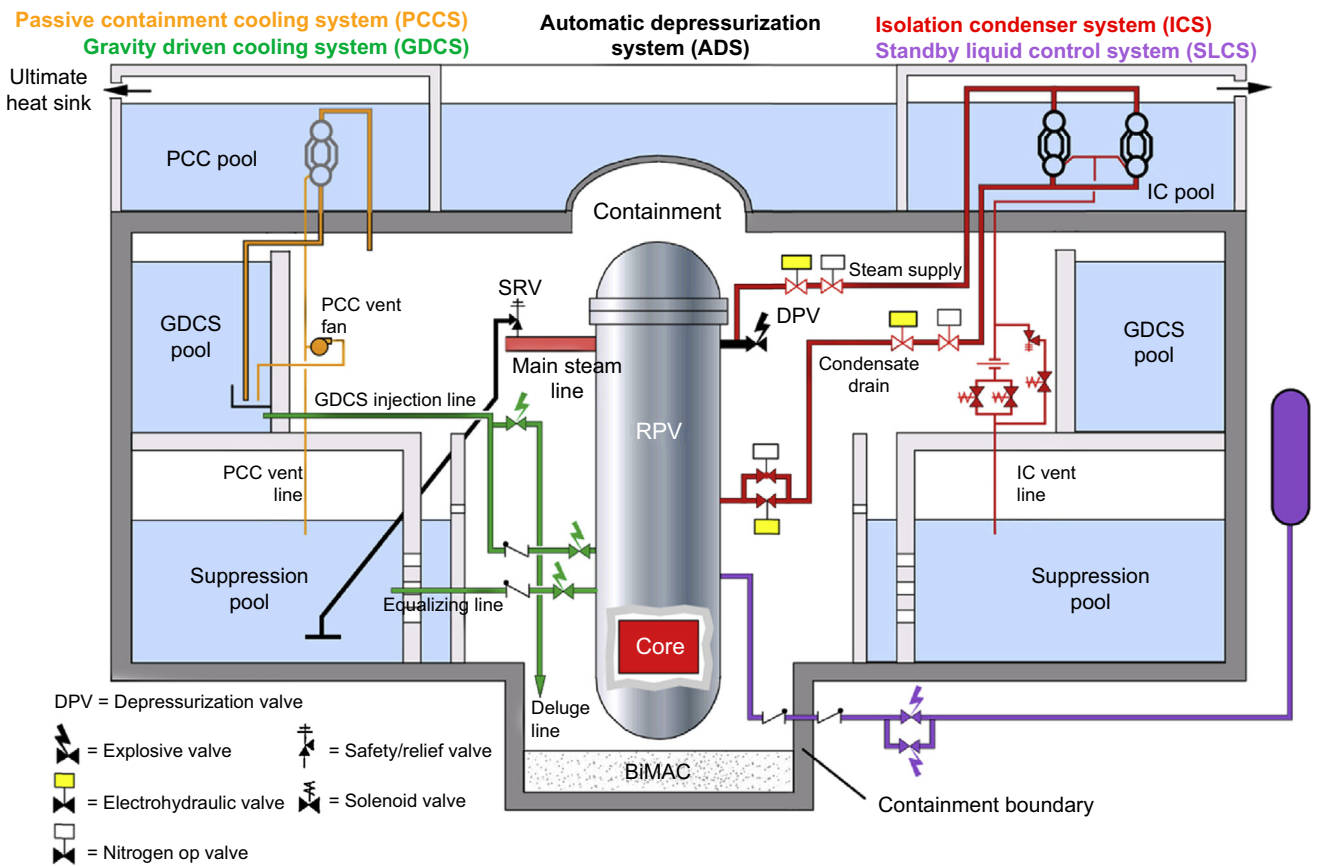


Figure 16.1 Schematic of economic simplified boiling water reactor with many different cooling systems (Saha et al., 2013). *DPV*, Depressurization Valve; *IC*, Isolation Condenser; *SRV*, Safety Relief Valve; *PCC*, Passive Containment Cooling; *RPV*, Reactor Pressure Vessel; *BiMAC*, Basemat Internal Melt Arrest and Coolability (Device)

In addition, because there is a criterion that "SSC functions (are) relied upon to ensure long-term safety (beyond 72 h) and to address seismic events….," and it is also required that

> *….the design certification applicant will use PRA insights, sensitivity studies, and deterministic methods to establish the ability of the design to maintain core cooling and containment integrity beyond 72 hours. Non-safety-related SSCs that are required to meet deterministic regulatory requirements, resolve the long-term safety and seismic issues, and prevent significant adverse systems interactions are subject to regulatory oversight.*
>
> *The staff expects regulatory oversight for all non-safety-related SSCs needed to meet NRC requirements, safety goal guidelines, and containment performance goals, as identified in the focused ESBWR PRA model.*

The requirements for the PRA are then stated as

> *This PRA includes all appropriate internal and external events for both power and shutdown operations. The process also includes adequate treatment of Risk Assessment uncertainties, long-term safety operation, and containment performance. A margins approach is used to evaluate seismic events. In addressing containment performance, the PRA considers the sensitivities and uncertainties in accident progression, as well as the inclusion of severe accident phenomena, including the explicit treatment of containment bypass. The PRA uses mean values to determine the availability of passive systems and the frequencies of core damage and large releases. The process estimates the magnitude of potential variations in these parameters and identifies significant contributors to these variations using appropriate uncertainty and sensitivity analyses.*

Similar quantified goals exist in other nations for new builds, and some have been promulgated as nominally "technology neutral" (ie, the requirements do not depend on the type of reactor). The safety submission must show that the proposed design is meeting certain overall quantified criteria (CNSC, 2008):

Core Damage Frequency (CDF)
The sum of frequencies of all event sequences that can lead to significant core degradation is less than 10^{-5} per reactor year.
Small Release Frequency (SRF)
The sum of frequencies of all event sequences that can lead to a release to the environment of more than 10^{15} becquerel of iodine-131 is less than 10^{-5} per reactor year. A greater release may require temporary evacuation of the local population.
Large Release Frequency (LRF)
The sum of frequencies of all event sequences that can lead to a release to the environment of more than 10^{14} becquerel of cesium-137 is less than 10^{-6} per reactor year. A greater release may require long-term relocation of the local population.

Despite its apparent simplicity and attractiveness, there are two simple issues with this type of methodology, as follows:

Firstly, the original focus of formal safety case reviews used for all existing designs was on analyzing design-basis transients and accidents, and conducting formalized PRAs that include external events, with the aim of demonstrating a low probability and managing the risk of core damage. The reactor accidents at Fukushima Daiichi demonstrated that the previous safety analyses and estimates were incomplete, overly optimistic, and did not adequately include extreme events, or even address the social consequences and public reaction to such accidents even when little radiation is released and no fatalities are directly attributable (ASME, 2012; Suzuki, 2014).

Secondly, as actual events to date have demonstrated, the nominal 72-h requirement or any such similar interval partly based on subjectively assessing the time scales available for potential emergency response and recovery actions as well as the viability and feasibility of providing back-up power and cooling is likely too short and somewhat arbitrary. Even if emergency measures are "credited" after this time, or require deployment of qualified equipment, there is still a significant and finite probability of not fully restoring needed power for cooling (Duffey and Ha, 2013).

16.2.2 The safety focus for advanced concepts

Current data for reactor accidents illustrate that the actual CDF is higher than predicted, primarily because of the inadequate prevention and control of extreme and unexpected events. Hence, the focus for AR concepts has moved from design-basis accidents (DBAs) to examining SAs, which include core damage; beyond-design−basis accidents (BDBAs), which challenge the safe "operating envelope" and safety systems and barriers; and rare or extreme events (REEs), which render multiple systems inoperable and require core cooling and/or emergency response actions over long time scales.

Hence, the modern safety analysis hierarchy has emerged as follows for the various classes and continuum of potential events:

DBAs: A formal definition of what constitutes the expected structural, seismic, accident, and transient loads and systems that must be "designed into" the system. Demonstrate defense-in-depth (DiD) and operational control by formal attention to structural integrity, engineering design, safety system operation, core physics, and physical barrier performance, and adopting relevant codes, best practices, and engineering standards.

BDBAs and SAs: An "extension" of the events that must be formally considered in safety analysis that takes the design well beyond its normal or limiting operational envelope and contains degradation of systems, components, and structures. Analyze and address weaknesses and inform risk-dominant accidents using probabilistic safety analyses, and develop emergency measures and procedures to manage the safety performance using state-of-the-art computer codes and applicable data.

REEs: A "stress test" of what extremes might evolve that challenge the integrity, coolability, operability, and controllability of the reactor, including consequence mitigation and social impacts. Develop emergency response and equipment measures

for responding to, and managing and coping with, major challenges and damage to entire systems, to minimize the impact and health effects of radioactive releases and avoid or reduce social disruption, and supporting strategic decision-making.

All Risk: Provide independent review and technical assessment of all aspects of analysis, design, construction, operation, licensing, maintenance, and management that impact process safety and challenge and require verification of all claims, decisions, and regulations.

This hierarchy of severity corresponds and aligns closely to adopting the proposed "All Risk" philosophy for reactor safety to "prevent large radioactive releases that could cause major disruption of society" (ASME, 2012, p. 53) and agrees with the original and fundamental Rickover Safeguards Model.

16.2.3 Emerging and new safety design criteria

To formalize these needs and hierarchy for supporting AR design and concept development, a listing of some 83 safety design criteria (SDC) have already been developed by the GIF. This list has evolved from specific considerations derived for the sodium-cooled fast reactor (SFR) but is generically applicable to ARs.

These SDCs are extensive. The full listing and explanation have not been openly published, but the scope and importance can be seen from the information given in a series of international workshops hosted by the International Atomic Energy Agency (IAEA) and are shown in the following list. (Note: Some of the key ones are highlighted in italics for later reference, and the currently publically unavailable criteria are left as deliberately unnumbered gaps.)

Safety Design Criteria: partial listing with edited NRC review comments. (Sofu, 2014; Nakai, 2013; information courtesy of the IAEA, Vienna)

- Criterion 1. Responsibilities in the management of plant design: Applicant shall be responsible for ensuring that the design meets all applicable safety and security requirements.
- Criterion 2. Management system for the plant design: Quality assurance (QA) requirements should extend beyond "design" considerations to address training of personnel, include a corrective action program, and address an inspection and test control program.
- Criterion 3. Safety of the plant design throughout the lifetime of the plant: Applicant should retain QA responsibility for tasks that are assigned to external organizations for design of specific parts.
- Criterion 4. Fundamental safety functions: Topic of "toxic chemicals" should be tied to nuclear safety (and) coolant inventory control should be a safety function.
- Criterion 5. Radiation protection: Use of As Low As Reasonably Achievable (ALARA) principle and acceptable dose limits for operational states and accident conditions.
- Criterion 6. Design for a nuclear power plant: Should minimize contamination of the facility. Reliance on passive systems or inherent features to perform fundamental safety functions should be emphasized. Design-basis threats (DBTs) should be included in the scope.
- Criterion 7. Application of DiD: Definition of events outside of established safety envelope should include DBTs. DiD (per IAEA definition) is a key element of safety philosophy but not a regulatory requirement in the United States.
- Criterion 8. Interfaces of safety with security and safeguards.

- Criterion 9. Proven engineering practices: Scope to address materials selection, fabrication, installation, examination, and testing.
- Criterion 10. Safety assessment: Definition of events outside of established safety envelope should include DBTs (and) include a QA provision for safety assessments and extended to include operational phase (not just design phase) to cover the changes in design.
- Criterion 11. Provision for construction: "Design" definition to include manufacturing, construction, assembly, and installation.
- Criterion 12. Features to facilitate waste management and decommissioning: Rad-waste minimization provision should be included.
- Criterion 14. Design basis for items important to safety: Definition of events outside of established safety envelope should include DBTs.
- Criterion 16. Postulated initiating events: Reliance on manual initiation of systems instead of automatic action to mitigate the response to an initiating event is allowed only in a limited number of circumstances (eg, fire protection) and definition of events outside of established safety envelope should include DBTs.
- Criterion 19. DBAs: No guidance in the United States on evaluation of DBAs using best-estimate methods including uncertainty; new criteria may be needed to delineate the design-basis sodium accidents for SFRs.
- Criterion 20. Design extension conditions: Limited set of events more severe than DBAs [station blackout, anticipated transients without scram (ATWS), aircraft impact, etc.] for "design extension" requirements. *The design shall be such that design extension conditions that could lead to significant radioactive releases are practically eliminated*.
- Criterion 21. Physical separation and independence of safety systems: Separation and independence should apply in providing DiD for the design of a physical protection system.
- Criterion 23. Reliability of items important to safety: Include the design of a physical protection system.
- Criterion 25. Single failure criterion: Design of a physical protection system should prevent a single failure that will render the security function ineffective or unavailable.
- Criterion 29. Calibration, testing, maintenance, repair, replacement, inspection, and monitoring of items important to safety: Include physical security systems; worker exposures should be ALARA (not just below specified limits).
- Criterion 31. Aging management: Provision should be made for providing adequate space in the facility to facilitate removal and repair/replacement of aging mechanisms/components.
- Criterion 32. Design for optimal operator performance: Include design of a physical protection system; qualification of personnel and considerations essential to ensure that operators can perform the functions associated with safe plant control (training and human performance trending) should be addressed.
- Criterion 33. Sharing of safety systems between multiple units of a nuclear power plant: Shall not be shared between multiple units unless this contributes to enhanced safety; it can be shown that such sharing will not significantly impair their ability to perform their safety functions, including, in the event of an accident in one unit, an orderly shutdown and cool down of the remaining units.
- Criterion 34. Systems containing fissile material or radioactive material: Should extend to facilitate physical protection of systems, including cybersecurity, to protect against radiological sabotage and the safeguards of special nuclear material from theft and diversion.
- Criterion 37. Communication systems at the plant: Reliability of communication should be required for use after all postulated initiating events and in accident conditions, including applicable DBTs.

- Criterion 38. Control of access to the plant: Specific physical access control measures should include those necessary for detecting, assessing, and delaying insider threats for systems and equipment designated as vital.
- Criterion 42. Safety analysis of the plant design: Anticipated operational occurrences (AOOs) and DBAs are evaluated in the safety analysis and include design of a physical protection system to protect against malevolent acts.
- Criterion 43. Performance of fuel elements and assemblies: Specified acceptable fuel design limits should not be violated for AOOs.
- Criterion 44. Structural capability of the reactor core: Addresses only internal events. Fuel assemblies are considered important to safety and therefore must accomplish their safety functions, allowing reactor shutdown and maintaining a coolable geometry, under internal and external DBA events.
- Criterion 45. *Control of the reactor core*: *The reactor core should have prompt inherent nuclear feedback characteristics to compensate for rapid reactivity insertions*.
- Criterion 46. Reactor shutdown: Implies the specified design limits for the fuel are not exceeded for AOOs.
- Criterion 50. Cleanup of reactor coolant: Introduction of chemicals should be addressed in a manner tied to nuclear safety and radiological risk and should address chemical protection.
- Criterion 54. Containment system for the reactor: Should specifically include "internal events" and address the question of "confinement" versus traditional use of "containment."
- Criterion 55. Control of radioactive releases from the containment: Require that leak rate testing be performed at design-basis pressures.
- Criterion 56. Isolation of the containment: Inconsistent with GDC 56, which states that check valves cannot be used as the automatic isolation valve outside of containment.
- Criterion 58. *Control of containment conditions: Containment is designed to withstand the worst DBA and/or SA conditions*.
- Criterion 61: Protection system: Protection system independence should consist of independent trains such that a single failure would not prevent the protective action.
- Criterion 66. Supplementary control room: Requirements for the control room should also apply to the supplementary control room.
- Criterion 71. Process sampling systems and postaccident sampling systems: Process sampling systems and postaccident sampling systems shall be designed so that the dose to an operator taking samples from these systems is ALARA.
- Criterion 75. Lighting systems: Redundant or extended service lamps should be used in high-radiation areas to maintain personnel exposures ALARA by reducing the frequency of lighting replacement. Design features should be provided to permit the servicing of lighting from lower radiation areas.
- Criterion 80. Fuel handling and storage systems: Fuel handling and storage systems for irradiated and nonirradiated fuel shall be designed to maintain doses to operators ALARA.
- Criterion 81. Design for radiation protection: The plant layout should be designed to minimize exposures and contamination of operating personnel by controlling access to areas with radiation hazards and areas of possible contamination. Ventilation systems shall be designed to minimize personnel exposures and control the spread of contamination.
- Criterion 82: Means of radiation monitoring: Facilities should be provided near the monitors for decontamination of contaminated personnel or equipment.

16.2.4 The safety goal and objective of "practical elimination"

A key point emerges. It is impossible for any design to survive extreme events such as a meteor impact, a major military attack, or the disintegration of society due to events such as political upheavals, "regime change," or massive supervolcanic eruptions, among others.

So within the confines of what is considered by reasoning and logic as feasible and necessary, any inherent issues in the design can be addressed so that the effects and consequences are minimized and controlled. In addition, it is well known that claiming or deriving small values of core damage frequencies or LRF, using current Probabilistic Safety Assessment (PSA)/PRA methods, leads to unreasonably low and basically unprovable numbers. It also leads to a subjective decision on what is or may be a lower bound or cutoff for event sequence frequency, and claims of calculating even a CDF of approximately 10^{-8} or less have been made, despite lack of data and the large uncertainty.

In part, these somewhat misleading low frequencies with large uncertainties have arisen because the initiating event frequencies and subsequent actions themselves are highly uncertain. These uncertainties are particularly important for the safety of ARs (eg, in potentially large seismic events; U.S. 1997; EPRI, U.S. DOE and U.S. NRC, 2012; TEPCO, 2012, p. 437 et seq.), but also because of the overwhelming role of human error and of improper organizational decision-making in all known accidents (Reason, 1997; Duffey and Saull, 2008), which contribution is also poorly represented, inadequately modeled, and often underestimated.

These difficulties, and the potentially large consequences and design implications, have led to the concept of "practical elimination," as italicized for emphasis in Criterion 20 and featured in Criterion 45.

The stated goal and concept of practical elimination (Dudour and Carluec, 2011; with italic emphasis added).

Mitigation of the consequences of some accident situation must be excluded by design:

- Either because implementation of mitigation devices is not reasonably feasible,
- Or, because the R&D to be developed for demonstrating their efficiency is not reasonably feasible.
- *The first design objective is to make such situations physically impossible*.
- In compliance with DiD, "practical elimination" is acceptable only for a limited number of very well identified situations.

The "practical elimination" of some accident situation requires implementation of independent reliable design features and a robust demonstration of their efficiency, for example:

- Combination of active and passive systems,
- Inherent characteristics, and
- Operating procedures for verifying efficiency of protection devices (eg, needs in-service inspection).

For implementing such an objective, principles for setting up a demonstration of practical elimination have been expounded (Okano, 2014) as follows and are

consistent with the coupled deterministic and probabilistic safety approaches previously given:

- Demonstration is made on a case-by-case approach
- Deterministic basis, supplemented by probabilistic studies
- General principles for deterministic demonstration:
  - Look for complete list of Practical Elimination situations
  - Introduce provisions to mitigate the consequences of initiating event
- Emphasis should be placed on:
  - Prevention of situations leading to "cliff edge effects"
  - Efficiency and reliability of mitigating provisions cover a wider domain
  - Less sensitive to common mode failure
- Probabilistic studies
  - To ensure completeness and to establish expected frequency

Whether and how such approaches, the concepts of which there are many candidates and proposals, are possible is the subject of current development and is specific to each AR.

16.3 Safety objectives and the classification of advanced reactor types

There is no global or international consensus on the details of nomenclature, safety criteria, or licensing methods for new concepts and designs. Given that it is not possible to cover or foresee all future possibilities or variations in design and principles, the task is how to ensure some uniformity of approach toward meeting some agreed-upon high-level safety goals. The important GIF effort has provided a common forum for such discussions, as have the efforts of some nuclear regulators to "harmonize" their differing approaches without relinquishing their statutory national regulatory authority. These efforts have resulted in so-called Safety Reference Levels (SRLs), which for existing reactors are summarized elsewhere (WENRA, 2014). For the new or ARs of interest here, there are seven high-level SOs promulgated and listed as follows (WENRA, 2009), with "SO" and italics added for clarity:

SO1. Normal operation, abnormal events, and prevention of accidents

- Reducing the frequencies of abnormal events by enhancing plant capability to stay within normal operation.
- Reducing the potential for escalation to accident situations by enhancing plant capability to control abnormal events.

SO2. Accidents without core melt

- Ensuring that accidents without core melt induce no offsite radiological impact or only minor radiological impact (in particular, no necessity of iodine prophylaxis, sheltering, or evacuation).
- Reducing, as far as reasonably achievable, the core damage frequency, taking into account all types of hazards and failures and combinations of events, and the releases of radioactive material from all sources, providing due consideration to siting and design to reduce the impact of all external hazards and malevolent acts.

SO3. Accidents with core melt

- Reducing potential radioactive releases to the environment from accidents with core melt, also in the long term, by following the qualitative criteria:
  Accidents with core melt that would lead to early or large releases must be practically eliminated; for accidents with core melt that have not been practically eliminated, design provisions have to be taken so that only limited protective measures in area and time are needed for the public (no permanent relocation, no need for emergency evacuation outside of the immediate vicinity of the plant, limited sheltering, no long-term restrictions in food consumption) and that sufficient time is available to implement these measures.

SO4. Independence between all levels of defense-in-depth

- Enhancing the effectiveness of the independence between all levels of DiD, in particular through diversity provisions (in addition to the strengthening of each of these levels separately as addressed in the previous three objectives) to provide, as far as reasonably achievable, an overall reinforcement of DiD.

SO5. Safety and security interfaces

- Ensuring that safety measures and security measures are designed and implemented in an integrated manner. Synergies between safety and security enhancements should be sought.

SO6. Radiation protection and waste management

- Reducing as far as reasonably achievable by design provisions, for all operating states, decommissioning and dismantling activities, individual and collective doses for workers, radioactive and nonradioactive discharges to the environment, and quantity and activity of radioactive waste.

SO7. Management of safety

- Ensuring effective management of safety from the design stage. This implies that the licensee establishes effective leadership and management of safety over the entire new plant project and has sufficient in-house technical and financial resources to fulfill its prime responsibility in safety; ensures that all other organizations involved in siting, design, construction, commissioning, operation, and decommissioning of new reactors demonstrate awareness among the staff of the nuclear safety issues associated with their work and their role in ensuring safety.

We can all agree to these ideals. These are all fine words and with noble intent, but they still mask the complexities of reality, and they do not reflect that safety is actually and in practice (as amply demonstrated by Fukushima and most industrial accidents) the responsibility of the operator/owner of the plant, not the regulator. The regulatory process, whatever it is and wherever it occurs, simply ultimately grants a license that sets minimum standards or expectations for compliance by the owner and operator, as all such rules and regulations are intended to do. Requiring and undertaking periodic safety reviews, audits and inspections of operations, desirable and necessary as they may be, cannot and must not be a substitute for the designer and operator to relentlessly improve safety experience, knowledge, skill, awareness, training, and commitment.

Setting aside for the moment the inevitable variability in design detail and in implementation, we can conveniently group the various Generation IV (Gen IV), SMR, and AR concepts simply according to the medium utilized and needed for cooling the primary reactor. These three media are water (Class W: water reactors), gas (Class G: gas reactors), and liquid metal or salt (Class L: liquid metal/salt

reactors) that also conveniently characterizes the safety analysis methods and claims relative to meeting the SOs.

From reviews and compendiums of the current concepts and design variants, we classify examples of the various concepts, listing their published names and acronyms in Table 16.1. This display makes it clear that despite the alphabetic plethora, with some no longer under active development or still purely paper concepts, and others (marked with an asterisk) under active construction, all are subject to the same overall SO of maintaining cooling, but by using differing means.

In the interest of minimizing undue complexity, and to aid classification, we have limited the listing in Table 16.1 to the major AR variants and more mature published concepts as an example of the many and varied different schemes. Interested readers will find many variants proposed that are at differing stages of maturity, viability, and development and can make their own judgments on the realities and feasibility of commercial deployment.

The basic configurations of the ARs are also similar. All have a primary loop for extracting heat from the reactor core, inside of some kind of pressure-retaining vessel, channel, or container, with a heat exchanger (HEX) or direct cycle to a turbine. The cycle efficiencies and physical layouts are all adequately described elsewhere (in Chapter: Introduction: a survey of the status of electricity generation in the world, Part 1 and Appendix: Additional materials (schematics, layouts, *T-s* diagrams, basic parameters, and photos) on thermal and nuclear power plants of this handbook, and the references given to Table 16.1), and need not be repeated here. However, the safety details between designs within a given class are different because of the inherent differences in operating temperatures and pressures, coolant heat capacity, natural-circulation flows, reactor reactivity coefficients, and physical power limits, which all give rise to differing accident possibilities and event progression. Any and all proponents will, and do, formally claim to meet the SO as a necessary condition for acceptance.

So are these concepts safe? Are some "safer" than others? And how do we know?

We cannot simply turn to results or deliberations in the licensing process here because these are not only still emerging but also deliberately avoid analyzing comparative safety, as is also the case with commercial aircraft. Technological innovation also generally leads to regulation and licensing, not the other way round, as clearly shown by the evolution of computers, automobiles, and modern medicines. The present approaches and origins to reactor safety and licensing are based on water reactor traditions and are not directly applicable to such different concepts in Table 16.1. In the United States, word changes to NRC licensing and regulations have been suggested to address this issue and to expand the applicability of existing methods and safety criteria to include selected others from Classes G and L than just Class W (INL, 2014).

Independent of reactor class, existing modern safety analyses are based on the twin directions of (1) assessing potential event initiators and quantifying estimates of the sequence evolution and responses using PSA/PRA and (2) Deterministic Analyses (DA) in which postulated events are analyzed largely independent of their likelihood. Combinations of many events, transients, and failures are considered, from simple upsets to loss of power, earthquakes, fires, and floods.

Table 16.1 Classifications of advanced reactors

Class W: water reactors	Class G: gas reactors	Class L: liquid metal/salt reactors
AFPR-100 (Atoms for Peace Reactor; PNNL)	GFR (Gas-cooled Fast Reactor)	Gen4 Module (Gen4 energy)
CAREM* (Spain)	HTGR (High-Temperature Gas-cooled Reactor; AREVA)	BREST* (lead-cooled fast reactor; Rosatom)
SMR-160 (Small Modular Reactor; Holtec International)	PBMR (Pebble-Bed Modular Reactor)	Traveling wave reactor (TerraPower)
mPower SMR (B&W)	GTHTR (Gas Turbine High-Temperature Reactor)	JSFR (Japan) SFR (Sodium-cooled Fast Reactor; United States)
Hyperion (Gen4 energy)	VHTR (Very-High−Temperature Reactor)	KALIMER-600 (Korea)
ACP100 SMR (China)	Antares (AREVA)	IMSR (Integral Molten Salt Reactor; Terrestrial Energy)
IRIS (International Reactor Innovative and Secure; Westinghouse)	ALLegro-ALLIANCE (gas fast reactor demonstrator; European Commission)	SSS
SMR natural-circulation pressurized water reactor (NuScale)	SC-HTGR (Steam Cycle High-Temperature Gas-cooled Reactor)	Astrid* (Advanced Sodium Technology Reactor for Industrial Demonstration) (CEA France)
W-SMR (Westinghouse Small Modular Reactor; Westinghouse)	EM^2 (Energy Multiplier Module; General Atomics)	PFBR* (Prototype Fast Breeder Reactor; India)
SCWR (SuperCritical Water Reactor; Supersafe; AECL)	Hybrid Power Technologies' advanced reactor	PRISM (Power Reactor Innovative Small Module; General Electric)
HPLWR (High-Pressure Light Water Reactor)	NGNP (Next-Generation Nuclear Plant; NGNP Industry Alliance)	LC-E-SSTAR (LakeChime Evolutionary Small Secure Transportable Reactor) BN-800* (Russia)

ANS, American Nuclear Society, 2014. Nuclear News 57, 43−85, U.S. DOE, United States Department of Energy Office of Nuclear Energy, 2014. Advanced Reactor Concepts Technical Review Panel Public Report. http://www.energy.gov/ne/downloads/advance-reactor-concepts-technical-review-panel-public-report, Goldberg, S.M., Rosner, R., 2011. Nuclear Reactors: Generation to Generation. American Academy of Arts and Sciences, Cambridge, MA, https://www.amacad.org/pdfs/nuclearReactors.pdf, and GIF, Generation IV International Forum, 2014b. Technology Roadmap Update for Generation IV Nuclear Energy Systems. Nuclear Energy Agency Organisation for Economic Co-operation and Development.

These two methods are consistent with the five stages of the generic Integrated Safety Analysis Methodology (ISAM) propounded by the GIF Risk and Safety Working Group (GIF, 2014b, p. 59). The overall methodology is openly published (GIF, 2011) and includes specific guidance for use (GIF, 2014a). The ISAM tools/stages are stated in the Roadmap Update as the following:

- Qualitative safety requirements/characteristic review,
- Phenomena Identification and Ranking Table,
- Objective provision tree,
- DA and phenomenological analyses, and
- PSA.

Because neither deterministic nor probabilistic methods are perfect for establishing safety margins or damage or activity release probabilities, nor do they allow inclusion of all possible scenarios, the obvious intent is that one should complement the other.

The contrasts and complementary aspects between the approaches were summarized at the top level in ASME (2012) and are shown in more detail in Table 16.2. PRA/PSA is nominally more inclusive, realistic, and general, and DA is much more stylized and arbitrary. As can be seen, both have limitations but provide excellent support to, but are not a substitute for, safety judgment.

Table 16.2 Summary and comparison of probabilistic risk assessment/probabilistic safety assessment and deterministic analysis approaches

Safety aspect	PRA/PSA approach	DA approach	Note
Method	Fault and event trees, plus scoping	Complex safety codes	Wide scope versus narrow focus
Initiating events	Frequency of occurrence	Selected major	Cover "what if" scenarios
Failures	Probabilistic	Single and/or worst	Judgment involved
Initial conditions	Nominal operating or "best estimate"	Limiting or "conservative"	Judgment involved
Number of sequences	Limited by cutoff and importance	Limited by edict and selection	Judgment involved
External events	Fire, flood, earthquake, tornado, threats	Boundary condition	Large uncertainty for "rare" events
Treatment of uncertainties	Included using distributions	Varying inputs and sampling outputs	Missing data and systematic errors

Continued

Table 16.2 Continued

Safety aspect	PRA/PSA approach	DA approach	Note
Safety measure	Core damage frequency	Safety limit margin	Both are failure to cool or control core
Consequences and off-site effects	Included and linked	Excluded	Supports emergency response measures
Safety systems operation	Reliability analysis	Defined functioning	Strong link to design
Human actions	Included and/or dynamic	Excluded and/or static	Large uncertainty
Passive safety systems	Included	In design basis	Claims vs. reality
Management culture	Included via HRA	Excluded	Not measurable
Equipment maintenance and operation	Included via reliability assessment	Unknown	Limited data
Results	Relative ranking of risk	Absolute margin	Used for design and licensing decisions
Limitations	Too small numbers and limited treatment of humans	Only arbitrary and stylized sequences	Potential for undue reliance on paper versus "real" safety
Licensing use	Risk informing and screening	Margin confirmation in design	Regulatory inflexibility

PRA, probabilistic risk assessment; *PSA*, probabilistic safety assessment; *DA*, deterministic analysis; *HRA*, human reliability analysis.

To address and improve safety analysis, and to address the key uncertainties in addressing extreme accidents, the key development approach therefore means radically enhancing and simplifying both design and licensing by

Improving and simplifying the safety analysis;
Making all safety and operating systems more robust;
Assuring more "inherent" safety;
Eliminating many possible initiating events;

Requiring less active systems valves, pumps, and actuators;
Reducing the need for human intervention and/or operator actions;
Providing indefinite cooling and/or heat rejection;
Eliminating or reducing the likelihood of core damage;
Enhancing emergency response effectiveness;
Reducing the potential for offsite releases;
Having more standardized or modular structures; and
Undertaking objective independent safety stress testing.

At the same time, the approach to reducing capital costs and risks often implies series building of multiple, perhaps smaller, units, sometimes utilizing common services and sites and reduced staffing, which all affect the potential for unexpected safety interactions. In addition, some options suggest using remote sites and alternative configurations, such as confinement buildings or underground silos, which also affect the geological and topological risk as well as logistical and emergency response aspects.

16.4 Generic safety objectives and safety barriers

Physically, meeting the SOs means providing and maintaining control at all times, plus ultimate and indefinitely lasting heat sinks (UIHS). In essence, we can simplify these by representing levels of process safety "barriers" (see eg, Bea and Gale, 2011, pp. 5−11), corresponding to deeply layered DiD. In that reference, the barriers are classified as proactive, reactive, and interactive and can be physical, procedural, and managerial. Hence, considering the failure or bypassing of one or multiple layers is necessary for setting the safety design philosophy, in which data and predictive uncertainties grow with the failure, bypass, or breaching of each layer.

The safety design objectives for barriers in all new technology systems are presented in the following.

16.4.1 Reduce the likelihood of initiating events

The chance of incidents and events is minimized by ensuring high reliability of active systems, effective actuation of passive systems, and imposing sufficient operating margins. In addition to robust design and construction of the primary system, buildings, components, pipes, and systems, additional margins are included in core thermal limits, in redundancy and diversity in shut-down and safety system deployment, and in safety and control equipment. This requires attention to the core physics and fuel design to provide void, temperature, and power reactivity coefficients having adequate margin, which ensures automatically reducing and/or limiting the reactor power for all conceivable and postulated transients [eg, ATWS or a loss of coolant accident (LOCA) coincident with loss of off-site power]. Multiple safety systems and instrumentation provide monitoring and control capability for all normal and upset conditions.

Almost all "routine" transients are expected to have benign results, without causing core damage. Therefore challenges only arise from major structural or system damage, primary system breaches, and/or severe extended loss of external power or cooling water.

The methods used include operating experience and event data, geotectonic historical records, coupled neutronic-thermal-hydraulic transient performance analysis codes, Computer Aided Design-Computer Aided Engineering (CAD-CAE) systems, structural finite element methods, materials stress analysis, Human Reliability Analysis, risk assessments and PRAs.

16.4.2 Ensure long-term cooling

Despite meeting Objective 1 stable long-term natural circulation and/or thermal radiation, heat removal from the core must be provided. This means ensuring removal of decay heat at all times to an ultimate heat sink such as the atmosphere, including situations in which all power (from outside grid cables and from inside generators and batteries) has been lost for extended times. The other intent is to minimize or obviate the need for human actions because these are themselves the cause of errors and accidents.

Some of the approaches that have been investigated for AR systems include the following:

- Provide natural-circulation loops for systems with inherently large heat capacity coolants or moderators.
- Design for rapid depressurization to allow water injection to be assisted by the use of relief or "squib" valves and multiple loops.
- Incorporate high hydrostatic heads, nonreturn valves, HEXs, and steam condensers to assist natural circulation, and water pools, without requiring operator actions for some extended time.

Therefore the only challenges are in ensuring adequate heat removal and sufficient water and power supply for the time scales and ensuring that the UIHS and system integrity is maintained.

The methods used include validated thermal-hydraulic codes (see Section 16.10), system and component reliability analysis, and PRAs.

16.4.3 Ensure effective elimination of emergency response

One GIF safety goal is to essentially eliminate the need for emergency response, thus avoiding evacuation requirements for surrounding people and any land contamination. Providing that Objectives 1 and 2 are met, but still assuming barrier failure, this goal requires essentially avoiding core damage; maintaining containment or confinement integrity; and providing completely robust seismic-, terrorist-, and tornado-proof systems and structures. Additional options also include underground reactor buildings to reduce the "target" and filtered venting to control potential overpressures and any potential for radioactivity release.

The challenges that remain are in actually proving that releases absolutely cannot occur (given it is hard to prove a negative and such data are scarce) and that all potential core damage states are either avoided and/or adequately cooled. The methods used include SA analysis codes; structural failure mode analysis; radionuclide transport in buildings and the environment; historical geotechnical, hydraulic, and seismic response analysis; and PRAs.

16.4.4 Manage rare and extreme events

Despite meeting Objective 3, REEs must be considered that address natural events in association with or causing failure of infrastructure (both on- and off-site) and intense social disruption. These may include extreme or tsunami-induced uncontrolled flooding, major ice storms, aircraft impact, fires, and seismic and terrorist threats, in conjunction or associated with major failures in power, control, and systems.

In so-called stress tests, such extreme scenarios are considered to test the ability to respond and maintain control, ensuring graceful degradation, and avoiding noncoolable molten core configurations (by providing "core catchers" or concrete building base mat protectors) and explosions due to uncontrolled hydrogen production (as occurred at Fukushima), including in more fragile structures. Therefore challenges are in determining the bounds of the scenarios to be considered, in predicting the course of such events, and in the deployment of emergency equipment in a timely manner (eg, as in the FLEX "coping strategies"; NEI, 2012), to help to ensure a managed response that avoids panic and dismay. The methods used include risk assessment, PRAs, gaseous mixing and explosion analysis, and SA and consequence codes.

16.4.5 Ensure Rickover safeguards for public well-being

Despite meeting Objectives 1−4, which are essential physical barriers, there are the other key aspects of corporate, management, and regulatory safety that require attention. All major events include a failure of safety performance at senior management levels as well as at the operational level, plus an inadvertent emphasis on process production over process safety.

These human performance barriers are not just the last line of defense; they are indeed the glue that holds the entire safety edifice together. It is well known that having the correct attitudes, training, emphasis, rewards structure, working environment, and philosophy, which all support safety, are key to effective implementation and to effective safety and process management. This actual human performance goes well beyond traditional Human Reliability Analysis on task performance to consider and represent the difference between the claims and reality about safety "culture" and risk adverse behaviors. It is a necessary but not sufficient condition that the licensed owner-operator and the design authority meet all regulations and requirements, but they must still solely bear the safety burden and the risk. The regulator sets the standards whereas management sets the expectations and meets the goals.

Therefore challenges remain not only in ensuring the highest standards of safety performance, personal accountability, and attitudes but also in measuring and continuously improving that same performance. Social and public acceptance must be won, not by slogans but by example, and retained by unending emphasis on safety. This is particularly true and needed for any new technology (viz. the commercial aviation industry).

The methods used include providing a learning environment and effective informal issue communication, independent analysis, Red Teams (critical independent reviewers), management benchmarking, inspections, safety performance audits, on-site presence, intensive "bottom-up" reporting, and most of all assuring personal responsibility and accountability.

The logical hierarchy invoked by ISAM is as follows [see Fig. 3 in GIF (2014a)]:

Safety goals and objectives
Fundamental safety functions
Probabilistic success criteria
Deterministic success criteria
DiD levels:
- 1st—Prevention
- 2nd—Surveillance and control
- 3rd—Accident management
- 4th—Control of severe conditions and mitigation
- 5th—Mitigation of radiological consequences

16.5 Risk informing safety requirements by learning from prior events

It is important to learn from actual events (Duffey and Saull, 2008), and ARs are no exception. Even with the massive rare events, there are many opportunities for learning from more frequent occurrences. For examining and learning from known events, precursors, and accidents, a certain procedural formality has emerged that is relevant to improving operational and "real" rather than hypothetical safety. Typical terminology that is used for event investigations, barrier failure allocation, "root cause analysis," and formal incident reviews is shown in the following.

Accident Investigation Terminology (see Figs. 1–9 in U.S. DOE (2015))

A **causal factor** is an event or condition in the accident sequence that contributes to the unwanted result. There are three types of causal factors: direct cause(s), which is the immediate event(s) or condition(s) that caused the accident; root cause(s), which is the causal factor that, if corrected, would prevent recurrence of the accident; and the contributing causal factors, which are the causal factors that collectively with the other causes increase the likelihood of an accident, but which did not cause the accident.

The **direct cause** of an accident is the immediate event(s) or condition(s) that caused the accident.

Root causes are the causal factors that, if corrected, would prevent recurrence of the same or similar accidents. Root causes may be derived from or encompass several contributing causes. They are higher-order, fundamental causal factors that address classes of deficiencies, rather than single problems or faults.
Systemic root causes involve a deficiency in a management system that, if corrected, would prevent the occurrence of a class of accidents.
Local root causes involve a specific deficiency that, if corrected, would prevent recurrence of the same accident.
Contributing causes are events or conditions that collectively with other causes increased the likelihood of an accident but that individually did not cause the accident. Contributing causes may be longstanding conditions or a series of prior events that, alone, were not sufficient to cause the accident, but were necessary for it to occur. Contributing causes are the events and conditions that "set the stage" for the event and, if allowed to persist or recur, increase the probability of future events or accidents.
Event and causal factors analysis includes charting, which depicts the logical sequence of events and conditions (causal factors that allowed the accident to occur), and the use of deductive reasoning to determine the events or conditions that contributed to the accident.
Barrier analysis reviews the hazards, the targets (people or objects) of the hazards, and the controls or barriers that management systems put in place to separate the hazards from the targets. Barriers may be physical or administrative.
Change analysis is a systematic approach that examines planned or unplanned changes in a system that caused the undesirable results related to the accident.
Error precursor analysis identifies the specific error precursors that were in existence at the time of or prior to the accident. Error precursors are unfavorable factors or conditions embedded in the job environment that increase the chances of error during the performance of a specific task by a particular individual or group of individuals. Error precursors create an error-likely situation that typically exists when the demands of the task exceed the capabilities of the individual or when work conditions aggravate the limitations of human nature.

Note that "barrier analysis" is a key step, because it fundamentally includes DiD, such as the those invoked against radioactivity release (fuel/primary system/containment), and is an adaptation of the "bow-tie" methodology that was commonly utilized in and by the oil and gas industry. However, it is now known that such physical, procedural, administrative, and managerial layers may be breached, bypassed, or made ineffective or aggravated by human actions and subsequent loss of control, as exemplified by multiple SAs, such as the Three Mile Island loss of coolant, Davis-Besse head corrosion, Fukushima core melts and explosions, the Concorde and Air France AF447 aircraft crash, and the Deepwater Horizon offshore oil-spill events (Duffey, 2015).

A notional example of a "barrier tree" for a loss-of-power Fukushima-type event is given in Fig. 16.2, which has some 10 levels of physical, procedural, operational, and managerial barriers. Data and analysis of major events indicate that such barriers are penetrated and bypassed by human actions, decisions, and behaviors with an overall probability that is greater than Order (10^{-3}), consistent with human learning and decision-making errors (Duffey, 2015).

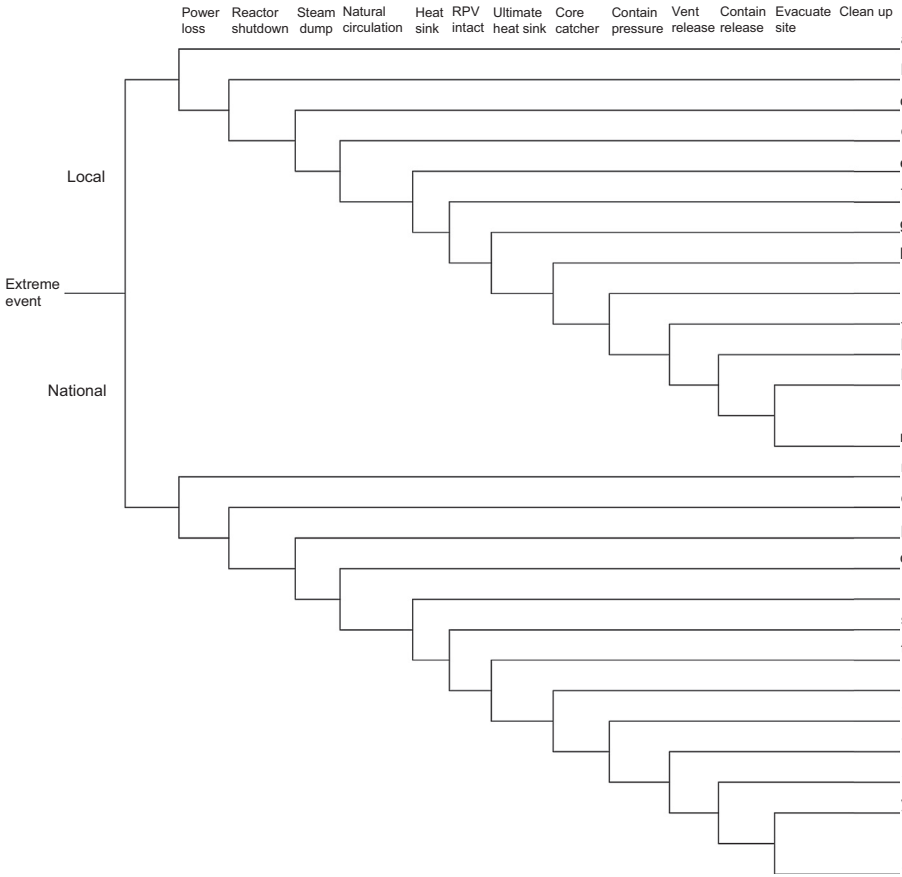


Figure 16.2 Notional barrier tree for nuclear plant.

16.6 Major technical safety issues

We may further classify the major generic technical safety issues for each of the three Classes, W, G, and L, using information derived from experience and the published literature as given in the following discussions based on material from the GIF (GIF, 2014b; Kelly, 2014; by permission).

Safety design approaches to achieving GIF goals (adapted from Kelly, 2014):

Very-high−temperature reactor (VHTR) safety (Class G): Restricted to 600 MW (thermal); huge thermal inertia of graphite structure and matrix; fuel not damaged below 1600°C, single-phase inert coolant.

SFR safety (Class L): Inherent features such as natural-circulation cooling and fuel expansion; single-phase coolant with high margin to boiling.

Supercritical water-cooled reactor (SCWR) safety (Class L): Single-phase coolant; passive safety systems.

Gas-cooled fast reactor (GFR) safety (Class G): Very-high−temperature fuel; complex engineered safety systems.
Liquid metal-cooled fast reactor (LMFR) safety (Class L): Single-phase, high-enthalpy coolant; large margin to boiling; amenable to natural-circulation cooling.
Molten salt reactor (MSR) safety (Class L): No possibility of fuel melt; low fissile inventory; relatively low fission product inventory.

These top-level goals have been extended in more detail as follows, in which we have made the GIF discussion generic to all systems for the appropriate AR class.

Class W (GIF, 2014b, p. 45):

> *The SCWR will be licensed only if it fulfills at least these stringent requirements. More specifically, the Fukushima Daiichi accident demonstrated the need for passive residual heat removal over long periods and the SCWR should be designed accordingly.*

For the SCWR, with a very high-pressure (25 MPa), high-temperature system the depressurization rates and forces are potentially larger than in current light water reactors (LWRs). For the two concepts of a reactor pressure vessel (RPV) or pressure tube (PT), both need to show that a simple LOCA, or RPV or PT failure by cracking or damage, does not lead to core damage.

In the basic concept of the RPV version (Oka and Mori, 2014), classic LWR transient analysis is used. For the PT version, total loss of flow and cooling is addressed as in the Class G systems, using radiation cooling to a UIHS. In both cases, the safety goal and requirement is to provide cooling and hence to avoid fuel melting and/or core damage for indefinite time scales, even for BDBAs and REEs (Yetisir et al., 2015).

For such Class W systems, the major heat removal mechanism invoked is natural circulation (often called "passive"), in not only the primary system, but in back-up cooling, and in the eventual heat rejection to a UIHS that is usually the atmosphere or the earth.

The decision to provide that there be no core melt for any and all loss-of-cooling events has led to the SCWR-PT concept having thermal radiation as the only cooling mechanism that ensures that clad and fuel melting is not possible (Yetisir et al., 2015). In the NuScale AR concept, the requirement to maintain cooling indefinitely has led to a series of natural-circulation paths.

Class G (GIF, 2014b, p. 21):

For GFRs,

> *The need (is) to ensure robust Decay Heat Removal (DHR) without external power input, even in depressurized conditions, is now regarded as a requirement. Previous concepts used electrical (battery) driven blowers to handle depressurized DHR. Although the DHR system has no diesel power units that would need protection from potential flooding, integrity of the electrical infrastructure following an extreme event is still required.*

> *Work is required on two fronts; first to reduce the likelihood of full depressurization and second, to increase the autonomy of the DHR system through the use of self-powered systems. While these self-powered systems cannot be considered passive, they do not require any external power input. Finally, the strategy to deal with severe accidents is to be established.*

The GFR also has a rapid heat up on loss of cooling, which as noted previously cannot be maintained unless power to gas circulators (pumps) is available, which then means high-temperature-resistant fuel is needed. This has led to the adoption of so-called particle or pebble fuel. In addition, RPV or primary system failure is difficult, and so attention has even been given in the past to Class G using prestressed concrete vessels.

The need to initiate and maintain some natural-circulation cooling is extremely demanding for such a high-power density concept, resulting in multiple layers of back-up gas circulators and power supplies.

Class G (GIF, 2014b, p. 51):

For VHTR,

> *passive DHR systems have been designed to facilitate operation of the VHTR, with a final goal of simple operation and transparent safety concepts. Demonstration tests are planned to verify the system's passive characteristics and to show that its safety margins are sufficient…..Design-basis and beyond-design-basis accident analyses for the VHTR will need to include phenomena such as chemical attack of graphitic core materials, typically by either air or water ingress. Adequacy of existing models will need to be assessed, and new models may need to be developed and validated."*

Further demonstrations of the safety performance for both the prismatic and pebble-bed concepts, at high-temperature test reactor (HTTR) and HTR-10, emphasize the benefit of the strong negative temperature coefficient of reactivity, the high heat capacity of the graphite core, the large temperature increase margin, and the robustness of TRi-ISOtropic fuel in producing a reactor concept that does not need off-site power to survive multiple failures or severe natural events as occurred at the Fukushima Daiichi nuclear station.

Because of the need to limit ingress of a moderator or water that can produce potentially explosive hydrogen on interaction with hot graphite (eg, $C + 2H_2O = CO_2 + 2H_2$), this has led to consideration of adopting inert gas HEXs (eg, using supercritical CO_2).

Class L (GIF, 2014b, p. 10 and p. 34):

For the SFR,

> *…efforts will be concentrated on…safety and operation (improving core inherent safety and I&C), prevention and mitigation of sodium fires, prevention and mitigation of severe accidents with large energy releases, and ultimate heat sink.*

In addition, specifically for the SFR, there is a "designer's choice" as a result of safety (Anzieu et al., 2014; subtitled Applied Gen IV Criteria to ASTRID), which partly states state that:

> *12. Prompt criticality shall not be reached either by core compaction or other core motion, or by a gas flow, or by collapse of the core support.*
>
> *13. Loss of the DHR function that could lead to a possible collapse of the primary circuit structures shall be practically eliminated.*
>
> *14. Core sodium de-flooding shall be practically eliminated.*
>
> *Comment: this criterion obviously includes leak of the two reactor vessels.*
>
> *15. Core melting during handling shall be practically eliminated, for instance thanks to appropriate prevention means and handling error detection system.*

None of these issues are new because the sodium reacts exothermically with water, and the core is not in its most reactive configuration. Hence, major core transients and prompt criticality is possible from reconfiguration or inadvertently adding moderator, or by voiding the central part of the core by boiling. In fact, leakage of sodium through small holes in the HEX has been a major inconvenience and difficulty.

Class L (GIF, 2014b, p. 29):

> *Molten Salt Fast Reactor (MSFR) systems have been recognized to have favourable features making them a potential long-term alternative to solid-fuelled fast-neutron systems. However, mastering the technically challenging technology will require concerted, long-term international R&D efforts, namely:*

- system design: development of advanced neutronic and thermal-hydraulic coupling models;
- analysis of salt interactions with air or water in case of a severe accident;
- analysis of the accident scenarios (eg, HEX loss);
- fluorides (Fluoride salt-cooled High-temperature Reactor (FHRs)) may offer large-scale power generation while maintaining full passive safety.

These issues are also well known because on loss of power or flow the reactor becomes subcritical as the core drains, and prototypes have been run to demonstrate feasibility.

16.7 Multiple modules and plant risk

Many of the ARs are designated as "modular" in design, meaning that multiple units can be mass produced with a common licensing basis and having shared siting. Such approaches are already successfully used in the design and construction of industrial

equipment and facilities and in reducing the construction time of large nuclear plants. The AR/SMR intent is to use more but smaller units to enable:

1. Assembly-line processes with just-in-time delivery and less field work,
2. Lower the initial capital investment and produce an earlier return on investment,
3. Shorter engineering and construction times,
4. Adding increments of power as demand requires and cash flow allows,
5. Reduced unit costs by series build rather than "on-off" or custom designs,
6. Upfront one-step review and licensing ("certification") of the duplicated design,
7. Sharing of common facilities and site infrastructure,
8. Reduction of staffing duplication for security and operations,
9. Reduced costs of unit downtime and flexible/standardized maintenance, and
10. Improved safety by system diversity and less activity release potential.

These are fine and desirable goals, but they do contain increased specific costs, at least for the first few units that have to bear the development, licensing, and production-line setup. In addition, the issue has been discussed of the relative safety for multiple units that are co-located and may share interactions between systems and shared facilities. To date, most licensing and builds had been on the basis of one unit at a time, despite the presence or co-location of other facilities. This was also highlighted by Fukushima, because of the presence of spent fuel pools at the site, with the potential for additional activity release.

Therefore the apparently simple safety question for ARs is whether multiple, say, 10 small units, have the same or more risk than one unit with some multiple of the power output, say, 10 times, and greater radioactive and spent fuel inventory per unit at the same site?

The considerations for multiple plant risk have already been addressed for the implications for PSA/PRA purposes (CNSC/OECD, 2014). The revisions needed to safety methods, assessments, rules, and regulations have been considered, and a practical approach has been suggested as to how to include multiple units (Vecchiarelli et al., 2014). The overall objective is simply to provide protection to the public and "practically eliminate the potential for extensive social disruption," in line with the ASME approach (ASME, 2012), and to aggregate (add) the individual CDFs to stay below some agreed overall site limit while excluding some low-frequency events.

It should be noted that the units sharing or on adjacent sites are partially independent and that unexpected interactions can exist, as has been demonstrated by Fukushima. This multitude of potential interactions has also been examined (Modarres, 2015). By examining the differing possible types of interactions, from an initial scoping study it was concluded that common cause failures dominated and were due to system, event, and human errors. In fact, considering the differing learning stages and operational experience levels, it has been shown that multiple facilities at multiple sites do indeed have higher risks (Duffey and Saull, 2008; Appendix F, p. 481). These results are not surprising by themselves because events or damage that affect multiple units simultaneously, or even propagate from unit to unit, or hinder the operation of shared systems, or are common to the design must now be included in the safety assessment, rather than using a single unit case as applicable to all other units.

16.8 The role of safety research and development for advanced reactors

Research and development (R&D) has a vital role in providing the methods, data, and sound judgments needed for developing and evaluating new technology. Adequate and exhaustive testing is essential, be it hardware, software, or firmware, for proving any new innovation or product, to establish or refute the safety claims, and to underpin system performance requirements.

Clearly all is not resolved for the formalization of the safety of ARs, and additional data, analyses, and thinking are all underway at the time of preparation this chapter. A useful summary is given by the GIF "Roadmap Update" (GIF, 2014b, p. 39) for the systems that they are pursuing:

> *Additional R&D on safety issues highlighted by the Fukushima Daiichi accident is foreseen….A primary focus on the following issues is anticipated:*
>
> - *robust and highly reliable systems for adequate cooling of safety-relevant components and structures;*
> - *geometric stability of the SFR core in case of a strong earthquake and assurance of reliable performance of the control rods;*
> - *seismic-resistant design of the spent fuel pools and fuel-handling devices;*
> - *integrity of the primary circuit and its cooling;*
> - *design features aimed at excluding the risk of flooding of the reactor building;*
> - *effective options for dealing with severe accidents.*

We now turn to the salient and key safety issue that is also the subject of extensive research. How can natural circulation and inherent and indefinite cooling be demonstrated for these seemingly many and varied AR systems?

We proceed by fully examining the state of the art for the analysis and modeling of natural-circulation flows and heat removal, which are so important to the effective long-term removal of heat to a UIHS in all AR concepts. We specifically avoid the analysis of heat removal for degraded cores and the role of "core catchers," which are added sacrificial and/or cooled and reinforced layers beneath the RPV. Instead, we rely simply on the empirical evidence from major and SAs to date (eg, Three Mile Island, Chernobyl, and Fukushima) that demonstrate that highly degraded and complex core configurations are ultimately coolable, and that the primary safety goal or aim for ARs, not for existing reactor designs, is really to ensure adequate cooling before the onset of limited core damage, core melt, and public panic.

16.9 Natural-circulation loop and parallel channel thermal-hydraulics

16.9.1 Introduction

Natural-circulation loop (NCL) thermal-hydraulics are an essential aspect in the design, operation, and safety of all Gen IV concepts. Some concepts rely on natural

circulation for normal operating conditions and off-normal safety conditions. Others depend on natural circulation only for passive off-normal safety conditions. The objective of natural-circulation passive safety systems is to maintain the system in safe shutdown states, for long periods of time, without the necessity of operator intervention or availability of electric power.

Passive safety systems based on natural circulation are intended to provide the ultimate heat sink in cases of failure of the normal operation of the reactor cooling system. Because of its critical importance, fundamental understanding of the properties and characteristics of natural-circulation hydrodynamics, thermal responses, and thermodynamics in the complex engineering equipment of nuclear reactor power systems is essential. For the Gen IV systems that are based on natural circulation at normal operating states the properties and characteristics under steady-state conditions must also be well understood.

In general, the natural-circulation flows encountered in nuclear power plants will be associated with closed loops composed of piping, flow channels of various shapes, and several equipment components. The loops are generally closed, but a failure in the piping that makes up the loop can disrupt the natural circulation and make the system useless for its intended purpose. The secondary side of steam generators (SGs), for plants using natural circulation for normal operations, is characterized as an NCL with throughput; feedwater input from the condenser and steam extraction at the SG exit to feed the turbines. All of these systems will have regions within which the flow is in parallel channels, such as fuel rods, and fuel-rod bundles, in the core, and tubing in SGs and HEXs.

Natural-circulation flows around loops and flows in parallel channels are both susceptible to departures from steady operation and excursions into oscillatory and, potentially, unstable states. Thus Gen IV nuclear reactor power systems combine the type of fluid flow and geometries that are known to potentially lead to undesirable states. In particular, undesirable oscillatory states under steady-state operation should be avoided. The complete system and associated operational envelope are designed to avoid unstable states.

The discussions in the following sections will focus on the thermal-hydraulic properties and characteristics of flows in parallel channels and NCLs. The literature on general aspects of the analytical, experimental, mathematical modeling, numerical solution methods, and computational aspects of these flows will be briefly reviewed. These aspects when associated with specific Gen IV systems will also be discussed.

16.9.2 Natural-circulation flows

The driving potential for natural-circulation flows is created by buoyancy within the fluid itself. This is in contrast to forced circulation flows that are driven by power external to, and supplied into, the fluid, generally by means of a pump or other mechanisms. The driving potential for natural-circulation flows is small relative to that which can be supplied from external power sources. At steady state the induced buoyancy forces are balanced by the pressure losses around the loop, and this determines

the steady-state mass flow rate in the NCL. The small, internally induced driving potentials make natural-circulation flows more susceptible to the onset of instability because perturbations in the flow rate or power source feed directly to changes in the driving potential. Any equipment part, or region of the complete system, and the physical phenomena and processes associated with the part or region, have the potential to introduce perturbations. For example, startup of nuclear-powered natural-circulation systems, or changes in the steady operating state, are perturbations that will occur during the lifetime of the system.

A rough working definition of instability might be stated as a departure from an intended course of operation of a thermal-hydrodynamic system. Observed departures include sustained periodic oscillations; damped oscillations that return to smooth operation; growing oscillations in systems that can inject power into the fluid; and aperiodic, chaotic, and oscillations. Nayak and Vijayan (2008) indicate that even at steady-state conditions, oscillations in natural-circulation systems, including boiling two-phase systems, are generally present. Amplitudes greater than $\pm 10\%$ of the mean state are sometimes classified as instabilities. Others consider that amplitudes greater than $\pm 30\%$ indicate instability. In complex engineered equipment systems the effects of interactions between the physical phenomena and processes that occur in the various components can be difficult to quantify. The chaotic response of deterministic mathematical models as discovered by Lorenz (1963) is closely related to idealized models of fluid flow and heat transfer in natural-circulation systems.

Ruspini et al. (2014) and Ruspini (2013) has given detailed descriptions of the physical phenomena and processes associated with each of the several types of instability. The following is taken, by permission (with slight changes in the display of a few of the words), from the Table of Contents of his PhD dissertation (Ruspini, 2013), *Two-Phase Flow Instability Mechanisms*.

- Characteristic pressure drop vs. flow rate instabilities
  - Ledinegg instability
  - Flow distribution instability
  - Flow pattern transition
  - Pressure Drop Oscillation (PDO)
- Density Wave Oscillations (DWO)
  - Type I: Due to gravity, DWO_I
  - Type II: Due to friction, DWO_{II}
  - Type III: Due to momentum, DWO_{III}
- Compound density wave phenomena
  - Density wave oscillation in parallel channels
  - Coupled neutronic thermo-hydraulic instabilities
- FlaSHing instability (FSH)
- Thermal Oscillations (ThO)
- GEySering (GES)
- Natural Boiling Oscillation (NBO)
- Thermo-Acoustic Oscillations (TAO)

Instabilities in Condensing flows
    Self-sustained oscillations
    Characteristic pressure drop vs. flow rate curve for condensing systems
    Oscillations in parallel condensing channels
Water-hammer phenomena
Flow-induced instabilities

This long list is an indication of the potential complexities that need to be considered for natural-circulation systems. Extensive discussions, including experimental observations, for each of these are covered in the text and associated papers by Ruspini et al. (2010, 2011a,b, 2012, 2014), Ruspini (2012). IAEA (2005) have summarized several of these as shown in Table 16.3.

Numerous factors have been determined to influence the performance, and especially the stability, of NCLs. Many of these were enumerated in the earliest investigations of flow and heat transfer in NCLs. Others have been encountered as the original idealizations, both analytical and experimental, have been generalized to include additional and realistic aspects of the physical domain. Some of these factors include, among others

1. The degree of subcooling of the fluid at the channel entrance,
2. The pressure gradient in the subcooled-liquid portion of a boiling channel,
3. The distribution of the pressure losses around the flow channel,
4. The operating pressure level,
5. The heat flux/channel power supplied to the fluid,
6. The void fraction/quality and its distribution, and the two-phase flow regime,
7. The mass flow rate of the fluid,
8. Geometric properties of the flow channels in the system,
9. The operating pressure level with larger regions of stability at increased pressure, and
10. The thermodynamic state of the coolant; single-or two-phase and its distribution.

Note that this list describes what can be characterized as a more or less pure thermally driven hydrodynamic NCL in that the effects of engineered equipment and the associated physical phenomena and processes are not listed. Some of these factors include power generation in nuclear fuel rods, heat conduction in all of the solid-material boundaries of the fluid, changes in flow-channel geometry around the loop, system-state-change perturbations introduced during normal operations, changes in boundary conditions (BCs), and operations of equipment that is coupled to the fluid. The list also does not address the known issues relative to numerical solution methods applied to mathematical models of NCLs, both simple and realistic, and the onset of flow instability (OFI) in single and parallel channels.

Although single-phase flow systems have been one focus of investigations of OFI, especially under natural-circulation conditions, two-phase flow systems, being inherently complex, have received more attention. Interest in boiling two-phase natural-circulation systems for nuclear power applications was present at the early stages of R&D of the systems. In general, these early developments were driven by the perceived advantages of natural-circulation systems for nuclear submarines.

Table 16.3 Classification of thermal-hydraulic instabilities

Class	Type	Mechanism	Characteristic
Static instabilities			
Fundamental (or pure) static instabilities	Flow excursion or Ledinegg instabilities	$\left.\frac{\partial \Delta p}{\partial G}\right\|_{\text{int}} \leq \left.\frac{\partial \Delta p}{\partial G}\right\|_{\text{ext}}$	Flow undergoes sudden, large amplitude excursion to a new, stable operating condition
	Boiling crisis	Ineffective removal of heat from heated surface	Wall temperature excursion and flow oscillation
Fundamental relaxation instability	Flow pattern transition instability	Bubbly flow has less void but higher ΔP than that of annular flow	Cyclic flow pattern transitions and flow rate variations
Compound relaxation instability	Bumping, geysering, or chugging	Periodic adjustment of metastable condition, usually due to lack of nucleation sites	Period process of superheat and violent evaporation with possible expulsion and refilling
Dynamic instabilities			
Fundamental (or pure) dynamic instabilities	Acoustic oscillations	Resonance of pressure waves	High frequencies (10−100 Hz) related to the time required for pressure wave propagation in system
	Density wave oscillations	Delay and feedback effects in relationship among flow rate, density, and pressure drop	Low frequencies (1 Hz) related to transit time of a continuity wave
Compound dynamic instabilities	Thermal oscillations	Interaction of variable heat transfer coefficient with flow dynamics	Occurs in film boiling
	Boiling water reactor instability	Interaction of void-reactivity coupling with flow dynamics and heat transfer	Strong only for small fuel time constant and under low pressures
	Parallel channel instability	Interaction among small number of parallel channels	Various modes of flow redistribution
Compound dynamic instability as secondary phenomena	Pressure drop oscillations	Flow excursion initiates dynamic interaction between channel and compressible volume	Very-low−frequency periodic process (0.1 Hz)

Used with permission from IAEA, 2005. Natural Circulation in Water-Cooled Nuclear Power Plants Phenomena, Models, and Methodology for System Reliability Assessments, IAEA-TECDOC-1474. IAEA, Vienna, p. 23.

Pressure loss distributions around the loop are known to be first-order effects relative to stability properties and characteristics under natural-circulation conditions. The locations of singular, reversible and irreversible, pressure changes and losses, respectively, associated with geometry changes have been determined to be important. Local losses at the entrance and exits of energy supply or exchange components have been shown to be especially important. Pressure losses at the entrance are critically important relative to promoting stability, and those at an exit to a lesser degree. Large losses at an exit can induce instability. The reversible pressure changes associated with continuous or abrupt changes in flow-channel geometry, such as nozzles and chimneys and abrupt expansions or contractions, are also important. Wall-to-fluid friction, a distributed resistance to fluid motion, and its distribution along the flow channel, is also important.

Physical instabilities arise whenever discontinuities and/or adverse gradients are present in a flow field. Classical situations that have been thoroughly investigated include discontinuities in velocity, temperature, pressure, and density or combinations of these. In the case of mathematical modeling of NCLs, discontinuities introduced into algebraic representations of model closures for wall; interphase, friction, heat, and mass transfer; and the equation of state (EoS) can also introduce instabilities. These are purely artifacts of mathematical constructs and are not encountered in the physical domain. The stopping criterion for numerical iterative methods must also be checked that the calculated results are independent of its value.

Representation of the wall-friction factor correlation in the transition between laminar and turbulent friction, for example, has been shown to have the potential to introduce artificial instability (Ambrosini et al., 2004; for an example). At the same time, in the physical domain, transition between laminar and turbulent flow due to variations in the fluid thermodynamic states around a loop can introduce instability. Such changes can be due to the dependency of the fluid viscosity on temperature, for example, or for changes in the flow area around the loop. Boiling and condensing two-phase flows are especially important examples of significant changes in the thermodynamic state. Likewise, fluids operating at supercritical thermodynamic states, receiving renewed interest for nuclear reactor designs, experience significant state changes around an NCL.

16.10 Literature review

In the following paragraphs a brief summary of some of the literature associated with thermal-hydraulic properties and characteristics and performance, including onset of instability, in NCLs and parallel channels is given. In general, the literature on NCLs and associated physical phenomena and processes is far too enormous to be reviewed in detail here. Instead, many of the reviews already, and especially recently, given will be mentioned along with some of the earlier literature associated with nuclear power systems.

Several reviews of many aspects of single- and two-phase flows, including flows in NCLs and parallel channels, have recently appeared as follows. Ruspini et al. (2014),

based on Ruspini's doctoral thesis (Ruspini, 2013), have given an exhaustive review, citing more than 200 literature sources. Ruspini (2013) has additionally investigated mathematical modeling and numerical solution methods, including error estimates, for application to various experimental and analytical data. Related investigations developed during the course of his research are reported in Ruspini et al. (2010, 2011a,b, 2012), Ruspini (2012).

Basu et al. (2014) have reviewed applications of single-phase NCLs for nuclear power applications, and Misale (2014) presented a summary of the status of single-phase NCLs. Sarkar et al. (2014) present a review of supercritical NCLs. Previous reviews that supplement these include Prasad et al. (2007), Nayak and Vijayan (2008), and Vijayan and Nayak (2010), who reviewed instabilities for boiling two-phase NCLs, including natural-circulation boiling water reactors (BWRs). The latter reference has a list of instability events that have occurred in operating machines.

Manavela Chiapero et al. (2012, 2013a,b) have reviewed pressure drop oscillations in boiling systems. The exhaustive nature of the research at the Norwegian University of Science and Technology cannot be overemphasized. Reviews of instabilities in the case of single and parallel channels include Ozawa et al. (1989), Tadrist (2007), and Kakac and Bon (2008). The latter is especially complete. March-Leuba and Rey (1993) presented a state-of-the-art review for the case of coupled thermo-hydraulic-neutronic instabilities in BWRs.

The IAEA have provided reports on both the general concepts and some focused aspects of Gen IV nuclear reactors (IAEA, 2001, 2002, 2004, 2005, 2009, 2012, 2014). Saha et al. (2013) provide a summary of the general concepts of Gen IV machines and the thermal-hydraulics R&D that will be required to develop and validate multiphase, multiscale, multiphysics advanced computational models and methods. Rowinski et al. (2015) provided a review of the various implementations of SMR concepts.

Additional literature reviews that generally predate those mentioned will be noted in the following discussions. The discussions in this report will focus more on nuclear reactor applications instead of the general case of parallel channels and NCLs. However, both situations arise in nuclear power applications. The general cases have been extensively covered by the literature just cited.

16.10.1 The early investigations

The concept of using natural circulation in nuclear-powered energy production systems dates from the earliest days, the early 1950s, of nuclear energy applications. The question of the hydrodynamic stability of NCLs was first investigated, analytically and experimentally, in this early period. Representative publications include Hamilton et al. (1954), Wissler et al. (1956a,b), Chilton (1957), Lowdermilk et al. (1958), Garlid et al. (1961), Anderson et al. (1962), Lottes et al. (1963), and Jain (1965), among several others. An electronic literature search will produce many citations to early publications from the 1950s that are difficult to obtain. In the United States this research was underway in a few national laboratories, universities, and private organizations.

The latter were generally supported by way of government contracts. Some of the work was directed toward applications to nuclear-powered naval vessels.

Creveling and Schoenhals (1966), Keller (1967), and Welander (1967) performed fundamental work on highly idealized systems. These papers are considered landmark initial studies and continue to be cited to this day. However, note that experimental and analytical research had been underway for more than a decade when the papers were published. The report by Garlid et al. (1961) has extensive citations to the very early literature including analytical and experimental investigations. The report also contains an analog computer program for the model equations. Alstad et al. (1956) investigated single-phase NCLs and Wissler et al. (1956a,b), Anderson et al. (1962), Jeglic and Grace (1965), Grace and Krejsa (1967), and Yadigaroglu and Bergles (1969) investigated two-phase loops.

The concept of a SCWR based on natural circulation was also investigated in the 1960s (see Harden, 1963; Cornelius, 1965a,b, for examples). The renewed interest in supercritical reactors has recently driven significant additional research.

The early work in the United States was directed toward the various models of BWRs then under experimental and analytical investigations. These operating machines included the experimental boiling water reactor (EBWR), Special Power Excursion Reactor Test Program (SPERT), SPERT-I, and the BOiling water ReActor eXperiment (BORAX), and BORAX I−V machines (Lottes et al., 1963). Stability of boiling two-phase flow and heat transfer, OFI, and critical heat flux or Departure from Nucleate Boiling were all investigated. Berenson (1964) has a summary of the experimental results up to that time. In general the stability of BWRs during various phases of operation continues to be an active area of research. All findings to date indicate that startup and operation of nuclear-powered natural-circulation systems is readily achieved.

Most of the early research involved coupled experimental and analytical efforts, and that coupling continues to the present time. Analytical approaches were somewhat straightforward because the mathematics leads to tractable problem statements for simple NCLs. Findings from the early analytical investigations indicated that careful attention must be given to discretization and numerical solution of model equations when applied to investigations of the onset of instability. At the present time early in the 21st century, applications of multidimensional computational fluid dynamics (CFD) is proving to be helpful in graining deeper understanding of the physical phenomena and processes that can lead to the onset of instability. CFD is also proving useful for identifying deficiencies in the classical zero- and one-dimensional analytical modeling of NCLs.

The early experimental data and associated analyses indicated that oscillatory behavior, although present, did not always lead to growth to divergence. Closed regions of instability, bounded by both lower and higher power additions into the systems, were observed. The boundaries and range of the closed regions varied with the operating pressure level and the thermodynamic state of the fluid. The diameter and length of the piping in the simple experimental systems, and other geometric details, were also found to affect the stability properties of the systems.

The onset of instability in NCLs closely correlated with significant differences between the gradients in driving potential and the flow resistance around the loop. In this respect the onset is exactly analogous to the onset of instabilities in the case of flows in single and parallel channels. The significant effects of the magnitudes of the flow resistances at the incoming and outgoing legs of the loops at the energy supply were also noted. Increases in resistance on the incoming side increased the size of the region of stability whereas the converse was found for the outgoing side. Increasing the local flow resistance at the inlet side continues to be a common method to avoid onset of instability. At the same time the effects of the resistance on the power capacity of the system must be considered.

Most of the original and early experimental and analytical investigations were based on simple idealized experimental loops and one-dimensional formulations of the model equations. Even at this early phase of investigations, all of the citations previously listed utilized mathematical models as a means to gain deeper understanding. One-dimensional, area-averaged mathematical models of the governing equations generally coincided with the level of measurements in experimental facilities. In addition, the earliest investigations more or less omitted considerations of almost all aspects of loops in the physical domain: nonuniform flow-channel geometry, latencies associated with energy transfer and transport processes such as conduction in all of the solid material surrounding the fluid, and changes in the state of BCs that arise in HEXs, among others. The effect of neutron-transport and energy production and void-power coupling in the core of nuclear reactors was a focus.

Analytical investigations in the frequency domain, based on linearization of the model equations, are useful for natural-circulation systems. In general, as the model equation system grows to account for additional physical phenomena and processes and greater detail in engineered equipment systems, the linear system gets too complex for carrying to completion. At this point the linear systems and numerical solution, including numerical inversion of Laplace transformed systems, are incorporated into computer software. Frequency domain models and codes continue to be used for real-world systems. However, the ultimate investigations and quantifications are generally based on simulations in the time domain. Much of the available experimental data have been used to validate time-domain models and methods and gain approval for applications of these to safety issues.

BCs in the earlier mathematical models relied on (1) specifications of the energy supply into the system and equality of the energy rejection or (2) specification of the temperature at the energy source and sink. This approach neglects the temporal response of the energy-transfer processes from the BCs of an ultimate source and to the BCs of the ultimate sink. For applications to Gen IV nuclear power production the engineered equipment that makes up the source and sink and the processes occurring within that equipment are required to be included in an analysis and prototypical experimental facilities.

Rao et al. (2005a,b,c,d, 2008) and Kumar and Gopal (2009) have generalized the mathematical models to include more nearly realistic BCs by considering HEXs for the energy source and sink. Additional generalization can be obtained by use of more detailed modeling of the physical phenomena and processes that occur within

the HEXs and the fluid states at the entrances to these (eg, flow rate and thermodynamic state perturbations).

Fundamental analytical and experimental work continued throughout the 1950s into the 1970s. Various issues associated with BWRs, including stability and the onset of instability and effects of neutronic power feedback, were primary areas of focus. BWRs were considered in the early literature, primarily relating to the EBWR, SPERT I, and the variations of the BORAX I−V (Berenson et al., 1964; Levy and Beckjord, 1960). The BORAX operating machines were constructed at the National Reactor Testing Station near Idaho Falls, Idaho beginning in the very early 1950s. Boiling, stability, and neutrons have a very long history (Haroldsen, 2008). These experiments were the first to investigate void-reactivity coupling and feedback. The results of geysering instabilities could be observed from a nearby public transportation roadway.

Experimental and analytical work was also underway in Europe at AB Atomicenergi associated with the Marviken and Halden boiling heavy water reactor machines (Becker et al., 1963, 1964) and in Italy at Centro Informazioni, Studi ed Esperienze (CISE). The AB Atomenergi work included extensive experimental facilities and mathematical modeling. In some regards these efforts confirmed, and significantly supplemented the findings of, the earlier work of the 1950s.

At this time it had been established that (1) as the pressure increases the power at the onset of instability increases, and the frequency of oscillations increase; (2) the onset of instability decreases as the inlet subcooling increases so that lower values are preferred relative to ensuring stable states; (3) as the local pressure loss at the inlet to the energy supply is increased, the region of stable operation is increased; and (4) as the local pressure loss at the outlet is increased, the region of stable operation decreases. In the latter case the loop flow is less stable.

Review of the literature was given by Boure et al. (1973), in which the physical mechanisms and mathematical models in use up to that time are discussed. The report has a summary of the computer codes that had been applied to the problem in the frequency and time domains. Saha (1974), Ishii (1976), Saha et al. (1976), and Saha and Zuber (1978) provided initial investigations into effects of thermal nonequilibrium between the liquid and vapor phases. Lahey and Drew (1980) discussed instability issues associated with LWRs.

16.10.2 Three Mile Island issues

After the incident at the Three Mile Island nuclear plant in 1979, the nuclear industry as a whole around the world intensified experimental and analytical investigations into all aspects of natural-circulation thermal-hydraulics. The small-break loss of coolant accident (SBLOCA) nature of the incident revealed the critical importance of natural circulation to understanding the response of such systems under these conditions. The entire industry worked to ensure that understanding of all aspects SBLOCAs, for existing and future systems, was correct and complete.

Major experimental programs were devised, developed, constructed, and successfully completed, including LOBI-MOD2, SPES, ROSA-III, ROSA-IV LSTF, BETHSY, and FIST. Experimental facilities originally built for large-break loss of

coolant accident (LBLOCA) investigations (eg, Semiscale and LOFT) were modified to look into the SBLOCA case. Data from these facilities continue to be used as validation exercises for mathematical models and computer codes. Aksan (2008) has given a summary of activities associated with SBLOCA and major system-analysis codes such as TRACE (U.S. NRC, 2008), TRAC-P (LANL, 1986), TRAC-B (Spore et al., 1981; INEL, 1992), RELAP5 (INEL, 1995; ISL, 2001), CATHARE (Bazin and Pelissier, 2006), and ATHLET (Austregesilo et al., 2006; Lerchel and Austregesilo, 2006). Interest in Gen IV machines has driven development of other models and codes.

Zvirin (1982) reviewed experimental data and analytical approaches appropriate for natural circulation and SBLOCA, with a focus on pressurized water reactors. Results of other investigations led by the Electric Power Research Institute include Zvirin (1979, 1985), Zvirin et al. (1981), Duffey and Sursock (1987), Greif et al. (1979), Mertol et al. (1981), and Mertol (1980) among others. Greif (1988) presented a literature survey and summary to that time. Gruszynski and Viskanta (1983) conducted and experimental investigation of a rectangular NCL using tube bundles for the energy source and sink. They report that the friction factor correlation for natural-circulation flows is different from that for forced circulation.

The 1980s, and continuing, saw an ever-increasing number of publications addressing experimental, analytical, numerical, and system-code applications to NCLs. The extensive citations in the recent reviews previously listed can be used to follow-up on any aspects of NCLs and parallel channels. The most recent activities have been driven by the proposed applications to Gen IV, and beyond, nuclear power reactors.

16.10.3 Boiling water reactor stability in the time and frequency domains

Renewed focus was on instabilities in operating BWR systems, especially the effects of neutronics, power feedback, and patterns of oscillatory flow in parallel channels, which are enclosed fuel rod arrays in these systems. Extensive effort was applied to models and analyses in the frequency domain and several computer codes were devised, developed, and applied (Peng et al., 1984, 1986; Lahey et al., 1990; March-Leuba, 1984; March-Leuba and Rey, 1993). Various frequency domain analysis methods have also been developed including LAPUR (Escriva et al., 2008) and NUFREQ-NP (Peng et al., 1984), among others.

The mathematical models and numerical solution methods used in the major systems-analysis computer codes used in the industry were the subjects of research relative to applications to SBLOCA and natural circulation. During this period of intensive research, the critical importance of the discretization of the continuous equations and the associated numerical solution methods used in systems-analysis computer codes for nonlinear analyses in the time domain was one area of primary focus.

Some of these codes include RETRAN (Computer Simulation & Analysis, 1998), RELAP5 (Information Systems Laboratories, 2001), TRAC-BWR (Spore et al., 1981), CATHENA (Richards et al., 1985), CATHARE (Bazin and Pelissier, 2006), ATHLET (Austregesilo et al., 2006; Lerchl and Austregesilo, 2006), and RAMONA

(Rohatgi et al., 1998), along with variations of these as they are developed for new applications. In addition to constant updating of these major codes to gain applicability to new analyses, models, methods, and code development continues around the world. For example, Korea has developed the TASS/SMR code (Hwang et al., 2005, 2006), among others. In addition to these major codes, other time- and frequency domain models and methods have been developed for local, special-purpose analyses of experimental data and numerical solution methods. These special-purpose models and methods are generally not freely available.

Low-flow stability tests conducted at the Peach Bottom nuclear plant in the United States (Woffinden and Niemi, 1981) have been used for validation of system-analysis models, codes, and application procedures. Costa et al. (2008) applied the coupled RELAP5/MOD3.3 thermal-hydraulic code and PARCS-2.4 three-dimensional neutronics code to simulate these tests. D'Auria (1997) pulled together an Organisation for Economic Co-Operation and Development state-of-the-art report. Mori (1998) used the RETRAN-3D (CSA, 1998) code and Wulff et al. (1992) and Rohatgi et al. (1994) applied the Brookhaven National Laboratory Engineering Plant Analyzer approach. Costa et al. (2008) have summarized other events that have occurred in operating plants. These data are also used for validation.

Aguirre et al. (2005) presented an extensive summary of the analytical, experimental, and model and code validation research conducted in support of gaining deep understanding of the natural-circulation and stability issues for BWRs. Four major experimental facilities—CLOTAIRE (Gouirand, 1988), DESIRE (van de Graaf et al., 1994), CIRCUS (de Kruijf et al., 2000), and PANDA (Dreier et al., 1996)—and seven major system-analysis models and codes—MONA (Hoyer, 1994), ATHLET (Krepper and Prasser, 1999), RAMONA (Grandi et al., 1998), LAPUR (Otaduy and March-Leuba, 1990), FLICA (Toumi et al., 2000), RELAP5/MOD3 (INEL, 1995), and TRAC-BF1/MOD1 (INEL, 1992)—have been applied to the problem. CFD codes were utilized for specific issues, and a linear stability model and code were developed within the project. Kozmenkov et al. (2012) have used CIRCUS data for validation of the RELAP5 models and code.

Investigations into various aspects of stability issues in BWRs, especially natural-circulation BWRs, continue to the present time. Faculty and staff at the Delft University of Technology, likely because of the presence of the operating Dodewaard machine, have researched several aspects of BWR stability (Furuya, 2006; Marcel, 2007; Stekelenburg, 1994; van Bragt, 1998). van der Hagen et al. (2000) have reviewed information on BWR stability experiments. Activities have continued after the state-of-the-art review (Hu, 2010; Hu and Kazimi, 2011, 2012; Xu et al., 2009; Lakshmanan and Pandey, 2009; Rohde et al., 2010), among others.

16.10.4 Numerical methods and artifacts

Almost all numerical methods implicitly introduce artifacts into numerical solutions applied to the discrete approximations to the continuous model equations. These artifacts significantly affect the dispersion and dissipation of the calculated response, thus introducing errors into the calculated decay ratio. Because investigation of the stability

of natural-circulation flows is a primary objective of the analyses, it must be demonstrated that the numerical method itself does not introduce artificial instability or artificial stability. Implicit numerical solution methods, developed so that larger values of the discrete time step can be used, especially introduce artificial stability into calculations. Thus numerical solutions must be determined to be true instability or stability and not instability or stability introduced by the numerical methods themselves. Numerical methods can result in false positives and false negatives; it must be determined that no artifacts are introduced into calculations by numerical solution methods.

The numerous complexities of the physical domain represented by all of the components and associated detailed aspects of a system that affect the stability of the system must be (1) realistically included into the mathematical models, (2) accurately resolved by the numerical solution methods, and (3) shown to not have introduced artifacts into the calculations. The numerically enhanced mathematical stability of implicit methods, the potential numerical instability of explicit methods, and the dissipative and dispersive characteristics of implicit and explicit methods require careful investigations. Jensen (1992) has given examples of some of these effects.

Professors W. Ambrosini and J. Ferreri, in a collaborative effort over a period of approximately 10 years, and with others, have presented an exhaustive investigation of the effects of numerical approximations to the continuous model equations, and the numerical solution method for these, on calculations of the onset of instability for natural-circulation and parallel-channel flows. A few examples are Ferreri and Ambrosini (1999, 2002), Ambrosini and Ferreri (1997a,b, 1998, 2000, 2003, 2006, 1999), Ferreri et al. (1995), Ambrosini et al. (2001), and Ambrosini (2001, 2008), among many others. The investigations have used special-purpose computer codes in the frequency and time domains, and the RELAP5 system-analysis code. Mangal et al. (2012) have also compared RELAP5 calculations with NCL properties.

16.10.5 Generation IV passive residual heat removal systems

Most of the analytical and experimental investigations into NCLs have been based on a single isolated loop. In contrast, passive cooling of nuclear power plants based on natural-circulation operation requires coupled loops as follows. For the safe shutdown condition for natural-circulation Gen IV machines, the passive residual heat removal system (PRHRS) is made up of two coupled natural-circulation systems: one that transports the energy from the RPV and the second that deposits the energy into the ultimate heat sink. The latter process is the second NCL and the coupling to the primary loop is through an intermediate HEX. That HEX is generally the same as that used during normal operation of the machine—the SG. The energy is deposited into the ultimate heat sink, generally a large pool of water, by means of a second HEX.

The source of the energy in the primary NCL is the fuel rods in the reactor core, the coupling mechanism between the two loops is the SG, and a second HEX is used in the secondary loop to deposit the energy into the heat sink. All of this equipment, and the associated single- and two-phase thermal-hydraulic phenomena and processes, must be accounted for in the mathematical models developed for the system.

The fluid flow through the core, through the SG and the PRHRS HEX, is characterized by flow through parallel channels. The channels in the core are formed by the fuel rods and those in the SG and PRHRS by closed flow-tube channels. Such flow configurations, parallel flow channels, are susceptible to instabilities for single- and two-phase flows. Under long-term safe shut-down conditions the PRHRS is expected to be a two-phase flow system.

For Gen IV systems that have an integral containment and for the case of a piping break internal to the containment, three coupled NCLs must correctly operate to ensure removal of the energy from the core. An opening low in the RPV must be provided so that the expelled coolant can return from the containment back to the core region for the SG to transport energy to the PRHRS HEX.

In general, the major system-analysis codes are equipped to model all of the equipment components and associated physical phenomena and processes that are expected to occur. The codes and modeled natural-circulation and parallel-channel flows for the coupled NCL case require validation by comparisons of predictions with experimental data. The major codes, the several locally developed special-purpose models and codes, and application procedures have been validated by use of many of the simple pure thermal-hydro experiments and analytical results for NCLs and parallel-channel flows. However, in general, the general-purpose major codes must be validated for applications to complete coupled-loop systems for design, development of deep understanding, and safety-grade analyses.

16.10.6 Coupled natural-circulation loops

The few investigations into the properties and characteristics of coupled NCLs include Salazar et al. (1988) for idealized coupled loops with specified energy input and extraction over the primary and secondary loops, respectively. Wu (2011) has analyzed the case of a general number of coupled loops following the idealized approach of Welander. The mathematical model reduces to a system of coupled ordinary differential equations (ODEs) analogous to a coupled system of the equations developed by Lorenz (1963).

The major experimental loop for investigations of PRHRS coupled loops, and individual components, seems to be the VISTA facility (Park et al., 2014) in Korea. This facility, named Verification by Integral Simulation of Transients and Accident—Integral Test Loop (VISTA-ITL), has been developed to allow experiments involving coupled NCLs. The experimental data have been used for validation of the TASS/AMR-S (Yang et al., 2008) and MARS-KS thermal-hydraulic models and codes (Park et al., 2008, 2014). The data also can be used by other organizations for validation analyses. The VISTA-ITL facility is also used for experiments on the components that make up the complete system (Kim et al., 2013). A small-scale NCL, the Purdue University Multidimensional integral test Assembly (PUMA), has been constructed at Purdue University (Ishii et al., 1996). The Oregon State University—Multi-Application Small Light Water Reactor (OSU-MASLWR) loop in the United States is a scaled model of the complete NuScale natural-circulation machine (Mascari et al., 2012).

Men et al. (2014) have conducted experiments on the natural convection heat transfer for a PRHRS HEX in an in-containment refueling water storage tank. Several empirical correlations for the forced convection flow internal to the HEX tube and the natural convection heat transfer outside of the tube in the tank, for the vertical and horizontal portion of the tube, were compared with experimental data. The Dittus-Boelter forced convection correlation and the McAdams correlations for natural convection proved to give the better model of the data. Wenbin et al. (2014) have conducted experiments for the secondary loop of the Chinese Advance Pressurized Water Reactor for validation of the MISAP20 models and code. These and other papers are in a special issue of the *Science and Technology of Nuclear Installations* journal published in 2014 as indicated by the cited references.

16.10.7 Supercritical fluid states and natural-circulation loops

The historical investigations in the 1960s into supercritical fluids for NCLs and nuclear-powered machines were mentioned earlier. Chatoorgoon (1986, 2001) and Chatoorgoon et al. (2005a,b) presented additional early sources in addition to making new contributions. The renewed interest in supercritical fluid states for nuclear power applications has resulted in many new experimental, analytical, and numerical investigations.

The IAEA (2014) has produced a detailed summary of many aspects of supercritical natural-circulation thermal hydraulics and heat transfer for water reactors. The IAEA has identified SCWR concepts in Canada, China, Japan, Korea, Russia, and the Euratom organization. A report on the seventh International Symposium on SCWRs has been released (Penttila, 2015). Supercritical CO_2 has also been proposed as the working fluid. Sarkar et al. (2014) gave a state-of-the-art review for supercritical water, and Vijayan et al. (2013) have investigated the steady-state and stability properties of supercritical CO_2 NCLs. Ampomah-Amoako and Ambrosini (2013) have applied CFD for analyses of stability of flows of supercritical flows.

The significant rapid changes in thermodynamic state, transport, and thermophysical properties encountered when dealing with fluids under supercritical conditions open a potential for instabilities. Accounting for these variations, and the associated effects on fluid flow and heat transfer, also makes development of heat transfer and friction factor engineering models and correlations difficult. The significant changes act directly in the fluid and so directly affect the flow under natural-circulation conditions. Ambrosini (2007) has drawn an analogy between supercritical states and boiling.

The heat transfer and friction factor correlations for supercritical fluid states, and the stability of the flows used in the experiments, have been the subjects of many studies over the years. Pioro and Duffey (2003, 2005), Duffey and Pioro (2005), and Pioro et al. (2004) completed exhaustive and comprehensive reviews of the literature to that time, compiling massive amounts of literature, and reviewing friction factor and heat transfer coefficient correlations, and stability, among other issues. Cheng and Schulenberg (2001) reviewed the literature for applications to the high-performance LWR. Recent investigations that supplement that information include Zhang et al. (2010), Bae and Kim (2009), Bae (2011), Chen et al. (2014), Zhao et al. (2014),

Gu et al. (2015a,b), and Tilak and Basu (2015). The IAEA report (2014) and the conference proceedings by Penttila (2015) summarize the most recent information.

Swapnalee et al. (2012) and Chatoorgoon (2013) have validated the dimensionless numbers developed by Ambrosini and Sharabi (2008) and Debrah et al. (2013) for supercritical fluid data. Zhang et al. (2010) have given a three-dimensional model and numerical solution method for the case of a supercritical CO_2 rectangular NCL.

Jain and Conradini (2006) reported a difference between model predictions and experimental data with a time-domain model indicating instability and supercritical CO_2 NCL data indicating stability. For supercritical water a change to a more nearly accurate EoS in the frequency domain analysis indicated stability. The frequency domain studies continued to indicate instability for the supercritical CO_2 system; thus they are still not in agreement with experimental data. The frequency domain analyses for supercritical water and CO_2 did not always agree with the time domain results.

Jain and Rizwan-uddin (2008) report that the significant deviations from the results reported by Chatoorgoon et al. (2005b) of the numerical predictions with the Flow Instability Analysis under SuperCritical Operating conditions (FIASCO) model and code are likely due to the larger time step sizes used in previous studies. A larger time-step size increases numerical dissipation and dispersion and thus indicates stable states that are due to numerical artifacts and not physical reality. Chatoorgoon et al. (2007) reported that a time-step size refinement study leads to results that are in agreement with Jain and Rizwan-uddin. Increase in the pressure level with supercritical CO_2 shows a stabilizing effect similar to that observed in boiling two-phase NCLs. At a fixed power, an increase in pressure leads to reduced void fraction, which in turn leads to a decrease in wall friction and momentum flux pressure gradients—a stabilizing effect. The threshold power for OFI does not correspond to the maximum in the flow versus power curve.

16.10.8 Computational fluid dynamics

Considerations of distributions across the flow channel, transverse to the primary flow direction, were first included in basically one-dimensional models by approximating the temperature distribution in the fluid parallel to the flow direction. Recently there is an increasing application of CFD to various single- and two-phase thermal-hydraulic analyses, including NCLs and supercritical fluid states, in nuclear power systems. These approaches also allow for resolution of the thermal stratification in horizontal and vertical sections of the loop as well as resolution of gradients normal to the primary flow direction and the consequent effects on calculated stability. Fully three-dimensional analyses are becoming the norm, but only for simple idealized single-phase cases.

Burroughs (2003) and Burroughs et al. (2005) applied analytical and numerical methods to laminar flow in the standard NCL geometry and observed behavior of stable response at Prandtl numbers less than those observed in the usual Lorenz (1963) ODE model. Pilkhwal et al. (2007) observed that CFD results demonstrated the onset of instabilities that could not have been observed with standard

one-dimensional analyses. Angelo et al. (2012) have applied CFD to the steady-state analysis of an operating NCL.

Yadav et al. (2012a,b) applied CFD modeling to determine heat transfer and friction factor correlations for CO_2 flows in NCLs, and investigated performance and stability of supercritical CO_2 NCLs having HEX BCs. He et al. (2004, 2008) and Sharabi et al. (2008b) applied CFD and turbulence modeling to heat transfer analysis of supercritical states. Jackson (2013), one of the pioneers in the mixed-convection heat transfer area, has presented a nice summary of many aspects. Angelo et al. (2012), Ampomah-Amoako and Ambrosini (2013), Desrayaud et al. (2013), Jingjing et al. (2015), and Sharabi et al. (2008a) also investigated supercritical NCLs for stability by a CFD approach. Misale et al. (2000) introduced the effects of two-dimensional heat conduction into NCL stability analyses.

16.10.9 Nanofluids

NCLs based on working fluids containing nanoparticles have been investigated (eg, Misale et al., 2012). Yu et al. (2015) have experimentally investigated the effects of nanoparticles on the onset of nucleate boiling (ONB) and OFI. Both of these subjects are in the initial stages of investigations. Interaction of the nanoparticles with the microscopic structure of a boiling surface is indicated.

16.10.10 Sodium fast reactors

Aoto et al. (2014) presented a summary of recent SFR developments. Sabharwall et al. (2012) investigated the effects of axial conduction in the fluid of a liquid metal reactor and concluded that the effect is small for the fluids of interest and natural-circulation conditions.

The Experimental Breeder Reactor (EBR-II) development activities in the United States in the 1980s included studies of natural circulation in this machine (Gillette et al., 1980; Planchon et al., 1985; Singer et al., 1980). Ha et al. (2010) validated the MARS models and code with EBR-II test data. The IAEA (2013) conducted a blind benchmark exercise using data from the PHENIX sodium-cooled reactor.

16.10.11 Parallel channels

The core of nuclear reactors is an example of a component in an NCL in which flow in parallel channels occurs. The stability of the parallel-channel flow through the core must be investigated, and these investigations include effects of conjugate heat conduction and energy production by fission in the material adjacent to the fluid. Single- and two-phase flows under steady-state and transient conditions are important considerations relative to safety analyses of Gen IV machines.

As in the case of the previous sections, there is an enormous literature on stability of fluid flow in single and multiparallel channels. The review by Kakac and Bon (2008) is especially complete to that time. Ruspini (2013) and Ruspini et al. (2014) include this situation in their review. Munoz et al. (2002) and Vyas et al. (2010) studied

parallel-channel instability in BWRs. Recent activity has focused on supercritical thermodynamic states. Xiong et al. (2013, 2012), Gu et al. (2015a,b), and Dutta et al. (2015) have all investigated the onset of instability, in single and parallel channel, for the supercritical thermodynamic state fluid case.

The RELAP5 models and code have been validated with fundamental data for OFI in single and parallel channels (Hamidouche and Bousbia-salah, 2006; Gartia et al., 2007; Colombo et al., 2012a). Kommer (2015) has tested the TRACE code (U.S. NRC, 2008) by simulations of OFI for simple and parallel channels.

The parallel flow channels in the helical-coil SG that is used in integral SMRs represents a potential for instabilities. Experimental and theoretical research on the stability characteristics of this parallel channel flow has been given by Guo et al. (2001) and Colombo (2013). Colombo et al. (2012b) and Papini et al. (2014) have validated the RELAP5 models and code for this application.

16.11 Modeling natural-circulation loops

Single NCLs have been the subject of experimental, analytical, and numerical research for several decades since the early 1950s. The literature is very extensive with investigations continuing to this day. Much of the research has been directed toward various systems of electric power generation by nuclear power plants. A brief review of some of the literature has been given earlier in this chapter.

On the other hand, systems composed of two or more coupled NCLs have not been much investigated. The objectives of the present notes include development of model equations for steady-state and transient flows in coupled NCLs, including realistic BC representations. The design of such systems, an interesting optimization problem, is not addressed here.

16.11.1 Single channels and parallel channels

Before considering NCLs, a brief summary of the basic equations used for stability modeling and analysis for a single channel, or parallel channels, is given in the following paragraphs. The potential for instabilities to occur in equipment based on parallel-channel flows exists in the core and SG of Gen IV machines.

The model equations for mass, momentum, and energy balance and the EoS that will be useful in the following discussions are summarized in the following paragraphs. Any number of textbooks have detailed derivations and discussions (eg, Todreas and Kazimi, 1990; Collier and Thome, 1996). An area-averaged, transient, one-dimensional formulation for compressible fluids will be sufficient for the applications considered in this chapter. Some aspects of accounting for separate speeds for the vapor and liquid phases in a two-phase mixture are also included.

Mass conservation for the mixture of liquid plus vapor is

$$\frac{\partial}{\partial t}\rho A_f + \frac{\partial}{\partial z}W = 0 \qquad [16.1]$$

The mixture mass flow rate is the sum of the liquid and vapor flows,

$$W = W_\mathrm{l} + W_\mathrm{g} \qquad [16.2]$$

where $W = \rho u A_\mathrm{f}$, $W_\mathrm{l} = \alpha_\mathrm{l}\rho_\mathrm{l}u_\mathrm{l}A_\mathrm{f}$, and $W_\mathrm{g} = \alpha_\mathrm{g}\rho_\mathrm{g}u_\mathrm{g}A_\mathrm{f}$; α is the void fraction; ρ is the density of the fluid mixture; and u is the mixture fluid speed in the axial direction parallel to the flow channel walls. The flow area might vary in the direction of flow. Other quantities that are needed in the following developments are the mass fraction occupied by each phase or fluid in a volume of fluid mixture, $\overline{X}_\mathrm{l}^\mathrm{m} = M_\mathrm{l}/M \quad \overline{X}_\mathrm{g}^\mathrm{m} = M_\mathrm{g}/M \quad M = \rho V$, where $M_\mathrm{l} = \alpha_\mathrm{l}\rho_\mathrm{l}V$ and $M_\mathrm{g} = \alpha_\mathrm{g}\rho_\mathrm{g}V$. Mass conservation for the vapor phase is

$$\frac{\partial}{\partial t}\alpha_\mathrm{g}\rho_\mathrm{g}A_\mathrm{f} + \frac{\partial}{\partial z}W_\mathrm{g} = \dot{m}_\mathrm{lg}A_\mathrm{f} \qquad [16.3]$$

where $\dot{m}_\mathrm{lg}$ is the net mass exchange, per unit fluid volume, between the liquid and vapor with conversion of liquid to vapor taken as positive. For example, in the case of subcooled boiling, the net mass exchange is given by the difference between the portion of the heat transfer that goes to phase change and the recondensation of that vapor into the subcooled liquid (eg, Hughes et al., 1981).

A momentum balance model for the mixture of liquid plus vapor is

$$\begin{aligned}\frac{\partial}{\partial t}\frac{W}{A_\mathrm{f}} + \frac{\partial}{\partial z}\frac{W^2}{\rho A_\mathrm{f}^2} + \frac{\partial}{\partial z}\overline{X}_\mathrm{g}^\mathrm{m}\overline{X}_\mathrm{l}^\mathrm{m}\rho V_\mathrm{SL}^2 = &-\frac{\partial}{\partial z}P - K_\mathrm{wf}\frac{W|W|}{\rho A_\mathrm{f}^2} \\ &- K_\mathrm{ll}\frac{1}{2}\frac{W^2}{\rho A_\mathrm{f}^2}\delta(z - z_\mathrm{ll}) - \rho g\cos\theta\end{aligned} \qquad [16.4]$$

where θ is the angle between the flow direction and the vertically upward positive z-axis and $\delta(z - z_\mathrm{ll})$ is the Dirac-delta function, where z_ll is the location of a local flow perturbation. The third term on the left-hand side accounts in the momentum flux term for the speed difference between the vapor and liquid, $V_\mathrm{SL} = (u_\mathrm{g} - u_\mathrm{l})$, and is usually denoted as the slip velocity. The second and third terms on the right-hand side must account for the two-phase nature of the mixture usually by means of two-phase multipliers or a mechanistic model of the flow field. The third term accounts for irreversible pressure losses at significant geometric features in the flow field. A contribution to the momentum balance due to mass exchange has been neglected because it is generally small and usually does not significantly affect the motion of either phase parallel to the flow channel walls.

The speed of each phase or fluid can be expressed in terms of the mixture speed and the slip speed by $u_\mathrm{l} = u - \overline{X}_\mathrm{g}^\mathrm{m}V_\mathrm{SL}$ and $u_\mathrm{g} = u + \overline{X}_\mathrm{l}^\mathrm{m}V_\mathrm{SL}$. A model is needed for the slip velocity, and a few options are available. The momentum equation models for the liquid and vapor can be subtracted to get a fully dynamic model for the difference. That equation can additionally be simplified to the interphase-friction-and-gravity

dominated case to get an algebraic equation for the velocity difference. This simplified dynamic slip approach forms a basis for a drift-flux model approach that is frequently used for a velocity difference. Alternatively, any of the many algebraic slip ratio models and correlations can be used.

The two momentum equations and development of the velocity slip from them are not considered in this chapter. In general, the more detailed two-phase flow models are applied to problems by use of computer models that are based on the more detailed approaches.

The energy conservation model for the mixture based on the enthalpy formulation is

$$\frac{\partial}{\partial t}\rho h A_f + \frac{\partial}{\partial z}\left(Wh + \overline{X}_g^m \overline{X}_l^m \rho A_f (h_g - h_l) V_{SL}\right) = p_{wh} q''_w \qquad [16.5]$$

where p_{wh} is the heated perimeter of the wall and q''_w is the wall-to-mixture heat flux.

The EoS returns the density and temperature as functions of two thermodynamically independent state properties; for example, $\rho_l = \widehat{\rho_l}\,(P, h_l)\; T_l = \widehat{T_l}\,(P, h_l)$. Instead of treating the full thermal nonequilibrium, unequal-temperature case, a less general approach is to take the vapor to be at the saturation temperature corresponding to the local pressure $\rho_g = \widehat{\rho_{gs}}\,(P)\; T_g = \widehat{T_{gs}}\,(P)\; h_g = \widehat{h_{gs}}\,(P)$ (Hughes et al., 1981; Hughes and Katsma, 1983). This assumption has been proven to be good for most two-phase flow regimes, but in general it cannot be extended to all two-phase flow situations. The model balance equations with an equation for the velocity difference and the EoS are sufficient to solve the system.

The wall heat flux, q''_w, can be handled in several ways: (1) as a specified constant; (2) as a specified function of location along the flow channel; (3) provided by nuclear reactions within the solid wall bounding the fluid and that described by point kinetics or temporal and spatial variations in neutron transport and coupled to heat transfer between the fluid and wall as

$$q''_w = h_{cw}(T_w - T) \qquad [16.6]$$

where h_{cw} is the wall-to-fluid convective heat transfer coefficient, or (4) determined by the performance of an HEX.

For boiling of a saturated mixture the mass exchange per unit volume is

$$\dot{m}_{lg} = \frac{h_{cw}\overline{A}_{wh}(T_w - T)}{(h_{gs} - h_{ls})} \qquad [16.7]$$

where $\overline{A}_{wh}$ is the heated wall area per unit fluid volume. For bulk temperature less than the saturation value, models will be needed for the wall-to-phase energy and mass exchange.

The case of boiling in the flow channels, the most interesting case, calls for a somewhat detailed treatment of the wall-to-fluid heat transfer mechanisms along the channel. In general, for vertical upflow in a heated channel in order from a subcooled

inlet the state of the wall is usually described as follows. Convection heat transfer to subcooled liquid, onset of nucleation (OON) with superheated fluid adjacent to the heated wall and a subcooled bulk fluid state, ONB, partial subcooled boiling, onset of significant void (OSV), fully developed subcooled boiling, and on through saturated boiling and high void fraction liquid film vaporation, to dispersed flow boiling, and finally to heat transfer to superheated single-phase vapor. In general, the details of the boiling between the OON and bubble departure are not resolved.

All of these might occur under natural convection, mixed convection, or natural-circulation conditions and each of these as laminar or turbulent flow. At the same time, detailed descriptions of the wall-to-fluid friction must also consider the states of the fluid near the wall and in the bulk. The number of empirical correlations needed to cover all possibilities for heat transfer and wall friction is large.

Close accounting for the boiling mechanisms led to early successes in prediction of stability boundaries (Grace and Krejsa, 1967; Jeglic and Grace, 1965; Lowdermilk et al., 1958). In general, when the focus is on a point of significant change, in contrast to distributions, close consideration of each term in the model equations is required. For example, the individual terms in these equations can be mapped to the list of instability initiating phenomena given in Section 16.10.

Supercritical fluid states, although avoiding some of these mechanisms, have unique heat transfer and wall friction characteristics that must be addressed. The rapid changes in the thermodynamic state and thermophysical and transport properties of supercritical fluid states is (very) roughly somewhat analogous to the changes encountered during boiling of normal fluids. The change in mixture density due to boiling and flashing, or condensation, is an example.

Detailed descriptions of all of the flow and heat transfer mechanisms is beyond the scope of the present text. Furthermore, it is difficult to provide a definitive list of suggested data sets and correlations for all possible combinations of flow and heat transfer mechanisms, especially when flow-channel geometry effects and supercritical fluid states are taken into consideration. See the literature review in this chapter for additional information.

Initial conditions and BCs must be specified for transient applications and BCs alone for steady-state applications. Typical BC sets include (1) flow and thermodynamic state provided at the inlet to a flow channel and pressure specified at the outlet and (2) the pressure change across the flow channel is specified. In the first case the calculations yield the pressure at the inlet, and all along the channel, and the distribution of the thermodynamics state along the channel. In the second case, the calculations give the flow and the pressure and temperature distribution along the channel.

Almost all analytical investigations into parallel channel and NCL instability are based on a subset of the general equations previously given. Muñoz-Cobo et al. (2002) use a zero-dimensional approach, and Ambrosini et al. (2001) use one-dimensional models, accurate finite-difference approximations, and numerical solution methods. Investigations based on a more general formulation of the problem are usually performed with computer models of the flow situation (Ambrosini and Ferreri, 2006). Data from experiments that were developed to test the less general formulations are used for validation exercises for the more general computer models. As time

progresses both the experiments and the computer model calculations move toward increased spatial resolution and more detailed mathematical models of the physical domain. Several of the detailed investigations have been summarized in the literature review in this chapter.

The zero-dimensional approach is frequently applied to the separate regions of boiling channels and system. The general equations are specialized and applied to the single-phase, nonboiling, and subcooled partial boiling portions; the saturated boiling boundary; the riser above the heated energy source; and so forth (eg, Ishii, 1976; Anderson et al., 1962; Yadigaroglu and Bergles, 1969). The zero-dimensional approach has an advantage in that accounting for the thermal response of the solid material adjacent to the fluid is straightforward. The zero-dimensional approach also has the advantage that a system of ODEs is obtained and these can be solved, to any order of accuracy required, by off-the-shelf ODE system solvers.

Studies of the static OFI are performed with the steady-state form of the earlier equations (eg, Duffey and Hughes, 1991; Rohatgi and Duffey, 1998; Duffey and Sursock, 1987; Zvirin et al., 1981). Chatoorgoon (2001, 2013) has applied the approach to supercritical fluid states. The correlation by Whittle and Forgan (1967) has been shown to be a good fit to the experimental data. The authors suggested that OFI roughly corresponds to bubble detachment, OSV, for the case of boiling of subcooled water.

Constant total pressure drop across the channel BCs is typically imposed by use of a large bypass channel or by attaching large plena to the entrance and exit. Parallel-channel tests are also conducted with large plena. Channels in which the pressure drop is imposed by pumping power injected into the fluid are usually not constant-pressure drop systems. For applications in the frequency domain the equation system is linearized about a uniform initial state.

The phase change number and the subcooling number are dimensionless groups that are used to display the regions of stable and unstable responses—the stability map (see Ishii, 1976; Rohatgi and Duffey, 1998, among dozens of others).

$$N_{\mathrm{ph}} = \frac{Q}{Wh_{\mathrm{fg}}}\rho_{\mathrm{f}s}\left(\frac{1}{\rho_{\mathrm{gs}}} - \frac{1}{\rho_{\mathrm{ls}}}\right) \qquad [16.8]$$

and

$$N_{\mathrm{sub}} = \frac{(h_{\mathrm{ls}} - h_{\mathrm{in}})}{h_{\mathrm{fg}}}\rho_{\mathrm{fs}}\left(\frac{1}{\rho_{\mathrm{gs}}} - \frac{1}{\rho_{\mathrm{ls}}}\right) \qquad [16.9]$$

Experimental studies have indicated the following characteristics:

Instability can be introduced by an increase in the power supplied to the fluid and by a decrease in the mass flow rate.
An increase in local pressure loss at the inlet is always stabilizing whereas an increase in the local loss at a two-phase exit is always highly destabilizing.

A compressible volume following the inlet restriction leads to instability.
In general, distributed wall friction and local losses in a single-phase region are always stabilizing.

These properties are in complete agreement with those that were discovered in the 1950s for stability of NCLs.

Validation of system-analysis codes by comparisons of predictions with experimental data is necessary for applications of the models and codes to Gen IV machines. Rohde et al. (2010) have compared ATHLET and TRAGG code predictions with data from the scaled GENESIS facility for applications to the ESBWR. Colombo (2013), Colombo et al. (2012a,b), and Papini et al. (2014) have applied the RELAP5/MOD3.3 models and code to experimental data for two-phase flows in models of a helically coiled SG of the type to be used in Gen IV SMRs. Gartia et al. (2007) have applied the RELAP5 systems-analysis code to the case of an NCL with parallel channels. Vyas et al. (2010) conducted an experiment with boiling and 10 parallel channels. Xiong et al. (2012, 2013) presented modeling and analysis of supercritical water flows in parallel channels. Walter and Linzer (2006) studied the effects of pressure level in an NCL with two unequally heated parallel pipes.

16.11.2 Single natural-circulation loop

Before taking up the coupled NCL case, the single NCL case will be briefly summarized. A sketch of a single NCL is shown in Fig. 16.3. The BC at the source is assumed to be a constant energy supply, and the sink is assumed to be supplied by a constant heat transfer coefficient and sink temperature. These are relatively simple BCs, and the horizontal source and sink also simplify the modeling and analysis. Rao et al. (2005a,b,c,d, 2008) seem to be the first to have considered realistic BCs represented by HEXs. Kumar and Gopal (2009) have also analyzed an NCL with HEX BCs.

Note that the energy source and sink are shown to be horizontal in Fig. 16.3. Other arrangements include having the source and/or sink in a vertical segment, or having one or the other of the source or sink vertical and the other horizontal. The source is always at a lower elevation that the sink in all cases. In the case of horizontal source and sink the thermal center of both the source and sink are determined solely by the geometry of the system and are not a function of the thermal processes occurring within the BCs.

The flow direction is shown to be in the clockwise sense, but NCLs will operate in either direction, unless means are employed to ensure unidirectional flow. In addition, the very simple geometry of the loop shown in Fig. 16.3 is an idealization of the possible geometry of NCLs, which instead may be complex, having different path lengths, flow areas, and plumbing fixtures.

The NCL system shown in Fig. 16.3 should include a means to maintain the pressure level in the system (eg, a pressurizer partially filled with liquid and the remaining filled with a gas or vapor, connected to the loop piping). Even a simple model of a

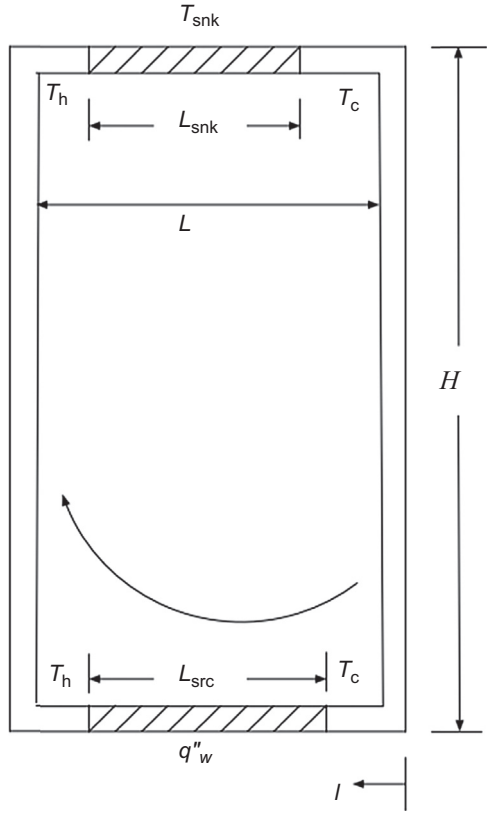


Figure 16.3 Single natural-circulation loop.

pressurizer would introduce additional degrees of freedom that are not needed for the following discussions. However, note that the dynamics of the pressurizer will affect the dynamics of the system. These effects are generally not included in most analytical models.

No leakage paths are considered for most analyses of simple NCLs; the loop is closed, therefore the mass in the system is constant. For example, steam extraction and condensate injection, an NCL with through-flow (Mertol et al., 1981), is not considered here. Note that the dynamics of the BCs and the dynamics of these additional considerations in reality have a potential to affect the dynamic response of the system.

Only the single-phase flow case is considered in this chapter. In general, modeling and analyses of two-phase flow NCLs are conducted in the time domain by applications of system-analysis models and computer codes, and these are based on highly detailed and complex models of two-phase flows. Analyses based on these detailed models are basically analytically intractable.

This initial summary will consider only constant-diameter loops and all of the usual assumptions and idealizations applied to NCL flows. These idealizations include the following:

1. Constant thermophysical and transport properties for the fluid.
2. Uniform distributions of all flow-field quantities across the flow channels.
3. The fluid is thermally expandable: variations in density with pressure are neglected.
4. Buoyancy forces due to fluid density variations are accounted for by the linear Bousinesq approximation.
5. Conduction heat transfer characteristics of the all piping-wall materials can be neglected when modeling transient response.
6. Axial heat conduction in the working fluids and piping materials is neglected.
7. Energy losses from the outside of the piping is neglected.
8. Conversion of mechanical energy into thermal energy by means of viscous dissipation is neglected.
9. Pressure-volume work terms in the energy equation model are also neglected.
10. Parallel flow paths everywhere in the systems are not accounted for.

These idealizations are usually applied to analyses of natural convection and natural-circulation flows. Note that use of these assumptions introduces the likelihood that important aspects of the onset of instabilities will not be correct. Each of these assumptions must be validated because potential effects on the onset of instability are subtle. In general, all assumptions and idealizations require in-depth justification in order that false positives and false negatives are eliminated.

All mathematical models and computer codes that are used for safety-grade steady-state and transient analyses of nuclear reactor systems are sufficiently general that almost none of these assumptions are necessary. Two-phase fluid states are the norm for these models and codes. Although many include axial heat conduction in piping materials, two- and three-dimensional modeling within the working fluids is a specialized application and has recently begun to receive attention.

With these assumptions and applying the general equations given previously, the following system of model equations is obtained. Mass conservation, Eq. [16.1], gives

$$\frac{\partial}{\partial l} W = 0 \qquad [16.10]$$

which gives

$$W = W(t) \qquad [16.11]$$

where l measures the distance along the loop. The mass flow rate is everywhere the same and is a function of time alone. At steady state $W = W_{ss}$.

Integrating the momentum balance, Eq. [16.4], around the loop gives

$$\frac{L_t}{A_f} \frac{d}{dt} W = \oint \rho(T) g \cos\theta dl - R_{wf}(W) \frac{W|W|}{\rho A_f^2} \qquad [16.12]$$

where the fluid density, $\rho(T)$, is assumed to be a function of temperature alone,

$$\rho = \rho_0[1 - \beta(T - T_0)] \qquad [16.13]$$

and the loop flow resistance is composed of distributed wall friction and local losses

$$R_{\mathrm{wf}}(W) = \left[\frac{1}{8}\overline{A}_{\mathrm{wf}} f_{\mathrm{wf}} L_{\mathrm{t}} + \frac{1}{2}\sum_j K_{j\mathrm{ll}}\right] \qquad [16.14]$$

where $R_{\mathrm{wf}}(W)$indicates a function of the mass flow rate, about which more is given in Section 16.11.3.

For the loop in Fig. 16.3, with the source and sink horizontal, Eq. [16.12] gives

$$\frac{L_{\mathrm{t}}}{A_{\mathrm{f}}}\frac{d}{dt}W = \rho_0\beta g H(T_{\mathrm{h}} - T_{\mathrm{c}}) - R_{\mathrm{wf}}(W)\frac{W|W|}{\rho_0 A_{\mathrm{f}}^2} \qquad [16.15]$$

The energy conservation model, Eq. [16.5], for the flow direction shown, is

$$\frac{\partial}{\partial t}T + \frac{W}{\rho_0 A_{\mathrm{f}}}\frac{\partial}{\partial l}T = \frac{p_{\mathrm{wh}}}{\rho_0 C_{\mathrm{p}} A_{\mathrm{f}}} q''_{\mathrm{w}} \qquad [16.16]$$

for the energy supply source at the bottom of the loop,

$$\frac{\partial}{\partial t}T + \frac{W}{\rho_0 A_{\mathrm{f}}}\frac{\partial}{\partial l}T = 0 \qquad [16.18]$$

for the unheated sections of the loop, and

$$\frac{\partial}{\partial t}T + \frac{W}{\rho_0 A_{\mathrm{f}}}\frac{\partial}{\partial l}T = \frac{p_{\mathrm{wh}}}{\rho_0 C_{\mathrm{p}} A_{\mathrm{f}}} h_{\mathrm{csnk}}(T_{\mathrm{snk}} - T) \qquad [16.19]$$

for the energy sink at the top of the loop.

The recipe for performing a stability analysis of the model equations is as follows. Set and solve the steady-state form of the equations previously listed. This gives the mass flow rate as a function of the loop resistance

$$R_{\mathrm{wf}}(W_{\mathrm{ss}})\frac{W_{\mathrm{ss}}|W_{\mathrm{ss}}|}{\rho_0 A_{\mathrm{f}}^2} = \rho_0\beta g H(T_{\mathrm{hss}} - T_{\mathrm{css}}) \qquad [16.20]$$

The temperature difference across the energy source from Eq. [16.16] is

$$T_{\mathrm{hss}} = T_{\mathrm{css}} + \frac{p_{\mathrm{wh}} L_{\mathrm{src}}}{W_{\mathrm{ss}} C_{\mathrm{p}}} q''_{\mathrm{w}} \qquad [16.21]$$

The temperature ratio at the outlet from the sink is

$$\frac{(T_{\text{snk}} - T_{\text{css}})}{(T_{\text{snk}} - T_{\text{hss}})} = \text{e}^{-\frac{h_{\text{c snk}}\, p_{\text{wh}}\, L_{\text{snk}}}{W_{\text{ss}} C_{\text{p}}}} \qquad [16.22]$$

so the cold side outlet temperature is

$$T_{\text{css}} = T_{\text{snk}} + \frac{p_{\text{wh}} L_{\text{src}}}{W_{\text{ss}} C_{\text{p}}} q''_{\text{w}} \left[\text{e}^{\frac{h_{\text{c snk}}\, p_{\text{wh}}\, L_{\text{snk}}}{W_{\text{ss}} C_{\text{p}}}} - 1 \right]^{-1} \qquad [16.23]$$

where the exponent is the Stanton number times an area ratio

$$\frac{h_{\text{c snk}}\, p_{\text{wh}}\, L_{\text{snk}}}{W_{\text{ss}} C_{\text{p}}} = \mathbf{St} \frac{A_{\text{hsrc}}}{A_{\text{f}}} \qquad [16.24]$$

The factor on the right-hand side of Eq. [16.24] represents the overall thermal conductance between the sink temperature and the energy source.

Because the energy exchange at the sink is a temperature-controlled process, design of the energy exchange device at the sink requires an iterative approach. Some kind of control system will be necessary to maintain the system at approximate steady conditions when operating. The results of this simple system are often expressed in terms of dimensionless numbers (eg, Todreas and Kazimi, 1990), and Eq. [16.20] can be written as

$$\frac{b}{2} \mathbf{Re}^{2-m} = \mathbf{Gr}_{D_{\text{he}}} \left(\frac{H}{L_{\text{t}}} \right) \qquad [16.25]$$

where the Grashof number is in terms of the heated equivalent diameter of the loop piping

$$\mathbf{Gr}_{D_{\text{he}}} = \frac{g\beta(T_{\text{hss}} - T_{\text{css}}) D_{\text{he}}^3}{\upsilon^2}$$

and the value of m is given by the distributed wall-friction factor correlation

$$f_{\text{wf}} = C_{\text{wf}} / \mathbf{Re}^m$$

Stability is investigated in the frequency domain by considering the linearized form of the transient equations. The linear system can usually be analytically solved; if not, then numerical methods are then used. The algebra getting to the final characteristic equation is straightforward but somewhat lengthy and tedious and is not included here. Again, numerical methods might be needed to solve the characteristic equation. Many of the papers listed in the previous section can be consulted for details. Rao et al. (2005d, 2008) and Sabharwall et al. (2012) have worked out the details for somewhat

complex cases. Stability in the time domain is investigated by means of numerical methods applied to the nonlinear equations.

This analysis is an example of the classic approach to analysis of NCLs. However, as noted in the previous discussions, several aspects of actual NCLs in the physical domain are not included in the approach. In practice, each of the omitted factors needs to be addressed for its potential to lead to instabilities.

16.11.3 Coupled natural-circulation loops

The corresponding modeling for coupled NCLs is summarized in the following paragraphs.

A sketch of two coupled NCLs is shown in Fig. 16.4, in which the loops are vertically adjacent. Energy addition into the system is represented by a horizontal section at the bottom of the bottom primary loop and energy rejection by a horizontal section at the top of the top secondary loop. A horizontal HEX section between the loops represents the thermal coupling. The figure indicates that pressurizers are attached to each loop for pressure regulation. Leakage paths, and other physical domain equipment, are not included.

A system that is based on NC flow through the reactor core and has NC flow on the secondary side of the SG is, in effect, two coupled NCLs. The secondary loop is the fluid system on the secondary side of the SG, and the ultimate energy sink in that loop is the condenser downstream of the turbines. Of course, the turbines also remove energy from that fluid stream. The SG loop has through-flow with the extraction being the vapor and the injection being the return of the condensate into the secondary side of the SG.

The sketch in Fig. 16.4 indicates clockwise flow in the hot primary loop and the cool secondary loop. This arrangement indicates countercurrent flow in the BCs and coupling HEXs. Note that there are four equally likely arrangements of the flow in the loops for the system shown in the figure: clockwise or counter-clockwise in either loop.

An analysis of NCLs requires that the spatial distributions of the state of the fluid around the loops be known. Thus each flow direction arrangement must be accounted for in the development of the model equations and the associated solutions. NCLs such as shown in Fig. 16.4 will operate in either direction. Properly located supplemental energy addition and rejection could be used to ensure the flow directions at steady-state conditions.

The temperature distribution in the working fluids in the HEX BCs is also required. Thus the inlet and outlet ends of the source and sink HEXs must be specified. The sketch indicates countercurrent flow in the boundary HEXs. The fluid temperature at the inlet to the energy source and sink will be specified and might be a function of time.

A different arrangement is shown in Fig. 16.5, which shows a horizontal energy addition at the bottom of the left-side primary loop, a vertical HEX coupling the loops, and energy rejection in a horizontal section at the top of the right-side secondary loop.

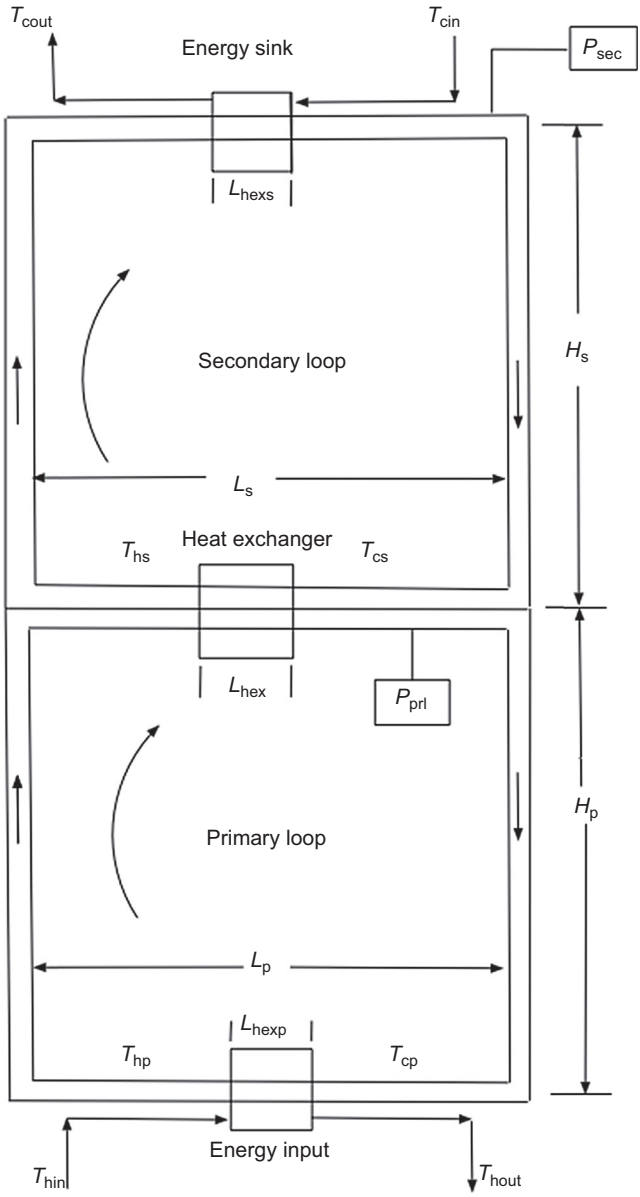


Figure 16.4 Two vertical coupled natural-circulation loops.

The energy source and sink are represented by arbitrary spatial distributions, and these can also be time dependent.

If instability results in reverse-flow direction in either or both of the loops, then the distributions in the working fluids must account for the new alignments. Accounting

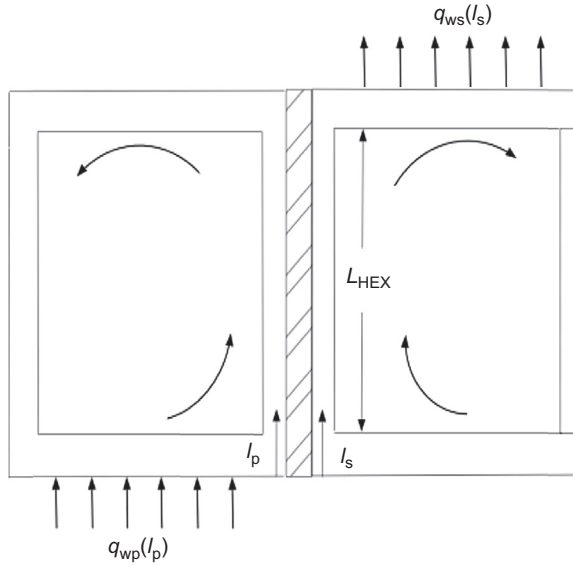


Figure 16.5 Two horizontal coupled natural-circulation loops.

for all possible combinations of flow directions in the loops and BC HEXs leads to a large number of possibilities, and these cannot all be captured in a single system of model equations.

In general, the dimensions of the loops can be different and variable around the loops. For example, in Figs. 16.4 and 16.5, although the horizontal and vertical dimensions are shown to be somewhat symmetrical, that is not a requirement. All of the dimensions of both loops and all HEXs can be different. For example, a nuclear reactor will generally involve several flow-area changes in the primary and secondary loops. Constant cross-sectional flow area is assumed here. This simplification is applied solely to ease the equation processing and can be incorporated in a straightforward manner.

The modeling is based on adaptation of the equations in the previous section to the coupled loops case. The model equations developed herein will be written for the case of single-phase flow in the primary and secondary loops. Both steady-state and off-normal transient conditions in the Gen IV nuclear reactor case involve two-phase fluid states. Safety-grade analyses of design and off-normal states will generally be handled by systems-analysis models and codes that easily accommodate generalized geometry, fluid states, and flow directions.

A statement of conservation of mass for one-dimensional flow is

$$\frac{\partial}{\partial t}\rho A_f + \frac{\partial}{\partial l}\rho u A_f = 0 \qquad [16.26]$$

where l measures the distance along a loop. Integration around the hot primary loop for the case that there might be leakage from the loop gives

$$\frac{d}{dt}M = w_{\mathrm{lpin}} - w_{\mathrm{lpout}} \qquad [16.27]$$

where w_{lp} is a leakage flow for the primary loop, or through-flow as in the case of steam extraction from an SG and condensate return back into the loop. If these mass flows are equal, then Eq. [16.27] indicates that the mass of fluid in the loop is constant. Failure to maintain the mass and energy content of a loop opens significant potential for failure of the natural circulation to be maintained. In particular, loss of fluid without the possibility of replenishing the loss will very likely lead to complete failure of the operation of the systems. In a general case, the leakage flows might be functions of time.

When the vapor off-take and condensate input are equal and do not vary in time, the mass in the hot primary loop is constant. The same considerations apply to the secondary loop whenever it is operational. Likewise, application of the considerations to the energy conservation models for both loops shows that the energy content will change if the extraction and injection are not equal. The developments carried out in the following will not consider the general case of loss of fluid from the systems.

If there is no loss of fluid, then the mass content is always constant and Eq. [16.26] gives

$$\frac{d}{dl}W = 0 \qquad [16.28]$$

Application to each loop gives $W_{\mathrm{p}} = W_{\mathrm{p}}(t)$ and $W_{\mathrm{s}} = W_{\mathrm{s}}(t)$. For steady-state conditions, $W_{\mathrm{p}} = W_{\mathrm{pss}}$ and $W_{\mathrm{s}} = W_{\mathrm{sss}}$.

In the absence of extraction and re-injection, the mass flow around the loop is a function of time alone and is everywhere constant. If extraction and re-injection are present, then the mass flow rate varies with time and space along the flow paths, the mass and energy content changes as a function of time, and the operation as an NCL can be destroyed. If the SG operation is modeled, then the flow is constant but different in various parts of the system: the total flow for those parts that include the energy source and a reduced flow downstream of the extraction point. If the steam flow is w_{stmp}, and the flow through the energy source in the primary loop is W_{p}, then the flow downstream of the steam-extraction location is $W_{\mathrm{p}} - w_{\mathrm{stmp}}$.

A one-dimensional form of the momentum balance equation for engineering applications in flow networks and engineered equipment is (Todreas and Kazimi, 1990)

$$\frac{\partial}{\partial t}\frac{W}{A_{\mathrm{f}}} + \frac{\partial}{\partial z}\frac{W^2}{\rho A_{\mathrm{f}}^2} = -\frac{\partial}{\partial l}P - K_{\mathrm{wf}}\frac{W|W|}{\rho_0 A_{\mathrm{f}}^2} - K_{\mathrm{ll}}\frac{1}{2}\frac{W|W|}{\rho_0 A_{\mathrm{f}}^2}\delta(z - z_{\mathrm{ll}}) - \rho g\cos\theta \qquad [16.29]$$

where θ is the angle between the flow direction and the vertically upward positive z-axis, $\delta(z - z_{ll})$ is the Dirac-delta function, and ρ_0 is the reference density used in the EoS.

The momentum balance model for the NCLs in Figs. 16.4 and 16.5 is obtained by integration of Eq. [16.29] around a loop to get

$$\frac{L_{tp}}{A_{fp}}\frac{\partial}{\partial t}W_p = \oint_{L_{tp}} g\rho_p(T_p)\cos\theta_p dl_p - R_{wfp}(W_p)\frac{W_p|W_p|}{\rho_{0p}A_{fp}^2} \quad [16.30]$$

for the primary hot loop and

$$\frac{L_{ts}}{A_{fs}}\frac{\partial}{\partial t}W_s = \oint_{L_{ts}} g\rho_s(T_s)\cos\theta_s dl_s - R_{wfs}(W_s)\frac{W_s|W_s|}{\rho_{0s}A_{fs}^2} \quad [16.31]$$

for the secondary cool loop.

The loop flow resistance, the last term on the right-hand side of Eqs. [16.30] and [16.31], is

$$R_{wf}(\cdot) = \left[\frac{1}{8}\overline{A}_{wf}f_{wf}L_t + \frac{1}{2}\sum_j K_{jll}\right] \quad [16.32]$$

where $R_{wf}(\cdot)$ indicates a function of the respective mass flow rates and the geometric details of the loop. The first contribution in Eq. [16.32] is due to distributed wall friction and the second is due to local irreversible losses at location j.

For the case of steam extraction and injection, Eq. [16.30] obtains from the injection location to the extraction location, and

$$\frac{L_{tp}}{A_{fp}}\frac{\partial}{\partial t}(W_p - w_{stmp}) = \oint_{L_{tp}} g\rho_p(T_p)\cos\theta_p dl_p - R_{wfp}(W_p - w_{stmp})\frac{(W_p - w_{stmp})|W_p - w_{stmp}|}{\rho_{0p}A_{fp}^2} \quad [16.33]$$

holds from the extraction location to the injection location. A model equation for the loss of fluid, a momentum balance for example, is needed for w_{stmp}.

Note that integration completely around the loop has averaged out all spatial locations for the pressure gradients due to distributed wall friction and local losses and changes in flow area. The latter are represented by the second term on the left-hand side of Eq. [16.29].

The wall-to-fluid friction factor can be represented in a general form by

$$f_{wf} = C_{wf}/\mathbf{Re}^m \quad [16.34]$$

where the Reynolds number is

$$\mathbf{Re} = \frac{WD_{\text{hy}}}{A_{\text{f}}\mu} \qquad [16.35]$$

For forced convection flows in round tubes, the usual values are $C_{\text{wf}} = 64.0$ and $m = 1$ for laminar flow, $C_{\text{wf}} = 0.3164$ and $m = 0.25$ for lower values of the Reynolds number ($\mathbf{Re} < 10^5$), and $C_{\text{wf}} = 0.184$ and $m = 0.20$ for high Reynolds number fully developed turbulent flow.

The specific form of the distributed wall friction factor, Eq. [16.34], for natural-circulation flows, has been the subject of extensive investigations. Todreas and Kazimi (1990) present a summary to that time, including rod bundle data by Gruszynski and Viskanta (1983). Swapnalee and Vijayan (2011) and Ambrosini et al. (2004) are additional examples. The special consideration required for supercritical thermodynamic states has been noted earlier in this chapter (eg, Pioro and Duffey, 2003; Yadav et al., 2012b). Natural-circulation flows, having bulk motions, are somewhat different from natural convection and low-flow forced convection. The necessity for a continuous representation of the friction factor for wall-distributed resistance is an additional critical aspect of stability of NCLs as discussed in Section 16.10.

$\overline{A}_{\text{wf}}$ is the wall area per unit fluid volume for friction

$$\overline{A}_{\text{wf}} = \frac{A_{\text{wf}}}{V} = \frac{p_{\text{w}} l}{A_{\text{f}} l} = \frac{4}{D_{\text{hy}}} \qquad [16.36]$$

where p_{w} is the wetted perimeter and l is an increment of length in the direction of flow.

Local irreversible losses have been included into the flow resistance model only for completeness; these will not be considered further in this chapter. The numerical value of the local loss factor depends on the geometry of the flow channel at the location of the loss. The issues associated with correct and accurate representations of the wall flow resistance, both distributed and local, are not addressed in these notes; these have been covered in detail in the literature.

Note that although the flow resistance has been represented in a general manner to cover the case of reversed flow, it is not always carried through in the development of the model equations. In general, unless otherwise noted, these notes assume that the flow does not change direction. That is, oscillatory motions about zero are not necessarily covered. As noted in the introduction, the energy distribution around the loops must account for the flow direction.

The loop flow resistance is specialized to the cases that are considered in this chapter as follows. The local irreversible losses are neglected, mainly to save on equation processing. The distributed wall friction factor correlation formulation is considered in the following.

For laminar flow, Eqs. [16.32], [16.34], and [16.35] give

$$R_{\text{wf}} \frac{W|W|}{\rho_0 A_{\text{f}}^2} = \frac{1}{2} \frac{1}{D_{\text{hy}}} \frac{C_{\text{wf,lam}}}{\mathbf{Re}} \frac{W^2}{\rho_0 A_{\text{f}}^2} L_{\text{t}} = \frac{1}{2} \frac{L_{\text{t}}}{D_{\text{hy}}} C_{\text{wf,lam}} \mathbf{Re} \frac{\mu^2}{\rho_0 D_{\text{hy}}^2} \qquad [16.37]$$

For constant wall-friction factor in the turbulent flow regime,

$$R_{\mathrm{wf}}\frac{W|W|}{\rho_0 A_{\mathrm{f}}^2}=\frac{1}{2}\frac{L_{\mathrm{t}}}{D_{\mathrm{hy}}}C_{\mathrm{wf,tur}}\frac{W|W|}{\rho_0 A_{\mathrm{f}}^2}=\frac{1}{2}\frac{L_{\mathrm{t}}}{D_{\mathrm{hy}}}C_{\mathrm{wf,tur}}\mathbf{Re}^2\frac{\mu^2}{\rho_0 D_{\mathrm{hy}}^2} \qquad [16.38]$$

For the general formulation for turbulent flow, Eq. [16.34] for example, gives

$$R_{\mathrm{wf}}\frac{W|W|}{\rho_0 A_{\mathrm{f}}^2}=\frac{1}{2}\frac{L_{\mathrm{t}}}{D_{\mathrm{hy}}}\frac{C_{\mathrm{wf,tur}}}{\mathbf{Re}^m}\frac{W|W|}{\rho_0 A_{\mathrm{f}}^2}=\frac{1}{2}\frac{L_{\mathrm{t}}}{D_{\mathrm{hy}}}\frac{C_{wf,tur}}{\mathbf{Re}^m}\mathbf{Re}^2\frac{\mu^2}{\rho_0 D_{\mathrm{hy}}^2} \qquad [16.39]$$

The representation of distributed wall friction for all flow regimes from laminar to fully turbulent is required to be mathematically continuous. If this requirement is not met, then artificial modes of instability can be introduced; all discontinuities present potential for introduction of instability. For sufficiently low flow rates, the changes in the fluid viscosity as the temperature changes round the loop can introduce laminar and turbulent friction flow regimes.

Energy conservation model equations are required for all segments of the primary and secondary loops. These segments are (1) the energy input segment in the primary loop, (2) unheated horizontal and rising segments of both loops, (3) the coupling HEX segment, (4) unheated falling segments for both loops, and (5) the energy rejection HEX segment in the secondary loop. General formulations of the model equations are given first in the following sections.

The energy conservation model equations are written for the directions of flow shown in Fig. 16.4. To save on the equation processing, the case of loss and injection of fluid from/to the loops is not considered in detail. The situation as outlined for the mass conservation equation holds by direct analogy. Note that net loss, without replacement, of mass and energy from either loop can lead to situations for which the intended natural circulation will not be present.

The energy equation models for the primary loop are

$$\frac{\partial}{\partial t}T_{\mathrm{p}}+\frac{W_{\mathrm{p}}}{A_{\mathrm{fp}}\rho_{\mathrm{p0}}}\frac{\partial}{\partial l_{\mathrm{p}}}T_{\mathrm{p}}=\frac{p_{\mathrm{whp}}q''_{\mathrm{wp}}}{A_{\mathrm{fp}}\rho_{\mathrm{p0}}C_{\mathrm{pp}}} \qquad [16.40]$$

for the energy supply segment of the hot primary loop, where p_{whp} is the heated perimeter of the wall for the HEX and q''_{wp} is the wall heat flux from the energy source HEX to the primary loop. The wall heat flux is determined by the flow arrangement and the boundary temperatures for the energy supply HEX or by the temporal and spatial distribution of the energy source internal to the primary loop.

The energy conservation model for the unheated horizontal and rising segments of the primary loop accounting for the potential for energy exchange between the fluid and the wall during transients is

$$\frac{\partial}{\partial t}T_{\mathrm{p}}+\frac{W_{\mathrm{p}}}{A_{\mathrm{fp}}\rho_{\mathrm{p}_0}}\frac{\partial}{\partial l_{\mathrm{p}}}T_{\mathrm{p}}=\frac{p_{\mathrm{whp}}h_{\mathrm{cwp}}}{A_{\mathrm{fp}}\rho_{\mathrm{p0}}C_{\mathrm{pp}}}(T_{\mathrm{whp}}-T_{\mathrm{p}}) \qquad [16.41]$$

At steady state the right-hand side is zero.

For the primary side of the coupling HEX the temperature gradient in the fluid is negative,

$$\frac{\partial}{\partial t}T_{\mathrm{p}} + \frac{W_{\mathrm{p}}}{A_{\mathrm{fp}}\rho_{\mathrm{p0}}}\frac{\partial}{\partial l_{\mathrm{p}}}T_{\mathrm{p}} = \frac{U_{\mathrm{cHEX}}p_{\mathrm{whp}}}{A_{\mathrm{fp}}\rho_{\mathrm{p0}}C_{\mathrm{pp}}}(T_{\mathrm{s}} - T_{\mathrm{p}}) \qquad [16.42]$$

and

$$\frac{\partial}{\partial t}T_{\mathrm{p}} + \frac{W_{p}}{A_{\mathrm{fp}}\rho_{\mathrm{p}_0}}\frac{\partial}{\partial l_{\mathrm{p}}}T_{\mathrm{p}} = \frac{p_{\mathrm{whp}}h_{\mathrm{cwp}}}{A_{\mathrm{fp}}\rho_{\mathrm{p0}}C_{\mathrm{pp}}}(T_{\mathrm{wcp}} - T_{\mathrm{p}}) \qquad [16.43]$$

for the unheated horizontal and falling segments of the primary loop past the coupling HEX, again allowing for energy exchange between the fluid and wall.

Using a zero-dimensional lumped approach for the heat exchange between the fluid and the wall in the non-HEX segments,

$$\frac{d}{dt}T_{\mathrm{whp}} = \frac{p_{\mathrm{whp}}h_{\mathrm{cwhp}}}{M_{\mathrm{whp}}C_{\mathrm{pwhp}}}(T_{\mathrm{p}} - T_{\mathrm{whp}}) \qquad [16.44]$$

for the hot segments of the primary loop and

$$\frac{d}{dt}T_{\mathrm{wcp}} = \frac{p_{\mathrm{whp}}h_{\mathrm{cwcp}}}{M_{\mathrm{wcp}}C_{\mathrm{pwcp}}}(T_{\mathrm{p}} - T_{\mathrm{wcp}}) \qquad [16.45]$$

for the cold segments of the primary loop. The zero-dimensional modeling neglects the variation of the wall temperature along the direction of flow.

The transient response of the wall materials in the energy source HEX is

$$\frac{d}{dt}T_{\mathrm{wpHEX}} = \frac{p_{\mathrm{wo}}q''_{\mathrm{o}}}{M_{\mathrm{wpHEX}}C_{\mathrm{pwpHEX}}} - \frac{p_{\mathrm{wi}}q''_{\mathrm{i}}}{M_{\mathrm{wpHEX}}C_{\mathrm{pwpHEX}}} \qquad [16.46]$$

The transient response of the wall materials in the coupling HEX is given by

$$\frac{d}{dt}T_{\mathrm{wcHEX}} = \frac{p_{\mathrm{wo}}q''_{\mathrm{o}}}{M_{\mathrm{wcHEX}}C_{\mathrm{pwcHEX}}} - \frac{p_{\mathrm{wi}}q''_{\mathrm{i}}}{M_{\mathrm{wcHEX}}C_{\mathrm{pwcHEX}}} \qquad [16.47]$$

The denominators of Eqs. [16.46] and [16.47] represent the thermal mass of the metal in the respective HEX.

At steady-state conditions, the temperature distribution in the energy source and coupling HEX is obtained by integrating Eqs. [16.40] and [16.42] along the flow path in these devices. The models for various energy supply methods, Eq. [16.40], are discussed in these notes.

The corresponding model equations for the cool secondary loop are

$$\frac{\partial}{\partial t}T_s - \frac{W_s}{A_{fs}\rho_{s0}}\frac{\partial}{\partial l_s}T_s = \frac{U_{cHEX}p_{whs}}{A_{fs}\rho_{s0}C_{ps}}(T_p - T_s) \quad [16.48]$$

for the coupling HEX, where the temperature gradient in the fluid in the direction of flow is positive. Note that in the coupling HEX the distance coordinates are the same. An energy equation model for the horizontal and rising hot side of the unheated segments of the secondary loop is

$$\frac{\partial}{\partial t}T_s + \frac{W_s}{A_{fs}\rho_{s0}}\frac{\partial}{\partial l_s}T_s = \frac{p_{whs}h_{cws}}{A_{fs}\rho_{s0}C_{ps}}(T_{whs} - T_s) \quad [16.49]$$

and

$$\frac{\partial}{\partial t}T_s + \frac{W_s}{A_{fs}\rho_{s0}}\frac{\partial}{\partial l_s}T_s = \frac{\overline{A}_{whs}q''_{ws}}{\rho_{s0}C_{ps}} \quad [16.50]$$

for the energy sink in the cool secondary loop and

$$\frac{\partial}{\partial t}T_s + \frac{W_s}{A_{fs}\rho_{s0}}\frac{\partial}{\partial l_s}T_s = \frac{p_{whs}h_{cws}}{A_{fs}\rho_{s0}C_{ps}}(T_{wcs} - T_s) \quad [16.51]$$

for the falling cooler fluid in the unheated segments of the secondary loop. The coupling HEX provides the physical and mathematical coupling between the primary and secondary loops.

The transient response of the wall materials when modeled as a zero-dimensional lumped parameter approach is more useful when the fluid in the respective segments is also modeled on a zero-dimensional basis. When modeling an entire system in some detail, conduction in the surrounding solid materials will frequently be assumed to be one dimensional and coupled one to one with fluid control volumes.

If in the case of a boiling two-phase loop zero-dimensional lumped models are used for the various boiling-state regions, then the thermal response of the wall material can be directly considered.

An assumption frequently used in highly idealized modeling is that the energy rejection from the secondary loop can be carried out as a constant heat flux manner and is equal to the energy source. In general that is not possible to directly arrange in the physical domain. Slight generalizations, which will be developed in the following, lead to more physically realistic representations.

The BCs for the equation system, in the general case considered in Fig. 16.4, are given by the inlet temperature at the hot end of the energy supply HEX, T_{hin}, and the inlet temperature at the cold end of the energy sink HEX, T_{cin}. In the general case, these BCs can be taken to be functions of time to allow introductions of perturbations in the BCs. The steady-state performance of the coupled loops is determined by

the overall thermal conductance from $T_{\text{hin}}$to T_{cin}. Analyses of idealized NCL systems are sometimes directly based on specification of the source and sink temperature difference. Others are based on specification of constant source and sink temperature on one side of the HEX BCs. Less general analyses can be based on specification of the energy supply on the primary loop, Eq. [16.40], and the corresponding energy sink on the secondary loop, Eq. [16.50].

The fluid in both loops is taken to be thermally expandable and the density a linear function of temperature alone, as in the single-loop case, Eq. [16.13]. Specific aspects of the energy source and sink are considered in the following paragraphs.

The heat flux on the right-hand side of Eq. [16.40] for the primary loop energy supply can be taken to be a constant,

$$q''_{\text{wp}} = q''_{0\text{wp}} \tag{16.52}$$

which is a common BC for analyses of idealized single NCLs, or a function of the location within the energy source device

$$q''_{\text{wp}} = q''_{\text{wp}}(l_{\text{p}}) \quad (L_{\text{pHEXi}} \leq l_{\text{p}} \leq L_{\text{pHEXo}}) \tag{16.53}$$

where the distribution on the right-hand side of Eq. [16.53] can be explicitly specified for each physical situation. The steady-state axial heat flux distribution in a reactor core is an example. The energy source can also be modeled by use of a heat transfer coefficient and a specified temperature for the energy source

$$q''_{\text{wp}} = h_{\text{cpsrc}}(T_{\text{psrc}} - T_{\text{p}}) \quad (L_{\text{pHEXi}} \leq l_{\text{p}} \leq L_{\text{pHEXo}}) \tag{16.54}$$

where h_{cpsrc} is the convective heat transfer coefficient for the primary loop energy source and T_{psrc} is the specified constant temperature for the energy source. Each of these gives different distributions of the primary-loop fluid temperature in the energy-source segment. The limits on the location in the hot primary loop correspond to the inlet and outlet side of the energy source HEX segment. For these idealizations the specified quality can also be taken to be a function of time so that the effects of perturbations of the energy supply on the onset of instability can be investigated.

The energy source can also be modeled by an HEX as shown in Figs. 16.3. This model is not addressed in detail in these notes. The modeling for the coupling HEX given in these notes, using Eqs. [16.42] and [16.48], can be adapted to cover this situation.

Not all of the possible representations of the energy supply will be treated in detail. The constant energy source and constant energy supply temperature models are developed in the following.

If the primary loop energy source heat flux is constant, then Eq. [16.40] gives the distribution

$$T_{\text{pss}}(l_{\text{p}}) = T_{\text{cpss}} + q''_{0\text{wp}} \frac{p_{\text{whp}}}{W_{\text{pss}} C_{\text{pp}}} l_{\text{p}} \quad (L_{\text{pHEXi}} \leq l_{\text{p}} \leq L_{\text{pHEXo}}) \tag{16.55}$$

and the outlet temperature is

$$T_{\mathrm{hpss}} = T_{\mathrm{cpss}} + q''_{0\mathrm{wp}} \frac{A_{\mathrm{whpsrc}}}{W_{\mathrm{pss}} C_{\mathrm{pp}}} \quad (l_{\mathrm{p}} = L_{\mathrm{pHEXo}}) \qquad [16.56]$$

where A_{whpsrc} is the total wall area for heat transfer for the hot primary loop energy source and T_{cpss} is the primary-loop fluid temperature at the inlet to the energy-addition segment. This latter quantity is a result of the performance of the coupled loops.

The right-hand sides of these can be written in terms of the total power addition into the fluid,

$$Q_{\mathrm{src}} = q''_{0\mathrm{wp}} A_{\mathrm{whpsrc}} \qquad [16.57]$$

If the energy source is represented by Eq. [16.54], then Eq. [16.40] becomes

$$\frac{d}{dl_{\mathrm{p}}} T_{\mathrm{pss}} = \frac{p_{\mathrm{whp}}}{W_{\mathrm{pss}} C_{\mathrm{pp}}} h_{\mathrm{cpsrc}} (T_{\mathrm{psrc}} - T_{\mathrm{pss}}) \qquad [16.58]$$

and, with T_{psrc} constant, integration gives

$$T_{\mathrm{pss}}(l_{\mathrm{p}}) = T_{\mathrm{psrc}} - (T_{\mathrm{psrc}} - T_{\mathrm{cpss}}) \mathrm{e}^{-\frac{h_{\mathrm{cpsrc}} p_{\mathrm{whp}}}{W_{\mathrm{pss}} C_{\mathrm{pp}}} (l_{\mathrm{p}} - L_{\mathrm{pHEXi}})} \quad (L_{\mathrm{pHEXi}} \le l_{\mathrm{p}} \le L_{\mathrm{pHEXo}}) \qquad [16.59]$$

and the hot temperature for the primary loop at the outlet of the energy supply segment is

$$T_{\mathrm{hpss}} = T_{\mathrm{psrc}} - (T_{\mathrm{psrc}} - T_{\mathrm{cpss}}) \mathrm{e}^{-\frac{h_{\mathrm{cpsrc}} A_{\mathrm{whpsrc}}}{W_{\mathrm{pss}} C_{\mathrm{pp}}}} \quad (l_{\mathrm{p}} = L_{\mathrm{pHEXo}}) \qquad [16.60]$$

As in the case of the single NCL previously considered, the exponent can be written in terms of the Stanton number.

The energy equation models for the coupling HEX are coupled and must be solved together. The energy equation for the primary side fluid, Eq. [16.42], for steady state is

$$\frac{\partial}{\partial l_{\mathrm{p}}} T_{\mathrm{pss}} = \frac{U_{\mathrm{cHEX}} p_{\mathrm{whp}}}{W_{\mathrm{pss}} C_{\mathrm{pp}}} (T_{\mathrm{sss}} - T_{\mathrm{pss}}) \qquad [16.61]$$

and Eq. [16.48] for the secondary-side fluid is

$$\frac{\partial}{\partial l_{\mathrm{p}}} T_{\mathrm{sss}} = -\frac{U_{\mathrm{cHEX}} p_{\mathrm{whs}} (T_{\mathrm{pss}} - T_{\mathrm{sss}})}{W_{\mathrm{sss}} C_{\mathrm{ps}}} \qquad [16.62]$$

where both of these apply in the segments assigned to the coupling HEX, which is denoted by cHEX in the subscripts. Within the coupling HEX the coordinates are the same.

The energy balance for the primary fluid stream through the coupling HEX is

$$q''_{0\text{wp}} = W_{\text{pss}} C_{\text{pp}} (T_{\text{cpss}} - T_{\text{hpss}}) \quad [16.63]$$

which has been written as a decrease in the energy content of the primary fluid. For the secondary fluid stream

$$q''_{0\text{wp}} = W_{\text{sss}} C_{\text{ps}} (T_{\text{hsss}} - T_{\text{csss}}) \quad [16.64]$$

The solutions for the temperature and temperature difference distributions are straightforward but are not included here. Rao et al. (2005d, 2008) and Sabharwall et al. (2012) have developed the solutions in some detail. If HEXs are used to add energy into the primary loop and extract energy from the secondary fluid, then the modeling is analogous to that used for the coupling HEX.

The energy sink on the secondary loop can be modeled in three ways: (1) as a constant sink analogous to the energy source in the primary loop, (2) with a heat transfer coefficient and constant specified sink temperature, or (3) as an HEX, again analogous to the modeling of the energy supply in the primary loop.

If the heat flux on the right-hand side of Eq. [16.50] is a constant, then the temperature at the outlet from the energy sink is

$$T_{\text{csss}} = T_{\text{hsss}} - q''_{0\text{ws}} \frac{A_{\text{whssnk}}}{W_{\text{sss}} C_{\text{ps}}} \quad [16.65]$$

where A_{whssnk} is the total wall heat transfer area for the cool secondary loop energy sink.

If the energy sink is represented by the model corresponding to Eq. [16.54], then Eq. [16.50] gives the cool temperature for the secondary loop at the outlet of the energy-sink device,

$$T_{\text{csss}} = T_{\text{ssnk}} - (T_{\text{ssnk}} - T_{\text{hsss}}) \text{e}^{-\frac{h_{\text{cssnk}} A_{\text{whssnk}}}{W_{\text{sss}} C_{\text{ps}}}} \quad [16.66]$$

The model equations developed in these sections are summarized here for later reference. The steady-state forms of the general model equations given in the previous section are developed in the following paragraphs.

For the system in Fig. 16.4, all of the energy-exchange components are horizontal so that the momentum balance models, Eqs. [16.30] and [16.31], integrated around the loops give

$$R_{\text{wfp}}(W_{\text{pss}}) \frac{W_{\text{pss}} |W_{\text{pss}}|}{\rho_{0\text{p}} A_{\text{fp}}^2} = g \rho_{0\text{p}} \beta_{\text{p}} \left(T(\bullet)_{\text{hpss}} - T(\bullet)_{\text{cpss}} \right) H_{\text{p}} \quad [16.67]$$

for the hot primary loop and

$$R_{\mathrm{wfs}}(W_{\mathrm{sss}})\frac{W_{\mathrm{sss}}|W_{\mathrm{sss}}|}{\rho_{0\mathrm{s}}A_{\mathrm{fs}}^2}=g\rho_0\beta\left(T(\bullet)_{\mathrm{hsss}}-T(\bullet)_{\mathrm{csss}}\right)H_{\mathrm{s}} \qquad [16.68]$$

for the cold secondary loop. The notation $T(\bullet)$ means that the temperature is a function of $(W_{\mathrm{pss}},W_{\mathrm{sss}};T_{\mathrm{src}},T_{\mathrm{snk}})$.

For the general case of HEXs at the energy source and sink, there are eight unknowns—W_{p}, T_{ph}, T_{pc}, T_{srco}, for the primary loop and W_{s}, T_{ps}, T_{ps}, T_{snko}—and eight equations—two momentum and energy balances for both streams in all three HEXs. This counting is for the case of pure thermally driven hydrodynamic NCLs. The number of parameters associated with the hydrodynamic case is also very large, even if the geometry is not included. The problem rapidly becomes intractable if modeling and responses for the solid materials surrounding the fluid, and additional necessary realisms, are included. It is clear that analytical solutions will be very difficult to obtain and that might be possible, if at all, only under very special conditions. Salazar et al. (1988) and Wu (2011) have given highly idealized representations of coupled NCLs.

The natural recourse for this situation is to use numerical solution methods for both steady-state and transient analyses. The systems-analysis codes that are used for design and safety studies can all handle the coupled NCL case. At the same time, local special- and general-purpose natural-circulation models, methods, and codes are being developed for applications to Gen IV reactor concepts.

Given the complexity of coupled NCL systems, especially for operating reactor design, bypassing the usual frequency domain analyses and going directly to time domain analyses will prove to be efficient. Detailed descriptions of the systems, along with analyses in the time domain, will ultimately be required; therefore starting the required effort is a good idea. The literature review given previously clearly indicates that validation of many systems-analysis models and codes for applications to Gen IV machines is well underway.

16.12 Conclusions

The literature review indicates that validation of the models and codes that will likely be used for exploration and licensing is a top focus. Generalized frequency and time domain codes are readily available. There are abundant fundamental experimental data for the onset of instabilities in simple channels such as single and parallel tubes and simple NCLs. Experimental facilities for critical aspects of specific Gen IV designs will likely evolve as R&D continues. There seems to be worldwide coordination, cooperation, and collaboration.

Nomenclature

A	Area, m^2
$\overline{A}$	Area per unit fluid volume, 1/m
A_f	Flow area, m^2
C_p	Specific heat at constant pressure, J/kg K
D	Diameter, m
D_{he}	Heated equivalent diameter, m
D_{hy}	Wetted equivalent diameter, m
f_w	Friction factor
g	Gravitational body force, kg m/s^2
G	Mass flux, kg/m^2s
h	Enthalpy, J/kg
h_c	Heat transfer coefficient, W/m^2K
h_g	Vapor phase enthalpy, J/kg
h_{fg}	Enthalpy of evaporation, J/kg
h_l	Liquid phase enthalpy, J/kg
H	Vertical height, m
K_{ll}	Local pressure loss factor
l	Distance along loop, m
L	Horizontal length, m
M	Mass, kg
N_{pch}	Phase change number
N_{sub}	Subcooling number
p	Perimeter, m
q''_w	Wall heat flux, W/m^2
Q	Power, W
R_w	Flow resistance factor
t	Time, s
u	Speed, m/s
U	Overall heat transfer factor, W/m^2K
V	Fluid volume, m^3

Continued

V_{SL}	Slip velocity, m/s
W	Mass flow rate, kg/s
$\overline{X}^{m}$	Mass fraction
z	Axial direction, m

Greek symbols

α	Void fraction
β	Coefficient of thermal, 1/K expansion
δ	Dirac-delta function
μ	Dynamic viscosity, Pa s
ρ	Density, kg/m^3
ν	Kinematic viscosity, m^2/s

Nondimensional numbers

Gr	Grashof Number, $\frac{g\beta\Delta T D_{he}^3}{\upsilon^2}$
Re	Reynolds number, $\frac{WD_{hy}}{A_f\mu}$
St	Stanton number, $\frac{h_c}{\rho u C_p}$

Subscripts

c	Cool, cooled, coupling
cp	Cool temperature primary loop
cs	Cool temperature secondary loop
ext	External
g	Vapor
gs	Saturated vapor state
h	Hot, heated

hp	Hot temperature primary loop
hs	Hot temperature secondary loop
hex	Heat exchanger
i, in	Inlet
int	Internal
l	Liquid
lam	Laminar
lgs	Saturated liquid and vapor
ls	Saturated liquid state
0	Reference state
o	Out, outlet
p	Primary loop
pri	Primary side of HEX
S	Secondary loop
sec	Secondary side of HEX
snk	Sink
src	Source
ss	Steady state
t	Total length
tur	Turbulent
w	Wall, wetted
wh	Wall heat
wf	Wall friction

Acronyms and abbreviations

ALARA	As Low As Reasonably Achievable
AOOs	Anticipated Operational Occurrences
ARs	Advanced Reactors
ASME	American Society of Mechanical Engineers
ASTRID	Advanced Sodium Technological Reactor for Industrial Demonstration
ATHLET	Analysis of THermal-hydraulics of LEaks and Transients
ATWS	Anticipated Transients Without Scram

Continued

BCs	Boundary Conditions
BDBA	Beyond-Design-Basis Accidents
BHWR	Boiling Heavy Water Reactor
BIMAC	Basement Internal Melt Arrest and Coolability (Device)
BORAX	BOiling water Reactor eXperiment
BWR	Boiling Water Reactors
CAPWR	Chinese Advance Pressurized Water Reactor
CATHARE	Code for Analysis of THermalhydraulics during an Accident of Reactor and safety Evaluation
CATHENA	Canadian Algorithm for THErmalhydraulic Network Analysis
CDF	Cumulative Damage Function
CDFs	Core Damage Frequencies
CFD	Computational Fluid Dynamics
CHF	Critical Heat Flux
CNSC	Canadian Nuclear Safety Commission
COL	Combined Operating License
DA	Deterministic Analyses
DBAs	Design Basis Accidents
DBTs	Design Basis Threats
DHR	Decay Heat Removal
DiD	Defense in Depth
DNB	Departure from Nucleate Boiling
DPV	DePressurization Valve
EBR	Experimental Breeder Reactor
EBWR	Experimental Boiling Water Reactor
EPRI	Electric Power Research Institute
ESBWR	Economic Simplified Boiling Water Reactor
EoS	Equation of State
FHRs	Fluoride salt-cooled High-temperature Reactor
FIST	Full-height Integral Simulation Test
Gen IV	Generation IV
GIF	Generation IV International Forum
HEX	Heat EXchanger

HPLWR	High Performance Light Water Reactor
HRA	Human Reliability Analysis
HTGR	High-Temperature Gas-cooled Reactor
HTTR	High Temperature Test Reactor
Hz	Hertz
I&C	Instruments & Control
IAEA	IAEA International Atomic Energy Agency
IC	Isolation Condenser
ICs	Initial Conditions
IRWST	In-containment Refueling Water Storage Tank
ISAM	Integrated Safety Analysis Methodology
LBLOCA	Large-Break Loss of Coolant Accident
LOBI	LOop Blowdown Investigation
LOCA	Loss Of Coolant Accident
LOFT	Loss Of Fluid Test
LRF	Large Release Frequency
LWRs	Light Water Reactors
MSFR	Molten Salt Fast Reactor
NC	Natural Circulation
NCL	Natural Circulation Loop
NEI	Nuclear Energy Institute
NRTS	National Reactor Testing Station
OCED	Organization for Economic Co-operation and Development
ODEs	Ordinary Differential Equations
OFI	Onset of Flow Instability
ONB	Onset of Nucleate Boiling
OON	Onset of Nucleation
OSU-MASLWR	Oregon State University − Multi-Application Small Light Water
OSV	Onset of Significant Void
PBMR	Pebble Bed Modular Reactor
PIRT	Phenomena Identification and Ranking Table
PRA	Probabilistic Risk Assessment

Continued

PRHRS	Passive Residual Heat Removal System
PSA	Probabilistic Safety Assessment
PSB	Partial Subcooled Boiling
PT	Pressure Tube
PUMA	Purdue University Multidimensional integral test Assembly
PWR	Pressurized Water Reactor
QA	Quality Assurance
R/A	Reliability/Availability
R&D	Research & Development
REE	Rare or Extreme Events
RELAP	Reactor Excursion and Leak Analysis Program
RETRAN	REactor TRANsient
ROSA-III	Rig Of Safety Assessment-III
ROSA-IV LSTF	Rig Of Safety Assessment-IV Large Scale Test Facility
RPV	Reactor Pressure Vessel
SAs	Severe Accidents
SB	Station Blackout
SCB	Fully Developed Subcooled Boiling
SBLOCA	Small-Break Loss of Coolant Accident
SDC	Safety Design Criteria
SFRs	Sodium Fast Reactors
SG	Steam Generator
SMRs	Small Medium and/or Modular Reactors
SO	Safety Objective
SPERT	Special Power Excursion Reactor Test Program
SPES	Simulatore Pressurizzato per Esperienze di Sicurezza
SRF	Small Release Frequency
SRLs	Safety Reference Levels
SRV	Safety Relief Valve
SSCs	Structures, Systems and Components
TMI	Three Mile Island
TRAC	Transient Reactor Analysis Code
TRAC-B	Transient Reactor Analysis Code-Boiling water reactor

TRACE	TRAC/RELAP Advanced Computational Engine
TRAC-P	Transient Reactor Analysis Code-Pressurized water reactor
TRISO	TTIstructural-ISOtropic
U.S. DOE	United States Department Of Energy
U.S. NRC	United States Nuclear Regulatory Commission
UIHS	Ultimate and Indefinitely lasting Heat Sinks
VISTA-ITL	Verification by Integral Simulation of Transients and Accident − Integral Test Loop
WENRA	Western European Nuclear Regulators Association

References

Aguirre, C., Caruge, D., Castrillo, F., Dominicus, G., Geutjes, A.J., Saldob, V., van der Hagen, T.H.J.J., Hennig, D., Huggenberger, M., Ketelaar, K.C.J., Manera, A., Munoz-Cobo, J.L., Prasser, H.-M., Rohde, U., Royer, E., Yadigaroglu, G., 2005. Natural circulation and stability performance of BWRs (NACUSP). Nuclear Engineering and Design 235, 401−409.

Aksan, N., 2008. International standard problems and small break loss-of-coolant accident (SBLOCA). Science and Technology of Nuclear Installations. http://dx.doi.org/10.1155/2008/814572. Article ID 814572, 22 p.

Alstad, C.D., Isbin, H.S., Amundson, N.R., 1956. The Transient Behavior of Single-Phase Natural Circulation Water Loop Systems. Argonne National Laboratory Report, ANL-5409.

Ambrosini, W., Ferreri, J.C., 1997a. Numerical analysis of single-phase, natural circulation in a simple closed loop. In: Proceedings of 11th Meeting on Reactor Physics and Thermal Hydraulics, Pocos de Caldas, MG, Brazil, August 18−22th 1997, pp. 676−681.

Ambrosini, W., Ferreri, J.C., 1997b. Stability analysis of single-phase thermosyphon loops by finite-difference numerical methods. In: Proceedings of Post SMIRT 14 Seminar 18 on 'Passive Safety Features in Nuclear Installations', Pisa, August 25−27th 1997, pp. E21−E210.

Ambrosini, W., Ferreri, J.C., 1998. The effect of truncation error on the numerical prediction of linear stability boundaries in a natural circulation single-phase loop. Nuclear Engineering and Design 183, 53−76.

Ambrosini, W., Ferreri, J.C., 2000. Stability analysis of single-phase thermosyphon loops by finite-difference numerical methods. Nuclear Engineering and Design 201, 11−23.

Ambrosini, W., D'Auria, F., Pennati, A., Ferreri, J.C., 2001. Numerical effects in the prediction of single-phase natural circulation stability. In: National Heat Transfer Conference of UIT, Modena, Italy, June 25−27.

Ambrosini, W., 2001. On some physical and numerical aspects in computational modelling of one-dimensional flow dynamics. In: 7th International Seminar on Recent Advances in Fluid Mechanics, Physics of Fluids and Associated Complex Systems (Fluidos 2001), Buenos Aires, Argentina, October 17−19.

Ambrosini, W., Ferreri, J.C., 2003. Prediction of stability of one-dimensional natural circulation with a low diffusion numerical scheme. Annals of Nuclear Energy 30, 1505−1537.

Ambrosini, W., Forgione, N., Ferreri, J.C., Bucci, M., 2004. The effect of wall friction in single-phase natural circulation stability at the transition between laminar and turbulent flow. Annals of Nuclear Energy 31, 1833−1865.

Ambrosini, W., Ferreri, J.C., 2006. Analysis of basic phenomena in boiling channel instabilities with different flow models and numerical schemes. In: Proceedings of on Density Wave Instability Phenomena − Modelling and Experimental Investigation, 14th International Conference on Nuclear Engineering (ICONE 14), Miami, Florida, USA, July 17−20, 2006.

Ambrosini, W., 2007. On the analogies in the dynamic behaviour of heated channels with boiling and supercritical fluids. Nuclear Engineering and Design 237, 1164−1174.

Ambrosini, W., 2008. Lesson learned from the adoption of numerical techniques in the analysis of nuclear reactor thermal-hydraulic phenomena. Progress in Nuclear Energy 50, 866−876.

Ambrosini, W., Sharabi, M.B., 2008. Dimensionless parameters in stability analysis of heated channels at supercritical pressures. Nuclear Engineering and Design 238, 1917−1929.

Ampomah-Amoako, E., Ambrosini, W., 2013. Developing a CFD methodology for the analysis of flow stability in heated channels with fluids at supercritical pressures. Annals of Nuclear Energy 54, 251−262.

Anderson, R.P., Bryant, L.T., Carter, J.C., Marchaterre, J.F., 1962. Transient Analysis of Two-Phase Natural-Circulation Systems. Argonne National Laboratory Report, ANL-6653.

Angelo, G., Andrade, D.A., Angelo, E., Torres, W.M., Sabundjian, G., Macedo, L.A., Silva, A.F., 2012. A numerical and three-dimensional analysis of steady state rectangular natural circulation loop. Nuclear Engineering and Design 244, 61−72.

ANS, American Nuclear Society, 2014. Nuclear News 57.

Anzieu, P., Guidez, J., Sauvage, J.-F., Carluec, B., 2014. France proposal of applied Generation IV SFR SDC. In: Joint IAEA-GIF SFR Safety Workshop, June.

Aoto, K., Dufour, P., Hingyi, Y., Glatz, J.P., Kim, T.-I., Ashurko, Y., Hill, R., Uto, N., 2014. A summary of sodium-cooled fast reactor development. Progress in Nuclear Energy 77, 247−265.

ASME, American Society of Mechanical Engineers, 2012. Forging a New Nuclear Safety Construct. Presidential Task Force on response to Japan nuclear power plant events. ASME, New York, ISBN 978-0-7918-3435-0.

Austregesilo, H., Bals, C., Lerchl, G., Romstedt, 2006. ATHLET Mod 2.1 Cycle a Models and Methods. Gesellschaft für Anlagen und- Reaktorsicherheit (GRS) gGmbH Report GRS-P-1/Vol. 4.

Bae, Y.-Y., Kim, H.-Y., 2009. Convective heat transfer to CO_2 at supercritical pressure flowing vertically upward in vertical tubes and an annular channel. Experimental Thermal and Fluid Science 33, 329−339.

Bae, Y.-Y., 2011. Mixed convection heat transfer to carbon dioxide flowing upward and downward in a vertical tube and an annular channel. Nuclear Engineering and Design 241, 3164−3177.

Basu, D.N., Bhattacharyya, S., Das, P.K., 2014. A review of modern advances in analyses and applications of single-phase natural circulation loop in nuclear thermal hydraulics. Nuclear Engineering and Design 280, 326−348.

Bazin, P., Pelissier, M., 2006. CATHARE 2 V25_1: Description of the Base Revision 6.1 Physical Laws Used in the 1D, 0D and 3D Modules. CEA Report CEA/DER/SSTH/LDAS/EM/2005-038.

Bea, R.G., Gale, W.E., 2011. Rule 26 Report on BP's Deepwater Horizon Macondo Blowout. US District Court, Eastern District of Louisiana, TREX-2001.

Becker, K.M., Jahnberg, S., Haga, I., Hansson, P.T., Mathisen, R.P., 1963. Hydrodynamic Instability and Dynamic Burnout in Natural Circulation Two-Phase Flow an Experimental and Theoretical Study. AB Atomenergi Report AE-156.

Becker, K.M., Mathisen, R.P., Eklind, O., Norman, B., 1964. Measurements of Hydrodynamic Instabilities, Flow Oscillations and Burnout in a Natural Circulation Loop. AB Atomenergi Report AE-131.

Berenson, P.J., 1964. Flow Stability in Multi-tube Forced-convection Vaporizers. Air Force Aero Propulsion Laboratory Report APL TDR 64-117.

Bhatt, S.C., Wachowiak, R.M., 2006. ESBWR Certification Probabilistic Risk Assessment. General Electric Company Report NEDO-33201, Rev. 1.

Boure, J.A., Bergles, A.E., Tong, L.S., 1973. Review of two-phase flow instability. Nuclear Engineering and Design 25, 165−192.

Burroughs, E., 2003. Convection in a Thermosyphon, Bifurcation and Stability Analysis (Ph.D. dissertation). The University of New Mexico, Albuquerque, New Mexico.

Burroughs, E.A., Coutsias, E.A., Romero, L.A., 2005. A reduced-order partial differential equation model for the flow in a thermosyphon. Journal of Fluid Mechanics 543, 203−237.

Chatoorgoon, V., 1986. A simple thermal hydraulic stability code. Nuclear Engineering and Design 93, 51−67.

Chatoorgoon, V., 2001. Stability of supercritical fluid flow in a single channel natural-convection loop. International Journal of Heat and Mass Transfer 44, 1963−1972.

Chatoorgoon, V., Voodi, A., Fraser, D., 2005a. The stability boundary for supercritical flow in natural circulation loops part I, H_2O studies. Nuclear Engineering and Design 235, 2570−2580.

Chatoorgoon, V., Voodi, A., Upadhye, P., 2005b. The stability boundary for supercritical flow in natural circulation loops part II, CO_2 and H_2. Nuclear Engineering and Design 235, 2581−2593.

Chatoorgoon, V., 2013. Non-dimensional parameters for static instability in supercritical heated channels. International Journal of Heat and Mass Transfer 64, 145−154.

Chatoorgoon, V., Shah, M., Duffey, R., 2007. Linear predictions of supercritical flow instability in parallel channels. In: Proceedings of 3rd International Symposium on SCWR-Design and Technology, Shanghai, China, March 12−15, 2007 (Paper SCR2007-P009).

Chen, Y., Yang, C., Zhao, M., Bi, K., Du, K., 2014. Forced convective heat transfer experiment of supercritical water in different diameter of tubes. Journal of Energy and Power Engineering 8, 1495−1504.

Cheng, X., Schulenberg, T., 2001. Heat Transfer at Supercritical Pressure − Literature Review and Application to an HPLWR. Scientific Rept. FZKA6609, Forschungszentrum Karlsruhe, Germany.

Chilton, H., 1957. A theoretical study of stability in water flow through heated passages. Journal of Nuclear Energy 5, 273−284.

CNSC, Canadian Nuclear Safety Commission, 2008. Design of New Nuclear Power Plants. CNSC Report RD-337.

CNSC/OECD, Canadian Nuclear Safety Commission, 2014. In: International Workshop on Multi-Unit Probabilistic Safety Assessment (PSA), Ottawa, Canada, November 17−20.

Collier, J.G., Thome, J.R., 1996. Convective Boiling and Condensation, third ed. Oxford Science Publications, Clarendon Press, Oxford.

Colombo, M., 2013. Experimental Investigation and Numerical Simulation of the Two-Phase Flow in the Helical Coil Steam Generator. Doctoral Thesis. Politecnico di Milano.

Colombo, M., Cammi, A., Papini, D., Ricotti, M.E., 2012a. Numerical investigation on boiling channel instabilities by imposing constant pressure drop boundary conditions via a large bypass. In: Proceedings of the International Conference Nuclear Energy for New Europe 2010, Portoroz, Slovenia September 6−9, Paper Number 413.

Colombo, M., Cammi, A., Papini, D., Ricotti, M.E., 2012b. RELAP5/MOD3.3 study on density wave instabilities in single channel and two parallel channels. Progress in Nuclear Energy 56, 15−23.

Cornelius, A., 1965a. An Investigation of Instabilities Encountered during Heat Transfer to a Supercritical Fluid (Ph.D. thesis). Oklahoma State University.

Cornelius, A.J., 1965b. An Investigation of Instabilities Encountered during Heat Transfer to a Supercritical Fluid. Argonne National Laboratory Report, ANL-7032.

Costa, A.L., Petruzzi, A., D'Auria, F., Ambrosini, W., 2008. Analyses of instability events in the Peach Bottom-2 BWR using thermal-hydraulic and 3D neutron kinetic coupled codes technique. Science and Technology of Nuclear Installations 2008. Article ID 423175, 17 p. http://dx.doi.org/10.1155/2008/423175.

Creveling, H.F., Schoenhals, R.J., 1966. Steady Flow Characteristics of a Single-Phase Natural Circulation Loop. Technical Report No 15. Purdue Research Foundation. COO-1177-15.

CSA, Computer Simulation & Analysis, Inc., 1998. RETRAN-3D-A Program for Transient Thermal-Hydraulic Analysis of Complex Fluid Flow Systems Volume 1, Theory and Numeric. Electric Power Research Institute Report, NP-7405, Volume 1, Revision 3.

D'Auria, F. (Ed.), 1997. State-of-the-Art Report on Boiling Water Reactor Stability. OECD Report NEA/CSNI/R(96)21, OECD/GD(97)13.

Debrah, S.K., Ambrosini, W., Chen, Y., 2013. Discussion on the stability of natural circulation loops with supercritical pressure fluids. Annals of Nuclear Energy 54, 47−57.

de Kruijf, W.J.M., van der Hagen, T.H.J.J., Mudde, R.F., 2000. CIRCUS; a natural circulation two-phase flow facility. In: Eurotherm Seminar No. 63, 6−8 September 1999, Genoa, Italy, 391−395.

Desrayaud, G., Fichera, A., Lauriat, G., 2013. Two-dimensional numerical analysis of a rectangular closed-loop thermosiphon. Applied Thermal Engineering 50, 187−196.

Dreier, J., Huggenberger, M., Aubert, C., Bandurski, T., Fischer, O., Healzer, J., Lomperski, S., Strassberger, H.-J., Varadi, G., Yadigaroglu, G., 1996. The PANDA facility and first test results. Kerntechnik 61, 214−222.

Duffey, R.B., 2015. Extreme events: causes and predictions. In: Proceeding of the Probabilistic Safety Analysis Conference PSA 2015. American Nuclear Society, Sun Valley, Idaho. Paper 12222.

Duffey, R.B., Ha, T., 2013. The probability and timing of power system restoration. IEEE Transactions on Power Systems 28, 3−9.

Duffey, R.B., Hughes, E.D., 1991. Static flow instability onset in tubes, channels, annuli, and rid bundles. International Journal of Heat and Mass Transfer 34, 2483−2496.

Duffey, R.B., Pioro, I.L., 2005. Experimental heat transfer of supercritical carbon dioxide flowing inside channels (survey), Nuclear Engineering and Design, 235, 913−924.

Duffey, R.B., Saull, J.W., 2008. Managing Risk: The Human Element. John Wiley and Sons, Chichester, United Kingdom.

Duffey, R.B., Sursock, J.P., 1987. Natural circulation phenomena relevant to small breaks and transients. Nuclear Engineering and Design 102, 115−128.

Dudour, P., Carluec, B., 2011. Safety implication in the light of the Fukushima NPP accident. In: GIF-INPRO Workshop, 30th November−1st December. IAEA, Vienna.

Dutta, G., Zhang, C., Jiang, J., 2015. Analysis of parallel channel instabilities in the CANDU supercritical water reactor. Annals of Nuclear Energy 83, 264−273.

EPRI, U.S. DOE, U.S. NRC, 2012. Technical Report: Central and Eastern United States Seismic Source Characterization for Nuclear Facilities. EPRI 1021097, DOE/NE-0140, NUREG-2115.

Escriva, A., Cobo, J.L.M., San Roman, J.M., Darriba, M.A., March-Leuba, J., 2008. LAPUR 60 Manual. Oak Ridge National Laboratory Report NUREG/CR-6958.

Ferreri, J.C., Ambrosini, W., D'Auria, F., 1995. On the convergence of RELAP5 calculations in a single-phase, natural circulation test problem. In: Proceedings of X-ENFIR, 7−11th August 1995, as de Lindoia, SP, Brazil, pp. 303−307.

Ferreri, J.C., Ambrosini, W., 1999. Verification of RELAP5/MOD31 with Theoretical Stability Results. United State Nuclear Regulatory Commission Report NUREG-IA-0151.

Ferreri, J.C., 1999. Single-phase natural circulation in simple circuits − reflections on its numerical simulation. In: Invited Lecture at the Eurotherm Seminar No 63 on Single and Two-Phase Natural Circulation, September 6−8 1999, Genoa, Italy.

Ferreri, J.C., Ambrosini, W., 2002. On the analysis of thermal-fluid-dynamics instabilities via numerical discretization of conservation equations. Nuclear Engineering and Design 215, 153−170.

Furuya, M., 2006. Experimental and Analytical Modeling of Natural Circulation and Forced Circulation BWR − Thermal-Hydraulic, Core-Wide, and Regional Stability Phenomena (Doctoral thesis). Delft University of Technology.

Garlid, K., Amundson, N.R., Isbin, H.S., 1961. A Theoretical Study of the Transient Operation and Stability of Two-Phase Natural Circulation Loops. Argonne National Laboratory Report, ANL-6381.

Gartia, M.R., Pilkhwal, D.S., Vijayan, P.K., Saha, D., 2007. Analysis of metastable regimes in a parallel channel single phase natural circulation system with RELAP5/MOD3.2. International Journal of Thermal Sciences 46, 1064−1074.

GIF, Generation IV International forum, 2011. An Integrated Safety Assessment Methodology (ISAM) for Generation IV Nuclear Systems. GIF/RSWG/2010/002/rev1, Version 1.1.

GIF, Generation IV International Forum, 2014a. Guidance Document for Integrated Safety Assessment Methodology (ISAM) − (GDI). European Commission Joint Research Centre Report for GIF Risk and Safety Working Group, GIF/RSWG/2014/001, Version 1.0.

GIF, Generation IV International Forum, 2014b. Technology Roadmap Update for Generation IV Nuclear Energy Systems. Nuclear Energy Agency Organisation for Economic Co-operation and Development.

Goldberg, S.M., Rosner, R., 2011. Nuclear Reactors: Generation to Generation. American Academy of Arts and Sciences, Cambridge, MA. https://www.amacad.org/pdfs/nuclearReactors.pdf.

Gouirand, J.M., 1988. CLOTAIRE Program, Description and Manufacturing of the Mock-up. CEA, Cadarache. DRE/STRE/LGV 88−876.

Grace, T.M., Krejsa, E.A., 1967. Analytical and Experimental Study of Boiler Instabilities Due to Feed-system − Subcooled Region Coupling. National Aeronautics and Space Administration Report NASA TN D-3961.

Gillette, J.L., Singer, R.M., Tokar, J.V., Sullivan, J.E., 1980. Experimental study of the transition from forced to natural circulation in EBR-II at low power and flow. Journal of Heat Transfer 102, 525−530. http://dx.doi.org/10.1115/1.3244335.

Grandi, G., Hoyer, N., Belblidia, L., 1998. Two-fluid thermal hydraulics capabilities of RAMONA-5. In: Proceedings of the International Conference on the Physics of Nuclear Science and Technology, October 5−8, 1998, Long Island, NY, USA, pp. 1621−1625.

Greif, R., Zvirin, Y., Mertol, A., 1979. The transient and stability behavior of a natural convection loop. Journal of Heat Transfer 101, 684−688.

Greif, R., 1988. Natural circulation loops. Journal of Heat Transfer 110, 1243−1258.

Gruszynski, M.J., Viskanta, R., 1983. Heat Transfer to Water from a Vertical Tube Bundle under Natural-Circulation Conditions. Argonne National Laboratory Report NUREG/CR-3167, ANL-83-7.

Gu, H.Y., Li, H.B., Hua, Z.X., Liu, D., Zhao, M., 2015a. Heat transfer to supercritical water in a 2×2 rod bundle. Annals of Nuclear Energy 83, 114−124.

Gu, H.Y., Zhao, M., Cheng, X., 2015b. Experimental studies on heat transfer to supercritical water in circular tubes at high heat fluxes. Experimental Thermal and Fluid Science 65, 22−32.

Guo, L.-J., Feng, Z.-P., Chen, X.-J., 2001. Pressure drop oscillation of steam-water two-phase flow in a helically coiled tube. International Journal of Heat and Mass Transfer 44, 1555−1564.
Ha, K.-S., Jeong, H.-Y., Cho, C., Kwon, Y.-M., Lee, Y.-B., Hahn, D., 2010. Simulation of the EBR-II loss-of-flow tests using the MARS code. Nuclear Technology 169, 134−142.
Hamidouche, T., Bousbia-salah, A., 2006. RELAP5/3.2 assessment against low pressure onset of flow instability in parallel heated cannels. Annals of Nuclear Energy 33, 510−520.
Hamilton, D.C., Lynch, F.E., Palmer, L.D., 1954. The Nature of Flow of Ordinary Fluids in a Thermal Convection Harp. ORNL-1624.
Harden, D.G., 1963. Transient Behavior of a Natural-circulation Loop Operating Near the Thermodynamic Critical Point. Argonne National Laboratory Report, ANL-6710.
Haroldsen, R., 2008. The Story of the BORAX Nuclear Reactor and the EBR-1 Meltdown. http://www.ne.anl.gov/pdfs/reactors/Story-of-BORAX-Reactor-by-Ray-Haroldsen-v2.pdf (accessed 23.08.15.).
He, S., Kim, W.S., Jiang, P.X., Jackson, J.D., 2004. Simulation of mixed convective heat transfer to carbon dioxide at supercritical pressure. International Journal of Mechanical Engineering Science 218, 1281−1296.
He, S., Kim, W.S., Jackson, J.D., 2008. A computational study of convective heat transfer to carbon dioxide at a pressure just above the critical value. Applied Thermal Engineering 28, 1662−1675.
Howlett II, R.C., 1995. The Industrial Operator's Handbook. Techstar Inc, Pocatello, Idaho.
Hoyer, N., 1994. MONA, a 7-Equation transient two-phase flow model for LWR dynamics. In: Proceedings of the International Conference on New Trends in Nuclear System Thermo-hydraulics, pp. 271−280.
Hu, R., 2010. Stability Analysis of the Boiling Water Reactor: Methods and Advanced Designs (Ph.D. dissertation). Massachusetts Institute of Technology.
Hu, R., Kazimi, M.S., 2011. Flashing-induced instability analysis and the start-up of natural circulation boiling reactors. Nuclear Technology 176, 57−71.
Hu, R., Kazimi, M.S., 2012. Boiling water reactor stability analysis by TRACE/PARCS: modeling effects and case study of time versus frequency domain approach. Nuclear Technology 177, 8−28.
Hughes, E.D., Paulsen, M.P., Agee, L.J., 1981. A drift-flux model of two-phase flow for RETRAN. Nuclear Technology 54, 410−421.
Hughes, E.D., Katsma, K.R., 1983. Numerical solution method improvements for RETRAN. Nuclear Technology 61, 167−180.
Hwang, Y.D., Yang, S.H., Kim, S.H., Lee, S.W., Kim, H.K., Yoon, H.Y., Lee, G.H., Bae, K.H., Chung, Y.J., 2005. Model Description of TASS/SMR Code. Korea Atomic Energy Research Institute. KAERI/TR-3082/2005.
Hwang, Y.D., Lee, G.H., Chung, Y.J., Kim, H.C., Chang, D.J., 2006. Assessment of the TASS/SMR Code Using Basic Test Problems. Korea Atomic Energy Research Institute. KAERI/TR-3156/2006.
IAEA, 2001. Thermohydraulic Relationships for Advanced Water Cooled Reactors. IAEA-TECDOC-1203, Vienna.
IAEA, 2002. Natural Circulation Data and Methods for Advanced Water Cooled Nuclear Power Plant Designs. IAEA-TECDOC-1281, Vienna.
IAEA, 2004. Status of Advanced Light Water Reactor Designs, 2004, IAEA-TECDOC-1391, Vienna, Austria.
IAEA, 2005. Natural Circulation in Water Cooled Nuclear Power Plants, Phenomena, Models, and Methodology for System Reliability Assessments. IAEA-TECDOC-1474. IAEA, Vienna.

IAEA, 2009. Passive Safety Systems and Natural Circulation in Water Cooled Nuclear Power Plants. IAEA-TECDOC-1624. IAEA, Vienna, Austria.
IAEA, 2013. Benchmark Analyses on the Natural Circulation Test Performed During the PHENIX End-of-Life Experiments. TECDOC No. 1703. IAEA, Vienna, Austria.
IAEA, 2012. Natural Circulation Phenomena and Modelling for Advanced Water Cooled Reactors. IAEA-TECDOC-1677, Vienna.
IAEA, 2014. Heat Transfer Behaviour and Thermohydraulics Code Testing for Supercritical Water Cooled Reactors (SCWRs). IAEA-TECDOC-1746, Vienna.
INEL, Idaho National Engineering Laboratory, 1995. RELAP5/MOD3 Code Manual, Vols. 1−6. INEL-95/0174, NUREG/CR-5535.
INEL, Idaho National Engineering Laboratory, 1992. TRAC-BF1/MOD1; an Advanced Best-estimate Computer Program for BWR Accident Analysis, Vols. 1−3. EGG-2626, NUREG/CR-4356.
INL, Idaho National Laboratory, 2014. Guidance for Developing Principal Design Criteria for Advanced (Non-light Water) Reactors. Idaho National Laboratory Report INL/EXT-14-31179 Rev. 1.
Ishii, M., 1976. Study on Flow Instabilities in Two-Phase Flow Mixtures. Argonne National Laboratory Report ANL-76-23.
Ishii, M., Revankar, S.T., Dowlati, R., Bertodano, M.L., Babelli, I., Wang, W., Pokharna, H., Ransom, V.H., Viskanta, R., Wilmarth, T., Han, J.T., 1996. Scientific Design of Purdue University Multi-Dimensional Integral Test Assembly (PUMA) for GE SBWR. U.S. Nuclear Regulatory Commission Report NUREG/CR-6309.
ISL, Information Systems Laboratories, Inc., 2001. RELAP5/MOD33 Code Manual Volume I, Code Structure, System Models, and Solution Methods. United States Nuclear Regulatory Commission Report, NUREG/CR-5535/Rev 1-Volume I.
Jackson, J.D., 2013. Fluid flow and convective heat transfer to fluids at supercritical pressure. Nuclear Engineering and Design 264, 24−40.
Jain, K.C., 1965. Self-Sustained Hydrodynamic Oscillations in a Natural-circulation Two-Phase-Flow Boiling Loop. Argonne National Laboratory Report ANL-7073.
Jain, P.K., Rizwan-uddin, 2008. Numerical analysis of supercritical flow instabilities in a natural circulation loop. Nuclear Engineering and Design 238, 1947−1957.
Jain, R., Conradini, M.L., 2006. A linear stability analysis for natural-circulation loops under supercritical conditions. Nuclear Technology 155, 312−323.
Jeglic, F.A., Grace, T.M., 1965. Onset of Flow Oscillations in Forced-Flow Subcooled Boiling. National Aeronautics and Space Administration Report NASA TN D-2821.
Jensen, P., 1992. BWR Stability Analysis Methods and Sensitivities. Nuclear Safety Analysis Center Report NSAC-172.
Jingjing, L., Tao, Z., Mingqiang, S., Qijun, H., Yanping, H., Zejun, A., 2015. CFD analysis of supercritical water flow instability in parallel channels. International Journal of Heat and Mass Transfer 86, 923−929.
Kakac, S., Bon, B., 2008. A review of two-phase flow dynamic instabilities in tube boiling systems. International Journal of Heat and Mass Transfer 51, 399−433.
Keller, J.B., 1967. Periodic oscillations in a model of thermal convection. Journal of Fluid Mechanics 26 (Part 3), 599−606.
Kelly, J.E., 2014. Generation IV International Forum: a decade of progress through international cooperation. Progress in Nuclear Energy 77, 240−246.
Kim, S., Bae, B.-U., Cho, Y.-J., Park, Y.-S., Kang, K.-H., Yun, B.-J., 2013. An experimental study on the validation of cooling capability for the Passive Auxiliary Feedwater System (PAFS) condensation heat exchanger. Nuclear Engineering and Design 260, 54−63.

Kommer, E.M., 2015. Numerical modeling of flow boiling instabilities using TRACE. Annals of Nuclear Energy 76, 263−270.

Kozmenkov, Y., Rohde, U., Manera, A., 2012. Validation of the RELAP5 code for the modeling of flashing-induced instabilities under natural-circulation conditions using experimental data from the CIRUS test facility. Nuclear Engineering and Design 243, 168−175.

Krepper, E., Prasser, H.-M., 1999. Natural circulation experiments at the ISB-VVER integral test facility and calculations using the thermal-hydraulic code ATHLET. Nuclear Technology 128, 75−86.

Kumar, K.K., Gopal, M.R., 2009. Steady-state analysis of CO_2 based natural circulation loops with end heat exchangers. Applied Thermal Engineering 29 (10), 1893−1903.

LANL, Los Alamos National Laboratory, 1986. TRAC-PFl/MODl: An Advanced Best-Estimate Computer Program for Pressurized Water Reactor Thermal-Hydraulic Analysis. NUREG/CR-3858, LA-10157-MS.

Lowdermilk, W.H., Lanzo, C.D., Siegel, B.L., 1958. Investigation of Boiling Burnout and Flow Instability for Water Flowing in Tubes. National Advisory Committee for Aeronautics Report NACA TN 4382.

Lahey Jr., R.T., Drew, D., 1980. An Assessment of the Literature Related to LWR Instability Modes. U.S. Nuclear Regulatory Commission Report NUREG/CR-1414.

Lahey Jr., R.T., Podowski, M.Z., Clausse, A., DeSanctis, N., 1990. A linear analysis of channel-to-channel instability modes. Chemical Engineering Communications 93, 75−81.

Lakshmanan, S.P., Pandey, M., 2009. Analysis of startup oscillations in natural circulation boiling systems. Nuclear Engineering and Design 239, 2391−2398.

Lerchel, G., Austregesilo, H., 2006. ATHLET Mod 2.1 Cycle a, User's Manual. Gesellschaft für Anlagen und- Reaktorsicherheit (GRS) GmbH Report GRS-p-1/Vol. 1, Rev. 4.

Levy, S., Beckjord, E.S., 1960. Hydraulic instability in a natural circulation loop with net steam generation at 1000 psia. In: Heat Transfer Conference, Paper No 60-HT-27. American Society of Mechanical Engineers, Buffalo, New York.

Lorenz, E.N., 1963. Deterministic non-periodic flow. Journal of Atmospheric Sciences 20, 130−141.

Lottes, P.A., Anderson, R.P., Hoflund, B.M., Marchaterre, J.F., Petrick, F.M., Popper, G.F., Weatherhead, R.J., 1963. Boiling Water Reactor Technology Status of the Art Report. Argonne National Laboratory Report, ANL-6561.

Manavela Chiapero, M., Fernandino, M., Dorao, C.A., 2012. Review on pressure drop oscillations in boiling systems. Nuclear Engineering and Design 250, 436−447.

Manavela Chiapero, M., Fernandino, M., Dorao, C.A., 2013a. On the influence of heat flux updating during pressure drop oscillation − a numerical analysis. International Journal of Heat and Mass Transfer 63, 31−40.

Manavela Chiapero, E., Fernandino, M., Dorao, C.A., 2013b. Numerical analysis of pressure drop oscillations in parallel channels. International Journal of Multiphase Flow 56, 15−24.

Mangal, A., Jain, V., Nayak, A.K., 2012. Capability of the RELAP5 code to simulate natural circulation behavior in test facilities. Progress in Nuclear Energy 61, 1−16.

Marcel, C.P., 2007. Experimental and Numerical Stability Investigations on Natural Circulation Boiling Water Reactors (Doctoral thesis). Delft University of Technology.

March-Leuba, J., 1984. Dynamic Behavior of Boiling Water Reactors (Doctoral dissertation). University of Tennessee—Knoxville.

March-Leuba, J., Rey, J., 1993. Coupled thermo-hydraulic-neutronic instabilities in boiling water nuclear reactors, A review of the state of the art. Nuclear Engineering and Design 145, 97−111.

Mascari, E., Vella, G., Woods, B.G., D'Auria, F., 2012. Analyses of the OSU-MASLWR experimental test facility. Science and Technology of Nuclear Installations 2012. http://dx.doi.org/10.1155/2012/528241. Article ID 528241.

Men, Q., Wang, X., Zhou, X., Meng, X., 2014. Heat transfer analysis of passive heat removal heat exchanger under natural convection condition on tank. Science and Technology of Nuclear Installations 2014. Article ID 279791, 8 p.

Mertol, A., 1980. Heat Transfer and Fluid Flow in Thermosyphons (Ph.D. dissertation). University of California at Berkeley.

Mertol, A., Grief, R., Zvirin, Y., 1981. The transient, steady state and stability behavior of a natural convection loop with a throughflow. International Journal of Heat and Mass Transfer 24, 621−633.

Misale, M., 2014. Overview on single-phase natural circulation loops. In: Proceedings of the International Conference on Advances in Mechanical and Automation Engineering − MAE 2014. http://dx.doi.org/10.15224/978-1-63248-022-4-101.

Misale, M., Ruffino, P., Frogheri, M., 2000. The influence of the wall thermal capacity and axial conduction over a single-phase natural circulation loop, 2-D numerical study. International Journal of Heat and Mass Transfer 36, 533−539.

Misale, M., Devia, F., Garibaldi, P., 2012. Experiments with Al_2O_3 nanofluid in a single-phase natural circulation mini-loop, preliminary results. Applied Thermal Engineering 40, 64−70.

Modarres, M., 2015. Multi-unit nuclear plant risks and implications of the quantitative health objectives. In: Proceedings of the American Nuclear Society Probabilistic Safety Analysis Conference (PSA2015), Sun Valley, Idaho, April 26−30.

Mori, M., 1998. Benchmarking and qualification of RETRAN-03 for BWR stability analysis by comparison with frequency-domain stability analysis code. Nuclear Technology 121, 260−274.

Muñoz-Cobo, J.L., Podowski, M.Z., Chiva, S., 2002. Parallel channel instabilities in boiling water reactor systems: boundary conditions for out of phase oscillations. Annals of Nuclear Energy 29, 1891−1917.

Nayak, A.K., Vijayan, P.K., 2008. Flow instabilities in boiling two-phase natural circulation systems, a review. Science and Technology of Nuclear Installations 2008. http://dx.doi.org/10.1155/2008/573192. Article ID 573192, 15 p.

Nakai, R., 2013. In: 3rd Joint GIF-IAEA Workshop on SDC for SFRs, February 26−27, Vienna.

NEI, Nuclear Energy Institute, 2012. Diverse and Flexible Coping Strategies (FLEX) Implementation Guide. Nuclear Energy Institute Report NEI 12-06 [Draft Rev. 0], Washington, D.C. (U.S. NRC Accession number ML122221A205).

Oka, Y., Mori, H. (Eds.), 2014. Supercritical-Pressure Light Water Cooled Reactors. Springer, Tokyo, ISBN 978-4-431-55024-2.

Okano, T., 2014. SDC discussions related to practical elimination: of accident situations. In: IAEA-GIF Workshop on Safety of SFR, IAEA, Vienna, 10−11 June.

Otaduy, P.J., March-Leuba, J., 1990. LAPUR User's Guide. NUREG/CR-542, ORNL/TM-11285.

Ozawa, M., Akagawa, K., Sakaguchi, T., 1989. Flow instabilities in parallel-channel flow systems of gas−liquid two-phase mixtures. International Journal of Multiphase Flow 15, 639−657.

Papini, D., Colombo, M., Cammi, A., Rocotti, M.E., 2014. Experimental and theoretical studies on density wave instabilities in helically coiled tubes. International Journal of Heat and Mass Transfer 68, 343−356.

Park, H.-S., Min, B.-Y., Jung, Y.-G., Shin, Y.-C., Ko, Y.-J., Yi, S.-J., 2014. Design of the VISTA-ITL test facility for an integral type reactor of SMART and a post-test simulation

of a SBLOCA test. Science and Technology of Nuclear Installations 2014. Article ID 840109, 14 p.

Park, H.-S., Choi, K.-Y., Cho, S., Yi, S.-Y., Park, C.-K., Chung, M.-K., 2008. Experimental study on the natural circulation of a passive residual heat removal system for an integral reactor following a safety related event. Annals of Nuclear Energy 35, 2249−2258.

Peng, S.J., Podowski, M.Z., Lahey Jr., R.T., Becker, M., 1984. NUFREQ-NP, a computer code for the stability analysis of boiling water nuclear reactors. Nuclear Science and Engineering 88, 404−411.

Peng, S.J., Podowski, M.Z., Lahey Jr., R.T., 1986. BWR linear stability analysis. Nuclear Engineering and Design 93, 25−37.

Penttila, S. (Ed.), 2015. 7th International Symposium on Supercritical Water-Cooled Reactors, ISSCWR-7, March 15−18, 2015, Helsinki, Finland, VTT Technology Report VTT 216.

Pilkhwal, D.S., Ambrosini, W., Forgione, N., Vijayan, P.K., Saha, D., Ferreri, J.C., 2007. Analysis of the unstable behavior of a single-phase natural circulation loop with one-dimensional and computational fluid-dynamic models. Annals of Nuclear Energy 34, 339−355.

Pioro, I.L., Duffey, R.B., 2003. Literature Survey of Heat Transfer and Hydraulic Resistance of Water, Carbon Dioxide, Helium and Other Fluids at Supercritical and Near-critical Pressures. Atomic Energy of Canada Report AECL-12137, FFC-FCT-409.

Pioro, I.L., Khartabil, H.F., Duffey, R.B., 2004. Heat transfer to supercritical fluids flowing in channels − empirical correlations (survey). Nuclear Engineering and Design 230, 69−91.

Pioro, I.L., Duffey, R.B., 2005. Experimental heat transfer in supercritical water flowing inside channels (survey). Nuclear Engineering and Design 235, 2407−2430.

Prasad, G.V.D., Pandey, M., Kalra, M.S., 2007. Review of research on flow instabilities in natural circulation boiling systems. Progress in Nuclear Energy 49 (6), 429−451.

Planchon, H.P., Singer, R.M., Mohr, D., Feldman, E.E., Chang, L.K., Betten, P.R., 1985. The EBR-II inherent shutdown and heat removal tests − a survey of test results. paper CONF-850410-6. In: Presented at the International Topical Meeting on Fast Reactor Safety April 21−25, 1985, Knoxville, Tennessee.

Rao, N.M., Maiti, B., Das, P.K., 2005a. Comparison of dynamic performance for direct and fluid coupled indirect heat exchange systems. International Journal of Heat and Mass Transfer 48, 3244−3252.

Rao, N.M., Maiti, B., Das, P.K., 2005b. Dynamic performance of a natural circulation loop with end heat exchangers under different excitations. International Journal of Heat and Mass Transfer 48, 3185−3196.

Rao, N.M., Maiti, B., Das, P.K., 2005c. Pressure variation in a natural circulation loop with end heat exchangers. International Journal of Heat and Mass Transfer 48, 1403−1412.

Rao, N.M., Maiti, B., Das, P.K., 2005d. Stability behavior of a natural circulation loop with end heat exchangers. Journal of Heat Transfer 127, 749−756.

Rao, N.M., Maiti, B., Das, P.K., 2008. Steady state performance of a single phase natural circulation loop with end heat exchangers. Journal of Heat Transfer 130, 084506.

Reason, J., 1997. Managing the Risks of Organizational Accidents. Ashgate Publishing, Aldershot, United Kingdom.

Richards, D.J., Hanna, B.N., Hobson, N., Ardron, K.H., 1985. ATHENA, a two-fluid code for CANDO LOCA analysis. In: Third International Topical Meeting on Reactor Thermal Hydraulics, Newport, Rhode Island, USA, October 15−18, 1985, 7E-1 thru 7E-14 (CATHENA Formerly Named ATHENA).

Rickover, H.G., 1970. Testimony, hearing before the Joint Committee on Atomic energy. In: 91st Congress, 2nd Session, March 19−20.

Rohatgi, U.S., Mallen, A.N., Cheng, H.S., Wulff, W., 1994. Validation of the engineering plant analyzer methodology with peach bottom 2 stability tests. Nuclear Engineering and Design 151, 145−156.

Rohatgi, U.S., Cheng, H.S., Khan, H.J., Mallen, A.N., Neymotin, L.Y., 1998. RAMONA-4B a Computer Code with Three-dimensional Neutron Kinetics for BWR and SBWR System Transient − Models and Correlations. Brookhaven National Laboratory Report BNL-NUREG-52471−1.

Rohatgi, U.S., Duffey, R.B., 1998. Stability, DNB, and CHF in natural circulation two-phase flow. International Communications in Heat and Mass Transfer 25, 161−174.

Rohde, M., Marcel, C.P., Manera, A., Van der Hagen, T.H.J.J., Shiralkar, 2010. Investigating the ESBWR stability with experimental and numerical tools: a comparative study. Nuclear Engineering and Design 240, 375−384.

Rowinski, M.K., White, T.J., Zhao, J., 2015. Small and medium sized reactors (SMR), a review of technology. Renewable and Sustainable Energy Reviews 44, 643−656.

Ruspini, L.C., Dorao, C.A., Fernandino, M., 2010. Dynamic simulations of Ledinegg instability. Journal of Natural Gas Science and Engineering 2, 211−216.

Ruspini, L.C., Dorao, C.A., Fernandino, M., 2011a. Simulation of a natural circulation loop using a least squares hp-adaptive solver. Mathematics and Computers in Simulation 81, 2517−2528.

Ruspini, L.C., Dorao, C.A., Fernandino, M., 2011b. Modeling of dynamic instabilities in boiling systems. In: ICONE-19: 19th International Conference on Nuclear Engineering; Osaka (Japan); October 24−25, 2011. Japan Society of Mechanical Engineers, Tokyo, Japan [3427 p.]; 2011; [9 p.].

Ruspini, L.C., 2012. Inertia and compressibility effects on density waves and Ledinegg phenomena in two-phase flow systems. Nuclear Engineering and Design 250, 60−67.

Ruspini, L.C., Dorao, C.A., Fernandino, M., 2012. Two-phase flow instabilities in boiling and condensing systems. Journal of Power and Energy Systems 6 (2), 302−313.

Ruspini, L.C., 2013. Experimental and Numerical Investigation on Two-Phase Flow Instabilities (Doctoral thesis). Norwegian University of Science and Technology.

Ruspini, L.C., Marcel, C.P., Clausse, A., 2014. Two-phase flow instabilities: a review. International Journal of Heat and Mass Transfer 71, 521−548.

Sabharwall, P., Yoo, Y.J., Wu, Q., Sienicki, J.J., 2012. Natural circulation and linear stability analysis for liquid metal reactors with the effect of fluid axial conduction. Nuclear Technology 178, 298.

Saha, P., Aksan, N., Anderson, J., Yan, J., Simoneau, J.P., Leung, L., Bertrand, F., Aoto, K., Kamide, H., 2013. Issues and future direction of thermal-hydraulics research and development in nuclear power reactors. Nuclear Engineering and Design 264, 3−23.

Saha, P., 1974. Thermally Induced Two-Phase Flow Instabilities, Including the Effects of Thermal Non-Equilibrium between the Phases (Ph.D. dissertation). Georgia Institute of Technology, Atlanta, Georgia.

Saha, P., Ishii, M., Zuber, N., 1976. An experimental investigation of the thermally induced flow oscillations in two-phase systems. ASME Journal of Heat Transfer 98, 616−622.

Saha, P., Zuber, N., 1978. An analytical study of the thermally induced two-phase flow instabilities including the effect of thermal non-equilibrium. International Journal of Heat and Mass Transfer 21, 415−426.

Salazar, O., Mihir, S., Ramos, E., 1988. Flow in conjugate natural circulation loops. AIAA Journal of Thermophysics 2, 180−183.

Sarkar, M.K.S., Tilak, A.K., Basu, D.N., 2014. A state-of-the-art review of recent advances in supercritical natural circulation loops for nuclear applications. Annals of Nuclear Energy 73, 250–263.

Sharabi, M.B., Ambrosini, W., He, S., 2008a. Prediction of unstable behaviour in a heated channel with water at supercritical pressure by CFD models. Annals of Nuclear Energy 35, 767–782.

Sharabi, M., Ambrosini, W., He, S., Jackson, J.D., 2008b. Prediction of turbulent convective heat transfer to a fluid at supercritical pressure in square and triangular channels. Annals of Nuclear Energy 35, 993–1005.

Singer, R.M., Gillette, J.L., Mohr, D., Tokar, J.V., Sullivan, J.E., Dean, E.M., 1980. Response of EBR-II to a complete loss of primary forced flow during power operation. In: Specialists' Meeting on Decay Heat Removal and Natural Convection in FBR's, Brookhaven National Laboratory Upton, Long Island, New York, February 28–29, 1980.

Sofu, T., 2014. In: 4th IAEA-GIF Technical Meeting/Workshop on Safety of SFRs, June 10–11, Vienna.

Spore, J.W., Giles, M.W., Singer, G.L., Shumway, R.W., 1981. TRAC-BD1/MOD1, an Advanced Best Estimate Computer Program for Boiling Water Reactor Transient Analysis Volume 1 Model Description. Idaho National Engineering Laboratory Report, NUREG/CR-2178, EGG-2109.

Stekelenburg, A.J.C., 1994. Statics and Dynamics of a Natural Circulation Cooled Boiling Water Reactor (Doctoral thesis). Delft University of Technology.

Suzuki, A., 2014. Managing the Fukushima challenge. Risk Analysis 34, 1–17.

Swapnalee, B.T., Vijayan, P.K., 2011. A generalized flow equation for single phase natural circulation loops obeying multiple friction laws. International Journal of Heat and Mass Transfer 54, 2618–2629.

Swapnalee, B.T., Vijayan, P.K., Sharma, M., Pilkhwal, D.S., 2012. Steady state flow and static instability of supercritical natural circulation loops. Nuclear Engineering and Design 245, 99–112.

Tadrist, L., 2007. Review on two-phase flow instabilities in narrow spaces. International Journal of Heat and Fluid Flow 28 (1), 54–62.

TEPCO, 2012. Fukushima Nuclear Accident Analysis Report. Tokyo Electric Power Company Inc.

Tilak, A.K., Basu, D.N., 2015. Computational investigation of the dynamic response of a supercritical natural circulation loop to aperiodic and periodic excitations. Nuclear Engineering and Design 284, 251–263.

Todreas, N.E., Kazimi, M.S., 1990. Nuclear Systems I: Thermal Hydraulic Fundamentals and Nuclear Systems II: Elements of Thermal Hydraulic Design. Hemisphere Publishing Corporation, New York.

Toumi, I., Bergeron, A., Gallo, D., Royer, E., Caruge, D., 2000. FLICA-4: a three-dimensional two-phase flow computer code with advanced numerical methods for nuclear applications. Nuclear Engineering and Design 200, 139–155.

U.S. DOE, United States Department of Energy Office of Nuclear Energy, 2014. Advanced Reactor Concepts Technical Review Panel Public Report. http://www.energy.gov/ne/downloads/advance-reactor-concepts-technical-review-panel-public-report.

U.S. DOE, United States Department of Energy Office of Environmental Management, 2015. Accident Investigation Report, Phase 2: Radiological Release Event at the Waste Isolation Pilot Plant. http://energy.gov/sites/prod/files/2015/04/f21/WIPP%20Rad%20Event%20Report%20Phase%202%2004.16.2015.pdf.

U.S. NRC, United States Nuclear Regulatory Commission, 1997. Recommendations for Probabilistic Seismic Hazard Analysis: Guidance on Uncertainty and Use of Experts. CR-6372 UCRL-ID-122160, Vols. 1 and 2.

U.S. NRC, United States Nuclear Regulatory Commission, 2004. Nuclear Power Plant Licensing Process. NUREG/BR-0298, Rev. 2.

U.S. NRC, U.S. Nuclear Regulatory Commission, 2008. TRACE V5.0 Theory Manual, Field Equations, Solution Methods and Physical Models. Draft Report. Division of Risk Assessment and Special Projects, Office of Nuclear Regulatory Research, Washington, DC. Pdf File created August 15, 2007. Available on NRC's online document retrieval system ADAMS since February 2009 with Reference No."ML071000097".

U.S. NRC, United States Nuclear Regulatory Commission, 2014. Final safety evaluation report related to the certification of the economic simplified boiling-water reactor standard design. NUREG-1966, ADAMS Accession number ML14100A187.

van Bragt, D.D.B., 1998. Analytical Modeling of Boiling Water Reactor Dynamics (Doctoral thesis). Delft University of Technology.

van de Graaf, R., van der Hagen, T.H.J.J., Mudde, R.F., 1994. Two-phase flow scaling laws for a simulated BWR assembly. Nuclear Engineering and Design 148, 455–462.

van der Hagen, T.H.J.J., Stekelenburg, A.J.C., van Bragt, D.D.B., 2000. Reactor experiments on type-I and type-II BWR stability. Nuclear Engineering and Design 200, 177–185.

Vecchiarelli, J., Dinnie, K., Luxat, J., 2014. Development of a Whole-Site PSA Methodology. CANDU Owners Group. COG-13-9034 r0.

Vijayan, P.K., Nayak, A.K., 2010. Introduction to instabilities in natural circulation systems. In: IAEA Training Course on Natural Circulation Phenomena and Passive Safety Systems in Advanced Water-cooled Reactors, ICTP, Trieste, Italy, 17–21 May 2010.

Vijayan, P.K., Sharma, M., Pilkhwal, D.S., 2013. Steady State and Stability Characteristics of a Supercritical Pressure Natural Circulation Loop (SPNCL) with CO_2. Bhabha Atomic Research Centre Report BARC/2013/003.

Vyas, H.P., Venkat Raj, V., Nayak, A.K., 2010. Experimental investigations on steady state natural circulation behavior of multiple parallel boiling channel system. Nuclear Engineering and Design 240, 3862–3867.

Walter, H., Linzer, W., 2006. The influence of the operating pressure on the stability of natural circulation systems. Applied Thermal Engineering 26, 892–897.

Welander, P., 1967. On the oscillatory instability of a differentially heated fluid loop. Journal of Fluid Mechanics 29, 17–30.

Wenbin, Z., Yanping, H., Zejun, X., Chuanxin, P., Sansan, L., 2014. Experimental research on passive residual heat removal system of Chinese advanced PWR. Science and Technology of Nuclear Installations 2014. Article ID 325356, 8 p.

WENRA, Western European Nuclear Regulators Association, 2009. Safety Objectives for New Power Reactors. Study by WENRA Reactor Harmonization Working Group, pp. 9–10.

WENRA, Western European Nuclear Regulators Association, 2014. Safety Reference Level for Existing Reactors. Available at: http://www.wenra.org/harmonisation/reactor-harmonisation-working-group.

Whittle, R.H., Forgan, R., 1967. A correlation for the minima in the pressure drop versus flow-rate curves for sub-cooled water flowing in narrow heated channels. Nuclear Engineering and Design 6, 89–99.

Wissler, E.H., Isbin, H.S., Amundson, N.R., 1956a. The oscillatory behavior of a two-phase natural circulation loop. In: Presented at the Nuclear Engineering and Science Congress, Cleveland, Ohio. AIChE Preprint 59, 1955. See also American Institute of Chemical Engineers Journal, 2, 157–162.

Wissler, E.H., Isbin, H.S., Amundson, N.R., 1956b. Oscillatory behavior of a two-phase natural circulation loop. AIChE Journal 2, 157–162.

Woffinden, F.B., Niemi, R.O., 1981. Low-Flow Stability Tests at Peach Bottom Atomic Power Station Unit 2 during Cycle 3. Electric Power Research Institute Report NP-972.

Wu, Y., 2011. On the modeling and control of coupled multi-loop thermosyphons. In: Applications of Mathematics and Computer Engineering, 2011 American Conference on Applied Mathematics, pp. 105−110.

Wulff, W., Cheng, H.S., Mallen, A.N., Rohatgi, U.S., 1992. BWR Stability Analysis with the BNL Engineering Plant Analyzer. Brookhaven National Laboratory Report NUREG/CR-5816; BNL-NUREG-52312.

Xiong, T., Yan, X., Huang, S., Yu, J., Huang, Y., 2013. Modeling and analysis of supercritical flow instability in parallel channels. International Journal of Heat and Mass Transfer 57, 549−557.

Xiong, T., Yan, X., Xiao, Z.J., Li, Y.L., Huang, Y.P., Yu, J.C., 2012. Experimental study on flow instability in parallel channels with supercritical water. Annals of Nuclear Energy 48, 60−67.

Xu, Y., Downar, T., Walls, R., Ivanov, K., Staudenmeier, J., March-Lueba, J., 2009. Application of TRACE/PARCS to BWR stability analysis. Annals of Nuclear Energy 36, 317−323.

Yadav, A.K., Gopal, M.R., Bhattacharyya, S., 2012a. CFD analysis of a CO2 based natural circulation loop with end heat exchangers. Applied Thermal Engineering 36, 288−295.

Yadav, A.K., Gopal, M.R., Bhattacharyya, S., 2012b. CO_2 based natural circulation loops, new correlations for friction and heat transfer. International Journal of Heat and Mass Transfer 55, 4621−4630.

Yadigaroglu, G., Bergles, A.E., 1969. An Experimental and Theoretical Study of Density-Wave Oscillation in Two-Phase Flow. Massachusetts Institute of Technology Report DSR 74629-3.

Yang, S.H., Chung, Y.-J., Kim, K.-K., 2008. Experimental validation of the TASS/SMR code for an integral type pressurized water reactor. Annals of Nuclear Energy 35, 1903−1911.

Yetisir, M., Gaudet, M., Duffey, R., 2015. SuperSafe Reactor© (SSR): a supercritical water-cooled small reactor. In: Proceedings of the 22nd International Technical Meeting on Small Modular Reactors, Canadian Nuclear Society, Ottawa, Canada November 7−9.

Yu, L., Sur, A., Liu, D., 2015. Flow boiling heat and two-phase flow instability of nanofluids in a minichannel. Journal of Heat Transfer 137. http://dx.doi.org/10.1115/1.4029647. Paper No: HT-14-1408.

Zhang, X.-R., Chen, L., Yamaguchi, H., 2010. Natural convective flow and heat transfer of supercritical CO_2 in a rectangular natural circulation loop. International Journal of Heat and Mass Transfer 53, 4112−4122.

Zhao, M., Gu, H.Y., Cheng, X., 2014. Experimental study on heat transfer of supercritical water flowing downward in circular tubes. Annals of Nuclear Energy 63, 339−349.

Zvirin, Y., 1979. The effect of dissipation on free convection loops. International Journal of Heat and Mass Transfer 22, 1539−1545.

Zvirin, Y., 1982. A review of natural circulation loops in pressurized water reactors and other systems. Nuclear Engineering and Design 67, 203−225.

Zvirin, Y., 1985. The instability associated with the onset of motion in a thermosyphon. International Journal of Heat and Mass Transfer 28, 2105−2111.

Zvirin, Y., Jeuck III, P.R., Sullivan, C.W., Duffey, R.B., 1981. Experimental and analytical investigations of a natural circulation system with parallel loops. Journal of Heat Transfer 103, 645−652.

Nonproliferation for advanced reactors: political and social aspects

17

G. Clark [1], *R.B. Duffey* [2]
[1]Nuclear Adviser, Pell Frischmann Group, Manchester Square, London, UK; [2]DSM Associates Inc., Ammon, Idaho Falls, ID, United States

17.1 Introduction

Two fundamental goals of advanced reactors (ARs) and new Generation IV technologies rely on nuclear fuels and their use for providing globally sustainable energy supply while reducing the potential for abuse for nuclear weapons development and threats (Kelly, 2014), as follows:

Sustainability: Generation IV nuclear energy systems will provide sustainable energy generation that meets clean air objectives and promotes long-term availability of systems and effective fuel. They will minimize and manage their nuclear waste and notably reduce the long-term stewardship burden in the future, thereby improving protection for the public health and the environment.

Proliferation Resistance and Physical Protection: Generation IV nuclear energy systems will increase the assurance that they are a very unattractive and the least desirable route for diversion or theft of weapons-usable materials, and provide increased physical protection against acts of terrorism.

The underlying and existing technology of nuclear fuel is well described in standard textbooks, reference books, and handbooks (Murray and Holbert, 2015; Nuclear Energy Encyclopedia, 2011; Handbook of Nuclear Engineering, 2010; Nuclear Engineering Handbook, 2009; Lamarsh and Baratta, 2001; Hewitt and Collier, 2000; Glasstone and Sesonske, 1994), and in chapter 18 of this handbook.

Fundamentally, nuclear fission is a reaction in which the nucleus of a heavy nuclide splits into smaller nuclides, a few new neutrons are created, gamma rays are emitted, and a significant amount of energy is released. Since then, nuclear fission has been used as the basis for production of heat in all of the current nuclear reactors. Even though these reactors can be categorized based on their cooling medium, pressure boundary, type of nuclear fuel, or neutron spectrum, they all have one common feature, which is the production of heat via a fission chain reaction in the nuclear fuel.

An important part of every reactor design involves the selection of a nuclear fuel and design of the fuel assemblies. As general requirements, a nuclear fuel should have a high melting point, acceptable thermal conductivity, sufficient mechanical

Handbook of Generation IV Nuclear Reactors. http://dx.doi.org/10.1016/B978-0-08-100149-3.00017-3
Copyright © 2016 Elsevier Ltd. All rights reserved.

stability, good dimensional and irradiation stability, as well as chemical compatibility with the cladding and the coolant. Another important parameter that influences the design and selection of a nuclear fuel is the dominant neutron spectrum of the reactor. Thus, in the past, the emphasis has been on uranium-based fuels in commercial water-cooled reactors (PWRs, BWRs, and HWRs), and its ceramic oxide, UO_2, and U_3O_8, with only limited enrichment of the fissile ^{235}U isotope (<20%) as derived from gaseous diffusion and centrifuge separation technology (see, eg, the latest proposed Iran/US/IAEA/EU/UN Agreement, Joint Comprehensive Plan of Action (JCPOA) (2015)). To meet the demanding Generation IV goals, many future concepts and designs for ARs focus on one or more of the following ideas, selection depending on the design details and preferred fuel cycle:

- Extending the sustainability of the uranium and other fuel resources by enhancing the burnup or fraction of fissionable atoms used per unit energy produced;
- Using "breeding" fuel cycles and core designs that provide more fuel than is consumed, producing fissile plutonium (^{239}Pu) and uranium (^{233}U) isotopes from nonfissile material (^{238}U and ^{232}Th, respectively);
- Adopting recycling strategies by separating unusable fission products from "gently used" fuel and/or blending with virgin fuel for reuse, sometimes with an on-site facility to avoid transport and external facilities;
- Providing fuel and core designs that are more "accident resistant," using materials that are capable of withstanding higher temperatures before melting and/or damage occurs to the clad or fuel, or eliminating the possibility of core melt altogether, and avoiding the potential for hydrogen production and explosions;
- Reducing high-level waste streams in both amounts and toxicity, especially for very long-lived radionuclides, by recycling, isotopic conversion, and actinide burning; and
- Avoiding and limiting diversion opportunities by having "sealed" cores that can be removed and replaced infrequently only under outside or independent supervision, or having a so-called "closed" fuel cycle.

17.1.1 Nonproliferation: past influence and future directions

The whole issue of nonproliferation is fraught with the politics of power and influence. The starting point, the aims of Nuclear Non-Proliferation Treaty (NPT) of 1968 and the parallel development of the role of the International Atomic Energy Agency (IAEA) established in Vienna in 1957, tasked with (among other things) the policing of a safeguards regime, whose aim was to make certain that civil nuclear materials were not diverted to military purposes. Originally, this safeguards regime only applied to "declared" facilities, but following the first Iraq War in 1991, it has aimed to be more all embracing. The most recent amendments are supposed to allow surprise inspections, of anything, anywhere, at any time. The NPT has been surprisingly successful, despite the weapons states not relinquishing their own weapons. In place of pessimistic predictions that by the year 2000, there would be 30–35 nuclear-armed states, there are still less than 10. But as the Treaty contains no provision for amendment or for sanctions against member states that flout their obligations, the system of which it is the foundation is beginning to look somewhat frayed. The system has learnt from its failures, but it is finding it difficult to deal with a small minority of member states who have concluded

that the possession of nuclear weapons is a greater prize than continued membership of a nonproliferation club (NPTC) dominated by the weapons states. While the Indian and Pakistani weapons tests of May 1998 pose an insoluble formal difficulty, the substance looks set to be solved by pragmatic agreements in each case, aimed at bringing them into compliance. The motives for this small number of countries developing a weapons capability derive from their perception of their national needs, independence, defense, and pride, just as was the case earlier for the weapons states.

There are other shortcomings:

- Israel (although not a member of the Treaty) is known to have a clandestine weapons capacity, but this is passed over in silence by the USA;
- Iraq was revealed after the first Gulf War as having pursued a clandestine weapons program throughout the 1980s while appearing to be a model member of the Treaty. Following the Iraq revelations, an additional protocol was negotiated that allows the IAEA to be much more proactive in policing the system of which it is the guardian;
- Others—Iran, Libya, and North Korea—have also flouted their obligations as Treaty members. External political pressure brought Libya back into compliance. It remains to be seen whether the agreement reached in 2015 with Iran on nuclear fuel limitation will have the declared effect of limiting Iran's capacity to develop nuclear weapons. North Korea has demonstrated its ability to make a modest nuclear weapon-type explosion, and remains defiant in the face of pressure to abandon its nuclear weapons ambitions. This still leaves India, Pakistan, Israel, and others unresolved; and
- Isolation as a policy of containment and retribution manifestly does not work; see the cases of Israel, India, Pakistan, Iran, and North Korea. The NPT has in consequence become inconsistent in application, ineffective in adoption, and inequitable in practice.

As also noted in a fairly recent Massachusetts Institute of Technology (MIT) report (The Future of Nuclear Power, 2003):

> *The current international safeguards regime is inadequate to meet the security challenges of the expanded nuclear deployment contemplated in the global growth scenario. The reprocessing system now used in Europe, Japan, and Russia that involves separation and recycling of plutonium presents unwarranted proliferation risk.*

Specifically, this inadequacy placed MIT in the difficult position of proposing that "…over at least the next 50 years, the best choice to meet these challenges is the open, once-through fuel cycle. We judge that there are adequate uranium resources available at reasonable cost to support this choice under a global growth scenario."

We return to this key issue of global sustainability of nuclear fuels beyond the next decades later, simply noting that this statement is rather myopic or US-centric. It implies these significant weaknesses, in their view, would not allow the full use of the nuclear fuel energy source. This is only reasonable if many other sustainable fuels exist, domestically and globally, and is at the heart of the NPT debate and the need for revision.

In the discussion of fuel cycle issues, the United States particularly, but the other weapons states also, have tended to adopt a hypocritical position, arguing for keeping

the existing distribution of skills and services as they are. At the beginning of the first preparatory committee in April 2007 for the review conference of the NPT in 2010, the US delegate delivered a long speech full of self-praise about the great efforts the United States had undertaken to promote the civilian uses of nuclear energy, concentrating on power generation and the peripheral uses—medical isotopes, the use of nuclear techniques in agriculture, industrial measurement, and so on—but skating over the tough efforts it has made over the years, decades even, to keep enrichment and reprocessing out of the hands of the nonweapons states. Originally these efforts were directed to keeping a US monopoly of enrichment and insisting that US-tagged material had eventually to be returned to the United States. Arguing from the general to the particular, the purpose of this speech was to attempt to demonstrate that Iran had no right under Article IV of the NPT to assistance in the development of a native fuel cycle, which could incidentally be used for weapons production, whatever Iran's declared intentions, and arguing that its civil needs could be met by an internationally backed guaranteed supply of fuel for its planned reactor if commercial channels failed to deliver.

Despite all these difficulties, the international safeguards system does have real value. The key to it lies in the scientific detail, which forces the exploiters of nuclear energy to discriminate between deploying it in weaponry and using it as a source of energy for the generation of electricity. While the two branches have much in common, from the earliest days, military programs have been developed separately from all the civil uses of nuclear energy.

An issue which has come to the fore recently, but was always there, even in the early years, is the exploitation by the weapons states of a de facto monopoly on (closely held) enrichment technology for commercial advantage in international trade and nuclear energy deployment to the disadvantage of the rest. Thus commercial gains became entwined with policy games. One way to strengthen the international safeguards system as a generally effective defense against proliferation is by:

- Deploying licensed enrichment technology; and
- Switching to more sustainable nonplutonium fuel cycles.

This would make it possible for civil nuclear power to spread to areas of the world that it has not yet reached, but needs to do.

We discuss the shortcomings of the Treaty, the measures that have been taken to improve matters, the actions of rogue states, the easier implications for resistance to global terrorism, and the points of weakness or danger for the future. *These lie in the nuclear fuel cycle rather than in the spread of nuclear power reactors*. Just as the Treaty, at its inception, reflected the political balance between the superpowers in the Cold War, the world's defenses against nuclear proliferation are likely to be more assisted by the continuing political commitment of its leading member states, especially, the United States, than by formal attempts to amend the Treaty to take account of exceptions which have arisen in its 40-year history. It thus points out how unhelpful the recent selectivity, persecution, and bullying tactics of the United States have been. Finally, the paper reaffirms the continuing support of the civil nuclear industry, in whose interest it was created, to the international safeguards system.

Table 17.1 Typical military nuclear stockpiles

Country	Stockpile (est.)	Comment[a]
China	125	M, A
France	300	S, M
India	50	M
Israel	80	Undeclared
North Korea	~10	M
Pakistan	60	M
Russia	14,000	S, M, A, W
UK	160	S, M, A
USA	10,000	S, M, A, W

[a]*S*, submarine; *M*, missile; *A*, aircraft; *W*, shell delivery systems.
The Independent, April 2009.[1]

17.1.2 Past dreams and present realities of the politics of power

President Obama's 2009 initiative aimed at negotiating, once again, a reduction in the number of nuclear weapons in the world. He declared in Prague on April 5, 2009, that he wanted "a new treaty to end the production of fissile materials and, although this was probably not feasible in his lifetime, a world free of such weapons altogether." A desirable, almost altruistic goal, such a reduction was intended to be approached step-by-step under the US–Russia bilateral Strategic Arms Reduction Treaty (START) talks, which foundered on the principles of the need to "trust but verify," and the inability to achieve "zero." The magnitude of the nuclear disarmament task is easily seen from the present declared or known weapons stockpiles that have their origins in regional and global conflicts.

There is some "surplus" weapons material (some in warhead form) that is just being stored or has been down-blended for making commercial fuel under the Gore–Chernomyrdin Agreement. There is clearly a small quantity in North Korea and perhaps also some already in Israel and Iran. For estimates of current stockpiles, see Table 17.1.

For the past few years, Iran's construction of a working uranium enrichment plant, avowedly for peaceful purposes, has dominated the headlines, along with North Korea's avowed pursuit of nuclear and rocket technology. The United States and the European Union (rather less confrontationally) have expressed determination to prevent Iran from going ahead. What is it all about? Why the apoplexy in Washington?

[1] Although precise numbers are cited here, they are in fact approximations. Even if exact numbers were available for one specific moment in time, continuing stockpile changes as a result of deployment shifts and inspection and maintenance actions cause actual numbers to fluctuate.

Why do even the Russians and the Chinese pay lip service to the objective of preventing the Iranian enrichment plant, or the North Korea nuclear missile program, even if they do not show much solidarity with the western powers in taking measures in the Security Council to deter the Iranians?

Iran has asserted its rights under Article IV to develop enrichment technology for peaceful purposes, a position not palatable to those weapons states (notably the USA) that see the potential for weapons production. Iran's[2] position depends on its persuading people that it is fulfilling its obligations under Article II. It has not been entirely successful on this front, largely because of its evasive accounts of earlier history. Meanwhile, North Korea alternates positions over peaceful versus military use, and between multilateral negotiations and unilateral withdrawal.

The essence is political: revolutionary Iran, ever since the fall of the Shah in 1979, has been adamantly opposed to the United States, excoriated by Iran as the great Satan. The US, which was humiliated in a number of incidents during the revolution and by the fiasco of its claim of weapons of mass destruction (WMDs) in Iraq, is unwilling to take an objective view of the situation. Although it routinely denounces Iran as a supporter of terrorism and finds it difficult to conceive that the Iranians could have neutral or benign objectives in developing a technology ostensibly for civilian use, it has tried to strike a compromise. The enrichment of uranium to the degree necessary to enable them to produce nuclear weapons in the relatively near future is a short step beyond using it to produce nuclear fuel. Therefore, to the chagrin of Israel, recent agreements between the US, EU, UN, and Iran aim to set thresholds on amounts, centrifuge counts, and enrichment levels that hopefully delay the potential for weapons manufacture or deployment. Iran, meanwhile, continues to test missiles with the potential capability for weapons delivery.

For their part, the Iranians claim that their intention is the peaceful development of nuclear energy, as is their right under the NPT. They assert that in an uncertain and generally hostile world, it is a prime national interest of theirs to develop a complete nuclear fuel cycle rather than having to rely on outside supply for crucial parts of it. They are made more intransigent, just like anyone else, by being threatened, bullied, and pilloried. They are not the first country to have thought or reacted in this way, as India had already demonstrated in the face of US objections and international boycotts and embargoes. However, many of the states that have viable civil nuclear programs have found it acceptable to import some of their key constituent parts, including enriched uranium fabricated into fuel for civil reactors. There are, in fact, good economic arguments for so doing, especially if a country possesses only a small number of reactors. Russia, seeing an export opportunity, has made the Iranians an offer of guaranteed supplies of reactor fuel, which takes at face value the latter's claim that they are only seeking to guarantee their supplies of fuel for their planned civilian reactors, the first of which has been completed with Russian assistance and Russian fueling.

[2] For an extensive discussion of the Article IV problem, see Christopher Ford's recent paper: "Nuclear Technology Rights and Wrongs: The NPT, Article IV, and Non-proliferation," which can be found on the NPEC website.

Similarly, Communist North Korea warred against US and UN armies, withstood them, and, backed militarily by China, established the armistice line at the end of the War in 1953, close to the famous 38th parallel as the dividing line. It has held it ever since. As a result, the US invested heavily in South Korea's economy, trade, and technology, even supplying whole factories and designs for deploying commercial nuclear power plants, while trying to isolate North Korea, or offering similar technology and energy supplies as a quid pro quo for stopping nuclear weapons development. Thus was born the "Axis of Evil" of President George Bush, portrayed as arrayed against the forces of good.

To set this in context so as to make sensible recommendations for the future, we shall also look at the history and present needs for energy independence, not allowing foreign policies to be dictated by the weapons states (like US, Russia, and France), and at national pride in self-reliance in the newly emerging economic powerhouses of the world (China and India), and the supply stranglehold of the major oil and gas producers (Russia and OPEC) on the US and EU users. Couple that with the needs of nations to grow, both economically and politically, and we have the elements of a world scene that must be and is changing. In fact, we may summarize the interests of many nations and their aspirations, given recent statements and trends diagrammatically in Table 17.2, which follows below.

The aim of the table is to show how widespread is the interest in the development of the fuel cycle, both actually and potentially. *It also shows how "containing" or restricting enrichment and commercial nuclear technology to a few countries (weapons states) is unrealizable and unreasonable*. What everyone really wants are cheap, assured, sustainable and secure energy supply, using proven and economic designs.

This nonproliferation story has all the makings of a saga, which is a long way from resolution, with a long back history. The aim of this chapter is to clarify the issues, which have led to the present position and to propose some new solutions and attitudes, not the least from the existing weapons states that recognize today's realities and needs.

One major new subplot is the widespread realization that to make a real difference a *massive* global deployment of nuclear energy (some 10 times the present) will be needed if nuclear energy is used to resolve future energy sustainability and climate change-driven reduced emission targets and requirements. Existing regimes, paradigms, and mechanisms are plainly inadequate faced with such a new era. The weapons states' offering of special "proliferation resistant" reactors and "assured fuel supply" is little better than applying a band-aid to a broken leg and likely to be counterproductive.

17.1.3 The genesis of the NPT and its bargain

The foundation of the current international regime for containing the spread of nuclear weapons is the nuclear NPT. It was a product, following the ugly Cold War race to mutually assured destruction, of a realization that WMDs were potentially highly unstable as a national policy tool. It was opened for signature in 1968 and came into force

Table 17.2 Typical national fuel cycle capabilities and reactor types (disclosed, past, present, real, or proposed)

	Supply	Reprocess	Enrich	Fast	Thermal	Open	Closable
USA	√	√	√	√	√	√	√
Russia	√	√	√	√	√	√	√
France		√	√	√	√	√	√
China	√	√	√	√	√		√
UK		√	√		√	√	√
Japan		√	√	√	√	√	√
Canada	√	√	√		√	√	√
India		√	√	√	√		√
Pakistan			√		√		√
Portugal	√						
Australia	√		√				√
Turkey							√
Germany					√	√	
Finland					√	√	√
Lithuania					√	√	√
South Korea				√	√	√	√
South Africa			√		√	√	√
Switzerland					√	√	√
Argentina		√	√			√	√
Brazil	√	√	√		√	√	√
Mexico					√	√	
Romania					√	√	√
Israel			√				
Iran		√			√		√
North Korea		√	√				√
Belgium					√	√	
Sweden			√		√	√	√
Spain					√	√	

in the spring of 1970 when sufficient (40) ratifications of the Treaty had been collected by the three depository powers (the United States, Britain, and the Soviet Union).

The NPT itself was the culmination of a lengthy process set in motion by President Eisenhower's speech to the General Assembly of the United Nations in December 1953, known ever since as his "Atoms for Peace" speech. The speech also proposed the establishment of an International Atomic Energy Agency under the aegis of the United Nations, which would promote the benefits of the peaceful uses of nuclear energy at the same time as facilitating practical measures of military nuclear disarmament. One of its prime objectives was to develop a system whereby the proliferation of military technologies could be controlled by the application of "safeguards" on all nuclear establishments. What this meant was measuring, tracking, and labeling every

atom of fissionable material in circulation or use in a safeguards regime, which had two main variants: installation-specific safeguards, as set out in INFCIRC/66, and "full-scope safeguards," set out in INFCIRC/153,[3] in which all a member state's nuclear installations became subject to international safeguards policed by the inspectors of the IAEA.

The purpose of an inspection is to demonstrate the truth of a member state's claim that there has been no diversion of material, based on a voluntary declaration of the usage and facilities to be "under safeguards." If the inspector should find otherwise, he would have to report in the first instance through the Director General to the Board of Governors of the IAEA, who in turn decide whether to appeal to the Security Council for action to deal with the breach. The fallout from the fallacy of voluntary disclosure was yet to emerge.

The creation of this system was strongly influenced by the more or less simultaneous creation of European Atomic Energy Community (Euratom) and its system of safeguards in 1957 by the six founder member countries of the European Community (see Appendix 1 on Euratom).

While the establishment of the IAEA was a deal between the United States and its allies on one side and the Soviet Union and its cohorts on the other, tension between the two camps rose over the next 5 years, culminating in the Cuban Missile Crisis of October 1962. The diffusion of the crisis without, fortunately, any of the threatened exchanges of nuclear missiles led to the negotiation of a number of international agreements aimed at reducing the risk of a repetition of this blood-curdling crisis in which disaster was avoided by a whisker. The nuclear NPT was one of these. By this time two more states had joined the ranks of those who possessed nuclear weapons, France in 1961 and the People's Republic of China in 1964, both doing so without any declarations, prior permissions, or global agreement; they did so in pursuit of their own national and political self-interests, under President de Gaulle and Chairman Mao, thus setting a precedent. *They did so well before the Treaty was presented for signature, so they were not (and rejected being) bound by its later aims*.

The Treaty bargain (see Appendix 2 for the full text) recognized straightforwardly that there were five nuclear weapons states at the time of signature, and its prime aim was to devise a way forward that would limit the total number of weapons states to those who already had them. It did this by enjoining on the weapons states not to pass on the technology of nuclear weapons to any nonweapons states (Article I), and by rewarding the self-denial of the nonweapons states (Article II) with promises of *equal access* for all "states parties" to the development of civilian nuclear power and other civilian technologies (Article IV).

These included what now seems bizarre: any civil spinoff from "peaceful nuclear explosions" (Article V). (In the 1960s, there were both in the Soviet Union and in the United States enthusiastic supporters of using specially designed nuclear explosions to simplify mega civil works projects such as the diversion of the Yenesei River

[3] Easily found on the IAEA's website: www.iaea.org.

or the excavation of a second Panama Canal! Fortunately, wiser heads prevailed on both sides of the Iron Curtain before anything was done to implement these projects!)

Nonweapons states were enjoined to negotiate with the IAEA a full-scope safeguards agreement, together with specific "facilities attachment agreements" covering all their nuclear installations within 180 days of joining the Treaty (Article III). Some did, but many did not, or at least not for a number of years. The number of inspections under "full-scope safeguards" is supposedly proportionate to the amount of civilian-use nuclear material, and their frequency depends in part on the ease with which the material could theoretically be diverted from civilian to military use and the length of time that this would take.

Further, the weapons states committed themselves to begin negotiations in good faith to end the nuclear arms race at an early date, and to work toward *complete* nuclear disarmament (Article VI). The insertion of Article VI was not entirely cynical. The Cuban Crisis of 1962 had brought home, even to the superpowers, that their rivalry could lead to universal nuclear annihilation if not carefully regulated. The aspiration toward nuclear disarmament remained little more than an aspiration for the first 20 years of the Treaty's life. As a result, this key part of the bargain has not yet been fulfilled, which has lent support to accusations that the Treaty remains discriminatory and inequitable.

In essence, the case for reform can be summed up as follows:

> *Non-proliferation is a set of bargains whose fairness must be self-evident if the majority of countries is to support their enforcement. The only way to achieve this is to enforce compliance universally, not selectively, including the obligations the nuclear states have taken on themselves.*

Nonnuclear weapons states such as Australia, Argentina, Brazil, Canada, and South Africa do not want to get shut out of an enrichment market that will grow if nuclear energy enjoys a renaissance. Other states resent being denied access to additional nuclear technologies when they feel that they have not benefited from nuclear cooperation as it is, and the nuclear weapons states have not delivered on the original disarmament bargain.[4]

The IAEA was formally given the responsibility of policing the Treaty. This resulted in a significant extension of its international safeguards system.

The Treaty originally was limited to 25 years duration, with provision for five yearly reviews, and consideration after 25 years of possible further extension. These provisions reflected the uncertainty among its sponsors when it was introduced. The very notion of international inspection of installations, which went close to the heart of what individual countries would regard as their most important security interests, was in the circumstances of the time (late 1960s) an amazing innovation. A number of countries held back from joining for a variety of reasons: they still had ambitions to become nuclear weapons states (Argentina, Brazil, South Africa), they wanted to

[4] Carnegie Foundation's 2007 scorecard.

retain the freedom to help their allies or clients (France, China[5]), they disliked the discriminatory nature of the Treaty (India), they did not want to fall in with the dictates of the superpowers (France), or because of regional political rivalries (Pakistan).

Some 185 countries have now signed up, the only exceptions being India, Pakistan, Israel, who have never joined, and North Korea (the DPRK), who withdrew from the Treaty in 2003. South Africa and Libya gave up their weapons programs for different reasons: South Africa as it underwent internal political changes, and Libya because the exposure of its involvement in A.Q. Khan's network made it realize that compliance with its NPT obligations was a more advantageous policy than proliferation.

17.1.4 Effects of the treaty

The NPT is an interstate treaty aimed at creating trust between states, and therefore, hopefully, at diminishing the desire of states to possess nuclear weapons. The International Safeguards System, administered by the IAEA, was designed in the first place to demonstrate that member states were doing what they declared they were doing, and thus to provide reassurance to other states. It was up to the states themselves to ensure that their employees were carrying out their instructions.

From some points of view, the NPT has been the most successful arms control treaty ever. Certainly at the time of its inception, it was generally believed that by the end of the 20th century, there would be 30−35 nuclear weapons states. In practice, there are still less than 10, with only 8 clearly acknowledged nuclear-armed states. Pakistan and India broke cover in May 1998 and carried out a series of underground tests. Israel is widely assumed to have weapons capability and has even on occasion admitted it, but has never carried out an observed weapons test. North Korea claimed that it carried out a nuclear test in October 2006 and a further test on a larger scale in April 2009. It has been suggested that although North Korea has been openly threatened by the US, it did not fear them, as it had already defeated them in battle in the Korean War, and China has, until recently, shown reluctance to bully or enrage a neighboring Communist state, which was its ally in that same war.

Shortly before it handed over power to the African National Congress, the apartheid regime in South Africa confessed to having developed nuclear weapons but announced that it had decided to dismantle them. It surrendered its accumulated stockpile of fissionable material to the depository powers of the Treaty, allowed the IAEA to inspect its installations and their dismantlement in 1991, and joined the Treaty as a nonweapons state. The buildings and facilities stand as empty shells and monuments.

To put all this history another way, in the past 50 years, a universalistic system of control of fissionable material has been established under the detailed supervision of the IAEA in Vienna. The NPT is its key document. The system has worked to the

[5] At the opening for signature of the NPT China had still not replaced Taiwan as a member of the United Nations and the Security Council.

extent that the weapons states established by 1965 still dominate the division of the world into weapons and nonweapons states. This is what the system was designed to achieve, but it is fraying at the edges. It has NOT worked, for example, when disclosure was not complete and undisclosed facilities have concealed weapons work. Further, two important states have demonstrably mastered the production of nuclear weapons, two others have probably done so, and several more have flirted with it and have only been prevented by strong-arm tactics, which have little to do with the formal system and much to do with the projection of the military power of the United States. Despite four quinquennial review conferences of the Treaty since India and Pakistan drove a coach and horses through the formal system in 1998, the governments of the acknowledged weapons states, for 10 years, made no move to amend the Treaty, or even to engage in serious multilateral discussion of what might be done. (The British Foreign Office, however, issued a discussion paper on February 4, 2009, in preparation for the 2010 Review Conference.[6])

One reason for this inaction is that the IAEA/NPT system, which some say has served reasonably well for the past 50 years, is a product of the wider political shape of the world.

It is worth stressing at this point that the strategic aims of the superpowers were little affected by the NPT. Until the late 1980s, the development of nuclear weapons by both the United States and the Soviet Union paid no attention to the aims of Article VI of the Treaty, but reflected the evolving strategies of both sides in their respective bids for supremacy. Even though they were sponsors of the Treaty, the pieties of Article VI in no way hindered their arms race. The virtue of the Treaty as perceived in Moscow and in Washington was that it was a device, in practice quite an effective device, through which they were able to repress the complications that the entry of numerous other powers into the nuclear contest could have caused.

The Treaty was never perfect even as a system of superpower control, but has been used as a rationale for "regime change," meaning invasions related to stopping "WMDs" and the imposition of "economic sanctions."

China had been disappointed in the late 1950s in its expectations of nuclear assistance from Moscow. By the time, it acquired its own nuclear weapons in 1964. It was already engaged in a bitter ideological struggle with the Soviet Union. India, smarting from its defeat in the Himalayan confrontation with China in 1962 and from lack of Soviet support, clearly decided to bolster nonalignment and self-reliance with its own nuclear arsenal. The proliferation path opened: even though Pakistan was in theory covered by the US nuclear shield, nonaligned India was much nearer and militarily much more powerful than Pakistan, a fact demonstrated forcibly by its support for the transformation of East Pakistan into independent Bangladesh; Pakistan sought assistance from China in order to match Indian developments. In South America, the rivalry of Argentina and Brazil for leadership prevented them for many years from accepting the protection of the IAEA's nonproliferation regime before finally signing

[6] "Lifting the nuclear shadow: creating the conditions for abolishing nuclear weapons" an FCO Information Paper.

a mutual pact of inspection and cessation. Israel had to develop a deterrent, having been invaded in 1948, and having fought bloody wars in 1967 and 1973 against Egypt in Sinai and Syria in the Golan Heights.

The world today is more fragmented, threatened, and volatile than for 50 years, despite the peace, and the balance of global and political power is shifting to those who control regional energy resources, away from those who control weapons. The new emergence of the government control of global oil supply by the "Seven Stars" (Russia, Iran, Saudi Arabia, Venezuela, the United Arab Emirates, China, and Brazil) has changed the balance of global influence, where the producer states now own and control the world's major natural resources of oil and gas in place of yesterday's "Seven Sisters" of the US and other global oil corporations (Mobil, Exxon, BP, Chevron, Shell, etc.). The reemergence of the US as an oil (and gas) exporter has also lead to quasiinstability in traditional energy pricing in the never-ending struggle for global market share, economic growth, international political power, and national and business revenue.

Paradoxically, in uranium resources, where many of the major resources are in local ownership in Canada, Kazakhstan, and Australia, we see an opposite trend, with the weapons states' fuel cycle companies seeking to expand their positions in resource control because they either never had, or now do not have, large domestic uranium resources. The globalization of the nuclear fuel market will inevitably complicate proliferation control.

17.1.5 Shortcomings of the treaty

Its successes are clearly impressive, but all is not well with the system. The first Gulf War of 1991 revealed that the assumption that members of the NPTC would play by the rules (as it was so clearly in their interests to do so) was unduly complacent. Iraq had previously, for a number of years, been attempting to develop a nuclear weapon in defiance of the objectives of the Treaty of which Iraq was a founder member, even though the threat was greater than the reality.

The IAEA came in for much criticism from the US for its failure to detect, still less to prevent, this gross breach of its rules. In its defense, it would say that those rules were not sufficiently stringent, as disclosure was voluntary. But more stringent rules would have been unacceptable to the member states in the mid-1960s when the Treaty and its rules were negotiated. Furthermore, there was an unspoken but nevertheless real bargain at the Agency that the superpowers would keep their own clients in order and not interfere with the activities of the clients of the other.

Iraq was not the only player who hoped to avoid detection in clandestine disregard of their NPT obligations. Libya, Iran, and North Korea were all engaged in undeclared attempts to develop enrichment technology, weapons materials, and missile delivery systems. NB[7]: *Israel was not and is not a member of the Treaty. While the role of Israel is a sensitive issue for the US and Europe who supported its founding as a*

[7] NB is the standard abbreviation for "Note Bene," the Latin for "note well."

nation-state, the final report of the WMD Commission deals with Israel dispassionately and comprehensively.[8]

A safeguards system is only as good as the member states' ability, not to say willingness, to police it. This is exemplified in Iran's moves to develop a civilian nuclear power program as its right, and the NPT and others countries desire to ensure there is not a clandestine weapons development effort at the same time. The NPT-based idea is to place limits on the level of U^{235} fuel enrichment (20% or less to avoid an efficient bomb), reduce the amounts produced by centrifuges and reactors (to be less than that required for easily making a bomb), and the avoidance of U^{238}-fueled plutonium production reactors (to minimize a Pu^{239} threat). But the Agreement is limited in its scope, inspection regime, and timescale, reflecting the low level of trust between the parties.

Even when the NPT was not as universal as it now is, informal meetings of possible supplier states played a significant role in supporting the safeguards system. There were two main groupings: the so-called Zangger Committee (named after its first chairman) and the Nuclear Suppliers Group (NSG), who developed voluminous lists of so-called "sensitive" materials to be interdicted and/or not delivered without agreement or license. This was foreign policy hard at work, trying to be effective. Discussion of "diversion" tends to be in terms of diversion of fissionable material, but the development of viable military nuclear facilities also depends on the acquisition of the appropriate technologies. Many of the technologies that are useable in weapons production, of course, have other, civilian uses. Drawing up codes of conduct that took account of these complications and sought to deny would-be proliferators the means to do so, was (and is) a complex and frustrating business in which a state's national export interests are often in conflict with its NPT obligations. Lists include various types of steel or zirconium tubing, uranium ore, explosives, and propellants, and even certain radioisotopes (while uranium ore itself is not subject to safeguards, countries that export it are expected to report their exports to the IAEA). All too often, the export interests of specialized manufacturers prevailed over the wishes of bureaucrats in government ministries. Meetings of the Zangger Committee and the NSG endeavored to square this circle. Whatever modest success they may have had to begin with, it was in practice undermined by the advent of globalization of international trade in the 1980s and 1990s, as has been very clearly shown in the IISS's chilling account of the successes of A.Q. Khan's network.[9] Here, and apparently with the connivance or at least the acquiescence of his government, the leading weapons designer from Pakistan sold, smuggled, and supplied design details, materials, and drawings, getting rich in the process.

A reassuring aspect of this, from one point of view, is the fact that the customers of A.Q. Khan's designs and materials continued to be would-be proliferating states: Libya, North Korea, or Iran. No one has as yet uncovered any conclusive signs that

[8] Weapons of Mass Destruction Commission, final report, "Weapons of Terror: Freeing the World of Nuclear, Biological, and Chemical Arms," Stockholm, Sweden, June 1, 2006.

[9] "Nuclear Black Markets: Pakistan, A.Q. Khan and the rise of proliferation networks," an IISS strategic dossier, 2007.

individuals, whether oligarchs or tribal chieftains, have developed coherent plans to be the possessors of nuclear weapons, but the design details are out of the genie's bottle too.

17.1.6 Attempts to improve the treaty system

A key discovery in 1991 was that Iraq had cynically been cheating for at least a decade and probably longer. This revelation gave a much needed impetus to the search for improvements in the system, and although the IAEA was attacked for its earlier complacency, there seemed, in practice, little alternative to strengthening its rules and to encouraging it to be much more proactive in pursuit of breaches of those rules. An "Additional Protocol" was negotiated, which authorized the Agency to take the initiative in bringing to international attention any breaches or apparent breaches in the system and increased its powers of intervention. Twenty years later, this Protocol is far from being ratified universally[10]: China ratified in 2002, while Euratom and its member states all ratified on April 30, 2004. The United States finally ratified the Protocol and brought it into force on January 6, 2009. Iran signed it in December 2003, but following its dispute with the Agency over its enrichment program, has not brought it into force.

But the remaining issue is that the NPT is, in a key respect, de facto discredited. From the start, India openly defied the pressure to join, developed and tested weapons, possessing and developing enrichment technology and plutonium producing facilities (some diverted from peaceful research purposes after being supplied by the US and Canada). A cynic would argue that because of its recent economic performance, global role, and trade growth, it is now "forgiven" in the sense that new agreements are being written to allow the export of nuclear reactors and fuel to India to supply its industries and grid. The side agreements are not yet finalized but aim to separate the weapons and civilian uses and facilities, but the truth is that India has won by ignoring everyone and the NPT. The example or model has been set: go your own way, ignore the NPT, become successful, be a key global commercial player, and be forgiven. The reason is simple: the NPTC members can make money by selling nuclear reactors, natural uranium, and enriched fuel to India, so the Club's commercial interests prevail, while at the same time, the Club is pretending to control Indian access to nuclear materials. The cobbled-up agreement is therefore a sham. The Indians argue that they were forced to proliferate by the challenges and threats they were subjected to by China and Pakistan (this argument is not quite consistent with the normal Indian position that they are, in principle, opposed to the discriminatory nature of the Treaty. Nor is it entirely propaganda. A careful reading of the Indian program shows them stalling development for a long time until the threats from China and Pakistan tipped the balance, with the US refusing to back or protect them against these two, while at the same time funding the Pakistan program. (Moreover, Pakistan is, strictly speaking, not a weapons state, as defined by Article I of the Treaty, as it is not a member of the Treaty!)

[10] The IAEA's latest status report listing those states who have signed or ratified the Additional Protocol can be found on its website at www.iaea.org/OurWork/SV/Safeguards/sg_protocol.html.

This is the nub of the problem: we have "declared" and "undeclared" weapons states and different "rights" claimed as a result.

We also have the Christian Bomb (US, France, and UK), the Communist Bomb (Russia, North Korea, and China), the Jewish Bomb (Israel), and the Hindi Bomb (India). It is not surprising that there has been persistent pressure for a Muslim Bomb.

This "cynical" view is not new or even eccentric. Throughout its history, there has been a persistent conventional consensus that the NPT has failed, that it is on the verge of failure, or that an inevitable cascade of proliferation following the diffusion of technical know-how will cause it to fail. But the real world has presented very little evidence in support of this consensus. For example, the rate of proliferation peaked in the 1960s, before the entry into force of the Treaty, and then declined over the next 30 years. The percentage of countries that acquired nuclear weapons is only about 25% of those who could have because they considered, inherited, or acquired a nuclear option, but decided in the end to remain nonweapons states. Fewer countries are today seeking nuclear status than at any point since the end of WWII. The international safeguards system is not perfect, but it has achieved much since it was first introduced. It evolves in a positive direction with ever-increasing support.[11]

Meanwhile, global stability and nongovernmental threats exist in the form of Islamist pressure spearheaded by the Taliban in the North-West Frontier Province and numerous groups elsewhere (notably ISIS/ISIL, Al Qaeda, etc.).

17.2 Nuclear history and basic science

So far, we have concentrated on the political issues presented by the division (in Articles I and II of the NPT) of the world into states that have and those that do not have nuclear weapons, and hence enrichment capacity for nuclear fuel production and sales. It is worth setting out why this is not simply a matter of political choice.

The so-called "critical mass" for a bomb is reached when the chain reaction of fissions is so self-sustaining that it becomes explosive from producing so much energy from fission so quickly as to vaporize the materials. Nuclear reactors are not designed to explode, and although they contain enough material for criticality (a self-perpetuating chain reaction), the rate of increase in neutron number (and hence, power) is controlled by poison rods that absorb neutrons, and by overpower trips and shutdown devices. The "reactivity margin" for the fuel has design limits on the core configuration and the enrichment.

While the Second World War was underway, making the atom bomb first was a target for both the Allies and the Axis powers. It was perceived as a matter of survival. A huge effort was therefore put into the Manhattan Project, launched in March 1942

[11] For a sophisticated account of the effects on policy of NPT membership see "Learning from Past Success: the NPT and the future of Non-proliferation": Jim Walsh, for the Weapons of Mass Destruction Commission, 2005. See also Etel Solingen: "Nuclear Logics."

by the US and its allies, which demonstrates a key facet of the problem. The atom bomb came first; civil nuclear power came later. All subsequent efforts to develop nuclear weapons have done so through dedicated weapons programs, quite separate from attempts to achieve electricity generation (see below).

Anyone seeking to produce nuclear weapons today has to follow one or both of the Manhattan routes, and the technologies have of course been refined and improved. Gas centrifuge-based separation of the uranium isotopes is a far more efficient technique than the electromagnetic induction and gaseous diffusion-based separation used in the Manhattan Project. To manufacture reliable centrifuges is not easy. They have to be engineered to the precise tolerances necessary, require spinning at very high speed, use special tube materials, and are connected in what are called cascades of many thousands of centrifuges. This is the technology of choice today, and three more plants are now being built (in Europe, the US, and Japan) to produce nuclear fuel.

These details are fundamental. They have a major bearing on the nature of the threat of nuclear proliferation and on the measures taken to prevent it. An efficient (ie, small) uranium bomb has, in practice, to contain around 93% U^{235}. Likewise, the plutonium weapons in the arsenals of the weapons states are over 90% Pu^{239}. The cleverest weapons designers employed at Los Alamos claim (controversially) that it is possible to create a weapon of some sort from any isotopic composition of plutonium and an inefficient bomb from uranium above around 20% enrichment. As they also admit, this would certainly be inferior to using virtually pure Pu^{239}, and advance calculation of its effects would be much more difficult; the weapons states have, in practice, stuck to the latter.

To manufacture weapons-grade material in sufficient quantities for an "efficient" (read, high explosive) yield is a major industrial operation. It requires the level of technical attainment and the resources of a nation-state. In the face of modern satellite observational technologies, it is not so easy to hide the fabrication plants, though underground siting is obviously preferred and is known to occur.

It was not entirely a coincidence that the first five weapons states were the five permanent members of the Security Council!!!

17.2.1 Commercial nuclear power

The proliferation problem arises from the fact that power reactors, research reactors, and nuclear weapons programs make use of the same applications of nuclear fission, and require the same skills, but in very different degrees, as well as to very different ends. The problem is becoming more acute, as after 30 years of hesitation and stagnation, the civil nuclear power industry is on the threshold of a worldwide revival, with many "new" countries examining adopting nuclear energy (eg, UAE, Jordan, Egypt, Malaysia, Saudi Arabia, Chile, Turkey, South Africa) and others expanding (eg, China, Russia, India), while some even contract (eg, Germany, France, Japan, and UK). This prospect has understandably fueled renewed concerns about an increased danger of nuclear proliferation. However, we shall show below that proliferation does not arise from commercial power plants.

In contrast to the very high levels of uranium enrichment required by weapons programs, power reactors use either natural (unenriched) uranium as the basis of their fuel, or relatively low levels of enrichment, up to about 4%. Similarly with plutonium, the isolation of pure Pu^{239} required for successful weapons design is not a priority for plutonium use in breeder reactors or for its recycling as Mixed OXide fuel (MOX) for use in current thermal reactors. The resultant fuels are not bomb material and cannot be used directly for weapons production. However, the processes that are essential for the enrichment of uranium or for the separation of plutonium from irradiated fuel are essentially the same in both civil and military applications.

The main differences lie in the length of time the processes continue: enrichment to weapons grade takes much longer; in contrast, the extraction of pure Pu^{239} has to take place very soon after irradiation with neutrons begins. In both cases, "criticality" issues have to be taken into account; in other words, precautions have to be taken to avoid the accumulation in a single vessel of a sufficient quantity of the fissile material that would permit a chain reaction (and therefore a burst of neutron discharge or even a spontaneous explosion) to occur.

In the 50 odd years of nuclear power generation since the opening of Calder Hall in 1956, *there has not been a single instance among the NPT's member states of diversion of nuclear material from the power sector* to potential military ends. The main reason is obvious. Light water reactors (LWRs) are some 80% of those in operation, and are designed only to be fueled when they are offline, ie, not generating electricity, and have been mainly located in countries with weapons stocks and enrichment technology (eg, US, Russia, India, France, and China) or have disavowed its use (eg, Japan and Canada).

The cases which have given rise to so much anxiety in recent years—Iraq, Libya, North Korea, and now Syria and Iran—are all countries, **which originally do not have nuclear power in operation**, though Iraq and Iran have both set out down the road of building civil nuclear power station systems. In practice, all of them had and have research reactors in nuclear research establishments, which have been subject to safeguards. It has been an objective in all these cases to present a compliant front, and only when the façade could no longer be maintained, has a public international row developed about those countries' observance (or lack of it) of their safeguards obligations.

India and Pakistan are awkward exceptions to this on the whole favorable narrative. But neither is a member of the NPT, and both have maintained consistent opposition to it from the outset on the true grounds that it is *discriminatory*. India has recently signed onto nuclear cooperation agreements covering their civilian program, and this is directly related to the fuel cycle. Without indigenous uranium supplies, they must relay on imported fuel (and also LWRs) until their own thorium cycle is established. Both India and Pakistan made use of installations that were originally presented as civilian power stations to develop nuclear weapons. India has, however (as explained above), now negotiated an accommodation with the international system in order to overcome bottlenecks caused by its isolation, and Pakistan, under US pressure, has abandoned the proliferating practices of Dr. A.Q. Khan, primarily for political reasons, which have little to do with nuclear policy.

17.2.2 Present situation and issues on research and sustainability

The Indian and Pakistani tests in May 1998 created a great formal problem for the nonproliferation regime. Paradoxically, they cannot now join the NPT unless they abandon their weapons, of which there is no sign, either as weapons states or as nonweapons states. It remains to be seen whether the deal that India has struck with the NSG led by the United States will cause the NPT bargain of 1968 to unravel. After all, the integration of India, a nuclear-armed state, into the system in this way reduces the value of the benefits supposed to be received (under Articles II–IV of the Treaty) by the nonnuclear weapons states (NNWS) as a result of their abandonment of the weapons option. The alleged development of "WMDs," meaning primarily nuclear weapons, was one of the principal overt excuses for the invasion of Iraq in the spring of 2003. Others have also been accused (by the United States) of harboring such designs: Libya, North Korea, most recently Syria, and above all, Iran. It is notable that none of these had a working power reactor until the Russians completed one reactor at Bushehr in Iran and brought it online, just 37 years after the Deposed Shah gave the project the go-ahead. The new US/EU/UN/Iran Joint Agreement leaves Russia poised to supply and complete more units sometime after 2015, and may even have been approved with different terms by Iran, who, like North Korea, also persists in pursuing "peaceful" rocket launch development.

But there are some obvious points of weakness and even danger in the system.

17.2.2.1 Research for advanced reactors

Research reactors have been mentioned several times already as sources of weakness and known proliferation in the system, and of course are used to develop Generation IV and AR concepts, materials, and fuels. They are, of course, included in a member state's full-scope safeguards declaration to the IAEA, and therefore subject to inspection. How frequently depends on the nature of the material they contain. Unlike power reactors, which are large-scale well-protected industrial installations, research reactors are usually situated in academic institutions as one part of their scientific installations. They are much softer (easier) targets for theft of nuclear materials than power stations. Security is often lax, and if, for example (as it often is), the research reactor is an open pool reactor, physical protection is minimal compared with a massive pressurized power reactor. In the early days of the atomic age, the enrichment of the research reactor fuel was high, comparable with bomb material. In the past 20 years, however, the United States, backed by Russia and Britain, has campaigned with some success for the modification of these research reactors so that they use uranium enriched to less than 20%. However, there are still about 120 fueled with so-called "weapons grade" HEU, as the US pursued a policy of repatriating as much fuel as possible by paying for it and its replacement.

But it is clear that in a world where we may expect more, not fewer, research reactors, and medical isotopes, and fuel production, a new attitude is needed.

Nuclear reactor development and deployment entails expansion also of the fuel cycle; after all, that is the driver and enables energy security and independence without greenhouse gas emissions. World nuclear use will grow as energy demand, economic needs, environment issues, and supply security concerns grow. So the race is on to secure nuclear fuel supplies, particularly uranium for short term, hence large price increases (good news, up to a point, for those with resources).

17.2.2.2 Commercial fuel supply

There is a major unspoken issue: supplies of uranium ore at reasonable economic prices are finite. This tends to be denied by uranium suppliers, who, just like the oil and gas producers, rightly assert that there is no shortage of supply today for the present, but omit to mention the price it will cost and what will happen if demand grows by a factor of 10, as it could. Drivers for increased demand are increasing need for energy security and price changes in competitor fuels, coupled with climate change needs and concerns. With over 400 reactors operating today, the present world demand is ~70,000 tU/a. A tenfold increase would give an upper-bound estimate of demand for 4000 reactors needing ~700,000 tU/a by 2050. The present 400 reactors could be kept going for another 150 years, but that would leave a shortfall of over 3000 reactors (or some three-fourths of the postulated need) in the near foreseeable future.

Today's estimates of identified reserves are about 5 MtU, recoverable at a cost of <$130/kg. Even allowing a doubling or tripling of this estimate to, say, 10 MtU, just 1000 reactors operating for 60 years will consume all the world's cheapest uranium (in about 60,000 reactor operating years) with present fuel cycles technology. So, as uranium producers say, there is no present shortage, but there is a long-term point of danger.

There is an unofficial "Nuclear Fuel Cycle Club" (US, France, Japan, Russia, EU, UK) who currently possess enrichment technology (and most of them nuclear weapons too). Under the banner of "nonproliferation," these same present uranium enrichment technology owners would restrict others' access to enrichment technology (see the most recent agreement between the United States and Abu Dhabi[12]). After first using all of today's cheap(er) uranium, these same nations (Japan, US, France, and Russia) openly say they would deploy plutonium-fueled, hopefully self-sustaining, "fast" reactors, whose design, technology, and commercial exploitation they would also control. Those countries, such as those in the Club with large fuel reserves, favor "regional fuel centers" which carve out the world, and which de facto they wish to control.

17.2.2.3 Alternate fuel cycles for advanced reactors

Those without large uranium reserves favor alternate thorium cycles (India, China, Turkey). Moves to restrict acquisition of enrichment and recycling technology have recently included efforts by the US to define "fuel cycle nations" and form the Global

[12] Signed January 17, 2009.

Nuclear Energy Partnership (US DOE, 2007). So attempts to form energy policy, to influence global and national alliances, and simple economic and commercial pragmatism are now all intertwined with the NPT.

Unfortunately, not only are the present efforts and aims misdirected, there is a major issue of unintended consequences. The past inconsistent and selective use of the nonproliferation banner to further foreign policy and security aims has both been ineffective, and given the admirable aim of nonproliferation of nuclear arms, a bad reputation as a cloak for cynical political interference in other nations' internal affairs.

There are some other main points of danger.

The possibility that hitherto nonnuclear countries may soon acquire nuclear power stations is a neuralgic issue for the Greens. However, the further construction of power stations is not the real issue. The US government may have pressurized Siemens not to proceed with the construction of the power station at Bushehr after the fall of the Shah in 1979, but now all the major players, with the encouragement of their governments, are seeking to gain contracts for the construction of power reactors round the globe. As the controversies over Iran (and to a lesser extent, North Korea) and the proposed agreements decisively show, the real proliferation fear is the fuel cycle.

Firstly, it is more difficult to police than power stations and more difficult to separate in the public mind, as the processes for fuel production and for bomb material have elements in common. Secondly, as the history of Dr. A.Q. Khan's network shows, would-be proliferators have so far aimed at procuring their essential materials and equipment afresh. In other words, they have attempted to exploit the weaknesses of the export control regimes of potential supplier states rather than to steal existing machinery and material.

The two most obvious points in the fuel cycle at which proliferation could take place are enrichment of uranium and reprocessing of spent fuel. To do either on an industrial as opposed to laboratory scale requires huge and expensive establishments. The earliest such establishments grew out of the needs of the weapons programs of the weapons states, but when the civil power programs of the developed world required greater supplies of enriched uranium fuel, expansion programs got underway. The United States has persistently argued that such production facilities should be in the hands of existing weapons states, and has over the years fought a rearguard battle against the establishment of enrichment facilities in other countries such as Brazil and Japan. Iran is just the latest example.

17.2.2.4 Enrichment

Enrichment is just one, albeit the most sensitive, stage in the transformation of the refined ore (ie, yellowcake for uranium) into fresh fuel. The enriched uranium oxide has to be fabricated into fuel to fit the reactor design for which it has been ordered. In many discussions of the problem of proliferation control, the fact that nuclear fuel is like a bespoke suit tends to be overlooked. The fuel fabricator has to take account of the precise degree of enrichment specified by the reactor operator and to set the fuel in assemblies that will deliver the most efficient neutron flux for the reactor

management's needs. One should not, of course, exaggerate the difficulties that this causes, but it is a weakness of calls (such as Senator Nunn's and others) for international fuel banks that they ignore it. Commercial interests of course dominate; the fuel cycle is where money can be made. So Russia offers an "international" fuel bank, using, of course, Russian fuel.

It is clear that providing "black box" or "sealed" enrichment technology will be possible, provided the supplier retains all the technology rights and the plant is inspectable. This does not seem to be the preferred approach of the present centrifuge owners, who wish to maintain their monopoly for commercial reasons and to own and operate their own plants and not to license the technology. This approach can actually encourage proliferation. If a nation wishes to achieve energy independence and policy freedom, then they *cannot* allow other nations to control their energy supply. And use this as a political lever. The client–customer basis has to take into account the marketplace realities, not just the political–commercial interests and overtones. If not, the nation will decide to "do it themselves," whatever the cost (as the Iran, India, Pakistan, North Korea, and other cases demonstrate).

17.2.2.5 Reprocessing and recycling

An alternative fuel cycle is to reprocess irradiated fuel with the aim of separating the plutonium-239 or thorium-233 it has created from the rest of the material. Again, this is a technique that has been in use since the beginning of the nuclear age, and one embarrassing consequence of this was the creation of large stockpiles of separated plutonium. The present practice of combining plutonium oxide with uranium oxide to make MOX is a relatively recent development. In a period of cheap and plentiful uranium, there has been little or no economic incentive to use MOX, as it is more expensive. Even with much more expensive raw uranium, there is still little incentive, as handling MOX in a reactor is more complicated than straightforward fuel made of freshly enriched uranium.

If a "nuclear renaissance" does take place, these proliferation points of anxiety in the fuel cycle will increase. Countries outside the present limits of the nuclear power world will enter it, perhaps at a much slower rate than current hype suggests. But the struggle of the Iranians to realize an ambition that goes back to the Shah in the 1970s will have its imitators in many other countries in the developing world. The issues are not simply technical. They are also political and commercial. It is clear that on a technical level, an entrant county is not well placed to develop all stages of the fuel cycle at the same time. Nor is there any commercial incentive to do so. Autarky is a very expensive policy, even when it seems to be the only answer to political pressures. Iran might do well to take note of recent statements by USEC, the world's largest enrichment company with the widest customer base, complaining of the difficulties of financing the centrifuge enrichment plant it is currently building, and its reported difficulties in obtaining Department of Energy financial support!

It is given, as mentioned above, that within each state, the state has the duty of making sure that none of its citizens is breaking the law and indulging in proliferating activity or actions that can be construed as likely to support proliferation. For the first

few decades of the Treaty's existence, this was a reasonable assumption, but the world has changed. Terrorists bring a new aspect to the whole story.

Terrorists are not the subjects of the NPT. They are not "states parties," but renegades who do not follow the "rules," the niceties or words of a Treaty. They represent a threat to what is called "physical protection" aspects of nonproliferation, the "guns, guards, and gates" mentality of the military, security, and sanity. This aspect is dealt with by spending vast sums on clearances, background checks, identity tags, detection equipment, controls, procedures, scanners, and such, of the type so familiar in airports. But terrorists are really interested in attacking and dislocating high-profile and payoff "soft" targets, not defended ones. The aim is, as in the military war, the supplies, infrastructure, communication, and soft underbelly of the opponent. Nuclear systems and sites are already "hardened," resistant to terrorists, unless a real whole-scale nation-to-nation war breaks out.

The mechanisms of the Treaty are not well adapted to limiting the opportunities of opposition or terrorist groupings. By definition, the first line of defense against them must be the member state whose installations are targets for the postulated subversive activity.

17.2.2.6 Future policy implications of nuclear fuel cycles

Major anomalies exist at present, being two declared nuclear-armed states not listed in Article I: India and Pakistan. Israel keeps its own counsel generally, but is universally regarded as a nuclear-armed state, and the fact that it provokes tension throughout the Middle East. Iran is widely suspected of pursuing nuclear weapons under cover of developing civil nuclear power, and North Korea pursues a strange weaving path, which has included several underground nuclear test explosions, the first of which was probably a failure.

The Treaty has no real means of dealing with any of these anomalies. It makes the benign assumption that its member states will obey its rules; there are no provisions for punishment if they do not do so or if any of them decide to leave the Treaty. Such sanctions have to be sought elsewhere, for example, at the UN Security Council or through the determination of one or another of the superpowers, in practice, the United States.

US policy toward India, North Korea, and Iran has been violently inconsistent, as it is not governed by any obvious principle apart from expediency and a desire to maintain US supremacy by whatever deal seems locally appropriate. The latest deal with India is a good example of the pragmatism of United States policy. The nuclear isolation of India following the 1974 nuclear test had outlasted its usefulness. After the 1998 tests, some means had to be found of bringing India into the international nonproliferation system. The deal that has been struck separates the civil from the military sector in a way not dissimilar to what prevails in the acknowledged weapons states; it also provides the United States (and other keen nuclear exporters, such as France) with an entrée into the rapidly expanding Indian civil nuclear construction scene. While there is a now significant constraint that did not previously exist on India's freedom of action, the cause of much political difficulty in India, the benefit to India is access to the international fuel market and to the international construction market

denied her for over 30 years. As isolated India's nuclear progress was much hampered by shortages of indigenous uranium and other bottlenecks, the price seemed worth paying. In 2005, the Indian government tacitly recognized the great disadvantages of this isolation by seeking an agreement, first with the United States, and then with other prominent members of the NSG, which would put an end to it.

As to North Korea, two whole nuclear reactors now lie in storerooms in South Korea, the US having abandoned building of them in North Korea by US contractors as failed "compensation" for giving up on their weapons program.

Taking the long view, it is possible to argue that in some respects, the pragmatism of US policy has been more successful in restraining the rebels than adherence to the orthodoxies of the international nonproliferation system.

US policy toward Iran has been the exact opposite of its policy toward North Korea: initially refusing to build the sort of reactors that have been promised to the North Koreans as compensation for dropping their ambitions to have a nuclear weapon. This inconsistency may have contributed to Iranian intransigence. It also gave the Russians more than one unexpected export opportunity. Iran's intransigence has been intensified by the US use of sanctions (just as Saddam Hussein's defiance was in the 1990s), and has not been eased by the EU's attempt to mediate. Whereas North Korea was a comparatively isolated problem, Iran is embroiled in the Middle East crisis generally: the Arab–Israeli dispute and the continuing travail in Iraq and Afghanistan. More important than any of these, Iran is an oil-rich nation, which is much less subject to economic pressure than the comparatively poverty stricken North Koreans.

Israel cannot be ignored altogether, although many discussions do just that. But whether or not Israel has the nuclear weapons usually accredited to her, she is unlikely to be a proliferator. She acquired the necessary materials and skills for her weapons program well before the NPT became the cynosure of arms control treaties that it is today. Her existence as a presumed weapons state is a serious lump of grit in an otherwise smooth system. It causes not only oceans of rhetoric, but also misplaced ambitions by other Middle Eastern states to match this presumed status, and is thus a weakness in the NPT system. Whether it is a direct threat to it is less clear.

17.3 A look at the future

This previous review of the present situation explains how we got to where we are, and points out areas of difficulty and weakness, even danger, in the present situation. But apart from the current usual global crises, there are at least three explosive issues which will challenge the comfortable assumptions of the supporters of the NPT and affect the deployment of advanced and Generation IV reactors on a global scale.

These are, firstly, the increasing recognition of the value of civil nuclear power as a possible means, perhaps the only effective possible means, of replacing hydrocarbons as our prime energy source if we are to make inroads into combating the threat of global warming. For this to work, the deployment of nuclear energy has not only to

be at least 10 times its present deployment. It has also to penetrate the world outside the OECD countries on the same massive scale.

If the threat of global warming seems too far off to warrant such a spectacular shift, secondly, security of energy supply has at last been recognized as a major desideratum. Those countries with indigenous energy resources have an economic advantage over those without, but the majority of the world's population resides in areas of relative energy poverty. They must rely on imported supplies of coal, oil, gas, and nuclear fuel for now, but obviously will be looking at alternate fuel cycles and recycling as necessary means of supporting economic, national, and political survival.

Thirdly, two-thirds of the projected rise in energy demand over the next 50 years will be in this developing world and its huge populations. Faced with declining oil and gas supplies, developing countries will not wish to be excluded from the possibility of acquiring large-scale installations of nuclear energy, as one can see from the rash of announced plans to build nuclear reactors in many countries that so far have never had them. Even oil-rich countries such as Abu Dhabi and Iran are in the forefront of such schemes.

To satisfy this demand in the medium and long term, is impossible if the world remains restricted to the once-through cycle.

A transition through Generation IV designs to a wholesale adoption of breeder reactors is thus inevitable.

17.3.1 Alternate fuel cycles

For those without access to large uranium reserves, or needing energy supply surety, a new alternate cycle (AC) is needed that will ensure sustainable supply and smaller waste streams. There should be a more intrinsically proliferation-resistant cycle, with no significant plutonium generation, thus not requiring all of today's policing and international stress. It also must not require introducing a new reactor technology, and acknowledge the ownership and deployment of uranium enrichment technology as a proliferation concern while still allowing vastly expanded reactor builds.

Such a fuel cycle is available now using thorium, which is more globally plentiful (perhaps three times more) than uranium, and so could meet the medium-term future need. With careful fuel design and recycling, a thorium reactor would give a near breeding cycle and so is more sustainable with much lower (up to 10 times less) waste amounts and storage needs. This thorium switch would enable more reactor deployment using today's reactor technologies and help stabilize fuel cost and supply, and avoids having to introduce many fast reactors.

Such an AC path is already being explored (eg, notably by India, Norway, China, Canada, and others), with the transition to a near self-sustaining predominantly thorium-fueled cycle being initiated by burning plutonium as the start-up fuel. The cycle thus reduces plutonium inventories/stocks during transition to a primarily thorium near breeder cycle using separated U^{233}.

This transition is real and could totally alter the global fuel cycle and reactor deployment opportunities. In fact, some of India has already chosen to develop this AC route

as a national priority. Such AC concepts are, in fact, not new; what is new is the concept that an alternate sustainable and closable fuel cycle may enable greater benefits to be gained from nuclear energy deployment worldwide.

Because of inherent technical characteristics, D_2O moderation, and distributed channels with flexible fueling, HWRs have a great deal of fuel cycle flexibility, and this has been the subject of significant research and development by AECL and others. The combination of relatively high neutron efficiency (provided by heavy water moderation and careful selection of core materials), online fueling capability, and simple fuel bundle design mean that HWR reactors can use not only natural and enriched uranium, but also a wide variety of other fuels. These include:

1. recycled uranium;
2. thorium-based fuels with U^{233} recycle (see above);
3. minor actinides "intermediate burner";
4. MOX fuels; and
5. recycled LWR fuels.

17.3.2 Advanced reactors and the Nuclear Non-Proliferation Treaty

In the future, beyond, say, 2030, the aim will be to provide highly efficient AR concepts, such as the use of Generation IV systems, which can couple thermal efficiencies of some 50% using a proliferation-resistant thorium cycle with a near breeder cycle. In addition, this advanced concept lends itself to indirect and direct hydrogen production, which can be coupled with a power grid, which then allows a greater usage of wind power. This, in turn, leads to wider deployment of nuclear energy. The development of criteria for assessing the proliferation resistance of AR systems has been proposed (GIF, 2014, 2011).

Against this projection of demand and the likely ways of satisfying it, the worldview of the NPT seems hopelessly restrictive. It is questionable that what made good sense when nuclear technology was confined to a few countries (primarily the weapons states, but also including a raft of allied or client states who were content to let the weapons states take the lead, in most of whom it was still very much a minority supplier of energy) could be extended without modification to a scene in which civil nuclear power is the energy of choice of most countries, because the obvious alternatives (coal, oil, gas) are becoming unavailable, impossibly expensive, or unacceptably polluting. For example, the air in Beijing has become so bad that all industry in the region had to be closed for 2 months so as to purify the air, which the[13] competing athletes were going to breathe during the 2008 Olympic Games!

As mentioned earlier, economic and commercial factors lie behind the unwillingness of the have-powers to spread the rewards of the fuel cycle more thinly. It has been convenient commercially for the weapons states to argue that the possession of

[13] Sharon Sassquoni: Looking Back: the 1978 Nuclear Non-proliferation Act; Arms Control Association, December 2008.

enrichment or reprocessing plants should be confined to the existing weapons states. But the practice has never been pure. Germany and the Netherlands (both NNWS) have enrichment plants tied by the Treaty of Almelo to the United Kingdom (a weapons state). The United States has had to accept that Japan and Brazil should now operate commercial enrichment plants. The US rearguard action to defend its fraying monopoly was undermined originally by its inability to supply what it had contracted to its customers during the first great expansion of nuclear power in the 1970s, and by the great superiority of the URENCO centrifuge technology over their old gaseous diffusion plants at Piketon and Paducah. But commercial centrifuge plants are very expensive—even USEC, still the largest enricher in the world, has run into financing difficulties arising from the huge cost of building its new centrifuge plant—and make little sense in economic terms until a country can provide sufficient customers for their output.

The same is true of reprocessing plants, which are even more rare in a world that is still wedded to the once-through cycle. Originally the aim of reprocessing was to provide plutonium suitable for weapons use (see above). It then became a possible way of reducing the volume of spent fuel, aka, high-level waste. More recently, a number of technologies have been developed to enable reuse of the energy-rich components of spent fuel. The most obvious of these is MOX fuel (described above), which also has the advantage of being a way of reabsorbing the separated plutonium that had already accumulated in some countries. Other processes have been tested in the laboratory, but not yet on a commercial scale, whereby the plutonium is not released on its own but only in conjunction with other fission products. These would make it unusable as a source of weapons material.

Underlying all the above discussion is the assumption that it is not in our interest generally and not in the interests of the civil nuclear supplier companies (see next section), regardless of whatever point of the nuclear fuel cycle they operate, that there should be an increase in the number of weapons states. Ideally, there should be fewer. This was the main motive for introducing the NPT in the first place, and it remains the obvious driving force to continuing with the international safeguards system, improving it where possible. The fact that there has not been any practical use of a nuclear weapon since the Treaty came into force should not make us complacent. It is difficult and invidious to argue that some countries are more "responsible" in nuclear matters than others. The factors which have made the present weapons states "responsible" have little to do with the NPT, though peer group pressure has played a role, as it is clearly in no one's interest that a country should run amok brandishing nuclear weapons.

The civil nuclear industry, which wishes to profit from the so-called nuclear renaissance, and those who would promote the substitution of nuclear power for the declining attractions of the hydrocarbon-based economy have a duty to ensure that the separation of the benefits to civil society of civil nuclear power from the temptations of nuclear arms are maintained. Systems of control are not impossible to devise and are significantly easier to monitor than reductions in CO_2 emissions through

so-called carbon trading, which has become the fashionable nostrum in the face of public fears of global warming. A more certain route to this end is to substitute fission for combustion as the principal form of energy production.

It will be easier to achieve acceptance of this if more progress is made to bring the original bargain of the NPT to fruition. In this regard, the initiative of the British Foreign Secretary in February 2009, a move clearly coordinated with Washington, in launching a campaign to make progress on Article VI before the next review conference of the Treaty in 2010 was commendable. It goes some way toward providing a way to retreat from the less defensible decision of Tony Blair, just before he left office, to launch renewal of Trident, the British submarine-based nuclear deterrent.

17.4 The wider context

In conclusion, it is worth reminding ourselves that nuclear power does not exist in a vacuum. It is one of many ways of generating electricity. Compared with its competitors, it has a number of characteristics, which add up, in the eyes of its supporters, to a compelling advantage over those competitors:

- It is a large-scale base-load generator. After half a century's experience, it is a reliable mature technology.
- The fuel is amazingly energy dense. One kilogram of uranium has the energy equivalent of 17,000 tons of coal. Stockpiling the fuel or the raw material from which it is made is easy and takes up minimum space.
- Uranium ore bodies are mostly in stable countries (Australia, Canada, etc.).
- Transporting yellowcake or fabricated fuel is low-cost, small-scale compared with coal or oil; a year's worth of fuel for Sizewell B barely fills the equivalent of one floor of a double-decker bus.
- Its "carbon footprint" is minuscule compared with most of its competitors, including wind.
- Existing known reserves are sufficient for the next half century's projected use. More will undoubtedly be discovered, as the element is omnipresent in the earth's crust (2−3 parts per million) and existing known ore bodies are the fruit of the last great expansion of nuclear power in the 1970−80s. In practice, they were far more than sufficient to fuel what was actually built, leading to a slump in uranium prices, which lasted until 2002. The recent spike in uranium spot prices has led, as one would expect, to a revival of exploration and the first steps in the development of new mines.
- But even without dramatic new discoveries of ore bodies, the generating technology is poised (and has done the groundwork for) a number of great leaps in the efficiency of fuel exploitation. The first is straightforward recycling of spent fuel in thermal reactors, using MOX or DUPIC. The second is Generation IV designs. The third is a return to the fast breeder, which, in principle, can extract all the latent energy in uranium, 97% of which remains in spent fuel from the once-through cycle used today. These advances in energy efficiency (a great clarion call of the antinuclear Greens) will be comparable to the improvements between James Watt's first steam engine (1% efficient) and modern generating turbines, some 35−40% efficient, even before the introduction of combined heat and power techniques.

So why is it not an open and shut case? Basically public hostility, because of:

1. Fear of nuclear weapons: though one of the aims of this chapter has been to show that these are two separate technologies, which the international nuclear nonproliferation system has been spectacularly successful in keeping apart;
2. Fears about the safety of the technology, especially after Chernobyl. The industry (coming from a very secretive, even hermetic culture) has been very incompetent in rebutting the wilder fears, or in developing reassurance[14]; and
3. In a world of plentiful cheap fuels, nuclear seemed (and was) expensive and inflexible.

But in a world facing an impending energy crisis because of surging demand exceeding supply, and awareness of the ill effects of carbon emissions from hydrocarbon-based fuels, the balance of advantage for nuclear power looks different.

It is therefore vital for the future of nuclear generation as a means both of combating "global warming" and as a part of the answer to the cycles of "peak oil" and "cheap gas" (which should be the subject of another full paper) that the international safeguards system should be maintained and improved. The improved version should command public confidence. Extending it without those improvements, and without solving the problems posed by Iran or North Korea described above, may not command the public support necessary for it to function effectively.

It will also be vital for the preservation of the advanced technological civilization that we all enjoy, and even aspire to, that nuclear power (despite the misgivings of some) does expand into the vacuum left by the forthcoming retreat of oil. The eagerness with which oil-rich states like Iran and Abu Dhabi are striving to establish nuclear power in their territories is not based primarily on a covert desire to become weapons states, though they may flirt with that idea too, but on their need to survive the demise of oil.

As part of the bargain with the NNWS, the weapons states committed themselves in Article VI of the Treaty to work toward divesting themselves of nuclear weapons and toward complete and universal disarmament. As adumbrated earlier, for the first 20 years of the Treaty, this was little more than a pious ambition. The Treaty reflected the reality of superpower relationships and was not itself the motive force behind their development. Both the superpowers piled up colossal quantities of nuclear weapons in what was eventually admitted to be a futile attempt to intimidate each other.

With the change of regime in Washington, this has been recognized there. One of President Obama's first foreign policy initiatives was to call on the Russian government to revisit the START agreements and take them further, suggesting that neither superpower required more than 1000 warheads, a reduction to about a third of what they at present deploy, and that it should be a priority task to come to an agreement of the modalities of making such a reduction.

The minor weapons states (Britain, France, and China) have shunned the limelight and have usually said little about their levels of nuclear armaments, but these are measured in hundreds rather than thousands.

[14] The two totemic disasters of Chernobyl and Three Mile Island were the result of incompetent practice in two experienced nuclear countries; to spread the technology to new countries inevitably gives rise to nervousness. But consider the record of South Korea over the last 40 years.

Discussion of the politics of the weapons states tends to concentrate on the United States and, to some degree, on Russia. China maintains a very low profile, often siding with the Russians, eg, over discussion of possible sanctions against Iran, provoked by Security Council discussion to state a position. The British and French keep very quiet about their own nuclear armaments, but both, especially the British, tend to echo US positions on avoidance of proliferation. The position of all three is influenced by extraneous factors and their perception of their own fundamental national interests: the Chinese have strong oil import links with Iran; the French were certainly influenced by the contracts they had established with Saddam's regime in Iraq in opposing US/UK plans for invading Iraq in the spring of 2003. There is nothing surprising in this; the NPT was created, after all, as a means of codifying the national interests of the nuclear powers that supported it.

The NPT remains the main instrument for achieving a framework that would and should allow peaceful deployment of ARs, but as we have noted, the Treaty has some major shortcomings that need to be remedied if it is to remain useful and effective in the longer term.

Finally, the dangers of global warming and climate change have done much to change the public perception of nuclear power and the use of plutonium and other fuel cycles. The civil nuclear industry believes, with good reason, that it has much to offer by way of mitigation of climate change. If it is to take its rightful place as one of the principal means of our reducing manmade greenhouse gas emissions, it will be vital to reinforce the message to the public that the spread of civil nuclear power to regions that, up to now, have not had it, and the deployment in the medium term of large numbers of breeder reactors can be done without increasing the dangers of nuclear weapons proliferation. The civil nuclear industry knows that a necessary condition for carrying the public with it is the continued existence of a respected and effective international safeguards regime.

Any great expansion in nuclear power stations will lead inexorably to the implementation of advanced fuel cycles, including thorium and the breeder economy. The IAEA supported by the industry will have to devise systems of safeguarding that give similar security in that context as they have achieved for the once-through cycle. It will be obliged to do so because of global warming and peak oil because no one will wish either to lead to nuclear war. To achieve this, the Agency will need vastly more resources and trained personnel. Strengthening the IAEA would also reduce the tendency of powerful players to use their weight to bully mavericks or to exert illegitimate commercial pressure.

17.5 Fuel cycles: sustainable recycling of used fuel compared to retrievable storage

17.5.1 Introduction: the cost of not burying the past

Using fuel just once, irradiating for a few years in a thermal reactor to, say, 30−50,000 MWD/t, leaves about 99% of the fertile material (U^{238}) unused, and

some equivalent 30% or more of the original fissile material (U^{235}) still available. So it is widely known that reuse of the fuel to extract more energy and reduce waste makes technical sense. The fuel goes in at a few percent of U^{235} and comes out as "spent" while still containing about 0.3% Pu^{239}, and is still capable of making more energy but is presently labeled as "waste." This fissile material and the U^{238} fertile component could make more energy if converted (= upgraded) by breeding in a different reactor. There are many potential fuel cycles using different fissile fuels as their starting point and reprocessing and final radioactive waste storage (see Fig. 17.1).

However, in both the US and Canada, there is no recycling of used fuel allowed by political edict, which is not the case in, say, India, Russia, and France. This ban is a legacy again of Cold War thinking and public antipathy to the use of nuclear energy.

Instead, once used fuel is stored and allowed to cool (decay) on site at operating LWRs and HWRs, with the intent it be sent to an ultimate (underground) storage facility. After over 20 years of study and debate, that was the purpose of the ill-fated Yucca Mountain site, where about $10 billion has been spent to date without completing the facility due to deliberate political dallying and delay. In Canada, the idea is to use "retrievable storage," presuming some use might be found for the fuel in the future.

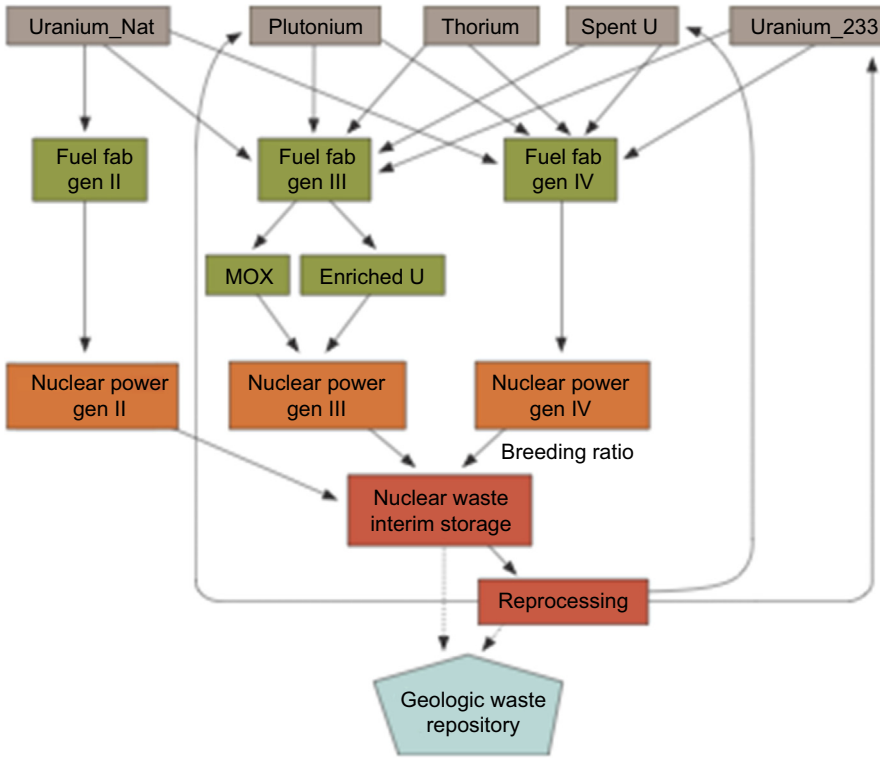


Figure 17.1 The various global nuclear fuel cycles (Edmonds et al., 2007).

The rationale for not recycling used fuel is largely a socio-technological one. Perhaps it is too deadly or toxic to be kept in "interim storage," and requires expensive facilities for millennia to avoid leaking into ground water. If recycling is "allowed," some plutonium or other fissile material might be diverted for some evil purpose (eg, for atomic or radioactive bombs). Today, once-used fuel in the US is stored on-site in flask or as in the Zwileg facility in Switzerland. Indeed, the NRC 1310-page Generic Environmental Impact Statement for continued and generally unplanned on-site storage found the environmental impacts for almost everything to be "small" (ie, negligible risk), while assuming some long-term repository is available in about 60 years (NRC, 2014). It has been reported that as of January 11, 2013, following yet another special Commission report (Blue Ribbon Commission on America's Nuclear Future, 2012), that the Obama administration will ask Congress to approve a plan by building a pilot interim storage facility for nuclear storage by 2021 and a larger facility by 2025 "based on consent" of the host state.

The DOE reportedly has said: "the administration has now decided to pursue the siting and licensing of two interim storage facilities by 2025. The first initially would focus on accepting used nuclear fuel from reactor sites that have been shut down. The second site, to be available by 2025, would accept enough fuel to reduce expected government liabilities." Another goal is to "make demonstrable progress," meaning the legal costs and fines incurred by not accepting fuel as had been promised, including "the siting of permanent repository sites that could start accepting waste by 2048."

This idea is similar in scope and timing to the ongoing activity by the Nuclear Waste Management Organization (NWMO) in Canada that has been focused on achieving consensus, and social acceptance and funding volunteer sites (NWMO, 2005). In that report, Table 8.1, the cost of an "Adaptive Phased Management" (APM) approach to a geologic facility is about $20 billion over 350 years to be largely funded by the electric utilities (ie, by the customers via a surcharge).[15] To ensure funding surety, "waste" fuel owners are required to deposit $550 million immediately, and then $110 million a year into a trust, depending on how much once-used fuel they have or expect. This is in addition to the some $8.5 billion that was already set aside in guarantees. There are no incentives in the NWMO report, or in their official mandate, for the NWMO to reduce the amounts of fuel stored, the timescales, or the expected costs.

Apparently, US nuclear utilities pay about $750 million into the Nuclear Waste Fund every year, plus several $100 million on dry storage casks and their secure storage on-site. For 60 years, as in the NRC scenario, this would be about $45 billion collected from customers via a surcharge, plus any other interim storage costs.

Now, future ARs would be expected to have a more sophisticated energy and resource efficient fuel cycle, and satisfy some sustainability argument. This concept

[15] Accounting techniques can estimate the "net present value" by assuming the funds are all invested upfront in some hypothetical fund; this technique is used to lower the apparent cost of future expenditures, but does not reduce the real dollar amounts of money actually spent, both now and in the future.

of fuel reuse is often called "closing the fuel cycle" and involves treatment, separation, and new fuels. Indeed, the NRC defines this possibility as follows:

> ***Fuel reprocessing (recycling)****: The processing of reactor fuel to separate the unused fissionable material from waste material. Reprocessing extracts isotopes from spent fuel so they can be used again as reactor fuel.*

Generally, present fuel cycle policy in states with ample uranium and plutonium resources (eg, UK, US, and Canada) favors long-term geologic storage of once-used fuel, with or without retrievable options, independent of the cost and recycling technology. In fact, reuse of CANDU fuel is only possible at present in China.

Many options, studies, and tests have already been performed for existing reactor designs (IAEA-TECDOC-1122, 1999). There appears to be no "in principle" technical problems for recycling, particularly as additional irradiation reduces the long-lived actinides and radio-toxicity, and hence can reduce storage times needed before decaying to safe or background levels.

Paradoxically and ironically, recycling has already occurred by "disposing" of excess weapons material, eg, Pu^{239} of and Th^{233} originally produced by military "production" reactors for use in now retired nuclear bombs. The US has down-blended and used material from Russia as fuel for commercial reactors, and the UK is looking at some similar approaches to reduce its plutonium "inventory."

Since used fuel is radioactive and contains fission products, it must be placed in heavy containers and shielding, well sealed against leakage, and any potential underground dissolution and migration into groundwater minimized. This APM is based on the concept of being able to retrieve the fuel at some unspecified point in the future if desired, for whatever reason. But all the costing and planning is based on essentially indefinite (or "passive APM") safe storage below ground in a deep geologic repository (DGR) consisting of underground tunnels, canisters, vaults, and removable sealing. The timescales for storage are truly glacial, being envisaged as up to millions of years until the radiation decays to its premined or background levels, so the DGR would have assured storage and disposal facilities for many thousands, if not millions, of years.

The siting process for the DGR/APM facility has itself been glacial and is taking many years due to lengthy dialog and legalistic processes designed to be consensual, consultative, normative, sociologically acceptable, and fully transparent. After much such consultation with "stakeholders," the NWMO has unsurprisingly selected DGR/APM as the "preferred" technical and social option. Costing for such a DGR using APM has been estimated by the NWMO at about \$12−24 billion in present worth moneys, for storing all the four to eight million once-used fuel bundles produced to date. This DGR cost then represents an average upper limit storage and disposal cost per bundle of about \$20,000,000,000/4,000,000 ∼ \$5000/bundle. Since each bundle weighs about 20 kgHM, this represents a cost of the "waste" disposal of ∼\$250/kgHM, which is even somewhat higher than so-called "natural" or nonenriched uranium, presently sells for as fuel in the open market (a range depending on demand and speculation of, say, about \$60 to 130/kgHM).

This immediately raises an interesting question: why not resell, recycle, or reuse this asset? This idea has not escaped the notice of the public, the media, or the technical community who have variously stated in debate, comment, and input sessions:

> *There is no such thing as nuclear waste…it gives us the chance to follow France's lead in developing complete reprocessing for nuclear material.*
>
> *Tucker (2009)*

17.5.2 Economic and social aspects of recycling

Instead of burying used nuclear fuel, for ARs, one can consider the sustainable option of actively recycling and reusing as being socially, economically, environmentally, and technically more attractive and sensible. Reusing this fuel would help provide an assured future energy supply, reduce storage times by factors of thousands, provide value by turning what is presently designated as "waste" into "energy," and reduce ultimate storage liabilities, including the social and political costs. The goal is, in fact, "zero waste," thus avoiding the embarrassment and social stigma if not being reused.

Such "advanced fuel cycles" have been examined in detail already (eg, see Fig. 17.2).

Extensive analyses have also been made of the economics of recycling, albeit commissioned on behalf of a fuel manufacturer (The Boston Consulting Group, 2006), which concludes:

"In addition, recycling, as part of a portfolio strategy, presents a number of benefits:

- Eliminates the need for additional repository capacity, beyond the initial 83,800 ton capacity at Yucca Mountain, until 2070.
- Contributes to early reduction of used fuel inventories at reactor sites – in particular, removing newer, hotter fuel for recycling within three years of discharge and eliminating the need for additional investments in interim storage capacity.
- Relies on existing technology – with appropriate modifications – and can provide an operational transition to future technology developments such as Advanced Fuel Cycles and fast reactors.
- Shows cash flow requirements that could fit until 2030 within the current financing resources available for the once-through strategy, or even until 2050+ if acceptance of used fuel at Yucca Mountain begins only after the first years of operation of the recycling plant.
- Offers a tool for nuclear power sector to protect against potential rises in uranium prices, by providing MOX and recycled UOX (uranium oxide) fuel 5, whose production cost is independent of uranium prices and enrichment costs."

Since the NWMO and US Yucca Mountain process started and this "spent" fuel was first formed, much has happened in our increased awareness of the earth's finite and precious resources and in our enhanced understanding the fragile global ecosystem and the sensitive role of climate change, plus real recognition of the burgeoning needs for energy in China, India, and other countries that are home for most of the human race and now of its factories and production lines, and even new reactor concepts. These trends and realizations place new pressures and obligations on the custodians of one of the world's major energy resources, to respond and position globally to the needs for a sustainable future, whereby the classic definition, present practices do not endanger or restrict the options of future generations.

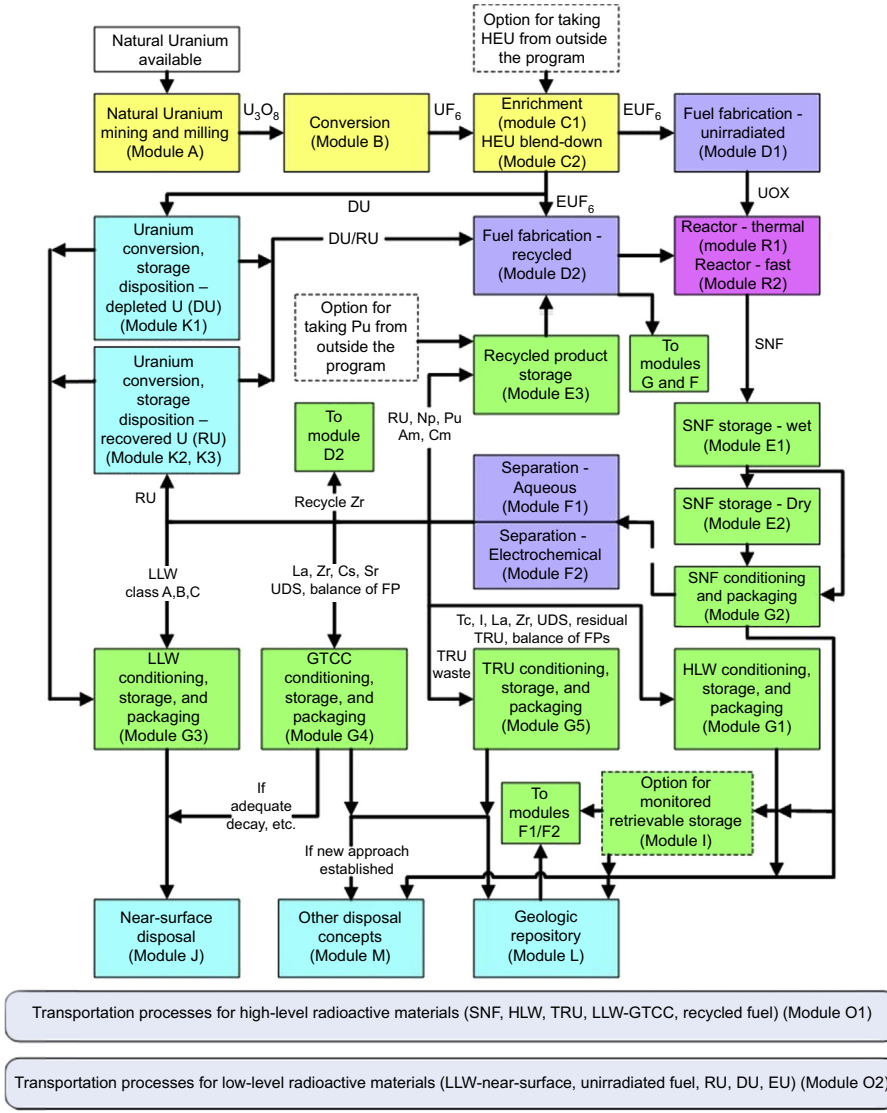


Figure 17.2 Example of advanced uranium fuel cycle (Shropshire et al., 2008).

In fact, it is well known that modern processing and fuel cycle technology allows for a sustainable, and perhaps even a perpetually renewable, future energy scenario using nuclear energy. Future ARs will breed and recycle fuel. Therefore, "waste" streams will be drastically reduced, separation and "burning" of long-lived actinides will occur, and repositories will only be needed just for less than a thousand, not for the unnecessary million years (US DOE, 2007, 2006).

In today's modern world, inaction is unacceptable both technically and morally.

17.5.3 The cost savings of the future

A review of LWR reprocessing costs has been given (Rothwell, 2009), which established an estimate reprocessing cost range for a facility of between $500 and $4000/kgHM.

There is indeed a price for recycling, just like the blue box we use today for disposing and reusing household goods. But does "waste to energy" have to be cheaper than whatever we use or do today? Or does it just need to be cheaper than the alternates like DGR/APM?

There was and is no recycling of anything in the original once-through cycle (OTC), as this meant separations and enrichment of plutonium and other isotopes (see the above sections on nonproliferation implications). The OTC was born in the days after WWII when nuclear energy was in its infancy, and the concept of finite energy resources seemed irrelevant when compared to the impacts of atomic energy, oil cartels, and hydrogen bombs. However, this attitude was and is not true for those countries without large uranium reserves, notably France, Japan, Russia, India, China, and Korea, where a longer-term view is taken, since "raw" fuel ores must be bought abroad. For these uranium resource-poor countries, recycling and breeding are seen as the ultimate answer to sustainable nuclear energy supply using thorium-, plutonium-, and enrichment-based cycles while also endowing the countries with energy independence.

The OTC is not sustainable, a fact not overlooked by nuclear energy opponents, and is actually a relic of the past decisions and norms. The global uranium resources of about 5 MMt U^{235} were regarded as large, at least compared to oil and gas, and the world did not envisage thousands of reactors with a global energy demand 5 to 10 times that of today. There has always been enough uranium to supply today's several hundred units, and the uranium suppliers, like oil producers, always assure the markets that there is no shortage and ample present supply. A quick calculation shows that with over 400 reactors operating today, present world uranium (U^{235}) demand is $\sim$70,000 ton per annum U^{235}, or low enough for another 100−150 years or so based on present so-called recoverable reserves.

But we can provide an upper-bound estimate of the demand for 4000 reactors needing $\sim$700,000 ton per annum U^{235} by 2050. Today's estimates of identified reserves are about 5 MMtU U^{235} at a cost of <$130/kg (Duffey, 2008). Even allowing a doubling or tripling of this resource estimate to, say, 10 MMtU of U^{235}, just 1000 reactors operating for 60 years, which is their stated life, will use all the world's cheapest uranium (or by about 60,000 reactor operating years) with present, mainly OTC, technology.

Another way to state it is that although the present 400 reactors could be kept going for another 150 years, this leaves a shortfall of about 3000 reactors (or some three-fourths of the need) in the near or not too distant future. Some 1000 reactors are easily envisaged by 2040 or so (ie, after the era of "cheap gas"), not coincidentally just using up the cheapest uranium. This is not a cause for alarm; there is plenty of uranium, and more uranium reserves will be found but, of course, at steadily

higher prices (cf. oil, gas, and other commodity markets). Aggressively adopting recycling and increased fuel utilization might even allow up to 1500 reactors, but at increased cost of those processes and facilities, which are all known and/or existing technology.

This consideration of uranium cost leads to an analysis of the price natural uranium fuel would have to be at to make recycling attractive pricewise. The answer is a price that is two to three times today's, or about \$240−360/kgHM, almost exactly the same range (at least within the accuracy of these estimates) as the present cost of the DGR/APM storage at about \$300/kgHM.

So the order of magnitude of the costs is clear and supports recycling as being about equal to the cost of using a DGR for disposal if the future includes about 10 times more reactors. But there are also some other technical advantages and economic business opportunities for mining nations and the fuel (waste) owners, as well as massive social benefits.

17.5.4 Waste to energy: burning the benefits

It would seem a no-brainer: recycling is good. But there are other considerations, like owners' liabilities, obligations, and choices; waste disposal funds of many billions already exist. As a simple worked example, consider that used fuel from CANDU reactors, which is being produced at the rate of about 100,000 bundles per year, or about 2000 MMT HM/year, of which 0.3% is useful fissile material (Pu^{239} and related isotopes) that can be separated and used again. This means CANDUs are producing about:

$$1000{,}000 \text{ bundles} \times 20 \text{ kg/bundle} \times 0.3\% = 6000 \text{ kg Pu/year} = 6 \text{ Mt Pu/year}$$

From a proliferation and security perspective, it would be preferable to destroy or use this plutonium, rather than entomb it, presuming no access ("intrusion") or use is allowed or possible for a historic timescale of a million or so years. Interestingly, LWR spent fuel is at about 0.9% fissile, which is why France can and does recycle today, and why this used recycled fuel could also be recycled again directly again in CANDU (in the so-called DUPIC cycle).

Assuming this once-used fuel can be safely processed (see below), the 6 Mt Pu/year would be processed into ~5% enriched plutonium−thorium fuel to kick start the Pu^{239}−Th^{232}−U^{233} cycle, which can be reused as fuel and burnt to about 40,000 MW(t) d/t using present fuel technology.

The U^{233} so produced would then be separated and reused in an endless chain, replacing the plutonium as the starter fuel. Assuming just 35% for the nominal thermal to electricity conversion efficiency, which is a low present design estimate as future reactor designs intend to reach 50%, then the electricity produced from just this recycled fuel is:

$$6 \text{ Mt/year at } 40 \text{ MWd/kg at } 35\% = 40{,}320{,}000{,}000 \text{ kWh/year} = 40 \text{ TkWh/year}$$

or about the equivalent of the full electrical output from six or more small reactors. At the assumed equilibrium use rate of 6 Mt/year, the lower life estimate of the existing Pu^{239} resource in Canadian used fuel alone is:

$$20 \text{ kg/bundle} \times 4 \text{ million bundles} \times 0.3\%/6 \text{ Mt/year} = 2400/6 = 40 \text{ years}$$

This timescale is fully sufficient to start, transition to, and implement a full $Pu-Th^{232}-U^{233}$ fuel cycle facility not just in Canada, but globally with India and China, who both possess ample thorium reserves, including fuel manufacturing, plutonium destruction, and actinide separations.

The key is also a global transition to a parallel full thorium-based fuel cycle, as envisaged by India and China based on their small uranium but large nuclear energy and thorium resources. A full near breeding thorium fuel cycle is envisaged in an optimized reactor concept, with the thorium cost being at about current market spot price of ~$120/kg, or again not coincidentally about the natural uranium price.

Also key is the actinide separation as a technology step. By separating out from the "residual" waste streams, the long-lived transuranics or actinides, namely americium and curium, removes over 90% of the DGR waste heat load and radioactivity but only <0.1% of the used fuel mass. Removal and "burning" these actinides in thermal reactors is then feasible, since the actinide destruction is about 90% or more. This is also desirable as it allows for lower decay heats and smaller timescales of about 1000 years for the DGR. These timeframes are at least comparable to human experience with large structures and geologic knowledge (cf. the pyramids, Greco–Roman buildings, and natural caverns).

So the benefits are indeed burnt. Moreover, there is a positive income stream, assuming that the electricity produced is sold in or to the open market at ~5c/kWh using existing reactors or even new special purpose ones. The income is then of order:

$$40 \text{ TWh/year} \times \$0.05/\text{kWh} = \$2 \text{ B/year}$$

For a 40-year reactor life, this is about $80 billion income. This income must offset and pay for the cost of processing and fuel manufacture, which over the same 40 years is ~$10–20 billion for the fuel and reprocessing plants and 6 Mt/year × range of ($500–4000/kgHM) = $3 million to $24 million/year, or an upper limit of about $1 billion, plus any other operating costs (say about $200 million/year) to give a total lifetime expense of about $30 billion.

Such a waste-to-energy facility has a return on equity of about three times, and the lower estimate of the business benefit-to-cost ratio is then of order 1.5, assuming a 10% IR. This estimate is made without counting any of the "softer" societal benefits, increased jobs, future investment, spinoffs, sustainability returns, carbon credits, and global market share, etc., that any such business case would have to be made.

This type of "storage cost recycling versus benefit" analysis can be generalized for any in-principle fuel cycle. But the fact that the costs (outlays) and the benefits (returns) are even remotely similar is amazing and clearly represents a business and market opportunity in addition to the purely social job and technology advantages.

17.5.4 Overcoming the ostrich syndrome

If it cannot be seen, perhaps we can pretend that it does not exist. So it is with once-used nuclear fuel, originally seen by antinuclear activists as the Achilles heel of nuclear energy; if used fuel cannot be stored, then it is not a closable or viable system, but remains an open running sore. Sociology reigned, and desperate for a solution, the response was to bury it, "out of sight, out of mind," and to undertake endless study and consultation with stakeholders and the "public." The problem then was to find a socially and politically acceptable, even low-profile approach, with the soluble technology considerations of mining, geology, tectonics, and chemical effects, not the insoluble not in my backyard (NIMBY) ones. This has led to the Yucca Mountain fiasco, where after spending perhaps $10 billion or so and after 20 years of study, politics and sociology have finally said that NIMBY prevails and the used fuel cannot be buried after all. The only option is to literally "burn" it as a useful resource.

Appendix 1: Euratom

Around the same time as the foundation of the IAEA, the original six member states of the European Coal and Steel Community negotiated the establishment of two further Communities, the European Common Market and the European Atomic Energy Community (Euratom), enshrined in the Treaty of Rome. At this time, none of the six had nuclear weapons, nor indeed had developed civilian nuclear power. The Euratom Treaty reflects the issues that were paramount at the time (which included French and others' fears of a revived Germany), and among its objectives, as with the IAEA, was **to make certain that civil nuclear materials are not diverted to other (particularly military) purposes**.

The Treaty introduced an extremely comprehensive and strict system of safeguards to ensure that civil nuclear materials were not diverted from the civil use declared by the member states. The EU has exclusive powers in this domain, which it exercises through a team of 300 inspectors who enforce the Euratom safeguards throughout the EU.

These Euratom safeguards are now applied in conjunction with those of the IAEA under tripartite agreements concluded between the member states, the community, and the IAEA, and even though they are to some degree more stringent, are best regarded as a subclass of the Agency's international safeguards (this regional arrangement has, of course, been extended with the expansion of the European Communities' original six members over the past 50 years into the 27 current members of the Union).

Appendix 2: The 1997 IAEA additional protocol at a glance

In the 1980s, Iraq, an NPT state party, had successfully circumvented IAEA safeguards by exploiting the Agency's original system of confining its inspection and

monitoring activities to facilities or materials explicitly declared by each state in its safeguards agreement with the agency. To close the "undeclared facilities" loophole, the IAEA initiated a safeguards improvement plan known as "Program 93+2." The plan's name reflected the fact that it was drafted in 1993 with the intention of being implemented in 2 years.

Putting "Program 93+2" into effect, however, took more time than expected, and the program has, in practice, been implemented in two parts. The IAEA, within its existing authority, initiated the first part in January 1996. This first step added new monitoring measures, such as environmental sampling, no-notice inspections at key measurement points within declared facilities, and remote monitoring and analysis. The second part of "Program 93+2" required a formal expansion of the agency's legal mandate in the form of an additional protocol to be adopted by each NPT member to supplement its existing IAEA safeguards agreement. The IAEA adopted a Model Additional Protocol on May 15, 1997, which it encouraged its members to follow.

The additional protocol

Its essence was to reshape the IAEA's safeguards regime from a quantitative system focused on accounting for known quantities of materials and monitoring declared activities to a qualitative system aimed at gathering a comprehensive picture of a state's nuclear and nuclear-related activities, including all nuclear-related imports and exports. The Additional Protocol also substantially expands the IAEA's ability to check for clandestine nuclear facilities by providing the agency with authority to visit any facility, declared or not, to investigate questions about or inconsistencies in a state's nuclear declarations. NPT states parties are not required to adopt an additional protocol, although the IAEA is urging all to do so.

The model protocol outlined four key changes that must be incorporated into each NPT state-party's additional protocol.

First, the amount and type of information that states will have to provide to the IAEA is greatly expanded. In addition to the former requirement for data about nuclear fuel and fuel cycle activities, states will now have to provide an "expanded declaration" on a broad array of nuclear-related activities, such as "nuclear fuel cycle-related research and development activities—not involving nuclear materials" and "the location, operational status and the estimated annual production" of uranium mines and thorium concentration plants. (Thorium can be processed to produce fissile material, the key ingredient for nuclear weapons.) All trade in items on the NSG trigger list will have to be reported to the IAEA as well.

Second, the number and types of facilities that the IAEA will be able to inspect and monitor is substantially increased beyond the previous level. In order to resolve questions about the information a state has provided on its nuclear activities, the new inspection regime provides the IAEA with "complementary," or preapproved, access to "any location specified by the Agency," as well as all of the facilities specified in the "expanded declaration." By negotiating an additional protocol, states will, in effect, guarantee the IAEA access on short notice to all of their

declared and, if necessary, undeclared facilities in order "to assure the absence of undeclared nuclear material and activities."

Third, the agency's ability to conduct short notice inspections is augmented by streamlining the visa process for inspectors, who are guaranteed to receive within 1 month's notice "appropriate multiple entry/exit" visas that are valid for at least a year.

Fourth, the Additional Protocol provides for the IAEA's right to use environmental sampling during inspections at both declared and undeclared sites. It further permits the use of environmental sampling over a wide area rather than being confined to specific facilities.

Acronym

NPT	Non-Proliferation Treaty

References

Blue Ribbon Commission on America's Nuclear Future, January 2012. Report to the Secretary of Energy. NRC accession No. ML120970375DOE, Washington, DC, USA, 180 pages.

Duffey, R.B., 2008. Future fuel cycles: a global perspective. In: Proceedings of the 16th International Conference on Nuclear Engineering (ICONE-16), May 11−15, Orlando, FL, USA.

Edmonds, J.A., Wise, M.A., Dooley, J.J., Kim, S.H., Smith, S.J., Runci, P.J., Clarke, L.E., Malone, E.L., Stokes, G.M., 2007. Global Energy Technology Strategy: Addressing Climate Change Phase 2 Findings. Pacific Northwest National Laboratory, Joint Global Change Research Institute, College Park, MD, USA (Chapter 6) "Nuclear Energy", p. 75.

Glasstone, S., Sesonske, A., 1994. Nuclear Reactor Engineering. Reactor Systems Engineering, fourth ed., vol. 2. Chapman & Hall, New York, NY, USA. 867 pages.

Generation IV International Forum (GIF), 2011. Evaluation Methodology for Proliferation Resistance and Physical Protection of Generation IV Energy Systems. Proliferation Resistance and Physical Protection Working Group. Report GIF/PRPPWG/2011/003 Rev. 6, and IAEA CN_220 289.

Generation IV International Forum (GIF), 2014. Annual Report, Section 4.2, pp. 105−106. Accessed at: www.gen-4.org/gif/upload/docs/application/pdf/gif_2014_annual_report_final.pdf.

Cacuci, D.G. (Ed.), 2010. Handbook of Nuclear Engineering, vol. 5. Springer, New York, NY, USA.

Hewitt, G.F., Collier, J.G., 2000. Introduction to Nuclear Power, second ed. Taylor & Francis, New York, NY, USA. 304 pages.

IAEA-TECDOC-1122, November 1999. Fuel Cycle Options for LWRS and HWRs. IAEA, Vienna.

Joint Comprehensive Plan of Action (JCPOA), 2015. Vienna, 14 July, Full text, www.state.gov/documents/245317.pdf, 18 pages plus Annexes 1−5 (see also: www.whitehouse.gov/sites/default/files/docs/jcpoa_what_you_need_to_know.pdf (accessed January 2016), and the Iran commentary at www.beibert.com of October 2015).

Kelly, J.E., 2014. Generation IV international forum: a decade of progress through international cooperation. Progress in Nuclear Energy 77, 240−246.

Lamarsh, J.R., Baratta, A.J., 2001. Introduction to Nuclear Engineering, third ed. Prentice Hall, Upper Saddle River, NJ, USA. 783 pages.

Murray, R.L., Holbert, K.E., 2015. Nuclear Energy, seventh ed. Elsevier, Waltham, MA, USA. 550 pages.

NRC, September, 2014. Generic Environmental Impact Statement for Continued Storage of Spent Nuclear Fuel: Final Report, vol. 1 (NUREG-2157). Washington, DC, USA, 687 pages.

Krivit, S.B., Lehr, J.H., Kingery, T.B. (Eds.), 2011. Nuclear Energy Encyclopedia: Science, Technology, and Applications. J. Wiley & Sons, Hoboken, NJ, USA, 595 pages.

Kok, K.D. (Ed.), 2009. Nuclear Engineering Handbook. CRC Press, Boca Raton, FL, USA, 768 pages.

Nuclear Waste Management Organization (NWMO), November 2005. Choosing a Way Forward, Final Study. Toronto, ON, Canada, 454 pages.

Rothwell, G., 2009. Forecasting light water reactor fuel reprocessing costs. In: Proceedings of the Global Conference, Paris, France, September 6−11, 2009, Paper No. 9228, pp. 2959−2964.

Shropshire, D.E., Williams, K.A., Boore, W.B., et al., March 2008. Advanced Fuel Cycle Cost Basis. INL/EXT-07-12107, 613 pages.

The Boston Consulting Group, July 2006. Economic Assessment of Used Nuclear Fuel Management in the United States. Report, Boston MA, USA, 96 pages.

The Future of Nuclear Power, 2003. An Interdisciplinary MIT Study. Massachusetts Institute of Technology (MIT), Cambridge, MA, USA, ISBN 0-615-12420-8, 26 pages.

Tucker, W., March 13, 2009. There is no such thing as nuclear waste. Wall Street Journal.

U.S. Department of Energy (DOE), January 2007. Global Nuclear Energy Partnership Strategic Plan. Office of Nuclear Energy, Office of Fuel Cycle Management. GNEP-167312, Rev 0.

U.S. Department of Energy (DOE), January 2006. Advanced Fuel Cycle Initiative (AFCI). Office of Nuclear Energy, Science and Technology, U.S. Department of Energy, 2 pages.

Thermal aspects of conventional and alternative fuels

18

W. Peiman, I.L. Pioro, K. Gabriel, M. Hosseiny
University of Ontario Institute of Technology, Oshawa, Ontario, Canada

18.1 Introduction

The genesis of nuclear power, similar to many advanced technologies that are available to humanity today, is considered to be esteemed in the 19th century. A series of unprecedented scientific discoveries opened a new vista for releasing an enormous amount of energy from the atom. Through these discoveries, nuclear science and nuclear fission were developed. Nuclear fission is a reaction in which the nucleus of a heavy nuclide splits into smaller nuclides, a few new neutrons are created, gamma rays are emitted, and a significant amount of energy is released. Since then, nuclear fission has been used as a basis for production of heat in all the current nuclear reactors. Even though these reactors can be categorized based on their cooling medium, pressure boundary, type of nuclear fuel, or neutron spectrum, they all have one common feature, which is the production of heat via a fission chain reaction in the nuclear fuel.

An important part of every reactor design involves the selection of a nuclear fuel and design of fuel assemblies. As general requirements, a nuclear fuel should have a high melting point, acceptable thermal conductivity, sufficient mechanical stability, good dimensional and irradiation stability, as well as chemical compatibility with the cladding and the coolant. Another important parameter that influences the design and selection of a nuclear fuel is the dominant neutron spectrum of a reactor. In this context, nuclear reactors can be categorized as fast neutron spectrum, epithermal neutron spectrum, and thermal neutron spectrum. This classification is based on the energy group of neutrons that maintain the fission chain reaction. In a fast neutron spectrum reactor, the chain reaction is sustained mainly by fission of fast (eg, high-energy) neutrons, while in an epithermal or thermal reactor, fission of epithermal (intermediate energy) or thermal (low energy) neutrons, respectively, maintain the chain reaction.

The neutron spectrum has an impact on the reactor design, selection of materials for the reactor core, the type of nuclear fuel, and the associated fuel cycle. Unlike fast neutron spectrum reactors, thermal neutron spectrum reactors utilize a moderator such as water, heavy water, or graphite (C) in order to thermalize (reduce the energy of) high-energy neutrons. Coolant is also different in these two types of reactors. Thermal neutron spectrum reactors utilize coolants such as water or CO_2, which are composed of light elements, especially those having high scattering cross sections, compared to liquid metal coolants, such as sodium or lead, which are used in some fast neutron spectrum reactors (Alexander, 1964). However, it should be mentioned

Handbook of Generation IV Nuclear Reactors. http://dx.doi.org/10.1016/B978-0-08-100149-3.00018-5
Copyright © 2016 Elsevier Ltd. All rights reserved.

that gas-cooled fast reactors are also considered (Waltar et al., 2012). The neutron spectrum also affects the isotopic concentration of fissile and fertile nuclides in the fuel. As shown in Table 18.1, fast neutron spectrum reactors require a higher percentage of fissile nuclides compared to thermal neutron spectrum reactors. The majority of the current commercial nuclear reactors have been designed as thermal neutron spectrum reactors. Table 18.1 provides a summary of these reactors based on the data at the end of 2013 (WNA, 2015c).

In a nuclear fuel, the fission chain reaction is maintained by fission of fissile elements, which are capable of sustaining the fission reaction with neutrons of all energy. As such, fissile nuclides are used in the fuel of both thermal neutron spectrum and fast neutron spectrum reactors. The fissile nuclides of importance for nuclear reactors are ^{233}U, ^{235}U, ^{239}Pu, and ^{241}Pu. Among these fissile nuclides, only ^{235}U is a naturally occurring nuclide, while others are produced by neutron capture of other nuclides during operation of a nuclear reactor. For instance, ^{239}Pu is bred by neutron capture of ^{238}U, ^{241}Pu is bred by neutron capture of ^{240}Pu, and ^{233}U is bred by neutron capture of ^{232}Th. Hence, the current nuclear reactors rely on ^{235}U as the primary fissile element. In terms of the fuel composition, the nuclear fuel of the most nuclear reactors consists primarily of ^{238}U, which is a fissionable element that undergoes fission only with high-energy neutrons, with a smaller fraction of ^{235}U. As shown in Table 18.1, fast neutron spectrum reactors require a higher percentage of fissile elements than thermal neutron spectrum reactors as the probability of fission reaction of fissile elements, such as ^{235}U and ^{239}Pu, with fast neutrons is lower.

Even though the majority of commercial nuclear reactors are thermal neutron spectrum reactors, there has been a continuous scientific effort for design and operation of fast neutron spectrum reactors since the inception of the nuclear technology. First experimental fast neutron spectrum reactors (or fast reactors) such as Clementine, Experimental Breeder Reactor I (EBR-I), the experimental BR-10 reactor, Fast Breeder Test Reactor (FBTR) EBR-I, BR-10, and FBTR reached their first criticality, respectively, in 1946, 1951, 1958, and 1985. Later in the 1970s through the 1990s, first prototype fast reactors, Phenix, PFR, BN-600, and Monju SFR began their operation (Waltar et al., 2012). There is a renewed interest in fast neutron spectrum reactors to be included as part of the overall nuclear fuel cycle because of the advantages that these reactors offer. Since 2000, an international collaboration has focused on the development of six concepts of the Generation IV nuclear reactors. There are several fast neutron spectrum reactors among the selected designs. Table 18.2 provides a summary of the Generation IV nuclear-reactor concepts (WNA, 2015d).

Nuclear reactors can be designed on the basis of their fuel cycle such that they breed more fissile nuclides than what they use. Breeder reactors can utilize uranium, thorium, and plutonium resources more efficiently. There are two types of breeder reactors: (1) fast neutron spectrum breeder; and (2) thermal neutron spectrum breeder reactors, which are designed based on ^{238}U (99.2% natural abundance) and ^{232}Th (100% natural abundance), respectively. Fertile nuclides ^{238}U and ^{232}Th capture neutrons and transform, respectively, to fissile nuclides ^{239}Pu and ^{233}U. Through this process, which is known as breeding, the reactor produces more fissile nuclides than what it consumes. Fast-breeder reactors (FBRs) can also be used in order to transmute the long-lived

Table 18.1 Fuels, coolants/moderators, and neutron spectrums of various types of operating nuclear power reactors

Reactor type	Main countries	Number	GWe[a]	Fuel	^{235}Uranium enrichment, wt%	Coolant/ moderator	Neutron spectrum
Pressurized Water Reactor (PWR)	USA, France, Japan, Russia, China	276	253	UO_2	2.1−3.1[b] 4.5−5.5[c]	Water/water	Thermal
Boiling Water Reactor (BWR)	USA, Japan, Sweden	80	76	UO_2	2.6−3.05[d]	Water/water	Thermal
CANada Deuterium Uranium (CANDU) or Pressurized Heavy Water Reactor (PHWR)	Canada, India	48	24	UO_2	0.71[e]	Heavy water/ heavy water	Thermal
Advance Gas-cooled Reactor (AGR) and Magnox	UK	15	8	UO_2[f] Natural U (metal)[g]	2.3 0.7	CO_2/graphite	Thermal
Light-water cooled, Graphite-moderated Reactor (LGR) RBMK (Russian: High Power Channel-Type Reactor) EGP (scaled down version of the RBMK)	Russia	11 + 4	10.2	Enriched UO_2	2.4[h]	Water/graphite	Thermal
Sodium-cooled fast reactor (BN-600)	Russia	1	0.6	UO_2 and PuO_2	17, 21, and 26[i]	Liquid sodium/ none	Fast

[a]GWe = capacity in thousands of megawatts (gross).
[b]Westinghouse design (Westinghouse Electric Corporation, 1984).
[c]Water-Water Power Reactor (VVER) (Muraviev, 2014).
[d]General Electric design (GE Nuclear Energy, 1972); initial enrichment is 1.7−2.0 wt% ^{235}U.
[e]EC6 Design (Candu Energy, 2012).
[f]AGR design.
[g]Magnox.
[h]RBMK design(Muraviev, 2014).
[i]BN-600 design (WNA, 2015b).

Table 18.2 Neutron spectrum, coolant, temperature/pressure, and fuel of Generation IV nuclear-reactor concepts (WNA, 2015d)

Reactor	Neutron spectrum	Coolant	Temperature °C	Pressure[a]	Fuel	Fuel cycle	Uses
GFR	Fast	Helium	850	High	^{238}U +[b]	Closed, on site	Electricity and hydrogen
LFR	Fast	Lead or lead−bismuth	480−800	Low	^{238}U +	Closed, regional	Electricity (hydrogen)
MSR	Fast	Fluoride salts	700−800	Low	UF in salt	Closed	Electricity and hydrogen
MSR − advanced high-temperature reactor	Thermal	Fluoride salts	750−1000	−	UO_2 particles in prism	Open	Hydrogen
SFR	Fast	Sodium	550	Low	^{238}U and mixed oxide	Closed	Electricity
Supercritical water-cooled reactor	Thermal or fast	Water	510−625	Very high	UO_2	Open (thermal) closed (fast)	Electricity (hydrogen)
Very high temperature reactor	Thermal	Helium	700−950 (1000 later)	high	UO_2 prism or pebbles	Open	Hydrogen and electricity

[a]High = 7−15 MPa and very high = ~25 MPa.
[b]+ = with some ^{235}U or ^{239}Pu.

minor actinides in the spent fuel to radionuclides with shorter half-lives. Thermal breeder reactors, on the other hand, produce less minor actinides in the spent fuel. $^{232}Th-^{233}U$ breeding cycle can be utilized in both fast and thermal reactors (Waltar et al., 2012). Even though both fast and thermal breeder reactors have been designed, FBRs are more efficient breeders. It is also notable that FBRs utilize the same fuel, uranium dioxide (UO_2)−plutonium dioxide (PuO_2), which has been used in some of the current commercial nuclear reactors.

The $^{232}Th-^{233}U$ cycle is of interest due to that the abundance of thorium in the Earth's crust is between three to five times that of uranium (OECD/NEA and IAEA, 2014). In addition, there are large thorium deposits in some countries such as India, Brazil, Australia, and the USA (WNA, 2015a). The $^{238}U-^{239}Pu$ cycle is the most effective with fast neutrons. For ^{239}Pu, the number of emitted neutrons in a fission reaction per absorbed neutrons is greater when fission is induced by fast neutrons rather than thermal neutrons. The additionally emitted neutrons can be utilized for transforming more ^{238}U nuclides to ^{239}Pu. Hence, the FBRs are based on $^{238}U-^{239}Pu$ in which ^{239}Pu and ^{238}U in the core undergo fission. In a two-region reactor, ^{238}U nuclides in the core and in the blanket[1] are transmuted to ^{239}Pu (Alexander, 1964; Waltar et al., 2012).

Even though ^{235}U is used as the primary fissile nuclide in the fuel of nuclear reactors, the fuel is designed in various geometrical configurations and chemical forms. In terms of geometrical configuration, nuclear fuels have been designed in the forms of cylindrical pellets, annular pellets, pebbles, plates and TRIstructural ISOtopic (TRISO) pellets. Cylindrical pellets are used in PWRs, BWRs, and CANDU reactors, annular pellets are used in VVER and RBMK designs (IAEA-TECDOC-1578, 2007), pebbles are used in PBMR (Kadak, 2005), TRISO pellets are used in very high temperature reactors (VHTRs) (OECD, 2014), and plates are used in some research reactors, such as advanced test reactors (Stanley and Marshall, 2008). In terms of the chemical structure, nuclear fuels can be classified into four categories: (1) metallic fuels; (2) ceramic fuels; (3) hydride fuels; and (4) composite fuels. This section provides an overview of these nuclear fuels.

18.2 Metallic fuels

Uranium, plutonium, and thorium are the most common metallic fuels (Kirillov et al., 2007). These metallic fuels have high thermal conductivity, high fissile atom density, good neutron economy, and good fabrication (Ma, 1983). On the other hand, metallic fuels suffer from irradiation instability, poor mechanical properties, and corrosion resistance, especially at high temperatures when exposed to air or water. The exposure of the metallic fuels to a neutron flux results in fuel swelling and has negative effects on the thermal conductivity (Kirillov et al., 2007). In addition, metallic fuels suffer from low melting points, and also, the fuel undergoes a phase change. A phase transformation results in a volume change in the fuel. For instance, α-phase of uranium metal is stable up

[1] The blanket, which surrounds the reactor core, is the region containing the fertile nuclides.

to 670°C, the β-phase exists between 670 and 776°C, and the γ-phase exists from 776°C up to the melting point of ~1135°C (Kirillov et al., 2007). Consequently, the use of metallic uranium fuel is limited to temperatures below 660°C (ORNL, 1965).

To improve these undesirable characteristics of the metallic uranium, uranium alloys such as uranium−aluminum, uranium−magnesium, and uranium−molybdenum have been developed (Ma, 1983). Metallic fuels have been used in some power reactors and research reactors with relatively low operating temperatures. For instance, a uranium alloy has been used in Magnox reactors (Simnad, 1992). Magnox reactors are subject to two design temperature limits at steady state conditions. First, the fuel temperature should be below 660°C. Second, the cladding temperature should be below 420°C (Zakova, 2012). Metallic fuels, such as uranium and plutonium fuels, were also used in the first generation of FBRs (Hafele et al., 1970).

For use in high-temperature applications, a potential fuel must have a high melting point, high thermal conductivity, and good irradiation and mechanical stability (Ma, 1983). These requirements eliminate the use of metallic fuels mainly due to their low melting points and high irradiation creep and swelling rates (Ma, 1983). On the other hand, ceramic fuels have promising properties, which have made these fuels as the fuels of choice for the current commercial nuclear reactors and suitable candidates for high-temperature applications. The next section provides more information on ceramic fuels.

18.3 Ceramic fuels

Ceramic fuels have high melting points, good dimensional and radiation stability, and are chemically compatible with most coolants and sheath materials. In addition to melting point, the thermal conductivity of a fuel is a critical property that affects the operating temperature of the fuel (the highest temperature in a reactor is the fuel centerline temperature, for hollow pellets it will be the internal wall temperature). UO_2 has been used as the fuel of choice in BWRs, PWRs, and CANDU reactors. The thermal conductivity of UO_2 is between approximately 2 and 4 W/m K within the operating temperature range of 1000−2800°C. On the other hand, fuels such as uranium dicarbide (UC_2), uranium carbide (UC), and uranium mononitride (UN) have significantly higher thermal conductivities compared to that of UO_2 and other oxide fuels, as shown in Fig. 18.1. The higher thermal conductivities of these fuels result in lower fuel temperatures compared to those of UO_2 under the same operating conditions (Peiman et al., 2015; Miletic et al., 2015; Abdalla et al., 2012; Grande et al., 2011).

Considering chemical structures of ceramic fuels, these fuels can be categorized as oxide fuels, carbide fuels, and nitride fuels. Oxide fuels such as UO_2, mixed oxide (MOX), and thorium dioxide (ThO_2) have low thermal conductivities compared to carbide and nitride fuels. Hence, from the heat transfer point of view, oxide fuels can also be identified as low thermal conductivity fuels. On the other hand, carbide (eg, UC and UC_2) and nitride (eg, UN) fuels are identified as high thermal conductivity fuels. Table 18.3 lists basic properties of these fuels at 0.1 MPa and 25°C.

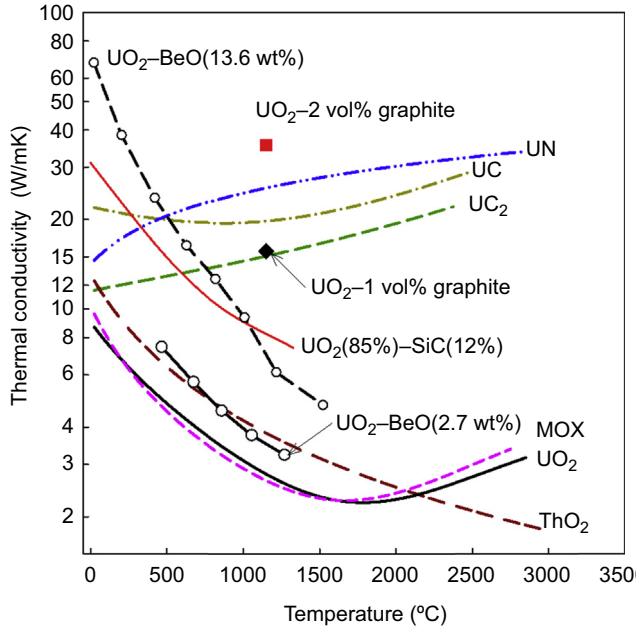


Figure 18.1 Thermal conductivity of several nuclear fuels (Cox and Cronenberg, 1977; Frost, 1963; IAEA, 2008; Ishimoto et al., 1996; Leitnaker and Godfrey, 1967; Khan et al., 2010; Kirillov et al., 2007; Lundberg and Hobbins, 1992; Solomon et al., 2005).

18.3.1 Oxide fuels

Oxides of uranium, thorium, and plutonium have been used as nuclear fuels (ie, UO_2, PuO_2, and MOX) have good corrosion resistance, high melting point, and excellent mechanical and irradiation stability. As such, UO_2, PuO_2, and MOX have been used as fuels in commercial nuclear reactors such as PWRs, BWRs, CANDU reactors, etc. In addition, oxide fuels are chemically compatible with the cladding materials and water, which is used as the coolant in these reactors. On the other hand, the disadvantages of oxide fuels include low uranium atom density, low thermal conductivity, and poor thermal-shock resistance (Simnad, 1992). A literature survey on properties of UO_2, MOX, and ThO_2 fuels is provided in the following sections with a focus on thermophysical properties.

18.3.1.1 Uranium dioxide

As a ceramic fuel, UO_2 is a hard and brittle material due to its ionic or covalent interatomic bonding. In spite of that, UO_2 is currently used in PWRs, BWRs, CANDU reactors, and others due to its properties. Oxygen has a very low thermal neutron absorption cross section, which does not result in a serious loss of neutrons. UO_2 is chemically stable and does not react with water within the operating temperatures of these reactors. UO_2 is structurally very stable. The crystal structure of the UO_2 fuel

Table 18.3 **Basic properties of selected fuels at 0.1 MPa and 25°C (Chirkin, 1968; IAEA, 2008; Frost, 1963; Cox and Cronenberg, 1977; Leitnaker and Godfrey, 1967; Lundberg and Hobbins, 1992)**

Property	Unit	UO_2	MOX[a]	ThO_2	UC	UC_2	UN
Molecular mass	amu	270.3	271.2	264	250.04	262.05	252.03
Theoretical density	kg/m^3	10,960	11,074	10,000	13,630[b]	11,680[1]	14,420
Melting point	°C	2847 ± 30	2750 ± 50[c]	3378 ± 17[d]	2507[e] 2520 2532[f]	2375[2] 2562[3]	2850 ± 30[g]
Heat capacity	J/kg K	235	240	235	203[h]	233[4]	190
Heat of Vaporization	kJ/kg	1530	1498	–	2120	1975 ± 20[3]	1144[i] 3325[j]
Thermal conductivity	W/mK	8.7	7.8[k]	9.7	21.2	11.57	14.6
Linear expansion coefficient, $\times 10^{-6}$	1/K	9.75	9.43	8.9[l]	10.1	18.1[l]	7.52
Electric resistivity, $\times 10^{-8}$	Ω m	7.32	–	–	250	120	146
Crystal structure	–	FCC[m]	FCC	FCC	FCC	BCT[n], $t < 1820$°C FCC, $t > 1820$°C	FCC

[a]MOX—mixed oxides $(U_{0.8}Pu_{0.2})O_2$, where 0.8 and 0.2 are the molar parts of UO_2 and PuO_2.
[b]Frost (1963).
[c]Popov et al. (2000).
[d]IAEA-TECDOC-1496.
[e]Cox and Cronenberg (1977).
[f]Lundberg and Hobbins (1992).
[g]At nitrogen pressure ≥0.25 MPa.
[h]Leitnaker and Godfrey (1967).
[i]$UN(s) = U(l) + 0.5N_2(g)$, Gingerich (1969).
[j]$UN(s) = U(g) + 0.5N_2(g)$, Gingerich (1969).
[k]At 95% density.
[l]At 1000°C, Bowman et al. (1966).
[m]*FCC*, face-centered cubic.
[n]*BCT*, body-centered tetragonal.

retains most of the fission products even at high burnups (Cochran and Tsoulfanidis, 1999). The thermal conductivity of the fuel is an important thermophysical property in the computation of the fuel temperature. The thermal conductivity of 95% theoretical density (*TD*) UO_2 can be calculated using the Frank correlation, shown as Eq. [18.1] (Carbajo et al., 2001). In Eq. [18.1], T is the temperature in K. This correlation is valid for temperatures in the range of 25−2847°C. Even though UO_2 has a high melting point, its thermal conductivity is very low compared to those of high thermal conductivity or composite fuels. The properties of other fuels are discussed in the following sections.

$$k_{UO_2}(T) = \frac{100}{7.5408 + 17.692 \times (10^{-3}T) + 3.6142 \times (10^{-3}T)^2} + \frac{6400}{(10^{-3}T)^{5/2}} \exp^{-16.35/(10^{-3}T)} \quad [18.1]$$

The thermal conductivity of the fuel varies with temperature and is affected by manufacturing methods, the percentage of the porosity of the fuel, burnup, fission gas release, and deviation from stoichiometry. As such, there are uncertainties in the reported thermal conductivities. For UO_2, the uncertainty is about 10% for temperatures below 1727°C (2000 K), while the uncertainty increases up to 20% for temperatures between 1727°C (2000 K) and 2847°C (3120 K) (IAEA-TECDOC-1496, 2006). Fig. 18.2 shows UO_2 thermal conductivity profiles as a function of fuel temperature for various percentages of theoretical fuel density, manufacturing, stoichiometry, and irradiation. Fig. 18.3 shows the impact of porosity and irradiation on thermal conductivity of UO_2. Thermal conductivity is shown for unirradiated UO_2 and irradiated UO_2 with a neutron flux of 1.16×10^{19} neutrons/cm^2 at 527°C (800 K) before testing. In addition, Fig. 18.4 shows the uncertainty associated with the thermal conductivity of UO_2 for various percentages of fuel porosity. In these figures, the *TD* of UO_2 is considered to be 10,960 kg/m^3.

18.3.1.2 Mixed oxide

MOX fuel refers to nuclear fuels consisting of UO_2 and PuO_2. MOX fuel was initially designed for use in liquid metal fast breeder reactors and in light water reactors (LWRs) when reprocessing and recycling of the used fuel is adopted (Cochran and Tsoulfanidis, 1999). The UO_2 content of MOX may be natural, enriched, or depleted uranium, depending on the application of MOX fuel. In general, MOX fuel contains between 3% and 5% PuO_2 blended with 95−97% natural or depleted UO_2 (Carbajo et al., 2001). The small fraction of PuO_2 slightly changes the thermophysical properties of MOX fuel compared with those of UO_2 fuel.

Most thermophysical properties of UO_2 and MOX (3−5% PuO_2) have similar trends. For instance, thermal conductivities of UO_2 and MOX fuels decrease as the temperature increases up to 1700°C (see Fig. 18.1). Despite similar trends in thermal conductivity, UO_2 and MOX fuels have different densities and melting points.

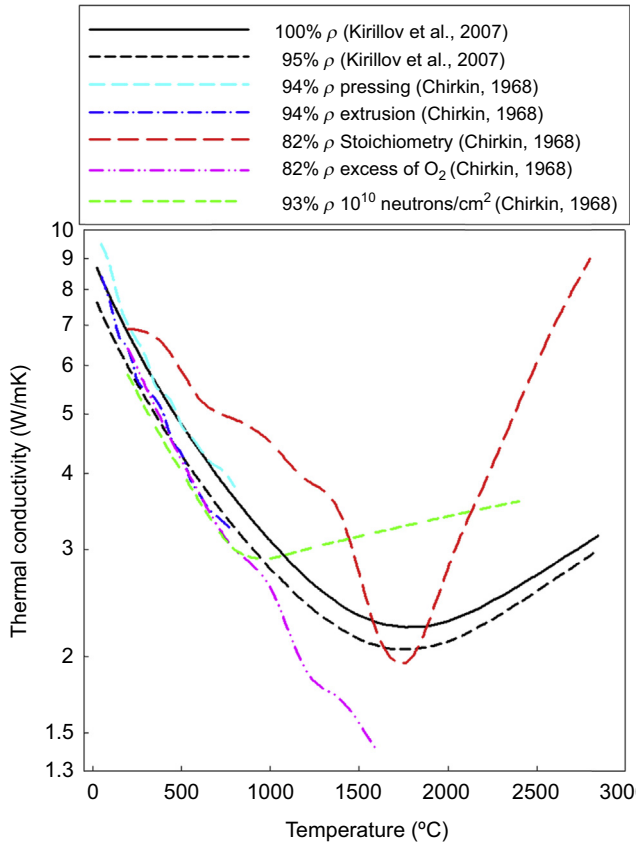


Figure 18.2 Thermal conductivity of UO_2 as a function of percentage of *TD*, manufacturing, stoichiometry and irradiation.

The density of MOX fuel is slightly higher than that of UO_2 fuel. MOX fuel has a lower melting temperature, lower heat of fusion, and lower thermal conductivity than those of UO_2 fuel. For the same power, MOX fuel has a higher stored energy, which results in a higher fuel centerline temperature compared with that of UO_2 fuel. The fission gas release rate from MOX is higher compared to that from UO_2 because of the lower thermal conductivity of MOX up to temperatures around 1500°C, which results in higher fuel temperatures. The most significant differences between these two fuels have been summarized in Table 18.3.

The thermal conductivity of a fuel is of importance in the computation of the fuel centerline temperature. The thermal conductivities of MOX and UO_2 decrease as functions of temperature up to temperatures around 1527 and 1727°C, respectively, and then they increase as the temperature increases (see Fig. 18.1). In general, the thermal conductivity of MOX fuel is slightly lower than that of UO_2. In other words, the addition of small amounts of PuO_2 decreases the thermal conductivity of the mixed fuel. However, the thermal conductivity of MOX does not decrease significantly when

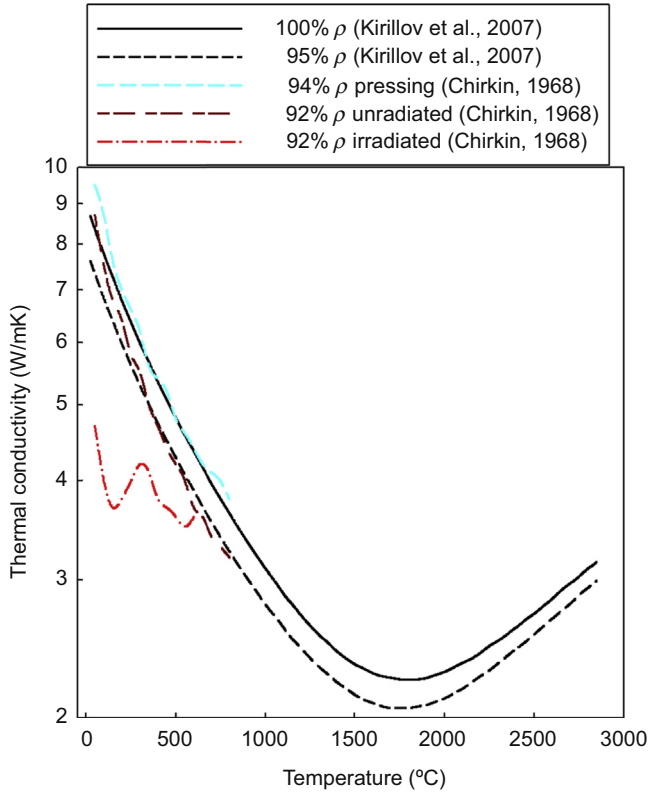


Figure 18.3 Impact of porosity and irradiation of thermal conductivity of UO_2.

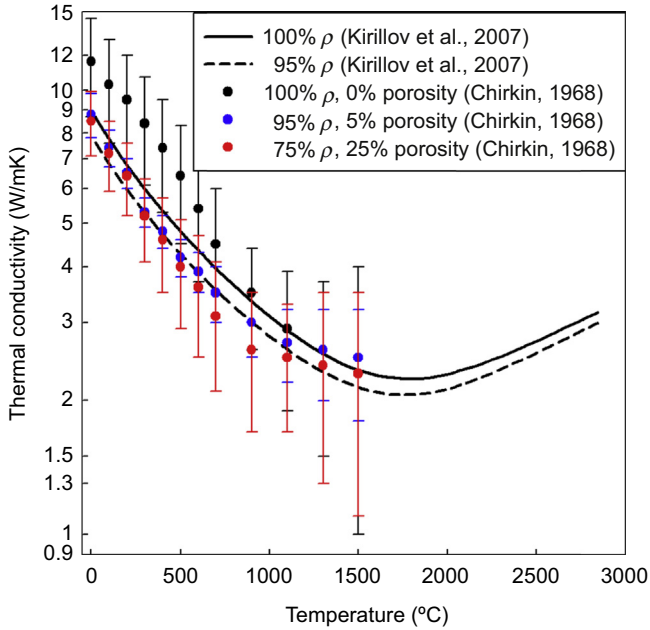


Figure 18.4 Uncertainty in thermal conductivity of UO_2.

the PuO_2 content of the fuel is between 3% and 15%. The thermal conductivity of MOX fuel decreases as the concentration of PuO_2 increases beyond 15%. As a result, the concentration of PuO_2 in commercial MOX fuels is kept below 5% (Carbajo et al., 2001; Popov et al., 2000). Carbajo et al. (2001) recommend the following correlation shown as Eq. [18.2] for the calculation of the thermal conductivity of 95% *TD* MOX fuel. This correlation is valid for temperatures between 427°C and 2827°C, x less than 0.05, and PuO_2 concentrations between 3% and 15%. In Eq. [18.2], T is the temperature in K. The uncertainty associated with Eq. [18.2] is 7% for temperatures between 427°C (700 K) and 1527°C (1800 K). For temperatures above 2827°C (3100 K), the uncertainty increases to 20%.

$$k(T,x) = \frac{1}{A + C(10^{-3}T)} + \frac{6400}{(10^{-3}T)^{5/2}} \exp^{-16.35/(10^{-3}T)} \qquad [18.2]$$

where x is a function of oxygen to heavy metal ratio $\left(x = 2 - \frac{O}{M}\right)$ and

$$A(x) = 2.58x + 0.035\ (\text{mK/W}), \quad C(x) = (-0.715x + 0.286)(\text{m/W})$$

18.3.1.3 Thorium dioxide

Currently, there is an interest in using thorium-based fuels in nuclear reactors. Thorium is widely distributed in nature and is approximately three times as abundant as uranium. However, ThO_2 does not have any fissile elements to fission with thermal neutrons. Consequently, ThO_2 must be used in combination with a "driver" fuel (eg, UO_2, UC, or PuO_2), which has ^{235}U as its initial fissile elements. The presence of a driver fuel such as UO_2 in a nuclear reactor core results in the production of enough neutrons, which in turn start the thorium cycle. In this cycle, ^{232}Th is converted into ^{233}Th, which decays to ^{233}Pa. Eventually, ^{233}U, which is a fissile element, is formed by the β^- decay of ^{233}Pa (Cochran and Tsoulfanidis, 1999).

The use of thorium-based fuels in nuclear reactors requires information on the thermophysical properties of these fuels. Jain et al. (2006) have conducted experiments on thorium and the solid solutions of ThO_2 and lanthanum oxide ($LaO_{1.5}$). As a result of their experiments, Jain et al. (2006) have determined the density, thermal diffusivity, and specific heat for several compositions of ThO_2 and $LaO_{1.5}$ ranging from pure thorium to10 mol% $LaO_{1.5}$. These properties were measured for temperatures between 100 and 1500°C (Jain et al., 2006).

In their analysis, the thermal conductivity values have been calculated based on Eq. [18.3], which requires the measured values of the thermal diffusivity, specific heat, and density of these solid solutions. In the current study, the correlation developed by Jain et al. (2006), which is shown as Eq. [18.4], has been used in order to calculate the thermal conductivity of ThO_2 fuel for the purpose of the calculation of the fuel centerline temperature. In Eq. [18.4], T is the temperature in K.

$$k = \alpha \rho c_p \qquad [18.3]$$

$$k_{ThO_2} = \frac{1}{0.0327 + 1.603 \cdot 10^{-4} T} \quad [18.4]$$

Bakker et al. (1977) proposed a correlation, which is shown as Eq. [18.5], for the calculation of the thermal conductivity of ThO_2 with 95% *TD*. This correlation is valid for the temperature range between 27°C (300 K) and 1727°C (2000 K) (Das and Bharadwaj, 2013). Eq. [18.5], T is the temperature in K.

$$k_{ThO_2} = \frac{1}{4.20 \times 10^{-4} + 2.25 \times 10^{-4} T} \quad [18.5]$$

Belle and Berman (1984) also developed a correlation for the calculation of the thermal conductivity of ThO_2. This correlation is shown as Eq. [18.6], which is valid for ThO_2 with 100% *TD* and in the temperature range between 25°C (298 K) and 2677°C (2950 K). In Eq. [18.6], T is the temperature in K.

$$k_{ThO_2} = \frac{1}{0.0213 + 1.597 \times 10^{-4} T} \quad [18.6]$$

Even though the above equations capture the variation in thermal conductivity of ThO_2 as a function of temperature, the thermal conductivity of ThO_2 also changes due to manufacturing methods, the percentage of the porosity of the fuel, burnup, fission gas release, and deviation from stoichiometry. Fig. 18.5 shows the variation in thermal conductivity of ThO_2 for various porosities and densities as a function of temperature.

ThO_2 is used in combination with UO_2 or PuO_2 in solid solutions. Solid solutions of ThO_2−UO_2 and ThO_2−PuO_2 have different thermophysical properties. IAEA-TECDOC-1496 (2006) recommends Eq. [18.7] for the calculation of the thermal conductivity of $(Th_{1-y}U_y)O_2$ with 95% *TD* for the temperature range between 600°C (873 K) and 1600°C (1873 K). In this equation, T is the temperature in Kelvin, and y is the weight percent of UO_2.

$$k_{(Th_{1-y}U_y)O_2} = \frac{1}{-0.0464 + 0.0034y + (2.5185 \times 10^{-4} + 1.0733 \times 10^{-7} y)T} \quad [18.7]$$

IAEA-TECDOC-1496 (2006) recommends Eq. [18.8] for the calculation of the thermal conductivity of $(Th_{1-y}Pu_y)O_2$ for the temperature range between 600°C (873 K) and 1700°C (1873 K). In this equation, T is the temperature in K and y is the weight percent of PuO_2. Valuable information about the thermophysical and impact of irradiation on thermophysical properties of ThO_2 is provided by Das and Bharadwaj (2013), IAEA-TECDOC-1496 (2006), and Belle and Berman (1984).

$$k_{(Th_{1-y}Pu_y)O_2} = \frac{1}{-0.08388 + 1.7378y + (2.62524 \times 10^{-4} + 1.7405 \times 10^{-4} y)T} \quad [18.8]$$

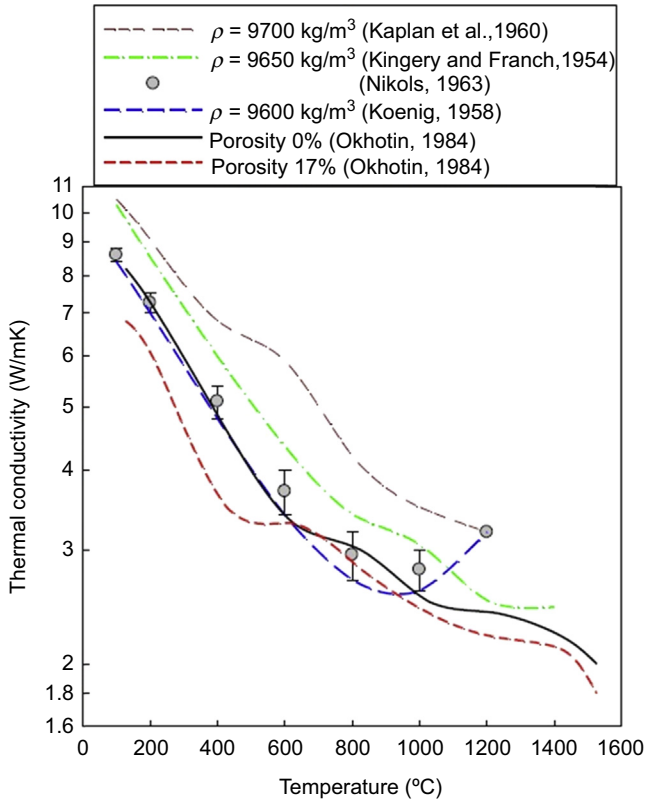


Figure 18.5 Thermal conductivities of ThO_2 for various porosities and densities.

The thermal conductivities of ThO_2, ThO_2—UO_2 and ThO_2—PuO_2 are shown in Fig. 18.6 as a function of temperature.

18.3.2 Carbide fuels

Carbides of uranium and thorium have been considered as nuclear fuels (Simnad, 1992). The use of carbides of plutonium has also been investigated but as mixed carbides such as UC—PuC (Ogard and Leary, 1970). Compared to MOX fuel, mixed carbide fuel has a higher thermal conductivity, higher heavy metal density, and better neutron economy. Carbides of thorium, ThC, and ThC_2 are the most stable compounds of thorium after ThO_2. ThC is stable up to temperatures close to its melting point. Carbides of uranium have desirable properties such as high thermal conductivities and high melting points. UC and UC_2 are two carbides of uranium, which can be used as nuclear fuels. Uranium sesquicarbide (U_2C_3) is another carbide of uranium. U_2C_3 cannot be manufactured through casting or compaction of a powder. But, UC_2 may transform to U_2C_3 at high temperatures and under stress (Frost, 1963). The following two sections provide a literature survey on thermophysical, mechanical, and irradiation properties of UC and UC_2.

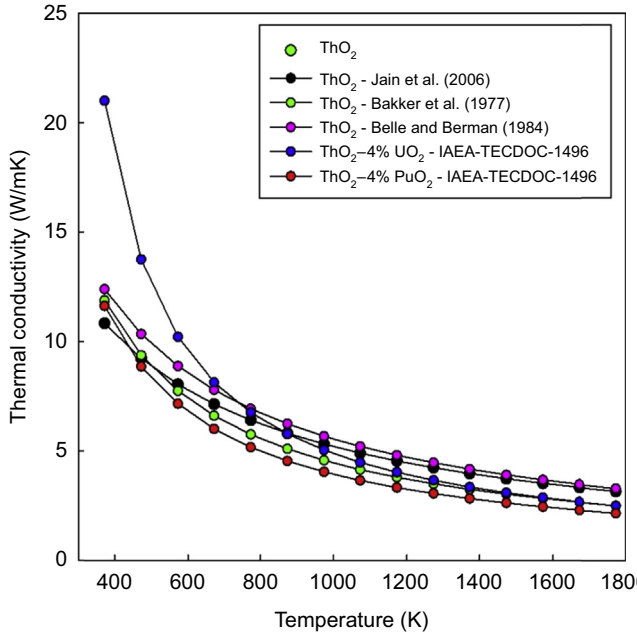


Figure 18.6 Thermal conductivity of ThO_2.

18.3.2.1 Uranium carbide

UC, which has a faced-centered cubic (FCC) crystal structure similar to those of UN and NaCl, has a high melting point approximately 2507°C and a high thermal conductivity, above 19 W/m K at all temperatures up to the melting point. UC has a density of 13,630 kg/m^3, which is lower than that of UN but higher than those of UO_2 and UC_2. It should be noted that the density of hypostoichiometric UC is slightly higher than that of stoichiometric UC, which is listed in Table 18.3. Coninck et al. (1975) report densities between 13,730 and 13,820 kg/m^3 at 25°C for hypostoichiometric UC. Moreover, uranium atom density of UC is higher than that of UO_2 but lower than that of UN. The uranium atom densities of UC and UN are 1.34 and 1.4 times that of UO_2.

Many researchers have studied thermophysical properties of UC. Coninck et al. (1975) conducted experiments on hypostoichiometric and stoichiometric UC, and determined the thermal diffusivity, thermal conductivity, and spectral emissivity of UC. For hypostoichiometric UC, the thermal diffusivity α, in m^2/s, and thermal conductivity k, in W/m K, correlations are valid for a temperature range of 570−2000°C. In Eqs. [18.9] and [18.10], T is the temperature in K (Coninck et al., 1975).

$$\alpha = 10^{-4} \cdot \left[5.75 \cdot 10^{-2} + 1.25 \cdot 10^{-6}(T - 273.15)\right] \quad [18.9]$$

$$k = 100 \cdot \left[2.04 \cdot 10^{-1} + 2.836 \cdot 10^{-8}(T - 843.15)^2\right] \quad [18.10]$$

Coninck et al. (1975) provide two correlations for the calculation of the spectral emissivity of hypostoichiometric UC. Eq. [18.11] has been suggested for pure UC when temperature varies between 1100 and 2000°C. Moreover, Eq. [18.12] can be used in order to determine the spectral emissivity of oxidized samples for temperatures between 1100 and 1600°C. In Eqs. [18.11] and [18.12], T is the temperature in K.

$$\varepsilon = 5.5\cdot10^{-1} - 8.5\cdot10^{-5}(T - 273.15) \quad [18.11]$$

$$\varepsilon = -4.666\cdot10^{-1} + 1.050\cdot10^{-1}(T - 273.15) - 7.627\cdot10^{-5}(T - 273.15)^2 + 1.813\cdot10^{-8}(T - 273.15)^3 \quad [18.12]$$

Coninck et al. (1975) provided two correlations, shown as Eqs. [18.13] and [18.14], which can be used to determine the mean values of the thermal diffusivity and thermal conductivity of stoichiometric UC for a temperature range between 850 and 2250°C, in m^2/s and W/m K, respectively. In addition, Eq. [18.15] can be used to calculate the spectral emissivity of stoichiometric UC for temperatures between 1100 and 2250°C (Coninck et al., 1975). In Eqs. [18.13]–[18.15], T is the temperature in K.

$$\alpha = 10^{-4}\cdot\left[5.7\cdot10^{-2} + 1.82\cdot10^{-12}(T - 1123.15)^3\right] \quad [18.13]$$

$$k = 100\cdot\left[1.95\cdot10^{-1} + 3.57\cdot10^{-8}(T - 1123.15)^2\right] \quad [18.14]$$

$$\varepsilon = 5.65\cdot10^{-1} - 5\cdot10^{-5}(T - 273.15) \quad [18.15]$$

In addition to Eqs. [18.10] and [18.14], Kirillov et al. (2007) have recommended another correlation, shown as Eqs. [18.16] and [18.17], for the calculation of the thermal conductivity of UC in W/m K. Fig. 18.7 shows the thermal conductivity calculated using Eqs. [18.10], [18.14], [18.16], and [18.17] as a function of temperature. It is recommended to use Eq. [18.14] for the calculation of the thermal conductivity of UC fuel because this equation provides the lowest thermal conductivity values for a wide temperature range, leading to a conservative calculation of the fuel centerline temperature. In Eqs. [18.16] and [18.17], T is the temperature in K.

$$k = 21.7 - 3.04\cdot10^{-3}(T - 273.15) + 3.61\cdot10^{-6}(T - 273.15)^2, \quad 323 < T < 973\ \text{K} \quad [18.16]$$

$$k = 20.2 + 1.48\cdot10^{-3}(T - 273.15), \quad 973 < T < 2573\ \text{K} \quad [18.17]$$

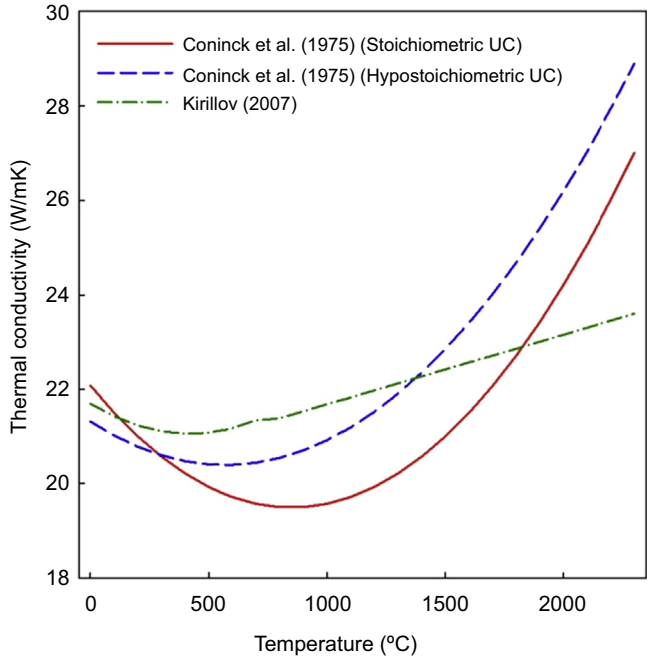


Figure 18.7 Thermal conductivity of UC resulted from various correlations.

Leitnaker and Godfrey (1967) have conducted experiments on UC in a temperature range between 298.15 and 2800 K. As a result, they have provided Eqs. [18.18] and [18.19], which can be used in order to calculate the specific heat and the enthalpy of UC based on the results of Leitnaker and Godfrey (1967), where T is the temperature in K and the specific heat and enthalpy are in J/kg K and J/kg, respectively. The average percent error associated with Eq. [18.19] is ±0.84%.

$$c_p = 6\cdot10^{-15}T^5 - 6\cdot10^{-11}T^4 + 2\cdot10^{-7}T^3 - 3\cdot10^{-4}T^2 + 0.2655\,T + 147.34 \quad [18.18]$$

$$H(T) - H(298\ \mathrm{K}) = \frac{4184}{250.04}\left[14.430\,T - 1.074\cdot10^{-3}T^2 + 1.890\cdot10^{5}T^{-1} + 3.473\cdot10^{-5}T^{5/2} - 4.894\cdot10^{3}\right] \quad [18.19]$$

The linear thermal expansion of UC, in 1/K, for a temperature range of 0−2000°C, can be calculated using a correlation shown as Eq. [18.20] (IAEA, 2008) with an uncertainty of ±15%. In Eq. [18.20], T is the temperature in K. Fig. 18.8 shows the

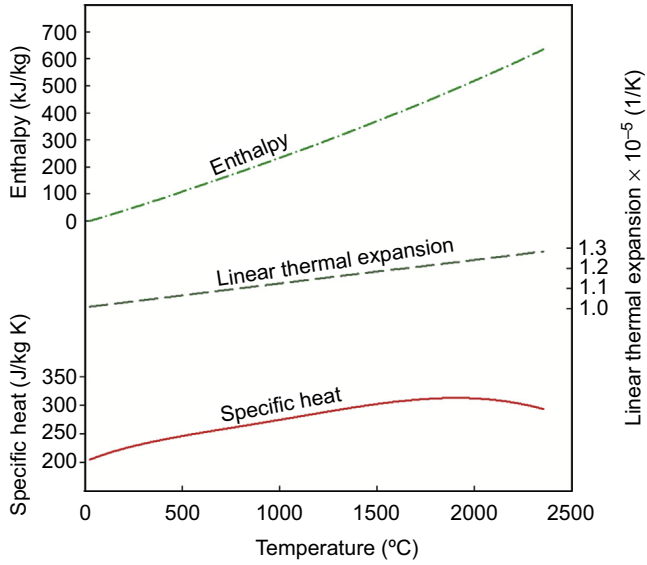


Figure 18.8 Thermodynamic properties of UC as function of temperature (IAEA, 2008; Leitnaker and Godfrey, 1967).

variations in the specific heat, enthalpy, and linear thermal expansion of UC as functions of temperature.

$$\alpha = 1.007 \cdot 10^{-5} + 1.17 \cdot 10^{-9}(T - 273.15) \quad [18.20]$$

Frost (1963) has developed a correlation shown as Eq. [18.21], which can be used to determine the diametric increase of UC fuel as a function of time-averaged fuel centerline temperature. According to Eq. [18.21], UC fuel undergoes significant swelling for temperatures above 1000°C. In Eq. [18.21], R_D and T are percent diametric increase per atom percent burnup and time-averaged fuel centerline temperature in K, respectively. In addition, Harrison (1969) provides the volumetric swelling of UC as a function of burnup for various temperatures. Fig. 18.9 shows the result of the analysis conducted by Harrison (1969) on the volumetric swelling of UC.

$$R_D = 0.6 + 0.77(9T/5000 - 1) \quad [18.21]$$

Stellrecht et al. (1968) have developed a correlation, shown as Eq. [18.22], which can be used to determine the compressive creep rate of UC in 1/h for temperatures between 1200 and 1600°C and stress values between 20.68 and 68.95 MPa. This correlation was developed specifically based on data obtained on hyperstoichiometric UC (eg, $UC_{1.08}$). Seltzer et al. (1975) have studied the effects of deviation from stoichiometry on the creep rate of UC and found that the creep rate decreases by increasing the atomic ratio of carbon to uranium (C/U) due to precipitation strengthening. Tokar et al.

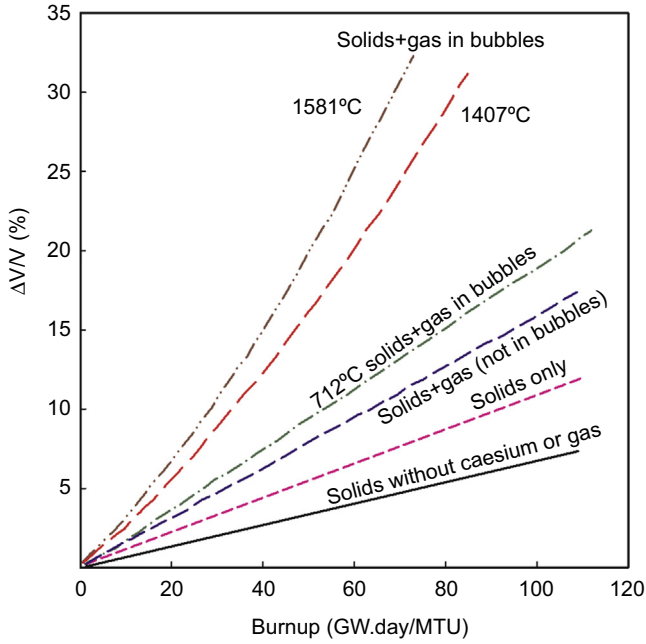


Figure 18.9 Volumetric swelling of UC as function of temperature and burnup.
Based on Harrison, J.W., 1969. The irradiation-induced swelling of uranium carbide. Journal of Nuclear Materials 30, 319–323.

(1970) also demonstrate that the creep rate is higher for hypostoichiometric UC than hyperstoichiometric UC due to the existence of free uranium in the microstructure of hypostoichiometric UC. However, this reduction in the creep rate depends on temperature and only exhibits at temperatures up to 1700°C. Fig. 18.10 shows the creep rate of UC as a function of temperature for several selected stress values. In Eq. [18.22], σ is the stress in Pa, R is the gas constant in cal/K mol, and T is the temperature in K. As shown in Fig. 18.10, the creep rate increases as the temperature increases; this indicates that the creep rate proportionally depends on temperature. In addition, the increase in temperature changes the creep mechanism from vacancy migration to dislocation motion (Tokar et al., 1970).

$$\varepsilon' = 1.8 \cdot 10^{-3} (\sigma/6894.76)^3 e^{-\left(\frac{90{,}000}{RT}\right)} \qquad [18.22]$$

18.3.2.2 Uranium dicarbide

UC_2 is a carbide of uranium, which has a high melting point and a high thermal conductivity. UC_2 has a body-centered tetragonal (BCT) crystal structure up to the transformation temperature of 1820 ± 20°C, where it transforms to a face-centered cubic (FCC) structure, similar to that of UO_2 (Frost, 1963). Frost (1963) has indicated that UC_2 has always been found in hypostoichiometric forms such

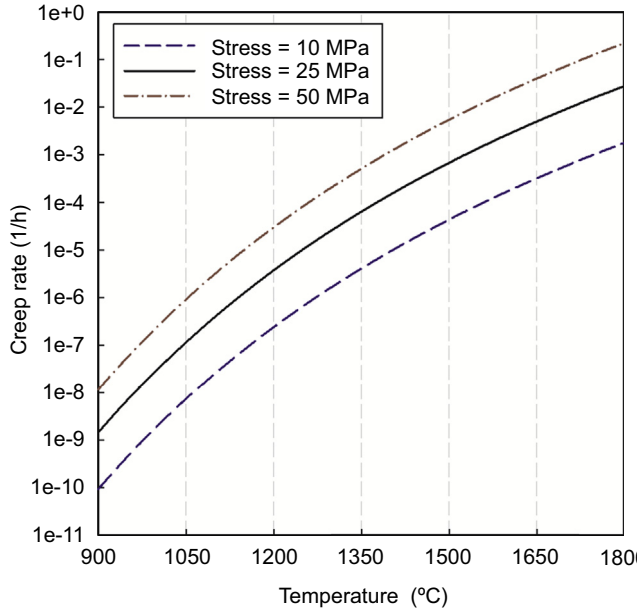


Figure 18.10 Creep rate of UC as function of temperature (Stellrecht et al., 1968).

as $UC_{1.75-1.90}$. The most common and probable composition of UC_2 is $UC_{1.8}$, which is often written as UC_2 (Frost, 1963). In a VHTR design, UO_2 and UC_2 have been considered as the fuel with a ratio of 3:1 (Olander, 2009). The function of UC_2 is to reduce the UO_2 fuel back to UO_2 when oxygen is released from the UO_2 fuel.

The thermodynamic properties of UC_2 have been studied by several scientists. Coninck et al. (1976) conducted experiments on UC_2 and provided correlations for the calculation of the thermal diffusivity, thermal conductivity, and emissivity of UC_2 as functions of temperature. Coninck et al. (1976) used the modulated electron beam technique in order to determine the thermal diffusivity of UC_2 samples. In this technique, an electron gun is used to bombard a material in the form of a thin solid plate from one face. The electron gun is modulated to vary sinusoidally as a function of time. The phase difference between the temperature fluctuations of the two faces of the plate is measured, which is used to determine the thermal diffusivity of the material (Wheeler, 1965). Then, thermal conductivity is calculated as the multiplication of thermal diffusivity, density, and specific heat as shown in Eq. [18.3].

Coninck et al. (1976) have developed two correlations shown as Eqs. [18.23]–[18.26] for the calculation of the thermal diffusivity, in m^2/s, and thermal conductivity, in W/m K, of the nearly stoichiometric UC_2. The correlations for slightly hypostoichiometric UC_2 and hypostoichiometric UC_2 have been shown as Eqs. [18.27]–[18.32]. In Eqs. [18.23]–[18.32], T is the temperature in K.

$$\alpha = 10^{-4}\cdot\left[0.0398 - 1.775\cdot10^{-6}(T - 273.15) - 8.65\cdot10^{-10}(T - 273.15)^2\right],\quad 873 < T < 2013\ \text{K} \tag{18.23}$$

$$\alpha = 0.0375\cdot10^{-4},\quad 2103 < T < 2333\ \text{K} \tag{18.24}$$

$$k = 100\cdot\left[0.115 + 2.7\cdot10^{-5}(T - 273.15) + 2.8\cdot10^{-10}(T - 273.15)^2 + 3.035\cdot10^{-12}(T - 273.15)^3\right],\quad 873 < T < 2013\ \text{K} \tag{18.25}$$

$$k = 100\cdot\left[0.082 + 5.64\cdot10^{-5}(T - 273.15)\right],\quad 2103 < T < 2333\ \text{K} \tag{18.26}$$

Slightly hypostoichiometric:

$$\alpha = 10^{-4}\cdot\left[0.0454 - 4.73\cdot10^{-6}(T - 273.15) - 5.8\cdot10^{-10}T^2\right],\quad 873 < T < 1993\ \text{K} \tag{18.27}$$

$$\alpha = 0.045\cdot10^{-4},\quad 2093 < T < 2343\ \text{K} \tag{18.28}$$

$$k = 100\cdot\left[0.1182 + 2.895\cdot10^{-5}(T - 273.15) + 3.8\cdot10^{-9}(T - 273.15)^2 + 1.9\cdot10^{-12}(T - 273.15)^3\right],\quad 873 < T < 1993\ \text{K} \tag{18.29}$$

$$k = 100\cdot\left[0.102 + 4.88\cdot10^{-5}(T - 273.15)\right],\quad 2093 < T < 2343\ \text{K} \tag{18.30}$$

Hypostoichiometric UC_2:

$$\alpha = 10^{-4}\cdot\left[0.043 - 1.9\cdot10^{-6}(T - 273.15) - 1.2\cdot10^{-9}(T - 273.15)^2 - 4.11\cdot10^{-13}(T - 273.15)^3\right],\quad 873 < T < 1973\ \text{K} \tag{18.31}$$

$$k = 100\cdot\left[0.132 + 1.9\cdot10^{-5}(T - 273.15) + 4.3\cdot10^{-9}(T - 273.15)^2\right],\quad 873 < T < 1973\ \text{K} \tag{18.32}$$

Figs. 18.11 and 18.12 show the thermal conductivity and thermal diffusivity for stoichiometric, slightly hypostoichiometric, and hypostoichiometric UC_2 as functions

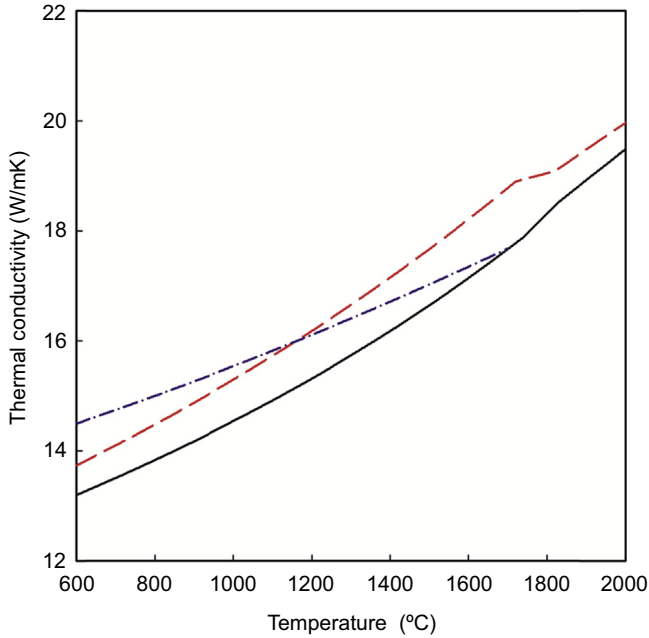


Figure 18.11 Thermal conductivity for stoichiometric, slightly hypostoichiometric, and hypostoichiometric UC_2 as function of temperature (Coninck et al., 1976).

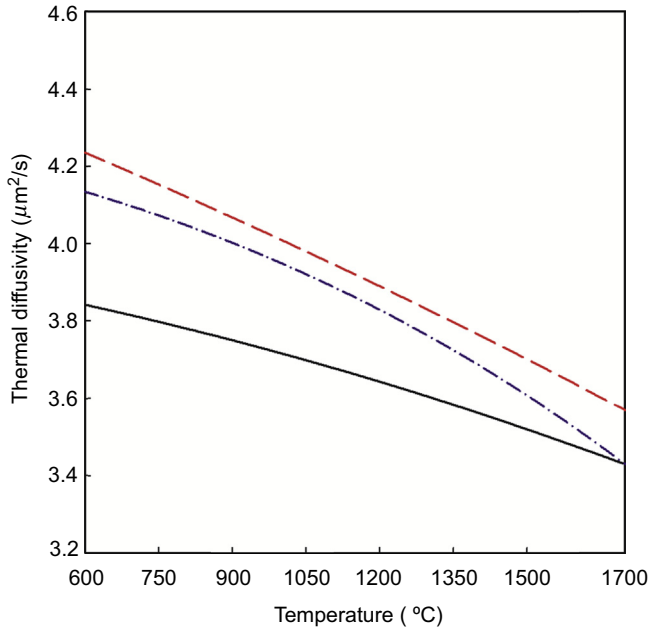


Figure 18.12 Thermal diffusivity for stoichiometric, slightly hypostoichiometric, and hypostoichiometric UC_2 as function of temperature (Coninck et al., 1976).

of temperature. As shown in Fig. 18.11, the deviation from stoichiometry does not significantly change the thermal conductivity of UC_2. For all cases, the thermal conductivity increases, and the thermal diffusivity (see Fig. 18.12) decreases as temperature rises.

Leitnaker and Godfrey (1967) have conducted experiments on a mixture consisting of 5.5% UC, 94.5% $UC_{1.91}$, and 7% carbon in a temperature range between 25 and 2727°C. They have provided the values of the specific heat of the mixture, as shown in Fig. 18.13. Eq. [18.33] can be used in order to calculate the specific heat of the mixture in J/kg K for a temperature range between 25 and 1787°C. Moreover, Leitnaker and Godfrey (1967) provided Eqs. [18.34] and [18.35], which can be used for the calculation of enthalpy in J/kg. Eqs. [18.34] and [18.35] are valid for temperature ranges between 25 and 1787°C, and 1787 and 2308°C, respectively. The average percent errors associated with Eqs. [18.34] and [18.35] are ±0.25% and ±0.30%, respectively (Leitnaker and Godfrey, 1967). In Eqs. [18.33]−[18.35], T is the temperature in K.

$$c_p = -1\cdot10^{-10}T^4 + 7\cdot10^{-7}T^3 - 11\cdot10^{-4}T^2 + 0.8401\,T + 65.088 \qquad [18.33]$$

$$H(T) - H(298\ \text{K}) = \frac{4184}{262.05}\cdot\left[4.076\,T + 2.631\cdot10^{-2}T^2 - 2.332\cdot10^{-5}T^3 + 1.025\cdot10^{-8}T^4 - 1.573\cdot10^{-12}T^5 - 3.013\cdot10^{3}\right], \quad 298.15 < T < 2060\ \text{K} \qquad [18.34]$$

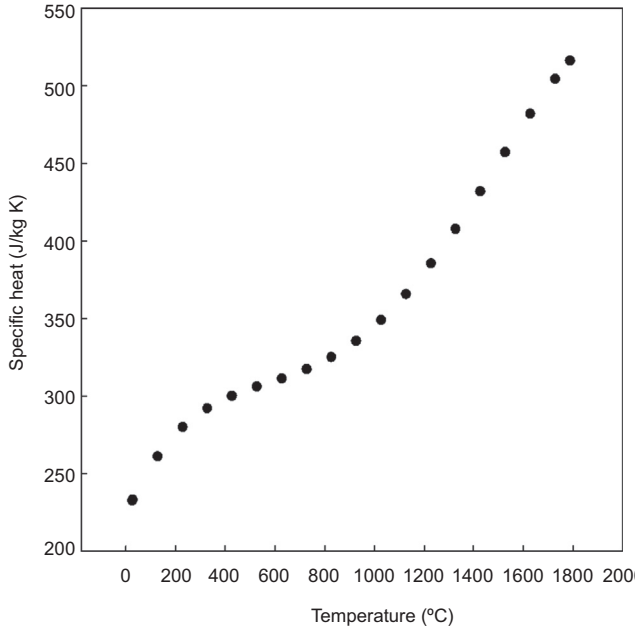


Figure 18.13 Specific heat of UC_2 as a function of temperature (Leitnaker and Godfrey, 1967).

$$H(T) - H(298\ \mathrm{K}) = \frac{4184}{262.05} \cdot \left[-2.512\,T + 6.894 \cdot 10^{-3} T^2 + 1.806 \cdot 10^4 \right], \quad 2060 < T < 2581\ \mathrm{K} \qquad [18.35]$$

There has been a renewed interest in UC_2. UC_2 is used in combination with UO_2 as the fuel of choice for the VHTR in the United States (Olander, 2009). For this reactor design, the ratio of UO_2:UC_2 is 3:1. In addition to increasing the effective thermal conductivity of the fuel, another advantage of using UC_2 is that UC_2 reduces the UO_2 fuel to UO_2 when oxygen is released from the UO_2.

18.3.3 Nitride fuels

There are three compounds of uranium nitride system, namely, UN, uranium dinitride (UN_2), and uranium sesquinitride (U_2N_3). Among these compounds, UN has been considered as nuclear fuel for use in space nuclear reactors and sodium cooled fast-breeder reactors (Matthews et al., 1988) because of its superior properties, such as high thermal conductivity, high melting point, and high uranium atom density. The fuel residence time in the reactor core can be increased when UN is used as a fuel (Zakova, 2012). The following section provides a literature survey on properties of UN.

18.3.3.1 Uranium mononitride

Uranium mononitride or uranium nitride (UN) can be produced by several methods, including: (1) hot pressing; (2) cold pressing and sintering; and (3) carbothermic reduction of UO_2 plus carbon in nitrogen (Simnad, 1992; Shoup and Grace, 1977). The latter process produces UN with densities in the range of 65−90% of *TD* (Shoup and Grace, 1977). UN has a high melting point, high thermal conductivity, and high radiation stability. These properties enhance the safety of operation and allow the fuel to achieve high burnups (IAEA, 2008). In addition, UN has the highest fissile atom density, which is approximately 1.4 times that of UO_2 and greater than those of other fuels, such as UC. In other words, when UN is used as a fuel, a smaller volume of fuel is required, which leads to a smaller core. Even though UN is more stable in air than UC (Simnad, 1992), one disadvantage of the UN fuel is that under some conditions, it decomposes to liquid uranium and gaseous nitrogen (IAEA, 2008), which in turn results in the formation of cracks in the fuel. The formation of cracks increases the possibility of the release of gaseous fission products and has adverse effects on the mechanical and thermophysical properties of the fuel.

It is significantly important to establish a temperature−pressure relationship for the melting point of UN fuel in order to establish temperature limits for UN fuel elements. UN melts congruently at high nitrogen pressures. In contrast, at high nitrogen pressures, UN melts incongruently, which means UN decomposes to liquid uranium and releases nitrogen gas. Therefore, it is expected to measure low UN vapor pressure over UN fuel due to its tendency to decompose. In comparison with UO_2 fuel, the

vapor pressure of UN over UN fuel is four orders of magnitude less than the vapor pressure of UO_2 over UO_2 fuel. UN fuel melts congruently at high partial pressures of nitrogen; however, the decomposition of UN occurs at low nitrogen partial pressures. Therefore, the partial pressure of UN fuel is an indication of melting or decomposition of the fuel, which in turn can be used to establish engineering limits for UN fuel (Hayes et al., 1990c).

Hayes et al. (1990c) have developed an empirical correlation shown as Eq. [18.36], which can be used to calculate the melting point of UN, in K, as a function of partial pressure of nitrogen that depends on temperature. Eq. [18.36] is valid when the partial pressure of nitrogen is between 10^{-8} and 10^5 Pa. The partial pressure of nitrogen in Eq. [18.36] can be calculated using Eq. [18.37]. In addition, Eq. [18.38] can be used in order to calculate the vapor pressure of uranium over UN in Pascal (Hayes et al., 1990c). The total vapor pressure over UN is the sum of the partial pressures of N_2 and U. Figs. 18.14–18.16 show the partial pressures of nitrogen and uranium over UN as functions of temperature, and the melting point of UN as a function of partial pressure of nitrogen over UN, respectively. In Eqs. [18.37] and [18.38], T is the temperature in K.

$$T_m = 3035.0\left(P_{N_2}/1.01\cdot 10^5\right)^{0.02832} \quad [18.36]$$

$$\log_{10}(P_{N_2}) = 1.01\cdot 10^5\left(1.8216 + 1.882\cdot 10^{-3}T - 23543.4/T\right), \quad 1400 < T < 3170\ \text{K} \quad [18.37]$$

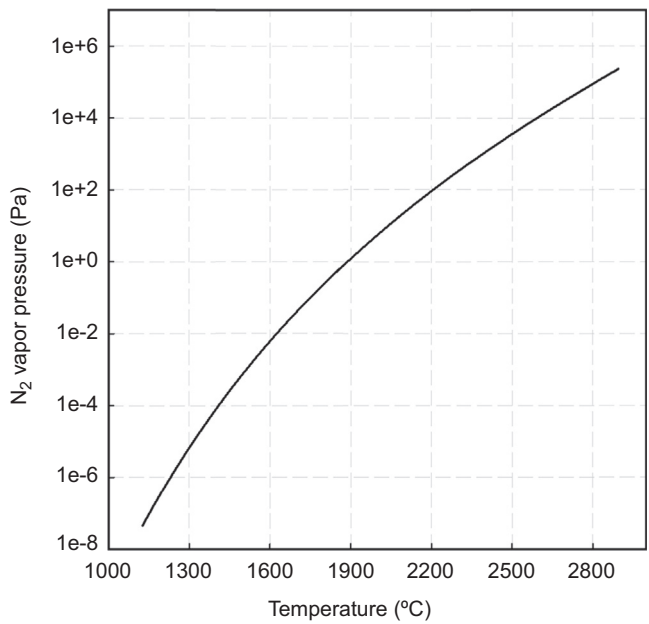


Figure 18.14 Vapor pressure of nitrogen as function of temperature.

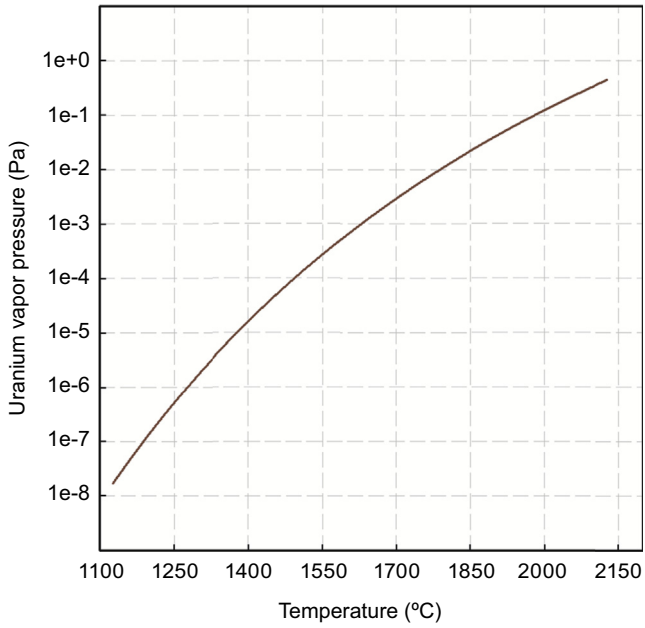


Figure 18.15 Vapor pressure of uranium as function of temperature.

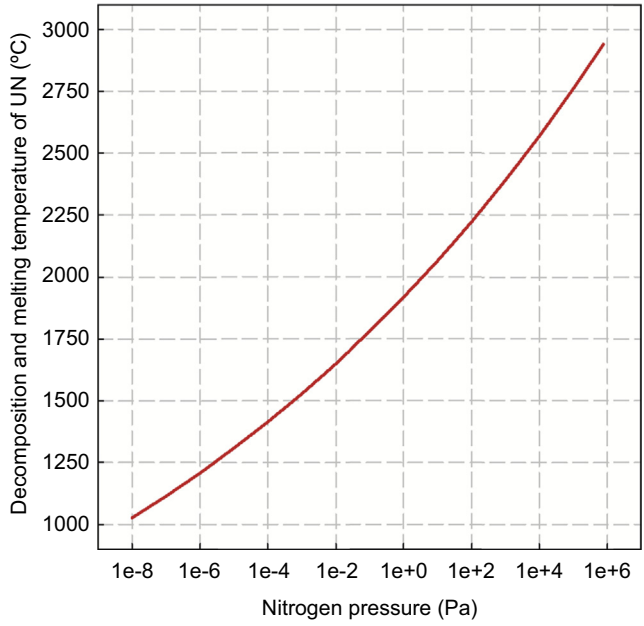


Figure 18.16 Melting point of UN as function of partial pressure of nitrogen.

$$\log_{10}(P_U) = 1.01\cdot 10^5\left(6.9654 - 5.137\cdot 10^{-4}T - 26616.1/T\right), \quad 1400 < T < 2400\ \text{K} \qquad [18.38]$$

Ross et al. (1988) have developed a correlation, shown as Eq. [18.39], for the calculation of the thermal conductivity of UN, in W/m K. In Eq. [18.39], T is the temperature in K. This correlation, which has an uncertainty within ±10%, calculates the thermal conductivity of UN fuel with 100% of *TD*. In general, nuclear fuels are manufactured with porosity to accommodate for the gaseous fission products. Therefore, it is necessary to determine the thermal conductivity of a fuel based on its porosity. Kikuchi et al. (1972) have developed a correlation, shown as Eq. [18.40], which can be used to calculate the effective thermal conductivity of porous UN fuel as a function of percent porosity. In Eq. [18.40], the coefficient β is independent of temperature and has a value of 1.79 ± 0.05 for porosities below 10%. Nevertheless, β becomes temperature dependent when porosity increases beyond 12%. The value of β varies from 1.38 ± 0.12 at 300°C to -0.09 ± 0.05 at 1300°C (Kikuchi et al., 1972).

$$k_{100\%TD} = 1.37\ T^{0.41} \qquad [18.39]$$

$$k_p = k_{100\%TD}\left(\frac{1-P}{1+\beta P}\right) \qquad [18.40]$$

In addition to the Ross et al. correlation, Hayes et al. (1990a) developed another correlation shown as Eq. [18.41], which calculates the thermal conductivity of UN in W/m K. This correlation, which is a function of both temperature and percent porosity, can be applied when porosity changes between 0% and 20% for temperatures in the range of 25−1650°C (Hayes et al., 1990a). Fig. 18.17 shows the thermal conductivity of UN with 5% porosity as a function of temperature, calculated based on the two studied correlations. As shown in Fig. 18.17, the Hayes et al. correlation results in lower thermal conductivity values for temperatures approximately above 700°C. In other words, the Hayes et al. correlation is more conservative than the Ross et al. correlation in the prediction of the thermal conductivity of UN at temperatures above 700°C. In addition, the standard deviation of the Hayes et al. correlation is ±2.3% compared to ±3.2% for the Ross et al. correlation. Therefore, as a conservative approach, the Hayes et al. correlation may be used for the calculation of the thermal conductivity of UN fuel. In Eq. [18.41], T is the temperature in K.

$$k = 1.864\mathrm{e}^{-2.14P}T^{0.361} \qquad [18.41]$$

Hayes et al. (1990c) developed correlations for the calculation of the thermodynamic properties of UN including specific heat, enthalpy, entropy, and Gibbs free energy as functions of temperature; these correlations are shown as Eqs. [18.42]−[18.45],

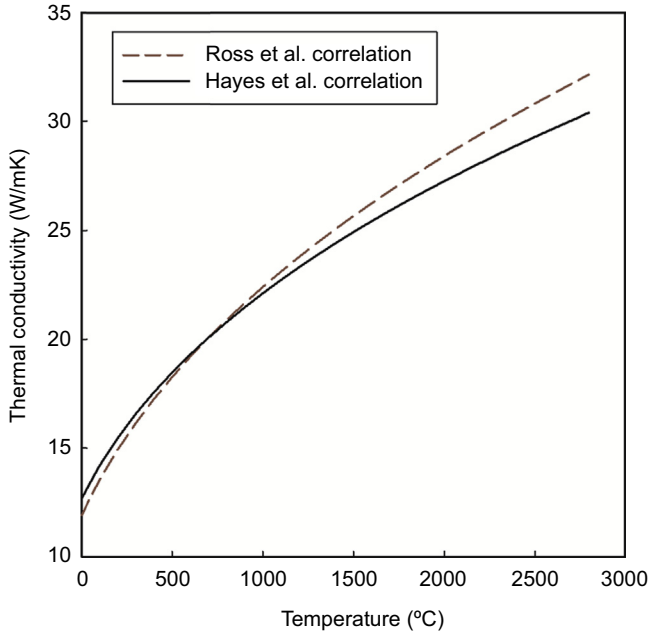


Figure 18.17 Thermal conductivity of 95%*TD* UN fuel.
Based on the Ross, S.B., El-Genk, M.S., Matthews, R.B., 1988. Thermal conductivity correlation for uranium nitride fuel. Journal of Nuclear Materials 151, 313–317 and Hayes, S., Thomas, J., Peddicord, K., 1990a. Material properties of uranium mononitride-III transport properties. Journal of Nuclear Materials 171, 289–299 correlations.

respectively. The specific heat and the entropy are in J/kg K. The enthalpy and the Gibbs free energy are in J/kg. In Eqs. [18.42]–[18.45], T is the temperature in K.

$$c_p = \frac{1000}{252.04}\cdot\left[51.14(\Theta/T)\frac{\exp(\Theta/T)}{[\exp(\Theta/T)-1]^2} + 9.491\cdot10^{-3}\,T + \frac{2.642\times10^{11}}{T^2}\exp(-18{,}081/T)\right] \quad [18.42]$$

$$H(T) - H(298\text{ K}) = \frac{1000}{252.04}\cdot\left[\frac{51.14\Theta}{\exp(\Theta/T)-1} + 4.746\cdot10^{-3}T^2 - 8148.34 + 1.461\cdot10^{7}\exp(-18,081/T)\right] \quad [18.43]$$

$$S = \frac{1000}{252.04} \cdot \left[\frac{51.14(\Theta/T)}{\exp(\Theta/T) - 1} - 51.14 \ln\{1 - \exp(\Theta/T)\} + 9.491 \cdot 10^{-3}\, T + 16.31 \right] \quad [18.44]$$

$$G = \frac{1000}{252.04} \cdot \left[51.14\, T \ln\{1 - \exp(-\Theta/T)\} - 4.746 \cdot 10^{-3} T^2 - 16.31 + 1.461 \cdot 10^{7} \exp(-18,081/T) \right] \quad [18.45]$$

The specific heat correlation is valid for temperatures between 25 and 2355°C, where T is the temperature in K, and Θ is the empirically determined Einstein temperature, which is 92.55°C (365.7 K) for UN. Fig. 18.18 shows the selected thermodynamic properties of UN.

It is essential for a fuel to maintain its structural integrity under the conditions of a nuclear reactor. In other words, the fuel must have an adequate mechanical stability

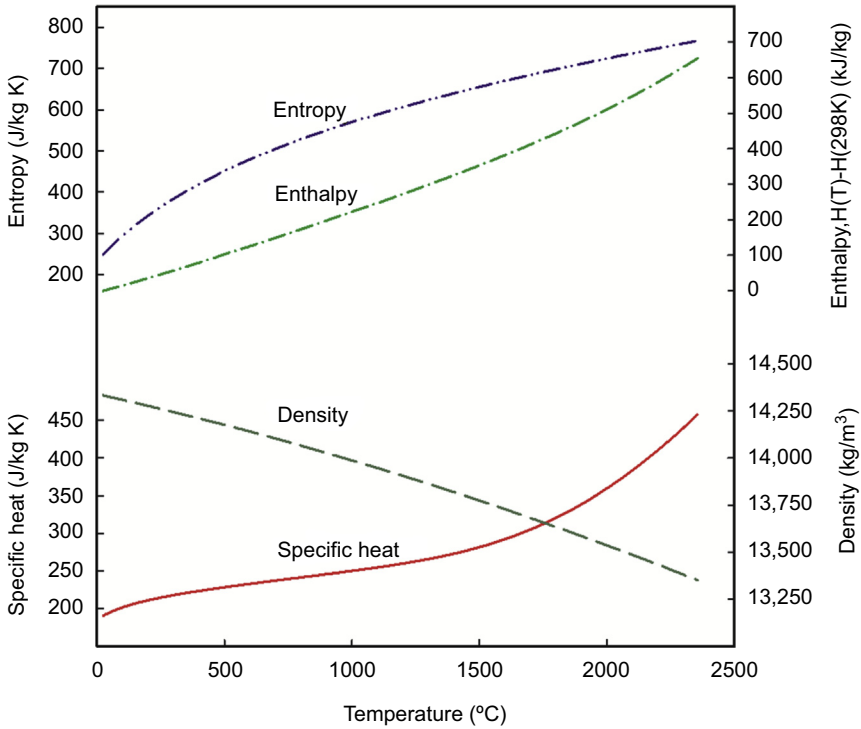


Figure 18.18 Thermodynamic properties of UN as function of temperature.

and withstand stresses under operating conditions. The mechanical stability of a fuel is related to its mechanical properties. Thus, the study of mechanical properties of the fuel is an inseparable part of a safe design.

Mechanical properties of UN such as modulus of elasticity, shear modulus, and Poisson's ratio can be determined using Eqs. [18.46]–[18.48], where E, G, v, and TD are the Young's modulus, Shear modulus, Poisson's ratio, and TD (eg, $TD = 95$ for a fuel with a 95% TD), respectively (Hayes et al., 1990b). Fig. 18.19 shows the Young's modulus and shear modulus of UN, both in MPa, as functions of temperature for 95% TD UN. Eqs. [18.46]–[18.48] were developed based on percent theoretical densities between 70% and 100%; however, they can be used for fuels with higher porosities. In addition, Hayes et al. (1990b) provided a correlation, shown as Eq. [18.49], for the calculation of the hardness of UN in MPa. The latter correlation is valid for temperatures in the range of 25–1400°C, and porosities between 0.0 and 0.26°C. Moreover, the density and linear expansion coefficient of UN, in kg/m^3 and 1/K, can be calculated using Eqs. [18.50] and [18.51], respectively, which are valid for temperatures between 25 and 2250°C (IAEA, 2008). Fig. 18.20 shows the linear thermal expansion of UN as a function of temperature. In Eqs. [18.42]–[18.51], T is the temperature in K.

$$E = 0.258\, TD^{3.002}\left[1 - 2.375\cdot 10^{-5}T\right], \quad 298\ \text{K} < T < 1473\ \text{K} \qquad [18.46]$$

$$G = 1.44\cdot 10^{-2} TD^{3.446}\left[1 - 2.375\cdot 10^{-5}T\right], \quad 298\ \text{K} < T < 1473\ \text{K} \qquad [18.47]$$

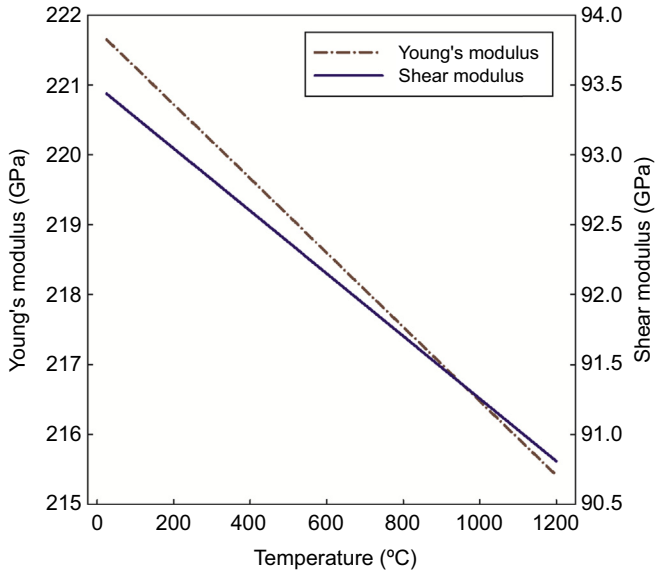


Figure 18.19 Young's and Shear moduli of UN with 95% TD as function of temperature.

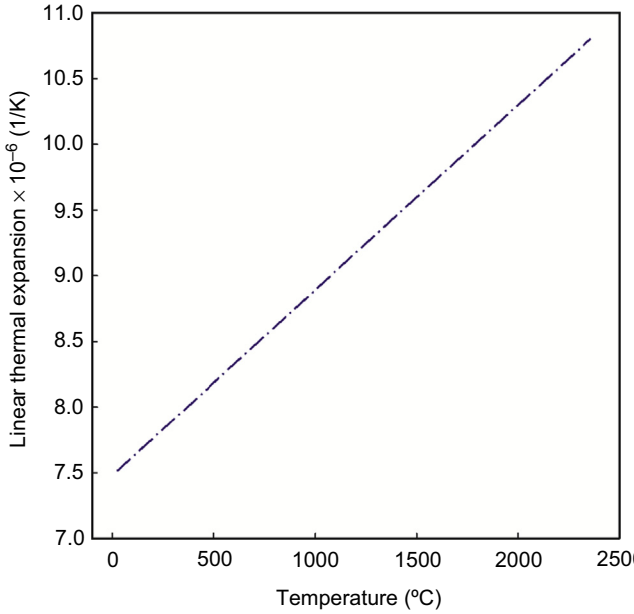


Figure 18.20 Linear thermal expansion of UN as function of temperature.
Based on IAEA, 2008. Thermophysical Properties of Materials for Nuclear Engineering: A Tutorial and Collection of Data (Vienna, Austria).

$$v = 1.26 \cdot 10^{-3} TD^{1.174}, \quad 298\ \text{K} < T < 1473\ \text{K} \tag{18.48}$$

$$HD = 9.807 \cdot \left[951.8\{1 - 2.1P\}\exp\left(-1.882 \cdot 10^{-3} T\right)\right] \tag{18.49}$$

$$\alpha = 7.096 \cdot 10^{-6} + 1.409 \cdot 10^{-9}\ T \tag{18.50}$$

$$\rho = 14,420 - 0.2779\ T - 4.897 \cdot 10^{-5} T^2 \tag{18.51}$$

Irradiation swelling, growth, and creep are the primary effects of irradiation on the fuel. Irradiation swelling results in volumetric instability of the fuel at high temperatures, while irradiation growth causes dimensional instability of the fuel at temperatures lower than two-thirds of the melting point of the fuel (Ma, 1983). In addition to dimensional and volumetric instability, a continuous and plastic deformation of the fuel due to creep may adversely affect its mechanical properties. Thus, it is required to study the behavior of the fuel under irradiation, specifically the irradiation-induced swelling, irradiation-induced growth, and irradiation-induced creep of the fuel.

Ross et al. (1990) have developed a correlation for the calculation of the percent volumetric swelling of UN fuel. This correlation is shown as Eq. [18.52], where T_{avg} is the volume average fuel temperature in K, B is the fuel burnup in MW day/M g(U), and $\rho_{\%TD}$ is the percent TD of the fuel (eg, $\rho_{\%TD}$ equals to 0.95 for a fuel

with 5% porosity). In addition to this correlation, the volumetric swelling of UN can be calculated based on the fuel centerline temperature using Eq. [18.53] (Ross et al., 1990), where T is the temperature in K. The uncertainty of the volumetric swelling correlation, Eq. [18.53], is ±25% for burnups above 10,000 MW day/Mg (U). On the other hand, the uncertainty associated with this correlation increases to ±60% at lower burnups (Ross et al., 1990). Fig. 18.21 shows the volume expansion of UN as a function of temperature for selected burnup values.

$$\Delta V/V(\%) = 4.7 \cdot 10^{-11} T_{\text{avg}}^{3.12} \left(\frac{B}{9008.1} \right)^{0.83} \rho_{\%TD}^{0.5} \quad [18.52]$$

$$\Delta V/V(\%) = 1.16 \cdot 10^{-8} T_{\text{CLT}}^{2.36} \left(\frac{B}{9008.1} \right)^{0.82} \rho_{\%TD}^{0.5} \quad [18.53]$$

In addition, Hayes et al. (1990b) have developed a correlation shown as Eq. [18.54], which gives the steady state creep rate of dense UN with 100% *TD,* in 1/h. In Eq. [18.54], T is the temperature in K. This correlation is valid for temperatures between 1497 and 1810°C and stresses, σ, in the range of 20−34 MPa. To account for the porosity of the fuel, Eq. [18.54] should be multiplied by the creep porosity

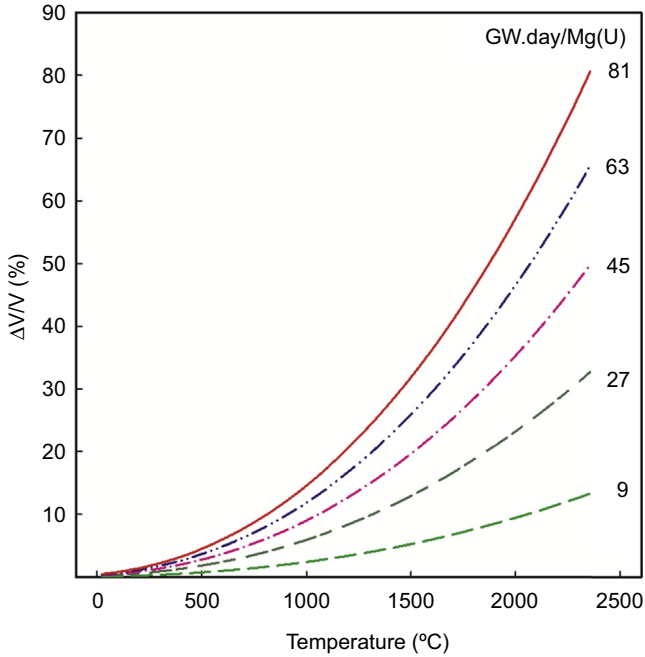


Figure 18.21 Percent volumetric swelling (V/V) of UN as function of burnup and temperature. Based on Ross, S.B., El-Genk, M.S., Matthews, R.B., 1990. Uranium nitride fuel swelling correlation. Journal of Nuclear Materials 170, 169−177.

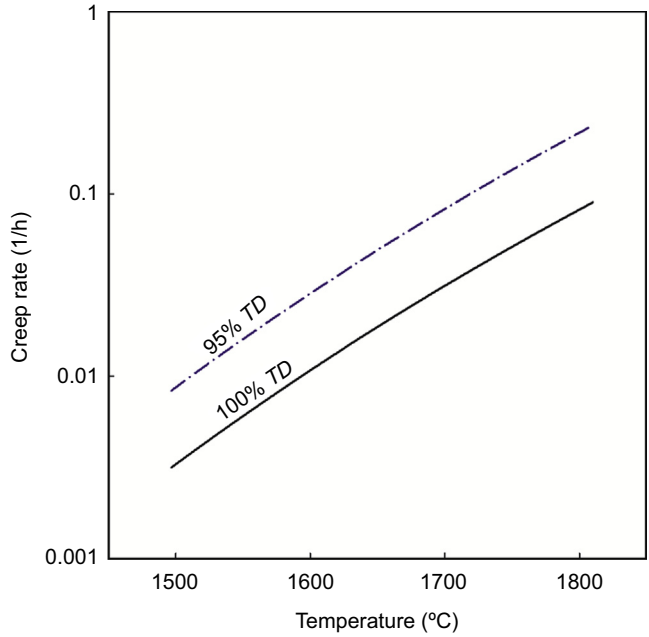


Figure 18.22 Steady state creep rate of UN at 25 MPa stress as function of temperature. Based on Hayes, S., Thomas, J., Peddicord, K., 1990b. Material property correlations for uranium mononitride-II mechanical properties. Journal of Nuclear Materials 171, 271−288.

correlation factor shown as Eq. [18.55] (Hayes et al., 1990b). In Eq. [18.55], P is the porosity in volume fraction. Fig. 18.22 shows the creep of UN with 100% *TD* and 95% *TD* as a function of temperature for a stress value of 25 MPa. Fig. 18.22 also indicates that the creep rate increases by increasing the porosity.

$$\dot{\varepsilon} = 3600 \cdot 2.054 \cdot 10^{-3} \sigma^{4.5} \exp(-39,369.5/T) \quad [18.54]$$

$$f(P) = \frac{0.987}{(1-P)^{27.6}} \exp(-8.65\,P) \quad [18.55]$$

18.3.4 Discussion

The most important factors associated with nuclear fuels for high-temperature applications include melting point, phase change, evaporation, high-temperature chemical stability, release of fission products, radiation-induced swelling, thermal-shock resistance, density, high-temperature creep, and mass of fissile elements (Lundberg and Hobbins, 1992). High thermal conductivity fuels (eg, UN and UC) have high melting points and high thermal conductivities, which lead to lower fuel centerline temperatures compared to those of low thermal conductivity fuels (eg, UO_2, MOX, or ThO_2) for a given thermal power. Thus, the other factors should be considered in order to determine the best fuel option(s).

One of these factors is phase change. Among high thermal conductivity fuels, UC_2 undergoes a phase change at temperatures within the range between 1765°C (Bowman et al., 1966) and 1820°C (Frost, 1963). This phase change results in an increase in the volume of the fuel, which in turn may jeopardize the mechanical integrity of the fuel and the sheath. This phase change significantly reduces the possibility of using UC_2 as a nuclear fuel in high-temperature applications. As a result, a comparison of the other factors has been drawn mainly among UN, UC, and UO_2. The latter fuel has been taken into consideration because UO_2 is widely used in nuclear reactors.

The atom density of uranium is another important factor, especially in fast neutron spectrum reactors because fission probability is significantly lower for fast neutrons compared to those of thermal neutrons. Both UN and UC have high uranium atom density, approximately 1.40 and 1.34 times that of UO_2. Hence, use of UC or UN leads to smaller core sizes compared to that of UO_2 fuel.

Stellrecht et al. (1968), Routbort (1972), Routbort and Singh (1975), and Hayes et al. (1990b) studied the steady state creep strength and irradiation-induced creep of UN and UC fuels, and provided several correlations for the calculation of the steady state and irradiation-induced creep rates. These correlations can be used in order to predict the mechanical behavior of these fuels (eg, dimensional stability and integrity) under operating conditions. Further studies have calculated the creep rates of fully dense UN and UC for a stress of 25 MPa (see Figs. 18.22 and 18.10). In terms of irradiation-induced creep, both UN and UC have significantly lower irradiation-induced creep rates compared to UO_2 (Routbort and Singh, 1975). The results demonstrate that when UC and UN fuels are compared, the irradiation-induced creep rate of UC was lower than of UN at 1500°C. In other words, UC has a better creep strength and resistance to deformation than UN. With UC fuel, it is recommended to use hyperstoichiometric UC (Routbort, 1972) because it has a lower steady state creep rate compare to hypostoichiometric UC. In addition, hyperstoichiometric UC has a higher mechanical strength than hypostoichiometric UC due to higher values of long-range stress (Routbort, 1972), which result in higher proportional limit values. As a result, hyperstoichiometric UC has better mechanical behavior at high temperatures than hypostoichiometric UC and UN.

In addition to creep resistance, hardness is another mechanical property, which is an indication of the resistance of a material to deformation. Routbort and Singh (1975) have identified the grain size, porosity, impurity contents, C/U or N/U ratios, and temperature as the most important factors affecting the hardness. They also have provided the hardness values at room temperature and 1000°C for UC and UN. For both UN and UC, the hardness decreases as the temperature increases. According to Routbort and Singh (1975), the hardness values, in kg/mm^2, are 100, 120, and 50 for $UC_{1.05}$, $UC_{0.98}$, and UN, respectively. The result of their investigation shows that UC has a higher hardness compared to UN; therefore, UC has a higher resistance against deformation, which in turn increases the mechanical integrity of the fuel under operating conditions of high-temperature nuclear applications.

The fission reaction in a nuclear fuel results in the production of gaseous fission products. These fission products are either contained in the fuel or released, which in turn exert stress on the sheath. In addition, the containment of the fission products

in the fuel results in the swelling (eg, a reduction in density due to a volume increase) of the fuel. Thus, it is essential to study the swelling rate of nuclear fuels to ensure that the fuel and the cladding will withstand the stresses exerted on them and maintain their mechanical integrity under the operating conditions of a nuclear reactor, especially when high burnups are required.

A comparison between the volumetric swelling of UN and UC fuels shows that the percent volumetric swelling of UN is higher than that of UC (see Figs. 18.21 and 18.9). For instance, the percent volumetric swelling of UN is approximately 17% and that of UC 12%, approximately at 1400°C and a burnup of 40 GW day/Mg(U). It should be noted that the temperature of 1400°C has been chosen because of the available experimental data related to the swelling of UC. In addition, it should be noted that the swelling of both fuels can be reduced by increasing the porosity of the fuel (Frost, 1963). In contrast, Ma (1983) demonstrates that the fission gas release is higher for porous fuels compared with dense fuels, which have less porosity. Nevertheless, UC has a lower percent volumetric swelling compared to UN.

The thermal shock resistance of a nuclear fuel is an indication of the degree to which the fuel withstands sudden changes in temperature. A low thermal shock resistance may result in the formation of cracks in the fuel, which in turn reduces the mechanical integrity of the fuel and increases the fission product release rate. As indicated by Eq. [18.56] (Kutz, 2005), the thermal shock resistance of a fuel depends on its thermal conductivity, compressive strength, Poisson's ratio, the coefficient of thermal expansion, and Young' modulus of elasticity. The thermal shock resistances of UC, UN, and UO_2 have been calculated based on Eq. [18.56] for a temperature range between 800 and 1800°C. In Eq. [18.56], R' is the thermal shock resistance in W/m, k is the thermal conductivity in W/mK, σ is the compressive strength in MPa, ν is the Poisson's ratio, α is the coefficient of thermal expansion in cm/cm K, and E is the Young' modulus of elasticity in MPa. All required properties were determined for 95% *TD* fuels except the linear thermal expansion coefficient, which was based on 100% *TD* fuels. The result shows that the thermal shock resistances of both UN and UC are 5−15 times higher than those of UO_2 within the examined temperature range. The low thermal shock resistance of UO_2 is mostly due to its low thermal conductivity, which makes this fuel vulnerable to sudden temperature changes at high operating temperatures. Thus, UN and UC have significantly higher thermal shock resistances compared with UO_2 and are more suitable for high-temperature applications.

$$R' = \frac{k \cdot \sigma(1-\nu)}{\alpha \cdot E} \qquad [18.56]$$

The chemical compatibility of a nuclear fuel with coolant, which is an essential factor that affects the integrity of the fuel, can be studied in terms of the oxidation behavior of the fuel when exposed to the coolant. For instance, UO_2 fuel is stable in water and has a high oxidation resistance in light water and heavy water at the LWR and heavy water reactor conditions (eg, up to 320°C). However, UO_2 oxidizes at temperatures above 320°C if it comes in direct contact with air or water in the case of

a sheath breach (Ma, 1983). Similarly, UC has a poor oxidization resistance when it comes in contact with water, even at temperatures as low as 55°C (Ma, 1983). Likewise, UN oxidizes in water at temperatures above 100°C due to the deformation of the protective layer, which is formed on the surface of UN. The protective layer on the surface of UN is eventually lost at high temperatures, and cracks are formed. In addition, the oxidization resistance of UN is highly dependent on deviation from stoichiometry (Ma, 1983). In other words, the presence of free uranium or U_2N_3 significantly increases the oxidization rate. On the other hand, Kirillov et al. (2007) imply that UC and UN have better compatibility with coolant and cladding compared to UO_2. Therefore, further study is required on the chemical compatibility of UC and UN with water due to the discrepancy between the two available sources.

In terms of high-temperature stability, a great number of studies have been conducted on hypostoichiometric and hyperstoichiometric UN. The results of these studies indicate that hyperstoichiometric UN coexists with U_2N_3 in the temperature range of 1075−1375°C for hyperstoichiometric UN with N/U atomic ratios approximately between 1.2 and 1.5°C (Matthews et al., 1988). According to the phase diagram provided by Matthews et al. (1988), U_2N_3 decomposes to UN and nitrogen at temperatures approximately above 1375°C. The release of nitrogen gas results in severe cracking of the fuel. This problem can be solved by using hypostoichiometric UN. However, it should be noted that Matthews et al. (1988) demonstrate that the fission gas release rate is higher for hypostoichiometric UN than hyperstoichiometric UN. If UN is chosen as a nuclear fuel, hypostoichiometric UN with adequate porosity should be utilized in order to minimize the negative impacts of the decomposition of U_2N_3 and accommodate for the fission products.

Another issue related to UN fuel is that hypostoichiometric UN decomposes to uranium and nitrogen gas, which leads to cracking of the fuel due to the release of nitrogen. The results of several studies have shown that the incongruent vaporization of hypostoichiometric UN leads to the release of nitrogen and the formation of free uranium (Balankin et al., 1978). Balankin et al. (1978) report of the appearance of free uranium in the temperature range between 1500 and 1800°C. Moreover, Gingerich (1969) indicates that the incongruent vaporization of hypostoichiometric UN occurs in the temperature range between 1130 and 1800°C for N/U atomic ratios of 1.0 and 0.92, respectively. Gingerich (1969) also provides the results of experiments, which were conducted by Covert and Bonham, Vozzella and DeCrescente, and Inouye and Leitnaker, on the decomposition of UN. Their experimental results, which are in agreement with Gingerich's results, indicate that incongruent decomposition of UN occurs at temperature ranges of 1600−2000°C (based on Covert and Bonham), 1645 and 1992°C (based on Vozzella and DeCrescente), and 1300°C (based on Inouye and Leitnaker). In addition, Oggianu et al. (2003) indicate that UN dissociates at temperatures higher than 1600°C, which is in agreement with other values published in the literature. Therefore, the release of nitrogen gas and formation of cracks in the fuel should be studied thoroughly if UN is chosen as the fuel of choice for high-temperature applications, but it should be mentioned that this effect might not be significant when the maximum fuel temperature of UN fuel is below 1300°C under normal operating conditions.

The study of neutronic properties of a nuclear fuel is as essential as analyzing its thermodynamic and mechanical properties. Oggianu et al. (2003) draw a comparison between neutronic properties of UO_2, UC, and UN, which have been summarized in Table 18.4. According to Oggianu et al. (2003), UN has higher fission and absorption cross sections for the thermal neutrons than UC. These two parameters can be used to calculate the fission-to-capture ratio, which indicates that 43.7% of absorbed neutrons results in fission in UN fuel compared to 54.3% in UC. This shows that a higher neutron economy is achieved when UC fuel is used. It should be noted that the fission-to-capture ratio for UO_2 is higher than that of UC. On the other hand, UO_2 has a smaller uranium atom density compared to those of UN and UC. A high uranium atom density indicates a smaller core size, which in turn reduces the costs. Thus, both UN and UC result in smaller core sizes.

It is beneficial to demonstrate an economic assessment among UO_2, UC, and UN fuels in order to provide a comparison between the fuel cycle costs of these fuels. The result of the study conducted by Oggianu et al. (2003) shows that the cost of fuel is lower for UC compared to UN (Oggianu et al., 2003). This higher fuel cost for UN might be due to the necessity to enrich nitrogen to ^{15}N to avoid the formation of ^{14}C. Oggianu et al. (2003) have calculated the cost of the fuel cycle plus the cost of forced outages, which indicates that still the overall cost is lower for UC fuel. Thus, UC fuel is economically more attractive than UN fuel.

As has been noted, each fuel exhibits both desirable and detrimental properties, all of which should be considered to ensure that the integrity and longevity of the fuel in the reactor is maintained. The study of the deleterious behavior of these fuels provides the means to select the most suitable fuel for the use in advanced reactors. As a summary, the perceived issues associated with UO_2, UN, and UC fuels have been listed in Table 18.5.

With an objective to illustrate the difference in fuel temperatures of the low thermal conductivity and high thermal conductivity fuels, a thermal power distribution inside a reactor core was calculated based on the neutronic properties of a fresh and symmetric core of a pressure channel (PCh) supercritical water-cooled reactor (SCWR).

Table 18.4 Neutronic properties of UO_2, UC, and UN (Oggianu et al., 2003)

Parameter	UO_2	UC	UN
Fission cross section for natural uranium (at 0.025 eV), cm^{-1}	0.102	0.137	0.143
Absorption cross-section for natural uranium (at 0.025 eV), cm^{-1}	0.185	0.252	0.327
$\alpha = \Sigma_c/\Sigma_f$ (capture to fission ratio)	0.831	0.839	1.286
η (average number of neutrons emitted per neutron absorbed)	1.34	1.34	1.08
Uranium atom density based on 100% theoretical density, g/cm^3	9.67	12.97	13.52

Table 18.5 Issues related to UO_2, UN, and UC fuels

Fuel	Problem		References
UO_2	Low thermal conductivity and high linear thermal expansion coefficient at high temperatures		INSC (2010)
	Low thermal shock resistance at high operating temperatures (eg, above 1100°C)		–
	Higher irradiation-induced creep than UN and UC		Routbort and Singh (1975)
	High fission product at $T > 1725$°C		Lundberg and Hobbins (1992)
	High evaporation rate		Lundberg and Hobbins (1992)
	Lower uranium density compared to UC and UN		Ma (1983)
	Lower fuel density compared to UC and UN		Ma (1983)
UN	UN dissociates at	$T > 1130$°C	Gingerich (1969)
		$T > 1500$°C	Balankin et al. (1978)
		$T > 1600$°C	Oggianu et al. (2003)
	Hyperstoichiometric UN coexists with U_2N_3, which decomposes to UN and nitrogen at temperatures approximately above 1375°C		Matthews et al. (1988)
	Higher irradiation-induced creep compared with UC		Routbort and Singh (1975)
	Oxidation reaction with water		Oggianu et al. (2003)
	Relatively higher volumetric swelling compared with UO_2		Ross et al. (1990)
	The necessity to enrich in ^{15}N to minimize the ^{14}C production		Oggianu et al. (2003)
	Lower hardness compared with UC		Routbort and Singh (1975)
	Relatively high gaseous fission products release from hypostoichiometric UN		Matthews et al. (1988)
UC	Speculative chemical compatibility with water (eg, reacts with water)		Ma (1983); Kirillov et al. (2007)
	Relatively higher volumetric swelling compared with UO_2		Frost (1963)
	~12% lower melting point compared with UO_2 and UN		Cox and Cronenberg (1977) Lundberg and Hobbins (1992)

The analyzed reactor core consists of 336 high-efficiency reentrant fuel channels. The inlet temperature of the coolant is 350°C at a pressure of 25 MPa, and the outlet temperature is 625°C. As a conservative approach, the thermal power corresponding to a fuel channel with the maximum thermal power was used in order to calculate the fuel centerline and sheath temperatures with the use of a one-dimensional thermal–hydraulic code. The temperature variation of the fuel hottest element in the radial direction is shown in Fig. 18.23. The maximum fuel centerline temperature of the UO_2 fuel reaches 2196°C in the hottest fuel element of a fuel channel with a maximum thermal power of 10.23 MW_{th}. The temperature profiles of the coolant and the cladding (ie, CLaDding Temperature (CLDT)), as well as the Heat Transfer Coefficient (HTC) are shown in Fig. 18.24.

Fig. 18.25 shows heat-flux profiles used in the calculation of the fuel centerline and cladding temperatures.

It should be noted that there are many power/heat flux profiles in a reactor core. In other words, the axial heat flux profile (AHFP) in each fuel assembly differs from those of the other fuel assemblies. This variation in power profiles is due to the radial and axial power distribution, fuel burnup, presence of reactivity control mechanisms, and refueling scheme. Considering the shape of AHFPs, these heat flux profiles can be categorized as cosine, upstream-skewed cosine, and downstream-skewed cosine. In terms of the sheath/cladding and fuel centerline temperatures, upstream-skewed cosine AHFP is the most ideal heat flux profile, as it results in lower cladding and fuel centerline temperatures. On the other hand, the downstream-skewed cosine AHFP results in the highest temperatures. Thus, for design purposes, it is a

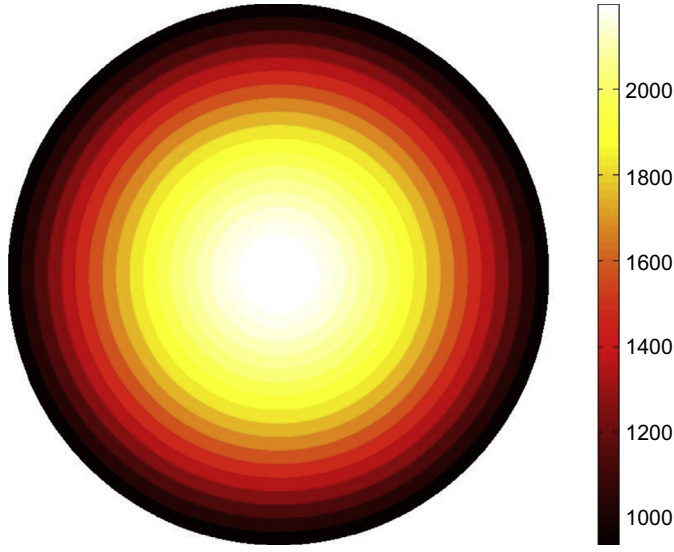


Figure 18.23 Temperature variation in degrees Celsius across UO_2 fuel element at location of maximum temperature.

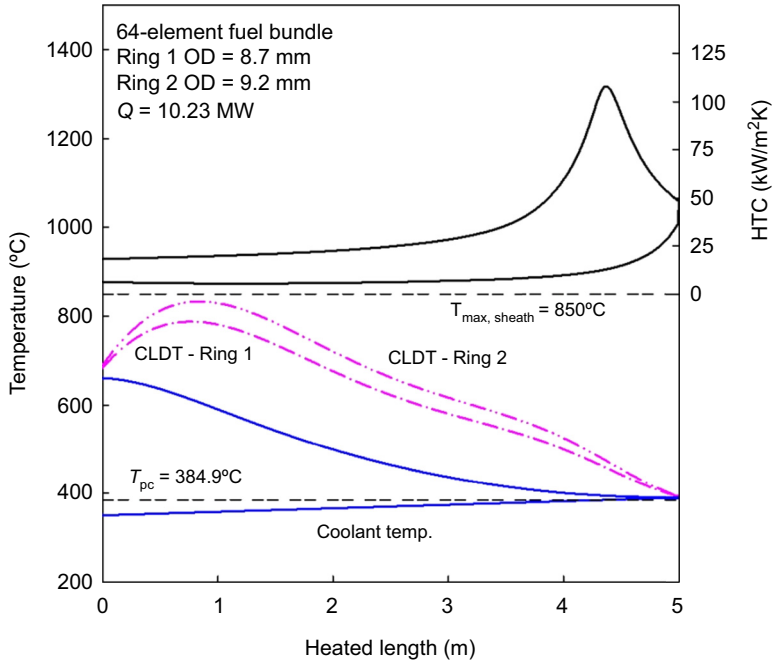


Figure 18.24 Coolant- and cladding- (sheath-) temperature profiles and Heat Transfer Coefficient (HTC) variation along fuel channel (CLDT).

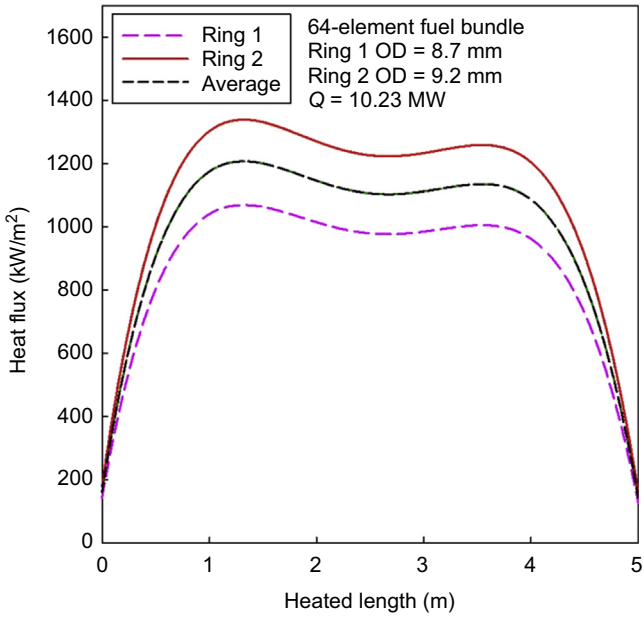


Figure 18.25 Heat-flux profiles associated with UO_2 fuel elements in Ring 1 and Ring 2 of fuel bundle and average heat flux for fuel channel with maximum thermal power of 10.23 MW.

conservative approach to determine the sheath and fuel centerline temperatures based on a downstream-skewed AHFP.

For the same fuel bundle design and heat flux profile, a high thermal conductivity fuel such as UC or UO_2−silicon carbide (SiC) shows significantly less fuel centerline temperatures. Figs. 18.26 and 18.27 show the temperature variation of the fuel hottest

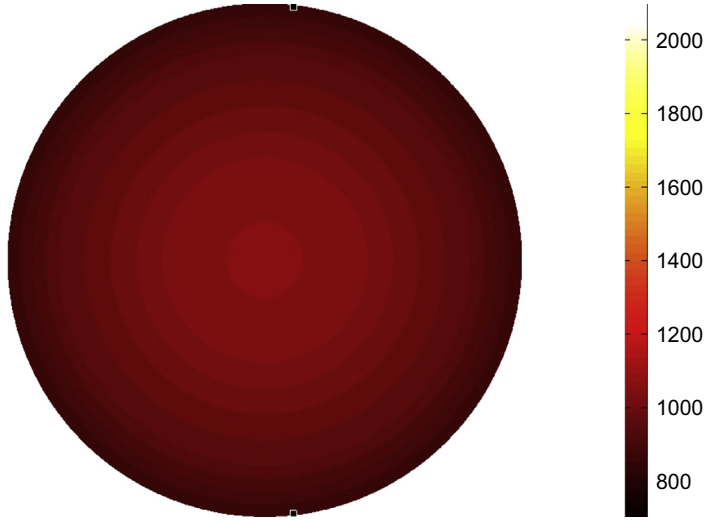


Figure 18.26 Temperature variation in degrees Celsius across UC fuel element at location with maximum temperature.

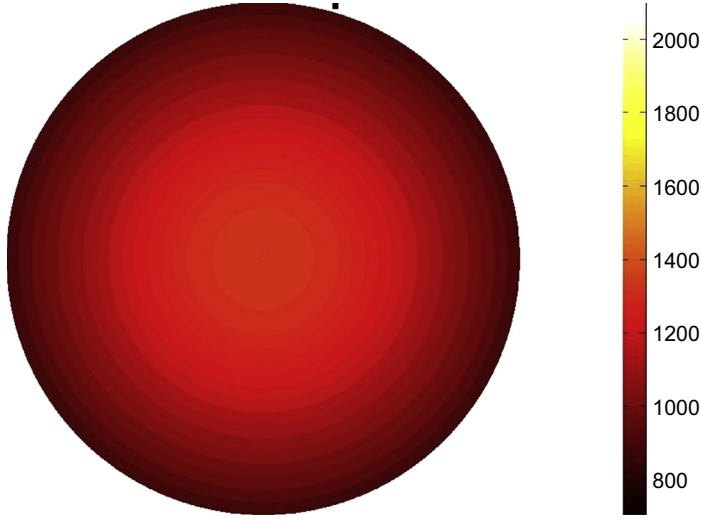


Figure 18.27 Temperature variation in degrees Celsius across UO_2−SiC fuel element at location with maximum temperature.

element in the radial direction, respectively, for UC and UO_2−SiC. The maximum fuel centerline temperature of UC is approximately 1063°C. Similarly, the maximum fuel centerline temperature for UO_2−SiC reaches 1312°C.

In another study, Kovaltchouk et al. (2015a) calculated the power distribution inside the core of a PCh SCWR with the high-efficiency re-entrant channel and the 64-element fuel bundle as their reference fuel channel and fuel bundle. Similarly, Kovaltchouk et al. (2015b) calculated the power distribution based on the high-efficiency channel and the 78-element fuel bundle. In order to determine the power distribution inside the core, Kovaltchouk et al. (2015a,b) conducted thermal−hydraulic and neutronic coupling with the use of a diffusion code, DONJON, and an in-house one-dimensional thermal−hydraulic code. In both studies, the maximum fuel temperature was calculated for two cases. In the first case, the fuel centerline temperature was calculated for a homogenous mixture of ThO_2 and PuO_2. In the second case, a two-layer fuel was modeled where ThO_2 was located at the center of each fuel pin, while PuO_2 was modeled as the medium of the outer layer. The results of their analyses showed that the maximum fuel temperature is significantly lower for the two-layer fuel.

18.4 Hydride fuels

18.4.1 Uranium−zirconium hydride fuel

A promising fuel for future use in light-water reactors is the hydride fuel, which has been used in Training, Research, Isotopes, General Atomics (TRIGA) reactors. In the uranium−zirconium hydride fuel, U−$ZrH_{1.6}$, uranium metal phase is dispersed in the continuous $ZrH_{1.6}$ phase. The density of the hydride fuel is 8.256 g/cm^3. The atom density of uranium in U−$ZrH_{1.6}$ is less than that of the oxide fuels (ie, UO_2). Hence, a higher enrichment of uranium is required in order to achieve the same burnup with the same power density (Galahom et al., 2014). The thermal conductivity of U−$ZrH_{1.6}$ is significantly higher than that of oxide fuels such as UO_2. High thermal conductivity reduces the temperature gradient across the fuel, which in turn decreases the release of gaseous fission products (Olander et al., 2009). Simnad (1980) recommended a thermal conductivity of 17.6 ± 0.8 W/m K for design purposes. An investigation showed that for U−$ZrH_{1.6}$ with a hydrogen-to-zirconium ratio of 1.6, the thermal conductivity is insensitive to temperature and weight fraction of uranium (Simnad, 1980).

Tsuchiya et al. (2001) calculated the thermal conductivity of U−ZrH_x for hydrogen-to-zirconium ratios between 1.6 and 2.0 ($1.6 \leq x \leq 2.0$) (see Fig. 18.28). Tsuchiya et al. (2001) experimentally measured the thermal diffusivity of ZrH_x and calculated the thermal conductivity based on the relationship among the thermal diffusivity, density, and specific heat. Further, they calculated the thermal conductivity of U−ZrH_x using the rule of mixture as expressed in Eq. [18.57]. In Eq. [18.57], V_i and k_i are the volume fraction and thermal conductivity of the constituent phase i.

$$k_{\mathrm{U–ZrH}_x} = V_{\mathrm{U}} k_{\mathrm{U}} + V_{\mathrm{ZrH}_x} k_{\mathrm{ZrH}_x} \qquad [18.57]$$

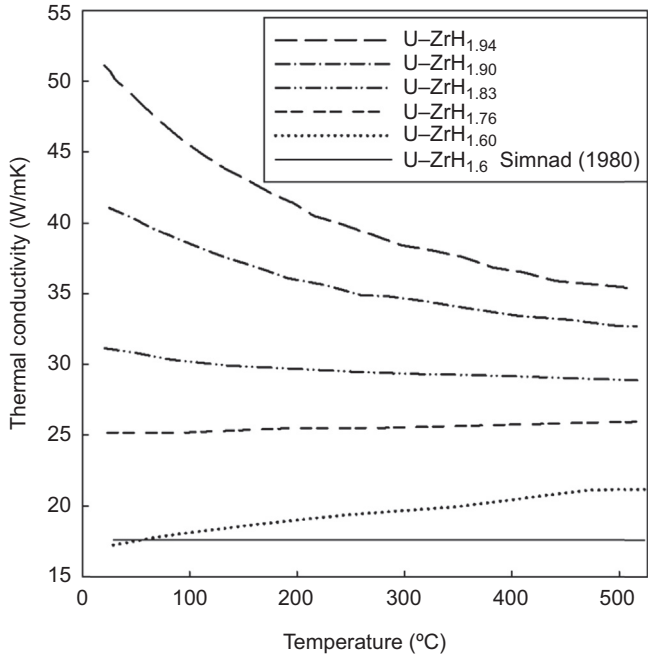


Figure 18.28 Thermal conductivity of U−ZrH_x (Simnad, 1980; Tsuchiya et al., 2001).

In addition to its relatively high thermal conductivity, another advantage of U−$ZrH_{1.6}$ fuel is that it has a large prompt negative temperature coefficient of reactivity (Zakova, 2012), which is caused by higher fuel temperatures due to an increase in reactor power. The reduction in reactivity, in turn, reduces the reactor power and hence the fuel temperature. On the other hand, U−$ZrH_{1.6}$ has a large fission product swelling, which is approximately three times that of oxide fuels. Due to large early swelling rates of the fuel, the maximum design temperature limit of the fuel is around 750°C for steady state conditions and 1050°C during transients (Olander et al., 2009). Fig. 18.29 shows the swelling of U−$ZrH_{1.6}$ as a function of burnup (Huang et al., 2001).

U−$ZrH_{1.6}$ has chemical compatibility with water. Zirconium hydride has low reactivity rates when exposed to water, steam, or air up to temperatures around 600°C. The corrosion rate of the fuel is very low. The results of water quench tests, for the purpose of investing the corrosion resistance and thermal shock resistance of the fuel, have shown no damaging effects on the fuel heated to 800°C. A surface discoloration was observed when fuel samples, which were heated up to 900°C, were quenched in water. Further experiments with fuel rods heated up to 1200°C showed cracks on the fuel pellets after being quenched in water. Nevertheless, no safety concern was caused, and the pellets were in good condition (Simnad, 1980).

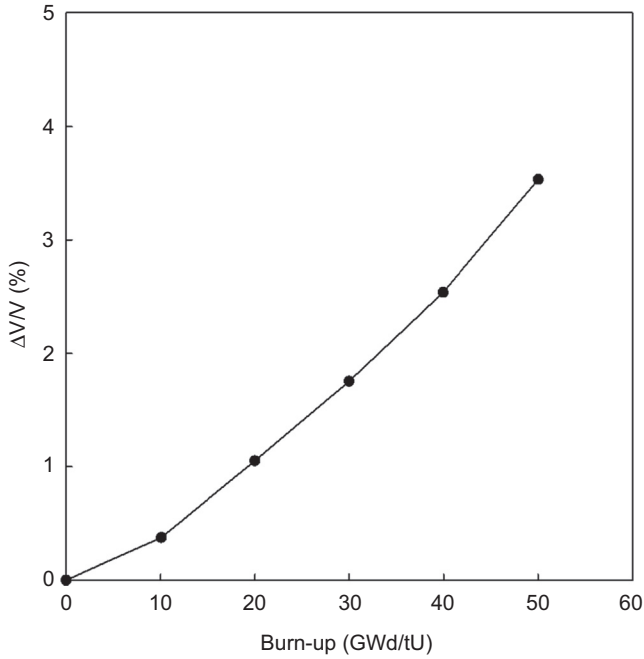


Figure 18.29 Calculated solid swelling of U−$ZrH_{1.6}$ with 45 wt% uranium as a function of burnup at 600°C (873 K) (Huang et al., 2001).

18.4.2 Uranium−thorium−zirconium fuels

Uranium−thorium−zirconium fuels ($UTh_4Zr_{10}H_x$) are also of interest due to a significant amount of thorium resources and utilization of the fuels in breeder reactors. In $UTh_4Zr_{10}H_x$, metallic uranium is dispersed in $ThZr_2H_{7-x}$ and ZrH_{2-x} hydrides. Similar to U−ZrH1.6, $UTh_4Zr_{10}H_x$ ($x = 20$, 24, and 27) fuels have higher thermal conductivities compared to those of oxide fuels, such as UO_2 and ThO_2. Tsuchiya et al. (2000) calculated the thermal conductivity of three $UTh_4Zr_{10}H_x$ ($x = 20$, 24, and 27) fuels. The thermal conductivities are shown in Fig. 18.30 as a function of temperature.

The density of $UTh_4Zr_{10}H_x$ fuels is calculated using Eq. [18.58] as a function of the ratio of hydrogen to UTh_4Zr_{10} at a temperature of 296 K. In comparison with UO_2, which has a density of 10,960 kg/cm^3, the density of uranium−thorium hydride fuels are less. For instance, the density of $UTh_4Zr_{10}H_{20}$ is estimated to be 7.8 g/cm^3 at 25°C (298 K) based on Eq. [18.58].

$$\rho = 8.40 - 2.99 \times 10^{-2}x \qquad [18.58]$$

The specific heat of $UTh_4Zr_{10}H_x$ ($x = 20$, 24, and 27) can be calculated using Eq. [18.59]. Fig. 18.31 shows the specific heat of $UTh_4Zr_{10}H_{20}$, $UTh_4Zr_{10}H_{24}$, and

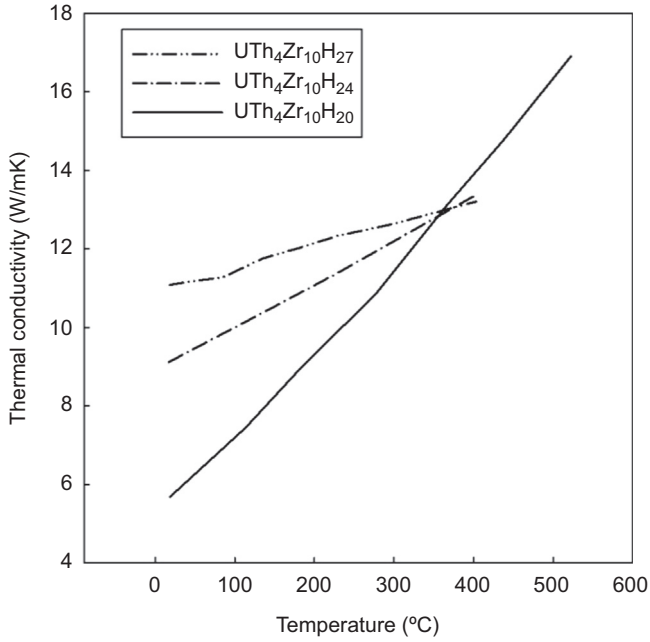


Figure 18.30 Thermal conductivity of $UTh_4Zr_{10}H_x$ as a function of temperature (Tsuchiya et al., 2000).

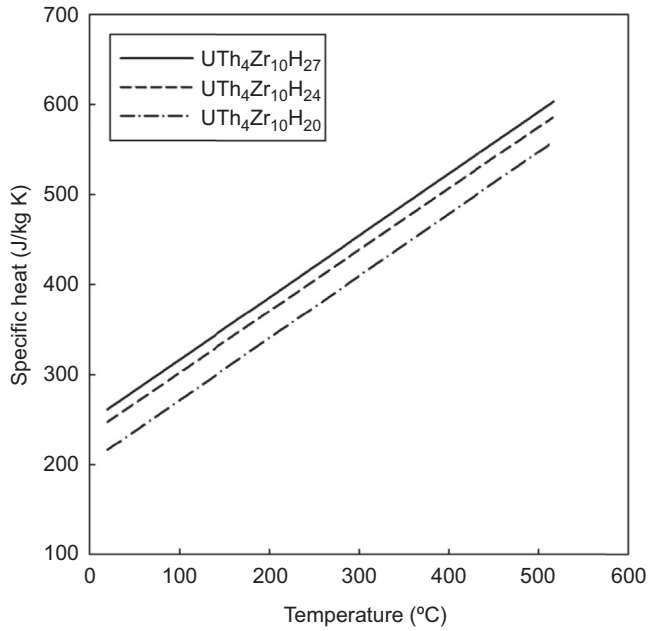


Figure 18.31 Calculated specific heats of $UTh_4Zr_{10}H_{20}$, $UTh_4Zr_{10}H_{24}$, and $UTh_4Zr_{10}H_{27}$ (Tsuchiya et al., 2000).

$UTh_4Zr_{10}H_{27}$ fuels as a function of temperature based on Eq. [18.59] (Tsuchiya et al., 2000). The calculated specific heat values based on Eq. [18.59] are in kJ/kg K, and the temperature is in K.

$$C_p = -0.110 + 6.87 \times 10^{-4}T + 6.36 \times 10^{-3}x \quad [18.59]$$

18.5 Composite fuels

Over the past decade, there has been a great interest in developing high thermal conductivity fuel and/or improving the thermal conductivity of low thermal conductivity fuels, such as UO_2. High thermal conductivities result in lower fuel centerline temperatures and limit the release of gaseous fission products (Hollenbach and Ott, 2010). As shown previously, UO_2 has a very low thermal conductivity, especially at high temperatures compared to other fuels such as UC, UC_2, and UN. However, research has shown that the thermal conductivity of oxide fuels such as UO_2 can be increased by either adding a continuous solid phase or long, thin fibbers of a high thermal conductivity material (Hollenbach and Ott, 2010; Solomon et al., 2005).

A high thermal conductivity material must have a low neutron absorption cross section depending on the reactor (Hollenbach and Ott, 2010). In addition, it must have a high melting point and be chemically compatible with the fuel, the cladding, and the coolant. The need to meet these requirements narrows the potential materials to SiC, beryllium oxide (BeO), and C. The following sections provide a literature survey on UO_2 fuels composed of SiC, C, and BeO.

18.5.1 Uranium dioxide–silicon carbide

The thermal conductivity of UO_2 fuel can be improved by incorporating SiC into the matrix of the fuel. SiC has a high melting point approximately at 2800°C, high thermal conductivity (78 W/m K at 727°C), high corrosion resistance even at high temperatures, low thermal neutron absorption, and dimensional stability (Khan et al., 2010). Therefore, when used with UO_2, SiC can address the problem of the poor thermal conductivity of UO_2 fuel.

Calculation of the thermal conductivity of UO_2 plus SiC fuel falls under the theories of composites. Generally, theories contemplating the thermal conductivity of composites are classified into two categories. One category assumes that inclusions are randomly distributed in a homogeneous mixture. The effective thermal conductivities (ETCs) of the composites, based on the aforementioned principle, are formulated by Maxwell. The other category, which is based on the work performed by Rayleigh, assumes that particles are distributed in a regular manner within the matrix.

Khan et al. (2010) provided the thermal conductivity of UO_2–SiC fuel as a function of temperature and weight percent of SiC. Khan et al. (2010) assumed that the thin coat of SiC covered UO_2 particles and determined the thermal conductivity of the composite fuel for three cases. These cases, which are described in the following paragraph, were solved based on the Rayleigh equation shown as Eq. [18.60] (Khan et al., 2010).

$$k_{\text{eff}_{R(\psi)}} = k_{\text{SiC}} \cdot \left[1 + 3 \frac{\psi}{\left[\frac{k_{\text{UO}_2} + 2 \cdot k_{\text{SiC}}}{3k_{\text{UO}_2} - k_{\text{SiC}}}\right] - \psi + 1.569 \left[\frac{k_{\text{UO}_2} - k_{\text{SiC}}}{3k_{\text{UO}_2} - 4k_{\text{SiC}}}\right] \cdot \psi^{10/3}} \right] \quad [18.60]$$

In Case I, it was assumed that all UO_2 particles are completely covered within a layer of SiC. In Case II, the coating on UO_2 particles is not complete. In other words, it was assumed that there were blocks of UO_2 covered with SiC along the radial direction of the fuel. Finally, in Case III, it was assumed that there were blocks of UO_2 coated with SiC. The SiC coating in the latter case was discontinued such that SiC covered only two opposite sides of each UO_2 block.

For all three examined cases, the thermal conductivities were calculated for 97% *TD* and when the weight percent of SiC was 12% and 8%. The results indicate a small difference between the ETC of Case I and Case II. This small difference was due to the continuity of SiC layer in Cases I and II. However, in Case III, the discontinuity of SiC resulted in little improvement in the ETC of the fuel. Therefore, the addition of a continuous solid phase of SiC to UO_2 fuel increases the ETC of the fuel. In the present study, UO_2−SiC fuel with 12 wt% SiC has been examined, and its thermal conductivity has been calculated using Eq. [18.61]. Eq. [18.61] has been developed based on the analysis conducted for Case I. In Eq. [18.61], T is the temperature in K.

$$k_{\text{eff}} = -9.59 \times 10^{-9} T^3 + 4.29 \times 10^{-5} T^2 - 6.87 \times 10^{-2} T + 4.68 \times 10^{+1} \quad [18.61]$$

18.5.2 Uranium dioxide−graphite

Hollenbach and Ott (2010) have studied the effects of the addition of C fibbers on thermal conductivity of UO_2 fuel. Theoretically, the thermal conductivity of C varies along different crystallographic planes. For instance, the thermal conductivity of perfect C along basal planes is more than 2000 W/m K (Hollenbach and Ott, 2010). On the other hand, it is less than 10 W/m K in the direction perpendicular to the basal planes. Hollenbach and Ott (2010) have performed computer analyses in order to determine the effectiveness of adding long, thin fibbers of high thermal conductivity materials to low thermal conductivity materials to determine the effective thermal conductivity. In their studies, the high thermal conductivity material had a thermal conductivity of 2000 W/m K along the axis and a thermal conductivity of 10 W/m K radially, similar to perfect C. The low thermal conductivity material had properties similar to UO_2 (eg, with 95% *TD* at ∼1100°C) with a thermal conductivity of 3 W/m K.

Hollenbach and Ott (2010) have examined the effective thermal conductivity of the composite for various volume percentages of the high thermal conductivity material, varying from 0% to 3%. Fig. 18.32 shows that the addition of just one volume percent of high thermal conductivity material increases the effective thermal conductivity of the composite approximately by a factor of 5. Moreover, if the amount of the high thermal conductivity material increases to 2% by volume, the effective thermal conductivity of the composite reaches the range of high thermal conductivity fuels, such as UN and UC.

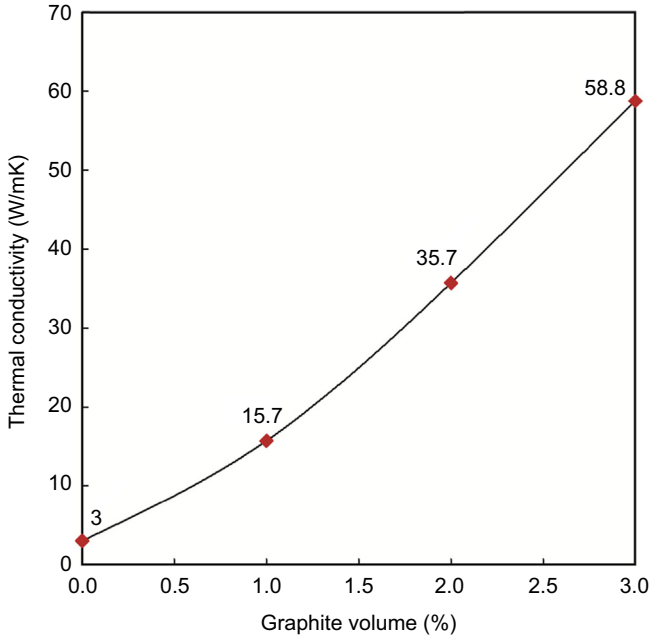


Figure 18.32 Thermal conductivity of UO_2 as function of C fibber volume percent (Hollenbach and Ott, 2010).

18.5.3 Uranium dioxide–beryllium oxide

BeO is a metallic oxide with a very high thermal conductivity. BeO is chemically compatible with UO_2, most sheath materials including zirconium alloys, and water. In addition to its chemical compatibility, BeO is insoluble with UO_2 at temperatures up to 2160°C. As a result, BeO remains as a continuous second solid phase in the UO_2 fuel matrix while being in good contact with UO_2 molecules at the grain boundaries. BeO has desirable thermochemical and neutronic properties, which have resulted in the use of BeO in aerospace, electrical, and nuclear applications. For example, BeO has been used as the moderator and the reflector in some nuclear reactors. However, the major concern with beryllium is its toxicity. But the requirements for safe handling of BeO are similar to those of UO_2. Therefore, the toxicity of BeO is not a limiting factor in the use of this material with UO_2 (Solomon et al., 2005).

Similar to other enhanced thermal conductivity fuels, the thermal conductivity of UO_2 can be increased by introducing a continuous phase of BeO at the grain boundaries. The effects of the present of such second solid phase on the thermal conductivity of UO_2 is significant such that only 10% by volume of BeO would improve the thermal conductivity of the composite fuel by 50% compared to that of UO_2 with 95% *TD*. Fig. 18.33 shows the thermal conductivity of UO_2–BeO as a function of temperature for 0.9 wt%, 2.7 wt%, 10.2 wt%, and 20.4 wt% of BeO (Ishimoto et al., 1996; Latta et al., 2008; McDeavitt, 2009; Solomon et al., 2005).

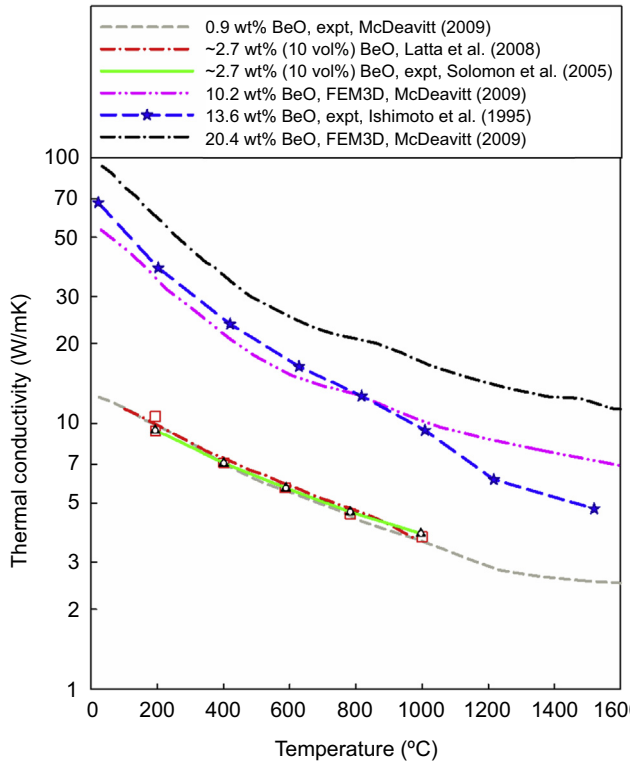


Figure 18.33 Thermal conductivity of UO_2−BeO as function of temperature (Ishimoto et al., 1996; Latta et al., 2008; McDeavitt, 2009; Solomon et al., 2005).

Zhou et al. (2015) have used the finite element modeling method in ANSYS (an engineering simulation software) to determine the thermal conductivity of UO_2−BeO. In their analysis, Zhou et al. (2015) investigated the thermal conductivity of UO_2−BeO based on the characteristics of the two available manufacturing methods, namely, slug bisque (SB) and green granule (GG) (Solomon et al., 2005). They found the UO_2−BeO manufacturing based on the GG method possesses a higher thermal conductivity compared to those manufactured using the SB method. Zhou et al. (2015) have provided correlations for the calculation of the thermal conductivity of the UO_2−BeO for a wide range of volume percent of BeO varying from 0 to 10. Zhou et al. (2015) have provided Eqs. [18.62] and [18.63] for the calculation of the thermal conductivity of UO_2−BeO with 10% volume percentage of BeO, respectively, for the SB and GG manufacturing methods. In these correlations, which are valid for a temperature range between −173°C (100 K) and 1800°C (2073 K), the temperature is in K.

$$k_{\text{eff}}(T) = 497.6\ T^{-0.679} \qquad [18.62]$$

$$k_{\text{eff}}(T) = 3348.5\ T^{-0.928} \qquad [18.63]$$

References

Abdalla, A., Peiman, W., Pioro, I., Gabriel, K., 2012. Sensitivity analysis of fuel centerline temperature in SCWRs. In: Proceedings of the 20th International Conference on Nuclear Engineering (ICONE-20) − ASME 2012 POWER Conference, July 30−August 3, Anaheim, California, USA. Paper #54530, 9 pp.

Alexander, L.G., 1964. Breeder reactors. Annual Review of Nuclear Science 14, 287−322.

Bakker, K., Cordfunke, E.H.P., Konings, R.J.M., Schram, R.P.C., 1997. Critical evaluation of the thermal properties of ThO_2 and $(Th_1-yUy)O_2$ and a survey of the literature data on $(Th_1-yPuy)O_2$. Journal of Nuclear Materials 250 (1), 1−12.

Balankin, S.A., Loshmanov, L.P., Skorov, D.M., Sokolov, V.S., 1978. Thermodynamic Stability of Uranium Mononitride. Soviet Atomic Energy 44 (4), 374−376.

Belle, J., Berman, R.M., 1984. Thorium Dioxide: Properties and Nuclear Applications. Naval Reactors Office, United State Department of Energy, Government Printing Office, Washington, DC, USA.

Bowman, A.L., Arnold, G.P., Witteman, W.G., Wallace, T.C., 1966. Thermal expansion of uranium dicarbide and uranium sesquicarbide. Journal of Nuclear Materials 19, 111−112.

Candu Energy, 2012. Enhanced CANDU 6 Technical Summary. http://www.candu.com/site/media/Parent/EC6%20Technical%20Summary_2012-04.pdf.

Carbajo, J.J., Yoder, G.L., Popov, S.G., Ivanov, V.K., 2001. A review of the thermophysical properties of MOX and UO_2 fuels. Journal of Nuclear Materials 299, 181−198.

Chirkin, V., 1968. Thermophysical Properties of Materials for Nuclear Engineering (in Russian). Atomizdat Publishing House, Moscow, Russia.

Cochran, R.G., Tsoulfanidis, N., 1999. The Nuclear Fuel Cycle: Analysis and Management, second ed. American Nuclear Society, Illinois, USA.

Coninck, R.D., Lierde, W.V., Gijs, A., 1975. Uranium carbide: thermal diffusivity, thermal conductivity spectral emissivity at high temperature. Journal of Nuclear Materials 57, 69−76.

Coninck, R.D., Batist, R.D., Gijs, A., 1976. Thermal diffusivity, thermal conductivity and spectral emissivity of uranium dicarbide at high temperatures. Journal of Nuclear Materials 8, 167−176.

Cox, D., Cronenberg, A., 1977. A theoretical prediction of the thermal conductivity of uranium carbide vapor. Journal of Nuclear Materials 67, 326−331.

Das, D., Bharadwaj, S.R., 2013. Thoria-based Nuclear Fuels. Springer, London, UK.

Frost, B.R., 1963. The carbides of uranium. Journal of Nuclear Materials 10, 265−300.

Galahom, A., Bashter, I.I., Aziz, M., 2014. Study the neutronic analysis and burnup for BWR fueled with hydride fuel using MCNPX code. Progress in Nuclear Energy 77, 65−71.

GE Nuclear Energy, 1972. BWR/6 General Description of a Boiler Water Reactor. Retrieved from NC State University: http://www4.ncsu.edu/∼doster/NE405/Manuals/BWR6GeneralDescription.pdf.

Gingerich, K.A., 1969. Vaporization of uranium mononitride and heat of sublimation of uranium. Journal of Chemical Physics 51 (10), 4433−4439.

Grande, L., Villamere, B., Allison, L., Mikhael, S., Rodriguez-Prado, A., Pioro, I., 2011. Thermal aspects of uranium carbide and uranium di-carbide fuels in supercritical water-cooled nuclear reactors. Journal of Engineering for Gas Turbines and Power 133 (2). February, 7 pp.

Hafele, W., Faude, D., Fischer, E.A., Laue, H.J., 1970. Fast breeder reactors. Annual Review of Nuclear Science 20, 393−434.

Harrison, J.W., 1969. The irradiation-induced swelling of uranium carbide. Journal of Nuclear Materials 30, 319−323.

Hayes, S., Thomas, J., Peddicord, K., 1990a. Material properties of uranium mononitride-III transport properties. Journal of Nuclear Materials 171, 289−299.

Hayes, S., Thomas, J., Peddicord, K., 1990b. Material property correlations for uranium mononitride-II mechanical properties. Journal of Nuclear Materials 171, 271−288.

Hayes, S., Thomas, J., Peddicord, K., 1990c. Material property correlations for uranium mononitride-IV thermodynamic properties. Journal of Nuclear Materials 171, 300−318.

Hollenbach, D.F., Ott, L.J., 2010. Improving the thermal conductivity of UO_2 fuel with the addition of graphite fibers. In: Transactions of the American Nuclear Society and Embedded Topical Meeting "Nuclear Fuels and Structural Materials for the Next Generation Nuclear Reactors", June 13−17, San Diego, CA, USA, pp. 485−487.

Huang, J., Tsuchiya, B., Konashi, K., Yamawaki, M., 2001. Thermodynamic analysis of chemical states of fission products in uranium-zirconium hydride fuel. Journal of Nuclear Materials 294, 154−159.

IAEA, 2008. Thermophysical Properties of Materials for Nuclear Engineering: A Tutorial and Collection of Data (Vienna, Austria).

IAEA-TECDOC-1496, 2006. Thermophysical Properties Database of Materials for Light Water Reactors and Heavy Water Reactors (Vienna, Austria).

IAEA-TECDOC-1578, 2007. Computational Analysis of the Behaviour of Nuclear Fuel under Steady State, Transient and Accident Conditions (Vienna, Austria).

INSC, 2010. Thermal Conductivity of Solid UO2. Retrieved June 28, 2010, from International Nuclear Safety Center. http://www.insc.anl.gov/matprop/uo2/cond/solid/index.php.

Ishimoto, S., Hirai, M., Ito, K., Korei, Y., 1996. Thermal conductivity of UO_2-BeO pellet. Journal of Nuclear Science and Technology 33 (2), 134−140.

Jain, D., Pillai, C., Rao, B.K., Sahoo, K., 2006. Thermal diffusivity and thermal conductivity of Thoria−Lanthana solid solutions up to 10 mol.% LaO (1.5). Journal of Nuclear Materials 353, 35−41.

Kadak, A.C., 2005. A future for nuclear energy: pebble bed reactors. International Journal of Critical Infrastructures 1 (4).

Khan, J.A., Knight, T.W., Pakala, S.B., Jiang, W., Fang, R., 2010. Enhanced thermal conductivity for LWR fuel. Journal of Nuclear Technology 169, 61−72.

Kikuchi, T., Takahashi, T., Nasu, S., 1972. Porosity dependence of thermal conductivity of uranium mononitride. Journal of Nuclear Materials 45, 284−292.

Kirillov, P.L., Terent'eva, M.I., Deniskina, N.B., 2007. Thermophysical Properties of Nuclear Engineering Materials, third ed. revised and augmented. IzdAT Publishing House, Moscow, Russia. 194 pp.

Kovaltchouk, V., Nichita, E., Saltanov, E., 2015a. Temperature distribution inside fresh-fuel pins of pressure-tube SCWR. In: Proceedings of the 7th International Symposium on Supercritical Water-cooled Reactors, ISSCWR-7, 15−18 March, Helsinki, Finland. Paper # ISSCWR7-2017.

Kovaltchouk, V., Nichita, E., Saltanov, E., 2015b. Axial power and coolant-temperature profiles for a Non-Re-entrant PT-SCWR fuel channel. In: Proceedings of the 7th International Symposium on Supercritical Water-cooled Reactors, ISSCWR-7, 15−18 March, Helsinki, Finland. Paper # ISSCWR7-2018.

Kutz, M., 2005. Mechanical Engineers' Handbook. Materials and Mechanical Design, third ed. John Wiley and Sons.

Latta, R., Revankar, S.T., Solomon, A.A., 2008. Modeling and measurement of thermal properties of ceramic composite fuel for light water reactors. Journal of Heat Transfer Engineering 29 (4), 357−365.

Leitnaker, J.M., Godfrey, T.G., 1967. Thermodynamic properties of uranium carbide. Journal of Nuclear Materials 21, 175−189.

Lundberg, L.B., Hobbins, R.R., 1992. Nuclear fuels for very high temperature applications. In: Intersociety Energy Conversion Engineering Conf., San Diego, CA, USA, 9 pp.

Ma, B.M., 1983. Nuclear Reactor Materials and Applications. Van Nostrand Reinhold Company Inc., New York, NY, USA.

Matthews, R.B., Chidester, K.M., Hoth, C.W., Mason, R.E., Petty, R.L., 1988. Fabrication and testing of uranium nitride fuel for space power reactors. Journal of Nuclear Materials 151, 334−344.

McDeavitt, S.M., 2009. High Conductivity Fuel Concept UO_2 − BeO Composite (Zr Cermet). Retrieved from. http://www.tamu.edu/.

Miletic, M., Peiman, W., Farah, F., Samuel, J., Dragunov, A., Pioro, I., 2015. Study on neutronics and thermalhydraulics characteristics of 1200-MWel pressure-channel SuperCritical Water-cooled Reactor (SCWR). ASME Journal of Nuclear Engineering and Radiation Science 1 (1), 10 pp.

Muraviev, E.V., 2014. Fuel Supply of nuclear power industry with the introduction of fast reactors. Journal of Thermal Engineering 61 (14), 1030−1039.

OECD Nuclear Energy Agency, 2014. Technology Roadmap Update for Generation IV Nuclear Energy Systems. Retrieved 12.06.15, from The Generation IV International Forum: https://www.gen-4.org/gif/upload/docs/application/pdf/2014-03/gif-tru2014.pdf.

OECD/NEA and IAEA, 2014. Uranium 2014: Resources, Production and Demand. http://www.oecd-nea.org/ndd/pubs/2014/7209-uranium-2014.pdf.

Ogard, A.E., Leary, J.A., 1970 (August). Plutonium Carbides. Retrieved 15.06.15, from US Department of Energy: http://www.osti.gov/scitech/servlets/purl/4102301/.

Oggianu, S.M., No, H.C., Kazimi, M.S., 2003. Analysis of Burnup and Economic Potential of Alternative Fuel Materials in Thermal Reactors. Journal of Nuclear Technology 143, 256−269.

Olander, D., Greenspan, E., Garkisch, H.D., Petrovic, B., 2009. Uranium−zirconium hydride fuel properties. Journal of Nuclear Engineering and Design 239, 1406−1424.

Olander, D., 2009. Nuclear fuels − present and future. Journal of Nuclear Materials 389, 1−22.

ORNL, 1965. Properties of Thorium, Its Alloys, and Its Compounds. Retrieved from Oak Ridge National Laboratory: http://web.ornl.gov/info/reports/1965/3445601336962.pdf.

Peiman, W., Pioro, I., Gabriel, K., 2015. Thermal-hydraulic and neutronic analysis of a re-entrant fuel channel design for pressure-channel supercritical water-cooled reactors. ASME Journal of Nuclear Engineering and Radiation Science 1 (2), 10 pp.

Popov, S.G., Carbajo, J.J., Ivanov, V.K., Yoder, G.L., 2000 (November). Thermophysical Properties of MOX and UO_2 Fuels Including the Effects of Irradiation. Retrieved 12.07.15, from Oak Ridge National Lab: http://web.ornl.gov/∼webworks/cpr/v823/rpt/109264.pdf.

Ross, S.B., El-Genk, M.S., Matthews, R.B., 1988. Thermal conductivity correlation for uranium nitride fuel. Journal of Nuclear Materials 151, 313−317.

Ross, S.B., El-Genk, M.S., Matthews, R.B., 1990. Uranium nitride fuel swelling correlation. Journal of Nuclear Materials 170, 169−177.

Routbort, J.L., 1972. High-Temperature Deformation of Polycrystalline Uranium Carbide. Journal of Nuclear Materials 44, 24−30.

Routbort, J.L., Singh, R.N., 1975. Elastic, Diffusional, and Mechanical Properties of Carbide and Nitride Nuclear Fuels - A Review. Journal of Nuclear Materials 58, 78−114.

Seltzer, M.S., Wright, T.R., Moak, D.P., 1975. Creep behavior of uranium carbide-based alloys. Journal of American Ceramic Society 58, 138−142.

Shoup, R.D., Grace, W.R., 1977. Process variables in the preparation of UN microspheres. Journal of American Ceramic Society 60 (7−8), 332−335.

Simnad, M.T., 1980. The U-Zrh Alloy: Its Properties X and Use in TRIGA Fuel, General Atomic Report GA-A16029. Retrieved from. http://citeseerx.ist.psu.edu/viewdoc/download?doi=10.1.1.456.7994&rep=rep1&type=pdf.

Simnad, M.T., 1992. Nuclear Reactor Materials and Fuels. http://www.cryptocomb.org/Nuclear%20Reactor%20Materials%20and%20Fuels.pdf.

Solomon, A.A., Revankar, S., McCoy, J.K., 2005. Enhanced Thermal Conductivity Oxide Fuels. Retrieved from OSTI: http://www.osti.gov/scitech/servlets/purl/862369-iDA0bI/.

Stanley, C.J., Marshall, F.M., 2008. Advanced test reactor − a national scientific user facility. In: Proceedings of the 16th International Conference on Nuclear Engineering (ICONE-16), May 11−15, Orlando, FL, USA.

Stellrecht, D.E., Farkas, M.S., Moak, D.P., 1968. Compressive creep of uranium carbide. Journal of American Ceramic Society 51 (8), 455−458.

Tokar, M., Nutt, A.W., Leary, J.A., 1970. Mechanical properties of carbide and nitride reactor fuels. Journal of Reactor Technology. http://www.osti.gov/bridge/purl.cover.jsp?purl=/4100394-tE8dXk/.

Tsuchiya, B., Huang, J., Konashi, K., Saiki, W., Onoue, T., Yamawaki, M., 2000. Thermal diffusivity measurement of uranium−thorium−zirconium hydride. Journal of Alloys and Compounds 312, 104−110.

Tsuchiya, B., Huang, J., Konashi, K., Teshigawara, M., Yamawaki, M., 2001. Thermophysical properties of zirconium hydride and uranium-zirconium hydride. Journal of Nuclear Materials 289, 329−333.

Waltar, A.E., Todd, D.R., Tsvetkov, P.V., 2012. Fast Spectrum Reactors. Springer, New York, NY, USA.

Westinghouse Electric Corporation, 1984. The Westinghouse Pressurized Water Reactor Nuclear Power Plant. http://www4.ncsu.edu/∼doster/NE405/Manuals/PWR_Manual.pdf.

Wheeler, M.J., 1965. Thermal diffusivity at incandescent temperatures by a modulated electron beam technique. British Journal of Applied Physics 16, 365−376.

WNA, April 2015a. Thorium. Retrieved 21.06.15, from World Nuclear Association: http://www.world-nuclear.org/info/Current-and-Future-Generation/Thorium/.

WNA, June 17, 2015b. Fast Neutron Reactors. Retrieved 21.06.15, from World Nuclear Association: http://www.world-nuclear.org/info/Current-and-Future-Generation/Fast-Neutron-Reactors/.

WNA, June 2015c. Nuclear Power Reactors. Retrieved 28.06.15, from World Nuclear Association: http://www.world-nuclear.org/info/Nuclear-Fuel-Cycle/Power-Reactors/Nuclear-Power-Reactors/.

WNA, August 2015d. Generation IV Nuclear Reactors. Retrieved 05.09.15, from World Nuclear Association: http://www.world-nuclear.org/info/nuclear-fuel-cycle/power-reactors/generation-iv-nuclear-reactors/.

Zakova, J., 2012. Advanced Fuels for Thermal Spectrum Reactors (Doctoral Thesis, Stockholm, Sweden).

Zhou, W., Liu, R., Revankar, S.T., 2015. Fabrication methods and thermal hydraulics analysis of enhanced thermal conductivity UO_2-BeO fuel in light water reactors. Journal of Annals of Nuclear Energy 81, 240−248.

Hydrogen cogeneration with Generation IV nuclear power plants

19

O.A. Jianu [1], *G.F. Naterer* [2], *M.A. Rosen* [1]
[1]University of Ontario Institute of Technology, Oshawa, Ontario, Canada; [2]Memorial University of Newfoundland, St. John's, NL, Canada

19.1 Introduction

A nuclear power plant's main output is electricity that is distributed via distribution networks. Cogeneration of hydrogen is an additional promising use of plants that can reduce greenhouse gas emissions with clean fuel production for homes and vehicles, among other uses. Naturally occurring elemental hydrogen is rare on earth, as it is only found in hydrogen-rich compounds, and its production necessitates energy input. Some hydrogen-rich compounds include natural gas and coal; however, producing it from hydrocarbons releases greenhouse gases. Another hydrogen-rich compound found in abundance and that is not comprised of hydrocarbons is water. Water may be split into its constituents through artificial photosynthesis and photobiological techniques based on algae, electrolysis, and water splitting systems using high temperatures obtained by nuclear or concentrated solar power plants (Rosen, 2015). The most common commercial method for hydrogen production is water electrolysis, but this uses significant amounts of electricity. Promising methods to produce hydrogen using lower amounts of electricity coupled with process and/or waste heat from nuclear power plants are thermochemical cycles for water decomposition. These cycles have the ability to produce large amounts of hydrogen that can meet industrial demands without releasing harmful by-products into the atmosphere. Industrial hydrogen demand occurs mainly for heavy oil refining, fertilizers, transportation fuels, and manufacturing applications, among others. Hydrogen production has become a rapidly growing and profitable industry. This chapter examines hydrogen cogeneration with Generation IV nuclear power plants and particularly water-splitting technologies.

19.2 Hydrogen review

Although hydrogen is the most abundant element in the universe, filling stars and gas planets, it seldom exists in its natural free state on Earth. Hydrogen bonds to other elements, such as oxygen, to form water. When ignited in the presence of the oxygen in air, hydrogen releases heat, which can be used for various purposes. When the reaction

Handbook of Generation IV Nuclear Reactors. http://dx.doi.org/10.1016/B978-0-08-100149-3.00019-7
Copyright © 2016 Elsevier Ltd. All rights reserved.

takes place in the presence of oxygen only, the only by-product is water. Since hydrogen is first created elsewhere and it stores that energy until it oxidizes, it is considered an energy carrier. Hydrogen is, in many ways, an excellent alternative energy carrier that can be produced from a number of different energy sources. By employing different production techniques, hydrogen has the potential to assist in the global transition to alternative clean energy sources.

In water splitting processes, water is decomposed into its constituents by the formula:

$$2H_2O \xleftrightarrow{\text{Heat}} 2H_2 + O_2 \qquad [19.1]$$

Hydrogen is a promising energy carrier in several ways.

- It can be safely transported in many ways, such as by pipeline, road, rail, and ship.
- It has many uses, including as a fuel in industrial, transportation, residential, and commercial activities, and for electricity generation in devices such as fuel cells (Rosen, 2015).
- When used as fuel, it causes little impact on the environment since the output of its oxidation is water.

Due to its flammable nature, hydrogen is a dangerous gas in confined spaces (Marbán and Valdés-Solís, 2007). But hydrogen can be handled safely, like other flammable and explosive gases and fuels.

Hydrogen has many uses and has significant potential for the transportation sector. In fact, hydrogen is presently employed as a fuel for spaceship propulsion systems. Although hydrogen is a promising fuel for ground vehicles, it is mostly used for demonstration purposes, in part due to the lack of a hydrogen infrastructure. However, there is a push toward developing a hydrogen infrastructure within the transportation sector, in large part due to hydrogen's main advantages when employed as a fuel: the absence of CO_2 emissions and thermal NO_x emissions. Additionally, hydrogen has the ability to be integrated with renewable energy sources of an intermittent character (ie, wind and solar energy). However, since hydrogen is not an energy source itself, it is only as clean as the method and energy source employed for its production.

Many uses of hydrogen are discussed in more detail in the next section.

19.2.1 Uses of hydrogen

Identifying potential markets for hydrogen is important for energy systems and for the research and development of hydrogen production technologies. Based on the end usage, the markets can be split into centralized and decentralized demands. Centralized plants are more economic when the end usage is accurately known, since the plants have the capacity to produce large amounts of hydrogen. One drawback is related to the transportation of the gas over large distances, because of its very low density, which requires the development of costly infrastructure. Decentralized plants produce smaller amounts of hydrogen and are set up where the feedstock is readily available. The main advantage is that costs associated with infrastructure are diminished. But costs associated with carbon capture can be restrictive, potentially making these plants infeasible when integrated with centralized plants.

To date, there are two main technologies for large-scale centralized hydrogen production, namely with inputs based on nuclear or hydrocarbon energy. The former produces large amounts of electricity and heat, and hence has the potential of being combined with electrolysis or thermochemical cycles. The latter produces hydrogen from fossil fuels using steam reforming, gasification, and other processes. Although steam reforming is a mature technology, it releases CO_2 that is either released to the environment or must be sequestered to avoid environmental impacts.

Regardless of the technology employed to produce large amounts of hydrogen, the main end use market sectors are identified as transportation, industrial, electrical, and commercial (Forsberg, 2007).

19.2.1.1 Transportation

About a third of the world's energy resources are consumed by the transportation sector, which operates almost entirely on fossil fuels. This is not a long-term sustainable option, since the Earth's fossil fuels are being depleted while releasing pollutants into the atmosphere during their extraction, conversion to usable fuels, and utilization. Additionally, the transportation sector's technology is responsible for over a third of the global greenhouse gases produced during the burning of fossil fuels using the internal combustion engine. Hence, alternatives to petroleum-driven vehicles are being sought, with electric vehicles and fuel cell vehicles being top candidates. When comparing four hypothetical candidates for fueling light vehicles, it was found that on a sun-to-tank basis, electricity and hydrogen from sustainable methods are more efficient than gasification and liquefaction of organic combustible compounds (Elder and Allen, 2009). Taking the comparison further and investigating different methods to produce electricity and hydrogen to power vehicles, the authors determined that it was slightly more efficient to power an electric vehicle using photovoltaic energy to produce electricity than to power a fuel cell vehicle using hydrogen produced through electrolysis.

An investigation of the electricity necessary to sustain hydrogen production for vehicles on an annual basis shows that even after developing more efficient systems for hydrogen production, it is necessary to increase electricity generation facilities significantly (Elder and Allen, 2009). This is attributed to electrolysis requiring electricity to split water into hydrogen and oxygen. Research also shows that electric vehicles are currently dominating the market compared to fuel cell vehicles, since they currently deliver practical on-road performance at a lower cost (Elder and Allen, 2009). However, even electric vehicles need much improvement to be viable options in today's competitive market. The main improvement pertains to the battery, which requires over 4 h to fully charge while providing a maximum range of around 360 km per charge (Sharma and Ghoshal, 2015). Since electric vehicles only provide enough fuel for relatively short trips, alternative options are being investigated; one of which is the hybrid electric vehicle. These vehicles operate on batteries for short trips and on liquid fuel for long trips. All these options are promising alternatives to gasoline vehicles; however, these technologies need further development before they can compete with the internal combustion engine in terms of cost and practicability. Hence, these

technologies will likely become transport options in the future only when these concerns are resolved.

For this reason, there has been a shift from using hydrogen in fuel cells for transportation to using it to manufacture synthetic motor fuel from heavy hydrocarbons and biomass. This is achieved through hydrocracking, a process in which the heavy molecules are cracked into gasoline in the presence of hydrogen and a catalyst. The advantage of this process is that it provides the consumer with jet fuel, diesel, or gasoline with low sulfur content. This method is advantageous in producing fuel for the matured internal combustion engine technology from poorer grades of crude oil such as bituminous shells, residues, and oil sands. Additionally, hydrogen can be used to produce synthetic fuel from coal through the Fischer–Tropsch process (Sharma and Ghoshal, 2015).

19.2.1.2 Industrial

Hydrogen has many uses in the industrial sector. Aside from the petroleum industry where hydrogen is used to process fossil fuels, it is used in the chemical industry for the production of ammonia and other chemicals. The ammonia production industry consumes about half of the hydrogen produced today (Forsberg, 2007). The produced ammonia is then used in the agricultural industry to produce fertilizer. Other chemical products formed using hydrogen are methanol and hydrochloric acid (HCl). Additionally, hydrogen is used in the food industry as a hydrogenating agent, since it has the ability of increase the level of saturation in unsaturated fats and oils. One food item produced using hydrogen is margarine. Hydrogen is also used on a large scale in the direct reduction of iron ore (Sharma and Ghoshal, 2015). Other industrial applications are found in engineering where hydrogen is used as a shielding gas during welding. Due to hydrogen having the highest thermal conductivity and specific heat of any gas, it is increasingly chosen as coolant in electrical generators. Heavy hydrogen or deuterium, one of hydrogen's stable isotopes, also has nuclear applications where it is used as fuel in nuclear fusion (O'Leary, 2012; Günay et al., 2014) and moderator in thermal nuclear fission reactions (Arias and Parks, 2015).

19.2.1.3 Electrical

It is important for system operators to match electricity supply to demand in real time. This can be challenging, for example with intermittent renewable energy, where both supply and demand can change throughout the day and throughout the year. As a result of these fluctuations, the cost of electricity also varies significantly. Consequently, it is necessary to introduce systems that can produce backup electricity when supply cannot match demand. A hydrogen market that produces electricity at times of high demand could be a viable option.

A hydrogen intermediate and peak electrical system using nuclear hydrogen that produces electricity when necessary has been implemented (Forsberg, 2007). These systems consist of hydrogen production, hydrogen storage, and peak electrical production. The feasibility of these systems depends on the cost and efficiency of hydrogen production and storage as well as the efficiency of fuel cells. Nonetheless, these

systems have the potential to alleviate problems associated with matching electricity production—often from renewable energy technologies—to demand.

19.2.1.4 Commercial

For electricity generation, hydrogen is mainly used to power fuel cells. A fuel cell converts the chemical energy of the fuel into electricity. This electrochemical conversion takes place as a result of a chemical reaction of positively charged ions of hydrogen with oxygen or other oxidizing agents. Fuel cells are different than batteries, since they do not store chemical energy; rather, they rely on a fuel supply such as hydrogen, hydrocarbons, or alcohols. The conversion takes place across a proton exchange membrane that acts as an electrolyte. In this process, hydrogen diffuses to the anode dissociating into hydrogen ions (protons) and electrons. Electricity is produced when the dissociated electrons travel around an external circuit. The protons diffuse through the electrolyte, combining with the electrons and oxygen at the cathode to form water (Elder and Allen, 2009). This clearly demonstrates a key advantage of a fuel cell: it converts chemical energy into electricity with water vapor being the only product. However, the technology needs further improvement to increase the efficiency of conversion and address other problems. The interest in the use of hydrogen in these sectors is motivated by the depletion of fossil fuel resources and the need to reduce greenhouse gas and other environmental emissions. This demonstrates some of the many benefits of employing hydrogen as an energy carrier.

19.2.2 Benefits of hydrogen

Hydrogen is a flammable gas that will burn in air at volumetric concentrations between 4% and 75%, and spontaneously ignites in air at 500°C. Hence, a hydrogen–air mixture with a concentration of approximately 20% hydrogen can be ignited by spark, sunlight, or heat where the minimum ignition energy is 0.02 mJ (Dryer et al., 2007; Ono et al., 2007). During combustion, hydrogen releases the highest amount of energy compared to any other fuel on a mass basis. Hydrogen's low heating value is 2.4, 2.8, and 4 times higher than that of methane, gasoline, and coal, respectively (Safari et al., 2015). The enthalpy of combustion of hydrogen is −242 kJ/mol, and the combustion reaction can be expressed as follows (Ahmed and Krumpelt, 2001):

$$2H_2(g) + O_2(g) \rightarrow 2H_2O(l) \qquad [19.2]$$

Due to the relatively high amount of energy release and clean combustion, hydrogen can alleviate two major energy concerns. It can reduce dependence on the depleting reserves of fossil fuels while reducing pollution and greenhouse gas emissions. Although hydrogen is the most abundant element in the universe, it rarely exists on Earth's surface in its primary form, being found mostly in water and organic compounds. Similar to electricity, hydrogen is an energy carrier that is only as clean as the

energy source from which it is produced. An assessment based on factors such as carbon dioxide emissions, availability of primary energy, cost of production, and use of land shows a clear advantage in using hydrogen over traditional fossil fuels or renewable technologies (Ewan and Allen, 2005). This was concluded based on a figure of merit assessment, giving the overall value of different routes to hydrogen. It was found that although renewable technologies have the lowest carbon dioxide emissions, they require large land areas and are not the most economic. Traditional fossil fuel technologies are lowest in cost due in part due to their maturity, but they produce the highest emissions while depleting the Earth's reserves.

Together, these factors suggest that a "hydrogen economy" is a promising alternative type of energy system, based on the vision of using hydrogen as a chemical energy carrier, and developing the associated energy infrastructure to support that vision. As an energy carrier, hydrogen has the ability to store the energy generated by nuclear power plants or by renewable energy sources such as solar or wind for use during peak demands (Elder and Allen, 2009).

19.3 Hydrogen production methods

Hydrogen is considered a promising energy carrier. Additionally, hydrogen is relatively benign environmentally, releasing water with very little other pollutants when burned. The majority of global hydrogen production is from fossil fuels (see Fig. 19.1) through a variety of processes. In general, these all release harmful pollutants into the atmosphere.

One of the least expensive processes for production of hydrogen is steam methane reforming, for which the overall reaction is (Armaroli and Balzani, 2011):

$$CH_4 + 2H_2O \rightarrow 4H_2 + CO_2 \qquad [19.3]$$

Alternative hydrogen production methods involve the splitting of water, which is considered one of the most advantageous ways, since it produces hydrogen via an

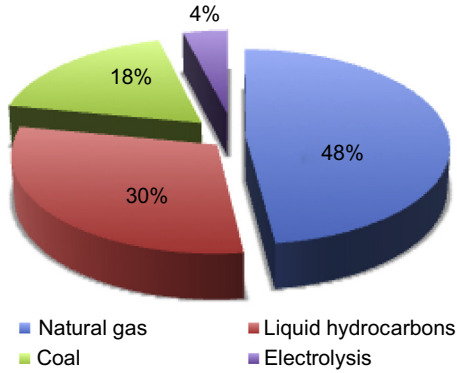


Figure 19.1 Common hydrogen production methods.

environmentally benign reaction (Eq. [19.1]). This process is less economic and only employed when high purity hydrogen is needed; hence, only about 4% of hydrogen is produced by this method at present (Armaroli and Balzani, 2011). Direct water thermolysis is another method to dissociate water; however, this method is not favored thermodynamically, as it requires significant amounts of energy. Additionally, the hydrogen and oxygen gases form an explosive mixture at elevated temperatures, necessitating that a gas separator be introduced to prevent the formation of this mixture. This significantly increases the overall cost of the production process, making it unattractive in today's market. Since the direct dissociation of water is not practical due to the high temperature for operation and safety associated with explosive gas mixture, attempts to achieve safer hydrogen production at lower temperatures via the water splitting reaction are underway. One promising option for large-scale production is thermochemical cycles, which achieve the overall reaction of Eq. [19.1] via intermediate steps. Several thermochemical cycles have been proposed and investigated over several decades, such as the iron oxide cycle, the zinc (Zn)/zinc oxide (ZnO) cycle, the ceria cycle, the sulfur−iodine (S−I) cycle, the hybrid sulfur (HyS) cycle, and the copper−chlorine (Cu−Cl) cycle. Many of these are described in this chapter.

19.3.1 Hydrogen production from fossil fuels

Hydrogen production is mainly carried out by reforming of natural gas and heavy oil, and by gasification of coal, heavy oil, and petroleum coke (Sharma and Ghoshal, 2015). The first of these involves the extraction of hydrogen from fossil fuels through steam methane reforming. In this process, natural gas, biogas, or landfill gas reacts with steam in the presence of a catalyst to produce hydrogen and carbon dioxide via the overall reaction given by Eq. [19.3]. In gasification, hydrogen is generated through the partial oxidation of hydrocarbons such as coal, heavy residual oils, and low-value refinery products. In this process, the hydrocarbon fuel reacts with oxygen at 1200−1350°C, yielding a mixture of carbon monoxide and hydrogen. Coal is converted to a gas by partial oxidation with oxygen and steam at elevated temperatures and pressures. A syngas containing mostly carbon monoxide and hydrogen is created and further treated with steam to increase the hydrogen yield. Since the gas produced contains impurities such as sulfur compounds, it is cleaned and the hydrogen is recovered. For this method to be environmentally benign, the carbon dioxide produced should be captured and sequestrated into geological formations or depleted oil and gas reservoirs. However, the capturing and sequestration of CO_2 produced in large amounts from coal is expensive and could be dangerous. Furthermore, there are several complex and unresolved problems associated with sequestrating the CO_2 produced, one of which includes the disposal of solid residues. Also, although coal reserves are abundant, they are nonrenewable; hence this method of producing hydrogen would only be a temporary option in terms of sustainability. Therefore, the move toward a hydrogen economy is likely only possible if more sustainable methods for hydrogen production are developed (Marbán and Valdés-Solís, 2007).

19.3.2 Hydrogen production by electrolysis

Electrolysis is a technology employed for the production of hydrogen from water splitting, and has existed since the early 19th century. The advantage of this technology is that the hydrogen produced has a purity of 99.99% compared with 98% purity obtained from fossil fuel based methods (Wang et al., 2012a). The input is water and electricity and hence the process does not pollute the Earth's atmosphere as the outputs from its production are hydrogen and oxygen. Hence, when combined with solar photovoltaic or wind power systems, hydrogen produced from water through electrolysis could play an important role in the future as an energy carrier for sustainable development. The disadvantage of electrolysis is the cost, which is higher than that of fossil fuel methods such as steam methane reforming. In water electrolysis, the water is split into hydrogen and oxygen using an electric current. Direct current passes through two electrodes immersed in water, and the following reactions occur on the surfaces of the electrodes (Wang et al., 2012b):

$$2H_2O(l) = O_2(g) + 4H^+(aq) + 4e^- \quad [19.4]$$

$$2H^+(aq) + 2e^- = H_2(g) \quad [19.5]$$

The electricity-to-hydrogen performance of this process is related to mass transfer effects, which in turn are influenced by the dynamics of the fluids in motion. This means that the electrolytic cell performance is affected by gas bubbles formed (ie, oxygen and hydrogen); their formation on the electrode as well as their motion affects the electrical and thermal properties of the electrolyte, diffusive transport of electroactive species, and current density (Bockris et al., 1985). Fluid flow in the electrolytic cell depends on the release of the dispersed phases. Thus, an understanding of gas–liquid flows in electrolytic systems for hydrogen production is important from the viewpoint of mass transfer and can aid in system optimization and improving efficiency. Hydrogen and oxygen bubbles start forming at the electrode surface during hydrogen production. Once detached from the surface, these bubbles rise due to buoyancy. The presence of these gas bubbles at the electrodes' surfaces can be detrimental to the overall process performance, due to the increase in the resistance of the electrolyte due to the bubbles blocking the active surface (Mat and Aldas, 2005).

Investigations to determine gas bubble formation, detachment, and flow to improve the efficiency of the electrolyzer have been reported (Wang et al., 2012a,b; Bockris et al., 1985). The velocity field of bubbles forming and detaching in an electrolytic cell with vertical electrodes was studied in order to relate gas evolution to hydrodynamics of electrolyte flow. Although the fluid flow in the system studies was laminar in terms of the Reynolds number, local turbulence due to the interactions with the continuous phase was determined (Boissonneau and Byrne, 2000). Additionally, the effects of gas evolution on hydrodynamics of water electrolysis for various electrode designs and different operating conditions, such as voltage and concentration, have been studied to improve the performance of electrolysis.

19.3.3 Hydrogen production by photoelectrolysis

Photoelectrolysis uses sunlight as the source of energy to directly decompose water into hydrogen and oxygen. The process uses two doped semiconductor materials: p-type and n-type. These semiconductors are brought together to form a p−n junction (Wang et al., 2012b; Ashraf Ali and Pushpavanam, 2011). When the charges in the n-type semiconductor material rearrange, a permanent electric field is created at the p−n junction. Furthermore, an electron is released, and a hole is created, as a photon with energy greater than that of the semiconductor material's band gap is absorbed at the junction (Holladay et al., 2009). A band gap is defined as the energy difference between the top of the valence bond and the bottom of the conduction band. The hole and electron are forced to move in opposite directions due to the electric field created due to the rearrangement of the charges in the n-type semiconductor. Due to these phenomena and in the presence of an external load, an electric current is created (Kim et al., 2011). In photoelectrolysis, a photocathode is a p-type semiconductor with excess holes, whereas a photoanode is an n-type semiconductor with excess electrons. As these semiconductors are immersed in an aqueous solution, water is split into hydrogen and oxygen. The four steps involved in this process can be summarized as follows:

- The anode is struck by a photon with greater energy than the band gap, and an electron−hole pair is created.
- Water at the anode's front surface is decomposed through the holes to form hydrogen ions and gaseous oxygen. The electrons flow through the back of the anode, which is electrically connected to the cathode.
- Hydrogen ions then pass through the electrolyte and form hydrogen gas as they react with the electrons at the cathode.
- A semipermeable membrane separates the oxygen and hydrogen gases, which are then processed and stored.

The efficiency is directly related to the semiconductor band gap as well as to the band edge alignments, since the material or device must have the correct energy to split water (Holladay et al., 2009). Electron transfer catalysts have been used in order to increase the efficiency of the system. One disadvantage of these catalysts is that they can lower the surface overpotentials in relation to the water and facilitate the reaction kinetics, which in turn increases the electricity losses in the system (Holladay et al., 2009). As a result, appropriate surface catalysts for the systems that have the ability to remain active for as many as 10^8 redox reaction cycles (ie, equivalent to 20 years of operation) are being investigated (Wang et al., 2012b). Promising options include the use of suspended metal complexes in solution as the photochemical catalysts, with nanoparticles of ZnO, Nb_2O_5, and TiO_2 typically being used (Ashraf Ali and Pushpavanam, 2011; Holladay et al., 2009; Aroutiounian et al., 2005).

19.3.4 Hydrogen production from solar energy

Another promising option to hydrogen production is water splitting using solar energy, which is an abundant albeit intermittent renewable energy source. In this method, the

electricity produced by solar radiation in photovoltaic or photoelectrochemical cells is used to split water. However, large amounts of electricity can only be produced when large areas of land are covered with solar panels. Also, the efficiencies of Si and three-junction and four-junction panels are approximately 20%, 36%, and 39%, respectively (Green et al., 2015). Certainly, there are many industrial and commercial roofs, highways, and roads that could be used rather than covering useful land. Still, compared to other means of producing electricity such as nuclear, solar is an expensive way to generate electricity. Improved efficiencies and/or the use of thin film technologies, nanostructured films, organic polymers, and concentrators may reduce the cost of solar electricity and thus of hydrogen production. Solar photovoltaic methods can contribute significantly to the development of a hydrogen economy; however, its costs have to be further reduced and its efficiency improved (Armaroli and Balzani, 2011; Bhosale et al., 2015).

19.3.5 Thermochemical cycles

Thermochemical cycles decompose water into hydrogen and oxygen using heat and a series of chemical reactions in a closed cycle. They are advantageous to direct one-step thermal water decomposition due to their ability to achieve water splitting at much lower temperatures (usually below 1000°C). Additionally, they recycle the chemicals internally without emitting wastes to the environment, making them preferable environmentally to fossil fuel-based hydrogen production systems. One promising thermochemical cycle that operates at lower temperatures than most thermochemical cycles is the Cu−Cl thermochemical cycle, which splits water into hydrogen and oxygen through intermediate copper and chlorine compounds. Due to its low temperature requirements, this cycle can be integrated with various nuclear power plants. This aspect is discussed in the next section.

19.4 Thermochemical cycles for hydrogen production

Thermochemical cycles can produce hydrogen in large quantities on a continuous basis with little impact on the environment compared to other means of hydrogen production. The only inputs to the cycles are water and heat (ie, heat from nuclear power plants), whereas the outputs are hydrogen and oxygen.

The thermolysis reaction can be accomplished under less extreme conditions when metal oxide thermochemical cycles are employed. These cycles split water through two intermediate reactions. The cycle can be described by the redox pair according to the following expressions (Charvin et al., 2007):

$$MO_{ox} \rightarrow MO_{red} + \frac{1}{2}O_2 \qquad [19.6]$$

$$MO_{red} + H_2O \rightarrow MO_{ox} + H_2 \qquad [19.7]$$

where M denotes a metal, the subscript "ox" denotes oxidation, and subscript "red" denotes reduction. In an ideal system, these two reactions are repeated cyclically and continually to produce H_2 and O_2, utilizing heat as an energy source.

The most common thermochemical cycles based on this redox pair are the iron oxide, cerium−cerium oxide, and Zn−ZnO cycles. Many other thermochemical cycles are being developed, some of which are discussed below, in terms of reactions used to split water, advantages, and disadvantages.

19.4.1 Sulfur−iodine cycle

The S−I thermochemical cycle is a well-known process for hydrogen production that involves three separate reactions. The first occurs in the Bunsen section in which water is reacted with iodine and sulfur dioxide (SO_2) to form sulfuric and hydriodic acids, as follows:

$$I_2 + SO_2 + 2H_2O \rightarrow 2HI + H_2SO_4 \quad [19.8]$$

During this exothermic reaction at around 120°C and at certain reactant concentrations, an excess of iodine causes a phase separation to occur between the two acid products. That is, the H_2SO_4 phase is entirely free of the HI phase and vice versa.

In the second section, sulfuric acid is decomposed via the following endothermic reaction:

$$2H_2SO_4 \rightarrow 2SO_2 + 2H_2O + O_2 \quad [19.9]$$

This reaction decomposes in two stages. During the first stage, the acid decomposes to SO_3 at temperatures between 400°C and 500°C. Then, it further decomposes to SO_2 in the presence of a solid catalyst at 800°C.

The third section of the overall cycle involves the decomposition of hydriodic acid to form hydrogen and iodine:

$$2HI \rightarrow I_2 + H_2 \quad [19.10]$$

This is a slightly endothermic reaction and can take place in the liquid or gas phase (Elder and Allen, 2009).

The advantage of this cycle is that all chemicals are in liquid or gaseous phases; hence without the need for solid transport and suitable for continuous operation. Additionally, it operates on a closed cycle without releasing effluents, the only outputs being hydrogen and oxygen. The main disadvantage is the high temperature requirement, which can be provided by solar, nuclear power plants or fossil fuels. Another disadvantage is the highly corrosive working fluids in the cycle, which necessitates suitable materials for operation.

19.4.2 Hybrid sulfur cycle

The HyS cycle, or Westinghouse cycle, is a combination of electrochemical and thermochemical processes (Elder and Allen, 2009). Compared to the S−I cycle, this cycle is advantageous in that it only consists of two main stages. The first stage involves the electrolysis of water and SO_2 as follows:

$$SO_2 + 2H_2O \rightarrow H_2SO_4 + H_2 \quad [19.11]$$

This reaction takes place at 87°C and yields hydrogen and sulfuric acid (H_2SO_4). In the second stage H_2SO_4 is decomposed to form water, oxygen, and SO_2, as follows:

$$H_2SO_4 \rightarrow H_2O + SO_2 + \frac{1}{2}O_2 \quad [19.12]$$

There is however an intermediate decomposition step, sulfuric acid decomposing first to sulfur trioxide and steam and then further to SO_2 and oxygen. This decomposition reaction at around 800°C is common to the S−I cycle described previously. To further improve the S−I and HyS cycles, metal oxides are used as catalytic materials. These cycles are then converted into "metal oxide-metal sulfate" cycles with the potential to achieve H_2 production at moderate temperatures (Bhosale et al., 2015).

19.4.3 Copper−chlorine cycle

The Cu−Cl cycle has become increasingly attractive to scientists and engineers due to its lower temperature requirement (ie, less than 600°C) compared to most other thermochemical cycles. These cycles achieve the overall splitting of water into its constituents through a series of reactions while internally recycling the reaction components. Thermochemical water decomposition generally involves at least three distinct steps: hydrogen production, oxygen production, and intermediate steps. Aside from its lower temperatures for operation, the advantage of this cycle is that chemical reactions form a closed internal loop, and all chemicals are reused on a continuous basis without emitting greenhouse gases to the atmosphere.

A simplified schematic of a Cu−Cl cycle for thermochemical water decomposition, showing overall inputs and outputs, operation temperatures, and intermediate steps, is shown in Fig. 19.2.

Several variations of the Cu−Cl cycle have been reported in the literature, including 5-step, 4-step, and 3-step cycles (Naterer et al., 2011). A 4-step cycle with its chemical reactions, temperatures of operation, and thermodynamic and kinematic implications is discussed here.

The first stage of the cycle is electrolysis in which hydrogen is generated as a result of oxidizing cuprous chloride (CuCl) in the presence of HCl during an electrochemical reaction. The overall cell reaction is given by:

$$2CuCl_{(aq)} + 2HCl_{(aq)} \rightarrow 2CuCl_{2(aq)} + H_{2(g)} \quad [19.13]$$

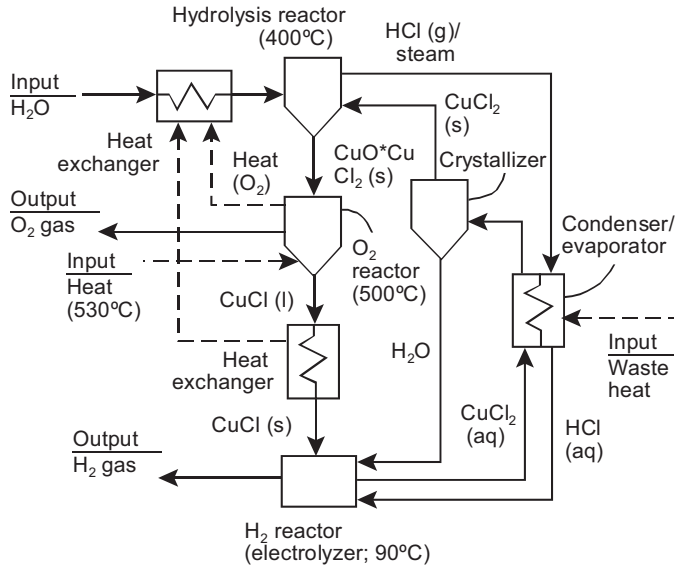


Figure 19.2 Schematic of a Cu−Cl thermochemical cycle showing overall inputs and outputs, temperature requirements, and recycling of chemicals.
Naterer, G., Suppiah, S., Lewis, M., Gabriel, K., Dincer, I., Rosen M.A., et al., 2009. Recent Canadian advances in nuclear-based hydrogen production and the thermochemical Cu−Cl cycle. International Journal of Hydrogen Energy 34, 2901−2917.

The efficiency of this cell depends on the electrode materials and their ability to produce hydrogen at low potentials, on the performance of the membrane, and on the electrolytic solution. Various relatively inexpensive electrode materials have been developed, and hydrogen production has been achieved at potentials as low as 0.5 V with ceramic carbon electrodes (Ranganathan and Easton, 2010). Additionally, several membranes have been investigated to identify those with lower copper diffusion rates but similar proton conductivities (Naterer et al., 2014; Ranganathan and Easton, 2010). Depending on these aspects and hence the current density, efficiencies ranging from 15% to 95% have been achieved (Hall et al., 2014).

The reactant system in electrolysis is a ternary system composed of CuCl, HCl, and H_2O. Improving the kinetics of electrolytic reaction for this hydrogen production process may return an improved hydrogen production rate while decreasing the reactor size (Naterer et al., 2014). The general form of the reaction kinetics may be written as:

$$k_{\text{electrolysis}} = k(C_{\text{CuCl}}, C_{\text{HCl}}, T) \qquad [19.14]$$

where C_{CuCl} and C_{HCl} are the concentrations of CuCl and HCl, respectively, in units of mol/L or kg/L, depending on the usage, T is temperature, and $k_{\text{electrolysis}}$ is the electrolytic reaction kinetics whose units depend on the form of the equation. As a result of proof-of-principle experiments, it has been determined that an option for improving

the kinetics is to increase the concentrations of both CuCl and HCl. However, the limiting factor of the increase in the electrolytic reaction kinetics is the thermodynamic solubility equilibrium of CuCl and HCl in water. That is, the boundary or constraining condition of the electrolytic solution kinetics is the solubility equilibrium, which is currently being examined in detail (Jianu et al., 2013).

The second step of the cycle consists of removing the water from aqueous cupric chloride ($CuCl_2$). Crystallization is an effective method to recover solids from solution due to its relatively low energy utilization, low material requirements, and lower cost compared to other alternatives. Hence, crystallization is of particular interest in the thermochemical Cu−Cl cycle for hydrogen production as an energy saving means to extract solid $CuCl_2$ from its aqueous solution. It has been determined from experiments that there is a range of concentrations that will demonstrate crystallization. If the initial concentration exceeds the upper bound of this range, the solution will be saturated and instantly become paste-like without forming crystals. Conversely, if the initial concentrations fall below the lower bound of a specified range, the solution will remain liquid upon cooling. As a result, it has been observed that crystallization does not occur for HCl concentrations below 3 Molar and above 9 Molar. Also, it has been found that anhydrous $CuCl_2$ does not crystallize under any of the conditions tested.

The third step involves supplying the water-free $CuCl_2$ solid to the hydrolysis reactor to produce copper oxychloride (Cu_2OCl_2) and HCl gas (Naterer et al., 2011). This is achieved in an endothermic noncatalytic gas−liquid or gas−solid reaction, expressible by the following equation:

$$2CuCl_2 + H_2O \rightarrow CuO \cdot CuCl_2 + 2HCl \qquad [19.15]$$

The chemical equilibrium and gaseous product fraction of this reaction predict the ability to effectively integrate the hydrolysis reactor and the downstream electrolytic processes. For this reason, the multiphase gas−solid flow involving hydrolysis of $CuCl_2$ and steam in a packed bed reactor was examined, and the experimental results demonstrate that an HCl fraction above 0.3 can be achieved. Thus, integration is possible without introducing costly HCl/steam separation processes (Pope et al., 2012).

The last step in the cycle is the decomposition reaction. This reaction is expressed by:

$$CuO \cdot CuCl_2 \rightarrow 2CuCl + \frac{1}{2}O_2 \qquad [19.16]$$

This is a decomposition reaction in which oxygen gas and molten CuCl are obtained from Cu_2OCl_2. Several gaseous products exit the reactor, such as oxygen gas, CuCl vapor, and some products from side reactions, such as HCl gas, Cl_2 gas, and water vapor. When particles enter the reactor at a temperature below 430°C, bubbles may develop in the molten salt. These bubbles and their aggregate formation decrease the contact area between the reactant particle and heating medium; therefore, aggregations may float to the surface. This is a major safety concern, as reported in Naterer et al. (2011).

Proof-of-principle experiments for each of the reactions in Eqs. [19.13]−[19.16] have been performed (Naterer et al., 2014; Marin et al., 2011; Dincer, 2012). Experimental results have been reported for most of the processes of the Cu−Cl cycle, and laboratory-scale reactors for the processes have been tested successfully in the Clean Energy Research Laboratory at the University of Ontario Institute of Technology (Wang et al., 2012b). Although the summation of the reactions can form a closed cycle, most previous studies have focused on individual reactors rather than an integrated Cu−Cl cycle with a holistic approach. Nonetheless, because of the lower operating temperatures, these reactors could use process and/or waste heat from nuclear power plants and successfully produce hydrogen.

19.4.4 Iron oxide cycle

The iron oxide cycle is one of the metal cycles that operates according to the pair of redox expressions given by Eqs. [19.6] and [19.7]. In the first reaction, the solid is reduced, releasing oxygen:

$$Fe_3O_4 \rightarrow 3FeO + \frac{1}{2}O_2 \qquad [19.17]$$

This is an endothermic reduction reaction at a temperature of 2000°C. The conversion of this reaction is highly dependent on the atmosphere in which it occurs. It was shown that 80% of a 0.8-g sample was converted within 5 min in the presence of argon, whereas the conversion was only half of that in air (Charvin et al., 2007).

The second reaction is an oxidation of the reduced solid with steam that yields H_2 and the original oxide according to the following expression:

$$3FeO + H_2O \rightarrow Fe_3O_4 + H_2 \qquad [19.18]$$

This oxidation reaction requires temperatures below 800°C. The conversion of this reaction is influenced not only by the temperature, but also by the particle size and the atmosphere in which the reaction takes place. Research shows that 92% chemical conversion can be achieved at 575°C and 29% conversion at 525°C. The theoretical energy required to generate 1 mol of hydrogen is given by the summation of the energy required to heat 1 mol of Fe_3O_4 to the temperature of Eq. [19.17], the energy input to heat water to the temperature desired in Eq. [19.18], and the enthalpy of the endothermic reduction. Based on these temperatures and on the high heating value of hydrogen, the theoretical energy yield of this cycle is about 37% (Charvin et al., 2007). The endothermic reaction of this cycle occurs at high temperature, necessitating directed solar thermal power for operation. Hence, to improve the efficiency of the cycle, high-temperature heat from nuclear plants could be utilized.

The iron oxide-based cycle is an attractive thermochemical cycle due to its less complex chemical steps and reactants compared to other cycles, which could result in less irreversibility and hence a higher cycle efficiency. Another advantage of this cycle is the use of noncorrosive materials, decreasing the costs associated with material development.

Like many other thermochemical cycles, it also avoids the problem of hydrogen and oxygen gas recombination at high temperatures, therefore making it a safe cycle to operate. It avoids gas recombination during quenching encountered with volatile metal oxides, such as Zn or cadmium oxides, due to only solid and gas being present. Another key feature is that iron oxide is nonvolatile, and therefore, it makes it possible for the continuous removal of the evolved oxygen from the condensed phase during the solar reduction step, increasing high reduction rates (Charvin et al., 2007). The main disadvantage of this cycle is that it requires high temperatures for operation. Also, a slight temperature drop can significantly affect the chemical conversion rates to hydrogen, affecting its efficiency. Another disadvantage is that it necessitates large amounts of magnetite, and the shape of the particles plays a key role in the chemical conversion. This requires careful production of the particles in the desired shape, which can be costly.

19.4.5 Cerium–cerium oxide cycle

The ceria-based thermochemical redox cycle offers a promising pathway to split water while storing intermittent sunlight in the form of hydrogen. Similar to other metal oxide thermochemical cycles, the cerium–cerium oxide cycle consists of two steps. The first reaction is the reduction of ceria (CeO_2) to form cerium (III) oxide:

$$2CeO_2 \rightarrow Ce_2O_3 + \frac{1}{2}O_2 \qquad [19.19]$$

In this reduction step, ceria is thermally dissociated during an endothermic reaction, generally at above 1400°C. Since there is a low oxygen partial pressure in a nonstoichiometric state, O_2 is released. To achieve such high temperatures, this step is usually driven by solar energy.

The second step is the oxidation of the cerium (III) oxide back to its original form, in the presence of water, given by:

$$Ce_2O_3 + H_2O \rightarrow 2CeO_2 + H_2 \qquad [19.20]$$

An important factor in the efficiency of this cycle is ceria's fluorite structure, which permits oxygen ions to move with relative ease. Therefore, migrating these oxygen vacancies could improve the reaction and cycle efficiency. The migration of such vacancies is controlled by the activation energy and the clustering with dopants. Hence, doping the ceria has been considered, and zirconia (Zr) is a promising dopant. The amounts of oxygen released during the reduction steps as well as the formation and stability of cerium (III) oxide are highly dependent on the presence of Zr in the different materials. When comparing the reduction yields of doped and undoped materials, it was found that values range from 6% for pure ceria to 27.9% for 50% Zr during the first cycle. Additionally, the reduction yields increase linearly by increasing the amount of Zr; hence, reduction is favored in the presence of Zr (Le Gal et al., 2013). Other studies have investigated the thermodynamics of ceria dopants such as yttrium (III) oxide, samarium oxide, gadolinium oxide, calcium oxide, and strontium oxide

(Scheffe and Steinfeld, 2012). Although the doped ceria shows improved efficiency compared to pure ceria, the selected dopants in that study had lower potential to split H_2O than pure ceria, as described in Furler et al. (2012).

The cerium–cerium oxide thermochemical cycle is promising due to ceria's stable crystallographic structure, having a cubic fluorite structure when reduced to nonstoichiometries of up to 0.25. Also, complications, such as extensive sintering, that arise from solid-to-solid and solid-to-liquid transitions are avoided (Ackermann et al., 2014). Other chemistry considerations are summarized below:

- Reactions do not need a catalyst, as steam hydrolysis chemistry features rapid kinetics and complete reactions at 400–600°C.
- Cerium oxide reactivity with water is high, and therefore, particle sieving is not required.
- Thermal quenching is not necessary.
- H_2 and O_2 are produced separately, so a high temperature gas phase separation step is not required.
- The produced H_2 is pure, and emissions are not released into the environment.

The advantage of this process is that heat from the high temperature solar step could be recovered and used in the downstream reactor. Also, technologies for gas–solid solar reactors have been developed previously; hence implementation with solar concentrating systems is possible for a large-scale cycle. The main drawback of the cerium–cerium oxide thermochemical cycle relates to the temperature of operation, the endothermic step requiring optimization before being compatible with other technologies, and to reduce sample vaporization (Abanades and Flamant, 2006). Also, cerium (III) oxide is highly unstable, quickly becoming ceria in conditions that are not optimal. Hence, the cycle has to be optimized before it can become commercial.

19.4.6 Zinc–zinc oxide cycle

Another cycle for hydrogen production of special interest is the solar thermochemical cycle based on Zn–ZnO redox reactions. This cycle splits water into its constituents via two steps. In the first step, ZnO is dissociated thermally into Zn gas and O_2 during an endothermic reaction at temperatures of above 2000°C. Since this temperature is difficult to achieve, concentrated solar energy is used as the heat source. This reaction is given by the following expression:

$$\mathrm{ZnO} \rightarrow \mathrm{Zn} + \frac{1}{2}\mathrm{O_2} \qquad [19.21]$$

The second step involves the hydrolysis of liquid Zn to form H_2 and solid ZnO:

$$\mathrm{Zn} + \mathrm{H_2O} \rightarrow \mathrm{ZnO} + \mathrm{H_2} \qquad [19.22]$$

This is a non-solar, exothermic step at 425°C in which solid ZnO separates naturally from hydrogen. The oxide is then recycled back into the first step while the hydrogen is processed and stored.

The major disadvantage of this thermochemical cycle is the high energy required for the dissociation of ZnO. Several chemical aspects of the thermal dissociation have been previously investigated, and an apparent activation energy in the range 310−350 kJ/mol has been reported (Steinfeld, 2002). Similar to most thermochemical cycles, the advantage is that hydrogen and oxygen are derived in different steps, hence eliminating the need for gas separation at high temperature. Another advantage pertains to the number of reactions needed to produce hydrogen, this cycle only necessitating two steps.

19.5 Hydrogen cogeneration with Generation IV reactors

Nuclear energy has the potential to be utilized as the main energy source in centralized large-scale hydrogen production systems. High-temperature thermochemical processes, water electrolysis, and high-temperature steam electrolysis all require large amounts of energy for operation; hence, energy efficiency is important for a hydrogen economy operating in an environmentally benign manner. For more efficient thermochemical and electrochemical hydrogen production cycles, waste heat from nuclear energy could be employed (Elder and Allen, 2009; Orhan et al., 2012; Naterer et al., 2013; Yildiz and Kazimi, 2006). Hence, high temperature reactors that can be integrated with hydrogen production cycles are the gas-cooled, molten salt-cooled, and liquid metal-cooled reactor technologies (Yildiz and Kazimi, 2006). For successful cogeneration of hydrogen with Generation IV nuclear reactors, some process requirements have to be met. Nuclear steam reforming of methane, hot electrolysis, and thermochemical cycles impose similar requirements on the nuclear reactor (Forsberg, 2003). Some of these requirements follow:

- The reactor power of a typical nuclear reactor matches well with scaled up hydrogen production facilities. However, the plant size varies depending on specific applications, and economic considerations have to be addressed.
- Hydrogen production cycles require peak temperatures between 500°C and 2000°C. Hence, only some reactors of all thermochemical cycles have the potential to use heat from nuclear power plants.
- The endothermic high-temperature chemical reactions of dissociation require constant temperatures; therefore, waste must be delivered over small temperature ranges.
- Low pressures are required for completion of the chemical reactions, since high pressures reverse the desired chemical reactions.
- The hydrogen production facilities should be isolated from the nuclear power plants, so problems generated in one facility would not impact the performance of the other facility, and to prevent tritium transport into the hydrogen production facility.

The critical requirement for successful integration of the hydrogen production systems with nuclear power plants is the delivery of the heat from the reactor core to the thermochemical plant for hydrogen production under appropriate conditions. Characteristics of the reactor are used to meet these conditions.

19.5.1 Heat requirements for hydrogen production

Operating temperatures play a key role in electrolytic and thermochemical methods of hydrogen production. All the thermochemical cycles for hydrogen production require large amounts of high-temperature heat to drive the disassociation reactions. One key condition for successful integration is the near constant temperature in order to drive the dissociation reactions. From an engineering point of view, these are very high temperatures that should be reduced to lower thermal and pressure stresses. To reduce peak temperature in nuclear reactors, a liquid or gas reactor coolant could be used. The advantage of liquid over gas coolants is that they have good heat transfer capabilities and lower pumping power costs. Additionally, liquid-cooled reactors can deliver most of their heat at near constant temperatures, which satisfies the heat requirement for successful integration. Although gas-cooled reactors have the ability to deliver the heat at near constant temperatures, costs associated with pumping increase significantly, making the integration less economic. For example, when a temperature of 750°C is needed, the coolant temperature of a liquid-cooled reactor is less than 850°C, whereas the temperature in a gas-cooled reactor may be above 1000°C. The higher temperatures in a gas-cooled reactor would require different materials that could withstand high stresses from the pressurized gas coolant. Liquid-cooled reactors are thus preferred, since they lower peak temperatures (Forsberg, 2003).

19.5.2 Pressure considerations

As previously mentioned, thermochemical cycles split water through a series of chemical reactions. The chemicals used in these facilities are often hazardous, and when under pressure reactions, could reverse. High-pressure reactor coolants create the potential for a number of safety concerns such as pressurization, which could reverse reactions and release toxic gases. Additionally, the demand on the materials of high-pressure rector coolants is much greater than those for low-pressure. Hence, from a safety and materials point of view, a low-pressure, nonchemically reactive coolant should be used. Since hydrogen production systems do not require high pressures, these low-pressure liquid coolants could match the pressures of the hydrogen production systems. Salts that avoid the potential for pressurization due to high boiling points, such as Nuoride, could be used. Aside from a high boiling point, about 1400°C, Nuoride is a suitable candidate, since it does not react with air and only slowly reacts with water (Forsberg, 2003).

19.5.3 Isolation

Successful hydrogen cogeneration with Generation IV nuclear power plants would require the two facilities to be separated by some distance. The heat losses between the two facilities could be minimized with the use of a high heat capacity, low-pressure, molten salt coolant. This is a mature technology with molten salts typically being used to transfer heat at high temperatures. Another benefit of using molten salts for the cogeneration of hydrogen with nuclear power plants is the ability of the molten salts to absorb tritium. Tritium is a radioactive form of hydrogen that can diffuse

through hot metals; thus, the reactor design must be chosen to minimize the amount of tritium entering the hydrogen production facility. There are three methods to avoid tritium contamination: design the reactor to avoid tritium production, choose a coolant that traps tritium, and design heat exchangers that minimize tritium transport. When designing specifically for hydrogen production, minimizing the tritium inventory is the preferred option, whereas when designing for reactors that produce electricity, tritium is trapped in the power cycle, and hence it is not a major issue (Forsberg, 2003).

Nonetheless, thermodynamic investigations demonstrate that the thermochemical Cu−Cl cycle at relatively low temperatures is a feasible and promising pathway to sustainable production of hydrogen with Canada's future nuclear reactors, namely the supercritical water-cooled reactor (Rosen et al., 2012). Also, efficiency can be further improved with pinch analysis and improved design of the chemical reactors for hydrogen production (Ghandehariun et al., 2012).

19.6 Conclusions

Coupling hydrogen production with nuclear power plants is a promising technology for addressing society's economically and environmentally unsustainable dependence on fossil fuels. Hydrogen produced in this manner would be available for sectors where large-scale quantities of hydrogen would be required. The utilization of heat from nuclear reactors is beneficial, since the efficiencies of the facilities increase and costs associated with generating heat at temperatures required by hydrogen production facilities are reduced. Additionally, nuclear energy is a large-scale energy resource that can consistently be provided to the hydrogen production facility. Since hydrogen is an energy carrier as clean as the method used to produce it, coupling the two technologies provides an important pathway for mitigating climate change and depletion of fossil fuel reserves.

References

Abanades, S., Flamant, G., 2006. Thermochemical hydrogen production from a two-step solar-driven water-splitting cycle based on cerium oxides. Solar Energy 80 (12), 1611−1623.

Ackermann, S., Scheffe, J.R., Steinfeld, A., 2014. Diffusion of oxygen in ceria at elevated temperatures and its application to H_2O/CO_2 splitting thermochemical redox cycles. Journal of Physical Chemistry C 118 (10), 5216−5225.

Ahmed, S., Krumpelt, M., 2001. Hydrogen from hydrocarbon fuels for fuel cells. International Journal of Hydrogen Energy 26 (4), 291−301.

Arias, F.J., Parks, G.T., 2015. On the feasibility of self-sustainable deuterium production in fusion reactors using an ionization chamber. Journal of Fusion Energy (2), 5−7.

Armaroli, N., Balzani, V., 2011. The hydrogen issue. ChemSusChem 4 (1), 21−36.

Aroutiounian, V.M., Arakelyan, V.M., Shahnazaryan, G.E., 2005. Metal oxide photoelectrodes for hydrogen generation using solar radiation-driven water splitting. Solar Energy 78 (5), 581−590.

Ashraf Ali, B., Pushpavanam, S., 2011. Analysis of liquid circulation and mixing in a partitioned electrolytic tank. International Journal of Multiphase Flow 37 (9), 1191−1200.

Bhosale, R.R., Kumar, A., van den Broeke, L.J.P., Gharbia, S., Dardor, D., Jilani, M., Folady, J., Al-Fakih, M.S., Tarsad, M.A., 2015. Solar hydrogen production via thermochemical iron oxide−iron sulfate water splitting cycle. International Journal of Hydrogen Energy 40 (4), 1639−1650.

Bockris, J., Dandapani, B., Cocke, D., Ghoroghchian, J., 1985. On the splitting of water. International Journal of Hydrogen Energy 10 (3), 179−201.

Boissonneau, P., Byrne, P., 2000. Experimental investigation of bubble-induced free convection in a small electrochemical cell. Journal of Applied Electrochemistry 30 (7), 767−775.

Charvin, P., Abanades, S., Flamant, G., Lemort, F., 2007. Two-step water splitting thermochemical cycle based on iron oxide redox pair for solar hydrogen production. Energy 32 (7), 1124−1133.

Dincer, I., 2012. Green methods for hydrogen production. International Journal of Hydrogen Energy 37 (2), 1954−1971.

Dryer, F.L., Chaos, M., Zhao, Z., Stein, J.N., Alpert, J.Y., Homer, C.J., 2007. Spontaneous ignition of pressurized releases of hydrogen and natural gas into air. Combustion Science and Technology 179 (4), 663−694.

Elder, R., Allen, R., 2009. Nuclear heat for hydrogen production: coupling a very high/high temperature reactor to a hydrogen production plant. Progress in Nuclear Energy 51 (3), 500−525.

Ewan, B.C.R., Allen, R.W.K., 2005. A figure of merit assessment of the routes to hydrogen. International Journal of Hydrogen Energy 30 (8), 809−819.

Forsberg, C.W., 2003. Hydrogen, nuclear energy, and the advanced high-temperature reactor. International Journal of Hydrogen Energy 28 (10), 1073−1081.

Forsberg, C.W., 2007. Future hydrogen markets for large-scale hydrogen production systems. International Journal of Hydrogen Energy 32 (4), 431−439.

Furler, P., Scheffe, J., Gorbar, M., Moes, L., Vogt, U., Steinfeld, A., 2012. Solar thermochemical CO_2 splitting utilizing a reticulated porous ceria redox system. Energy and Fuels 26 (11), 7051−7059.

Ghandehariun, S., Rosen, M.A., Naterer, G.F., Wang, Z., 2012. Pinch analysis for recycling thermal energy in the Cu−Cl cycle. International Journal of Hydrogen Energy 37 (21), 16536−16541.

Green, M.A., Emery, K., Hishikawa, Y., Warta, W., Dunlop, E.D., 2015. Solar cell efficiency tables (version 46). Progress in Photovoltaics Research and Applications 23 (7).

Günay, M., Şarer, B., Kasap, H., 2014. Contributions of each isotope in some fluids on neutronic performance in a fusion−fission hybrid reactor: a Monte Carlo method. Indian Journal of Physics 88 (8), 861−866.

Hall, D.M., Akinfiev, N.N., LaRow, E.G., Schatz, R.S., Lvov, S.N., 2014. Thermodynamics and efficiency of a CuCl(aq)/HCl(aq) electrolyzer. Electrochimica Acta 143, 70−82.

Holladay, J.D., Hu, J., King, D.L., Wang, Y., 2009. An overview of hydrogen production technologies. Catalysis Today 139 (4), 244−260.

Jianu, O.A., Wang, Z., Rosen, M.A., Naterer, G.F., 2013. Shadow imaging of particle dynamics and dissolution rates in aqueous solutions for hydrogen production. Experimental Thermal and Fluid Science 51, 297−301.

Kim, S., Schatz, R., Khurana, S., Fedkin, M., Wang, C., Lvov, S.N., 2011. Advanced CuCl electrolyzer for hydrogen production via the Cu-Cl thermochemical cycle. ECS Transactions 35 (32), 257−265.

Le Gal, A., Bion, N., Le Mercier, T., Harle, V., 2013. Reactivity of doped ceria-based mixed oxides for solar thermochemical hydrogen generation via two-step water-splitting cycles. Energy and Fuels 27, 6068−6078.

Marbán, G., Valdés-Solís, T., 2007. Towards the hydrogen economy? International Journal of Hydrogen Energy 32 (12), 1625−1637.

Marin, G.D., Wang, Z., Naterer, G.F., Gabriel, K., 2011. X-ray diffraction study of multiphase reverse reaction with molten CuCl and oxygen. Thermochimica Acta 524 (1−2), 109−116.

Mat, M., Aldas, K., 2005. Application of a two-phase flow model for natural convection in an electrochemical cell. International Journal of Hydrogen Energy 30 (4), 411−420.

Naterer, G.F., Suppiah, S., Stolberg, L., Lewis, M., Ferrandon, M., Wang, Z., Dincer, I., Gabriel, K., Rosen, M.A., Secnik, E., Easton, E.B., Trevani, L., Pioro, I., Tremaine, P., Lvov, S., Jiang, J., Rizvi, G., Ikeda, B.M., Lu, L., Kaye, M., Smith, W.R., Mostaghimi, J., Spekkens, P., Fowler, M., Avsec, J., 2011. Clean hydrogen production with the Cu−Cl cycle − progress of international consortium, I: experimental unit operations. International Journal of Hydrogen Energy 36 (24), 15486−15501.

Naterer, G.F., Dincer, I., Zamfirescu, C., 2013. Hydrogen Production from Nuclear Energy. Springer, London.

Naterer, G.F., Suppiah, S., Stolberg, L., Lewis, M., Ahmed, S., Wang, Z., Rosen, M.A., Dincer, I., Gabriel, K., Secnik, E., Easton, E.B., Lvov, S.N., Papangelakis, V., Odukoya, A., 2014. Progress of international program on hydrogen production with the copper−chlorine cycle. International Journal of Hydrogen Energy 39 (6), 2431−2445.

O'Leary, D., 2012. The deeds to deuterium. Nature Chemistry 4 (3), 236.

Ono, R., Nifuku, M., Fujiwara, S., Horiguchi, S., Oda, T., 2007. Minimum ignition energy of hydrogen-air mixture: effects of humidity and spark duration. Journal of Electrostatics 65 (2), 87−93.

Orhan, M.F., Dincer, I., Rosen, M.A., 2012. Investigation of an integrated hydrogen production system based on nuclear and renewable energy sources: a new approach for sustainable hydrogen production via copper−chlorine thermochemical cycles. International Journal of Energy Research 36 (15), 1388−1394.

Pope, K., Wang, Z.L., Naterer, G.F., Secnik, E., 2012. Interfacial thermodynamics and X-ray diffraction of hydrolysis products in multiphase reacting flow of the Cu−Cl cycle. International Journal of Hydrogen Energy 37 (20), 15011−15019.

Ranganathan, S., Easton, E.B., 2010. Ceramic carbon electrode-based anodes for use in the Cu−Cl thermochemical cycle. International Journal of Hydrogen Energy 35 (10), 4871−4876.

Rosen, M.A., Naterer, G.F., Chukwu, C.C., Sadhankar, R., Suppiah, S., 2012. Nuclear-based hydrogen production with a thermochemical copper−chlorine cycle and supercritical water reactor: equipment scale-up and process simulation. International Journal of Energy Research 36 (4), 456−465.

Rosen, M.A., 2015. The prospects for renewable energy through hydrogen energy systems. Journal of Power and Energy Engineering 3, 373−377.

Safari, F., Tavasoli, A., Ataei, A., Choi, J.-K., 2015. Hydrogen and syngas production from gasification of lignocellulosic biomass in supercritical water media. International Journal of Recycling of Organic Waste in Agriculture 4 (2), 121−125.

Scheffe, J.R., Steinfeld, A., 2012. Thermodynamic analysis of cerium-based oxides for solar thermochemical fuel production. Energy and Fuels 26 (3), 1928−1936.

Sharma, S., Ghoshal, S.K., 2015. Hydrogen the future transportation fuel: from production to applications. Renewable and Sustainable Energy Reviews 43, 1151−1158.

Steinfeld, A., 2002. Solar hydrogen production via a two-step water-splitting thermochemical cycle based on Zn/ZnO redox reactions. International Journal of Hydrogen Energy 27 (6), 611−619.

Wang, Z., Roberts, R.R., Naterer, G.F., Gabriel, K.S., 2012a. Comparison of thermochemical, electrolytic, photoelectrolytic and photochemical solar-to-hydrogen production technologies. International Journal of Hydrogen Energy 37 (21), 16287−16301.

Wang, Z., Daggupati, V.N., Marin, G., Pope, K., Xiong, Y., Secnik, E., Naterer, G.F., Gabriel, K.S., 2012b. Towards integration of hydrolysis, decomposition and electrolysis processes of the Cu−Cl thermochemical water splitting cycle. International Journal of Hydrogen Energy 37 (21), 16557−16569.

Yildiz, B., Kazimi, M.S., 2006. Efficiency of hydrogen production systems using alternative nuclear energy technologies. International Journal of Hydrogen Energy 31 (1), 77−92.

Advanced small modular reactors

20

F. Aydogan
University of Idaho, Idaho Falls, ID, United States

20.1 Introduction

The key words of "small" and "modular" make the small modular reactors (SMRs) different than other reactors. "Small" denotes the reactor's decreased power size. "Modular" denotes (1) the primary coolant system (such as the reactor (RX) component in a light water SMR) enveloped by a pressure boundary; and (2) modular construction of components. Modular design requires compact architecture that is built in facility. For instance, the term of "modular" for a light water SMR (LW-SMR) is used for the RX, since it covers the reactor core and primary coolant system so that the overall power of a power plant can easily be increased by increasing the modular units.

There is no concrete definition for the upper limit of SMRs' power rating, but 300 MWe is usually used for a rough upper limit of SMRs. In addition to the reduced power level, most of the SMRs offer reduced spatial footprints and modularized compact designs fabricated in factories and transported to the intended sites, as well as improved safety features (such as passive safety, inherent or intrinsic safety, and safety-by-design). LW-SMRs employ a significantly less number of components in order to decrease costs and increase simplicity of design. However, new physical challenges have appeared with these changes. At the same time, advanced (ADV) SMR designs (such as Pebble Bed Modular Reactor, MHR Antares, Prism, 4S, Hyperion, etc.) are being developed that have improved passive safety and other features. Among the new SMRs, the US Department of Energy (DOE) has begun to support SMR activities in US since 2012 years by issuing solicitations, such as "Financial Assistance Funding Opportunity Announcement – Cost-Shared Development of Innovative Small Modular Reactor Designs." DOE supports SMRs because of safety and economical benefits (Lyons, 2012):

1. Passive/inherent/safety-by-design safety systems, which do not require an operator or control system action;
2. Reduced source term inventory;
3. Elimination of postulated accidents by simplified design;
4. Reduction in Emergency Planning Zone;
5. Below-grade construction of the RX;
6. Flexibility to add reactor units;
7. Decreased financial risk and initial investment;
8. Potential replacement of old coal plants;
9. Usage of domestic resources, such as forgings and manufacturing;

Handbook of Generation IV Nuclear Reactors. http://dx.doi.org/10.1016/B978-0-08-100149-3.00020-3
Copyright © 2016 Elsevier Ltd. All rights reserved.

10. Flexible power range with multiple units for various power grid needs and regional load growth;
11. Transportable modular components from factory to the site; and
12. Below-grade design of the RX and spent fuel storage pool for greater safety and security performance against external attacks and seismic events.

This support in the US motivates US-based SMR vendors to compete with international (non-US) SMR companies. Some of the international SMR designs are given as,

Russian designs:	KLT-40S (OKBM, 2015), VBER-150/300 (OKBM, 2015), VK-300 (Kuznetsov et al., 1999), ABV (OKBM, 2015), SVBR-100 (AKME, 2015),
Korean designs:	SMART (Park, 2011c), VHTR
Chinese designs:	CAP100/ACP100 (Mingguang, 2013), HTR-PM (Li, 2014),
Argentinean design:	CAREM-25 (Magan et al., 2014),
Japanese designs:	IMR, CCR, DMS, GTHTR300, 4S.

Several SMRs have been discussed by categorizing SMRs in different ways. For instance, the International Atomic Energy Agency (IAEA) categorizes the small and midsize reactors based on primary coolant types (IAEA, 2002). For the current chapter, IAEA's lists are updated by removing the midsize reactors (which produce more than 300 MWe/reactor unit) and adding the recent SMRs, as shown in Fig. 20.1.

SMRs are classified into two groups in the scope of this study (Fig. 20.1):

1. LW-SMR:
   LW-SMRs can be considered in the category of Generation III+ (Gen-III+). Some of the LW-SMRs, such as Westinghouse Small Modular Reactor (W-SMR), have inherited some safety features of licensed Gen-III+ reactors, such as the AP1000, which is the licensed commercial design. LW-SMRs generally use integrated RXs, which envelop the core, steam generator (SG), the pump, and the pressurizer (PRZ).
2. Non-LW-SMRs:
   Non-LW-SMRs can be considered in the category of Generation IV (Gen-IV) reactors in that they are highly economical with improved passive safety and reduced levels of radioactive waste.

However, most of the non-LW-SMRs are in the early phase of development and are therefore unable to easily inherit significant licensed features of other commercial Gen-IV reactors because even these reactors are still in the development phase. Even though LW-SMRs are relatively similar to each other, Gen-IV designs include a wide range of design varieties, such as coolant types, control systems, fuels, etc.

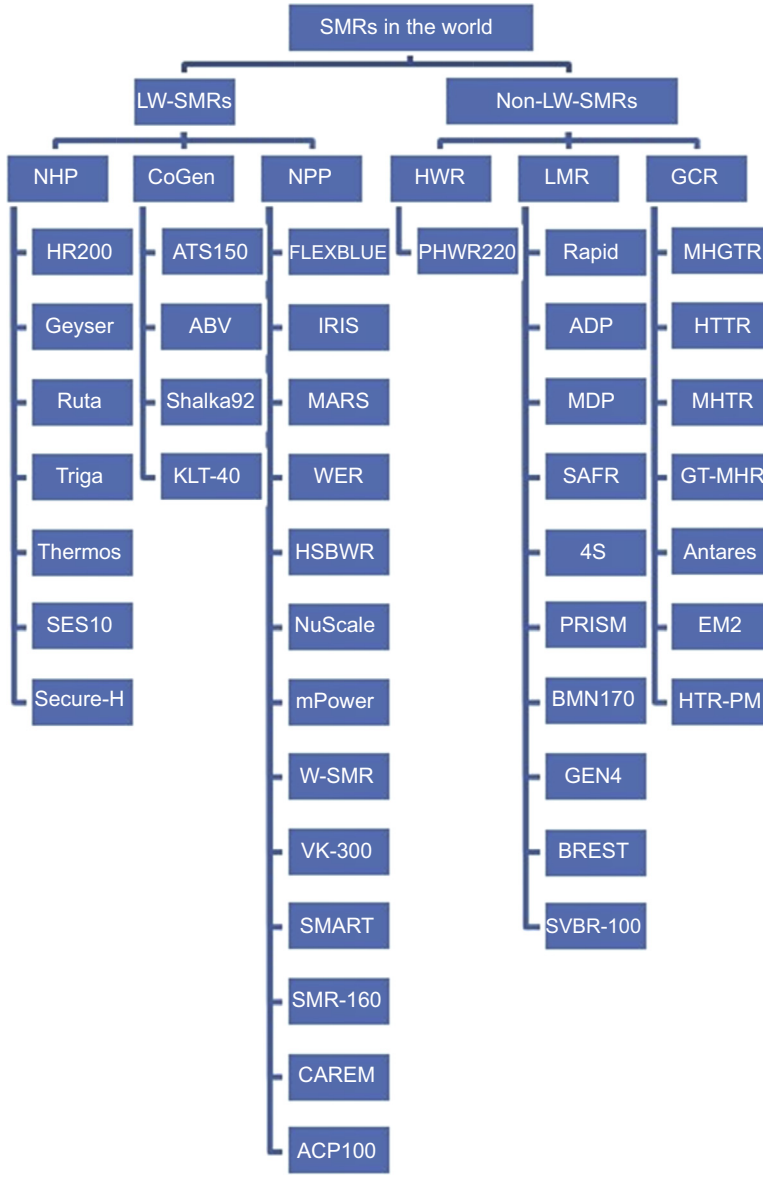


Figure 20.1 SMRs categorized based on coolant type (IAEA, 2002).

This chapter firstly discusses the early designs of SMRs. Then it selects and compares some of the SMR designs between LW and ADV SMRs. The selection has been performed to include variety of SMRs based on nuclear reactors, reactor coolant systems (RCSs), containment designs, and emergency core coolant system.

Selected designs are NuScale (IAEA, 2011a), SMART (System-integrated Modular Advanced Reactor) (Matzie, 2015; Park, 2011c), W-SMR (W, 2013), mPower (Babcock, 2013; IAEA, 2011b), International Reactor Innovative and Secure (IRIS) (Carelli et al., 2004) from LW-SMRs, and Power Reactor Innovative Small Module (PRISM) (PRISM, 1994), Super Safe, Small and Simple reactor (4S) (NRC, 2013), and Hyperion (Gen4energy, 2013) from ADV SMRs. Selected SMRs are compared based on: (1) nuclear reactors; (2) RCS components; (3) fuels; (4) containment; (5) Emergency Core Cooling System (ECCS); (6) cost evaluation; (7) security evaluation; and (8) flexibility of SMRs.

20.2 Early designs of small modular reactors

The first small size reactors have been designed in the 1960s for commercial and military applications. Some of these reactors are Shippingport in 1958, Yankee Rowe in 1960, Indian Point One in 1962, Dresden in 1960, TES-3 in 1961, US Savannah in 1962, OK-150 in 1957, and Otto Hahn in 1968. Even though there were several small size reactors designed in the 1960s, only a few of them inspired the current SMRs. Since most of the SMRs use integral/integrated design for RX, the following section will start to discuss the early integrated designs for naval and terrestrial applications.

Early integrated designs in which SGs and pumps are within the RX inspired the current SMR designs. One of the early designs is the Safe Integral Reactor (SIR) (Fig. 20.2) that introduces a tall riser to enhance natural circulation just above the core (Forsberg and Reich, 1991). Sealed circulation pumps are located just below the PRZ. SGs are placed around the periphery of the vessel. A passive PRZ is at the top of the pressure vessel because of the presence of vapor. This design makes an LB loss of coolant accident (LB-LOCA) impossible because there is no primary coolant pump.

Hannerz (Forsberg, 1983) proposed a new concept that is a combination of an updated integrated design and a pool type reactor design. This concept is called the Process Inherent Ultimate Safety (PIUS) (Fig. 20.3) design (Forsberg, 1983). The core is located at the bottom of riser. The hot flow at the exit of the riser conducts to the entrance of circulating flow pipes. These pipes connect the vessel and both SG and circulation pumps. The pump is attached to the exit of SG to decrease the pressured head required for circulation flow. The water is returned to the vessel from the pump and flows through a downcomer to the core. There is a connection gap between standpipe and pool at the lower end of standpipe. In the case of the LB-LOCA design, even though the pump head keeps the water flow through the downcomer to the reactor core at operating conditions, borated water in the pool starts to enter though a lower density lock so that natural circulation starts between the lower and upper density lock connections. In other words, the pool water is not used in operating

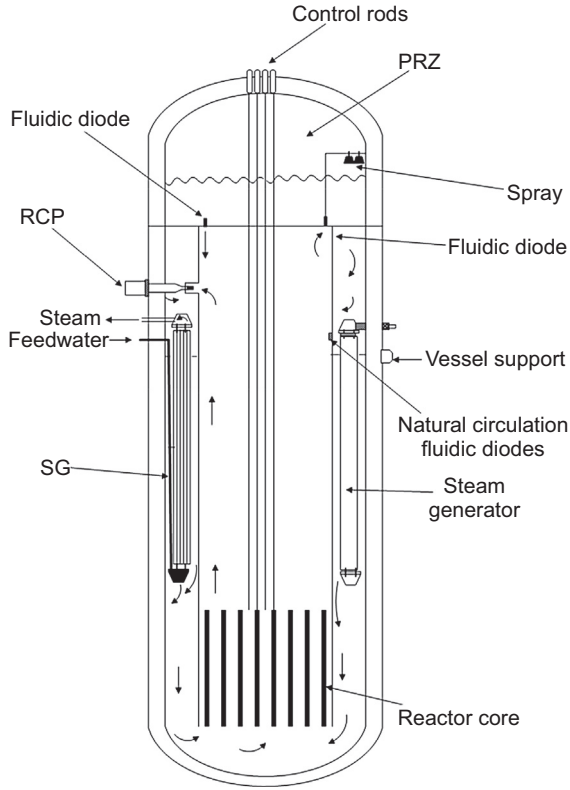


Figure 20.2 Configuration of SIR (Forsberg and Reich, 1991; Forsberg, 1983). *PRZ*, pressurizer; *RCP*, reactor circulation pump; SG, steam generator.

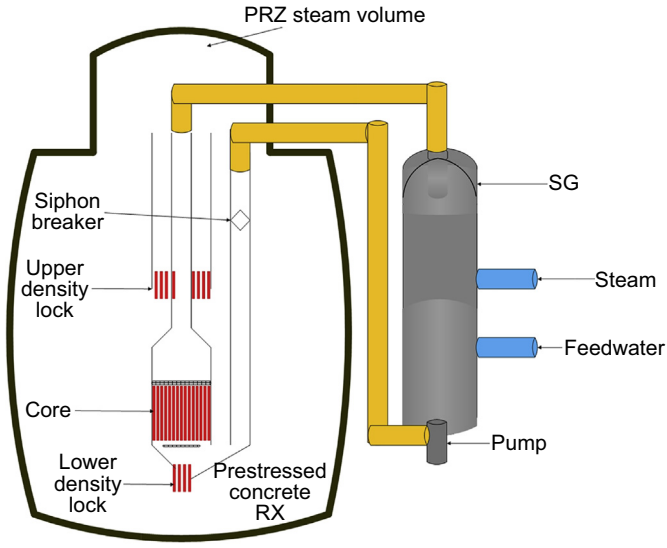


Figure 20.3 Configuration of PIUS (Forsberg and Reich, 1991; Forsberg, 1983). *PRZ*, pressurizer; *SG*, steam generator.

conditions. Even though there are circulation pipes connecting RX and SG, the vessel is located in a pool consisting of a large water inventory. Even though there might be an LB-LOCA on circulation pipes, the PIUS design is designed to handle even LB-LOCA with its large water inventory in the pool. The pool water inventory is cooled with the air to keep the pool temperature in a desired range in both accident and operating conditions. The water pool, the PRZ, and the core are enveloped with a prestressed concrete pressure vessel. The leakage from vessel is barred with a double stainless steel liner and concrete wall. PIUS's PRZ, similar to SIR, is at the top of the vessel.

Another design similar to SIR is the integrated reactor of Otto Hahn (Fig. 20.4). This reactor was designed for a commercial ship in 1960s.

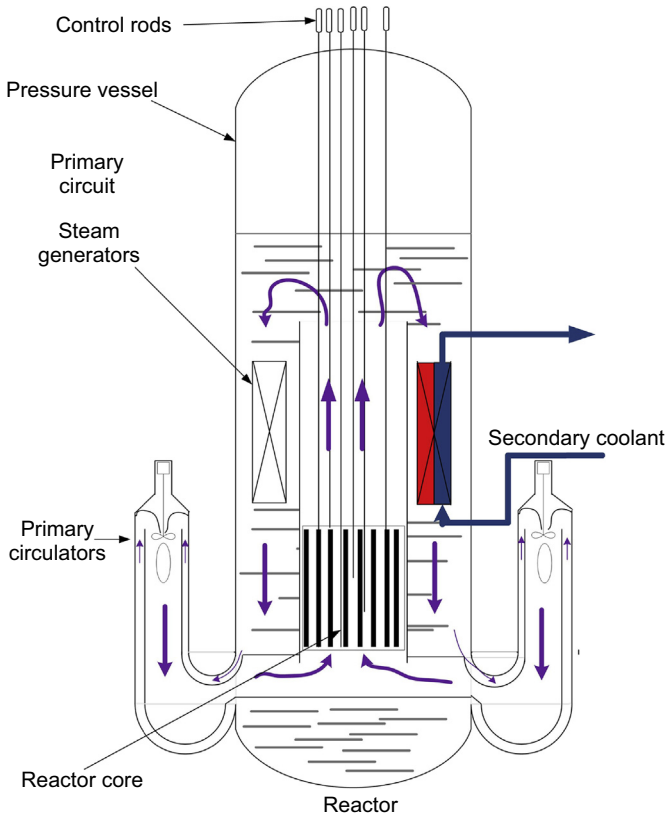


Figure 20.4 RX of Otto Hahn (Von Deobschuetz, 2005).

20.3 Nuclear reactors

Most of LW-SMR vessels are compact and integrated designs, which contain all the major RCSs along with SGs and an integral PRZ. Typical outlet temperatures are at around 300°C in LW-SMRs, which are much lower compared to ADV SMRs (non-LW-SMRs) as shown in Table 20.1. Outlet temperature could range from about 500°C to 1000°C.

Among the LW-SMRs, the IRIS vessel diameter is larger than other LW-SMRs because IRIS designers have increased the RCS inventory, and the IRIS power output is higher than other LW-SMRs. Obviously, increased RCS inventory increases the ratio of RCS inventory to produced power. In other words, there is more coolant inventory in the RCS to cool down the decay heat in accident conditions. This yields to flexibility for the safety margins, especially using US Nuclear Regulatory Commission (NRC)'s accident regulations for LWRs, defined in 10.CFR.50-46 regulations of NRC, for loss of coolant accident (LOCA). For instance, increased RCS coolant inventory provides better cooling in RX so that peak clad temperature is decreased.

Only W-SMR and mPower use internal control rod drive mechanism (CRDM) among LW-SMRs. This new design of CRDM eliminates the CRDM penetrations from the top of the RV to the core region. In addition, this new design provides free volume in the PRZ, upper plenum (UP), and in the riser of the RX. In addition, it not only simplifies the internal design of the reactor, but also decreases the pressure drop of the coolant and eliminates the maintenance of the penetrations including slaves, forging, etc.

Some of the non-LW-SMRs offer load following capability even though most of the LW-SMRs work with base load. The following needs can be met with load following capability of some SMRs (IAEA, 2002; NRC, 2014a; Kumar et al., 2012):

1. Replace fossil fuel burning power plants with SMRs because both of them have the same range or power level;
2. Use SMRs in rural places where there are limited power grids; and
3. Integrate SMRs in hybrid energy systems.

Even though load following capability gives flexibility to SMRs to change power in response to changing demands, the power change rate should never exceed 5% per min to prevent the pellet clad interaction resulting in clad rupture (Bruynooghe et al., 2010). Therefore, SMRs employing load following capability, such as W-SMR, limit linear power rate increase with the value of 5% power change per min (NRC, 2014a). Mortensen et al. (1998) identifies the typical power change of various power plants during load following: %8/min power change is a typical power change for oil, even though this change is %4/min for gas and coal-fired units. Mortensen's power change values show that SMRs' power change is in the range of other thermal gas and coal fired units.

Reactor designs of LW and non-LW-SMRs are given in Figs. 20.5−20.11.

Table 20.1 Comparison of nuclear reactors

Light water small modular reactor					
	NuScale (IAEA, 2013; NuScale, 2013a,b; IAEA, 2011a; Reyes, 2012)	**W-SMR** (Matzie, 2015; NRC, 2014a; W, 2013)	**IRIS** (Carelli et al., 2004, 2003a,b,c)	**SMART** (Park, 2011a, 2011c; Kim et al., 2014)	**mPower** (Babcock, 2013; IAEA, 2011b; State of New Jersey, 2014; ANSI, 2012; Ghosh et al., 2014)
Vessel diameter (m)	~2.7	3.5	6.21	5.99	3.924
Vessel height (m)	~14	~27	22	~16.1	25.2984
Vessel penetration	SSP	SSP	SSP	SSP	NPBTC
Control rod drive mechanism	External	Internal	External	External	Internal
Thermal power MW_{th})	160	~800	1000	330	530
Electricity power (MW_e)	45	~225	335	100	155 (for air-cooled condenser) 180 (for water-cooled condenser)
Capacity factor (%)	>95	–	>95	–	>95
Designer	NuScale	Westinghouse	IRIS Consortium	KAERI	Babcock & Wilcox
Mode of operation	BL	BL and LF	BL	BL and LF	BL and LF

Non-LW-SMR			
	PRISM (Power Reactor Innovative Small Module) (PRISM, 1994; GE Hitachi, 2015; Van Tuyle et al., 1989)	**4S (Super Safe, Small and Simple reactor) (NRC, 2013; Toshiba CREIPI, 2013)**	**Hyperion (GEN4) (Gen4energy, 2013)**
Reactor vessel Dimensions (m × m)	5.74 × 16.9	2.5 × 23	1.5 × 2
Thermal power (MW_{th})	840	30–135	70
Electricity power (MW_e)	311	10–50	25
Moderator	No Mod.	No Mod.	No Mod.
Designer	GE	Toshiba	GEN4
Mode of operation	BL and LF	BL and LF	BL

Where *SSP*, secondary side penetrations; *BL*, base load; *LF*, load following.

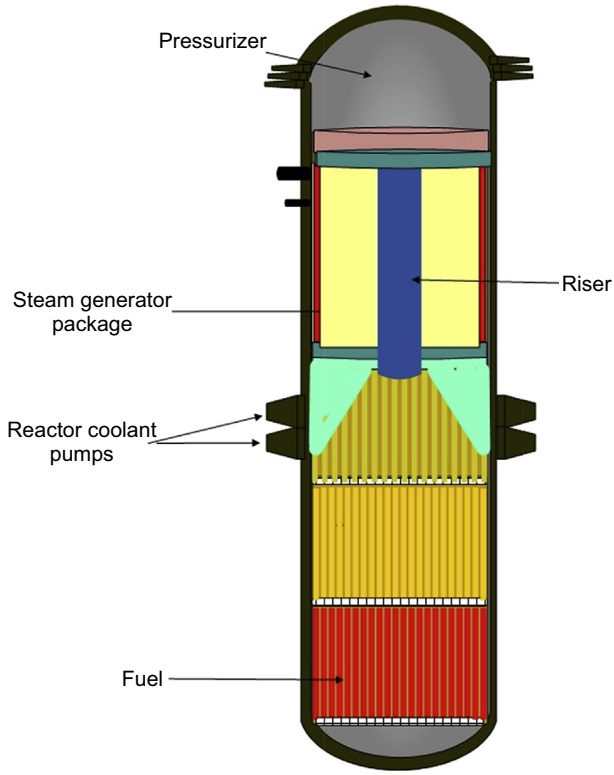


Figure 20.5 RX of W-SMR (Wheeler, 2012).

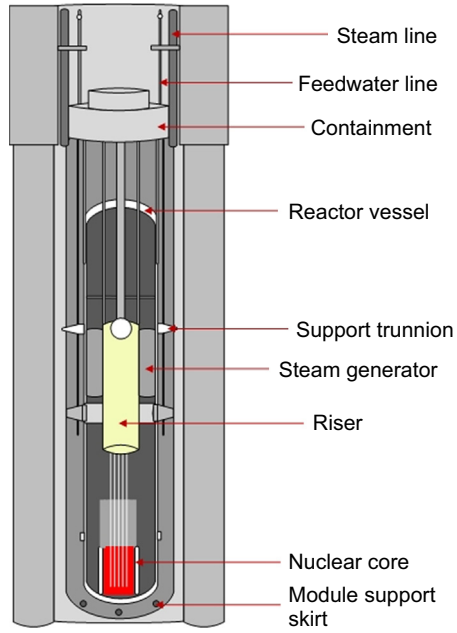


Figure 20.6 RX of NuScale (NRC, 2014b).

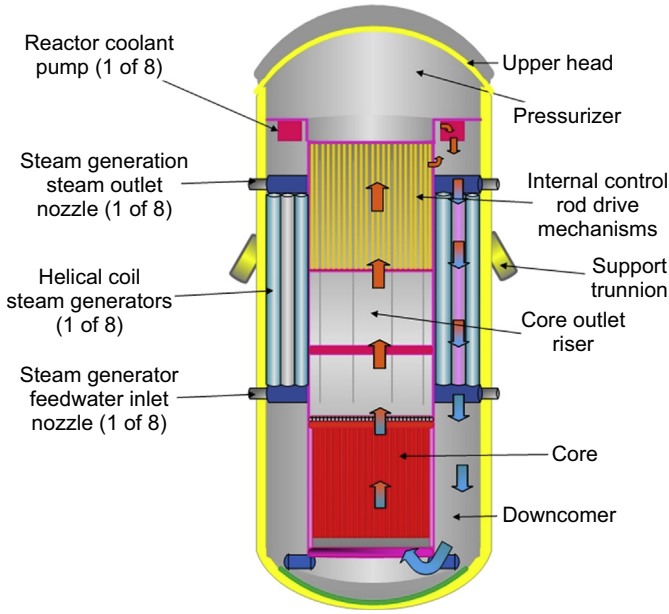


Figure 20.7 RX of IRIS (Carelli et al., 2003b).

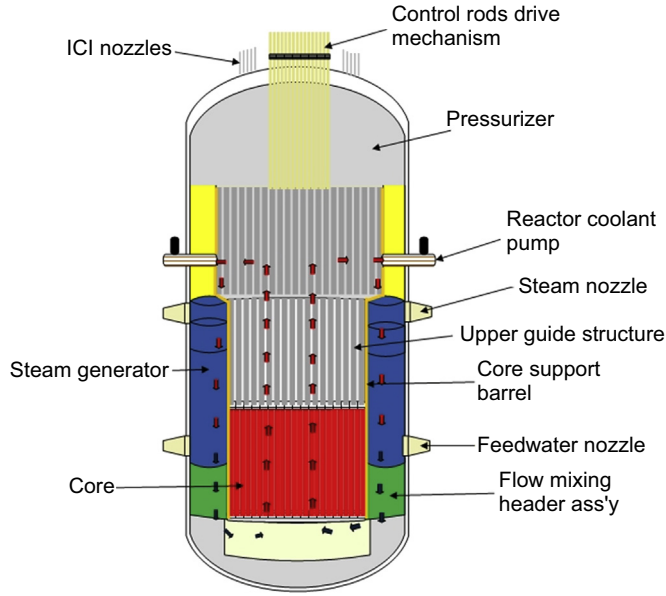


Figure 20.8 RX of SMART (IAEA, 2011a; Park, 2011a) *ICI*, in-core insturments; *Ass'y*, assembly.

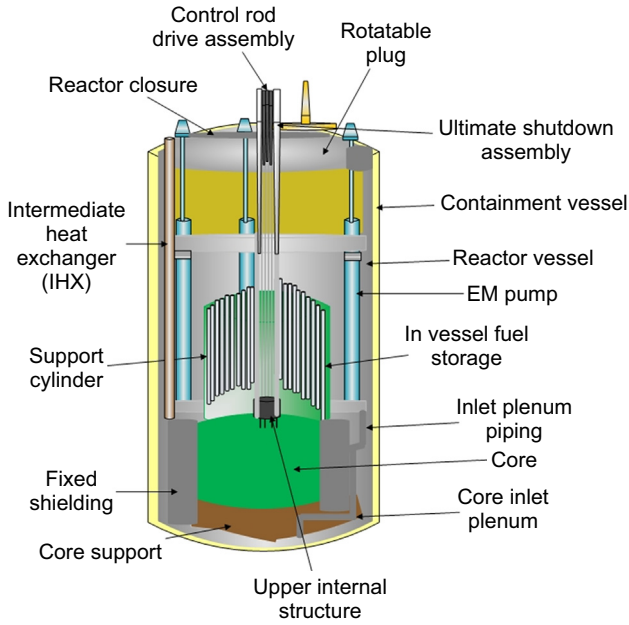


Figure 20.9 RX of PRISM (Nathan, 2013). *EM*, electromagnetic pump.

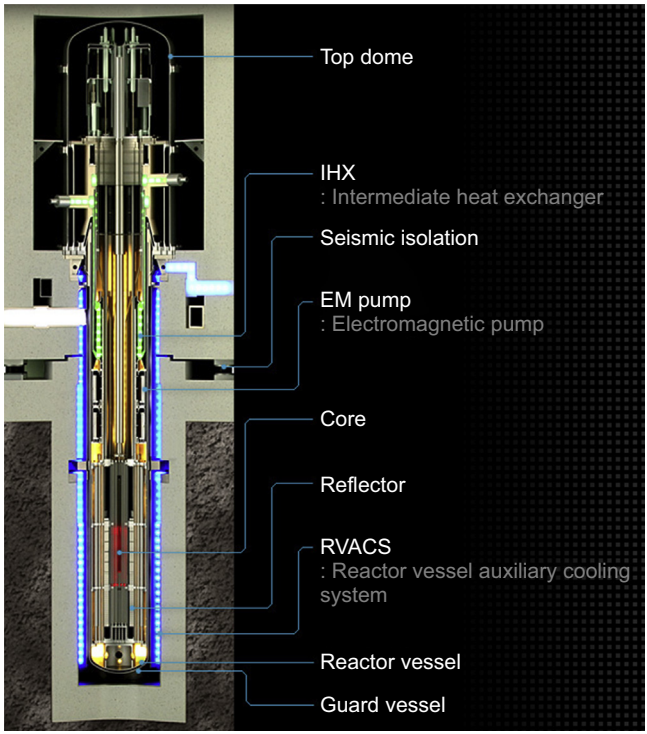


Figure 20.10 RX of 4S (Toshiba, 2015).
Courtesy of Toshiba Corporation.

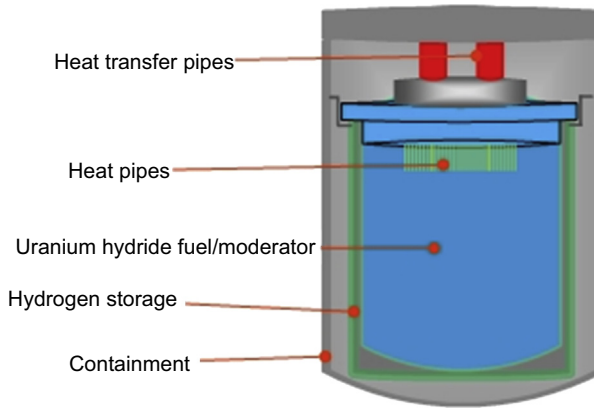


Figure 20.11 RX of Hyperion (Ganino, 2014).

20.4 Reactor coolant system components

The RCS is used to cool down the reactor core under operating conditions. Losing RCS coolant inventory will lead to core heat-up. In addition, the RCS coolant is enveloped generally within the pressure boundary, which is generally provided by the RV. Therefore, the penetrations on RV are eliminated to avoid large break (LB) or small break LOCA. Therefore, most of the integrated designs envelop RCS components in the pressure boundary.

Similar layouts (employing PRZ, SG, pump, etc.) are seen in most of the LW-SMRs, as shown in Figs. 20.1–20.3 and 20.5–20.8. PRZ is located at the top of the RV since PRZ employs 2-phase flow. Even though long and thin PRZs are desired to decrease the water level uncertainty, PRZs of LW-SMRs are short. Even though PRZ designs in LW-SMRs are similar to each, IRIS PRZ is slightly different than other PRZs. The IRIS PRZ uses only PRZ heaters instead of heaters and sprays. Increasing PRZ volume allows IRIS to eliminate sprays.

Another challenge for LW-SMRs is the limited room in the RV. Therefore, sizing of each RCS component is challenging. For instance, W-SMR solves the sizing issue about SG by using two components (a low quality SG and a steam dome) instead of one typical commercial SG component (Fig. 20.12) to produce high-quality vapor for turbines. The first component produces steam, which has small vapor fraction percentage that is not suitable for steam turbines. The second component separates the steam from liquid in the steam dome. This simple and effective approach is very common in early designs of navy reactors. By using this design, only secondary coolant is moved outside of the RV and enables a decrease in the size of RV.

NuScale is the only LW-SMR that uses natural circulation in operating conditions, as shown in Table 20.2. This feature decreases the number of RCS components. Since natural circulation is a challenging issue to get licensed in the US, NuScale (like the AP1000) uses the scaled integrated experimental facility in Oregon State University for design of NuScale SMR and validation of code predictions.

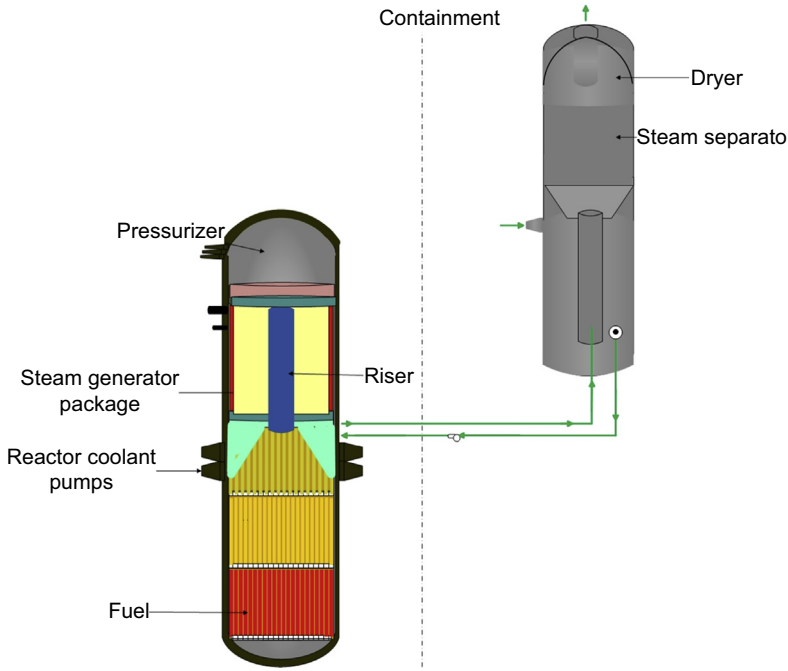


Figure 20.12 Split SG of W-SMR (Carelli et al., 2004; NRC, 2014a).

High core outlet temperature of coolant can only be provided by the non-LW-SMRs. Therefore, N = non-LW-SMRs can be used to produce high temperature steam for facilities/factories and to generate electricity with high efficiency.

The RCS comparison of SMRs is given in Table 20.2.

20.5 Fuels

Fuels used in SMRs are generally selected from the existing fuel designs. For instance, most of the LW-SMRs employ a 17 × 17 bundle design by decreasing its length. Using existing fuel designs decreases number of experiments required for validation, thereby reducing development costs for LW-SMRs. However, non-LW-SMRs use relatively new fuel designs so that all these new fuel designs must be validated against experimental results, especially using radiation conditions. These kinds of uncompleted tasks for the licensing of the non-LW-SMRs may cause design changes in the future.

Typical 17 × 17 fuel assemblies are used in LW-SMRs (Table 20.3). The differences between fuels assemblies used in LW-SMRs and commercial LWRs (such as AP1000) are the height and fuel cycle length of the fuel. Most of the non-LW-SMRs utilize unique fuel designs, as shown in Table 20.3.

Table 20.2 Comparison of RCS components

Light water small modular reactors					
	NuScale (IAEA, 2013, 2011b; Babcock, 2013; NuScale, 2013a,b; Reyes, 2012)	**W-SMR (Carelli et al., 2004; NRC, 2014a)**	**IRIS (Gen4energy, 2013; Carelli et al., 2003a,b,c)**	**SMART (Park, 2011a,c; Kim et al., 2014)**	**mPower (PRISM, 1994; NRC, 2013; State of New Jersey, 2014; ANSI, 2012; Ghosh et al., 2014)**
Outlet condition (°C)	~300°C (At 1500 psig/10.3421 MPa)	343°C (at 2500 psig/ 17.2368 MPa)	330°C	323°C	320°C (at 2050 psi/14.1342 MPa)
Steam generator type	Helical	Straight tube	Helical	Helical	Helical
Pressurizer in reactor vessel	Yes	Yes	Yes	Yes	Yes
Pressurizer active components	Heaters and sprays	Heaters and sprays	Heaters, No spray	–	Integral electric heaters
Circulation type	Natural	Forced	Forced	Forced	Forced

Non-LW-SMR			
	PRISM (PRISM, 1994; GE Hitachi, 2015; Van Tuyle et al., 1989)	**4S (NRC, 2013; Toshiba CREIPI, 2013)**	**Hyperion (Gen4energy, 2013)**
Outlet condition (°C)	~500	510	500
Operating pressure (MPa)	Low pres.	0.3	Ambient pressure
Steam generator type	Helical	Straight tube	Helical
Circulation type	Natural	Forced (two electromagnetic pumps in series)	Forced
Coolant type	Sodium	Sodium	Lead–bismuth eutectic

LW-SMRs generally employ 5% fuel enrichment, and non-LW-SMRs can have much higher fuel enrichment value (Table 20.3). For example, Hyperion uses about 20% enriched U-235 and U-238.

Table 20.3 Comparison of fuel components

Light water small modular reactors					
	NuScale (IAEA, 2013, 2011a; NuScale, 2013a,b; IAEA, 2011a; Reyes, 2012)	**W-SMR** (Matzie, 2015; NRC, 2014a; W, 2013)	**IRIS** (Carelli et al., 2003a,b,c, 2004)	**SMART** (Park, 2011a,c; Kim et al., 2014)	**mPower** (Babcock, 2013; IAEA, 2011b; State of New Jersey, 2014; ANSI, 2012; Ghosh et al., 2014)
Bundle type	17 × 17	17 × 17	17 × 17	17 × 17	17 × 17
Fuel length (m)	1.8288	2.4384	4.2672	2.01168	2.4130
Maximum fuel enrichment (w%)	4.95	<5	<5	<5	<5
Refueling frequency (years)	2−2.5	2	3.5	>3	4+
Control rod drive mechanisms	External	Internal	External	External	Internal
Fuel type	UO_2 pin	UO_2 pin	UO_2 pin	UO_2 pin	UO_2 pin
Active core height (m)	2	~2.4	~4.3	2	N/A
Cladding material	Zr-4 or advanced cladding	ZIRLO	Zr Alloy	Zr-4	Stainless steel

Lattice geometry	Square	Square	Square	Square	Square
Mode of reactivity control	Control rods, boric acid	Control rods, boric acid	Control rods, boric acid	Control rods, integrated B/A	Control rods, burnable poison
Mode of reactor shutdown	Control rods	Control rods	Control rods	Control rods, soluble boron	Control rods
Non-LW-SMR					
	PRISM (PRISM, 1994; GE Hitachi, 2015; Van Tuyle et al., 1989)		**4S (NRC, 2013; Toshiba CREIPI, 2013)**	**Hyperion (Gen4energy, 2013)**	
Bundle type	–		Hexagonal	–	
Fuel length (m)	–		2.5	–	
Maximum fuel enrichment (%)	26		18–19	<5	
Refueling frequency (years)	2		30	7–10	
Reactivity control system	Control rods + B4C Spheres		Axially movable reflectors	Hydrogen gas	
Fuel type	U-TRU-Zr (uranium–transuranic–zirconium alloy–metal fuel)		U–Zr (metal fuel)	UN	

Where *B/A*, burnable absorber.

LW-SMRs control the reactivity by using very commonly used techniques, such as soluble boron, burnable absorbers, and control rods. However, non-LW-SMRs use innovative techniques to control reactivity. For instance, 4S uses movable reflectors to control the reactivity. Using movable reflectors instead of chemical shim in the RCS eliminates the chemical control of chemical shim and chemical interaction between chemical shim and internal components of RCS. In addition, using a reflector around the reactor core is used as a passive (and/or an inherent) safety system to make the reactor subcritical in an accident condition. Economically, there is tradeoff between using a mechanical component to move the reflector and neglecting chemical control system for chemical shim. Another interesting example is Hyperion to control the reactivity since it uses hydrogen gases for reactivity control. The economical challenge for using hydrogen is its high production cost.

20.6 Containment

Containment is the last barrier in the defense in-depth strategy. Therefore, the containment vessel has to cover the components that may leak radioactive materials. In case of an accident, the containment wall has to be strong enough to handle high containment pressure. Ideally, a spherical containment shape is ideal for mechanical challenges. However, this design increases the capital cost of an SMR. Therefore, all the SMRs except IRIS use cylinder geometry (Table 20.4).

Containment designs are shown in Figs. 20.13–20.17. NuScale's containment design is the simplest containment design among SMRs. The reason is NuScale's ECCS system, Triple Crown (NuScale, 2013a,b), does not need several emergency tanks. This design simplifies the ECCS as well as decreases ECCS components significantly. Triple Crown system is discussed in the ECCS section of this article in detail.

20.7 Emergency core cooling system

ECCS removes the decay heat during accident conditions. Because the DOE tends to fund passive safety systems, almost all the SMR designs employ passive safety systems. However, some of them can remove the decay heat for a limited time without operator and/or active component action.

NuScale's ECCS, Triple Crown (NuScale, 2013a,b), employing ECCS, can remove the decay heat indefinitely without an external power source such as a battery, operator action, and additional coolant (Fig. 20.18). Safety valves in the NuScale design are opened without using an external power source just after an accident has been recognized. Then, the Triple Crown system removes the decay heat by using natural circulation (Fig. 20.18). At the first step, water has been circulated between the RV

Table 20.4 Comparison of containments

Light water small modular reactor					
	NuScale (IAEA, 2013, 2011a; NuScale, 2013a, 2013b; Reyes, 2012)	**W-SMR** (Matzie, 2015; NRC, 2014a; W, 2013)	**IRIS** (Carelli et al., 2003a,b,c, 2004)	**SMART** (Park, 2011a,c; Kim et al., 2014)	**mPower** (Babcock, 2013; IAEA, 2011b; State of New Jersey, 2014; ANSI, 2012; Ghosh et al., 2014)
Containment shape	Cyl.	Cyl.	Sph.	Cyl.	Cyl
Containment size (ft × ft)	80 × 15 (24.384 × 4.572 m)	~89 × 32 (26.2128 × 9.7536 m)	82 (24.9936 m)	~144 (43.8912 m)	N/A

Non-LW-SMR			
	PRISM (PRISM, 1994; GE Hitachi, 2015; Van Tuyle et al., 1989)	**4S** (NRC, 2013; Toshiba CREIPI, 2013)	**Hyperion**
Containment geometry	Cylinder (cont. vessel and dome)	Cyl./cph. geometry (guard vessel and top dome)	N/A
Containment size (m × m)	6.04 m diameter	3.65 × 8	N/A

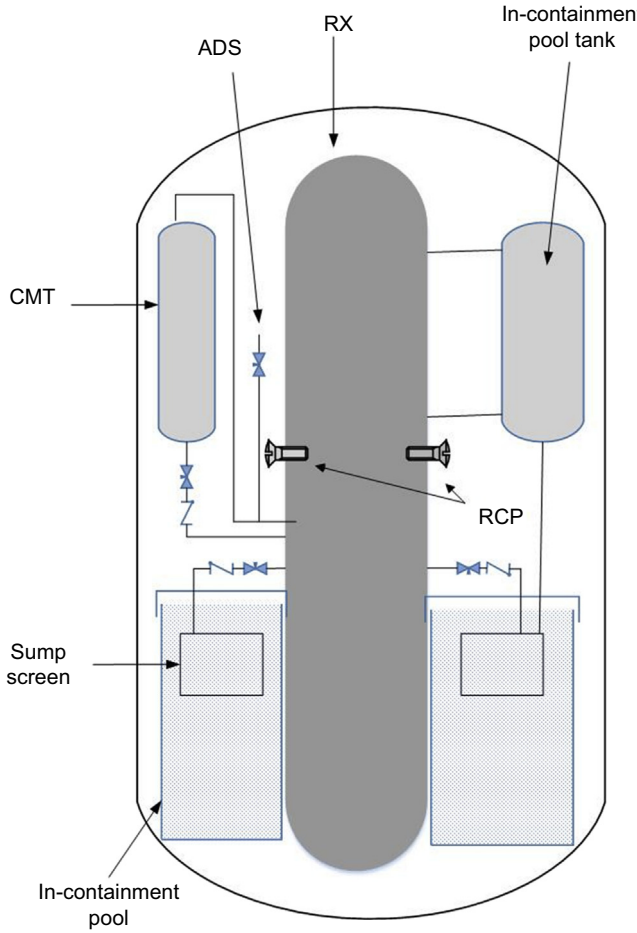


Figure 20.13 Containment of W-SMR (Carelli et al., 2004; NRC, 2014a). *ADS*, automatic depressurization system; *CMT*, core makeup tank; *RX*, reactor.

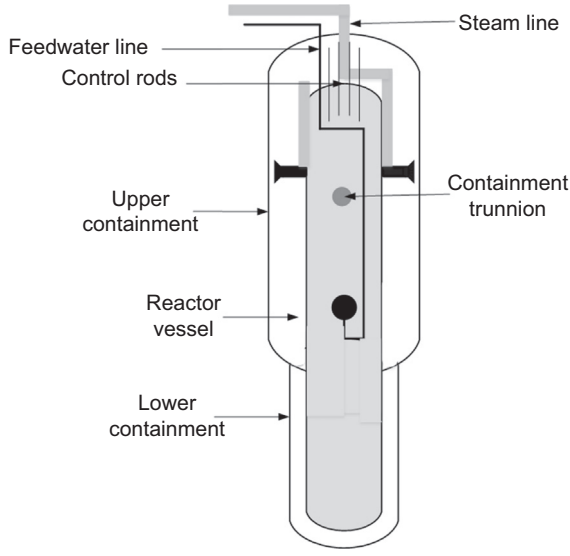


Figure 20.14 Containment of NuScale (NuScale, 2014).

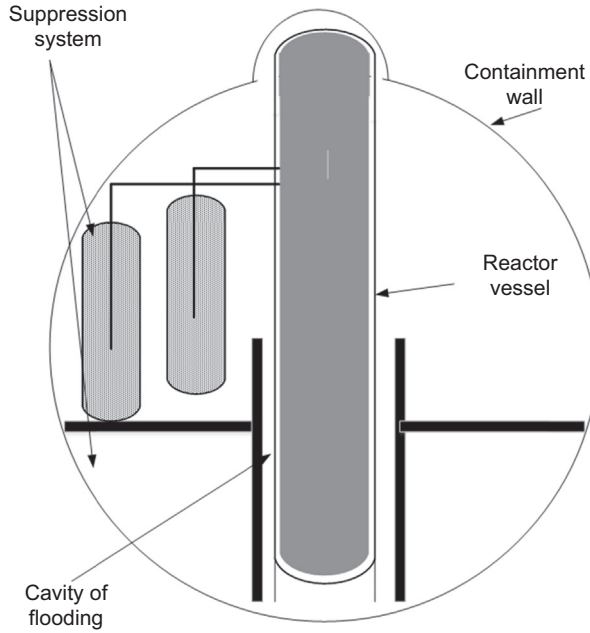


Figure 20.15 Containment of IRIS (Carelli et al., 2003b, 2004).

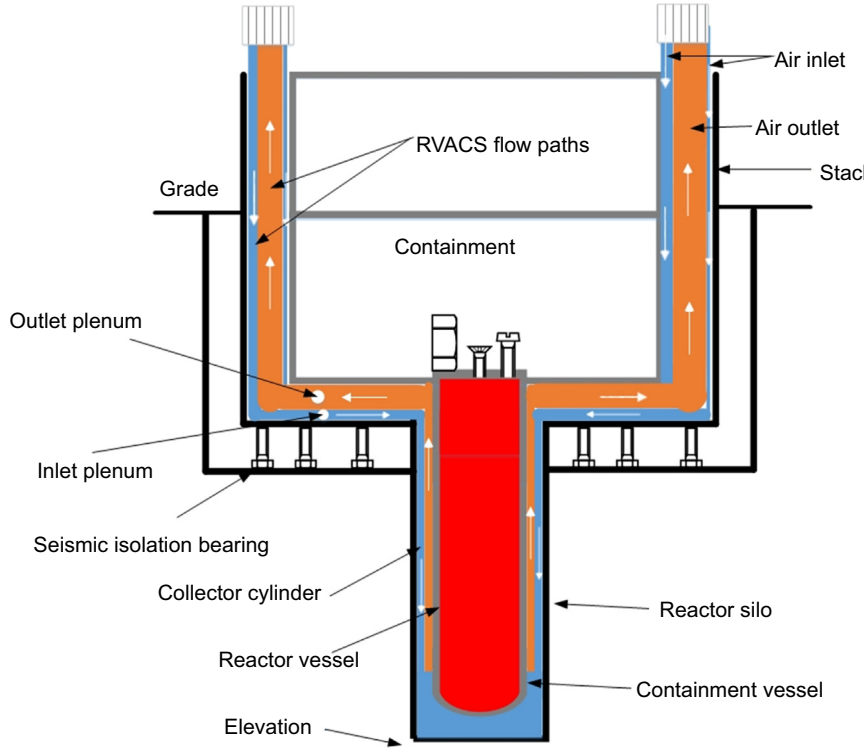


Figure 20.16 Containment of PRISM (GE Hitachi, 2015). *RVAC*, reactor vessel auxiliary cooling system.

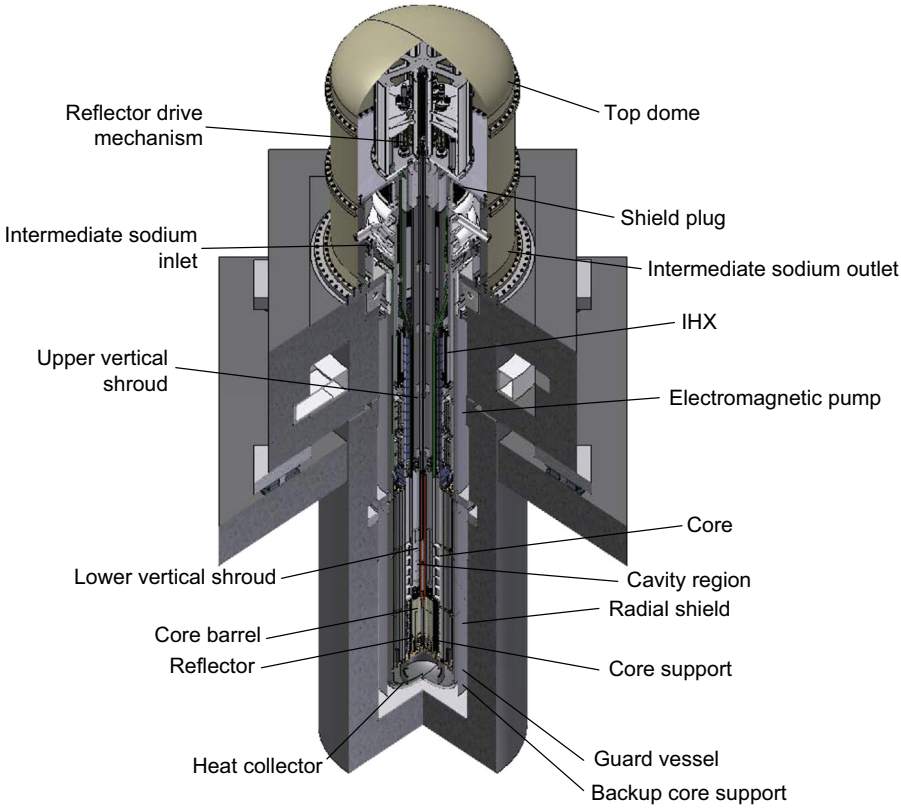


Figure 20.17 Containment of 4S (Toshiba, 2015). *IHX*, intermediate heat exchanger. Courtesy of Toshiba Corporation.

and the coolant inventory in the containment. Then, latent heat removes the heat in the second stage. Finally, air cools the RV wall at the decreased level of decay heat, which is in the long-term cooling stage.

W-SMR employs several safety tanks to remove the decay heat at least 7 days, as summarized in Table 20.5 and shown in Fig. 20.19.

IRIS's ECCS system is similar to W-SMR, as shown in Fig. 20.20.

The safety system (Fig. 20.21) of SMART includes a shutdown cooling system, residual heat removal system, safety injection system, reactor overpressure protection system, and emergency boron injection tank. Each of the four independent passive residual heat removal systems with 50% capacity can remove the core decay heat through natural circulation at any design basis events. This feature can keep the core undamaged for 72 h without any corrective action by operators in a design basis accident (Kim et al., 2014).

ECCS of PRISM has varied shutdown features (IAEA, 2003). The passive safety system of PRISM has been supported by inherent safety features, such as Doppler

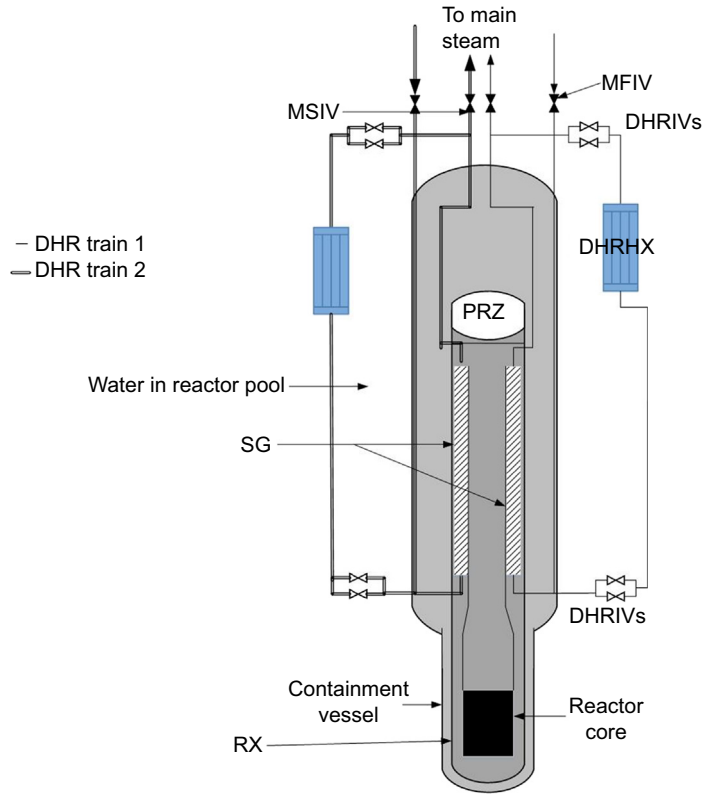


Figure 20.18 ECCS of NuScale (Reyes, 2012). *DHRIV*, decay heat removal isolation valve; *MSIV*, main steam isolation valve; *RX*, reactor; *MFIV*, main feedwater isolation valve; *DHRHX*, decay heat removal heat exchanger; *DHRIV*, decay heat removal isolation valve.

Table 20.5 W-SMR nuclear safety components

Nuclear safety related actions	Which component is used for the nuclear safety action?
Short-term reactivity controls	Control rods
Long-term reactivity controls	Core makeup tanks
Decay heat removal	Passive residue heat removal heat exchanger/ultimate heat sink tank(s)
Long-term makeup water supply	In-containment pool tanks/sump
Ultimate heat sink	Ultimate heat sink tank (7 days)
Severe accident management	In-vessel retention

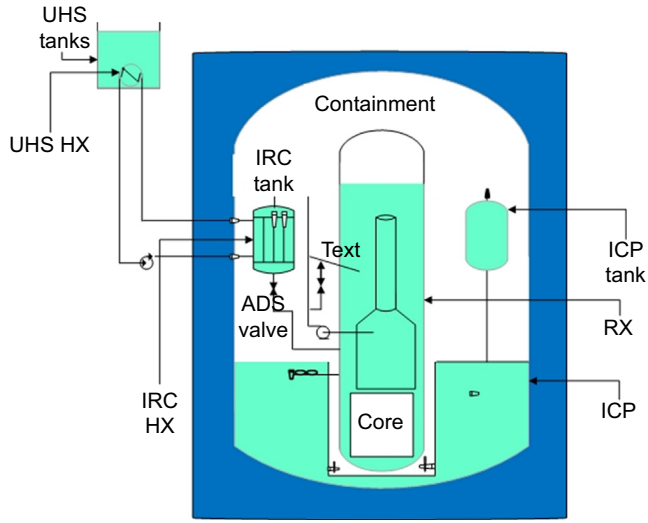


Figure 20.19 ECCS of W-SMR (Matzie, 2015; NRC, 2014a). *IRC*, inside reactor containment; *UHS*, ultimate heat sink; *HX*, heat exchanger; *RX*, reactor; *ADS*, automatic depressurization system.

effect, multidimensional fuel expansion, sodium density decrease, and also RV expansion. In addition, the passive reactor vessel auxiliary cooling system (RVACS) is the primary heat removal during not only anticipated transients without scram, but also all design basis accident conditions. Like NuScale's ECCS, PRISM's safety system can remove the decay heat in infinite time by using passive safety features. Similar to high temperature gas reactors' reactor core cavity system, the decay heat is transferred from the RV to the containment vessel via thermal radiation. Containment is cooled by natural convection of air outside of containment. On top of typical passive safety systems in PRISM, auxiliary cooling system can also be used to remove decay heat by utilizing natural circulation of air past the SG.

4S has several safety systems: active, passive, and inherent (IAEA, 2003) (see Fig. 20.22). Active shutdown systems are: (1) inserting reflectors by using gravitational force; and (2) inserting black control rods. The passive safety system of 4S uses natural circulation in RVACS and Intermediate Reactor Auxiliary Cooling System (IRACS). In addition, inherent safety system uses Doppler effect via metallic fuel and large inventory of coolant.

Gen4 or HYPERION's safety system can remove the decay heat in two ways: (1) dumping the steam to the condenser; and (2) if first decay heat removal way is not sufficient, back up decay heat removal system is used. This system utilizes natural circulation of primary coolant through bypass path in the core. The surface of Gen-IV module is cooled with latent of heat via water sprays provided by emergency cooling tank. The water inventory in this tank can be injected due to gravitational force to remove the decay heat for 2 weeks. The second system works as a passive safety system.

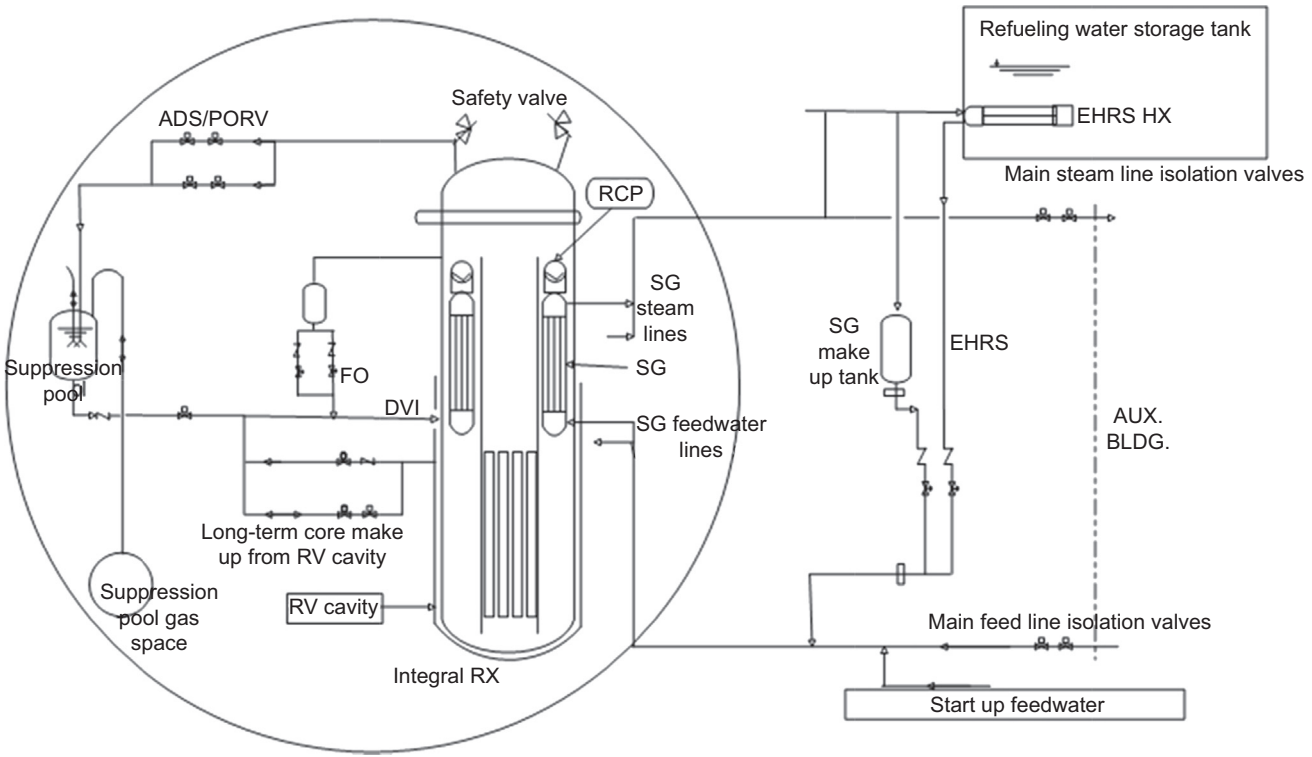


Figure 20.20 IRIS ECCS system (Carelli et al., 2003b, 2003c). *PORV*, power-operated relief valve; *SG*, steam generator; *RCP*, reactor circulation pump; *EHRS*, emergency heat removal system; *ADS*, automatic depressurization system; *RV*, reactor vessel; *FO*, fail open valve; *DVI*, direct vessel injection.

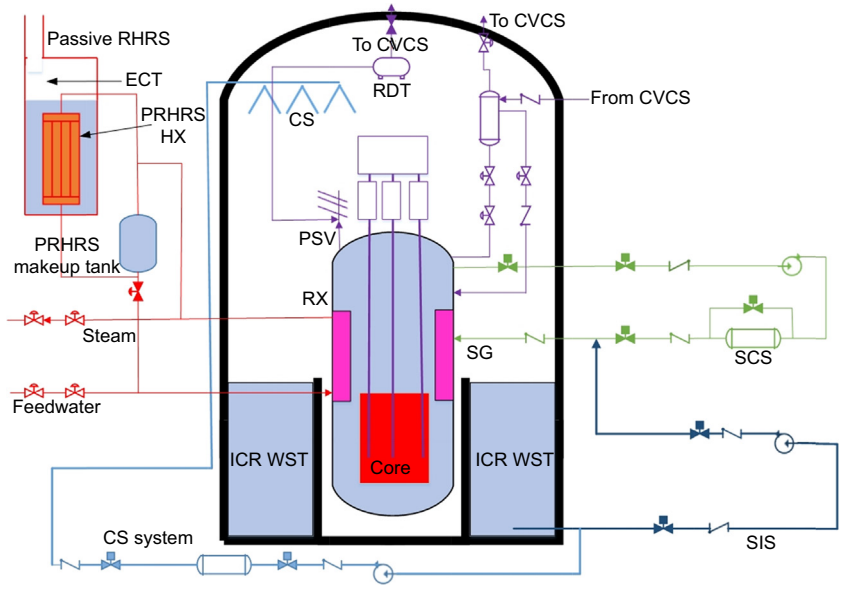


Figure 20.21 SMART ECCS system (Park, 2011c, 2011b). *PRHRS*, passive residual heat removal system; *RHRS*, residual heat removal system; *CVCS*, chemical and volume control system; *ICRWST*, in-containment refueling water storage tank; *SG*, steam generator; *RDT*, reactor drain tank; *SIS*, safety injection system; *ECT*, emergency cooldown tank; *HX*, heat exchanger; *RX*, reactor; *CS*, containment system.

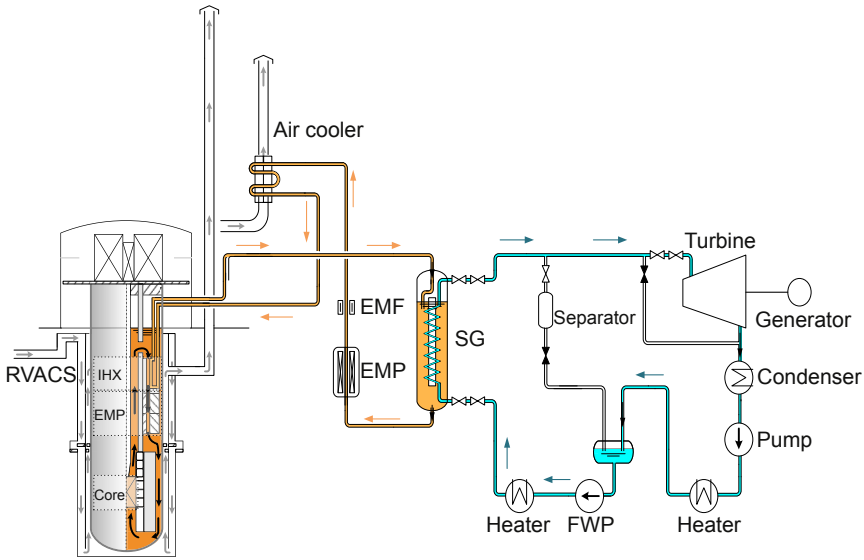


Figure 20.22 ECCS system of 4S (Prasad, 2012). *EMP*, electromagnetic pump; *EMF*, electromagnetic field; *SG*, steam generator; *EMP*, electromagnetic pump; *IHX*, intermediate heat exchanger; *FWP*, feedwater pump.

20.8 Economic and financing evaluation

Given the early stage of SMR development, there is no directly applicable historical cost information available, nor is there any publicly available detailed vendor cost information. It is clear, however, that in line with the preceding review of SMR designs, there are several design features that not only make SMRs significantly different from typical large nuclear power plants (NPPs), but also impact their projected costs. Most apparent is that their smaller reactor size and power output are substantially different from traditional NPPs. Some earlier studies attribute significant economies of scale to the construction of large nuclear plants (Christiensen and Greene, 1976; Krautmann and Solow, 1988). Under this assumption, the relationship between the overnight capital costs and the size of reactors of similar design and characteristics can be expressed as:

$$\mathrm{OCC_{SMALL}} = \mathrm{OCC_{LARGE}} \times (\mathrm{Size_{SMALL}}/\mathrm{Size_{LARGE}})^{n}$$

where $\mathrm{OCC_{SMALL}}$ and $\mathrm{OCC_{LARGE}}$ are the overnight capital costs of small and large NPPs, respectively, and $\mathrm{SIZE_{SMALL}}$ and $\mathrm{SIZE_{LARGE}}$ are respective reactor sizes, in MWe, and n is the scaling factor, often taken to be in the range of 0.4 to 0.7 (Phung, 1987). Based on this view, scaling down from gigawatt-sized NPPs to smaller SMRs would result in a significant loss of scale economies with a resulting increase in overnight capital costs.

There are, however, several factors that contrast with this view. The first stems from the failure of anticipated declines in unit costs to be realized with the dramatic increase in the size of NPPs during the 1970s−1980s. This has led many to maintain that scale economies in NPPs are likely very modest and may, in fact, be negative [see, for example, Kessides, 2012a,b; Grubler, 2010]. Second, the relationship between reactor size and costs, as stated above, is estimated for reactors of similar design and characteristics. The comparisons of different SMR designs in the present study demonstrate that SMRs have several features that are significantly different from conventional large nuclear plant designs that are likely to offset any loss scale economies that may exist.

The simplified SMR design features described earlier result in a reduction in the number of components along with a reduction in overnight costs. In addition, the safety characteristics of SMR designs are enhanced due not only to smaller reactor sizes, but also to the use of passive cooling systems. Further, the modularity of SMR designs enables the fabrication of the major components of the power unit, including the RV, steam supply, and cooling system in centralized manufacturing facilities and shipped in component parts via rail, truck, or ship for on-site installation (Carelli et al., 2010). Modularity has several advantages, including standardization of both components and design and resulting significant economies of mass production.

Further, “economies of mass manufacturing” are achieved when the SMR modules are manufactured in centralized, large-scale manufacturing facilities rather than on-site

for a large NPP. These economies of mass manufacturing have been shown to account for significant reductions in per unit manufacturing costs (Rosner et al., 2011; Boarin et al., 2012). The scale economies gained from modularization and mass manufacturing are enhanced from lessons learned during the manufacturing process. These result in productivity and efficiency gains with increases in the number of successive modules over the deployment schedule, and further reduce per unit overnight costs. Modularity also results in lower capital costs and reduced construction and installation times as compared to large nuclear or fossil fuel power plants. These, thereby, further reduce both financing costs and risk levels.

These cost advantages of SMRs suggest that SMRs can be economically competitive with large NPPs as well as energy production from fossil fuel and renewable energy facilities. Cost estimates include $50,000/kWh for the SMART design (Vujic et al., 2012), $4000/kWh for the NuScale design, and $5000/kW$_e$ for the IRIS design (World Nuclear Association, 2008). These estimates imply that the levelized cost of electricity from SMRs will be cost competitive with renewables and coal facilities and with natural gas facilities outside of North America (World Nuclear Association, 2008). Further, the cost advantages of SMRs extend beyond the initial capital costs in that SMRs are subject to much lower fuel price sensitivity risk than large coal or natural gas facilities because fuel costs comprise a much lower share of operating costs than is the case for fossil fuel plants (Pratson et al., 2013). This is apparent in the relative stability of nuclear energy production operating costs over time, as shown in Fig. 20.23 (NEI, 2014).

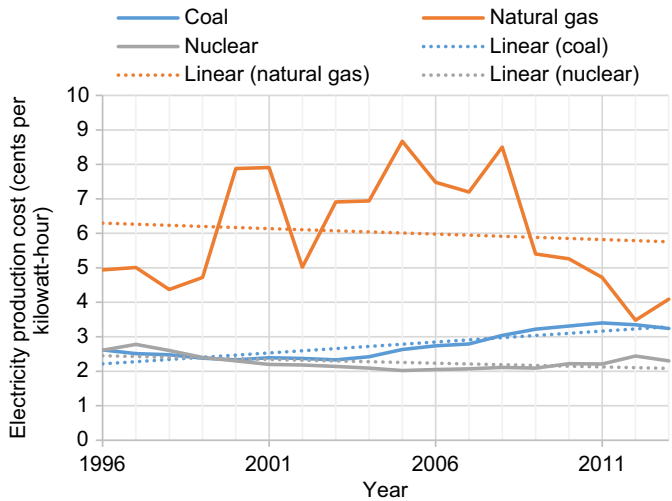


Figure 20.23 US electricity production costs (NEI, 2014). Where Production Costs = Operations and Maintenance Costs + Fuel Costs. Production costs do not include indirect costs and are based on Federal Energy Regulatory Commission (FERC) Form 1 filings submitted by regulated utilities. Production costs are modeled for utilities that are not regulated.
Ventyx Velocity Suite (NEI, 2014. http://www.nei.org/Knowledge-Center/Nuclear-Statistics/Costs-Fuel,-Operation,-Waste-Disposal-Life-Cycle/US-Electricity-Production-Costs-and-Components).

Besides overnight capital costs and all-in costs that include financing and construction, there are costs relating to development, design certification, and licensing. SMRs present new challenges for the industry and the NRC. With industry stakeholder input, the NRC has slowly but methodically been addressing issues for both light water (LW) and non-LW reactors relating to insurance requirements (US Nuclear Regulatory Commission, 2011a), the security regulatory framework (US Nuclear Regulatory Commission, 2011b), and mechanistic source term (US Nuclear Regulatory Commission, 2013), among others. The NRC is focusing primarily on the LW designs that have Department of Energy licensing support: mPower and NuScale. NRC policy papers, memoranda, and a 2012 report to Congress (US Nuclear Regulatory Commission, 2012) express the need for more research resources and international cooperation to fully address the human resource requirements to certify and license advanced designs. Advanced reactor high temperature and liquid metal design and development costs would be negatively impacted if the NRC does not keep pace with development and research advances more quickly than anticipated.

The US also provides incentives for SMRs that will assist with bringing all-in costs down for the first orders, assuming SMR development continues to advance. Eligibility for US incentives is predicated on domestic manufacturing and/or domestic installation and power production, depending on the particular incentive. The US issued a draft federal loan guarantee solicitation announcement for advanced nuclear energy projects, of which $10.6 billion is available for nuclear power facilities, including SMRs (US Department of Energy Loan Programs Office, 2014). The US currently provides a production tax credit (PTC) for a limited amount of nuclear capacity (Solan et al., 2010); it is possible that power for SMRs in the future may be eligible for remaining capacity under the PTC or a new set-aside for an SMR-specific PTC.

While the US has taken some steps to incentivize nuclear power projects, including SMRs, one of the major hindrances to the building of new large nuclear projects at the global level is the lack of financing. Commercial banks, multilateral development banks (MDBs), and export/import credit agencies provided funding in the past, but have not been willing to provide funds for nuclear projects. For commercial banks, high initial capital costs and extended construction periods, during which costs escalate have combined to increase the financing risk for nuclear builds. These projects also have significant delays in financing returns on investment, especially in liberalized electricity markets.

The decrease in funding from commercial banks has been accompanied by a commensurate decrease in lending on the part of MDBs over the same period. Indeed, some MDBs have placed moratoria on funding nuclear power projects. Major examples include the World Bank, which, while acknowledging that nuclear power can contribute to climate change goals, has not yet altered its policies against lending for nuclear projects, and the Asian Development Bank, which recently reaffirmed its policy of not funding nuclear power facilities (Findlay, 2012). The reluctance on the part of MDBs to invest in large nuclear power projects stems largely from the high up-front capital costs, the widespread underestimation of true final costs, and the inflexibility of NPPs as electricity generators, particularly for emerging economies (World Bank Technical Paper #154, 1994). These issues are mitigated by the features of SMRs, including reduced

cost and financing risks, the ability to be integrated with other sustainable energy sources, and nonenergy applications. In addition, increasing energy demands can be met incrementally without tying up large amounts of money for long periods of time.

Since the financial crisis, there has been a dramatic increase in funding for low-carbon energy projects on the part of MDBs (Bloomberg New Energy Finance Report, 2010). For example, The Asian Development Bank, Inter-American Development Bank, and the European Investment Bank all list low-carbon energy projects among their top priorities, with the latter listing renewable energy, energy efficiency, and nuclear projects as part of its corporate investment plan (Fu-Bertaux, 2011). The World Bank has significantly increased funding for low-carbon projects as well as district heating and displacement of carbon-intensive fuels as part of its energy strategy. The features of SMRs can further the achievement of these goals, and funding from MDBs for SMR deployment will increase. In addition, both SMR vendor countries and importing nations can use export/import credit agencies to assist with financing SMRs. Canada, for example, has used this route to promote its Canadian Deuterium Uranium reactor to developing countries (Bratt, 2006).

SMR development is also likely to take advantage of some of the new financing arrangements that have been established to compensate for the decrease in traditional funding options for nuclear builds. With the escalation of costs and changing revenue streams in liberalized energy markets, vendors have taken on more of the risk from operators for both large nuclear and other large power facilities such as coal and hydro projects. Three possible avenues are fixed construction price contracts, fixed power price contracts, and build−own−operate (BOO) contracts between vendors and operators. In fixed-price construction contracts, vendors agree to build the facility for an agreed upon price, effectively isolating operators from cost overruns. Such an agreement was used in the construction of the Olkiluoto 3 plant in Finland between AREVA (a French multinational group headquartered in Paris, France) and Finland's Teollisuuden Voima Oyj. In guaranteed price contracts, the operator's selling price for power is guaranteed when the investment decision is made, thereby reducing operator risk on the revenue side. This was the agreement between Electricité de France and AREVA for the UK's $26 billion Hinkley Point C nuclear plant (Kidd, 2014; Reuters International, 2014), which has received approval from the European Commission. In BOO agreements, the vendor agrees to build and operate the plant and in return for selling power at fixed prices to domestic power companies. Since domestic economies do not have to finance such projects or bear the financial risk associated with them, BOO agreements are currently underway or being developed for nuclear projects in Turkey, Vietnam, Bangladesh, and other developing economies, and are a viable option for increasing the use of SMRs going forward.

20.9 Security of small modular reactors

The realm of nuclear security is centered upon the "intentional misuse of nuclear or radioactive materials" for the purpose of causing harm (Safety of Nuclear Power Reactors, 2015). The security of the SMRs for proliferation resistance and physical protection is increased for every SMR. Proliferation resistance is feature of an SMR that

controls the fissile materials that can be used for weapons. In addition, a key emphasis is placed on potential threats to structural facilities, such as an RX, containment building, or a nuclear materials facility.

SMR designs claim that they have made improvements to nuclear security concerns. Most of the SMRs enhance the nuclear security by:

1. Housing the reactor underground: This feature protects the RX from an external threat, such as an airplane crash. In addition, this provides a physical barrier of ground for radiation leakage.
2. Limiting the access to the reactor building and control room. Since the most of the components [RX, control room, reactor circulation pump, SG, and other primary components] are underground, the access to this components are limited to protect for NPP for threats.
3. Decreasing the number of components in SMRs. Number of components of SMRs are reduced significantly. The security of the SMRs can be focused on the significantly decreased number of components that are potential for threats.
4. Improved safety systems by using passive, inherent safety or safety-by-design features eradicate the (un)intentional misuse of nuclear components.

20.10 Flexibility of small modular reactors

The power level of SMRs varies from 10 to 300 MW_e. Retired gas and coal power plants can easily be replaced with SMRs since SMRs' power and physical size are decreased significantly. In addition, the SMRs can be used for hybrid energy systems (HES) (Fig. 20.24).

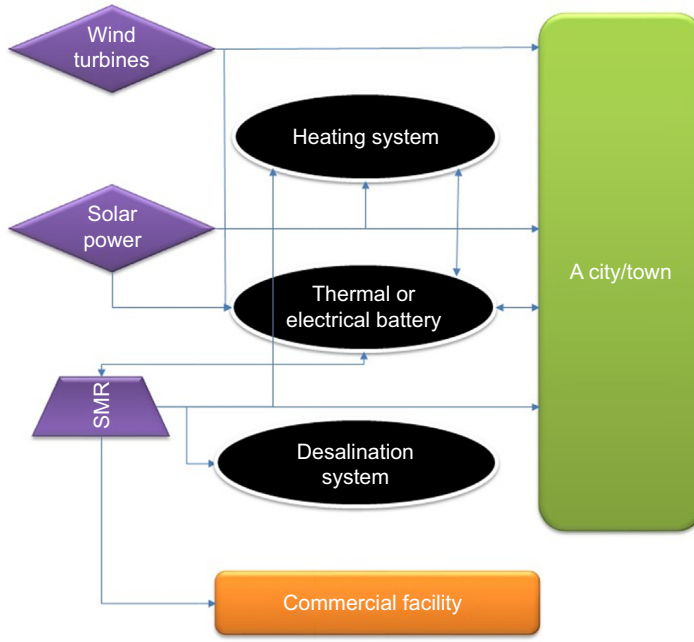


Figure 20.24 HES utilizing SMRs.

The overall power can easily be managed in the power grids by using the SMRs in an HES. When the power demand decreases, the SMR power is used either in a heating system or a desalination system or a battery. If the energy is stored in a battery, the stored energy can be used when the electrical demand of a city or town increases. In the HES, solar power plants, wind turbines are cardinally is employed with SMRs-based variation of power generation and consumptions. Since the generation of power from solar power plants and wind turbines are not constant, the load following feature of SMRs are used to provide the necessary power when power demand is higher than power generation from power plants of solar and wind. Thermal and electrical batteries are the power buffer for this power network (Fig. 20.24).

20.11 Conclusions and future trends

The historical development of SMRs started with integrated reactor designs, such as SIR and PIUS. The integrated design's major advantage is envelopment of majority (or all) RCS components. In addition, integrated design eliminates the pipe connections between the RCS components. For instance, there are hot leg, cold leg, surge line, and other pipes in integrated SMRs. Most of the integrated RVs are slim and tall to take advantage of chimney effect—movement of the coolant in the riser component, resulting from coolant buoyancy—in especially accident conditions.

This chapter compares selected LW and non-LW-SMRs in respect to nuclear reactors, fuels, containment, and ECCS. Even though there is no clear winner in this comparison, the following conclusions are highlighted:

- All SMR designs motivate US-based organizations to compete with their international peers. DOE financially supports two SMR projects, NuScale and mPower, to accelerate the development of LW-SMRs.
- Internal CRDM designs of NuScale and W-SMR eliminate the CRDM penetrations from top of the vessel (RV) to the core region. It also provides free volume in PRZ, UP, and in the riser of the RV. Since internal CRDM does not occupy space in the UP and PRZ in integrated RX, pressure drop due to friction on corresponding internals for CRDM decreases. This will yield to improve the flow distribution in RX.
- Some of the LW and non-LW-SMRs offer load following capability. Even though the power of these SMRs cannot be changed as quickly as coal or natural gas power plants, load following capability gives flexibility to the utilities to change the power based on electricity demand in the power grids.
- IRIS's PRZ design is slightly different than other LW-SMRs, since it eliminates the sprays in PRZ. This elimination requires bigger PRZ volume than other LW-SMRs' PRZ volumes.
- W-SMR's SG consists of two parts. This design decreases the size of the SG, which is in RV.
- IRIS's containment size is the largest among LW-SMRs to provide a large volume for safety. In addition, IRIS's containment is in a spherical shape to avoid edges and sides, which decreases the resistance of containment against a high pressure, different between the containment and air in the accident conditions.

- NuScale's safety system can remove the decay heat indefinitely, even though other LW-SMRs can remove for a limited period (generally 7 days).
- 4S's safety system has several active, passive, and inherent safety features. Especially advanced inherent safety feature and 30 years refueling frequency makes 4S different than other non-LW-SMRs.

SMRs have the potential to offset the traditionally perceived economies of scale for large NPPs with cost reductions from several types of economies, including cost savings due to modularization, mass manufacturing, reduced components from design simplicity, and passive safety systems. In addition to reducing the cost of manufacturing and installing SMR units, there are also associated reductions in operating costs. The financing community needs to be assured that the costs of building and operating SMRs are reasonable. Further, this technology needs to demonstrate a high capacity to contribute to carbon reduction goals while providing a viable route to meeting future energy demands. Ultimately, in addition to reducing uncertainty about the costs, sustained government support for SMR development is critical for the designs to be licensed for commercial operation. SMRs in HES will likely be employed because of flexible features of SMRs.

Abbreviations

4S	Super-Safe, Small and Simple
ABV	Nuclear, modular, water in Russian
ACS	Auxiliary cooling system
ADS	Automatic depressurization system
ADV	Advanced
Antares	AREVA New Technology Advanced Reactor Energy System
AP1000	Advanced Passive 1000
ATWS	Anticipated transient without scram
AUX BLDG	Auxiliary building
BL	Base load
BOO	Build−own−operate
CAP100/ACP100	Chinese Advanced Passive 100/Advanced China Power 100
CAREM-25	Central Argentina de Elementos Modulares − 25
CCR	Compact containment water reactor
CVCS	Chemical and volume control system

Continued

CMT	Core makeup tank
CS	Containment spray
CRDM	Control rod drive mechanism
CoGen	CoGeneration
DHR	Decay heat removal
DHRHX	Decay heat removal heat exchanger
DHRIV	Decay heat removal isolation valve
DMS	Double modular simplified and medium small reactor
DVI	Direct vessel injection
ECCS	Emergency core coolant system
ECT	Emergency cooldown tank
EDF	Electricité de France
EHRS	Emergency heat removal system
EMF	Electromagnetic field
EMP	Electromagnetic pump
FO	Fail open valve
FWP	Feedwater pump
Gen-III+	Generation III+
GT-MHR	Gas turbine modular helium reactor
GTHTR300	Gas turbine high temperature reactor 300 MWe
HES	Hybrid energy systems
HR200	Nuclear heating reactor with 200 MW of thermal power
HSBWR	Hitachi Small Boiling Water Reactor
IMR	Integrated modular water reactor
IRC	Inside reactor containment
ICRWST	In-containment refueling water storage tank
IRIS	International Reactor Innovative and Secure
KAERI	The Korea Atomic Energy Research Institute
LB	Large break
LF	Load following
LOCA	Loss of coolant accident
LW	Light water
MDBs	Multilateral development banks

MFIV	Main feedwater isolation valve
MHGTR	Modular high-temperature gas-cooled reactor
MHR	Modular helium reactor
MHTR	Modular high-temperature reactor
MSIV	Main steam isolation valve
NHP	Nuclear hydrogen production
Non-LW	Non-light water
OCC	Overnight capital cost
OSU	Oregon State University
PCT	Peak clad temperature
PHWR220	Pressurized Heavy water reactor
PIUS	Process inherent ultimate safety
PORV	Power-operated relief valve
PRHRS	Passive residual heat removal system
PRZ	Pressurizer
PSV	Pressurizer safety valve
PTC	Production tax credit
RCP	Reactor circulation pump
RCS	Reactor coolant system
RDT	Reactor drain tank
RHR	Residual heat removal
RV	Reactor vessel
RVACS	Reactor vessel auxiliary cooling system
RX	Reactor
SAFR	Sodium advanced fast reactor
SB	Small break
SCS	Shutdown cooling system
SG	Steam generator
SIR	Small innovative reactor
SIS	Safety injection system
SMART	System-Integrated Modular Advanced ReacTor
SPWR	Simplified pressurized water reactor

Continued

SVBR	Svintsovo-vismutovyi bystryi reactor (or in English "lead−bismuth fast reactor")
Triga	Training, research, isotopes, general atomic
TVO	Teollisuuden Voima Oyj
UHS	Ultimate heat sink
UN	Uranium nitride
UP	Upper plenum
U-TRU-Zr	Uranium−transuranic−zirconium alloy
VBER-150/300	Vodyanoi Blochnyi Energetichesky 150/300
VHTR	Very high temperature reactor
W-SMR	Westinghouse small modular reactor
ZIRLO	Zirconium low oxidation

Acknowledgment

The images of 4S reactor has been used by using "Courtesy of Toshiba Corporation." The author thanks Toshiba Corporation.

References

AKME, 2015. http://www.akmeengineering.com/svbr100.html.

ANSI, 2012. http://publicaa.ansi.org/sites/apdl/NESCCDocs/NSECC%2012-036%20-%20BM%20mPower%20Reactor%20Design%20Overview.pdf.

Babcock, 2013. http://www.babcock.com/library/Documents/SP201−100.pdf.

Bloomberg New Energy Finance Report, November 2010. Weathering the Storm: Public Funding for Low-Carbon Energy in the Post Financial Crisis Era. United Nations Environment Programme and SEF Alliance.

Boarin, S., Locatelli, G., Mancini, M., Ricotti, M., 2012. Financial case studies on small- and medium-size modular reactors. Nuclear Technology 178 (2), 218−232.

Bratt, D., 2006. The Politics of CANDU Exports. University of Toronto Press.

Bruynooghe, C., Eriksson, A., Fulli, G., 2010. Load-Following Operating Mode at Nuclear Power Plants (NPPs) and Incidence on Operation and Maintenance (O&M) Costs. JRC Scientific and Technical Reports, EUR 24583EN.

Carelli, M.D., Conway, L.E., Oriani, L., April 06−11, 2003a. Safety features of the IRIS reactor. In: Nuclear Mathematical and Computational Sciences: A Century in Review, a Century Anew. Gatlinburg, Tennessee.

Carelli, M.D., Conway, L.E., Oriani, L., 2003b. The design and safety features of the IRIS reactor. In: ICONE11−36564, 11th International Conference on Nuclear Engineering, Tokyo, Japan.

Carelli, M.D., Conway, L.E., Collado, J., Cinotti, L., Moraes, M., Lombardi, C., Kujawski, J., 2003c. Integral layout of the IRIS reactor. In: Proceedings of ICAPP'03, May 4−7, Cordoba, Spain.

Carelli, M.D., Conway, L.E., Oriani, L., Petrović, B., Lombardi, C.V., Ricotti, M.E., Barroso, A.C.O., Collado, J.M., Cinotti, L., Todreas, N.E., Grgić, D., Moraes, M.M., Boroughs, R.D., Ninokata, H., Ingersoll, D.T., Oriolo, F., 2004. The design and safety features of the IRIS reactor. Nuclear Engineering and Design 230 (1−3), 151−167.

Carelli, M., Garrone, P., Locatelli, G., Mancini, M., Mycoff, C., Trucco, P., 2010. Economic features of integral, modular, small-to-medium size reactors. Progress in Nuclear Energy 52 (4), 403−414.

Christiensen, L., Greene, W., 1976. Economies of scale in U.S. electric power generation. Journal of Political Economy 84 (1), 655−676.

Findlay, T., 2012. Nuclear Energy and Global Governance: Ensuring Safety, Security and Non-proliferation. Routledge, London, p. 85.

Forsberg, C.W., Reich, W.J., 1991. Worldwide Nuclear Power Reactors with Passive and Inherent Safety. Oak Ridge National Lab, Oak Ridge, TN. Report, ORNL/TM-11907.

Forsberg, C.W., 1983. A Process-Inherent, Ultimate-Safety (PIUS), Boiling Water Reactor. CONF-850610−34.

Fu-Bertaux, X., May 2011. Financing the Sustainable Energy Transition: Rising Support from Multilateral Development Banks. Worldwatch Institute.

Ganino, 2014. http://www.ganino.com/hyperion_power_generation_accumulators.

GE Hitachi, 2015. http://gehitachiprism.com/what-is-prism/how-prism-works/.

Gen4energy, 2013. http://www.gen4energy.com/.

Ghosh, A., Das, K., Basu, D., Miller, L., 2014. Soil Structure and Fluid interaction Assessment of new modular reactor: Part-2-Numerical study of Soil reactor Structure interaction. In: Proceedings of the ASME 2014 Small Modular Reactors Symposium, April 15−17, Washington DC.

Grubler, A., 2010. The costs of the French nuclear scale-up: a case of negative learning by doing. Energy Policy 38, 5174−5188.

IAEA, 2002. Small and medium sized reactors: status and prospects. In: International Seminar, Egypt, ISBN 92-0-114802-X.

IAEA, 2003. http://www.iaea.org/NuclearPower/Downloadable/FR/booklet-fr-2013.pdf.

IAEA, 2011a. Status of Small Medium Sized Reactor Designs. IAEA.

IAEA, 2011b. http://www.iaea.org/NuclearPower/Downloads/Technology/meetings/2011-Jul-4-8-ANRT-WS/3_USA_mPOWER_BABCOCK_DELee.pdf.

IAEA, 2013. https://aris.iaea.org/sites/..%5CPDF%5CNuScale.pdf.

Kessides, I., 2012a. The Future of the Nuclear Industry Reconsidered: Risks, Uncertainties, and Continued Potential. World Bank Policy Research Working Paper 6112.

Kessides, I., May 2012b. Economies of scale and the economics of smaller sized nuclear reactors. In: Platts International Annual Small Modular Reactor Conference, Arlington, VA.

Kidd, S., March 12, 2014. Financing Nuclear Projects − New Options? Nuclear Engineering International.

Kim, K.K., Lee, W.J., Choi, S., Kim, H.R., Ha, J.J., 2014. SMART: the first licensed advanced integral reactor. Journal of Energy and Power Engineering 8, 94−102.

Krautmann, A., Solow, J., 1988. Economies of scale in nuclear power generation. Southern Economic Journal 55 (1), 70−85.

Kumar, N., Besuner, P.M., Lefton, S.A., Agan, D.D., Douglas, D.H., 2012. Power Plant Cycling Costs. AES 12047831-2-1. Aptertek Aptech, National Renewable Energy Laboratory. http://wind.nrel.gov/public/WWIS/APTECHfinalv2.pdf.

Kuznetsov, Y.N., Lisitsa, F.D., Romenkov, A.A., Tokarev, Y.I., 1999. Nuclear plant with VK-300 boiling water reactors for power and district heating grids. In: ICONE-7335, ICONE-ASME Conference, Japan.

Li, F., 2014. http://www.iaea.org/NuclearPower/Downloadable/Meetings/2014/2014-04-08-04-11-TM-NPTDS/2_Li01.pdf.

Lyons, P., 2012. Small Modular Reactors − Why Are SMR Technologies of Interest to DOE? DOE Presentation, 3/16/2012.

Magan, H.B., et al., 2014. CAREM Prototype Construction and Licensing Status. IAEA-CN-164−5S01. IAEA.

Matzie, R., 2015. Small Modular Reactors: A Call for Action. http://www.hoover.org/sites/default/files/pages/docs/matzie_smr_diagram_presentation_2015_0.pdf.

Mingguang, Z., 2013. https://www.iaea.org/NuclearPower/Downloadable/Meetings/2013/2013-06-18-06-20-TWG-NPTD/36-snerdi-china-smr.pdf.

Mortensen, J.H., Moelbak, T., Andersen, P., Pedersen, T.S., December 1998. Optimization of boiler control to improve the load-following capability of power-plant units. Control Engineering Practice. ISSN: 0967-0661 6 (12), 1531−1539.

Nathan, S., May 13, 2013. Prism Project: A Proposal for the UK's Problem Plutonium. The Engineer.

NEI, 2014. http://www.nei.org/Knowledge-Center/Nuclear-Statistics/Costs-Fuel,-Operation,-Waste-Disposal-Life-Cycle/US-Electricity-Production-Costs-and-Components.

NRC, 2013. http://www.nrc.gov/reactors/advanced/4s.html.

NRC, 2014a. http://www.nrc.gov/reactors/advanced/advanced-files/smr.jpg.

NRC, 2014b. http://www.nrc.gov/reactors/advanced/nuscale.html.

NuScale, April 16, 2013a. NuScale Announces Major Technology Breakthrough − Safe Cooldown Over Indefinite Timeframe Achievable with No Operator Action, No Power, No Additional Water. Wall Street Journal.

NuScale, 2013b. http://www.nuscalepower.com/triplecrown.aspx.

NuScale, October 22, 2014. Retrieved February 3, 2015, from: http://www.nrc.gov/reactors/advanced/nuscale.html.

OKBM, 2015. http://www.okbm.nnov.ru/npp#regional.

Park, K.B., 2011a. https://www.iaea.org/INPRO/3rd_Dialogue_Forum/08.Park.pdf.

Park, K.B., 2011b. SMARTm INPRO Dialogue Forum on nuclear energy innovations, Austria. In: Lee, W.J. (Ed.), The SMART Reactor. 4th Annual Asian-Pacific Nuclear Energy Forum.

Park, K.B., 2011c. SMART design and technology features. In: Interregional Workshop on Advanced Nuclear Reactor Technology for Near Term Deployment, Austria.

Phung, D., 1987. Theory and Evidence for Using the Economy-of-Scale Law in Power Plant Economics. Oak Ridge National Laboratory. Report ORNL/TM-10195.

Prasad, S., 2012. http://www.andrew.cmu.edu/user/ayabdull/Prasad_SMRDesc.pdf.

Pratson, L., Haerer, D., Patino-Echeverri, D., 2013. Fuel prices, emission standards, and generation costs for coal vs natural gas power plants. Environmental Science and Technology 47 (9), 426−433.

PRISM, 1994. NUREG-1368.

Reuters International, October 08, 2014. Update 5 − First New British Nuclear Plant in Decades Wins EU Funding Fight.

Reyes, J.N., 2012. NuScale Plant Safety in Response to Extreme Events. NT 5-11-56. In: Nuclear Technology, vol. 178. http://www.nuscalepower.com/images/our_technology/NuScale-Safety-Nucl-Tech-May12-pre.pdf.

Rosner, R., Goldberg, S., Hezir, J., 2011. Small Modular Reactors − Key to Future Nuclear Power Generation in the U.S. Energy Policy Institute of Chicago (EPIC).

Safety of Nuclear Power Reactors, February 2015. Retrieved February 15, 2015, from: http://world-nuclear.org/infor/Safety-and-Security/Safety-of-Plants/Safety-of-Nuclear-Power-Reactors/.

Solan, D., Black, G., Louis, M., Peterson, St., Carter, L., Peterson, Sa, Bills, R., Morton, B., Arthur, E., June 2010. Economic and Employment Impacts of Small Modular Nuclear Reactors. Center for Advanced Energy Studies' Energy Policy Institute. http://epi.boisestate.edu/download.aspx?File=/3494/economic%20and%20employment%20impacts%20of%20smrs.pdf.

State of New Jersey, 2014. http://www.state.nj.us/dep/cleanair/hearings/.../09_mpower.ppt.

Toshiba CREIPI, June 03, 2013. Super-Safe, Small and Simple Reactor (4S, Toshiba Design). Retrieved February 03, 2015, from: https://aris.iaea.org/sites/..%5CPDF%5C4S.pdf.

Toshiba, 2015. http://www.toshiba.co.jp/nuclearenergy/english/business/4s/features.htm.

US Department of Energy Loan Programs Office, October 2014. Federal Loan Guarantees for Advanced Nuclear Projects. OMB Control Number: 1910-5134.

US Nuclear Regulatory Commission, December 22, 2011a. Policy Issue Information: Insurance and Liability Regulatory Requirements for Small Modular Reactor Facilities. http://pbadupws.nrc.gov/docs/ML1133/ML113340133.pdf.

US Nuclear Regulatory Commission, December 29, 2011b. Policy Issue Information: Security Regulatory Framework for Certifying, Approving, and Licensing Small Modular Nuclear Reactors (M110329). http://pbadupws.nrc.gov/docs/ML1129/ML112991113.pdf.

US Nuclear Regulatory Commission, August 2012. Report to Congress: Advanced Reactor Licensing. http://pbadupws.nrc.gov/docs/ML1215/ML12153A014.pdf.

US Nuclear Regulatory Commission, May 30, 2013. Memorandum to Commissioners: Current Status of the Source Term and Emergency Preparedness Policy Issues for Small Modular Reactors. http://pbadupws.nrc.gov/docs/ML1310/ML13107A052.pdf.

Van Tuyle, G.J., et al., 1989. Examining the inherent safety of PRISM, SAFR, and the MHTGR. Nuclear Safety 91, 185−202.

Von Deobschuetz, P., 2005. https://www.iaea.org/OurWork/ST/NE/NEFW/CEG/documents/ws052005_6E.pdf.

Vujic, J., Bergmann, R., Skoda, R., Miletic, M., 2012. Small modular reactors: simpler, safer, cheaper? Energy 45, 288−295.

W, 2013. http://www.westinghousenuclear.com/SMR/index.htm.

Wheeler, B., April 01, 2012. Developing Small Modular Reactor Designs in the U.S. Power Engineering. http://www.power-eng.com/articles/npi/print/volume-5/issue-2/nucleus/developing-small-modular-reactor-designs-in-the-us.html.

World Bank Technical Paper #154, April 1994. Environmental Assessment Sourcebook Volume III: Guidelines for Environmental Assessment of Energy and Industry Projects by the World Bank Environment Department, pp. 83−89.

World Nuclear Association, 2008. The Economics of Nuclear Power. Available at: http://www.world-nuclear.org/uploadedfiles/org/info/pdf/economicsnp.pdf.

Appendix A1: Additional materials (schematics, layouts, $T-s$ diagrams, basic parameters, and photos) on thermal and nuclear power plants[1]

I.L. Pioro[1], P.L. Kirillov[2]
[1]University of Ontario Institute of Technology, Oshawa, Ontario, Canada, [2]State Scientific Centre of the Russian Federation - Institute of Physics and Power Engineering (IPPE) named after A.I. Leipunsky, Obninsk, Russia

This appendix provides additional materials (schematics, layouts, $T-s$ diagrams, basic parameters, and photos) on advanced thermal (combined cycle and supercritical pressure Rankine steam turbine cycle) power plants and nuclear power plants with modern nuclear power reactors [pressurized water reactors (PWRs), boiling water reactors (BWRs), pressurized heavy water reactors (PHWRs), advanced gas-cooled reactors (AGRs), gas-cooled reactors (GCRs), light water-cooled graphite-moderated reactors (LGRs) (RBMKs and EGPs), and liquid metal fast-breeder reactors (LMFBRs) (BN-600 and BN-800)].

A1.1 Fossil fuel thermal power plants (listed here just for reference purposes)

A1.1.1 Combined cycle power plants

Natural gas is considered as a clean fossil fuel compared to coal and oil, but still, due to the combustion process, emits a lot of carbon dioxide when it used for electrical generation. The most efficient modern thermal power plants with thermal efficiencies within a range of 50–60% (up to 62%) are, so-called combined cycle power plants (combination of Brayton gas turbine and Rankine steam turbine power cycles) (see Figs. A1.1–A1.4, and Tables A1.1 and A1.2), which use mainly natural gas[2] as a fuel.

[1] This appendix is partially based on papers by Pioro and Duffey (2015) and Dragunov et al. (2015), and chapters by Pioro and Kirillov (2013a–d).
[2] In general, these plants can use any clean gaseous fuels; for example, liquefied natural gas (LNG), blast-furnace gas, etc.

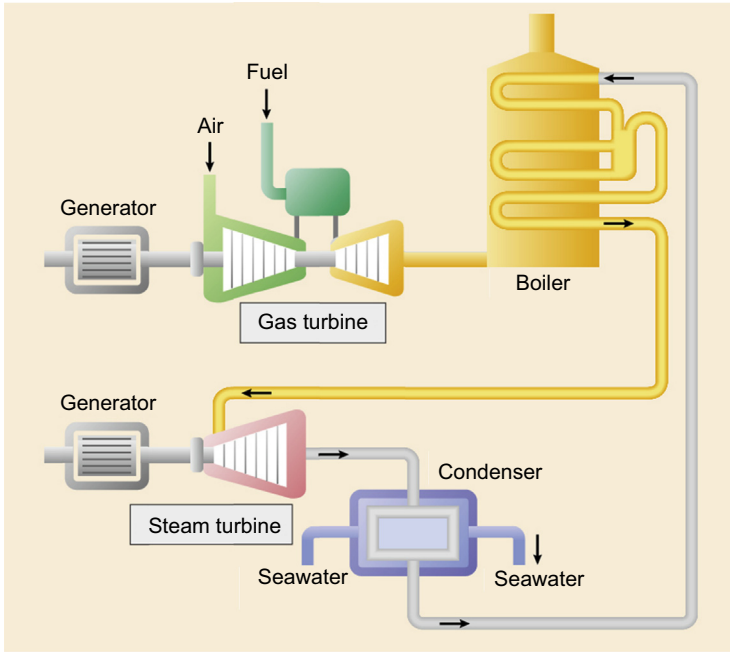


Figure A1.1 Simplified schematics of combined cycle power plant (courtesy and copyright of Mitsubishi Heavy Industries; MHI). Thermal efficiencies are the highest in power industry, up to 62% (Brayton cycle: 30%; and Rankine cycle: 40%). Current level of inlet temperatures to gas turbine is about 1600−1650°C and to steam turbine, 620°C.

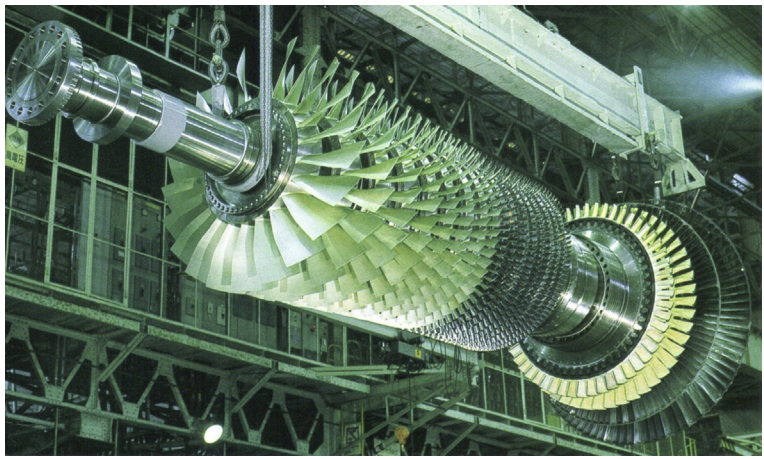


Figure A1.2 Photo of combined cycle power plant gas turbine rotor with compressor blades (at front) and turbine blades (at rear).
Courtesy and copyright of MHI.

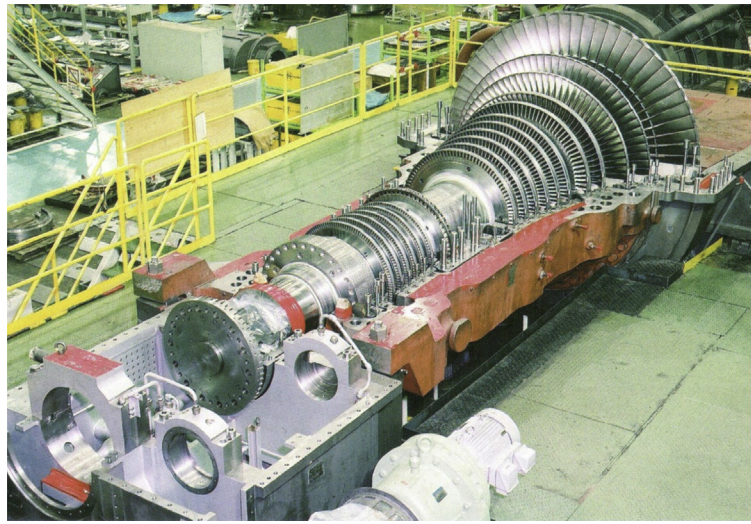


Figure A1.3 Photo of combined cycle power plant steam turbine with open cover (courtesy and copyright of MHI). Single-cylinder reheat turbines are used.

A1.1.2 Coal-fired power plants

For thousands of years, mankind used, and still is using, wood and coal for heating purposes. For about 100 years, coal is used for generating electrical energy at coal-fired thermal power plants worldwide. Usually, coal-fired power plants operate based on the so-called steam Rankine cycle, which can be organized at two different levels of pressures: (1) older or smaller capacity power plants operate at steam pressures no higher than ~16 MPa (~157 technical atmospheres); and (2) modern large capacity power plants (see Figs. A1.5–A1.9) operate at supercritical pressures from 23.5 MPa and up to 38 MPa. Supercritical pressures mean pressures above the critical pressure of water, which is 22.064 MPa. From thermodynamics, it is well known that higher thermal efficiencies correspond to higher temperatures.

Therefore, usually subcritical pressure plants have thermal efficiencies of about 36–40% and modern supercritical pressure plants of 43–50% (up to 55%). Steam generator outlet temperatures or steam turbine inlet temperatures have reached a level of about 625°C at pressures of 25–30 (up to 38) MPa. However, a common level is about 535–585°C at pressures of 23.5–25 MPa. Fig. A1.10 shows possible solutions for carbon dioxide capture and storage (CCS) at thermal power plants.

In spite of advances in coal-fired power plants' design and operation worldwide, they are still considered as not environmental friendly due to producing a lot of carbon dioxide emissions as a result of the combustion process plus ash, slag, and even acid rains. However, it should be admitted that known resources of coal worldwide are the largest compared to those of other fossil fuels (natural gas and oil).

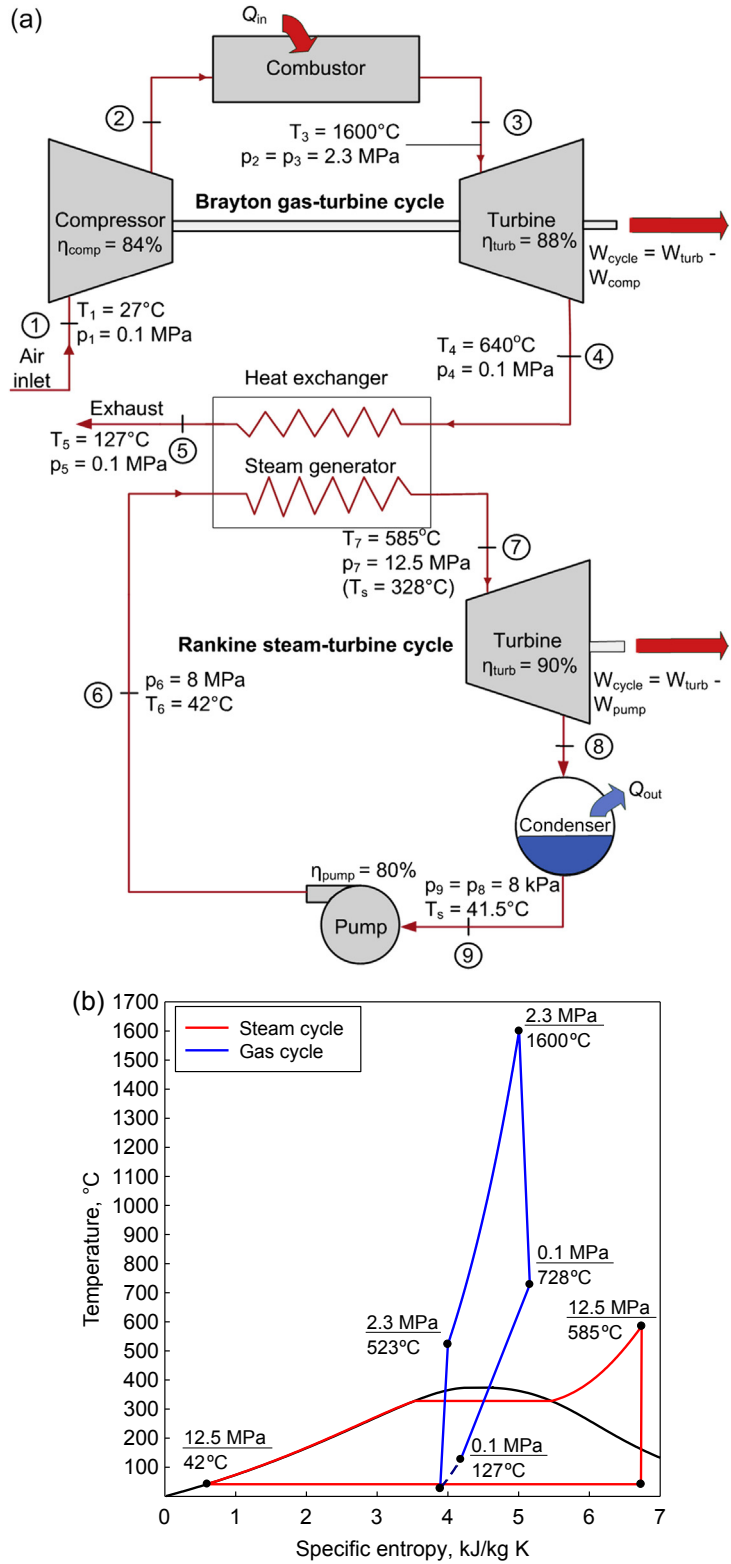


Figure A1.4 (a) Modern combined cycle power plant schematic and (b) T−s diagram. Partially based on data from MHI and Siemens.

Table A1.1 Reference data on selected combined cycle power plants designed and manufactured by MHI

	Plant output	LHV heat rate			Plant efficiency	Gas turbine power	Steam turbine power	No. of gas turbines
Model	**kW**	**kJ/kWh**	**kcal/kWh**	**Btu/kWh**	**%**	**kW**	**kW**	**–**
50 Hz								
M701DA	212,500	7000	1673	6635	51.4	142,100	70,400	1
M701F4	477,900	6000	1433	5687	60.0	319,900	158,000	1
	958,800	5981	1429	5668	60.2	639,800	319,000	2
M701F5	525,000	5902	1410	5594	61.0	354,000	171,000	1
	1,053,300	5883	1405	5576	61.2	708,000	345,300	2
M701G2	498,000	6071	1450	5755	59.3	325,700	172,300	1
	999,400	6051	1445	5735	59.5	651,400	348,000	2
M701J	680,000	5835	1394	5531	61.7	463,000	217,000	1
60 Hz								
M501DA	167,400	7000	1673	6635	51.4	112,100	55,300	1
M501F3	285,100	6305	1506	5976	57.1	182,700	102,400	1
	572,200	6283	1501	5955	57.3	365,400	206,800	2
M501GAC	404,000	6080	1452	5763	59.2	269,000	135,000	1
	810,700	6060	1447	5744	59.4	538,000	272,700	2
	1,216,000	6060	1447	5744	59.4	807,000	409,000	3
M501J	470,000	5854	1398	5549	61.5	322,000	148,000	1
	942,900	5835	1394	5531	61.7	644,000	298,900	2

LHV, lower heating value.
Courtesy of MHI.

Table A1.2 Reference data on selected gas turbines for combined cycle power plants designed and manufactured by MHI

	ISO-Base rating*	LHV heat rate			*P* ratio	Air flow	Turbine speed	Exhaust temp.
Model	**kW**	**kJ/kWh**	**kcal/kWh**	**Btu/kWh**	**–**	**kg/s**	**rpm**	**°C**
50 Hz								
M701DA	144,090	10,350	2473	9810	14	441	3000	542
M701F4	324,300	9027	2156	8556	18	712	3000	592
M701F5	359,000	9000	2150	8530	21	712	3000	611
M701G2	334,000	9110	2175	8630	21	737	3000	587
M701J	470,000	8783	2098	8325	23	861	3000	638
60 Hz								
M501DA	113,950	10,320	2465	9780	14	346	3600	543
M501F3	185,400	9740	2325	9230	16	458	3600	613
M501GAC	272,000	9074	2167	8600	20	598	3600	614
M501J	327,000	8783	2098	8325	23	598	3600	636
MF-111	14,570	11,630	2,778	11,020	15	55	9660	530
MF-221	30,000	11,260	2,688	10,670	15	108	7200	533
MFT-8	26,780	9310	2223	8820	21	86	5000	464

*Combined cycle power plants have relatively small gas ans steam turbines.
Courtesy of MHI.

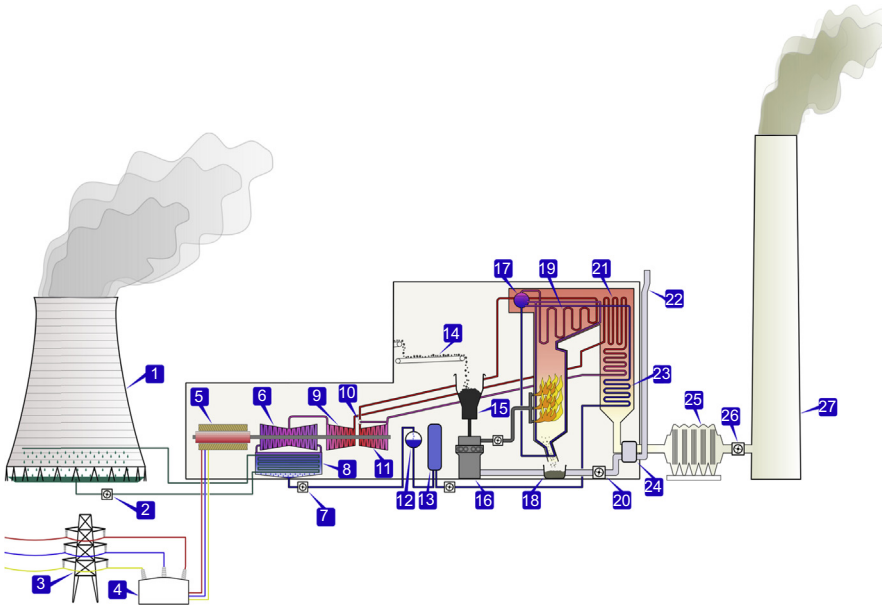


Figure A1.5 Typical scheme of coal-fired thermal power plant *(Author/User: BillC; https://commons.wikimedia.org/wiki/File:PowerStation2.svg; website approached January 26, 2016)*: (1) Cooling tower; (2) cooling-water pump; (3) transmission line (3-phase); (4) step-up transformer (3-phase); (5) electrical generator (3-phase); (6) low-pressure (LP) steam turbine; (7) condensate pump; (8) surface condenser; (9) intermediate-pressure steam turbine; (10) steam control valve; (11) high-pressure (HP) steam turbine; (12) deaerator; (13) feedwater heater; (14) coal conveyor; (15) coal hopper; (16) coal pulverizer; (17) boiler steam drum; (18) bottom ash hopper; (19) superheater; (20) forced draught (draft) fan; (21) reheater; (22) combustion air intake; (23) economizer; (24) air preheater; (25) precipitator; (26) induced-draught fan; and (27) flue gas stack.

A1.2 Current nuclear power reactors and nuclear power plants (listed here just for reference purposes)

The current section is dedicated to modern nuclear power reactors and corresponding to that, nuclear power plants (NPPs), and includes their layouts, $T-s$ diagrams, basic parameters, and photos. Nuclear power reactors and corresponding NPPs are listed in the following sequence: (1) PWRs/advanced PWRs; (2) BWRs/advanced boiling water reactors (ABWRs); (3) PHWRs; (4) AGRs; (5) GCRs[3]; (6) LGRs (RBMKs and EGPs); and (7) LMFBRs (BN-600 and BN-800), ie, the sequence is based on the decreasing number of particular types of reactors currently operated in the world (see Table 1.7 in Chapter: 1). All of the power conversion cycles for current NPPs are based solely on the subcritical-pressure Rankine steam turbine cycle.

[3] Currently, ie, april of 2016, all GCRs have been shut down. And this type of reactors cooled with carbon dioxide will not be built again.

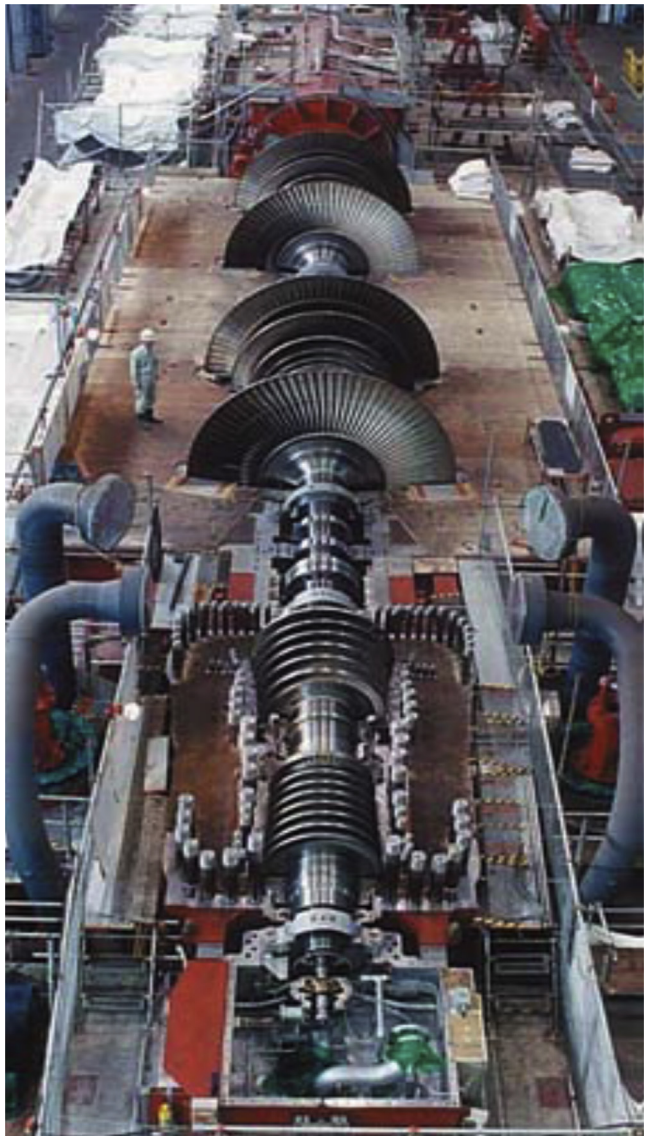


Figure A1.6 Photo of Tomato-Atsuma (Japan) coal-fired power plant Unit No. 4: supercritical pressure steam turbine: one HP, one intermediate pressure, and two double-flow LP cylinders (courtesy and copyright by Hitachi, Ltd.): 700 MW_{el}, TC4F-43, 3000 rpm, steam parameters: 25.0 MPa pressure, and 600/600°C (primary steam/reheat) temperature.



Figure A1.7 Photo of LP double-flow steam turbine rotor with blades for supercritical pressure coal-fired power plant.
Siemens press photo; courtesy and copyright by Siemens AG, Munich/Berlin, Germany.

Fig. A1.11 shows typical operating conditions of all water[4]-cooled reactors on the pressure−temperature diagram. And Table A1.3 lists major parameters of Russian power reactors and NPPs because Russia has quite a wide range of various types of operating nuclear power reactors.

A1.2.1 Pressurized water reactors

Accounting on the available information in the open literature and figures provided by major nuclear vendors (ROSATOM/ROSENERGOATOM, MHI, and AREVA) and US NRC, it was decided to show the following reactors and NPPs:

1. 1000-MW_{el} VVER-1000-reactor NPP (Russian design) (see Figs. A1.12−A1.14). Basic parameters of VVER-1000 are listed in Table A1.3. Reference parameters of Generation III+ VVER are listed in Table A1.4 and additional parameters in Table A1.5;
2. Typical US PWR NPP (see Fig. A1.15). Basic parameters of US PWR NPP and AP-1000 NPP (Generation III+) are listed in Tables A1.6 and A1.7, respectively;
3. MHI advanced PWR NPP layout and typical PWR fuel assembly (see Figs. A1.16 and A1.17, respectively); and
4. Main design and operating parameters for EPR (AREVA) (see Table A1.8).

It should be noted that in all NPPs with PWRs, ABWRs, BWRs, PHWRs, and LGRs, subcritical-pressure Rankine steam turbine cycle is used. Primary steam is a saturated steam at the corresponding pressure. For the reheat, the primary saturated steam is used. Therefore, the reheat temperature is lower than the primary steam temperature. In general, the primary steam and secondary steam parameters at NPPs are significantly lower than those at thermal power plants. Due to this, thermal efficiencies of these NPPs equipped with water-cooled reactors are lower than those of NPPs equipped with AGRs and LMFBRs (sodium-cooled fast reactors, SFRs), and

[4] Including reactors with light- and heavy-water coolants.

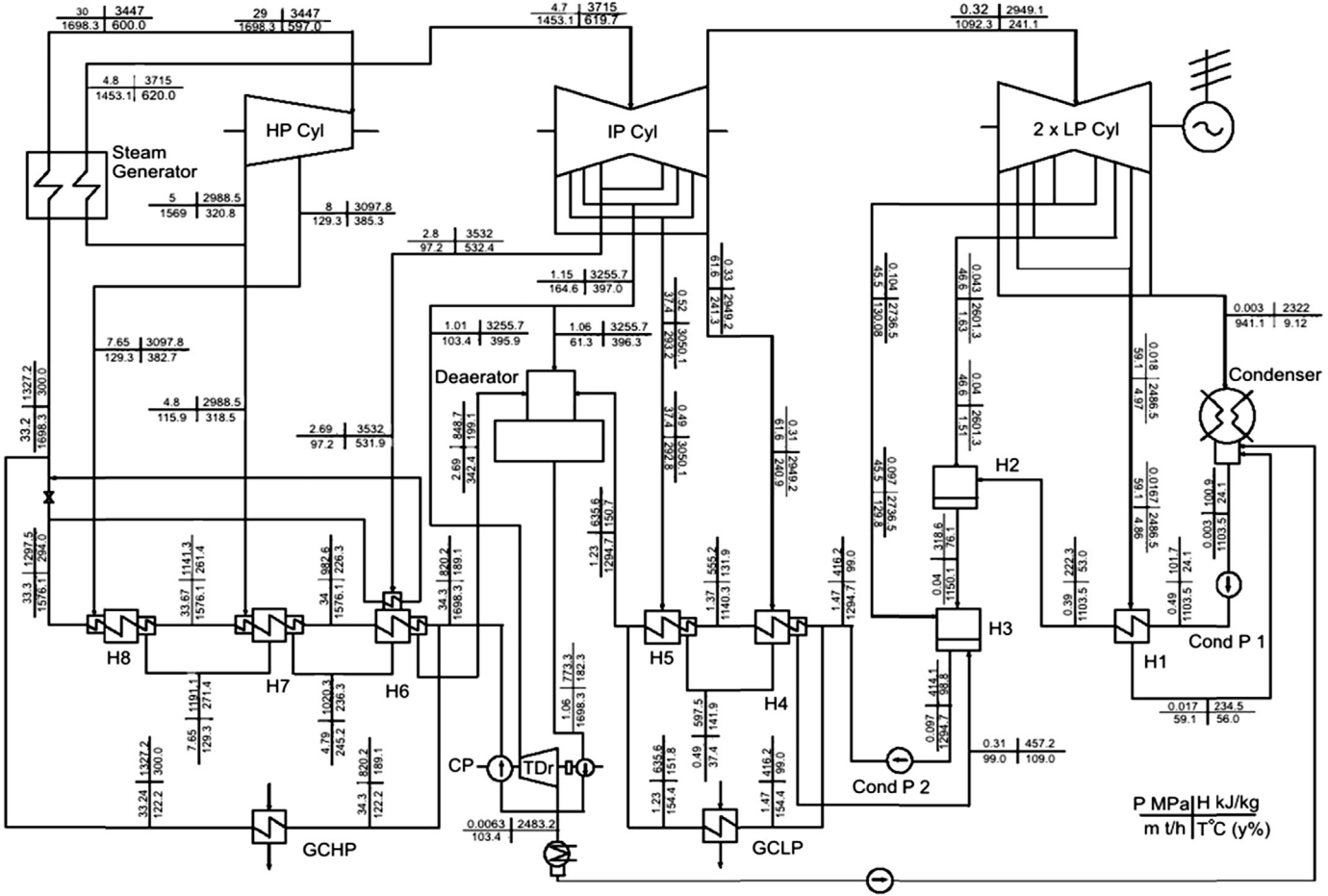


Figure A1.8 Single reheat regenerative cycle 600-MW_{el} Tom'-Usinsk thermal power plant (Russia) layout (Kruglikov et al., TsKTI, Russia, 2009): *Cyl*, cylinder; *H*, heat exchanger (feedwater heater); *CP*, circulation pump; *TDr*, turbine drive; *Cond P*, condensate pump; *GCHP*, gas cooler of high pressure; and *GCLP*, gas cooler of low pressure.

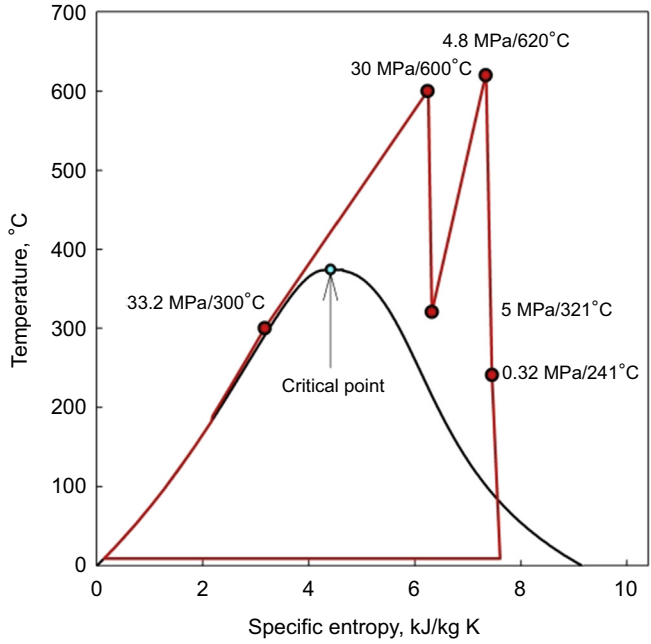


Figure A1.9 Simplified $T-s$ diagram for Tom'-Usinsk thermal power plant supercritical-pressure Rankine steam turbine cycle.

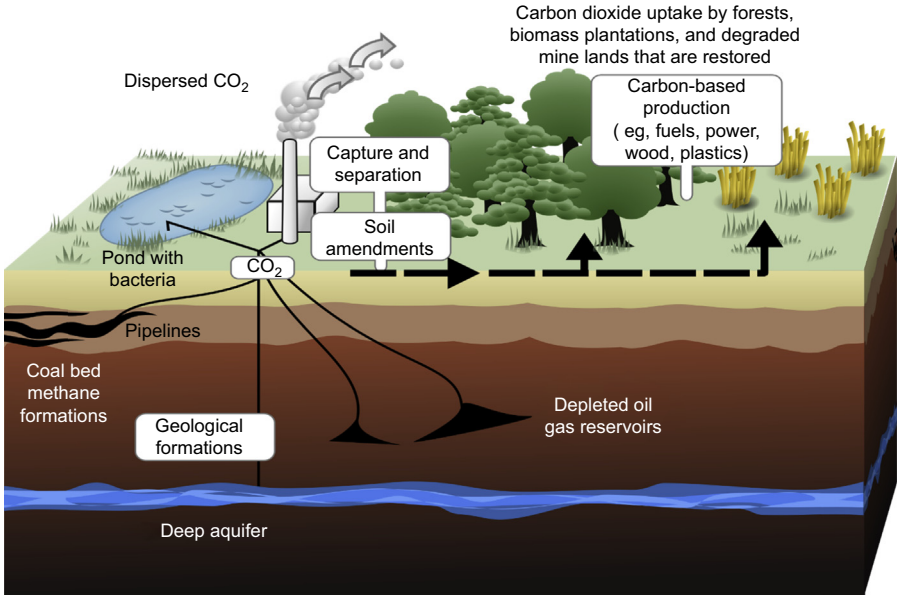


Figure A1.10 Possible solutions for CCS (courtesy of the Oak Ridge National Laboratory, US Dept. of Energy): Schematic showing terrestrial and geological sequestration of carbon dioxide emissions from coal-fired power plant.
Rendering by L. Hardin and J. Payne: http://www.ornl.gov/info/ornlreview/v33_2_00/research.htm.

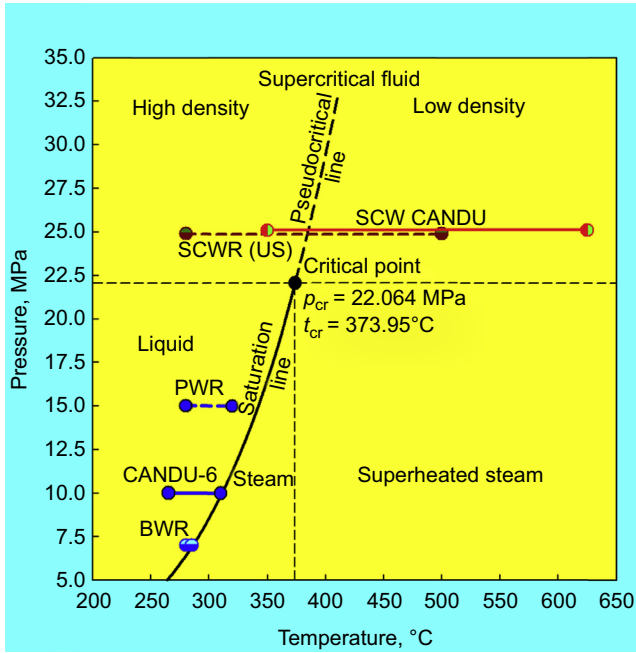


Figure A1.11 Typical operating conditions (pressure drop is not accounted for) in *P-T* coordinates for BWRs, CANDU reactors, PWRs, and SCWRs (Generation IV concept).

Table A1.3 Major basic parameters of Russian power reactors and NPPs

Parameter	VVER-440	VVER-1000 (Fig. A1.12)	EGP-6 (Fig. A1.36)	RBMK-1000 (Fig. A1.33)	BN-600 (Fig. A1.37)
Thermal power, MW_{th}	1375	3000	65	3200	1470
Electrical power, MW_{el}	440	1000	12	1000	600
Thermal efficiency, %	32.0	33.3	18.5	31.3	40.8
Coolant pressure, MPa	12.3	15.7	6.2	6.9	~0.1
Coolant flow, t/h	44,050	64,800	600	32,000	21,800
Coolant temperature, °C	270/298	290/322	265	284	380/550
Steam flow rate, t/h	2700	5880	100	5600	640
Steam pressure, MPa	4.3	5.9	6.5	6.4	15.3
Steam temperature, °C	256	276	280	280	505
Core: Diameter/height, m/m	3.8/11.8	4.5/10.9	4.2/3.0	11.8/7	2.05/0.75
Fuel enrichment, %	3.6	4.3	3.0; 3.6	2.0–2.4	21; 29.4
No. of fuel assemblies	349	163	273	1580	371[a]

[a]Inside zone 209; Outer zone 162; Screen 380.

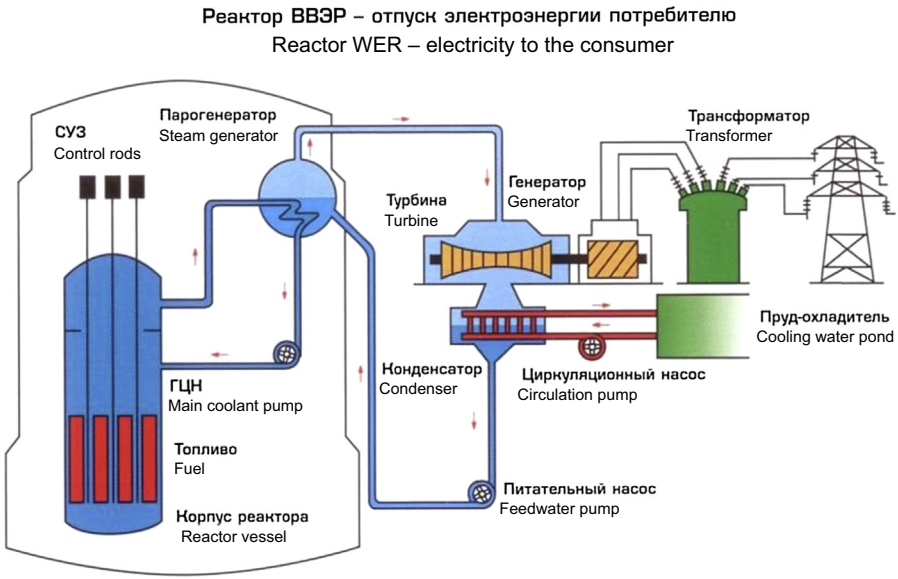


Figure A1.12 Simplified scheme of typical PWR (Russian VVER-1000) NPP (ROSENERGOATOM, 2004) (courtesy of ROSENERGOATOM): General basic features: (1) thermal neutron spectrum; (2) uranium dioxide (UO_2) fuel; (3) fuel enrichment about 4%; (4) indirect cycle with steam generator(s) (also, a pressurizer required (not shown)), ie, double-flow circuit (double loop); (5) reactor pressure vessel (RPV) with vertical fuel rods (elements) assembled in bundle strings cooled with upward flow of light water; (6) reactor coolant and moderator are the same fluid; (7) reactor coolant outlet parameters: pressure 15−16 MPa (T_{sat} = 342−347°C) and temperatures inlet/outlet 290−325°C; and (8) power cycle−subcritical-pressure regenerative Rankine steam turbine cycle with steam reheat (working fluid: light water, turbine steam−inlet parameters: saturation pressure of 6−7 MPa and saturation temperature of 276−286°C).

significantly lower than those of modern advanced combined cycle and supercritical-pressure thermal power plants.

Table A1.6 lists main design and operating parameters for EPR, French PWR of Generation III+ (AREVA company).

A1.2.2 Boiling water reactors

Accounting on the available information in the open literature and figures is provided by major nuclear vendors (Hitachi and Toshiba) and US NRC. It was decided to show the following reactors and NPPs as typical representatives of Generation III and III+ BWR NPPs:

1. Typical US BWR NPP layout (see Fig. A1.18) and its parameters (see Table A1.9);
2. Layout of ABWR Hitachi, Ltd. (see Fig. A1.19), and comparison of ABWR and BWR basic parameters (see Table A1.10); and
3. ABWR NPP (see Fig. A1.20, for layout Fig. A1.21, for T-S diagram) (based on data from Toshiba company).

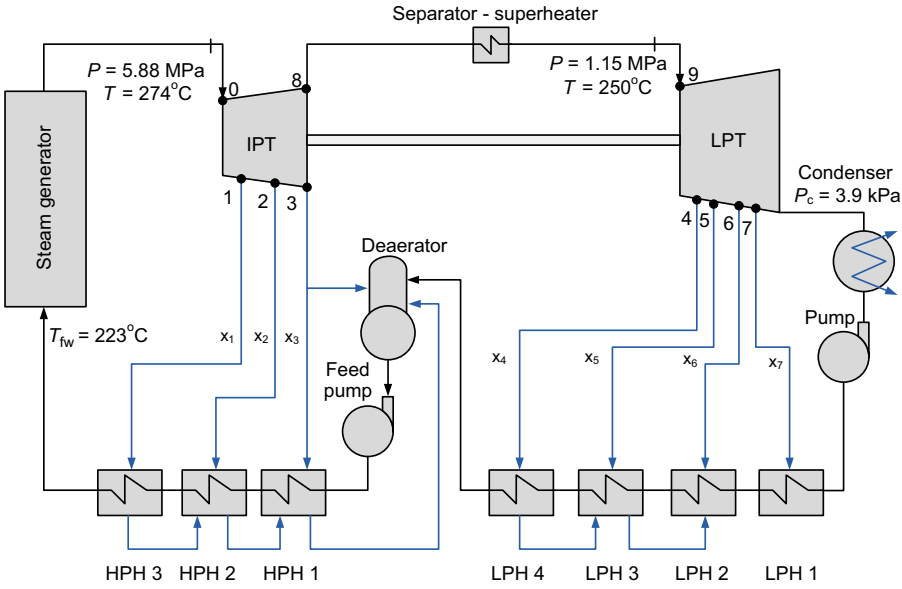


Figure A1.13 Simplified thermodynamic layout of 1000-MW_{el} VVER-1000 PWR NPP. Based on Grigor'ev, V.A., Zorin, V.M. (Eds.), 1988. Thermal and Nuclear Power Plants. Handbook, (In Russian), second ed. Energoatomizdat Publishing House, Moscow, Russia, 625 pp.; Margulova, T.C., 1995. Nuclear Power Plants, (In Russian). Izdat Publishing House, Moscow, Russia, 289 pp.

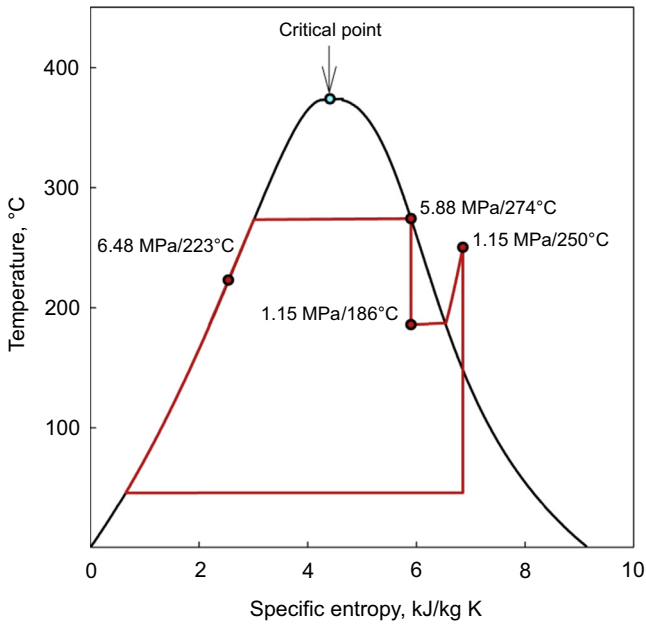


Figure A1.14 Temperature-specific entropy diagram for VVER-1000 turbine cycle.

Table A1.4 Reference parameters of Generation III+ VVER

Parameter	Value
Thermal power, MW_{th}	3200
Electric power, MW_{el}	1160
NPP thermal efficiency, %	36
Primary coolant pressure, MPa	16.2
Steam-generator pressure, MPa	7.0
Coolant temperature at reactor inlet, °C	298
Coolant temperature at reactor outlet, °C	329
Steam generator pressure/temperature, MPa/°C	6.27/278
Nuclear power plant service life, years	50
Main equipment service life, years	60
Replaced equipment service life, years, not less than	30
Capacity factor, %	Up to 90
Load factor, %	Up to 92
Equipment availability factor	99
Length of fuel cycle, years	4–5
Frequency of refueling, months	12–18
Fuel assembly maximum burn up, MW day/kgU	Up to 60–70
Interrepair period length, years	4–8
Annual average length of scheduled shutdowns (for refueling, scheduled maintenance work), days per year	16–40
Refueling length, days per year	$\leq$16
Number of not scheduled reactor shutdowns per year	$\leq$1
Frequency of severe core damage, 1/year	$<10^{-6}$
Frequency of limiting emergency release, 1/year	$<10^{-7}$
Efficient time of passive safety and emergency control system operation without operator's action and power supply, hour	$\geq$24
OBE/SSE, magnitude of MSK-64 scale	6 and 7
Compliance with EUR requirements, yes/no	Yes

Mainly based on data from Ryzhov, S.B., Mokhov, V.A., Nikitenko, M.P., et al., 2010. Advanced designs of VVER reactor plant. In: Proceedings of the 8th International Topical Meeting on Nuclear Thermal-Hydraulics, Operation and Safety (NUTHOS-8), Shanghai, China, October 10–14.

Table A1.5 Additional typical parameters of latest VVER-1000 series 300 and 400 (for basic parameters, see Table A1.3)

Parameter	Value
Pressure vessel ID, m	4.14
Reactor pressure vessel (RPV) wall thickness, m	0.19
RPV height without cover, m	10.9
Core equivalent diameter, m	3.12
Core height, m	3.56
Volumetric heat flux, MW/m^3	110
Average volumetric flow rate in assembly, m^3/h	515 ± 55
No. of fuel assemblies	163
No. of rods per assembly	317
Fuel mass, ton of UO_2	80
Part of fuel reloaded during year	1/3
Fuel	UO_2
Fuel enrichment, %	4

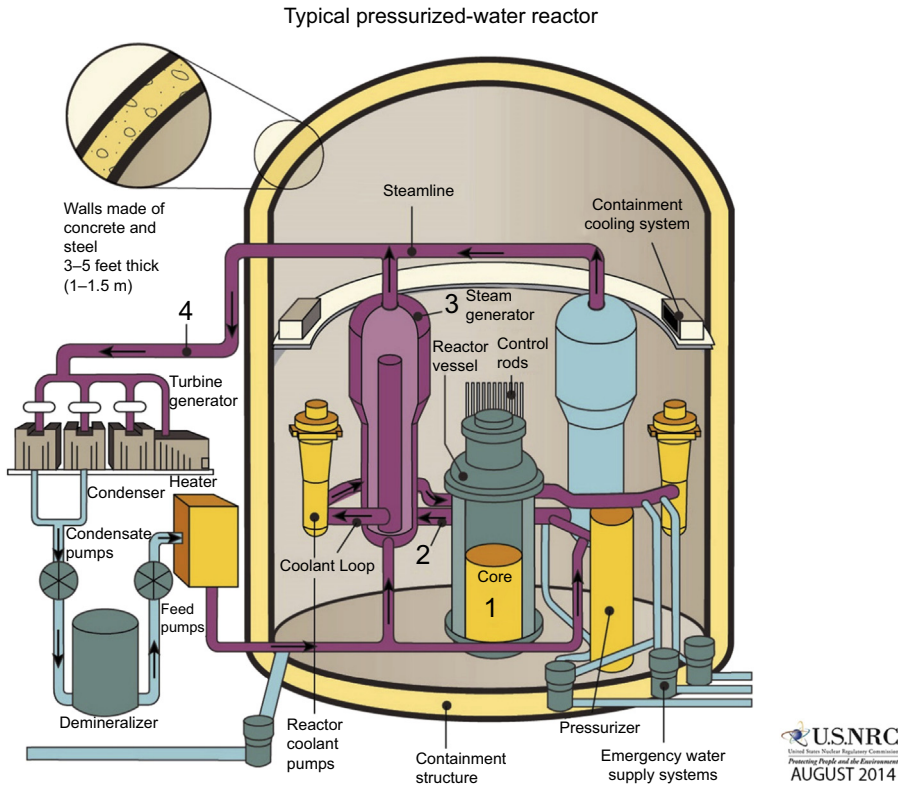


Figure A1.15 Simplified layout of typical US PWR NPP. Courtesy of US NRC.

Table A1.6 Typical basic parameters of US PWR NPP (Shultis and Faw, 2007)

Parameter	Value
Thermal power, MW_{th}	3800
Electrical power, MW_{el}	1300
Thermal efficiency, %	34
Specific power, kW/kg (U)	33
Power density, kW/L	102
Average linear heat flux, kW/m	17.5
Rod heat flux average/max, MW/m^2	0.584/1.46
Core	
Length, m	4.17
OD, m	3.37
Reactor coolant system	
Pressure, MPa	15.5
Inlet temperature, °C	292
Outlet temperature, °C	329
Mass flow rate (m), kg/s	531
Steam generators	
Total number	4
Outlet pressure, MPa	6.9
Outlet temperature, °C	284
Mass flow rate, kg/s	528
Reactor pressure vessel (RPV)	
OD, m	4.4
Height, m	13.6
Wall thickness, m	0.22
Fuel	
Fuel pellets	UO_2
Pellet OD, mm	8.19
Rod OD, mm	9.5
Zircaloy clad thickness, mm	0.57

Continued

Table A1.6 Continued

Parameter	Value
Rods per bundle (17 × 17)	264
Bundles in core	193
Fuel loading, ton	115
Enrichment, %	3.2
Reactivity control	
No. of control assemblies	68
Shape	Rod clusters
Absorber rods per assembly	24
Neutron absorber	Silver-in-Cadmium and/or B_4C
Soluble poison shim	Boric acid H_3BO_3

Table A1.7 Basic parameters of AP-1000 US Generation III+ PWR NPP (Shultis and Faw, 2007; http://www.westinghousenuclear.com/New-Plants/AP1000-PWR)

Parameter	Value
Thermal power, MW_{th}	3415
Electrical power, MW_{el}	1110
Thermal efficiency, %	33
Number of loops	2
Hot leg temperature, °C	321
No. of fuel bundles	157
Type of fuel assembly	17 × 17
Active fuel height, m	4.3
Linear heat flux, kW/m	18.7
Control rod clusters assemblies	53 (16 Gy)
Reactor vessel ID, m	3.99
Vessel flow, m^3/h	68,100

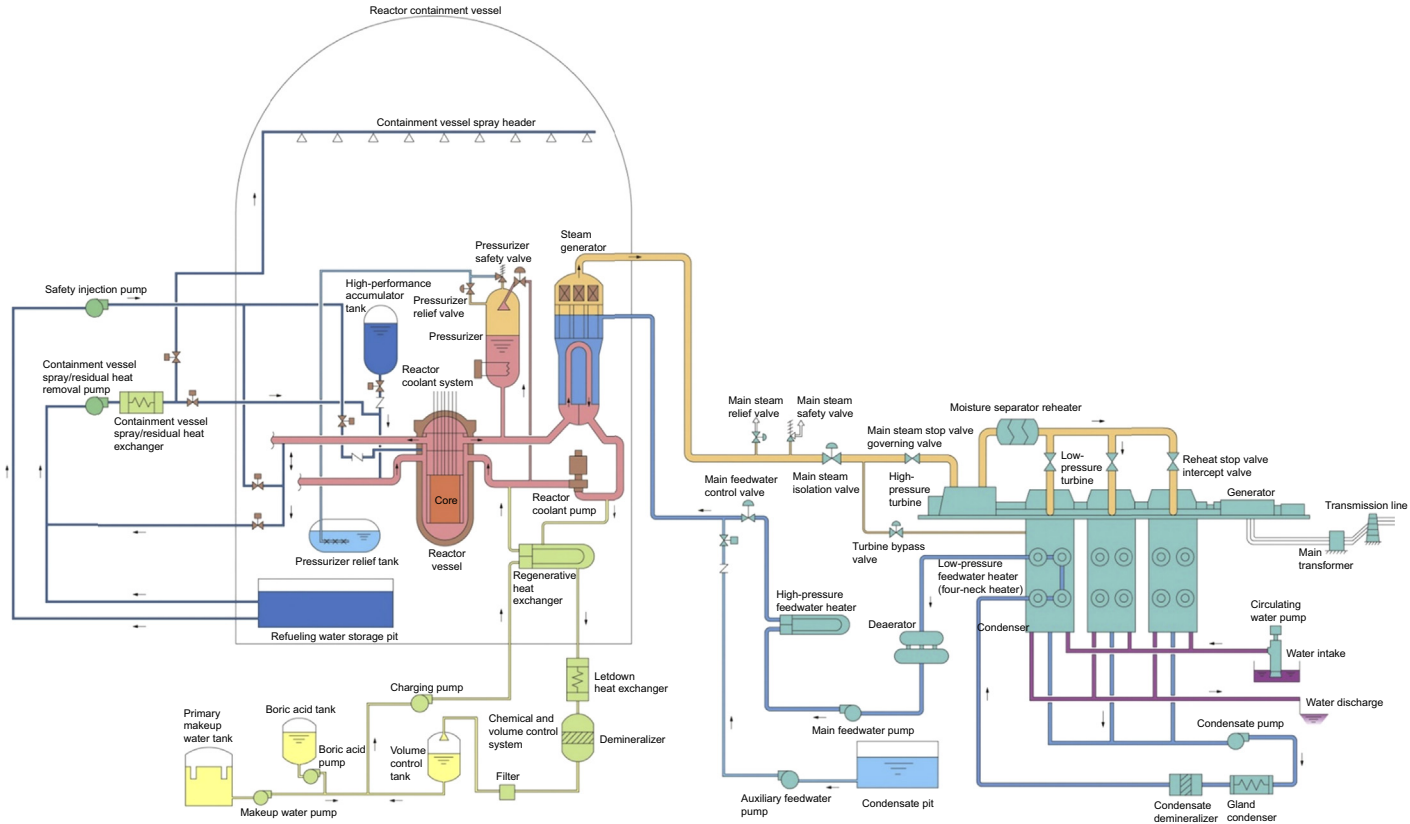


Figure A1.16 MHI 1500-MW_{el} advanced PWR NPP simplified layout (two-stage reheat cycle). Courtesy and copyright of MHI.

Table A1.8 Main design and operating parameters for EPR (AREVA)

Parameter	Value
Thermal power, MW_{th}	4590
Electric power, MW_{el}	1650
Gross thermal efficiency, %	36−37
No. of loops	4
Operating/design pressure, MPa	15.5/17.6
RPV inlet/outlet temperatures, °C	295.2/330 (T_{sat} at 15.5 MPa = 345°C)
Total flow/loop, m^3/h	28,315
Main steam operating/design pressure, MPa	7.72/10
Core	
Active height, m	4.2
No. of fuel assemblies	241
No. of rod cluster control assemblies	89
Fuel-assembly array (bundle)	17 × 17
No. of fuel rods	63,865
Average linear heat flux, kW/m	16.7

Based on data from AREVA, France: http://www.areva.com/EN/operations-5444/epr-reactor-fact-sheet.html.

Toshiba's ABWR is a reactor that has been in operation since 1996 on the basis of proven technologies of BWRs around the world. In 1996, Unit 6 at the Kashiwazaki-Kariwa NPP was put into operation as the world's first ABWR plant. In 1997, Unit 7 has started its operation at the same plant. In 2005, another ABWR started to operate as Unit 5 at the Hamaoka NPP.[5]

An important feature in the ABWR is that the condenser plays a role of a deaerator. The system consists of the main deaerating condenser connected with air ejector and off-gas treatment system.

The corresponding layout and $T-s$ diagram of a typical ABWR NPP are shown in Figs. A1.18 and A1.19, respectively (Fig. A1.21).

A1.2.3 Pressurized heavy water reactors

According to the information in Nuclear News (March 2016), the vast majority of PHWRs in the world are CANDU-type reactors designed by the Atomic Energy of

[5] It should be noted that due to the earthquake and tsunami disaster in Japan in March of 2011, which resulted in the Fukushima NPP accident, all that was left after this accident, Japanese 43 reactors, have been shut down. Recently, ie, January of 2016, just a couple of reactors have been restarted.

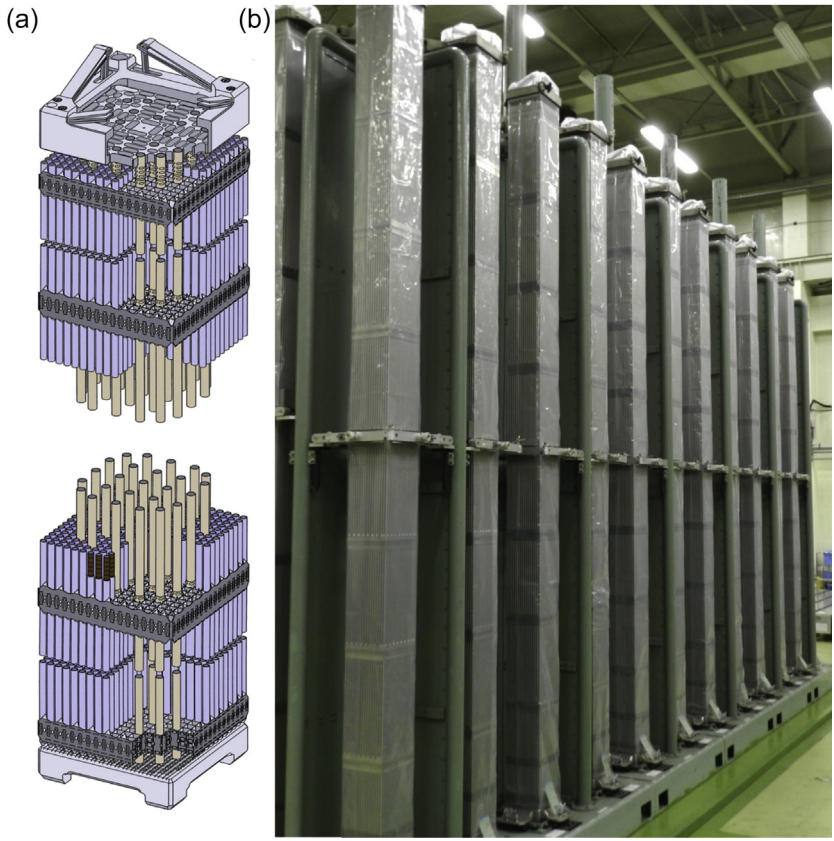


Figure A1.17 Typical PWR fuel assembly.
Courtesy and copyright by MHI.

Table A1.9 Typical parameters of US BWR (Shultis and Faw, 2007)

Parameter	Value
Thermal output, MW_{th}	3830
Electrical output, MW_{el}	1330
Thermal efficiency, %	34
Specific power, kW/kg (U)	26
Power density, kW/L	56
Average linear heat flux, kW/m	20.7
Rod heat flux average/max, MW/m^2	0.51/1.12
Core	
Length, m	3.76
OD, m	4.8

Continued

Table A1.9 Continued

Parameter	Value
Reactor coolant system	
Pressure, MPa	7.17
Feedwater temperature, °C	216
Outlet steam temperature, °C	290
Outlet steam flow rate, kg/s	2083
Core flow rate, kg/s	14,167
Core void fraction average/max	0.37/0.75
Reactor pressure vessel	
ID, m	6.4
Height, m	22.1
Wall thickness, m	0.15
Fuel	
Fuel pellets	UO_2
Pellet OD, mm	10.6
Rod OD, mm	12.5
Zircaloy clad thickness, mm	0.86
Rods per bundle (8 × 8)	62
Bundles in core	760
Fuel loading, ton	168
Enrichment, %	1.9
Reactivity control	
No. of control assemblies	193
Shape	Cruciform
Overall length, m	4.42
Length of poison section, m	3.66
Neutron absorber	Boron carbide
Soluble poison shim	Gadolinium

Canada Limited (AECL). Currently, the CANDU reactor technology in Canada is being developed by the CANDU Energy Inc. (http://www.candu.com/en/home/aboutcandu/default.aspx), a member of the SNC-Lavalin Group (Mississauga, Ontario, Canada). Therefore, all information on CANDU reactors presented in this section is based on brochures obtained from the CANDU Energy Inc., and figures on

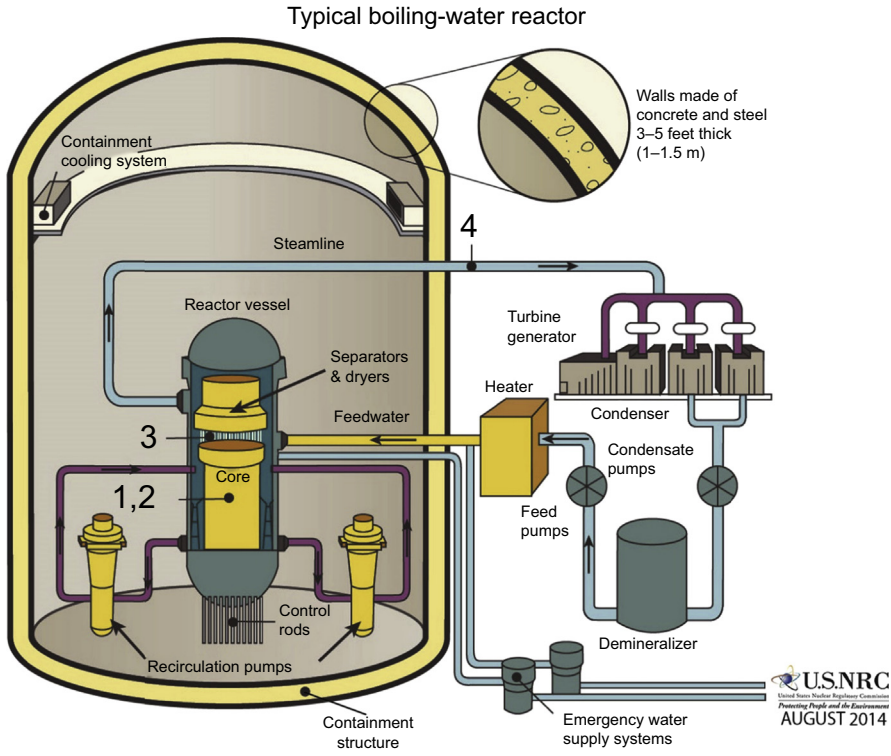


Figure A1.18 Simplified layout of typical BWR NPP (courtesy of US NRC): general basic features: (1) thermal neutron spectrum; (2) UO_2 fuel; (3) fuel enrichment about 3%; (4) direct cycle with steam separator (steam generator and pressurizer are eliminated), ie, single-flow circuit (single loop); (5) RPV with vertical fuel rods (elements) assembled in bundle strings cooled with upward flow of light water (water and water−steam mixture); (6) reactor coolant, moderator, and power cycle working fluid are the same fluid; (7) reactor coolant outlet parameters: pressure about 7 MPa and saturation temperature at this pressure is about 286°C; and (8) power cycle: subcritical-pressure regenerative Rankine steam turbine cycle with steam reheat.

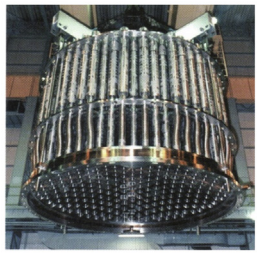
CANDU reactors/NPPs have been also provided by the CANDU Energy Inc., and published here with their permission. For the latest data and developments in the CANDU reactor technologies, please, refer to CANDU Energy Inc., website.

Therefore, basic information on PHWRs is provided based on Enhanced CANDU 6 (EC6) (for details, see Figs. A1.22−A1.26) and a brief description is provided below. EC6 is an evolutionary design based on the operating CANDU 6 reactors. The CANDU 6 reactors were designed and constructed after the successful operation of the four unit Pickering reactors (for details, see Figure A1.27). A simplified layout of the PHWR NPP (Siemens design) (Atucha, Argentina) is also shown in Figure A1.28. This is a PHWR design that uses a reactor vessel as the reactor coolant pressure boundary with fuel channels inside while CANDU type of PHWR uses the pressure tube in the fuel channel as the pressure boundary. (For PHWRs operated in India, see Chapter 15).

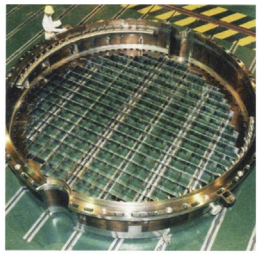
Table A1.10 Key specifications of ABWR and BWR-5

Parameter	Item	ABWR	BWR-5
Power	Electrical	1350 MW_{el}	1100 MW_{el}
	Thermal	3926 MW_{th}	3293 MW_{th}
Thermal efficiency (gross), %		34	33.4
Reactor core	Fuel assemblies	872	764
	Control rods	205	185
Reactor equipment	Recirculation system	Internal pump method	External recirculation type
	Control rod drive	Hydraulic/electric motor drive methods	Hydraulic drive
Reactor containment vessel		Reinforced concrete with built-in liner	Free-standing vessel
Residual heat removal system		3 systems	2 systems
Turbine systems	Thermal cycle	Two-stage reheat	Nonreheat
	Turbine (blade length)	1.32 m (52″)	1.09 m (43″)
	Moisture separation method	Reheat type	Nonreheat type
	Heater drain	Drain-up type	Cascade type

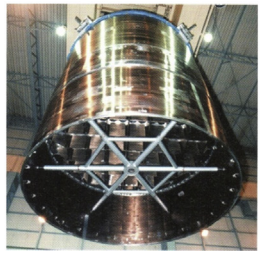
Courtesy of Hitachi-GE Nuclear Energy.



Steam separator



Top guide



Shroud

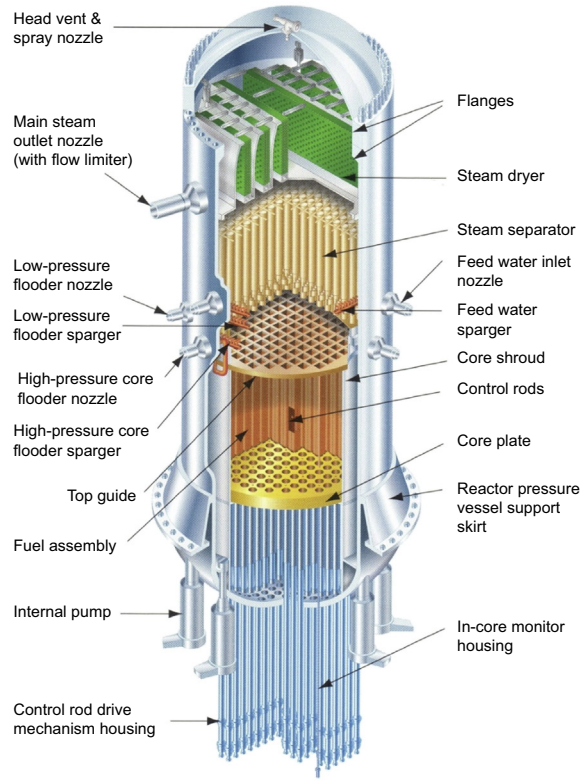


Figure A1.19 Simplified layout of typical ABWR NPP.
Courtesy and copyright by Hitachi, Ltd.

The EC6 is a 700 MW_{el}-class heavy water-moderated and heavy water-cooled pressure tube (pressure-channel) reactor (see Figs. A1.22−A1.25). Basic features and parameters of this reactor and corresponding NPP are as the following: (1) thermal neutron spectrum; (2) natural uranium-dioxide UO_2 fuel; (3) fuel enrichment about 0.71wt.%U^{235} ie, natural uranium; (4) indirect cycle with steam generator, ie, double-flow circuit (double loop); (5) pressure-channel design: Calandria vessel with horizontal fuel channels; (6) reactor coolant and moderator separated, but both are heavy water; (7) reactor coolant parameters: (a) inlet-header operating pressure 11.05 MPa and temperature 265°C; (b) outlet-header operating pressure 9.89 MPa and temperature 310°C (close to saturation temperature); and (c) maximum single-channel mass flow rate 28.5 kg/s; (8) on-line refueling; and (9) power cycle-subcritical-pressure regenerative Rankine steam turbine cycle with steam reheat (working fluid light water, turbine: one HP and two double-flow LP cylinders; net thermal output 2080 MW_{th}; gross/net electrical output (nominal) 740/690 MW_{el}; turbine

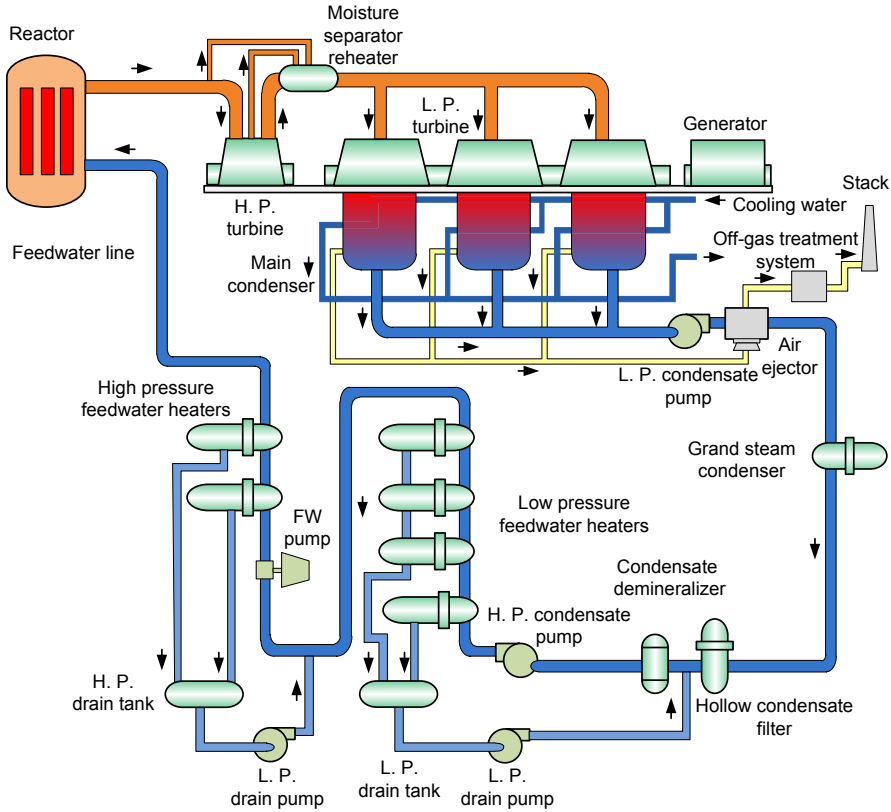


Figure A1.20 Simplified layout of ABWR NPP.
Based on data from Toshiba, 2011. Leading Innovation. Advanced Boiling Water Reactor (ABWR), Booklet. Toshiba Corporation, Japan.

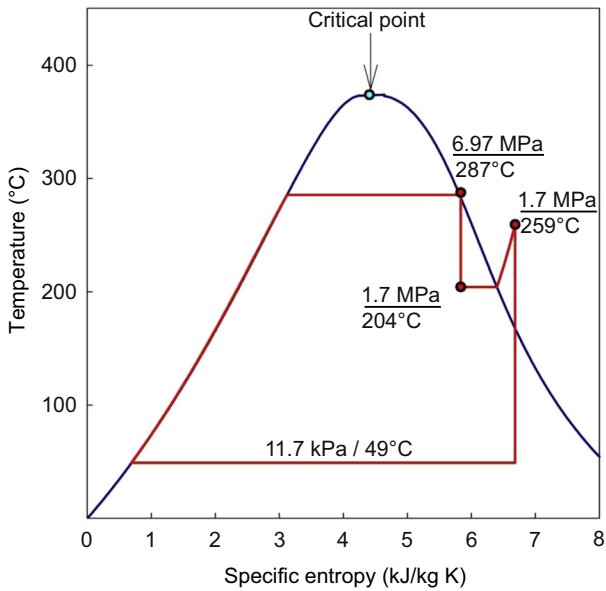


Figure A1.21 *T*–*s* diagram for typical ABWR NPP turbine cycle (reheat pressure was assumed to be one-quarter of the main steam pressure).

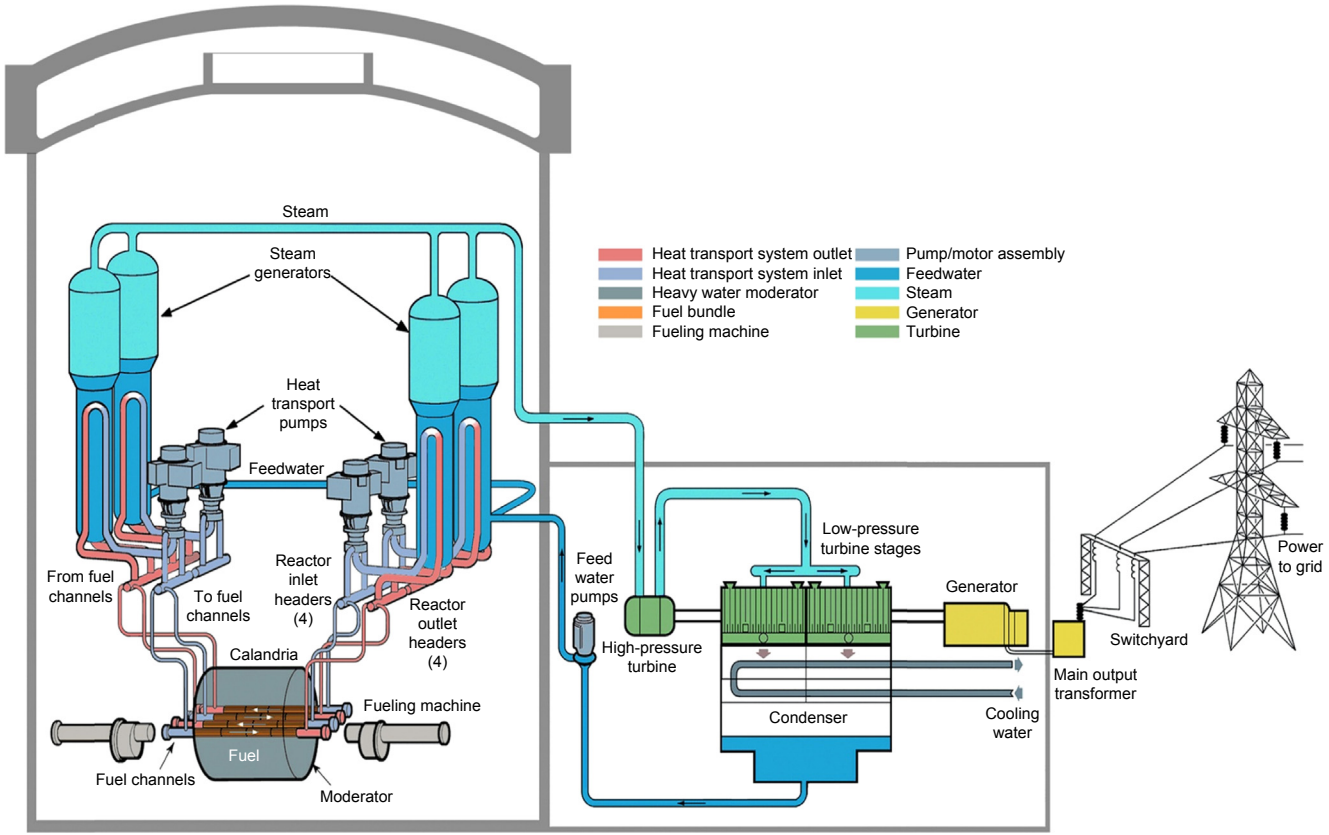


Figure A1.22 Simplified CANDU NPP flow diagram (courtesy of SNC-Lavalin): moisture separator and reheater are not shown.

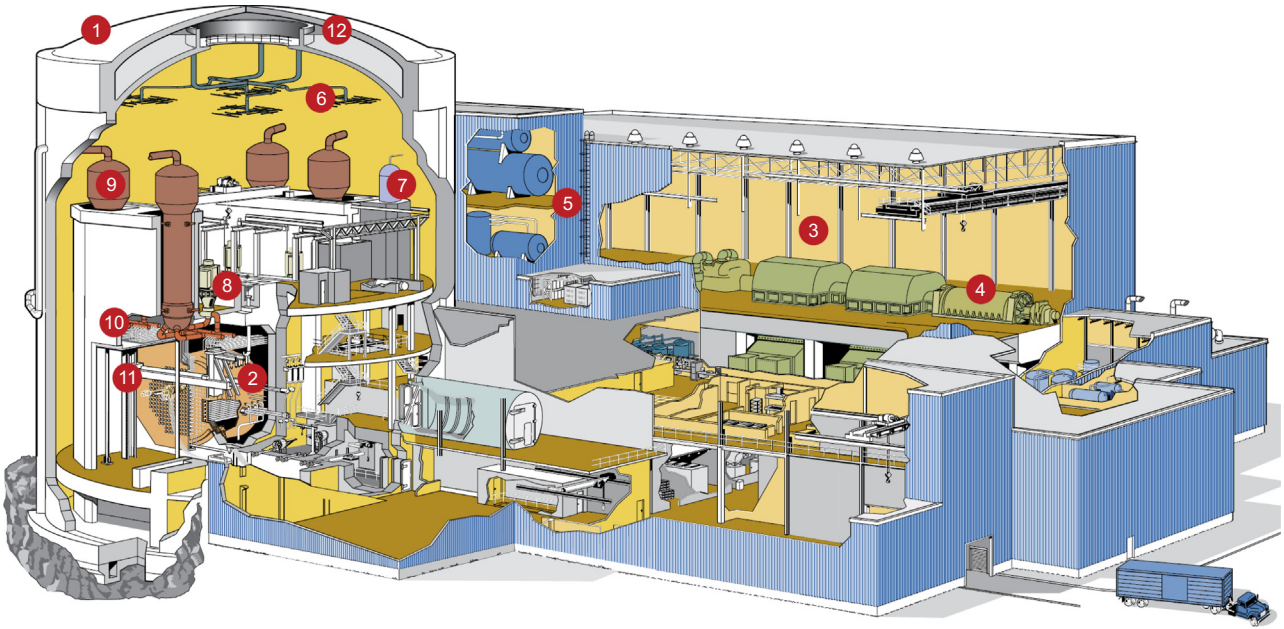


Figure A1.23 Layout of EC-6 NPP (courtesy of SNC-Lavalin): 1) Reactor building; 2) Calandria vessel; 3) Turbine building; 4) Turbine generator; 5) Service building; 6) Spray system; 7) Pressurizer; 8) Heat-transport pumps; 9) Steam generators; 10) Heat-transport system; 11) Fuelling machine: and 12) Reserve water tank.

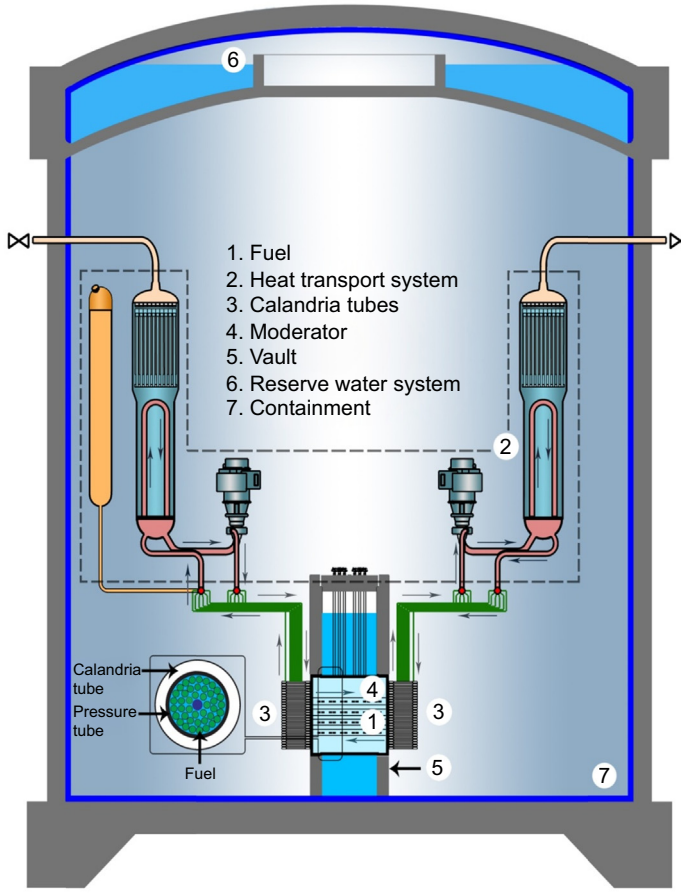


Figure A1.24 Barriers for prevention of releases.
Courtesy of SNC-Lavalin.

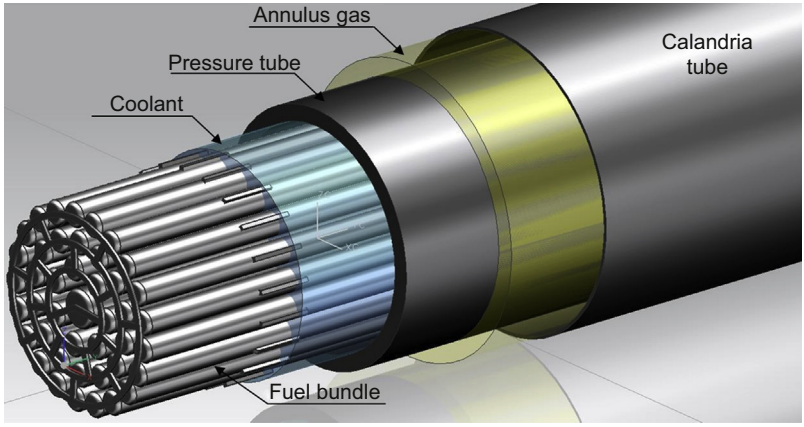


Figure A1.25 3-D image of CANDU-reactor fuel channel with bundle.
Based on data from AECL.

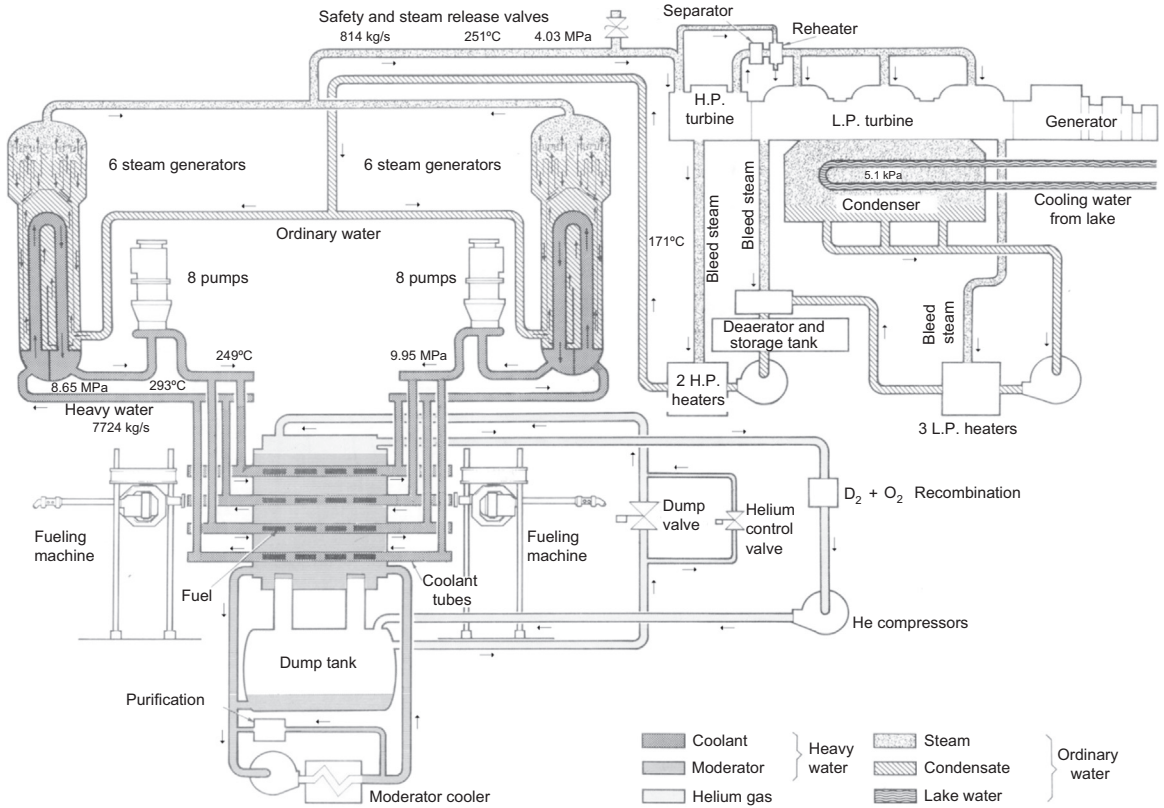


Figure A1.26 Simplified flow diagram of 515-MW_{el} CANDU reactor NPP (Pickering Power Plant, Ontario, Canada) (AECL Report, 1969): these 515-MW_{el} CANDU reactors are the smallest ones in Canada, and first two of them were put into operation in 1971.

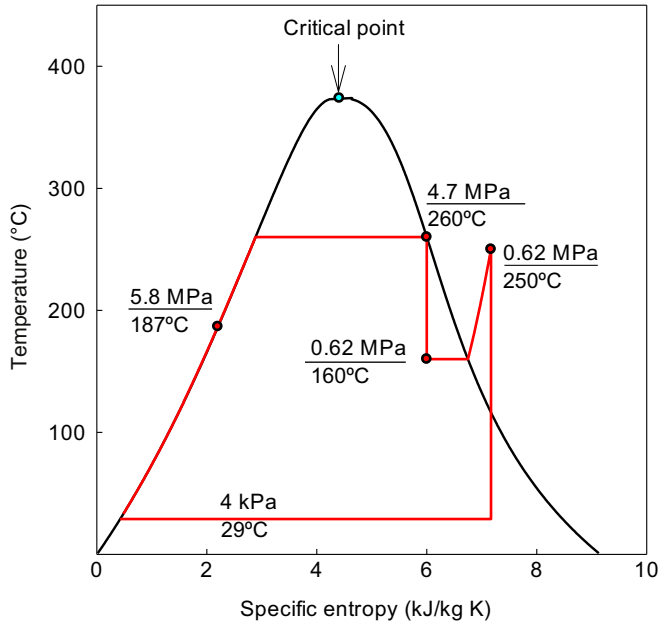


Figure A1.27 $T-s$ diagram of 740-MW_{el} of typical Ec6 CANDU-reactor turbine cycle.

steam inlet parameters: saturation pressure 4.69 MPa and temperature 260°C; feedwater − 5.8 MPa (T_{sat} = 273.4°C) and 187°C; also, condenser back pressure ranges from 3.74 kPa to 4.9 kPa depending on condenser cooling temperature. The T-s diagram for a typical EC6 is shown in Figure A1.26.).

A1.2.4 Advanced gas-cooled reactors and gas-cooled reactors

Accounting on the available information in the open literature, it was decided to show a simplified schematic of an AGR/ribbed fuel element; thermodynamic layout, and $T-s$ diagram of the AGR Torness NPP (see Figs. A1.29−A1.31, respectively) and just a simplified schematic of a GCR NPP (see Fig. A1.32).

A1.2.5 Light water-cooled graphite-moderated reactors: RBMK and EGP

Accounting on the available information in the open literature, it was decided to show a simplified schematic, thermodynamic layout and $T-s$ diagram of a 1000-MW_{el} RBMK NPP (see Figs. A1.33−A1.35, respectively) and just a simplified schematic of an 11-MW_{el} EGP-6 NPP (see Fig. A1.36). Basic data on these two reactors are listed in Table A1.3.

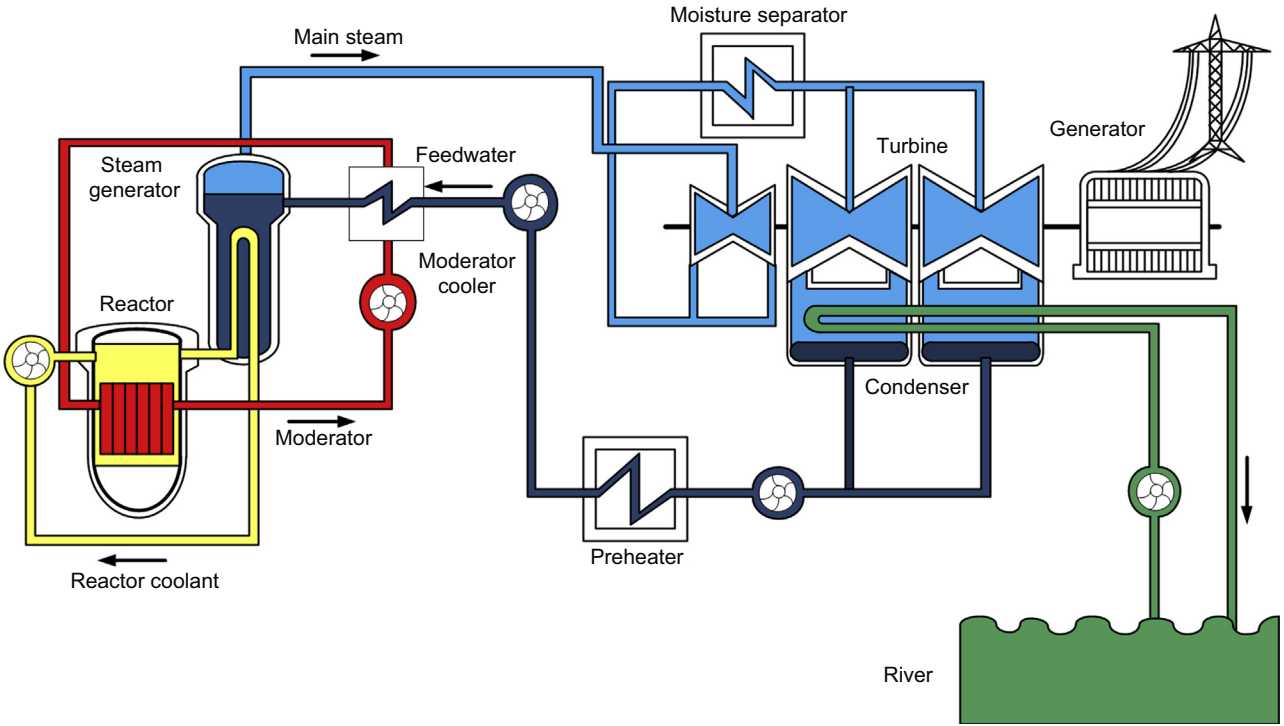


Figure A1.28 Simplified PHWR NPP flow diagram (Siemens design) (Atucha, Argentina) *(based on Nuclear Engineering International, Sept. 1982, England)*. Currently, both Unit 1 (335 MW_{el}) and Unit 2 (692 MW_{el}) are in operation.

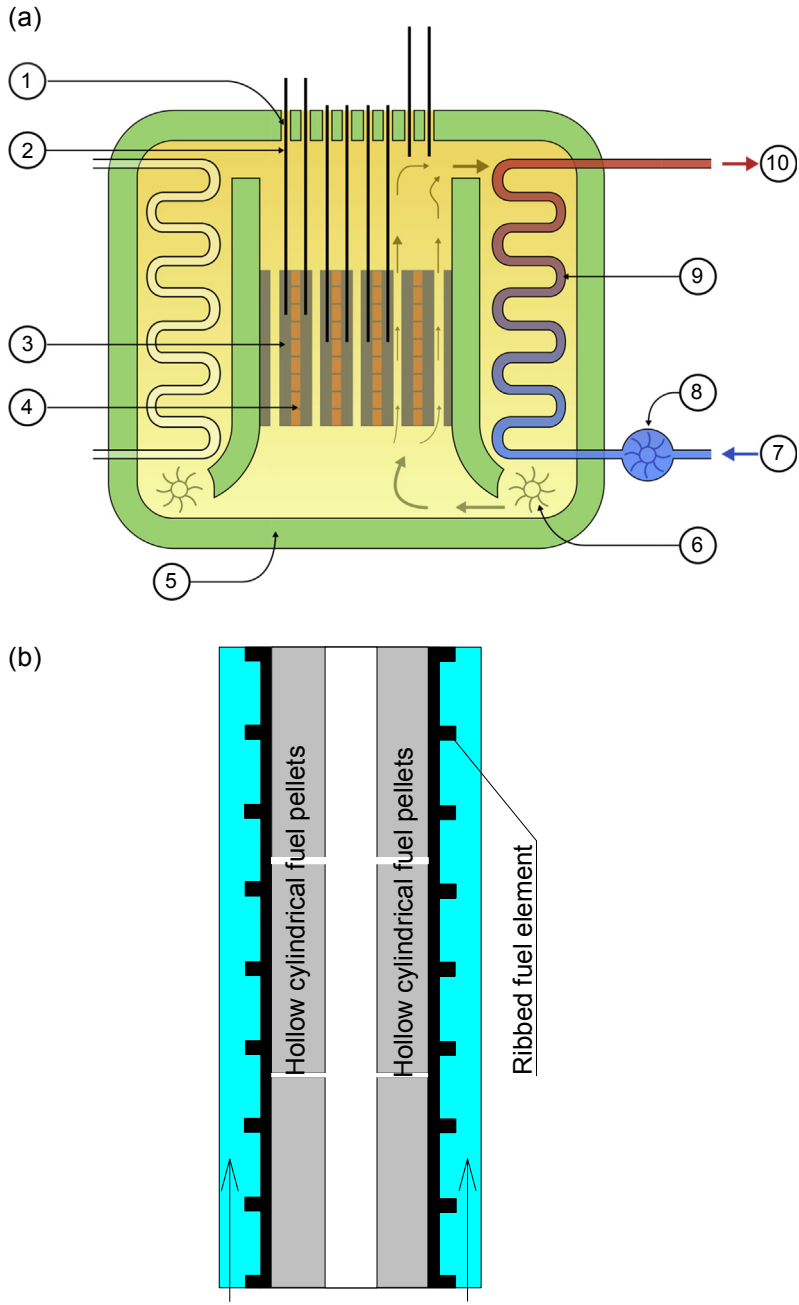


Figure A1.29 (a) Simplified schematic diagram of an AGR (*Author: Messer Woland, https://commons.wikimedia.org/wiki/File:AGR_reactor_schematic.svg*; website approached on January 28, 2016): (1) charge tubes; (2) control rods; (3) graphite moderator; (4) fuel assemblies; (5) concrete pressure vessel and radiation shielding; (6) gas circulator; (7) water; (8) water circulator; (9) heat exchanger; and (10) steam. Heat exchanger is contained within steel-reinforced concrete combined pressure vessel and radiation shield; and (b) AGR ribbed fuel element with hollow fuel pellet (Hewitt and Collier, 2000).

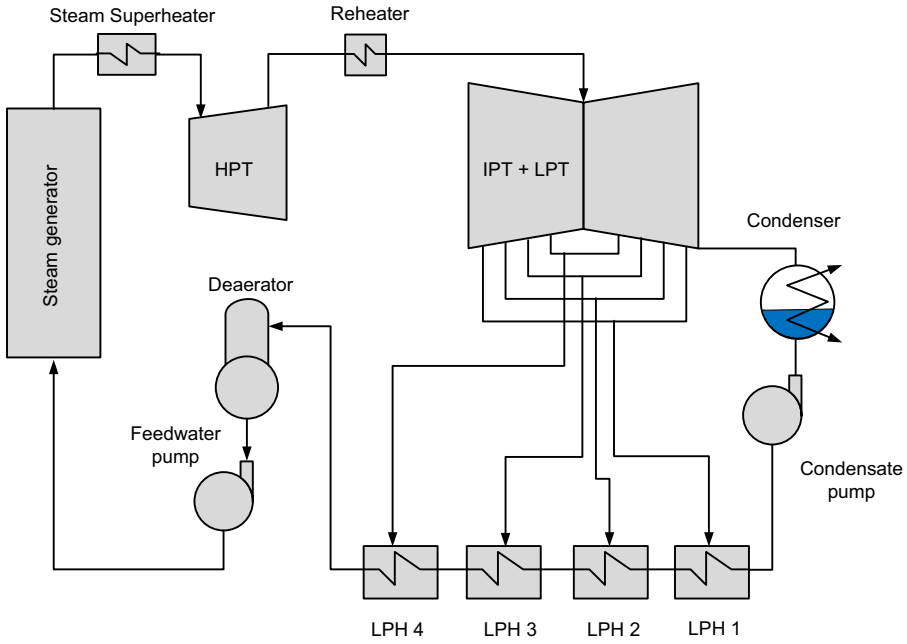


Figure A1.30 Thermodynamic layout of AGR Torness NPP.
Based on data from Nonbel, E., 1996. Description of the Advanced Gas Cooled Type of Reactor (AGR), Report NKS/RAK2(96)TR-C2, November. RisØ National Laboratory, Roskilde, Denmark, 88 pp.

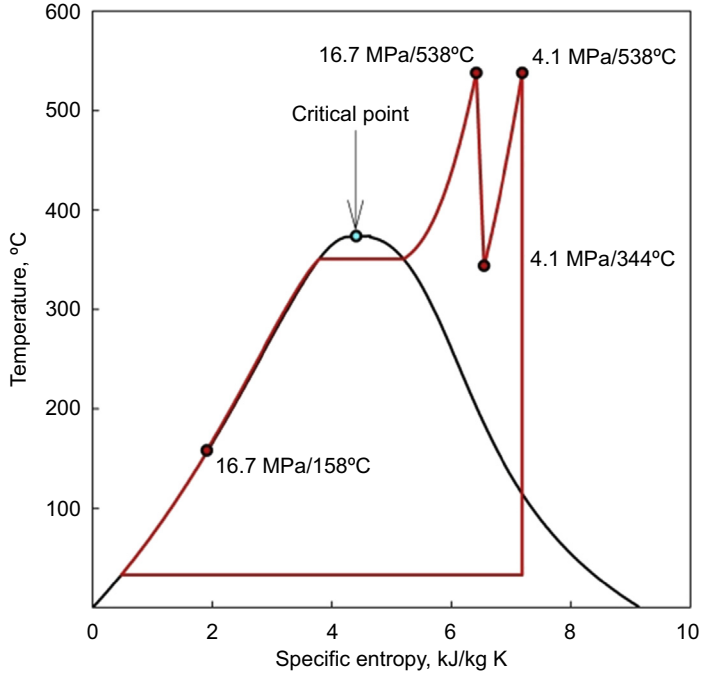


Figure A1.31 *T*−*s* diagram for AGR Torness NPP turbine cycle.

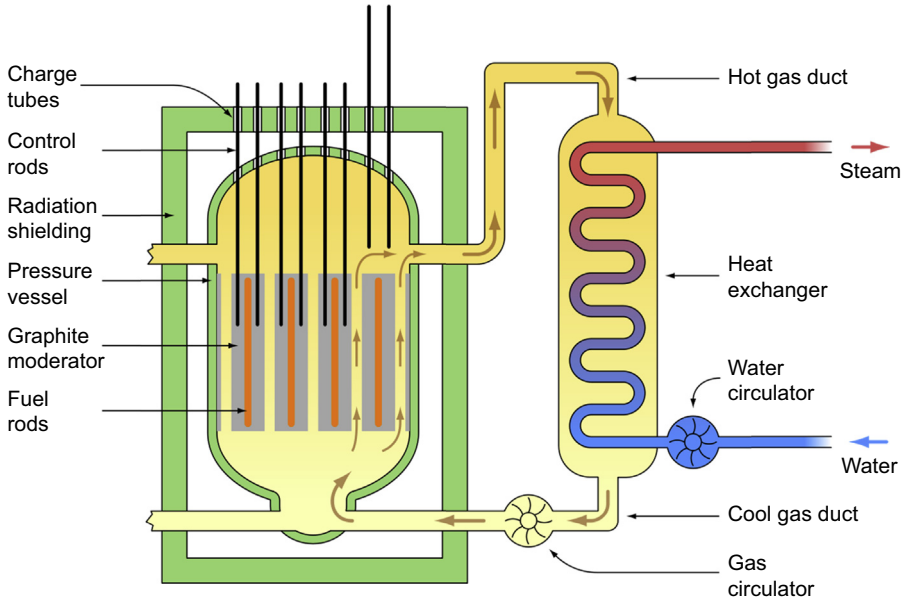


Figure A1.32 Simplified schematic of GCR (early Magnox nuclear reactor design with cylindrical, steel, pressure vessel) (**Original** drawn by **Emoscopes**; Converted to SVG by **Sakurambo**; https://commons.wikimedia.org/wiki/File:Magnox_reactor_schematic.svg; website approached on January 28, 2016). Heat exchanger is outside concrete radiation shielding.

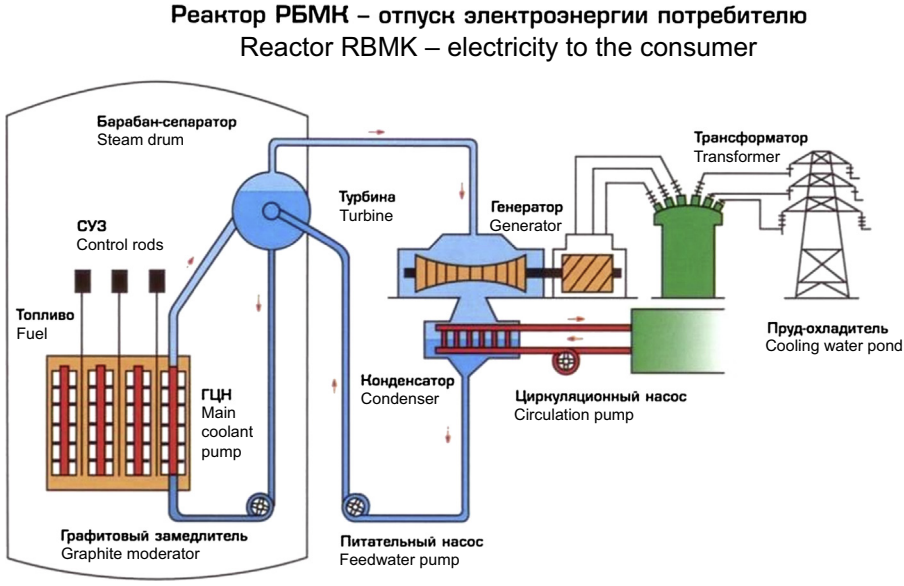


Figure A1.33 Simplified schematic of 1000-MW_{el} LGR (Russian RBMK) NPP (ROSENERGOATOM, 2004).
Courtesy of ROSENERGOATOM.

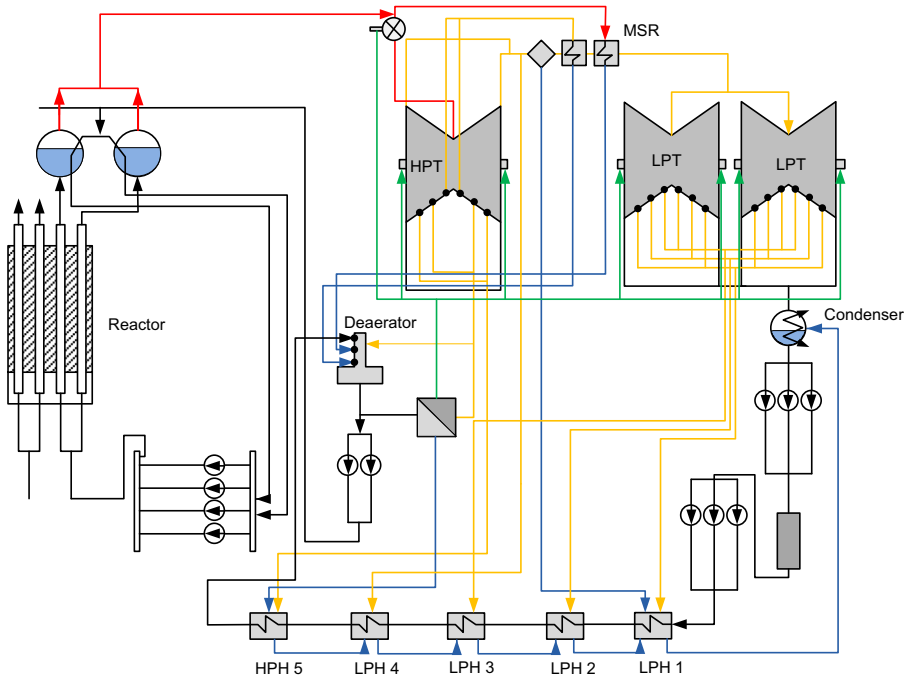


Figure A1.34 Thermodynamic layout of RBMK-1000 NPP.
Adapted and simplified from Cherkashov, Yu.M. (Eds.), 2006. Channel Nuclear Power Reactor (RBMK) (Канальный Ядерный Энергетический Реактор РБМК (In Russian)), 2006. Publishing House GUP NIKIET, Moscow, Russia, 631 pp.

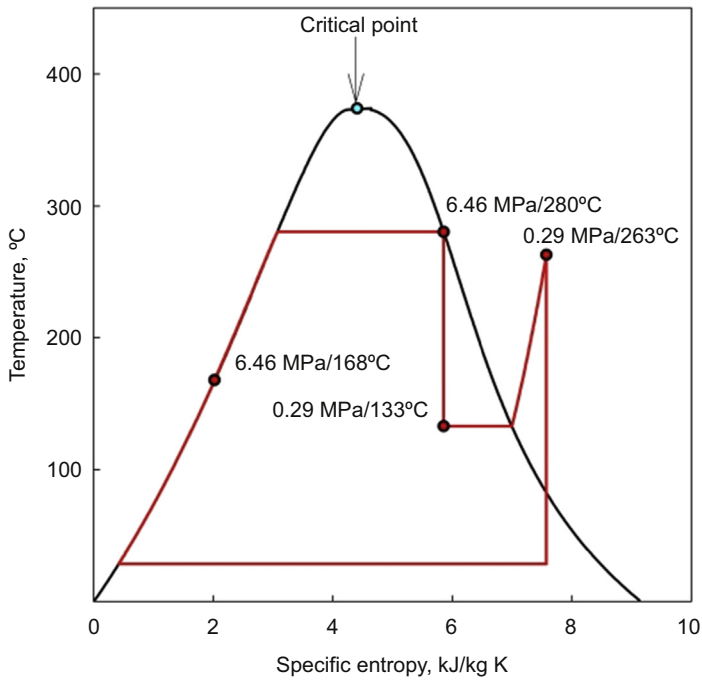


Figure A1.35 *T*−*s* diagram for RBMK-1000 NPP turbine cycle.

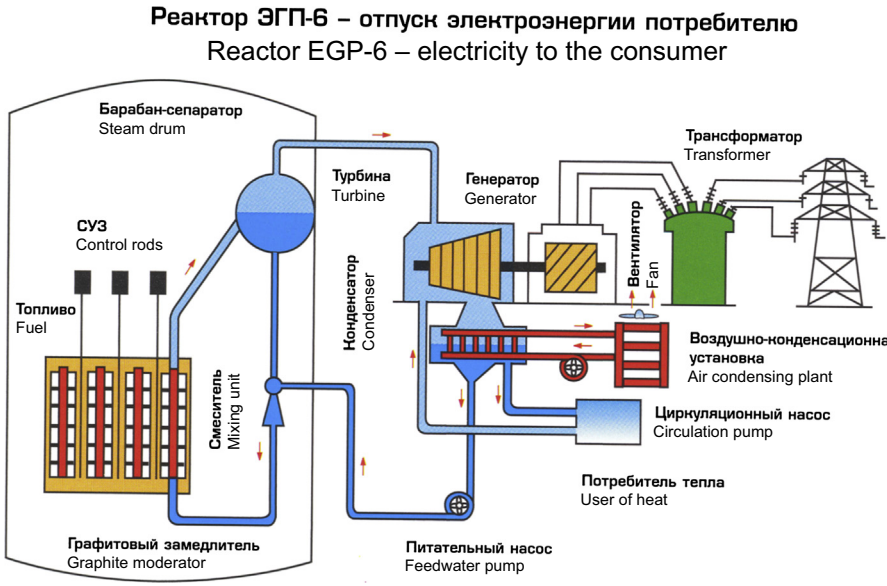


Figure A1.36 Simplified schematic of 11-MW_{el} EGP-6 (power heterogeneous loop reactor) NPP: graphite-moderated, boiling light water-cooled with natural circulation (also, LGR), pressure channel power reactor for production of electricity and heat, air-cooled condenser; prototype of RBMK; and smallest operating reactor by power.

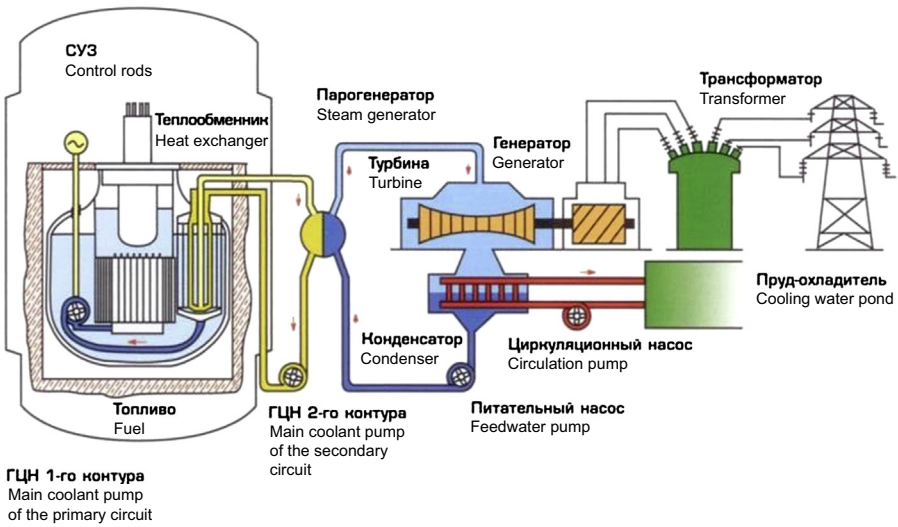


Figure A1.37 Scheme of LMFBR or SFR (Russian BN-600) NPP (ROSENERGOATOM, 2004).
Courtesy of ROSENERGOATOM.

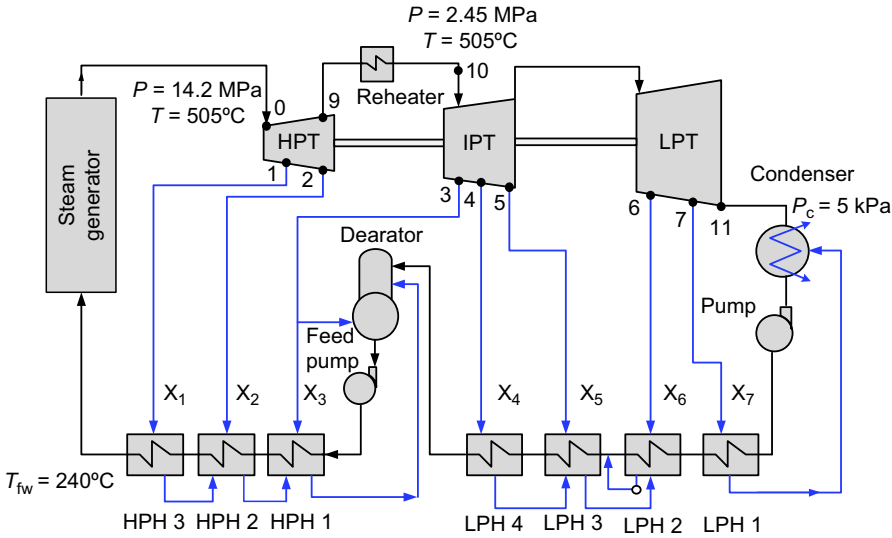


Figure A1.38 Thermodynamic layout of 600-MW_{el} BN-600 SFR NPP.
Based on data from Grigor'ev, V.A., Zorin, V.M. (Eds.), 1988. Thermal and Nuclear Power Plants. Handbook, (In Russian), second ed. Energoatomizdat Publishing House, Moscow, Russia, 625 pp.; Margulova, T.C., 1995. Nuclear Power Plants, (In Russian). Izdat Publishing House, Moscow, Russia, 289 pp.

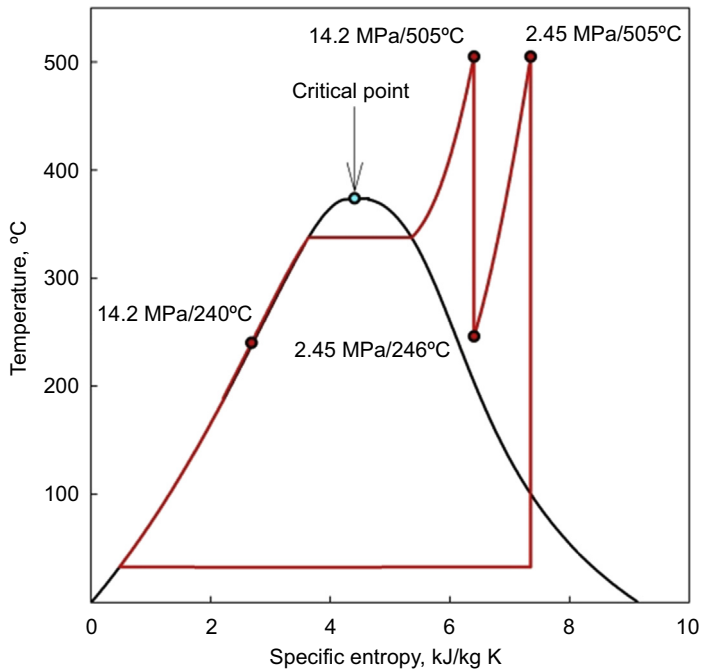


Figure A1.39 $T-s$ diagram for the 600-MW_{el} BN-600 SFR NPP turbine cycle.

Table A1.11 Key-design parameters of Russian SFRs—BN reactors (www.proatom.ru)

No.	Parameter	BN-600[a]	BN-800[a]	BN-1200[b]
1	Thermal power, MW_{th}	1470	2100	2800
2	Electrical power, MW_{el}	600	880	1220
3	Basic components No. of turbines × type No. of generators × type	 3 × K-200-130 3 × ТГВ-200-М	 1 × K-800-130 1 × ТЗВ-800-2	 1 × K-1200-160 1 × ТЗВ-1200-2
4	Pressure vessel Diameter, m Height, m	12.86 12.60	12.96 14.82	16.9 20.72
5	No. of heat transfer loops	3	3	4
6	Temperature of reactor coolant: sodium, primary loop − T_{in}/T_{out}, °C	377/550	354/547	410/550
7	Temperature of intermediate coolant: sodium, secondary loop − T_{in}/T_{out}, °C	328/518	309/505	355/527
8	Temperature of power cycle working fluid: water/steam − T_{in}/T_{out}, °C	240/505	210/490	275/510
9	Pressure at steam generator outlet, MPa	13.7	14.0	17.0
10	Scheme of steam reheat with	Sodium	Steam	Steam
11	Basic unchangeable components service term, years	30	40	60
12	NPP thermal efficiency (gross), %	42.5	41.9	43.6
13	NPP thermal efficiency (net), %	40.0	38.8	40.5

[a]BN-600 and BN-800 are currently in operation at the Beloyarsk NPP; BN-600 commercial start − 1981 and BN-800 − 2016.
[b]BN-1200: concept of future Russian SFR.

A1.2.6 Sodium-cooled fast reactor: BN-600 and BN-800

Accounting on the available information in the open literature, it was decided to show a simplified schematic, thermodynamic layout and $T-s$ diagram of a 600-MW_{el} BN-600 NPP (see Figs. A1.37−A1.39, respectively). Basic data on Russian SFRs−BN reactors are listed in Table A1.11.

Nomenclature

OBE	Operating Basis Earthquake ground motion
SSE	Safe-Shutdown Earthquake ground motion

Acknowledgments

Authors would like to express their great appreciation to Mr. Sumio Fujii (Mitsubishi Heavy Industries (MHI)), Mr. Yuchiro Yoshimoto (Hitachi GE Nuclear Energy, Ltd.), Mr. Ala Alizadeh and Mr. Stephen Yu (CANDU Energy Inc., SNC-Lavalin Group), US NRC, US DOE, Oak Ridge National Laboratory (US Dept. of Energy), ROSENERGOATOM, ROSATOM, Siemens AG (Germany), Toshiba, and authors of figures from the Wikimedia-Commons website for their materials used in this appendix.

References

AECL Report, 1969. Pickering Generation Station. Design Description. Report prepared by Atomic Energy of Canada Limited, 229 pp.

Cherkashov, Yu.M. (Ed.), 2006. Channel Nuclear Power Reactor (RBMK) (Канальный Ядерный Энергетический Реактор РБМК (In Russian)), 2006. Publishing House GUP NIKIET, Moscow, Russia, 631 pp.

Dragunov, A., Saltanov, Eu., Pioro, I., Kirillov, P., Duffey, R., 2015. Power cycles of generation III and III+ nuclear power plants. ASME Journal of Nuclear Engineering and Radiation Science 1 (2), 10 pp.

Grigor'ev, V.A., Zorin, V.M. (Eds.), 1988. Thermal and Nuclear Power Plants. Handbook, (In Russian), second ed. Energoatomizdat Publishing House, Moscow, Russia. 625 pp.

Hewitt, G.F., Collier, J.G., 2000. Introduction to Nuclear Power, second ed. Taylor & Francis, New York, NY, USA. 304 pp.

Kruglikov, P.A., Smolkin, Yu.V., Sokolov, K.V., 2009. Development of engineering solutions for thermal scheme of power unit of thermal power plant with supercritical parameters of steam, (In Russian). In: Proc. Int. Workshop "Supercritical Water and Steam in Nuclear Power Engineering: Problems and Solutions", Moscow, Russia, October 22−23, 6 pp.

Margulova, T.C., 1995. Nuclear Power Plants, (In Russian). Izdat Publishing House, Moscow, Russia, 289 pp.

Nonbel, E., 1996. Description of the Advanced Gas Cooled Type of Reactor (AGR). Report NKS/RAK2(96)TR-C2, November. RisØ National Laboratory, Roskilde, Denmark, 88 pp.

Pioro, I., Duffey, R., 2015. Nuclear power as a basis for future electricity generation. ASME Journal of Nuclear Engineering and Radiation Science 1 (1), 19 pp. Free download from: http://nuclearengineering.asmedigitalcollection.asme.org/article.aspx?articleID=2085849.

Pioro, I., Kirillov, P., 2013a. In: Méndez-Vilas, A. (Ed.), Current Status of Electricity Generation in the World, Chapter in the Book: Materials and Processes for Energy: Communicating Current Research and Technological Developments, Energy Book Series #1. Formatex Research Center, Spain, pp. 783–795. Free download from: http://www.formatex.info/energymaterialsbook/book/783-795.pdf.

Pioro, I., Kirillov, P., 2013b. In: Méndez-Vilas, A. (Ed.), Current Status of Electricity Generation at Thermal Power Plants, Chapter in the Book: Materials and Processes for Energy: Communicating Current Research and Technological Developments, Energy Book Series #1. Formatex Research Center, Spain, pp. 796–805. Free download from: http://www.formatex.info/energymaterialsbook/book/796-805.pdf.

Pioro, I., Kirillov, P., 2013c. In: Méndez-Vilas, A. (Ed.), Current Status of Electricity Generation at Nuclear Power Plants, Chapter in the Book: Materials and Processes for Energy: Communicating Current Research and Technological Developments, Energy Book Series #1. Formatex Research Center, Spain, pp. 806–817. Free download from: http://www.formatex.info/energymaterialsbook/book/806-817.pdf.

Pioro, I., Kirillov, P., 2013d. In: Méndez-Vilas, A. (Ed.), Generation IV Nuclear Reactors as a Basis for Future Electricity Production in the World, Chapter in the Book: Materials and Processes for Energy: Communicating Current Research and Technological Developments, Energy Book Series #1. Formatex Research Center, Spain, pp. 818–830. Free download from: http://www.formatex.info/energymaterialsbook/book/818-830.pdf.

ROSENERGOATOM, 2004. Russian Nuclear Power Plants. 50 Years of Nuclear Power. Moscow, Russia, 120 pp.

Ryzhov, S.B., Mokhov, V.A., Nikitenko, M.P., et al., 2010. Advanced designs of VVER reactor plant. In: Proceedings of the 8th International Topical Meeting on Nuclear Thermal-Hydraulics, Operation and Safety (NUTHOS-8), Shanghai, China, October 10–14.

Shultis, J.K., Faw, R.E., 2007. Fundamentals of Nuclear Science and Engineering, second ed. CRC Press, Boca Raton, FL, USA. 591 pp.

Toshiba, 2011. Leading Innovation. Advanced Boiling Water Reactor (ABWR), Booklet. Toshiba Corporation, Japan.

Appendix A2: Comparison of thermophysical properties of reactor coolants[1]

I.L. Pioro, A. Dragunov, Eu. Saltanov, B. Ikeda
University of Ontario Institute of Technology, Oshawa, Ontario, Canada

A2.1 Introduction

A2.1.1 Generations II, III, and III+ reactor coolants

The current fleet of nuclear power reactors uses the following reactor coolants (see also Table A2.1):

1. Light water (H_2O) at subcritical pressures and temperatures[2] in pressurized water reactors (PWRs) (single-phase cooling, ie, liquid cooling); boiling water reactors (BWRs) (two-phase cooling, ie, with flow boiling, outlet reactor steam quality is usually about 10%), and light water-cooled graphite-moderated reactors (LGRs) [two-phase cooling, ie, with flow boiling, outlet fuel-channel steam quality is usually about 14% (maximum, 20%)];
2. Heavy water (D_2O) at subcritical pressures and temperatures[3]: in pressurized heavy water reactors (PHWRs) (single-phase cooling; however, there is a possibility for boiling within some subchannels at the fuel channel outlet, steam quality usually does not exceed 5%);
3. Carbon dioxide (CO_2) at subcritical pressures, but at supercritical temperatures[4] an advanced gas-cooled reactors (AGRs); and
4. Liquid sodium (Na)[5] in a sodium-cooled fast reactor (SFR).

Power cycles of Generation III and III+ NPPs are shown in Dragunov et al. (2015).

A2.1.2 Generation IV reactor coolants

Generation IV nuclear reactor concepts proposed have identified the use of the following reactor coolants (see also, Table A2.2):

1. H_2O at supercritical pressures and temperatures[3] in supercritical water-cooled reactors (SCWRs) (single-phase cooling because at supercritical pressures, fluids are considered single-phase substances);

[1] This chapter is partially based on the paper by Dragunov et al. (2013).
[2] Water: critical pressure—22.064 MPa and critical temperature—373.95°C (NIST REFPROP, 2010).
[3] D_2O: critical pressure—21.671 MPa and critical temperature—370.7°C (NIST REFPROP, 2010).
[4] CO_2: critical pressure—7.3773 MPa and critical temperature—30.978°C (NIST REFPROP, 2010).
[5] Na: melting temperature—97.7°C and boiling temperature—882.8°C.

2. Helium (He) at supercritical pressures and temperatures[7] in GFRs and very high temperature reactor (VHTRs);
3. Liquid Na[6] in SFRs;
4. Liquid lead (Pb)[8] in lead-cooled fast reactors (LFRs);

Table A2.1 Typical ranges of thermal efficiencies (gross[6]) for selected modern nuclear power plants (NPPs arranged by decreasing values of thermal efficiency) (Pioro and Duffey, 2015)

No	Nuclear power plant	Gross efficiency, %
1	AGR NPP (based on Torness NPP, UK) (Generation III); thermal neutron spectrum; moderator—graphite; reactor coolant—CO_2: $P = 4$ MPa, $T_{in} = 290°C$ & $T_{out} = 650°C$; indirect cycle (double loop, ie, CO_2−water/superheated steam); Rankine power cycle with single steam reheat—primary steam (turbine inlet): $P_{in} = 16.7$ MPa ($T_{sat} = 351°C$) and $T_{in} = 538°C$; secondary steam: $P_{in} = 4.1$ MPa ($T_{sat} = 252°C$) and $T_{in} = 538°C$ ($T_{cr} = 374°C$)	Up to 42
2	SFR (based on Russian BN-600 reactor) NPP (Generation IV); fast neutron spectrum; no moderator; reactor coolant: $P \approx 0.1$ MPa and $T_{in} = 380°C$ and $T_{out} = 550°C$; indirect cycle (triple loop, ie, sodium−sodium−water/superheated steam); Rankine power cycle with single steam reheat—primary steam (turbine inlet): $P_{in} = 14.2$ MPa ($T_{sat} = 338°C$) and $T_{in} = 505°C$; secondary steam: $P_{in} = 2.45$ MPa ($T_{sat} = 223°C$) and $T_{in} = 505°C$ ($T_{cr} = 374°C$)	Up to 40
3	PWR NPP (Generation III+, to be implemented within next 1−10 years); thermal neutron spectrum; moderator and reactor coolant—H_2O: $P = 15.5$ MPa ($T_{sat} = 345°C$) and $T_{out} = 327°C$; indirect cycle (double loop, ie, water−water/saturated steam); Rankine power cycle with single steam reheat−primary steam (turbine inlet): $P_{in} = 7.8$ MPa & $T_{in/sat} = 293°C$	Up to 38

[6] Gross thermal efficiency (gross eff.) of a unit during a given period of time is the ratio of the gross electrical energy generated by a unit to the thermal energy of a fuel consumed during the same period by the same unit. The difference between gross and net thermal efficiencies includes internal needs for electrical energy of a power plant, which might not be small (5% or more).

[7] He: critical pressure—0.2276 MPa and critical temperature—−267.95°C (NIST REFPROP, 2010).

[8] Lead: melting temperature—327.5°C and boiling temperature—1750°C.

Table A2.1 Continued

No	Nuclear power plant	Gross efficiency, %
4	PWR (based on Russian VVEP-1000 reactor) NPP (Generation III); thermal neutron spectrum; moderator and reactor coolant—H_2O: $P = 15.7$ MPa ($T_{sat} = 346°C$) & $T_{out} = 322°C$; indirect cycle (double loop, ie, water—water/saturated steam); Rankine power cycle with single steam reheat—primary steam (turbine inlet): $P_{in} = 5.9$ MPa and $T_{in/sat} = 274°C$; secondary steam: $P_{in} = 1.15$ MPa ($T_{sat} = 186°C$) & $T_{in} = 250°C$	Up to 36
5	ABWR NPP (Generation III+); thermal neutron spectrum; direct cycle (single loop); moderator/reactor coolant/working fluid in Rankine power cycle with single steam reheat—H_2O; primary steam (turbine inlet): $P_{in} = 6.97$ MPa & $T_{in/sat} = 286°C$; secondary steam: $P_{in} = 1.7$ MPa ($T_{sat} = 204°C$) & $T_{in} = 259°C$	Up to 34
6	PHWR (based on Pickering 740-MW_{el} EC6 reactor) NPP (Generation III); thermal neutron spectrum; moderator—D_2O: $P = 0.1$ MPa and $T \approx 70°C$; reactor coolant—D_2O: $P_{in} = 11$ MPa; $T_{in} = 265°C$; and $T_{out} = 310°C$; indirect cycle (double loop, ie, D_2O–H_2O/saturated steam); Rankine power cycle with single steam reheat—primary steam (turbine inlet): $P_{in} = 6$ MPa and $T_{in/sat} = 260°C$; secondary steam: $P_{in} = 0.62$ MPa ($T_{sat} = 160°C$) and $T_{in} = 250°C$	Up to 32
7	LGR (based on Russian RBMK—pressure channel boiling reactor) NPP (Generation III); thermal neutron spectrum; moderator—graphite; direct cycle (double loop with steam separator in between); reactor coolant/working fluid in Rankine power cycle with single steam reheat—H_2O; primary steam (turbine inlet): $P_{in} = 6.46$ MPa & $T_{in/sat} = 280°C$; secondary steam: $P_{in} = 0.29$ MPa ($T_{sat} = 132°C$) and $T_{in} = 263°C$	Up to 34

Table A2.2 Estimated ranges of thermal efficiencies (gross) of Generation IV NPP concepts (NPP concepts shown according to the decreasing values of thermal efficiency) (Pioro and Duffey, 2015)

No	Nuclear power plant	Gross efficiency, %
1	VHTR NPP; thermal neutron spectrum; moderator graphite; reactor coolant—He: $P = 7$ MPa and $T_{in} = 640$°C and $T_{out} = 1000$°C; primary power cycle—direct Brayton gas turbine cycle; possible backup—indirect Rankine steam cycle	≥55
2	Gas-cooled fast reactor (GFR) or high temperature reactor (HTR) NPP; fast neutron spectrum; no moderator; reactor coolant—He: $P = 9$ MPa and $T_{in} = 490$°C & $T_{out} = 850$°C; primary power cycle—direct Brayton gas turbine cycle; possible backup—indirect Rankine steam cycle	≥50
3	SCWR NPP (one of Canadian concepts, ie, pressure channel reactor); thermal neutron spectrum; moderator—D_2O; reactor coolant—H_2O: $P = 25$ MPa ($P_{cr} = 22.064$ MPa) and $T_{in} = 350$°C and $T_{out} = 625$°C ($T_{cr} = 374$°C); direct cycle, ie, single loop; supercritical pressure Rankine power cycle with single steam reheat—primary steam (turbine inlet): $P_{in} = 25$ MPa ($P_{cr} = 22.064$ MPa) and $T_{in} = 625$°C ($T_{cr} = 374$°C); secondary steam: $P_{in} = 5.7$ MPa ($T_{sat} = 252$°C) and $T_{in} = 625$°C; possible backup—indirect supercritical pressure Rankine steam cycle with single steam reheat (superheat)	45−50
4	MSR NPP; thermal neutron spectrum (moderator—graphite) or fast neutron spectrum (no moderator); reactor coolant—sodium-fluoride salt with dissolved uranium fuel: $P \approx 0.1$ MPa and $T_{out} \approx 800$°C; primary power cycle—indirect supercritical pressure CO_2 Brayton gas turbine cycle; possible backup—indirect Rankine steam cycle	~50
5	LFR NPP (based on Russian design Brest-300 reactor); fast neutron spectrum; no moderator; reactor coolant—liquid Pb: $P \approx 0.1$ MPa and $T_{in} = 420$°C and $T_{out} = 540$°C; primary power cycle—indirect supercritical pressure Rankine steam cycle: $P_{in} \approx 24.5$ MPa ($P_{cr} = 22.064$ MPa) and $T_{in} = 340$°C and $T_{out} = 520$°C ($T_{cr} = 374$°C) or subcritical pressure Rankine steam cycle with superheated steam; single steam reheat; possible backup in some other countries—indirect supercritical pressure CO_2 Brayton gas turbine cycle	~43

Table A2.2 Continued

No	Nuclear power plant	Gross efficiency, %
6	SFR (based on Russian BN-600 reactor) NPP (Generation IV); fast neutron spectrum; no moderator; reactor coolant—Na: $P \approx 0.1$ MPa, $T_{in} = 380°C$, and $T_{out} = 550°C$; indirect cycle (triple loop, ie, Na−Na−water/superheated steam); Rankine power cycle with single steam reheat—primary steam (turbine inlet): $P = 14.2$ MPa ($T_{sat} = 338°C$) and $T_{in} = 505°C$ ($T_{cr} = 374°C$); secondary steam: $P = 2.45$ MPa ($T_{sat} = 223°C$) and $T_{in} = 505°C$; possible backup in some other countries—indirect supercritical pressure CO_2 Brayton gas turbine cycle	~40

5. Liquid lead−bismuth eutectic (LBE) [44.5% Pb and 55.5% bismuth (Bi)][9] in liquid metal-cooled reactors, for example, in Russian *Svintsovo-Vismutovyi Bystryi Reaktor* (SVBR); and
6. Molten fluoride salts (for example, FLiNaK)[10] in molten salt reactors (MSRs).

For a better understanding of the thermodynamic terms such as subcritical/supercritical pressures, supercritical fluid, superheated/saturated steam, etc., thermodynamic diagrams for H_2O, CO_2, and He are shown in Figs. A2.1−A2.3 [partially based on figures in Mann and Pioro (2015)].

A glossary of the terms used in Figs. A2.1−A2.3 and used elsewhere in the text is given below:

Compressed fluid is a fluid at a pressure above the critical pressure but at a temperature below the critical temperature.
Critical point (also called a critical state) is a point at which the distinction between the liquid and gas (vapor) phases disappears, ie, both phases have the same temperature, pressure, and specific volume or density. The critical point is characterized using the phase state parameters T_{cr}, P_{cr}, and v_{cr} (or ρ_{cr}), which have unique values for each pure substance.
Pseudocritical line is a line that consists of pseudocritical points.
Pseudocritical point (characterized with P_{pc} and T_{pc}) is a point at a pressure above the critical pressure where the temperature ($T_{pc} > T_{cr}$) corresponds to the maximum value of the specific heat for this particular pressure.
Pseudocritical region is a narrow region around a pseudocritical point where all thermophysical properties of a pure fluid exhibit rapid variations. For H_2O, it is about ±25°C from pseudocritical temperature.

[9] LBE: melting temperature—123.5°C and boiling temperature—1670°C.
[10] FLiNaK (LiF−NaF−KF): Melting temperature—454°C and boiling temperature—1570°C.

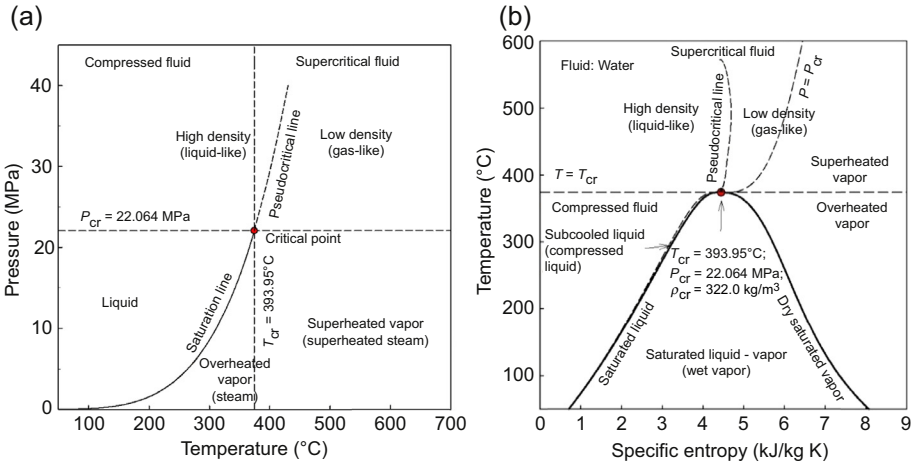


Figure A2.1 Thermodynamic diagrams for H_2O: (a) pressure−temperature diagram; and (b) temperature−specific entropy diagram.

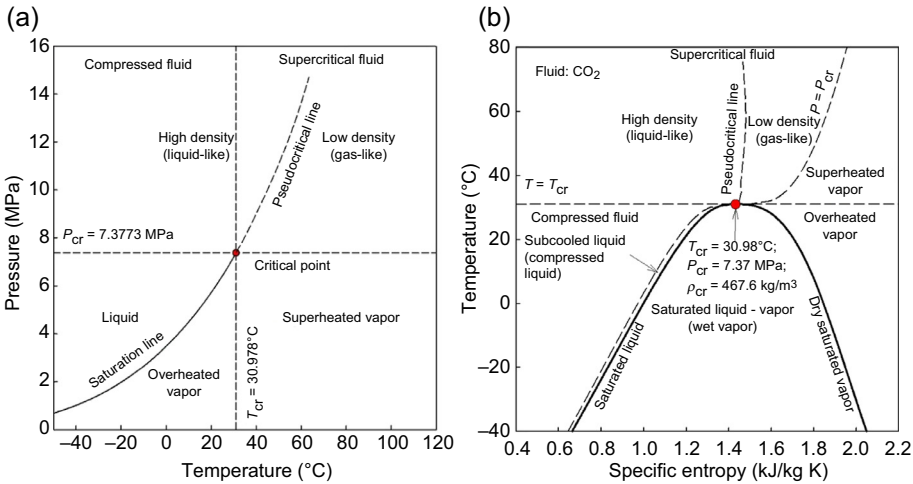


Figure A2.2 Thermodynamic diagrams for CO_2: (a) pressure−temperature diagram; and (b) temperature−specific entropy diagram.

Supercritical fluid is a fluid at pressures and temperatures that are higher than its critical pressure and critical temperature. However, often in various publications, a term supercritical fluid includes both terms: supercritical fluid and compressed fluid.

Overheated vapor is a dry vapor at a pressure and temperature below the critical pressure and temperature, respectively, but above the corresponding parameters of dry saturated vapor.

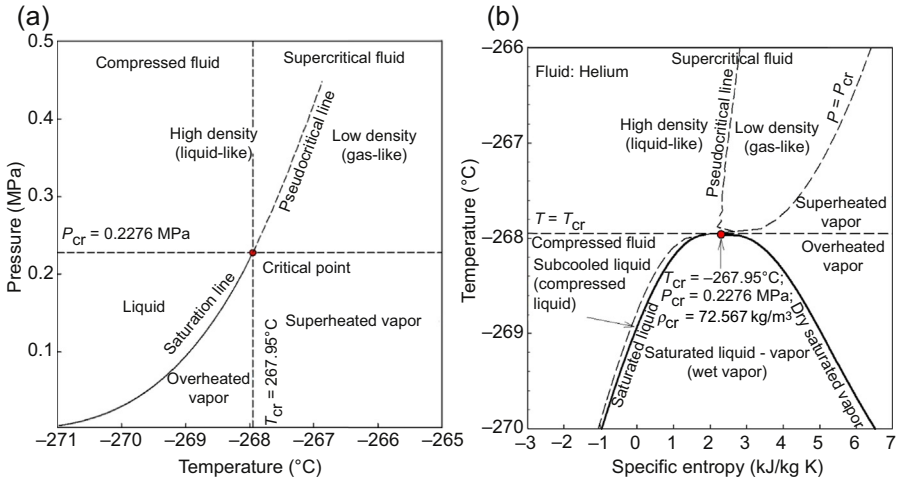


Figure A2.3 Thermodynamic diagrams for He: (a) pressure−temperature diagram; and (b) temperature−specific entropy diagram.

Supercritical "steam" is actually supercritical water (SCW) because at supercritical pressures, the fluid is considered as a single-phase substance. However, this term is widely (and incorrectly) used in the literature in relation to supercritical "steam" generators and turbines.
Superheated vapor is a vapor at pressures below the critical pressure, but at temperatures above the critical temperature.

A2.2 Reactor coolants by type

A2.2.1 Fluid coolants

Subcritical pressure H_2O is very well known and is the most used reactor coolant. Due to that, it will be used in the subsequent comparisons as a reference case. In general, D_2O has many thermophysical properties and behaviors that are close to those of H_2O (for details, see Table A2.3). However, D_2O has a significantly lower neutron capture cross section compared to H_2O, which allows for more thorough moderation. Therefore, only the heat transfer characteristics of subcritical pressure D_2O will be compared with those of other coolants.

One of the advantages of H_2O and D_2O is the high heat transfer coefficients at forced convection and at flow boiling. However, there is a limit for efficient heat transfer, called critical heat flux (CHF), which usually cannot be exceeded during nuclear reactor operation.

In Table A2.3:

$$\Delta = \frac{Property_{D_2O} - Property_{H_2O}}{Property_{D_2O}} \times 100\%$$

Table A2.3 Comparison of selected thermophysical properties of D_2O and H_2O

(a) At subcooled conditions: $P = 11$ MPa and $T = 260°C$ (approximately CANDU reactor fuel channel inlet conditions)

Coolant	ρ kg/m^3	c_p J/kg K	k W/m K	μ μPa s	Pr –
D_2O	875.4	4657.1	0.536	114.7	0.997
H_2O	791.5	4887.5	0.618	103.7	0.820
Δ, %	9.6	−5.0	−15.3	9.6	17.7

(b) At saturated conditions: $P = 10$ MPa and $T_{sat} = 310°C$ for D_2O (approximately CANDU reactor fuel channel outlet conditions) and $T_{sat} = 311°C$ (Δ = 0.3%) for H_2O

Coolant	$\frac{\rho_f}{\rho_v}$ kg/m^3	$\frac{c_{pf}}{c_{pv}}$ J/kg K	$\frac{k_f}{k_v}$ W/m K	$\frac{\mu_f}{\mu_v}$ μPa s	$\frac{Pr_f}{Pr_v}$ –	h_{fg} kJ/kg
D_2O	$\frac{760.0}{62.5}$	$\frac{5823.6}{6730.7}$	$\frac{457.7}{82.0}$	$\frac{89.2}{20.2}$	$\frac{1.13}{1.66}$	1178.8
H_2O	$\frac{688.4}{55.5}$	$\frac{6123.7}{7140.8}$	$\frac{526.8}{76.6}$	$\frac{81.7}{20.2}$	$\frac{0.95}{1.88}$	1317.4
Δ, %	$\frac{9.4}{11.2}$	$\frac{-5.2}{-6.1}$	$\frac{-15.1}{6.6}$	$\frac{8.4}{0}$	$\frac{16.3}{-13.5}$	−11.8

Data based on National Institute of Standards and Technology, 2010. NIST Reference Fluid Thermodynamic and Transport Properties—REFPROP. NIST Standard Reference Database 23, Ver. 9.1. Department of Commerce, Boulder, CO, USA.

SCW is a coolant in an SCWR concept with an operating pressure of about 25 MPa, and reactor inlet and outlet temperatures of about 350 and 625°C (max.), respectively. Specifics of SCW thermophysical properties and heat transfer are discussed in Appendix A3 and in the following publications: IAEA-TECDOC-1746 (2014), Gupta et al. (2013), Pioro (2011), Pioro et al. (2011), Pioro and Mokry (2011), NIST REFPROP (2010), and Pioro and Duffey (2007).

The main disadvantage of water as a reactor coolant is that to reach higher thermal efficiencies of NPP, higher temperatures are needed, which in turn requires high or even supercritical pressures.

A2.2.2 Gas coolants

For comparison purposes in this Appendix, it was decided to consider subcritical pressure CO_2. CO_2 at subcritical pressures is currently being used in the most efficient nuclear power reactors: AGRs. In general, CO_2 is not a strong absorber of thermal neutrons and does not become very radioactive. Other advantages of CO_2 are its chemical stability within the operating range of temperatures (292−650°C). In addition, CO_2 does not react with either the moderator or fuel.

Using He as a reactor coolant at high outlet temperatures (850 and 1000°C in GFR and VHTR, respectively) makes it possible to achieve very high thermal efficiencies of

the plant that are close to those of modern advanced thermal power plants. The major advantages of He are: (1) a relatively high thermal conductivity compared to that of other gases (an exception is hydrogen), which is close to that of liquids; and (2) its behavior as a noble or inert gas.

In general, the advantages of gaseous reactor coolants compared to water are a possibility to achieve high, or even very high, temperatures at the reactor outlet using significantly lower pressures, and there is no CHF phenomena at gas cooling, which limits heat transfer in fluid cooling. However, the heat transfer coefficients at gas forced convection cooling are usually significantly lower than those at water cooling.

A2.2.3 Liquid metal coolants

Liquid Na is currently used in the Russian BN-600 and BN-800—the only ones operating SFR so far in the world—and is proposed to be used in Generation IV SFRs. Na is a well-known low melting point (97.7°C) alkali metal, which has the main advantages of high thermal conductivity and low neutron absorption cross section. Also, the relatively high boiling point (882.8°C) of Na allows a reactor to operate at pressures close to ~0.1 MPa. In addition, very high heat transfer coefficients can be achieved with Na cooling.

However, Na is very chemically reactive substance, which requires special precautions to be taken when it used as a reactor coolant. Therefore, for improved reactor safety, a secondary Na loop is utilized, which acts as a buffer between the radioactive Na—reactor coolant in the primary loop and the water/steam in the third loop—a steam Rankine power cycle.

Pb is proposed for use in an LFR at pressures close to ~0.1 MPa. Pb has a higher melting point (327.5°C) and a significantly higher boiling point (1750°C) compared to that of Na, which significantly impacts the manner of operating a reactor. Also, it is a more inert liquid metal than Na. Due to that, the LFR has only two loops: (1) a primary loop with Pb as a reactor coolant; and (2) a secondary loop with water/steam as a steam Rankine power cycle.

LBE is a eutectic alloy of Pb (44.5%) and Bi (55.5%), being considered instead of Pb as an option for the LFR. One of the main advantages of LBE is its melting point of 123.5°C, which is significantly lower than that of Pb and close to that of Na. Neither the Pb nor LBE react readily with water or air, in contrast to Na, which allows for the elimination of the intermediate coolant loop used in SFRs. Moreover, LBE is not a new technology; it has been proven by years of reliable experience as a coolant in nuclear powered submarines operated by the Soviet Union since the 1970s.

A major advantage of liquid metal reactor coolants is the low operating pressures inside a reactor (close to atmospheric one) with a possibility to achieve high temperatures. Also, all current liquid metal reactors use a fast neutron spectrum, which allows for more efficient fuel cycles.

More information on liquid metal reactor coolants can found in the following publications: Beznosov et al. (2007), Todreas et al. (2004), Dementyev (1990), IAEA (1985), and Waltar and Reynolds (1981).

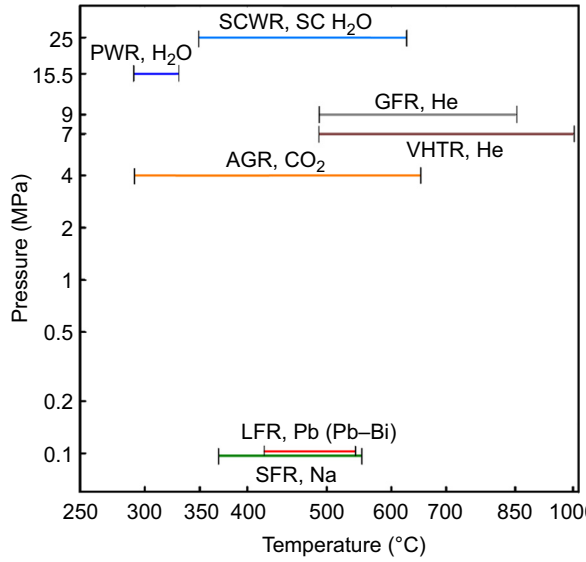


Figure A2.4 Pressure−temperature diagram showing operating ranges of coolants for PWR, AGR, SFR, and proposed Generation IV reactor concepts (pressure drop is not considered).

A2.2.4 Molten salt coolants

Molten salt fluorides, which are proposed as coolants for MSR, have promising thermophysical and thermal hydraulic properties. Molten salts, similar to liquid metals, have a low vapor pressure even at high temperatures, which is attractive compared to water and gaseous coolants. The salts are less chemically reactive than Na. In addition, salts can provide moderation due to their light element composition, like fluorine (F), lithium (Li), and beryllium (Be) in FLiBe.

In the next section, a comparison of the main thermophysical properties will be conducted for all the coolants mentioned above. The range of temperatures investigated covers the operating ranges of the corresponding reactors (see Tables A2.1 and A2.2, and Fig. A2.4). Basic averaged parameters for the coolants used in each of the reactors utilized are listed in Table A2.4.

A2.3 Thermophysical properties of proposed Generation II, III, III+, and IV reactor coolants

In this section, a comparison of the main thermophysical properties of various coolants for Generation IV reactor systems is presented. It is important to note that the basic properties are shown for a wide range of temperatures (from 250 to 1000°C) that covers the operating ranges of current and Generation IV reactors (see Fig. A2.4 and Tables A2.1 and A2.2).

Table A2.4 Basic reference parameters of selected Generations II, III, III+, and IV nuclear power reactors/concepts

Reactor	Neutron spectrum	Core design		Reactor coolant	Moderator	Reactor cycle	No of circuits	*P*	*T*
								MPa	°C
PWR	Thermal	Heterogeneous	PV	Water		Indirect	2	~15.5	292−329
AGR	Thermal	Heterogeneous	PV[a]	CO_2	Graphite	Indirect	2	4	292−650
SFR	Fast	Heterogeneous	PV	Na	−	Indirect	3	~0.1	370−550
GFR	Fast	Heterogeneous	PV	He	−	Direct	1	9	490−850
						Indirect	2		
VHTR	Thermal	Heterogeneous	PV	He	Graphite	Direct	1	7	490−1000
						Indirect	2		
LFR	Fast	Heterogeneous	PV	Pb (LBE)	−	Indirect	2	~0.1	550−800 (420−540)
MSR	Epithermal	Homogeneous	PV	Sodium fluoride with dissolved uranium	Graphite	Indirect	3	~0.1	$T_{out} = 700-800$
MSFR	Fast	Homogeneous	PV	Sodium fluoride with dissolved uranium	−	Indirect	3	~0.1	$T_{out} = 700-800$
SCWR	Thermal	Heterogeneous	PV	Water	Water	Direct	1	~25	300−625
			PCh (PT)		D_2O	Indirect	2		
	Fast		PV	Water	−	Direct	1		300−625
			PCh (PT)			Indirect	2		

MSFR, molten salt fast reactor.
[a]Though coolant flows through individual channels inside graphite moderator, the actual pressure boundary is the vessel surrounding the moderator.

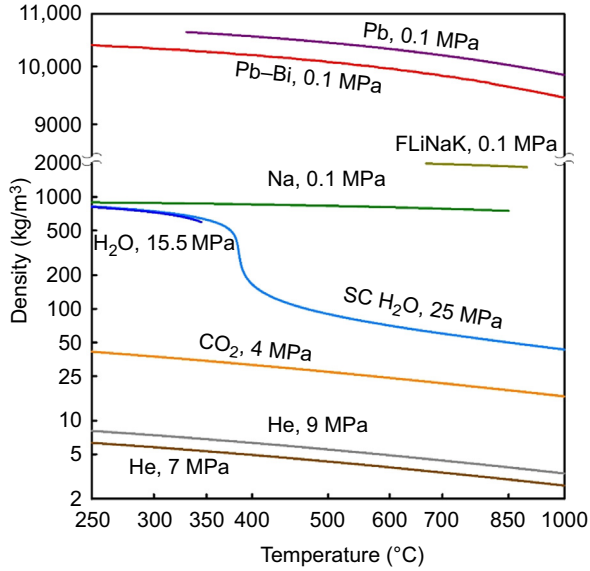


Figure A2.5 Density of selected coolants versus temperature.

Properties of subcritical and supercritical water, CO_2, and He-4 were obtained from NIST REFPROP software (2010). Properties of Na were taken from Kirillov et al. (2007). Properties of other coolants were calculated either using the original correlations presented in NEA (2007) or using correlations recommended by authors of this book.

Before comparing thermophysical properties of the coolants, it is reasonable to have a general overview of the desired characteristics of a generic reactor coolant. Nuclear reactors have certain specific requirements for coolants, such as:

- high specific heat, thermal conductivity, and low viscosity;
- low corrosive and low erosive effects on all the reactor materials;
- high boiling point and low melting point (not related to gaseous coolants);
- high thermal resistance and radiation resistance;
- low neutron absorption cross section;
- explosion-proof, noncombustible, nontoxic;
- widely available (not rare); and
- low neutron activation.

Fig. A2.5 shows densities profiles of reactor coolants versus temperature. As expected, molten Pb and Pb−Bi alloy have the highest densities, followed by molten salt and Na. Actually, at ~250°C, the densities of molten Na, subcritical pressure water, and SCW are close. However, with temperature increase, the densities of water and SCW steadily decline. Within the pseudocritical range, the SCW density drops significantly due to the transition from a "liquid-like" fluid to a "gas-like" fluid. Gases, especially He, have the lowest densities. The density of CO_2 is significantly higher than that of He.

In general, the densities of the reactor coolants (with exception of SCW) decline almost linearly with increasing temperature (see Fig. A2.5). The densities of gases

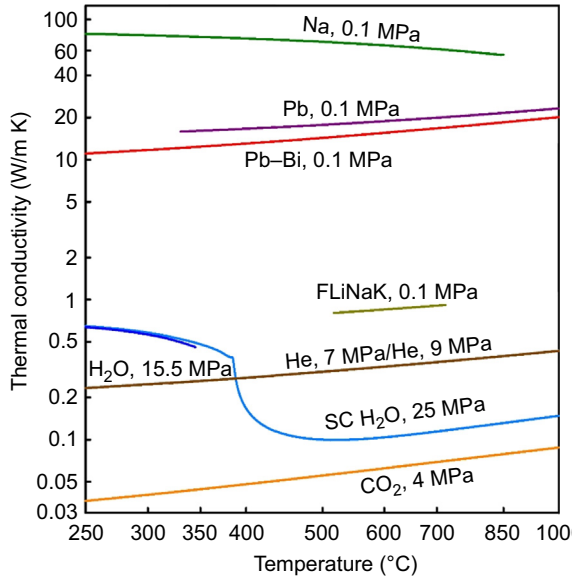


Figure A2.6 Thermal conductivity of selected coolants versus temperature.

(He and CO_2) decrease about 1.6 times, but the density change for liquid metals is insignificant. For SCW, the density drops by almost 8 times in the pseudocritical region.

As one would expect, the thermal conductivity of liquid metals is significantly higher than that of gases (50−3000 times, see Fig. A2.6). The thermal conductivity of Na drops slightly, while that for Pb, LBE, He, and CO_2 increases linearly with the temperature. The thermal conductivity behavior of SCW is special. The thermal conductivity decreases linearly for temperature between 250−350°C and then goes through a small peak in the pseudocritical point before decreasing smoothly from about 0.4 to 0.1 W/m K. As the temperature increases above 500°C, the thermal conductivity increases linearly to values higher than those of CO_2, but lower than those of He.

The majority of the thermal properties[11] of FLiNaK molten salt have intermediate values between those of liquid metals and fluids. However, the viscosity of FLiNaK appears to be significantly higher than that of the rest of the coolant. This also causes the Prandtl number (**Pr**) to be very high.

The temperature dependence of the viscosity of liquid metals is quite the opposite behavior to that of gases (Fig. A2.7). The viscosity of Na and Pb drop linearly over the whole range of temperature, while the viscosity of Pb−Bi has a slower linear drop, up to 600°C, and then the viscosity increases for temperatures between 600 and 1000°C. Near 1000°C, the viscosity returns to a value close to that measured at 250°C. The viscosities of gases increase linearly with temperature, and the viscosity of SCW at

[11] Thermal properties of FLiNaK were calculated based on Sohal et al. (2010); Khokhlov et al. (2009), Williams et al. (2006), and Chrenkova et al. (2003).

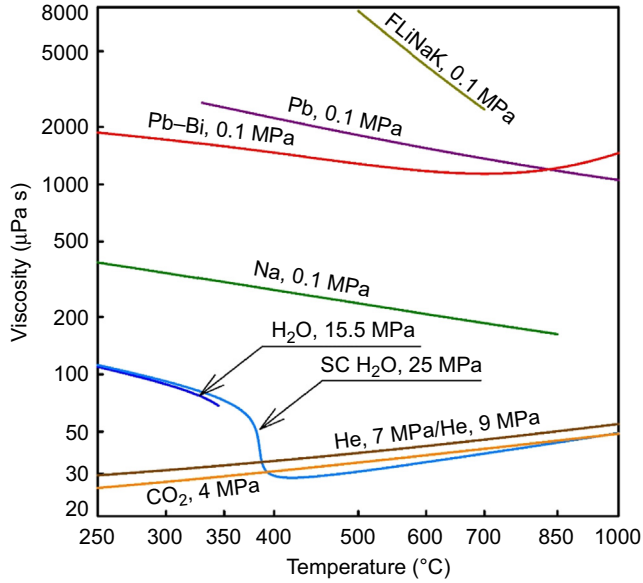


Figure A2.7 Dynamic viscosity of selected coolants versus temperature.

temperatures beyond the pseudocritical range behave in a fashion similar to that of gases. In general, the shape of the viscosity−temperature curve for SCW is similar to that of its thermal conductivity. However, the viscosity does not exhibit a peak in the pseudocritical point.

The specific heat of He, Na, Pb, and Pb−Bi (Fig. A2.6) is nearly constant over the whole range of operational parameters. In the case of CO_2, the specific heat increases linearly and reaches the same value as Na at around 750°C. The specific heat of water goes through a peak (where its value increases almost 8 times) within the pseudocritical region. The specific heats of Pb and LBE are nearly identical and 10 times less than those of Na and CO_2, and almost 40 times less than that of He. At temperatures higher than 450°C, the specific heat of He is higher than that of SCW.

Figs. A2.8 and A2.9 shows the enthalpy increase versus temperature for all reactor coolants. The enthalpy increase is straight forward and is related to the behavior of the specific heat. Therefore, the highest increase in enthalpy is in SCW, especially in the pseudocritical range where the specific heat has a peak. Eventually, SCW, water, and He show close trends in enthalpy increase. The enthalpy increases for Na and CO_2 and lie in the middle of the range. The lowest enthalpy increases are shown by the Pb−Bi alloy and especially by Pb itself. The enthalpy rise for the molten salt is very sharp, starting from relatively low values (below that for Pb and Pb−Bi alloy) and almost reaching values for CO_2 and Na at higher temperatures.

The dependence of **Pr** (which is defined as a ratio of product of viscosity and specific heat to thermal conductivity) on temperature for different coolants is shown in Fig. A2.10. As follows from the definition, the shape of **Pr** is governed by the more

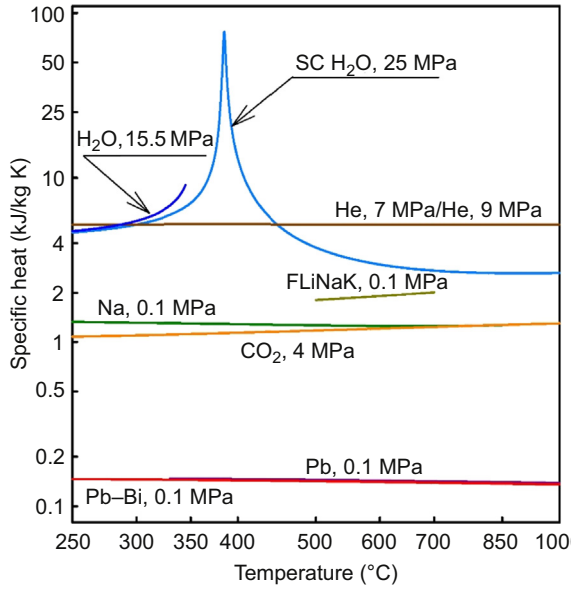


Figure A2.8 Specific heat of selected coolants versus temperature.

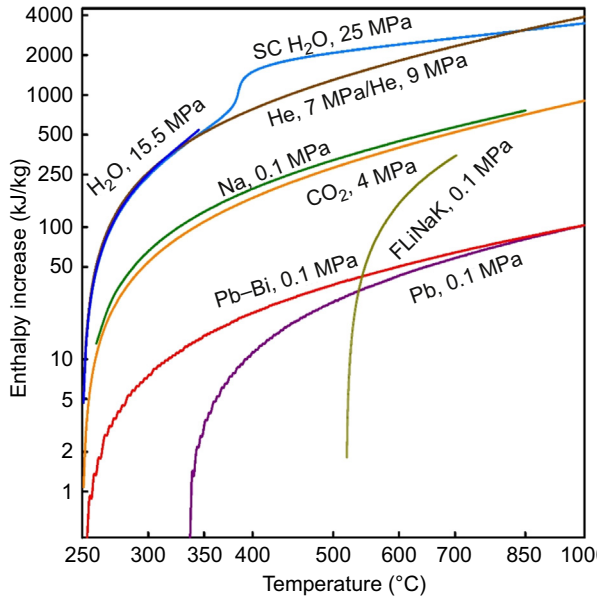


Figure A2.9 Enthalpy of selected coolants versus temperature.

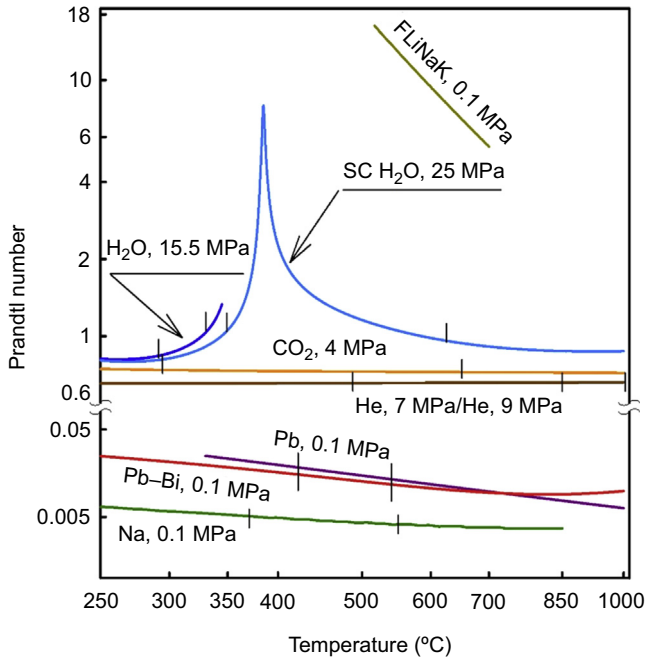


Figure A2.10 **Pr** of selected coolants versus temperature.

significantly changing property of the coolant. It was found that the specific heat is nearly constant for all of the Generation IV reactors coolants except for SCW. Therefore, for most of the coolants, the ratio of the viscosity to the thermal conductivity will affect the shape of the **Pr**/temperature curve.

As we see from Fig. A2.6, the changes in the viscosity and thermal conductivity of the gases are such that they compensate each other, and the **Pr** of gases is virtually constant over most of the 750°C temperature span. However, for the liquid metals, the viscosity drops more significantly than the thermal conductivity increases. As a result, the **Pr** of liquid metals drops almost linearly with temperature. Due to an increase in viscosity of LBE at high temperatures, the corresponding value of **Pr** for Pb—Bi also increases. Since the specific heat of SCW goes through the most rapid changes compared with its other thermophysical properties, the **Pr** of SCW behaves similar to its specific heat. At high temperatures (>500°C), the **Pr** of SCW behaves similar to that of the gases.

The volumetric expansivity of liquid metals is much smaller than that of the remaining coolants and stays almost constant (see Fig. A2.11). The volumetric expansivity of gases drops almost twice, in a linear fashion, from 250 to 1000°C. Remarkably, the values of volumetric expansivity for SCW at temperatures below the pseudocritical point are close to those for gases. Near the pseudocritical point, the volumetric expansivity of SCW peaks. At higher temperatures, the volumetric expansivity of SCW gradually reaches values corresponding to those of gases.

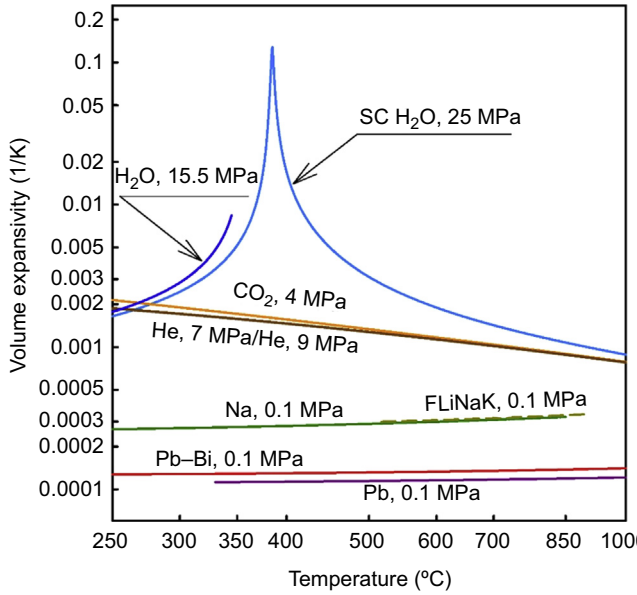


Figure A2.11 Volume expansivity of selected coolants versus temperature.

To summarize the above, the thermophysical properties of liquid metals and gases experience only minor linear changes with increasing temperature. However, all the properties of water at pseudocritical conditions go through very rapid changes. The basic properties of He, CO_2, and water are summarized in Table A2.5. Basic properties of Pb, molten salt (FLiNaK), and Na are summarized in Table A2.6.

A2.4 Heat transfer coefficients in nuclear power reactors

Typical heat transfer coefficient ranges for various reactor coolants are listed in Table A2.7. It shows that Na has the highest heat transfer coefficient among all the proposed coolants, making it a more competitive fluid for power conversion.

Fig. A2.12 shows calculated heat transfer coefficients at conditions corresponding to those of the operating reactors. The calculated values fall very close to those presented in Table A2.7. Among the coolants considered, Na, in conditions close to SFR, has the highest heat transfer coefficient of all the proposed coolants (70−80 kW/m^{2}K). Conditions achieved in a generic CANDU reactor (added for comparison purposes) allow heat transfer coefficients above 60 kW/m^2 K. Calculations also showed that in a PWR, the heat transfer coefficients are about 45 kW/m^2 K. Pb, as expected, has heat transfer coefficients around 25 kW/m^2 K, which is lower than that of another liquid metal: Na. Heat transfer coefficients of SCW (5−15 kW/m^2 K) and CO_2 (1.8−2.5 kW/m^2 K) also lie within the typical ranges of values.

Table A2.5 Basic properties of He, CO_2, and water

No	Properties	Fluids		
		Helium	Carbon dioxide	Water
1	Chemical formula	He	CO_2	H_2O
2	Molar mass, kg/kmol	4.0026	44.01	18.015
3	Triple point, °C	−270.97	−56.558	0.01
4	Normal boiling point temperature, °C	−268.93	−78.464	99.974
5	Critical point temperature, °C	−267.95	30.978	373.95
6	Critical point pressure, MPa	0.2276	7.3773	22.064
7	Critical point density, kg/m^3	72.567	467.6	322.0
8	Flammability	–	–	–
9	Explosion hazard	–	–	–
10	Chemical reactivity	Inert gas	Moderate	Moderate–high
11	Toxicity	–	–	–
12	Corrosiveness	Inert gas	Yes	Very

Based on National Institute of Standards and Technology, 2010. NIST Reference Fluid Thermodynamic and Transport Properties–REFPROP. NIST Standard Reference Database 23, Ver. 9.1. Department of Commerce, Boulder, CO, USA.

Table A2.6 Basic properties of Pb, Pb−Bi, molten salt, and Na

No	Properties	Fluids			
		Lead	Lead −bismuth	Fluoride salt[a]	Sodium
1	Chemical formula	Pb	44.5 Pb-55.5 Bi	FLiNaK	Na
2	Molar mass, kg/kmol	207.2	~208	41.3	23
3	Density at 20°C, kg/m^3	11,340	10,500	–	968
4	Melting point temperature, °C	327.5	123.5	454	97.8
5	Boiling point temperature, °C	1749	1670	1570	883
6	Heat of fusion, kJ/mol (kJ/kg)	4.77 (23.0)	8.08 (38.8)	–	2.60 (113.0)
7	Heat of vaporization, kJ/mol (kJ/kg)	179.5 (866.3)	178.1 (856.3)	–	97.42 (4236)
8	Flammability	Highly purified Pb fine powder can ignite in air	Fine powder can ignite in air	–	Spontaneously ignites when heated above 115°C in air that has even modest moisture content; generates flammable H_2 and caustic Na hydroxide upon contact with water

Continued

Table A2.6 Continued

No	Properties	Fluids			
		Lead	Lead −bismuth	Fluoride salt[a]	Sodium
9	Explosion hazard	Fine powder can ignite in air	Fine powder can ignite in air	−	Na powder is highly explosive in water and may spontaneously explode in the presence of oxygen
10	Chemical reactivity	Reactive (oxidized in air)	Corrosive	−	Highly reactive
11	Toxicity	Poisonous	Poisonous	−	Can be poisonous
12	Corrosiveness	Yes Can embrittle metals	Yes	Yes	High

[a]Williams et al. (2006).

Table A2.7 Typical ranges of heat transfer coefficients, heat fluxes, and sheath temperatures for reactor coolants, and capacities per reactor core volume

Typical ranges of heat transfer coefficients for reactor coolants	
Coolant	**Heat transfer coefficient, kW/m^2 K**
Na (forced convection) (~SFR conditions)	50–80
Boiling water (flow boiling) (~BWR conditions)	~40
CANDU reactor	~50
Water (single-phase forced convection)	~30
SCW (~SCWR conditions)	7–10
Pb (forced convection) (~LFR conditions)	25–35
Pb–Bi (forced convection) (~SVBR conditions)	20–30
He (rough surface)	10
CO_2 (high pressure) (~AGR conditions)	2–5

Typical ranges of heat fluxes for reactors' coolants		
Coolant	**Heat flux, kW/m^2**	**$T_{sheath}-T_{coolant}$, ^oC**
Na (forced convection) SFR	2000 (1800–2400)	25–30
Water (single-phase forced convection)	1500	50
Boiling water (flow boiling) BWR	1000	15
CANDU reactor	625	15
Boiling water in a kettle	150	15

Reactor type	**Sheath temperature, ^oC**
AGR	750
SFR	700
GCR (MAGNOX)	450
PWR	390
BWR	300

Typical ranges of average capacity (kW) per reactor core volume (liter)	
Reactor type	**kW/L**
Magnox	1
AGR, high temperature gas reactor (HTGR), VHTR	6–10
RBMK	4–6

Continued

Table A2.7 Continued

Typical ranges of average capacity (kW) per reactor core volume (liter)	
Reactor type	**kW/L**
BWR	40–50
PWR, VVER	100–150
SCWR, VVER-SKD[a]	100
SFR, BN	400–550

[a]*SKD*, supercritical pressure in Russian abbreviations.
Based on Hewitt, G.F., Collier, J.G., 2000. Introduction to Nuclear Power, second ed. Taylor and Francis Publishing Office, USA, 304 pages and data provided by P.L. Kirillov.

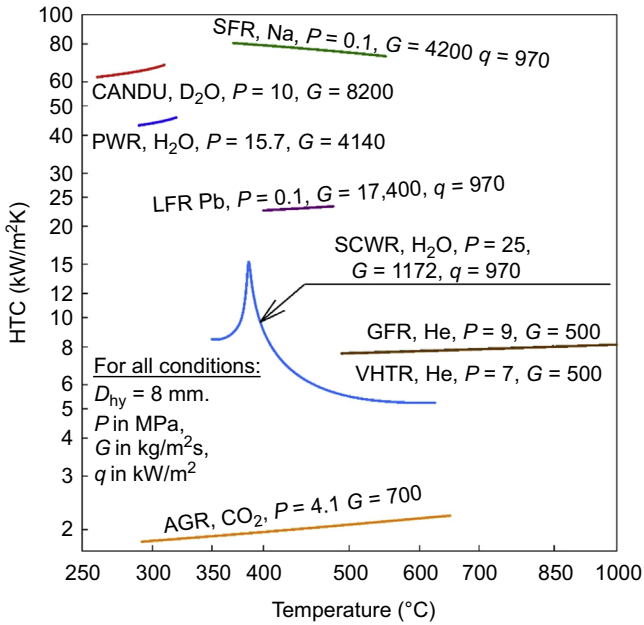


Figure A2.12 Heat transfer coefficients calculated for a flow of coolants in Generation IV, AGR, and PWR reactors in a bare tube at nominal operating pressures and at mass fluxes close to actual mass fluxes for the respective reactor.

For calculations of subcritical H_2O, D_2O, CO_2, and He, the value of heat flux was not taken into account, while for SCW, Pb, and Na, the value of heat flux was assumed to be 970 kW/m^2. A hydraulic-equivalent diameter of 8 mm was used in the calculations for all the coolants.

Fig. A2.13 shows heat transfer coefficients calculated for all coolants (including FLiNaK) for the generic conditions: $G = 1000$ kg/m^2 s, $q = 970$ kW/m^2 K, $D_{hy} = 8$ mm.

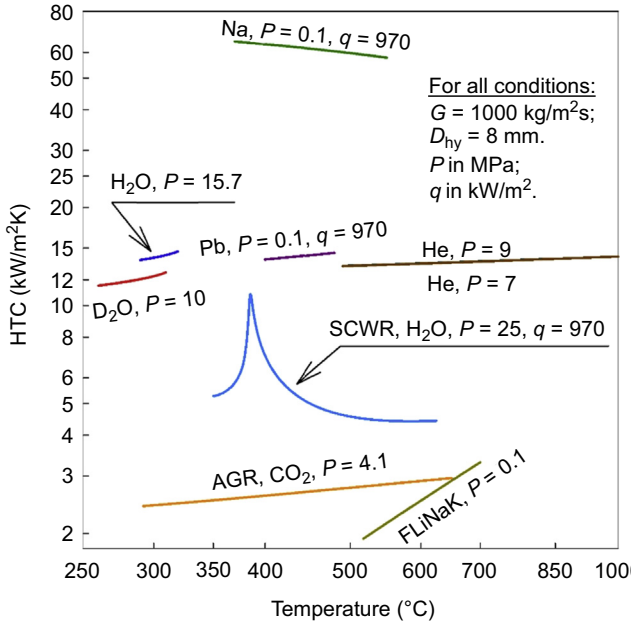


Figure A2.13 Heat transfer coefficients calculated for a flow of coolants in Generation IV, AGR, and PWR reactors in a bare tube at generic operating conditions.

It can be seen that at the chosen generic conditions, a Na coolant has the highest heat transfer coefficients, ranging from 58−96 kW/m^2 K, while CO_2 and FLiNaK have the lowest heat transfer coefficients, ranging from 1−4 kW/m^2 K. The heat transfer coefficient of SCW starts at ~5 kW/m^2 K, then goes through a peak in the pseudocritical region where its value increases by almost two times, and after that, drops close to 4 kW/m^2 K at temperatures above 450°C. The heat transfer coefficients of the gases, water, D_2O, and Pb increase slightly with temperature. Heat transfer coefficients of the molten salt increase significantly with temperature. The heat transfer coefficient of Na drops linearly with temperature increase.

A2.5 Conclusions

Based on the above, the following conclusions can be made.

- In general, liquid metal coolants have high thermal stability, high boiling points, and very low saturated vapor pressures, which distinguish them from other types of nuclear coolants.
- The specific heats of Pb and LBE are nearly identical and 10 times less than those of Na and CO_2, and are almost 40 times less than that of He. At temperatures higher than 450°C, the specific heat of He is even higher than that of SCW.
- As one would expect, the thermal conductivity of liquid metals is significantly higher than that of gases (50−3000 times). The highest thermal conductivity was for Na (60−70 W/m K).

- The volumetric expansivity of liquid metals is much lower than that of the other coolants examined, and stays almost constant.
- The thermophysical properties of liquid metals and gases show only small linear changes with temperature. However, all the properties of SCW go through very rapid changes in the pseudocritical range.
- The thermophysical properties of LBE, except for the thermal conductivity, are close to the average values of those of Pb and Bi.
- At high temperatures (more than 500°C), the **Pr** of SCW behaves similar to gases.
- One of the least desirable properties of water is its high vapor pressure, which increases rapidly with temperature. Its relatively low critical temperature (∼374°C) limits the maximum temperature of the coolant and significantly limits the efficiency of the power conversion cycle.
- The specific heat of He is higher than that of CO_2 and liquid metals. The thermal conductivity of He is 10 times greater than that of CO_2. This characteristic facilitates heat transfer and reduces the size of heat exchangers. He is far more inert than CO_2, does not absorb neutrons, and cannot become radioactive on its own.

Nomenclature

c_p	specific heat at constant pressure, J/kg/K
D_{hy}	Hydraulic-equivalent diameter, m
G	Mass flux, kg/m^2 s
h_{fg}	Latent heat of evaporation, J/kg
k	Thermal conductivity, W/m/K
q	Heat flux, W/m^2/K
v	Specific volume, m^3/kg

Greek symbols

Δ	Difference
μ	Dynamic viscosity, Pa·s
ρ	Density, kg/m^3

Nondimensional Numbers

Pr	Prandtl number $\left(\frac{\mu \cdot c_p}{k}\right)$

Subscripts

f	Fluid
g	Gas
hy	Hydraulic equivalent
In	Inlet
Out	Outlet
scw	Supercritical water
v	Vapor

Acronyms

LBE	Lead−bismuth eutectic
LMR	Liquid metal-cooled reactor
FLiNaK	LiF **+ NaF + KF salt**
PCh	Pressure channel
PT	Pressure tube
PV	Pressure vessel
SC	Supercritical
SCW	Super critical water

References

Beznosov, A.V., Dragunov, Yu.G., Rachkov, V.I., 2007. Heavy-liquid Metal Coolants in Nuclear Engineering (In Russian). IzdAt Publishing House, Moscow, Russia, 434 pages.

Chrenkova, M., Danek, V., Vasiljev, R., Silny, A., Kremenetsky, V., Polyakov, E., 2003. Density and viscosity of the $(LiF\text{-}NaF\text{-}KF)_{eut}-KBF_4-B_2O_3$ melts. Journal of Molecular Liquids 102 (1), 213−226.

Dementyev, B.D., 1990. Nuclear Power Reactors (In Russian). Energoatomizdat Publishing House, Moscow, Russia, 352 pages.

Dragunov, A., Saltanov, Eu., Pioro, I., Kirillov, P., Duffey, R., 2015. Power cycles of Generation III and III+ nuclear power plants. ASME Journal of Nuclear Engineering and Radiation Science 1 (2), 10 pages.

Dragunov, A., Saltanov, Eu., Pioro, I., Ikeda, B., Miletic, M., Zvorykina, A., 2013. Investigation of thermophysical and nuclear properties of prospective coolants for Generation-IV nuclear reactors. In: Proceedings of the 21st International Conference on Nuclear Engineering (ICONE-21), July 29−August 2, Chengdu, China, Paper #16020, 11 Pages.

Gupta, S., Saltanov, Eu., Mokry, S.J., Pioro, I., Trevani, L., McGillivray, D., 2013. Developing empirical heat-transfer correlations for supercritical CO_2 flowing in vertical bare tubes. Nuclear Engineering and Design 261, 116−131.

Hewitt, G.F., Collier, J.G., 2000. Introduction to Nuclear Power, second ed. Taylor and Francis Publishing Office, USA. 304 pages.

IAEA-TECDOC-1746, 2014. Heat Transfer Behaviour and Thermohydraulics Code Testing for Supercritical Water Cooled Reactors (SCWRs), IAEA TECDOC Series. September, Vienna, Austria, 496 pages. Free download from: http://www-pub.iaea.org/books/IAEABooks/10731/Heat-Transfer-Behaviour-and-Thermohydraulics-Code-Testing-for-Supercritical-Water-Cooled-Reactors-SCWRs.

IAEA, 1985. Status of Liquid Metal Cooled Fast Reactors. Technical Report Series No. 246. IAEA, Vienna, Austria.

Khokhlov, V., Ignatiev, V., Afonichkin, V., 2009. Evaluating physical properties of molten salt reactor fluoride mixtures. Journal of Fluorine Chemistry 130, 30−37.

Kirillov, P.L., Terentieva, M.I., Deniskina, N.B., 2007. Thermophysical Properties of Materials for Nuclear Engineering, second ed. IzdAT Publishing House, Moscow, Russia. 192 pages.

Mann, D., Pioro, I., 2015. Study on specifics of thermophysical properties of supercritical fluids in power engineering applications. In: Proceedings of the 23rd International Conference on Nuclear Engineering (ICONE-23), May 17−21, Chiba, Japan, Paper #1730, 11 Pages.

NEA No 6195, 2007. Handbook on Lead-bismuth Eutectic Alloy and Lead Properties, Materials Compatibility, Thermal-hydraulics and Technologies. Nuclear Energy Agency (NEA) and Organisation for Economic Co-operation and Development (OECD), France, 693 pages. Free download from: https://www.oecd-nea.org/science/reports/2007/pdf/lbe-handbook-complete.pdf.

National Institute of Standards and Technology, 2010. NIST Reference Fluid Thermodynamic and Transport Properties−REFPROP. NIST Standard Reference Database 23, Ver. 9.1. Department of Commerce, Boulder, CO, USA.

Pioro, I., 2011. The potential use of supercritical water-cooling in nuclear reactors. In: Krivit, S.B., Lehr, J.H., Kingery, Th.B. (Eds.), Nuclear Energy Encyclopedia: Science, Technology, and Applications. J. Wiley & Sons, Hoboken, NJ, USA, pp. 309−347.

Pioro, I., Duffey, R., 2015. Nuclear power as a basis for future electricity generation. ASME Journal of Nuclear Engineering and Radiation Science 1 (1), 19 pages. Free download from: http://nuclearengineering.asmedigitalcollection.asme.org/article.aspx?articleID=2085849.

Pioro, I.L., Duffey, R.B., 2007. Heat Transfer and Hydraulic Resistance at Supercritical Pressures in Power Engineering Applications. ASME Press, New York, NY, USA, 334 pages.

Pioro, I., Mokry, S., 2011. Thermophysical properties at critical and supercritical conditions. In: Belmiloudi, A. (Ed.), Heat Transfer. Theoretical Analysis, Experimental Investigations and Industrial Systems. INTECH, Rijeka, Croatia, pp. 573−592. Free download from: http://www.intechopen.com/books/heat-transfer-theoretical-analysis-experimental-investigations-and-industrial-systems/thermophysical-properties-at-critical-and-supercritical-pressures.

Pioro, I., Mokry, S., Draper, S., 2011. Specifics of thermophysical properties and forced-convective heat transfer at critical and supercritical pressures. Reviews in Chemical Engineering 27 (3−4), 191−214.

Sohal, M., Ebner, M., Sabharwall, P., Sharpe, P., 2010. Engineering Database of Liquid Salt Thermophysical and Thermochemical Properties. INL/EXT-10−18297 report, 70 pages, retrieved from: http://www.inl.gov/technicalpublications/Documents/4502650.pdf (on 01.09.14).

Todreas, N.E., MacDonald, P.E., Heizlar, P., Buongiorno, J., Loewen, E., 2004. Medium-power lead−alloy reactors: missions for this reactor technology. Nuclear Technology 147 (3), 305.

Waltar, A.E., Reynolds, A.B., 1981. Fast Breeder Reactors. Pergamon Press, USA, 853 pages.

Williams, D.F., Toth, L.M., Clarno, K.T., ORNL-TM-12−2006, 2006. Assessment of Candidate Molten Salt Coolants for the Advanced High-Temperature Reactor (AHTR). ORNL/TM-2006/12 report, 86 pages, retrieved from: http://web.ornl.gov/∼webworks/cppr/y2006/rpt/124584.pdf (on 19.08.14).

Appendix A3: Thermophysical properties of fluids at subcritical and critical/ supercritical conditions[1]

I.L. Pioro[1], C.O. Zvorykin[2]
[1]University of Ontario Institute of Technology, Oshawa, Ontario, Canada, [2]National Technical University of Ukraine, Kyiv Polytechnic Institute, Peremohy Ave, Kiev, Ukraine

A3.1 Introduction

A3.1.1 Historical note on using supercritical pressure fluids

The use of supercritical fluids in different processes is not new, nor was it a human invention. Mother Nature has been processing minerals in aqueous solutions at near or above the critical point of water for billions of years (Levelt Sengers, 2000). It was only in the late 1800s when scientists started to use this natural process, called hydrothermal processing, in their labs for creating various crystals. During the last 50–60 years, this process (operating parameters: water pressures from 20 to 200 MPa and temperatures from 300 to 500°C) has been widely used in the industrial production of high-quality single crystals (mainly gemstones) such as quartz, sapphire, titanium oxide, tourmaline, zircon, and others.

The first works devoted to the problem of heat transfer at supercritical pressures started as early as the 1930s. Schmidt et al. (1946) investigated free convection heat transfer of fluids at the near critical point with the application to a new effective cooling system for turbine blades in jet engines. They found that the free convection heat transfer coefficient at the near critical state was high, and decided to use this advantage in single-phase thermosiphons with an intermediate working fluid at the near critical point (Pioro and Pioro, 1997).

In the 1950s, the idea of using supercritical water (SCW) appeared to be rather attractive for steam generators/turbines in the thermal power industry. The objective was to increase the total thermal efficiency of coal-fired thermal power plants. At supercritical pressures, there is no liquid–vapor phase transition; therefore, there is no such phenomenon as critical heat flux or dryout. It is only within a certain range of parameters that deteriorated heat transfer may occur. Work in this area was mainly

[1] This Appendix is partially based on the following publications: Pioro (2014); Pioro et al. (2011); Pioro and Mokry (2011); Pioro and Duffey (2007); Mann and Pioro (2015), and Gupta et al. (2013).

performed in Germany, the former USSR, and the US in the 1950s−1980s (Pioro and Duffey, 2007).

In general, the gross thermal efficiency of modern thermal power plants with subcritical parameter steam generators [for details, see Appendix: A1 on thermal and nuclear power plants and Pioro and Duffey (2007)] is about 36−40%, but reaches 45−50% or even higher with supercritical parameters ie, with a "steam" pressure of 23.5−26 MPa and inlet turbine temperatures within the range of 535−585°C; the thermal efficiency is about 50−55% at ultra-supercritical parameters (25−38 MPa and 600−625°C).

Near the end of the 1950s and at the beginning of the 1960s, several studies were conducted on the potential use of SCW as a coolant in nuclear reactors (Pioro and Duffey, 2007). However, these activities were abandoned for some time and regain momentum in the 1990s (for the latest achievements in development of SCWRs, see Chapter: 8). The primary objectives for using SCW as a coolant in nuclear reactors are: (1) increasing thermal efficiency of modern water-cooled nuclear power plants (NPPs), which is currently 30−36% to approximately 40−45% or even higher; (2) decreasing operational and capital costs by eliminating steam generators, steam separators, steam dryers, etc.; and (3) possibility for co-generation of hydrogen through thermochemical cycles (for details, see Chapter: 19).

At the end of the 20th century and the beginning of the 21st century, helium became quite attractive as a reactor coolant in a gas-cooled fast reactor (GFR) concept and in a very high-temperature reactor (VHTR) concept (for details, see Chapters: 3 and 4). Helium within the operating conditions of these reactors is a supercritical fluid (Pioro and Duffey, 2007).

In addition, supercritical carbon dioxide (Pioro and Duffey, 2007) was considered as a modeling fluid instead of water due to significantly lower critical parameters. Also, in the 2000s, supercritical carbon dioxide Brayton gas turbine cycle became quite attractive in some countries, including the US as an alternative power conversion cycle compared to subcritical and supercritical pressure Rankine steam turbine cycle for a number of Generation IV nuclear reactor concepts.

In general, possible applications of supercritical fluids in Generation IV nuclear reactor concepts are as the following (also, for details, see chapters in Parts I and II):

1. Supercritical fluids as reactor coolants
   a. Supercritical water-cooled reactors (SCWRs) will use SCW ($P_{cr} = 22.064$ MPa; $T_{cr} = 373.95$°C);
   b. Both GFRs and VHTRs will use supercritical helium[2] ($P_{cr} = 0.2276$ MPa; $T_{cr} = -267.95$°C (5.1953 K)).
2. Supercritical pressure power cycles working fluids
   a. SCWRs with direct or indirect cycles will use supercritical pressure "steam" Rankine cycle;
   b. Lead-cooled fast reactor (Russian design) might use supercritical pressure "steam" Rankine cycle (there is a possibility that GFRs in other countries might use supercritical

[2] It should be noted that within the operating conditions for both GFR and VHTR, helium behaves as a compressed gas because these operating conditions way above the critical point or pseudo-critical points at corresponding operating pressures.

pressure carbon dioxide Brayton gas turbine cycle ($P_{cr} = 7.3773$ MPa; $T_{cr} = 30.978°C$));

c. Both GFRs and VHTRs might use supercritical pressure helium (or helium−nitrogen mixture) Brayton gas turbine cycle (there is a possibility that GFRs might use supercritical pressure carbon dioxide Brayton gas turbine cycle ($P_{cr} = 7.3773$ MPa; $T_{cr} = 30.978°C$)); and

d. Sodium-cooled fast reactors (US concept) and molten salt reactors might use supercritical pressure carbon dioxide Brayton gas turbine cycle ($P_{cr} = 7.3773$ MPa; $T_{cr} = 30.978°C$).

Therefore, the most widely used supercritical fluids as of today and possibly in the future are water, carbon dioxide, helium, and refrigerants. Often, refrigerants, similar to carbon dioxide, are considered as modeling fluids instead of water due to significantly lower critical pressures and temperatures (for example, R-134a: $P_{cr} = 4.0593$ MPa; $T_{cr} = 101.06°C$), which decreases the complexity and costs of thermal hydraulic experiments. Based on the above mentioned, knowledge of thermophysical properties specifics at critical and supercritical pressures is very important for safe and efficient use of fluids in power and other industries.

A3.1.2 Definitions of terms and expressions related to critical and supercritical regions

Prior to a general discussion on specifics of thermophysical properties and forced convective heat transfer at critical and supercritical pressures, it is important to define special terms and expressions used at these conditions. For a better understanding of these terms and expressions, their definitions are listed below together with complementary (Figs. A3.1−A3.4).

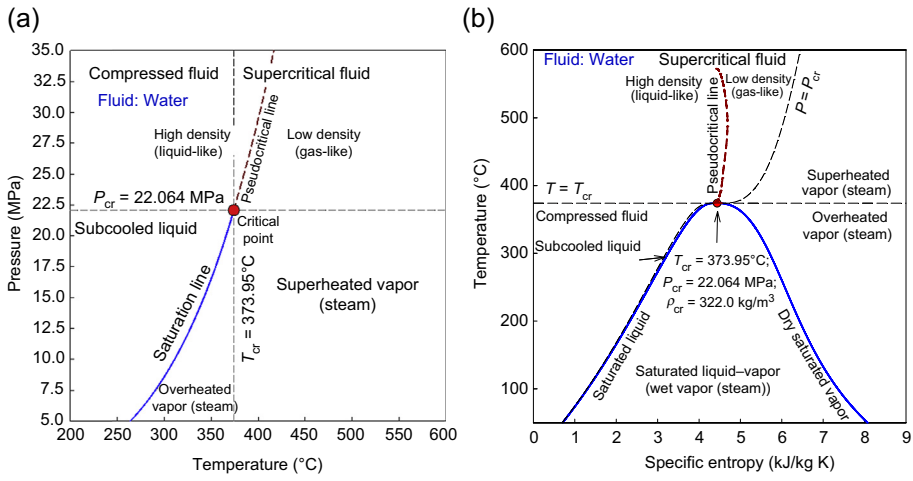


Figure A3.1 Thermodynamics diagrams for water: (a) pressure−temperature and (b) temperature−specific entropy.

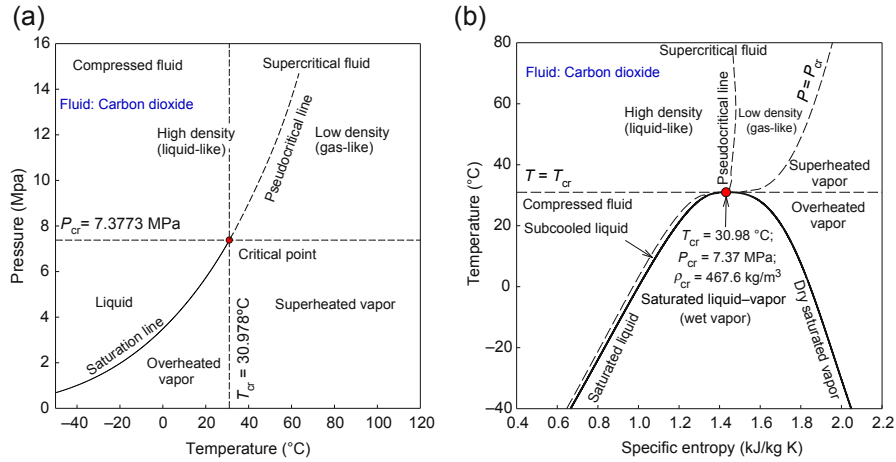


Figure A3.2 Thermodynamics diagrams for carbon dioxide: (a) pressure−temperature and (b) temperature−specific entropy.

Compressed fluid is the fluid at a pressure above the critical pressure but at a temperature below the critical temperature.

Critical point (also called a *critical state*) is the point in which the distinction between the liquid and gas (or vapor) phases disappears, ie, both phases have the same temperature, pressure, and specific volume or density. The *critical point* is characterized with the phase−state parameters: T_{cr}, P_{cr}, and v_{cr} (or ρ_{cr}), which have unique values for each pure substance.

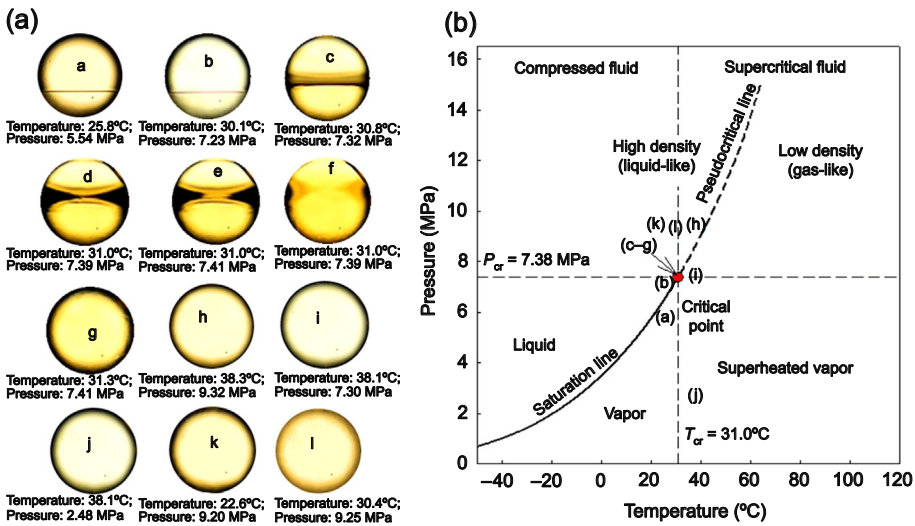


Figure A3.3 Photos of carbon dioxide during transition through (a) critical and pseudocritical points and (b) corresponding pressure−temperature diagram (Gupta et al., 2013).

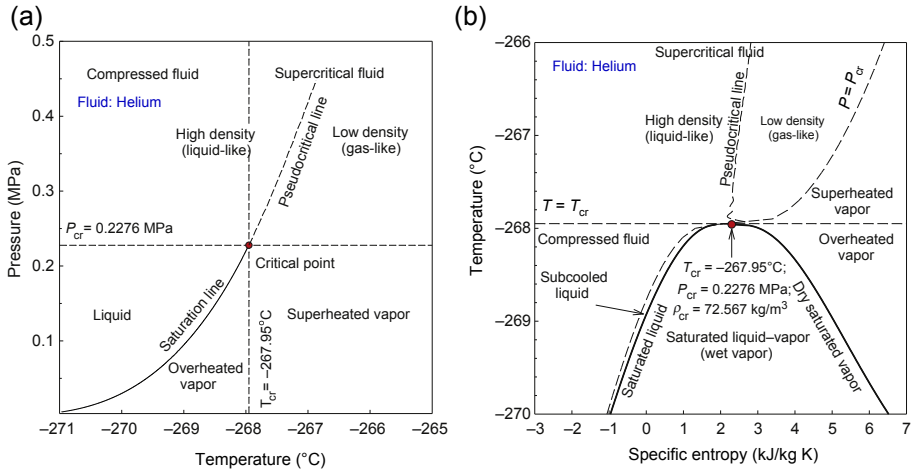


Figure A3.4 Thermodynamics diagrams for helium: (a) pressure−temperature and (b) temperature−specific entropy.

Near critical point is actually a narrow region around the critical point where all thermophysical properties of a pure fluid exhibit rapid variations.

Pseudocritical line is the line that consists of pseudocritical points.

Pseudocritical point (characterized with P and T_{pc}) is the point at a pressure above the critical pressure and at a temperature ($T_{pc} > T_{cr}$) corresponding to the maximum value of specific heat at this particular pressure.

Supercritical fluid is the fluid at pressures and temperatures that are higher than the critical pressure and critical temperature. However, in the present handbook, the term *supercritical fluid* usually includes both terms: a *supercritical fluid* and *compressed fluid*.

Supercritical "steam" is actually SCW because at supercritical pressures, fluid is considered as a single-phase substance. However, this term is widely (and incorrectly) used in the literature in relation to supercritical "steam" generators and turbines.

Superheated steam is the steam at pressures below the critical pressure but at temperatures above the critical temperature.

Note: All thermophysical properties of fluids presented in this appendix were calculated through the NIST REFPROP software (2010).

A3.2 Thermophysical properties at critical and supercritical pressures

Critical parameters of selected fluids are listed in Table A3.1. For better understanding of general trends and specifics of various thermophysical properties near critical and pseudocritical points, it was decided to show these properties in comparison with subcritical properties for water (see Figs. A3.5−A3.12). Also, thermophysical

Table A3.1 Critical parameters of selected fluids (NIST, 2010)

Fluid	P_{cr} (MPa)	T_{cr} (°C)	ρ_{cr} (kg/m^3)
Carbon dioxide (CO_2)	7.3773	30.98	467.6
Freon-134a (1,1,1,2-tetrafluoroethane, CH_2FCF_3)	4.0593	101.06	511.9
Helium (He)	0.2276	−267.95	72.567
Water (H_2O)	22.064	373.95	322.0

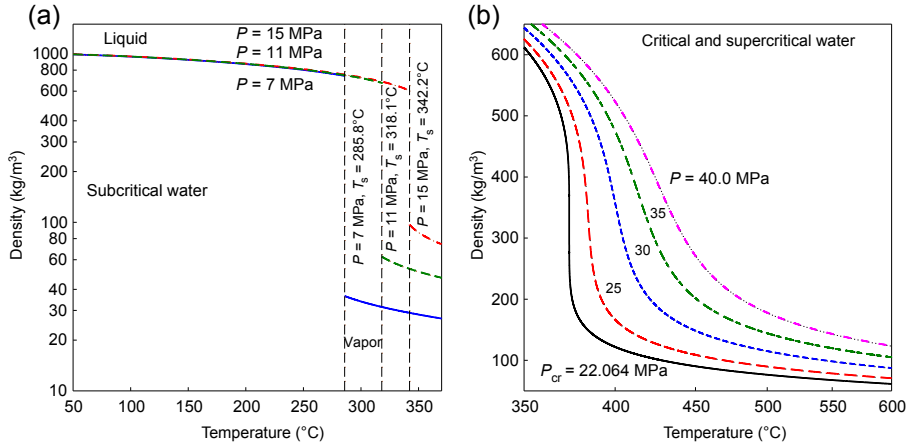


Figure A3.5 Density versus temperature: (a) subcritical pressure water and (b) critical and supercritical pressure water.

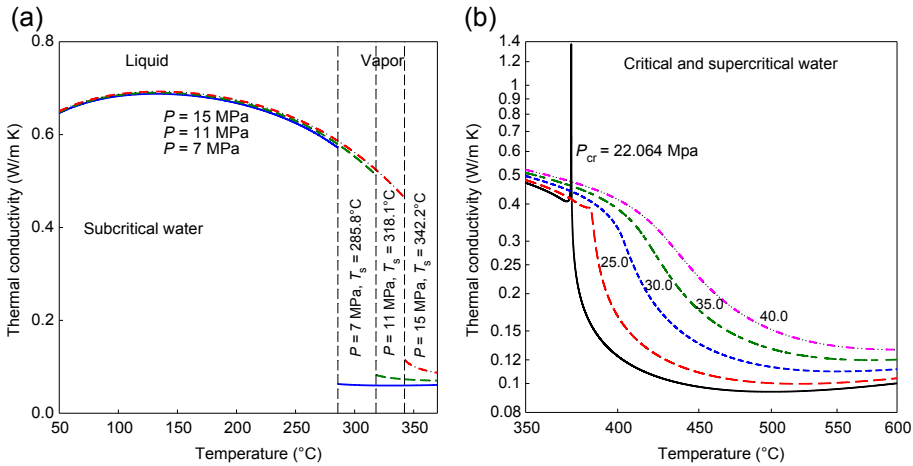


Figure A3.6 Thermal conductivity versus temperature: (a) subcritical pressure water and (b) critical and supercritical pressure water.

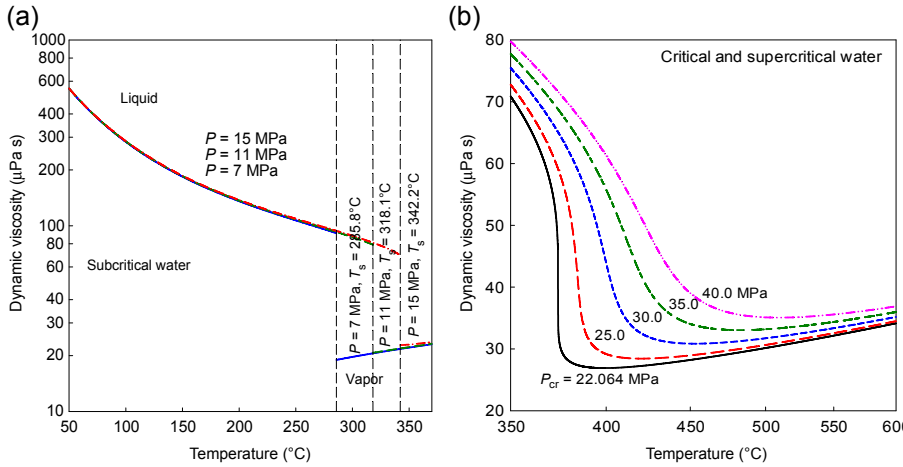


Figure A3.7 Dynamic viscosity versus temperature: (a) subcritical pressure water and (b) critical and supercritical pressure water.

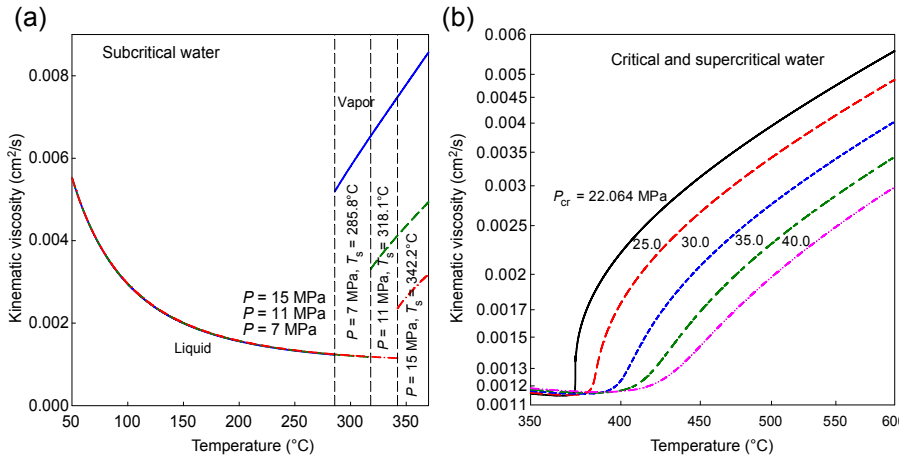


Figure A3.8 Kinematic viscosity versus temperature: (a) subcritical pressure water and (b) critical and supercritical pressure water.

properties of critical/supercritical carbon dioxide are shown in Figs. A3.14−A3.22, A3.23(b), A3.24(b); and selected properties of critical/supercritical helium in Figs. A3.25−A3.27. Other properties of supercritical helium and properties of supercritical R-134a are shown in the book by Pioro and Duffey (2007).

In addition, thermophysical properties of all current and Generation IV nuclear power reactors within operating ranges are shown in Appendix A2 and thermophysical properties of selected gases including helium and carbon dioxide at 0.1 MPa are shown in Appendix A6.

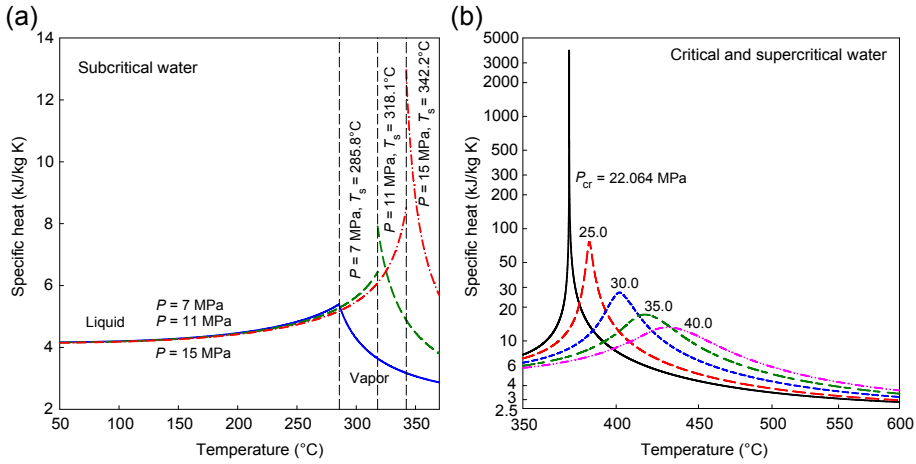


Figure A3.9 Specific heat at constant pressure versus temperature: (a) subcritical pressure water and (b) critical and supercritical pressure water.

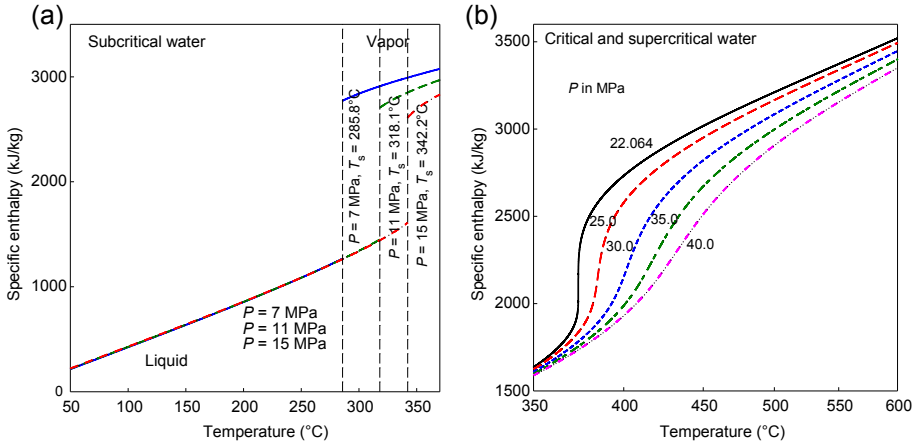


Figure A3.10 Specific enthalpy versus temperature: (a) subcritical pressure water and (b) critical and supercritical pressure water.

Figs. A3.5–A3.12 show variations in the basic thermophysical properties of water at three subcritical pressures [all **(a)** figures]: (1) 7 MPa—usual operating pressure of boiling water reactors (BWRs) and many Rankine steam turbine cycles in pressurized water reactor (PWR), BWR, and RBMK NPPs; (2) 11 MPa—usual inlet pressure for CANDU reactors; and (3) 15 MPa—usual pressure for PWRs; and the critical ($P_{cr} = 22.064$ MPa) and four supercritical pressures ($P = 25$, 30, 35, and 40 MPa) [all **(b)** figures]. The range of critical and supercritical pressures covers current range

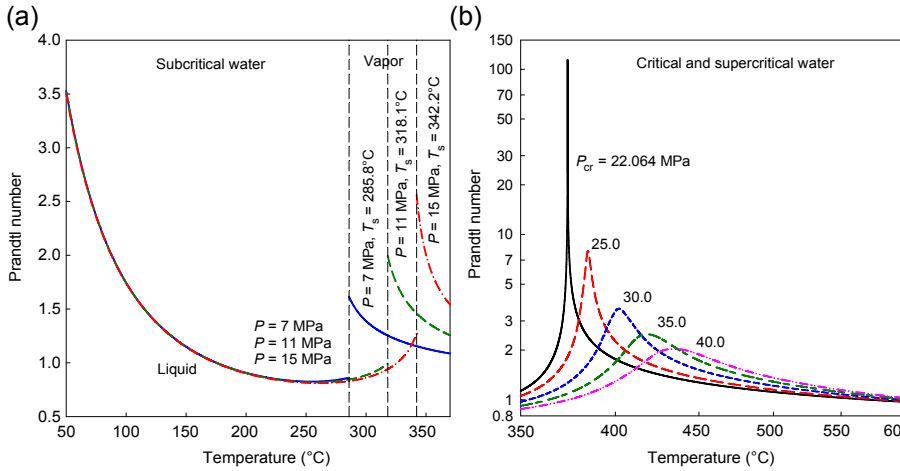


Figure A3.11 Prandtl number versus temperature: (a) subcritical pressure water and (b) critical and supercritical pressure water.

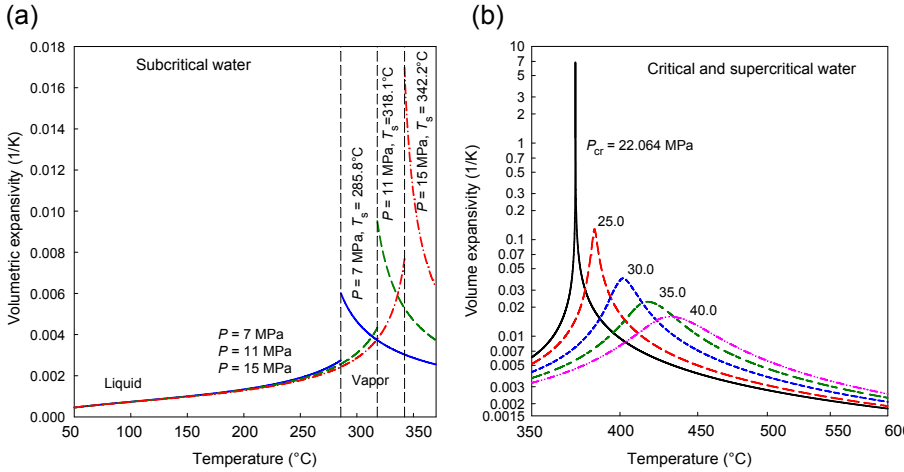


Figure A3.12 Volumetric expansivity versus temperature: (a) subcritical pressure water and (b) critical and supercritical pressure water.

of pressures in thermal power industry used at supercritical pressure coal-fired power plants. Fig. A3.13 shows selected thermophysical properties near the pseudocritical point of water at 25 MPa.

Also, in addition to variations of thermophysical properties of water, the same properties of carbon dioxide at the equivalent pressures to those of water (the conversion is based on $\left(\frac{P}{P_{cr}}\right)_{H_2O} = \left(\frac{P}{P_{cr}}\right)_{CO_2}$) are shown in Figs. A3.14–A3.21. Fig. A3.22 shows

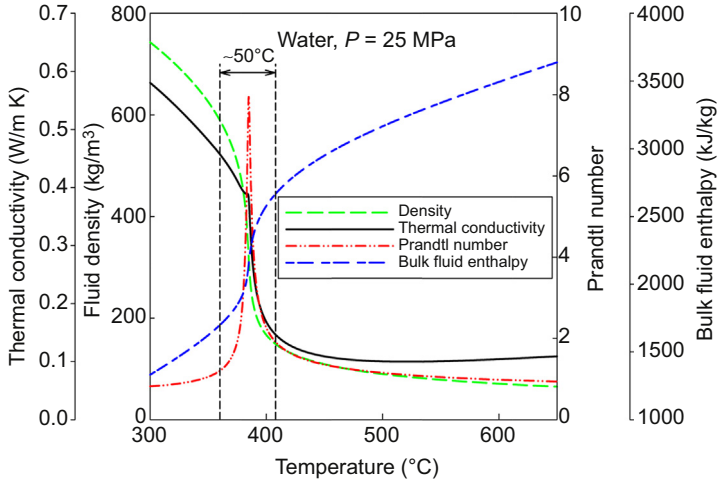


Figure A3.13 Variations of selected thermophysical properties of water near pseudocritical point (384.9°C at 25 MPa): pseudocritical region is about ±25°C around pseudocritical point.

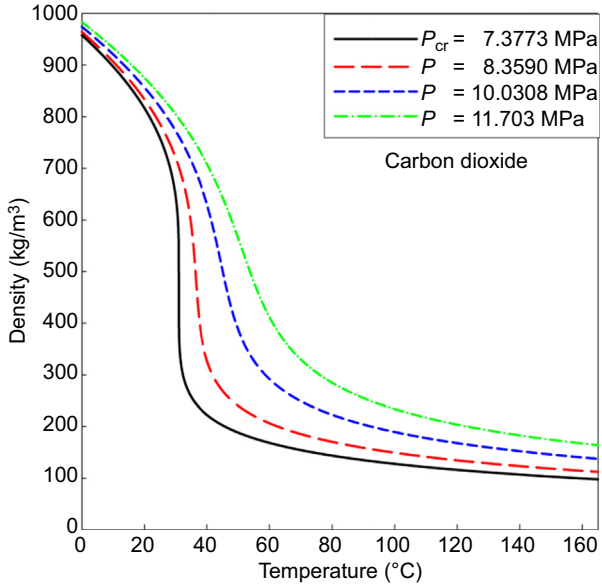


Figure A3.14 Density versus temperature: carbon dioxide.

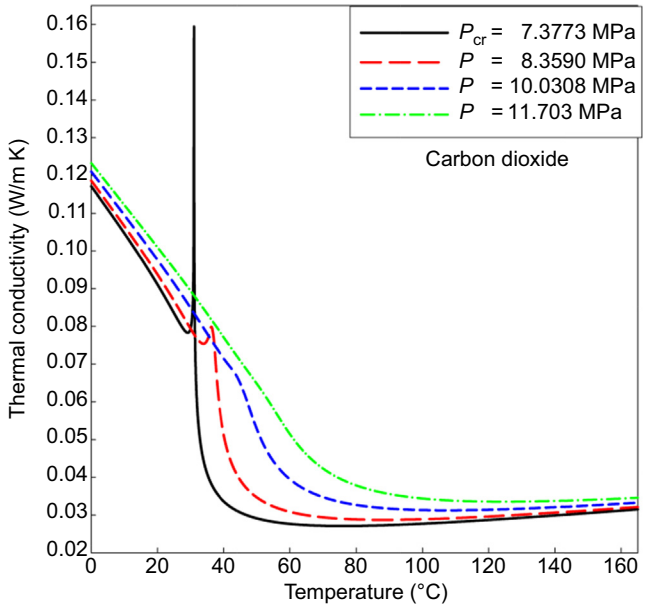


Figure A3.15 Thermal conductivity versus temperature: carbon dioxide.

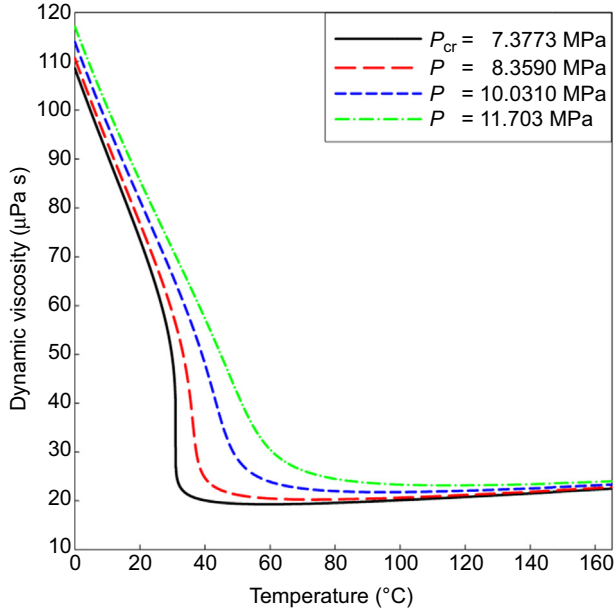


Figure A3.16 Dynamic viscosity versus temperature: carbon dioxide.

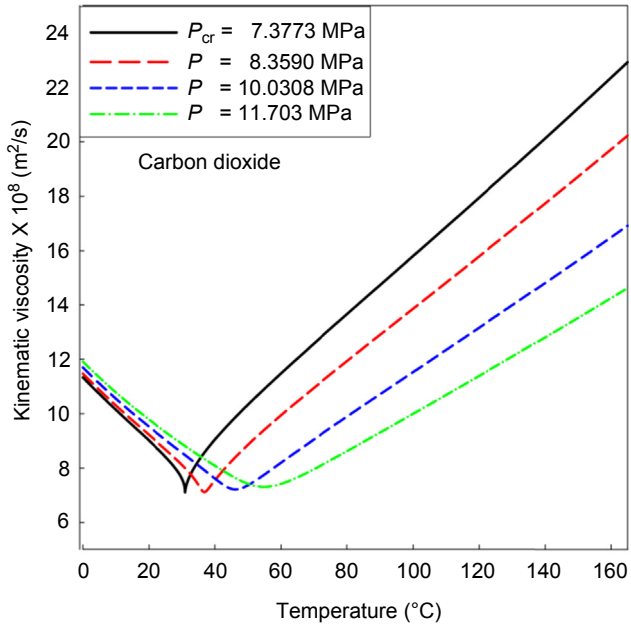


Figure A3.17 Kinematic viscosity versus temperature: carbon dioxide.

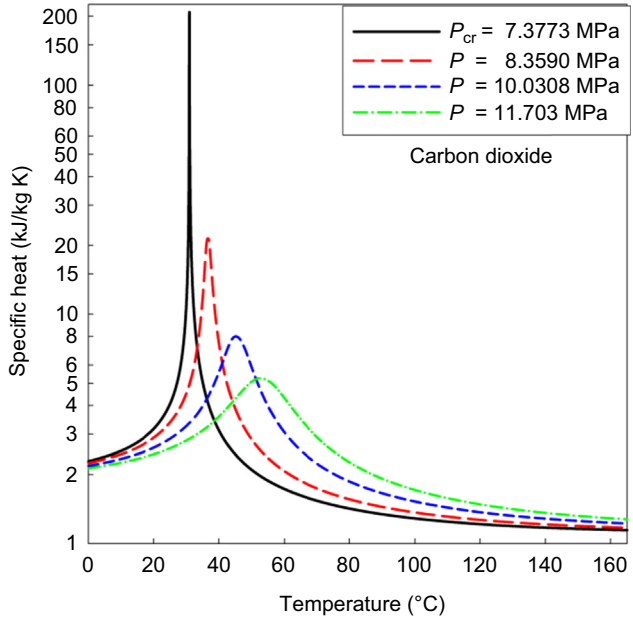


Figure A3.18 Specific heat at constant pressure versus temperature: carbon dioxide.

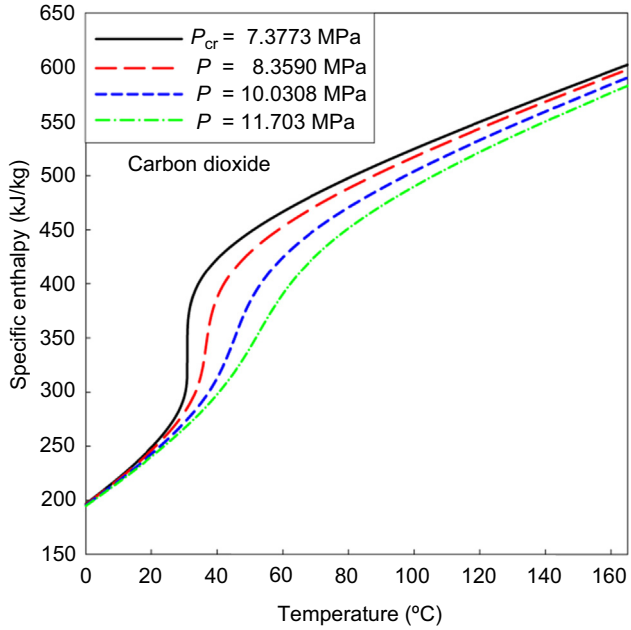


Figure A3.19 Specific enthalpy versus temperature: carbon dioxide.

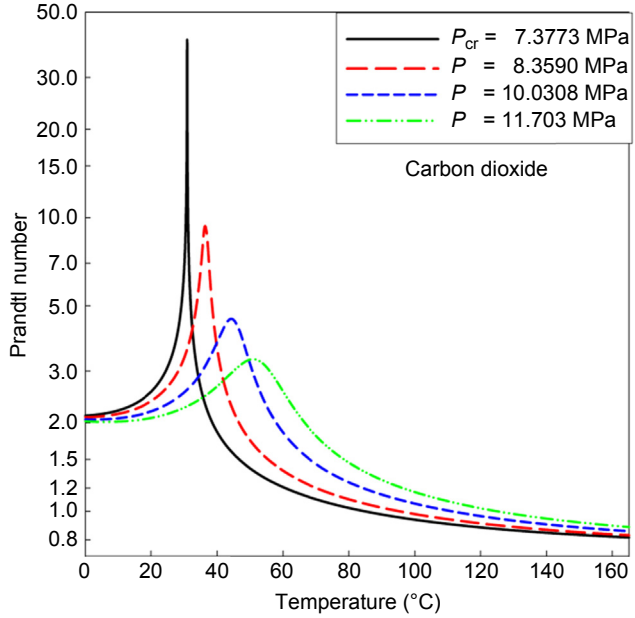


Figure A3.20 Prandtl number versus temperature: carbon dioxide.

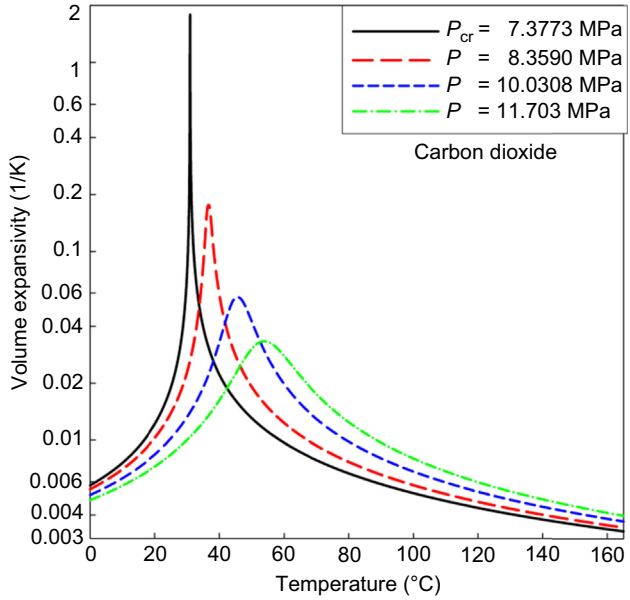


Figure A3.21 Volume expansivity versus temperature: carbon dioxide.

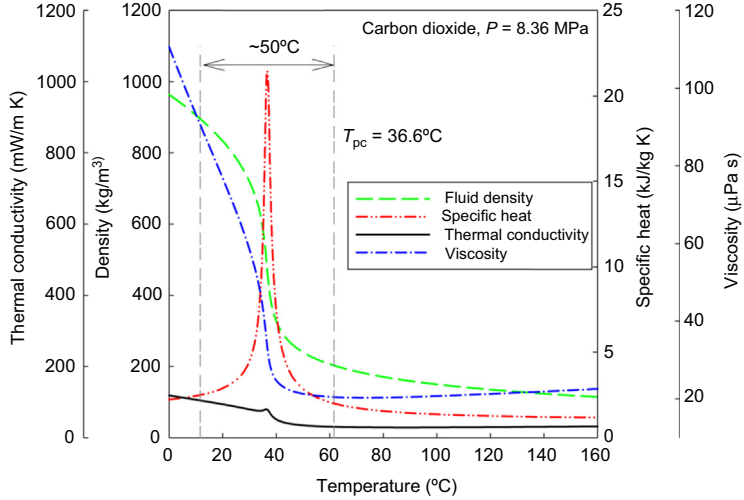


Figure A3.22 Variations of selected thermophysical properties of carbon dioxide near pseudocritical point (36.6°C at 8.36 MPa): pseudocritical region is about ±25°C around pseudocritical point. Carbon dioxide pressure of 8.36 MPa corresponds to water pressure of 25 MPa.

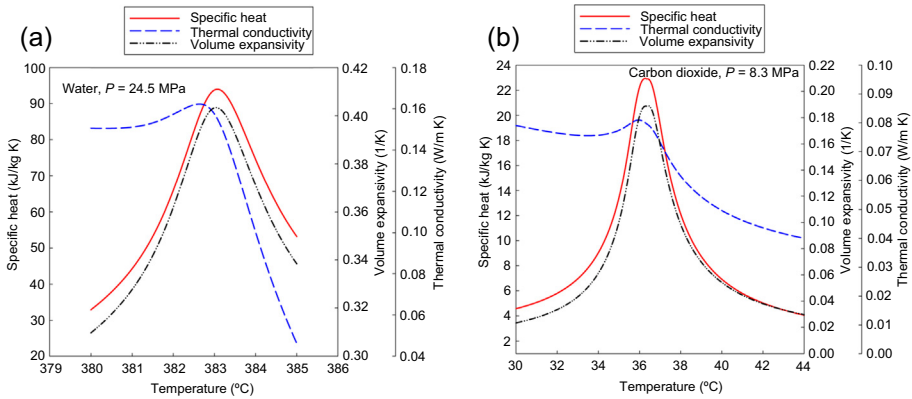


Figure A3.23 Specific heat, volume expansivity, and thermal conductivity vs. temperature: (a) water, $P = 24.5$ MPa, and (b) carbon dioxide, $P = 8.3$ MPa. It can be seen that maximum values of expansivity and thermal conductivity might not be in the pseudocritical point, which is based on the maximum value of specific heat. However, these deviations are usually small (within a degree or so).

selected thermophysical properties near the pseudocritical point of carbon dioxide at 8.36 MPa, which is the equivalent pressure of 25 MPa in water.

It should be noted that thermophysical properties of 121 pure fluids, including water, carbon dioxide, helium, refrigerants, etc.; 5 pseudo-pure fluids (such as air); and mixtures with up to 20 components at different pressures and temperatures, including critical and supercritical regions, can be calculated using the NIST REFPROP software (2010), Version 9.1.

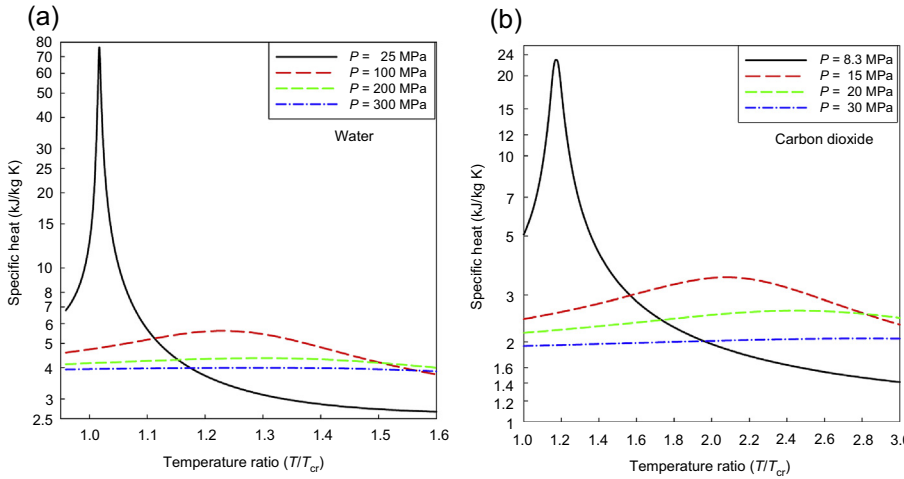


Figure A3.24 Specific heat profiles at various pressures: (a) water and (b) carbon dioxide.

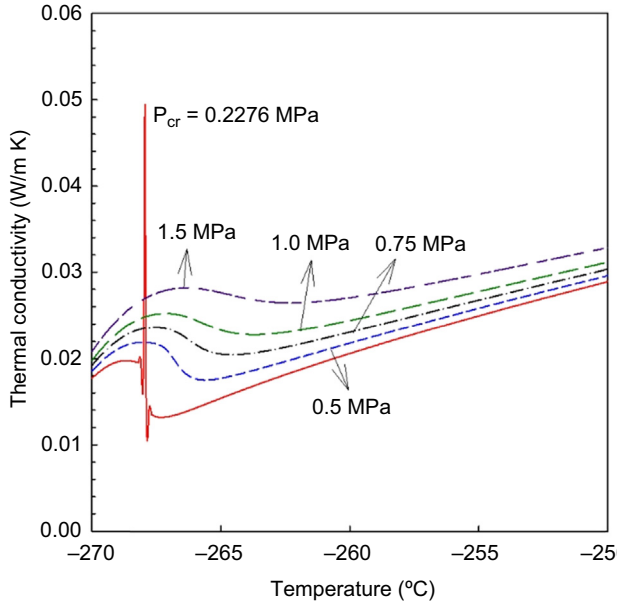


Figure A3.25 Thermal conductivity versus temperature: helium.

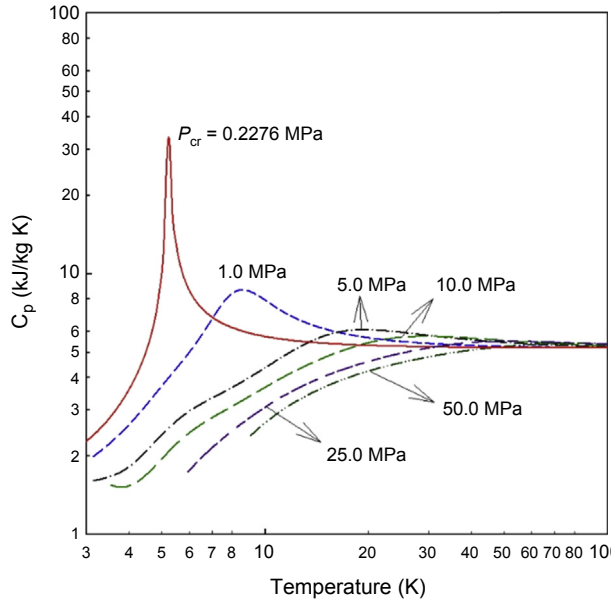


Figure A3.26 Specific heat versus temperature: helium.

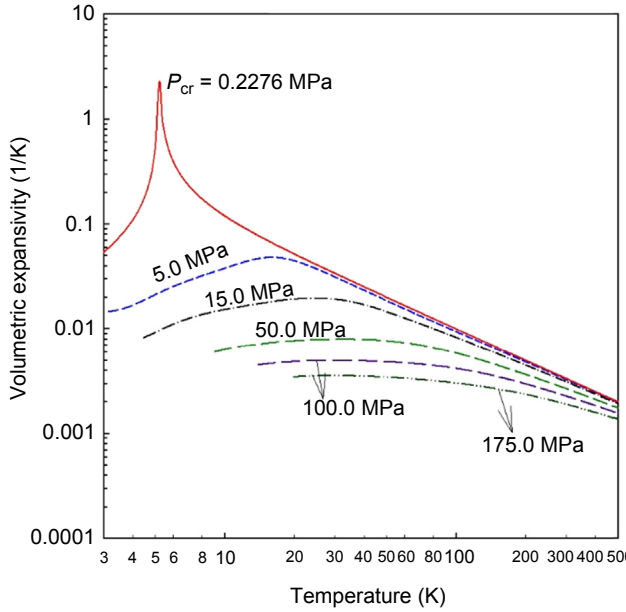


Figure A3.27 Volumetric expansivity versus temperature: helium.

Analysis of profiles shown in Figs. A3.5−A3.12 for subcritical water [figures **(a)**] and critical/supercritical water [figures **(b)**] shows similar trends. However, for subcritical water, there are two different values of any thermophysical property on the saturation line: one for liquid and one for vapor (steam). However, for example, at pressure of 7 MPa, values of specific heat of water (5.4025 kJ/kg K) and steam (5.3566 kJ/kg K) can be very close (see Fig. A3.9(a)). Also, it can be clearly seen that pressure has almost negligible effect of liquid properties. Just closer to the saturation line, some small differences can be seen in property profiles at various pressures.

At critical and supercritical pressures, a fluid is considered to be a single-phase substance, ie, at any critical/supercritical pressure, all properties have just a single value for any pressure−temperature combination, in spite of the fact that all thermophysical properties undergo significant changes within the critical and pseudocritical regions. Near the critical point, these changes are dramatic (see Figs. A3.5(b)−A3.13(b) for water and A3.14−A3.22 for carbon dioxide). In the vicinity of pseudocritical points, with an increase in pressure, these changes become less pronounced (see Figs. A3.5(b)−A3.12(b) for water and Figs. A3.14−A3.21 for carbon dioxide).

Also, it can be seen that properties such as density and dynamic viscosity undergo a significant drop (near the critical point this drop is almost vertical) within a very narrow temperature range (see Figs. A3.5(b) and A3.7(b), respectively, for water, and Figs. A3.14 and A3.16 for carbon dioxide), while the kinematic viscosity and specific

enthalpy undergo a sharp increase (see Figs. A3.8(b) and A3.10(b), respectively, for water, and Figs. A3.17 and A3.19 for carbon dioxide).

Thermal conductivity, specific heat, Prandtl number, and volume expansivity have peaks (or "humps" at higher supercritical pressures) near the critical and pseudocritical points (see Figs. A3.6(b), A3.9(b), A3.11(b), and A3.12(b), respectively, for water, and Figs. A3.15, A3.18, A3.20, and A3.21 for carbon dioxide; also, see Fig. A3.23(a) and (b) for water and carbon dioxide). The magnitude of these peaks decreases very quickly with an increase in pressure (see Fig. A3.24 for water and carbon dioxide). Also, "peaks" transform into "humps" profiles at pressures beyond the critical pressure. It should be noted that the thermal conductivity, dynamic viscosity, and kinematic viscosity undergo through their minimum right after the critical and pseudocritical points (see Figs. A3.6(b), A3.7(b), and A3.8(b), respectively, for water, and Figs. A3.15−A3.17 for carbon dioxide).

The specific heat of water (see Fig. A3.9(b)) (as well as of other fluids, for example, for carbon dioxide, see Fig. A3.18; and Fig. A3.26 for helium) has a maximum value at the critical point. The exact temperature that corresponds to the specific heat peak above the critical pressure is known as the pseudocritical temperature (see also Figs. A3.23 and A3.24, and Table A3.2 for water and carbon dioxide). For water at pressures approximately above 300 MPa and for carbon dioxide at pressures above 30 MPa (see Fig. A3.24), a peak (here, it is better to say a "hump") in specific heat almost disappears; therefore, the term such as a *pseudocritical point* no longer exists. The same applies to the *pseudocritical line*.

In general, it is very difficult or, actually impossible, to define the exact pressure at which a maximum value of specific heat will disappear or cannot be defined. The major problem here is that we need to know uncertainties of specific heat at these very high supercritical pressures, which are not easy to find. If a maximum value of specific heat is within these uncertainties compared to those on a base line, we can assume that at this pressure, a pseudocritical point does not exist!

It should be noted that peaks in the thermal conductivity and volume expansivity may not correspond to the pseudocritical temperature (see Table A3.3 and Fig. A3.23).

In early studies, ie, approximately before 1990, a peak in thermal conductivity was not taken into account. Later, this peak was well established (see Fig. A3.6(b) for water and Fig. A3.15 for carbon dioxide) and included into thermophysical properties data and software. The peak in thermal conductivity diminishes at about 25.5 MPa for water (see Fig. A3.6(b) and Table A3.3) and at about 8.4 MPa for carbon dioxide (see Fig. A3.15 and Table A3.3).

In general, crossing the pseudocritical line from left to right is similar to crossing the saturation line from liquid to vapor. The major difference in crossing these two lines is that all changes (even drastic variations) in thermophysical properties at critical and supercritical pressures are continuous and gradual, and take place within a certain temperature range (see Figs. A3.13 and A3.22). On the contrary, at subcritical pressures, there are properties discontinuity on the saturation line: one value for liquid and another for vapor (see Figs. A3.5(a)−A3.12(a) for water). Therefore, critical and supercritical fluids behave as single-phase substances. However, still it can be noted that below critical/pseudocritical temperatures, fluids behave as "liquid-like"

Table A3.2 Values of pseudocritical temperature and corresponding peak values of specific heat within wide range of pressures for water and carbon dioxide

Water			Carbon dioxide		
Pressure (MPa)	Pseudocritical temperature (°C)	Peak value of specific heat (kJ/kg K)	Pressure (MPa)	Pseudocritical temperature (°C)	Peak value of specific heat (kJ/kg K)
23	377.5	284.3	7.5	31.7	228.1
24	381.2	121.9	8	34.7	35.3
25	384.9	76.4	8.5	37.4	18.7
26	388.5	55.7	9	40.0	12.8
27	392.0	43.9	9.5	42.6	9.9
28	395.4	36.3	10.0	45.0	8.1
29	398.7	30.9	10.5	47.4	6.9
30	401.9	27.0	11.0	49.7	6.1
31	405.0	24.1	11.5	51.8	5.5
32	408.1	21.7	12.0	53.9	5.0
33	411.0	19.9	12.5	55.9	4.6
34	413.9	18.4	13.0	57.8	4.3
35	416.7	17.2	13.5	59.5	4.1

Table A3.3 Peak values of specific heat, volume expansivity, and thermal conductivity in critical and near pseudocritical points: (a) water and (b) carbon dioxide

Pressure (MPa)	Pseudocritical temperature (°C)	Temperature (°C)	Specific heat (kJ/kg K)	Volume expansivity (1/K)	Thermal conductivity (W/m K)
(a) Water					
$P_{cr} = 22.064$	$T_{cr} = 374.1$	–	∞	∞	∞
22.5	375.6	–	690.6	1.252	0.711
23.0	–	377.4	–	–	0.538
	377.5	–	284.3	0.508	–
23.5	–	379.2	–	–	0.468
	–	379.3	–	0.304	–
	379.4	–	171.9	–	–
24.0	–	381.0	–	–	0.429
	381.2	–	121.9	0.212	–
24.5	–	382.6	–	–	0.405
	–	383.0	–	0.161	–
	383.1	–	93.98	–	–
25.0	–	384.0	–	–	0.389
	384.9	–	76.44	–	–
	–	385.0	–	0.128	–

25.5	386.7	–	64.44	0.107	No peak
26.0	388.5	–	55.73	0.090	0.355
27.0	392.0	–	43.93	0.069	0.340
28.0	395.4	–	36.29	0.056	0.329
29.0	398.7	–	30.95	0.046	0.321
30.0	401.9	–	27.03	0.039	0.316
(b) Carbon dioxide					
$P_{cr} = 7.3773$	$T_{cr} = 30.978$	–	∞	∞	∞
7.5	31.7	–	228.06	2.025	0.160
8.0	–	34.5	–	–	0.089
	34.7	–	35.27	0.300	–
8.5	–	36.9	–	–	0.078
	37.4	–	18.67	0.151	–
9.0	40.0	–	12.83	–	–
	–	40.1	–	0.0992	No peak
9.5	42.6	–	9.86	–	–
	–	42.8	–	0.0733	No peak
10.0	45.0	–	8.08	–	
	–	45.4	–	0.058	No peak
10.5	47.4	–	6.91	–	–
	–	480	–	0.048	No peak

Continued

Table A3.3 Continued

Pressure (MPa)	Pseudocritical temperature (°C)	Temperature (°C)	Specific heat (kJ/kg K)	Volume expansivity (1/K)	Thermal conductivity (W/m K)
11.0	49.7	–	6.07	–	–
	–	50.4	–	0.040	No peak
11.5	51.8	–	5.46	–	–
	–	52.8	–	0.035	No peak
12.0	53.9	–	4.99	–	–
	–	55.2	–	0.031	No peak
12.5	55.9	–	4.61	–	–
	–	57.4	–	0.028	No peak
13.0	57.8	–	4.30	–	–
	–	59.5	–	0.025	No peak
15.0	64.2	–	3.50	–	–
	–	67.5	–	0.018	No peak
20.0	75.8	–	2.62	–	–
	–	84.3	–	0.011	No peak
25.0	82.3	–	2.26	–	–
	–	97.4	–	0.008	No peak
30.0	86.4	–	2.06	–	–
	–	107.5	–	0.006	No peak

substances, and above critical/pseudocritical temperatures, as "gas-" or "vapor-like" substances (for details, see Fig. A3.5 for densities of subcritical and supercritical water).

Analyses of Figs. A3.25−A3.27 for helium show that helium as a reactor coolant will perform as a compressed gas because of operating range of pressures and, especially because temperatures are way above those of critical/pseudocritical regions.

A3.3 Conclusions

Supercritical fluids are used intensively in various industries. Therefore, understanding specifics of thermophysical properties and their behavior at critical and supercritical pressures is an important task. Supercritical fluids are considered as single-phase substances in spite of significant variations of all thermophysical properties within critical or pseudocritical regions. Some of these variations in thermophysical properties are similar to those at subcritical pressures during crossing of the saturation line.

Nomenclature

C_p	Specific heat at constant pressure, J/kg K
v	Specific volume, m^3/kg

Greek letters

ρ	Density, kg/m^3

References

Gupta, S., Saltanov, E., Mokry, S.J., Pioro, I., Trevani, L., McGillivray, D., 2013. Developing empirical heat-transfer correlations for supercritical CO_2 flowing in vertical bare tubes. Nuclear Engineering and Design 261, 116−131.

Levelt Sengers, J.M.H.L., 2000. Supercritical fluids: their properties and applications. In: Kiran, E., et al. (Eds.), Supercritical Fluids, NATO Advanced Study Institute on Supercritical Fluids − Fundamentals and Application, NATO Science Series, Series E, Applied Sciences, vol. 366. Kluwer Academic Publishers, Netherlands, pp. 1−29.

Mann, D., Pioro, I., 2015. Study on specifics of thermophysical properties of supercritical fluids in power engineering applications. In: Proceedings of the 23rd International Conference on Nuclear Engineering (ICONE-23), May 17−21, Chiba, Japan, Paper #1730, p. 11.

National Institute of Standards and Technology, 2010. NIST Reference Fluid Thermodynamic and Transport Properties-REFPROP. NIST Standard Reference Database 23, Ver. 9.1. Department of Commerce, Boulder, CO, USA.

Pioro, I., 2014. Application of supercritical pressures in power engineering: specifics of thermophysical properties and forced-convective heat transfer. In: Anikeev, V., Fan, M. (Eds.), Supercritical Fluid Technology for Energy and Environmental Applications. Elsevier, pp. 201−233.

Pioro, I.L., Duffey, R.B., 2007. Heat Transfer and Hydraulic Resistance at Supercritical Pressures in Power Engineering Applications. ASME Press, New York, NY, USA, p. 334.

Pioro, I., Mokry, S., 2011. Thermophysical properties at critical and supercritical conditions. In: Belmiloudi, A. (Ed.), Heat Transfer. Theoretical Analysis, Experimental Investigations and Industrial Systems. INTECH, Rijeka, Croatia, pp. 573−592. Free download from: http://www.intechopen.com/books/heat-transfer-theoretical-analysis-experimental-investigations-and-industrial-systems/thermophysical-properties-at-critical-and-supercritical-pressures.

Pioro, I., Mokry, S., Draper, S., 2011. Specifics of thermophysical properties and forced-convective heat transfer at critical and supercritical pressures. Reviews in Chemical Engineering 27 (3−4), 191−214.

Pioro, L.S., Pioro, I.L., 1997. Industrial Two-Phase Thermosyphons. Begell House, New York, NY, USA, p. 288.

Schmidt, E., Eckert, E., Grigull, V., 1946. Heat transfer by liquids near the critical state, AFF Translation, No. 527, Air Materials Command. Wright Field, Dayton, OH, USA. April.

Appendix A4: Heat transfer and pressure drop in forced convection to fluids at supercritical pressures[1]

I.L. Pioro
University of Ontario Institute of Technology, Oshawa, Ontario, Canada

A4.1 Introduction

A4.1.1 Historical note on using supercritical pressure fluids

The first works devoted to the problem of heat transfer at supercritical pressures started as early as the 1930s. Schmidt et al. (1946) investigated free convection heat transfer of fluids at the near critical point with the application to a new effective cooling system for turbine blades in jet engines. They found that the free convection heat transfer coefficient (HTC) at the near critical state was high, and decided to use this advantage in single-phase thermosiphons with an intermediate working fluid at the near critical point.

In the 1950s, the idea of using supercritical water appeared to be rather attractive for steam generators/turbines in the thermal power industry. The objective was to increase the total thermal efficiency of coal-fired thermal power plants. At supercritical pressures, there is no liquid−vapor phase transition; therefore, there is no such phenomenon as critical heat flux or dryout. It is only within a certain range of parameters that deteriorated heat transfer may occur. Work in this area was mainly performed in the former USSR and in the US in the 1950s−1980s.

At the end of the 1950s and the beginning of the 1960s, early studies were conducted to investigate a possibility of using supercritical water in nuclear reactors. Several concepts of nuclear reactors using supercritical water were developed in Great Britain, France, the US, and the former USSR. However, this idea was abandoned for almost 30 years with the emergence of light water reactors (LWRs), but regained interest in the 1990s following LWRs' maturation [see Chapters: 2 and 8; IAEA TECDOC (2014); Schulenberg and Starflinger (2012); Pioro (2011); Oka et al. (2010); Pioro and Duffey (2007)].

The most widely used supercritical fluids are water, and after that, carbon dioxide, helium, and refrigerants. Often, carbon dioxide and refrigerants are considered as

[1] This Appendix is partially based on the following publications: Pioro (2014) and Pioro and Mokry (2011).

modeling fluids and used instead of water due to significantly lower critical pressures and temperatures, which decreases the complexity and costs of thermal hydraulic experiments.

A4.1.2 Definitions of terms and expressions related to supercritical pressure heat transfer

Prior to a general discussion on specifics of forced convective heat transfer at critical and supercritical pressures, it is important to define special terms and expressions used at these conditions. For a better understanding of these terms and expressions, their definitions are listed below together with complementary Fig. A4.1 [for further details, see also Appendix: A3 and book by Pioro and Duffey (2007)].

Deteriorated Heat Transfer (DHT) is characterized with lower values of the HTC compared to those for normal heat transfer (NHT), and hence has higher values of wall temperature within some part or within the entire heated channel.

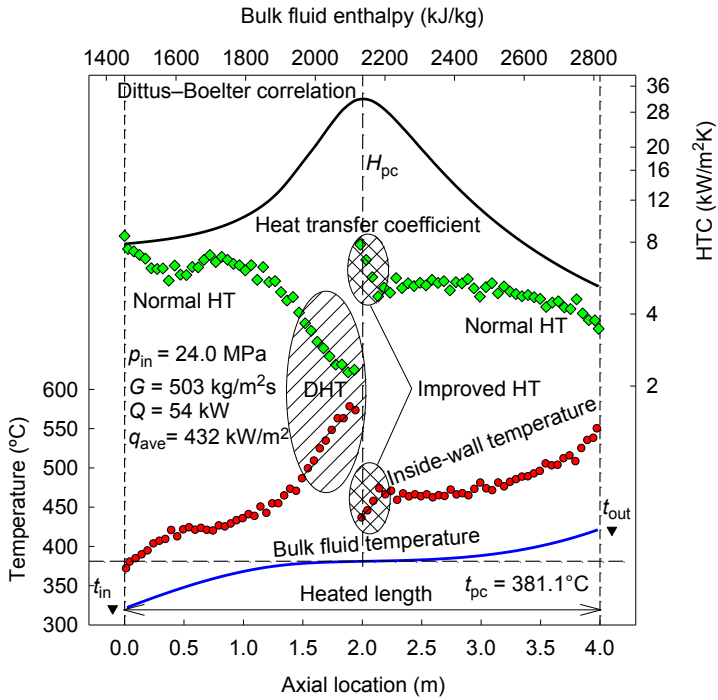


Figure A4.1 Temperature and HTC profiles along heated length of vertical circular tube: water, $D = 10$ mm and $L_h = 4$ m.
Data by Kirillov, P.L., Lozhkin, V.V., Smirnov, A.M, 2003. Investigation of Borders of Deteriorated Regimes of a Channel at Supercritical Pressures (in Russian). State Scientific Center of Russian Federation Institute of Physics and Power Engineering by the name of A.I. Leypunskiy, FEI-2988, Obninsk, Russia, p. 20.

Improved Heat Transfer (IHT) is characterized with higher values of the HTC compared to those for NHT, and hence lower values of wall temperature within some part or within the entire heated channel. In our opinion, the improved heat transfer regime or mode includes peaks or "humps" in the HTC near the critical or pseudocritical points.

NHT can be characterized, in general, with HTCs similar to those of subcritical convective heat transfer far from the critical or pseudocritical regions, when they are calculated according to the conventional single-phase Dittus−Boelter-type correlations: $\mathbf{Nu} = 0.023\ \mathbf{Re}^{0.8}\mathbf{Pr}^{0.4}$.

Pseudo-boiling is a physical phenomenon similar to subcritical pressure nucleate boiling, which may appear at supercritical pressures. Due to heating of a supercritical fluid with a bulk fluid temperature below the pseudocritical temperature (high-density fluid, ie, "liquid"), some layers near the heating surface may attain temperatures above the pseudocritical temperature (low-density fluid, ie, "gas"). This low-density "gas" leaves the heating surface in a form of variable density (bubble) volumes. During the pseudo-boiling, the HTC usually increases (improved heat transfer regime).

Pseudo-film boiling is a physical phenomenon similar to subcritical pressure film boiling, which may appear at supercritical pressures. At pseudo-film boiling, a low-density fluid (a fluid at temperatures above the pseudocritical temperature, ie, "gas") prevents a high-density fluid (a fluid at temperatures below the pseudocritical temperature, ie, "liquid") from contacting ("rewetting") a heated surface. Pseudo-film boiling leads to the deteriorated heat transfer regime.

A4.2 Specifics of forced convection heat transfer at supercritical pressures

Water is the most widely used coolant or working fluid at supercritical pressures. The largest application of supercritical water is in supercritical "steam" generators and turbines, which are widely used in the thermal power industry worldwide. Currently, upper limits of pressures and temperatures used in the thermal power industry are about 30−38 MPa and 600−625°C, respectively. A new direction in supercritical water application in the power industry has been the development of supercritical water-cooled reactor (SCWR) concepts, as part of the Generation IV International Forum initiative (for details, see Chapters: 2 and 8; IAEA TECDOC (2014); Schulenberg and Starflinger (2012); Pioro (2011); Oka et al. (2010); Pioro and Duffey (2007); Peiman et al. (2015)) and proceedings of the International Symposiums on SCWRs (ISSCWR); the latest ISSCWR-7 was in 2015 and selected augmented, and revised papers have been published in the ASME Journal of Nuclear Engineering and Radiation Science in 2016, Vol. 2, No. 1. However, other areas of using supercritical water exist (Pioro and Duffey, 2007).

Supercritical carbon dioxide is mainly used as a modeling fluid instead of water, due to its significantly lower critical parameters (see Appendix: A3). However, currently,

new areas of using supercritical carbon dioxide as a coolant or as a working fluid have emerged, for example, in the Brayton gas turbine cycle, which considered as prospective power cycle in a number of Generation IV reactor concepts. The third supercritical fluid used in some special technical applications is helium. Supercritical helium is used in experimental or test helium-cooled reactors, in the cooling coils of superconducting electromagnets, superconducting electronics, and power-transmission equipment. Also, refrigerant R-134a is being considered as a prospective modeling fluid due to its low critical parameters compared to those of water. Additional information can be found in Pioro and Duffey (2007).

Experiments at supercritical pressures are very expensive and require sophisticated equipment and measuring techniques. Therefore, some of these studies (eg, heat transfer in fuel bundles) are proprietary and hence are not published in open literature.

The majority of studies deal with heat transfer and hydraulic resistance of working fluids, mainly water, carbon dioxide, and helium, in circular bare tubes (Pioro and Duffey, 2007). In addition to these fluids, forced and free convection heat transfer experiments were conducted at supercritical pressures, using liquefied gases such as air, argon, hydrogen; nitrogen, nitrogen tetroxide, oxygen, and sulfur hexafluoride; alcohols such as ethanol and methanol; hydrocarbons such as n-heptane, n-hexane, di-iso-propyl-cyclo-hexane, n-octane, iso-butane, iso-pentane, and n-pentane; aromatic hydrocarbons such as benzene and toluene, and poly-methyl-phenyl-siloxane; hydrocarbon coolants such as kerosene, TS-1 and RG-1, jet propulsion fuels RT and T-6; and refrigerants. A limited number of studies were devoted to heat transfer and pressure drop in annuli, rectangular-shaped channels, and bundles (Razumovskiy et al., 2015; IAEA TECDOC, 2014; Richards et al., 2013; Pioro and Duffey, 2007).

Accounting that supercritical water and carbon dioxide are the most widely used fluids and that the majority of experiments were performed in circular tubes, specifics of heat transfer and pressure drop, including generalized correlations, will be discussed in this paper based on these conditions. Specifics of heat transfer and pressure drop at other conditions and/or for other fluids are discussed in the book by Pioro and Duffey (2007).

A4.2.1 Basics of supercritical heat transfer

All primary sources (ie, all sources found by the authors from a total of 650 references dated mainly from 1950 till beginning of 2006) of heat transfer experimental data for water and carbon dioxide flowing inside circular tubes at supercritical pressures are listed in the book by Pioro and Duffey (2007).

In general, three major heat transfer regimes (for their definitions, see the beginning of this Appendix) can be noticed at critical and supercritical pressures (for details, see Fig. A4.1):

1. NHT;
2. IHT; and
3. DHT.

Also, two special phenomena (for their definitions, see the beginning of this appendix) may appear along a heated surface: (1) pseudo-boiling and (2) pseudo-film boiling.

These heat transfer regimes and special phenomena appear to be due to significant variations of thermophysical properties near the critical and pseudocritical points (see Appendix: A3) and due to operating conditions.

Therefore, the following conditions can be distinguished at critical and supercritical pressures (partially shown in Figs. A4.1−A4.3):

1. Wall and bulk fluid temperatures are below a pseudocritical temperature within a part of or for the entire heated channel;
2. Wall temperature is above, and bulk fluid temperature is below a pseudocritical temperature within a part of or for the entire heated channel;
3. Wall temperature and bulk fluid temperature is above a pseudocritical temperature within a part of or for the entire heated channel;
4. High heat fluxes;
5. Entrance region;
6. Upward and downward flows;
7. Horizontal flows; and
8. Effect of gravitational forces at lower mass fluxes, etc.

All these conditions can affect supercritical heat transfer.

Fig. A4.4 shows temperature and thermophysical properties profiles along the heated length of vertical circular tube (operating conditions in this figure correspond to those in Fig. A4.2(c)).

Some researchers have suggested that variations in thermophysical properties near critical and pseudocritical points result in the maximum value of HTC. Thus, Yamagata et al. (1972) found that for water flowing in vertical and horizontal tubes, the HTC increases significantly within the pseudocritical region (Fig. A4.5). The magnitude of the peak in HTC decreases with increasing heat flux and pressure. The maximum HTC values correspond to a bulk fluid enthalpy, which is slightly less than the pseudocritical bulk fluid enthalpy.

Results of Styrikovich et al. (1967) are shown in Fig. A4.6. Improved and deteriorated heat transfer regimes, as well as a peak ("hump") in HTC near the pseudocritical point are clearly shown in this figure. The deteriorated heat transfer regime appears within the middle part of the test section at a heat flux of about 640 kW/m^2, and it may exist together with the improved heat transfer regime at certain conditions. With the further heat flux increase, the improved heat transfer regime is eventually replaced with that of DHT.

Vikhrev et al. (1971, 1967) found that at a mass flux of 495 kg/m^{2}s, two types of DHT existed (Fig. A4.7): (1) the first type appeared within the entrance region of the tube $L/D < 40-60$; and (2) the second type appeared at any section of the tube, but only within a certain enthalpy range. In general, the DHT occurred at high heat fluxes.

The first type of DHT observed was due to the flow structure within the entrance region of the tube. However, this type of DHT occurred mainly at low mass fluxes

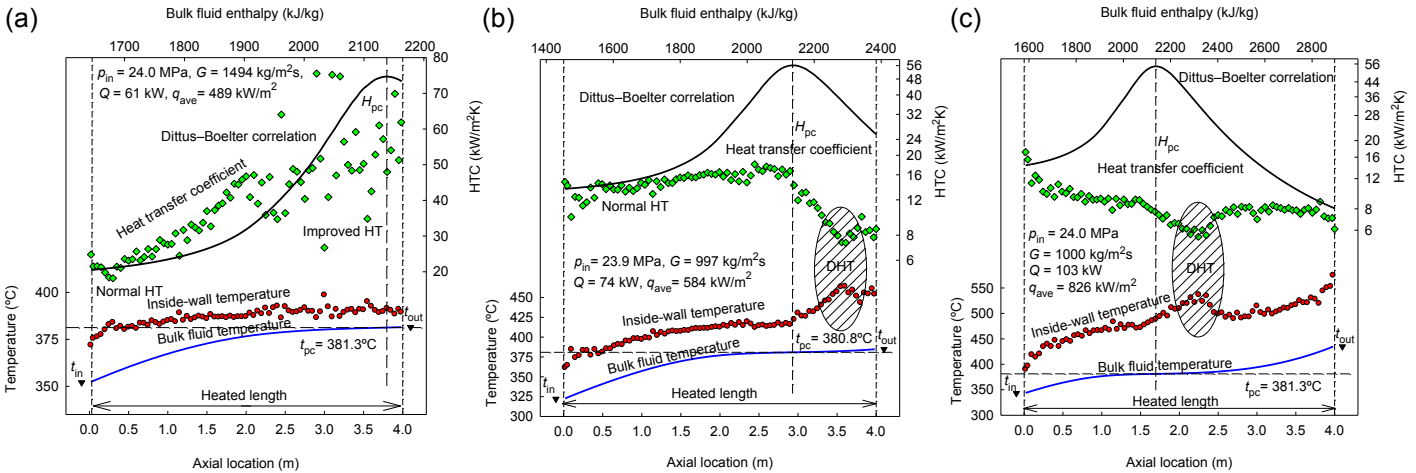


Figure A4.2 Temperature and heat transfer coefficient profiles along heated length of vertical circular tube: water, $D = 10$ mm and $L_h = 4$ m; (a) bulk fluid temperature ranges from below to the pseudocritical temperature; (b) bulk fluid temperature ranges from below to slightly above the pseudocritical temperature; and (c) bulk fluid temperature ranges from below to above the pseudocritical temperature.
Data by Kirillov, P.L., Lozhkin, V.V., Smirnov, A.M, 2003. Investigation of Borders of Deteriorated Regimes of a Channel at Supercritical Pressures (in Russian). State Scientific Center of Russian Federation Institute of Physics and Power Engineering by the name of A.I. Leypunskiy, FEI-2988, Obninsk, Russia, p. 20.

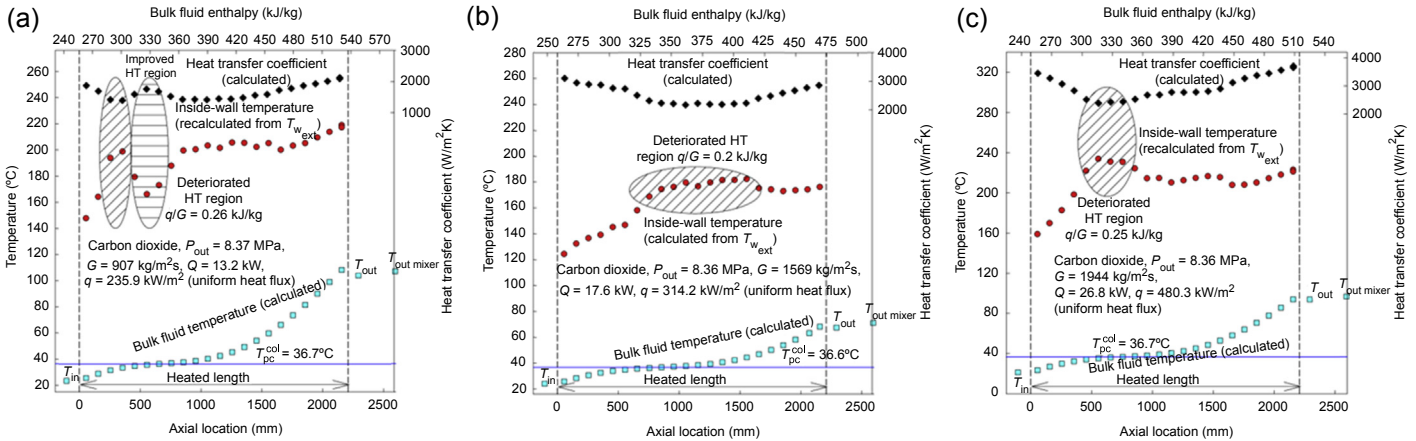


Figure A4.3 Temperature and heat transfer coefficient variations along heated length of vertical circular Inconel-600 test section: carbon dioxide, $D = 8$ mm and $L_h = 2.4$ m; (a) variations of heat transfer regimes at lower mass flux (907 kg/m^{2}s); (b) at medium mass flux (1569 kg/m^{2}s); and (c) at higher mass flux (1994 kg/m^{2}s).

Data from Pioro, I.L., Duffey, R.B., 2007. Heat Transfer and Hydraulic Resistance at Supercritical Pressures in Power Engineering Applications. ASME Press, New York, NY, USA, p. 328

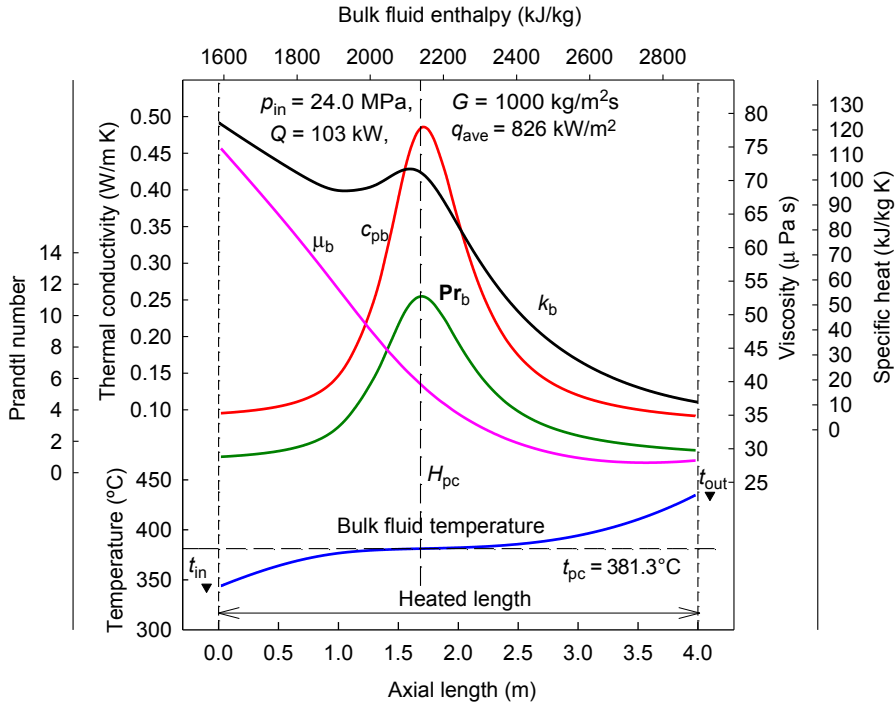


Figure A4.4 Temperature and thermophysical properties profiles along heated length of vertical circular tube (operating conditions in this figure correspond to those in Fig. A4.2): water, $D = 10$ mm and $L_h = 4$ m; thermophysical properties based on bulk fluid temperature.

and at high heat fluxes (Fig. A4.7(a,b)) and eventually disappeared at high mass fluxes (Fig. A4.7(c,d)).

The second type of DHT occurred when the wall temperature exceeded the pseudocritical temperature (Fig. A4.7). According to Vikhrev et al. (1967), the DHT appeared when $q/G > 0.4$ kJ/kg (where q is in kW/m^2 and G is in kg/m^{2}s). This value is close to that suggested by Styrikovich et al. (1967) ($q/G > 0.49$ kJ/kg). However, the above-mentioned definitions of two types of DHT are not enough for their clear identification.

A4.2.2 Pseudo-boiling and pseudo-film boiling phenomena

Ackerman (1970) investigated heat transfer to water at supercritical pressures flowing in smooth vertical tubes, with and without internal ribs, within a wide range of pressures, mass fluxes, heat fluxes, and diameters. He found that the pseudo-boiling phenomenon could occur at supercritical pressures. The pseudo-boiling phenomenon is thought to be due to large differences in fluid density below the pseudocritical point (high-density fluid, ie, "liquid") and beyond (low-density fluid, ie, "gas"). This heat transfer phenomenon was affected by pressure, bulk fluid temperature, mass flux, heat flux, and tube diameter.

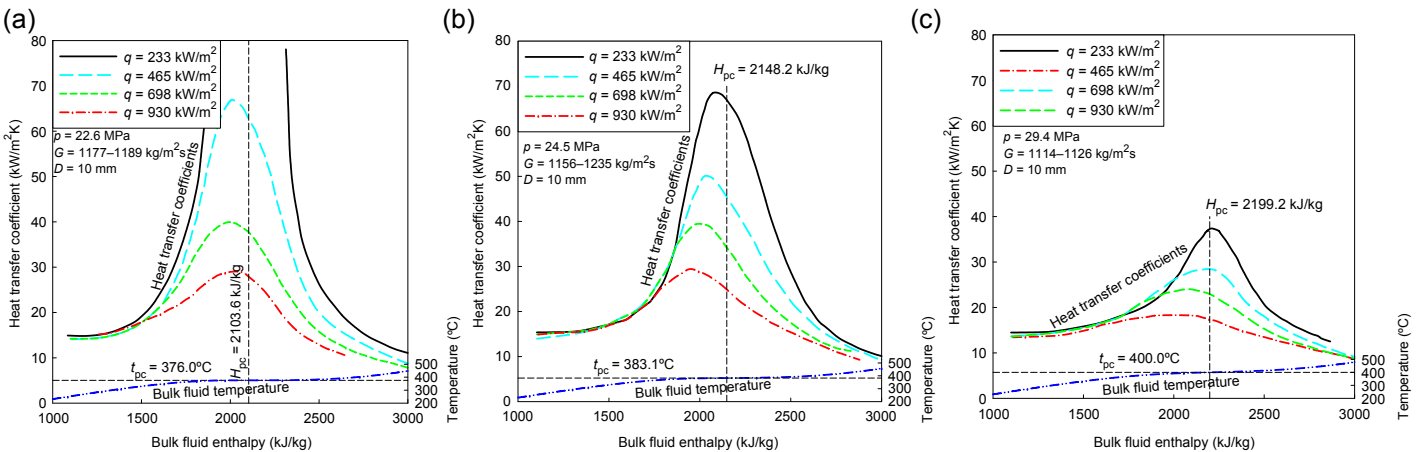


Figure A4.5 HTC versus bulk fluid enthalpy in vertical tube with upward flow at various pressures: water: (a) $p = 22.6$ MPa; (b) $p = 24.5$ MPa; and (c) $p = 29.4$ MPa.

Data from Yamagata, K., Nishikawa, K., Hasegawa, S., et al., 1972. Forced convective heat transfer to supercritical water flowing in tubes. International Journal of Heat & Mass Transfer 15 (12), 2575−2593.

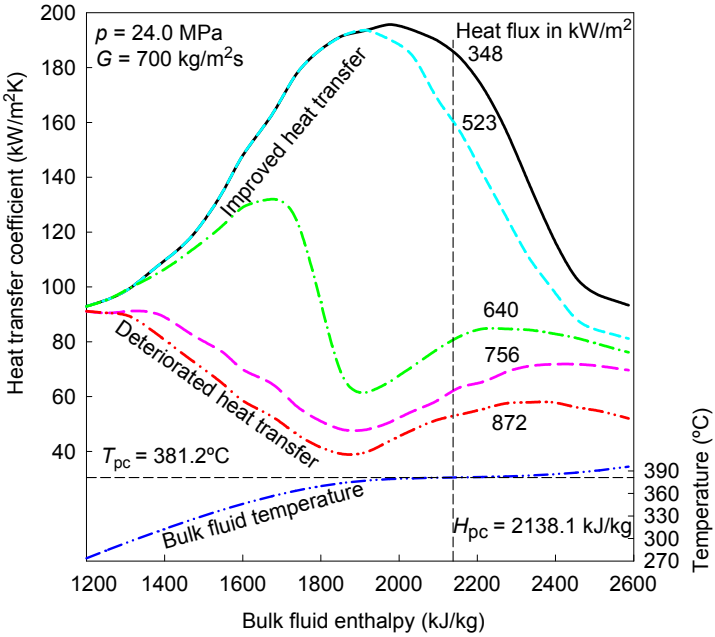


Figure A4.6 Variations in heat transfer coefficient values of water flowing in tube.
Data from Styrikovich, M.A., Margulova, T.K., Miropol'skii, Z.L., 1967. Problems in the development of designs of supercritical boilers. Thermal Engineering (Теплоэнергетика, стр. 4–7) 14 (6), 5–9.

The process of pseudo-film boiling (ie, low-density fluid prevents high-density fluid from "rewetting" a heated surface) is similar to film boiling, which occurs at subcritical pressures. Pseudo-film boiling leads to DHT. However, the pseudo-film boiling phenomenon may not be the only reason for DHT. Ackerman (1970) noted that unpredictable heat transfer performance was sometimes observed when the pseudocritical temperature of the fluid was between the bulk fluid temperature and the heated surface temperature.

Kafengaus (1975, 1986), while analyzing data of various fluids (water, ethyl and methyl alcohols, heptane, etc.), suggested a mechanism for pseudo-boiling that accompanies heat transfer to liquids flowing in small-diameter tubes at supercritical pressures. The onset of pseudo-boiling was assumed to be associated with the breakdown of a low-density wall layer that was present at an above-pseudocritical temperature, and with the entrainment of individual volumes of the low-density fluid into the cooler (below pseudocritical temperature) core of the high-density flow, where these low-density volumes collapse with the generation of pressure pulses. At certain conditions, the frequency of these pulses can coincide with the frequency of the fluid column in the tube, resulting in resonance and in a rapid rise in the amplitude of pressure fluctuations. This theory was supported with experimental results.

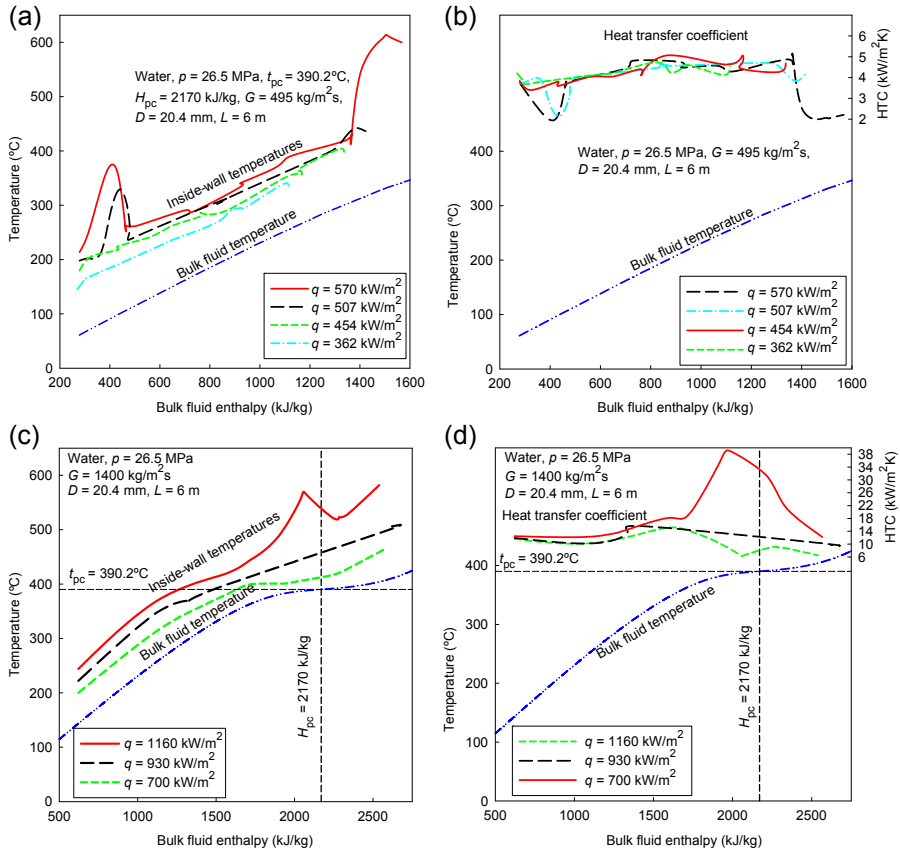


Figure A4.7 Temperature profiles (a) and (c) and heat transfer coefficient values (b) and (d) along heated length of a vertical tube: Heat transfer coefficient values were calculated by the author of the current appendix using the data from the corresponding figure; several test series were combined in each curve in figures (c) and (d).
Data by Vikhrev, Y.V., Kon'kov, A.S., Lokshin, V.A., et al., 1971. Temperature regime of steam generating tubes at supercritical pressure (in Russian). In: Transactions of the IVth All-Union Conference on Heat Transfer and Hydraulics at Movement of Two-phase Flow inside Elements of Power Engineering Machines and Apparatuses, Leningrad, Russia, pp. 21−40 and Vikhrev, Y.V., Barulin, Y.D., Kon'kov, A.S., 1967. A study of heat transfer in vertical tubes at supercritical pressures. Thermal Engineering (Теплоэнергетика, стр. 80−82) 14 (9), 116−119.

A4.2.3 Horizontal flows

All primary sources (ie, all sources found by the authors from a total of 650 references dated mainly from 1950 till beginning of 2006) of experimental data for heat transfer to water and carbon dioxide flowing in horizontal test sections are listed in Pioro and Duffey (2007).

Krasyakova et al. (1967) found that in a horizontal tube, in addition to the effects of nonisothermal flow that is relevant to a vertical tube, the effect of gravitational forces is important. The latter effect leads to the appearance of temperature differences between the lower and upper parts of the tube. These temperature differences depend on flow enthalpy, mass flux, and heat flux. A temperature difference in a tube cross section was found at $G = 300-1000\ \text{kg/m}^2\text{s}$ and within the investigated range of enthalpies ($H_b = 840-2520\ \text{kJ/kg}$). The temperature difference was directly proportional to increases in heat flux values. The effect of mass flux on the temperature difference is the opposite, ie, with an increase in mass flux, the temperature difference decreases. DHT was also observed in a horizontal tube. However, the temperature profile for a horizontal tube at locations of DHT differs from that for a vertical tube, being smoother for a horizontal tube compared to that of a vertical tube with a higher temperature increase on the upper part of the tube than on the lower part.

A4.2.4 Heat transfer enhancement

Similar to subcritical pressures, turbulization of flow usually leads to heat transfer enhancement at supercritical pressures (Pioro and Duffey, 2007).

Shiralkar and Griffith (1970) determined both theoretically (for supercritical water) and experimentally (for supercritical carbon dioxide) the limits for safe operation, in terms of the maximum heat flux for a particular mass flux. Their experiments with a twisted tape inserted inside a test section showed that heat transfer was enhanced by this method. Also, they found that at high heat fluxes, DHT occurred when the bulk fluid temperature was below and the wall temperature was above the pseudocritical temperature.

Lee and Haller (1974) found heat flux and tube diameter to be the important parameters affecting the minimum mass flux limits to prevent pseudo-film boiling. Multilead ribbed tubes were found to be effective in preventing pseudo-film boiling.

A4.2.5 Practical prediction methods for forced-convection heat transfer at supercritical pressures

Unfortunately, satisfactory analytical methods for practical prediction of forced convection heat transfer at supercritical pressures have not yet been developed due to the difficulty in dealing with steep property variations, especially in turbulent flows and at high heat fluxes. Therefore, generalized correlations based on experimental data are used for HTC calculations at supercritical pressures.

There are numerous correlations for convective heat transfer in circular tubes at supercritical pressures [for details, see in Pioro and Duffey (2007)]. However, an analysis of these correlations has shown that they are more or less accurate only within the particular dataset, which was used to derive the correlation, but show a significant deviation in predicting other experimental data. Therefore, only selected correlations are listed below.

In general, many of these correlations are based on the conventional Dittus–Boelter-type correlation (see Eq. [A4.1]) in which the regular specific heat is replaced with the cross-sectional averaged specific heat within the range of $(T_w - T_b)$; $\left(\frac{H_w - H_b}{T_w - T_b}\right)$, J/kg K (see Fig. A4.8). Also, additional terms, such as: $\left(\frac{k_b}{k_w}\right)^k$; $\left(\frac{\mu_b}{\mu_w}\right)^m$; $\left(\frac{\rho_b}{\rho_w}\right)^n$, etc., can be added into correlations to account for significant variations in thermophysical properties within a cross section due to a nonuniform temperature profile, ie, due to heat flux.

It should be noted that usually generalized correlations, which contain fluid properties at the wall temperature, require iterations to be solved, because there are two unknowns: (1) HTC and (2) the corresponding wall temperature. Therefore, the initial wall temperature value at which fluid properties will be estimated should be "guessed" to start iterations.

The most widely used heat transfer correlation at subcritical pressures for forced convection is the Dittus–Boelter (1930) correlation. In 1942, McAdams proposed

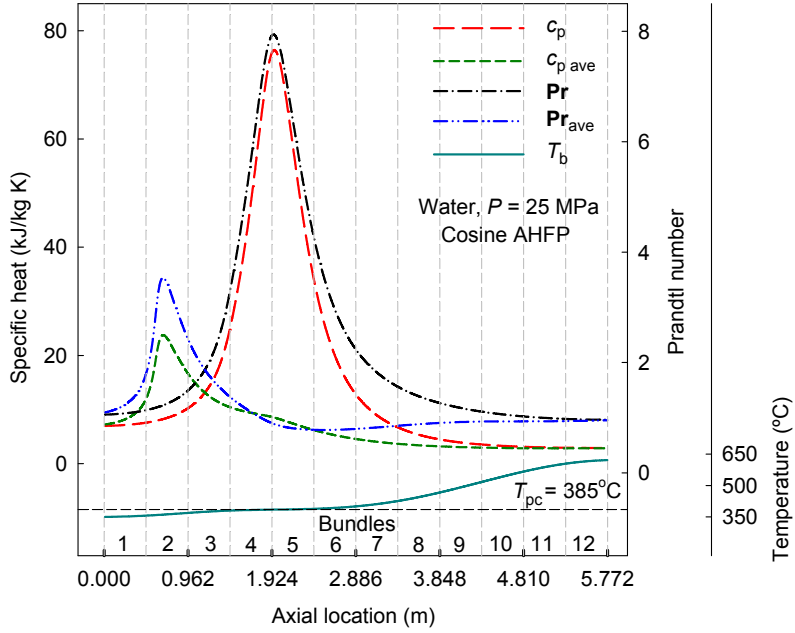


Figure A4.8 Regular and averaged Prandtl number and specific heat profiles for water along heated length of fuel channel. *AHFP*; axial heat flux profile.
Data from Mokry, S., Naidin, M., Baig, F., et al., 2008. Conceptual thermal-design options for pressure-tube SCWRs with thermochemical co-generation of hydrogen. In: Proc. 16th Int. Conf. On Nuclear Engineering (ICONE-16), Orlando, FL, USA, May 11–15, Paper #48313, p. 13.

to use the Dittus–Boelter correlation in the following form for forced convective heat transfer in turbulent flows at subcritical pressures:

$$\mathbf{Nu_b} = 0.0243 \ \mathbf{Re_b^{0.8} Pr_b^{0.4}}. \qquad [A4.1]$$

However, it was noted that Eq. [A4.1] might produce unrealistic results within some flow conditions (see Figs. A4.1, A4.3, and A4.9), especially near the critical and pseudocritical points because it is very sensitive to properties variations.

In general, experimental heat transfer coefficient values show just a moderate increase within the pseudocritical region. This increase depends on flow conditions and heat flux: higher heat flux—less increase. Thus, the bulk fluid temperature might not be the best characteristic temperature at which all thermophysical properties should be evaluated. Therefore, the cross-sectional averaged Prandtl number (see Fig. A4.8), which accounts for thermophysical properties variations within a cross section due to

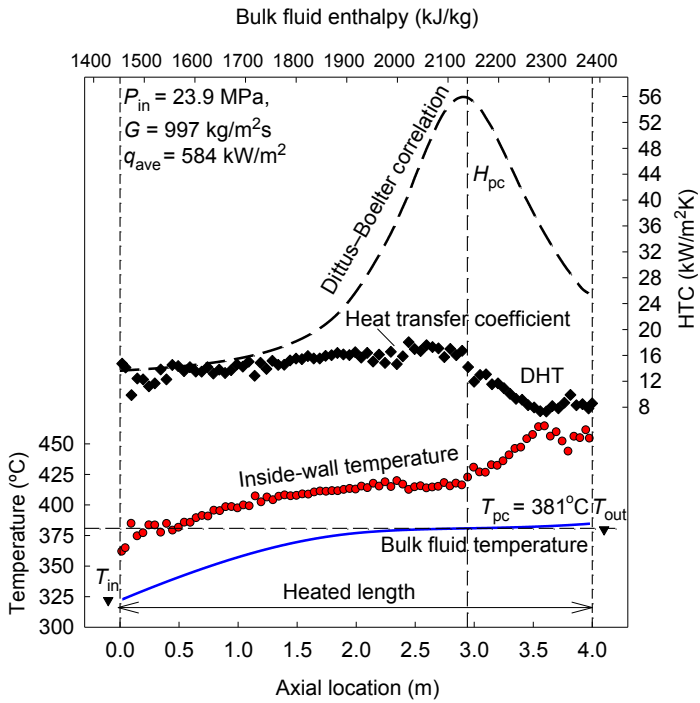


Figure A4.9 Temperature and heat transfer coefficient (experimental and calculated values) profiles along heated length of bare vertical tube. $G = 1500$ kg/m^{2}s and $q = 884$ kW/m^2. Data from Pioro, I.L., Kirillov, P.L., Mokry, S.J. Gospodinov, Y.K., 2008. Supercritical water heat transfer in a vertical bare tube: normal, improved and deteriorated regimes. In: Proc. 2008 International Congress on Advances in Nuclear Power Plants (ICAPP'08), Anaheim, CA, USA, June 8–12, Paper #8333, p. 10.

heat flux, was proposed to be used in many supercritical heat transfer correlations instead of the regular Prandtl number. Nevertheless, this classical correlation (Eq. [A4.1]) was used extensively as a basis for various supercritical heat transfer correlations (Pioro and Duffey, 2007).

The majority of empirical correlations were proposed in the 1960s−1970s (Pioro and Duffey, 2007), when experimental techniques were not at the same level (ie, advanced level) as they are today. Also, thermophysical properties of water have been updated since that time (eg, a peak in thermal conductivity in critical and pseudocritical points within a range of pressures from 22.1 to 25 MPa for water (see Appendix: A3) was not officially recognized until the 1990s).

Therefore, recently, a new correlation, based on a new set of heat transfer data and the latest thermophysical properties of water (NIST, 2010) within the SCWRs operating range, was developed and evaluated (Mokry et al., 2011):

$$\mathbf{Nu_b} = 0.0061\ \mathbf{Re_b^{0.904}}\overline{\mathbf{Pr_b}}^{0.684}\left(\frac{\rho_w}{\rho_b}\right)^{0.564}. \qquad [A4.2]$$

Fig. A4.10 shows scatter plots of experimental HTC values versus calculated HTC values according to Eq. [A4.2], and calculated and experimental values for wall temperatures. Both plots lie along a 45° straight line with an experimental data spread of ±25% for the HTC values and ±15% for the wall temperatures. This correlation was verified within the following operating conditions: water, upward flow, vertical bare tubes with inside diameters of 3−38 mm, pressure of 22.8−29.4 MPa, mass flux of 200−3000 kg/m^{2}s, and heat flux of 70−1250 kW/m^2. This correlation can be also used for supercritical carbon dioxide and other fluids. However, its accuracy might be less in these cases.

Figs. A4.11 and A4.12 show a comparison of Eq. [A4.2] with the experimental data by Kirillov et al. (2003). Fig. A4.13 shows a comparison between experimentally obtained HTC and wall temperature values and those calculated with the computational fluid dynamics (CFD) code FLUENT and Eq. [A4.2]. It is worth noting that in CFD codes, not all turbulent models are applicable to heat transfer at supercritical pressures. These models need to be tuned on the basis of experimental data prior their use in similar conditions (Miletic et al., 2015).

Figs. A4.11−A4.13 show that the latest correlation (Eq. [A4.2]) closely represents experimental data and follows trends closely even within the pseudocritical range. It should be noted that all heat transfer correlations presented in this paper are intended only for the normal and improved heat transfer regimes. The following empirical correlation was proposed for calculating the minimum heat flux at which the deteriorated heat transfer regime appears:

$$q_{dht} = -58.97 + 0.745 \cdot G, \quad \mathrm{kW/m^2}. \qquad [A4.3]$$

A recent study was conducted by Zahlan et al. (2010, 2011) in order to develop a heat transfer lookup table for the critical/supercritical pressures. An extensive literature

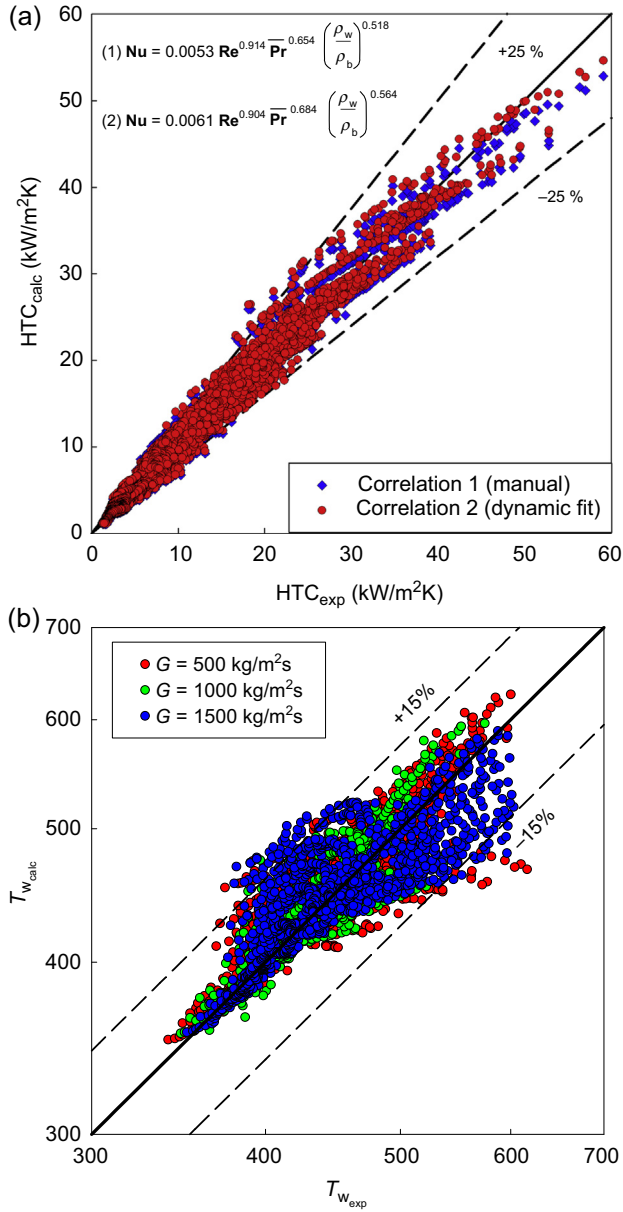


Figure A4.10 Comparison of data fit through Eq. [A4.2] with experimental data by Kirillov et al. (2003): (a) for HTC and (b) for wall temperature.

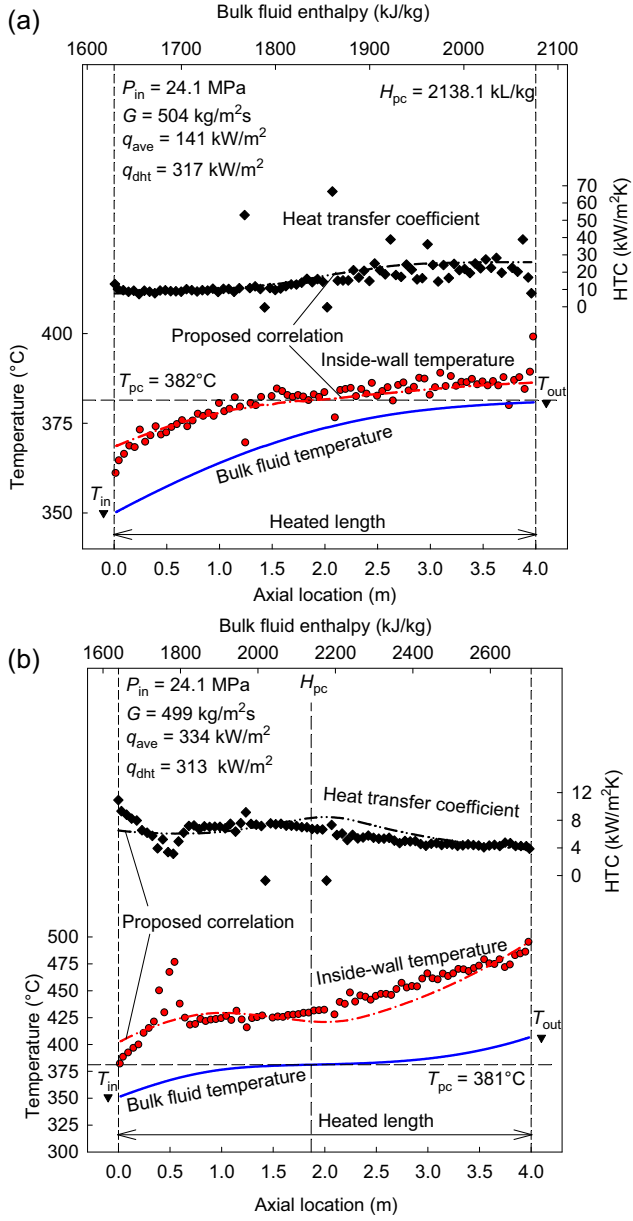


Figure A4.11 Temperature and heat transfer coefficient profiles at various heat fluxes along 4-m circular tube ($D = 10$ mm): $P_{in} \approx 24$ MPa and $G \approx 500$ kg/m^{2}s; "proposed correlation"—Eq. [A4.2]: (a) $q_{ave} \approx 140$ W/m^2 and (b) $q_{ave} \approx 330$.
Data by Kirillov, P.L., Lozhkin, V.V., Smirnov, A.M, 2003. Investigation of Borders of Deteriorated Regimes of a Channel at Supercritical Pressures (in Russian), State Scientific Center of Russian Federation Institute of Physics and Power Engineering by the name of A.I. Leypunskiy, FEI-2988, Obninsk, Russia, p. 20.

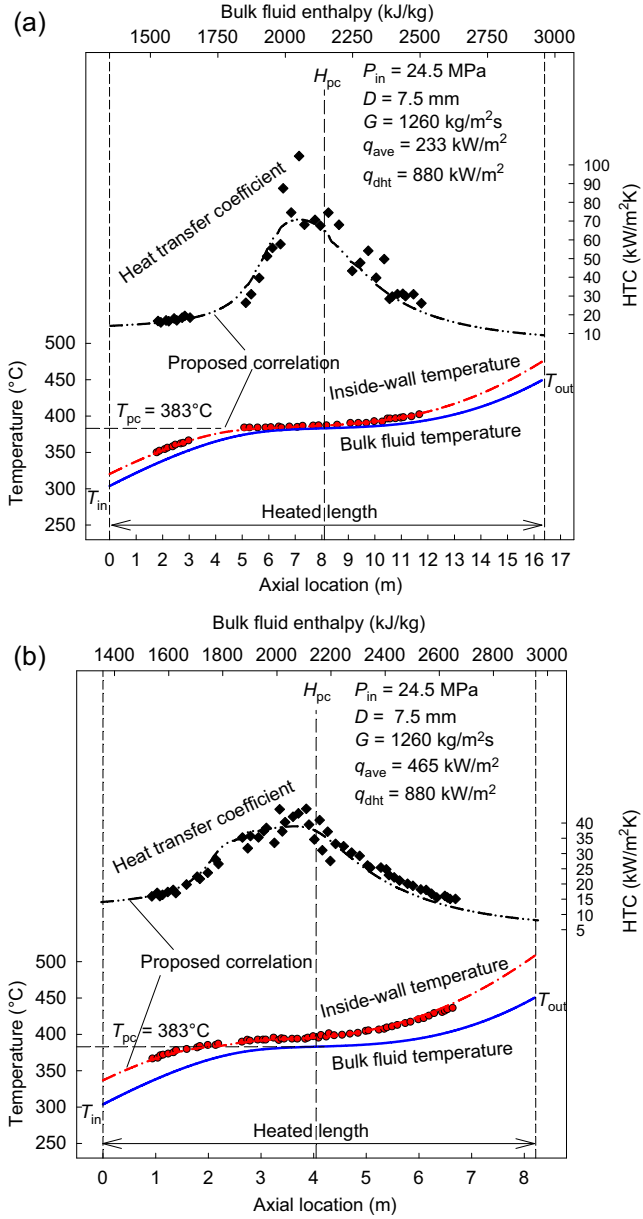


Figure A4.12 Temperature and heat transfer coefficient profiles along circular tube at various heat fluxes: nominal operating conditions—$P_{in} = 24.5$ MPa, $G = 1260$ kg/m^{2}s, and $D = 7.5$ mm; "proposed correlation"—Eq. [A4.2]: (a) $q_{ave} = 233$ W/m^2 and (b) $q_{ave} = 465$ W/m^2.
Data by Yamagata, K., Nishikawa, K., Hasegawa, S., et al., 1972. Forced convective heat transfer to supercritical water flowing in tubes. International Journal of Heat & Mass Transfer 15 (12), 2575−2593.

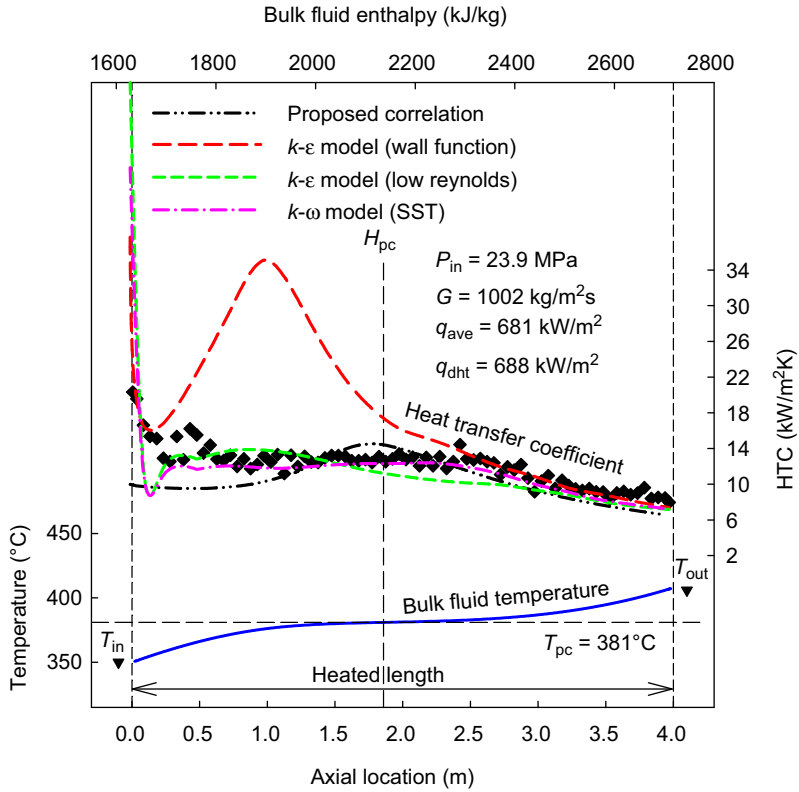


Figure A4.13 Comparison of heat transfer coefficient and wall temperature values calculated with proposed correlation (Eq. [A4.2]) and FLUENT CFD-code (based on data from Vanyukova et al. (2009)) with experimental data along 4-m circular tube ($D = 10$ mm): $P_{in} = 23.9$ MPa and $G = 1002$ kg/m^{2}s.

review was conducted, which included 28 datasets and 6663 trans-critical heat transfer data. Tables A4.1 and A4.2 list results from this study in the form of the overall weighted average and root mean square (RMS) errors: (a) within three supercritical subregions and (b) for subcritical liquid and superheated steam. Many of the correlations listed in these tables can be found in Pioro and Duffey (2007). In their conclusions, Zahlan et al. (2011, 2010) determined that within the supercritical region, the latest correlation by Mokry et al. (2011) (Eq. [A4.2]) showed the best prediction for the data within all three subregions investigated (based on RMS error). Also, the Mokry et al. correlation showed good predictions for subcritical liquid and superheated steam compared to other several correlations.

The latest information on heat transfer correlations can be found in the IAEA TECDOC (2014), Gupta et al. (2013), and Saltanov et al. (2015).

Table A4.1 Overall weighted average and RMS errors within three supercritical subregions (Zahlan et al., 2010, 2011)

	Supercritical region				Region	
	Liquid-like		Gas-like		Critical or pseudocritical	
	Errors (%)					
Correlation*	Average	RMS	Average	RMS	Average	RMS
Bishop et al. (1965)	6.3	24.2	5.2	18.4	20.9	28.9
Swenson et al. (1965)	1.5	25.2	−15.9	20.4	5.1	23.0
Krasnoshchekov et al. (1967)	15.2	33.7	−33.6	35.8	25.2	61.6
Watts and Chou (1982)	4.0	25.0	−9.7	20.8	5.5	24.0
Griem (1996)	1.7	23.2	4.1	22.8	2.7	31.1
Jackson (2002)	13.5	30.1	11.5	28.7	22.0	40.6
Mokry et al. (2011)	−3.9	**21.3**	−8.5	**16.5**	**−2.3**	**17.0**
Kuang et al. (2008)	−6.6	23.7	**2.9**	19.2	−9.0	24.1
Cheng et al. (2009)	**1.3**	25.6	**2.9**	28.8	14.9	90.6
Hadaller and Banerjee (1969)	7.6	30.5	10.7	20.5	–	–
Sieder and Tate (1936)	20.8	37.3	93.2	133.6	–	–
Dittus and Boelter (1930)	32.5	46.7	87.7	131.0	–	–
Gnielinski (1976)	42.5	57.6	106.3	153.3	–	–

In bold: the minimum values.

Table A4.2 Overall average and RMS error within subcritical region (Zahlan et al., 2010, 2011)

Correlation	Subcritical liquid		Superheated steam	
	Error (%)			
	Average	RMS	Average	RMS
Sieder and Tate (1936)	27.6	37.4	83.8	137.8
Gnielinski (1976)	−4.3	**18.3**	80.3	130.2
Hadaller and Banerjee (1969)	27.3	35.9	19.1	34.4
Dittus and Boelter (1930)	10.4	22.5	75.3	127.3
Mokry et al. (2011)	**−1.1**	19.2	**−4.8**	**19.6**

In bold: the minimum values.

A4.3 Hydraulic resistance

In general, the total pressure drop for forced convection flow inside a test section, installed in a closed-loop system, can be calculated according to the following expression (Pioro and Duffey, 2007):

$$\Delta p = \sum \Delta p_{fr} + \sum \Delta p_{\ell} + \sum \Delta p_{ac} + \sum \Delta p_{g}, \qquad [A4.4]$$

where Δp is the total pressure drop, in Pa.

The pressure drop due to frictional resistance, Δp_{fr} (Pa), is defined as

$$\Delta p_{fr} = \left(\xi_{fr} \frac{L}{D} \frac{\rho u^2}{2}\right) = \left(\xi_{fr} \frac{L}{D} \frac{G^2}{2\rho}\right), \qquad [A4.5]$$

where ξ_{fr} is the frictional coefficient, which can be obtained from appropriate correlations for different flow geometries. For smooth circular tubes, ξ_{fr} is given by Filonenko (1954):

$$\xi_{fr} = \left(\frac{1}{(1.82\ \log_{10}\mathbf{Re_b} - 1.64)^2}\right). \qquad [A4.6]$$

Eq. [A4.6] is valid within a range of $\mathbf{Re} = 4 \times 10^3 - 10^{12}$.

Usually, thermophysical properties and the Reynolds number in Eqs. [A4.5] and [A4.6], respectively, are based on arithmetic average of inlet and outlet values. The pressure drop due to local flow obstruction, Δp_{ℓ} is (Pa), is defined as

$$\Delta p_{\ell} = \left(\xi_{\ell} \frac{\rho u^2}{2}\right) = \left(\xi_{\ell} \frac{G^2}{2\rho}\right), \qquad [A4.7]$$

where ξ_ℓ is the local resistance coefficient, which can be obtained from appropriate correlations for different flow obstructions. The pressure drop due to acceleration of flow, Δp_{ac} (Pa), is defined as

$$\Delta p_{ac} = \left(\rho_{\text{out}} u_{\text{out}}^2 - \rho_{\text{in}} u_{\text{in}}^2\right) = G^2 \left(\frac{1}{\rho_{\text{out}}} - \frac{1}{\rho_{\text{in}}}\right). \quad [A4.8]$$

The pressure drop due to gravity, Δp_{g} (Pa), is defined as

$$\Delta p_g = \pm g \left(\frac{\rho_{\text{out}} + \rho_{\text{in}}}{2}\right) L \sin\theta, \quad [A4.9]$$

where θ is the test section inclination angle to the horizontal plane, sign "+" is for the upward flow, and sign "−" is for the downward flow. The arithmetic average value of densities can be used only for short sections in the case of strongly nonlinear dependency of the density versus temperature. Therefore, in long test sections at high heat fluxes and within the critical and pseudocritical regions, the integral value of densities should be used (see Eq. [A4.10]).

Ornatskiy et al. (1980) and Razumovskiy (2003) proposed that Δp_{g} at supercritical pressures can be obtained by:

$$\Delta\, p_g = \pm g \left(\frac{H_{\text{out}}\rho_{\text{out}} + H_{\text{in}}\rho_{\text{in}}}{H_{\text{out}} + H_{\text{in}}}\right) L \sin\theta. \quad [A4.10]$$

Eq. [A4.4] is applicable for subcritical and supercritical pressures. However, adjustment of this expression to conditions of supercritical pressures, with single-phase dense gas and significant variations in thermophysical properties near the critical and pseudocritical points, was the major task for the researchers and scientists. In general, two major approaches to solve this problem were taken: an analytical approach (including numerical approach) and an experimental (empirical) approach.

For reference purposes, selected results obtained at Chalk River Laboratories (Pioro and Duffey, 2007) are shown in Fig. A4.14. In these experiments, the local pressure drop due to obstructions along the heated length was 0 because of a smooth test section. Therefore, the measured pressure drop consists only of three components:

$$\Delta p_{meas} = \Delta p_{fr} + \Delta p_{ac} + \Delta p_g. \quad [A4.11]$$

Additional details of pressure drop at supercritical pressures are listed in Pioro and Duffey (2007). An important issue at supercritical and subcritical pressures is uncertainties of measured and calculated parameters. Appendix D in the book by Pioro and Duffey (2007) is dedicated to this important issue.

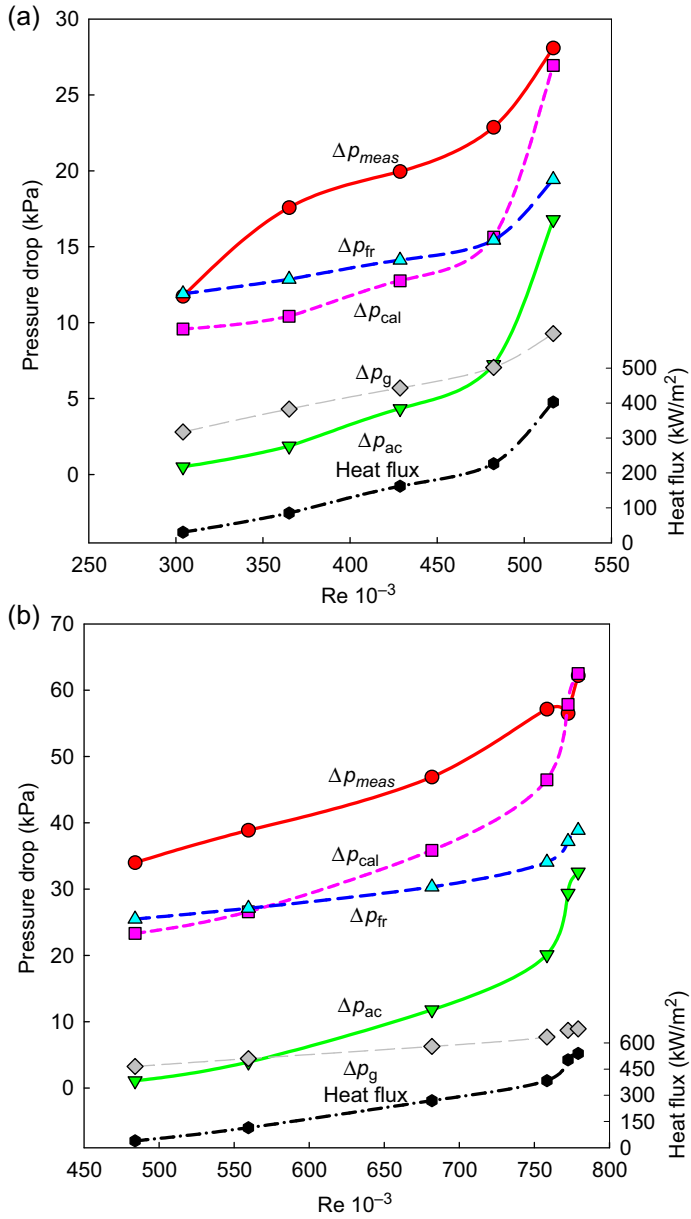


Figure A4.14 Effect of Reynolds number on total pressure drop (measured and calculated) and its components (calculated values) in supercritical carbon dioxide flowing in vertical circular tube: $p_{out} = 8.8$ MPa; (a) $G = 2040$ kg/m^{2}s, $t_{in} = 32°$C; and (b) $G = 3040$ kg/m^{2}s, $t_{in} = 31°$C.

A4.4 Conclusions

Supercritical fluids are used intensively in various industries. Therefore, understanding specifics of heat transfer and pressure drop in various flow geometries at supercritical pressures is an important task.

In general, three major heat transfer regimes were noticed at critical and supercritical pressures: (1) NHT; (2) IHT; and (3) DHT. Also, two special phenomena may appear along a heated surface: (1) pseudo-boiling and (2) pseudo-film boiling. These heat transfer regimes and special phenomena appear to be due to significant variations of thermophysical properties near the critical and pseudocritical points and due to operating conditions.

The current analysis of several well-known heat transfer correlations for supercritical fluids showed that the Dittus−Boelter correlation (1930) significantly overestimates experimental HTC values within the pseudocritical range. The Bishop et al. (1965) and Jackson (2002) correlations tend also to deviate substantially from the experimental data within the pseudocritical range. The Swenson et al. (1965) correlation provided a better fit for the experimental data than the previous three correlations within some flow conditions, but does not follow up closely the experimental data within others.

Therefore, a new correlation was developed by Mokry et al. (2011), which showed the best fit for the experimental data within a wide range of flow conditions. This correlation has an uncertainty about ±25% for HTC values and about ±15% for calculated wall temperature. Also, based on an independent study performed by Zahlan et al. (2010, 2011), this heat transfer correlation (given as Eq. [A4.2]) is the best within the supercritical region and for superheated steam compared to other well-known correlations. Also, this correlation showed good predictions for subcritical fluids.

The derived correlation can be used for supercritical fluid heat transfer calculations, in circular and other flow geometries, for heat exchangers, steam generators, nuclear reactors and other heat transfer equipment, for future comparison with other datasets, and for verification of computer codes and scaling parameters between water and modeling fluids. This correlation can be also used for supercritical carbon dioxide and other fluids. However, its accuracy might be less in these cases. Some specifics of pressure-drop calculations were also listed in the paper.

Nomenclature

A	Flow area, m^2
c_p	Specific heat at constant pressure, J/kg K
$\overline{c}_p$	Averaged specific heat within the range of $(t_w - t_b)$; $\left(\frac{H_w - H_b}{T_w - T_b}\right)$, J/kg K

D	Inside diameter, m
G	Mass flux, kg/m^{2}s; $\left(\frac{m}{A_{\mathrm{fl}}}\right)$
g	Gravitational acceleration, m/s^2
H	Specific enthalpy, J/kg
h	Heat transfer coefficient, W/m^{2}K
k	Thermal conductivity, W/m K
L	Heated length, m
m	Mass-flow rate, kg/s; $(\rho \cdot V)$
q	Heat flux, W/m^2; $\left(\frac{Q}{A_{\mathrm{h}}}\right)$
u	Axial velocity, m/s
V	Volume-flow rate, m^3/kg or volume, m^3
v	Specific volume, m^3/kg; $\left(\frac{1}{\rho}\right)$

Greek letters

α	Thermal diffusivity, m^2/s; $\left(\frac{k}{c_{\mathrm{p}} \cdot \rho}\right)$
Δ	Difference
θ	Test section inclination angle, degree
μ	Dynamic viscosity, Pa s
ξ	Friction coefficient
ρ	density, kg/m^3
υ	Kinematic viscosity, m^2/s; $\left(\frac{\mu}{\rho}\right)$

Non-dimensional numbers

Nu	Nusselt number; $\left(\frac{h \cdot D}{k}\right)$
Pr	Prandtl number; $\left(\frac{\mu \cdot c_p}{k}\right) = \left(\frac{\upsilon}{\alpha}\right)$
$\overline{\mathbf{Pr}}$	cross-sectional average Prandtl number within the range of $(t_{\mathrm{w}} - t_{\mathrm{b}})$; $\left(\frac{\mu \cdot \bar{c}_p}{k}\right)$
Re	Reynolds number; $\left(\frac{G \cdot D}{\mu}\right)$

Subscripts or superscripts

ac	Acceleration
ave	Average
b	Bulk
calc	Calculated
dht	Deteriorated heat transfer
exp	Experimental
fl	Flow
fr	Friction
g	Gravitational
h	Heated
in	Inlet
ℓ	Local
max	Maximum
meas	Measured
out	Outlet or outside
w	Wall

Abbreviations and acronyms

DHT	Deteriorated heat transfer
HT	Heat transfer
HTC	Heat transfer coefficient
IHT	Improved heat transfer
NHT	Normal heat transfer
RMS	Root mean square (error)

References

Ackerman, J.W., 1970. Pseudoboiling heat transfer to supercritical pressure water in smooth and ribbed tubes. Journal of Heat Transfer, Transactions of the ASME 92 (3), 490−498 (Paper No. 69-WA/HT-2, pp. 1−8).

Bishop, A.A., Sandberg, R.O., Tong, L.S., 1965. Forced convection heat transfer to water at near-critical temperatures and supercritical pressures. In: A.I.Ch.E.-I.Chem.E. Symposium Series, No. 2, pp. 77–85.

Cheng, X., Yang, Y.H., Huang, S.F., 2009. A Simple Heat Transfer Correlation for SC Fluid Flow in Circular Tubes. In: NURETH-13, Kanazawa City, Ishikawa Prefecture, Japan, September 27–October 2.

Dittus, F.W., Boelter, L.M.K., 1930. Heat Transfer in Automobile Radiators of the Tubular Type. University of California, Berkeley, Publications in Engineering, vol. 2, No. 13, pp. 443–461 (or Int. Communications in Heat and Mass Transfer, 1985, vol. 12, pp. 3–22).

Filonenko, G.K., 1954. Hydraulic resistance of pipelines (in Russian). Thermal Engineering (4), 40–44.

Gnielinski, V., 1976. New equation for heat and mass transfer in turbulent pipe and channel flow. International Journal of Chemical Engineering 16 (2), 359–366.

Griem, H., 1996. A new procedure for the at near-and supercritical prediction pressure of forced convection heat transfer. Heat and Mass Transfer 3, 301–305.

Gupta, S., Saltanov, E., Mokry, S.J., Pioro, I., Trevani, L., McGillivray, D., 2013. Developing empirical heat-transfer correlations for supercritical CO_2 flowing in vertical bare tubes. Nuclear Engineering and Design 261, 116–131.

Hadaller, G., Banerjee, S., 1969. Heat Transfer to Superheated Steam in Round Tubes. AECL Report.

IAEA TECDOC, 2014. Heat Transfer Behaviour and Thermohydraulics Code Testing for Supercritical Water Cooled Reactors (SCWRs). In: IAEA TECDOC Series. IAEA-TECDOC-1746, September, Vienna, Austria, 496 p. Free download from: http://www-pub.iaea.org/books/IAEABooks/10731/Heat-Transfer-Behaviour-and-Thermohydraulics-Code-Testing-for-Supercritical-Water-Cooled-Reactors-SCWRs.

Jackson, J.D., 2002. Consideration of the heat transfer properties of supercritical pressure water in connection with the cooling of advanced nuclear reactors. In: Proc. 13th Pacific Basin Nuclear Conference, Shenzhen City, China, October 21–25.

Kafengaus, N.L., 1975. The mechanism of pseudoboiling. Heat Transfer –Soviet Research 7 (4), 94–100.

Kafengaus, N.L., 1986. About some Peculiarities in fluid Behaviour at supercritical pressure in conditions of intensive heat transfer. Applied Thermal Sciences, (ПроМышленная Теплотехника, стр. 6–10) 8 (5), 26–28.

Kirillov, P.L., Lozhkin, V.V., Smirnov, A.M., 2003. Investigation of Borders of Deteriorated Regimes of a Channel at Supercritical Pressures (in Russian), p. 20. State Scientific Center of Russian Federation Institute of Physics and Power Engineering by the name of A.I. Leypunskiy, FEI-2988, Obninsk, Russia.

Krasnoshchekov, E.A., Protopopov, V.S., Van, F., Kuraeva, I.V., 1967. Experimental investigation of heat transfer for carbon dioxide in the supercritical region. In: Gazley Jr., C., Hartnett, J.P., Ecker, E.R.C. (Eds.), Proc. 2nd All-soviet Union Conf. On Heat and Mass Transfer, Minsk, Belarus, May, 1964, Published as Rand Report R-451-PR, vol. 1, pp. 26–35.

Krasyakova, L.Y., Raykin, Y.M., Belyakov, I.I., et al., 1967. Investigation of temperature regime of heated tubes at supercritical pressure (in Russian). Soviet Energy Technology (Энергомашиностроение) (1), 1–4.

Kuang, B., Zhang, Y., Cheng, X., 2008. A New, Wide-Ranged Heat Transfer Correlation of Water at Supercritical Pressures in Vertical Upward Ducts. NUTHOS-7, Seoul, Korea, October 5–9.

Lee, R.A., Haller, K.H., 1974. Supercritical water heat transfer developments and applications. In: Proc. 5th Int. Heat Transfer Conference (IHTC), Tokyo, Japan, September 3−7, vol. IV, pp. 335−339. Paper No. B7.7.

McAdams, W.H., 1942. Heat Transmission, second ed. McGraw-Hill, New York, NY, USA, p. 459.

Miletic, M., Peiman, W., Farah, F., Samuel, J., Dragunov, A., Pioro, I., 2015. Study on neutronics and thermalhydraulics characteristics of 1200-MW_{el} pressure-channel Supercritical water-cooled reactor (SCWR). ASME Journal of Nuclear Engineering and Radiation Science 1 (1), 10.

Mokry, S., Pioro, I.L., Farah, A., et al., 2011. Development of supercritical water heat-transfer correlation for vertical bare tubes. Nuclear Engineering and Design 241, 1126−1136.

National Institute of Standards and Technology, 2010. NIST Reference Fluid Thermodynamic and Transport Properties-REFPROP. NIST Standard Reference Database 23, Ver. 9.1. Department of Commerce, Boulder, CO, US.

Oka, Y., Koshizuka, S., Ishiwatari, Y., Yamaji, A., 2010. Super Light Water Reactors and Super Fast Reactors. Springer, New York, NY, USA, p. 416.

Ornatskiy, A.P., Dashkiev, Yu.G., Perkov, V.G., 1980. Supercritical Steam Generators (in Russian). VyshchaShkola Publishing House, Kiev, Ukraine, p. 287.

Peiman, W., Pioro, I., Gabriel, K., 2015. Thermal-hydraulic and neutronic analysis of a re-entrant fuel channel design for pressure-channel supercritical water-cooled reactors. ASME Journal of Nuclear Engineering and Radiation Science 1 (2), 10.

Pioro, I., 2014. Application of supercritical pressures in power engineering: specifics of thermophysical properties and forced-convective heat transfer. In: Anikeev, V., Fan, M. (Eds.), Supercritical Fluid Technology for Energy and Environmental Applications. Elsevier, pp. 201−233.

Pioro, I., 2011. The potential use of supercritical water-cooling in nuclear reactors. In: Krivit, S.B., Lehr, J.H., Kingery, Th.B. (Eds.), Nuclear Energy Encyclopaedia: Science, Technology, and Applications. J. Wiley & Sons, Hoboken, NJ, USA, pp. 309−347.

Pioro, I.L., Duffey, R.B., 2007. Heat Transfer and Hydraulic Resistance at Supercritical Pressures in Power Engineering Applications. ASME Press, New York, NY, USA, p. 328.

Pioro, I.L., Kirillov, P.L., Mokry, S.J., Gospodinov, Y.K., 2008. Supercritical water heat transfer in a vertical bare tube: normal, improved and deteriorated regimes. In: Proc. 2008 International Congress on Advances in Nuclear Power Plants (ICAPP'08), Anaheim, CA, USA, June 8−12, Paper #8333, p. 10.

Pioro, I., Mokry, S., 2011. Heat transfer to fluids at supercritical pressures. In: Belmiloudi, A. (Ed.), Heat Transfer. Theoretical Analysis, Experimental Investigations and Industrial Systems. INTECH, Rijeka, Croatia, pp. 481−504.

Razumovskiy, V.G., 2003. Private Communications. National Technical University "KPI", Kiev, Ukraine.

Razumovskiy, V.G., Pis'mennyi, E.N., Sidawi, K., Pioro, I.L., Koloskov, A.E., 2015. Experimental heat transfer in 7 an annular channel and 3-rod 8 bundle cooled with upward flow of supercritical water. ASME Journal of Nuclear Engineering and Radiation Science 2 (1), 8.

Richards, G., Harvel, G.D., Pioro, I.L., Shelegov, A.S., Kirillov, P.L., 2013. Heat transfer profiles of a vertical, bare, 7-element bundle cooled with supercritical Freon R-12. Nuclear Engineering and Design 264, 246−256.

Saltanov, E., Pioro, I., Mann, D., Gupta, S., Mokry, S., Harvel, G., 2015. Study on specifics of forced-convective heat transfer in supercritical carbon dioxide. ASME Journal of Nuclear Engineering and Radiation Science 1 (1), 8.

Schmidt, E., Eckert, E., Grigull, V., 1946. Heat Transfer by Liquids Near the Critical State, AFF Translation, No. 527, Air Materials Command. Wright Field, Dayton, OH, USA, April.

Schulenberg, T., Starflinger, J. (Eds.), 2012. High Performance Light Water Reactor. Design and Analyses. Scientific Publishing, Karlsruher Institut fūr Technologie (KIT), Germany, p. 241.

Shiralkar, B.S., Griffith, P., August 1970. The effect of swirl, inlet conditions, flow direction, and tube diameter on the heat transfer to fluids at supercritical pressure. Journal of Heat Transfer, Transactions of the ASME 92 (3), 465–474.

Seider, N.M., Tate, G.E., 1936. Heat transfer and pressure drop of liquids in tubes. Industrial and Engineering Chemistry 28 (12), 1429–1435.

Styrikovich, M.A., Margulova, T.K., Miropol'skii, Z.L., 1967. Problems in the development of designs of supercritical boilers. Thermal Engineering (Теплоэнергетика, стр. 4–7) 14 (6), 5–9.

Swenson, H.S., Carver, J.R., Kakarala, C.R., 1965. Heat transfer to supercritical water in smooth-bore tubes. Journal of Heat Transfer, Transactions of the ASME, Series C 87 (4), 477–484.

Vanyukova, G.V., Kuznetsov, YuN., Loninov, A.Y., Papandin, M.V., Smirnov, V.P., Pioro, I.L., 2009. Application of CFD-code to calculations of heat transfer in a fuel bundle of SCW pressure-channel reactor. In: Proc. 4th Int. Symp. on Supercritical Water-Cooled Reactors, March 8–11, Heidelberg, Germany, Paper No. 28, p. 9.

Vikhrev, Y.V., Barulin, Y.D., Kon'kov, A.S., 1967. A study of heat transfer in vertical tubes at supercriticaressures. Thermal Engineering (Теплоэнергетика, стр. 80–82) 14 (9), 116–119.

Vikhrev, Y.V., Kon'kov, A.S., Lokshin, V.A., et al., 1971. Temperature regime of steam generating tubes at supercritical pressure (in Russian). In: Transactions of the IVth All-Union Conference on Heat Transfer and Hydraulics at Movement of Two-phase Flow Inside Elements of Power Engineering Machines and Apparatuses, Leningrad, Russia, pp. 21–40.

Watts, M.J., Chou, C.-T., 1982. Mixed convection heat transfer to supercritical pressure water. In: Proc. 7th Int. Heat Transfer Conference (IHTC), Munich, Germany, pp. 495–500.

Yamagata, K., Nishikawa, K., Hasegawa, S., et al., 1972. Forced convective heat transfer to supercritical water flowing in tubes. International Journal of Heat & Mass Transfer 15 (12), 2575–2593.

Zahlan, H., Groeneveld, D., Tavoularis, S., 2010. Look-up table for trans-critical heat transfer. In: Proc. 2nd Canada-China Joint Workshop on Supercritical Water-Cooled Reactors (CCSC-2010), Toronto, Ontario, Canada: Canadian Nuclear Society (CNS), April 25–28.

Zahlan, H., Groeneveld, D.C., Tavoularis, S., Mokry, S., Pioro, I., 2011. Assessment of supercritical heat transfer prediction methods. In: Proc. 5th Int. Symp. on SCWR (ISSCWR-5), Vancouver, BC, Canada, March 13–16, Paper P08, p. 20.

Appendix A5: World experience in nuclear steam reheat[1]

Eu. Saltanov, I.L. Pioro
University of Ontario Institute of Technology, Oshawa, Ontario, Canada

A5.1 Introduction

Concepts of nuclear reactors cooled with water at supercritical pressures were studied as early as the 1950s and 1960s in the US and Russia. After a 30-year break, the idea of developing nuclear reactors cooled with supercritical water (SCW) became attractive again as the ultimate development path for water cooling. This statement is based on the known history of the thermal power industry, which made a "revolutionary" step forward from the level of subcritical pressures (15–16 MPa) to the level of supercritical pressures (23.5–35 MPa) more than 50 years ago with the same major objective as that of supercritical water-cooled reactors (SCWRs): to increase thermal efficiency of power plants. The main objectives of using SCW in nuclear reactors are: (1) to increase the thermal efficiency of modern nuclear power plants (NPPs) from 30–35% to about 45–50%; and (2) to decrease capital and operational costs and, hence decrease electrical energy costs.

To achieve higher thermal efficiency, nuclear steam reheat has to be introduced inside a reactor. Currently, all supercritical turbines at thermal power plants have a steam reheat option. In the 1960s and 1970s, Russia, the US, and some other countries have developed and implemented nuclear steam reheat at subcritical pressures in experimental reactors. Therefore, it is important to summarize the worldwide experience of implementing nuclear steam reheat at several experimental boiling water reactors (BWRs) and utilize it in the context of development of SCWRs concepts with a steam reheat option.

A5.2 US experience in nuclear steam reheat[2]

An active program for the development and demonstration of BWRs with nuclear steam reheat was implemented and directed by the United States Atomic Energy Commission (USAEC). Two general types of the reactors were pursued:

1. Reactors with integral reheating design (steam was generated and reheated in the same core); and

[1] This chapter is mainly based on Saltanov, Eu. and Pioro, I., 2011. World Experience in Nuclear Steam Reheat, Chapter in book "Nuclear Power: Operation, Safety and Environment", Editor: P.V. Tsvetkov, INTECH, Rijeka, Croatia, pp. 3–28. Free download from: http://www.intechopen.com/books/nuclear-power-operation-safety-and-environment/world-experience-in-nuclear-steam-reheat.

[2] This chapter is based on the paper by Novick et al. (1965).

2. Reactors with separate reheating design (steam supplied from another source was superheated in the core).

Under the USAEC program, the following reactors were built: Boiling Reactor Experiment V (BORAX−V, started operation in December of 1962), BOiling NUclear Superheater (BONUS, started operation in December of 1964), and Pathfinder (started operation in July of 1966). The main parameters of these reactors are listed in Tables A5.1 and A5.2 (Novick et al., 1965).

At the design stage of these reactors, several problems related to the implementation of steam reheat were encountered and addressed. Below is the highlight of those problems:

1. Fuel element sheath performance and corrosion resistance at high temperatures;
2. Corrosion, erosion, and deposits on fuel element surfaces due to ineffective steam separation prior to the reheating zone inlet;
3. Keeping the desired power ratio between the evaporating and reheating zones during extended reactor operation;
4. Fission products carryover in direct cycle systems; and
5. Reactivity changes as a result of inadvertent flooding of the reheating zone.

In search of the solutions to these problems, USAEC also instituted a number of programs to determine long-term integrity and behavior of the fuel element sheath. Since May of 1959, the Superheat Advance Demonstration Experiment (SADE) and the subsequent Expanded SADE loops had been utilized to irradiate a total of 21 fuel elements in the Vallecitos BWR. Saturated steam at about 6.9 MPa from the Vallecitos BWR was supplied to the fuel element section, where it was superheated to temperatures of 418−480°C. The results of those irradiation tests combined with out-of-core corrosion tests led to the following conclusions (Novick et al., 1965):

1. Commercial 18-8 stainless steel was not satisfactory for fuel sheath material in the superheated steam (SHS) environment;
2. Materials with higher nickel alloy content, such as Inconel and Incoloy, appeared to perform satisfactorily as a sheath material in the SHS environment; and
3. Strain cycling coupled with environmental chemistry was significant in the failure rate of sheath materials for reactors with steam reheat.

Additional information on design of these reactors constructed under the USAEC program can be found in USAEC reports (1959, 1961, and 1962) and in the publication by Ross (1961).

Based on the US experience with nuclear steam reheat, it may be concluded that the nuclear steam reheat is possible and higher thermal efficiencies can be achieved; however, this implementation requires more complicated reactor core design and better materials.

A5.3 Russian experience in nuclear steam reheat

This section presents a unique compilation of materials that overviews all major aspects of operating experience of the first in the world industrial NPP with implemented nuclear steam reheat.

Table A5.1 Main general parameters of BWR NPPs with integral reheat design (Novick et al., 1965)

	BORAX−V		BONUS		Pathfinder	
	Zone		Zone		Zone	
Parameters	**Boiling**	**SHS**	**Boiling**	**SHS**	**Boiling**	**SHS**
Structural material (core)	A1(X8001)	SS	Zr−2	SS-248	Zr−2	SS
Fuel type	Rod	Plate	Rod	Rod	Rod	Annular
Fuel material	UO_2	UO_2−SS cermet	UO_2	UO_2	UO_2	UO_2−SS cermet
Fuel enrichment, %	4.95	93	2.4	3.25	2.2	93
Sheath material	SS-304	SS-304 L	Zr−2	Inconel	Zr−2	SS-316L
Control rod shape	Cruciform and "T"	Cruciform and "T"	Cruciform	Slab	Cruciform	Round rod
Control rod material	Boral	Boral	1.0% $_{wt}$ ^{10}B in SS	1.0% $_{wt}$ ^{10}B in SS	2% $_{wt}$ ^{10}B in SS	2% $_{wt}$ ^{10}B in SS
Average power density, MW_{th}/m^3	42.5	40.5	33.6	11.5	45.2	46.5

Table A5.2 Main thermal parameters of BWR NPPs with integral reheat design (Novick et al., 1965)

Parameters	BORAX−V	BONUS	Pathfinder
Electric power, MW_{el} (gross)	3.5	17.5	66
Electric power, MW_{el} (net)	3.5	16.5	62.5
Thermal power, MW_{th}	20	50	200
Reheat loop to evaporating loop power ratio	0.21	0.35	0.22
Gross cycle thermal efficiency, %	–	35	33
Net cycle thermal efficiency, %	–	33	31
NPP steam cycle	Direct	Direct	Direct
Reheating-zone location	Central or peripheral	Peripheral	Central
Nominal operating pressure, MPa	4.1	6.7	4.1

A5.3.1 General information

Reactors with nuclear steam reheat were also developed in the former Soviet Union. The Beloyarsk Nuclear Power Plant (BNPP) was the first NPP in the world where nuclear steam reheat was implemented on industrial level. Two reactors (100 MW_{el} and 200 MW_{el}) were installed with identical steam parameters at the turbine inlet ($P_{in} = 8.8$ MPa and $T_{in} = 500–510°C$). The first reactor (Unit 1) was put into operation on April 26, 1964, and the second reactor (Unit 2) on December 29, 1967. Both reactors had similar dimensions and design. However, the flow diagram and the core arrangement were significantly simplified in Unit 2 compared to that of Unit 1. Schematics and simplified layouts of the BNPP Units 1 and 2 are shown in Figs. A5.1 and A5.2.

Operation of BNPP proved the feasibility of steam reheat implementation on an industrial scale (Baturov et al., 1978). Major results of the BNPP operation are listed below (Petrosyants, 1969):

1. The reactor was started up from the cold state without external heat sources. The reactor heat-up was carried out at 10% power until the water temperature in the separators reached 285−300°C at 8.8 MPa. Levels in the separators were formed during the heat-up. Transition from cooling with water to cooling with steam in the SHS channels did not cause significant reactivity changes.
2. The radial neutron flux flattening achieved was one of the best among operating reactors. The radial neutron flux irregularity coefficient, K_{ir}, for both units was 1.28−1.30, while the design values were: $K_{ir} = 1.46$ for Unit 1 and $K_{ir} = 1.24$ for Unit 2.

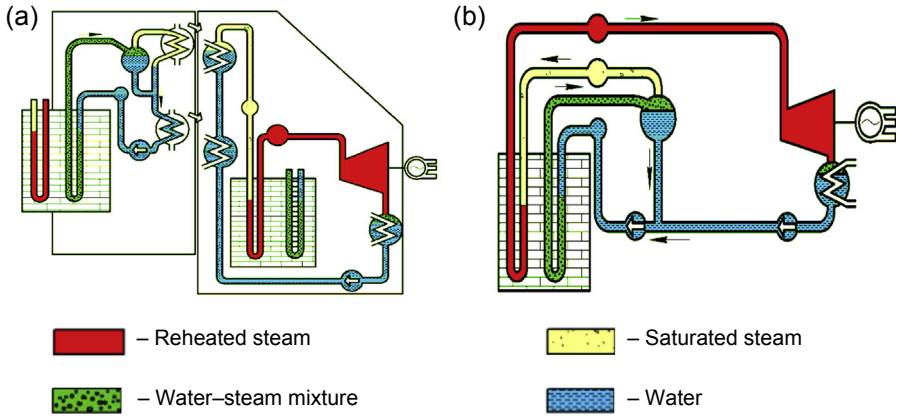


Figure A5.1 BNPP Unit 1 (a) and Unit 2 (b) general schematics of thermodynamic cycle. Based on the paper by Yurmanov, V.A., Belous, V.N., Vasina, V.N., Yurmanov, E.V., 2009a. Chemistry and corrosion issues in supercritical water reactors. Proceedings of the IAEA International Conference on Opportunities and Challenges for Water Cooled Reactors in the 21st Century, Vienna, Austria, October 26–30.

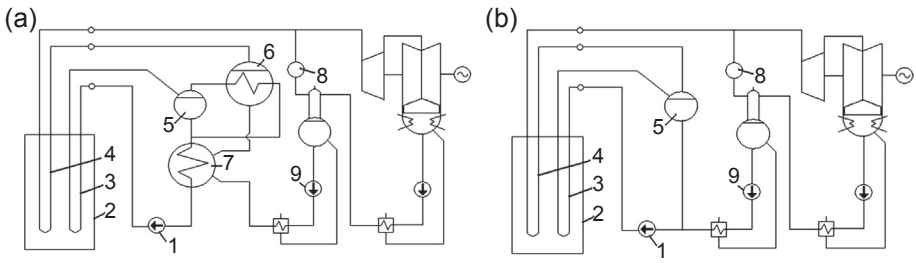


Figure A5.2 Simplified layout of BNPP Unit 1 (a) and Unit 2 (b): (1) circulation pump; (2) reactor; (3) boiling-water channels; (4) superheated steam channels; (5) steam separator; (6) steam generator (SG); (7) economizer; (8) bubbler; and (9) feedwater pump.
Based on the paper by Petrosyants, A.M., 1969. Power reactors for nuclear power plants (from the first in the world to the 2-GW electrical power NPP), (In Russian). Atomic Energy 27 (4), 263–274.

3. Radioactivity in the turbine and technological equipment of the plant were below the prescribed limits. Radiation rates did not exceed 10 μR/s at the high-pressure cylinders and did not exceed 8 μR/s at the low-pressure cylinders. Such low dose rates were attained by implementing the fuel elements that eliminated the possibility of fission–fragment activity transported via the coolant loop. BNPP operation experience showed that radiation levels near Unit 1 equipment were significantly lower than that of other operating reactors, and releases of radioactive products into the atmosphere were 5–10 times lower than allowed by the regulations.

A5.3.2 Thermodynamic cycle development

Reliability, simple design, and efficiency are the main criteria when choosing the flow diagram for both the fossil and NPPs. Special requirements for impermeability and water regime are specified for NPPs.

Several layouts of thermodynamic cycles for an NPP with a uranium−graphite reactor were considered for the BNPP (see Fig. A5.3). In the considered layouts, the coolant was either boiling water (BW) or SHS. Feasibility of the NPP designs was also taken into account (Dollezhal et al., 1958).

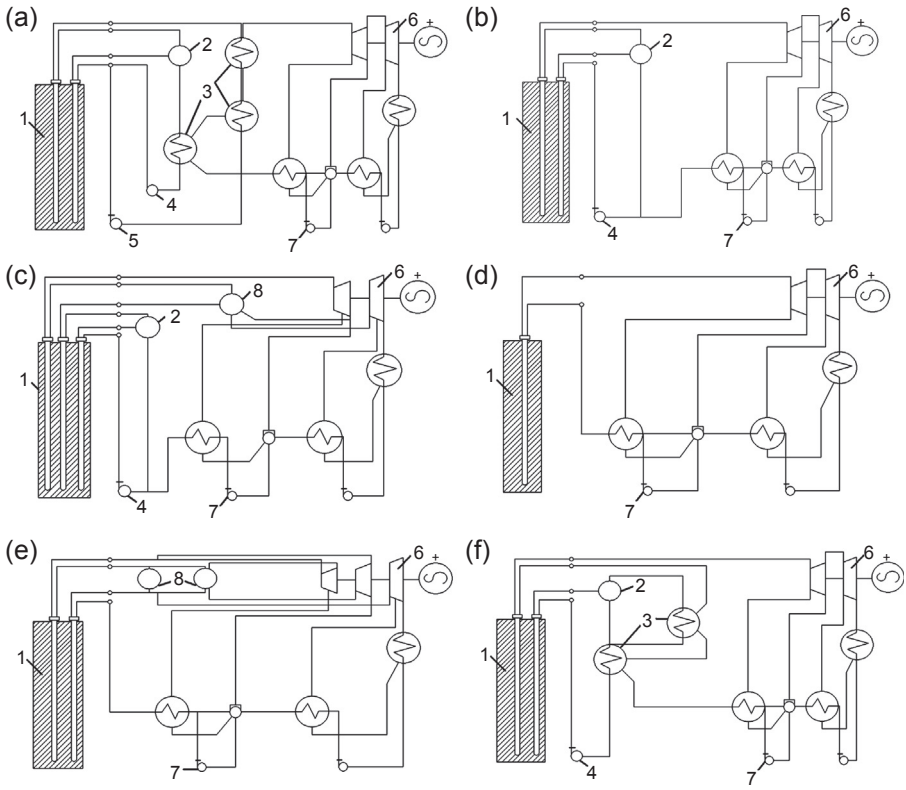


Figure A5.3 Possible layouts of NPPs with steam reheat: (1) reactor; (2) steam separator; (3) steam generator; (4) main circulation pump; (5) circulation pump; (6) turbine with electrical generator; (7) feedwater pump; and (8) intermediate steam reheater.
Based on the paper by Dollezhal, N.A., Krasin, A.K., Aleshchenkov, P.I., Galanin, A.N., Grigoryants, A.N., Emel'anov, I.Ya., Kugushev, N.M., Minashin, M.E., Mityaev, Yu.I., Florinsky, B.V., Sharapov, B.N., 1958. Uranium-graphite reactor with reheated high pressure steam. Proceedings of the 2nd International Conference on the Peaceful Uses of Atomic Energy, United Nations, Session G-7, P/2139, vol. 8, 398−414.

A5.3.2.1 Layout (a)

A steam separator, SG (consisting of preheating, boiling, and steam superheating sections), and two circulation pumps are included in the primary coolant loop. Water and very high-pressure steam are the primary coolants. High- and intermediate-pressure steam is generated in the secondary loop and directed to the turbine.

A5.3.2.2 Layout (b)

This is a direct cycle layout. Steam from a reactor flows directly to a turbine. The turbine does not require an intermediate steam reheat.

A5.3.2.3 Layout (c)

Steam from a reactor flows directly to a turbine. The turbine requires the intermediate steam reheat. The reactor has three types of fuel channels depending on their purpose: (1) to preheat water to the saturation temperature; (2) to boil and partial evaporate water; and (3) to superheat steam.

A5.3.2.4 Layout (d)

This is a direct cycle layout. The evaporation and reheat are achieved inside a reactor. The turbine does not require the intermediate steam reheat.

A5.3.2.5 Layout (e)

This is another direct cycle layout. One or two intermediate steam reheats are required.

A5.3.2.6 Layout (f)

Water circulates in the closed loop consisting of a reactor, steam separator, preheater, and a circulation pump. Partial evaporation is achieved in the first group of channels. Steam exiting the steam separator is directed to the boiling section of the SG and condenses there. Condensate from the boiler is mixed with water from the separator. The cooled water is fed to a preheater and then directed to circulation pumps. The generated steam on the secondary side is superheated in the second group of channels and then directed to the turbine.

Layouts (b–e) were not recommended due to unpredictable water chemistry regimes at various locations throughout the thermodynamic cycle. Layout (a) with the secondary steam reheat required high pressures and temperatures in the primary loop. Circulation pumps with different parameters (power and pressure) would have to be used to feed common header upstream of the channels of the primary group. In this respect, Layout (a) was considerably more complex and expensive than Layout (f). Activation of SHS, which could occur in Layout (f), was not considered to be posing any significant complications to the turbine operation and hence remained a viable option (Dollezhal et al., 1958).

From the considerations above, Layout (f) was chosen to be developed at the BNPP Unit 1. Surface corrosion products in the secondary loop and salts in condenser coolant

were trapped in the SG and removed from it during purging. Additionally, modern separators provided steam of high quality, which resulted in very low salt deposits in the turbine.

A5.3.3 Beloyarsk NPP reactor design

The reactor was placed in a cylindrical concrete cavity, where the 3-m-thick wall served as a part of the biological shield. A cooled reinforced concrete base of the reactor with six base jacks was implemented on the bottom of the cavity. The bottom bedplate attached to the bottom supporting ring was held by jacks. Cooling coils were placed on the bottom of the bedplate to provide cooling.

The cylindrical graphite stack (3-m diameter and 4.5-m height) of the reactor was installed on the bottom bedplate. The stack was made of columns, assembled of hexagonal blocks (0.12-m width across corners) in the center and of sectors in the periphery. The central part of the stack was penetrated by vertical operating channels (long graphite cylinders containing inner thin steel tubes with fuel elements). The reactor core (7.2-m diameter and 6-m height) was surrounded with a 0.8-m-thick graphite reflector. An additional 1-m-thick graphite layer and an approximately 0.5-m cast iron layer over the upper reflector formed the principal part of the biological shield. A 0.6-m-thick graphite layer serving as the lower neutron shield was located below the lower reflector.

The graphite stack (9.6-m overall diameter and 9.0-m height) was enclosed in a gas-tight cylindrical carbon steel shell filled with nitrogen to prevent graphite deterioration. The outer graphite blocks were penetrated by steel uprights with horizontal lateral braces in several places along their height. The entire stack rested on the bottom bedplate. The graphite stack was covered on the top with a plate carrying standpipes with openings for the insertion of operating channels. The piping for feeding the coolant to the fuel bundles and for removing the coolant water from control rods was located between the standpipes. The piping of the operating channels and protective coating failure detection system was also located between the standpipes. The plate rested on supports installed on the tank of the side water shield. The plate was connected with the graphite stack shell by means of a compensator, which allowed both for vertical elongations of the shell and horizontal elongations of the plate, which occurred during heating (Yemelyanov et al., 1982).

As shown in Fig. A5.4, the reactor had 1134 operating channels and contained 998 fuel channels, 6 automatic control rods, 78 channels for reactivity compensating rods, 16 shutdown rods, and 36 channels for ionization chambers and counters. The fuel channels were comprised of 730 BW channels, also referred to in the literature as evaporating channels, and 268 SHS channels, also referred to in the literature as steam reheat channels.

The main parameters of the BNPP reactors are listed in Table A5.3.

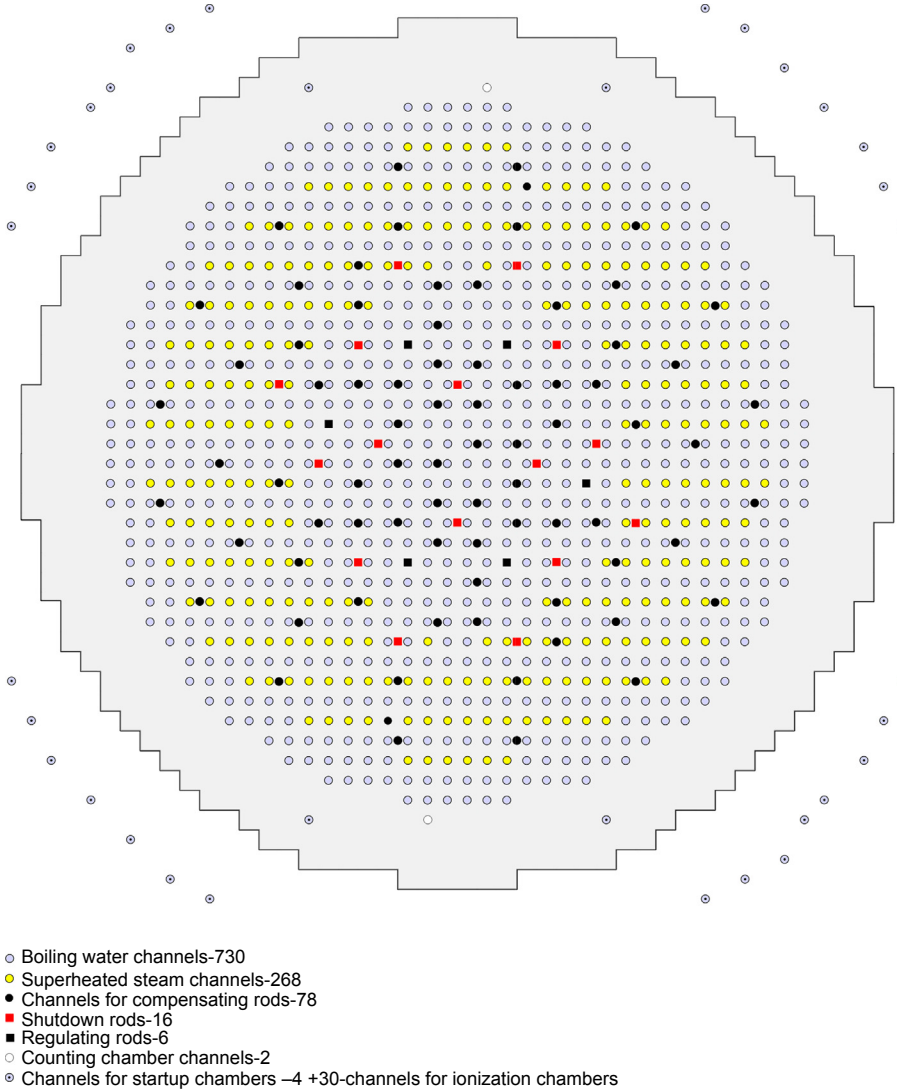


Figure A5.4 BNPP Unit 1 channels layout (Pioro et al., 2010).
This figure is based on the paper by Dollezhal, N.A., Krasin, A.K., Aleshchenkov, P.I., Galanin, A.N., Grigoryants, A.N., Emel'anov, I.Ya., Kugushev, N.M., Minashin, M.E., Mityaev, Yu.I., Florinsky, B.V., Sharapov, B.N., 1958. Uranium-graphite reactor with reheated high pressure steam. Proceedings of the 2nd International Conference on the Peaceful Uses of Atomic Energy, United Nations, Session G-7, P/2139, vol. 8, 398−414.

Table A5.3 Main parameters of BNPP reactors (Aleshchenkov et al., 1964; Dollezhal et al., 1969, 1971)

Parameters	BNPP Unit 1 (730 BWs and 268 SHSs)	BNPP Unit 2 (732 BWs and 266 SHSs)
Electrical power, MW_{el}	100	200
Number of K-100-90-type turbines	1	2
Inlet steam pressure, MPa	8.5	7.3
Inlet steam temperature, °C	500	501
Gross thermal efficiency, %	36.5	36.6
Total metal content (top and bottom plates, vessel, biological shielding tank, etc.), t	1800	1800
Weight of separator drums, t	94	156
Weight of circulation loop, t	110	110
Weight of graphite stacking, t	810	810
Uranium load, t	67	50
Specific load, MW_{th}/t	4.3	11.2
Uranium enrichment, %	1.8	3.0
Specific electrical energy production, MW_{el} days/t	4000	10,000
Square lattice pitch, mm	200	200
Core dimensions, m: diameter Height	7.2 6	7.2 6

A5.3.4 Physical parameters of Beloyarsk NPP reactors

Flattening of the power distribution was achieved at the BNPP with physical profiling: appropriate distribution of control rods and fuel channels of different uranium enrichment (for fresh load) and profiling of burnup fuel along the reactor radius. The reactor load consisted of SHS channels of 2% and 3% uranium enrichments (SHS-2 and SHS-3, respectively) and BW channels. The BW channels were located in rings in alternate locations with SHS-2. SHS-3 was located along the circumference and had lower pressure losses in the steam circuit (Dollezhal et al., 1964).

Neutronics calculations were made to choose optimal distribution of channels to achieve required power shape. Most of the calculations for the core reactor physics were performed in the two-group approximation. In accordance with the fuel channels distribution, the core was represented by four cylindrical regions with the radii: $R_1 = 175$ cm (234 fuel channels), $R_2 = 268$ cm (324 fuel channels), $R_3 = 316$ cm (220 fuel channels), and $R_4 = 358$ cm (220 fuel channels). The previous calculations

and operating experience of large uranium−graphite reactors with relatively small neutron leakage showed that a simplified schematic could be used when neutron distribution in the reactor was determined by the multiplication characteristics of the reactor regions. The multiplications constants obtained for the four regions ($k_{inf,1} = 1.013$, $k_{inf,2} = 1.021$, $k_{inf,3} = 1.043$, and $k_{inf,4} = 1.045$) allowed flattening of the neutron distribution along the reactor radius with $K_{ir} = 1.20-1.25$. The increase in the multiplication constants values towards the periphery of the reactor was attained by placing fuel channels with 3% uranium enrichment. Refueling schemes and, therefore, fuel burnup at different regions were chosen such as to allow designed power flattening in the end of the fuel campaign, with corresponding values of $k_{inf,i}$. Control rods insertion in the core maintained $k_{inf,i}$ values in the necessary limits during normal operation (Vikulov et al., 1971).

One of the requirements to be met when implementing nuclear steam reheat was to maintain a constant specified power ratio (π) between SHS and BW channels during the operating period. The SHS channel temperature up to 520°C at the BNPP was obtained by setting $\pi = 0.41$, which corresponded to the optimum parameters of the thermodynamic cycle. The number of SHS channels was chosen to provide a π value of 0.41 at the partial refueling scheme where the $K_{ir} \approx 1.25$. The steady-state regime was characterized with small fluctuations of approximately 1% in the π-value between the refuelings. Circular arrangement of SHS channels (Unit 1) had an advantage of small π sensitivity to the changes in radial neutron flux distributions, while for central arrangement of SHS channels (Unit 2), π values were more sensitive (see Table A5.4).

However, preference was given to the central arrangement of SHS channels because this allowed attaining a higher π value (around 12% higher) with the same number of SHS channels. Additionally, central arrangement of SHS channels provided better multiplication characteristics than BW channels. SHS channels were placed in the central region to increase average fuel burnup by 10%. It should be noted that during the initial operation period, the burnup rates were different for BW and SHS channels of fresh load, which led to an unbalance of power between superheating and boiling zones. Fig. A5.5 shows the calculated dependence of π values as well as ratios of power for different types of fuel channels to the power generated by the reactor (Vikulov et al., 1971).

Calculations were performed assuming $K_{ir} \approx 1.25$. A fast decrease in the superheating zone power relative to that of the boiling zone in the initial period was accounted for by a lower power change in SHS channels due to slightly higher fuel

Table A5.4 Steam superheating zone power-to-boiling zone power ratio (π) dependence on neutron flux K_{eff} for BNPP Unit 2 (Vikulov et al., 1971)

π	0.408	0.429	0.452	0.494
K_{eff}	1.20	1.36	1.53	1.78

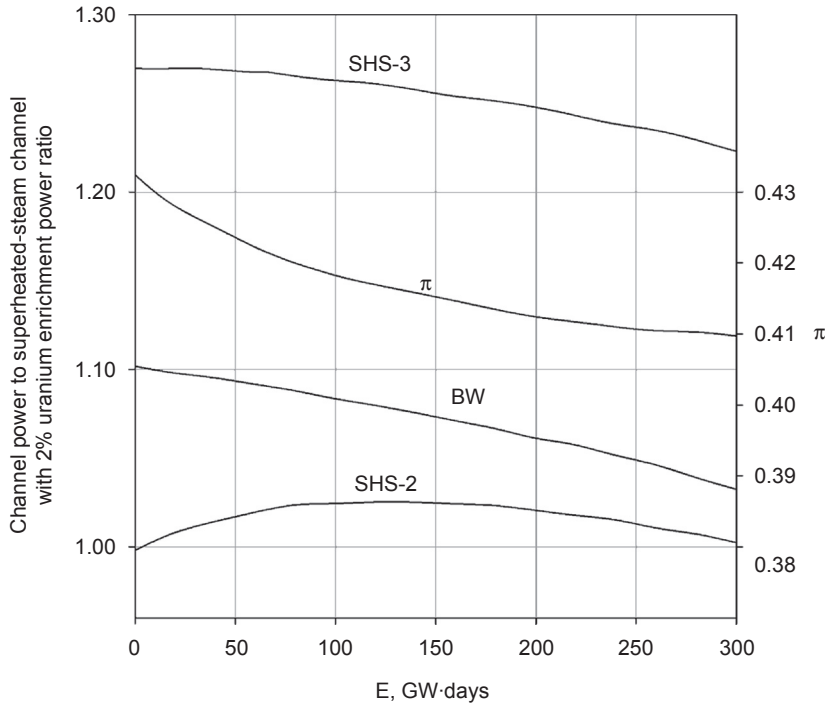


Figure A5.5 Channel power ratios and power split between SHS and BW channels (π) dependences on burnup produced by BNPP Unit 2 during the first operating period: SHS-3—superheated-steam channel with 3% uranium enrichment and SHS-2—superheated-steam channel with 2% uranium enrichment.
Based on the paper by Vikulov, V.K., Mityaev, Yu.I., Shuvalov, V.M., 1971. Some issues on Beloyarsk NPP reactor physics, (In Russian). Atomic Energy 30 (2), 132–137.

conversion in the low-enriched SHS-2. Practically achieved values of K_{ir} were approximately 1.4 for Unit 1 and 1.3 for Unit 2.

One of the features of the uranium–graphite reactors cooled with water was the possibility of reactivity change with water content change in the reactor. Substitution of BW with steam in the operating channels lead to the rapid change of coolant average density. Failure of a fuel element sheath was another possibility of water content change that was considered while designing the BNPP reactors. The chosen core lattice with respect to reactivity change turned out to be weakly dependent on water content changes. It was explained by the combination of the effects of increased resonance neutrons captured by increased water content and an increase at the same time of nonproductive neutrons absorption (Dollezhal et al., 1964). Normalized thermal neutrons distribution along the operating channel cell was studied experimentally for the reactor lattice as shown in Fig. A5.6. The gradients in the normalized thermal neutrons distributions along the reactor radius and height for both units indicated a significant disturbance in the normalized thermal neutron flux near the outer edge of the reactor

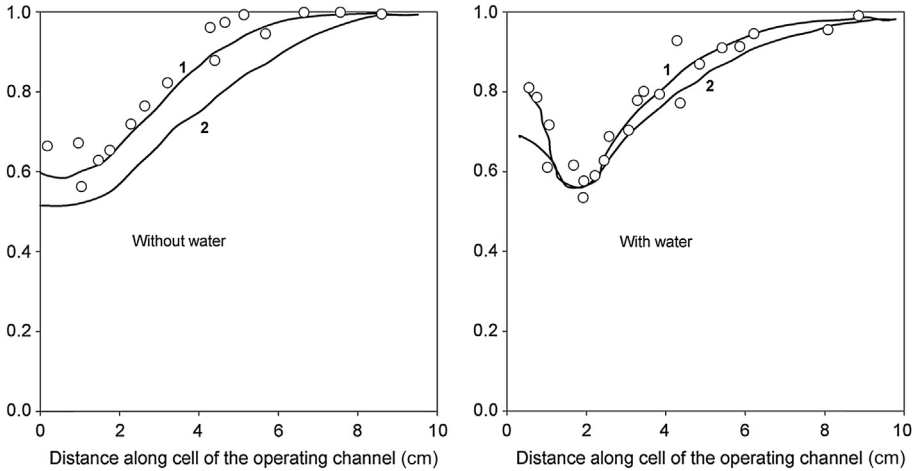


Figure A5.6 Normalized thermal neutrons density distribution along cell of the operating channel: (1) experimental curve; and (2) design curve.
Based on the paper by Dollezhal, N.A., Krasin, A.K., Aleshchenkov, P.I., Galanin, A.N., Grigoryants, A.N., Emel'anov, I.Ya., Kugushev, N.M., Minashin, M.E., Mityaev, Yu.I., Florinsky, B.V., Sharapov, B.N., 1958. Uranium-graphite reactor with reheated high pressure steam. Proceedings of the 2nd International Conference on the Peaceful Uses of Atomic Energy, United Nations, Session G-7, P/2139, vol. 8, 398–414.

likely where the steam reheat channels end, affecting the power distribution. The results indicated a more stable distribution for the BNPP Unit 2.

Distribution deformation near the end of operating period was explained by the nonuniform fuel burnup. The results proved a possibility of elementary diffusion theory application for determining neutron density distributions and showed the impact of the arrangement of the superheated steam channels on power distribution.

A5.3.5 Boiling water channels

Fault-free operation of BW channels was achieved with reliable crisis-free cooling of bundles and avoiding interchannel and subchannel pulsations of the coolant flow rate. The appropriate experiments were performed during design of the BNPP. As the result of the increased design power, the inner diameter of the fuel element was increased from 8.2 mm for Unit 1 to 10.8 mm for Unit 2. Note that an annular fuel design was used; thus an increased inner diameter resulted in thinner fuel and lower-centerline temperatures. Coolant was on the inside of the annular fuel and graphite was on the outside of the fuel.

Experiments were performed at different pressures and constant heat flux, steam content, and coolant mass fluxes. The experiments showed that wall temperature increase at the boiling crisis was higher when coolant pressure was lowered. At the same time, with the lowered coolant pressure, the critical steam content increased. The experiments on hydrodynamic stability showed that mass flux pulsations within

the region of high steam content did not introduce danger for the BNPP reactors because nominal pressure in the evaporating loop was 8.8 MPa, and steam content at the channels outlet was not higher than 35%. Wall temperature oscillations were in the phase with the subchannel flow rate pulsations. With the increased pressure, both the amplitude of temperature oscillations and coolant flow rate decreased. The same effect occurred at the decreased heat flux and increased flow rate per channel. Wall temperature oscillations were within the range of 65°C at 1000 kg/h flow rate and 30°C at 1500 kg/h flow rate at constant pressure of 4.9 MPa and 0.2 MW power (Dollezhal et al., 1964).

Fuel elements of larger inner diameter used at Unit 2 compared to that of Unit 1 allowed to lower heat flux and hydraulic resistance. With the equal outer diameter (20 mm), fuel elements inner diameter of the BWs at Unit 1 were 9.4 × 0.6 mm while that of Unit 2 were 12 × 0.6 mm. Diameter of the central tube for feeding the coolant was also increased. There were no other differences in the BWs construction used at BNPP Units 1 and 2. Uranium−molybdenum alloy with magnesium filler was used as fuel in the BWs.

A5.3.6 Superheated steam channels

At the BNPP, SHS channels were operated at higher temperatures compared to those in the BW channels and therefore limited the choice of fuel composite and materials. The development of fuel elements for SHS channels underwent several stages. Preliminary tests on the manufacturing technology and performance of fuel elements of various designs were made. As the result, a tubular fuel element with a stainless steel sheath and a uranium dioxide fuel composite was chosen for further development (Samoylov et al., 1976). Fuel elements in the initial modification had a tubular design. The elements were formed by two coaxial stainless steel sheaths (9.4 × 0.6 and 20 × 0.3 mm, respectively). Thus, SHS channels with such fuel elements did not differ significantly from BW channels (Fig. A5.7), consisting of six fuel elements arranged in a graphite collar with a central steam feeding tube. Steam entered the central tube and was superheated while passing along the fuel bundles.

Later, a U-shaped (or reentrant) design was developed. The central tube (9.4 × 0.6 mm) was replaced with an absorbing soft control rod (12 × 0.6 mm). The decreased width of the active material decreased nonproductive neutron absorption and allowed some power flattening. The steam was reheated, first passing downward along three fuel bundles and then passing upwards along another three fuel bundles. Such design reduced temperature conditions for SHS channels and allowed usage of simpler and cheaper materials. Also, reactor graphite stack temperature was lowered by 100°t at a channel power of 0.36 MW. This was achieved with the transfer of heat released in the graphite stack to the downward flow fuel elements that operated at intermediate temperatures (Dollezhal et al., 1964).

Efforts for further improvement of heat and physical parameters led to another modification of channels and fuel elements. One upward flowing fuel element was eliminated, inner fuel element sheath was increased to the size of 16 × 0.7 mm, and outer sheath size was increased to 23 × 0.3 mm.

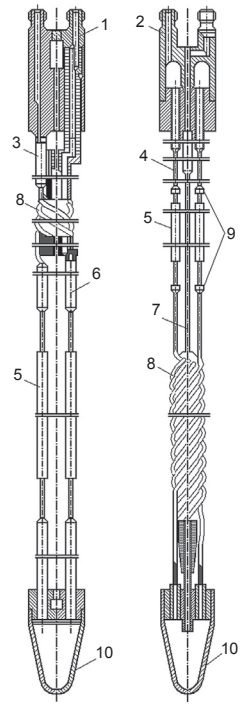


Figure A5.7 Principal design scheme of boiling-water and superheated steam channels: (1) head of boiling-water channel; (2) head of superheated-steam channel; (3) three downward-flow strings; (4) six upward-flow strings; (5) fuel bundle strings; (6) three upward-flow strings; (7) downward-flow strings; (8) compensators; (9) welded joints of tubes; and (10) tail. Based on the paper by Yemelyanov, I.Ya., Shasharin, G.A., Kyreev, G.A., Klemin, A.I., Polyakov, E.F., Strigulin, M.M., Shiverskiy, E.A., 1972. Assessment of the pumps reliability of the Beloyarsk NPP from operation data, (In Russian). Atomic Energy 33 (3), 729−733.

Physical and thermal parameters improved sharply after such a modification due to decreased matrix material in the fuel elements and increased flow cross section. Six element channels were gradually replaced by five element channels during refueling of the operating reactor. The removal of one of the elements allowed for an increase in steam velocity in the upward flowing fuel elements (Samoylov et al., 1976). Stainless steel was used as the outer sheath material. Uranium dioxide dispersed in matrix alloy was used as fuel elements in SHS channels. Improvements in the performance of various BNPP parameters are listed in Tables A5.5 and A5.6.

A5.3.7 Hydrodynamic stability of the Beloyarsk NPP channels during reactor startup

During startup and nominal operating conditions, it was necessary to provide reliable cooling of fuel bundles (crisis-free heat transfer and hydrodynamic stability).

Table A5.5 Average parameters of BNPP Unit 1 before and after installation of superheated steam channels (Dollezhal et al., 1969)

Parameters	Before SHSs installation	After SHSs installation
Electrical power, MW_{el}	60–70	100–105
Steam P_{in}, MPa	5.9–6.3	7.8–8.3
Steam T_{in}, °C	395–405	490–505
Exhaust steam P, kPa	9–11	3.4–4.0
Mass flow rate of water in 1st loop, kg/h	1400	2300–2400
P in separators, MPa	9.3–9.8	11.8–12.7
Gross thermal efficiency, %	29–32	35–36
Electrical power for internal needs, %	10–12	7–9

Experiments on setups simulating Units 1 and 2 were performed for determining safe operating conditions for coolant flow rate with no pulsations during the startup.

Both SHS and BW channels of the BNPP were filled with water in the initial state. During reactor startup, the water in the SHS channels was to be discharged, and a transition to cooling by steam was to be performed. Additionally, the units were preheated and started without external heat sources.

The coolant flow rate stability in the BW channels was studied for wide ranges of pressures, flow rates, and powers (Smolin et al., 1965). Special attention was paid to the determination of pressure, flow rate, steam content, and power. Various combinations of these parameters created conditions leading to pulsations. When they occurred, flow rate pulsations took place when coolant reached saturation temperature at the outlet of the BWs. Pulsations were in the form of coolant flow rate periodical oscillations in peripheral tubes. Oscillations were phase shifted in different tubes while the total flow rate was constant.

Two pulsation regions were determined as the result of the experiments: small steam content region ($x =$ 0–15%, 3–6 oscillations per min) and high steam content region ($x = 25$–80%, 15–20 oscillations per min). Flow rate pulsations in tubes were accompanied by wall tube temperature oscillations along its length with the frequency being equal to that of flow rate oscillations. Wall temperature oscillations in the top cross sections of the heating zone within the small steam content region occurred with a shift to the smaller values in the surface or volumetric boiling zones and to both the smaller and higher values in the economizer zone. Wall temperature oscillations in the top cross sections of the heating zone within the high steam content shifted only to the higher values causing boiling crisis (Smolin et al., 1965).

Table A5.6 Design parameters and operating conditions of superheated steam channels (Dollezhal et al., 1964)

Parameters	BNPP Unit 1	BNPP Unit 2 (U-shaped channel with 6 fuel elements)	
		Downward-flow fuel elements	Upward-flow fuel elements
Max. channel power, kW	368	767	
Min. channel power, kW	202	548	
Steam mass flow rate through max. power channel, kg/h	1900	3600	
Steam mass flow rate through channel operating at minimal power, kg/h	1040	2570	
Steam P_{in}/P_{out}, MPa	10.8/9.81	12.9/12.3	12.2/10.8
Steam T_{in}/T_{out}, °C	316/510	328/399	397/508
Max heat flux, MW/m^2	0.56	0.95	0.79
Max steam velocity, m/s	57	76	112
Max T, °C			
Sheath	530	426	531
Fuel	550	482	565
Graphite	725	735	735

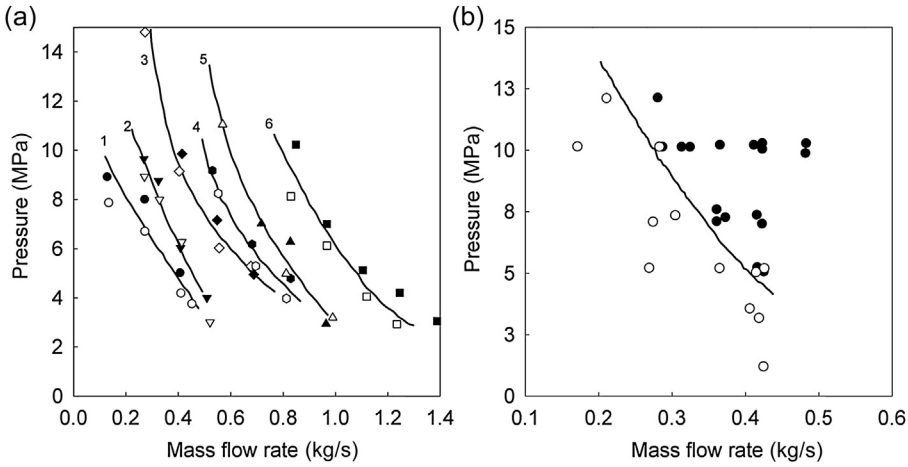


Figure A5.8 Ranges of hydrodynamic stability in BW (a) and SHS (b) channels of BNPP Unit 2 at different channel power (regions of channels stable operation are above curves, closed symbols): (1) 50 kW; (2) 100 kW; (3) 200 kW; (4) 300 kW; (5) 400 kW; and (6) 800 kW. Based on the paper by Smolin, V.N., Polyakov, V.K., Esikov, V.I., Shuyinov, Yu.N., 1965. Test stand study of the start-up modes of the Kurchatov's Beloyarsk nuclear power plant, (In Russian). Atomic Energy 19 (3), 261–269.

The curves distinguishing stability zones (above the curves) from pulsation zones (below the curves) for the BW and SHS channels of the BNPP Unit 2 are shown in Fig. A5.8.

As seen in Fig. A5.8, the range of stable operation of channels broadens with the increase in pressure or increase in flow rate. The stable operation range contracts with the increase in power. The operating conditions that provided stable flow rate and reliable cooling of the BW and SHS channels at the startup and nominal operating conditions were chosen based on the performed research. The method of replacing water coolant by steam coolant in SHS channels using accumulated heat was accepted for experimental testing of startup conditions on Unit 1. The method of gradual replacement of water in the SHS channels first by a water–steam mixture and then by steam was accepted for experimental tests of startup regime on Unit 2 (Smolin et al., 1965). The experimentally obtained data are presented in Figs. A5.9 and A5.10.

Both methods were elaborately tested and proved to provide reliable cooling of the BW and SHS channels during the startup. They were adapted for the development of the BNPP startup conditions.

A5.3.8 Startup of Beloyarsk NPP reactors

The startup testing of the Unit 1 and Unit 2 reactors of the BNPP is described in this section. During the Unit 1 startup: (1) both loops were filled with deaerated water; (2) water circulation was established; (3) air was removed; and (4) the pressure was raised up to 10 and 3 MPa in the primary and secondary loops, respectively (Aleshchenkov et al., 1971).

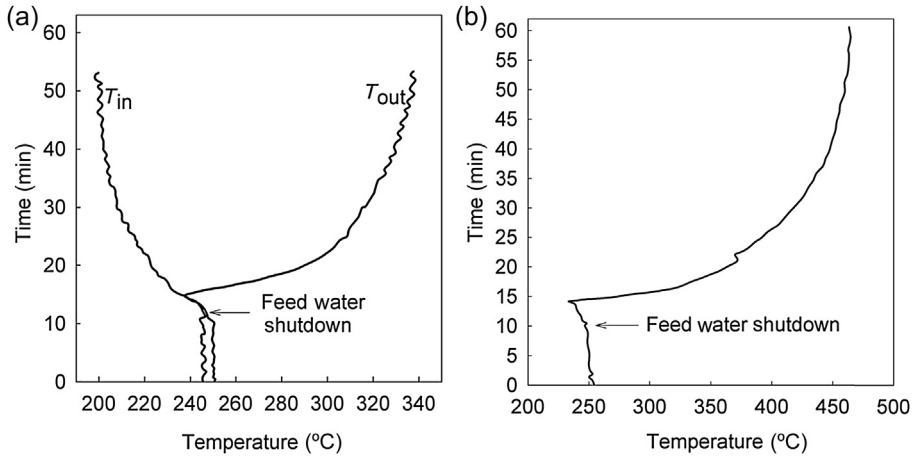


Figure A5.9 Temperature variations at BNPP Unit 1 SHS channels at transitional regime: (a) coolant inlet (T_{in}) and outlet temperatures (T_{out}), and (b) sheath temperature.
Based on the paper by Smolin, V.N., Polyakov, V.K., Esikov, V.I., Shuyinov, Yu.N., 1965. Test stand study of the start-up modes of the Kurchatov's Beloyarsk nuclear power plant, (In Russian). Atomic Energy 19 (3), 261−269.

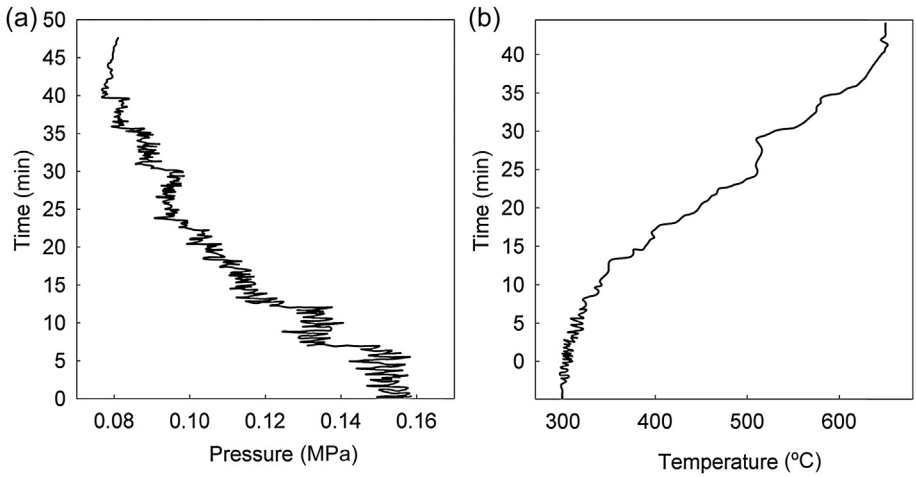


Figure A5.10 Variations of pressure drop (a) and sheath temperature (b) at BNPP Unit 2 during high-power startup.
Based on the paper by Smolin, V.N., Polyakov, V.K., Esikov, V.I., Shuyinov, Yu.N., 1965. Test stand study of the start-up modes of the Kurchatov's Beloyarsk nuclear power plant, (In Russian). Atomic Energy 19 (3), 261−269.

Equipment was heated up at 10−14% of reactor power. Average heat-up rate was kept at 30°C/h as measured at the separators. This value was chosen based on experience of drum boilers operation, though reactor equipment allowed significantly higher heat-up rate. No heat removal was provided during the heat-up to the 160°C coolant temperature at the reactor outlet. The water level was formed at 160°C in the bubbler, and the excess heat started being released to the turbine condenser. When water temperature at the outlet of the SHS channels reached 230°C, the heat-up was terminated. Total heat-up time was about 9 h.

At the next step, water was purged from SHS channels. The transient processes took place in the second loop, while constant pressure and boiling-free cooling of BWs were provided in the primary loop. Reactor power was rapidly reduced to ~2% of its nominal level and feedwater flow rate was reduced to provide water level in the SGs to purge SHS channels. The water−steam mixture from evaporators and steam from the steam loop were directed to the bubbler and then to the deaerator and the turbine condenser.

The purging of SHS channels started after the level in the SGs had been formed. The purging regime was monitored by the pressure drop between the reactor inlet and outlet steam headers and the coolant temperature at the outlet of each SHS channel. Additional steam discharge by increased pressure drop rate was achieved, and consequently, the purging was accelerated by opening gate valves in front of the bubbler for 1−2 min. The pressure drop rate was chosen based upon the allowed temperature condition and was set to ~0.15 MPa/min. Overall time for the level formation in the evaporators was ~8−10 min, and the time of purging ~6−10 min. The gate valves in front of bubblers were closed, and reactor power was increased after the purging had finished. Thus, the pressure and the temperature in SHS channels were increased. After 2 h, the purging of SHS channels had been finished, and the reactor achieved a stable operation at 10% power level. Heating of steam pipes and the turbine was initiated, and the turbine connection to the power line was prepared. Further power increase was made once the turbine had been connected to the power line.

The first loop was transitioned to the boiling flow regime, and the separators levels were formed at 35% reactor power and ~6 MPa pressure. During the transient to the boiling regime, the operating conditions of the main circulation pumps (MCPs) were continuously monitored. Water temperature was maintained at 5−6°C below the boiling margin for intake pipes of the MCPs. Level formation in the separators was accompanied by a smooth pressure change. It took about 3 h for the water to reach controlled level in the separators, the time being dependent only on the separator bleed lines throughput.

The specifics of a single-circuit flow design of the BNPP Unit 2 made its sequence startup operations somewhat different. SHS channels purging and transition to boiling regime in the BW channels took place simultaneously. Filling of the circuits and equipment heat-up were the same as in Unit 1. The terminal heat-up parameters were higher ($P \approx 9.3$ MPa and $T \approx 290$°C). Two MCPs were used to drive coolant circulation in the evaporating loop. SHS channels purging and transition to boiling regime in the BW channels took place after the heat-up. The feedwater flow rate was considerably reduced, water was purged out of the separators, and the flow rate to the bubblers was increased to form levels in the separators. As a result, the water in the fuel channels and separators boiled, causing the purging of water and water−steam mixture

from SHS channels. The monitoring of the purging process was the same as at the Unit 1. After SHS channels purging had been completed, the reactor power was increased, and steam flow into the bubbler was reduced at the reheated steam temperature rise rate of about 1°C/min with the pressure drop between the steam headers of at least ~50−60 kPa. The automatic level control system was put into operation as soon as the water in the separators reached the rated level. The subsequent reactor power increase, turbine preparation, and connection of the turbine to the power line were the same as for Unit 1 (Aleshchenkov et al., 1971).

A5.3.9 Pumps

All pumps at the BNPP were of high-speed type (3000 rpm). Serial high-power feeding pumps were used. Other pumps were of special canned type in which the motor spindle and pump spindle were revolved in a pumped medium and were separated from the motor stator by a thin hermetic nichrome plate. Bearing pairs of the pumps were lubricated and cooled by pumped water. The revolving details of bearings were made of advanced hard alloys and bearing bushes were made of special plastics. Some minor failures were observed in operation of MCP (Yemelyanov et al., 1972). Those were due to: (1) cracks in nichrome jacket; (2) malfunctioning of fan of the stator front parts; (3) pilot-valve distribution system imperfections; and (4) failures of the fasteners in the pump interior. Modernizations of some individual elements of the MCP and reconstruction of independent pump cooling loops improved optimal on-stream time between maintenance and repairing (16,000 h). As a result, the failure probability of the MCP was reduced to minimum. Operating experience of the MCPs showed that serial pumps could be used instead of specially designed canned pumps under no fragment activity in the loops conditions that were achieved at BNPP.

A5.3.10 Water chemistry

The experiments on effectiveness of water and steam radiolysis suppression by hydrogen in BW and SHS channels were performed after 16 months of Unit 1 operation. Water and steam samples were taken at the drum separator, MCPs, inlet, and outlet of SHS channels. Ammonia dosing was terminated before the test for determination of the required amount of hydrogen that was necessary to suppress water and steam radiolysis that was partially caused by ammonia decomposition (Yurmanov et al., 2009b). Hydrogen concentration in saturated steam at the separator was found to be 45−88 nmL/kg, and in circulation water at the main circulation pump was found to be 2.75−12.8 nmL/kg. Despite some hydrogen excess, oxygen concentration decreased from 2.28 to 0.1 mg/dm^3. Dissolved oxygen concentration in the circulating water at the MCP did not exceed 0.01−0.03 mg/dm^3. At the next stage of experiments, steam radiolysis in SHS channels and the possibility of suppressing it by hydrogen concentration levels were studied. Hydrogen concentration was set to 1.2−6.2 nmL/kg in steam and 1.2−1.8 nmL/kg in circulating water. Oxygen concentration was below 0.15 mg/kg in steam and about 0.02 mg/dm^3 in the circulating water. The obtained results demonstrated effective suppression of water radiolysis.

Additional research was carried out at 60% reactor power. The results showed that the oxygen concentration was decreased to 0.03 mg/kg at the SHS channels outlet only at 45-nmL/kg hydrogen concentration. The water−steam mixture at the turbine ejector consisted of hydrogen (62−65%) and oxygen (8−10%) at a hydrogen concentration of 40−45 nmL/kg. The water−steam mixture had to be diluted with air to a nonexplosive state, ie, hydrogen volume fraction was to be decreased below 2−3% (Shitzman, 1983).

The equipment for Unit 2 was made from the following constructional materials: stainless steel (5500 m^2, 900 m^2 of which were used for the core), carbon steel (5600 m^2), brass and cupronickel (14,000 m^2), and stellite (4.8 m^2). The studies showed that radiolytic gases production rate was approximately five times lower than that of a BWR of the same power. Water radiolysis at the BW channels of the BNPP Unit 1 was suppressed by ammonia dosing. This kept radiolytic oxygen content in water at several hundredths of a milligram per liter. Ammonia dosing was not used at Unit 2 due to the danger of corrosion of the condenser tubes and low-pressure heaters. Radiolytic fixation of oxygen in the steam that was bled to high-pressure heaters was achieved by hydrazine hydrate dosing. The operation norms and the actual quality of coolant at the BNPP Unit 2 are listed in the Table A5.7. Additional information on water flow regime may be found in paper by Konovalova et al. (1971).

All the indicators of coolant quality were in the range set by the water regime regulations during normal operating period.

In August 1972 (after 4.5 years of operation), neutral no-correction water was implemented at Unit 2 (Dollezhal et al., 1974). Operation in the new conditions revealed the following advantages over the ammonia-treated state:

1. The cease of feedwater ammonia treatment led to the zero nitrate content in the reactor circulation water. This allowed an increase of the pH from 4.8 to the neutral level at the 300°C operating temperature.
2. Balance of the corrosion products content in the circulation water and chemical flushing of the BW channels showed that the rate of metallic oxide deposits formation on the fuel bundles surfaces in the evaporating zone of the reactor was three times lower using no-correction water.
3. The Co-60 deposition rate outside the core was 7−10 times lower using no-correction water.
4. Condensate purification experience using no-correction water allowed a six-fold increased filter service cycle.

A5.3.11 Modular reactor with steam reheat

The BNPP became the first in the world industrial NPP with a uranium−graphite power reactor. Examination of the main characteristics of the BNPP reactors (for example, see Table A5.3) shows that performance of such type of reactors could be improved. BNPP used slightly enriched uranium, and the calculations showed that increasing enrichment to 5% would increase fuel burnup 4−10 times (up to 40,000 MW days/t).

Table A5.7 Actual parameters of BNPP Unit 2 coolant quality during period of normal operation (Konovalova et al., 1971)

Parameters	Feedwater	Reactor circulating water	Reactor bleed water	Saturated/reheated steam	Turbine condensate
SiO_3^{2-}, μg/kg	–	–	100–300	5–15/5–15	–
Chlorides, μg/kg	25	25	25	–/–	–
Iron oxides, μg/kg	20–60	20–60	30–60	20–30/20–30	0
Copper, μg/kg	–	–	7–30	0.4/–	0.8
Specific activity, Ci/L	–	–	10^{-5}	$-/10^{-7}$	–
Oxygen, μg/kg	10–15	30	30	$(5–6) \times 10^3/(5–6) \times 10^3$	40–50
Ammonia, mg/kg	1–25	0.6–1.4	0.6–1.4	0.8–2/0.8–2	1–2
pH	9.2–9.5	8–9	9–9.5	9–9.5/9–9.5	9–9.5

All channel reactors were constructed with traditional cylindrical shape of core. Therefore, power increase in such a reactor could be attained by increasing the number of working channels in the core and a proportional increase in diameter size. However, increase in power per reactor would then be limited by the maximum size of the reactor upper plate that could be built and withstand a high load. A solution to this situation was found in modular design of the channel reactor with a rectangular core. Such a shape would allow separating not only the core, but also the reactor as a whole into equal geometry sections. Then the reactor of a specified capacity can be constructed of the required number of modules. Each module would stay the same for reactors of different power outputs, and, consequently, core width and maximum size of the upper metalwork would stay the same too. Therefore, the power of a modular power would not be limited by the size of the upper plate (Yemelyanov et al., 1982).

A modular-type reactor with coolant at supercritical fluid conditions (see Fig. A5.11) was developed at Research and Development Institute of Power Engineering (RDIPE, Moscow, Russia) as an improvement to the existing RBMK (Russian acronym for Pressure Channel Reactor of High Power).

Rod fuel bundles were inserted into zirconium SHS (SHS-Z) channels (see Fig. A5.12) on the core level. UO_2 fuel elements with steel sheath were designed. Fuel bundles were covered by a sheath to hold SHS-Z channel wall below 360°C (Grigoryants et al., 1979). Therefore, saturated steam entering the channel was split into two streams. About 25% of the steam flowed through the annular gap cooling the SHS-Z channel wall. Both streams mixed at the core exit. Steam mixture was at about 455°C. Tests with SHS-Z channels were performed in BNPP Unit 1 to check design decisions. SHS-Z channels were tested during 23–24 start-ups–shutdowns,

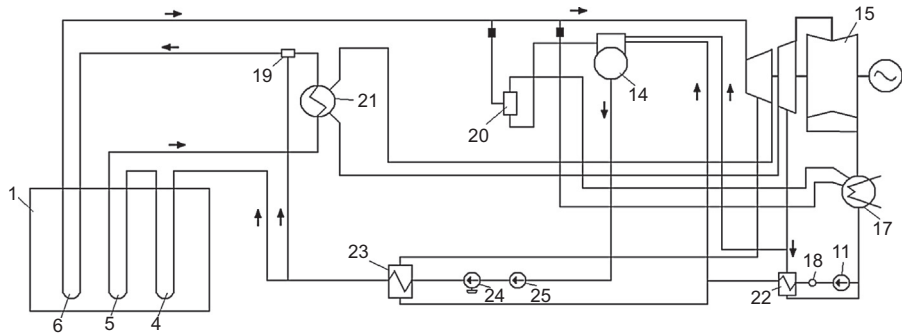


Figure A5.11 Schematic of RDIPE SCW NPP: (1) reactor; (4) preheating channel; (5) first SHS; (6) second SHS; (11) condensate extraction pump; (14) deaerator; (15) turbo-generator; (17) condenser; (18) condenser purifier; (19) mixer; (20) startup separator; (21) intermediate steam reheater; (22) low-pressure regenerative preheater; (23) high-pressure regenerative preheater; (24) feed turbo-pump; and (25) booster pump.
Based on the paper by Aleshchenkov, P.I., Zvereva, G.A., Kireev, G.A., Knyazeva, G.D., Kononov, V.I., Lunina, L.I., Mityaev, Yu.I., Nevskii, V.P., Polyakov, V.K., 1971. Start-up and operation of channel-type uranium-graphite reactor with tubular fuel elements and nuclear steam reheating, Atomic Energy (Атомная Энергия, Стр. 137–144) 30 (2), 163–170.

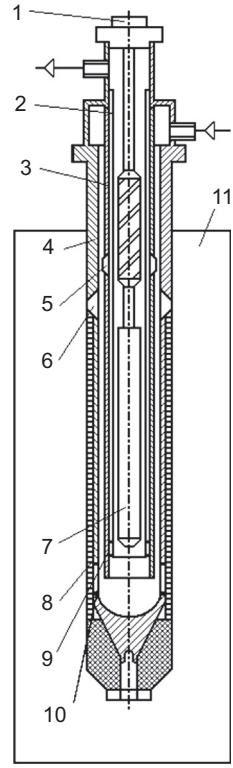


Figure A5.12 Principal scheme of SHS-Z: (1) suspension rod; (2) thermal screen; (3,4) outer and inner tubes of bearing body; (5) inner tube reducer; (6) upper reducer of outer tube; (7) fuel bundle; (8) graphite sleeves; (9) thermal screen and inner tube seal; (10) lower reducer of outer tube; and (11) reactor.
Based on paper by Mikhan, V.I., Glazkov, O.M., Zvereva, G.A., Mihaylov, V.I., Stobetskaya, G.N., Mityaev, Yu.I., Yarmolenko, O.A., Kozhevnikov, Yu.N., Evdokimov, Yu.V., Sheynkman, A.G., Zakharov, V.G., Postnikov, V.N., Gladkov, N.G., Saraev, O.M., 1988. Reactor testing of zirconium steam-reheat channels with rod fuel elements in reactors of the first stage of BNPP (In Russian). In: BNPP Operating Experience: Information Materials (In 4 Volumes). USSR Academy of Sciences, Ural Branch, 207 pp.

including 11 emergency shutdowns of the reactor when the steam temperature rate of change was 20−40°C/min during the first 3 min of an automatic control system operation, and 5°C/min after that.

SHS-Z channel wall temperature reached 400−700°C and that of the fuel bundles sheath reached 650−740°C during startup operation at the steam pressure of 2.45−4.9 MPa. Channels were operated about 140 h at high temperature conditions. Studies showed that fuel element seal failures were mainly due to short-duration overheating (Mikhan et al., 1988).

Additional information on SHS-Z-channel tests in BNPP Unit 1 may be found in the papers by Grigoryants et al. (1979) and by Mikhan et al. (1988).

A5.4 Conclusions

The worldwide operating experience of the reactors with nuclear steam reheat provides vital information on physical and engineering challenges associated with implementation of steam reheat in conceptual SCWRs. Major advancements in implementation of steam reheat inside the reactor core were made in the US and Russia in 1960s−70s. Three experimental reactors were designed and tested in the 1960s−70s in the US. In the former Soviet Union, nuclear steam reheat was implemented at two units at the Beloyarsk NPP. Operating experience of the units showed a possibility of reliable and safe industrial application of nuclear steam reheat right up to outlet temperatures of 510−540°C after over a decade of operation. Thermal efficiency of the Beloyarsk NPP units was increased by from ∼33% to ∼38% as the result of implementing nuclear steam reheat. The introduction of nuclear steam reheat was economically justified in cases where the steam was superheated up to 500°C and higher with the use of stainless steel sheath fuel elements.

The experiments and operating experience obtained to date also indicate that further improvements in SHS channel design and in reactor design are possible.

Nomenclature

k	Multiplication constant
K_{ir}	Neutron flux irregularity coefficient
R	Radius, m

Greek letters

π	Power split between superheated steam and boiling water and channels

Subscripts

In	Inlet
inf	Infinite
Out	Outlet

Abbreviations and acronyms

BNPP	Beloyarsk nuclear power plant
BONUS	BOiling NUclear Superheater
BORAX	BOiling Reactor Experiment
BW	Boling water (channel)
ESADE	Expanded Superheat advance demonstration experiment
FWP	Feedwater pump
MCP	Main circulation pump
NSERC	Natural Sciences and Engineering Research Council
RBMK	Russian acronym for channel reactor of high power
RDIPE	Research and development Institute of Power Engineering (Moscow, Russia)
SADE	Superheat Advance Demonstration Experiment
SCW	Supercritical water
SG	Steam generator
SHS	SuperHeated steam (channel)
SS	Stainless steel
USAEC	United States Atomic Energy Commission
Z	Zirconium

References

Aleshchenkov, P.I., Mityaev, Yu.I., Knyazeva, G.D., Lunina, L.I., Zhirnov, A.D., Shuvalov, V.M., 1964. The Kurchatov's Beloyarsk nuclear power plant (In Russian). Atomic Energy 16 (6), 489–496.

Aleshchenkov, P.I., Zvereva, G.A., Kireev, G.A., Knyazeva, G.D., Kononov, V.I., Lunina, L.I., Mityaev, Yu.I., Nevskii, V.P., Polyakov, V.K., 1971. Start-up and operation of channel-type uranium-graphite reactor with tubular fuel elements and nuclear steam reheating. Atomic Energy (Атомная Энергия, Стр. 137–144) 30 (2), 163–170.

Baturov, B.B., Zvereva, G.A., Mityaev, Yu.I., Mikhan, V.I., 1978. Nuclear reheating of steam, results and prospects at the present stage. Atomic Energy (Атомная Энергия, стр. 126–131) 44 (2), 131–137.

Dollezhal, N.A., Krasin, A.K., Aleshchenkov, P.I., Galanin, A.N., Grigoryants, A.N., Emel'anov, I.Ya., Kugushev, N.M., Minashin, M.E., Mityaev, Yu.I., Florinsky, B.V., Sharapov, B.N., 1958. Uranium-graphite reactor with reheated high pressure steam. In: Proceedings of the 2nd International Conference on the Peaceful Uses of Atomic Energy, United Nations, vol. 8, pp. 398–414. Session G-7, P/2139.

Dollezhal, N.A., Emel'yanov, I.Ya., Aleshchenkov, P.I., Zhirnov, A.D., Zvereva, G.A., Morgunov, N.G., Mityaev, Yu.I., Knyazeva, G.D., Kryukov, K.A., Smolin, V.N., Lunina, L.I., Kononov, V.I., Petrov, V.A., 1964. Development of power reactors of BNPP-type with nuclear steam reheat (In Russian). Atomic Energy (11), 335–344 (Report No. 309, 3rd International Conference on Peaceful Uses of Nuclear Energy, Geneva, 1964).

Dollezhal, I.Ya., Aleshchenkov, P.I., Evdokimov, Yu.V., Emel'yanov, I.Ya., Ivanov, B.G., Kochetkov, L.A., Minashin, M.E., Mityaev, Yu.I., Nevskiy, V.P., Shasharin, G.A., Sharapov, V.N., Orlov, K.K., 1969. BNPP operating experience (In Russian). Atomic Energy 27 (5), 379–386.

Dollezhal, N.A., Aleshchenkov, P.I., Bulankov, Yu.V., Knyazeva, G.D., 1971. Construction of uranium-graphite channel-type reactors with tubular fuel elements and nuclear-reheated steam. Atomic Energy (Атомная Энергия, стр. 149–155) 30 (2), 177–182.

Dollezhal, N.A., Malyshev, V.M., Shirokov, S.V., Emel'yanov, I.Ya., Saraev, Yu.P., Aleshchenkov, P.I., Mityaev, Yu.I., Snitko, E.I., 1974. Some results of operation of the I.V. Kurchatov nuclear power station at Belyi Yar. Atomic Energy (Атомная Энергия, Стр. 432–438) 36 (6), 556–564.

Grigoryants, A.N., Baturov, B.B., Malyshev, V.M., Shirokov, S.V., Mikhan, V.I., 1979. Tests on zirconium SRCh in the first unit at the Kurchatov Beloyarsk nuclear power station. Atomic Energy (Атомная Энергия, Стр. 55–56) 46 (1), 58–60.

Konovalova, O.T., Kosheleva, T.I., Gerasimov, V.V., Zhuravlev, L.S., Shchapov, G.A., 1971. Water-chemical mode at the NPP with channel reactor and nuclear steam reheat (In Russian). Atomic Energy 30 (2), 155–158.

Mikhan, V.I., Glazkov, O.M., Zvereva, G.A., Mihaylov, V.I., Stobetskaya, G.N., Mityaev, Yu.I., Yarmolenko, O.A., Kozhevnikov, Yu.N., Evdokimov, Yu.V., Sheynkman, A.G., Zakharov, V.G., Postnikov, V.N., Gladkov, N.G., Saraev, O.M., 1988. Reactor testing of zirconium steam-reheat channels with rod fuel elements in reactors of the first stage of BNPP (In Russian). In: BNPP Operating Experience: Information Materials (In 4 Volumes). USSR Academy of Sciences, Ural Branch, 207 pp.

Novick, M., Rice, R.E., Graham, C.B., Imhoff, D.H., West, J.M., 1965. Developments in nuclear reheat. In: Proceedings of the 3rd International Conference, Geneva, vol. 6, pp. 225–233.

Petrosyants, A.M., 1969. Power reactors for nuclear power plants (from the first in the world to the 2-GW electrical power NPP) (In Russian). Atomic Energy 27 (4), 263–274.

Pioro, I., Saltanov, Eu.., Naidin, M., King, K., Farah, A., Peiman, W., Mokry, S., Grande, L., Thind, H., Samuel, J., Harvel, G., 2010. Steam-reheat option in SCWRs and experimental BWRs. In: Report for NSERC/NRCan/AECL Generation IV Energy Technologies Program (NNAPJ) Entitled "Alternative Fuel-channel Design for SCWR" with Atomic Energy of Canada Ltd., Version 1, UOIT, Oshawa, on, Canada, March, 128 pp.

Ross, W.B., 1961. Pathfinder Atomic Power Plant, Superheater Temperature Evaluation Routine, an IBM-704 Computer Program. United States Atomic Energy Commission, Office of Technical Information, Oak Ridge, TN, 49 pp.

Samoilov, A.G., Pozdnyakova, A.V., Volkov, V.S., 1976. Steam-reheating fuel elements of the reactors in the I.V. Kurchatov Beloyarsk nuclear power station. Atomic Energy (Атомная Энергия, стр. 371–377) 40 (5), 451–457.

Shitzman, M.E., 1983. Neutral-oxygen Water Regime at Supercritical-pressure Power Units (In Russian). Energoatomizdat Publishing House, Moscow, Russia.

Smolin, V.N., Polyakov, V.K., Esikov, V.I., Shuyinov, Yu.N., 1965. Test stand study of the start-up modes of the Kurchatov's Beloyarsk nuclear power plant (In Russian). Atomic Energy 19 (3), 261–269.

USAEC Report ACNP-5910, 1959. Allis-Chalmers Manufacturing Co., Pathfinder Atomic Power Plant (Final Safeguards Report, May).

USAEC Report PRWRA-GNEC 5, 1962. General Nuclear Engineering Corp., BONUS (Final Hazards Summary Report, February).

USAEC Report (MaANL-6302), 1961. Design and Hazards Summary Report—Boiling Reactor Experiment V (Borax-v). Argonne National Laboratory.

Vikulov, V.K., Mityaev, Yu.I., Shuvalov, V.M., 1971. Some issues on Beloyarsk NPP reactor physics (In Russian). Atomic Energy 30 (2), 132−137.

Yemelyanov, I.Ya., Shasharin, G.A., Kyreev, G.A., Klemin, A.I., Polyakov, E.F., Strigulin, M.M., Shiverskiy, E.A., 1972. Assessment of the pumps reliability of the Beloyarsk NPP from operation data (In Russian). Atomic Energy 33 (3), 729−733.

Yemelyanov, I.Ya., Mikhan, V.I., Solonin, V.I., Demeshev, R.S., Rekshnya, N.F., 1982. Nuclear Reactor Design (In Russian). Energoizdat Publishing House, Moscow, Russia, 400 pp.

Yurmanov, V.A., Belous, V.N., Vasina, V.N., Yurmanov, E.V., 2009a. Chemistry and corrosion issues in supercritical water reactors. In: Proceedings of the IAEA International Conference on Opportunities and Challenges for Water Cooled Reactors in the 21st Century, Vienna, Austria, October 26−30.

Yurmanov, V.A., Vasina, V.N., Yurmanov, E.V., Belous, V.N., 2009b. Water regime features and corrosion protection issues in NPP with reactors at supercritical parameters (In Russian). In: Proceedings of the IAEA International Conference on Opportunities and Challenges for Water Cooled Reactors in the 21st Century, Vienna, Austria, October 26−30.

Appendix A6: Comparison of thermophysical properties of selected gases at atmospheric pressure

I.L. Pioro[1], *P.L. Kirillov*[2]
[1] University of Ontario Institute of Technology, Oshawa, Ontario, Canada, [2] State Scientific Centre of the Russian Federation - Institute of Physics and Power Engineering (IPPE) named after A.I. Leipunsky, Obninsk, Russia

This appendix shows various thermophysical properties of selected gases at atmospheric pressure (0.1 MPa). Application of selected gases in nuclear power and other industries is based on some specific properties of selected gases. Selected gases and their basic properties are listed in Table A6.1. Thermophysical property profiles versus temperature of selected gases at 0.1 MPa are shown in Fig. A6.1. Summary data on current and future applications of selected gases are listed in Table A6.2.

Table A6.1 Basic properties of selected gases

No.	Gas	Molar mass kg/kmol	Triple point (T) K / °C	Normal boiling (T) K / °C	T_{cr} K / °C	P_{cr} MPa	ρ_{cr} kg/m^3
1	Air, N_2 (78%) + O_2 (21%) + Ar (1%)	28.965	59.75 −213.4	78.903 −194.25	132.53 −140.62	3.786	342.68
2	Argon, Ar	39.95	83.806 −189.34	87.302 −185.85	150.69 −122.46	4.863	536.6
3	Carbon dioxide, CO_2	44.01	**216.59** **−56.56**	**194.69** **−78.46**	**304.13** **30.98**	**7.377**	467.6
4	Helium, He	4.00	***2.1768*** ***−270.97***	***4.222*** ***−268.93***	***5.1953*** ***−267.95***	***0.228***	72.6
5	Hydrogen, H_2	***2.02***	13.957 −259.19	20.369 −252.78	33.145 −240.01	1.296	***31.3***
6	Krypton, Kr	**83.80**	115.78 −157.37	119.73 −153.42	209.48 −63.67	5.525	**909.2**

Bold and italic indicate the lowest value. *Bold* indicates the highest value.
Data from NIST REFPROP, Ver. 9.1. http://www.nist.gov/srd/nist23.cfm.

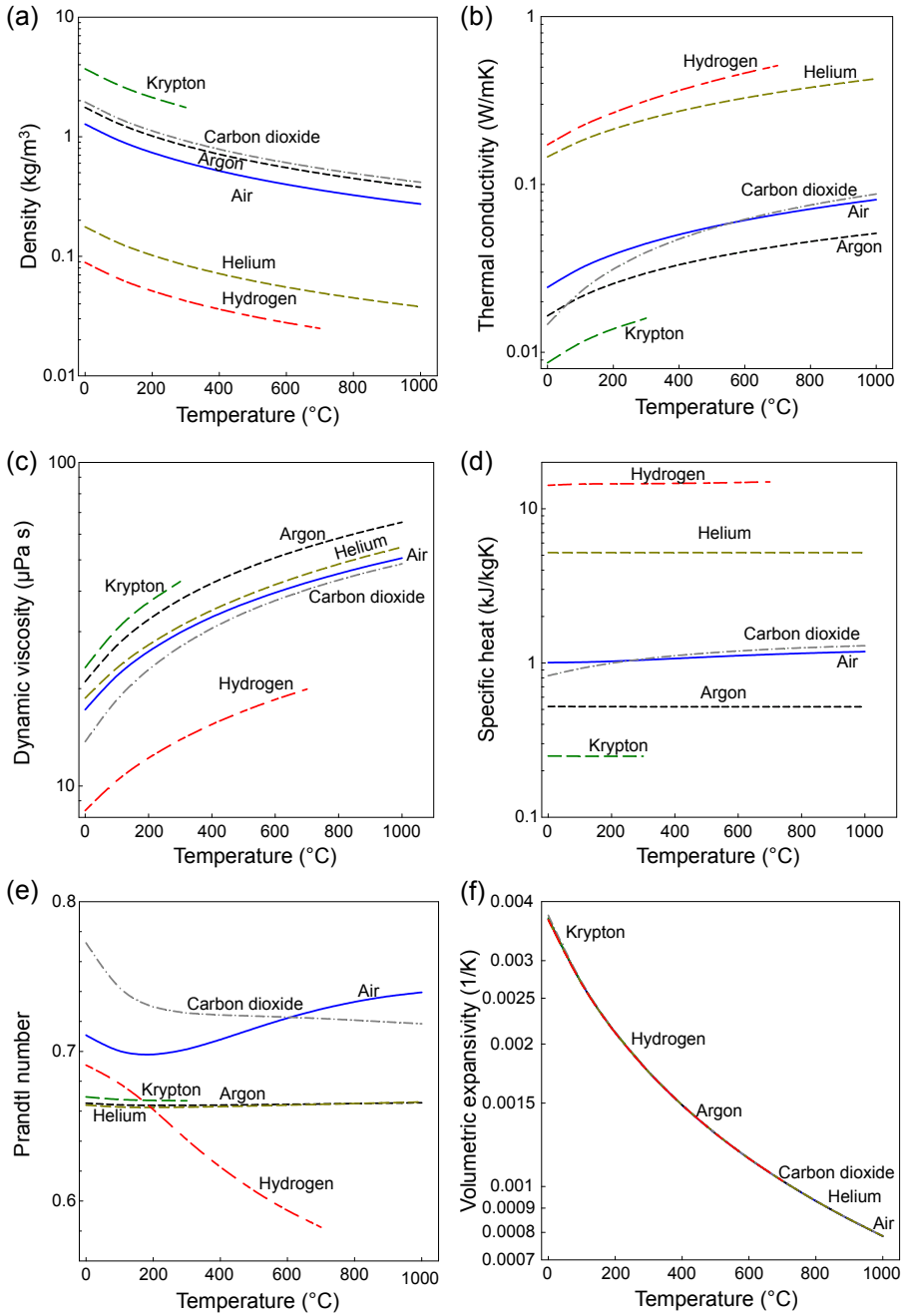


Figure A6.1 Thermophysical property profiles versus temperature of selected gases at 0.1 MPa: (a) density, (b) thermal conductivity, (c) dynamic viscosity, (d) specific heat at constant pressure, (e) Prandtl number, and (f) volumetric expansivity.
Based on data from NIST REFPROP, ver. 9.1.

Table A6.2 Applications of selected gases in nuclear power and other industries

No.	Gas	Most important properties	Properties' effect	Application
1	Helium	Stable in neutron flux	Can be used inside reactor core	Reactor coolant in VHTRs and GFRs; working fluid in Brayton power cycle
		Noble/inert gas	Does not participate in chemical reactions	
		2nd highest thermal conductivity	High heat-transfer rates	
		2nd highest specific heat	Store and retrieve more energy	
2	Carbon dioxide	Stable in neutron flux	Can be used inside reactor core	Reactor coolant in GCRs and AGRs; filling gas[a] in CANDU reactors in gap between pressure tube and calandria tube; working fluid in supercritical CO_2 Brayton power cycle
		Close to being an inert gas		
		Average thermal conductivity		
		Average specific heat		
3	Hydrogen	Highest thermal conductivity	High heat-transfer rates	Coolant inside sealed large electrical generators
		Highest specific heat	Store and retrieve more energy per 1°C	
		Lowest density	Low friction	
		Lowest viscosity	Low friction	
4	Argon	Stable in neutron flux	Can be used inside reactor core	Separates SFR sodium core from contact with air; filling gas in insulated glass units (windows)
		Noble/inert gas	Does not participate in chemical reactions	
		2nd lowest thermal conductivity	Decreases conduction heat transfer	
		2nd lowest specific heat		

Continued

Table A6.2 Continued

No.	Gas	Most important properties	Properties' effect	Application
		3rd highest density	Heavier than air	
		2nd highest viscosity	Decreases convection heat transfer	
5	Krypton	Noble/inert gas	Does not participate in chemical reactions	Best filling gas in insulated glass units (windows)
		Lowest thermal conductivity	Lowest conduction heat transfer	
		Lowest specific heat		
		Highest density	Heaviest gas	
		Highest viscosity	Lowest convection heat transfer	

VHTR, very high temperature reactor; *GFR*, gas-cooled fast reactor; *GCR*, gas-cooled reactor; *AGR*, advanced gas-cooled reactor; *CANDU*, CANada deuterium uranium; *SFR*, sodium-cooled fast reactor.
[a]Used to prevent heat losses and to monitor any cracks in a pressure tube.

Appendix A7: Supplementary tables

I.L. Pioro, R. Panchal
University of Ontario Institute of Technology, Oshawa, Ontario, Canada

Table A7.1 Population, electrical energy consumption per [a]capita, and Human Development Index in various countries worldwide

No.	Country	Population in millions (July 2015)	EEC		HDI (2014)	
			TWh (2012–2014)	W/ capita	Rank	Value
1	Norway	5.21	119.5	2618	1	0.944
2	Australia	22.75	222.6	1116	2	0.935
3	Switzerland	8.12	58.0	815	3	0.93
4	Denmark	5.58	32.0	653	4	0.923
5	Netherlands	16.95	116.8	786	5	0.922
6	Ireland	4.89	24.2	565	6	0.916
7	Germany	80.85	540.1	762	6	0.916
8	United States	321.37	3832.0	1360	8	0.915
9	New Zealand	4.44	40.3	1036	9	0.913
10	Canada	35.10	524.8	1706	9	0.913
11	Singapore	5.67	47.2	948	11	0.912
12	Hong Kong	7.14	44.2	706	12	0.91
13	Liechtenstein	0.038	1.4	4124	13	0.908
14	United Kingdom	64.09	319.1	568	14	0.907
15	Sweden	9.80	130.5	1519	14	0.907
16	Iceland	0.332	16.9	5822	16	0.899
17	South Korea	49.12	482.4	1120	17	0.898
18	Israel	8.05	59.8	848	18	0.894
19	Luxembourg	0.570	6.1	1222	19	0.892
20	Japan	126.92	921.0	828	20	0.891
21	Belgium	11.32	81.9	825	21	0.89
22	France	66.55	451.1	773	22	0.888
23	Austria	8.67	69.0	908	23	0.885
24	Finland	5.48	82.0	1709	24	0.883

Continued

Table A7.1 Continued

No.	Country	Population in millions (July 2015)	EEC		HDI (2014)	
			TWh (2012−2014)	W/ capita	Rank	Value
25	Slovenia	1.98	13.0	749	25	0.88
26	Spain	48.15	243.1	576	26	0.876
27	Italy	61.86	303.1	559	27	0.873
28	Czech Republic	10.64	60.6	649	28	0.87
29	Greece	10.78	57.7	611	29	0.865
30	Estonia	1.27	8.2	741	30	0.861
31	Brunei Darussalam	0.430	3.5	916	31	0.856
32	Cyprus	1.19	4.3	412	32	0.85
33	Qatar	2.19	30.5	1587	32	0.85
34	Andorra	0.086	0.6	750	34	0.845
35	Slovakia	5.45	28.7	601	35	0.844
36	Poland	38.56	139.0	411	36	0.843
37	Lithuania	2.88	9.7	382	37	0.839
38	Malta	0.414	2.1	568	37	0.839
39	Saudi Arabia	27.75	231.6	952	39	0.837
40	Argentina	43.43	117.1	308	40	0.836
41	United Arab Emirates	5.78	93.3	1841	41	0.835
42	Chile	17.51	63.4	413	42	0.832
43	Portugal	10.83	46.3	487	43	0.83
44	Hungary	9.90	36.8	424	44	0.828
45	Bahrain	1.35	11.7	990	45	0.824
46	Latvia	1.99	7.1	410	46	0.819
47	Croatia	4.46	17.0	434	47	0.818
48	Kuwait	2.79	50.0	2045	48	0.816
49	Montenegro	0.647	3.5	611	49	0.802
50	Belarus	9.59	37.9	451	50	0.798
51	Russia	142.42	1037.0	831	50	0.798

Table A7.1 Continued

No.	Country	Population in millions (July 2015)	EEC		HDI (2014)	
			TWh (2012−2014)	W/ capita	Rank	Value
52	Romania	21.67	49.7	262	52	0.793
53	Uruguay	3.34	9.6	326	52	0.793
54	Oman	3.29	20.4	707	52	0.793
55	Bahamas	0.325	1.7	603	55	0.79
56	Kazakhstan	18.16	80.3	504	56	0.788
57	Barbados	0.291	0.9	368	57	0.785
58	Antigua and Barbuda	0.092	0.3	362	58	0.783
59	Bulgaria	7.19	28.5	452	59	0.782
60	Panama	3.66	7.1	223	60	0.78
61	Malaysia	30.51	118.5	443	62	0.779
62	Mauritius	1.34	2.7	226	63	0.777
63	Seychelles	0.092	0.3	363	64	0.772
64	Trinidad and Tobago	1.22	8.4	781	64	0.772
65	Serbia	7.18	26.9	428	66	0.771
66	Cuba	11.03	16.2	168	67	0.769
67	Lebanon	6.18	12.9	239	67	0.769
68	Costa Rica	4.81	9.0	213	69	0.766
69	Iran	81.82	195.3	272	69	0.766
70	Venezuela	29.28	97.7	381	71	0.762
71	Turkey	79.41	197.0	283	72	0.761
72	Sri Lanka	22.05	10.2	53	73	0.757
73	Mexico	121.74	234.0	219	74	0.756
74	Brazil	204.26	483.5	270	75	0.755
75	Georgia	4.93	8.5	196	76	0.754
76	Saint Kitts and Nevis	0.052	0.1	286	77	0.752
77	Azerbaijan	9.78	17.8	207	78	0.751

Continued

Table A7.1 Continued

No.	Country	Population in millions (July 2015)	EEC		HDI (2014)	
			TWh (2012−2014)	W/ capita	Rank	Value
78	Grenada	0.111	0.2	183	79	0.75
79	Jordan	8.12	14.6	205	80	0.748
80	Macedonia	2.10	7.0	379	81	0.747
81	Ukraine	44.43	159.8	410	81	0.747
82	Algeria	39.54	42.9	124	83	0.736
83	Peru	30.44	35.7	134	84	0.734
84	Armenia	3.06	5.0	188	85	0.733
85	Albania	3.03	7.8	293	85	0.733
86	Bosnia and Herzegovina	3.87	12.6	371	85	0.733
87	Ecuador	15.87	19.0	137	88	0.732
88	Saint Lucia	0.164	0.3	234	89	0.729
89	Fiji	0.909	0.8	98	90	0.727
90	Mongolia	2.99	4.2	160	90	0.727
91	China	1367.49	5523.0	461	90	0.727
92	Thailand	67.98	155.9	262	93	0.726
93	Dominica	0.074	0.1	139	94	0.724
94	Libya	6.41	27.5	490	94	0.724
95	Tunisia	11.04	13.3	138	96	0.721
96	Colombia	46.74	49.4	121	97	0.72
97	St. Vincent and Grenadines	0.103	0.1	142	97	0.72
98	Jamaica	2.95	3.0	116	99	0.719
99	Tonga	0.107	0.04	48	100	0.717
100	Dominican Republic	10.48	11.9	130	101	0.715
101	Belize	0.347	0.6	199	101	0.715
102	Suriname	0.580	1.6	309	103	0.714
103	World	7256.49	19,710.0	310	103	0.711

Table A7.1 Continued

No.	Country	Population in millions (July 2015)	EEC		HDI (2014)	
			TWh (2012−2014)	W/ capita	Rank	Value
104	Maldives	0.393	0.3	77	104	0.706
105	Samoa	0.198	0.1	52	105	0.702
106	Botswana	2.18	3.2	168	106	0.698
107	Moldova	3.55	5.1	163	107	0.693
108	Egypt	88.49	135.6	175	108	0.69
109	Turkmenistan	5.23	11.8	256	109	0.688
110	Indonesia	255.99	167.5	75	110	0.684
111	Gabon	1.71	1.7	112	110	0.684
112	Paraguay	6.78	8.1	137	112	0.679
113	Uzbekistan	29.20	45.2	177	114	0.675
114	Philippines	101.00	61.3	69	115	0.668
115	El Salvador	6.14	5.7	105	116	0.666
116	Vietnam	94.35	108.3	131	116	0.666
117	South Africa	53.68	211.6	450	116	0.666
118	Bolivia	10.80	6.5	68	119	0.662
119	Kyrgyzstan	5.66	9.9	200	120	0.655
120	Iraq	37.06	53.4	164	121	0.654
121	Cabo Verde	0.546	0.3	60	122	0.646
122	Micronesia	0.105	0.2	194	123	0.64
123	Guyana	0.735	0.6	87	124	0.636
124	Nicaragua	5.91	3.6	69	125	0.631
125	Morocco	33.32	26.7	91	126	0.628
126	Namibia	2.21	4.2	219	126	0.628
127	Guatemala	14.92	8.2	62	128	0.627
128	Tajikistan	8.19	14.4	201	129	0.624
129	India	1251.70	864.7	79	130	0.609
130	Honduras	8.75	5.0	66	131	0.606
131	Bhutan	0.742	1.6	252	132	0.605
132	Timor-Leste	1.23	0.1	12	133	0.595
133	Vanuatu	0.272	0.05	21	134	0.594

Continued

Table A7.1 Continued

No.	Country	Population in millions (July 2015)	EEC		HDI (2014)	
			TWh (2012−2014)	W/ capita	Rank	Value
134	Syria	17.06	25.7	172	134	0.594
135	Congo, Republic of the	4.76	0.7	18	136	0.591
136	Kiribati	0.106	0.02	26	137	0.59
137	Equatorial Guinea	0.741	0.1	14	138	0.587
138	Zambia	15.07	8.3	63	139	0.586
139	Ghana	26.33	10.6	46	140	0.579
140	Laos	6.91	2.9	47	141	0.575
141	Bangladesh	168.96	41.5	28	142	0.57
142	Cambodia	15.71	3.6	26	143	0.555
143	Sao Tome and Principe	0.194	0.06	36	143	0.555
144	Nepal	31.55	3.2	12	145	0.548
145	Kenya	45.93	6.6	17	145	0.548
146	Pakistan	199.09	80.3	46	147	0.538
147	Angola	19.63	4.8	28	149	0.532
148	Swaziland	1.44	1.3	103	150	0.531
149	Tanzania	51.05	4.5	10	151	0.521
150	Nigeria	181.56	24.8	16	152	0.514
151	Cameroon	23.74	5.5	27	153	0.512
152	Madagascar	23.81	1.9	9	154	0.51
153	Zimbabwe	14.23	6.8	55	155	0.509
154	Solomon Islands	0.622	0.1	15	156	0.506
155	Mauritania	3.60	1.0	31	156	0.506
156	Papua New Guinea	6.67	3.1	53	158	0.505
157	Comoros	0.781	0.04	6	159	0.503
158	Yemen	26.74	3.8	16	160	0.498
159	Lesotho	1.95	0.7	41	161	0.497
160	Togo	7.55	1.0	15	162	0.484
161	Rwanda	12.66	0.4	3	163	0.483
162	Haiti	10.11	0.5	5	163	0.483

Table A7.1 Continued

No.	Country	Population in millions (July 2015)	EEC		HDI (2014)	
			TWh (2012−2014)	W/ capita	Rank	Value
163	Uganda	37.10	2.8	9	163	0.483
164	Benin	10.45	0.9	10	166	0.48
165	Sudan	36.11	5.7	18	167	0.479
166	Djibouti	0.828	0.3	43	168	0.47
167	South Sudan	12.04	0.7	7	169	0.467
168	Senegal	13.98	2.6	21	170	0.466
169	Afghanistan	32.56	3.9	14	171	0.465
170	Cote D'Ivoire	23.30	4.7	23	172	0.462
171	Malawi	17.96	2.0	13	173	0.445
172	Ethiopia	99.47	5.2	6	174	0.442
173	Gambia	1.97	0.2	13	175	0.441
174	Congo	79.38	7.3	11	176	0.433
175	Liberia	4.20	0.3	8	177	0.43
176	Guinea-Bissau	1.73	0.05	3	178	0.42
177	Mali	16.96	0.9	6	179	0.419
178	Mozambique	25.30	11.3	51	180	0.416
179	Sierra Leone	5.88	0.1	3	181	0.413
180	Guinea	11.78	0.9	9	182	0.411
181	Burkina Faso	18.93	1.0	6	183	0.402
182	Burundi	10.74	0.3	3	184	0.4
183	Chad	11.63	0.2	2	185	0.392
184	Eritrea	6.53	0.3	5	186	0.391
185	Central African Republic	5.39	0.2	4	187	0.35
186	Niger	18.05	0.9	6	188	0.348

[a]United Nations, "Table 1: Human development index and its components," in *UNITED NATIONS DEVELOPMENT PROGRAMME*. [Online]. Available: http://hdr.undp.org/en/composite/HDI. Accessed: Jan. 16, 2016.
Central Intelligence Agency, "The World Factbook: Electricity Consumption," in *CIA.org*. [Online]. Available: https://www.cia.gov/library/publications/the-world-factbook/rankorder/2233rank.html. Accessed: Jan. 16, 2016.
Central Intelligence Agency, "The World Factbook: Population," in *CIA.org*. [Online]. Available: https://www.cia.gov/library/publications/the-world-factbook/rankorder/2119rank.html. Accessed: Jan. 16, 2016.

Table A7.2 Power reactors by nation as per March of 2015[a]

No.	Nation	Number of units (reactor type) (in operation)	Net MW_{el}	Units (forthcoming)	Net MW_{el}
1	Argentina	2 (PHWRs)	935	1	717
2	Armenia	1 (PWR)	375	0	0
3	Bangladesh	0 (PWR)	0	2	2000
4	Belarus	0 (PWR)	0	2	2400
5	Belgium	7 (PWRs)	5885	0	0
6	Brazil	2 (PWRs)	1901	1	1275
7	Bulgaria	2 (PWRs)	1906	0	0
8	Canada	19 (PHWRs)	13,472	0	0
9	China	28 (26 PWRs; 2 PHWRs)	24,268	37	37,630
10	Czech Republic	6 (PWRs)	3678	0	0
11	Finland	4 (2 PWRs; 2 BWRs)	2716	2	2800
12	France	58 (PWRs)	63,130	1	1600
13	Germany	8 (6 PWRs; 2 BWRs)	10,783	0	0
14	Hungary	4 (PWRs)	1889	2	2400
15	India	21 (18 PHWRs; 2 BWRs; 1 PWR)	5308	8	5257
16	Iran	1 (PWR)	915	0	0
17	Japan	43 (20 PWRs; 18 BWRs; 5 ABWRs)	40,179	3	3002
18	Mexico	2 (BWRs)	1300	0	0
19	Netherlands	1 (PWR)	487	0	0
20	Pakistan	3 (2 PWRs; 1 PHWR)	725	5	3600
21	Romania	2 (PHWRs)	1300	2	1240
22	Russia	34 (18 PWRs; 15 LGRs; 1 LMFBR)	24,593	11	8760
23	Slovakia	4 (PWRs)	1816	2	810
24	Slovenia	1 (PWR)	666	0	0
25	South Africa	2 (PWRs)	1800	0	0
26	South Korea	24 (20 PWRs; 4 PHWRs)	21,697	7	9400
27	Spain	7 (6 PWRs; 1 BWR)	7068	0	0

Table A7.2 Continued

No.	Nation	Number of units (reactor type) (in operation)	Net MW_{el}	Units (forthcoming)	Net MW_{el}
28	Sweden	10 (3 PWRs; 7 BWRs)	9303	0	0
29	Switzerland	5 (3 PWRs; 2 BWRs)	3238	0	0
30	Taiwan	6 (4 BWRs; 2 PWRs)	4884	2	2600
31	Turkey	0 (PWRs)	0	4	4600
32	Ukraine	15 (PWRs)	13,107	3	2850
33	United Arab Emirates	0 (PWRs)	0	4	5600
34	United Kingdom	15 (14 AGRs; 1 PWR)	8723	0	0
35	United States	99 (65 PWRs; 34 BWRs)	101,057	8	9490
Total		**436**	**379,463**	**107**	**107,031**

[a]Nuclear News, March 2016, Publication of American Nuclear Society (ANS), pp. 35–67.

Table A7.3a Effects of US Department of Energy's loan-guarantee program on economics of electric power plant generating technologies, 2015 (2005 dollars per megawatt-hour)

No.	Technology	Levelized cost of generation			
		Without loan guarantee	With loan guarantee	Cost reduction	Percent cost reduction
1	Pulverized coal	53.6	53.6	0.0	0
2	Advanced combined cycle	55.3	55.3	0.0	0
3	IGCC	56.1	46.6	9.5	17
4	Nuclear	63.3	47.8	15.5	25
5	Wind	68.0	50.6	17.5	26
6	IGCC with carbon sequestration	73.7	60.3	13.4	18
7	Advanced combined cycle with carbon sequestration	75.9	67.0	8.9	12

IGCC, integrated coal gasification combined cycle. To convert the value in US dollars/MWh into US Cent/kWh—divide by 10. Data from http://www.eia.gov/oiaf/aeo/otheranalysis/pdf/tbl9.pdf.

Table A7.3b Projected levelized cost of electricity (LCOE)[a] in the United States by 2020 (as of 2015)

No.	Power generating technology	Projected LCOE in US dollars/MWh		
		Min.	Average	Max.
1	Geothermal	43.8	**47.8**	52.1
2	NG advanced combined cycle	68.6	**72.6**	81.7
3	Wind onshore	65.6	**73.6**	81.6
4	NG conventional combined cycle	70.4	**75.2**	85.5
5	Hydro	69.3	**83.5**	107.2
6	Conventional coal	87.1	**95.1**	119
7	Advanced nuclear	91.8	**95.2**	101
8	NG advanced combined cycle with CCS	93.3	**100.2**	110.8
9	Biomass	90	**100.5**	117.4
10	NG advanced combustion turbine	94.6	**113.5**	126.8
11	IGCC	106.1	**115.7**	136.1
12	Solar PV	97.8	**125.3**	193.3
13	NG conventional combustion turbine	107.3	**141.5**	156.4
14	IGCC with CCS	132.9	**144.4**	160.4
15	Wind offshore	169.5	**196.9**	269.8
16	Solar thermal	174.4	**239.7**	382.5

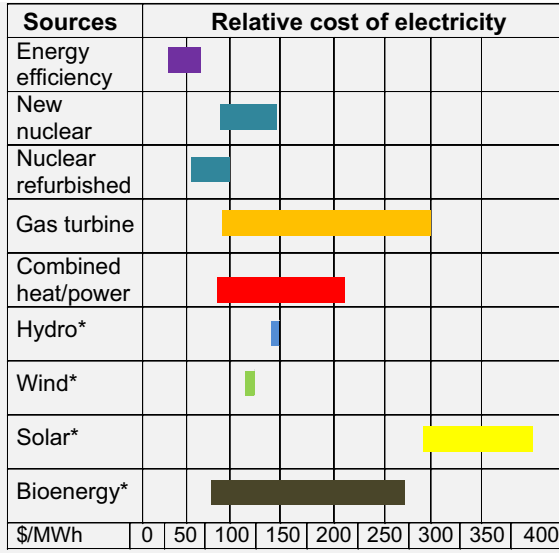
LCOE, levelized cost of electricity; *NG*, natural gas; *CCS*, carbon capture and storage; *IGCC*, integrated gasification combined cycle; *PV*, photovoltaic.
[a]The LCOE is a measure of a power source that attempts to compare different methods of electricity generation on a comparable basis. It is an economic assessment of the average total cost to build and operate a power-generating asset over its lifetime divided by the total energy output of the asset over that lifetime. The LCOE can also be regarded as the minimum cost at which electricity must be sold to break even over the lifetime of the project.
Data from https://en.wikipedia.org/wiki/Cost_of_electricity_by_source.

Table A7.4 Levelized cost of electricity in Germany in 2013

No.	Power-generating technology	LCOE in €/MWh		
		Min.	Average	Max.
1	Coal-fired power plants (brown coal)	38	45.5	53
2	Coal-fired power plant (hard coal)	63	71.5	80
3	Onshore wind farms	45	76.0	107
4	CCGT power plants (co-generation)	75	86.5	98
5	PV systems	78	110.0	142
6	Offshore wind power	119	156.5	194
7	Biogas power plant	135	192.5	250

LCOE, levelized cost of electricity; *CCGT*, combined cycle gas turbine; *PV*, photovoltaic.
Data from https://en.wikipedia.org/wiki/Cost_of_electricity_by_source.

Table A7.5 Relative cost of electricity from various energy sources in Ontario in Canadian $/MWh in 2013–2014



Based on data from Ontario's Long-Term Energy Plan, Ministry of Energy, Toronto, Canada, 2013; from http://www.energy.gov.on.ca/en/files/2014/10/LTEP_2013_English_WEB.pdf.

Appendix A8: Unit conversion

A8.1 Primary or fundamental dimensions and their units in SI (International System)

Dimension	Unit
1 Length	meter (m)
2 Mass	kilogram (kg)
3 Time	second (s)
4 Temperature	kelvin (K)
5 Electric current	ampere (A)
6 Amount of light	candela (cd)
7 Amount of matter	mole (mol)

A8.2 Standard prefixes in SI units

Multiple	Prefix
10^{12}	tera (T)
10^{9}	giga (G)
10^{6}	mega (M)
10^{3}	kilo (k)
10^{2}	hector (h)
10^{1}	deka (d)
10^{-1}	deci (d)
10^{-2}	centi (c)
10^{-3}	milli (m)
10^{-6}	micro (μ)
10^{-9}	nano (n)
10^{-12}	pico (p)

A8.3 Unit conversion

A8.3.1 Area

$1\ m^2 = 10.76391\ ft^2$.
$1\ ft^2 = 0.092903\ m^2$; $1\ in^2 = 6.4516\ cm^2 = 645.16\ mm^2$; $1\ mil^2 = 6.452 \cdot 10^{-4}\ mm^2$; 1 circular mm = 0.7853982 mm^2; 1 circular (circ.) in = 506.707479 mm^2; 1 circ. mil = $5.0671 \cdot 10^{-4}\ mm^2$; $1\ yd^2 = 0.8361\ m^2$; 1 acre = 4840 yd^2 = 4046.86 m^2; $1\ mi^2 = 2.59\ km^2$.

A8.3.2 Density

$1\ kg/m^3 = 6.24280 \cdot 10^{-2}\ lb/ft^3$.
$1\ lb/ft^3 = 16.0185\ kg/m^3$; $1\ slug/ft^3 = 515.38\ kg/m^3$.

A8.3.3 Electrical resistivity specific

$1\ \Omega \cdot$circ. mil/ft $= 1.6624261 \cdot 10^{-9}\ \Omega$ m; $1\ \Omega \cdot$in $= 0.0254\ \Omega$ m.
Sometimes instead of "Ohm" is used symbol "Ω".

A8.3.4 Energy, work, and heat amount

Units	J[a]	erg	kg_f m	kcal	kW h
1 J = 1 Ws	1.0	10^7	0.101972	$2.38846 \cdot 10^{-4}$	$2.7778 \cdot 10^{-7}$
1 erg	10^{-7}	1.0	$1.01972 \cdot 10^{-8}$	$2.38846 \cdot 10^{-11}$	$2.7778 \cdot 10^{-14}$
1 kg_f m	9.80665	$9.80665 \cdot 10^7$	1.0	$2.34228 \cdot 10^{-3}$	$2.724 \cdot 10^{-6}$
1 kcal	$4.1868 \cdot 10^3$	$4.1868 \cdot 10^{10}$	$4.26935 \cdot 10^2$	1.0	$1.163 \cdot 10^{-3}$
1 kW h	$3.6 \cdot 10^6$	$3.6 \cdot 10^{13}$	$3.67098 \cdot 10^5$	$8.59845 \cdot 10^2$	1.0

[a]Units based on names of scientists (researchers etc.) should be capitalized.

1 horsepower per hour (hp · h) = 2647.8 kJ; $1\ eV = 1.602 \cdot 10^{-19}$ J; 1 erg = 1 dyne (dyn) cm = $0.1 \cdot 10^{-6}$ J, 1 L (L, l, or ℓ) atm = 101.33 J.

1 British thermal unit (Btu or BTU) (thermal) = 1.05435 kJ; 1 Btu = 1.055056 kJ; 1 Btu (mean) = 1.05587 kJ.

1 calorie (cal) (thermal) = 4.184 J; 1 cal = 4.1868 J; 1 cal (at 15°C) = 4.1858 kJ; 1 cal (at 20°C) = 4.1819 J; 1 cal (mean) = 4.19002 J; 1 Calorie (Cal) (food) = 4.1868 kJ.

1 lb_f ft = 1.355817 J; 1 poundal (pdl) ft = 0.04214 J; 1 therm = 105,506 kJ; 1 pound centigrade unit (pcu) = 1.8 Btu = 1.8978 kJ.

A8.3.5 Specific Enthalpy

1 kcal/kg = 1 cal/g = 4.1868 kJ/kg; 1 Btu/lb = 2.326 kJ/kg; 1 chu/lb = 4.1868 kJ/kg; 1 ft lb_f/lb = 0.00299 kJ/kg.

A8.3.6 Flow rate volumetric (or volume flow rate)

1 gallon (US)/min (gpm) = 0.06309 dm^3/s; 1 ft^3/min (cfm) = 471.95 dm^3/s.

A8.3.7 Force

1 N = 10^5 dyn = 0.101972 kg_f; 1 kg_f = 9.80665 N.

1 lb_f = 4.448222 N; 1 cental = 100 lb_f = 444.822 N; 1 kip = 1000 lb_f = 4448.222 N; 1 poundal (pdl) = 1 lb_f ft/s^2 = 0.138255 N; 1 grain = $0.6355 \cdot 10^{-3}$ N; 1 stone = 62.2751 N.

1 lb_f = 0.01 cental = 0.001 kip = 32.174 pdl = 7000.00 grain = 16 ozf.

A8.3.8 Heat flux

1 W/m^2 = 0.8598 kcal/h m^2 = 7.988 · 10^{-2} kcal/h ft^2 = 0.31791 Btu/h ft^2 = 0.17611 centigrades heat unit (chu)/h ft^2.

1 kcal/h m^2 = 1.163 W/m^2; 1 cal/s cm^2 = 41,868 W/m^2.

1 kcal/h ft^2 = 12.5184 W/m^2; 1 Btu/h ft^2 = 3.154 W/m^2; 1 chu/h ft^2 = 5.6783 W/m^2.

A8.3.9 Heat flux volumetric

1 Btu/h ft^3 = 10.35 W/m^3.

A8.3.10 Heat transfer coefficient

1 Btu/h $ft^{2\circ}$F = 5.6782 W/m^2 K.

A8.3.11 Heat transfer rate and power

Units	W	kcal	kg_f m/s	hp (metric)
1 W = 1 J/s	1.0	0.86	0.102	$1.36 \cdot 10^{-3}$
1 kcal/h	1.163	1.0	0.118	$1.58 \cdot 10^{-3}$
1 kg_f m/s	9.81	8.44	1.0	$1.33 \cdot 10^{-2}$
1 hp (metric)	735.5	633	75	1.0

1 W = 10^7 erg/s; 1 m^3 atm/h = 28.146 W; 1 hp (el.) = 746 W.

1 horsepower (hp) (UK) = 745.7 W; 1 Btu/h = 0.29307 W; 1 lb_f ft/min = 0.022597 W; 1 lb_f ft/s = 1.35582 W; 1 cheval-vapor = 1 hp (metric) = 735.5 W; 1 chu/h = 0.52753 W.

A8.3.12 Length

1 m = 3.2808 ft.

1 yard (yd) = 0.9144 m = 3 ft (3′); 1 ft = 12 inch (in) (12″).

1 ft = 0.3048 m; 1 in (1″) = 25.4 mm; 1 mil = 0.001 in = 0.0254 mm; 1 μm = 10^{-6} m; 1 mile (mi) = 5280 ft = 1609.344 m; 1 nautical mile (nmi) = 6076.1 ft = 1852 m.

A8.3.13 Mass

1 pound (lb) = 16 ounces (oz) = 453.59237 g; 1 oz = 28.3495 g; 1 slug = 32.174 lb = 14.594 kg; 1 short ton (or tonne) (t) (US 2000 lb) = 0.9072 metric ton; 1 long ton (imperial ton, UK 2240 lb) = 1.016 metric ton.

A8.3.14 Pressure

Units	Pa	bar	kg_f/cm^2	atm (phys.[a])	mm Hg	mm H_2O
1 Pa = 1 N/m^2 =	1	10^{-5}	$1.02 \cdot 10^{-5}$	$0.987 \cdot 10^{-5}$	$7.5024 \cdot 10^{-3}$	0.10197
1 bar =	10^5	1.0	1.02	0.98692	$7.5024 \cdot 10^2$	$1.02 \cdot 10^4$
1 kg_f/cm^2 = 1 at (tech. [a]) =	$9.80665 \cdot 10^4$	0.980665	1.0	0.9678	735.56	10^4
1 atm (phys.) =	$1.01325 \cdot 10^5$	1.01325	1.0332	1.0	760.0	$1.0332 \cdot 10^4$
1 mm Hg = 1 torr =	133.322	$1.33 \cdot 10^{-3}$	$1.36 \cdot 10^{-3}$	$1.316 \cdot 10^{-3}$	1.0	13.595
1 mm H_2O = 1 kg_f/m^2 =	9.80665	$9.80665 \cdot 10^{-5}$	10^{-4}	$9.678 \cdot 10^{-5}$	$7.356 \cdot 10^{-2}$	1.0

[a] *phys*., physical; *tech*., technical.

1 bar = 10^6 dyn/cm^2 = 14.5038 lb_f/in^2 (psi) = 2088.543 lb_f/ft^2 = 29.530 inches of Hg = 401.463 inches of water = $1.4504 \cdot 10^{-2}$ kip/in = 69,053.14 poundal/ft^2.

1 lb_f/in^2 (pounds per square inch absolute, psia) = 6894.76 Pa; 1 lb_f/ft^2 = 47.88 Pa; 1 inch of Hg = 3.3864 kPa; 1 inch of water = 249.1 Pa; 1 kip/in = 6894.76 kPa.

A8.3.15 Specific heat

1 Btu/lb Ra = 4186.9 J/kg K; 1 ft lb_f/slug·Ra = 0.16723 J/kg K.

A8.3.16 Temperature scales

Scale	K (T)	°C (t)	Ra (T)	°F (t)	°R (t)
Kelvin K =	1.0	$t + 273.15$	$5/9T$	$5/9t + 255.37$	$5/4t + 273.15$
Celsius °C =	$T - 273.15$	$1.0t$	$5/9t - 273.15$	$5/9(t - 32)$	$1.25t$
Rankine Ra =	$1.8T$	$1.8(t + 273.15)$	$1.0T$	$t + 459.67$	$1.8(1.25t + 273.15)$
Fahrenheit °F =	$1.8T - 459.67$	$1.8t + 32$	$T - 459.67$	$1.0t$	$2.25t + 32$
Réaumur °R =	$0.8(T - 273.15)$	$0.8t$	$0.8(5/9T - 273.15)$	$(t-32)4/9$	$1.0t$

The Rankine temperature scale (widely used in the United States, Canada, and other countries) is the absolute scale, 0 Ra = 0 K, at the same time 1 Ra = 1°F; sometimes degrees of Rankine have a symbol "R," for example 0 R; the same symbol is related to degrees of Réaumur; however, the sign of degree should be used in this case, ie, 0°R.

The temperature scale of Fahrenheit is the practical scale (also widely used in the United States, Canada, and other countries), 32°F = 0°C and 212°F = 100°C.

The Réaumur temperature scale is the practical scale, 0°R = 0°C, but 80°R = 100°C (currently, this scale rarely used).

A8.3.17 Temperature difference

$\Delta T = 1$ K = 1°C = (9/5) Ra = (9/5)°F.

Degrees of absolute scales are more preferable to be used for the temperature difference.

A8.3.18 Thermal conductivity

1 W/m K = 1 W/m °C = 0.8598 kcal/h m °C = 2.3885 cal/s cm °C = 0.5778 Btu/h ft °F = 0.5778 chu/h ft °C.

1 kcal/h m °C = 1.163 W/m K; 1 cal/s cm °C = 418.68 W/m K; 1 Btu/h ft °F = 1 chu/h ft °C = 1.7307 W/m K; 1 Btu in/h °F ft^2 = 0.144 W/m K.

A8.3.19 Viscosity dynamic

Units	Pa s	kg/m s	kg_f s/m^2	P (poise)
1 Pa s = 1 N s/m^2 =	1.0	1.0	0.101972	10.0
1 kg/m s =	1.0	1.0	0.101972	10.0

Continued

Units	Pa s	kg/m s	$kg_f\ s/m^2$	P (poise)
1 $kg_f\ s/m^2$ =	9.80665	9.80665	1.0	98.0665
P (poise) =	0.1	0.1	$0.101972 \cdot 10^{-1}$	1.0

1 Pa s = 0.671969 lb/ft s = 2419.088 lb/ft h = $2.08855 \cdot 10^{-2}$ $lb_f\ s/ft^2$.

1 lb/ft s = 1.4882 Pa s; 1 lb/ft h = $0.41338 \cdot 10^{-3}$ Pa s; 1 $lb_f\ s/ft^2$ = 1 slug/ft s = 47.8803 Pa s.

A8.3.20 Viscosity kinematic

1 $m^2/s = 1 \cdot 10^4$ St (stokes) = 10.7639 ft^2/s = 38,750.0775 ft^2/h = 91,440.0 L (L, l, or ℓ)/in·h.

1 St = $1 \cdot 10^{-4}$ m^2/s.

A8.3.21 Volume

1 m^3 = 35.3147 ft^3; 1 L = 1 dm^3 = 0.001 m^3.

1 ft^3 = 0.028317 m^3; 1 in^3 = 16.3871 cm^3; 1 gallon liquid US = 3.7854 L and 1 gallon UK = 4.54609 L; 1 fluid oz (UK) = 28.413 mL; 1 fl oz (US) = 29.574 mL; 1 pint (pt) (UK) = 0.5683 dm^3.

Notes: *at*, atmosphere (technical); *atm*, atmosphere (physical); *Btu* (Btu or BTU), British thermal unit; *cal*, calorie; *cc*, cubic centimeter; *chu*, centigrades heat unit; *1 circular mil*, area of circle with diameter of 1 mil; *dyn*, dyne; *eV*, electronvolt; *f*, force; *fl*, fluid; *ft*, foot or feet; *h*, hour; *Hg*, mercury; *in*, inch; *J*, joule; *h*, hour; *hp*, horsepower; *L (L or l)*, liter (litre); *lb* (from Latin: *libra*), pound or lb_m (lbm), pound of mass; *lb_f (lbf)*, pound of force; *m*, meter (metre); *mi*, mile; *mil*, unit of length equal to one thousandth of an inch; *min*, minute; *μm*, micrometer; *N*, newton; *nmi*, nautical mile; *oz*, ounce; *P*, poise; *Pa*, pascal; *pcu*, pound centigrade unit; *pdl*, poundal; *psi*, pounds per square inch; *psia*, psi absolute; *psig*, psi gauge; *s*, second; *St*, stoke; *UK*, United Kingdom (ie, British unit); *US*, United States (ie, US unit); *yd*, yard; *W*, watt.

A8.4 Some physical constants and definitions

Normal acceleration due to gravity: $g_n = 9.80665\ m/s^2 = 32.174\ ft/s^2$;

Universal gas constant: $R = 8.31451$ J/mol K = 8.31447 kPa m^3/kmol K = 0.0831447 bar m^3/kmol K = 82.05 L atm/kmol K = 1.9858 Btu/lbmol Ra = 1545.37 ft lb_f/lbmol Ra = 10.73 psia ft^3/lbmol Ra.

Normal conditions: Physical conditions at a pressure of p = 101,325 Pa = 1.01325 bar = 14.696 psi = 760 mm Hg (normal atmosphere) = 29.9213 in Hg = 10.3323 m

H_2O and a temperature of $t = 273.15$ K $= 0°C$ at which a molar gas volume is $V_o = 2.24141 \cdot 10^{-2}$ m^3/mol.

A8.5 Thermophysical property software for gases and liquids

Thermophysical properties of gases, liquids, and fluids at supercritical pressures used in publications of Dr. I. Pioro were calculated according to the National Institute of Standards and Technology software (2010) (http://www.nist.gov/srd/nist23.cfm).

"Version 9.1 includes 121 pure fluids, five pseudo-pure fluids (such as air), and mixtures with up to 20 components (this statement is taken from: http://www.nist.gov/srd/nist23.cfm, the website accessed on January 9, 2016):

- The typical natural gas constituents methane, ethane, propane, butane, isobutane, pentane, isopentane, hexane, isohexane, heptane, octane, nonane, decane, undecane, dodecane, carbon dioxide, carbon monoxide, hydrogen, nitrogen, and water.
- The hydrocarbons acetone, benzene, butene, *cis*-butene, cyclohexane, cyclopentane, cyclopropane, ethylene, isobutene, isooctane, methylcyclohexane, propylcyclohexane, neopentane, propyne, *trans*-butene, and toluene.
- The HFCs R23, R32, R41, R125, R134a, R143a, R152a, R161, R227ea, R236ea, R236fa, R245ca, R245fa, R365mfc, R1233zd(E), R1234yf, and R1234ze(E).
- The refrigerant ethers RE143a, RE245cb2, RE245fa2, and RE347mcc (HFE-7000).
- The HCFCs R21, R22, R123, R124, R141b, and R142b.
- The traditional CFCs R11, R12, R13, R113, R114, and R115.
- The fluorocarbons R14, R116, R218, R1216, C4F10, C5F12, and RC318.
- The "natural" refrigerants ammonia, carbon dioxide, propane, isobutane, and propylene.
- The main air constituents nitrogen, oxygen, and argon.
- The noble elements helium, argon, neon, krypton, and xenon.
- The cryogens argon, carbon monoxide, deuterium, krypton, neon, nitrogen trifluoride, nitrogen, fluorine, helium, methane, oxygen, normal hydrogen, parahydrogen, and orthohydrogen.
- Water (as a pure fluid, or mixed with ammonia).
- Miscellaneous substances including carbonyl sulfide, diethyl ether, dimethyl carbonate, dimethyl ether, ethanol, heavy water, hydrogen chloride, hydrogen sulfide, methanol, methyl chloride, nitrous oxide, Novec-649, sulfur hexafluoride, sulfur dioxide, and trifluoroiodomethane.
- The xylenes *m*-xylene, *o*-xylene, *p*-xylene, and ethylbenzene.
- The FAMES (fatty acid methyl esters, ie, biodiesel constituents) methyl oleate, methyl palmitate, methyl stearate, methyl linoleate, and methyl linolenate.
- The siloxanes octamethylcyclotetrasiloxane, decamethylcyclopentasiloxane, dodecamethylcyclohexasiloxane, decamethyltetrasiloxane, dodecamethylpentasiloxane, tetradecamethylhexasiloxane, octamethyltrisiloxane, and hexamethyldisiloxane.
- 79 predefined mixtures (such as R407C, R410A, and air); the user may define and store others.

The program uses the most accurate equations of state and models currently available:

- High accuracy Helmholtz energy equations of state, including international standard equations for water, R134a, R32, and R143a and equations from the literature for ethane, propane, R125, ammonia, carbon dioxide, and others.
- High accuracy MBWR equations of state, including the international standard EOS for R123.
- The Bender equation of state for several of the "older" refrigerants, including R14, R114, and RC318.
- An extended corresponding states model for fluids with limited data.
- An excess Helmholtz energy model for mixture properties.
- Experimentally based values of the mixture parameters are available for hundreds of mixtures.
- The American Gas Association equation AGA8 for natural gas properties (as an alternative to the Helmholtz model).
- Viscosity and thermal conductivity are based on fluid-specific correlations (where available), a modification of the extended corresponding states model, or the friction theory model.

Available properties:

Temperature (T), pressure (p), density, energy, enthalpy, entropy, specific heat at constant pressure, specific heat at constant volume, sound speed, compressibility factor, Joule–Thomson coefficient, quality, second and third virial coefficients, second and third acoustic virial coefficients, Helmholtz energy, Gibbs energy, heat of vaporization, fugacity, fugacity coefficient, chemical potential, k value, molar mass, B12, thermal conductivity, viscosity, kinematic viscosity, thermal diffusivity, Prandtl number, surface tension, dielectric constant, gross and net heating values, isothermal compressibility, volume expansivity, isentropic coefficient, adiabatic compressibility, specific heat input, exergy, Gruneisen, critical flow factor, excess values, dp/dr, d^2p/dr^2, dp/dT, dr/dT, dp/dr, d^2p/dr^2."

"The mini-REFPROP program is a sample version of the full REFPROP program (located at www.nist.gov/srd/nist23.cfm) and is meant for use as a teaching tool in the introduction of thermodynamics to students. It contains a limited number of pure fluids (water, CO_2, R134a, nitrogen, methane, propane, hydrogen, and dodecane) and also allows mixture calculations of nitrogen with methane for teaching Vapor–Liquid Equilibrium (VLE). The program expires Aug. 31, 2016, at which point a new set of install files will be uploaded here." (This statement is taken from http://www.boulder.nist.gov/div838/theory/refprop/MINIREF/MINIREF.HTM, the website accessed on January 9, 2016).

Index

Note: Page numbers followed by “f” indicate figures, “t” indicate tables.

A
ABWRs. *See* Advanced boiling water reactors (ABWRs)
AC. *See* Alternate cycle (AC); Alternating current (AC)
ACC. *See* Accumulators (ACC)
Accelerator driven system (ADS), 120−121
Accident investigation terminology, 474−475
Accumulators (ACC), 390
Active decay heat removal systems (ADHRSs), 346
Active shut-down systems, 109, 684
Adaptive Phased Management (APM), 572
Additional Generation IV systems, 137−142
  Chinese CLEAR-I reactor, 140, 141f
  PBWFR, 140−141
  South Korea URANUS-40 system, 137−138
  SVBR-100 reactor, 141−142
ADHRSs. *See* Active decay heat removal systems (ADHRSs)
Adiabatic core, 129
ADS. *See* Accelerator driven system (ADS); Automatic depressurization system (ADS)
ADV SMR. *See* Advanced small modular reactors (ADV SMR)
Advanced boiling water reactors (ABWRs), 223, 391, 707. *See also* Boiling water reactors (BWRs); Lead-cooled fast reactors (LFRs)
  key specifications of ABWR and BWR-5, 724t
  simplified layout of ABWR NPP, 726f
  simplified layout of typical ABWR NPP, 725f
  T−*s* diagram for typical ABWR NPP turbine cycle, 726f
Advanced gas reactor. *See* Advanced gas-cooled reactors (AGRs)
Advanced gas-cooled reactors (AGRs), 57, 701, 731, 733f, 743
  thermodynamic layout of AGR Torness NPP, 734f
  T−*s* diagram for AGR Torness NPP turbine cycle, 734f
Advanced heavy water reactor (AHWR), 414
  AHWR-300 design features, 414−417
  design features of AHWR-300, 414−417
  enhanced safety features, 417
    accidents and Fukushima types of scenarios, 418
    inherent safety features, 418
    passive safety systems, 418
  fuel cluster, 416f
  fuel cycle for, 416f
  improving economics, 419−420
  and major systems, 415f
  physical protection system, 419
  proliferation resistance, 419
  research and development activities, 420
  safety goals, 418−419
Advanced Lead Fast Reactor European Demonstrator (ALFRED), 120, 257
Advanced nuclear reactors in China, 374−375
Advanced reactors (ARs), 37, 455, 541, 566−568
Advanced seismic isolation system, 299−300
Advanced small modular reactors (ADV SMR), 661−662
  containment, 678
  economic and financing evaluation, 687−690
  emergency core cooling system, 678−684

Advanced small modular reactors (ADV SMR) (*Continued*)
fuels, 674–678
international SMR designs, 662
nuclear reactors, 667
comparison, 668t–669t
RCSs components, 673–674
Advanced Sodium Technological Reactor for Industrial Demonstration (ASTRID), 98, 256
AECL. *See* Atomic Energy of Canada Limited (AECL)
AGRs. *See* Advanced gas-cooled reactors (AGRs)
AHFP. *See* Axial heat flux profile (AHFP)
AHWR. *See* Advanced heavy water reactor (AHWR)
AKME Engineering, 321
ALARA. *See* As Low As Reasonably Achievable (ALARA)
ALFRED. *See* Advanced Lead Fast Reactor European Demonstrator (ALFRED)
ALLEGRO, 257
Alternate cycle (AC), 565
Alternate fuel cycles, 565–566
Alternating current (AC), 301
AMBIDEXTER-NEC. *See* Advanced Molten-salt Breakeven Inherently-safe Dual-function EXcellen Tly-Ecological Reactor Nuclear Energy Complex (AMBIDEXTER-NEC)
Anticipated operational occurrences (AOOs), 463
Anticipated transient without scram (ATWS), 58–59, 290–291, 301–302, 462
AOOs. *See* Anticipated operational occurrences (AOOs)
APM. *See* Adaptive Phased Management (APM)
ARs. *See* Advanced reactors (ARs)
As Low As Reasonably Achievable (ALARA), 263, 461
Asian Development Bank, 689–690
ASTRID. *See* Advanced Sodium Technological Reactor for Industrial Demonstration (ASTRID)
Atmospheric air heat exchangers, 211
Atomic Energy of Canada Limited (AECL), 720–723
Atomic Minerals Directorate for Exploration and Research, 413–414
"Atoms for Peace" speech, 548–549
ATWS. *See* Anticipated transient without scram (ATWS)
Autarky policy, 562
Automatic depressurization system (ADS), 209, 380
Axial heat flux profile (AHFP), 621–623

B

Backup RSSs, 288
BARC. *See* Bhabha Atomic Research Center (BARC)
Barrier analysis, 475
Base metal (BM), 355–356
"Basic Safety Standards" Directive (BSS Directive), 246
BCC models. *See* Body center cubic models (BCC models)
BCs. *See* Boundary conditions (BCs)
BCT crystal structure. *See* Body-centered tetragonal crystal structure (BCT crystal structure)
BDBAs. *See* Beyond-design–basis accidents (BDBAs)
Beginning of equilibrium cycle (BOEC), 343
Beloyarsk Nuclear Power Plant reactor (BNPP reactor), 828, 829f
design, 832
hydrodynamic stability, 839–842
physical parameters, 834–837
startup, 842–845
Benefit-to-cost ratio, 578
Beryllium oxide (BeO), 630–631
Beyond-design–basis accidents (BDBAs), 460
Bhabha Atomic Research Center (BARC), 413–414
Bismuth (Bi), 310
Blanket assemblies, 200
Blanket fuel, 100, 103
BM. *See* Base metal (BM)
BN-600 reactor, 98, 312, 740
BN-800 reactor, 98, 312–313, 314t, 315f, 315t, 740

BN-1200 design, 98, 317–320, 319f, 320t
BNPP reactor. *See* Beloyarsk Nuclear Power Plant reactor (BNPP reactor)
Body-centered tetragonal crystal structure (BCT crystal structure), 601–602
Body center cubic models (BCC models), 394
BOEC. *See* Beginning of equilibrium cycle (BOEC)
BOiling Nuclear Superheater (BONUS), 826
Boiling Reactor Experiment V (BORAX–V), 826
Boiling water (BW), 830
  channels, 837–838
BOiling water ReActor eXperiment (BORAX), 488
Boiling water reactors (BWRs), 25f–26f, 189, 223, 247, 487, 701, 709–720, 743, 778–779. *See also* Advanced boiling water reactors (ABWRs)
  parameters of AP-1000 US Generation III+ PWR NPP, 718t
  parameters of US BWR, 721t–722t
  simplified layout of typical BWR NPP, 723f
  stability, 491–492
Bologna 1999 process, 242
BONUS. *See* BOiling Nuclear Superheater (BONUS)
BOO. *See* Build–own–operate (BOO)
BOR-60, 312
BORAX. *See* BOiling water ReActor eXperiment (BORAX)
Boric acid, 200
Boron carbide (B_4C), 65, 100
Boundary conditions (BCs), 484
BR. *See* Breeding ratio (BR); Bystryi Reactor (BR)
Brayton cycle, 94
  gas-turbine cycle, 17
Breeder reactors, 584–587
Breeding process, 584–587
Breeding ratio (BR), 260
BREST. *See* Bystry Reaktor so Svintsovym Teplonositelem (BREST)
BREST-1200, 327, 328t–329t
BREST-OD-300 reactor, 133–136, 135t, 136f, 324–327
  characteristics, 326t
  primary system layout, 325f
BSS Directive. *See* "Basic Safety Standards" Directive (BSS Directive)
Build–own–operate (BOO), 690
Burgers vortex model, 293–294
BWRs. *See* Boiling water reactors (BWRs)
Bystry Reaktor so Svintsovym Teplonositelem (BREST), 120
Bystryi Reactor (BR), 310

C
CABRI
  program, 292
  safety research reactor, 111
Calandria vessel, 197
Canadian SCWR concept, 194, 196f
  fuel assembly concept, 201–205, 202f
Candu Energy Inc., 720–723
CANDU reactors, 577
CANLUB coating of standard CANDU PHWR fuel cladding, 203–204
CAPP code, 350–351
Capture and storage (CCS), 703
  possible solutions, 711f
Carbide fuels, 596
  uranium carbide, 597–601
  uranium dicarbide, 601–606
Carbon dioxide (CO_2), 743, 750
  basic properties, 760t
  density *vs*. temperature, 780f
  dynamic viscosity *vs*. temperature, 781f
  kinematic viscosity *vs*. temperature, 782f
  peak values of specific heat, volume expansivity, and thermal conductivity, 790t–792t
  photos during transition, 774f
  Prandtl number *vs*. temperature, 783f
  specific enthalpy *vs*. temperature, 783f
  specific heat, volume expansivity, and thermal conductivity *vs*. temperature, 785f
  specific heat at constant pressure *vs*. temperature, 782f
  specific heat profiles at various pressures, 785f
  thermal conductivity *vs*. temperature, 781f
  thermodynamic diagrams, 748f
  thermodynamics diagrams for, 774f
  values of pseudocritical temperature, 789t

Carbon dioxide (CO_2) (*Continued*)
variations of selected thermophysical properties, 784f
volumetric expansivity *vs*. temperature, 784f
Carbon footprint, 568
Carbon trading, 567–568
CAS pilot projects. *See* Chinese Academy of Sciences pilot projects (CAS pilot projects)
Causal factor, 474
CCFR-B. *See* Chinese commercial breeding fast reactor (CCFR-B)
CCFR-T. *See* Chinese commercial transmutation fast reactor (CCFR-T)
CCS. *See* Capture and storage (CCS)
CCWS. *See* Components cooling water system (CCWS)
CDA. *See* Core disruptive accident (CDA)
CDF. *See* Core damage frequency (CDF); Cumulative damage fraction (CDF); Cumulative damage function (CDF)
CDFR. *See* Chinese demonstration fast reactor (CDFR)
CEFR. *See* Chinese experimental fast reactor (CEFR)
Ceramic coatings, 149
Ceramic fuels, 588
carbide fuels, 596–606
discussion, 615–624
nitride fuels, 606–615
oxide fuels, 589–596
properties, 590t
temperature variation in degrees Celsius, 621f
Ceria (CeO_2), 652
Cerium–cerium oxide cycle, 652–653
CFD. *See* Computational fluid dynamics (CFD)
CFR-1000, 98
CFR-600, 98
CFV. *See* Coeurà Faible Vidange (CFV)
Chalk River Laboratories, 816
Change analysis, 475
China Generation IV concepts
current status of nuclear power in, 373–374
plans for advanced nuclear reactors in, 374–375
sodium-cooled fast reactor research and development, 375
lead-cooled fast reactor research and development, 401–405
molten salt reactor research and development, 393–401
research before SFR construction, 375
SFR development strategy, 376–380
supercritical water-cooled reactor research and development, 385–393
VHTR research and development, 380–385
China HuaNeng Group (CHNG), 384
China Institute of Atomic Energy (CIAE), 375
China LEad Alloy-cooled Reactor (CLEAR), 120–121, 140, 401–402, 402f
CLEAR-v, 402–403
China National Nuclear Corporation (CNNC), 378
China Nuclear Engineering and Construction (CNEC), 384
Chinese Academy of Sciences pilot projects (CAS pilot projects), 375
Chinese CLEAR-I reactor, 140, 141f, 142t
Chinese commercial breeding fast reactor (CCFR-B), 380
Chinese commercial transmutation fast reactor (CCFR-T), 380
Chinese demonstration fast reactor (CDFR), 378–380, 379f
Chinese experimental fast reactor (CEFR), 374–378, 376f–377f
CHF. *See* Critical heat flux (CHF)
CHNG. *See* China HuaNeng Group (CHNG)
Chromium (Cr), 321–322, 360–362
CHTR. *See* Compact high-temperature reactor (CHTR)
CIAE. *See* China Institute of Atomic Energy (CIAE)
Civil nuclear industry, 567–568
CLaDding Temperature (CLDT), 619–621
Clean Burn concept, 63
CLEAR. *See* China LEad Alloy-cooled Reactor (CLEAR)
Closed fuel cycles, 95, 107, 114, 309–310, 317–318

Closing fuel cycle, 542, 572–573
CNEC. *See* China Nuclear Engineering and Construction (CNEC)
CNNC. *See* China National Nuclear Corporation (CNNC)
Coal-fired power plants, 7–9, 703, 707f
  Tomato-Atsuma coal-fired power plant, 708f
Coeurà Faible Vidange (CFV), 102–103
Cogeneration, 78–81, 229
  desalination, 80–81
  hydrogen, 79–80
  thermochemical iodine sulfur process, 79f
COL. *See* Combined Operating License (COL)
Cold traps (CTs), 286–288
"Collapsible cladding" concept, 203
Combined cycle, 17
Combined cycle power plants, 701, 702f
  gas turbine rotor, 702f
  modern, 704f
  reference data, 705t
    on selected gas turbines, 706t
  steam turbine, 703f
Combined Operating License (COL), 457
Commercial uses of hydrogen, 641
Common mode failure, 296
Compact high-temperature reactor (CHTR), 414, 421
Compact reactor system, 293–294
Components cooling water system (CCWS), 288–289
Composite fuels, 628
  uranium dioxide–beryllium oxide, 630–631
  uranium dioxide–graphite, 629
  uranium dioxide–silicon carbide, 628–629
Compressed fluid. *See* Supercritical fluid
Computational fluid dynamics (CFD), 162, 393, 488, 496–497, 809
Concept viability, 176–181
Containment, 678
  comparison, 679t
  4S, 682f
  IRIS, 681f
  measures, 111
  NuScale, 680f
  pool, 208–209
  PRISM, 681f
  steam condenser gallery, 209
  W-SMR, 680f
Containment vessel (CV), 289
Contemporary nuclear power technologies, 224–226, 225t
Contributing causes, 475
Control rod drive mechanism (CRDM), 667
Control system, 75, 76f
Conventional SFR power conversion, 113–114
Coolant, 583–584
  Generation IV nuclear-reactor, 586t
  injection system, 105
  plenums, 421
  types of operating nuclear power reactors, 585t
COPA, 355
Copenhagen 2002 process, 242
Copper oxychloride (Cu_2OCl_2), 650
Copper–chlorine cycle (Cu–Cl cycle), 642–643
Core barrel, 192
Core damage frequency (CDF), 313, 418–419, 459
Core design, 190–192
Core disruptive accident (CDA), 437–439
Core fuel, 100
CORONA code, 352
Coupled natural-circulation loops, 494–495, 508–520
Coupled neutronics/CFD simulations, 162
CRDM. *See* Control rod drive mechanism (CRDM)
Critical heat flux (CHF), 749
Critical point, 747–749, 774
Critical pressure
  critical parameters of selected fluids, 776t
  definitions of terms and expressions, 773–775
  density *vs*. temperature, 776f
  dynamic viscosity *vs*. temperature, 777f
  kinematic viscosity *vs*. temperature, 777f
  Prandtl number *vs*. temperature, 779f
  specific enthalpy *vs*. temperature, 778f
  specific heat at constant pressure *vs*. temperature, 778f
  thermal conductivity *vs*. temperature, 776f
  thermophysical properties, 775–777

Critical pressure (*Continued*)
variations of selected thermophysical properties, 780f
volumetric expansivity *vs*. temperature, 779f
Critical state. *See* Critical point
Crystallization, 650
CTs. *See* Cold traps (CTs)
Cu−Cl cycle, 648−651, 649f
Cu−Cl cycle. *See* Copper−chlorine cycle (Cu−Cl cycle)
Cumulative damage fraction (CDF), 343
Cumulative damage function (CDF), 457
Cupric chloride ($CuCl_2$), 650
Cuprous chloride (CuCl), 648
Curie point-type SASS, 290−291
CV. *See* Containment vessel (CV)
Cyberterrorism, 270

D
DA. *See* Deterministic Analyses (DA)
DAE. *See* Indian Department of Atomic Energy (DAE)
DBAs. *See* Design-basis accidents (DBAs)
DBEs. *See* Design-basis events (DBEs)
DBTs. *See* Design-basis threats (DBTs)
DCs. *See* Dip coolers (DCs)
"Decarbonization scenarios", 244−245
Decay heat, 105
Decay Heat eXchanger (DHX), 346
Decay heat removal (DHR), 109−110, 126, 175, 477−478
Decay heat removal system (DHRS), 285, 288, 335−336, 439−440
DECs. *See* Design extension conditions (DECs)
Deep geologic repository (DGR), 573
Defense-in-depth (DiD), 172−173, 205, 288, 460
DEG. *See* Double-ended guillotine (DEG)
DELIGHT, 63
Demonstration reactors, 108
Density wave oscillations (DWO), 483
Dependent double failure, 296
Depleted uranium (DU), 129
Desalination cogeneration, 80−81, 80f, 80t
cost, 86
Design extension conditions (DECs), 288
DEC-1, 437−439
DEC-2, 437−439
Design measures, 110
Design-basis accidents (DBAs), 288, 417, 460
Design-basis events (DBEs), 437−439
Design-basis threats (DBTs), 461
Deteriorated heat transfer (DHT), 796, 799, 802
Deterministic Analyses (DA), 467
Deterministic and Phenomenological Analyses (DPA), 263
Deterministic approach, 288
DG. *See* Directorate General (DG)
DGR. *See* Deep geologic repository (DGR)
DHR. *See* Decay heat removal (DHR)
DHRS. *See* Decay heat removal system (DHRS)
DHT. *See* Deteriorated heat transfer (DHT)
DHX. *See* Decay Heat eXchanger (DHX)
DiD. *See* Defense-in-depth (DiD)
Dip coolers (DCs), 127
Dip plates (DPs), 286−288
Dirac-delta function, 499, 511−512
Direct cycle, 42
Direct reactor auxiliary cooling system (DRACS), 285
Direct reactor cooling (DRC), 127
Direct steam cycle with moisture separator reheater, 194, 195f
Direct water thermolysis, 642−643
Directorate General (DG), 242
Displacement per atom (DPA), 401
DOE. *See* US Department of Energy (DOE)
DOE Generation IV program, 234
Domestic US energy markets, 230−231
Double-boundary failure modes, 296−297
Double-ended guillotine (DEG), 297
DPA. *See* Deterministic and Phenomenological Analyses (DPA); Displacement per atom (DPA)
DPs. *See* Dip plates (DPs)
DRACS. *See* Direct reactor auxiliary cooling system (DRACS)
DRC. *See* Direct reactor cooling (DRC)
DU. *See* Depleted uranium (DU)
DUPIC cycle, 577
DWO. *See* Density wave oscillations (DWO)
Dynamic operation, 75−77
Dynamic simulation, 75

E
EAGLE project, 292
EBR-II. *See* Experimental Breeder Reactor (EBR-II)
EBWR. *See* Experimental boiling water reactor (EBWR)
EC6. *See* Enhanced CANDU 6 (EC6)
EC. *See* European Commission (EC)
ECCS. *See* Emergency core cooling system (ECCS)
Economic and financing evaluation, 687−690
Economic simplified boiling water reactor (ESBWR), 223, 457
Economics Modelling Working Group (EMWG), 268
"Economy of scale", 284
EEC. *See* Electrical energy consumption (EEC)
EED. *See* Electro-electrodialysis (EED)
Effective delayed neutron fraction (β_{eff}), 162
Effective full power day (EFPD), 63−65
Effective thermal conductivities (ETCs), 628
EFPD. *See* Effective full power day (EFPD); Equivalent full power day (EFPD)
EFR. *See* European Fast Reactor (EFR)
EFSI. *See* European Fund for Strategic Investments (EFSI)
EFTS. *See* Euratom Fission Training Schemes (EFTS)
EGE. *See* European Group on Ethics (EGE)
Electric power generation usage, 1
Electric vehicles, 639−640
Electrical energy consumption (EEC), 3f
Electricity, 641
  electrical grid integration, 231−232
  electrical resistivity specific, 872
  electrical uses of hydrogen, 640−641
Electricity generation, 4f
  cost, 82−84
    capital cost, 82, 83f
    fuel cost, 83, 84f
    operating cost, 83, 83f
    power generation cost, 84, 84f
  modern nuclear power plants, 21−29
  statistics, 1−14
    1. 2-MW_{el} concentrated photovoltaic solar power plant, 16f
    781-MW_{el} onshore Roscoe wind turbine power plant, 10f
    aerial view of largest concentrated solar thermal power plant, 12f
    average capacity factors, 18t
    electrical energy consumption per capita, 2t
    Gemasolar, 14f
    improper and "proper", installation of photovoltaic panels, 17f
    installed capacity and electricity generation, 19f−20f
    largest hydroelectric power plant in world, 9f
    largest operating power plants of world, 8t
    map of annual average direct normal solar resource data distribution, 15f
    map of wind speed distribution over United States, 11f
    power generated and capacity factors, 19f−20f
    power generation, 6f
    power plants of world, 7t
    SEGS, 13f
    test system, 16f
  thermal power plants, 14−18
Electro-electrodialysis (EED), 79
Electrolysis, hydrogen production by, 644
Electron transfer catalysts, 645
ELFR. *See* European Lead-Cooled Fast Reactor (ELFR)
ELSY project. *See* European Lead-cooled SYstem project (ELSY project)
Emergency core cooling system (ECCS), 418, 663−664, 678−684
  IRIS ECCS system, 685f
  NuScale, 683f
  SMART ECCS system, 686f
  system of 4S, 686f
  W-SMR, 684f
    nuclear safety components, 683t
EMWG. *See* Economics Modelling Working Group (EMWG)
Encapsulated Nuclear Heat Source (ENHS), 359−360
Energy
  conservation model equations, 514
  sources, 7

Energy (*Continued*)
work, and heat amount, 872
Enhanced CANDU 6 (EC6), 723, 725–731
Enhanced sustainability, 40
ENHS. *See* Encapsulated Nuclear Heat Source (ENHS)
Enthalpy, 609–611, 873
EoS. *See* Equation of state (EoS)
EPR. *See* European Pressurized Reactor (EPR); Evolutionary power reactor (EPR)
Equation of state (EoS), 486
Equivalent full power day (EFPD), 312–313
Error precursor analysis, 475
ESBWR. *See* Economic simplified boiling water reactor (ESBWR)
ESNII. *See* European Sustainable Nuclear Industrial Initiative (ESNII)
ETCs. *See* Effective thermal conductivities (ETCs)
EU. *See* European Union (EU)
"EU Energy Roadmap 2050", 244–245
EUR. *See* European Utility Requirement (EUR)
Euratom Fission Training Schemes (EFTS), 242
Euratom research and training program in Generation IV systems
developing/teaching science, 270–272
within Energy Union, 241–246
ESNII, 251–255
Generation I, II, III, and IV of nuclear fission reactors, 246–251
goals for generation-IV nuclear energy systems, 247–251
proliferation resistance and physical protection, 267–270
safety and reliability, 259–262
socioeconomics, 262–267
sustainability, 258–259
technology roadmap for six GIF systems, 247–251
European Commission (EC), 120, 242
European Fast Reactor (EFR), 255–258
European Fund for Strategic Investments (EFSI), 245
European Group on Ethics (EGE), 256
European Lead Fast Reactor. *See* European Lead-Cooled Fast Reactor (ELFR)
European Lead-Cooled Fast Reactor (ELFR), 120, 131–133, 132f, 133t–134t
European Lead-cooled SYstem project (ELSY project), 120, 125, 125f
European Pressurized Reactor (EPR), 251
European Sustainable Nuclear Industrial Initiative (ESNII), 120, 251–255
European Technology Platforms, 244
European Union (EU), 241
European Utility Requirement (EUR), 263
Evaluation and Viability Of Liquid fuel fast reactor systems (EVOL), 266
Event and causal factors analysis, 475
EVOL. *See* Evaluation and Viability Of Liquid fuel fast reactor systems (EVOL)
Evolutionary power reactor (EPR), 166–167
Ex-vessel storage tank (EVST), 298
Experimental boiling water reactor (EBWR), 488
Experimental Breeder Reactor (EBR-II), 497
"Extended conditions", 457
External costs, 267
External hazards, 288–289

F

FA. *See* Framework Agreement (FA); Fuel assembly (FA)
Face center cubic models (FCC models), 394
crystal structure, 597, 601–602
FaCT project. *See* Fast Reactor Cycle Technology Development project (FaCT project)
FAIDUS. *See* Fuel assembly with inner duct structure (FAIDUS)
Failure Modes, Effects, and Criticality Analysis (FMECA), 268
FALCON. *See* "Fostering ALFRED Construction" (FALCON)
Fast breeder reactor (FBR), 260, 426, 428f, 584–587. *See also* Advanced heavy water reactor (AHWR); High-temperature reactors (HTRs); Lead-cooled fast reactors (LFRs); Molten salt reactors (MSRs)

conceptual design features of FBR-600, 436
control and safety rod drive mechanism, 438f
decay heat removal systems, 442f
enhanced safety features, 437–441
fast breeder test reactors and current status, 430–432
fast reactor program in India, 430
motivation for improvements for future, 435
PFBR, 432–435
heat transport systems, 431f
operating parameters, 434t
reactor assembly for FBR-600, 433f
research and development status, 441–442
Fast neutron reactors, 260
Fast Reactor. *See* Bystryi Reactor (BR)
Fast reactor cycle systems (FS), 283
Fast Reactor Cycle Technology Development project (FaCT project), 283–284
Fast reactor fuel assembly concept, 200
"Fast Reactor with Lead Coolant", 120
Fast spectrum reactors, 119
"Fast-response" gas-fired power plants, 7–9
FB-CVD technology. *See* Fluidized bed chemical vapor deposition technology (FB-CVD technology)
FBR. *See* Fast breeder reactor (FBR)
FBR-600, conceptual design features of, 436
fuel handling scheme for, 436f
FCC models. *See* Face center cubic models (FCC models)
FCD. *See* First concrete date (FCD)
Federal Target Program, 309
Federation of Electric Power Companies (FEPC), 82
FEPC. *See* Federation of Electric Power Companies (FEPC)
FFFER. *See* Forced Fluoride Flow for Experimental Research (FFFER)
FHM. *See* Fuel handling machine (FHM)
FHR. *See* Fluoride-salt–cooled high-temperature reactor (FHR)
FHR Safety Analysis Code (FSAC), 397
FHS. *See* Fuel handling system (FHS)
FHX. *See* Forced-draft sodium-to-air heat eXchanger (FHX)
FIASCO model, 496
First concrete date (FCD), 383–384
Fischer–Tropsch process, 640
Fissile nuclides, 100, 584
Fission gas plenum, 101–102
Fission products (FPs), 107, 119, 157–158
Fission technologies, 243–244
Fixed deck, 286–288
FlaSHing instability (FSH), 483
FLiNaK molten high-temperature salt test loop, 399–401, 400f
Fluid coolants, 749–750
Fluidized bed chemical vapor deposition technology (FB-CVD technology), 354
Fluoride-salt–cooled high-temperature reactor (FHR), 393, 479
FMECA. *See* Failure Modes, Effects, and Criticality Analysis (FMECA)
Forced convection heat transfer, 797–813
basics of supercritical heat transfer, 798–802
heat transfer enhancement, 806
horizontal flows, 805–806
practical prediction methods, 806–813
pseudo-boiling and pseudo-film boiling phenomena, 802–804
temperature and heat transfer coefficient profiles, 800f
variations, 801f
Forced Fluoride Flow for Experimental Research (FFFER), 178, 179f
Forced-draft sodium-to-air heat eXchanger (FHX), 346
Fort St. Vrain (FSV), 55
Fossil fuels, 639
hydrogen production from, 643
thermal power plants
coal-fired power plants, 703, 707f
combined cycle power plants, 701, 702f
"Fostering ALFRED Construction" (FALCON), 257
4S containment, 682f
4S ECCS system, 686f

4S reactor. *See* Super Safe, Small and Simple reactor (4S reactor)
FPs. *See* Fission products (FPs)
Framework Agreement (FA), 249
FREDOCSR1000. *See* FREquency DOmain analysis of CSR1000 (FREDOCSR1000)
Free surface vortex, 293–294
FREquency DOmain analysis of CSR1000 (FREDOCSR1000), 393
FS. *See* Fast reactor cycle systems (FS)
FSAC. *See* FHR Safety Analysis Code (FSAC)
FSH. *See* FlaSHing instability (FSH)
FSL. *See* Refueling sodium level (FSL)
FSV. *See* Fort St. Vrain (FSV)
Fuel assembly (FA), 198–205, 387–388, 388f
  Canadian SCWR FA concept, 201–205, 202f
  fast reactor fuel assembly concept, 200
  HPLWR, 198–200
  reactor core with fast neutron spectrum, 201f
Fuel assembly with inner duct structure (FAIDUS), 288, 291, 292f
Fuel handling machine (FHM), 289
Fuel handling system (FHS), 105, 289
Fuel(s), 674–678. *See also* Nuclear fuel
  bundle concept, 201–202, 203f
  burnup, 63–65
    plutonium fuel, 63–65, 66t–67t
    uranium fuel, 63, 64t–65t
  cells, 641
  cladding material candidates, 203, 204t
  comparison of components, 676t–677t
  cost, 83, 84f
  cycles
    advanced uranium fuel cycle, 575f
    cost, 570–574
    cost savings of future, 576–577
    economic and social aspects of recycling, 574–575
    global nuclear fuel cycles, 571f
    overcoming ostrich syndrome, 579
    technology, 106–107, 197–198
    waste to energy, 577–578
  design, 60–63, 62t
  development, 424–425
  elements, 102
  Fuel pin, 101–102
  Fuel rods, 128
  subassembly, 101–102
  supplier nations, 272
Fukushima accidents, 373–374
  and Fukushima types of scenarios, 418
  Fukushima-Daiichi accident, 300–302
    nuclear power plant accident, 108

G

G4-Econs, 268
GAMMA+ code, 351
Gas turbine combined cycle (GTCC), 86
Gas turbine generator (GTG), 288–289
Gas turbine modular helium-cooled reactor (GT-MHR), 234–236
Gas-cooled fast reactors (GFRs), 39, 43–44, 43f, 91, 227, 772. *See also* Sodium-cooled fast reactors (SFRs); Lead-cooled fast reactors (LFRs)
  in-core design options, 94t
  rationale and generational research and development bridge, 91–93
  safety, 477
  technology, 93–95
Gas-cooled reactors (GCRs), 701, 731, 735f, 743
Gas(es)
  at atmospheric pressure
    in nuclear power and industries, 857–858
    properties, 855
    thermophysical properties comparison, 855
    thermophysical property profiles *vs.* temperature, 856
  bubbling, 164–166
  coolants, 750–751
  entrainment, 293–294, 293f
GCRs. *See* Gas-cooled reactors (GCRs)
GDCS. *See* Gravity-driven cooling systems (GDCS)
Gen-I. *See* Generation I (Gen-I)
Gen4 safety system, 684
Generation I (Gen-I), 246–247
Generation II, III, III+, and IV reactor coolants, 752–759
  basic properties of He, CO_2, and water, 760t

reference parameters, 753t
selected coolants *vs.* temperature
density, 754f
enthalpy, 757f
Pr, 758f
specific heat, 757f
thermal conductivity, 755f
viscosity, 756f
volume expansivity, 759f
Generation II (Gen-II), 247
Generation III (Gen-III), 247
Gen-III+, 662
Generation IV (Gen-IV), 98, 247, 309, 335–336, 413–414, 466–467, 662
contemporary nuclear power technologies, 224–226, 225t
deployment perspectives, 233–236
energy market in United States, 229–231
GFR, 92–94
hydrogen cogeneration with, 654
heat requirements for hydrogen production, 655
isolation, 655–656
pressure considerations, 655
lead-cooled fast reactor designs, 131–142
Additional Generation IV systems, 137–142
Reference Generation IV systems, 131–137
nuclear energy systems, 227
electrical grid integration, 231–232
industry and utilities interests in, 232–233, 233t
nuclear power technologies, 228t
passive residual heat removal systems, 493–494
potential role, 229–231
program evolution in United States, 223–229
reactor coolants, 743–749
estimated ranges of thermal efficiencies, 746t–747t
technologies, 541
Generation IV International Forum (GIF), 37, 98, 121, 226–227, 248, 335–336, 455–456
estimated ranges of thermal efficiencies, 53t
generation IV goals, 38–39
origins, 37–38
selection, 39–40
status of GIF system arrangements and memoranda, 39f
system development timelines, 40f
six generation IV nuclear energy systems, 40–52
Generations II, III, and III+ reactor coolants, 743
GEySering (GES), 483
GFRs. *See* Gas-cooled fast reactors (GFRs)
GG. *See* Green granule (GG)
Gibbs free energy, 609–611
GIF. *See* Generation IV International Forum (GIF)
GIF Policy Group, 226–227
GIF/MSR. *See* MSR System Steering Committee of the Generation IV International Forum (GIF/MSR)
GIF Technology Roadmap (2002), 253
Global Nuclear Energy Partnership (GNEP), 269
Goals for generation-IV nuclear energy systems, 247–251
Graphite
reflectors, 385
stack, 832
Gravity-driven cooling systems (GDCS), 390
Gravity-driven core flooding system, 209–210
Green granule (GG), 631
GT-MHR. *See* Gas turbine modular helium-cooled reactor (GT-MHR)
GTCC. *See* Gas turbine combined cycle (GTCC)
GTG. *See* Gas turbine generator (GTG)
GTHTR300 reactor, 67–68, 68f, 72, 72f
GTHTR300C + IS, 84–85, 85f
Guard vessel (GV), 288
GV. *See* Guard vessel (GV)

H

HAZard and Operability (HAZOP), 268
HDI. *See* Human Development Index (HDI)
HDPV. *See* Hot gas duct pressure vessel (HDPV)
Heat exchanger (HEX), 467
Heat flux, 873

Heat flux (*Continued*)
volumetric, 873
Heat requirements for hydrogen production, 655
Heat transfer
enhancement, 806
rate and power, 873–874
Heat transfer coefficient (HTC), 795, 796f, 799, 873
in nuclear power reactors, 759–765, 764f–765f
ranges of heat transfer coefficients, heat fluxes, and sheath temperatures, 763t–764t
Heavy liquid metal reactors (HLMRs), 320–321
BREST-1200, 327, 328t
BREST-OD-300, 324–327
characteristics, 326t
primary system layout, 325f
SVBR-100, 321–324, 322t, 323f
Heavy water (D_2O), 743, 749
thermophysical properties comparison, 750t
HELIOS, 360
Helium (He), 58–59, 743–747, 750–751
basic properties, 760t
specific heat *vs*. temperature, 786f
thermal conductivity *vs*. temperature, 786f
thermodynamic diagrams, 749f
thermodynamics diagrams for, 775f
volumetric expansivity *vs*. temperature, 787f
Heterogeneous core configuration, 100, 101f
HEX. *See* Heat exchanger (HEX)
High burn-up core, 289–290
High-performance light water reactor (HPLWR), 191–192, 198–200, 199f
High-precision simulation method, 293–294
High-pressure preheaters (HP preheaters), 190
High-temperature
materials, 355–356
systems, 40
High-temperature gas-cooled reactor (HTGR), 55, 56t, 380–381
early development of HTGR program, 381
High-temperature reactor module (HTR-Module), 381
High-temperature reactor-pebble bed module (HTR-PM), 55, 70f, 73f, 374–375
design, 385
parameters, 386t–387t
primary loop, 386f
project, 384
High-temperature reactors (HTRs), 91, 226, 248–249, 374, 413–414, 421. *See also* Advanced heavy water reactor (AHWR)
compact high-temperature reactors, 421
component layout, 422f
core cross section, 422f
design and operating parameters, 423t
fuel development, 424–425
inherent safety features, 426
innovative high-temperature reactor, 428–429, 429t
materials development, 425
molten salt natural-circulation loop, 428f
passive heat removal systems, 426
reactor physics design, 421–424
research and development activities, 427
thermal hydraulics design, 424
High-temperature test reactor (HTTR), 55, 67f, 74f–75f, 382f, 478
design and objectives, 382–383
engineering experiments, 383
experiences learning, 383–384
test module project, 381–382
HLMRs. *See* Heavy liquid metal reactors (HLMRs)
Homogeneous core, 100, 101f
Homogeneous reactor experiment (HRE-2), 157–158
Homogeneous reactors, 172
Horizontal flows, 805–806
Hot gas duct pressure vessel (HDPV), 385
Hot-leg piping design, 295, 295f
HP preheaters. *See* High-pressure preheaters (HP preheaters)
HPLWR. *See* High-performance light water reactor (HPLWR)
HRE-2. *See* Homogeneous reactor experiment (HRE-2)
HTC. *See* Heat transfer coefficient (HTC)

HTGR. *See* High-temperature gas-cooled reactor (HTGR)
HTR-10. *See* High-temperature test reactor (HTTR)
HTR-Module. *See* High-temperature reactor module (HTR-Module)
HTR-PM. *See* High-temperature reactor-pebble bed module (HTR-PM)
HTRs. *See* High-temperature reactors (HTRs)
HTTR. *See* High-temperature test reactor (HTTR)
Human Development Index (HDI), 3f
"Humps", 788, 799
150 MW_{el} prototype sodium-cooled fast reactor development
  configuration of fluid system, 345f
  core design, 343
  fluid system design, 345–346
  fuel design, 343–345
  mechanical structure design, 346
  top-tier design requirements, 341–342, 342t–343t
  U–Zr core design, 344t
Hybrid sulfur cycle (HyS cycle), 642–643, 648
Hybrid systems, 232
Hydraulic resistance, 815–816
Hydride fuels
  uranium–thorium–zirconium fuels, 626–628
  uranium–zirconium hydride fuel, 624–625
Hydro-fired power plants, 7–9
Hydrochloric acid (HCl), 640
Hydrocracking, 640
Hydrogen, 339, 637–638
  benefits, 641–642
  production, 336, 356–358
    cost, 84–85, 85t
    by electrolysis, 644
    from fossil fuels, 643
    methods, 642, 642f
    by photoelectrolysis, 645
    from solar energy, 645–646
    thermochemical cycles, 646–654
  uses, 638
    commercial, 641
    electrical, 640–641
    industrial, 640
    transportation, 639–640
  water splitting processes, 638
Hydrogen cogeneration, 79–80, 637
  with Generation IV reactors, 654
    heat requirements for hydrogen production, 655
    isolation, 655–656
    pressure considerations, 655
HYPERION's safety system, 684
HyS cycle. *See* Hybrid sulfur cycle (HyS cycle)

I

IAEA. *See* International Atomic Energy Agency (IAEA)
ICs. *See* Isolation condensers (ICs)
IFNEC. *See* International Framework for Nuclear Energy Cooperation (IFNEC)
IGCAR. *See* Indira Gandhi Center for Atomic Research (IGCAR)
IHT. *See* Improved Heat Transfer (IHT)
IHTR. *See* Innovative high-temperature reactor (IHTR)
IHTS. *See* Intermediate heat transport system (IHTS)
IHXs. *See* Intermediate heat exchangers (IHXs)
Improved Heat Transfer (IHT), 797
IMSBR. *See* Indian molten salt breeder reactor (IMSBR)
In-vessel retention (IVR), 301–302
Independent double failures, 297
India, Generation IV
  AHWR, 414–420
  FBR, 430–442
  HTRs, 421–429
  MSRs, 442–448
Indian Department of Atomic Energy (DAE), 413–414
Indian molten salt breeder reactor (IMSBR), 414, 442–445, 446f
  design and operating parameters, 448t
  pool-type, 447f
Indira Gandhi Center for Atomic Research (IGCAR), 413–414
Indirect cycle, 42
Industrial uses of hydrogen, 640

INET. *See* Institute of Nuclear Energy Technology (INET)
Inherent reactivity feedback, 109
Inherent safety features, 418
Inlet plenum, 194
Inner layer of high-density pyrolytic carbon (IPyC), 60–61
Innovative high-temperature reactor (IHTR), 414, 428–429, 429t
INPRO. *See* International Project on Innovative Nuclear Reactors and Fuel Cycles (INPRO)
Institut de Radioprotection et de Sûreté Nucléaire (IRSN), 251
Institute for Physics and Power Engineering (IPPE), 350
Institute of Nuclear Energy Technology (INET), 381–382
INTCA code, 352
Integrated Safety Analysis Methodology (ISAM), 265, 469
Interface-tracking approach, 293–294
Intermediate heat exchangers (IHXs), 75, 104, 284, 295–296, 296f, 346, 377, 432
Intermediate heat transport system (IHTS), 337
Intermediate reactor auxiliary cooling systems (IRACSs), 285
International Atomic Energy Agency (IAEA), 107–108, 242, 373–374, 461, 542–543, 662
International Framework for Nuclear Energy Cooperation (IFNEC), 269
International Project on Innovative Nuclear Reactors and Fuel Cycles (INPRO), 249
International Reactor Innovative and Secure (IRIS), 663–664
  containment, 681f
  ECCS system, 685f
International Symposiums on SCWRs (ISSCWR), 797
IPPE. *See* Institute for Physics and Power Engineering (IPPE); Institute of Physics and Power Engineering (IPPE)
IPyC. *See* Inner layer of high-density pyrolytic carbon (IPyC)
IRACSs. *See* Intermediate reactor auxiliary cooling systems (IRACSs)
Iran nuclear program, 270
IRIS. *See* International Reactor Innovative and Secure (IRIS)
Iron (Fe), 321–322, 360–362
  oxide cycle, 651–652
IRSN. *See* Institut de Radioprotection et de Sûreté Nucléaire (IRSN)
ISAM. *See* Integrated Safety Analysis Methodology (ISAM)
Isolation condensers (ICs), 133, 210
ISSCWR. *See* International Symposiums on SCWRs (ISSCWR)
IVR. *See* In-vessel retention (IVR)

J
JAEA. *See* Japan Atomic Energy Agency (JAEA)
Japan, Generation IV concepts, 283
  JSFR, 284–300
Japan Atomic Energy Agency (JAEA), 55, 283–284, 290
Japan Atomic Energy Commission, 283–284
Japan sodium-cooled fast reactor (JSFR), 98, 283–300, 287f
  bird's eye view of NSSS, 285f
  design specifications, 286t
  general design features, 284–289
  key innovative technologies in, 289–300
    advanced seismic isolation system, 299–300
    compact reactor system, 293–294
    high burn-up core, 289–290
    integrated IHX/pump component, 295–296
    natural-circulation decay heat removal system, 297–298, 298f
    reliable steam generator, 296–297
    safety enhancement, 290–292
    simplified fuel handling system, 298
    steam generator with double-walled straight heat transfer tubes, 297f
    steel plate–reinforced concrete containment vessel, 299
    two-loop cooling system, 294–295
  with lessons learned from Fukushima-Daiichi accident, 300–302

reactor vessel, 287f
JHR. *See* Jules Horowitz Reactor (JHR)
Joint Research Centre (JRC), 242
JOYO experimental reactor, 283, 290, 293
JRC. *See* Joint Research Centre (JRC)
JSFR. *See* Japan sodium-cooled fast reactor (JSFR)
Jules Horowitz Reactor (JHR), 258

K
KAEC. *See* Korea Atomic Energy Commission (KAEC)
KAERI. *See* Korea Atomic Energy Research Institute (KAERI)
KAERI−Dynamic Simulation Code (KAERI−DySCo), 356−357, 357f
KALIMER. *See* Korea Advanced LIquid Metal Reactor (KALIMER)
KALIMER-600, 337
Key water chemistry issues, 52
KIER. *See* Korea Institute of Energy Research (KIER)
KIST. *See* Korea Institute of Science and Technology (KIST)
Korea, Generation IV concepts
  current status of nuclear power, 335−336
  nuclear hydrogen project plan, 339f
  plans for advanced nuclear reactors
    sodium-cooled fast reactor, 336−338
    VHTR, 338−341
  research and development
    LFR, 358−363
    MSR, 363−365
    sodium-cooled fast reactor, 341−350
    very high temperature reactor, 350−358
Korea Advanced LIquid Metal Reactor (KALIMER), 337
Korea Atomic Energy Commission (KAEC), 337
Korea Atomic Energy Research Institute (KAERI), 335−336, 350, 351f
  CORONA code, 352
  FB-CVD technology, 354
  TRISO fuel particles, 354f
Korea Institute of Energy Research (KIER), 339
Korea Institute of Science and Technology (KIST), 339

L
Large break (LB), 673
Large early release frequency (LERF), 263
Large eddy simulation (LES), 293−294
Large release frequency (LRF), 313, 457, 459
Large-break loss of coolant accident (LBLOCA), 490−491, 664
Large-diameter fuel elements, 102
Large-scale sodium thermal−hydraulic test program, 346−347
LB. *See* Large break (LB)
LBE. *See* Lead−bismuth eutectic (LBE)
LBLOCA. *See* Large-break loss of coolant accident (LBLOCA)
LCOE. *See* Levelized cost of electricity (LCOE)
Lead (Pb), 310, 751
  basic properties, 761t−762t
  coolants, 119
  lead corrosion, protection from, 149−150
Lead fast reactor (LFR), 358−363
  Peacer Park with multinational control, 359f
  R&D at SNU, 358f
Lead-cooled European Advanced DEmonstration Reactor (LEADER), 120, 266
Lead-Cooled Fast Reactor−Amphora Shaped project (LFR-AS project), 145−148, 146f
Lead-cooled fast reactors (LFRs), 39, 46−47, 46f, 119, 227, 375, 743−747, 772−773
  advantages, 130
  basic design choices, 121−126
    comparative properties of liquid metal coolants, 121t
    design choices for reactors with lead as coolant, 122−123
    design parameters of Generation IV reference LFR concepts, 123t
    lead *vs*. LBE, 121−122
    primary system concept, 123−126
  fuel technology and fuel cycles, 128−129
    fuel assembly characteristics, 128−129
    transuranic masses, 129t
  future trends, 142−150

Lead-cooled fast reactors (LFRs) (*Continued*)
generation IV lead-cooled fast reactor designs, 131–142
key challenges, 131
overview and motivation, 119–121
research and development, 401–402
CLEAR, 401–402, 402f
safety principles, 126–128
Lead–bismuth eutectic (LBE), 46–47, 119, 358–359, 401–402, 421
Lead–Bismuth Fast Reactor. *See* Svintsovo-Vismutovyi Bystryi Reaktor (SVBR)
LEADER. *See* Lead-cooled European Advanced DEmonstration Reactor (LEADER)
LERF. *See* Large early release frequency (LERF)
LES. *See* Large eddy simulation (LES)
LEU. *See* Low enriched uranium (LEU); Low-enriched uranium (LEU)
Levelized cost of electricity (LCOE), 868t
in Germany, 868t
in United States, 868t
Levelized unit energy costs (LUEC), 266
LFR. *See* Lead fast reactor (LFR)
LFR-120 (LFR-AS) project, 143
LFR-AS project. *See* Lead-Cooled Fast Reactor–Amphora Shaped project (LFR-AS project)
LFRs. *See* Lead-cooled fast reactors (LFRs)
LGRs. *See* Light water-cooled graphite-moderated reactors (LGRs)
LHR. *See* Linear heat rating (LHR)
Liaison-POmpe-SOmmier (LIPOSO), 147
Licensing process, 226
Light water (LW), 689, 743
basic properties, 760t
subcritical pressure, 749
thermodynamic diagrams, 748f
thermophysical properties comparison, 750t
Light water reactors (LWRs), 40–42, 97, 164, 198, 223–224, 309, 384, 477, 558, 795
Light water SMR (LW-SMR), 661–662, 673, 678
Light water-cooled graphite-moderated reactors (LGRs), 701, 709–713, 731, 743
11-MW_{el} EGP-6, 737f
thermodynamic layout of RBMK-1000 NPP, 736f
T–s diagram for RBMK-1000 NPP turbine cycle, 736f
1000-$_{MWel}$ LGR NPP, 735f
Light water-cooled reactors. *See also* Light water reactors (LWRs)
Linear heat rating (LHR), 430
Lines of protection (LOP), 263
LIPOSO. *See* Liaison-POmpe-SOmmier (LIPOSO)
Liquid lead–bismuth eutectic (LBE), 743–747, 751
basic properties, 761t–762t
Pb–Bi coolant, 323–324
Pr for, 758
Liquid metal coolants, 751
Liquid metal fast reactors. *See* Liquid metal–cooled fast reactors (LMFRs)
Liquid metal fast-breeder reactors (LMFBRs), 701
Liquid metal–cooled fast reactors (LMFRs), 93, 226
safety, 477
Liquid Na, 751
basic properties, 761t–762t
Liquid-cooled reactors, 655
Liquid-fuel
reactor specificities, 172–174
single loop reactor, 178f
Liquid-fuel TMSR (TMSR-LF), 393
LMFBRs. *See* Liquid metal fast-breeder reactors (LMFBRs)
LMFRs. *See* Liquid metal–cooled fast reactors (LMFRs)
LOCA analysis. *See* Loss of coolant accident analysis (LOCA analysis)
LOCAs. *See* Loss-of-coolant accidents (LOCAs)
LOHRS. *See* Loss of heat removal system (LOHRS)
LOHS. *See* Loss of heat sink (LOHS)
Long-term cooling, 472
LOOP. *See* Loss of offsite power (LOOP)
Loop-type system, 105–106, 106t, 283
LOP. *See* Lines of protection (LOP)
LORL. *See* Loss of reactor level (LORL)
Loss of coolant accident analysis (LOCA analysis), 323–324, 390, 471, 667

Loss of flow, 176
Loss of heat removal system (LOHRS), 301, 302t
Loss of heat sink (LOHS), 176, 290–291
Loss of liquid fuel, 176
Loss of offsite power (LOOP), 395
Loss of reactor level (LORL), 288
Loss-of-coolant accidents (LOCAs), 208–209
Low enriched uranium (LEU), 198
Low-density "gas", 797
Low-enriched uranium (LEU), 414–417
Low-flow stability tests, 492
Low-pressure preheaters (LP preheaters), 190
LRF. *See* Large release frequency (LRF)
LUEC. *See* Levelized unit energy costs (LUEC)
LW. *See* Light water (LW)
LW-SMR. *See* Light water SMR (LW-SMR)
LWRs. *See* Light water reactors (LWRs)

M
MAC. *See* Multiple-channel analysis code (MAC)
Magnox reactors, 588
Main circulation pumps (MCPs), 844
Main heat transport system (MHTS), 420
Manganese (Mn), 349
Manhattan Project, 557
MARS. *See* Minor Actinides Recycling in Molten Salt (MARS)
MAs. *See* Minor actinides (MAs)
Mass, 874
  conservation, 505
Massachusetts Institute of Technology (MIT), 543
Master logic diagram (MLD), 395
MBIR. *See* Multipurpose fast neutron research reactor (MBIR)
MC approach. *See* Monte Carlo approach (MC approach)
MCNP. *See* Monte Carlo code for neutron and photon transport (MCNP)
MCPs. *See* Main circulation pumps (MCPs)
MDBs. *See* Multilateral development banks (MDBs)
MDEP. *See* Multinational Design Evaluation Program (MDEP)
Metal fuel development, 349
Metal-clad fuel elements, 94
Metallic fuels, 587–588
MHTS. *See* Main heat transport system (MHTS)
MINA. *See* MINI Sodium Fire Facility (MINA)
MINI Sodium Fire Facility (MINA), 441–442, 444f
Minor actinides (MAs), 107, 130, 157–158, 249, 310, 380
Minor Actinides Recycling in Molten Salt (MARS), 170, 266
MIT. *See* Massachusetts Institute of Technology (MIT)
Mixed oxide (MOX), 42, 378, 414–417, 588, 591–594
  fuel, 197–198, 259, 558
Mixed spectrum SCWR (SCWR-M), 385–390, 388f, 390f
  design parameters, 389t
Mixture mass flow rate, 499
MLD. *See* Master logic diagram (MLD)
Mod.9Cr-1Mo steel, 285, 289
Modern nuclear power plants, 21–29, 22t
  age of nuclear power reactors in selected countries, 27f
  casualties, 30t–31t
  generations of nuclear reactors, 23f
  number of nuclear power reactors, 24t, 25f–26f, 28t
  scenarios for future of nuclear power, 27f
  selected Generation III+ reactors, 29t
Modular nuclear power reactors, 248
Modular reactor with steam reheat, 846–849
Moisture separator reheater (MSR), 194
Molten salt
  basic properties, 761t–762t
  coolants, 752
  fluorides, 752
  test loops, 399–401
MOlten Salt Actinide Recycler and Transmuter (MOSART), 158, 395–397
Molten salt breeder reactor (MSBR), 157–158, 413–414

Molten Salt Breeder Reactor Development Facility (MSBRDF), 448
Molten salt fast reactor (MSFR), 48, 158–163, 159f, 479. *See also* Advanced heavy water reactor (AHWR); Fast breeder reactor (FBR); High-temperature reactors (HTRs); Lead-cooled fast reactors (LFRs)
  calculated neutron spectrum of reference MSFR, 160f
  characteristics, 160t
  concept viability, 176–181
  core and system description, 158–161
  fuel cycle scenarios, 166–170
    actinide stockpiles evolution, 170f
    French nuclear power deployment exercise, 169f
    time evolution of contributions, 171f
    time evolution up to equilibrium of heavy nuclei inventory, 168f
  fuel salt chemistry and material issues
    fuel salt treatment with two loops, 165f
    influence of batch reprocessing rate, 165f
    processing schemes, 164–166
    impact of salt composition on corrosion of structural materials, 166
  HRE-2, 157–158
  physicochemical properties, 161t
  safety issues, 170–176
    decay heat removal, 175
    liquid-fueled reactor specificities, 172–174
    main functions, 174f
    preliminary accidental transient identification, 176
    residual heat in different radioactive fluids, 175f
    resources and functions of fuel circuit subsystems, 173f
    safety approach and risk analysis, 171–172
  transient calculations, 162–163
    delayed and prompt neutron sources, 162f
    instantaneous load-following, 163f
    power, velocity, and temperature distribution, 164f
Molten salt natural-circulation loop, 428f
Molten salt reactor experiment (MSRE), 397
Molten salt reactors (MSRs), 39, 47–49, 48f, 157, 227, 363–365, 375, 442, 743–747. *See also* Advanced heavy water reactor (AHWR); Fast breeder reactor (FBR); High-temperature reactors (HTRs)
MONJU, 105–106
  design challenges, 445–447
  designs of IMSBR, 442–445
  research and development, 393
    material and salts research, 401
    molten salt test loops, 399–401
    neutronic modeling, 399
    thermal-hydraulic modeling and safety analysis, 394–398
    thermo-hydraulics and neutronics coupling analysis, 399
  research and development activities, 448
  safety, 477
  test facilities for, 447f
  prototype power reactor, 283, 293
Monte Carlo approach (MC approach), 162
Monte Carlo code for neutron and photon transport (MCNP), 399
MOSART. *See* MOlten Salt Actinide Recycler and Transmuter (MOSART)
MOX. *See* Mixed oxide (MOX)
MSBR. *See* Molten salt breeder reactor (MSBR)
MSBRDF. *See* Molten Salt Breeder Reactor Development Facility (MSBRDF)
MSF system. *See* Multistage flash system (MSF system)
MSFR. *See* Molten salt fast reactor (MSFR)
MSR. *See* Moisture separator reheater (MSR)
MSR System Steering Committee of the Generation IV International Forum (GIF/MSR), 158
MSRE. *See* Molten salt reactor experiment (MSRE)
MSRs. *See* Molten salt reactors (MSRs)
Multi-purpose hYbrid Research Reactor for High-tech Applications (MYRRHA), 120, 249

Multinational Design Evaluation Program (MDEP), 250
Multiple-channel analysis code (MAC), 399
Multipurpose fast neutron research reactor (MBIR), 313–317, 316f
  design characteristics, 318t
  testing capabilities, 317t
Multistage flash system (MSF system), 80–81
MYRRHA. *See* Multi-purpose hYbrid Research Reactor for High-tech Applications (MYRRHA)

N
Nanofluids, 497
National Major Science and Technology projects, 374–375
Natural Boiling Oscillation (NBO), 483
Natural circulation, 122, 127, 288
Natural convection, 112–113
Natural Science Foundation of China (NSFC), 393–394
Natural uranium (NU), 129
Natural-circulation decay heat removal system, 297–298, 298f
Natural-circulation loops (NCLs), 481–482, 495–496, 498
  modeling, 498
    coupled natural-circulation loops, 508–520
    parallel channels, 498–503
    single channels, 498–503
    single natural-circulation loop, 503–508, 504f
  natural-circulation flows, 482–486
  passive safety systems, 482
  thermal-hydraulic instabilities classification, 485t
NBO. *See* Natural Boiling Oscillation (NBO)
NCLs. *See* Natural-circulation loops (NCLs)
NEA. *See* Nuclear Energy Agency (NEA)
Near critical point, 775
Near-Term Deployment Group (NTDG), 234, 235t
Net capacity factor of power plant, 3
Neutron absorber, 100
Neutron spectrum, 583–584
  Generation IV nuclear-reactor, 586t
  types of operating nuclear power reactors, 585t
Neutronic(s), 834–835
  modeling, 399
  models, 399
Neutronics/thermo-fluid coupled analysis code system, 352, 352f
Next generation nuclear plant (NGNP), 55
NGOs. *See* Nongovernmental organizations (NGOs)
NHDD project. *See* Nuclear hydrogen development and demonstration project (NHDD project)
NHT. *See* Normal heat transfer (NHT)
Nickel (Ni), 321–322
  nickel-based alloys, 161
Niigata-ken Chuetsu-oki earthquake in 2007, 299–300
NIMBY. *See* Not in my backyard (NIMBY)
Nitride fuels, 100, 606
  uranium mononitride, 606–615
NNWS. *See* Nonnuclear weapons states (NNWS)
Non-LW-SMR, 662
Nongovernmental organizations (NGOs), 245
Nonnuclear weapons, 550
Nonnuclear weapons states (NNWS), 559
Nonproliferation, 542–544
  Euratom, 579
  fuel cycles, 570–579
  future, 564
    advanced reactors, 566–568
    alternate fuel cycles, 565–566
    nuclear non-proliferation Treaty, 566–568
  genesis of NPT and bargain, 547–551
  IAEA additional protocol (1997), 579–581
  military nuclear stockpiles, 545t
  national fuel cycle capabilities and reactor types, 548t
  nonproliferation, 542–544
  past dreams and present realities of politics of power, 545–547
  Treaty system
    attempts to improving, 555–556
    effects, 551–553
    shortcomings, 553–555
  wider context, 568–570

Nonproliferation club (NPTC), 542–543
Normal heat transfer (NHT), 796–797
Normal sodium level (NSL), 286–288
NPIC. *See* Nuclear Power Institute of China (NPIC)
NPPs. *See* Nuclear power plants (NPPs)
NPT. *See* Nuclear Non-Proliferation Treaty (NPT)
NPTC. *See* Nonproliferation club (NPTC)
NRC. *See* US Nuclear Regulatory Commission (NRC)
NSFC. *See* Natural Science Foundation of China (NSFC)
NSG. *See* Nuclear Suppliers Group (NSG)
NSL. *See* Normal sodium level (NSL)
NSSS. *See* Nuclear steam supply system (NSSS)
NTDG. *See* Near-Term Deployment Group (NTDG)
NU. *See* Natural uranium (NU)
Nuclear energy, 98, 244, 654
Nuclear Energy Agency (NEA), 243
Nuclear fission, 244–245, 541, 583
  nuclear fission reactors, generation I, II, III, and IV of, 246–251
Nuclear fuel, 584. *See also* Fuel(s)
  ceramic fuels, 588–624
  composite fuels, 628–631
  Generation IV nuclear-reactor, 586t
  hydride fuels, 624–628
  metallic fuels, 587–588
  types of operating nuclear power reactors, 585t
NUclear Generation-II and Generation-III Association (NUGENIA), 252
Nuclear history, 556
  commercial nuclear power, 557–558
  present situation and issues, 559
    alternate fuel cycles for advanced reactors, 560–561
    commercial fuel supply, 560
    enrichment, 561–562
    future policy implications of nuclear fuel cycles, 563–564
    reprocessing and recycling, 562–563
    research for advanced reactors, 559–560
  weapons-grade material, 557
Nuclear hydrogen development and demonstration project (NHDD project), 336, 340, 341f
Nuclear hydrogen production, 421
Nuclear Non-Proliferation Treaty (NPT), 542–543, 551, 566–568
Nuclear power, 21–22, 229
  generation, 335
  industry, 223
Nuclear Power Institute of China (NPIC), 385–387
Nuclear power plants (NPPs), 1, 3, 52, 242–243, 312, 373, 637, 639, 687, 707–740, 772, 825
  parameters, 712t
  typical ranges of thermal efficiencies, 744t–745t
Nuclear power reactors, 707–740
  AGRs, 731, 733f
  BWRs, 713–720
  GCRs, 731, 735f
  heat transfer coefficients in, 759–765, 764f–765f
    ranges of heat transfer coefficients, heat fluxes, and sheath temperatures, 763t–764t
  LGRs, 731
  PHWRs, 720–731
  PWRs, 709–713
  SFRs, 737f, 740
Nuclear reactors, 584–587, 667
  comparison, 668t–669t
  RX of 4S, 672f
Nuclear renaissance, 562, 567–568
Nuclear steam reheat
  BWR NPPs
    parameters, 827t
    thermal parameters, 828t
  nuclear reactors, 825
  Russian experience in, 826–849
  US experience in, 825–826
Nuclear steam supply system (NSSS), 72
Nuclear Suppliers Group (NSG), 554
Nuclear Transmutation Energy Research Center of Korea (NUTRECK), 359
Nuclear Waste Management Organization (NWMO), 572

NUGENIA. *See* NUclear Generation-II and Generation-III Association (NUGENIA)
Numerical methods and artifacts, 492−493
Nuoride, 655
NuScale, 673, 678
  containment, 680f
  ECCS, 683f
NUTRECK. *See* Nuclear Transmutation Energy Research Center of Korea (NUTRECK)
NWMO. *See* Nuclear Waste Management Organization (NWMO)

O
O&M. *See* Operation and maintenance (O&M)
Oak Ridge National Laboratory (ORNL), 157−158, 397
Objective Provision Tree (OPT), 263
ODEs. *See* Ordinary differential equations (ODEs)
ODS steel cladding material. *See* Oxide-dispersion-strengthened steel cladding material (ODS steel cladding material)
OECD. *See* Organisation for Economic Co-operation and Development (OECD)
OEM. *See* Original equipment manufacturer (OEM)
OFI. *See* Onset of flow instability (OFI)
OGDHR system. *See* Operating-grade decay heat removal system (OGDHR system)
ONB. *See* Onset of nucleate boiling (ONB)
Once-through cycle (OTC), 576
Once-through-then-out mode (OTTO mode), 381
Onset of flow instability (OFI), 484
Onset of nucleate boiling (ONB), 497
Onset of nucleation (OON), 500−501
Onset of significant void (OSV), 500−501
OON. *See* Onset of nucleation (OON)
Operating cost, 83, 83f
Operating-grade decay heat removal system (OGDHR system), 439−440
Operation and maintenance (O&M), 268
OPT. *See* Objective Provision Tree (OPT)
OPyC. *See* Outer layer of high-density pyrolytic carbon (OPyC)
Ordinary differential equations (ODEs), 494
Oregon State University−Multi-Application Small Light Water Reactor (OSU-MASLWR), 494
Organisation for Economic Co-operation and Development (OECD), 243
ORIGEN2, 399
Original equipment manufacturer (OEM), 86
ORNL. *See* Oak Ridge National Laboratory (ORNL)
OSU-MASLWR. *See* Oregon State University−Multi-Application Small Light Water Reactor (OSU-MASLWR)
OSV. *See* Onset of significant void (OSV)
OTC. *See* Once-through cycle (OTC)
Otto internal combustion engine cycle, 17
OTTO mode. *See* Once-through-then-out mode (OTTO mode)
Out-of-pile mock-up experiments, 291
Outer layer of high-density pyrolytic carbon (OPyC), 60−61
Overheated vapor, 747−749
Oxide coatings, 149
Oxide fuels, 589
  mixed oxide, 591−594
  thorium dioxide, 594−596
  uranium dioxide, 589−591
Oxide-dispersion-strengthened steel cladding material (ODS steel cladding material), 289−290

P
PALLAS reactor, 258
Pantograph-type fuel handling machine, 298, 299f
"Paper reactors", 92
Parallel channel(s), 497−503
  thermal-hydraulics, 481−482
    natural-circulation flows, 482−486
    passive safety systems, 482
    thermal-hydraulic instabilities classification, 485t
Particle fuel, 478
Passive DHRSs (PDHRSs), 346

Passive heat removal system, 397, 426
Passive moderator cooling system (PMCS), 211
Passive poison injection system (PPIS), 419
Passive residual heat removal (PRHR), 397, 397f–398f
Passive residual heat removal system (PRHRS), 493
Passive safety, 661–662, 678, 682–684
  features, 108
  systems, 418
Passive shut-down mechanism, 109
PATH. *See* Post-accident Thermal Hydraulics Facility (PATH)
PB-FHR. *See* Pebble-bed FHR (PB-FHR)
Pb–Bi. *See* Liquid lead–bismuth eutectic (LBE)
Pb–Bi-Cooled Direct Contact Boiling Water Fast Reactor (PBWFR), 140–141, 143t, 144f
PBMR. *See* Pebble bed modular reactor (PBMR)
PBWFR. *See* Pb–Bi-Cooled Direct Contact Boiling Water Fast Reactor (PBWFR)
PCh. *See* Pressure channel (PCh)
PCS. *See* Power conversion system (PCS)
PDHRSs. *See* Passive DHRSs (PDHRSs)
PDO. *See* Pressure drop oscillation (PDO)
PEACER-300, 360
Pebble bed
  core reactor design, 68–70
  reactor design, 57, 58f
  type, 42
Pebble bed modular reactor (PBMR), 234–236
Pebble fuel, 478
Pebble-bed FHR (PB-FHR), 393
PEC. *See* Practically eliminated condition (PEC)
Pellets, 204, 204f
PFBR. *See* Prototype fast breeder reactor (PFBR)
PGSFR. *See* Prototype Generation IV sodium-cooled fast reactor (PGSFR)
Phenomena Identification and Ranking Table (PIRT), 262
Photoelectrolysis, hydrogen production by, 645
PHTS. *See* Primary heat transport system (PHTS)
PHWRs. *See* Pressurized heavy water reactors (PHWRs)
Physical constants and definitions, 876–877
Physical protection, 419, 563
PIRT. *See* Phenomena Identification and Ranking Table (PIRT)
PIUS. *See* Process Inherent Ultimate Safety (PIUS)
PLD. *See* Pulsed laser deposition (PLD)
Plutonium (Pu), 40, 129, 343, 587–588
  fuel, 63–65, 66t–67t
Plutonium and Uranium Recovery by Extraction process (PUREX process), 262
Plutonium dioxide (PuO_2), 584–587
Plutonium Uranium Redox EXtraction process (PUREX process), 198
PMCS. *See* Passive moderator cooling system (PMCS)
Poisson's ratio, 617
Polonium (Po), 320–321
  Polonium-210, 122
Pool type, 105–106, 106t
Post-accident Thermal Hydraulics Facility (PATH), 441–442, 443f
Post-CDFR, 380
Powder metallurgy process, 290
Power conversion system (PCS), 345
Power generation, 78
  cost, 84, 84f
Power reactor fuels, 201
PPIS. *See* Passive poison injection system (PPIS)
PPs. *See* Primary pumps (PPs)
PR&PP. *See* Proliferation Resistance and Physical Protection (PR&PP)
PRA analysis. *See* Probabilistic Risk Assessment analysis (PRA analysis)
PRACS. *See* Primary reactor auxiliary cooling system (PRACS)
Practical prediction methods, 806–813
  comparison of data fit, 810f
  regular and averaged Prandtl number, 807f
  temperature and heat transfer coefficient, 808f, 811f–812f

weighted average and RMS errors, 814t–815t
Practically eliminated condition (PEC), 437–439
Prandtl number (Pr), 755
cross-sectional averaged, 808–809
dependence, 756–758
Preconceptual plant design, 51
Pressure, 874
vessel concept, 192–193, 193f
Pressure channel (PCh), 619–621
Pressure considerations, 655
Pressure drop oscillation (PDO), 483
Pressure tube (PT), 194–197, 477
Pressurized heavy water reactors (PHWRs), 413–414, 701, 709–713, 720–731, 743
barriers for prevention of releases, 728f
layout of generic PHWR NPP, 732f
simplified CANDU NPP flow diagram, 727f
simplified flow diagram of 515-MW_{el} CANDU reactor NPP, 729f
simplified PHWR NPP flow diagram, 731f
$T-s$ diagram for 515-MW_{el} CANDU reactor Pickering NPP turbine cycle, 730f
3-D image of CANDU-reactor fuel channel with bundle, 729f
Pressurized water reactor (PWR), 25f–26f, 166–167, 189, 223, 247, 341, 374, 701, 709–713, 713f, 743, 778–779
design and operating parameters for EPR, 720t
MHI 1500-MW_{el} advanced PWR NPP simplified layout, 719f
operating ranges of coolants, 752f
parameters of Russian power reactors, 712t
parameters of US PWR NPP, 717t–718t
reference parameters of Generation III+ VVER, 715t
simplified layout of typical US PWR NPP, 716f
simplified thermodynamic layout of 1000-MWel VVER-1000 PWR NPP, 714f
temperature-specific entropy diagram for VVER-1000 turbine cycle, 716f
typical operating conditions, 712f
typical parameters of latest VVER-1000 series 300 and 400, 716t
typical PWR, 713f
Pressurizer (PRZ), 662
PRHR. *See* Passive residual heat removal (PRHR)
PRHRS. *See* Passive residual heat removal system (PRHRS)
Primary coolant loop, 42
Primary cooling system, 104
Primary heat transport system (PHTS), 345
Primary pumps (PPs), 104, 125
Primary reactor auxiliary cooling system (PRACS), 288
Primary RSSs, 288
Primary system concept, 123–126
development and current conceptual designs, 124–126
early conceptual designs derived from sodium-cooled fast reactor concepts, 124
PRISM containment, 681f
Prismatic block type, 42
Prismatic core reactor design, 65–68
Prismatic reactor design, 57, 58f
Private costs, 267
Probabilistic Risk Assessment analysis (PRA analysis), 457
Probabilistic safety analysis (PSA), 263, 266, 395, 464
Probabilistic safety assessment. *See* Probabilistic safety analysis (PSA)
Process Inherent Ultimate Safety (PIUS), 664–666
configuration, 665f
"Product shifting" protocol, 229–230
Production tax credit (PTC), 689
"Program 93+2" plan, 579–580
Proliferation resistance, 419, 690–691
Proliferation Resistance and Physical Protection (PR&PP), 272
Prototype fast breeder reactor (PFBR), 98, 413–414, 432–435
heat transport systems, 431f
operating parameters, 434t
Prototype Generation IV sodium-cooled fast reactor (PGSFR), 335–336
PRZ. *See* Pressurizer (PRZ)

PSA. *See* Probabilistic safety analysis (PSA)
Pseudo-boiling, 797, 802–804
Pseudo-film boiling, 797, 802–804
Pseudocritical
  line, 747–749, 775, 788
  point, 747–749, 775, 788
  region, 747–749
PT. *See* Pressure tube (PT)
PTC. *See* Production tax credit (PTC)
Pulsed laser deposition (PLD), 150
PUMA. *See* Purdue University Multidimensional integral test Assembly (PUMA)
Purdue University Multidimensional integral test Assembly (PUMA), 494
PUREX process. *See* Plutonium and Uranium Recovery by Extraction process (PUREX process); Plutonium Uranium Redox EXtraction process (PUREX process)
PWR. *See* Pressurized water reactor (PWR)
PyC coating. *See* Pyrolytic carbon coating (PyC coating)
Pyrochemical salt batch reprocessing, 164–166
Pyrolytic carbon coating (PyC coating), 401
Pyroprocess Integrated Inactive Demonstration Facility, 338
Python script, 363–364

Q

Qualitative safety features review, 260
Quality assurance (QA), 461

R

R&D. *See* Research and development (R&D)
R/A missions. *See* Reliability/Availability missions (R/A missions)
Radioactive element stockpiles evolution, 169–170
Radiotoxicity reduction, 107
Rankine steam-turbine cycle, 14
Rankine temperature scale, 875
Rare or extreme events (REEs), 460, 473
Rated operation, 72–75
RCRs. *See* Reactivity control rods (RCRs)
RCSs. *See* Reactor coolant systems (RCSs)
RDIPE. *See* Research and Development Institute of Power Engineering (RDIPE)
Re-criticality free core concept, 288
Reactivity anomalies accident, 176
Reactivity control rods (RCRs), 57
Reactor coolant systems (RCSs), 663–664
  comparison of components, 675t
  components, 673–674
Reactor coolants
  fluid coolants, 749–750
  gas coolants, 750–751
  liquid metal coolants, 751
  molten salt coolants, 752
  supercritical fluids as, 772–773
  thermophysical properties
    Generation IV reactor coolants, 743–749
    Generations II, III, and III+ reactor coolants, 743
    of proposed Generation II, III, III+, and IV reactor coolants, 752–759
Reactor core, 190–191
Reactor modelization, 162
Reactor per year (RY), 418–419
Reactor physics, 163
  design, 421–424
  experiment, 350
Reactor pressure vessel (RPV), 57, 385, 477, 713f
Reactor shut-down (RSS), 109
  system, 288
Reactor vessel (RV), 128, 132, 286–288, 287f
Reactor vessel air cooling system (RVACS), 127, 682–684
Reactor vessel auxiliary cooling system. *See* Reactor vessel air cooling system (RVACS)
Recoverable reserves, 576
Recycling economic and social aspects, 574–575
REEs. *See* Rare or extreme events (REEs)
Reference Generation IV systems, 131–137
  BREST-OD-300 reactor, 133–136, 135t, 136f
  ELFR, 132–133, 132f, 133t
  SSTAR, 137
Refueling sodium level (FSL), 286–288

RELAP5 models, 498
Reliability/Availability missions (R/A missions), 457
Reliable steam generator, 296–297
Republic of Korea (ROK), 358
Request for Information (RFI), 234
Research and development (R&D), 37, 91–92, 97, 226, 243–244, 283–284, 309, 335–336, 375, 414, 481
  AHWR activities, 420
  HTR activities, 427
  molten salt reactors activities, 448
Research and Development Institute of Power Engineering (RDIPE), 327–328, 848
Reserve water pool, 210–211
"Rewetting", 797
Reynolds number (Re), 512–513
RFI. *See* Request for Information (RFI)
Rickover safeguards for public well-being, 473–474
Risk and Safety Working Group (RSWG), 265
Risk-informed approach, 288
RMS errors. *See* Root mean square errors (RMS errors)
Rod drive mechanisms, 324–325
"Rogue nations", 268
ROK. *See* Republic of Korea (ROK)
Root causes, 475
Root mean square errors (RMS errors), 809–813, 814t
Rotating plug (RP), 286–288
RP. *See* Rotating plug (RP)
RPV. *See* Reactor pressure vessel (RPV)
RSS. *See* Reactor shut-down (RSS)
RSWG. *See* Risk and Safety Working Group (RSWG)
Russian BREST-OD-300/1200 concepts, 125
Russian experience in nuclear steam reheat, 826
  Beloyarsk NPP reactor
    design, 832
    hydrodynamic stability, 839–842
    physical parameters, 834–837
    startup, 842–845
  BNPP operation, 828–829
  BNPP Unit 1 channels, 833f
  boiling water channels, 837–838
  design parameters and operating conditions, 841t
  modular reactor with steam reheat, 846–849
  parameters of BNPP, 834t, 847t
  pumps, 845
  RDIPE SCW NPP, 848f
  reactors with, 828
  superheated steam channels, 838–839
  thermodynamic cycle development, 830–832
  water chemistry, 845–846
RV. *See* Reactor vessel (RV)
RVACS. *See* Reactor vessel air cooling system (RVACS)
RY. *See* Reactor per year (RY)

S

SA. *See* Severe accident (SA)
SADE. *See* Superheat Advance Demonstration Experiment (SADE)
Safe Integral Reactor (SIR), 664
  configuration, 665f
Safeguards system, 554
Safety, Security, and Safeguards concept (3S concept), 247
Safety design criteria (SDC), 98–99, 107–108, 284, 461
  emerging and new, 461–463
Safety design guidelines (SDGs), 98–99
Safety Objective (SO), 456
Safety of advanced reactors
  classifications of advanced reactors, 468t
  generic safety objectives and safety barriers, 471
    ensuring effective elimination of emergency response, 472–473
    ensuring long-term cooling, 472
    ensuring Rickover safeguards for public well-being, 473–474
    managing rare and extreme events, 473
    reducing likelihood of initiating events, 471–472
  literature review, 486
    boiling water reactor stability, 491–492
    computational fluid dynamics, 496–497

Safety of advanced reactors (*Continued*)
coupled natural-circulation loops, 494–495
early investigations, 487–490
Generation IV passive residual heat removal systems, 493–494
nanofluids, 497
natural-circulation loops, 495–496
numerical methods and artifacts, 492–493
parallel channels, 497–498
sodium fast reactors, 497
supercritical fluid states, 495–496
Three Mile Island issues, 490–491
modeling natural-circulation loops, 498–520
multiple modules and plant risk, 479–480
natural-circulation loop, 481–486
parallel channel thermal-hydraulics, 481–486
risk informing safety requirements, 474–475
safety and reliability goals, 455–456
economic simplified boiling water reactor, 458f
emerging and new SDC, 461–463
licensing procedures, 456–457
safety focus for advanced concepts, 460–461
safety goal and objective of "practical elimination", 464–465
subsidiary safety requirements and licensing review, 457–460
safety objectives and classification, 465–471
safety principles, 455
safety research and development, 481
technical safety issues, 476–479
Safety Reference Levels (SRLs), 465–466
Safety system concept, 205–211
containment of HPLWR with safety systems, 208f
in pressure vessel-type supercritical water-cooled reactor concept, 206–207
pressure-tube type SCWR concept, 207–211, 212f
ADS, 209
atmospheric air heat exchangers, 211
containment pool, 208–209
gravity-driven core flooding system, 209–210
ICs, 210
PMCS, 211
reserve water pool, 210–211
Safety-grade decay heat removal system (SGDHR system), 439–440
SAs. *See* Subassemblies (SAs)
SASS. *See* Self-actuated shut-down system (SASS)
SB. *See* Slug bisque (SB)
SBLOCA. *See* Small-break loss of coolant accident (SBLOCA)
SBO-ATWS. *See* Station blackout anticipated transient without scram (SBO-ATWS)
SC. *See* Steel plate–reinforced concrete (SC)
Science, basic, 556
commercial nuclear power, 557–558
present situation and issues, 559
alternate fuel cycles for advanced reactors, 560–561
commercial fuel supply, 560
enrichment, 561–562
future policy implications of nuclear fuel cycles, 563–564
reprocessing and recycling, 562–563
research for advanced reactors, 559–560
weapons-grade material, 557
SCW. *See* Supercritical water (SCW)
SCWR. *See* Supercritical water-cooled reactor (SCWR)
SCWR-M. *See* Mixed spectrum SCWR (SCWR-M)
SDC. *See* Safety design criteria (SDC)
SDGs. *See* Safety design guidelines (SDGs)
SDS. *See* Shut-down system (SDS)
SEALER. *See* Swedish Advanced Lead Reactor (SEALER)
Secondary cooling system, 105
Secondary sodium circuits (SSDHRs), 439–440
Securing reactor shutdown, 288
Security of supply, 244–245, 270, 272
Segmented insulator concept, 204–205, 207f

SEGS. *See* Solar Energy Generating Systems (SEGS)
Seismic analysis code, 352
Self-actuated shut-down system (SASS), 288, 290–291, 291f
Senior industry advisory panel (SIAP), 249
"Sensitive" materials, 554
Seoul National University (SNU), 358
SERPENT MC code calculations, 163
Severe accident (SA), 457
SFEF. *See* Sodium Fire Experimental Facility (SFEF)
SFR. *See* Sodium-cooled fast reactor (SFR)
SG. *See* Steam generator (SG)
SG pressure vessel (SGPV), 385
SGDHR system. *See* Safety-grade decay heat removal system (SGDHR system)
SGPV. *See* SG pressure vessel (SGPV)
SGTR. *See* Steam generator tube rupture (SGTR)
Shanghai Institute of Applied Physics (SINAP), 393
Shanghai Jiaotong University (SJTU), 385–387
SHS. *See* Superheated steam (SHS)
SHS-Z channels. *See* Zirconium SHS channels (SHS-Z channels)
Shut-down system (SDS), 418
Shutdown, 72–75
S–I. *See* Sulfur–iodine (S–I)
SI units
  primary dimensions and units in, 871
  standard prefixes in, 871
SIAP. *See* Senior industry advisory panel (SIAP)
SiC. *See* Silicon carbide (SiC)
Silicon (Si), 360–362
Silicon carbide (SiC), 623–624
  layer, 60–61
SIMMER code, 292
Simplified fuel handling system, 298
SINAP. *See* Shanghai Institute of Applied Physics (SINAP)
Single channels, 498–503
Single natural-circulation loop, 503–508, 504f
SIR. *See* Safe Integral Reactor (SIR)
Six generation IV nuclear energy systems, 40–52, 41t
  GFR, 43–44, 43f
  LFR, 46–47, 46f
  MSR, 47–49, 48f
  SCWR, 49–52, 50f
  SFR, 44–46, 45f
  VHTR, 40–42, 41f
Six nuclear system concepts, 57
SJTU. *See* Shanghai Jiaotong University (SJTU)
Slug bisque (SB), 631
Small medium reactors. *See* Small modular reactors (SMRs)
Small modular reactors (SMRs), 37, 248, 456, 661
  on coolant type, 663f
  early designs, 664–666
  flexibility, 691–692
  HES utilizing, 691f
  RX of Otto Hahn, 666f
  security, 690–691
Small release frequency (SRF), 459
Small Secure Transportable Autonomous Reactor (SSTAR), 120–121, 126, 137, 138t, 139f, 249
Small-break loss of coolant accident (SBLOCA), 490
SMART. *See* System-integrated Modular Advanced Reactor (SMART)
SMRs. *See* Small modular reactors (SMRs)
SNETP. *See* Sustainable Nuclear Energy Technology Platform (SNETP)
SNF. *See* Spent nuclear fuel (SNF)
SNU. *See* Seoul National University (SNU)
SO. *See* Safety Objective (SO)
SOCA. *See* SOdium CAble Interaction Facility (SOCA)
SOdium CAble Interaction Facility (SOCA), 441–442, 445f
Sodium fast reactors. *See* Sodium-cooled fast reactor (SFR)
Sodium Fire Experimental Facility (SFEF), 441–442, 444f
Sodium pools, 377
Sodium Test Loop for Safety Simulation and Assessment (STELLA), 335–336
  STELLA program, 346–347, 348f
  STELLA-2 test loop, 346–347

Sodium-cooled fast reactor (SFR), 39, 44–46, 45f, 97, 103f–104f, 121, 166–167, 227, 283, 310, 312, 336–338, 374–375, 413–414, 461, 497, 709–713, 737f, 740, 743, 772–773. *See also* Gas-cooled fast reactors (GFRs)
BN-800, 312–313
BN-1200, 317–320
development history, 97–99
future trends and key challenges, 111–114
150 MW_{el} prototype development, 341–346
key-design parameters of Russian SFRs–BN reactors, 739t
lead-cooled fast reactor research and development, 401–405
MBIR, 313–317
molten salt reactor research and development, 393–401
Phts arrangement, 347f
research and development, 375
activities, 346–350
research before SFR construction, 375
safety issue
safety characteristics and safety design, 108–111
safety design criteria and safety design guidelines, 107–108
SFR development strategy, 376
CDFR, 378–380, 379f
CEFR, 376–378, 376f–377f
post-CDFR, 380
STELLA program, 348f
supercritical water-cooled reactor research and development, 385–393
system characteristics
consistency with fuel cycle system, 106–107
core configuration, 100–103, 102f
design features with sodium properties, 99–100, 99t
loop type and pool type, 105–106, 106t
plant system, 103–105
technology, 336–337
thermodynamic layout of 600-MW_{el} BN-600 SFR NPP, 738f
T–s diagram for 600-MW_{el} BN-600 SFR NPP turbine cycle, 738f
VHTR research and development, 380–385
SOdium-Fuel Interaction Facility (SOFI), 441–442, 443f
Sodium-to-AHX. *See* Sodium-to-air Heat eXchanger (Sodium-to-AHX)
Sodium-to-air Heat eXchanger (Sodium-to-AHX), 346
Sodium-water reaction, 110
SOFI. *See* SOdium-Fuel Interaction Facility (SOFI)
Solar energy, hydrogen production from, 645–646
Solar Energy Generating Systems (SEGS), 13f
Solid-fueled TMSR (TMSR-SF), 393
South Korea URANUS-40 system, 137–138, 139t, 140f
Soviet fast reactor program, 310–312
Special Power Excursion Reactor Test Program (SPERT), 488
Specific heat, 874
Spent fuel, 59
Spent nuclear fuel (SNF), 259, 310
SPERT. *See* Special Power Excursion Reactor Test Program (SPERT)
Spiral tube steam generator (STSG), 146
SRF. *See* Small release frequency (SRF)
SRLs. *See* Safety Reference Levels (SRLs)
SSCs. *See* Systems and Components (SSCs)
SSDHRs. *See* Secondary sodium circuits (SSDHRs)
SSTAR. *See* Small Secure Transportable Autonomous Reactor (SSTAR)
Stability, 215–216
START. *See* Strategic Arms Reduction Treaty (START)
Startup, 72–75, 213–215, 214f
pressure tube-type supercritical water-cooled reactor concept, 213–215
Station blackout anticipated transient without scram (SBO-ATWS), 397
Steam, 95
Steam generator (SG), 42, 44, 123, 285, 377–378, 430, 482, 662
Steam generator tube rupture (SGTR), 127
Steam Rankine cycle, 703
Steel core barrel, 67–68
Steel plate–reinforced concrete (SC), 289

containment vessel, 299, 300f
STELLA. *See* Sodium Test Loop for Safety Simulation and Assessment (STELLA)
Strategic Arms Reduction Treaty (START), 545
Stress tests, 243, 473
STSG. *See* Spiral tube steam generator (STSG)
Subassemblies (SAs), 430
Subchannel analysis models, 393
Submarine propulsion, 119–120
Sulfur dioxide (SO_2), 647
Sulfur–iodine (S–I), 642–643
  cycle, 642–643, 647
  process, 42
Super Safe, Small and Simple reactor (4S reactor), 663–664
Supercritical "steam", 747–749, 775
Supercritical carbon dioxide, 797–798
Supercritical fluid(s), 501, 747–749, 774–775
  as reactor coolants, 772–773
  states, 495–496
Supercritical fossil-fired power plant, 212–213
Supercritical heat transfer, 798–802
  HTC *vs*. bulk fluid enthalpy, 803f
  temperature and thermophysical properties profiles, 802f
  temperature profiles, 805f
  variations in heat transfer coefficient values, 804f
Supercritical pressure
  critical parameters of selected fluids, 776t
  density *vs*. temperature, 776f
  dynamic viscosity *vs*. temperature, 777f
  forced convection heat transfer at, 797–813
  heat transfer, 796–797
  historical note on using fluids, 771–775, 795–796
  kinematic viscosity *vs*. temperature, 777f
  power cycles working fluids, 772–773
  Prandtl number *vs*. temperature, 779f
  specific enthalpy *vs*. temperature, 778f
  specific heat at constant pressure *vs*. temperature, 778f
  thermal conductivity *vs*. temperature, 776f
  thermophysical properties, 775–777
  variations of selected thermophysical properties, 780f
  volumetric expansivity *vs*. temperature, 779f
Supercritical water (SCW), 747–750, 771–772, 825
Supercritical water-cooled reactor (SCWR), 39, 49–52, 50f, 189–190, 190f, 375, 619–621, 656, 743–747, 750, 797, 825. *See also* Very high temperature reactor (VHTR)
  advantages and disadvantages, 216–217
  core design options with multiple heat-up steps, 191f
  cutaway view of outlet sleeves, 196f
  direct steam cycle with moisture separator reheater, 195f
  dynamics and control, 212–213, 214f
  fuel assembly concept, 198–205
  fuel channel connection to outlet header, 197f
  fuel cycle technology, 197–198
  future trends, 218
  key challenges, 217–218
  pressure tube concept, 194–197
  pressure vessel concept, 192–193, 193f
  research and development, 385–387
    1000-MW_{el} Chinese supercritical water-cooled reactor, 390–393
    SCWR-M, 387–390
  safety, 476
    system concept, 205–211
  stability, 215–216
  start-up, 213–215
  system, 327–329
  types and system parameters, 190–192
Superheat Advance Demonstration Experiment (SADE), 826
Superheated steam (SHS), 775, 826
  channels, 838–839
Superheated vapor, 747–749
Supplementary tables
  LCOE
    in Germany, 868t
    in United States, 868t
  population, electrical energy consumption per capita, and HDI, 859t–865t
  power reactors by nation, 866t
  relative cost of electricity, 869t

Supplementary tables (*Continued*)
US Department of Energy's loan-guarantee program, 867t
Sustainability, 258–259
Sustainable Nuclear Energy Technology Platform (SNETP), 256–257
SVBR. *See* Svintsovo-Vismutovyi Bystryi Reaktor (SVBR)
SVBR-100 reactor, 120, 141–142, 144t, 145f, 321–324, 322t, 323f
Svintsovo-Vismutovyi Bystryi Reaktor (SVBR), 120, 743–747
Swedish Advanced Lead Reactor (SEALER), 143, 148–149, 149f
System-integrated Modular Advanced Reactor (SMART), 663–664
ECCS system, 686f
Systemic root causes, 475
Systems and Components (SSCs), 457

T

TAO. *See* Thermo-Acoustic Oscillations (TAO)
TD. *See* Theoretical density (TD)
Technical Review Panel (TRP), 234
Technical safety organizations (TSOs), 244
Technology roadmap for six GIF systems, 247–251
Temperature scales, 875
TFM approach. *See* Transient fission matrix approach (TFM approach)
TG. *See* Turbogenerator (TG)
^{232}Th–^{233}U cycle, 587
Theoretical density (TD), 589–591
Thermal conductivity, 875
Thermal hydraulics design, 424
Thermal Oscillations (ThO), 483
Thermal power plants, 3, 14–18
typical ranges of thermal efficiencies, 21t
Thermal-hydraulic(s)
issue, 294
modeling and safety analysis, 394–398
Thermo-Acoustic Oscillations (TAO), 483
Thermo-hydraulics and neutronics coupling analysis, 399
Thermochemical cycles, hydrogen production from, 646
cerium–cerium oxide cycle, 652–653
Cu–Cl cycle, 648–651, 649f
HyS cycle, 648
iron oxide cycle, 651–652
S–I cycle, 647
zinc–zinc oxide cycle, 653–654
Thermochemical water decomposition, 648
Thermodynamic cycle development, 830–832
Thermolysis reaction, 646–647
Thermophysical property software for gases and liquids, 877–878
30-MW_{th} HTTR, 55
ThO. *See* Thermal Oscillations (ThO)
THOREX technology. *See* Thorium Oxide Recovery by Extraction technology (THOREX technology)
Thorium (Th), 42, 59, 587–588, 594
fuel cycle, 167–169
Thorium dioxide (ThO_2), 588, 594–596
Thorium high-temperature reactor 300 (THTR-300), 55
Thorium molten salt reactor (TMSR), 393
Thorium Oxide Recovery by Extraction technology (THOREX technology), 262
Thorium-based accelerator driven system (Thorium-based ADS), 362–363, 362f
Thorium-based ADS. *See* Thorium-based accelerator driven system (Thorium-based ADS)
1000-MW_{el} Chinese supercritical water-cooled reactor, 390–393, 392f
3S concept. *See* Safety, Security, and Safeguards concept (3S concept)
Three Mile Island (TMI), 243, 490–491
Three-Stage Nuclear Power Program, 413–414
THTR-300. *See* Thorium high-temperature reactor 300 (THTR-300)
TIMe DOmain analysis of CSR1000 (TIMDO-CSR1000), 393
TMI. *See* Three Mile Island (TMI)
TMSR. *See* Thorium molten salt reactor (TMSR)
TMSR-LF. *See* Liquid-fuel TMSR (TMSR-LF)
TMSR-SF. *See* Solid-fueled TMSR (TMSR-SF)
Tom'-Usinsk thermal power plant

simplified $T-s$ diagram, 711f
single reheat regenerative cycle 600-MW_{el}, 710f
Tomato-Atsuma coal-fired power plant, 708f
Total loss of power, 176
Transient analysis, 398
Transient fission matrix approach (TFM approach), 162–163
Transient overpower or overcooling, 176
Transition phase, 111
Transmutation approach, 107
Transportation, 639–640
TRansUranics. *See* Transuranium (TRU)
Transuranium (TRU), 59, 157, 341, 358–359
TREAT
program, 292
safety research reactor, 111
Treaty system
attempts to improving, 555–556
effects, 551–553
shortcomings, 553–555
TRI-ISOtropic-coated particle fuel (TRISO-coated particle fuel), 42, 55, 60–61, 61f, 428–429
TRISO coating system, 354f
TRISO fuel
fabrication, 336
particles, 399
technology, 353–355
TRISO pellets, 587
TRISO-coated particle fuel. *See* TRI-ISOtropic-coated particle fuel (TRISO-coated particle fuel)
Tritium, 655–656
TRP. *See* Technical Review Panel (TRP)
TRU. *See* Transuranium (TRU)
TSOs. *See* Technical safety organizations (TSOs)
Tsunamis, 288–289
Tube-to-tube sheet weld failure, 297
Turbine inlet, 189–190
Turbogenerator (TG), 430
"2012 Interdisciplinary Study", 255–256
Two-loop cooling system, 294–295
Two-phase fluid, 505
TWOTRAN-2, 63

U
^{235}U, 106–107, 260, 584
^{238}U, 107
$^{238}U-^{239}Pu$ cycle, 587
UC. *See* Uranium carbide (UC)
UC_2. *See* Uranium dicarbide (UC_2)
UCB. *See* University of California–Berkeley (UCB)
UCO. *See* Uranium carbide (UC)
UIHS. *See* Ultimate and indefinitely lasting heat sinks (UIHS)
UIS. *See* Upper internal structure (UIS)
ULOF. *See* Unprotected loss of flow (ULOF)
Ulsan National Institute of Science and Technology (UNIST), 363
Ultimate and indefinitely lasting heat sinks (UIHS), 471
Ultimate shut-down systems (USD systems), 439
UN. *See* Uranium mononitride (UN)
UN Security Council, 563
Uncertainty analysis, 418–419
UNIST. *See* Ulsan National Institute of Science and Technology (UNIST)
Unit conversion, 872–876
United States Atomic Energy Commission (USAEC), 825–826
University of California–Berkeley (UCB), 364–365, 393
Unprotected loss of flow (ULOF), 395–397
Unprotected overcooling accident (UOC), 395–397
Unprotected transient overpower (UTOP), 395–397
UOC. *See* Unprotected overcooling accident (UOC); Uranium oxycarbide (UOC)
UP. *See* Upper plenum (UP)
Upper internal structure (UIS), 289
Upper plenum (UP), 667
Uranium (U), 40, 310, 336–337, 587–588
fuel, 63, 64t–65t
advanced cycle, 575f
uranium–thorium–zirconium fuels, 626–628
uranium–zirconium hydride fuel, 624–625
Uranium carbide (UC), 57, 588, 597–601
Uranium dicarbide (UC_2), 588, 601–606

Uranium dinitride (UN_2), 606
Uranium dioxide (UO_2), 59, 584–587, 589–591
  uranium dioxide–beryllium oxide, 630–631
  uranium dioxide–graphite, 629
  uranium dioxide–silicon carbide, 628–629
Uranium mononitride (UN), 588, 606–615
Uranium nitride (UN). *See* Uranium mononitride (UN)
Uranium oxycarbide (UOC), 59
Uranium sesquicarbide (U_2C_3), 596
Uranium sesquinitride (U_2N_3), 606
URANUS
  deploying underground for security enhancement, 361f
  design, 360–362
US Department of Energy (DOE), 37, 57, 226–227, 661–662
US domestic nuclear industry, 232
US experience in nuclear steam reheat, 825–826
US Nuclear Regulatory Commission (NRC), 226, 457, 667
US policy, 564
USAEC. *See* United States Atomic Energy Commission (USAEC)
USD systems. *See* Ultimate shut-down systems (USD systems)
User nations, 272
USSR and Russia, Generation IV
  HLMRs, 320–327
  Russian government, 309
  SCWR system, 327–329
  sodium fast reactors, 312–320
  Soviet fast reactor program, 310–312
UTOP. *See* Unprotected transient overpower (UTOP)
U–$ZrH_{1.6}$, 625

V

Verification by Integral Simulation of Transients and Accident–Integral Test Loop (VISTA-ITL), 494
Very high temperature reactor (VHTR), 39–42, 41f, 55, 227, 336–341, 380–381, 478, 587, 743–747, 772. *See also* Supercritical water-cooled reactor (SCWR)
  applications, 77–86
    energy and material balance, 81f
    industrial application, 81–82
  desalination cogeneration cost, 86
  design and analysis codes, 350–352
  detailed technical description
    fuel burnup, 63–65
    fuel design, 60–63, 62t
    plant design, 72
    plant operations, 72–77
    reactor design, 65–70, 69t
    reactor safety, 70–72, 71f
  development history and current status, 55–57
  economics, 82–86
    electricity generation cost, 82–84
    hydrogen production cost, 84–85, 85t
  gas turbine power generation cycle, 78f
  high-temperature materials, 355–356
  hydrogen production, 356–358
  research and development, 380–381
    early development of HTGR program, 381
    high-temperature reactor pebble-bed modular project, 384–385
    HTR-10 test module project, 381–384
  safety, 476
  technology overview
    design features, 58–60
    fuel cycle, 59
    multipurpose, 60
    reactor design types, 57
    safety, 58–59
  temperature range of VHTR and heat demand of industries, 60f
  TRISO
    coating system, 354f
    fuel technology, 353–355
VHTR. *See* Very high temperature reactor (VHTR)
Viscosity
  dynamic, 875–876
  kinematic, 876
VISTA-ITL. *See* Verification by Integral Simulation of Transients and Accident–Integral Test Loop (VISTA-ITL)
Vortex model, 293–294

W
W-SMR. *See* Westinghouse Small Modular Reactor (W-SMR)
Wall-to-fluid friction factor, 512–513
Waste to energy, 577–578
Water, 637, 797
  chemistry, 845–846
  electrolysis, 644
  mock-up of separator, 181f
  peak values of specific heat, volume expansivity, and thermal conductivity, 790t–792t
  specific heat, volume expansivity, and thermal conductivity *vs*. temperature, 785f
  specific heat profiles at various pressures, 785f
  splitting processes, 638
  thermodynamics diagrams for, 773f
  values of pseudocritical temperature, 789t
  water–steam loops, 127
"Weapons grade", 559
Weapons of mass destruction (WMDs), 546
Weld metal (WM), 355–356
Westinghouse cycle. *See* Hybrid sulfur cycle (HyS cycle)
Westinghouse Small Modular Reactor (W-SMR), 662, 684f
  containment, 680f
  nuclear safety components, 683t
WM. *See* Weld metal (WM)
WMDs. *See* Weapons of mass destruction (WMDs)
Wrapper tube, 101–102

X
Xi'an Jiaotong University (XJTU), 375

Y
Yttria-stabilized zirconia (YSZ), 359

Z
Zangger Committee, 554
Zero-dimensional approach, 502
Zinc (Zn), 642–643
Zinc oxide cycle (ZnO cycle), 642–643
Zinc–zinc oxide cycle (Zn–ZnO cycle), 653–654
Zirconium (Zr), 52, 338, 652–653
Zirconium carbide (ZrC), 63
Zirconium SHS channels (SHS-Z channels), 848–849, 849f
Zirconium-hydride (ZrH_2), 51, 200, 625
ZnO cycle. *See* Zinc oxide cycle (ZnO cycle)
Zn–ZnO cycle. *See* Zinc–zinc oxide cycle (Zn–ZnO cycle)
ZrC. *See* Zirconium carbide (ZrC)

Woodhead Publishing is an imprint of Elsevier
The Officers' Mess Business Centre, Royston Road, Duxford, CB22 4QH, UK
50 Hampshire Street, 5th Floor, Cambridge, MA 02139, USA
The Boulevard, Langford Lane, Kidlington, OX5 1GB, UK

Copyright © 2016 Elsevier Ltd. All rights reserved.

No part of this publication may be reproduced or transmitted in any form or by any means, electronic or mechanical, including photocopying, recording, or any information storage and retrieval system, without permission in writing from the publisher. Details on how to seek permission, further information about the Publisher's permissions policies and our arrangements with organizations such as the Copyright Clearance Center and the Copyright Licensing Agency, can be found at our website: www.elsevier.com/permissions.

This book and the individual contributions contained in it are protected under copyright by the Publisher (other than as may be noted herein).

Notices
Knowledge and best practice in this field are constantly changing. As new research and experience broaden our understanding, changes in research methods, professional practices, or medical treatment may become necessary.

Practitioners and researchers must always rely on their own experience and knowledge in evaluating and using any information, methods, compounds, or experiments described herein. In using such information or methods they should be mindful of their own safety and the safety of others, including parties for whom they have a professional responsibility.

To the fullest extent of the law, neither the Publisher nor the authors, contributors, or editors, assume any liability for any injury and/or damage to persons or property as a matter of products liability, negligence or otherwise, or from any use or operation of any methods, products, instructions, or ideas contained in the material herein.

British Library Cataloguing-in-Publication Data
A catalogue record for this book is available from the British Library

Library of Congress Cataloging-in-Publication Data
A catalog record for this book is available from the Library of Congress

ISBN: 978-0-08-100149-3 (print)
ISBN: 978-0-08-100162-2 (online)

For information on all Woodhead Publishing publications visit our website at https://www.elsevier.com/



Publisher: Joe Hayton
Acquisition Editor: Cari Owen
Editorial Project Manager: Alex White
Production Project Manager: Omer Mukthar
Designer: Greg Harris

Typeset by TNQ Books and Journals

Related titles

Handbook of Small Modular Nuclear Reactors
(ISBN 978-0-85709-851-1)

Small Modular Reactors: Nuclear Power Fad or Future?
(ISBN 978-0-08100-252-0)